Journal of Pharmaceutical and Biomedical Analysis 61 (2012) 1–7

Contents lists available at SciVerse ScienceDirect

Journal of Pharmaceutical and Biomedical Analysis

journal homepage: www.elsevier.com/locate/jpba

A solid phase extraction-liquid chromatographic–tandem mass spectrometry method for determination of concentrations of GDC-0941, a small molecule class I phosphatidylinositide 3-kinase inhibitor, to support clinical development

X. Ding[a,*], G. Morrison[b], B. Dean[a], C.E.C.A. Hop[a], L. Tobler[d], S. Percey[d], M. Meng[d], S. Reuschel[d], D.A. West[c], S. Holden[b], J.A. Ware[c]

[a] Genentech, Drug Metabolism and Pharmacokinetics, MS 412A, 1 DNA Way, South San Francisco, CA 94080, United States
[b] Genentech, Research and Early Development, Exploratory Clinical Development, United States
[c] Genentech, Research and Early Development, Small Molecule Clinical Pharmacology, United States
[d] Tandem Labs, 1121 East 3900 South, Salt Lake City, UT 84124, United States

ARTICLE INFO

Article history:
Received 26 July 2011
Received in revised form 3 November 2011
Accepted 7 November 2011
Available online 25 November 2011

Keywords:
GDC-0941
Class I phosphatidylinositide 3-kinase (PI3K)
96-Well SPE
Human plasma
LC–MS/MS

ABSTRACT

A solid phase extraction (SPE) liquid chromatographic–tandem mass spectrometry (LC–MS/MS) method for the determination of GDC-0941 concentrations in human plasma has been developed and validated to support clinical development. An Oasis MCX 10 mg 96-well SPE plate was used to extract plasma samples (50 μL) and the resulting extracts were analyzed using reverse-phase chromatography and mass spectrometer coupled with a turbo-ionspray interface. The method was validated over the calibration curve range 0.500–500 ng/mL with linear regression and $1/x^2$ weighting. Within-run relative standard deviation (%RSD) ranged from 1.5 to 11.5%, while the between-run %RSD varied from 0.0 to 4.4%. The accuracy ranged from 96.0% to 110.0% of nominal for within-run and 98.0% to 108.0% of nominal for between-run at all concentrations including the LLOQ quality control at 0.500 ng/mL. Extraction recovery of GDC-0941 was between 79.0% and 86.2%. Stability of GDC-0941 was established in human plasma for 602 days at −70 °C and 598 days at −20 °C, respectively, and established in reconstituted sample extracts for 167 h when stored at room temperature. Internal standard normalized matrix factor was 1.1, demonstrating that the use of the stable-labeled internal standard GDC-0941-d_8 effectively compensated observed matrix effect and resulting in no adverse impact on the quality of the data produced. This assay was used for the determination of GDC-0941 human plasma concentrations over a sufficient time period to determine pharmacokinetic parameters at relevant clinical doses.

© 2011 Elsevier B.V. All rights reserved.

1. Introduction

GDC-0941 (Fig. 1) is a small-molecule class I phosphatidylinositide 3-kinase (PI3K) inhibitor, which is currently in clinical development [1–5]. The PI3K signaling pathway is a major downstream effector of receptor tyrosine kinases that stimulate cell proliferation, promote survival, and inhibit apoptosis, such as human epidermal growth factor-2 (HER2), epidermal growth factor receptor (EGFR), and insulin like growth factor-1 receptor. Abnormal regulation of this central signaling pathway has been identified in a large number of cancer types, occurring through a variety of mechanisms. The pathway is constitutively activated by the loss of the tumor suppressor phosphatase and tensin homolog (PTEN), a phosphatase that counteracts the kinase activity of PI3K, in many tumor types [6,7]. AKT, a downstream target for PI3K, is overexpressed in some tumor types [8–10] and has been shown to be transforming [11]. Activating mutations of PI3K-α, which belongs to the class IA PI3K family, have been observed in a number of different tumor types [12,13]. These activating mutations have been shown to promote growth and invasion in cancer cells, effects that are abrogated by PI3K inhibitors. Taken together, these data provide a strong rationale for developing inhibitors of PI3K pathway signaling as a therapeutic strategy for human cancer.

A SPE LC–MS/MS method for the determination of GDC-0941 concentrations in human plasma was developed and validated using Oasis 96-well MCX SPE plates. The method was used for determination of GDC-0941pharmacokinetic behavior in a phase I trial utilizing healthy volunteers (GDC4740g, An Open-Label, Two-Part Study to Determine the Relative Bioavailability of Capsule and Tablet Formulations of GDC-0941 in Healthy Volunteer), the results of which are included in this paper. The method is also useful for

* Corresponding author. Tel.: +1 650 225 4102; fax: +1 650 467 3487.
E-mail address: ding.xiao@gene.com (X. Ding).

0731-7085/$ – see front matter © 2011 Elsevier B.V. All rights reserved.
doi:10.1016/j.jpba.2011.11.005

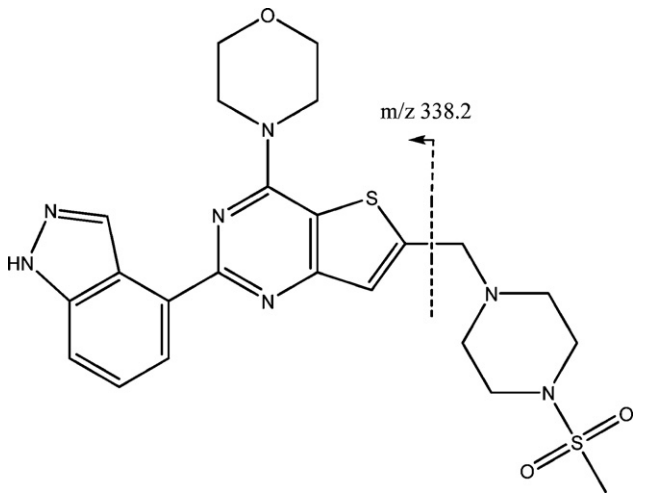

Fig. 1. Structure of GDC-0941.

the determination of GDC-0941 concentrations in human plasma in clinical trials.

2. Experimental

2.1. Materials

Test compound GDC-0941 and internal standard GDC-0941-d_8 were synthesized at Genentech with a purity of 97.4% and 96.5%, respectively. Acetonitrile (HPLC grade), methanol (HPLC grade), formic acid (ACS grade) and ammonium hydroxide (ACS grade) were obtained from EMD (Gibbstown, NJ, USA). N,N-dimethylformamide (HPLC grade) was obtained from Burdick and Jackson (Morristown, NJ, USA). Deionized water (type 1, typical 18.2 MΩ cm) or equivalent was generated at Tandem Labs (Salt Lake City, UT, USA). All reagents were used as received. Oasis MCX (10 mg) 96-well SPE plates were obtained from Waters Inc. (Milford, MA, USA). Human plasma (K_2EDTA) was obtained from Bioreclamation (Hicksville, NY, USA).

2.2. Instrumentation

The liquid chromatographic system consisted of a Shimadzu SCL-10A system controller and two LC-10AD Shimadzu pumps (Columbia, MD, USA). The detector was an API5000 mass spectrometer with a turbo-ionspray interface (ABSciex, Concord, Ontario, Canada). The separation was performed on a Metasil AQ 5 μm C_{18} 2.1 mm × 50 mm column (Varian, Inc., Palo Alto, CA USA) at a temperature of 55 °C controlled by a Cera column oven (SPEWare Corporation, Baldwin Park, CA, USA). Data was collected and processed using Analyst software (version 1.4.2, AB Sciex). The SPE procedure was performed using a Tomtec Quadra 96® (Hamden, CT, USA) and a CEREX® System 96 Multi-Channel SPE Positive Pressure Manifold from SPEWare Corp. (San Pedro, CA, USA). A Leap CTC PAL Autosampler (Chapel Hill, NC, USA) and an electronically actuated six-port high pressure switching valve (Valco Instruments Co., Houston, TX, USA) were used for introducing the samples to the LC–MS/MS system.

2.3. LC–MS/MS conditions

The three mobile phases (MP) used for separation and column cleaning were water containing 0.1% formic acid (mobile phase A), acetonitrile (mobile phase B), and 90:10 (v/v) acetonitrile:water (mobile phase C). Separation was achieved using reverse-phase liquid chromatography at a flow rate of 0.40 mL/min (typical column pressure 60 bar). An UNIGUARD guard cartridge (Thermo Fisher Scientific, Waltham, MA, USA) was used to protect the analytical column. The column cleaning was achieved by back flushing the analytical column for 1 min after elution of each sample with mobile phase C at a flow rate of 0.80 mL/min (back pressure ~200 bar). The following gradient conditions were used: equilibrate at 20% MP B for 1 min,ramp up from 20% MP B to 40% MP B in 0.5 min and hold at 40% B for 0.5 min, step down from 40% MP B to 20% MP B in 0.1 min, back flush for approximately 1 min with MP C, and re-equilibrate at 20% MP B for 0.5 min. Run time was 3.5 min and peak retention time was 1.8 min under the chromatographic conditions.

Mass spectrometer parameters were optimized by infusing a neat solution of GDC-0941 and the internal standard (IS) GDC-0941-d_8 separately using a Harvard Apparatus syringe pump (Holliston, MA, USA). GDC-0941 and GDC-0941-d_8 were ionized using a turbo-ionspray source operating in the positive ionization mode. The quantitation of GDC-0941 was performed using the selected reaction monitoring mode (SRM) with 100 ms dwell times for each transition, 5500 V ionspray voltage, 75 V declustering potential and 55 V collision energy. The SRM transitions monitored were m/z 514.3 to m/z 338.2 for GDC-0941 and m/z 522.3 to m/z 338.2 for GDC-0941-d_8. Analyst software 1.4.2 was used to optimize the MS parameters, data acquisition and data processing.

2.4. Preparation of standards and quality control samples

The initial standard stock solution containing GDC-0941 (1 mg/mL) was prepared in N,N-dimethylformamide (DMF) solvent and then diluted using DMF to give working standards ranging from 10 to 10,000 ng/mL.The working standards were spiked into plasma to prepare calibration standards at concentration 0.500, 1.00, 5.00, 25.0, 100, 300, 450 and 500 ng/mL.

High, middle, low, lower limit of quantitation (LLOQ) and dilution quality control (QC) samples containing GDC-0941 were prepared from a separate reference material weighing at concentrations of 400, 200, 1.50, 0.500 and 1,000 ng/mL, respectively, by diluting the stock solutions (1 mg/mL in DMF) with control human plasma. Following preparation, aliquots of quality control samples were transferred to cryogenic vials capped and stored at −60 °C to −80 °C.

The internal standard stock solution was prepared at 0.346 mg/mL in DMF. The working IS solution was prepared at 200 ng/mL by diluting the IS stock solution with DMF. The working IS solution (200 ng/mL) was diluted with water at 1:1 ratio, resulting in the final concentration of 100 ng/mL in 1:1 ratio of DMF:water (v/v), before spiking into the samples.

All stock solutions, working standards and working IS solution were stored at 1–8 °C. Working standards, QC samples and working IS solution were removed from freezer or refrigerator, thawed or equilibrated at room temperature, and used for the validation and the analysis of clinical human plasma samples.

2.5. Extraction of human plasma

To each well of a clean 96-well plate, was manually added 50 μL of each of calibration curve standards, QCs, control blanks, blanks or samples. To each well of the plate except for the wells containing the plasma blanks was manually added a 50 μL aliquot of diluted working IS solution (100 ng/mL in 1:1 ratio of DMF:water). The wells containing the plasma blanks received a 50 μL aliquot of DMF:water (1:1). Following the addition of 200 μL of water containing 5% formic acid to all wells of the plate, the plate was vortexed for 1 min and centrifuged at approximately 1500 × g for 1 min.

Methanol (400 μL) and 5% formic acid in water (400 μL) were added sequentially to each well of an Oasis MCX 96-well SPE plate to condition the plate. The buffered samples(300 μL) were then loaded to the plate and washed sequentially with 400 μL of 5% formic acid in water followed by 400 μL of methanol and eluted slowly with 400 μL of freshly prepared 5% (v/v) ammonium hydroxide in methanol into a 96-well collection plate. Eluted samples were evaporated to dryness using a turbovap set at 50 °C for approximately 30 min. Following reconstitution with 300 μL of 0.1% formic acid in water:acetonitrile (85:15, v/v), the 96-well collection plate was capped, vortexed and centrifuged at 1500 × *g* for 1 min. Ten μL of each of reconstituted samples was injected onto the LC–MS/MS system for analysis.

2.6. Stability

Low and high QC samples ($n = 6$ at each concentration) were subjected to five freeze–thaw cycles consisting of complete thawing at room temperature, vortexing, and then refreezing at −60 °C to −80 °C for at least 12 h. After five freeze–thaw cycles the samples were analyzed using freshly prepared calibration standards. Bench top stability was evaluated using low and high QC samples ($n = 6$ at each concentration) after sitting on the bench top at room temperature for 7 h prior to extraction. Long-term stability was also evaluated using low and high QC samples ($n = 6$ at each concentration). The QC samples were extracted after frozen storage at a temperature between −60 °C and −80 °C for 602 days and between −10 °C and −30 °C for 598 days separately. The reinjection reproducibility of extracted samples (or autosampler storage stability after extraction) was evaluated by letting extracted calibration standards ($n = 2$ at each concentration) and QC samples ($n = 6$ at low, medium and high QC concentrations) sit in the autosampler tray at room temperature for 167 h and then reinjecting them onto the LC–MS/MS system. To demonstrate that GDC-0941 blood samples were stable during the sample collection and processing of whole blood to plasma, the stability of GDC-0941 in whole blood was evaluated by spiking GDC-0941 into whole blood at a concentration of 300 ng/mL, storing the whole blood samples at room temperature or 1–8 °C for 2 h prior to analysis.

2.7. Pharmacokinetics of GDC-0941 in healthy volunteers

Pharmacokinetics of GDC-0941 was studied in an open-label, single-dose phase I study in eighteen healthy male and female subjects following Institutional Review Board approval of the protocol. Upon obtaining informed consent, meeting institutional and federal requirements and meeting study entry criteria, 60 mg of GDC-0941 was administered orally as a single, two-period randomized cross over between phase I capsule and prototype tablet with 240 mL room temperature tap water after a minimum of an 8-h fast. After drug administration, 12 serial blood samples were obtained over a 72 h sampling period and plasma was harvested for the determination of GDC-0941 plasma concentration over time.

Pharmacokinetic calculations were performed using WinNonlin® version 5.2.1 (Pharsight Corporation, Mountain View, CA). All AUC values were calculated using the linear trapezoidal method when the concentrations were rising and the logarithmic trapezoidal method when the concentrations were declining (linear up/Log down rule in WinNonlin®). Below the lower limit of quantitation (LLOQ) values at predose were considered as missing for PK analysis. Nominal blood collection time was used to calculate PK parameters. PK parameters were reported as their means and standard deviations (SD).

3. Results and discussion

3.1. LC–MS/MS

The quantitation of GDC-0941 was performed on the LC–MS/MS system described earlier using a turbo-ionspray source and SRM with positive ion mode. The predominant SRM transitions m/z 514.3 to m/z 338.2 for GDC-0941 and m/z522.3 to m/z 338.2 for IS GDC-0941-d_8 were monitored. Under the gradient chromatographic condition described earlier, the retention time was 1.8 min ($k' \sim 5.7$) for both GDC-0941 and GDC-0941-d_8 and the total HPLC run time was 3.5 min. Full scan product ion mass spectra of GDC-0941 and GDC-0941-d8 are shown in Fig. 2.

The need for column cleaning between injections was due to the low organic composition of the LC gradient, which caused endogenous phospholipids to be permanently retained on the LC column. Without this column cleaning step, the phospholipids can accumulate on the column and cause unwanted matrix effects such as divergent calibrations standards or random ion suppression. We therefore back flushed the column with a strong solvent at a high flow rate to remove the phospholipids from the column and improve the overall performance of the assay.

3.2. Accuracy and precision

Validation experiments were performed on three separate days with 2 calibration curves and 6 replicates of quality control samples at each concentration. Back-calculated concentrations of calibration Standards for GDC-0941 are listed in Table 1. Within-run and between-run accuracy and precision obtained from the validation experiments are summarized in Table 2. The within-run relative standard deviation (%RSD) from QC samples ranged from 1.5 to 11.5%, while the between-run %RSD from QC samples varied from 0.0 to 4.4%. The accuracy ranged from 96.0% to 110.0% of nominal for within-run and 98.0% to 108.0% of nominal for between-run at all concentrations including the LLOQ quality control at 0.500 ng/mL.

3.3. Sensitivity

Sensitivity was evaluated by extracting and analyzing six replicates of LLOQ QC samples at concentrations of0.500 ng/mL in three validation runs. Representative chromatograms of GDC-0941 at LLOQ and IS GDC-0941-d_8 at final concentration of 100 ng/mL are shown in Fig. 3. The accuracy at the LLOQ of 0.500 ng/mL was within 108.6% of nominal. The precision at the LLOQ was 11.5% (Table 2). The average signal to noise ratio of the LLOQ at 0.500 ng/mL was >10:1.

3.4. Selectivity and matrix effect

Selectivity was evaluated for GDC-0941 and IS GDC-0941-d_8 using six lots of blank plasma. Representative chromatograms of extracted blank plasma from GDC-0941 and IS GDC-0941-d_8 channels are shown in Fig. 4. Interference peaks in all six lots of blank plasma at the retention time of the GDC-0941 were ≤20% of the mean response for the GDC-0941 at the LLOQ. The interference peaks in all six lots of blank plasma at the retention time of the IS GDC-0941-d_8 were ≤5% of the mean response for the IS for all tested samples. No significant interference was observed at the retention time of the GDC-0941 and IS GDC-0941-d_8.

To further ensure the selectivity, the matrix effect was investigated using LLOQ QCs prepared in ten lots of blank plasma. The accuracy of the LLOQ QCs was within 109.0% of nominal and the precision was within 7.7% (Table 3).

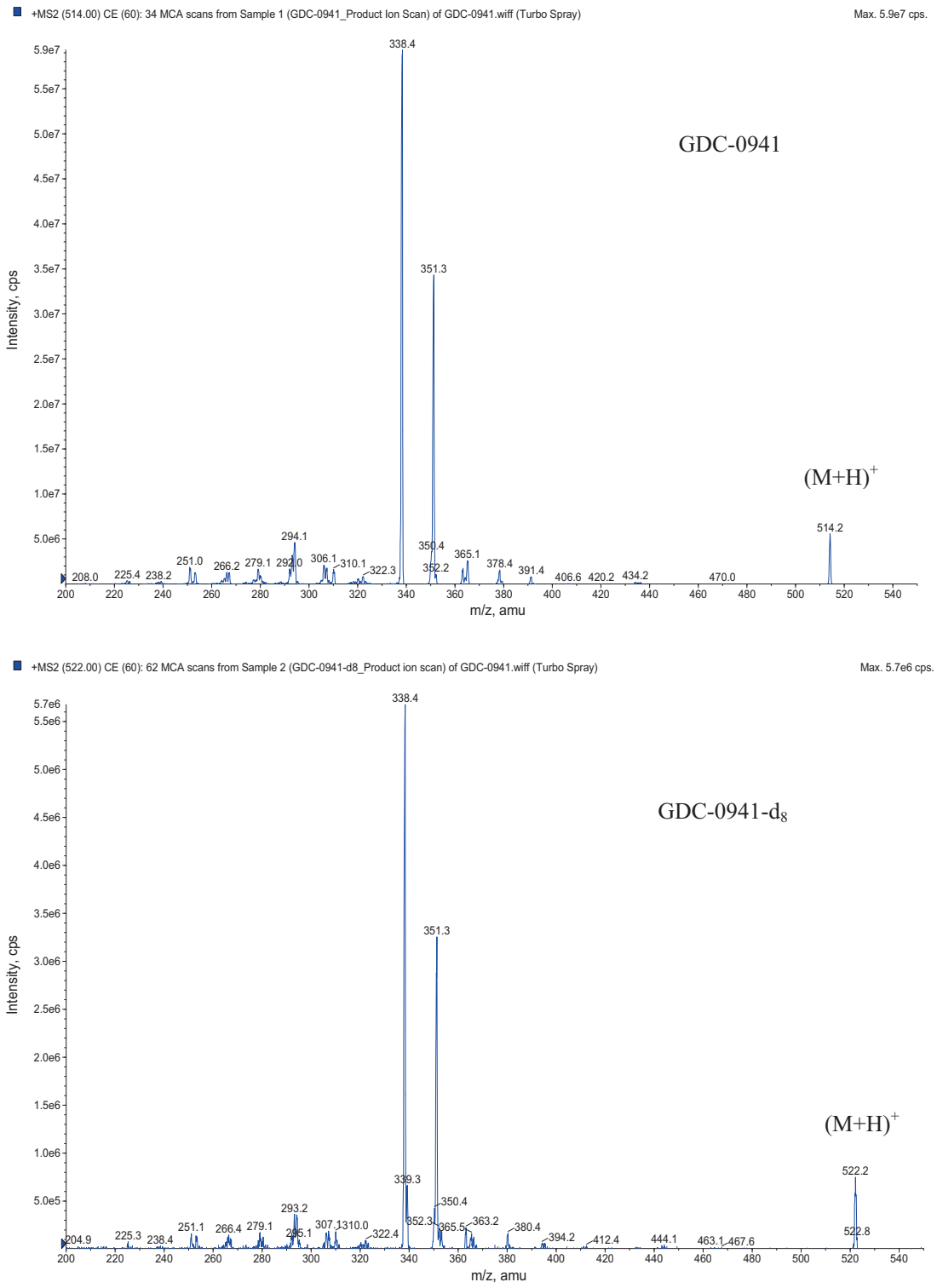

Fig. 2. Product ion mass spectra of GDC-0941 and GDC-0941-d_8.

The matrix effect was also evaluated quantitatively by measurement of the matrix factor, a ratio of the analyte peak response in the presence of matrix ions to the analyte peak response in the absence of matrix ions, i.e. in solvent [14]. Following the validated extraction procedure, six lots of blank human plasma were extracted and evaporated to dryness. An aliquot of 200 μL of solution containing 50 ng/mL GDC-0941 was spiked into the six tubes containing dried lots of blank plasma extract. The peak areas of the six resulting extracted solutions were compared to the peak areas of the six GDC-0941 neat solutions at 50 ng/mL concentration. The matrix factor, when measured by analyte or internal standard peak area, was 1.7 for GDC-0941 and 1.5 for IS GDC-0941-d_8 (Table 4), suggesting ionization enhancement for both GDC-0941 and IS GDC-0941-d_8. The internal standard normalized matrix factor, calculated using the area ratio of GDC-0941 to IS GDC-0941-d_8, was 1.1 (Table 4). The use of the stable-labeled internal standard GDC-0941-d_8 effectively compensated for the observed matrix effect and resulted in no adverse impact on the quality of the data produced.

Table 1
Back-calculated concentrations of calibration standards for GDC-0941 (linear weighted $1/x^2$).

	0.500 ng/mL	1.00 ng/mL	5.00 ng/mL	25.0 ng/mL	100 ng/mL	300 ng/mL	450 ng/mL	500 ng/mL	R^2
Run 1	0.482	1.01	4.94	25.6	91.6	303	463	528	0.9978
	0.519	1.00	4.57	25.4	104	286	459	509	
Run 2	0.496	0.960	5.33	27.1	101	290	450	479	0.9974
	0.504	1.01	5.27	25.7	103	280	423	478	
Run 3	0.495	0.959	5.36	27.3	101	286	437	477	0.9970
	0.499	1.04	5.23	26.2	102	283	436	468	
Mean	0.499	0.997	5.12	26.2	100	288	445	490	0.9974
Accuracy[a] (%)	98.0	97.0	102.4	104.8	100.0	96.0	98.9	98.0	
RSD[b] (%)	2.4	3.2	6.0	3.1	4.5	2.8	3.4	4.8	0.0
n	6	6	6	6	6	6	6	6	

[a] Expressed as [(mean observed concentration)/(nominal concentration)] × 100.
[b] Relative standard deviation: (standard deviation/mean) × 100.

Table 2
Within-run and between-run accuracy and precision of GDC-0941 quality control samples.

	LLOQ (0.500 ng/mL)	Low QC (1.50 ng/mL)	Middle QC (200 ng/mL)	High QC (400 ng/mL)	Dilution QC (1000 ng/mL)
Within-run mean (n = 6)	0.541	1.65	213	402	1020
Accuracy[a] (%)	108.2	110.0	106.5	100.5	102.0
RSD[b] (%)	11.5	5.0	2.0	4.6	1.6
Within-run mean (n = 6)	0.534	1.51	197	384	
Accuracy[a] (%)	106.8	100.7	98.5	96.0	
RSD[b] (%)	6.2	4.2	3.1	2.8	
Within-run mean (n = 6)	0.543	1.54	210	391	
Accuracy[a] (%)	108.6	102.7	105.0	97.8	
RSD[b] (%)	6.0	2.6	1.5	1.5	
Between-run mean (n = 18)	0.540	1.57	207	392	
Accuracy[a] (%)	108.0	104.7	103.5	98.0	
RSD[b] (%)	0.0	4.4	3.9	1.9	

[a] Expressed as [(mean observed concentration)/(nominal concentration)] × 100.
[b] Relative standard deviation: (standard deviation/mean) × 100.

3.5. Integrity of dilution

The ability to dilute samples with acceptable accuracy and precision was evaluated by preparation of a dilution QC containing GDC-0941 at a concentration of 1000 ng/mL, diluting it tenfold (n = 6) and then analyzing these diluted QC samples in one of the validation experiments. The accuracy of dilution QCs at 1000 ng/mL was within 102.0% of nominal and the precision was within 1.6% (Table 2).

3.6. Stability

Freeze–thaw, bench-top, long-term storage, sample collection (whole blood stability)and extracted sample stabilities were assessed under the conditions described earlier. It was demonstrated that GDC-0941 was stable in human plasma after five freeze–thaw cycles, stable in human plasma after storage on the bench-top at room temperature for 7 h prior to extraction, stable after extracted GDC-0941 QC plasma samples were stored in the autosampler tray at room temperature for 167 h, and stable in human plasma for 602 days at -70 ± 10 °C and 598 days at -20 ± 10 °C. Sample collection stability assessment demonstrated that GDC-0941 was stable in human whole blood for up to 2 h at both room temperature and 1–8 °C. The stability results are summarized in Table 5.

3.7. Extraction recovery

Extraction recovery was evaluated at low, medium and high QC concentrations (1500, 200 and 400 ng/mL) for GDC-0941 and at single concentration (200 ng/mL) for GDC-0941-d_8 using Oasis MCX SPE plate with a mixed-mode cation-exchange and reversed-phase sorbent. Through ionic interactions of GDC-0941 with the negatively charged MCX stationary phase at the acidic condition (5% formic acid in water) and hydrophobic interaction of GDC-0941 with the MCX reversed-phase sorbent, GDC-0941 was retained to the MCX mixed-mode sorbent, allowing removal of impurities that were not retained at acidic condition. Elution of GDC-0941 under basic conditions(5% ammonium hydroxide in methanol) allowed the neutralization of the ionic interaction between GDC-0941 and the stationary phase. Extraction recovery, measured by comparing the analyte/IS peak area ratio of the QC samples spiked in human plasma before extraction to control human plasma extracted in the same manner and then spiked post-extraction with a known

Table 3
Selectivity and matrix effect at the lower limit of quantitation for GDC-0941.

Nominal conc. (ng/mL)	LLOQ 1	LLOQ 2	LLOQ 3	LLOQ 4	LLOQ 5	LLOQ 6	LLOQ 7	LLOQ 8	LLOQ 9	LLOQ 10	Mean	Accuracy[a] (%)	RSD[b] (%)
0.500	0.545	0.597	0.544	0.569	[c]	0.490	0.485	0.551	0.503	0.587	0.545	109.0	7.7

[a] Expressed as [(mean observed concentration)/(nominal concentration)] × 100.
[b] Relative standard deviation: (standard deviation/mean) × 100.
[c] Sample deactivated due to analytical reason.

Table 4
Matrix Effect–Measured Matrix Factor for GDC-0941.

	Analyte in plasma extract	Analyte in neat solution
Mean area (6 lots)	635670	377310
RSD[a] (%)	14.4	5.0
Matrix factor[b]	1.7	
	IS in plasma extract	IS in neat solution
Mean area (6 lots)	885363	599086
RSD[a] (%)	10.1	3.7
Matrix factor[b]	1.5	
	Analyte in plasma extract	Analyte in neat solution
Mean area ratio (6 lots)	0.716	0.630
RSD[a] (%)	5.8	2.7
IS normalized matrix factor[c]	1.1	

[a] Relative standard deviation: (standard deviation/mean) × 100.
[b] Expressed as (mean area of plasma extract)/(mean area of neat solution).
[c] Expressed as (mean area ratio of analyte to IS in plasma extract)/(mean area ratio of analyte to IS in neat solution).

amount of the GDC-0941, was 82.7, 86.2 and 79.0%, respectively for GDC-0941 at 1.50, 200 and 400 ng/mL and 80.7% for IS GDC-0941-d_8.

3.8. Pharmacokinetic analysis

Validation was performed at a calibration curve range of 0.500–500 ng/mL. The lower limit of quantitation of 0.500 ng/mL was sufficient to detect the plasma concentrations at the 60 mg dose given in the study. The upper limit of quantitation of 500 ng/mL allowed minimum sample dilution and maximum sample throughput. Two standard curves were processed for each batch run. GDC-0941 concentrations were calculated from the equation $y = mx + b$, by weighted ($1/x^2$) linear least squares regression of the calibration line constructed from peak area ratios of GDC-0941 to internal standard versus nominal GDC-0941 concentrations (Table 1).

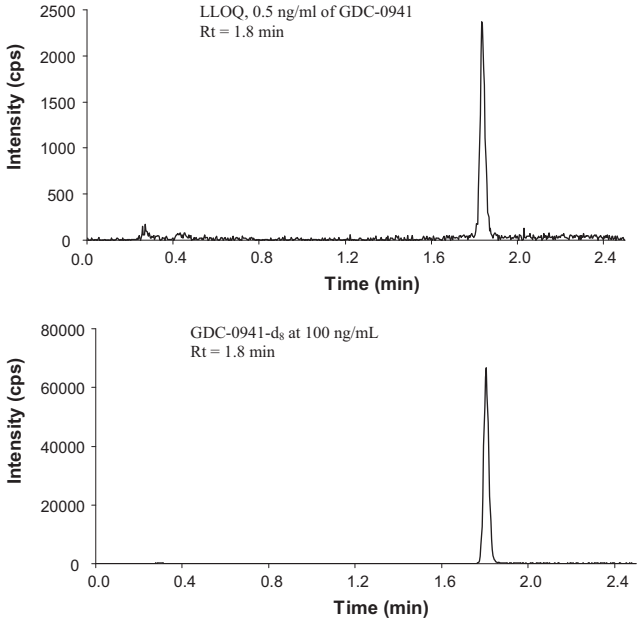

Fig. 3. Ion chromatograms for a GDC-0941 calibration standard at the LLOQ, 0.500 ng/mL, and internal standard GDC-0941-d_8 at concentration of 100 ng/mL.

Fig. 5 shows the representative GDC-0941 mean and standard deviation concentration versus time profiles for $n = 18$ healthy subjects enrolled in the clinical pharmacology study that were administered a 60 mg oral capsule dose of the phase I formulation. GDC-0941 plasma concentrations were within the calibration curve for all subjects and ranged from 0.599 to 376 ng/mL, with C_{max} ranging from 169 to 376 ng/mL and C_{last} ranging from 0.682 to 8.71 ng/mL. GDC-0941 was rapidly absorbed with a median T_{max} of 2 h. Over a 3-day blood sampling period, the area under the concentration–time curve and terminal elimination rate constant was adequately determined to estimate $T_{1/2}$.

Mean (standard deviation) pharmacokinetic data for these 18 healthy volunteers were: C_{max} = 252 (51.3) ng/mL, AUC_{0-t} = 2730 (833) ng h/mL, AUC_{0-inf} = 2800 (882) ng h/h, and $T_{1/2}$ = 13.7 (2.36) h.

Table 5
Stability assessments for GDC-0941.

Nominal conc. (ng/mL)	Determined mean (ng/mL, $n = 6$)	Mean %accuracy ($n = 6$)	RSD (%) ($n = 6$)
Bench-top stability at room temperature for 7 h			
1.50	1.51	100.7	2.1
400	395	98.8	5.3
Stability after 5 freeze–thaw cycles			
1.50	1.57	104.7	1.9
400	396	99.0	2.0
Storage at −70 ± 10 °C for 602 Days			
1.50	1.62	108.0	5.1
400	418	104.5	1.3
Storage at −20 ± 10 °C for 598 Days			
1.50	1.60	106.7	4.7
400	421	105.3	1.3
Storage in the autosampler at room temperature for 167 h			
1.50	1.72	114.7	3.7
200	213	106.5	1.1
400	415	103.8	1.9
Area ratio[a] at 300 ng/mL	Determined mean (ng/mL, $n = 6$)	Mean %accuracy ($n = 6$)	RSD (%) ($n = 6$)
Whole blood stability at room temperature (RT) and 1–8 °C for 2 h (compared to 0 h control)			
Control	3.200	–	8.4
RT	2.755	86.1	5.5
1–8 °C	2.905	90.8	6.6

[a] Area ratio: analyte area/internal standard area.

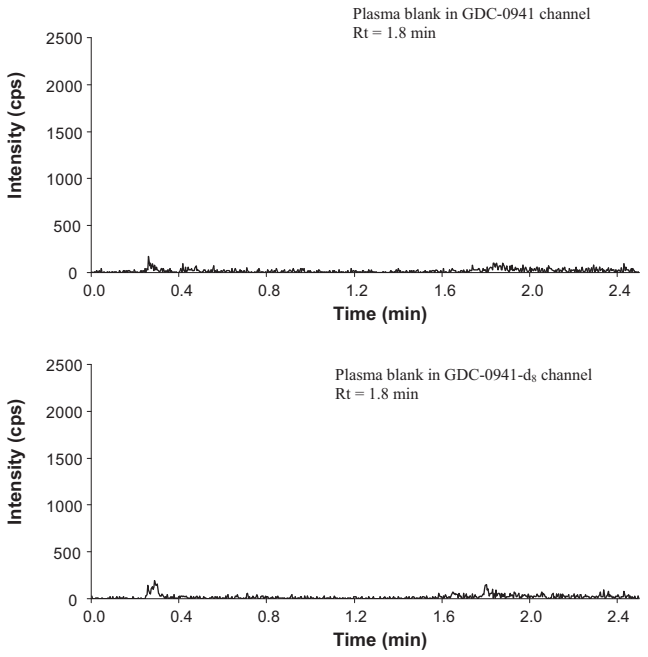

Fig. 4. Ion chromatograms of extracted blank plasma for the GDC-0941 and internal standard GDC-0941-d_8 channels.

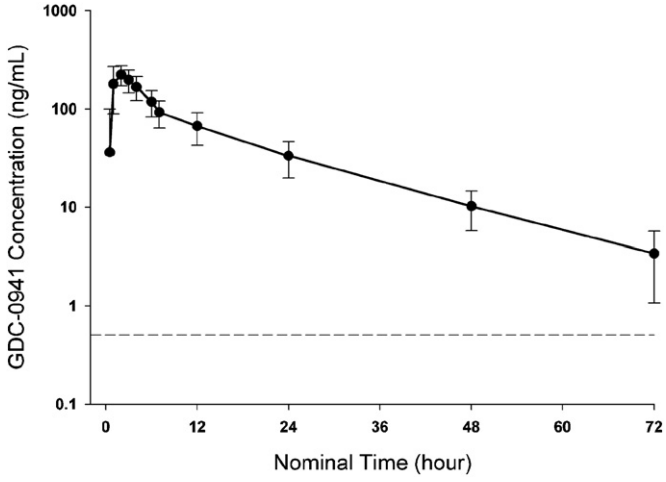

Fig. 5. Mean and standard deviation concentration versus time profiles for 18-healthy volunteers following a single 60 mg oral dose of GDC-0941 in a phase I clinical trial.

4. Conclusions

For the first time, an automated 96-well SPE LC–MS/MS method for the determination of GDC-0941 in human plasma was developed and validated. The LLOQ of 0.500 ng/mL is better than other methods developed for pre-clinical species (rat, dog, mouse and monkey). The validated method in human plasma met the regulatory requirements for accuracy, precision, selectivity and stability, and was applied successfully to the analysis of human plasma samples generated in a phase I clinical trial.

Acknowledgments

GDC-0941 was developed at Genentech, Inc. in collaboration with Piramed. The authors thank the healthy volunteers for enrolling in this study and taking valuable time away from their personal lives to advance science, Dr George Weissberger and the research staff at Institute for Translational and Experimental Medicine (ITEM), Strassbourg, FR for the conduct of the clinical study, our colleagues at Genentech – Drs. Jane Fridyland and Laurent Salphati. Their support is gratefully acknowledged.

References

[1] D. Sarker, R. Kristeleit, K.E. Mazina, J.A. Ware, Y. Yan, M. Dresser, M.A. Derynck, J.S. de Bono, A phase I study evaluating the pharmacokinetics (PK) and pharmacodynamics (PD) of the oral pan-phosphatidylinositol 3-kinase (PI3K) inhibitor GDC-0941, J. Clin. Oncol. ASCO Annu. Meet. Proc. 27 (2009) 3538.
[2] Multiple Clinical Trials Listed at http://clinicaltrials.gov/ct2/results?term=gdc-0941.
[3] C. O'Brien, J.J. Wallin, D. Sampath, D. GuhaThakurta, H. Savage, E.A. Punnoose, J. Guan, L. Berry, W.W. Prior, L.C. Amler, M. Belvin, L.S. Friedman, M.R. Lackner, Predictive biomarker of sensitivity to phosphatidylinositol 3′ kinase inhibitor GDC-0941 in breast cancer preclinical models, Clin. Cancer Res. 16 (2010) 3670–3683.
[4] L. Salphati, H. Wong, M. Belvin, D. Bradford, K.A. Edgar, W.W. Prior, D. Sampath, J.J. Wallin, Pharmacokinetic–pharmacodynamic modeling of tumor growth inhibition and biomarker modulation by the novel phosphatidylinositol 3-kinase inhibitor GDC-0941, Drug Metab. Dispos. 38 (2010) 1436–1442.
[5] F.I. Raymaud, S.A. Eccles, S. Patel, S. Alix, G. Box, I. Chuckowree, A. Folkes, S. Gowan, A.D.H. Brandon, F.D. Stefano, A. Hayes, A.T. Henley, L. Lensun, G. Pergl-Wilson, A. Robson, N. Saghir, A. Zhyvoloup, E. McDonald, P. Sheldrake, S. Shuttleworth, M. Valenti, N.C. Wan, P.A. Clarke, P. Workman, Biological properties of potent inhibitors of class I phosphatidylinositol 3-kinases: from PI-103 through PI-540, PI-620 to the oral agent GDC-0941, Mol. Cancer Ther. 8 (2009) 1725–1738.
[6] J. Li, C. Yen, D. Liaw, K. Podsypanina, S. Bose, S.I. Wang, J. Puc, C. Miliaresis, L. Rodgers, R. McCombie, S.H. Bigner, B.C. Giovanella, M. Ittmann, B. Tycko, H. Hibshoosh, M.H. Wigler, R. Parsons, PTEN, a putative protein tyrosine phosphatase gene mutated in human brain, breast and prostate cancer, Science 275 (1997) 1943–1947.
[7] P.A. Steck, M.A. Pershouse, S.A. Jasser, W.K.A. Yung, H. Lin, A.H. Ligon, L.A. Langford, M.L. Baumgard, T. Hattier, T. Davis, C. Frye, R. Hu, B. Swedlund, D.H.F. Teng, S.V. Tavtigian, Identification of a candidate tumor suppressor gene, MMACI, at chromosome 10q23.3 that i8s mutated in multiple advanced cancers, Net Gene 15 (1997) 356–362.
[8] S.P. Staal, Molecular cloning of the akt oncogene and its human homologues AKT1 and AKT2: amplification of AKT1 in a primary human gastric adenocarcinoma, Proc. Natl. Acad. Sci. U.S.A. 84 (1987) 5034–5037.
[9] A. Bellacosa, D. Defeo, A.K. Godwin, D.W. Bell, J.Q. Cheng, D.A. Altomare, M.H. Wan, L. Dubeau, G. Scambia, V. Masciullo, G. Ferrandina, P.B. Panici, S. Mancuso, G. Neri, J.R. Testa, Molecular alterations of the AKT2 oncogene in ovarian and breast carcinomas, Int. J. Cancer 64 (1995) 280–285.
[10] J.Q. Cheng, A.K. Godwin, A. Bellacosa, T. Taguchi, T.F. Franke, T.C. Hamilton, P.N. Tsichlis, J.R. Testa, AKT2, a putative oncogene encoding a member of a subfamily of protein–serine/threonine kinase, is amplified in human ovarian carcinomas, Proc. Natl. Acad. Sci. U.S.A. 89 (1992) 9267–9271.
[11] M. Aoki, O. Batista, A. Bellacosa, P. Tsichlis, P.K. Vogt, The Akt kinase: molecular determinants of oncogenicity, Proc. Natl. Acad. Sci. U.S.A. 95 (1998) 14950–14955.
[12] Y. Samuels, Z. Wang, A. Bardelli, N. Silliman, J. Ptak, S. Szabo, H. Yan, A. Gazdar, S.M. Powell, G.J. Riggins, High frequency of mutations of the PI3KCA gene in human cancers, Science 304 (2004) 554.
[13] K.E. Buchman, P. Argani, Y. Silliman, J. Ptak, S. Szabo, H. Konishi, B. Karakas, B.G. Blair, C. Lin, The PI3KCA gene is mutated with high frequency in human breast cancers, Cancer Biol. Ther. 3 (2004) 772–775.
[14] C.T. Viswanathan, S. Bansal, B. Booth, A.J. DeStefano, M.J. Rose, J. Sailstad, V.P. Shah, J.P. Skelly, P.G. Swann, R. Weiner, Workshop/conference report – quantitative bioanalysis methods validation and implementation: best practices for chromatographic and ligand binding assays, AAPS J. 9 (2007) E30–E42.

Journal of Pharmaceutical and Biomedical Analysis 61 (2012) 8–14

Contents lists available at SciVerse ScienceDirect

Journal of Pharmaceutical and Biomedical Analysis

journal homepage: www.elsevier.com/locate/jpba

Oral and topical pharmacokinetic studies of a novel TRPV1 antagonist, PAC-14028 in rats and minipigs using liquid chromatography/tandem mass spectrometric method

Yang-Hui Park[a], Kyung-Mi Joo[a], Byoung-Young Woo[a], Eui Dong Son[a,b], Sang Yo Byun[b], Hong-Ju Shin[a], Ki-Wha Lee[a], Young-Ho Park[a], Kyung-Min Lim[a,*]

[a] Amorepacific CO R&D Center, Yongin 446-729, Republic of Korea
[b] Department of Molecular Science & Technology, Ajou University, Suwon 443-749, Republic of Korea

ARTICLE INFO

Article history:
Received 31 August 2011
Received in revised form 7 November 2011
Accepted 8 November 2011
Available online 17 November 2011

Keywords:
Transient receptor potential vanilloid type I
PAC-14028
Pharmacokinetic
LC/MS/MS
Topical

ABSTRACT

PAC-14028 ((E)-N-((R)-1-(3,5-difluoro-4-methanesulfonylamino-phenyl)-ethyl)-3-(2-propyl-6-trifluoromethyl-pyridine-3-yl)-acrylamide) is a novel and potent transient receptor potential vanilloid type I (TRPV1) antagonist. We developed and validated a rapid, sensitive and selective liquid chromatography/tandem mass spectrometric method for determination of PAC-14028 in rat and minipig plasma. After protein precipitation PAC-14028 and internal standard (methylated analog, PAC-14026) were separated on a Symmetry C_{18} column (4.6 mm × 75 mm, 3.5 μm) with an isocratic mobile phase, acetonitrile: water (8:2, v/v) containing 0.2% formic acid and monitored by electrospray positive ionization with multiple reaction monitoring mode (PAC-14028, 492 → 156; IS, 506 → 156, *m/z*). The calibration curve was linear over the range of 1.0–500 ng/ml ($r^2 > 0.999$) and lower limit of quantitation (LLOQ) was 1 ng/ml. The precision and accuracy were within ±15% and the stability was acceptable during bench-top, auto-sampler, 3 freeze–thaw cycles and 4-week storage in a freezer at −80 °C. This method was successfully applied to the intravenous, oral and topical pharmacokinetic studies of PAC-14028 in rats and minipigs, which showed comparable pharmacokinetic parameters (T1/2, 2.1 h and 3.8 h; *F*%, 52.7% and 64.2% for rats and minipigs, respectively). Percutaneous absorption of PAC-14028 was negligible after topical application (*F*% 0.2–1.7%).

© 2011 Elsevier B.V. All rights reserved.

1. Introduction

The transient receptor potential vanilloid type 1 (TRPV1) is a calcium and non-selective cation channel activated by a pungent component of hot chilli pepper, capsaicin [1,2]. Expressed in peripheral nerve C-fibers, TRPV1 is also activated by noxious heat (>42 °C), proton and endogenous lipid mediators associated with inflammation and tissue injury [3], resulting in the release of neuropeptides and the initiation of painful, and itching sensation [1]. Various therapeutic utilities of TRPV1 antagonists have been investigated that include the management of somatic pain, migraine, respiratory diseases, bladder and gut associated inflammation [4–6]. Indeed, several potent and selective TRPV1 antagonists were discovered to be effective in the animal and human models of inflammatory, neuropathic and visceral diseases [7,8].

TRPV1 is also widely expressed in the skin tissues such as mast cells, keratinocytes, Langerhans cells, sebocytes and smooth muscle [9], suggesting the important role of TRPV1 in skin physiology. Recently, we discovered that a novel and potent TRPV1 antagonist, PAC-14028 ((E)-N-[(R)-1-(3,5-difluoro-4-methanesulfonylamino-phenyl)-ethyl]-3-(2-propyl-6-trifluoromethyl-pyridine-3-yl)-acrylamide) (Fig. 1A) can be effective in the treatment of refractory skin diseases such as atopic dermatitis [10] and pruritus [11]. PAC-14028 could prevent barrier damages, accelerate skin barrier recovery and suppress pruritus, showing a potential to open a new horizon for the treatment of atopic dermatitis. Moreover, it could suppress serum IgE increase, epidermal infiltration of inflammatory cells and mast cell degranulation associated with atopic dermatitis [12] without the serious side effects frequently encountered with corticosteroids [13] or calcineurin inhibitors [14]. Encouraged by the ideal efficacy and safety profiles of PAC-14028 for the management of refractory dermatological disorders, therapeutic modality of PAC-14028 is being actively explored in diverse dermatose models as well as other TRPV1-associated diseases. It is now undergoing through Phase I human clinical trial. Especially, for the use in the dermatological diseases, topical

* Corresponding author at: Amorepacific CO R&D Center, 314-1, Bora-dong, Giheung-gu, Yongin 446-729, Republic of Korea. Tel.: +82 31 280 5904; fax: +82 31 281 8391.
E-mail addresses: kimlim@amorepacific.com, eusapien@yahoo.com (K.-M. Lim).

0731-7085/$ – see front matter © 2011 Elsevier B.V. All rights reserved.
doi:10.1016/j.jpba.2011.11.011

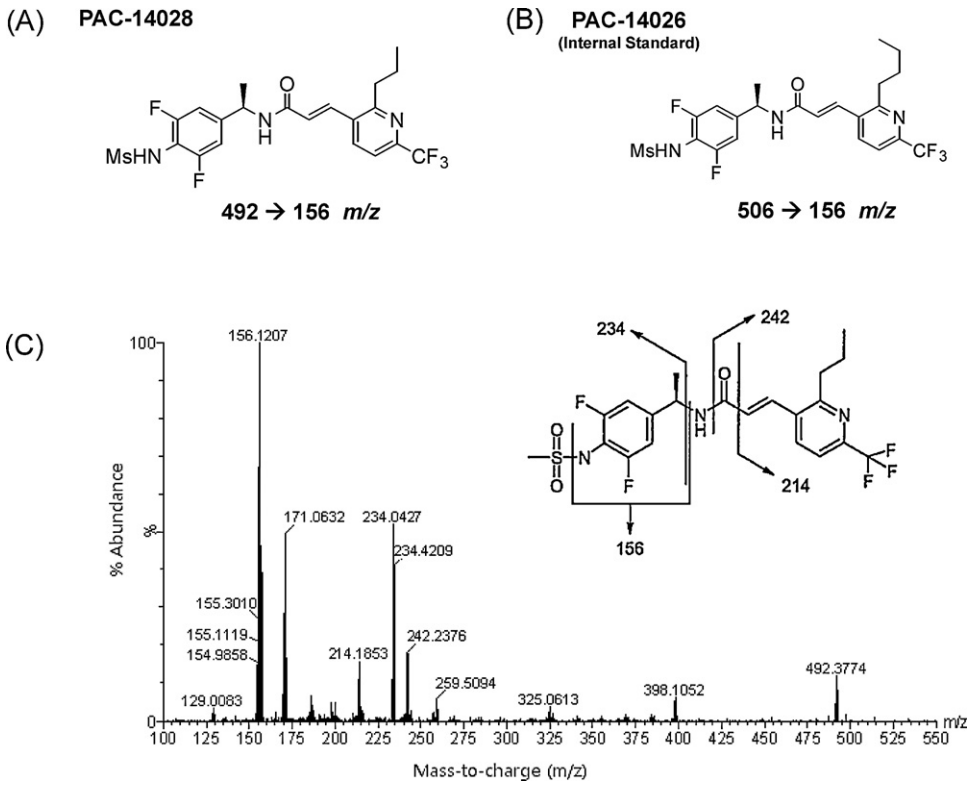

Fig. 1. Structures and product ion spectrum of analyte and internal standard. (A) Structure of PAC-14028; (B) structure of PAC-14026, IS; and (C) mass spectrum of PAC-14028 from precursor ions at *m/z* 492.

application is also being actively sought and being examined for the benefits of improved compliance and safety.

A series of pharmacokinetic studies has to be performed to warrant the accurate evaluation of systemic absorption of a drug after oral or topical administration. These studies are essential in the interpretation of pharmacological effects of a drug and prerequisite for the prediction of a safety margin. Regulatory bodies like FDA also reinforce the accurate assessment of systemic absorption profiles as a package of ADME for the entry into clinical trials [15]. However, in contrast to oral route, the percutaneous absorption after topical application is extremely low [16,17] and the development of sensitive bioanalytical methods is often required [18,19].

In this study, we developed a rapid, sensitive and selective quantitative bioanalytical method for the determination of PAC-14028 in blood plasma of rats and minipigs using liquid chromatography coupled to tandem mass spectrometry. The method was fully validated and successfully applied to pharmacokinetic studies following intravenous, oral and topical administration of PAC-14028 in rats. The pharmacokinetic study of PAC-14028 was also conducted in minipigs that have a skin penetration property similar to that of human skin [20,21], after oral and topical administration. We believe that this study may provide important information for the future studies of topical and oral efficacy of PAC-14028 and more importantly, will be a good example for the developers or investigators of topical drugs to conduct topical pharmacokinetics.

2. Experimental

2.1. Materials

PAC-14028 (purity > 98.5%) and PAC-14026 (internal standard, purity > 98.0%) were synthesized in Amorepacific R&D Center (Yongin, Korea). Methanol and acetonitrile were purchased from J.T. Baker (Phillipsburg, NJ), and formic acid, PEG400, methylcellulose and Tween80 from Sigma–Aldrich (St. Louis, MO). Ultrapure water was obtained from a Milli-Q PLUS PF water purification system (Billerica, MA). All solvents were of HPLC grade and reagents were of the highest quality available.

2.2. Preparation of stock solutions, calibration samples, and quality controls

Stock solution of PAC-14028 for calibration was prepared by dissolving 1 mg of PAC-14028 in 10 ml of methanol to obtain a concentration of 100 μg/ml. Fifty microliter of stock solution was added to 950 μl of blank plasma to obtain the 5000 ng/ml primary plasma stock. A series of calibration standard samples of PAC-14028 were prepared over the range from 1 ng/ml to 500 ng/ml (1, 2.5, 10, 25, 100, 250 and 500 ng/ml) by diluting the plasma stock with blank plasma. Final content of organic solvent was less than 1%. 100 μl of aliquot was taken from the spiked plasma for standard calibration. Quality control (QC) samples were prepared in the same manner at concentrations of 1(LLOQ), 3, 200 and 400 ng/ml by dilution the plasma stock (5000 ng/ml) with blank plasma. These samples were used to evaluate the intra- and inter-day precision and accuracy of the assay.

2.3. Sample preparation

Calibration standards, QC and plasma samples were extracted using a simple protein precipitation method. Hundred microliter of acetonitrile, 100 μl of 0.1 M HCl, and 100 μl of internal standard (100 μg/ml in acetonitrile) were added to 100 μl of plasma samples to clean up. After vortex-mixing for 15 min, samples were centrifuged for 10 min at 14,000 rpm (Eppendorf 5810R, Hamburg, Germany) and 4 °C. The supernatant was passed through a 0.45 μm PVDF syringe filter (National scientific, Rockwood, TN) and 10 μl of filtrate was injected onto LC/MS/MS for analysis.

Table 1
Matrix effect for PAC-14028 and PAC-14026 (internal standard).

Lot	Analyte (peak area)		Matrix factor[a]	Internal standard (peak area)		Matrix factor[a]
	Extracted matrix samples	Neat solution samples		Extracted matrix samples	Neat solution samples	
1	595,636	709,524	0.83	368,254	348,262	1.06
2	569,484	714,483	0.80	379,791	353,353	1.10
3	561,248	676,365	0.79	366,403	342,414	1.06
4	602,361	678,470	0.84	364,465	340,234	1.05
5	590,602	782,161	0.83	351,377	358,297	1.02
6	627,412	722,781	0.88	356,568	332,754	1.03
Mean	591,124	713,964	0.83	364,476	345,886	1.05
SD	23,768	38,528	0.03	9866	9294	0.03
CV(%)	4.0	5.4	4.02	2.7	2.7	2.71

PAC-14028 was 200 ng/ml and matrix (minipig plasma) was from 6 different animals.
[a] Matrix factor is a ratio of the response of the analyte in matrix relative to that of identically prepared analyte in mobile phase without matrix.

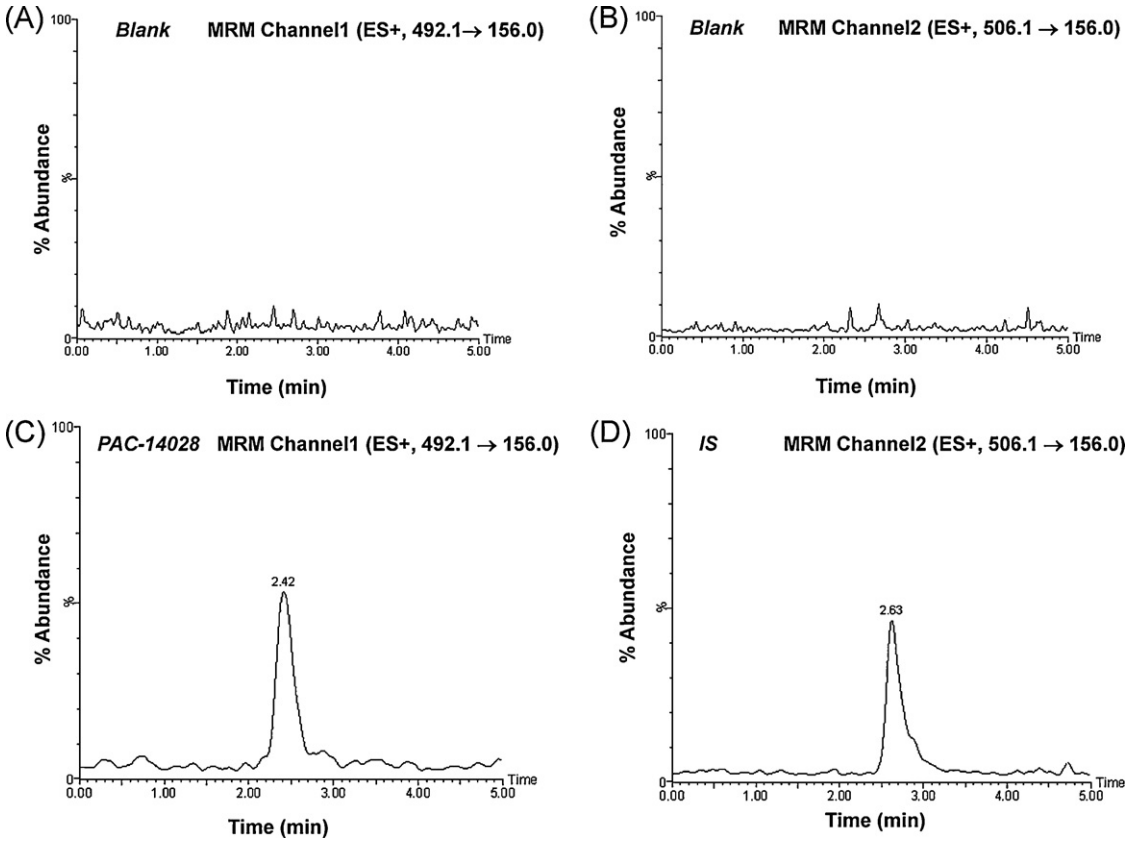

Fig. 2. Representative multiple reaction monitoring chromatograms of PAC-14028 (*m*/*z* 492) and PAC-14026 (*m*/*z* 506) in rat plasma. (A and B) Blank plasma; (C) plasma spiked with 1 ng/ml PAC-14028; and (D) plasma spiked with 10 ng/ml PAC-14026.

Table 2
Intra- and inter-day precision and accuracy ($n = 5$).

		Spiked conc. (ng/ml)	Detected conc. (ng/ml, mean ± SD)	Precision (RSD%)[a]	Accuracy (RE%)[b]
Rat	Intra-day	3	3.27 ± 0.1	3.3	8.8
		200	200.2 ± 4.2	2.1	0.1
		400	404.0 ± 8.6	2.1	1.0
	Inter-day	3	3.09 ± 0.2	5.2	3.0
		200	203.78 ± 2.3	2.3	1.6
		400	403.28 ± 6.4	1.9	0.8
Minipig	Intra-day	3	2.89 ± 0.1	3.2	−3.7
		200	198 ± 3.9	2.0	−1.0
		400	390 ± 8.8	2.3	−2.5
	Inter-day	3	2.92 ± 0.2	5.7	−2.7
		200	199 ± 12.2	6.1	−0.5
		400	399 ± 27.3	6.8	−0.3

[a] Precision was shown as relative standard deviation (RSD, %).
RSD (%) = standard deviation of calculated concentration/mean concentration × 100.
[b] Accuracy was shown as relative error (RE, %).
RE (%) = (calculated concentration − theoretical concentration)/theoretical concentration × 100.

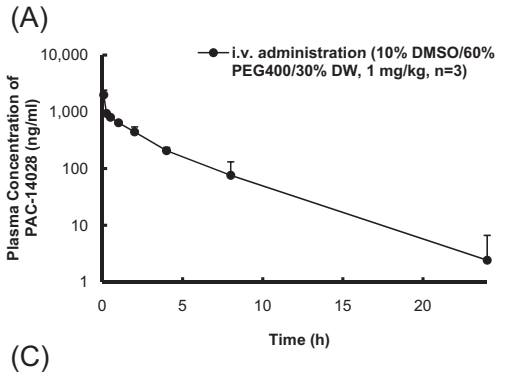

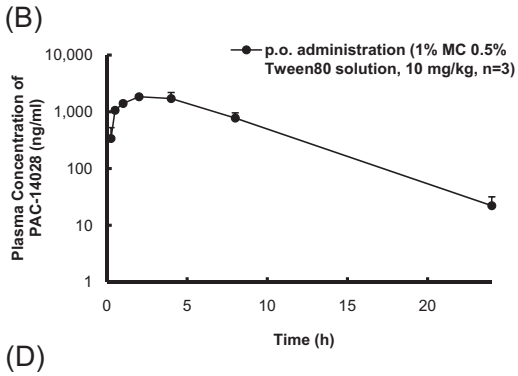

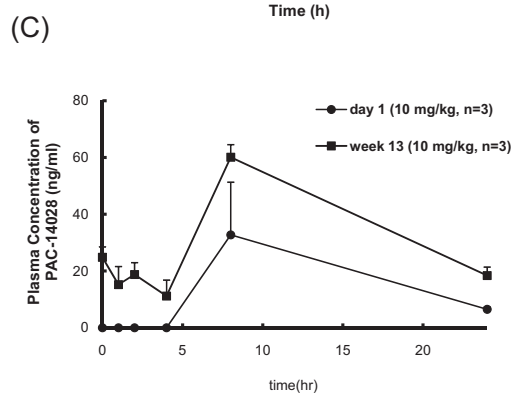

(D)

	i.v. (1 mg/kg)	p.o. (10 mg/kg)	topical[a] (10 mg/kg)
C_{max} (μg/ml)	-	1.84 ± 0.10	0.03 ± 0.02
T_{max} (h)	-	2.67 ± 1.15	8.00 ± 0.00
$AUC_{0\text{-}24\,h}$ (μg*h/ml)	3.44 ± 0.82	17.35 ± 0.99	0.38 ± 0.18
$T_{1/2}$ (h)	2.1	-	-
F (%)	-	52.7	1.2
CL (L/h/kg)	0.42 ± 0.30	-	-
Vss (L/kg)	1.85 ± 0.31	-	-

[a]parameters of day 1

Fig. 3. Mean plasma concentration–time curve and pharmacokinetic parameters of PAC-14028 in rats. (A–C) Time courses of plasma PAC-14028 concentrations after intravenous (A, 1 mg/kg (n = 3)), oral (B, 10 mg/kg (n = 3)), and topical (C, 10 mg/kg (n = 3)). (D) Pharmacokinetic parameters in rats. Values are the means ± SD.

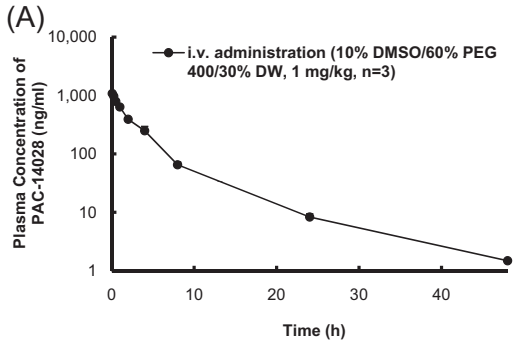

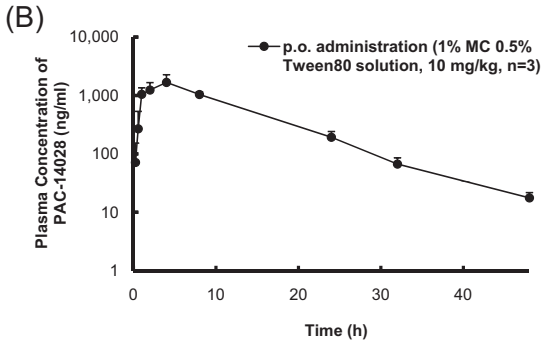

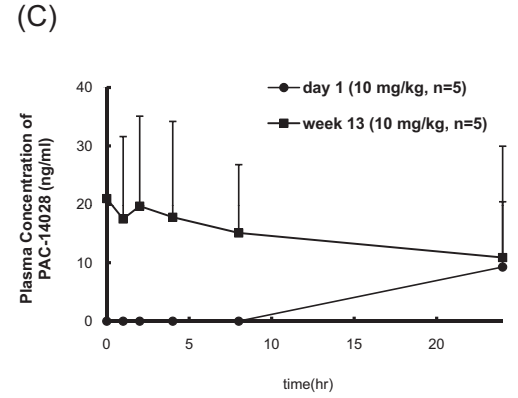

(D)

	i.v. (1 mg/kg)	p.o. (10 mg/kg)	topical[a] (10 mg/kg)
C_{max} (μg/ml)		1.81 ± 0.50	0.01 ± 0.02
T_{max} (h)		3.33 ± 1.15	24
$AUC_{0\text{-}24}$ h (μg*h/ml)	3.31 ± 0.20	20.35 ± 1.05	0.07±0.17
$T_{1/2}$ (h)	3.8	-	-
F (%)		64.2	0.2
CL (L/h/kg)	0.40 ± 0.24	-	-
Vss (L/kg)	1.59 ± 0.59	-	-

[a]parameters of day 1

Fig. 4. Mean plasma concentration–time curve and pharmacokinetic parameters in minipigs. (A–C) Time course of plasma PAC-14028 concentrations after intravenous (A, 1 mg/kg (n = 3)), oral (B, 10 mg/kg (n = 3)), and topical (C, 10 mg/kg (n = 5)). (D) Pharmacokinetic parameters in minipigs. Values are the means ± SD.

Table 3
Stability tests.

	Condition		Mean	SD	CV (%)	Stability (%)[a]
3 ng/ml	Short-term (RT, 4 h)	Initial	2.97	0.0	1.3	100.2
		After	2.98	0.0	1.1	
	Long-term (−80 °C, 4 weeks)	Initial	2.95	0.1	2.0	100.6
		After	2.97	0.0	0.7	
	Freeze–thaw	Initial	2.92	0.1	1.9	103.1
		After	3.01	0.0	1.0	
400 ng/ml	Short-term (RT, 4 h)	Initial	402.33	1.2	0.3	100.7
		After	405.33	1.5	0.4	
	Long-term (−80 °C, 4 weeks)	Initial	404.67	1.5	0.4	99.0
		After	400.67	3.1	0.8	
	Freeze–thaw	Initial	394.67	8.5	2.2	102.8
		After	405.67	3.1	0.8	

[a] Stability = mean conc. of stored samples × 100/mean conc. of initial samples ($n = 3$).

2.4. Chromatographic separation

Liquid chromatographic separation was performed with a Waters Alliance HPLC system (Waters, Milford, MA) equipped with a binary pump, an autosampler (maintained at 4 °C) and a solvent degasser. The isocratic mobile phase, acetonitrile: water (8:2, v/v) containing 0.2% formic acid, was delivered through a Symmetry C_{18} column (4.6 × 75 mm, 3.5 μm, Waters Co.) at room temperature and with a flow rate of 0.4 ml/min. Each run time was completed within 5 min.

2.5. Mass spectrometry instrumentation

The LC post-column effluents were introduced into a Waters Quattro Premier XE mass spectrometer with a Z-Spray ESI source (Micromass, Manchester, UK). The mass spectrometer was operated in the positive ion mode (ESI^+) in conditions: cone voltage, 40 V; and capillary voltage, 3.5 kV; desolvation gas flow, 850 l/h; cone gas flow, 100 l/h; collision gas flow, 0.15 ml/min; source temperature, 120 °C; and desolvation temperature, 350 °C. Two channels of mass-to-charge (m/z) ratio transitions were selected for the protonated analytes of PAC-14028 and internal standard in the mode of multiple reaction monitoring (MRM) as follows: PAC-14028, m/z 492 → 156; PAC-14026, m/z 506 → 156. The analytical data were processed with Masslynx 4.1 software (Waters Co.).

2.6. Method validation

The specificity or selectivity was examined by analyzing the processed blank plasmas from 6 individual animals. Specificity was confirmed by observing the absence of interfering peaks at the retention time both for PAC-14028 and IS, PAC-14026. Linearity was tested at 7 different concentrations at least four times, covering a calibration range of 1–500 ng/ml. The calibration curves were obtained through plotting the peak area ratio (peak area PAC-14028/peak area IS) versus concentration. The regression parameters of slope, intercept and correlation coefficient were calculated and fitted to "$y = mx + c$" with weighting factor $1/x^2$.

The lower limit of quantitation (LLOQ) of the assay was the lowest concentration on the calibration curve (1 ng/ml) that can be quantified within ±20% accuracy and precision. The LLOQ was confirmed by conducting 6 replicates.

The accuracy and precision of this analytical method were determined using QC samples in six replicates of 3 (3 X LLOQ), 200 (middle point of calibration curve) and 400 ng/ml (80% of ULOQ) of PAC-14028 in plasma. The intra- and inter-day accuracy and precision were determined by injection of 3 QC samples in 6 replicates for 3 days. Acceptance criteria were within ±15% both for precision and accuracy.

The recoveries were determined by comparing the mean peak area of the spiked samples with that of samples spiked after extraction. These experiments were performed in 6 replicate at 3 concentration levels of PAC-14028 (3, 200 and 400 ng/ml).

The stability test was designed to reflect the condition changes during sample handling that include bench-top (4 h at room temperature), autosampler (24 h at 4 °C), 3 freeze–thaw cycles and long-term storage in freezer (4 weeks at −80 °C) and analysis were done with 2 QC samples of PAC-14028 (3 and 400 ng/ml).

2.7. Pharmacokinetic study in rats and minipigs

The protocols or animal husbandry were approved prior to the start of experiments by local IACUCs of KIT (Daejun, Korea), MPI research (Kalamazoo, MI) and Amorepacific R&D center (Yongin, Korea). Male Sprague-Dawley rats (Orient Bio Inc., Sung-Nam, Korea), weighing from 210 to 230 g, and Gottingen minipigs (Marshall BioResources, North Rose, NY), weighing from 11 to 14 kg, were used for the study. Food was withheld for a day before dosing while water was available. Three rats/minipigs were given intravenously PAC-14028 at a single dose of 1 mg/kg, orally PAC-14028 at a single dose of 10 mg/kg as a suspension in 1% methylcellulose and 0.5% Tween80, or topically a single or multiple doses of 10 mg/kg as 1% PAC-14028 solution (gel form) in 68% PEG400 vehicle. For the topical application, dorsal area was shaved and painted with designated dose of PAC-14028 formulation. Occlusive dressing was placed on the applied region for 6 h to withhold licking or scratching the area. Blood samples were collected from the retro-orbital sinus or jugular vein into heparinized tubes at designated times after drug administration. Blood samples were centrifuged immediately, and the plasma was collected and stored at −70 °C until analysis. Samples that went beyond the linearity range were analyzed after dilution with blank plasma. To ensure the equivalence of diluted plasma, dilution QC was conducted with a standard sample spiked at 5000 ng/ml which showed acceptable accuracy and precision. The average of %RE and %RSD was −0.2% and 2.1%, respectively (within ±15.0%).

2.8. Statistics

The plasma concentration *vs* time data were analyzed by a non-compartmental method using the nonlinear least squares regression program WinNonlin (Scientific Consulting Inc., Cary, NC) and data were handled with Microsoft EXCEL®. All data were expressed as the mean ± standard deviation (SD).

3. Results and discussion

3.1. Development of bioanalytical method for the determination of PAC-14028 in rat and minipig plasma and method validation

In order to establish a mass spectrometric analysis condition, PAC-14028 and PAC-14026 (IS, a methylated analog of PAC-14028) were undergone mass scanning. PAC-14028 and IS formed protonated ion ($[M+H]^+$) in the positive ESI mode (Fig. 1A and B). The first quadrupole (Q1) mass spectra of PAC-14028 and IS showed their protonated ions at m/z 492 and 506, respectively. The corresponding product ions were both detected at m/z 156 of which structures were predicted as Fig. 1C. This was the most sensitive product ion for the quantification of both PAC-14028 and IS.

With this MRM mode (PAC-14028, m/z 492 → 156; IS, m/z 506 → 156), isocratic elution of acetonitrile: water (8:2, v/v) containing 0.2% formic acid, was sufficient to separate PAC-14028 and IS of which retention times were determined to be 2.4 and 2.6 min, respectively. There were no interfering peaks around the retention time of either PAC-14028 or IS. The selectivity or specificity of the method was confirmed by the absence of interferences in the matrix from 6 different sources (blank plasma from 6 different animals, Table 1) according to FDA guidline [22]. The average matrix factor for the analyte (the response of the analyte in matrix (minipig plasma) relative to that of identically prepared solutions without matrix) was determined to be 0.83 ± 0.03 (mean ± SD). The average matrix factor for the IS was determined to be 1.05 ± 0.03. Coefficient of variation (CV(%)) at LLOQ (1 ng/ml) was 5.9%, meeting the acceptance criteria of within ±15%. Fig. 2 represents typical chromatograms for the blank plasma (Fig. 2A and B), plasma spiked with 1 ng/ml of PAC-14028 (Fig. 2C) and 10 ng/ml of IS (Fig. 2D). The calibration curve provided a reliable response for PAC-14028 (1–500 ng/ml). The ratio of the peak area of PAC-14028 over IS was correlated well with the corresponding plasma concentration, and a good linearity was observed ($r^2 > 0.999$). The estimates of the intra- and inter-day precision and accuracy of the assay are presented in Table 2 . The recoveries determined at low (3 ng/ml), medium (200 ng/ml), high (400 ng/ml) QC concentrations were 96.9–100.2% for PAC-14028 and those of IS were 95.2–99.8%.

3.2. Stability of analytes in plasma

The stabilities of drug and IS in a biological matrix may be affected by the chemical properties of the compound, storage conditions and container systems. The stability test was designed to reflect the condition changes during sample handling and analysis with 2 QC samples of PAC-14028 (3 and 400 ng/ml). PAC-14028 in plasma was stable for at least 4 h at room temperature; it also remained intact at −80 °C for 4 weeks (Table 3). The stability of PAC-14028 in the plasma extract was also confirmed after 24 h of storage at 4 °C. In addition, no degradation of PAC-14028 was observed after 3 cycles of freezing and thawing. The concentration of PAC-14028 was within ±5% of changes during the storage conditions described above. On the basis of the results of stability test, PAC-14028 was considered to be stable during sample collection, handling and analysis.

3.3. Pharmacokinetic study of PAC-14028 following intravenous, oral and topical administration in rats and mini pigs

The validated method as developed above was used to evaluate the pharmacokinetics of PAC-14028 in rats and minipigs following intravenous, oral and topical administrations. Figs. 3A, B and 4A, B show the mean plasma concentrations after a single intravenous and oral administration of PAC-14028 in rats and minipigs. PAC-14028 showed a plasma half-life of 2.1 h in rats (Fig. 3D) while it was extended slightly to 3.8 h in minipigs (Fig. 4D). Oral bioavailability (F%) at 10 mg/kg dose was determined to be 52.7% and 64.2% in rats and minipigs, respectively suggesting that PAC-14028 was relatively well-absorbed through oral route. In contrast, the percutaneous absorption (AUC, F%) of PAC-14028 into systemic circulation after topical administration was shown to be extremely low, not exceeding 2% at day 1 (Figs. 3C and 4C). Even after repeated topical application once daily for 13 weeks, plasma concentrations of PAC-14028 remained below 100 ng/ml and F% was lower than 3%, suggesting that the systemic exposure of PAC-14028 may be low after topical administration in human.

Notably, while oral F% was similar between rats and minipigs, percutaneous absorption into systemic circulation was markedly lower in minipigs than rats (0.2% *vs* 1.2%) as shown in Figs. 3C and 4C. Rats displayed higher absorption following topical administration than minipigs. It is well known that the dense hair follicles in rats provide an easy access of topically applied drugs to dermis and thereby, the percutaneous absorption in rodents might be overestimated [21]. In this regard, minipigs are recommended as a choice of species in the pharmacokinetic study following topical administration[20] which is well in line with our results.

4. Conclusion

In this study, we developed a rapid, sensitive and specific bioanalytical method for the determination of a novel TRPV1 antagonist, PAC-14028 in rat and minipig plasma to investigate intravenous, oral and topical pharmacokinetics. A simple protein precipitation was sufficient for the sample clean-up and 5 min chromatographic run time was enough for the complete analysis with acceptable precision and accuracy. Most importantly, we demonstrated that this method could be successfully applied to the pharmacokinetic studies following intravenous, oral and topical administration of PAC-14028. Through these studies, PAC-14028 was shown to be well absorbed orally (F% 52.7–64.2%) while its percutaneous absorption after topical application was extremely limited, remaining below 3% even after the repeated treatment for 13 weeks. This result suggests that oral routes could be advantageous for obtaining a large plasma level of PAC-14028 for severe diseases whereas topical route may be ideal for restricting the drug exposure to affected skin lesions in the patients with a concern of safety.

Acknowledgement

This work was supported by a grant from the Ministry of Knowledge Economy (Bio-Star, 10031636).

References

[1] M.J. Caterina, D. Julius, The vanilloid receptor: a molecular gateway to the pain pathway, Annu. Rev. Neurosci. 24 (2001) 487–517.
[2] M.J. Gunthorpe, C.D. Benham, A. Randall, J.B. Davis, The diversity in the vanilloid (TRPV) receptor family of ion channels, Trends Pharmacol. Sci. 23 (2002) 183–191.
[3] S.W. Hwang, H. Cho, J. Kwak, S.Y. Lee, C.J. Kang, J. Jung, S. Cho, K.H. Min, Y.G. Suh, D. Kim, U. Oh, Direct activation of capsaicin receptors by products of lipoxygenases: endogenous capsaicin-like substances, Proc. Natl. Acad. Sci. U.S.A. 97 (2000) 6155–6160.
[4] Y. Jia, R.L. McLeod, J.A. Hey, TRPV1 receptor: a target for the treatment of pain, cough, airway disease and urinary incontinence, Drug News Perspect. 18 (2005) 165–171.
[5] A. Szallasi, D.N. Cortright, C.A. Blum, S.R. Eid, The vanilloid receptor TRPV1: 10 years from channel cloning to antagonist proof-of-concept, Nat. Rev. Drug Discov. 6 (2007) 357–372.
[6] J.E. Krause, B.L. Chenard, D.N. Cortright, Transient receptor potential ion channels as targets for the discovery of pain therapeutics, Curr. Opin. Investig. Drugs 6 (2005) 48–57.
[7] H.K. Rami, M. Thompson, P. Wyman, J.C. Jerman, J. Egerton, S. Brough, A.J. Stevens, A.D. Randall, D. Smart, M.J. Gunthorpe, J.B. Davis, Discovery of small molecule antagonists of TRPV1, Bioorg. Med. Chem. Lett. 14 (2004) 3631–3634.

[8] B.A. Chizh, M.B. O'Donnell, A. Napolitano, J. Wang, A.C. Brooke, M.C. Aylott, J.N. Bullman, E.J. Gray, R.Y. Lai, P.M. Williams, J.M. Appleby, The effects of the TRPV1 antagonist SB-705498 on TRPV1 receptor-mediated activity and inflammatory hyperalgesia in humans, Pain 132 (2007) 132–141.
[9] M. Steinhoff, J. Bienenstock, M. Schmelz, M. Maurer, E. Wei, T. Biro, Neurophysiological, neuroimmunological, and neuroendocrine basis of pruritus, J. Invest. Dermatol. 126 (2006) 1705–1718.
[10] J.W. Yun, J.A. Seo, Y.S. Jeong, I.H. Bae, W.H. Jang, J. Lee, S.Y. Kim, S.S. Shin, B.Y. Woo, K.W. Lee, K.M. Lim, Y.H. Park, TRPV1 antagonist can suppress the atopic dermatitis-like symptoms by accelerating skin barrier recovery, J. Dermatol. Sci. 62 (2011) 8–15.
[11] J.W. Yun, J.A. Seo, W.H. Jang, H.J. Koh, I.H. Bae, Y.H. Park, K.M. Lim, Antipruritic effects of TRPV1 antagonist in murine atopic dermatitis and itching models, J. Invest. Dermatol. 131 (2011) 1576–1579.
[12] C.A. Akdis, M. Akdis, T. Bieber, C. Bindslev-Jensen, M. Boguniewicz, P. Eigenmann, Q. Hamid, A. Kapp, D.Y. Leung, J. Lipozencic, T.A. Luger, A. Muraro, N. Novak, T.A. Platts-Mills, L. Rosenwasser, A. Scheynius, F.E. Simons, J. Spergel, K. Turjanmaa, U. Wahn, S. Weidinger, T. Werfel, T. Zuberbier, Diagnosis and treatment of atopic dermatitis in children and adults: European Academy of Allergology and Clinical Immunology/American Academy of Allergy, Asthma and Immunology/PRACTALL Consensus Report, J. Allergy Clin. Immunol. 118 (2006) 152–169.
[13] J.D. Ference, A.R. Last, Choosing topical corticosteroids, Am. Fam. Physician 79 (2009) 135–140.
[14] A. Qureshi, M.A. Fischer, Topical calcineurin inhibitors revisited, Arch. Dermatol. 143 (2007) 545–546.
[15] Food and Drug Administration, FDA Guidance for Industry: Bioanalytical Method Validation, 2001.
[16] C.J. Wang, Z. Tian, C. Gommoll, V. Reyes, C.C. Lin, A sensitive enzyme immunoassay (EIA) for quantitation of the topical anti-inflammatory agent SCH 40120 in unextracted human plasma, J. Pharm. Biomed. Anal. 11 (1993) 871–879.
[17] R.S. Gardner, M. Walker, D.A. Hollingsbee, A sensitive high-performance liquid chromatographic method for the assessment of percutaneous absorption of topical corticosteroids, J. Pharm. Biomed. Anal. 8 (1990) 1083–1085.
[18] R.W. Sparidans, S.G. van Velsen, M.P. de Roos, J.H. Schellens, C.A. Bruijnzeel-Koomen, J.H. Beijnen, Liquid chromatography–tandem mass spectrometric assay for clobetasol propionate in human serum from patients with atopic dermatitis, J. Chromatogr. B: Analyt. Technol. Biomed. Life Sci. 878 (2010) 2150–2154.
[19] R.S. Bhatta, H. Chandasana, C. Rathi, D. Kumar, Y.S. Chhonker, G.K. Jain, Bioanalytical method development and validation of natamycin in rabbit tears and its application to ocular pharmacokinetic studies, J. Pharm. Biomed. Anal. 54 (2011) 1096–1100.
[20] M.H. Qvist, U. Hoeck, B. Kreilgaard, F. Madsen, S. Frokjaer, Evaluation of Gottingen minipig skin for transdermal in vitro permeation studies, Eur. J. Pharm. Sci. 11 (2000) 59–68.
[21] T. Kurihara-Bergstrom, M. Woodworth, S. Feisullin, P. Beall, Characterization of the Yucatan miniature pig skin and small intestine for pharmaceutical applications, Lab. Anim. Sci. 36 (1986) 396–399.
[22] S. Bansal, A. DeStefano, Key elements of bioanalytical method validation for small molecules, AAPS J. 9 (2007) E109–E114.

Journal of Pharmaceutical and Biomedical Analysis 61 (2012) 15–21

Contents lists available at SciVerse ScienceDirect

Journal of Pharmaceutical and Biomedical Analysis

journal homepage: www.elsevier.com/locate/jpba

Determination of hydromorphone in human plasma by a sensitive RP-HPLC–ESI-MS method and its application to a clinical pharmacokinetic study in postoperative patients after low dose intravenous administration with infusion pump

Luning Sun[a,b], Yinbin Pan[c,1], Li Ding[a,*], Xuemei Luo[a], Zhengyu Yan[b,**,2], Cunming Liu[c], Yanning Qian[c], Yan Chu[a]

[a] Department of Pharmaceutical Analysis, China Pharmaceutical University, 24 Tongjiaxiang, Nanjing 210009, China
[b] Department of Analytical Chemistry, China Pharmaceutical University, 24 Tongjiaxiang, Nanjing 210009, China
[c] Department of Anesthesiology, First Affiliated Hospital of Nanjing Medical University, Nanjing 210029, China

ARTICLE INFO

Article history:
Received 16 August 2011
Received in revised form 9 November 2011
Accepted 10 November 2011
Available online 20 November 2011

Keywords:
Hydromorphone
Pharmacokinetics
RP-HPLC–ESI-MS
Postoperative patient

ABSTRACT

A sensitive reverse phase high performance liquid chromatography–electrospray ionization-mass spectrometry (RP-HPLC–ESI-MS) method has been developed and validated for the determination of hydromorphone in human plasma using naloxone as the internal standard (IS). After alkalization with saturated sodium bicarbonate, the plasma samples were extracted with ethyl acetate. Chromatographic separation was performed on a C18 column with the column temperature of 50 °C and a mobile phase of 5 mM ammonium acetate buffer containing 1% formic acid–methanol (88:12, v/v). Hydromorphone and the IS were detected by selected ion monitoring using the protonated molecules at *m/z* 286.2 for hydromorphone and *m/z* 328.2 for the IS. Calibration curve was linear over the range of 0.01–50 ng/mL. The lower limit of quantification was 0.01 ng/mL. The method was successfully applied to the pharmacokinetic study in postoperative patients after intravenous infusion of 1.5 mg hydromorphone hydrochloride. The obtained main pharmacokinetic parameters of hydromorphone in postoperative patients were as follows: the maximum hydromorphone plasma concentration (C_{max}) was (24.15 ± 12.51) ng/mL, the time to the C_{max} was (10.0 ± 0.0) min, and the elimination half-life was (2.7 ± 0.8) h.

© 2011 Elsevier B.V. All rights reserved.

1. Introduction

Hydromorphone (see Fig. 1), a semi-synthetic derivative of morphine, has been used extensively for the management of postoperative pain and morphine-resistant cancer-related pain [1], and has been considered as an alternative to morphine [2]. Although the pharmacokinetic characters of hydromorphone in healthy subjects have been studied [3–5], no data is available regarding this drug in postoperative patients or healthy Chinese subjects. Moreover, Chinese subjects have a higher clearance of morphine analogs compared with European subjects due to ethnical differences [6]. Therefore, in order to accurately elucidate the pharmacokinetics of hydromorphone hydrochloride injection in Chinese postoperative patients, it was necessary to develop a sensitive method for the determination of hydromorphone in human plasma. Various methods have been reported for the determination of hydromorphone in human plasma, which involved radioimmunoassay (RIA) [7], high performance liquid chromatography using electrochemical detector (HPLC–ECD) [8,9] and high performance liquid chromatography–tandem mass spectrometry (HPLC–MS/MS) [10–15]. The radioimmunoassay lacked of selectivity, while the HPLC–ECD methods [8,9] were not sensitive enough and required large plasma sample volume for assay. Among the six reported HPLC–MS/MS methods, four [10–13] of those methods focused on doping control or therapeutic drug monitoring of hydromorphone using the long HPLC–MS/MS run time, and were not sensitive enough for human pharmacokinetic study. The other two methods [14,15] were both normal phase high performance liquid chromatography–electrospray ionization-mass spectrometry (NP-HPLC–MS/MS) methods with the LLOQ of 0.1 ng/mL [14] and 0.05 ng/mL [15], respectively. But the need of automated SPE equipments [14] was not available in most laboratories. In these

* Corresponding author. Tel.: +86 25 83271289; fax: +86 25 83271289.
** Corresponding author.
E-mail addresses: dinglidl@hotmail.com (L. Ding), yanzhengyujiang@hotmail.com (Z. Yan).
[1] Co-first author.
[2] Co-corresponding author.

0731-7085/$ – see front matter © 2011 Elsevier B.V. All rights reserved.
doi:10.1016/j.jpba.2011.11.012

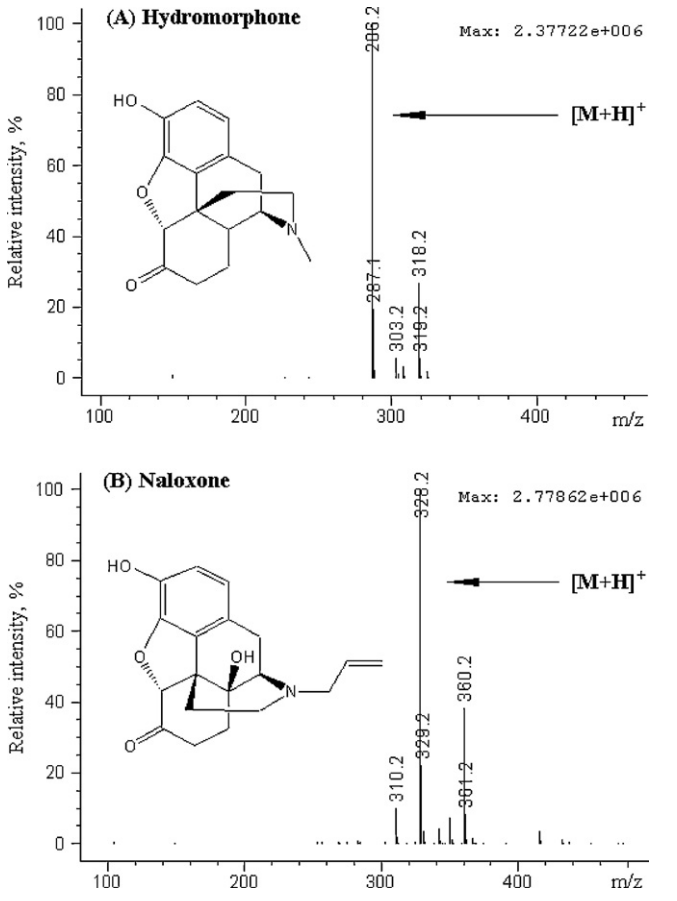

Fig. 1. Structures and mass spectra of hydromorphone (A) and naloxone (B).

two methods, to have to adopt the NP-HPLC system instead of the common and widely applied RP-HPLC system was mainly owing to the poor MS sensitivity and peak shape deterioration. However, these problems could also be solved by optimizing the RP-HPLC chromatographic and mass spectrometric conditions under the RP-HPLC system. The pilot study in our laboratory showed that an LLOQ of 0.01 ng/mL was necessary for our pharmacokinetic study. Therefore, the goal of this work was to develop a more sensitive RP-HPLC–MS method to determinate the hydromorphone in human plasma and illustrate the pharmacokinetics of hydromorphone in Chinese postoperative patients after 1.5 mg intravenous infusion administration of hydromorphone hydrochloride.

2. Experimental

2.1. Chemicals and reagents

The reference standard of hydromorphone hydrochloride (purity > 99.0%) was provided by Yichang Humanwell Pharmaceutical Co., Ltd. (Yichang, China). The reference standard of naloxone (see Fig. 1, purity > 99.0%) was purchased from National Institute for the Control of Pharmaceutical and Biological Products (Beijing, China). Methanol of HPLC grade was purchased from Merck KGaA (Darmstadt, German). Sodium bicarbonate, ethyl acetate, ammonium acetate and formic acid were of analytical grade purity and purchased from Nanjing Chemical Reagent Co., Ltd. (Nanjing, China). Distilled water was used throughout the study. Blank plasma was supplied by the Nanjing Branch of the Red Cross Society of China.

2.2. Instrumentation

The HPLC–ESI-MS methods were performed using an Agilent Technologies Series 1100 LC/MSD SL system (Agilent Technologies, Palo Alto, CA, USA), which included an Agilent 1100 G1312A binary pump, vacuum degasser (model G1322A), G1316A injection temperature controlled column compartment, Agilent 1100 autosampler (model G1313A), and an Agilent 1100 MSD single quadrupole mass spectrometer equipped with an electrospray source (model G1956B). The signal acquisition, peak integration and concentration determination were performed using the ChemStation software (10.02 A) supplied by Agilent Technologies.

2.3. LC–MS conditions

A Hedera ODS-2 column (5 μm, 150 mm × 2.1 mm i.d., Hanbon Science and Technology, Huaian, China) with a security Guard-C_{18} (5 μm, 4 mm × 2.0 mm, Phenomenex, Torrance, CA, USA) was used for the analytes separation. Isocratic elution employed a mobile phase of 5 mM ammonium acetate buffer solution containing 1% formic acid (pH 2.5)–methanol (88:12, v/v) at a flow rate of 0.20 mL/min. The column temperature was maintained at 50 °C. The autosampler was maintained at 8 °C.

The HPLC–ESI-MS method was carried out using nitrogen to assist nebulization. The quadrupole mass spectrometer equipped with an ESI source was set with the drying gas (N_2) flow of 10 L/min, the nebulizer pressure of 30 psig, the drying gas temperature of 350 °C, the capillary voltage of 4.0 kV and the positive ion mode. The fragmentor voltage was set at 160 V. The ESI-MS was performed in the selected ion monitoring (SIM) mode using the target ions $[M+H]^+$ at *m/z* 286.2 for hydromorphone and *m/z* 328.2 for the IS. Fig. 1 shows typical full-scan ESI mass spectra of hydromorphone and the IS.

2.4. Preparation of standard solutions

The stock solution of hydromorphone with a concentration of 1.0 mg/mL was prepared by dissolving hydromorphone in methanol. A series of standard working solutions with concentrations in the range of 0.5–10 μg/mL for hydromorphone were obtained by further dilution of the stock solution with methanol. The IS working solution (538 ng/mL) was prepared by diluting the stock solution of naloxone with methanol. All the solutions were stored at −20 °C and were brought to room temperature before use.

2.5. Plasma sample preparation

A plasma sample (1 mL) and 30 μL IS (538 ng/mL) were placed into a tube in turn. After vortex-mixing for 10 s, 1 mL saturated sodium bicarbonate was added and vortex-mixed for 30 s to alkalize the plasma. Then, the alkalized plasma sample was extracted with two 4 mL ethyl acetate by vortex for 5 min, and centrifuged at 4000 rpm for 8 min at room temperature. The supernatant was separated and evaporated to dryness under a gentle stream of nitrogen in a water bath of 40 °C. The residue was reconstituted with 120 μL mobile phase, and a 20 μL aliquot of the reconstituted solution was injected into the RP-HPLC–ESI-MS for analysis.

2.6. Preparation of calibration curves and quality control samples

The calibration standards of hydromorphone were prepared by spiking appropriate amount of hydromorphone working solutions into 1.0 mL blank plasma from healthy subjects. The standard curve was prepared for hydromorphone at concentration levels of 0.01024, 0.03072, 0.1024, 0.3072, 1.024, 3.072, 10.24, 25.60, 51.20 ng/mL. And those standard plasma samples were prepared according to the plasma sample preparation. The calibration curve

was prepared and assayed along with quality control (QC) samples and each run of the unknown plasma samples. The QC samples were prepared in 1.0 mL blank plasma at concentration levels of 0.02560, 2.048 and 40.96 ng/mL for hydromorphone. The results of the QC samples provided the basis of accepting or rejecting the run.

2.7. Method validation

2.7.1. Selectivity

The selectivity was assessed by comparing the chromatograms of six different sources of blank human plasma with the corresponding spiked plasma. Each blank plasma sample was tested using the proposed extraction procedure and RP-HPLC–ESI-MS conditions to ensure no interference of hydromorphone and the IS from plasma.

2.7.2. Extraction recovery and matrix effect

The extraction recovery was calculated by comparison of the peak areas of the analytes extracted from plasma samples with those of added standards dissolved in the reconstituted residue of the processed blank plasma. The matrix effect of the method was evaluated by comparing the peak areas of analytes resolved in blank plasma's reconstituted residue aqueous (the final solution of blank plasma after reconstituting) with that resolved in mobile phase. Three different concentration levels of hydromorphone at 0.02560, 2.048 and 40.96 ng/mL and the IS concentration level of 13.4 ng/mL were used to evaluate the extraction recovery and matrix effect by analyzing five replicates at each level. The blank plasma samples used in this study were obtained from five different batches of healthy human plasma. If the ratio <85% or >115%, a matrix effect was implied.

2.7.3. Linearity and lower limit of quantification

Calibration standards of hydromorphone at nine concentration levels of 0.01024, 0.03072, 0.1024, 0.3072, 1.024, 3.072, 10.24, 25.60, 51.20 ng/mL were extracted and assayed. To evaluate the linearity, the calibration curve was constructed by plotting peak-area ratios of hydromorphone to the IS versus the concentrations of hydromorphone, using weighted least squares linear regression (weighting factor, $1/C^2$). The LLOQ was defined as the lowest concentration on the calibration curve at which precision and accuracy were within ±20%, and it was established by using five samples independent of standards.

2.8. Precision and accuracy

The QC samples were prepared and analyzed on three separate analytical batches to evaluate the accuracy, intra- and inter-day precisions of the analytical method. The accuracy and precisions of the method were determined by analyzing five replicates of the QC samples at 0.02560, 2.048 and 40.96 ng/mL along with one calibration curve on each of three batches. Assay precision was calculated by using the relative standard deviation (RSD, %) and variance (ANOVA). Accuracy is evaluated by the relative deviation (RE, %) in the calculated value (E) of a standard from that of its true value (T) expressed as a percentage. It was calculated using the formula: $\mathrm{RE\%} = (E - T)/T \times 100$. The intra- and inter-day precisions were required to be less than 15%, and the accuracy to be within ± 15%.

2.9. Stability

The stability of hydromorphone in plasma was studied under a variety of storage and handling conditions using three aliquots at each QC level. The short-term temperature stability was evaluated by keeping the QC samples at room temperature for 10 h. The post-preparative stability was conducted by reanalyzing reconstituted QC samples for 12 h at 8 °C in the autosampler. Freeze and thaw stability was determined after three freeze and thaw cycles at −80 °C. The long-term stability of hydromorphone was determined by placing the QC samples at −80 °C for 8 weeks. Following above treatments, those samples were analyzed with calibration curves obtained from newly prepared standards and the results were compared with those of obtained from the samples immediately processed at 0 h. The analytes are considered to be stable when the values of the accuracies are in the range of 85%–115%, respectively, for all QC levels.

The stability of stock solutions of hydromorphone and the IS was evaluated at room temperature for 14 h and 16 h as well as in a refrigerator (−20 °C) for 9 weeks and 12 weeks, respectively. After completion of the desired storage time, the stability was tested by comparing the peak areas with those of freshly prepared solutions.

2.10. Pharmacokinetic study

The pharmacokinetic study was approved by the Ethics Committee of the First Affiliated Hospital of Nanjing Medical University and was conducted in accordance with guidelines for Good Clinical Practice in China, the Declaration of Helsinki, and all applicable national and local regulations. All patients signed an informed consent statement to express their willingness prior to the initiation of the study. Patients in this study were adult men and women, 18–45 years of age. All eligible patients were tobacco, alcohol and drug free and had a body mass index (BMI) between 18 and 25. Patients, who were subjected to elective minor surgery under general anesthesia with American Society of Anesthesiologists classifications as I to II, received an intravenous infusion of 1.5 mg hydromorphone hydrochloride injection in sterile saline solution (90 mL/9 mg/h, 10 min). The study drugs were administrated with micro-infusion pump (wz-50s, Smiths Medical, Zhejiang Province, China) and given through intravenous catheter in the antecubital vein opposite the one from which blood samples were taken. After a single intravenous infusion administration of 1.5 mg hydromorphone hydrochloride injection over 10 min, blood samples (3 mL) were collected at 0 h (pre-dose) and 5 min, 10 min, 15 min, 20 min, 30 min, 45 min, 1 h, 2 h, 3 h, 4 h, 6 h, 8 h, 10 h, 12 h and 14 h (post-dose). The beginning of the intravenous administration was considered time zero. The blood samples were transferred to heparinized tubes and centrifuged at 3000 rpm for 10 min. Plasma was separated and stored at −80 °C until analysis. The pharmacokinetic parameters were analyzed by non-compartmental model with Drug and Statistic (DAS) software (version 2.0, Rui-yuan Sun, Wuhu, China). The C_{max} and T_{max} were observed data. The apparent terminal elimination rate constants (λ_z) were determined by the absolute value of the slope of a linear regression of the natural logarithm of concentration–time. Elimination half-lives ($t_{1/2}$) were calculated as $0.693/\lambda_z$. The area under the plasma concentration versus time curve (AUC) from 0 to t (AUC_{0-t}), where t is the time of the last measurable concentration, was calculated with the trapezoidal method. The AUC from time 0 to infinity ($AUC_{0-\infty}$) was calculated as $AUC_{0-t} + C_t/\lambda_z$, where C_t is the last detectable concentration at time t.

3. Results and discussion

3.1. Method development and optimization

3.1.1. Conditions for mass spectrometry

Mass spectrometry operation parameters were carefully optimized for the determination of hydromorphone. The ESI in positive

ion mode could offer required sensitivity for the $[M+H]^+$ at m/z 286.2, so ESI in positive ion mode was adopted in the LC–MS assay. The fragmentor voltage was optimized in the SIM mode by comparing the intensities of hydromorphone target ion $[M+H]^+$ at different fragmentor voltages. The test results showed that the highest sensitivity could be obtained at the fragmentor voltage of 160 V. At this fragmentor voltage the most intensive ion of the IS was the ion $[M+H]^+$ at m/z 328.2. Therefore, the positive ion $[M+H]^+$ at m/z 328.2 was selected as the target ion for the IS. The parameters such as drying gas temperature, nebulizer pressure, capillary voltage and drying gas flow rate were optimized to obtain the highest intensity of protonated molecule of hydromorphone.

3.1.2. Conditions for chromatography

In practice, reverse phase separations are conducted far more frequently than normal phase for quantitative analysis of small analytes. Moreover, the reverse system provides both economic and ecological advantages for the low solvent consumption compared with normal phase system. Furthermore, there are too many types of underivatized and derivatized silica column, the reproducibility and reliability need to be conformed and improved. So, NP-HPLC–MS is a very important supplement but not an alternative to the RP-HPLC–MS for the analysis of polar compounds. Therefore, to develop and validate a more sensitive and reproducible RP-HPLC–MS method for the determination and pharmacokinetic study of hydromorphone in this study is necessary and valuable.

Due to the highly polar and stereo structure characters of hydromorphone, both previous studies [14,15] and our experiments suffered from peak shape deterioration and poor mass response in reverse system, however, we solved the problems successfully and developed a more sensitive and reproduced RP-HPLC–ESI-MS method. To get the sharp and symmetry peaks of analytes, the column temperature, the ionic strength and the pH value of the reconstituted solution, buffer concentration and the pH value of mobile phase were tested. The test results showed that the increasing column temperature led to improved peak shape and symmetry. The acceptable peak shape and symmetry was achieved at the column temperature of 50 °C, but the explanations for this phenomenon are not clear. The ionic strength and pH value of the reconstituted solution were not likely responsible for the improved peak shape because the same peak shape occurred when the different ionic strength and pH value of the reconstituted solution were investigated. Similarly, the buffer concentration and pH of mobile phase also had no significant impact on the peak shape of hydromorphone.

To enhance the MS response to hydromorphone, the organic content, flow rate, buffer concentration and pH value of the mobile phase were investigated. The higher content of organic solvent in the mobile phase was adopted, the better ionization efficiency for MS detection was observed. But, in order to retain the polar compound hydromorphone on the column, lower content of organic solvent in the mobile phase should be adopted in RP-HPLC–MS, which resulted in lower MS response due to the low ionization efficiency. Although the highly volatile organic mobile phases utilized in NP-HPLC–MS provided increased ESI-MS response, the adequate MS response could acquired by reducing the flow rate of mobile phase in RP-HPLC–MS. The experiment results exhibited that the MS response increased with the flow rate reducing, and the flow rate of 0.20 mL/min could provide the both suitable retention time and adequate MS response. So, we adopt the low flow rate instead of NP-HPLC to improve the ionization efficiency and get the adequate MS response. Although the experiments presented that ammonium acetate buffer or formic acid added in the mobile phase would decrease the MS response, acidifying the mobile phase with 1% formic acid could prevent retention time shifting and adding the mobile phase with 5 mM ammonium acetate could reduce matrix effects.

Therefore, the acceptable retention and separation of hydromorphone were performed on a C18 column with the column temperature of 50 °C, and a mobile phase of 5 mM ammonium acetate buffer containing 1% formic acid-methanol (88:12, v/v) at a flow rate of 0.20 mL/min.

3.1.3. Plasma sample preparation

A simple liquid–liquid extraction (LLE) was utilized for clean-up and extraction from the plasma. The experiment results presented that the extraction recovery of hydromorphone and the IS was sensitive to the pH of plasma. The adjustment of the plasma to a basic condition (pH 8.5) with saturated sodium bicarbonate solution could obtain the highest extraction efficiency for hydromorphone and the IS. Because they are all amphoteric compounds with tertiary amine and phenolic hydroxyl group in chemical structure, the extraction recovery would decrease if the adjusted plasma pH value was higher or lower than 8.5. Further test results proved that ethyl acetate exhibited higher extraction recovery to hydromorphone and the IS than diethyl ether, cyclohexane and their mixture solutions. Therefore, the ethyl acetate with 1 mL saturated sodium bicarbonate was finally adapted because of its high extraction efficiency and less interference of the analytes.

3.2. Method validation

3.2.1. Specificity, extraction recovery and matrix effect

Selectivity was assessed by comparing the chromatograms of six different batches of blank human plasma with the corresponding spiked plasma. Fig. 2 shows four typical SIM chromatograms. Retention times were approximately 4.3 min and 7.6 min for hydromorphone and the IS, respectively. The peak shapes of hydromorphone and IS were symmetrical, and meet the requirements for the assay. There was no interference observed at or close to the retention times of the analytes in human plasma samples.

The extraction recoveries of hydromorphone, determined at three QC concentration levels of 0.02560, 2.048 and 40.96 ng/mL, were (75.3 ± 9.6)%, (75.1 ± 1.7)% and (71.6 ± 2.8)% (n = 5), respectively, while the extraction recovery of IS was (82.6 ± 4.5)%. The matrix effects at three QC concentration levels of 0.02560, 2.048 and 40.96 ng/mL were (101.7 ± 4.4)%, (95.6 ± 1.0)% and (97.5 ± 2.3)% (n = 5) for hydromorphone, respectively, and (101.2 ± 2.9)% for the IS. No matrix effect for hydromorphone and the IS was observed, indicating that no co-eluting substance influenced the ionization of the analytes.

3.2.2. Linearity, lower limit of quantification, precision and accuracy

Visual inspection of the plotted duplicate calibration curves and correlation coefficients >0.998 confirmed that the calibration curves were linear over the concentration ranges of 0.01–50 ng/mL for hydromorphone. The typical standard curve was $f = 9.93 \times 10^{-2} C + 2.15 \times 10^{-4}$, where f represents the peak area ratio of hydromorphone to the IS and C represents the plasma concentration of hydromorphone. The LLOQ of this method was 0.01 ng/mL at which the signal-to-noise ratio (S/N) of hydromorphone was higher than 10, the precision expressed as RSD was 10.7% (n = 5), and the accuracy expressed as RE was 2.7% (n = 5).

Table 1 summarizes the intra- and inter-day precision and accuracy of the method evaluated by assaying the QC samples. The results demonstrated the acceptable accuracy and precision of the present method.

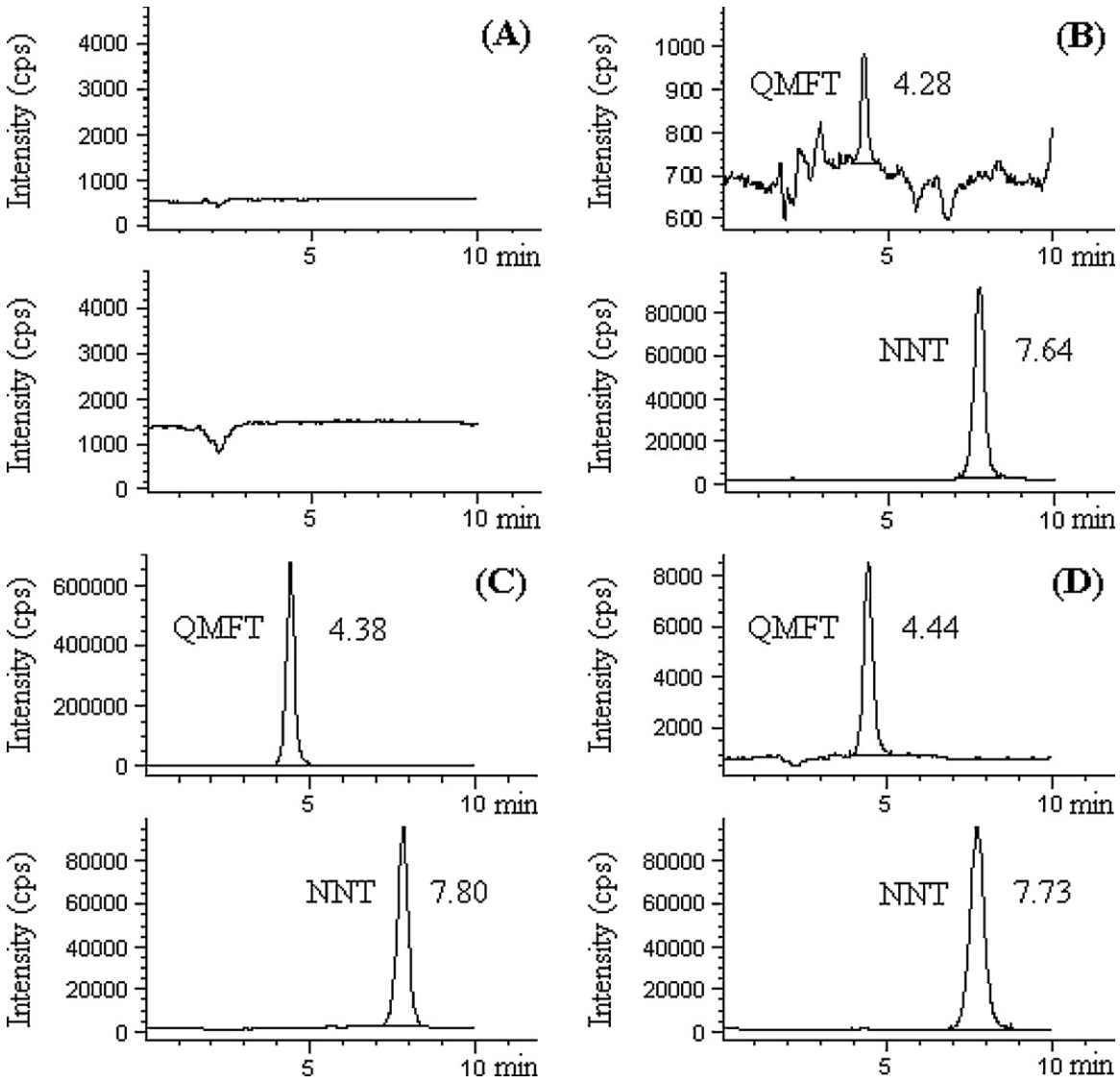

Fig. 2. Typical SIM chromatograms of blank plasma (A); LLOQ for hydromorphone (QMFT, 0.01 ng/mL) and the IS (NNT) in plasma (B); ULOQ for hydromorphone (50 ng/mL) and the IS in plasma (C); the plasma sample obtained from a subject at 4 h after intravenous infusion administration of 1.5 mg hydromorphone hydrochloride injection, the plasma concentration was estimated to be 0.2643 ng/mL (D).

3.2.3. Stability

The stability results are summarized in Table 2. The data showed that no significant degradation of hydromorphone in plasma was occurred at ambient temperature for 10 h and during three freeze-thaw cycles and at −80 °C for 8 weeks. The post-preparative stability test showed that the reconstituted samples in autosampler were stable at least 12 h at 8 °C. The stock solutions of hydromorphone and the IS in methanol were observed to remain stable for 2 months at −20 °C.

3.3. Pharmacokinetic study

The validated method was successfully applied in this pharmacokinetic study, and the plasma concentrations of hydromorphone in postoperative patients were determined up to 14 h after intravenous infusion of 1.5 mg hydromorphone hydrochloride injection over 10 min. The assay was capable of quantitating hydromorphone concentrations with all QC samples within 15% of their respective nominal value in the analytical run. The mean plasma

Table 1
Precision and accuracy validation results for hydromorphone determination.

Level	Nominal conc. (ng/mL)	Intra-day (n = 5)			Inter-day (n = 15)		
		Mean conc. found (ng/mL)	RE (%)	RSD (%)	Mean conc. found (ng/mL)	RE (%)	RSD (%)
Low QC	0.02560	0.02527	−1.3	8.4	0.02523	−1.4	10.8
Middle QC	2.048	2.181	6.5	2.6	2.176	6.3	3.0
High QC	40.96	41.70	1.8	2.8	41.25	0.7	2.1

Table 2
Stability of hydromorphone under different storage conditions ($n = 3$).

Storage conditions	Nominal conc. (ng/mL)	Mean conc. found (ng/mL)	Accuracy[a] (%)	RSD (%)	RE (%)
Short-term for 10 h	0.02560	0.02472	96.6	11.4	−3.4
	2.048	2.167	105.8	5.9	5.8
	40.96	42.25	103.2	4.5	3.2
Autosampler at 8 °C for 12 h	0.02560	0.02609	101.9	12.1	1.9
	2.048	2.163	105.6	1.5	5.6
	40.96	41.49	101.3	4.7	1.3
Three freeze–thaw cycles	0.02560	0.02527	98.7	3.9	−1.3
	2.048	2.113	103.2	3.7	3.2
	40.96	40.80	99.6	2.2	−0.4
Long-term at −80 °C for 8 weeks	0.02560	0.02769	108.2	2.1	8.2
	2.048	2.035	99.4	4.2	−0.6
	40.96	42.01	102.6	2.2	2.6

[a] Accuracy expressed as: 100 × (mean concentration found)/(nominal concentration).

Table 3
Pharmacokinetic parameters of hydromorphone in postoperative patients ($n = 9$) after continuous intravenous infusion of 1.5 mg hydromorphone hydrochlorate injection over 10 min.

Patient	Sex (M/F)	C_{max} (ng/mL)	T_{max} (min)	$t_{1/2}$ (h)	AUC_{0-t} (ng h/mL)	$AUC_{0-\infty}$ (ng h/mL)
1	F	22.01	10	2.1	9.483	9.538
2	F	16.15	10	1.9	12.23	12.26
3	F	42.53	10	4.4	11.39	11.49
4	F	13.55	10	2.1	8.601	8.676
5	F	30.14	10	2.9	13.41	13.47
6	M	11.70	10	3.2	11.30	11.44
7	F	39.91	10	1.9	15.87	15.90
8	M	9.076	10	3.1	7.758	7.821
9	M	32.28	10	2.3	13.94	13.98
Mean ± SD		24.15	10.0	2.7	11.55	11.62
		12.51	0.0	0.8	2.64	2.63

M: male; F: female; SD: standard deviation.

concentration–time curve of hydromorphone is shown in Fig. 3, and the pharmacokinetic parameters of hydromorphone are presented in Table 3. Fig. 3 shows that the plasma concentration of hydromorphone declines in a triphasic manner. The main pharmacokinetic parameters (C_{max} and AUC) obtained in this study are consistent with those in the previous studies [3–5] except for the $t_{1/2}$, which is slight shorter than that reported in the literatures (average 3–6 h) [3–5].

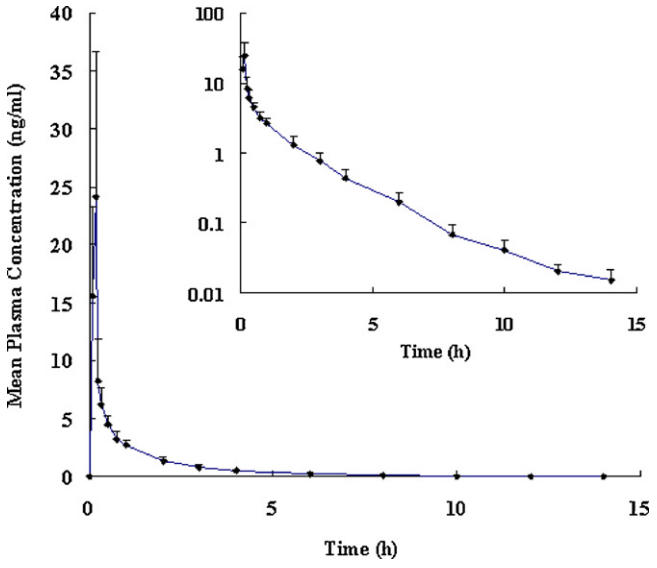

Fig. 3. Mean plasma concentration–time profile of hydromorphone in 9 postoperative patients after intravenous infusion administration of 1.5 mg hydromorphone hydrochloride injection.

4. Conclusion

A sensitive RP-HPLC–ESI-MS method for the quantification of hydromorphone in human plasma was established and successfully applied to the pharmacokinetic study of hydromorphone in postoperative patients after intravenous infusion administration of 1.5 mg hydromorphone hydrochloride injection. This method achieved an LLOQ of 0.01 ng/mL, and was suitable for the doping control, therapeutic drug monitoring and pharmacokinetic study of hydromorphone preparations. The pharmacokinetics of hydromorphone hydrochloride injection in postoperative patients was reported for the first time, and was valuable for the clinical application of hydromorphone hydrochloride injection.

References

[1] N. Sarhill, D. Walsh, K.A. Nelson, Hydromorphone: pharmacology and clinical applications in cancer patients, Support. Care Cancer 9 (2001) 84–96.
[2] A. Murray, N.A. Hagen, Hydromorphone, J. Pain Symptom Manage. 29 (2005) 57–66.
[3] B.A. Coda, A.C. Rudy, Pharmacokinetics and bioavailability of single-dose intranasal hydromorphone hydrochloride in healthy volunteers, Anesth. Analg. 97 (2003) 117–123.
[4] H.F. Hill, B.A. Coda, A. Tanaka, R. Schaffer, Multiple-dose evaluation of intravenous hydromorphone pharmacokinetics in normal human subjects, Anesth. Analg. 72 (1991) 330–336.
[5] B. Coda, A. Tanaka, R.C. Jacobson, G. Donaldson, C.R. Chapman, Hydromorphone analgesia after intravenous bolus administration, Pain 71 (1997) 41–48.
[6] H.H. Zhou, J.R. Sheller, H. Nu, M. Wood, A.J. Wood, Ethnic differences in response to morphine, Clin. Pharmacol. Ther. 54 (1993) 507–513.
[7] J.W. Lee, J.E. Pedersen, T.L. Moravetz, A.M. Dzerk, A.D. Mundt, K.V. Shepard, Sensitive and specific radioimmunoassays for opiates using commercially available materials. I. Methods for the determinations of morphine and hydromorphone, J. Pharm. Sci. 80 (1991) 284–288.
[8] N. Wetzelsberger, P.W. Lücker, W. Erking, High-pressure liquid chromatographic method for the determination of hydromorphone in human plasma with electrochemical detection, Arzneimittelforschung 36 (1986) 1707–1710.
[9] A.I. Bouquillon, D. Freeman, D.E. Moulin, Simultaneous solid-phase extraction and chromatographic analysis of morphine and hydromorphone in plasma by

high-performance liquid chromatography with electrochemical detection, J. Chromatogr. 577 (1992) 354–357.
[10] F. Musshoff, J. Trafkowski, U. Kuepper, B. Madea, An automated and fully validated LC–MS/MS procedure for the simultaneous determination of 11 opioids used in palliative care, with 5 of their metabolites, J. Mass. Spectrom. 41 (2006) 633–640.
[11] M. Barroso, E. Gallardo, D.N. Vieira, J.A. Queiroz, M. López-Rivadulla, Bioanalytical procedures and recent developments in the determination of opiates/opioids in human biological samples, Anal. Bioanal. Chem. 400 (2011) 1665–1690.
[12] T. Dahn, J. Gunn, S. Kriger, A.R. Terrell, Quantitation of morphine, codeine, hydrocodone, hydromorphone, oxycodone, oxymorphone, and 6-monoacetylmorphine (6-MAM) in urine, blood, serum, or plasma using liquid chromatography with tandem mass spectrometry detection, Methods Mol. Biol. 603 (2010) 411–422.
[13] R. Coles, M.M. Kushnir, G.J. Nelson, G.A. McMillin, F.M. Urry, Simultaneous determination of codeine, morphine, hydrocodone, hydromorphone, oxycodone, and 6-acetylmorphine in urine, serum, plasma, whole blood, and meconium, J. Anal. Toxicol. 31 (2007) 1–14.
[14] Y.L. Chen, G.D. Hanson, X. Jiang, W. Naidong, Simultaneous determination of hydrocodone and hydromorphone in human plasma by liquid chromatography with tandem mass spectrometric detection, J. Chromatogr. B 769 (2002) 55–64.
[15] W. Naidong, X. Jiang, K. Newland, R. Coe, P. Lin, J. Lee, Development and validation of a sensitive method for hydromorphone in human plasma by normal phase liquid chromatography–tandem mass spectrometry, J. Pharm. Biomed. Anal. 23 (2000) 697–704.

Journal of Pharmaceutical and Biomedical Analysis 61 (2012) 22–29

Contents lists available at SciVerse ScienceDirect

Journal of Pharmaceutical and Biomedical Analysis

journal homepage: www.elsevier.com/locate/jpba

In vivo microdialysis with LC–MS for analysis of spinosin and its interaction with cyclosporin A in rat brain, blood and bile

Rong-Hua Ma[a,1], Jie Yang[a,1], Lian-Wen Qi[a], Gui-Zhong Xin[a], Chong-Zhi Wang[b], Chun-Su Yuan[b], Xiao-Dong Wen[a,*], Ping Li[a,**]

[a] *State Key Laboratory of Natural Medicines (China Pharmaceutical University), Nanjing 210009, China*
[b] *Tang Center for Herbal Medicine Research and Department of Anesthesia & Critical Care, The Pritzker School of Medicine, The University of Chicago, 5841 South Maryland Avenue, Chicago, IL 60637, USA*

ARTICLE INFO

Article history:
Received 13 September 2011
Received in revised form
11 November 2011
Accepted 12 November 2011
Available online 22 November 2011

Keywords:
Spinosin
In vivo microdialysis
LC–/MS
Cyclosporin A
Drug–drug interactions

ABSTRACT

Spinosin, a major bioactive herbal ingredient isolated from Semen Ziziphi Spinosae, plays an important role in sedation and hypnosis. However, the pharmacokinetic behavior of spinosin in special sites has not been reported. Microdialysis (MD) technique, as a continuous, realtime monitoring sampling technique, is very suitable for the evaluation of the disposition of diverse drugs. To obtain more useful information on spinosin, an *in vivo* microdialysis sampling technique with High Performance Liquid Chromatography–mass spectrograph (HPLC–MS) method was developed to investigate the pharmacokinetics of spinosin and its interaction with cyclosporin A (CsA) in the brain, blood and bile of rats. The method was validated in terms of selectivity, linearity and sensitivity, and showed advantages in monitoring the pharmacokinetic behavior of drugs. The results revealed that CsA has obvious effects on the pharmacokinetic process of spinosin. When co-administered, the area under the curve (AUC) of spinosin in blood, bile and brain increased from 205.70 to 673.51 mg min/L, 7.77×10^4 to 1.25×10^5 mg min/L, and 2.09 to 5.58 mg min/L, respectively. The $t_{1/2}$ values of spinosin in blood, bile and brain also changed from 48.07 to 95.04 min, from 97.20 to 152.21 and from 42.18 to 73.83 min, respectively. These results demonstrated that the CsA decreased the efflux of spinosin through the inhibition of P-glycoprotein (P-gp) efflux transporter and it might be used as a group of P-gp substrate. Other transporters or pathways may also be involved in the metabolism of spinosin.

© 2011 Elsevier B.V. All rights reserved.

1. Introduction

Pharmacokinetic (PK) behavior of drugs plays a crucial role in the determination of their pharmacological actions. Any alterations in pharmacokinetic parameters will affect their therapeutic efficacy. Spinosin (2″-β-*O*-glucopyranosyl swertisin, $C_{28}H_{38}O_{15}$, Fig. 1), a bioactive herbal ingredient isolated from Semen Ziziphi Spinosae, plays an important role in sedation and hypnosis [1,2]. It significantly potentiated the hypnotic effect of pentobarbital by decreasing sleep latency, increasing sleeping time, and enhancing the rate of sleep onset induced by subhypnotic doses of pentobarbital [3]. The mechanism of this action may be related to postsynaptic 5-HT_{1A} receptors [4]. Although spinosin possesses significant activities, previous pharmacokinetic studies [5–9] are not sufficient for illustrating its mechanism of action and supplying research information for clinical use. The pharmacokinetic behavior of spinosin in special sites has not been reported elsewhere.

In recent decades, the crucial role of efflux transporters in drug absorption and disposition has gained considerable attention [10]. The inhibition or induction of transporters can lead to significant drug–drug interaction by affecting various pharmacokinetic parameters of the drug [11]. P-glycoprotein (P-gp), the most extensively studied ATP-binding cassette transporter, functions as a biological barrier by extruding toxic substances and xenobiotics out of cells [12]. The hypothesis that inhibition of P-gp improves the bioavailability of drugs that are substrate for this efflux transporter is gaining widespread recognition [13]. However, the role of P-gp efflux transporter in spinosin metabolism and disposition has not been investigated.

In many clinical cases, determining the total drug concentration does not always produce the designed data because only the free drug concentration is responsible for the distribution, elimination, and therapeutic effect of drugs [14]. MD is a sampling technique that not only enables direct measurement of free drug levels at the biophase and continuous sampling without net fluid loss, but also permits monitoring of local concentrations of drugs

* Corresponding author. Tel.: +86 25 8327 1379; fax: +86 25 8327 1379.
** Corresponding author. Tel.: +86 25 8327 1382; fax: +86 25 8327 1382.
E-mail addresses: endeavour@yahoo.cn (X.-D. Wen), liping2004@126.com (P. Li).
[1] These authors contributed equally to this work.

0731-7085/$ – see front matter © 2011 Elsevier B.V. All rights reserved.
doi:10.1016/j.jpba.2011.11.014

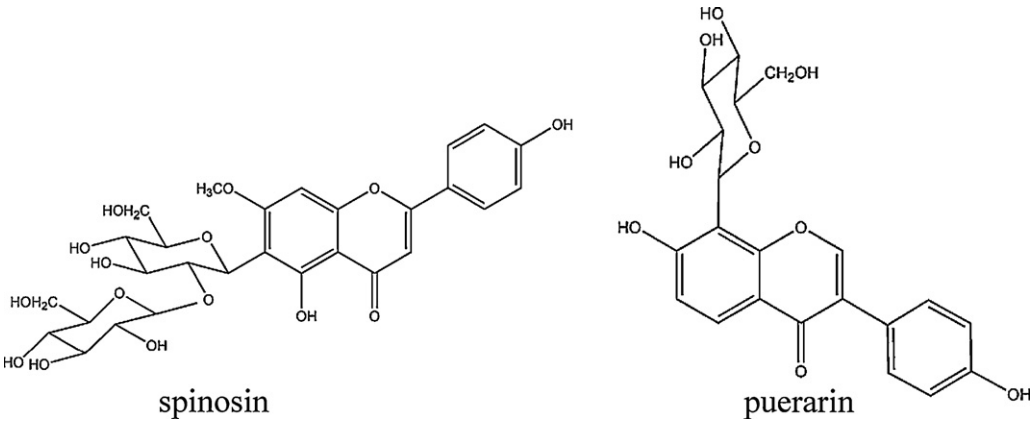

Fig. 1. The chemical structure of spinosin and puerarin (internal standard).

and metabolites at specific sites [15]. Recently, there has been growing interest in the use of microdialysis to evaluate the disposition of diverse drugs [16–18]. PK involving MD commonly requires an efficient and sensitive analytical method to measure considerably low concentration of the analyte in the microdialysate [15]. HPLC–MS with its high stability and sensitivity is particularly suitable for determination of compounds at low levels in biological fluids. Thus, microdialysis sampling techniques coupled with the HPLC–MS method provides an attractive tool for pharmacokinetic research.

To obtain more useful information on the metabolic fate of spinosin, this study aimed to investigate the pharmacokinetics of unbound spinosin in the brain, blood and bile of rats. For this purpose, an *in vivo* microdialysis sampling technique with the HPLC–MS method was developed and validated. The role of P-gp efflux transporter in spinosin metabolism and disposition was also investigated by comparing the PK of spinosin with and without CsA, a well-established P-gp inhibitor [19,20].

2. Experimental

2.1. Chemicals and materials

Spinosin was isolated from Semen Ziziphi Spinosae in the authors' laboratories and its structure in Fig. 1 was elucidated by Infrared Spectroscopy (IR), mass spectrography (MS), Carbon Nuclear Magnetic Resonance Spectroscopy (^{1}H NMR) and Nuclear Magnetic Resonance Spectroscopy (^{13}C NMR) methods and by comparison with the data in references [21]. The purity of this compound was determined to be higher than 98% by normalization of the peak area detected by HPLC. The internal standard (IS) Puerarin (Fig. 1) was purchased from the National Institute for Control of Pharmaceutical and Biological Products (Beijing, China). CsA was purchased from Novartis Pharma Stein AG (Basel, Switzerland). Acetonitrile was of HPLC grade from Merck (Darmstadt, Germany). Purified water prepared by the Millipore system (Millipore, Bedford, MA, USA) was used for all the preparations. Other chemicals were of analytical grade.

2.2. Experimental animals

Sprague–Dawley rats (280 ± 20 g) were obtained from Sino-British Sippr/BK Lab. Animal Co. Ltd. (Shanghai, China) and housed with unlimited access to food and water except for fasting 12 h before the experiment. The animals were maintained on a 12-h light/12-h dark cycle (light on at 8:00) at ambient temperature (22–25 °C) and 60% relative humidity. All experimental animal surgery procedures were reviewed and approved by the Institutional Animal Experimentation Committee of China Pharmaceutical University (Nanjing, China). The rats were anesthetized with urethane 1 g/kg (i.p.) and remained anesthetized throughout the experimental period. The femoral vein was exposed for further drug administration. The rat's body temperature was maintained at 37 °C during the experimental procedure.

2.3. Microdialysis experiments

Blood, brain and bile microdialysis systems consisted of a 3-syringe bracket microdialysis pump with a Bee Syringe Pump Controller (Bioanalytical System Inc., West Lafayette, IN, USA). Blood and bile duct microdialysis probes were constructed in-house based on a previous design [16]. A dialyzing membrane of 10 and 65 mm were used for blood and bile sampling, respectively. Under urethane anesthesia, the flexible blood microdialysis probe was implanted into the jugular vein toward the rat's right atrium, and then perfused with anticoagulant citrate dextrose (ACD) solution (3.5 mM citric acid, 7.5 mM sodium citrate, and 13.6 mM dextrose) at a flow rate of 2 μL/min. The bile microdialysis probe was perfused with Ringer's solution (147 mM NaCl, 2.4 mM $CaCl_2$, and 4.0 mM KCl with a pH of 7.3) at a flow rate of 2.0 μL/min.

For brain sampling, the rat was mounted on a stereotaxic frame (RWD Life Science Co. Ltd, Shenzhen China). An incision was made in the scalp, and a small hole was drilled for striatum implantation of a rigid brain microdialysis probe. Stereotaxic coordinates from bregma for ventral hippocampus (HC): −5.6 mm rostral, 5.0 mm medial, −3.4 mm ventral from the top of the skull according to the Paxinos and Watson. A microdialysis probe (MD-2204, 4 mm membrane, Bioanalytical system, Inc., USA) was lowered into the hippocampus of the anesthetized rat. Perfusion of the microdialysis probe with filtered Ringer's solution (147 mM NaCl, 2.4 mM $CaCl_2$, and 4.0 mM KCl with a pH of 7.3) was begun shortly before probe insertion and continued for the duration of the experiment delivered by a microinjection pump at a constant flow-rate of 2 μL/min. The blood, bile and brain samples were drawn at every 20 min after administration of spinosin until 6 h (interval of 10 min periods for the first 120 min). The midpoints of the sampling times were used for blood, bile and brain spinosin concentration-time profiles.

2.4. Drug administration

Spinosin (2 mg/mL) was dissolved in saline (containing 0.5% dimethyl sulfoxide (DMSO)). CsA was diluted with 0.9% (w/v) sodium chloride to 10 mg/mL. For the control group, 5 mg/kg of spinosin was administrated through the femoral vein to each rat 2 h after the blood, brain and bile probe were implanted for the equilibrium of the dialysis membrane. For CsA co-administration

groups, 10 mg/kg CsA was given through the femoral vein 10 min prior to spinosin injection. The volume of injection was 1 mL/kg.

2.5. Sample preparation

A stock solution of an internal standard (IS) of puerarin for blood was prepared in a concentration of 0.5 μg/mL in ACD solution. The blood analysis samples were prepared by spiking 3 μL (0.5 μg/mL) of the corresponding IS stock solutions into 12 μL dialysate followed by vortexing. And stock IS solutions of puerarin for bile and brain were prepared in Ringer's solution at 0.11 and 0.15 μg/mL, respectively. The bile analysis samples were prepared by spiking 18 μL (0.11 μg/mL) of the corresponding IS stock solutions into 2 μL dialysate followed by vortexing. And the brain analysis samples were prepared by spiking 3 μL (0.15 μg/mL) of the corresponding IS stock solutions into 12 μL dialysate followed by vortexing.

2.6. HPLC–MS system

Chromatographic analysis was performed on an Agilent 1100 series LC system (Agilent, Germany) equipped with a binary pump and a thermostatically controlled column apartment. Chromatographic separation was carried out at 25 °C on an Angilent extend-C_{18} column (50 mm × 4.6 mm I.D., 1.8 μm) with a C_{18} guard column (Hanbang, Jiangsu, China). The mobile phase consisted of 0.1% formic acid water (Solvent A) and acetonitrile (Solvent B). The injection volume of blood, brain, bile samples are 10 μL, 10 μL, 5 μL, respectively. The chromatograph was developed with a 10 min linear gradient from 15% Solvent A to 50% Solvent B followed by a 5 min re-equilibration. The flow rate was set at 0.5 mL/min. To avoid ion suppression, a post-column Diverter valve was applied to remove the ions in microdialysate. Detections were performed by a single quadrupole mass spectrometer (Product No. G2710BA, Agilent Corp, Santa Clara, CA, USA) equipped with an ESI source. The mass range was set at *m/z* 100–1000. The ESI-MS data were acquired in positive mode and conditions of MS analysis were as follows: drying gas (N_2) flow-rate, 10 L/min; drying gas temperature, 300 °C; nebulizing gas (N_2) pressure, 16 psi; capillary voltage, 3000 V; quad temperature, 100 °C; fragmentor, 100 V. The samples from the fast HPLC column were analyzed in selective ion monitoring (SIM) mode by monitoring the molecular ions *m/z* 417 for puerarin and *m/z* 609 for spinosin. SIM for each compound were restricted to specific retention time windows: 0–10 min, *m/z* 417, *m/z* 609 (retention time: 6.3 min, 7.4 min). All the operations, the acquiring and analysis of data were controlled by Chemstation software (Agilent Technologies, USA).

2.7. Method development

2.7.1. Selectivity

The selectivity of the method was tested by analyzing drug-free blood, bile and brain dialysate from five different rats. Each dialysate sample was tested using the HPLC–MS conditions proposed to insure no interference with spinosin and IS.

2.7.2. Calibration curves

Because of the differences in concentration ranges and matrix between blood, brain and bile dialysates, the calibration curves were prepared separately. The stock solution of spinosin for blood at 1.04 mg/mL was prepared in ACD solution (containing 10% DMSO), and then diluted with ACD solution to make the working standard solutions of different serial concentrations. Then, 10 μL of IS for blood and 10 μL of the corresponding working standard solutions were mixed with 80 μL of blank blood dialysate to form serial concentrations (1.04×10^{-2}, 3.12×10^{-2}, 1.04×10^{-1}, 3.12×10^{-1}, 1.04 and 3.12 μg/mL). Except for replacing ACD with Ringer's solution and forming different serial concentrations (2.00×10^{-2}, 5.00×10^{-2}, 1.00, 5.00, 10.0, 20.0, 50.0 μg/mL and 5×10^{-3}, 8×10^{-3}, 1.00×10^{-2}, 5.00×10^{-2}, 1.00×10^{-1}, 2.00×10^{-1}, 5.00×10^{-1} μg/mL in bile and brain, respectively), bile and brain calibration samples were prepared just as the same as blood samples. Standard working solutions were prepared every day, immediately before use.

The quality control (QC) samples with low, middle and high concentrations for blood (3.12×10^{-2}, 3.12×10^{-1} and 3.12 μg/mL), bile (5.00×10^{-2}, 1.00, 20.0 μg/mL) and brain (1.00×10^{-2}, 1.00×10^{-1}, 5.00×10^{-1} μg/mL) were also prepared one by one and daily in the same manner. All solutions were stored at −20 °C before use. For a standard curve, the ratio of the chromatographic peaks area (analytes/IS) as ordinate variables were plotted versus the concentration of spinosin as abscissa. The limit of detection (LOD) and limit of quantification (LOQ) determinations were considered as the final concentration producing a signal-to-noise ratio of 3 and 10, respectively. Both were measured with at least five replications.

2.7.3. Accuracy and precision

The intra-day precision and accuracy of the method were determined by analysis of the QC samples five times in a single day while its inter-day precision and accuracy were estimated by analysis of the QC samples three times in three consecutive days. The accuracy was calculated as mean percent deviation (RE) of the observed concentration (C_{obs}) from the nominal concentration (C_{nom}), accuracy (%RE) = $[(C_{obs} - C_{nom})/C_{nom}] \times 100$. The precision was expressed as percent of coefficient of variation (CV), precision (%CV) = [Standard deviation (SD)/mean C_{obs}) × 100. The acceptable intraday and interday precision is required to be less than 15% and the acceptable accuracy is required to be within 15% for all QC samples.

2.7.4. Matrix effect

Since the ionization of the analyte may influenced by the co-eluting, undetected endogenous matrix compounds, the matrix effect of analytes must be investigated during the analysis. It was evaluated by comparing the peak area of IS and spinosin in the blank dialysate with that at the same concentrations of IS and spinosin in methanol.

2.7.5. Stability

The stability of analytes was evaluated by analyzing QC samples at three concentrations exposed to different time and temperature conditions: modeling three freeze/thaw cycles (−20 °C to ambient temperature), 24 h storage at room temperature and frozen at −70 °C for 1 month.

2.7.6. Recoveries of microdialysis probes

A retrodialysis calibration technique was applied to recovery determination [22]. The experiment was carried as described in Section 2.3 except the perfusate was replaced by the spinosin ACD solution (for blood microdialysis) or Ringer's solution (for bile and brain microdialysis) in certain concentrations. The perfusate (C_{perf}) and dialysate (C_{dial}) concentrations of spinosin were determined by the HPLC–MS system. The *in vivo* relative recovery (R_{dial}) of spinosin across the microdialysis probe was calculated by the following equation: $R_{dial} = (C_{perf} - C_{dial})/C_{perf}$. Spinosin microdialysate concentrations (C_m) were converted to unbound concentration (C_u) by the estimated *in vivo* recoveries (R_{dial}) as follows: $C_u = C_m \times n/R_{dial}$ (*n*: microdialysis samples dilute multiples, the dilution multiples of samples are 1.25, 10 and 1.25 in blood, bile and brain, respectively).

2.8. Data analysis

Pharmacokinetic parameters in rats were estimated by a noncompartmental method using Drug and Statistics 2.0 (DAS

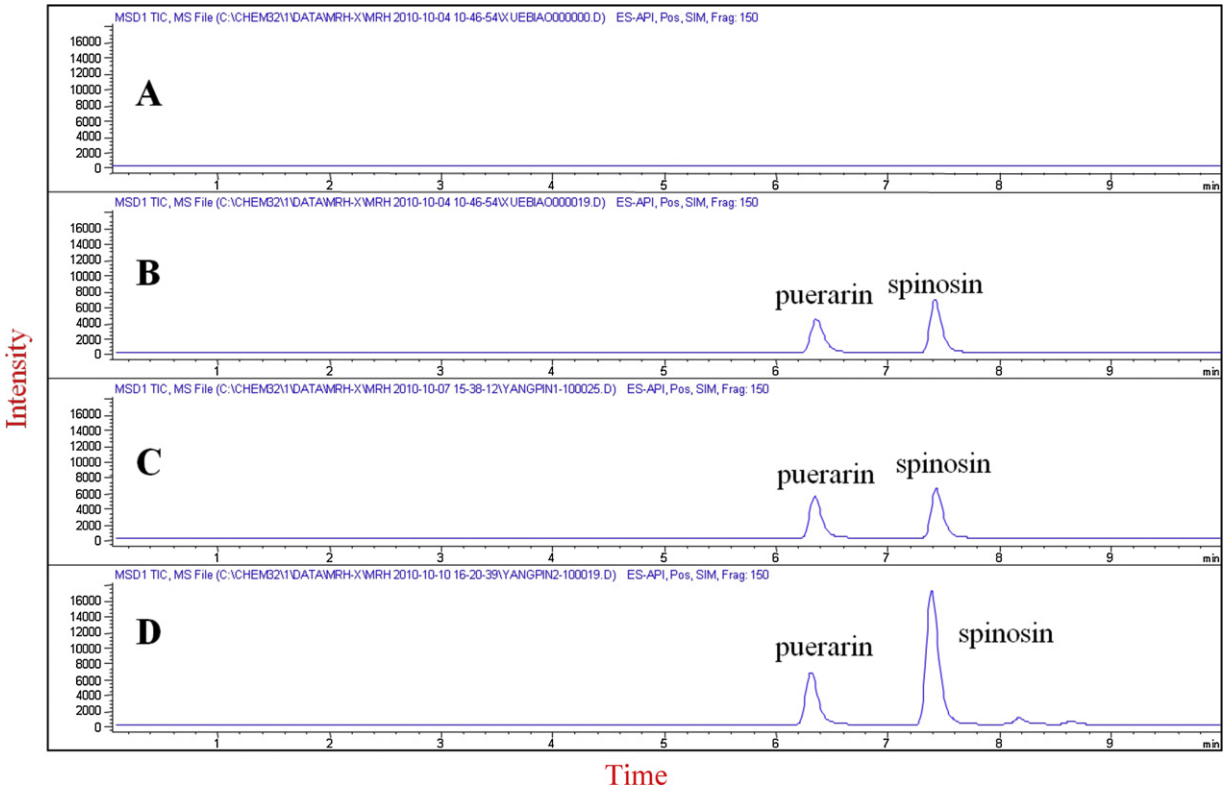

Fig. 2. Selected ion monitoring chromatograms from (A) blank blood dialysate; (B) blank blood dialysate spiked with spinosin and puerarin, the concentrations of spinosin and puerarin 0.624 μg/mL and 0.1 μg/mL, respectively; (C) blood dialysate collected at 20 min after administration, showing a spinosin concentration of 0.559 μg/mL; and (D) blood dialysate at 20 min after spinosin and CsA co-administration, showing a spinosin concentration of 1.247 μg/mL.

2.0) software package (Mathematical Pharmacology Professional Committee of China, Shanghai, China). The area under the concentration-time curve (AUC) was calculated according to the log linear trapezoidal method. The half-life ($t_{1/2}$) was calculated as follows: $t_{1/2} = 0.693/k$ (k is the elimination rate constant). All data were presented as mean ± S.D. Microsoft Excel was used for analysis with the t-test and $p < 0.05$ or $p < 0.01$ was used to determine significant differences between grouped measures.

3. Results and discussion

3.1. Method validation

3.1.1. Selectivity

Typical chromatograms of an extract from a dosed rat's dialysate (blood, bile and brain) and the blank samples are shown in Figs. 2–4. The retention times of spinosin and IS were 7.4 and 6.3 min, respectively. The results demonstrated that there is no interference in the determination of the analytes, suggesting good selectivity of the developed method.

3.1.2. Linearity and sensitivity

Three linear regressions of spinosin in blood, bile and brain dialysate exhibited good linear relationships over the range of 0.0104–3.12, 0.02–50 and 0.005–0.5 μg/mL, respectively. Each standard point was back calculated with the calibration, and all the non-zero samples showed less than 10.2% deviation except the LOQ of bile was less than 19.5%. The mean values of regression equation of the analyte in rat blood, bile and brain were: $y = 2.0755x + 0.0083$ ($r^2 = 0.9999$), $y = 2.1603x + 0.04$ ($r^2 = 0.9954$) and $y = 7.0339x - 0.0145$ ($r^2 = 0.9984$), respectively.

The LOD and LOQ for spinosin were found to be 3 and 10 ng/mL in blood dialysate, 10 and 20 ng/mL in bile dialysate, 1 and 5 ng/mL in brain dialysate, all of which were acceptable in the current assay. Intra-day accuracy and precision were determined by analyzing five replicates at three different concentration levels, five times at each concentration (Table 1). For all the samples evaluated, the variability was less than 15% (R.S.D.).

3.1.3. Matrix effect

The peak area ratio of the standard solutions mixed with methanol compared to that spiking into dialysates expresses the matrix effect in the sample matrix. The ratio value of 1 represented the response in the mobile phase and in the dialysate was the same and no significant matrix effect was observed. The average matrix effects of spinosin at three levels in blood (0.03, 0.3 and 3 μg/mL), bile (0.05, 1, 20 μg/mL) and brain (0.01, 0.1, 0.5 μg/mL) were 0.69 ± 0.02, 0.74 ± 0.04 and 0.71 ± 0.03, respectively. These results showed that endogenous substances slightly affected the ionization of the analytes under the present chromatographic and extraction conditions when the ESI interface was utilized. It reminds us that matrices ion suppression is an interesting point that we may develop new methods to reduce the effects.

3.1.4. Stability

Stability data are summarized in Table 2. The measured concentration in bile dialysate at 0.05 μg/mL is obviously lower than 0.05 μg/mL, suggesting spinosin is not stable at this concentration. Meanwhile, the solutions of spinosin at 1 μg/mL or 20 μg/mL were stable for three freeze/thaw cycles, 24 h at room temperature and at least 1 month when kept frozen at −70 °C. Thus, the concentration of spinosin in all the samples we used is higher than 1 μg/mL.

3.1.5. In vivo recovery of spinosin from microdialysis probe

Table 3 shows the average *in vivo* recovery levels of spinosin were 21.0% in blood dialysate, 59.3% in bile dialysate, and 22.35% in

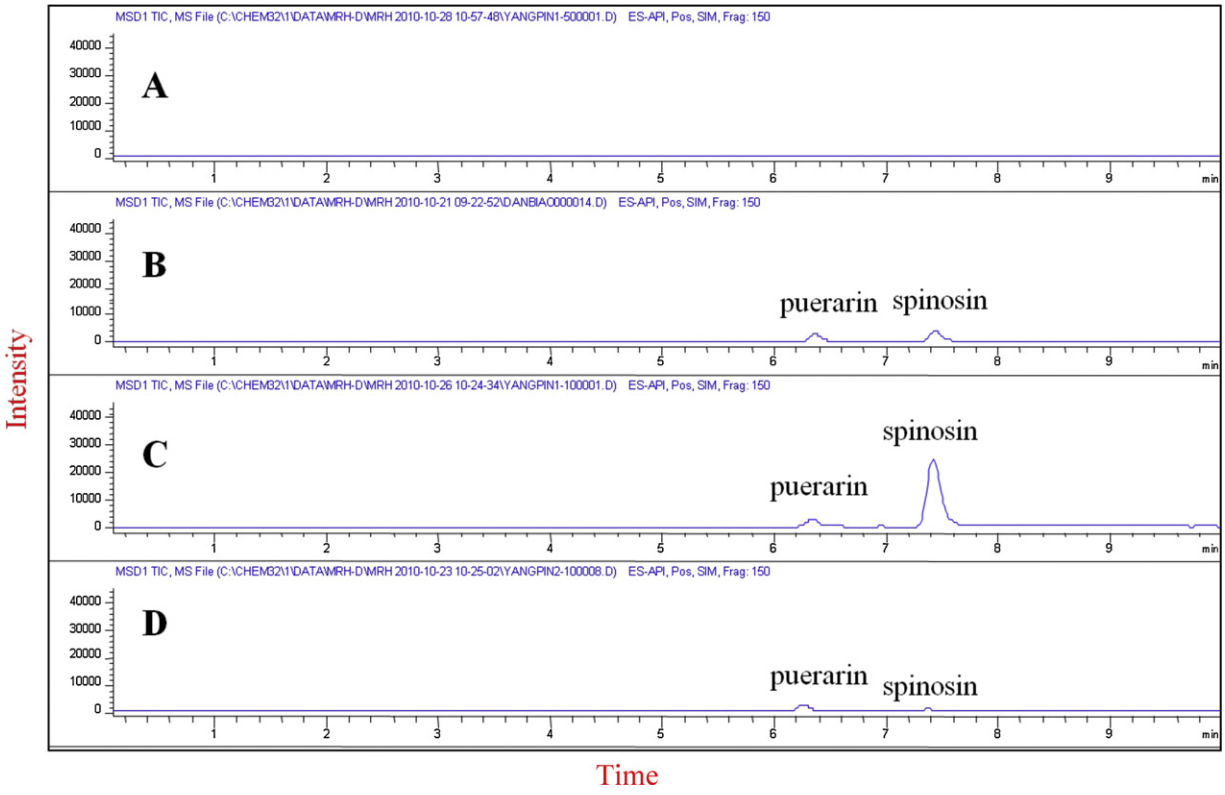

Fig. 3. Selected ion monitoring chromatograms from (A) blank bile dialysate; (B) blank bile dialysate spiked with spinosin and puerarin, the concentrations of spinosin and puerarin 0.5 μg/mL and 0.1 μg/mL, respectively; (C) bile dialysate collected at 10 min after administration, showing a spinosin concentration of 4.807 μg/mL; and (D) bile dialysate at 10 min after spinosin and CsA co-administration, showing a spinosin concentration of 0.141 μg/mL.

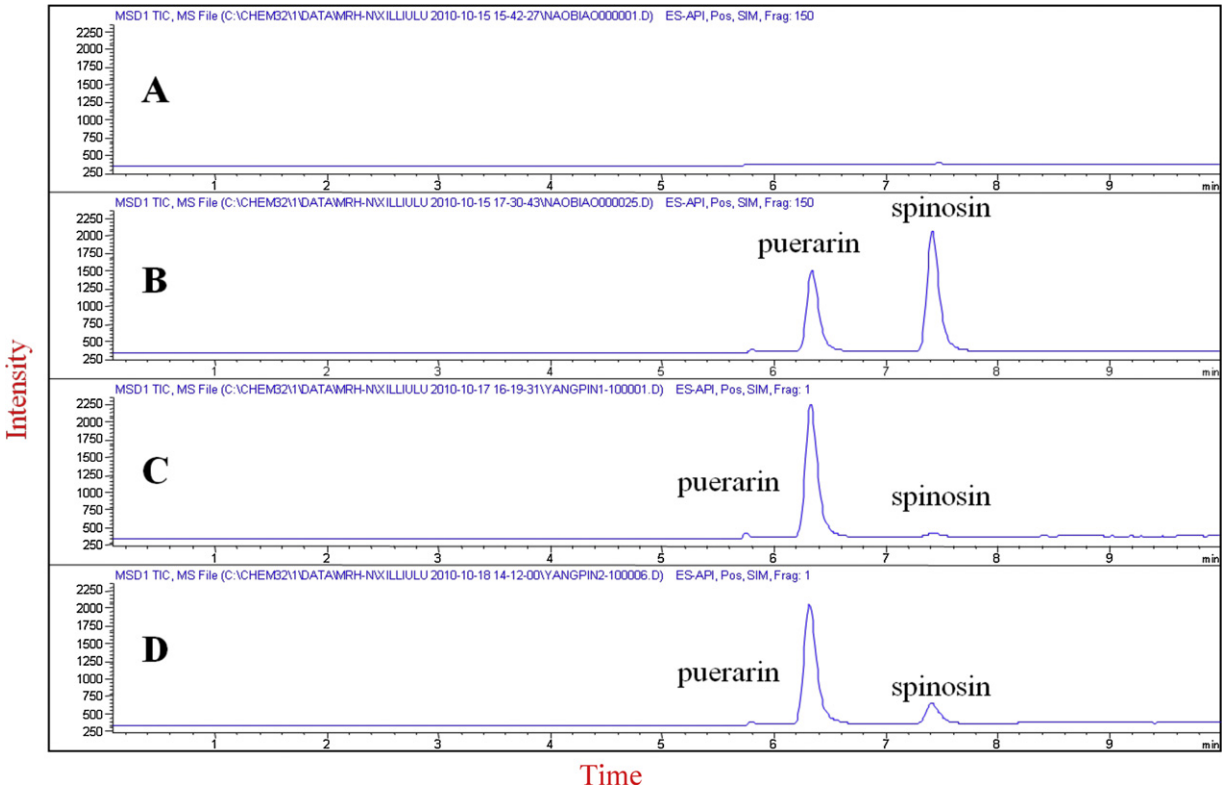

Fig. 4. Selected ion monitoring chromatograms from (A) blank brain dialysate; (B) blank brain dialysate spiked with spinosin and puerain, the concentrations of spinosin and puerarin 0.2 μg/mL and 0.03 μg/mL, respectively; (C) brain dialysate collected at 20 min after administration, showing a spinosin concentration of 6.677 ng/mL; and (D) brain dialysate at 20 min after spinosin and CsA co-administration, showing a spinosin concentration of 26.4 ng/mL.

Table 1
Intra- and inter-assay precision (% R.S.D.) and accuracy (% bias) of the method for the determination of spinosin ($n = 5$).

Biological specimen	Nominal concentration (μg/mL)	Observed concentration (μg/mL)	Precision (% RSD)	Accuracy (% bias)
Blood				
Intra-day	0.03	$2.80 \times 10^{-2} \pm 1.20 \times 10^{-3}$	4.41	−6.67
	0.3	$3.30 \times 10^{-1} \pm 2.80 \times 10^{-3}$	0.85	9.77
	3	$3.12 \pm 5.50 \times 10^{-2}$	1.78	4.04
Inter-day	0.03	$3.00 \times 10^{-2} \pm 6.70 \times 10^{-4}$	2.22	0.27
	0.3	$3.40 \times 10^{-1} \pm 2.50 \times 10^{-3}$	0.73	13.01
	3	$3.22 \pm 5.20 \times 10^{-2}$	1.35	7.20
Bile				
Intra-day	0.05	$4.60 \times 10^{-2} \pm 1.50 \times 10^{-3}$	3.27	−7.61
	1	$1.05 \pm 1.10 \times 10^{-2}$	0.73	4.57
	20	$22.80 \pm 1.40 \times 10^{-1}$	0.61	13.4
Inter-day	0.05	$4.80 \times 10^{-2} \pm 5.00 \times 10^{-3}$	13.02	−3.99
	1	$1.03 \pm 1.10 \times 10^{-2}$	0.85	3.39
	20	$19.95 \pm 4.30 \times 10^{-1}$	2.16	0.23
Brain				
Intra-day	0.01	$1.10 \times 10^{-2} \pm 7.30 \times 10^{-4}$	6.52	10.26
	0.1	$9.60 \times 10^{-2} \pm 4.20 \times 10^{-4}$	0.43	−3.69
	0.5	$4.90 \times 10^{-1} \pm 1.30 \times 10^{-2}$	2.71	−2.6
Inter-day	0.01	$1.50 \times 10^{-2} \pm 3.80 \times 10^{-4}$	0.03	5.32
	0.1	$9.70 \times 10^{-2} \pm 2.70 \times 10^{-3}$	3.45	2.63
	0.5	$4.76 \times 10^{-1} \pm 1.00 \times 10^{-2}$	2.37	4.88

Table 2
Stability of spinosin in dialysate ($n = 5$).

Microdialysis sampling	Nominal concentration (μg/mL)	Measured concentration (μg/mL) (RSD %) (RE %)					
		After three freeze/thaw cycles in dialysate		At room temperature for 24 h in dialysate		At −70 °C for 1 month in dialysate	
Blood	0.03	0.32	3.33	4.29	−6.67	6.19	−30
	0.3	1.27	23.33	0.85	10	0.77	16.7
	3	1.68	21.00	1.76	4	1.79	3.67
Bile	0.05	12.82	−22.00	2.6	−30	0.13	−22
	1	0.85	30.00	1.13	33	0.01	30
	20	2.16	−0.25	0.84	0.7	0.02	−0.25
Brain	0.01	6.37	10.00	6.73	10	0.25	30
	0.1	0.51	−16.00	0.44	−4	0.03	−21
	0.5	4.22	−10.00	2.65	−2	0.02	−14

brain dialysate. Sample concentrations were corrected by the probe recovery before pharmacokinetic data analysis.

3.2. Pharmacokinetics of spinosin in blood, bile and brain

The concentration versus time curves for spinosin in rat blood, bile, and brain dialysate after spinosin administration are shown in Fig. 5A–C. The peak concentration of spinosin in bile dialysate, which were significantly higher than that in blood and brain dialysate, was observed at about 15 min and could be detected until 6 h. The pharmacokinetic data of spinosin in blood, bile and brain dialysate are shown in Table 4.

The AUC of spinosin in blood, bile and brain were 205.70 ± 80.79 mg min/L, $7.77 \times 10^4 \pm 2.13 \times 10^4$ mg min/L and 2.09 ± 0.03 mg min/L, respectively. The amount of spinosin, as estimated from the AUC, $T_{1/2}$, in bile set against the concentration gradient was significantly greater than that in blood and brain, suggesting that spinosin might be actively excreted into the bile. The CL of spinosin in brain is significantly greater than that in blood and bile. The results indicated that spinosin entered into the brain rapidly (within 10 min) and it could be detected until 50 min after drug administration, suggesting that spinosin can effectively and rapidly penetrate the blood–brain barrier (BBB). This observation is consistent with a previous study [8]. It also supports the claim that the drug exerts it pharmacodynamic effect on the central nervous system [4].

3.3. Interaction of CsA with spinosin

After 10 mg/kg CsA was co-administered, the spinosin concentration in blood, bile and brain dialysate was significantly altered (Table 4 and Fig. 5). The AUC of spinosin in blood, bile and brain dialysate, at the dose of 5 mg/kg, increased from 205.70 to 673.51 mg min/L, 7.77×10^4 to 1.25×10^5 mg min/L and 2.09 to

Table 3
In vivo microdialysate recoveries (%) of spinosin from rat blood, bile and brain ($n = 5$).

Microdialysis sampling	Perfused concentration (μg/mL)	Recovery (%)	Average
Blood	0.02	25.10 ± 8.17	
	1	16.90 ± 2.97	21.0 ± 5.57
Bile	15	59.06 ± 9.96	
	150	59.54 ± 6.71	59.30 ± 8.34
Brain	0.01	30.04 ± 16.90	
	0.3	14.65 ± 1.62	22.35 ± 9.28

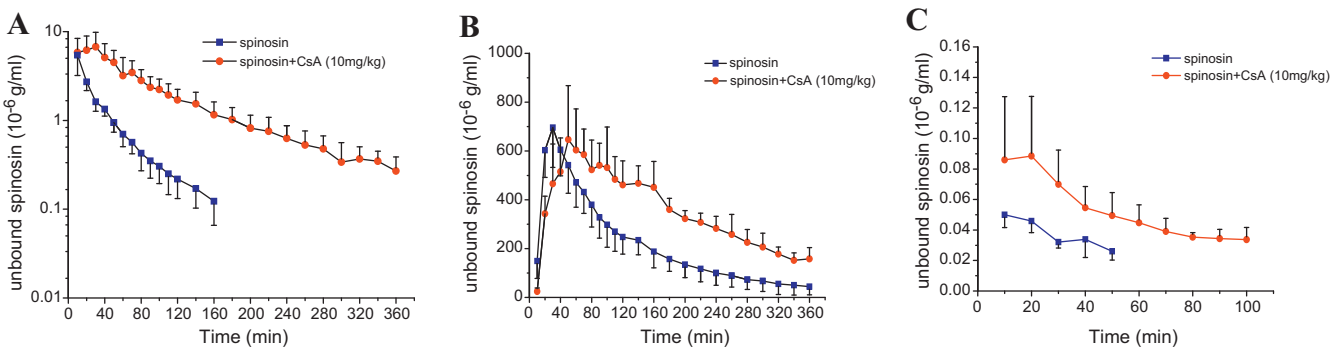

Fig. 5. Mean concentration–time profiles from (A) spinosin in rat blood dialysates after single administration of spinosin (5 mg/kg) and co-administration of spinosin and CsA (10 mg/kg); (B) spinosin in rat bile dialysates after single administration of spinosin (5 mg/kg) and co-administration of spinosin and CsA (10 mg/kg); and (C) spinosin in rat brain dialysates after single administration of spinosin (5 mg/kg) and co-administration of spinosin and CsA (10 mg/kg).

Table 4
Mean pharmacokinetic parameters of spinosin in dialysate after administration of spinosin (5 mg/kg).

Treatment	C_{max} (mg/L)	AUC (mg min/L)	$T_{1/2}$ (min)	CL (L/min/kg)	V (L/kg)
Blood					
Spinosin, 5 mg/kg	5.59 ± 2.65	205.70 ± 80.79	48.07 ± 4.71	$3.00 \times 10^{-2} \pm 5.10 \times 10^{-3}$	2.08 ± 0.35
+Cyclosprine, 10 mg/kg	7.76 ± 4.51	673.51 ± 327.19*	95.04 ± 30.39**	$9.00 \times 10^{-3} \pm 1.60 \times 10^{-3}$**	1.25 ± 0.19
Bile					
Spinosin, 5 mg/kg	695.40 ± 162.90	$7.77 \times 10^{4} \pm 2.13 \times 10^{4}$	97.20 ± 37.63	$1.00 \times 10^{-2} \pm 2.00 \times 10^{-3}$	$9.40 \times 10^{-2} \pm 1.80 \times 10^{-2}$
+Cyclosprine, 10 mg/kg	689.90 ± 191.10	$1.25 \times 10^{5} \pm 2.14 \times 10^{4}$**	152.21 ± 70.26	$2.00 \times 10^{-3} \pm 3.00 \times 10^{-4}$**	$7.00 \times 10^{-2} \pm 1.15 \times 10^{-2}$
Brain					
Spinosin, 5 mg/kg	$5.10 \times 10^{-2} \pm 7.5 \times 10^{-3}$	2.09 ± 0.03	42.18 ± 13.71	1.72 ± 0.28	101.67 ± 16.45
+Cyclosprine, 10 mg/kg	$9.00 \times 10^{-2} \pm 3.1 \times 10^{-2}$	5.58 ± 1.58**	73.83 ± 20.60*	$0.31 \pm 4.9 \times 10^{-2}$**	134.34 ± 17.77

Data expressed as means ± S.D. ($n = 5$). C_{max}: maximum concentration; AUC: area under the concentration vs. time curve; $t_{1/2}$: elimination half-life.
* $p < 0.05$ compared with single 5 mg/kg spinosin administration group.
** $p < 0.01$ compared with single 5 mg/kg spinosin administration group.

5.58 mg min/L respectively. The $t_{1/2}$ values of spinosin in blood, bile and brain dialysate also changed, respectively, from 48.07 to 95.04 min, from 97.20 to 152.21 and from 42.18 to 73.83 min when the drug was co-administered with CsA.

According to the results above, the AUC and $t_{1/2}$ values of spinosin in blood, bile and brain dialysate were significantly increased in CsA-added group, which suggested that CsA has obvious effects on the pharmacokinetic process of spinosin.

The increase of AUC and $t_{1/2}$ values of spinosin in the blood and brain could be due to the P-gp inhibition by CsA. CsA inhibited the efflux of spinosin by P-gp located on the membrane of the blood–brain barrier (BBB) and the blood–cerebrospinal fluid (BCSF) barrier, resulting in an increase of the spinosin concentration in the brain. Meanwhile, the inhibition of CsA on the excretion of spinosin may lead to the increase of its AUC in blood.

It has been extensively verified that CsA inhibits the hepatobiliary excretion of P-gp substrates from the liver into the bile [23]. Compared with the control group (given 5 mg/kg spinosin alone), the concentration of spinosin in bile dialysate was decreased in the period of 0–40 min when CsA was co-administered, suggesting CsA inhibits the P-gp transporter and thus decrease the hepatobiliary excretion of spinosin. Interestingly, after 40 min, the concentration of spinosin in bile was higher than that of control group, indicating that some other transporters, such as multispecific organic anion transporters [24], non-bile acid organic anion transporters [25], or conjugate export pumps [26] might be involved in the hepatobiliary excretion of spinosin.

In addition, the results of the present study indicate that the combining CsA with spinosin could provide an opportunity to achieve enhanced therapeutic effects of spinosin because of the increase of its concentration in blood and brain. The multi-drug treatment might be a useful way to reduce the dose of drugs and achieve better therapeutic effects in clinical practice.

4. Conclusions

In this study, a microdialysis technique with HPLC–MS method was developed to investigate the pharmacokinetics of unbound spinosin in the brain, blood and bile dialysate of rats. The work demonstrated this method can be conveniently and sensitively applied to monitor the pharmacokinetic behavior of drugs. The results revealed that CsA has obvious effects on pharmacokinetic process of spinosin since the AUC and $t_{1/2}$ values of spinosin in blood, bile and brain dialysate were significantly increased after drug co-administration. Since CsA is a well-established P-gp inhibitor, spinosin is also a substrate for P-gp transporter. Because hepatobiliary excretion of spinosin is also increased after co-administration, other transporters or pathways may also be involved in the metabolism of spinosin.

Acknowledgements

The authors greatly appreciate the financial support from the research project (No. 30973884) of the National Science Foundation of China, the program for Changjiang Scholars and Innovative Research Team in University, No. IRT0868, and the Postgraduate Innovative Projects of China Pharmaceutical University to Dr. Gui-Zhong Xin (No. ZJ10059).

References

[1] Y.J. Li, K.S. Bi, Study on the therapeutic material basis of traditional Chinese medicinal preparation Suanzaoren Decoction, Chem. Pharm. Bull. 56 (2006) 847–851.
[2] K. Kawashima, K. Saito, A. Yamada, S. Obara, T. Ozaki, Y. Kano, Pharmacological properties of traditional medicines. XXIII. Searching for active compounds in the blood and bile of rats after oral administrations of extracts of sansohnin, Biol. Pharm. Bull. 20 (1997) 1171–1174.

[3] L.E. Wang, Y.J. Bai, X.R. Shi, X.R. Shi, X.Y. Cui, S.Y. Cui, F. Zhang, Q.Y. Zhang, Y.H. Zhang, Y.Y. Zhao, Spinosin, a C-glycoside flavonoid from semen Ziziphi Spinozae, potentiated pentobarbital-induced sleep via the serotonergic system, Pharmacol. Biochem. Behav. 90 (2008) 399–403.
[4] L.E. Wang, X.Y. Cui, S.Y. Cui, J.X. Cao, J. Zhang, Y.H. Zhang, Q.Y. Zhang, Y.J. Bai, Y.Y. Zhao, Potentiating effect of spinosin, a C-glycoside flavonoid of Semen Ziziphi spinosae, on pentobarbital-induced sleep may be related to postsynaptic 5-HT(1A) receptors, Phytomedicine 17 (2010) 404–409.
[5] Y.J. Li, X.M. Liang, H.B. Xiao, K.S. Bi, Determination of spinosin in rat plasma by reversed-phase high-performance chromatography after oral administration of Suanzaoren decoction, J. Chromatogr. B 787 (2003) 421–425.
[6] Y.J. Li, M.C. Yao, S. Cheng, Quantitative determination of spinosin in rat plasma by liquid chromatography–tandem mass spectrometry method, J. Pharm. Biomed. Anal. 48 (2008) 1169–1173.
[7] Y.J. Li, X.M. Liang, H.B. Xiao, K.S. Bi, Pharmacokinetic study on spinosin in rat plasma after oral administration of suanzaoren extract at a single dose, Acta Pharm. Sin. 38 (2003) 448–450.
[8] Y.J. Li, Y.H. Dai, Y.L. Yu, Y. Li, Y.L. Deng, Pharmacokinetics and tissue distribution of spinosin after intravenous administration in rats, Yakugaku Zasshi 127 (2007) 1231–1235.
[9] K.D. Bao, P. Li, L.W. Qi, H.J. Li, L. Yi, W. Wang, Y.Q. Wang, Characterization of flavonoid metabolites in rat plasma, urine, and feces after oral administration of Semen Ziziphi Spinosae extract by HPLC–diode-array detection (DAD) and ion-trap mass spectrometry (MS(n)), Chem. Pharm. Bull. 57 (2009) 144–148.
[10] V.R. Tandon, B. Kapoor, G. Bano, S. Gupta, Z. Gillani, S. Gupta, D. Kour, P-glycoprotein: pharmacological relevance, Indian J. Pharmacol. 38 (2006) 13–24.
[11] M. Dorababu, A. Nishimura, T. Prabha, K. Naruhashi, N. Sugioka, K. Takada, N. Shibata, Effect of cyclosporine on drug transport and pharmacokinetics of nifedipine, Biomed. Pharmacother. 63 (2009) 697–702.
[12] J.H. Lin, Drug–drug interaction mediated by inhibition and induction of P-glycoprotein, Adv. Drug Deliv. Rev. 55 (2003) 53–81.
[13] J.H. Hamman, P.H. Demana, E.I. Olivier, Targeting receptors, transporters and site of absorption to improve oral drug delivery, Drug Target Insights 2 (2007) 71–81.
[14] J.D. Wright, F.D. Boudinot, M.R. Ujhelyi, Measurement and analysis of unbound drug concentrations, Clin. Pharmacokinet. 30 (1996) 445–462.
[15] M.L.T. Vieira, R.P. Singh, H. Derendorf, Simultaneous, HPLC analysis of triamcinolone acetonide and budesonide in microdialysate and rat plasma: application to a pharmacokinetic study, J. Chromatogr. B 878 (2010) 2967–2973.
[16] Q. Wu, X.D. Wen, L.W. Qi, W. Wang, L. Yi, Z.M. Bi, P. Li, An *in vivo* microdialysis measurement of harpagoside in rat blood and bile for predicting hepatobiliary excretion and its interaction with cyclosporin A and verapamil, J. Chromatogr. B 877 (2009) 751–756.
[17] C.F. Chien, Y.T. Wu, W.C. Lee, L.C. Lin, T.H. Tsai, Herb–drug interaction of *Andrographis paniculata* extract and andrographolide on the pharmacokinetics of theophylline in rats, Chem. Biol. Interact. 184 (2010) 458–465.
[18] W.H. Sheu, H.C. Chuang, S.M. Cheng, M.R. Lee, C.C. Chou, F.C. Cheng, Microdialysis combined blood sampling technique for the determination of rosiglitazone and glucose in brain and blood of gerbils subjected to cerebral ischemia, J. Pharm. Biomed. Anal. 54 (2011) 759–764.
[19] L. Kagan, T. Dreifinger, D. Mager, A. Hoffman, Role of p-glycoprotein in region-specific gastrointestinal absorption of talinolol in rats, Drug. Metab. Dispos. 38 (2010) 1560–1566.
[20] X.Y. Chu, K. Bleasby, J. Yabut, X.X. Cai, G.H. Chan, M.J. Hafey, S.Y. Xu, A.J. Bergman, M.P. Braun, D.C. Dean, R. Evers, Transport of the dipeptidyl peptidase-4 inhibitor sitagliptin by human organic anion transporter 3, organic anion transporting polypeptide 4C1, and multidrug resistance P-glycoprotein, J. Pharmacol. Exp. Ther. 321 (2007) 673–683.
[21] W.S. Woo, S.S. Kang, S.H. Shim, H. Wagner, V.M. Chari, O. Seligmann, G. Obermeier, The structure of spinosin (2″-*O*-β-glucosylswertisin) from *Zizyphus vulgaris* var.*Spinosus*, Phytochemistry 18 (1979) 353–355.
[22] T.H. Tsai, Assaying protein unbound drugs using microdialysis techniques, J. Chromatogr. B 797 (2003) 161–173.
[23] X.Y. Chu, Y. Kato, Y. Sugiyama, Possible involvement of P-glycoprotein in biliary excretion of CPT-11 in rats, Drug Metab. Dispos. 27 (1999) 440–441.
[24] Y. Kobayashi, R. Sakai, N. Ohshiro, M. Ohbayashi, N. Kohyama, T. Yamamoto, Possible involvement of organic anion transporter 2 on the interaction of theophylline with erythromycin in the human liver, Drug Metab. Dispos. 33 (2005) 619–622.
[25] C.D. Klaassen, L.M. Aleksunes, Xenobiotic, bile acid, and cholesterol transporters: function and regulation, Pharmacol. Rev. 62 (2010) 1–96.
[26] M.J. Zamek-Gliszczynski, K.A. Hoffmaster, K. Nezasa, M.N. Tallman, K.L.R. Brouwer, Integration of hepatic drug transporters and phase II metabolizing enzymes: mechanisms of hepatic excretion of sulfate, glucuronide, and glutathione metabolites, Eur. J. Pharm. Sci. 27 (2006) 447–486.

Journal of Pharmaceutical and Biomedical Analysis 61 (2012) 30–37

Contents lists available at SciVerse ScienceDirect

Journal of Pharmaceutical and Biomedical Analysis

journal homepage: www.elsevier.com/locate/jpba

Investigation of dried blood spot card-induced interferences in liquid chromatography/mass spectrometry

Xiaohui Chen*, Hongjuan Zhao, Panos Hatsis, Jakal Amin

Metabolism and Pharmacokinetics, Novartis Institutes for Biomedical Research Inc., 250 Massachusetts Avenue, Cambridge, MA 02139 USA

ARTICLE INFO

Article history:
Received 13 October 2011
Received in revised form
11 November 2011
Accepted 12 November 2011
Available online 23 November 2011

Keywords:
Liquid chromatography/mass spectrometry
Dried blood spotting
Interference
Ion-pairing
FTA® DMPK-A card

ABSTRACT

Unique and remarkable interferences were observed when dried blood spot (DBS) sampling was used in conjunction with liquid chromatography/mass spectrometry (LC/MS) assays. In particular, chromatographic retention time shifting and chromatographic peak shape distortion were observed, along with a severe suppression of MS signal intensity. The type of DBS cards, and chromatographic conditions were investigated using the same set of test compounds to gain insight into these interferences. It was determined that a constituent of the DBS cards, primarily sodium dodecyl sulfate (SDS), was responsible for the interferences by means of an ion-pairing mechanism. SDS formed ion pairs with compounds containing basic amine groups, which resulted in increased retention on a C_{18} stationary phase, peak shape distortion and ion suppression. These interferences were greatly alleviated and/or completely overcome with non-acidic mobile phases and/or DBS cards with no SDS coating. To the best of the authors' knowledge, this is the first in-depth report of interferences induced by DBS cards.

© 2011 Elsevier B.V. All rights reserved.

1. Introduction

Dried blood spotting (DBS) as a sample collection technique has been used to screen newborns for errors of metabolism since Dr. Robert Guthrie first collected blood samples on filter paper in 1963 [1]. In spite of this, the technique was limited in qualitative analysis because analytical instruments did not have the required sensitivity. Improvements in the sensitivity of analytical instrumentation, and in particular mass spectrometers, have recently given a new life to DBS, allowing the pharmaceutical industry to leverage its many benefits.

DBS is an alternative sample collection method with advantages over conventional sampling such as lower sample volumes, simpler sample collection and handling, as well as easier storage and transportation logistics [2]. Small sample volumes require less blood from humans during clinical trials, fewer animals for preclinical studies and serial bleeding sampling can be performed for small animals such as mouse which improves the quality of pharmacokinetic (PK) data. These advantages allow for significant savings in the cost of drug research and development. In addition, regulatory authorities have acknowledged that blood is an acceptable biological matrix for drug exposure measurements [3]. Therefore, DBS coupled with LC/MS/MS has been gaining momentum in the pharmaceutical industry, and has been recently applied in many areas such as PK, toxicokinetic, drug metabolism and clinical studies [2,4–7].

In spite of the potential benefits of a new technique, its implementation into a bioanalytical workflow demands careful and rigorous characterization to ensure reliable and robust assay performance. Over the years, bioanalytical scientists have come to recognize matrix effects and interferences as a potentially significant source of error in quantitative LC/MS assays, and appropriate strategies have been reported to deal with the most common of these, e.g., ionization suppression, chromatographic/isobaric interferences, etc. [8,9]. Herein, an interference unique to DBS was discovered and thoroughly examined as part of a larger effort in the authors' lab to characterize DBS in conjunction with quantitative LC/MS assays for support of PK studies in drug discovery. A group of compounds was chosen which covered a wide range in physical chemical properties to study this interference. It was discovered that certain compounds exhibited matrix effects/interferences, some of which were expected, e.g., severe ionization suppression, and others were not, e.g., chromatographic retention time (RT) shifting and chromatographic peak shape distortion. The interferences were observed only when a certain type of DBS card was used. This manuscript describes the investigation of these unique DBS-induced interferences to better understand the cause of the interferences and RT shifting, and the impact on the application of DBS for PK quantification.

Abbreviations: DBS, dried blood spotting; PK, pharmacokinetics; RT, retention time; WB, whole blood; SDS, sodium dodecyl sulfate; IS, internal standard; DMSO, dimethyl sulfoxide.

* Corresponding author. Tel.: +1 617 871 3818; fax: +1 617 871 4081.
E-mail address: xiaohui.chen@novartis.com (X. Chen).

0731-7085/$ – see front matter © 2011 Elsevier B.V. All rights reserved.
doi:10.1016/j.jpba.2011.11.015

2. Experimental

2.1. Reagents and materials

Lidocaine, erythromycin, dexamethasone (>98% purity), reserpine, cetirizine and glyburide were purchased from Sigma–Aldrich (St. Louis, MO). Fluoxetine hydrochloride and fexofenadine hydrochloride were purchased from ToCirs (Bristol, UK). Amitriptyline (98–102% purity) was purchased from Spectrum (Gardena, CA). Ethacrynic acid, cephalexin and taurocholic acid sodium salt were obtained from MP Biomedicals, LLC (Solon, Ohio). Mycophenolic acid was obtained from Calbiochem (Gibbstown, NJ). Sodium dodecyl sulfate was obtained from Thermo Scientific (Rockford, IL). HPLC grade acetonitrile, methanol, formic acid (88% purity), and dimethyl sulfoxide were purchased from Fisher Scientific (Fair Lawn, NJ). Ammonium formate (99% purity) was supplied by Acros (NJ, USA). Ultra-high purity nitrogen was supplied by an in-house nitrogen system. Water was in-house Milli-Q water generated by a Millipore lab water purification system (Billerica, MA). The blank Sprague Dawley rat whole blood was supplied by Bioreclamation, Inc. (Hicksville, NY). FTA® DMPK-A, FTA® DMPK-B and FTA® DMPK-C cards were supplied by Whatman plc (part of GE Healthcare) (Springfield Mill, UK). FTA® DMPK-A and DMPK-B cards are coated with different chemicals to lyse cells, denature proteins and/or inactivate pathogens. FTA® DMPK-C cards are uncoated.

2.2. Apparatus

Harris punches and cutting mats were obtained from Ted Pella, Inc. (Redding, CA). Microman positive displacement pipettes and tips used for blood spotting on cards were obtained from Gilson (Middleton, WI). A Tecan liquid handling system (Model Freedom EVO®) was obtained from Tecan Schweiz AG (Mannedorf, Switzerland). All experiments were performed on a HPLC-MS/MS system, which consisted of a CTC HTC PAL autosampler (Zwingen, Switzerland), an Agilent 1100 LC system with an integrated divert valve, and a Sciex API4000 (AB/Sciex, Canada) equipped with an electrospray ionization source. Post column infusion and infusion optimization of analyte MS/MS parameters were performed with a Harvard Pump 11 Plus syringe pump (Holliston, MA).

2.3. Sample preparation

Primary stock solutions for all test compounds and glyburide as internal standard (IS) were prepared at 1 mg/mL in dimethyl sulfoxide (DMSO). Working solutions for each compound were diluted from the primary stocks with DMSO to 50 μg/mL. All the solutions were stored at −20 °C and brought to room temperature before use. Test solutions were prepared fresh on the day of analysis by diluting the appropriate amount of the working solutions with blank Sprague-Dawley rat whole blood or the appropriate solvent to give a concentration of 500 ng/mL. Unless otherwise mentioned, this is the concentration of all test analytes used in this work. Extraction solution was prepared by mixing acetonitrile, methanol and water at the ratio of 1:1:1 (v/v/v) with or without 100 ng/mL glyburide.

2.4. LC/MS/MS analysis

Chromatographic separations employed an ACE C_{18}, 3 μm, 30 mm × 2.1 mm i.d. HPLC column (MAC-MOD Analytical, Inc. Chadds Ford, PA), and a solvent gradient employing two separate solvent systems. The default solvent system used acidic mobile phases consisting of 0.1% formic acid in water (A) and 0.1% formic acid in acetonitrile (B). The second solvent system used non-acidic mobile phases consisting of 10 mM ammonium formate in water (A) and 10 mM ammonium formate in methanol (B). Following sample injection of 10 μL, the mobile phase composition was held at 2% B for 0.5 min. It was then increased linearly to 98% B over 1.5 min and then held at 98% B for another 0.5 min. This was followed by re-equilibration of the column at the initial mobile phase conditions. The flow rate was 0.7 mL/min, and the column was maintained at 40 °C. The post column flow was diverted to waste for the first 0.5 min of each injection.

LC/MS/MS was performed in either positive (5500 V) or negative polarity (−4500 V) depending on the test compound. The source temperature was 550 °C. Gas 1 and Gas 2 settings for nitrogen were set to 60. The curtain gas and collision gas were also nitrogen and were set to 25 and 10 (arbitrary units). All test compounds were acquired with selected reaction monitoring (SRM) transitions with dwell times of 75 ms. Table 1 contains the chemical structure, molecular weight (MW), experimental pK_a value [10–14], SRM transition ($Q1 \rightarrow Q3$), declustering potential (DP, V) and collision energy (CE, V) of all test compounds. All data were acquired and quantified (peak integration) using Analyst® 1.4.2 software (AB/Sciex). Further data analysis and plotting were performed in Excel (Microsoft Corporation, Redmond, WA). All results are reported as the mean of three replicate analyses.

2.5. Recovery evaluation

The DBS recovery evaluation consisted of three parts, Experiment A, B and C as described in detail in Fig. 1. Experiment A was a complete DBS workup with analyte extraction from dried blood spots on DBS cards. An aliquot of 7 μL of a 500 ng/mLwhole blood (WB) sample was applied in triplicate to FTA® cards and allowed to dry at room temperature for at least 1 h. The blood spot was cut with a 6 mm diameter puncher and placed into a 96-deep well plate. The use of a small whole blood sample volume and a 6 mm puncher ensured that the applied samples were completely punched out of the DBS cards. Automated analyte extraction was performed on a Tecan by adding 300 μL of extraction solution with IS to the plate, sealing the plate and sonicating for 5 min without heat. The samples were centrifuged for 10 min at 2844 × g and 4 °C, and 125 μL of the supernatant was transferred to a new plate for LC/MS/MS analysis with the default acidic mobile phases. Experiment B was similar to Experiment A, however 500 ng/mL analyte was added to the sample after extraction. Experiment C of the evaluation used analytes prepared at the same 500 ng/mL concentration, but in neat solution, and served as a reference for Experiment A and B. Experiments B and C used 293 μL of extraction solution to compensate for the 7 μL of analyte added as a final step. The analytes' matrix effect, recovery and process efficiency were calculated using the following equations:

$$\text{Matrix effect} = \left(1 - \frac{\text{Peak area of analyte from Experiment B}}{\text{Peak area of analyte from Experiment C}}\right) \times 100$$

$$\text{Recovery} = \frac{\text{Peak area of analyte from Experiment A}}{\text{Peak area of analyte from Experiment B}} \times 100$$

$$\text{Process efficiency} = \frac{\text{Peak area of analyte from Experiment A}}{\text{Peak area of analyte from Experiment C}} \times 100$$

FTA® DMPK-A cards were the primary DBS cards used in the recovery evaluation based on a previous investigation into the stability of a set of proprietary test compounds in the authors' lab (data not shown). Surprisingly, RT shifting, ionization suppression and peak distortion were observed during the evaluation,

Table 1
All test compounds' structure, molecular weight (MW), experimental pK_a, SRM transition ($Q1 \rightarrow Q3$), declustering potential (DP) and collision energy (CE).

Compound	Structure	MW	pK_a	$Q1 \rightarrow Q3$	DP (V)	CE (V)
Amitriptyline	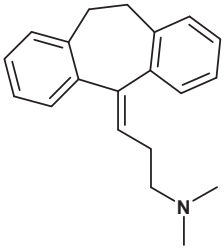	277.2	9.4	278.2 → 105.2	81	33
Cephalexin	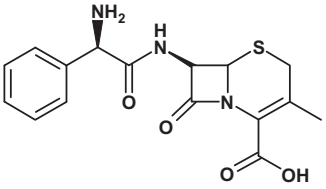	347.1	4.5	348.0 → 158.0	125	20
Cetirizine	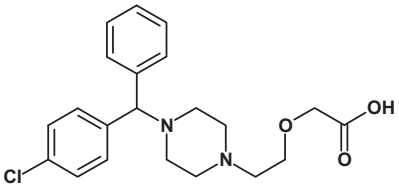	388.2	8.3	389.0 → 201.0	125	40
Dexa-methasone	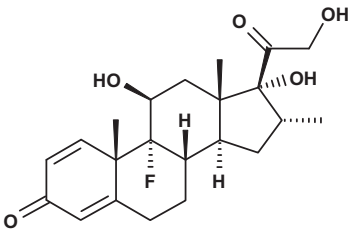	392.2	NA	393.2 → 373.1	86	13
Ethacrynic acid	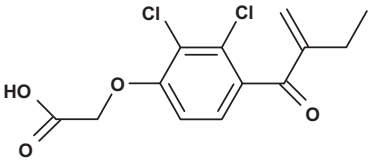	302.0	3.5	301.0 → 243.0	−100	−30
Erythromycin	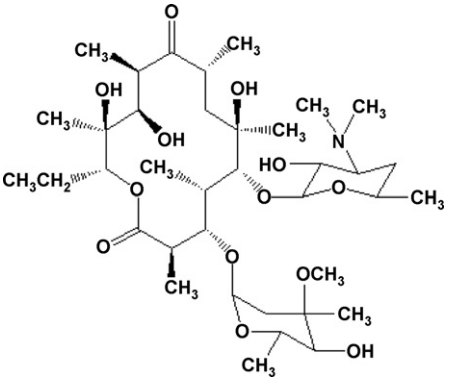	733.5	8.9	734.5 → 158.2	81	41
Fluoxetine	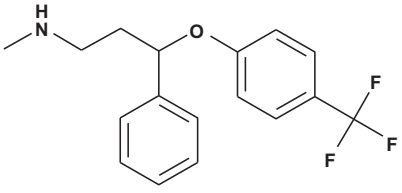	309.1	8.7	310.2 → 148.2	61	11

Table 1 (*Continued*)

Compound	Structure	MW	pK_a	$Q1 \rightarrow Q3$	DP (V)	CE (V)
Fexofenadine	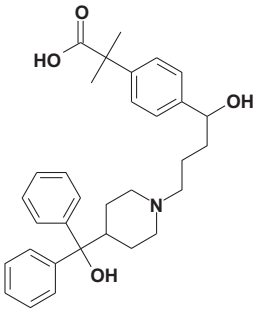	501.3	9.5	501.8 → 466.2	125	40
Lidocaine	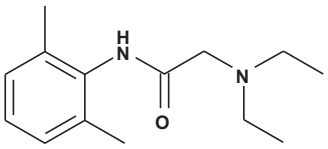	234.2	8.0	235.1 → 86.2	61	21
Mycophenolic acid	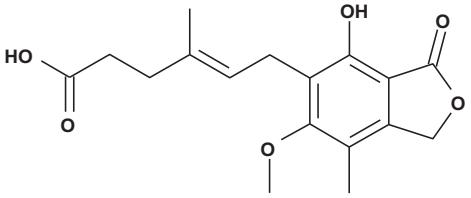	320.1	4.5	319.2 → 275.1	−55	−22
Reserpine	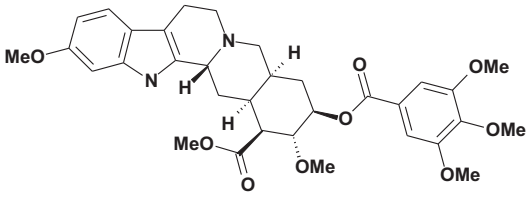	608.3	6.6	608.8 → 195.0	100	60
Taurocholic acid	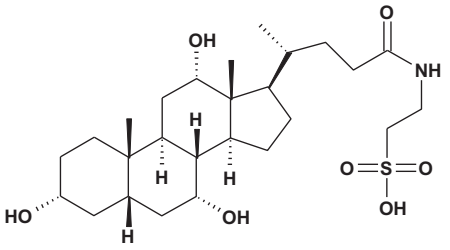	515.3	1.4	514.4 → 80.2	−160	−84

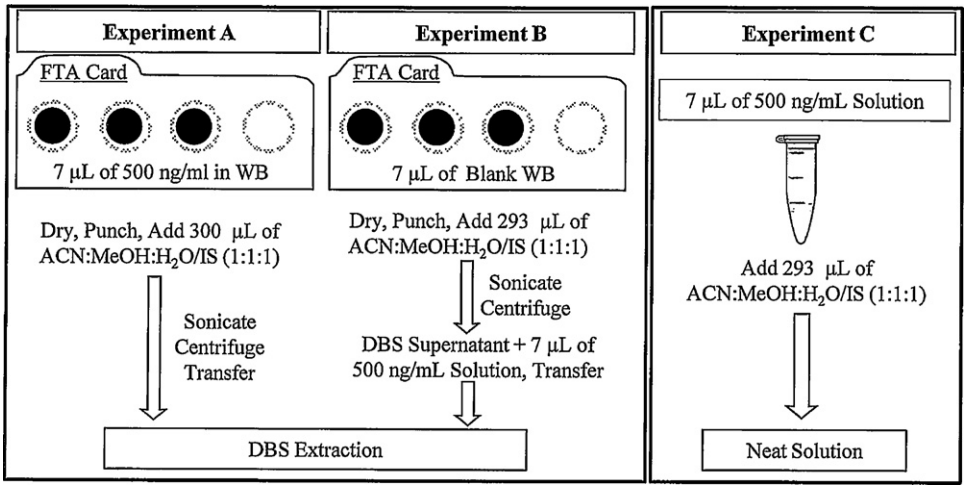

Fig. 1. Scheme of DBS recovery evaluation experiment.

Table 2
Matrix effect, recovery, process efficiency and retention time in solution and in matrix for all test compounds on FTA® DMPK-A cards with acidic mobile phase condition.

Compound	FTA® DMPK-A cards			RT (min)	
	Matrix effect (%)	Recovery (%)	Process efficiency (%)	In solution	In matrix
Amitriptyline	66	87	30	1.77	1.91
Cephalexin	18	89	73	1.46	1.46
Cetirizine	80	104	20	1.78	1.89
Dexamethasone	2	88	86	1.77	1.77
Ethacrynic acid	97	[a]	[a]	1.94	1.94
Erythromycin	99.6	95	0.4	1.69	1.86
Fluoxetine	58	96	41	1.80	1.92
Fexofenadine	40	74	44	1.76	1.89
Lidocaine	65	118	41	1.43	1.84
Mycophenolic acid	99.6	74	0.3	1.85	1.85
Reserpine	68	116	37	1.80	1.91
Taurocholic acid	61	71	28	1.75	1.72

[a] Below detection limit of 1 ng/mL.

which triggered an in-depth investigation. Control recovery experiments were performed using the identical sample preparation and instrument conditions but with different types of DBS cards: DMPK-B and DMPK-C cards. A control experiment was also performed using the identical sample preparation and instrument conditions but with non-acidic mobile phases containing 10 mM ammonium formate.

2.6. Effect of sodium dodecyl sulfate (SDS) concentrations on lidocaine

The DBS interference was further investigated by examining the effect of SDS concentration on the retention and peak shape of lidocaine in two separate experiments. The first experiment was to vary the concentration of SDS using blank DMPK-A discs. Lidocaine samples were prepared in triplicate as described in Experiment A of Section 2.5. Prior to extraction, a pre-punched DMPK-A disc was placed in one sample and two discs in the second sample. The third sample had no additional blank DMPK-A discs added. All three samples were extracted, centrifuged and analyzed by LC/MS/MS with acidic mobile phases as described in Section 2.5. The second experiment was to titrate lidocaine solution with increasing amounts of pure SDS and analyze the samples by LC/MS/MS. The DBS interference was characterized in terms of RT shifting and peak shape.

2.7. SDS elution monitoring

Certain samples from Experiment A of Section 2.5 were re-analyzed using two mobile phase systems, consisting of either 0.1% formic acid or 10 mM ammonium formate, to evaluate the elution of SDS off the chromatographic column. The SRM transition m/z 265.0 → 79.9 was monitored for SDS in negative ion mode. The problematic analytes were also simultaneously monitored to identify any co-elution with SDS, and thus explain the observed ionization suppression.

2.8. Post-column infusion

A post-column infusion experiment was performed with erythromycin to further investigate the observed ionization suppression with 3 types of DBS cards. Erythromycin and glyburide (IS) were infused post-column into the mass spectrometer, and the following five samples were injected for LC/MS/MS analysis: (1) 50:50 0.1% formic acid/acetonitrile; (2) protein precipitated blank rat plasma; (3) a blank DMPK-C card extraction; (4) a blank DMPK-B card extraction, and (5) a blank DMPK-A card extraction. The SRM transition of erythromycin was recorded to evaluate changes in MS response.

3. Results and discussion

3.1. Recovery/matrix effect characterization

The evaluation of DBS in the authors' laboratory began with a routine assessment of extraction recovery and interferences (Section 2.5) using DMPK-A cards. Table 2 shows the matrix effect, recovery, process efficiency and the retention time from Experiment A, B (in matrix) and C (in neat solution) for all test compounds on FTA® DMPK-A cards with acidic mobile phase conditions.

The results in Table 2 indicated that all test compounds had recovery greater than 70% with acetonitrile–methanol–water (1:1:1, v/v/v) as extraction solution except ethacrynic acid. Most of the compounds showed greater than 85% of recovery. However, there was a marked difference between test compounds in terms of DBS matrix effect. Some compounds such as cephalexin and dexamethasone demonstrated small matrix effects (18% and 2%), while others showed a significant drop in MS signal intensity compared with neat solution. The matrix effect for these compounds was greater than 40% of the intensity in a neat solution. For extreme instances such as erythromycin and mycophenolic acid, signal intensity in matrix was suppressed more than 1000 times. The process efficiencies were consequentially very poor for these compounds.

Furthermore, retention time shifting was observed for certain compounds. Most of these compounds were retained on column longer in matrix than their neat solutions. Chromatographic peak distortion and splitting were also observed. The first peak was of lower intensity with the same RT as in neat solution, and the other was of higher intensity eluting at a later RT.

In order to understand the cause of the observed RT shifting and peak distortion, control experiments were conducted with different types of DBS cards. Table 3 shows the matrix effect, recovery and process efficiency on FTA® DMPK-B cards (with different chemical coating) and FTA® DMPK-C cards (uncoated) respectively, using the

Table 3
Matrix effect, recovery and process efficiency with FTA® DMPK-B and DMPK-C cards and acidic mobile phase condition for the problematic compounds.

Compound	FTA® DMPK-B/DMPK-C cards		
	Matrix effect (%)	Recovery (%)	Process efficiency (%)
Amitriptyline	10/21	93/98	83/78
Cetirizine	60/8	96/90	38/83
Erythromycin	19/19	92/80	74/64
Fluoxetine	25/21	89/81	67/64
Fexofenadine	76/12	97/79	23/69
Lidocaine	8/−1	92/70	86/70
Reserpine	51/38	90/81	44/50

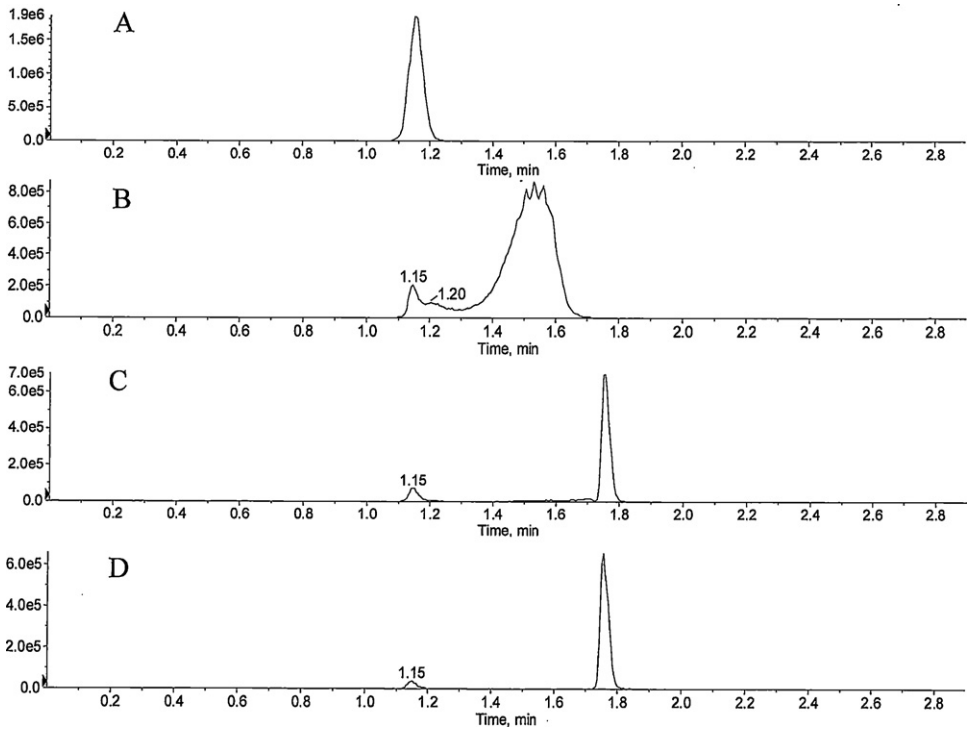

Fig. 2. The effect of SDS concentration on the chromatography of lidocaine. (A) Neat solution; (B) lidocaine spotted on a DMPK-A card; (C) lidocaine spotted on a DMPK-A card with one extra blank DMPK-A disc added before extraction; (D) lidocaine spotted on DMPK-A card with two extra discs added before extraction.

compounds that had the most pronounced RT shift. Interestingly, RT shifting and peak distortion were not observed with DMPK-B and -C cards (data not shown). Ionization suppression was also greatly improved. For example, the matrix effect for erythromycin was significantly decreased to 19% in B- and C-cards from 99.6% in A-cards. The results confirmed that the constituents of FTA® DMPK-A cards definitely played a role in the observed RT shifting and MS intensity loss.

3.2. Cause of retention time shifting with FTA® DMPK-A cards

An effort was undertaken to look for the chemical composition of DBS cards provided by GE Healthcare. Unfortunately, this was complicated by the fact that the chemistry of these cards is of a proprietary nature. Inspection of the corresponding MSDS sheets revealed that the ingredients on FTA® DMPK-A cards are sodium dodecyl sulfate (<5%) and tris (hydroxymethyl)aminomethane (<5%) [15]. The ingredient on FTA® DMPK-B cards is guanidinium thiocyanate (30–50%) [16]. The vendor did not specify the basis for the percentage of ingredients, i.e. (w/w) or (v/v).

The chemical structures and physical-chemical properties of all the test compounds were also carefully re-visited and evaluated. All the compounds that exhibited RT shifting with DMPK-A cards contained amine groups, and their pK_a values ranged from 6.6 to 9.5 (Table 1). The default mobile phase used in the recovery experiment consisted of 0.1% formic acid, and the pH* was measured 2.6. It was also noticed that the larger the difference between the analyte pK_a and the mobile phase pH*, the more RT shifting % was observed. The slope of a correlation plot of the test compounds' RT shifting % vs. the compounds' pK_a was 1.4. The linear correlation coefficient was 0.9 (data not shown).

The retention time shifting with DMPK-A cards could be best explained as a result of an ion-paring effect. Sodium dodecyl sulfate (SDS) coated on DMPK-A cards is a well known ion-pairing agent widely used in HPLC separation for poorly retained, positively-charged compounds. When the pH of the mobile phase was at least 2 units lower than the pK_a of the problematic compounds, the compounds' amine groups became protonated to produce cations. The cationic compounds could then ion pair with SDS anions extracted from DMPK-A cards, resulting in reversed phase and ion pair retention mechanisms.

This hypothesis was tested with the use of HPLC mobile phases modified with 10 mM ammonium formate. The pH* was measured 7.1. Basic compounds are expected to ionize to a smaller degree at this mobile phase pH although the exact amount depends on the particular test compound's pK_a. Given that the strength of association within ion pairs is a function of the degree of analyte protonation [17], this alteration in mobile phase pH had a dramatic reduction on ion-pair formation. As result, RT shifting was greatly alleviated for compounds such as amitriptyline and erythromycin. No RT shifting was observed for all other compounds (data not shown).

Neutral molecules, such as dexamethasone, or acidic molecules, such as ethacrynic acid, will never become positively charged in acidic mobile phase conditions, which results in retention being dominated by reversed phase interaction with the C_{18} stationary phase. Moreover, the presence of SDS may reduce the magnitude of reversed-phase interaction for acidic compounds due to competition for the stationary phase and an ion exclusion effect [17]. Taurocholic acid, for example, eluted slightly earlier when spotted on DMPK-A cards compared to neat solution.

This hypothesis was further tested with two experiments (Section 2.6) that demonstrated the effect of SDS concentration on lidocaine. The results of the first experiment using blank DMPK-A discs are shown in Fig. 2. Chromatogram A of Fig. 2 shows a retention time of lidocaine in a neat solution when there was no SDS in the sample. Retention followed conventional reversed-phase chromatography. Chromatogram B shows a broad and partially split chromatographic peak resulting from the presence of SDS in the form of one DMPK-A card disc. Addition of one and two more blank DMPK-A disc(s), further increased the amount of SDS in the lidocaine sample and resulted in chromatograms C and D,

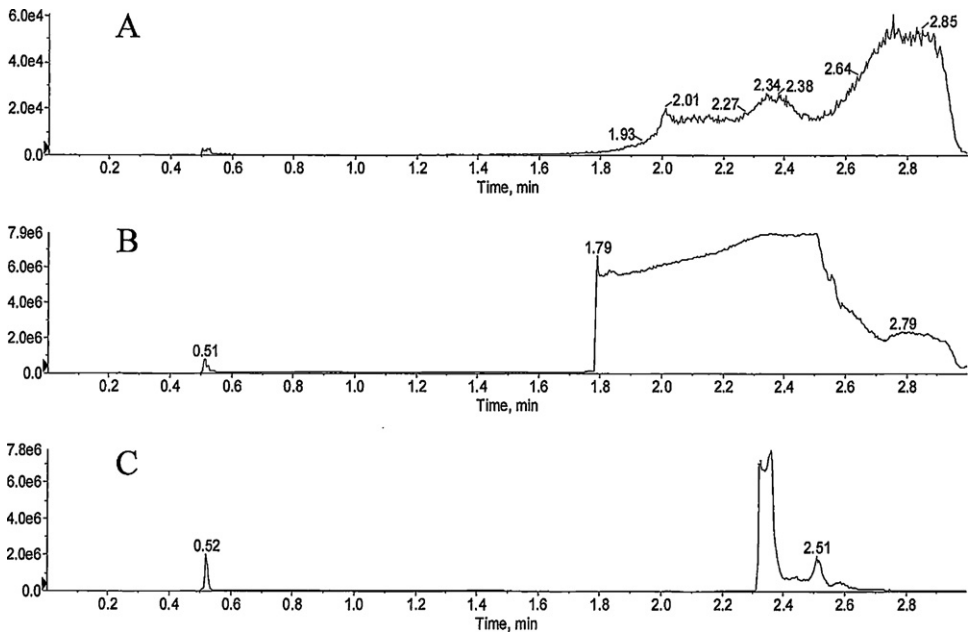

Fig. 3. SDS background from a blank injection (A) and SDS elution profile with mobile phases containing 0.1% formic acid (B) and containing 10 mM ammonium formate (C).

respectively. In going from chromatogram A to chromatogram B and C, the amount of SDS increased causing a decrease in the amount of retention due to reversed-phase interactions and an increase in ion pairing interactions. The addition of two discs of DMPK-A cards in chromatogram D showed that ion pairing became the dominant retention process.

The results of this experiment are supported by the SDS titration experiment. Once again, lidocaine appeared as a single peak when no SDS was present. This peak diminished and a second peak appeared with increasing intensity and retention on column when pure SDS was added. When the amount of SDS continued to increase, the lidocaine peaks kept shifting to higher retention time in a similar pattern. Eventually, a mole ratio of 2.7×10^6 was reached and lidocaine appeared as a single peak at a higher and constant retention time (data not shown).

3.3. Ion suppression caused by SDS

Retention time shifting was not the only manifestation of the SDS from DMPK-A cards. Significant ionization suppression of analyte was also observed, and was attributed to the presence of SDS, by means of SDS elution monitoring (Section 2.7 and Fig. 3) and a post-column infusion experiment (Section 2.8).

Chromatogram A of Fig. 3 indicated SDS background from a blank injection. When mobile phases containing 0.1% formic acid were used, SDS began to elute as a front at approximately 1.79 min and lasted for more than a half minute due to the high concentration present in DMPK-A cards (Chromatogram B of Fig. 3). Amine-containing compounds interacted with the SDS, which resulted in increased retention, and chromatographic peaks shifted into the SDS elution region. Analyte intensity was therefore suppressed due to the interference of the nonvolatile SDS in the electrospray process [18]. Furthermore, ion suppression may occur to any analytes if they elute within the SDS elution region even if they do not exhibit retention time shifting, e.g., ethacrynic acid and mycophenolic acid. When mobile phases containing 10 mM ammonium formate were used, SDS was observed to elute at 2.3 min as a much narrower peak (Chromatogram C of Fig. 3) and the test compounds eluted before SDS, thus mitigating ionization suppression.

The post-column infusion experiment (Section 2.8) performed with erythromycin further illustrated the ionization suppression caused by DMPK-A cards. There was a pronounced drop in erythromycin response during its peak elution window when a blank DMPK-A card extraction was injected onto the column. This clearly indicates co-elution of erythromycin with DMPK-A card components, thus resulting in the suppression in analyte response. In contrast, there was no interference with DMPK-B and -C card extractions for the compound (data not shown).

4. Conclusion

It is currently common practice that the choice of DBS cards is mainly determined by experiments and performance criteria, e.g., recovery and analyte stability improvement. There is minimum up-front guidance and prediction on which card to use without trial and error. Moreover, there is a paucity of knowledge and awareness of the ingredients on each type of card and what impact DBS cards may have in a bioanalytical assay. The significant and unique interferences caused by the ingredients of coated DBS cards demonstrated by our work may serve as a guide to fill in the blank. It is quite common that drug candidates contain amine functionalities in their structures. We have now obtained a better understanding and prediction on how amine-containing analytes will behave chromatographically with DMPK-A cards and acidic mobile phases. RT shifting may be used as an indicator of ion pairing formation and an alert for consequential interferences caused by the ion pairing formation. Our work also demonstrates the need for an extensive assay validation and careful assessment of DBS interaction and interferences. In our case, it was ion-pairing of analytes containing basic amine groups with SDS, but different cards with different chemistries can produce unique interferences. Therefore, DBS users should always be on the lookout for analyte interactions with DBS card constituents.

Acknowledgements

The authors would like to thank James Robbins and Julie Hilton from GE Healthcare for their support during our DBS evaluation and Upendra Argikar for helpful discussions.

References

[1] R. Guthrie, A. Susi, A simple phenylalanine method for detecting phenylketonuria in large populations of newborn infants, Pediatrics 32 (1963) 338–343.
[2] N. Spooner, R. Lad, M. Barfield, Dried blood spots as a sample collection technique for the determination of pharmacokinetics in clinical studies: considerations for the validation of quantitative bioanalytical method, Anal. Chem. 81 (2009) 1557–1563.
[3] FDA, Guideline for Industry Toxicokinetics: The Assessment of Systemic Exposure in Toxicity Studies, Fed. Regist. 60 FR 11264, 1995.
[4] T. Koal, H. Burhenne, R. Romling, M. Svoboda, K. Resch, V. Kaever, Quantification of antiretroviral drugs in dried blood spot samples by means of liquid chromatography/tandem mass spectrometry, Rapid Commun. Mass Spectrom. 19 (2005) 2995–3001.
[5] M. Barfield, N. Spooner, R. Lad, R. Parry, S. Fowles, Application of dried blood spots combined with HPLC–MS/MS for the quantification of acetaminophen in toxicokinetic studies, J. Chromatogr. B 870 (2008) 32–37.
[6] X. Liang, Y. Li, M. Barfield, Q.C. Ji, Study of dried blood spots technique for the determination of dextromethorphan and its metabolite dextrorphan in human whole blood by LC–MS/MS, J. Chromatogr. B 877 (2009) 8–9.
[7] W. Li, F.L.S. Tse, Dried blood spot sampling in combination with LC–MS/MS for quantitative analysis of small molecules, Biomed. Chromatogr. 24 (2010) 49–65.
[8] B.K. Matuszewski, M.L. Constanzer, C.M. Chaves-Eng, Strategies for the assessment of matrix effect in quantitative bioanalytical methods based on HPLC–MS/MS, Anal. Chem. 75 (2003) 3019–3030.
[9] M. Jemal, Y. Xia, LC–MS development strategies for quantitative bioanalysis, Curr. Drug Metab. 7 (2006) 491–502.
[10] D.S. Wishart, C. Knox, A.C. Guo, D. Cheng, S. Shrivastava, D. Tzur, B. Gautam, M. Hassanali., Drug Bank.ca: a knowledgebase for drugs, drug actions and drug targets, Nucleic Acids Res. (2008), 36 (Database issue): D901-6. PMID: 18048412.
[11] K. Balasubramaniam, K. Bindu, V.U. Rao, D. Ray, R. Haldar, A.W. Brzeczko, Impact of superdisintegrants on efavirenz release from tablet formulations, Disslution Technol. (2008) 18–25.
[12] Eli Lilly and Company Material Safety Data Sheet for Fluoxetine Hydrochloride Capsules and Tablets. Effective Date: 30 June 2005 http://www.ehs.lilly.com/msds/msds_fluoxetine_hydrochloride_capsules_and_tablets.pdf.
[13] C. Chen, Some pharmacokinetic aspects of the lipophilic terfenadine and zwitterionic fexofenadine in humans, Drugs in R&D 8 (2007) 301–314.
[14] M.J. O'Neil, A. Smith, P.E. Heckelman, et al., The Merck Index, 13th ed., Merck Research Laboratories, Division of Merck and Co., Inc., Whitehouse Station, NJ, 2001.
[15] GE Healthcare Safety Data Sheet for FTA DMPK-A; 100/Pack, Validation date: 25 August 2009 msdslifesciences@ge.com.
[16] GE Healthcare Safety Data Sheet for FTA DMPK-B; 100/Pack, Validation date: 25 August 2009 msdslifesciences@ge.com.
[17] R.F. Venn, Principles and Practice of Bioanalysis, 2nd ed., CRC Press, 2008.
[18] S.A. Gustarsson, J. Samskog, K.E. Markides, B. Langstrom, Studies of signal suppression in liquid chromatography–electrospray ionization mass spectrometry using volatile ion-pairing reagents, J. Chromatogr. A 937 (2001) 41–47.

Journal of Pharmaceutical and Biomedical Analysis 61 (2012) 38–43

Contents lists available at SciVerse ScienceDirect

Journal of Pharmaceutical and Biomedical Analysis

journal homepage: www.elsevier.com/locate/jpba

A rapid and sensitive HPLC–APCI-MS/MS method determination of fluticasone in human plasma: Application for a bioequivalency study in nasal spray formulations

Ricardo Martins Duarte Byrro[a,b,*], Isabela Costa César[a,b], Fabiana Fernandes de Santana e Silva Cardoso[a], Iram Moreira Mundim[a], Leonardo de Souza Teixeira[a], Ricardo Rodrigues Bonfim[a], Sandro Antônio Gomes[a], Gerson Antônio Pianetti[b]

[a] Instituto de Ciências Farmacêuticas, Alameda Coronel Eugênio Jardim 53, 74175-100 Goiânia, GO, Brazil
[b] Departamento de Produtos Farmacêuticos, Faculdade de Farmácia, Universidade Federal de Minas Gerais, Av. Pres. Antônio Carlos 6627, 31270-901 Belo Horizonte, MG, Brazil

ARTICLE INFO

Article history:
Received 8 August 2011
Received in revised form 7 October 2011
Accepted 16 November 2011
Available online 25 November 2011

Keywords:
Fluticasone
Nasal spray
HPLC–APCI-MS/MS
Plasma
Bioequivalence

ABSTRACT

A sensitive method for the determination of fluticasone in plasma was developed using high performance liquid chromatography with tandem mass spectrometric detection, whereas beclomethasone was used as internal standard. The analytes were extracted with a simple liquid–liquid extraction from the plasma samples and separated on an ACE C_{18} 50 × 4.6 mm i.d.; 5 μm particle size column with a mobile phase consisting of acetonitrile – 0.01% formic acid (48:52, v/v) at a flow rate of 1 ml/min. Detection was achieved by an Applied Biosystems API 5000 mass spectrometer (LC–MS/MS) set at unit resolution in the multiple reaction monitoring mode. Atmospheric pressure chemical ionization (APCI) was used for ion production. The mean recovery for fluticasone propionate was 85%, with a lower limit of quantification set at 2 pg/mL. The validated analytical method was applied to a bioequivalence study of fluticasone propionate administered by nasal spray formulations in human volunteers.

© 2011 Elsevier B.V. All rights reserved.

1. Introduction

Asthma and allergic rhinitis are common respiratory conditions associated with airway inflammation. Asthma is characterized by airway obstruction, which is at least partially reversible, and airway hyper-responsiveness to such stimuli as environmental allergens, viral respiratory-tract infections, irritants, drugs, food glucocoradditives, exercise, and cold air. Common symptoms of allergic rhinitis are nasal congestion, rhinorrhea, sneezing, nasal itch, and postnasal drainage [1,2]. As asthma and allergic rhinitis are inflammatory diseases, treatment with corticoids is recommended [2,3].

Inhaled corticosteroids have, over time, almost entirely replaced treatments based on oral corticosteroids, which commonly produced major adverse effects. These drugs, because of topical application, present a substantially better therapeutic index than oral steroids [4]. In addition, the treatment of allergic rhinitis has been revolutionized by the introduction of topical nasal steroid sprays, which are the most common medications prescribed by otolaryngology professionals, given that the regular use of these sprays reduces nasal obstruction, rhinorrhoea, and overall nasal symptom scores [5].

Fluticasone propionate (Fig. 1) is a corticosteroid available as aqueous nasal spray that has potent topical anti-inflammatory properties, with high topical activity in the nose, and is extremely effective in reducing nasal symptoms associated with rhinitis and asthma [6,7].

A nasally administered drug, intended for local action, can potentially produce systemic activity, although plasma levels generally do not reflect the amount of medication reaching the intended nasal sites of action. Systemic exposure following nasal administration can occur either by means of the medication absorbed within the systemic circulation of the nasal mucosa, or after ingestion and absorption within the gastrointestinal tract [8].

As the systemic absorption of fluticasone propionate after intranasal administration is low [9], the analytical method must be very sensitive in order to quantify the amount of the drug in plasma. The first methods reported in the literature employed the radioimmunoassay technique to quantify fluticasone. These methods quantified fluticasone with a lower limit of quantification (LLOQ) of approximately 500 pg/mL [1]. Despite the high sensitivity, these methods were substituted by chromatographic methods coupled to mass spectrometry detection. These techniques have proven to be more sensitive and there are several

* Corresponding author. Tel.: +55 31 34096967; fax: +55 31 34096976.
E-mail address: ricardobyrro@bol.com.br (R.M.D. Byrro).

0731-7085/$ – see front matter © 2011 Elsevier B.V. All rights reserved.
doi:10.1016/j.jpba.2011.11.018

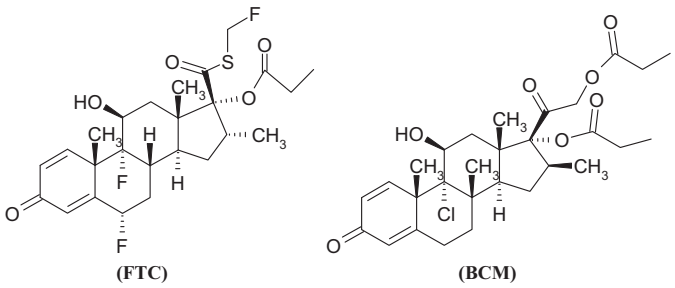

Fig. 1. Chemical structures of fluticasone propionate (FTC) and beclomethasone dipropionate (BCM).

methods reported in the literature for the quantitative analysis of fluticasone in plasma using HPLC–MS/MS [1,10–12]. The LOQ of some described methods was 10 pg/mL of fluticasone [11,12]. The pre-sample treatments in the literature were mainly performed by means of solid-phase extraction (SPE) [1,10–12].

Therefore, the present study aimed to develop and validate a new sensitive HPLC–APCI-MS/MS method for the quantitation of fluticasone propionate in human plasma, and quantify the drug at previously unheard of levels using a liquid–liquid extraction to treat the samples, and apply it to a bioequivalence study in healthy volunteers, who received fluticasone propionate through nasal spray administration.

2. Experimental

2.1. Chemicals and reagents

Fluticasone propionate (99.3% purity) and beclomethasone dipropionate (internal standard, 99.3% purity) reference standards were purchased from the United States Pharmacopoeia (Rockville, MD, USA). Ultra-pure water was obtained from a Millipore system (Bedford, MA, USA). Acetonitrile (HPLC grade) was purchased from Tedia (Fairfield, OH, USA), while formic acid, ammonium hidroxide, methylene chloride and methyl-*t*-butyl ether (analytical grade) were obtained from J.T. Baker (Phillipsburg, NJ, USA).

2.2. Instrumentation and analytical conditions

The HPLC–APCI-MS/MS analyses were carried out on an Agilent 1200 system (Santa Clara, CA, USA), composed of a quaternary pump, an autosampler, a column oven, and an API 5000 triple quadrupole mass spectrometer (MDS-SCIEX, Concord, Ontatio, Canada), equipped with an atmospheric pressure chemical ionization ion source. Analyst v.1.4.2 software was used for data acquisition and analysis. The liquid chromatography separation was performed on an ACE C_{18} column (50 × 4.6 mm i.d.; 5 μm particle size) at 40 °C. The mobile phase consisted of 0.01% formic acid and acetonitrile (48:52) at a flow rate of 1 mL/min. The run time was 3.5 min, and the injection volume was 40 μL.

Mass spectrometric detection was performed using atmospheric pressure chemical ionization ion source in positive ionization mode. The turbo-gas temperature was 350 °C, with an ion spray needle voltage of 4000 V, declustering potential of 76, nebulizer gas setting of 50 and curtain gas setting of 15. The collision energies were optimized at 23 V for fluticasone and 25 V for beclomethasone. Multiple reaction monitoring (MRM) was employed for data acquisition. The MRM fragmentation transitions were *m/z* 501 → *m/z* 293 and *m/z* 521 → *m/z* 337 for fluticasone and beclomethasone, respectively. The scan dwell time was set at 0.15 s for each channel.

2.3. Preparation of standard solutions

Stock solutions of fluticasone propionate and beclomethasone dipropionate were prepared by dissolving the accurately weighed reference substance in methanol. A working solution of fluticasone propionate was prepared by diluting the stock solution with acetonitrile and water (50:50) to a final concentration of 100 ng/mL.

The working solution of beclomethasone (IS) was prepared by diluting the stock solution with acetonitrile to a final concentration of 5 ng/mL. All stock solutions were prepared immediately before their use.

2.4. Preparation of calibration and quality control samples

Six calibration samples were prepared by spiking appropriate amounts of the working solution of fluticasone propionate in blank plasma obtained from healthy volunteers. The concentration of the calibration samples in plasma were 2, 10, 20, 30, 50, and 100 pg/mL of fluticasone propionate. Quality control (QC) samples in plasma were prepared in a similar manner, at low, middle, and high concentrations: 6, 40, and 80 pg/mL.

2.5. Sample preparation

A 50 μL aliquot of the IS solution (5 ng/mL of beclomethasone dipropionate in acetonitrile) and 200 μL of a 10% ammonium hydroxide solution were added to 500 μL of plasma sample. The sample was vortex mixed for 10 s. A 3 mL aliquot of methyl-*t*-butyl ether was then added and vortex mixed for 60 s. After, the samples were centrifuged at 3400 rpm for 6 min. A 2.4 mL portion of the organic layer was transferred and evaporated to dryness using an evaporator at 40 °C under a nitrogen stream. The dried extract was reconstituted with 60% acetonitrile (200 μL) and centrifuged at 3400 rpm for 4 min. A 40 μL aliquot was injected into the chromatographic system.

2.6. Method validation

The validation process was carried out according to Guidance for Industry – Bioanalytical Method Validation, recommended by the US Food and Drug Administration [13].

The selectivity of the method was evaluated by assaying human blank plasma samples from six different donors, including one lipemic and one hemolyzed plasma. These samples were compared to those containing fluticasone propionate at the LLOQ or beclomethasone at 5 ng/mL. In addition, plasma samples spiked with caffeine (1 μg/mL), chlorpheniramine (76 ng/mL), metamizole (5 μg/mL), and acetaminophen (20 μg/mL) were also evaluated to ensure no interference in the method.

Linearity was assessed by six-point calibration curves in human plasma in duplicate on three consecutive days. The curves were constructed by plotting the peak area ratio of fluticasone propionate to the IS versus the concentration. The evaluated concentration ranged from 2 to 100 pg/mL. The curves were evaluated by residuals and fitted by weighted linear regression. The LLOQ was established as the lowest concentration of the calibration curve, whose accuracy and precision were within 20%, as determined by the analyses of six replicates. Moreover, the analyte response at this concentration must be at least 5 times the baseline noise.

To evaluate the precision and accuracy of the method, QC samples at three concentration levels (6, 40, and 80 pg/mL of fluticasone propionate) were analyzed in six replicates on three different days. Intra-run and inter-run precision were calculated and expressed as relative standard deviation (R.S.D.%).

The extraction recovery of the method was determined by comparing the peak areas obtained from the plasma samples with those of direct injected standards at the same concentration. This recovery was evaluated by analyzing six replicates containing 6, 40, and 80 pg/mL of fluticasone propionate. The recovery of IS was determined in a similar manner within the working concentration (5 ng/mL of beclomethasone).

The stability of the analyte in plasma was evaluated under a variety of storage and handling conditions, using the low and high QC samples in six replicates. Freeze–thaw stability was evaluated after three complete freeze/thaw cycles (−80 to 23 °C) on consecutive days. Short-term temperature stability was assessed by analyzing samples that were kept at room temperature (23 °C) for 7 h. Long-term stability tests were performed on plasma samples that had been stored at −80 °C for 123 days. To evaluate the post-preparatory stability, QC samples were extracted and maintained in the autosampler (10 °C) for 16 h before the injection. The stabilities of fluticasone and IS working solutions, maintained at 4 °C for 4 days, were also evaluated. The analytes were considered stable when 85–115% of the initial concentrations could be identified.

The matrix effect was evaluated to verify whether or not the potential ion suppression or enhancement due to the co-elution matrix components existed in the analysis. The peak areas of fluticasone propionate and IS from the spike-after-extraction samples were compared to those of the standard solutions in the mobile phase at the same concentrations. This experiment was carried out with blank plasma samples from six different donors, at low and high QC concentrations of fluticasone propionate and working concentrations of beclomethasone (5 ng/mL).

2.7. Application to a bioequivalence study

The analytical validated method was used to determine the plasma concentration of fluticasone propionate and to evaluate the bioequivalence of two nasal spray formulations in a randomized, two-way, single-dose, crossover study. The drugs evaluated were the generic fluticasone propionate 50 μg (Neo Teuto Brasileiro Laboratory) and Flixonase® 50 μg (GlaxoSmithkline Brasil Ltda), test and reference respectively, both nasal sprays.

Eighty healthy volunteers (forty male and forty female) with a mean of 27.8 years of age and a mean weight of 66.17 kg participated in the study. Subjects underwent a physical examination, an electrocardiography, and laboratory testing (hematologic, biochemical, and urinalysis).

The administration of the drug was performed in a room isolated from external contamination and an adequate cleaning in the volunteers' nostrils was carried out before its administration. All subjects received either 10 sprays, five per nostril, alternately, corresponding to 500 μg of fluticasone propionate, under fasting conditions.

The blood samples (10 mL) were collected in heparinized tubes at 0, 10, 20, 30, 40, and 50 min, as well as at 1, 1.25, 1.5, 1.75, 2, 2.5, 3, 3.5, 4, 5, 6, 8, 12, 24, 48, and 72 h after drug administration. Plasma samples were obtained by centrifugation and frozen at −70 °C until analysis, at which time they were prepared according to that described in Section 2.5. The study protocol was approved by the Ethics Committee of Universidade Estadual de Campinas.

The pharmacokinetic parameters considered for the evaluation of the bioequivalence between test and reference products included: C_{max}—observed maximum plasma concentration of fluticasone; T_{max}—sampling time of the maximum plasma concentration; t_{half}—terminal elimination half-life time; AUC_{0-t}—area under plasma concentration/time plot until the last quantifiable value; $AUC_{0\rightarrow\infty}$—area under plasma concentration/time plot extrapolated to infinity. Analysis of variance was performed on the pharmacokinetic parameters. After, the 90% confidence intervals (CI) of the pharmacokinetic parameters characterizing the test/reference products were determined.

3. Results and discussion

3.1. Conditions for HPLC–APCI-MS/MS

The first step of the mass spectrometric detection consisted of recording the MS spectra of both fluticasone propionate and beclomethasone. From full scan MS, the protonated molecular ions $[M+H]^+$, with *m/z* 501 and *m/z* 521 for fluticasone propionate and beclomethasone, respectively, were selected as precursor ions and fragmented into the MS/MS mode (Fig. 2). The selected product ion was *m/z* 293 and *m/z* 337 for fluticasone propionate and beclomethasone, respectively. The HPLC–APCI-MS/MS conditions provided high signal intensities for both fluticasone propionate and beclomethasone. The addition of ammonium acetate buffer and formic acid in the mobile phase was important in improving the signal intensities in positive ion mode.

Nasally administered drugs, such as fluticasone propionate, provided a considerably technical difficulty in measuring the plasma concentrations due the reduced systemic absorption provided by these formulations. Daley-Yates noted that even the high doses used in his study produced a mean peak plasma concentration of only slightly above the method's LLOQ (20 pg/mL in this case) [9].

The pharmacokinetic evaluation of drugs administered using nasal sprays requires very sensitive methods that are able to quantify low amounts of the drug in the biological matrix. The method presented in this work provided an LLOQ of 2 pg/mL, thus producing reliable analytical measurements and allowing for an adequate characterization of the plasmatic concentration–time profiles of fluticasone propionate after the administration of the nasal spray. In addition to the high sensitivity, the method must be very robust and quick if it is to be successfully applied to a bioequivalence study. In this case, the method also had a short run time. The retention time for fluticasone propionate and beclomethasone dipropionate (IS) were 2.34 and 3.08 min, respectively (Fig. 3).

3.2. Sample extraction

In addition to the LLOQ, the method developed in this work presents a major advantage when compared to most trials performed to determine the presence of fluticasone propionate, especially when considering its sample treatment. The liquid–liquid extraction produces cleaner extracts than those produced with SPE and is less prone to matrix suppression [14]. Furthermore, this procedure has considerably lower cost than the SPE methods.

In the present study, various organic solvents were tested to develop an efficient liquid–liquid extraction procedure, and the simple use of methyl-*t*-butyl ether yielded the highest recoveries for both fluticasone propionate and IS from plasma. To enhance the recovery and reduce the matrix effects, the addition of acids and bases at different concentrations were also tested. The addition of 10% ammonium hydroxide results in cleaner extracts, which considerably decreased the occurrence of matrix effects. In addition, the extraction procedure employed proved to be robust.

3.3. Method validation

The mean recovery rate of fluticasone propionate ($n = 18$), determined at three concentrations, was 86.8%, whereas the recovery of IS proved to be 87.7% ($n = 18$). The recovery data are shown in Table 1.

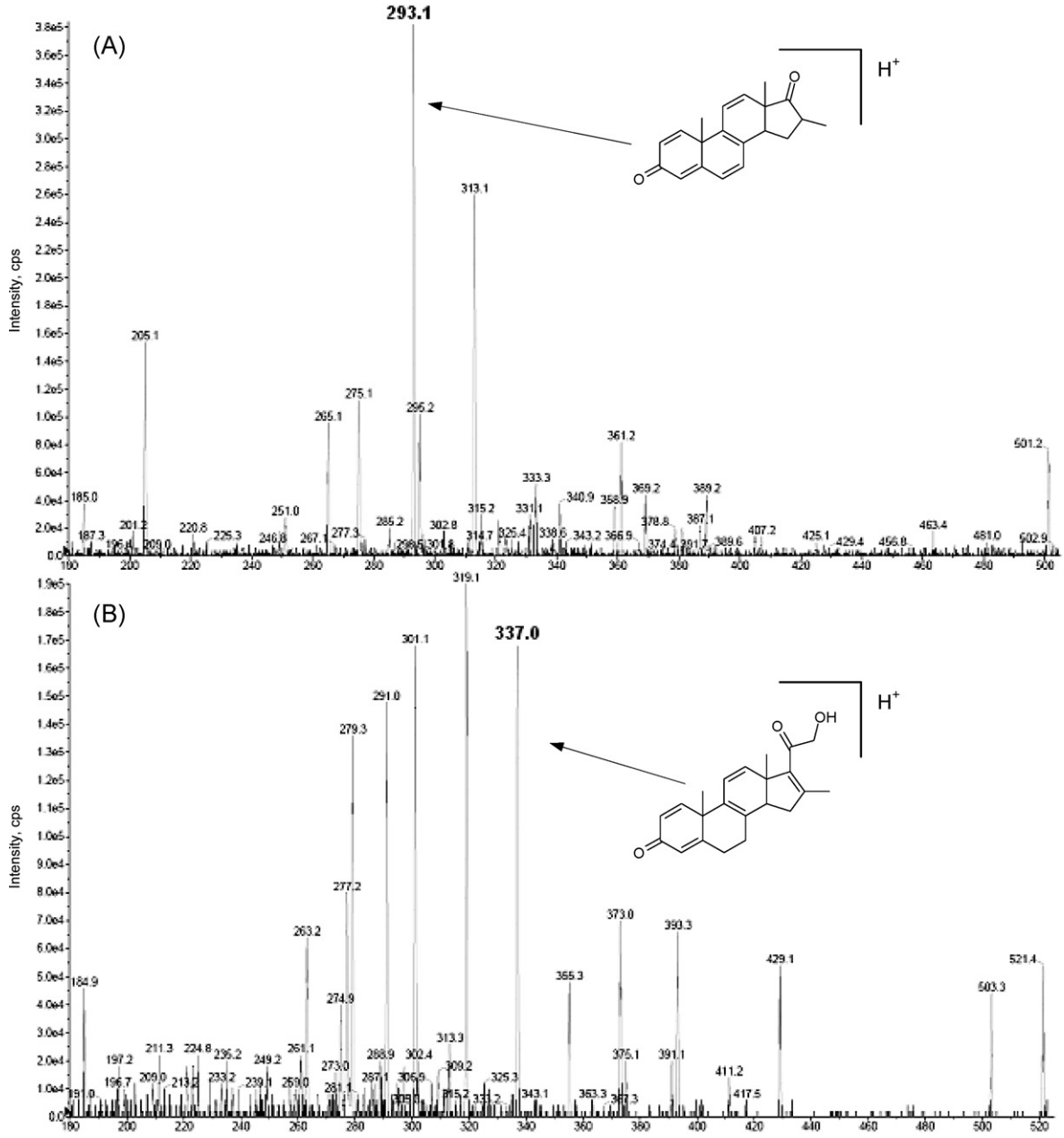

Fig. 2. Fragmentation mass spectra of fluticasone (A) and beclomethasone (B) obtained by APCI in positive ion mode.

The recoveries rates exceeded 85% and allowed, along with the other analytical conditions, for the quantitation of very small amounts of the analyte in plasma samples. This recovery rate (85%) is very similar to those described by SPE extraction.

Table 1
Precision and accuracy data for fluticasone propionate by HPLC–APCI-MS/MS.

Assay	Nominal concentration (pg/mL)	Observed concentration (pg/mL, mean ± S.D.)	Precision (%R.S.D.)	Accuracy (%)
Intra-run ($n = 6$)	6	5.45 ± 0.3	5.9	90.9
	40	39.85 ± 0.9	2.3	99.6
	80	82.01 ± 2.4	2.9	102.5
Inter-run ($n = 18$)	6	5.66 ± 0.4	7.5	94.3
	40	39.61 ± 1.0	2.5	99.0
	80	80.53 ± 2.2	2.7	100.7

S.D. = standard deviation.
R.S.D. = relative standard deviation.

Beclomethasone presented similar recovery, chromatographic and ionization properties of fluticasone propionate, which proved to be an adequate internal standard for the analysis.

No significant interference could be detected at the retention times of the analytes in the six different blank plasma chromatograms (Fig. 3). The plasma samples spiked with caffeine, chlorpheniramine, metamizole, or acetaminophen presented no response to the ion transitions selected for the quantitation of analytes.

The fluticasone propionate calibration curves proved to be linear, ranging from 2 to 100 pg/mL, with a regression coefficient of higher than 0.99. A typical standard curve was $y = 0.00549x + 0.00642$, with a weighted factor of $1/x$. The residuals showed no tendency of variation with concentration. The obtained LLOQ was 2 pg/mL, with a precision of 10.6% and 7.9% in terms of R.S.D. and accuracy, respectively. Linearity results obtained over the three consecutive days are presented in Table 2.

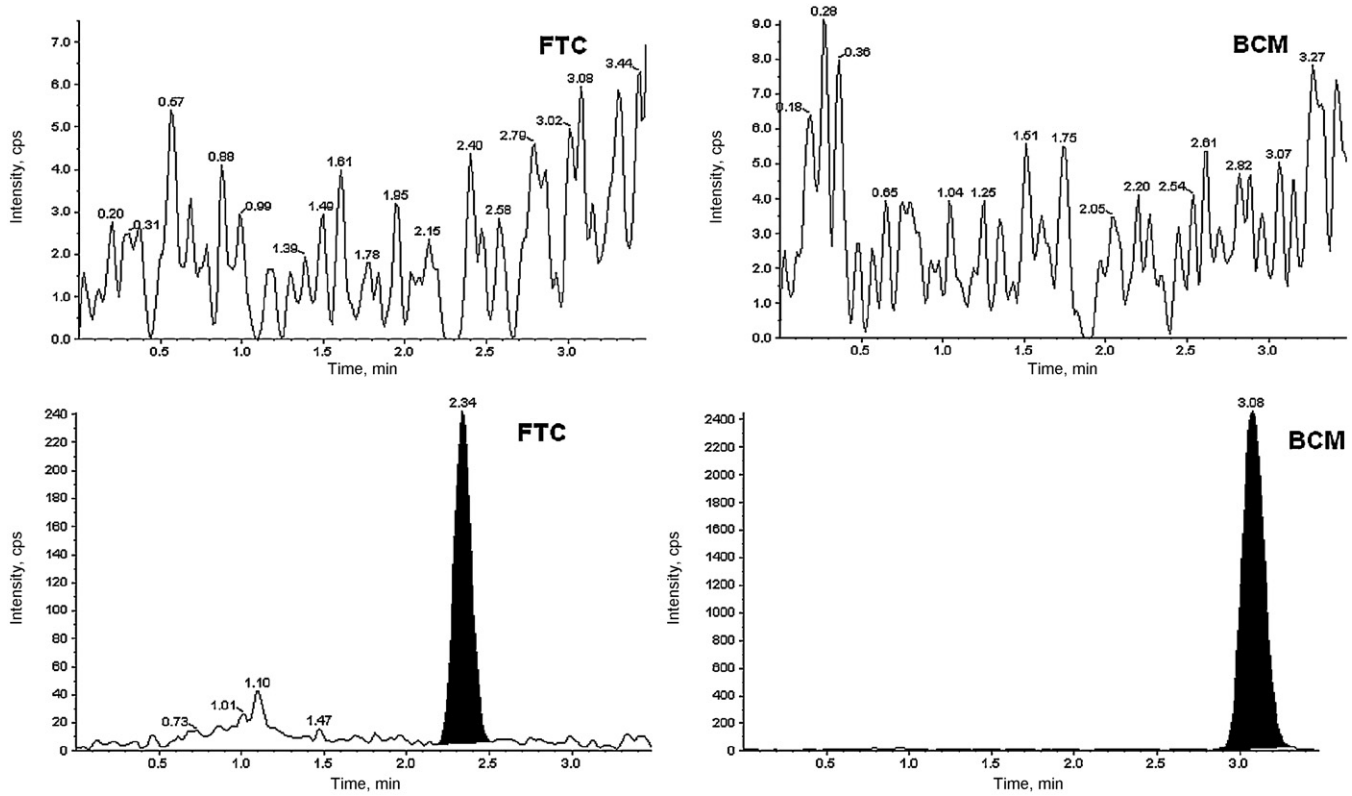

Fig. 3. SRM chromatograms of (A) blank plasma sample and (B) volunteer plasma collected 1 h after the administration of nasal spray (10.3 pg/mL of fluticasone (FTC) and spiked beclomethasone (BCM) at 500 pg/mL).

The intra-run and inter-run precision and accuracy were calculated by analyzing six replicates of QC samples at three concentration levels during three different days. The obtained data are shown in Table 3. The mean R.S.D. values were 3.68% and 4.23% for the intra-run and inter-run precision, respectively. The mean accuracy values were 98.1% and 97.79% for the intra-run and inter-run accuracy, respectively. These data indicated reproducible results and that the assay was accurate and reliable.

The matrix effect was evaluated by comparing the mean peak areas of fluticasone propionate and IS from the spike-after-extraction samples with those of the standard solutions in the mobile phase. The observed variation did not exceed the range from 85% to 115%. As such, in the present HPLC–MS/MS method, the matrix effects for the analytes proved to be insignificant.

The results of stability experiments showed that fluticasone propionate plasma samples were stable for up to 7 h at 23 °C for 123 days at −80 °C, for 16 h after extraction in the autosampler and after three complete freeze/thaw cycles on consecutive days, as the R.E values were within 15% for the analyte at low and high concentrations. Working solutions of fluticasone propionate and IS were stable for at least 4 days at 4 °C.

Table 2
Recovery data for fluticasone propionate by HPLC–APCI-MS/MS.

Analyte	Nominal concentration (pg/mL)	Recovery (%)	%R.S.D.
Fluticasone propionate ($n = 6$)	6	88.8	8.1
	40	89.1	2.7
	80	82.6	5.9
Beclometasone (IS) ($n = 18$)	500	87.7	4.0

Table 3
Precision and accuracy data of back-calculated concentrations of calibration samples for fluticasone in plasma.

Nominal concentration (pg/mL)	Observed concentration (pg/mL, mean ± S.D.)	Precision (%R.S.D.)	Accuracy (%)
2	2.14 ± 0.23	10.6	107.2
10	9.66 ± 0.34	3.5	96.6
20	19.31 ± 0.70	3.6	96.6
30	30.20 ± 0.83	2.7	100.7
50	48.87 ± 0.95	1.9	97.7
100	101.48 ± 3.48	3.4	101.8

S.D., standard deviation; R.S.D., relative standard deviation.

3.4. Application to a clinical bioequivalence study

The validated method was applied to determine the presence of fluticasone propionate in plasma samples in an attempt to establish the pharmacokinetic parameters in a bioequivalence study between two nasal spray formulations, the generic Fluticasone Propionate 50 μg (Neo Teuto Brasileiro Laboratory) and Flixonase® 50 μg (GlaxoSmithkline Brasil Ltda) test and reference respectively, in 80 healthy volunteers.

The nasal spray bottles were weighed before and after the administration in each volunteer. The bottle weight after the administration was used as an exclusion criterion, given that the weight of each bottle must be within the range of ±2 standard deviation, considering the mean weight of each bottle. Ten volunteers were excluded from the study due to this requirement. In addition, five volunteers were excluded due to nasal drip within 3 h

Table 4
Statistics of pharmacokinetic parameters of fluticasone propionate for reference and test formulations after nasal administration in human volunteers ($n = 64$).

Drug	Statistic	C_{max} (ng/mL)	T_{max} (h)	T_{half} (h)	AUC_{0-t} (ng/mL h)	$AUC_{0-\infty}$ (ng/mL h)
Reference (R)	Mean	29.15	1.12	14.27	236.36	340.77
	%R.S.D.	97.5	83.0	110.7	139.7	131.3
Tested (T)	Mean	25.85	1.54	13.53	227.05	364.17
	%R.S.D.	72.5	201.9	114.3	114.43	157.0

T_{max}, time to maximum concentration; C_{max}, maximum concentration; AUC_{0-t}, area under the curve of plasma concentration until the last concentration observed; $AUC_{0-\infty}$, area under the curve between the first sample and infinitive; T_{half}, elimination half life.

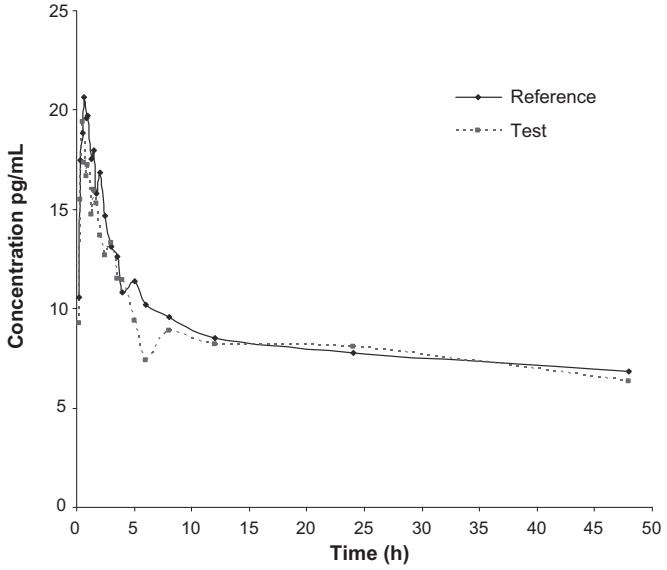

Fig. 4. Plasma mean concentration–time curves of fluticasone propionate for reference and test formulations after the administration of nasal spray in healthy volunteers ($n = 64$).

after administration, and one volunteer choose the withdraw from the study. Sixty-four volunteers finished the study, and the main pharmacokinetic parameters for the reference and test formulations were calculated (Table 4).

The extrapolated area of plasma concentration versus time was less than 20% of $AUC_{0-\infty}$, demonstrating the suitability of the method and experimental design. Fluticasone propionate was detected in plasma 10 min after its administration in the most of the subjects, demonstrating a rapid nasal absorption. The mean concentration profiles obtained for the reference (R) and test (T) formulations are shown in Fig. 4.

The most important objective of the bioequivalence study is to assure the safety and efficacy of the test product. According to the Food and Drug Administration (FDA) and the Brazilian regulatory agency for sanitation (Agência Nacional de Vigilância Sanitária – ANVISA), the equivalent range for basic pharmacokinetic parameters, such as C_{max}, AUC_{0-t}, and $AUC_{0\rightarrow\infty}$, must be within 80–125%. The mean and standard deviation of C_{max}, AUC_{0-t}, and $AUC_{0\rightarrow\infty}$ of the two formulations did not differ significantly, suggesting that the plasma profiles generated by the test formulation are comparable to those of the reference formulation. Therefore, the two nasal spray formulations can be considered bioequivalent regarding the extent and rate of absorption.

The ratios of the geometric means for C_{max} were 96.68%, while AUC_{0-t} proved to be 99.97%. For fluticasone, the 90% CI for the test formulation/reference formulation ratio for the logarithmic transformations of both C_{max} and AUC_{0-t} were within the bioequivalence limit of 80% to 125% (87.95–106.27 and 84.66–118.05%, respectively).

4. Conclusion

A simple, sensitive, and selective LC–MS/MS method was developed to quantify fluticasone propionate in human plasma. Validation results have shown that the method is robust and meets the requirements of the pharmacokinetic investigation after the nasal spray administration of therapeutic doses. To the best of our knowledge, this is the first HPLC–APCI-MS/MS method concerning the quantitation of fluticasone propionate in human plasma that has reached an LLOQ of 2 pg/mL and that also uses a liquid–liquid extraction in sample preparation. In addition, the relatively short run time required for analysis, as well as the sensitive and reliable results, contributed to the success of the method when it was applied to a bioequivalence study involving a large number of samples after the nasal spray administration of fluticasone propionate in human subjects.

References

[1] S.L. Callejas, R.A. Biddlecombe, A.E. Jones, K.B. Joyce, A.I. Pereira, S. Pleasance, Determination of the glucocorticoid fluticasone propionate in plasma by automated solid-phase extraction and liquid chromatography–tandem mass spectrometry, J. Chromatogr. B 718 (1998) 243–250.
[2] H. Herman, Once-daily administration of intranasal corticosteroids for allergic rhinitis: a comparative review of efficacy, safety, patient preference, and cost, Am. J. Rhinol. 21 (2007) 70–79.
[3] R. Fuller, M. Johnson, A. Bye, Fluticasone propionate – an update on preclinical and clinical experience, Respir. Med. 89 (1995) 3–18.
[4] M.H. Brutsche, I.C. Brutsche, M. Munavvar, S.J. Langley, C.M. Masterson, P.T. Daley-Yates, R. Brown, A. Custovic, T. A. Woodcock, Comparison of pharmacokinetics and systemic effects of inhaled fluticasone propionate in patients with asthma and healthy volunteers: a randomised crossover study, Lancet 356 (2000) 556–561.
[5] A.N. Waddell, S.K. Patel, A.G. Toma, A.R. Maw, Intranasal steroid sprays in the treatment of rhinitis: is one better than another? J. Laryngol. Otol. 117 (2003) 843–845.
[6] P.T. Daley-Yates, R.C. Baker, Systemic bioavailability of futicasone propionate administered as nasal drops and aqueous nasal spray formulations, Br. J. Clin. Pharmacol. 51 (2001) 103–105.
[7] P.T. Daley-Yates, A.C. Price, J.R. Sisson, A. Pereira, N. Dallow, Beclomethasone dipropionate: absolute bioavailability, pharmacokinetics and metabolism following intravenous, oral, intranasal and inhaled administration in man, Br. J. Clin. Pharmacol. 51 (2001) 400–409.
[8] W. Jeal, D. Faulds, Triamcinolone acetonide. A review of its pharmacological properties and therapeutic efficacy in the management of allergic rhinitis, Drugs 53 (1997) 257–280.
[9] P.T. Daley-Yates, R.L. Kunka, Y. Yin, S.M.##S. Andrews, C. Callejas, Ng Bioavailability of fluticasone propionate and mometasone furoate aqueous nasal sprays, Eur. J. Clin. Pharmacol. 60 (2004) 265–268.
[10] Y.N.B. Li, B.N. Tattam, K.F.##J. Brown, P. Seale, A sensitive method for the quantification of fluticasone propionate in human plasma by high-performance liquid chromatography/atmospheric pressure chemical ionization mass spectrometry, J. Pharm. Biomed. Anal. 16 (1997) 447–452.
[11] L. Laugher, T.G. Noctor, A. Barrow, J.M. Oxford, T. Phillips, An improved method for the determination of fluticasone propionate in human plasma, J. Pharm. Biomed. Anal. 21 (1999) 749–758.
[12] S. Krishnaswami, H. Mollmann, H. Derendorf, G. Hochhaus, A sensitive LC–MS:MS method for the quantification of fluticasone propionate in human plasma, J. Pharm. Biomed. Anal. 22 (2000) 23–129.
[13] Food and Drug Administration FDA Guidance for Industry: Bioanalytical Method Validation, U.S. Department of Health and Human Services, Food and Drug Administration, Center for Drug Evaluation and Research, 2001.
[14] G. Hopfgartner, E. Bourgogne, Quantitative high-throughput analysis of drugs in biological matrices by mass spectrometry, Mass Spectrom. Rev. 22 (2003) 195–214.

Journal of Pharmaceutical and Biomedical Analysis 61 (2012) 44–49

Contents lists available at SciVerse ScienceDirect

Journal of Pharmaceutical and Biomedical Analysis

journal homepage: www.elsevier.com/locate/jpba

Three-phase hollow fiber liquid phase microextraction of warfarin from human plasma and its determination by high-performance liquid chromatography

Mohammadreza Hadjmohammadi*, Hoda Ghambari

Department of Chemistry, University of Mazandaran, Babolsar 47416-95447, Iran

ARTICLE INFO

Article history:
Received 3 July 2011
Received in revised form
16 November 2011
Accepted 16 November 2011
Available online 25 November 2011

Keywords:
Hollow fiber
Liquid phase microextraction
Warfarin
HPLC
Plasma

ABSTRACT

A simple, inexpensive and efficient sample preparation technique, three-phase hollow fiber liquid phase microextraction (HF-LPME), followed by high-performance liquid chromatography–ultra violet detection (HPLC–UV) was used for the analysis of warfarin in human plasma. Warfarin was extracted from 11.0 ml of aqueous solution with pH = 2.3 (donor phase) into 1-octanol immobilized in the wall pores of a porous hollow fiber and then extracted into the acceptor phase with pH = 11.0 located in the lumen of the hollow fiber. After the extraction, the acceptor phase was directly injected into the HPLC system for quantification. Different factors affecting the HF-LPME including nature of organic extraction solvent, pH of donor and acceptor phases, stirring rate, extraction time and salt addition to the sample solution (donor phase) were investigated and optimized. Under the optimized conditions (1-octanol as organic solvent, pH_{donor} = 2.3, $pH_{acceptor}$ = 11.0, stirring speed of 1000 rpm, extraction time of 30 min, without addition of salt), limit of detection (LOD) of 5 ng ml^{-1} and enrichment factor of 225 were obtained. The calibration curve was linear within the range of 15–550 ng ml^{-1} with the square of correlation coefficient of 0.9984. The values of intra-day relative standard deviation (RSD) and inter-day RSD were 4.2% and 11.1%, respectively. The method was applied successfully for the analysis of warfarin in plasma sample from a patient under treatment with this drug and excellent sample clean-up was observed.

© 2011 Elsevier B.V. All rights reserved.

1. Introduction

Warfarin is a coumarin derivative which is the most commonly prescribed oral anticoagulant drug for the prophylaxis and treatment of venous and arterial thromboembolic disorders [1,2]. Due to the property of causing fatal hemorrhaging it is also used as a rodenticide. Warfarin exerts anticoagulant effect by decreasing the synthesis of vitamin K-dependent coagulation factors [3]. The therapeutic window of warfarin is very narrow: 0.5–3.0 μg ml^{-1} [4]. Exceeding the therapeutic window of this drug causes unwanted bleedings. In order to ensure the efficiency and safety of warfarin, the dosage must be adjusted accurately and frequently. Therapeutic monitoring of the effect of this drug is usually done by measuring a coagulation parameter, the international normalized ratio (INR). However, INR still has its limitations in detecting factors such as patient compliance, resistance to anticoagulant, drug interaction and food variety, etc. Although the INR is widely accepted as a gold standard for the monitoring of oral anticoagulation therapy, in order to adjust the dosage more objectively and accurately, concentration monitoring is essential in some situations for the confirmation of anticoagulant affecting factors, especially when the ideal INR is difficult to target [5]. Knowledge of the plasma concentration of warfarin is valuable for clinical decisions and allows for effective treatment of severe intoxication. The determination of plasma concentration can also be helpful in distinguishing non-compliance from genuine anticoagulant resistance.

Several methods such as high-performance liquid chromatography (HPLC) using ultraviolet or fluorescence detections [2,5–13], liquid chromatography–tandem mass spectrometry (LC–MS/MS) [14–16], micellar electrokinetic chromatography-electrospray ionization mass spectrometry (MEKC-ESI-MS) [17], supercritical fluid chromatography-tandem mass spectrometry (SFC-MS/MS) [18], capillary zone electrophoresis (CZE) [19–21] and square-wave adsorptive cathodic stripping voltammetry [22] have been reported for the determination of warfarin in the biological samples.

Biological sample analysis without sample preparation at low analyte concentrations, complex sample matrices and limited sample volumes available for the determinations, is very difficult [23]. Therefore, sample isolation as well as pre-concentration technique is necessary. Sample preparation is traditionally carried out by liquid–liquid extraction (LLE) or by solid-phase extraction (SPE). LLE offers high reproducibility and high sample capacity, but it is a tedious, time-consuming procedure, which can produce emulsions and requires large amounts of high purity organic solvents

* Corresponding author. Tel.: +981 125342350; fax: +981 125342350.
E-mail address: hadjmr@umz.ac.ir (M. Hadjmohammadi).

0731-7085/$ – see front matter © 2011 Elsevier B.V. All rights reserved.
doi:10.1016/j.jpba.2011.11.019

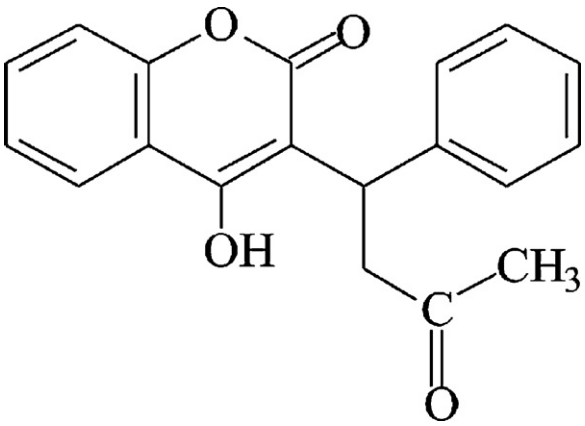

Fig. 1. Chemical structure of warfarin.

[24]. Although consumption of organic solvents is relatively low in SPE, it may require lengthy processing (i.e., conditioning, washing, eluting and drying) [25].

To overcome or reduce these problems, alternative sample preparation methods for drug analysis such as hollow fiber liquid phase microextraction (HF-LPME) have been developed. This technique was introduced by Pedersen-Bjergaard and Rasmussen in 1999 [26]. There are two modes of HF-LPME: three- and two-phase HF-LPME. In three-phase mode, three liquid phases participate in analyte extraction: (1) the sample solution (donor phase), with a pH that is adjusted to keep analytes neutrally charged, (2) the water-immiscible organic extractor phase, which is immobilized in the wall pores of the hollow fiber, and (3) the aqueous acceptor phase, with a pH that is adjusted to ionize the analytes. Compounds in their non-ionized form are extracted from the sample into the organic solvent and are subsequently extracted into the acceptor phase, which is directly compatible with HPLC and CE. This extraction mode is used for basic or acidic analytes with ionizable functionalities.

The major advantages of HF-LPME are simplicity, negligible volume of solvents used, high enrichment, low cost and excellent sample cleanup ability. Sample carry-over can be avoided because the hollow fibers are inexpensive enough to be single-used and disposable. In addition, HF-LPME tolerates a wide pH range, a feature which could not be done using SPE and solid-phase microextraction (SPME).

The aim of this study was to develop a sensitive and reliable method for analysis of warfarin in human plasma which is capable of complementing existing clinical methods. For this purpose, three-phase HF-LPME followed by HPLC–UV was applied for extraction and determination of warfarin in the plasma sample. Various parameters which affect the extraction efficiency of warfarin including pH of the donor and acceptor phases, the nature of organic phase, salt concentration, stirring rate and extraction time were studied and optimized in aqueous solutions of warfarin. Finally, the optimized conditions were applied to determine warfarin in plasma sample from a patient under warfarin treatment.

2. Experimental

2.1. Materials and solutions

Sodium warfarin (≥98%; Fig. 1) was purchased from Sigma–Aldrich (St. Louis, MO, USA). Methanol (HPLC-grade), sodium hydroxide, hydrochloric acid, phosphoric acid, formic acid, sodium chloride, 1-octanol and toluene were obtained from Merck (Darmstadt, Germany). Ammonium hydroxide, benzyl alcohol, n-dodecane and 1-undecanol were purchased from Fluka (Buchs, Switzerland). Water used was double distilled deionized. The Accurel Q3/2 polypropylene hollow fiber (200 μm wall thickness, 600 μm internal diameter and 0.2 μm average pore size), purchased from Membrana GmbH (Wuppertal, Germany), was used for all HF-LPME experiments.

Stock solution of warfarin (500.0 μg ml^{-1}) was prepared in methanol and stored in the dark at 4 °C. The working solutions were prepared daily by an appropriate dilution of the stock solution with double distilled deionized water.

2.2. Instrumentation

Chromatographic measurements were carried out using a HPLC system equipped with a series 10 LC pump, UV detector model LC-95 set at 254 nm and model 7125i manual injector with a 20 μl sample loop (Perkin-Elmer, Norwalk, CT, USA). Column used was C_{18} (250 mm × 4 mm, 5 μm particle size) from waters (Milford, MA, USA). A mixture of methanol and (0.5%) phosphoric acid (65:35, v/v) at a flow rate of 1.0 ml min^{-1} and room temperature was used as mobile phase. Measurement of solutions pH was done by a 3030 Jenway pH meter (Leeds, UK).

2.3. Extraction procedure

The hollow fiber was cut manually into 8.8 cm length pieces. Before using them, each piece was sonicated for 5 min in acetone to remove any possible contaminants in the fiber and then, dried in air. For each experiment, 11 ml of the sample solution was poured into a 12 ml sample vial. Then 30 μl of the acceptor phase (pH = 11.0) was withdrawn into the Hamiltone microsyringe and its needle was inserted into the lumen of the hollow fiber. The hollow fiber was submerged in the organic solvent (1-octanol) for 10 s to impregnate its pores with organic solvent. It was next placed into distilled water for 10 s in order to wash the extra organic solvent from the surface of the hollow fiber. The acceptor phase in the syringe was completely injected into the lumen of the hollow fiber and the end of the hollow fiber was sealed by a piece of aluminum foil. The fiber was bent to a U-shape and submerged in 11 ml of the sample solution. During extraction, sample was stirred using a 14 mm × 4 mm magnetic bar at 1000 rpm. After 30 min, the fiber was removed from the sample solution, and its closed end was cut and the extract was withdrawn into the microsyringe. Finally the extract was directly injected into the HPLC system. A fresh hollow fiber was used for each extraction to decrease the memory effect.

2.4. Plasma sample

Blank plasma was provided by healthy donors. Real plasma sample was obtained from a male hospitalized patient under warfarin treatment. In order to eliminate the protein binding of the drug in plasma (greater than 99%) [27], the pretreatment as outlined in the work of Tahmasebi et al. was performed [28]. For this purpose, 3 ml methanol was added to 2 ml of the plasma and the resulting mixture was strongly vortexed for 10 min. The mixture was placed for 10 min in an ice bath, followed by 10 min at ambient temperature and then centrifuged at 3500 rpm for 10 min. The supernatant was transferred into a 10 ml volumetric flask and diluted to the mark with double distilled deionized water. pH of the final solution was adjusted to 2.3 using 4 M HCl solution and the extraction procedure was done under the optimized conditions.

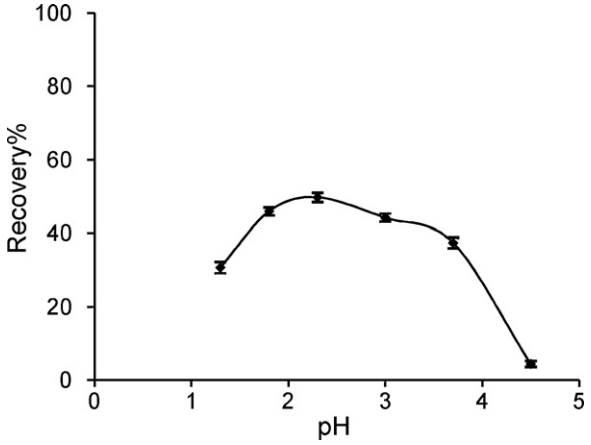

Fig. 2. Effect of donor phase pH on the extraction recovery of warfarin. Extraction conditions: 1-octanol as organic extraction solvent; donor phase, 11 ml of aqueous solution containing 0.1 μg ml^{-1} of warfarin; extraction time = 30 min; acceptor phase, 30 μl of 0.1 mM NaOH; stirring speed = 250 rpm; without addition of salt.

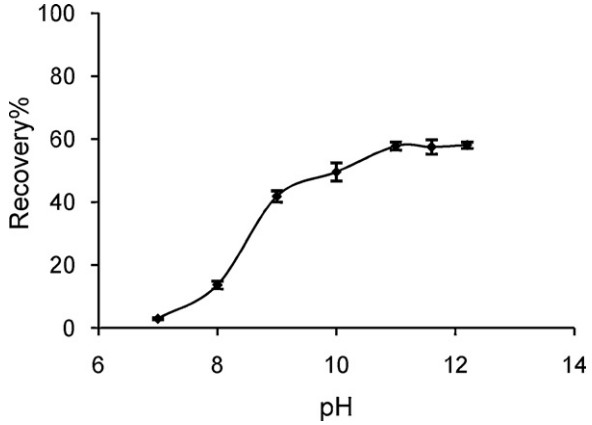

Fig. 3. Effect of pH of the acceptor phase on the extraction recovery of warfarin. Extraction conditions: pH $_{donor}$ = 2.3. Other conditions as Fig. 2.

3. Results and discussion

3.1. Optimization of HF-LPME

The effect of experimental variables such as the nature of organic solvent, pH of the donor and acceptor phases, stirring rate, salt concentration in the sample solution and extraction time on the extraction efficiency were investigated and optimized. For this purpose, HF-LPME was carried out using 11 ml of aqueous solution containing 0.1 μg ml^{-1} of warfarin. Extraction recovery was used to evaluate the extraction efficiency under different conditions and each experiment was repeated at least three times.

3.1.1. Selection of the organic extraction solvent

One of the critical steps in HF-LPME is to select an organic solvent for enrichment of the analyte. The selected organic solvent should be compatible with the fiber, immiscible with acceptor and donor phases, have low volatility to prevent solvent loss during the extraction and should present good affinity for the analyte [29]. On the basis of these considerations, 1-octanol, benzyl alcohol, *n*-dodecane, toluene and 1-undecanol were tested as the organic solvents. Among the organic solvents tested, 1-octanol showed the best extraction recovery for warfarin. Thus, 1-octanol was used in further experiments taking into account not only its good extraction recovery but also the low solvent loss compared to the other organic solvents tested (i.e. toluene and benzyl alcohol).

3.1.2. Optimization of donor phase pH

Warfarin is an acidic drug (pK_a = 5.0) [15]. To obtain high extraction efficiency for acidic compounds, the donor phase should be acidified to deionize the analytes and consequently increase their transfer from the donor phase into the organic phase. For this purpose, three different acids including hydrochloric, phosphoric and formic acid were tested at pH = 3.0. The highest warfarin recovery was obtained using HCl. Therefore, hydrochloric acid was used to adjust acidity (pH = 1.3–4.5). Results in Fig. 2 show that highest extraction recovery was obtained at pH = 2.3. In a more acidic solution, a decrease in the extraction recovery was observed. This can be attributed to protonation of the carbonyl groups of warfarin. Therefore, pH = 2.3 was used for subsequent experiments.

3.1.3. Optimization of acceptor phase composition

The acceptor phase should be basic to provide high solubility for the acidic analytes and ionize them to prevent re-entering of analytes into the organic phase. For determination of the composition of acceptor phase, sodium and ammonium hydroxide were tested (at pH = 10.0). Higher recovery was obtained with sodium hydroxide. Therefore, sodium hydroxide was used to adjust pH of acceptor phase in the range of 7.0–12.2. According to the obtained results, higher concentrations of NaOH in the acceptor phase provided highest recoveries for warfarin (Fig. 3). Therefore, pH of 11.0 was selected as the optimum pH value for further studies.

3.1.4. Effect of stirring speed

The extraction can be accelerated by stirring of the sample solution. Stirring facilitates analyte diffusion from donor phase, through the organic solvent, into the acceptor phase. Different stirring speeds from 100 to 1000 rpm were tested to determine their effect on the recovery of warfarin. According to Fig. 4, extraction recovery increased with increasing stirring speed. Therefore, 1000 rpm was selected as the optimum stirring speed in subsequent experiments.

3.1.5. Effect of extraction time

The extraction time is an important parameter in HF-LPME procedure because it influences the partition of the target analyte between the donor phase and organic phase and, subsequently, between the organic phase and acceptor phase. In this study, recovery of warfarin was investigated as a function of extraction time in the range of 10–120 min (Fig. 5). The recovery increased rapidly by the increasing of the extraction time up to 30 min but decreased thereafter as concluded in the reference [30]. Extending the extraction time to 120 min resulted in a marked decrease in the extraction

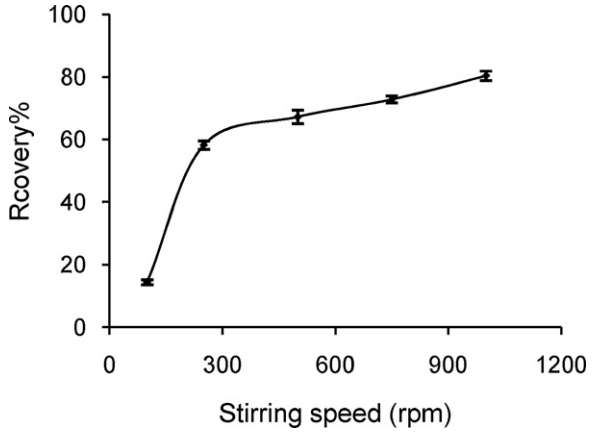

Fig. 4. Effect of stirring speed on the extraction recovery of warfarin. Extraction conditions: pH $_{acceptor}$ = 11.0 (adjusted with 1 M NaOH). Other conditions as Fig. 3.

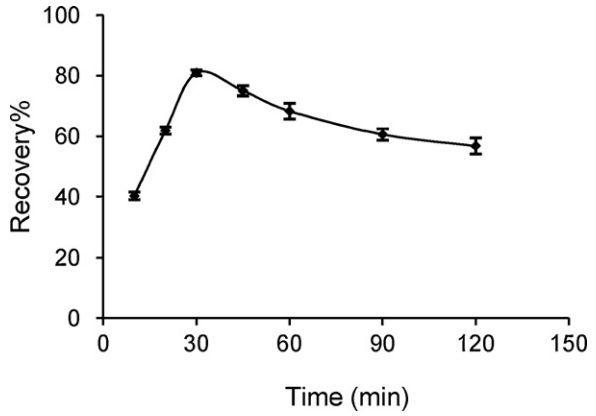

Fig. 5. Effect of extraction time on the extraction recovery of warfarin. Extraction conditions: stirring speed = 1000 rpm. Other conditions as Fig. 4.

Table 1
Figures of merit of the proposed method for the analysis of warfarin in human plasma.

LOD (ng ml^{-1})	5
Linear range (ng ml^{-1})	15–550
R^2	0.9984
EF	225
ER (%)	61.4
RSD (%) (intra-day, n = 5)	4.2
RSD (%) (inter-day, n =5)	11.1

recovery due to solvent dissolution [31]. Based on this observation the extraction time of 30 min was selected for all experiments.

3.1.6. Effect of salt addition to the sample solution

Some researchers have reported that the addition of salt to the sample solution has been beneficial for the extraction efficiency in microextraction procedures [32,33]. So, in this study, the effect of salt addition on the extraction recovery was examined by adding different amounts of NaCl into the sample solution in the range of up to 2.5 M. Recovery of analyte was decreased by increasing the salt concentration as was also found in other studies [24]. Most likely, a high salt concentration changes the physical properties of the diffusion film and reduces the rate of diffusion of analyte into the organic phase [34]. Hence, no salt was added in the subsequent experiments.

3.2. Method validation

To evaluate the analytical performance of the HF-LPME technique, figures of merit of this method including limit of detection (LOD), linear range, repeatability, reproducibility, extraction recovery and enrichment factor were investigated for extraction of warfarin from human plasma under the optimum conditions and were summarized in Table 1. The LOD value (5 ng ml^{-1}) was calculated based on the signal to noise ratio of 3. Linear correlation was obtained between peak area of analyte and its concentration in the range of 15–550 ng ml^{-1} with square of correlation coefficient (R^2)

Table 2
Determination of warfarin in patient plasma sample.

C_{added} (ng ml^{-1})	C_{found} (ng ml^{-1})	RSD (%) (n = 3) [a]	EF	ER (%)
–	117	5.1	–	–
100	207	3.9	220	60
400	543	3.7	216	58.9

[a] Intra-day RSD (%).

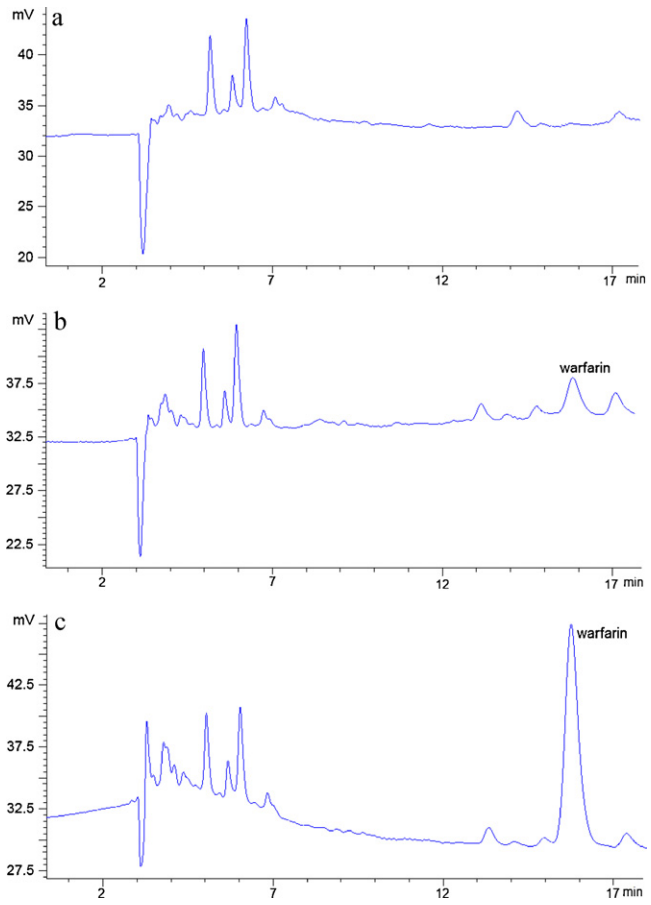

Fig. 6. HPLC chromatograms of (a) blank plasma sample, (b) patient plasma sample and (c) 400 ng ml^{-1} spiked patient plasma sample after extraction at optimum conditions. Mobile phase: methanol–(0.5%) phosphoric acid (65:35 v/v); flow rate: 1.0 ml min^{-1}; column: C_{18} (250 × 4 mm, 5 μm); UV detection at 254 nm.

of 0.9984. Under the optimum conditions, warfarin was extracted with satisfactory enrichment factor of 225 and the extraction recovery of 61.4%. The enrichment factor (EF) was defined as the ratio of the final concentration of warfarin in the acceptor phase to its initial concentration in the donor phase. The extraction recovery (ER) was calculated by the following equation:

$$\mathrm{ER} = \frac{C_a V_a}{C_d V_d} = \mathrm{EF} = \frac{V_a}{V_d}$$

where C_a and C_d are the final and initial concentrations of warfarin in the acceptor and the donor phases, respectively. C_a of the extracted drug was obtained from calibration curve of standard solutions. V_a and V_d are the volume of the acceptor phase (30 μl) and volume of the donor phase (11 ml), respectively.

The repeatability (intra-day) and reproducibility (inter-day) of the method were evaluated by carrying out five replicate extractions and determination of analyte at a concentration level of 0.1 μg ml^{-1} during a day (intra-day) and five replicates in five subsequent days (inter-day). The values of intra-day relative standard deviation (RSD) and inter-day RSD were 4.2% and 11.1%, respectively.

3.3. Application of HF-LPME for analysis of warfarin in real sample

Due to the importance of analysis of warfarin in plasma samples, the optimized method was applied to determine the concentration of this drug in the plasma sample from a patient under warfarin

Table 3
Comparison of the present method with other reported methods for the determination of warfarin.

Method	LOD ($ng\,ml^{-1}$)	Linear range ($ng\,ml^{-1}$)	RSD (%) (intra-day)	RSD (%) (inter-day)	Real sample	Reference
HF-LPME-HPLC-UV [a]	5	15–550	4.2	11.1	Plasma	This work
SPE-MEKC-ESI-MS [b]	100	250–5000	–	–	Plasma	[17]
LLE-HPLC-ESI-MS [c]	–	0.5–100	Less than 8.5	Less than 9.5	Serum	[35]
LLE-HPLC-UV [d]	–	120–3000	Less than 6.89	Less than 5.27	Plasma	[5]
Stripping voltammetry	0.3	15.4–123.3	–	–	Pharmaceutical Serum Urine	[22]

[a] Hollow fiber liquid phase microextraction-high performance liquid chromatography–ultra violet detection.
[b] Solid-phase extraction-micellar electrokinetic chromatography–electrospray ionization-mass spectrometry.
[c] Liquid–liquid extraction-high performance liquid chromatography–electrospray ionization-mass spectrometry.
[d] Liquid–liquid extraction-high performance liquid chromatography–ultra violet detection.

treatment, and the obtained results are summarized in Table 2. The chromatograms of HF-LPME extracts from blank plasma sample, patient plasma sample and spiked patient plasma sample are shown in Fig. 6(a–c). The chromatogram of blank plasma dose not show any interfering peak at the retention time of warfarin. This indicates that warfarin can be determined without any interference in the sample.

3.4. Comparison of the applied method with other reported methods

Table 3 shows LOD, linear range and RSD of the present method (HF-LPME-HPLC-UV) and those of other methods reported in literature for analysis of warfarin. Compared with other reported methods (Table 3), in most cases the present method exhibits adequately low LOD and broad linear range, and low quantities of the solvent were consumed.

4. Conclusions

A three-phase HF-LPME technique followed by HPLC–UV used for preconcentration and determination of warfarin in aqueous solution and plasma sample. This method presented a high enrichment and good sensitivity, while enabled efficient sample clean-up. Wide linear range of this method can be satisfactorily applied for warfarin in therapeutic drug monitoring. HF-LPME provides a simple, inexpensive, easy to use and benign to the environment method for extraction and preconcentration of warfarin from plasma samples.

References

[1] C. Huang, J. Yang, Y. Du, L. Miao, Measurement of free concentrations of highly protein-bound warfarin in plasma by ultra performance liquid chromatography–tandem mass spectrometry and its correlation with the international normalized ratio, Clin. Chim. Acta 393 (2008) 85–89.
[2] R. Denooz, Z. Douamba, C. Charlier, Fatal intoxications by acenocoumarol, phenprocoumon and warfarin: method validation in blood using the total error approach, J. Chromatogr. B 877 (2009) 2344–2348.
[3] D. de Orsi, L. Gagliardi, L. Turchetto, D. Tonelli, HPLC determination of warfarin and acenocoumarol in raw materials and pharmaceuticals, J. Pharm. Biomed. Anal. 17 (1998) 891–895.
[4] O. Osinbowale, M. Al Malki, A. Schade, J.R. Bartholomew, An algorithm for managing warfarin resistance, Clev. Clin. J. Med. 76 (2009) 724–730.
[5] S. Sun, M. Wang, L. Su, J. Li, H. Li, D. Gu, Study on warfarin plasma concentration and its correlation with international normalized ratio, J. Pharm. Biomed. Anal. 42 (2006) 218–222.
[6] A. Osman, K. Arbring, T.L. Lindahl, A new high-performance liquid chromatographic method for determination of warfarin enantiomers, J. Chromatogr. B 826 (2005) 75–80.
[7] I. Locatelli, V. Kmetec, A. Mrhar, I. Grabnar, Determination of warfarin enantiomers and hydroxylated metabolites in human blood plasma by liquid chromatography with achiral and chiral separation, J. Chromatogr. B 818 (2005) 191–198.
[8] P.R. Ring, J.M. Bostick, Validation of a method for the determination of (R)-warfarin and (S)-warfarin in human plasma using LC with UV detection, J. Pharm. Biomed. Anal. 22 (2000) 573–581.
[9] K.R. Henne, A. Gaedigk, G. Gupta, J.S. Leeder, A.E. Rettie, Chiral phase analysis of warfarin enantiomers in patient plasma in relation to CYP2C9 genotype, J. Chromatogr. B 710 (1998) 143–148.
[10] V.K. Boppana, W.H. Schaefer, M.J. Cyronak, High-performance liquid-chromatographic determination of warfarin enantiomers in plasma with automated on-line sample enrichment, J. Biochem. Biophys. Methods 54 (2002) 315–326.
[11] J.X. de Vries, E. Schmitz-Kummer, Direct column liquid chromatographic enantiomer separation of the coumarin anticoagulants phenprocoumon, warfarin, acenocoumarol and metabolites on an α_1-acid glycoprotein chiral stationary phase, J. Chromatogr. A 644 (1993) 315–320.
[12] S.D. McAleer, H. Chrystyn, A.S. Foondun, Measurement of the (R)- and (S)-isomers of warfarin in patients undergoing anticoagulant therapy, Chirality 4 (1992) 488–493.
[13] C. Banfield, M. Rowland, Stereospecific fluorescence high-performance liquid chromatographic analysis of warfarin and its metabolites in plasma and urine, J. Pharm. Sci. 73 (1984) 1392–1396.
[14] Z. Zuo, S. Kwan Wo, C.M.Y. Lo, L. Zhou, G. Cheng, J.H.S. You, Simultaneous measurement of S-warfarin, R-warfarin, S-7-hydroxywarfarin and R-7-hydroxywarfarin in human plasma by liquid chromatography–tandem mass spectrometry, J. Pharm. Biomed. Anal. 52 (2010) 305–310.
[15] W. Naidong, P.R. Ring, C. Midtlien, X. Jiang, Development and validation of a sensitive and robust LC–tandem MS method for the analysis of warfarin enantiomers in human plasma, J. Pharm. Biomed. Anal. 25 (2001) 219–226.
[16] Z. Zhang, B.M. King, Y.N. Wong, Quantitative liquid chromatography/mass spectrometry/mass spectrometry warfarin assay for in vitro cytochrome P450 studies, Anal. Biochem. 298 (2001) 40–49.
[17] J. Hou, J. Zheng, S.A. Shamsi, Separation and determination of warfarin enantiomers in human plasma using a novel polymeric surfactant for micellar electrokinetic chromatography–mass spectrometry, J. Chromatogr. A 1159 (2007) 208–216.
[18] R.A. Coe, J.O. Rathe, J.W. Lee, Supercritical fluid chromatography–tandem mass spectrometry for fast bioanalysis of R/S-warfarin in human plasma, J. Pharm. Biomed. Anal. 42 (2006) 573–580.
[19] W. Yau, E. Chan, Chiral CE separation of warfarin in albumin containing samples, J. Pharm. Biomed. Anal. 28 (2002) 107–123.
[20] P. Gareil, J.P. Gramond, F. Guyon, Separation and determination of warfarin enantiomers in human plasma samples by capillary zone electrophoresis using a methylated β-cyclodextrin-containing electrolyte, J. Chromatogr. B: Biomed. Sci. App. 615 (1993) 317–325.
[21] M. Balchen, A. Gjelstad, K.E. Rasmussen, S. Pedersen-Bjergaard, Electrokinetic migration of acidic drugs across a supported liquid membrane, J. Chromatogr. A 1152 (2007) 220–225.
[22] M.M. Ghoneim, A. Tawfik, Assay of anti-coagulant drug warfarin sodium in pharmaceutical formulation and human biological fluids by square-wave adsorptive cathodic stripping voltammetry, Anal. Chim. Acta 511 (2004) 63–69.
[23] H. Kataoka, New trends in sample preparation for clinical and pharmaceutical analysis, Trends Anal. Chem. 22 (2003) 232–244.
[24] E. Psillakis, N. Kalogerakis, Developments in liquid-phase microextraction, Trends Anal. Chem. 22 (2003) 565–574.
[25] J. Lee, H.K. Lee, K.E. Rasmussen, S. Pedersen-Bjergaard, Environmental and bioanalytical applications of hollow fiber membrane liquid-phase microextraction: a review, Anal. Chim. Acta 624 (2008) 253–268.
[26] S. Pedersen-Bjegaard, K.E. Rasmussen, Liquid–liquid microextraction for sample preparation of biological fluids prior to capillary electrophoresis, Anal. Chem. 71 (1999) 2650–2656.
[27] J.M. Steyn, H.M. Van Der Merwe, M.J. De Kock, Reversed-phase high-performance liquid chromatographic method for the determination of warfarin from biological fluids in the low nanogram range, J. Chromatogr. B: Biomed. Sci. Appl. 378 (1986) 254–260.
[28] E. Tahmasebi, Y. Yamini, A. Saleh, Extraction of trace amounts of pioglitazone as an anti-diabetic drug with hollow fiber liquid phase microextraction and determination by high-performance liquid chromatography–ultraviolet detection in biological fluids, J. Chromatogr. B 877 (2009) 1923–1929.
[29] K.E. Rasmussen, S. Pedersen-Bjegaard, Developments in hollow fibre-based, liquid-phase microextraction, Trends Anal. Chem. 23 (2004) 1–10.

[30] M. Mirzaei, H. Dinpanah, Three phases hollow fiber LPME combined with HPLC–UV for extraction, preconcentration and determination of valerenic acid in *Valeriana officinalis*, J. Chromatogr. B 879 (2011) 1870–1874.
[31] Z. Es'haghi, Determination of widely used non-steroidal anti-inflammatory drugs in water samples by in situ derivatization, continuous hollow fiber liquid-phase microextraction and gas chromatography-flame ionization detector, Anal. Chim. Acta 641 (2009) 83–88.
[32] D. Nagaraju, S. Huang, Determination of triazine herbicides in aqueous samples by dispersive liquid–liquid microextraction with gas chromatography–ion trap mass spectrometry, J. Chromatogr. A 1161 (2007) 89–97.
[33] A. Mohammadi, Y. Yamini, N. Alizadeh, Dodecylsulfate-doped polypyrrole film prepared by electrochemical fiber coating technique for headspace solid-phase microextraction of polycyclic aromatic hydrocarbons, J. Chromatogr. A 1063 (2005) 1–8.
[34] C. Yang, L. Guo, X. Liu, H. Zhang, M. Liu, Determination of tetrandrine and fangchinoline in plasma samples using hollow fiber liquid-phase microextraction combined with high-performance liquid chromatography, J. Chromatogr. A 1164 (2007) 56–64.
[35] M. Jin, X. Chen, H. Chen, Determination of warfarin and coumatetralyl in serum by HPLC coupled with electrospray ionization mass spectrometry, J. Liq. Chromatogr. Relat. Technol. 29 (2006) 2641–2650.

Journal of Pharmaceutical and Biomedical Analysis 61 (2012) 50–56

Contents lists available at SciVerse ScienceDirect

Journal of Pharmaceutical and Biomedical Analysis

journal homepage: www.elsevier.com/locate/jpba

Quantitative determination of exo- and endo-iohexol in canine and feline samples using high performance liquid chromatography with ultraviolet detection

S. De Baere[a,*], P. Smets[b], N. Finch[c], R. Heiene[d], P. De Backer[a], S. Daminet[b], S. Croubels[a]

[a] Dept. of Pharmacology, Toxicology and Biochemistry, Faculty of Veterinary Medicine, Ghent University, Salisburylaan 133, 9820 Merelbeke, Belgium
[b] Dept. of Medicine and Clinical Biology of Small Animals, Faculty of Veterinary Medicine, Ghent University, Salisburylaan 133, 9820 Merelbeke, Belgium
[c] School of Veterinary Science, University of Bristol, Langford, BS40 5DU, Bristol, United Kingdom
[d] Dept. of Companion Animal Clinical Sciences, Norwegian School of Veterinary Science, PO Box 8146 Dep, N-0033, Oslo, Norway

ARTICLE INFO

Article history:
Received 28 October 2011
Received in revised form
18 November 2011
Accepted 21 November 2011
Available online 28 November 2011

Keywords:
Iohexol
Cat
Dog
HPLC–UV
Plasma

ABSTRACT

A sensitive and specific high performance liquid chromatography–ultraviolet detection (HPLC–UV) method for quantitative determination of exo- and endo-iohexol in cat and dog serum/plasma is presented.

Sample preparation consisted of a protein precipitation step performed by adding 15 μL of trifluoroacetic acid to 100 μL of serum/plasma. Following vortexing and centrifugation, an aliquot of the supernatant was injected onto a polymeric PLRP-S column (250 mm × 4.6 mm i.d., dp: 8 μm, 100 Å), maintained at 30 °C. The mobile phase consisted of water (A) and methanol (B) and a gradient elution (flow-rate: 1.0 mL min^{-1}, total run-time: 21 min). The UV detector was set at a wavelength of 254 nm.

Matrix-matched calibration graphs were prepared for both exo- (0.44–657 μg mL^{-1}) and endo-iohexol (0.62–93.0 μg mL^{-1}). Correlation and goodness-of-fit coefficients were between 0.9985–0.9999 and 4.44–9.87%, respectively. Limits of quantification and detection were 0.44 and 0.15 μg mL^{-1} for exo-iohexol and 0.62 and 0.20 μg mL^{-1} for endo-iohexol, respectively. Results for within-day and between-day precision and accuracy fell within the ranges specified.

The reported method is simple and cost-effective. It has been successfully used for the analysis of exo- and endo-iohexol in serum/plasma samples of cats and dogs as part of pharmacokinetic studies with iohexol in order to determine plasma clearance of exo- and endo-iohexol. This indicates the usefulness of the developed method for application in the field of veterinary clinical practice and research.

© 2011 Elsevier B.V. All rights reserved.

1. Introduction

Iohexol (5-[(acetyl)(2,3-dihydroxypropyl)amino)]-*N*,*N*′-bis(2,3-dihydroxypropyl)-2,4,6,-tri-iodobenzene-1,3-dicarboxamide) (Fig. 1A) is a non-ionic, iodinated, water-soluble contrast medium of low osmolality, considered free from side effects in cats and dogs [1]. It consists of two stereoisomers (exo- and endo-iohexol) with exo-iohexol being the predominant isomer [2].

Following intravenous injection, iohexol does not bind to plasma proteins and enters the urine through glomerular filtration undergoing no tubular secretion or reabsorption. Hence, it is a suitable marker for glomerular filtration rate (GFR) determination [3–5].

As a non-radiolabeled contrast medium, iohexol has advantages over methods using other markers for determinating GFR, e.g. inulin which is considered to be the gold standard, but requires constant rate infusion and urinary catheterization; creatinine for which there is a lack of medical grade injectable formulation; radiolabeled chelating agents (e.g. ^{51}Cr-ethylenediaminetetraacetic acid (EDTA), ^{99m}Tc-diethylenetriaminepentaacetic acid (DTPA)) or radiological contrast media agents (e.g. ^{125}I-iothalamate), which require nuclear medicine facilities [5,6]. Since iohexol clearance is

Abbreviations: CRS, Chemical reference substance; CS, Cushing's syndrome; DTPA, Diethylenetriaminepentaacetic acid; EDTA, Ethylenediaminetetraacetic acid; g, Goodness-of-fit coefficient; GFR, Glomerular filtration rate; HPLC, High-performance liquid chromatography; IS, Internal standard; IV, Intravenous; LC–MS/MS, Liquid-chromatography–tandem mass spectrometry; LOQ, Limit of quantification; LOD, Limit of detection; MS/MS, Tandem mass spectrometry; QC, Quality control; *r*, Correlation coefficient; RSD, Relative standard deviation; S/N, Signal-to-noise ration; SPE, Solid-phase extraction; SS, Stock solution; UV, Ultraviolet detection; WS, Working solution.

* Corresponding author. Tel.: +32 9 264 73 48; fax: +32 9 264 74 97.
E-mail addresses: Siegrid.debaere@ugent.be (S. De Baere), Pascale.smets@ugent.be (P. Smets), Natalie.finch@bristol.ac.uk (N. Finch), Reidun.heiene@nvh.no (R. Heiene), Patrick.debacker@ugent.be (P. De Backer), Sylvie.daminet@ugent.be (S. Daminet), siska.croubels@ugent.be (S. Croubels).

0731-7085/$ – see front matter © 2011 Elsevier B.V. All rights reserved.
doi:10.1016/j.jpba.2011.11.022

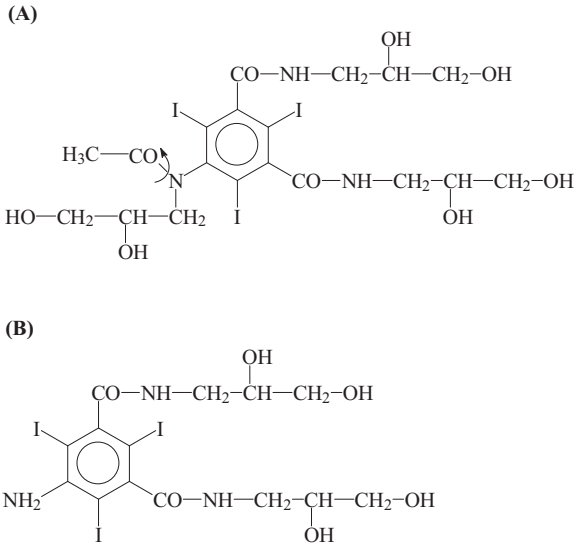

Fig. 1. Chemical structure of iohexol (A) and iohexol impurity J (B).

considered to provide an accurate estimate of GFR, it has now been adopted as a standard method by many clinicians/researchers both in human [1,5,6] and veterinary medicine [7–10].

Many analytical methods have been reported for the determination of iohexol in human serum or plasma, using HPLC–UV [1,3,6,11–15] or tandem mass spectrometric detection (MS/MS) [16–18], capillary electrophoresis [19–21], chemical measurement based on the colorimetric determination of iodine [22], X-ray fluorescence [6,23] or inductively coupled plasma-atomic emission spectroscopy [24]. Each technique has advantages and disadvantages. In contrast, only a few methods have been reported for the analysis of iohexol in animal body fluids (dog serum [25], dog plasma [26,27]).

Among these methods, HPLC–UV is generally preferred for its sensitivity and flexibility [1]. In addition, it offers the possibility to detect the exo- and endo-isomers of iohexol separately and is a cheaper and more accessible technique than LC–MS/MS.

Sample preparation has been performed by direct dilution [11], deproteinization using various protein precipitation agents [1,3,6,8,12,13,15,17,26,27], liquid–liquid extraction [14], solid-phase extraction (SPE) [25] or ultrafiltration [18]. The first two sample preparation techniques are simple and fast, but serum/plasma samples are frequently diluted by a factor 1–200, resulting in high limit of quantification (LOQ: 2–25 $\mu g\,mL^{-1}$) and detection (LOD: 1.2–10 $\mu g\,mL^{-1}$) levels. Sample preparation using an SPE column or an ultrafiltration device is expensive and time consuming and therefore, less appropriate for use in clinical samples.

Chromatography is generally accomplished using reversed-phase columns [1,6,8,11–13,15,16,18,25,27], but only a few methods mention the separation of exo- and endo-iohexol [1,8,13,15,25,27]. Since most authors quantitate only the major compound exo-iohexol, this isomer is generally used for the calculation of iohexol clearance and consequently as the marker for GFR determination. However, some authors described differences in plasma clearance between exo- and endo-iohexol in dogs and cats [8–10], but not in humans.

Because it was the aim to determine the plasma clearance of exo- and endo-iohexol, the present study focused on the development of a HPLC–UV method for the quantitative determination of both exo- and endo-iohexol at LOQ levels which were as low as possible (<1 $\mu g\,mL^{-1}$). The method was subjected to an in-house validation (linearity, within-run and between-run accuracy and precision, limit of quantification, limit of detection, specificity) and method performance characteristics were, to our knowledge, evaluated for the first time for both iohexol isomers. Thereafter, the applicability of the method was shown by the analysis of cat or dog serum/plasma samples, which were collected as a part of pharmacokinetic studies determining iohexol clearance.

2. Materials and methods

2.1. Standards and chemicals

Standards of iohexol and iohexol impurity J (5-amino-*N*,*N*′-bis(2,3-dihydroxypropyl)-2,4,6-tri-iodobenzene-1,3-dicarboxamide) (Fig. 1B), used as the internal standard (IS), were Chemical Reference Substances (CRS) of the European Pharmacopoeia (Strassbourg, France). The standards were stored at 2–8 °C and were replaced 6 months after opening the vial.

Stock solutions (SS) of 1 $mg\,mL^{-1}$ were prepared in methanol and stored at 2–8 °C for 12 months. Working solutions (WS) of iohexol (total iohexol concentrations: 100.0, 10.0, 1.0 and 0.1 $\mu g\,mL^{-1}$) were prepared by diluting the stock solution appropriately with HPLC water. The working solutions were stored at 2–8 °C for 6 months.

Trifluoroacetic acid was obtained from Sigma–Aldrich (Bornem, Belgium). Water and methanol, which were of HPLC grade, were purchased from VWR (Leuven, Belgium).

2.2. Patient samples

Known blank serum and plasma samples were obtained from healthy cats and dogs that did not receive iohexol.

2.2.1. Cat samples

The samples were collected from client owned cats undergoing iohexol clearance measurement to determine GFR. Data from this study have recently been published [28]. Briefly, serum samples were obtained from healthy cats ($n = 20$) which received an intravenous (IV) bolus of 647 $mg\,kg\,BW^{-1}$ of iohexol (Omnipaque300®). Blood samples were collected from the cephalic vein into a serum tube prior to iohexol administration and at 5, 15, 30, 60, 120, 180, 240 and 360 min after dosage. Serum samples were transferred to plastic tubes and stored at ≤−80 °C until analysis.

2.2.2. Dog samples

Following Ethical Committee approval (Faculty of Veterinary Medicine and Bioscience Engineering, Ghent University, authorization number: EC2008/066) and informed owner consent, plasma samples were obtained from healthy beagle dogs (control group; $n = 14$), from dogs suffering from Cushing's syndrome (CS; $n = 25$), and healthy client-owned dogs ($n = 12$) that were treated with one IV dose of iohexol (Omnipaque®, 64.7 $mg\,kg\,BW^{-1}$). Blood was sampled from the jugular vein into EDTA tubes prior to treatment and at 5, 15, 60, 120, 240, 360 and 480 min after dosage. Samples were centrifuged as soon as possible after collection (2054 × *g*, 10 min) and plasma was transferred to plastic tubes and stored at ≤−20 °C until analysis. It has previously been demonstrated by Lee et al. that iohexol is stable in serum/plasma under long-term storage conditions (2 months) at −20 °C [16]. More details concerning the canine measurements have been described by Smets et al. [29].

2.3. Sample preparation

2.3.1. Spiking of calibration curve and quality control (QC) samples

Appropriate volumes of the various working solutions were added to 100 µL of blank plasma/serum to

obtain calibrators with the following theorethical total exo-/endo-iohexol concentrations: 0.5 (0.44/0.06) $\mu g\,mL^{-1}$ (50 μL, WS: 1.0 $\mu g\,mL^{-1}$), 1 (0.88/0.12) $\mu g\,mL^{-1}$ (100 μL, WS: 1.0 $\mu g\,mL^{-1}$), 2.5 (2.19/0.31) $\mu g\,mL^{-1}$ (25 μL, WS: 10.0 $\mu g\,mL^{-1}$), 5 (4.38/0.62) $\mu g\,mL^{-1}$ (50 μL, WS: 10.0 $\mu g\,mL^{-1}$), 10 (8.76/1.24) $\mu g\,mL^{-1}$ (100 μL, WS: 10.0 $\mu g\,mL^{-1}$), 25 (21.9/3.10) $\mu g\,mL^{-1}$ (25 μL, WS: 100.0 $\mu g\,mL^{-1}$), 50 (43.8/6.20) $\mu g\,mL^{-1}$ (50 μL, WS: 100.0 $\mu g\,mL^{-1}$), 100 (87.6/12.4) $\mu g\,mL^{-1}$ (100 μL, WS: 100.0 $\mu g\,mL^{-1}$), 250 (219/31.0) $\mu g\,mL^{-1}$ (25 μL, SS: 1000 $\mu g\,mL^{-1}$), 500 (438/62.0) $\mu g\,mL^{-1}$ (50 μL, SS: 1000 $\mu g\,mL^{-1}$) and 750 (657/93.0) $\mu g\,mL^{-1}$ (75 μL, SS: 1000 $\mu g\,mL^{-1}$).

QC samples were spiked at a total iohexol concentration of 10 and 100 $\mu g\,mL^{-1}$.

Following spiking, samples were vortexed for 15 s, followed by the addition of HPLC water up to a final volume of 200 μL and additional vortexing.

2.3.2. Preparation of blank and incurred samples

One hundred microliters of blank plasma/serum or 100 μL of patient sample were added to 100 μL of HPLC water followed by a vortexing step (15 s).

2.3.3. Sample deproteinisation

Twenty-five microliters of the IS stock solution were added to each sample of an analytical batch (calibrators, QC and incurred samples). To the blank samples, no IS standard stock solution was added, but this was replaced by the addition of 25 μL of HPLC water. Samples were vortexed and equilibrated at room temperature for 5 min followed by the addition of 15 μL of trifluoroacetic acid and a further vortex mixing step of 15 s. The samples were centrifuged for 10 min at 7800 × *g*. The supernatant of the calibrators with a total iohexol concentration ranging from 0.5 to 10 $\mu g\,mL^{-1}$ and supernatant of the patient samples collected prior to and at >240 min after iohexol administration, were transferred to an autosampler vial.

Fifty microliters of the calibrator supernatant with a total iohexol concentration of 25 to 100 $\mu g\,mL^{-1}$ and 50 μL of the supernatant of the patient samples which were collected at 60 and 120 min after iohexol administration were transferred to an autosampler vial and diluted with 450 μL of HPLC water. For the remaining samples (i.e. calibrators with a total iohexol concentration >250 $\mu g\,mL^{-1}$ and patient samples collected at 5 and 15 min after treatment), 50 μL of supernatant were transferred to an autosampler vial and diluted with 950 μL of HPLC water.

Following vortexing, a 50-μL aliquot of each sample was injected onto the HPLC–UV instrument.

2.4. HPLC–UV analysis

The HPLC–UV system consisted of a P4000 gradient pump with vacuum degassing, an AS3000 autosampler, UV6000 detector, and a SN4000 module (Thermo Separations Products, Thermo Scientific, Breda, The Netherlands). The autosampler was set at a temperature of 10 °C.

Chromatographic separation was performed using a polymeric PLRP-S column (250 mm × 4.6 mm i.d., dp: 8 μm, 100 Å) in combination with a guard column of the same type (Agilent Technologies, Diegem, Belgium). The column was thermostatized at 30 °C. The mobile phase consisted of water (A) and methanol (B) and was delivered to the HPLC column at a flow-rate of 1.0 mL min^{-1}. A gradient elution was performed (0 min: 96% A – 4% B; 0–5 min: linear gradient to 80% A, 5–11 min: 80% A – 20% B, 11–15 min: linear gradient to 60% A, 15–15.5 min: linear gradient to 96% A, 15.5–21 min: 96% A – 4% B). Detection was performed at a wavelength of 254 nm.

Data processing was performed using the Chromquest version 4.1 software (Thermo Scientific).

2.5. In-house method validation

The proposed quantitative method was validated in-house for exo- and endo-iohexol in both feline serum and canine plasma, by evaluating the following parameters: linearity, within-run and between-run precision and accuracy, limit of quantification (LOQ), limit of detection (LOD), selectivity and carry-over. This is in compliance with the recommendations as defined by the European Community [30] and with reference guidelines defined in other EU and FDA documents [31–33].

2.5.1. Linearity

The linearity of the method was evaluated by analyzing calibration curve samples, which were prepared by spiking blank plasma/serum from dogs or cats not receiving iohexol. The calibration curve samples were analysed in the same way as the patient samples. The correlation coefficient (*r*) and the goodness-of-fit coefficient (*g*) were determined and were required to be ≥0.99 and ≤10%, respectively (see Table 1).

2.5.2. Accuracy and precision

Within-day precision and accuracy was evaluated by analyzing six blank plasma/serum samples, which were spiked with iohexol at low, medium and high concentration levels (see Table 2), on the same day. Between-day precision and accuracy was evaluated using the QC samples which were analysed with each batch of samples and run on different days. The acceptance criteria for accuracy were −20% to +10% of the theoretical concentration. For the precision, the relative standard deviation (RSD) was defined as $RSD_{max} = 2^{(1-0.5\log Conc)} \times 2/3$ for within-day precision and $2^{(1-0.5\log Conc)}$ for between-day precision.

2.5.3. Limit of quantification (LOQ)

The LOQ was defined as the lowest concentration of exo- and endo-iohexol for which the method was validated with a precision and accuracy that fell within the recommended ranges (see within-run accuracy and precision). The LOQ was also established as the lowest point of the calibration curve. The LOQ was determined by analyzing 6 spiked plasma/serum samples on the same day.

2.5.4. Limit of detection (LOD)

The LOD was defined as the lowest concentration of exo- and endo-iohexol which could be recognized by the detector with a signal-to-noise (S/N) ratio of ≥3. The LOD values were calculated by comparing the S/N ratios in the LOQ samples and in blank samples.

2.5.5. Selectivity

The selectivity of the method was evaluated with respect to interferences from endogenous compounds. The S/N ratio of a possible interfering peak in a blank sample had to be below to the S/N ratio of the analyte(s) in the same elution zone at the LOD level.

2.5.6. Carry-over

The carry-over was evaluated by analysing a water sample following analysis of the highest calibrator sample. The final analyte concentration in the water sample was required to be below the LOD.

Table 1
Evaluation of linearity for the analysis of exo- and endo-iohexol in dog plasma and cat serum.

	a	*b*	*r*	*g* (%)
Dog plasma				
Exo-iohexol: 0.44–657 μg mL^{-1} (*n* = 5)	$5.83 \times 10^{-6} \pm 4.83 \times 10^{-7}$	0.00396 ± 0.00514	0.9994 ± 0.0006	6.78 ± 1.84
Endo-iohexol: 0.62–93 μg mL^{-1} (*n* = 5)	$5.92 \times 10^{-6} \pm 3.54 \times 10^{-7}$	0.00379 ± 0.00303	0.9985 ± 0.0024	7.39 ± 1.87
Cat serum				
Exo-iohexol: 0.44–657 μg mL^{-1} (*n* = 2)	$6.24 \times 10^{-6} \pm 7.12 \times 10^{-7}$	0.00752 ± 0.00875	0.9999 ± 0.0001	4.44 ± 0.43
Endo-iohexol: 0.62–93 μg mL^{-1} (*n* = 2)	$8.32 \times 10^{-6} \pm 1.71 \times 10^{-6}$	0.00221 ± 0.00389	0.9998 ± 0.0001	9.87 ± 0.13

Note: *a*, slope; *b*, intercept; *r*, correlation coefficient (≥0.99); *g*, goodness-of-fit coefficient (< 10%); *n* = number of calibration curves.

3. Results and discussion

3.1. Sample clean-up

Extraction of iohexol from plasma or serum is aggravated due to its high polarity. In the literature several sample preparation techniques have been reported. Klenner et al. [25] performed a solid-phase extraction (SPE) using LiChrolut EN columns. One milliliter of sample was required to obtain a sensitivity that was sufficiently low (LOQ: 10 μg mL^{-1}). Following SPE, an evaporation step and filtration step was needed prior to injection onto the HPLC–UV system, making the method time consuming and expensive.

Many methods used an acid solution for protein precipitation (e.g. perchloric acid [1,3,6,13,15], trichloroacetic acid [26], trifluoroacetic acid [12,27], hydrochloric acid [8]). The volumes of acid that were added, were 2–15 times the initial volume of the plasma/serum samples, resulting in dilution of the sample prior to HPLC–UV analysis. Shihabi et al. [11] even diluted the serum sample 200 times prior to injection onto the HPLC apparatus. Sample dilution may possibly have a negative impact on the LOQ of the method, therefore, a small volume of trifluoroacetic acid was used in our method as a protein precipitation agent. The addition of only 15 μL was enough for precipitating serum/plasma proteins, resulting in clear supernatants. Sample dilution due to the addition of the precipitation agent was minimal, requiring only 100 μL of plasma for analysis. This is lower than the sample volume reported for other HPLC–UV methods (Klenner et al. [25]: 1000 μL, Farthing et al. [12]: 250 μL, Brändström et al. [6]: 200 μL).

In contrast to the method of Pöytäkangas et al., who did use 200 μL of a 10% solution of TFA in water for protein precipitation [27], the samples in the present study were clear enough for direct injection onto the HPLC–UV apparatus. Since filtration using a PVDF filter was not necessary, the time and costs for sample preparation were minimal in our method.

3.2. Chromatography

Special consideration was given to the choice of the analytical column and of the mobile phase, because it was the aim to separate the exo- and endo-iohexol isomers within a reasonable run-time. Two type of columns were tested, (Nucleosil 100 C18 (250 mm × 4.6 mm i.d.) and PLRP-S polymeric column (250 mm × 4.6 mm i.d.). Separation of exo- and endo-iohexol could be achieved using both columns, but the PLRP-S column was preferred due to its extended life-time.

The mobile phase consisted of water (A) and methanol (B) and a gradient elution was performed. Acetonitrile was also tested as organic modifier, however, it was observed that a better separation of the two isomers and better peak shape could be obtained using methanol.

The advantage of using non-volatile buffers (e.g. phosphate buffers [6,8,11,15,25], citrate buffer [1], trifluoroacetic acid [27]) in the aqueous part of the mobile phase, is that the chromatographic method can easily be transferred to LC–MS/MS if needed. Under the conditions used in the present method, endo- and exo-iohexol eluted at 9.1 and 10.3 min, respectively (Figs. 2B and 3B). Iohexol impurity J was used as internal standard and this compound eluted at approximately 15 min as a broad peak. The total run was accomplished in 21 min, which is considerably shorter than the method of Klenner et al. (45 min) [25]. Other methods report run-times lower than 20 min (HPLC–UV: Farthing et al.: 17 min [12], Soman et al.: 12 min [13], Pöytäkangas et al.: 13 min [27], LC–MS/MS: 1.5–17 min

Table 2
Results of the within-run precision and accuracy, LOQ and LOD evaluation for the analysis of exo- and endo-iohexol in dog plasma and cat serum.

Theoretical concentration (μg mL^{-1})	Mean ± SD actual concentration (μg mL^{-1})	Accuracy[a] (%)	Precision[a] (%)	RSD_{max} (%)	LOD (μg mL^{-1})
Dog plasma					
Exo-iohexol					
0.44 μg mL^{-1} (*n* = 6)	0.46 ± 0.01	5.5	2.2	12.1	0.15
8.76 μg mL^{-1} (*n* = 6)	8.15 ± 0.35	−7.0	4.3	7.7	
87.6 μg mL^{-1} (*n* = 6)	87.8 ± 0.25	0.2	0.3	5.4	
657.0 μg mL^{-1} (*n* = 6)	643.9 ± 2.95	−2.0	0.5	4.0	
Endo-iohexol					
0.62 μg mL^{-1} (*n* = 6)	0.62 ± 0.01	−0.2	1.6	11.5	0.20
1.24 μg mL^{-1} (*n* = 6)	1.21 ± 0.1	−2.1	8.2	10.3	
12.4 μg mL^{-1} (*n* = 6)	13.4 ± 0.14	7.9	1.0	7.3	
93.0 μg mL^{-1} (*n* = 6)	101.2 ± 2.80	8.8	2.8	5.4	
Cat serum					
Exo-iohexol					
0.44 μg mL^{-1} (*n* = 6)	0.45 ± 0.06	2.5	1.4	12.1	0.14
4.38 μg mL^{-1} (*n* = 6)	3.80 ± 0.13	−13.2	3.4	8.5	
87.6 μg mL^{-1} (*n* = 6)	88.0 ± 0.27	0.5	0.3	5.4	
657.0 μg mL^{-1} (*n* = 6)	646.5 ± 3.75	−1.6	0.6	4.0	
Endo-iohexol					
0.62 μg mL^{-1} (*n* = 6)	0.59 ± 0.04	−4.2	6.7	11.5	0.20
12.4 μg mL^{-1} (*n* = 6)	13.2 ± 0.12	6.5	0.9	7.3	
93.0 μg mL^{-1} (*n* = 6)	101.4 ± 3.17	9.0	3.1	5.4	

[a] *Acceptability ranges*: accuracy: conc. >10 ng mL^{-1}: −20% to +10%; precision: RSD ≤ RSD_{max}; LOD: S/N = 3.

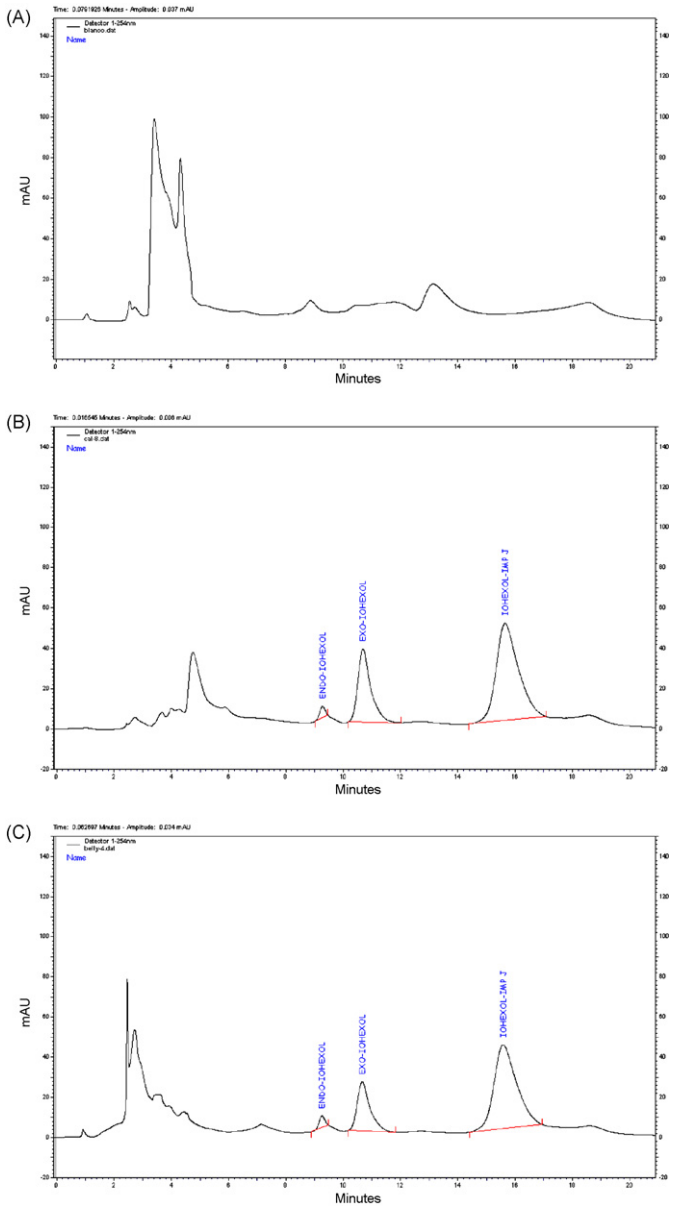

Fig. 2. HPLC–UV chromatogram of a blank dog plasma sample (A), a blank dog plasma sample spiked with iohexol at a concentration of 100 μg mL^{-1} (B) and a plasma sample collected from a dog at 60 min after IV iohexol administration (dose: 64.7 mg mL^{-1}, endo-iohexol concentration: 9.8 μg mL^{-1}, exo-iohexol concentration: 62.2 μg mL^{-1}) (C).

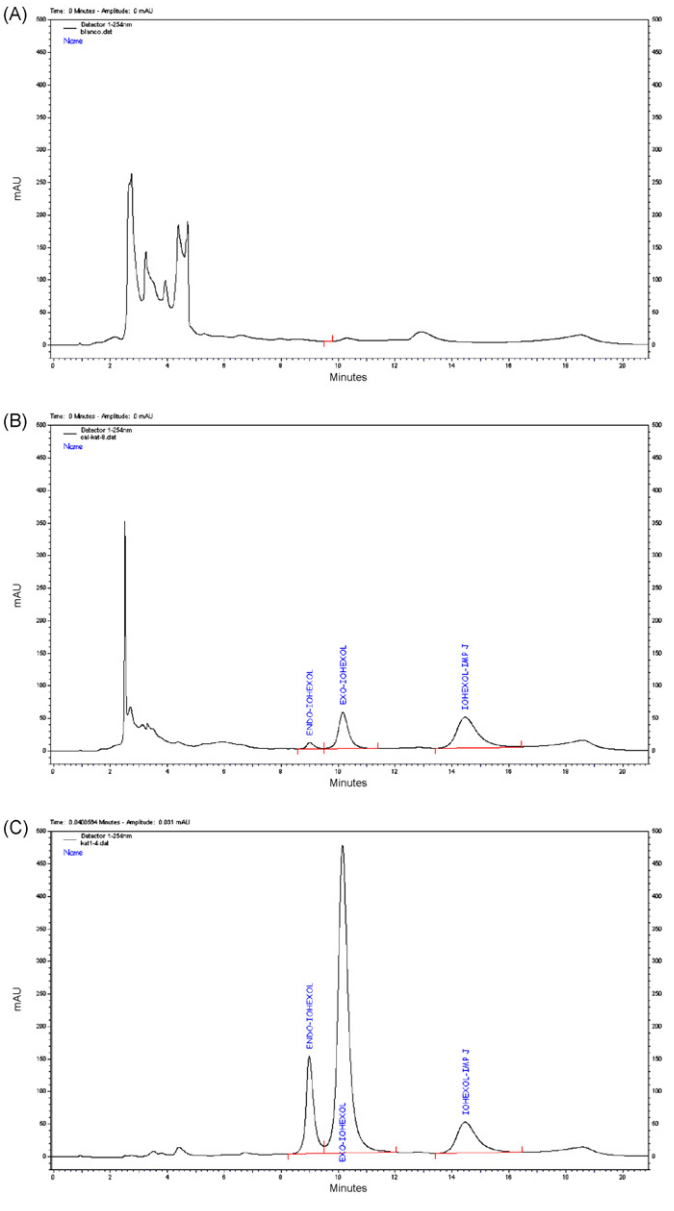

Fig. 3. HPLC–UV chromatogram of a blank cat serum sample (A), a blank cat serum sample spiked with iohexol at a concentration of 100 μg mL^{-1} (B) and a cat serum sample, taken at 60 min after IV iohexol administration (dose: 647 mg mL^{-1}, endo-iohexol concentration: 191.0 μg mL^{-1}, exo-iohexol concentration: 753.4 μg mL^{-1}) (C).

[16–18]), but did not discuss the quantitative determination of endo- and exo-iohexol. In addition, Farthing et al. reported that the pre-column required changing following analysis > 75 samples and that the analytical column required to be flushed for 1 h to eliminate interfering substances [12]. Using the method described in this paper, up to 500 samples could be analysed without changing the pre-column. In addition, retention times were stable (e.g. −0.76, −1.62 and −1.60% difference in retention time of endo-iohexol, exo-iohexol and the IS between sample 1 and sample 500, measured over 5 different analysis days). This demonstrates the robustness of the PLRP-S column used in the present study.

3.3. Internal standard

The method of internal standardization used in the present study was applied in order to compensate for analyte losses during sample preparation and for variations (retention time, sensitivity) during HPLC–UV analysis. For the presented method, it was decided to use iohexol impurity J as the internal standard. This is because this is a structural analog of iohexol, that is inexpensive and commercially available.

Internal standards used by other authors include *p*-aminobenzoic acid (PABA) [8,26,27] sodium diatrizoate dihydrate [25] and iohexol-related compound B [13]. *p*-Aminobenzoic acid has been used as IS by Laroute et al. and Meucci et al., because it was a structural analogous compound to *p*-amminohippuric acid, which was co-administered with iohexol. Sodium diatrizoate dihydrate is inexpensive. However, both compounds have less structural analogy to iohexol than iohexol impurity J. The disadvantage of using iohexol-related compound B as internal standard is the high cost of the pure standard.

3.4. Method validation

3.4.1. Linearity

Before constructing calibration curves, a standard solution of iohexol (1 μg mL^{-1}) was injected 6 times in order to determine the actual exo-/endo-iohexol ratio The mean ratio of the isomers in the iohexol standard was 87.6 ± 2.86% (range: 84.0–91.0%) exo-iohexol and 12.6 ± 2.86% (range: 9.0–16.0%) endo-iohexol. Using this ratio, the exo- and endo-iohexol concentration at each calibration level was calculated.

Results of the evaluation of linearity in dog plasma and cat serum for both exo- and endo-iohexol are shown in Table 1. Good results for linearity (r, g) were obtained for exo-iohexol over the complete range tested (0.44–657 μg mL^{-1}). For endo-iohexol, linearity was observed between 0.62 and 93.0 μg mL^{-1}. For all calibration curves, the y-intercepts were virtually zero, indicating the absence of endogenous interferences. The regression slopes showed a between-day variation ≤10%.

The calibration range was in the same order of magnitude as reported by other authors (Klenner et al.: 10–1000 μg mL^{-1} [25], Lee et al.: 10–1500 μg mL^{-1} [16], Soman et al.: 10–750 μg mL^{-1} [13]) and larger than Pöytäkangas et al.: 0.5–150 μg mL^{-1} [27]. If the analyte concentration fell above 110% of the concentration of the highest calibrator, the sample was reanalysed by increasing the amount of IS and diluting the sample in such a way that the analyte concentration fell within the calibration range.

3.4.2. Precision and accuracy

The results of the within-day precision and accuracy evaluation are summarized in Table 2. The acceptability ranges were met for both exo- and endo-iohexol at the specified levels. The between-run precision and accuracy was tested by the analysis of quality control samples, spiked at a level of 10 and 100 μg mL^{-1} and the results fell within the ranges specified (results not shown).

3.4.3. LOQ and LOD

The LOQ and LOD values for exo- and endo-iohexol in both dog plasma and cat serum are shown in Table 2. As can be seen, exo- and endo-iohexol can be quantified to levels of 0.44 μg mL^{-1}and 0.62 μg mL^{-1}, respectively. These levels were much lower than those reported for other HPLC–UV methods (LOQ ranging from 2 to 25 μg mL^{-1}, LOD ranging from 1 to 10 μg mL^{-1}) [6,8,11–14]). Pöytäkangas et al. [27] reported a similar LOQ value for exo-iohexol (0.5 μg mL^{-1}), but endo-iohexol was not quantitated in this method.

3.4.4. Selectivity

In Figs. 2A and 3A, chromatograms of blank dog plasma and cat serum samples, respectively, are shown. As can be seen, a small endogenous interference can be observed at the elution zone of endo-iohexol. This can explain the higher LOQ value for endo-iohexol, compared to exo-iohexol. At the elution zone of exo-iohexol, no endogenous interferences were observed.

3.4.5. Carry-over

In the water sample which was injected following the highest calibrator sample, no peaks were observed at the elution zone of endo- and exo-iohexol and the internal standard, indicating that no carry-over was present.

3.5. Analysis of patient samples

The applicability of the developed method described in this paper in clinical patients was shown by analysis of canine plasma and feline serum samples. The samples were collected following IV bolus administration of Omnipaque®.

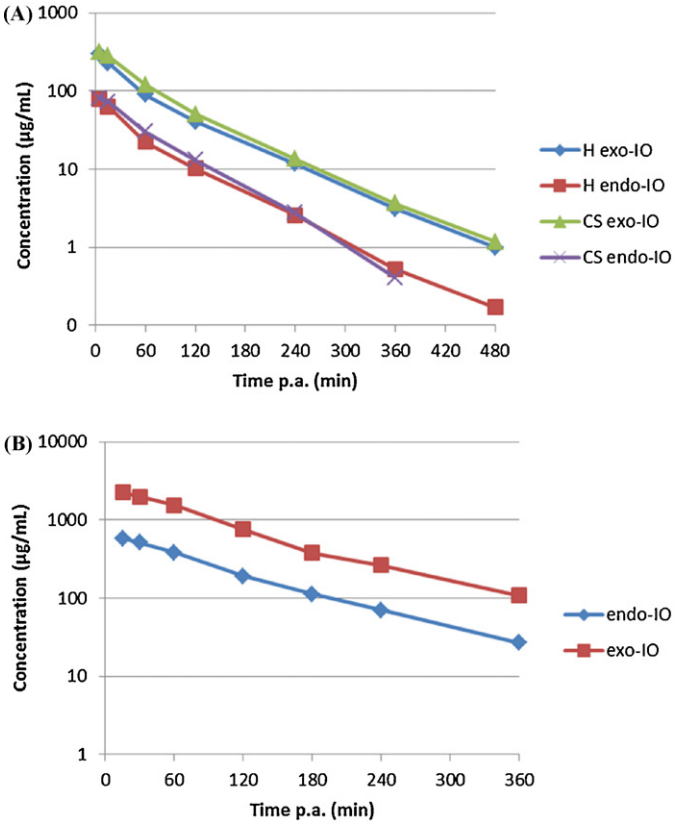

Fig. 4. Plasma/serum concentration versus time curves of exo- and endo-iohexol in (A) a healthy (H) and a Cushings' syndrom (CS) dog after the IV administration of 64.7 mg iohexol kg BW^{-1} and (B) in a healthy cat after the IV administration of 647 mg iohexol kg BW^{-1} (endo-IO, endo-iohexol; exo-IO, exo-iohexol).

3.5.1. Dog study

Iohexol analysis was performed as part of a study aiming to investigate the effect of *Cushing's syndrome* (CS) on kidney function by measuring the GFR using plasma clearance of exo- and endo-iohexol (multiple sampling method). Fig. 2C shows the chromatogram of a dog plasma sample. In Fig. 4A, the plasma concentration versus time curves for exo- and endo-iohexol in one animal of the control group and CS group, respectively, are shown. Detailed results of this study have been published by Smets et al. [29].

3.5.2. Cat study

Iohexol analysis was performed as part of a study to determine GFR using the plasma clearance of iohexol in cats. Data from this study has been published recently by Finch et al. [28]. Serum samples of all patients included in the study (n = 20) were analysed using the validated method described. Serum concentration versus time curves for exo- and endo-iohexol were constructed, as can be seen in Fig. 4B for one animal. Fig. 3C shows the chromatogram of a cat serum sample.

As can be seen from Figs. 2C and 3C and from Figs. 4A and 4B, both exo- and endo-iohexol could be quantified in dog plasma and cat serum samples. The method has already been applied to several pharmacokinetic studies measuring iohexol clearance in dogs and cats, proving the practicability and applicability of the developed method. All samples were analysed using the same analytical column, with the replacement of the guard column after analysis of approximately 500 samples. These findings indicate that plasma

preparation based on a simple deproteinisation step can be very useful and does not necessarily result in long run-times suggested by Klenner et al. [25] or shorter life-time of the guard/analytical column as suggested by Farthing et al. [12].

4. Conclusions

A rapid and sensitive HPLC–UV method for the quantitative determination of exo- and endo-iohexol in dog plasma and cat serum is described. The sample preparation procedure, consisting of a simple protein precipitation step using a strong acid, in combination with an acceptable HPLC run-time of 21 min, allowed the extraction and analysis of a large number of samples each day. The method was validated and results evaluated for both exo- and endo-iohexol. The HPLC–UV method was demonstrated to be inexpensive and robust with a short time of analysis.

The method was successfully applied to the determination of the plasma clearance of total, exo- and endo-iohexol for the calculation of the GFR in both canine and feline patients. This is important for use in veterinary research and clinical practice.

Acknowledgement

The authors wish to thank Ms. J. Lambrecht for her laboratory assistance.

References

[1] P. Nilsson-Ehle, Iohexol clearance for the determination of glomerular filtration rate: 15 years' experience in clinical practice, eJIFCC, 13, http://www.ifcc.org/ejifcc/vol13no2/1301200105.htm.
[2] S.J. Foster, M. Sovak, Isomerism in iohexol and ioxilan. Analysis and implications, Invest. Radiol. 23 (Suppl. 1) (1988) S106–S109.
[3] E. Krutzén, S.-E. Bäck, I. Nilsson-Ehle, P. Nilsson-Ehle, Plasma clearance of a new contrast agent, iohexol: a method for the determination of glomerular filtration rate, J. Lab. Clin. Med. 104 (1984) 955–961.
[4] P. Olofsson, E. Krutzén, P. Nilsson-Ehle, Iohexol clearance for assessment of glomerular filtration rate in diabetic pregnancy, Eur. J. Obstet. Gynecol. Reprod. Biol. 64 (1996) 63–67.
[5] B. Frennby, G. Sterner, Contrast media as markers for GFR, Eur. Radiol. 12 (2002) 475–484.
[6] E. Brändström, A. Grzegorczyk, L. Jacobsson, P. Friberg, A. Lindahl, M. Aurell, GFR measurement with iohexol and ^{51}-Cr-EDTA. A comparison of the two favoured GFR markers in Europe, Nephrol. Dial. Transplant. 13 (1998) 1176–1182.
[7] S.A. Brown, D.R. Finco, D. Boudinot, J. Wright, S.L. Tarver, T. Cooper, Evaluation of a single injection method, using iohexol, for estimating glomerular filtration rate in cats and dogs, Am. J. Vet. Res. 57 (1996) 105–110.
[8] V. Laroute, H.P. Lefebvre, G. Costes, P.-L. Toutain, Measurement of glomerular filtration rate and effective renal plasma flow in the conscious beagle dog by single intravenous bolus of iohexol and *p*-amminohippuric acid, J. Pharmacol. Toxicol. 41 (1999) 17–25.
[9] I. van Hoek, E. Vandermeulen, L. Duchateau, H. Lefebvre, S. Croubels, K. Peremans, I. Polis, S. Daminet, Comparison and reproducibility of plasma clearance of exogenous creatinine, exo-iohexol, endo-iohexol, and Cr-^{51}-EDTA in young adult and aged healthy cats, J. Vet. Intern. Med. 21 (2007) 950–958.
[10] A. Le Garreres, V. Laroute, F. De La Farge, K.G. Boudet, H.P. Lefebvre, Disposition of plasma creatinine in non-azotaemic and moderately azotaemic cats, J. Feline Med. Surg. 9 (2007) 89–96.
[11] Z.K. Shihabi, E.N. Thompson, M.S. Constantinescu, Iohexol determination by direct injection of serum on the HPLC column, J. Liq. Chromatogr. 16 (1993) 1289–1296.
[12] D. Farthing, D.A. Sica, I. Fakhry, T. Larus, S. Ghosh, C. Farthing, M. Vranian, T. Gehr, Simple HPLC–UV method for determination of iohexol, iothalamate, *p*-aminohippuric acid and *n*-acetyl-*p*-aminohippuric acid in human plasma and urine with ERPF, GFR and ERPF/GFR ratio determination using colorimetric analysis, J. Chromatogr. B 826 (2005) 267–272.
[13] R.S. Soman, H. Zahir, F. Akhlaghi, Development and validation of an HPLC–UV method for determination of iohexol in human plasma, J. Chromatogr. B 816 (2005) 339–343.
[14] J. Edelson, G. Palace, G. Park, High-performance liquid chromatographic determination of iohexol in plasma, urine and feces, J. Chromatogr. 274 (1983) 428–433.
[15] E. Cavalier, E. Rozet, N. Dubois, C. Charlier, Ph. Hubert, J.-P. Chapelle, J.-M. Krzesinski, P. Delanaye, Performance of iohexol determination in serum and urine by HPLC: validation, risk and uncertainty assessment, Clin. Chim. Acta 396 (2008) 80–85.
[16] S.-Y. Lee, M.-R. Chun, D.-J. Kim, J.W. Kim, Determination of iohexol clearance by high-performance liquid chromatography–tandem mass spectrometry (HPLC–MS/MS), J. Chromatogr. B 839 (2006) 124–129.
[17] Th.M. Annesley, L.T. Clayton, Ultraperformance liquid chromatography-tandem mass spectrometry assay for iohexol in human serum, Clin. Chem. 55 (2009) 1196–1202.
[18] M.C. Denis, K. Venne, D. Lesiège, M. Francoeur, S. Groleau, M. Guay, J. Cusson, A. Furtos, Development and evaluation of a liquid chromatography-mass spectrometry assay and its application for the assessment of renal function, J. Chromatogr. A 1189 (2008) 410–416.
[19] T. Kitahashi, I. Furuta, Method development for determining the iohexol in human serum by micellar electrokinetic capillary chromatography, J. Pharm. Biomed. Anal. 34 (2004) 153–158.
[20] M.V. Rocco, V.M. Buckalew Jr., L.C. Moore, Z.K. Shihabi, Capillary electrophoresis for the determination of glomerular filtration rate using nonradioactive iohexol, Am. J. Nephrol. 16 (1996) 138–143.
[21] Z.K. Shihabi, M.E. Hinsdale, Serum iohexol analysis by micellar electrokinetic capillary chromatography, Electrophoresis 27 (2006) 2458–2463.
[22] S.-E. Bäck, P. Masson, P. Nilsson-Ehle, A simple chemical method for the quantitation of the contrast agent iohexol, applicable for GFR measurements, Scand, J. Clin. Lab. Invest. 48 (1988) 825–829.
[23] T. Grönberg, S. Sjöberg, T. Almén, K. Golman, S. Mattsson, Noninvasive estimation of kidney function by X-ray fluorescence analysis. Elimination rate and clearance of contrast media injected for urography in man, Invest. Radiol. 18 (1983) 445–452.
[24] W.E. Braselton, K.J. Stuart, J.M. Kruger, Measurement of serum iohexol by determination of iodine with inductively coupled plasma-atomic emission spectroscopy, Clin. Chem. 43 (1997) 1429–1435.
[25] S. Klenner, C. Bergmann, K. Strube, W. Ternes, T. Spillmann, SPE for endo- and exo-iohexol analysis with HPLC in canine serum and rat urine, Chromatographia 65 (2007) 733–736.
[26] V. Meucci, A. Gasperini, G. Soldani, G. Guidi, M. Giorgi, A new HPLC method to determine glomerular filtration rate and effective renal plasma flow in conscious dogs by single intravenous administration of iohexol and *p*-aminohippuric acid, J. Chromatogr. Sci. 42 (2004) 107–111.
[27] M. Pöytäkangas, E. Saario-Paunio, T. Putkonen, I. Saastamoinen, R. Frias, Th. Spillmann, H. Saloniemi, Chromatographia 71 (2010) 211–216.
[28] N.C. Finch, H. Syme, J. Elliott, A.M. Peters, R. Gerritsen, S. Croubels, R. Heiene, Glomerular filtration rate estimation by use of a correction formula for slope-intercept plasma iohexol clearance in cats, Am. J. Vet. Res. 72 (12) (2011) 1652–1659.
[29] P.M.Y. Smets, H.P. Lefebvre, H.S. Kooistra, E. Meyer, S. Croubels, B.E.J. Maddens, S. Vandenabeele, J.H. Saunders, S. Daminet, Hypercortisolism affects glomerular and tubular function in dogs, Vet. J. (2011), doi:10.1016/j.tvjl.2011.05.027.
[30] Commision Decision 2002/657/EC implementing Council Directive 96/23/EC concerning the performances of analytical methods and the interpretation of results, Official Journal of the European Communities, No. L221, 17/08/2002, Decision of 12 August 2002, European Commision, Directorate General for Public Health and Consumers Protection.
[31] R.J. Heitzman (Ed.), Veterinary Drug Residues, Report Eur. 14126-EN, Commision of the EC, Brussels-Luxembourg, 1994.
[32] VICH GL 49 (MRK) draft 1, Guideline for the validation of analytical methods used in residue depletion studies, Brussels, Belgium, November 2009.
[33] J. Knecht, G. Stork, Percentage and logarithmic procedures for calculation of calibration curves, Fresen. Z. Anal. Chem. 270 (1974) 97–99.

Journal of Pharmaceutical and Biomedical Analysis 61 (2012) 57–63

Contents lists available at SciVerse ScienceDirect

Journal of Pharmaceutical and Biomedical Analysis

journal homepage: www.elsevier.com/locate/jpba

Pharmacokinetics and brain dispositions of tacrine and its major bioactive monohydroxylated metabolites in rats

Shuai Qian, Siu Kwan Wo, Zhong Zuo*

School of Pharmacy, Faculty of Medicine, The Chinese University of Hong Kong, Shatin, New Territories, Hong Kong Special Administrative Region

ARTICLE INFO

Article history:
Received 18 August 2011
Received in revised form
23 November 2011
Accepted 24 November 2011
Available online 3 December 2011

Keywords:
Tacrine
Hydroxytacrine
Pharmacokinetics
Brain disposition
Fluorescence

ABSTRACT

The current study aims to investigate the pharmacokinetics and brain disposition of tacrine and its three major bioactive monohydroxylated metabolites (1-hydroxytacrine, 2-hydroxytacrine and 4-hydroxytacrine). An assay for simultaneous quantification of tacrine and three above metabolites in rat plasma and brain tissue was developed. Four analytes together with internal standard were extracted from rat plasma or brain tissue homogenate by liquid–liquid extraction using ethyl acetate. Baseline separation of the four studied compounds was achieved by a Thermo Hypersil BDS C_{18} column with gradient elution using acetonitrile and ammonium formate-triethylamine (pH 4.0) under fluorescence detection. Extraction recoveries of all analytes ranged from 82.1% to 93.2% in both rat plasma and brain tissue. The intra- and inter-day precision and accuracy of each analyte at lower limit of quantification (LLOQ) and three quality control (QC) concentrations (low, middle and high) was within 12% RSD and within 11% bias in both biological matrices. The LLOQ for tacrine, 1-hydroxytacrine, 2-hydroxytacrine and 4-hydroxytacrine were found to be 2.5, 6.7, 2.1 and 2.1 ng/ml in plasma, and 12.3, 33.5, 10.6 and 10.5 ng/g in brain tissue, respectively. All four analytes were stable during analysis. The developed method provides a simple, sensitive and reproducible procedure for pharmacokinetics and brain disposition study of tacrine and its three major metabolites in rats after oral administration of tacrine. Pharmacokinetic study demonstrated that tacrine could be quickly absorbed and extensively metabolized to its monohydroxylated metabolites *in vivo*. In addition, rat brain disposition study showed that tacrine and its monohydroxylated metabolites were evenly distributed in different brain regions except for a slight lower concentration of tacrine in olfactory region. Moreover, tacrine and 4-hydroxytacrine exhibited a much higher brain-to-plasma ratio than that of 1-hydroxytacrine and 2-hydroxytacrine.

© 2011 Elsevier B.V. All rights reserved.

1. Introduction

Alzheimer's disease (AD) is a progressive neurodegenerative disorder characterized by deterioration of cognitive function, dementia, memory loss, altered behavior and mortality [1]. Although the exact mechanisms of AD are still not fully understood, it appears to involve a cholinergic deficiency by increasing evidences, and acetylcholinesterase inhibitors have produced the most successfully therapeutic results so far [2,3]. Tacrine (THA), a reverse and nonselective acetylcholinesterase inhibitor (AChEI), is the first approved drug to manage and improve the symptoms of AD. Due to its flat configuration and suitable lipophicility with a Log P of 2.71 [4,5], THA has a good intestinal permeability with an apparent permeability coefficient of 2.5×10^{-5} cm/s across rat jejunum [6]. However, the oral bioavailability of THA is relatively low (17–24% in human) because of its extensive first-pass metabolism [7]. Enzymatic investigations have implicated that cytochrome P450 1A2 plays a major role in the metabolism and biotransformation of THA [8,9]. Among all primary and secondary metabolites of THA, 1-hydroxytacrine (1-OH-THA), 2-hydroxytacrine (2-OH-THA) and 4-hydroxytacrine (4-OH-THA) have been identified as three major metabolites with different anti-AChE bioactivities in various species including human, rats and dogs [10–12] (Fig. 1). In addition, 1-OH-THA was proven to be the most abundant metabolite in all above mentioned species and had been selected as a potential candidate for treatment of AD [13,14]. Except for the anticholinesterase activity of THA, there also exists hypothesis that the hydroxylated metabolites of THA may act as the chelators of aluminum to remove it from brain so as to prevent the neurotoxicity effect of Al^{3+} ion [15,16]. THA is effective for Alzheimer's disease of mild to moderate severity. The main reasons for seldom usage of THA nowadays are related to its mild dose-dependent hepatotoxicity and other peripheral cholinergic side effects in clinical application. Patocka et al. proposed that the hepatotoxocity of tacrine was probably resulted from its reactive metabolite [15]. Therefore, it is worth to explore alternative routes

* Corresponding author. Tel.: +852 2609 6832; fax: +852 2603 5295.
E-mail address: joanzuo@cuhk.edu.hk (Z. Zuo).

0731-7085/$ – see front matter © 2011 Elsevier B.V. All rights reserved.
doi:10.1016/j.jpba.2011.11.025

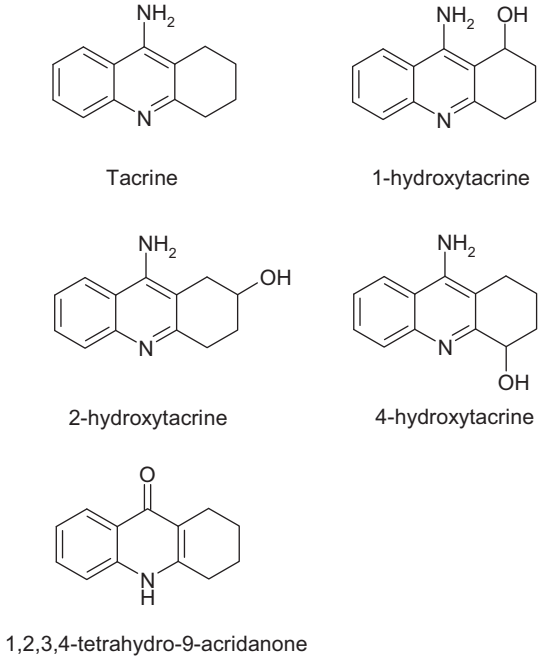

Fig. 1. Chemical structures of tacrine (THA), 1-hydroxytacrine (1-OH-THA), 2-hydroxytacrine (2-OH-THA), 4-hydroxytacrine (4-OH-THA) and 1,2,3,4-tetrahydro-9-acridanone (internal standard, IS).

of administration to avoid its first-pass metabolism as well as to enhance the bioavailability and brain targeting effect of THA.

During the past decades, nasal route of drug delivery is an attractive field and increasingly recognized to obtain modified drug metabolism, brain disposition as well as systemic exposure [17]. Although Jogani et al. has proved that intranasal delivery of THA could enhance its brain targeting effect [4,18], the modified dispositions of THA and its major metabolites have not been investigated. Therefore, there is a need to verify the pharmacokinetics and brain dispositions of both THA and its major active metabolites after intranasal administration of THA.

There are several published methods on the simultaneous identification of THA and its monohydroxylated metabolites in human, rat and bovine plasma/urine/microsomal incubate based on HPLC methods coupled with ultraviolet [11,19], fluorescence (FLD) [20–22], radioactive [9] or mass spectrometric detection [23–25]. In these methods, separation of THA from its metabolites can be easily achieved, but the baseline resolution among the three monohydroxylated metabolites is still challenging. For example, Hansen et al. has tried to determine the tacrine metabolites in human plasma and urine using a HPLC/FLD method, however, the separation of metabolites (especially for 1-hydroxytacrin and 2-hydroxytacrine) in the plasma sample was not fully resolved due to interference [20]. Although Cloos and Hondo has successfully demonstrated the separation of seven possible hydroxylated THA metabolites in microsomal incubate recently using ultra-high performance chromatographic column coupled with TOFMS [24], such method did not allocate the specific peaks for each hydroxytacrine in the reaction mixture. In summary, there is no existing analytical method that could simultaneously quantify THA and its three major hydroxylated metabolites in both plasma and tissue from either animal or human.

In the current study, in order to investigate the pharmacokinetics and brain disposition of THA and its major metabolites in rats, we plan to develop a simple, sensitive and reproducible HPLC/FLD assay performed on a Hypersil BDS C_{18} column for the simultaneous quantification and baseline separation of THA and its three major bioactive metabolites in rat plasma and brain tissue.

2. Materials and methods

2.1. Materials

Tacrine hydrochloride was purchased from Enzo Life Sciences Inc. (Farmingdale, NY, USA). 1-OH-THA, 2-OH-THA and 4-OH-THA were kindly gifted from Pfizer Inc. (Groton, CT, USA). 1,2,3,4-tetrahydro-9-acridanone (internal standard, IS) was obtained from Sigma (St. Louis, MO, USA). Ammonium formate, formic acid, sodium dihydrogen phosphate and triethylamine were purchased from BDH (Poole, England). Acetonitrile (HPLC grade) and ethylacetate (AR grade) were purchased from RCI Labscan (Bangkok, Thailand). All other reagents were of at least analytical grade and were used without further purification. Distilled and deionized water was used for the preparation of solutions.

2.2. Preparation of stock and working standard solutions, calibration standards and quality control (QC) samples

Individual stock solutions of THA, 1-OH-THA, 2-OH-THA and 4-OH-THA were prepared in 0.1 M hydrochloric acid (HCl) at concentration of around 1.2 mg/ml (free base). Appropriate amount of each stock solution was combined and further diluted with 0.02 M HCl to yield a stock standard mixture of THA, 1-OH-THA, 2-OH-THA and 4-OH-THA at concentrations of 61.6, 67.0, 21.3 and 21.0 μg/ml, respectively. Stock solution of IS were prepared by dissolving appropriate amount of 1,2,3,4-tetrahydro-9-acridanone in 0.1 M HCl at 1 mg/ml. All stock solutions were stored in glass vial and covered by aluminum foil for light protection and stored at −80 °C. Working standard solutions were prepared by serial dilution of the stock solutions with 0.02 M HCl.

To prepare calibration standards, blank plasma (100 μl) and whole brain tissue homogenate (0.1 g) were spiked with 10 μl of the working standard mixture and 10 μl of IS working solution (2 μg/ml) and followed by sample extraction in Section 2.3. The concentration range of THA and its monohydroxylated metabolites obtained from these calibration standards are listed in Table 1. Calibration curves were plotted by the peak area ratio of each analyte/IS *versus* concentrations of analytes in plasma and brain tissue. QC samples were prepared by spiking analytes of known concentration to blank plasma/brain tissue homogenate at three different concentrations (low, middle and high) within the calibration range.

2.3. Plasma and brain tissue sample preparations

Brain homogenate was freshly prepared by homogenizing rat brain tissue in 50 mM sodium phosphate buffer (pH 7.4) (1: 1.5, w/v). Homogenization was conducted in an ice bath using ultrasonic probe (Microson XL-2000, Misonix, USA) for 20–30 s.

To 100 μl plasma sample/0.1 g brain homogenate, an aliquot of 10 μl of IS working solution was added and the mixture was basified with 10 μl of 5 M sodium hydroxide before extraction with 1 ml ethyl acetate. After vortex mixing for 2 min, the mixture was centrifuged (10,000 × *g*) for 5 min at 4 °C. The organic phase was transferred to centrifuge tubes and the solvent was evaporated to dryness under a gentle stream of nitrogen at 37 °C. The obtained residue was reconstituted with 150 μl of ACN: 50 mM ammonium formate containing 0.5% triethylamine (pH4.0), 1:9 (v/v). After centrifugation (16,000 × *g*) for 5 min at 4 °C, an aliquot of 50 μl (for plasma samples) or 20 μl (for brain homogenate) supernatant was injected into the HPLC/FLD system.

Table 1
Linearity, recovery, intra-day and inter-day precision and accuracy of developed assay in rat plasma.

Compound	Linear range (ng/ml)	r^2	Spiked (ng/ml)	Recovery (%, $n=5$)	Intra-day ($n=5$)			Inter-day ($n=5$)		
					Determined (ng/ml)	Precision (% RSD)	Accuracy (% RE)	Determined (ng/ml)	Precision (% RSD)	Accuracy (% RE)
THA	2.5–307.9	0.9992	2.5 (LLOQ)	87.2 ± 6.3	2.4 ± 0.1	5.9	−4.2	2.4 ± 0.2	7.9	−4.8
			6.2	87.6 ± 2.8	5.6 ± 0.1	1.8	−8.6	5.6 ± 0.1	1.8	−9.6
			41.1	87.3 ± 8.3	39.3 ± 1.6	4.0	−4.3	40.1 ± 0.7	1.8	−2.4
			184.8	89.5 ± 5.5	182.9 ± 5.5	3.0	−1.0	185.3 ± 2.1	1.1	0.3
1-OH-THA	13–335.1	0.9997	6.7 (LLOQ)	84.8 ± 4.6	6.4 ± 0.3	4.4	−4.5	6.5 ± 0.1	1.9	−3.7
			10.1	91.9 ± 4.1	10.0 ± 0.9	8.5	−0.8	10.1 ± 0.8	8.1	0.0
			44.7	84.7 ± 6.3	44.8 ± 1.3	2.8	0.2	45.6 ± 1.0	2.2	2.0
			201.1	87.3 ± 3.6	196.7 ± 7.1	3.6	−2.2	204.4 ± 6.8	3.3	1.6
2-OH-THA	2.1–106.4	0.9990	2.1 (LLOQ)	85.2 ± 5.2	2.1 ± 0.2	7.5	−2.0	2.1 ± 0.0	1.7	−0.4
			3.2	82.5 ± 7.4	3.2 ± 0.2	6.7	1.4	3.3 ± 0.1	3.9	2.5
			14.2	83.6 ± 8.1	14.5 ± 0.4	3.0	2.0	14.6 ± 0.1	0.8	2.8
			63.8	82.1 ± 4.1	62.4 ± 2.8	4.6	−2.2	64.2 ± 1.6	2.5	0.6
4-OH-THA	2.1–105.2	0.9964	2.1 (LLOQ)	85.1 ± 7.9	2.1 ± 0.2	10.5	−0.9	2.1 ± 0.2	7.1	−0.2
			3.2	87.8 ± 5.1	3.2 ± 0.2	6.9	0.3	3.0 ± 0.3	9.2	−3.6
			14.0	86.0 ± 8.9	13.8 ± 0.5	3.4	−1.5	14.3 ± 0.8	5.2	2.1
			63.1	88.9 ± 2.5	63.2 ± 2.7	4.2	0.2	65.7 ± 2.5	3.7	4.1

2.4. Instrumentation and chromatographic conditions

The HPLC/FLD system consists of Waters 600 controller (pump), Waters 717 auto sampler and Waters 474 Scanning Fluorescence Detector. Instrumental control and data acquisition were controlled by Waters Millennium software (version 3). Chromatographic separation was performed on a Thermo BDS C_{18} Hypersil column (250 mm × 4.6 mm i.d., 5 μm particle size) protected by a guard column (Delta-Pak C_{18} Guard-Pak, Waters). Mobile phase consisting of eluent A [50 mM ammonium formate and 0.5% triethylamine (adjusted to pH 4.0 by formic acid) with 5% acetonitrile)] and eluent B [acetonitrile] was run at 1 ml/min. The gradient elution program was set as follow: 97.5% A (0–16 min), 97.5% → 87% A (16–16.5 min), 87% A (16.5–28 min), 87% → 25% A (28–28.5 min), 25% A (28.5–36 min), 25% → 97.5% A (36–36.5 min), and 97.5% A (36.5–44 min). Fluorescence detection was performed at an excitation wavelength of 330 nm and emission wavelength of 365 nm. The temperatures of column and autosampler were set at ambient and 4 °C, respectively.

2.5. Method validation

The method was validated on its specificity, sensitivity, linearity, intra-day and inter-day precision and accuracy, and stability testing according to the FDA guidance of bioanalytical method validation [26].

2.5.1. Specificity and sensitivity

The method specificity was evaluated by analysis of six separate blank sample matrix for interference. LLOQ was defined as the lowest concentration at which the signal-to-noise (S/N) ratio was larger than 5 and both the precision (the relative standard deviation, RSD) and accuracy (relative error, RE) were less than or equal to 20% by analyzing the five replicates of samples spiked with each analyte.

2.5.2. Precision and accuracy

The intra-day precision and accuracy were determined within 1 day by analysis of five replicates of QC samples at low, middle and high concentrations as described in Section 2.2. The inter-day precision and accuracy were determined on 3 separate days. Precision with RSD within 15% and accuracy within 15% were considered to be acceptable.

2.5.3. Recovery and stability

The recovery of each analyte was assessed by comparing the peak area of QC samples extracted from biological matrix with the peak area of reference standards prepared in reconstitute solvent.

Stability tests were evaluated at three different concentrations (low, middle and high) of QC samples. Freeze–thaw stability of analytes in the biological samples was evaluated by exposing QC samples to three cycles of freeze (−80 °C)–thaw (room temperature) process before sample preparation. Bench-top stability was determined by holding QC samples at room temperature for 3 h. Auto-sampler stability was evaluated by analyzing extracted and reconstituted QC samples after being placed in the auto-sampler (4 °C) for 24 h.

2.6. Pharmacokinetics and brain disposition of THA and its metabolites in rats

Adult male Sprague–Dawley rats, weighting 230–250 g, were provided by Laboratory Animal Services Center of The Chinese University of Hong Kong (Hong Kong, China). All experimental procedures were approved by the Department of Health of Hong Kong and Animal Ethics Committee at the Chinese University of Hong Kong.

One day before the study, the right jugular veins of five rats were cannulated with a polyethylene tubing (0.5 mm ID, 1 mm OD, Portex Ltd., England) for blood collection via a light surgery under anesthesia by intramuscular injection of a mixture containing ketamine (80 mg/kg) and xylazine (8 mg/kg). After a 24 h recovery and an overnight fasting (free access to water only), rats were orally administrated with 1 ml of THA solution (1 mg/ml) prepared in saline (4 mg/kg dose). Around 200 μl of blood was collected into a heparinized centrifuge tube at pre-determined time points (5, 10, 20, 30, 45, 60, 90, 120, 180, 240 and 360 min) post dosing. Plasma was obtained by centrifugation of blood at 16,000 × g for 5 min. Rats were allowed for free access to food and water 4 h after drug administration.

For brain distribution study, three rats were orally administrated with 1 ml of THA solution (3 mg/ml) prepared in saline

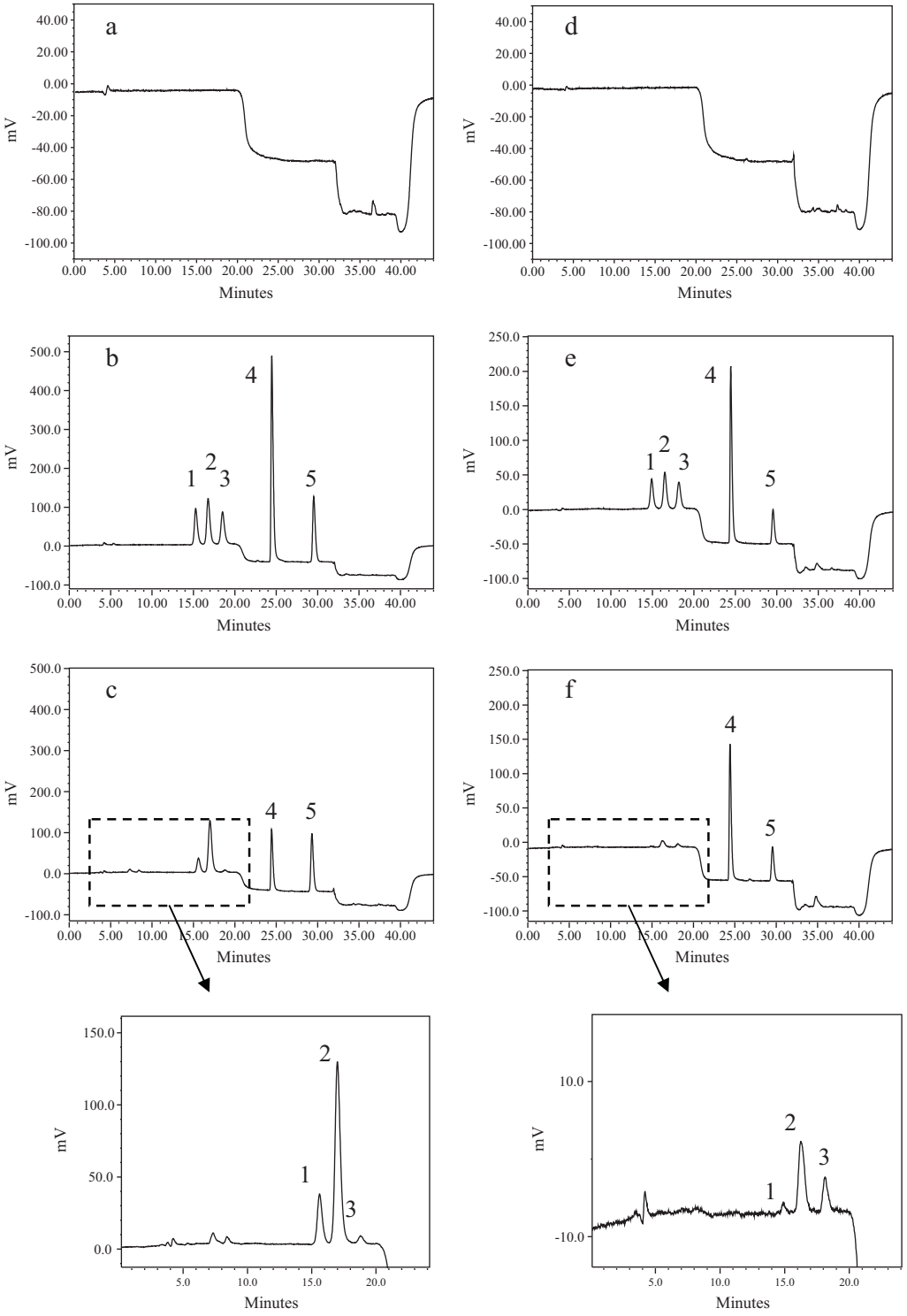

Fig. 2. Representative chromatograms of rat plasma and brain samples. For plasma: blank rat plasma (a), plasma spiked with analytes at high QC level (b), plasma sample at 45 min after oral administration of 4 mg/kg THA (c); for brain tissue: blank brain tissue homogenate (d), brain tissue homogenate spiked with analytes at high QC level (e), brain cortex sample obtained at 1 h after oral administration of 12 mg/kg THA (f). Peaks: 1 = 2-OH-THA; 2 = 1-OH-THA; 3 = 4-OH-THA; 4 = THA; 5 = IS (*note*: (i) the high QC levels of 2-OH-THA, 1-OH-THA, 4-OH-THA and THA in rat plasma are 63.8, 201.1, 63.1 and 184.8 ng/ml, respectively; (ii) the high QC levels of 2-OH-THA, 1-OH-THA, 4-OH-THA and THA in rat brain tissue are 266.0, 837.7, 263.0 and 769.8 ng/g, respectively; (iii) part of Fig. 2c and f are enlarged for clarification).

(12 mg/kg dose). At 1 h after administration, rats were sacrificed under anesthesia. Blood sample was collected by cardiac puncture and followed by centrifugation to obtain plasma. The whole brain was collected and quickly rinsed with ice-cold normal saline, and the surface water was blotted dry with paper towel. The brain tissue was then placed on ice pack and dissected into olfactory bulb, frontal cortex, cerebral cortex, hippocampus, striatum and other remaining (midbrain, thalamus, hypothalamus and cerebellum) regions. Blood vessels and meninges were carefully removed with forceps and each brain region was accurately weighted. All samples were stored at −80 °C for overnight and analyzed the next day.

Samples with analyte concentrations higher than the upper limit of quantification were diluted with the corresponding blank biological matrices to adjust the concentration within the linear range before sample preparation, and then reanalyzed. Pharmacokinetic parameters were calculated using WinNonlin software (Pharsight Corp., Version 2.1, Mountain View, CA) employing a non-compartmental model approach.

3. Results and discussion

3.1. Optimization of chromatographic conditions

Since 1-OH-THA, 2-OH-THA and 4-OH-THA (Fig. 1) are positional isomers, they share similar UV profiles, exhibit same fluorescence properties and cannot be distinguished via mass spectrometry. During assay development, we tried several types of column (including phenyl, ODS C_{18}, BDS C_8 and cyano) to separate these positional isomers, but failed to obtain baseline separation. Thermo BDS C_{18} Hypersil column was eventually selected for further evaluation. In addition, we found the composition and pH value of mobile phase had significant effects on the peak shape and separation of analytes. Either decreasing the ionic strength of ammonium formate from 75 mM to 10 mM or increasing the pH value of ammonium formate buffer from pH 2.5 to 7.0 would broaden the peak and increase peak tailing, resulting in poor separation of the three metabolites. Such problem can be overcome by addition of 0.5% (v/v) triethylamine in 50 mM ammonium formate (adjusted to pH 4.0 by formic acid). Consequently, Thermo BDS C_{18} Hypersil column and mobile phase consisting of 50 mM ammonium formate and 0.5% triethylamine (adjusted to pH 4.0 by formic acid) with 5% acetonitrile (eluent A) and acetonitrile (eluent B) was used in the study. Furthermore, high percentage (97.5%) of buffer (eluent A) for 16 min at the initial LC gradient profile is crucial for complete separation of the three positional isomers.

3.2. Method validation

3.2.1. Assay selectivity, sensitivity and linearity

Under the present chromatographic conditions, THA and its metabolites as well as IS are clearly baseline separated from each other with no interference from endogenous materials in rat plasma and brain tissue (Fig. 2b and e). The retention time for THA, 1-OH-THA, 2-OH-THA, 4-OH-THA and IS were 15.2, 16.7, 18.5, 24.4 and 29.5 min, respectively. The LLOQs for THA, 1-OH-THA, 2-OH-THA and 4-OH-THA were 2.5, 6.7, 2.1 and 2.1 ng/ml in rat plasma, and 12.3, 33.5, 10.6 and 10.5 ng/g in rat brain tissue, respectively. The precision (RSD, %) and accuracy (RE, %) of each analyte was less than 11.7% and 11.0%, respectively (Tables 1 and 2). Within the linear range, good linearities ($r^2 > 0.995$) are achieved for all analytes in both sample matrices (Tables 1 and 2). In addition, our developed method demonstrates good sensitivity with LLOQ of 2.1–6.7 ng/ml for all analytes in rat plasma, which is similar to those from literature [19], but offers superior advantage on the baseline separation of THA and its three monohydroxylated metabolites and smaller sample volume needed (100 μl vs. 1 ml from Hsu [19]).

3.2.2. Accuracy and precision

The intra-day and inter-day accuracy and precision of the assay method for all analytes in rat plasma and brain tissue are shown in Tables 1 and 2, respectively. For all the QC samples spiked with analytes at three concentration levels (low, middle and high) in both matrices, the % RSD of both intra-day and inter-day precision was below 10.8%, and the accuracy was within the range of −9.6 to 4.1% RE for all four analytes.

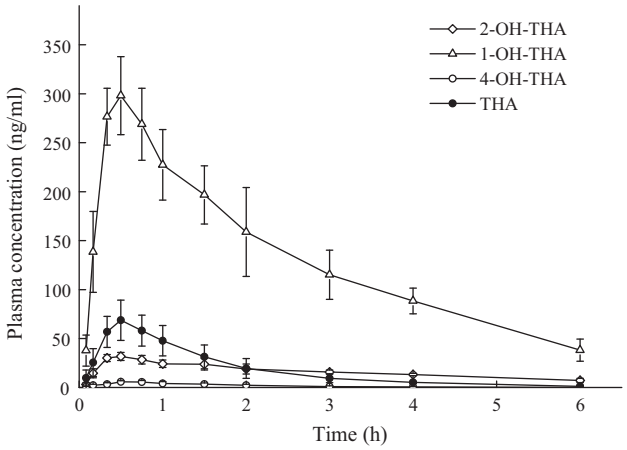

Fig. 3. Plasma concentration versus time profiles of THA and its metabolites after oral administration of THA at 4 mg/kg in rat plasma. Data represents mean ± SD ($n = 5$).

3.2.3. Recovery and stability

The mean extraction recoveries (Tables 1 and 2) of all four analytes in both rat plasma and brain tissue QC samples are found to be ranged from 81.5 to 93.2% and are consistent (less than 15% RSD) over the concentration range examined. The mean recovery for IS in rat plasma and brain tissue was 88.8% (with 4.5% RSD) and 90.8% (with 4.6% RSD), respectively. Such one-step liquid–liquid extraction approach (modified from the extraction method by Hansen [20]) used in this study provided comparable recoveries for all analytes to that reported by Hansen using ethyl acetate (84–105%), but much higher recoveries than that using chloroform/1-propanol mixture (68–83%) [22], cyclohexane/ethyl acetate mixture (35–96%) [19], and tertbutylmethyl-ether/*n*-hexane mixture (39–67%) [21]. The result suggests that the use of ethyl acetate for extracting THA and its major metabolites was effective and reproducible. Table 3 indicated that three freeze–thaw cycles, bench top for 3 h and storage in autosampler for 24 h did not affect the stability of the four analytes.

3.3. Pharmacokinetics and brain disposition of THA and its metabolites in rats

The developed and validated method has been applied to simultaneously determine THA and its major metabolites in rat plasma and brain tissue after oral administration of THA at 4 mg/kg. Typical chromatograms of rat plasma (45 min after dosing) and brain tissue (1 h after dosing) are shown in Fig. 2c and f, respectively. THA and its three bioactive metabolites were found in rat plasma with 1-OH-THA and 2-OH-THA being the two major metabolites. In rat brain tissue, two major metabolites of THA were 1-OH-THA and 4-O-THA, with trace amount of 2-OH-THA. The presence of 1-OH-THA, 2-OH-THA and 4-OH-THA in rat plasma and brain justified the need for complete separation of these metabolites (the enlarged figures of Fig. 2c and f).

The plasma concentration *versus* time profiles of THA and its metabolites after oral administration of THA at a dose of 4 mg/kg are shown in Fig. 3. The pharmacokinetic parameters of the studied analytes were summarized in Table 4. THA was quickly absorbed ($t_{max} \sim 0.5$ h) and extensively metabolized (AUC ratio of THA/sum of metabolites ~0.12) to 1-OH-THA, 2-OH-THA and 4-OH-THA in rat. 1-OH-THA has the highest concentration in plasma among three metabolites, while the plasma level of 4-OH-THA was relatively low and was close to its LLOQ (2.1 ng/ml). These results are in agreement with several previous reports [19,27], and such *in vivo* selective hydroxylation of THA was supported by the *in vitro* Phase

Table 2
Linearity, recovery, intra-day and inter-day precision and accuracy of developed assay in rat brain tissue.

Compound	Linear range (ng/g)	r^2	Spiked (ng/g)	Recovery (%, $n=5$)	Intra-day ($n=5$)			Inter-day ($n=5$)		
					Determined (ng/g)	Precision (% RSD)	Accuracy (% RE)	Determined (ng/g)	Precision (% RSD)	Accuracy (% RE)
THA	12.3–1539.5	0.9992	12.3 (LLOQ)	85.8 ± 8.3	12.1 ± 1.4	11.7	−1.9	11.6 ± 1.2	10.1	−5.5
			30.8	87.8 ± 3.9	31.2 ± 1.8	5.8	1.2	30.2 ± 1.3	4.3	−1.9
			230.9	92.5 ± 1.8	230.0 ± 5.3	2.3	−0.4	229.3 ± 5.4	2.3	−0.7
			769.8	93.2 ± 1.6	754.1 ± 20.3	2.7	−2.0	771.8 ± 25.5	3.3	0.3
1-OH-THA	33.5–1675.4	0.9993	33.5 (LLOQ)	90.2 ± 5.3	37.2 ± 1.5	4.0	5.5	35.5 ± 1.9	5.2	5.8
			83.8	82.1 ± 6.9	80.3 ± 8.1	10.0	−6.8	85.6 ± 8.8	10.2	2.2
			251.3	88.9 ± 4.0	257.4 ± 11.9	4.6	−2.4	259.4 ± 10.6	4.1	3.2
			837.7	89.6 ± 2.7	818.5 ± 37.8	4.6	−1.5	840.2 ± 35.7	4.3	0.3
2-OH-THA	10.6–532.0	0.9985	10.6 (LLOQ)	87.2 ± 3.8	11.2 ± 0.7	6.5	11.0	10.3 ± 0.7	7.2	−2.9
			26.6	84.3 ± 5.0	24.8 ± 1.5	6.0	−4.1	27.3 ± 3.0	10.8	2.8
			79.8	83.9 ± 4.1	77.9 ± 3.3	4.2	2.4	81.9 ± 5.5	6.7	2.6
			266.0	84.1 ± 2.9	262.0 ± 10.5	4.0	−2.3	269.8 ± 11.5	4.3	1.4
4-OH-THA	10.5–526.0	0.9994	10.5 (LLOQ)	82.4 ± 3.5	11.5 ± 0.3	2.9	9.5	11.0 ± 0.4	3.8	4.9
			26.3	89.5 ± 7.4	25.9 ± 1.8	7.0	−1.5	27.2 ± 1.8	6.8	3.5
			78.9	84.9 ± 3.5	79.8 ± 2.7	3.4	1.2	80.9 ± 2.8	3.4	2.5
			263.0	90.2 ± 1.5	252.2 ± 6.1	2.4	−4.1	263.4 ± 11.4	4.3	0.2

Table 3
Stability of THA and its metabolites in rat plasma and brain tissue during sample preparation and analytical process.

Biological matrices	Compounds	Spiked level	Determined concentration ($n=4$)		
			Freeze–thaw three cycles[a]	Bench top 3 h[b]	Autosampler 24 h[c]
Plasma (ng/ml)	THA	6.2	6.0 ± 0.1	6.0 ± 0.2	6.0 ± 0.2
		41.1	40.4 ± 0.6	40.0 ± 1.1	40.2 ± 0.7
		184.8	188.4 ± 2.9	187.0 ± 12.6	187.0 ± 0.8
	1-OH-THA	10.1	10.2 ± 1.0	9.4 ± 0.4	10.7 ± 0.7
		44.7	44.7 ± 2.8	45.8 ± 1.5	45.3 ± 0.5
		201.1	208.8 ± 11.0	201.0 ± 9.6	206.9 ± 4.1
	2-OH-THA	3.2	3.1 ± 0.3	3.3 ± 0.3	3.4 ± 0.0
		14.2	13.3 ± 1.7	14.3 ± 0.6	14.6 ± 0.4
		63.8	64.3 ± 7.0	62.7 ± 3.3	65.6 ± 1.5
	4-OH-THA	3.2	3.0 ± 0.3	3.0 ± 0.2	3.1 ± 0.1
		14.0	14.6 ± 0.3	14.0 ± 0.5	14.0 ± 0.5
		63.1	67.4 ± 2.3	65.3 ± 2.2	65.6 ± 1.2
Brain tissue (ng/g)	THA	30.8	29.8 ± 1.2	29.7 ± 1.6	29.7 ± 1.5
		230.9	239.5 ± 7.3	235.1 ± 6.5	238.5 ± 4.8
		769.8	808.2 ± 10.7	797.6 ± 22.6	797.8 ± 20.4
	1-OH-THA	83.8	86.7 ± 3.1	84.8 ± 2.2	82.1 ± 2.5
		251.3	265.7 ± 7.8	256.2 ± 8.2	254.4 ± 4.9
		837.7	861.9 ± 18.8	874.3 ± 11.3	874.8 ± 29.5
	2-OH-THA	26.6	27.2 ± 0.8	27.2 ± 1.1	26.1 ± 1.7
		79.8	85.6 ± 3.5	84.9 ± 3.6	82.7 ± 2.5
		266.0	281.5 ± 9.5	284.6 ± 12.2	286.7 ± 9.9
	4-OH-THA	26.3	27.4 ± 1.3	26.1 ± 2.3	25.3 ± 1.2
		78.9	84.4 ± 4.1	80.9 ± 3.3	80.8 ± 3.1
		263.0	273.1 ± 7.0	276.4 ± 8.1	280.3 ± 13.5

[a] Freeze–thaw at −80 °C and room temperature.
[b] Bench at ambient.
[c] Autosampler at 4 °C.

Table 4
Pharmacokinetic parameters of THA and its metabolites after oral administration of THA at 4 mg/kg in rats ($n=5$).

Parameters	THA	1-OH-THA	2-OH-THA	4-OH-THA
t_{max} (h)	0.5 ± 0.2	0.5 ± 0.2	0.6 ± 0.2	0.5 ± 0.1
C_{max} (ng/ml)	71.8 ± 18.6	303.5 ± 35.3	33.0 ± 3.2	5.6 ± 0.7
$t_{1/2}$ (h)	1.2 ± 0.4	2.0 ± 0.9	3.2 ± 2.0	N.D.
AUC_{0-6h} (ng h/ml)	109.1 ± 28.6	785.5 ± 80.0	99.2 ± 8.4	9.1 ± 2.1

t_{max}: time to the maximum plasma concentration; C_{max}: maximum plasma concentration; $t_{1/2}$: elimination half life; AUC_{0-6h}: area under the plasma concentration–time curve from 0 to 6 h; N.D.: not determined due to low concentration.

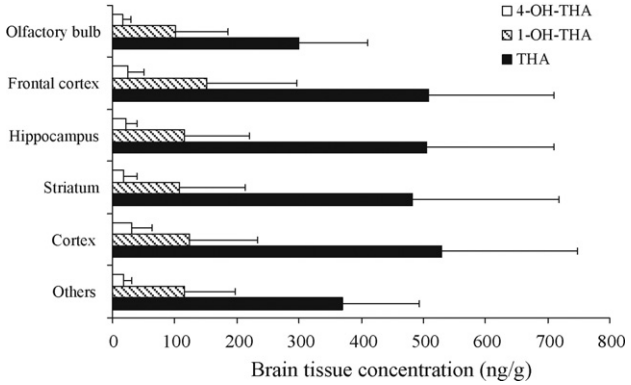

Fig. 4. Distribution of THA, 1-OH-THA and 4-OH-THA in various brain regions at 1 h after oral administration of 12 mg/kg THA (*note*: (i) 2-OH-THA was found to be lower than LLOQ and hence is not presented in this figure; (ii) data represents mean ± SD ($n = 3$); (iii) others represent mixture of midbrain, thalamus, hypothalamus and cerebellum).

I metabolism investigation in both human and rat liver microsomes by Madden [10] and Hooper [8,28].

Fig. 4 shows the brain regional distribution of THA and its major metabolites in rat at 1 h after oral administration of THA at a dose of 12 mg/kg. Plasma concentration of each analyte was also determined (86.1, 538.4, 38.8 and 6.3 ng/ml for THA, 1-OH-THA, 2-OH-THA and 4-OH-THA, respectively). In rat brain, THA was predominant followed by 1-OH-THA and 4-OH-THA. 2-OH-THA was found to be below LLOQ (<10.5 ng/g). In comparison to THA, the lack of 2-OH-THA in brain tissue probably resulted from its lower lipophilicity leading to limited penetration across the blood–brain barrier [27]. Both cortex and hippocampus, which have been associated with memory loss and considered as predominant target sites for AD [3,29], exhibited similar THA concentration level. Olfactory bulb exhibited a slightly lower THA concentration than that in other brain regions. In addition, 1-OH-THA and 4-OH-THA were found to be evenly distributed in all brain regions.

Comparing the average brain and plasma concentrations of the four analytes, THA and 4-OH-THA were found to be preferentially distributed in brain with brain-to-plasma ratios of 5.2 and 3.5, respectively. On the other hand, much lower concentrations of 1-OH-THA and 2-OH-THA were found in the same rat brain with both of their brain-to-plasma ratios less than 0.3. The high brain-to-plasma ratio of THA indicated that THA could easily across the blood–brain barrier.

4. Conclusion

A specific, sensitive and accurate analytical HPLC/FLD method with one-step liquid–liquid extraction has been established and validated for the determination of THA and its three monohydroxylated metabolites in rat plasma and brain tissue. Pharmacokinetic study in rats showed that THA could be rapidly absorbed followed by extensive metabolism into 1-OH-THA, 2-OH-THA and 4-OH-THA. In addition, both THA and 4-OH-THA achieved much higher brain-to-plasma ratios than that of 1-OH-THA and 2-OH-THA.

Acknowledgement

This work is supported by General Research Fund CUHK 480809.

References

[1] A.H. Friedlander, D.C. Norman, M.E. Mahler, K.M. Norman, J.A. Yagiela, Alzheimer's disease: psychopathology, medical management and dental implications, J. Am. Dent. Assoc. 137 (2006) 1240–1251.
[2] W. Li, M. Mak, H. Jiang, Q. Wang, Y. Pang, K. Chen, Y. Han, Novel anti-Alzheimer's dimer Bis(7)-cognitin: cellular and molecular mechanisms of neuroprotection through multiple targets, Neurotherapeutics 6 (2009) 187–201.
[3] D.G. Wilkinson, P.T. Francis, E. Schwam, J. Payne-Parrish, Cholinesterase inhibitors used in the treatment of Alzheimer's disease: the relationship between pharmacological effects and clinical efficacy, Drugs Aging 21 (2004) 453–478.
[4] V.V. Jogani, P.J. Shah, P. Mishra, A.K. Mishra, A.R. Misra, Nose-to-brain delivery of tacrine, J. Pharm. Pharmacol. 59 (2007) 1199–1205.
[5] W.K. Summers, Tacrine (THA, Cognex (R)), J. Alzheimers Dis. 2 (2000) 85–93.
[6] B.R. Jasti, V.P. Marasanapalle, J.R. Crison, J.W. Ma, X.L. Li, Investigation of some factors contributing to negative food effects, Biopharm. Drug Dispos. 30 (2009) 71–80.
[7] S. Madden, V. Spaldin, B.K. Park, Clinical pharmacokinetics of tacrine, Clin. Pharmacokinet. 28 (1995) 449–457.
[8] S. Madden, T.F. Woolf, W.F. Pool, B.K. Park, An investigation into the formation of stable, protein-reactive and cytotoxic metabolites from tacrine in vitro. Studies with human and rat liver microsomes, Biochem. Pharmacol. 46 (1993) 13–20.
[9] T.F. Woolf, W.F. Pool, S.M. Bjorge, T. Chang, O.P. Goel, C.F. Purchase II, M.C. Schroeder, K.L. Kunze, W.F. Trager, Bioactivation and irreversible binding of the cognition activator tacrine using human and rat liver microsomal preparations. Species difference, Drug Metab. Dispos. 21 (1993) 874–882.
[10] S. Madden, V. Spaldin, R.N. Hayes, T.F. Woolf, W.F. Pool, B.K. Park, Species variation in the bioactivation of tacrine by hepatic microsomes, Xenobiotica 25 (1995) 103–116.
[11] R.S. Hsu, G.M. Shutske, E.M. Dileo, S.M. Chesson, A.R. Linville, R.C. Allen, Identification of the urinary metabolites of tacrine in the rat, Drug Metab. Dispos. 18 (1990) 779–783.
[12] W.F. Pool, M.D. Reily, S.M. Bjorge, T.F. Woolf, Metabolic disposition of the cognition activator tacrine in rats, dogs, and humans. Species comparisons, Drug Metab. Dispos. 25 (1997) 590–597.
[13] J. Birks, G.G. Wilcock, Velnacrine for Alzheimer's disease, Cochrane Database Syst. Rev. (2004), CD004748.
[14] M.F. Murphy, S.T. Hardiman, R.J. Nash, F.J. Huff, J.J. Demkovich, C. Dobson, U.E. Knappe, Evaluation of HP 029 (velnacrine maleate) in Alzheimer's disease, Ann. N.Y. Acad. Sci. 640 (1991) 253–262.
[15] J. Patocka, D. Jun, K. Kuca, Possible role of hydroxylated metabolites of tacrine in drug toxicity and therapy of Alzheimer's disease, Curr. Drug Metab. 9 (2008) 332–335.
[16] J.L. Domingo, Aluminum and other metals in Alzheimer's disease: a review of potential therapy with chelating agents, J. Alzheimers Dis. 10 (2006) 331–341.
[17] Y.C. Wong, Z. Zuo, Intranasal delivery—modification of drug metabolism and brain disposition, Pharm. Res. 27 (2010) 1208–1223.
[18] V.V. Jogani, P.J. Shah, P. Mishra, A.K. Mishra, A.R. Misra, Intranasal mucoadhesive microemulsion of tacrine to improve brain targeting, Alzheimer Dis. Assoc. Disord. 22 (2008) 116–124.
[19] R.S. Hsu, E.M. DiLeo, S.M. Chesson, High-performance liquid chromatography for the determination of tacrine and its metabolites in plasma, J. Chromatogr. 530 (1990) 170–176.
[20] L.L. Hansen, J.T. Larsen, K. Brosen, Determination of tacrine and its metabolites in human plasma and urine by high-performance liquid chromatography and fluorescence detection, J. Chromatogr. B: Biomed. Sci. Appl. 712 (1998) 183–191.
[21] G. Aymard, M. Cayre-Castel, C. Fernandez, L. Lacomblez, B. Diquet, High-performance liquid chromatography with ultraviolet and fluorimetric detection for the simultaneous determination of tacrine, nimodipine, and their respective metabolites in the plasma of patients with Alzheimer disease, Ther. Drug Monit. 20 (1998) 422–429.
[22] D.B. Haughey, C.A. McNaney, M.S. Collis, R.R. Brown, P.H. Siedlik, L. Balogh, P.M. Klockowski, Simultaneous determination of tacrine and 1-hydroxy-, 2-hydroxy-, and 4-hydroxytacrine in human plasma by high-performance liquid chromatography with fluorescence detection, J. Pharm. Sci. 83 (1994) 1582–1585.
[23] D. Bao, V. Thanabal, W.F. Pool, Determination of tacrine metabolites in microsomal incubate by high performance liquid chromatography–nuclear magnetic resonance/mass spectrometry with a column trapping system, J. Pharm. Biomed. Anal. 28 (2002) 23–30.
[24] K.C. Cloos, T. Hondo, Rapid determination of tacrine and other drug metabolites in microsomal incubate by newly developed targeting algorithm on UHPLC/TOFMS, J. Chromatogr. B: Anal. Technol. Biomed. Life Sci. 877 (2009) 4171–4174.
[25] L.A. Marques, J. Kool, F. de Kanter, H. Lingeman, W. Niessen, H. Irth, Production and on-line acetylcholinesterase bioactivity profiling of chemical and biological degradation products of tacrine, J. Pharm. Biomed. Anal. 53 (2010) 609–616.
[26] US Food and Drug Administration, Guidance for Industry, Bioanalytical Method Validation, Centre for Drug Evaluation and Research (CDER), Rockville, 2001.
[27] W.P. McNally, W.F. Pool, M.W. Sinz, P. Dehart, D.F. Ortwine, C.C. Huang, T. Chang, T.F. Woolf, Distribution of tacrine and metabolites in rat brain and plasma after single- and multiple-dose regimens. Evidence for accumulation of tacrine in brain tissue, Drug Metab. Dispos. 24 (1996) 628–633.
[28] W.D. Hooper, W.F. Pool, T.F. Woolf, J. Gal, Stereoselective hydroxylation of tacrine in rats and humans, Drug Metab. Dispos. 22 (1994) 719–724.
[29] H. Yu, W.M. Li, K.K. Kan, J.M. Ho, P.R. Carlier, Y.P. Pang, Z.M. Gu, Z. Zhong, K. Chan, Y.T. Wang, Y.F. Han, The physicochemical properties and the in vivo AChE inhibition of two potential anti-Alzheimer agents, bis(12)-hupyridone and bis(7)-tacrine, J. Pharm. Biomed. Anal. 46 (2008) 75–81.

Journal of Pharmaceutical and Biomedical Analysis 61 (2012) 64–69

Contents lists available at SciVerse ScienceDirect

Journal of Pharmaceutical and Biomedical Analysis

journal homepage: www.elsevier.com/locate/jpba

Quantitative analysis of mephedrone using liquid chromatography tandem mass spectroscopy: Application to human hair

Syeda A.B. Shah[a], Nawed I.K. Deshmukh[a], James Barker[a,*], Andrea Petróczi[b], Paul Cross[c], Roland Archer[a], Declan P. Naughton[b]

[a] School of Pharmacy and Chemistry, Kingston University, London, UK
[b] School of Life Sciences, Kingston University, London, UK
[c] School of the Environment, Natural Resources and Geography, Bangor University, UK

ARTICLE INFO

Article history:
Received 12 October 2011
Received in revised form
10 November 2011
Accepted 24 November 2011
Available online 3 December 2011

Keywords:
Mephedrone
Metabolites
4-Methylephedrine
4-Methylnorephedrine: LC–MS/MS

ABSTRACT

Recent abuse of designer drugs such as mephedrone has presented a requirement for sensitive, reliable and reproducible methods for the detection of these controlled drugs in different matrices. This study focuses on a fully developed validated method for the quantitative analysis of mephedrone and its two metabolites 4-methylephedrine and 4-methylnorephedrine in human hair. The calibration curve was found to be linear in the range 5–100 pg/mg for mephedrone and 10–150 pg/mg for 4-methylephedrine and 4-methylnorephedrine. The method was successfully validated for the intraday precision, interday precision, limit of detection, accuracy and extraction recovery. Five out of 154 hair samples were confirmed to be positive for mephedrone. Due to the structural similarities to other methcathinones and amphetamines, one can propose the metabolism for mephedrone based on a similar pathway that has been previously used for these psychoactive drugs. The outlined method can be valuable for the future detection of mephedrone and its two metabolites in hair.

© 2011 Elsevier B.V. All rights reserved.

1. Introduction

'Legal high' is a term given to chemicals which possess psychoactive activity in humans, but are not subject to prohibition by law [1]. In the last few years, buying legal highs from the internet has become common practice for drug users. This is, in part, due to their structural similarity to controlled psychoactive substances such as phenethylamines and cathinones [2–4]. Mephedrone, sometimes referred to as 'meow', 'mcat' and 'bubbles' is a β-ketoamphetamine and has a structure similar to methcathinone, which in turn is the *N*-methyl analogue of the natural product cathinone [2]. Cathinone can be extracted from the leaves of an African and Middle Eastern plant *Catha edulis* or 'Khat' [4,5]. The alkaloid content of the fresh leaves is responsible for the psychoactive stimulating effects [4]. Mephedrone has been routinely sold on the internet as plant feed, with an accompanied warning of 'not suitable for human consumption'. However, in April 2010 it was specifically named and hence controlled in UK under the Misuse of Drugs Act 1971 as a Class B substance [1,6]. It has also been banned in the majority of other European countries [2]. The use of mephedrone is more common in males than females and it is reported to be one of the most commonly abused psychotropic drugs [1].

The popularity of use of these psychoactive drugs has created a demand for sensitive, robust and reliable analytical methods for their identification and quantification in different matrices. Gas chromatography mass spectrometry (GC–MS) has routinely been used for the detection of mephedrone in matrices such as blood and urine [3,6,7]. Recently, liquid chromatography mass spectroscopy (LC–MS) has also been employed for analysing blood samples for the detection of mephedrone [4]. Compared to urine and blood, hair samples can provide information on the long term history of the individual's intake of controlled drugs depending on the pharmacokinetic properties of the drug in question [8,9]. Also, blood and urine samples require storage at −20 °C in the presence of preservatives until analysis, for mephedrone [3]. Thus, hair is gaining potential interest for the detection of parent drugs in doping control [8]. The drugs bind to melanin which is the major component of hair [8]. Generally, urinalysis is carried out to determine the presence of metabolites of the controlled drugs and it is often difficult to detect the parent drug in urine. In addition, the matrix effects for urine and blood are much greater than hair [8].

In the scientific literature, there is limited information available on the metabolism of mephedrone in humans. As the structure of

* Corresponding author. Tel.: +44 020 8547 7981; fax: +44 020 8417 7562.
E-mail addresses: K0507911@kingston.ac.uk (S.A.B. Shah), K0630928@kingston.ac.uk (N.I.K. Deshmukh), J.Barker@kingston.ac.uk (J. Barker), A.Petroczi@kingston.ac.uk (A. Petróczi), paul.cross@bangor.ac.uk (P. Cross), RArcher@hssd.gov.gg (R. Archer), D.Naughton@kingston.ac.uk (D.P. Naughton).

0731-7085/$ – see front matter © 2011 Elsevier B.V. All rights reserved.
doi:10.1016/j.jpba.2011.11.026

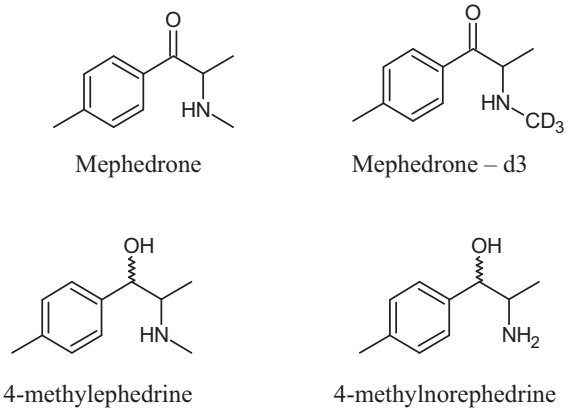

Fig. 1. Structures of mephedrone, 4-methylephedrine, 4-methylnorephedrine and mephedrone-d_3 (internal standard).

mephedrone is substantially similar to other psychoactive drugs such as methcathinone and methamphetamine, one can tentatively propose a metabolism of mephedrone on a similar basis. There are a number of different pathways by which this drug could be metabolised. The two metabolites analysed in this study are 4-methylephedrine and 4-methylnorephedrine [7,10–13]. The structures of mephedrone and its two metabolites are depicted in Fig. 1. The aim of this study was to develop an analytical method for the quantitative analysis of mephedrone and for two of its metabolites 4-methylephedrine and 4-methylnorephedrine in hair using LC–MS/MS.

2. Materials and methods

2.1. Hair specimen

Following ethical approval from two higher education institutions, hair samples were obtained from 154 healthy volunteers (95 male, 59 females) aged 18–56 years old [14]. Blank hair samples were obtained from two healthy individuals.

2.2. Chemicals and consumables

HPLC grade methanol, acetonitrile, water, and hexane, along with reagent grade ethyl acetate, ethanol, dichloromethane, chloroform and formic acid were purchased from Fisher Scientific UK Ltd. (Loughborough, UK). Tris HCl buffer and Cleland's reagent were obtained from VWR (Lutterworth, UK). Proteinase K was purchased from Sigma Aldrich (Dorset, UK). The metabolites 4-methylephedrine hydrochloride and 4-methylnorephedrine hydrochloride were synthesised in-house by borohydride reduction of mephedrone and 4-methylcathinone, respectively, at Kingston University (London, UK). Mephedrone hydrochloride and mephedrone-d_3 hydrochloride (internal standard) were purchased from LGC standards (Teddington, UK). An Agilent SB-C18 column (2.1 μm × 150 mm × 1.8 μm) was purchased from Agilent Technologies UK Ltd. (Wokingham, UK).

2.3. Instrumentation

Analyses were performed on a Thermoscientific liquid chromatography–tandem mass spectrometry (LC–MS/MS) system consisted of an Accela UPLC system (Thermo Scientific, UK Ltd., Loughborough, Leicestershire, UK) coupled to a Triple Quadrupole TSQTM mass spectrometer (Thermo Electron Corp., UK). This was operated in selective reaction monitoring (SRM) mode using the conditions given in Table 1 with detection parameters given in Table 2.

Table 1
Chromatography conditions for the separation of the compounds.

LC run time (min)	Acetonitrile (%)	Water (%)
0	65	35
3	100	0
4	100	0
5	65	35
10	65	35

The column was maintained at 50 °C and the auto sampler tray was set at 10 °C. The flow rate was 200 μL/min and the injection volume was 3.0 μL.

The capillary temperature was maintained at 300 °C and a voltage of 4000 V was employed. The collision pressure was kept at 1.5 mTorr. The fragmentation pathways of all the analytes are shown in Fig. 2.

2.4. Hair digestion and extraction

2.4.1. Decontamination

The hair samples were decontaminated by rinsing with 2 mL dichloromethane for 2 min (twice) at room temperature. Decontamination ensured the removal of contaminants from the surface of hair, which may interfere with the analysis [15]. After decontamination, the hair samples were air dried before cutting into very fine segments (*ca.* 1 mm length) using scissors.

2.5. Digestion

Initially, hair digestion was carried out by incubating the hair samples with 1 mL of 1 M sodium hydroxide solution at 95 °C for 10 min. However, this led to the complete degradation of analytes. Hence, enzymatic digestion was employed alternatively. Enzymatic digestion was carried out by placing the fine hair segments (50 mg) in a glass vial containing Cleland's reagent (100 mg) and enzyme proteinase K (15 mg). The internal standard mephedrone-d_3 (100 μL) at 40 pg/mg was added to the mixture. The mixture was finally incubated with Tris buffer (1 mL) for 2 h at 37.5 °C with constant stirring.

2.6. Extraction

Liquid–liquid extraction was optimised for mephedrone using hexane (3 mL), and for the metabolites using a mixture of chloroform, ethanol and diethyl ether (3 mL in total) with the ratio of 3:1:1. The contents were mixed using a vortex mixer and centrifuged at 5 °C for 5 min at 1750 × *g*. The organic layers were separated and pooled together in a glass tube. The organic layer was then dried using nitrogen gas and reconstituted with 200 μL of acetonitrile.

2.7. Method validation

Method validation was carried out in order to establish the sensitivity, specificity, selectivity, linearity, limit of detection (LOD), limit of quantification (LOQ), inter and intraday precision and accuracy and percentage recoveries. The metabolites when diluted in methanol gave better sensitivity as compared to acetonitrile, whereas mephedrone gave a similar sensitivity in both solvents. A calibration curve was obtained by spiking blank hair samples with known concentrations of the drugs in the range of 5–100 pg/mg for mephedrone and 10–150 pg/mg for 4-methylephedrine and 4-methylnorephedrine. The internal

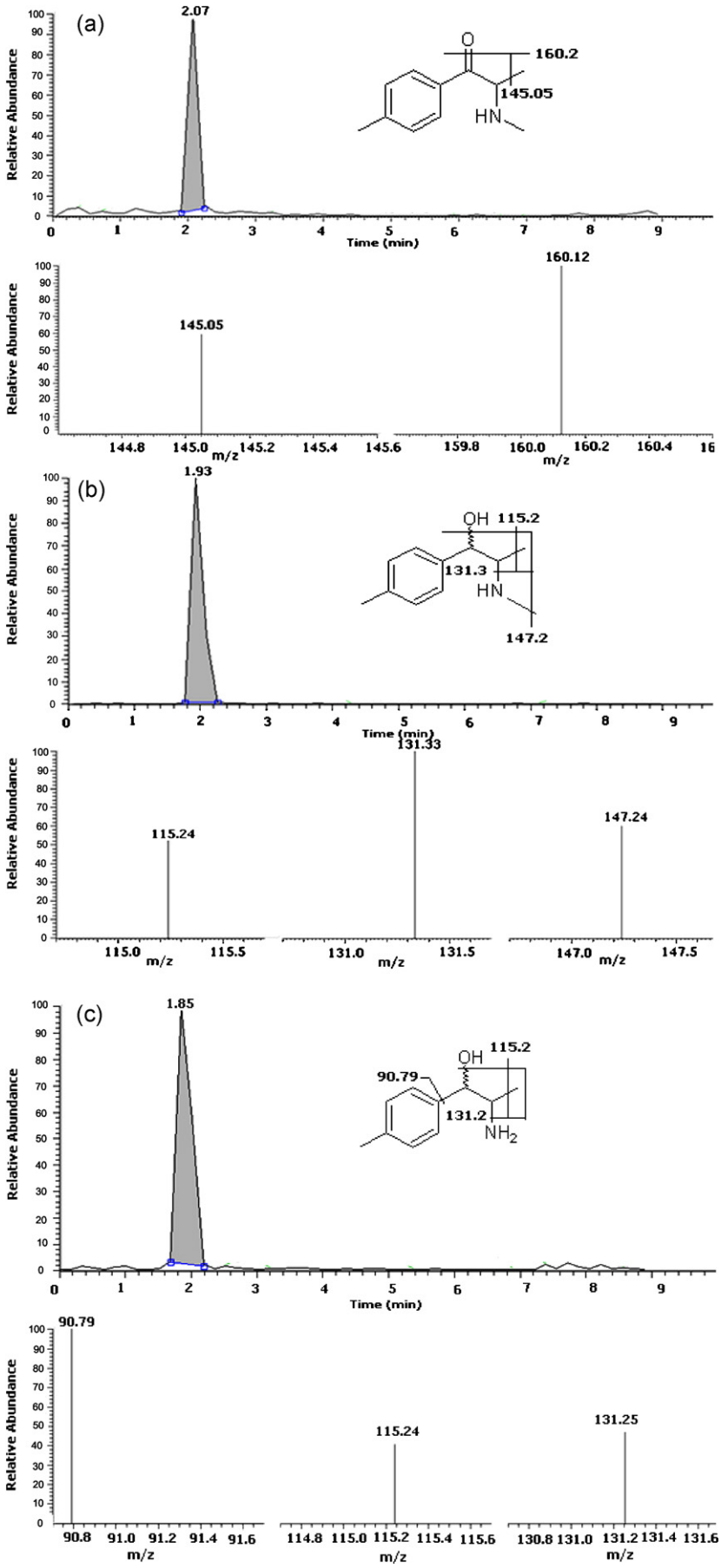

Fig. 2. LC–MS/MS chromatogram and CID spectra of (a) mephedrone, (b) 4-methylephedrine and (c) 4-methylnorephedrine in hair at concentrations of 10 pg/mg, 20 pg/mg and 20 pg/mg, respectively.

Table 2
Ion transitions, retention time (RT) and collision energies used for the analysis of the analytes and the internal standard.

Compound	RT (min)	Precursor ions (*m*/*z*)	Product ions (*m*/*z*)	Collision energy (eV)
Mephedrone	2.07	178.1	160.1	10
			145.1	18
4-Methylephedrine	1.93	180.2	147.2	19
			131.3	18
			115.2	39
4-Methylnorephedrine	1.85	166.2	131.2	14
			115.2	33
			90.8	24
Mephedrone-d_3	1.98	181.2	163.2	17
			148.2	20

Table 3
Precision and accuracy for intraday and interday of the three drugs at four different concentrations.

Compound	Concentration (pg/mg)	Precision RSD (%)		Accuracy %
		Intraday $N = 6+6+6+6$	Interday $N = 18+18+18+18$	
Mephedrone	5	0.62	0.8	99.15
	10	0.4	0.7	106.34
	20	2.11	1.7	103.16
	40	2.56	4.5	107.53
4-Methylephedrine	10	0.6	0.9	114.59
	20	0.75	0.7	110.76
	50	0.8	4	107.02
	100	4.92	3.4	98.52
4-Methylnorephedrine	10	0.54	1.1	107.98
	20	0.2	0.7	106.51
	50	2.91	2	97.6
	100	6.97	7.3	100.67

Table 4
Extraction recoveries of the three drugs at three different concentrations.

Compound	Concentration (pg/mg)	Recovery (%) $N = 6+6+6$	Regression coefficient	Regression equation
Mephedrone	5	90.36	0.999	$y = 0.112x + 0.429$
	20	110.37		
	40	108.10		
4-Methylephedrine	10	106.16	0.990	$y = 0.012x + 0.033$
	20	98.37		
	100	101.87		
4-Methylnorephedrine	10	100.23	0.990	$y = 0.008x + 1.389$
	20	96.78		
	100	101.32		

standard mephedrone-d_3 (100 μL) was added to all the standards with a final concentration of 40 pg/mg. The extraction recovery was validated for mephedrone and its metabolites at three different concentrations using six replicates by comparing the extracted samples with non-extracted samples.

3. Results and discussion

3.1. Validation results

There were no chromatographic interferences found due to the endogenous substances present in the blank (control) hair that was analysed using the above chromatographic conditions. The precision, accuracy and recoveries lie within the limits set by the FDA guidelines [16]. The validation data are given in Tables 3–5.

Table 5
Signal to noise ratios for the LOD and LOQ.

Compound	S/N for LOD $N = 6$	S/N for LOQ $N = 6$
Mephedrone	7	11
4-Methylephedrine	5	10
4-Methylnorephedrine	4	10

LOD and LOQ values for mephedrone were 2.5 pg/mg and 5 pg/mg, respectively. For 4-methylephedrine and 4-methylnorephedrine the LOD was 5 pg/mg and the LOQ 10 pg/mg.

Out of the 154 samples analysed, mephedrone was detected in only five samples. However, the metabolites were not detected in any of the samples analysed. However, owing to the method used for data and sample collection [14], it is impossible to link admission of mephedrone use to individuals, or individual samples. Out of the five samples, mephedrone could be successfully quantified in only one sample. It was found to be present at a concentration of 21.11 pg/mg. Fig. 3 shows the chromatogram and mass spectra of the quantified positive sample.

The results confirm that the LC–MS/MS method developed for mephedrone and its two metabolites is sensitive and robust. There was no significant change in column performance or the pressure after making several injections. Only 50 mg hair is required for the detection of the mephedrone and its metabolites. Hair analysis is capable of providing a long term history of drug use and any kind of hair treatment such as bleaching cannot affect the incorporation of the drug into hair. Thus, it can be used to compliment urinalysis for identifying routine drug users [17]. In this study, the metabolites could not be detected in the hair samples. In general, high polarity

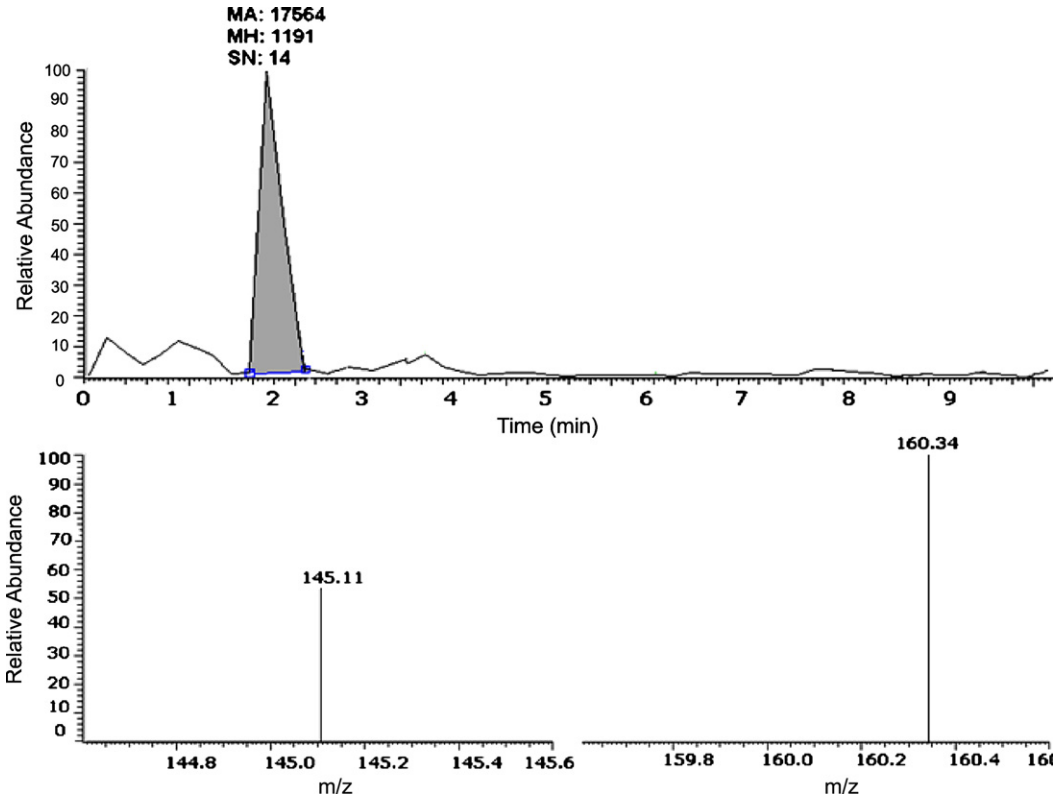

Fig. 3. LC–MS/MS chromatogram and CID spectra of the positive samples at concentrations of 21.11 pg/mg.

metabolites which are destined to be excreted in urine are difficult to detect in hair. In contrast, the parent drugs are lipophilic and can become incorporated into the hair [8]. It should be noted that as mephedrone is not smoked, the route of entry via environmental exposure would not provide a false positive for hair analyses.

There has been very little research carried out on the metabolism of mephedrone. Due to the structural similarities of mephedrone to methcathinones and methamphetamines, the metabolism of mephedrone has been proposed to follow a similar pathway. The pathway involves the hydroxylation of the methylene group and the second metabolite is formed by *N*-demethylation, thus forming a primary amine. However, there is a possibility of other pathways for the metabolism of mephedrone [7,10–13].

4. Conclusion

The present study describes a rapid and replicable method for the quantitative analysis of mephedrone and its two metabolites in human hair. The method is quite sensitive with an LOQ of 5 pg/mg for mephedrone and 10 pg/mg for its two metabolites. The absence of any interference on the chromatograms shows that the method is highly selective. The method is suitable for the future detection and quantification of mephedrone and its metabolites.

Author contributions

J.B., A.P. and D.P.N. conceived and designed the study. S.A.B.S. performed the analysis. R.A. synthesised and provided the metabolites. P.C. provided samples. S.A.B.S. and N.I.K.D. drafted the paper. J.B., A.P., D.P.N. and S.A.B.S. interpreted the results. All authors contributed to writing, and approved the final manuscript.

Acknowledgements

The authors thank Helen Taft and Christiana Adesanwo for their help with collecting hair samples.

References

[1] I. Vardakoua, C. Pistos, C.H. Spiliopouloua, Drugs for youth via internet and the example of mephedrone, Toxicol. Lett. 201 (2011) 191–195.
[2] E.Y. Santali, A. Cadogan, N. Daeid, K.A. Savage, O.B. Sutcliffe, Synthesis, full chemical characterisation and development of validated methods for the quantification of (±)-4'-methylmethcathinone (mephedrone): a new legal high, J. Pharm. Biomed. Anal. 56 (2011) 246–255.
[3] K.J. Lusthof, R. Oosting, A. Maes, M. Verschraagen, A. Dijkhuizen, A.G.A. Sprong, A case of extreme agitation and death after the use of mephedrone in The Netherlands, Forensic Sci. Int. 206 (2011) e93–e95.
[4] L.K. Sørensen, Determination of cathinones and related ephedrines in forensic whole-blood samples by liquid-chromatography–electrospray tandem mass spectrometry, J. Chromatogr. B 879 (2011) 727–736.
[5] D.M. Wood, D. Davies, M. Puchnarewicz, J. Button, R. Archer, H. Ovaska, J. Ramsey, T. Lee, D.W. Holt, P.I. Dargan, Recreational use of mephedrone (4-methylmethcathinone, 4-MMC) with associated sympathomimetic toxicity, J. Med. Toxicol. 6 (2010) 327–330.
[6] H. Torrance, G. Cooper, The detection of mephedrone (4-methylmethcathinone) in 4 fatalities in Scotland, Forensic Sci. Int. 202 (2010) e62–e63.
[7] M.R. Meyer, J. Wilhelm, F.T. Peters, Beta-keto amphetamines: studies on the metabolism of the designer drug mephedrone and toxicological detection of mephedrone, butylone, and methylone in urine using gas chromatography–mass spectroscopy, Anal. Bioanal. Chem. 397 (2010) 1225–1233.
[8] N. Deshmukh, I. Hussain, J. Barker, A. Petroczi, D.P. Naughton, Analysis of anabolic steroids in human hair using LC–MS/MS, Steroids 75 (2010) 710–714.
[9] P. Kintz, V. Cirimele, V. Demestre-Toulet, B. Ludes, Doping control for nandrolone using hair analysis, J. Pharm. Biomed. Anal. 24 (2001) 1125–1130.
[10] H.T. Kamata, N. Shima, K. Zaitsu, T. Kamata, A. Miki, M. Nishikawa, M. Katagi, H. Tsuchihashi, Metabolism of the recently encountered designer drug, methylone, in human and rats, Xenobiotica 36 (2006) 709–723.
[11] E. Pawlik, G. Plasser, H. Mahler, Studies on the phase I metabolism of the new designer drug 3-fluoromethcathinone using rabbit liver slices, Int. J. Legal. Med. (2011), doi:10.1007/s00414-011-0601-6.

[12] J. Caldwell, L.G. Dring, R.T. Williams, Metabolism of [^{14}C] methamphetamine in man, the guinea pig and the rat, Biochem. J. 129 (1972) 11–22.
[13] D.A. Williams, T.A. Lemke (Eds.), Foye's Principles of Medicinal Chemistry, 5th ed., Lippincott, Williams & Wilkins, USA, 2002, p. 227.
[14] A. Petróczi, T. Nepusz, P. Cross, H. Taft, S. Shah, N. Deshmukh, J. Schaffer, M. Shane, C. Adesanwo, J. Barker, D.P. Naughton, New non-randomised model to assess the prevalence of discriminating behaviour: a pilot study on mephedrone, Susbst. Abuse Treat. Prev. Policy 6 (2011) , doi:10.1186/1747-597X-6-20.
[15] F. Musshoff, B. Madea, New trends in hair analysis and scientific demands on validation and technical notes, Forensic Sci. Int. 165 (2007) 204–215.
[16] Guidance for Industry Bioanalytical Method Validation, http://www.fda.gov/downloads/Drugs/GuidanceComplianceRegulatoryInformation/Guidances/ucm070107.pdf, 2001 (accessed 16.09.11).
[17] R.L. DuPont, W.A. Baumgartner, Drug testing by urine and hair analysis: complementary features and scientific issues, Forensic Sci. Int. 70 (1995) 63–76.

Journal of Pharmaceutical and Biomedical Analysis 61 (2012) 70–77

Contents lists available at SciVerse ScienceDirect

Journal of Pharmaceutical and Biomedical Analysis

journal homepage: www.elsevier.com/locate/jpba

Determination of alamifovir disoproxil fumarate and its active metabolite 602076 in rat plasma by LC–MS/MS: Application to a pharmacokinetic study

Pingping Zhang[a,b], Jifen Guo[a,*], Fanhua Meng[a], Lu Sun[b], Bohua Zhong[a], Yimin Zhao[a]

[a] Beijing Institute of Pharmacology and Toxicology, 27 Taiping Road, Beijing 100850, PR China
[b] Shenyang Pharmaceutical University, 103 Wenhua Road, Shenyang 110016, PR China

ARTICLE INFO

Article history:
Received 23 September 2011
Received in revised form
25 November 2011
Accepted 27 November 2011
Available online 6 December 2011

Keywords:
Alamifovir disoproxil fumarate
LC–MS/MS
Pharmacokinetics
Metabolite

ABSTRACT

Alamifovir disoproxil fumarate (ADF) is a novel ester prodrug of alamifovir, which is currently as a promising antiviral candidate under investigation. This paper is aimed to develop rapid, sensitive and specific LC–MS/MS methods for the quantification of ADF and its active metabolite 602076 in rat plasma. According to the significantly different chemical properties of the compounds, two sets of liquid chromatography and ionization modes were used for determining the concentration of ADF and 602076 in rat plasma, separately. Following liquid–liquid extraction with *n*-hexane:dichloromethane:isopropanol (100:50:5, v/v/v), the ADF and internal standard (gliclazide) were separated on a Phenomenex Gemini C_{18} column (150 mm × 2.0 mm, 5 μm) with a mobile phase consisting of methanol:water:formic acid (70:30:0.1, v/v/v). A tandem mass spectrometer equipped with electrospray ionization (ESI) source was used as the detector and operated in positive ion mode. The metabolite 602076 and the internal standard ZHY81018 were extracted from plasma by protein precipitation with acetonitrile. Chromatographic separation was performed on a Capcell MG C_{18} column (150 mm × 2.0 mm, 5 μm) with a mobile phase consisting of acetonitrile and water (20:80, v/v). The MS/MS detection was operated in negative ion mode using an ESI source. The linear concentration ranges of the calibration curves were 2.5–500 ng/mL for ADF and 2.5–1000 ng/mL for 602076. The intra-assay RSD for quality control (QC) samples were from 3.3% to 6.7% for ADF, and 4.0% to 6.1% for 602076. The inter-assay RSD for QC samples were from 4.9% to 14.7% for ADF, and 2.6% to 4.4% for 602076. The relative errors for QC samples were from −10.6% to 1.9% for ADF, and 0.2% to 2.6% for 602076. The methods were successfully applied in the investigation of the pharmacokinetic profile of ADF, alamifovir and 602076 in rats. The results showed that ADF was rapidly metabolized to its active metabolite 602076 after oral absorption, with no detectable unchanged drug. The oral bioavailability of ADF was about 3 times higher than that of alamifovir.

© 2011 Elsevier B.V. All rights reserved.

1. Introduction

Hepatitis B virus (HBV) infection is a serious healthcare problem which caused global attention. Two billion people have evidence of HBV exposure worldwide, and an estimated 400 million are actively infected. In hyper endemic areas, such as China, Southeast Asia, Western Pacific, and sub-Saharan Africa, the carrier rate exceeds 8% [1,2]. Approximately 25% of the infected patients developed liver cirrhosis or hepatocellular carcinoma. Furthermore, all chronic carriers suffer from significant disease-associated malaise during their lifetime. HBV infection results in a million deaths each year and is among the 10 leading killer diseases listed by the World Health Organization [3].

Successful therapy of patients with hepatitis B requires long-term suppression of viral replication. Until now, there are only few agents, namely α-interferon and nucleoside analogues (lamivudine, adefovir dipivoxil, entecavir and tenofovir disoproxil) are approved for the treatment of HBV. However, all these drugs have been found to be able to cause serious side effects [4–6]. Thus, there is clearly the need for new antiviral agents in the treatment of HBV infection. Alamifovir {2-amino-6-(4-methoxyphenylthio)-9-[2-(phosphonomethoxy)ethyl]purine bis(2,2,2-trifluoroethyl)ester, also known as MCC-478}, is a novel nucleoside analogue which was synthesized as a derivative of adefovir [7]. It showed a substantially higher (ca. 80-fold) anti-HBV activity than lamivudine, despite no significant anti-human immunodeficiency virus activity [8]. Compared to the conventional nucleoside/nucleotide reverse transcriptase inhibitors, alamifovir appeared to have a novel mechanism of action by that it could inhibit protein priming and packaging reactions, and thereby decrease HBV replication [9]. Although alamifovir was rapidly absorbed, there was limited

* Corresponding author. Tel.: +86 10 66931614; fax: +86 10 68211656.
E-mail address: guojifen@sohu.com (J. Guo).

0731-7085/$ – see front matter © 2011 Elsevier B.V. All rights reserved.
doi:10.1016/j.jpba.2011.11.031

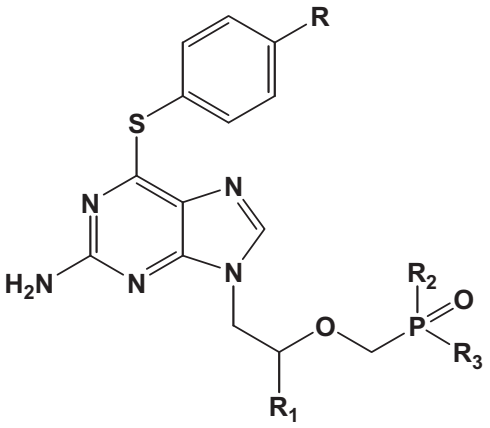

Compound	R	R_1	R_2	R_3
Alamifovir	OCH_3	H	OCH_2CF_3	OCH_2CF_3
602074	OCH_3	H	OCH_2CF_3	OH
602075	OH	H	OCH_2CF_3	OH
602076	OCH_3	H	OH	OH
ADF	OCH_3	H	$OCH_2OCOOCH(CH_3)_2$	$OCH_2OCOOCH(CH_3)_2$
ZHY81018	OCH_3	CH_3	OH	OH

Fig. 1. Chemical structures of alamifovir, 602074, 602075, 602076, ADF and ZHY81018.

systemic exposure due to its rapid hydrolysis and formation of at least three metabolites. This fact suggested that alamifovir acts as a prodrug. The major metabolites (chemical structures see Fig. 1) were 602074 and 602076, with 602075 detectable only in higher-dose groups [10]. These metabolites have also been found to have anti-HBV activity. However, the cytotoxicity of 602074, which is the major metabolite of alamifovir in humans, is significantly higher than that of the parent drug and the metabolite 602076. In order to diminish the side effects of alamifovir, some structural analogues of alamifovir were designed and synthesized. ADF (chemical structure see Fig. 1), a novel derivative of alamifovir, was synthesized and developed by Chinese scientists. It was found to be a promising anti-HBV candidate in primary evaluation [11]. The anti-HBV activity of ADF was 100 times higher than that of alamifovir [12].

The aim of this study is to develop rapid, sensitive and specific LC–MS/MS methods for the quantification of ADF and its active metabolite 602076 in rat plasma. To date, there is still no paper published that described in detail the measurement of alamifovir and its metabolites in biological samples, although individual labs may have validated assays. We report herein the validated LC–MS/MS methods for the detection of ADF and its active metabolite 602076 for the first time. The methods were successfully applied to determine the pharmacokinetic profile of ADF, alamifovir and 602076 in rats. The pharmacokinetic data measured for the active metabolite 602076 showed that the oral bioavailability of ADF was much higher (about 3 times) than that of alamifovir.

2. Experimental

2.1. Chemicals and reagents

ADF, alamifovir, 602076 and ZHY81018 were synthesized and supplied by the Beijing Institute of Pharmacology and Toxicology (Beijing, China). The purities of these compounds were found higher than 97% by HPLC analysis. Gliclazide was obtained from the National Institute for the Control of Pharmaceutical and Biological Products (Beijing, China). Methanol (HPLC grade) was purchased from Fischer Scientific (Fair Lawn, NJ, USA). Acetonitrile (HPLC grade), *n*-hexane and dichloromethane were purchased from Ourchem (Sinopharm Chemical Reagent Co., Ltd, Shanghai, China). All other chemicals and solvents used were purchased from Beijing Chemical Reagent Factory (Beijing, China). Wahaha (Hangzhou, China) deionized water was used throughout the study.

2.2. Instrumentation

An Agilent 1100 system (Palo Alto, CA, USA) consisting of a vacuum degasser, a quaternary pump, and an autosampler was used for solvent and sample delivery. An AB MDS Sciex API 3000 triple-quadrupole mass spectrometer (Concord, Ontario, Canada) equipped with a Turbo IonSpray ESI source was used for mass analysis and detection. Analyst 1.4 software (AB MDS Sciex) was used for data acquisition.

2.3. Liquid chromatographic and mass spectrometric conditions

The chromatographic separation for ADF was achieved by using a Phenomenex Gemini C_{18} column (150 mm × 2.0 mm, 5 μm; Phenomenex, Torrance, CA, USA) with the mobile phase consisting of methanol–water–formic acid (70:30:0.1, v/v/v). The analysis of 602076 was carried out on a Capcell Pak MG C_{18} column (150 mm × 2.0 mm, 5 μm; Shiseido, Japan) with the mobile phase consisting of acetonitrile–water (20:80, v/v). A C_{18} guard column (4.0 × 3.0 mm, 5 μm; Phenomenex, Torrance, CA, USA) was used throughout the entire study with isocratic elution. The flow rates for both acquisitions were set at 0.3 mL/min.

Mass spectrometric detection was conducted on an API 3000 triple quadrupole mass spectrometer equipped with an ESI

Table 1
Mass spectrometric conditions for the analytes and internal standards.

	Precursor ion	Product ion	CE (V)	DP (V)	FP (V)	NEB (Unit)	CUR (Unit)	CAD (Unit)	IonSpray (kV)
$[M+H]^+$									
ADF	644.3	394.2	35	60	160	3	12	4	5
Gliclazide	324.0	127.0	25	60	160	3	12	4	5
$[M-H]^-$									
602076	410.0	272.0	−32	−60	−140	8	11	5	−4.2
ZHY81018	424.3	272.1	−32	−60	−140	8	11	5	−4.2

interface operated in positive mode for ADF and negative mode for 602076. The optimized MS parameters were presented in Table 1.

2.4. Preparation of standard and quality control samples

Stock solutions of the analytes were prepared at 1 mg/mL in methanol and stored at −20 °C. A series of standard working solutions for ADF and 602076 were prepared by diluting stock solution with water. The IS solution was brought to a final concentration of 2500 ng/mL for gliclazide and 500 ng/mL for ZHY81018 in water. All working solutions were stored at 4 °C and brought to room temperature before use. Calibration standards and quality control samples were prepared by spiking 50 μL of the working solutions and 50 μL of IS into 100 μL of drug-free rat plasma. Matrix-matched ADF and 602076 calibration standards were prepared in plasma at concentrations of 2.5, 5, 10, 25, 50, 100, 250, 500 ng/mL and 2.5, 5, 10, 25, 100, 250, 500, 1000 ng/mL, respectively. Similarly, ADF and 602076 quality control (QC) samples were prepared separately in plasma to give concentrations of 5, 50, 500 ng/mL and 5, 100, 1000 ng/mL, respectively.

2.5. Sample preparation

Extraction of ADF and gliclazide was carried out by liquid–liquid extraction (LLE). First, 50 μL of the IS working solution (2500 ng/mL gliclazide), 50 μL of water and 100 μL 1% formic acid were added to 100 μL of rat plasma, and then 1 mL *n*-hexane:dichloromethane:isopropanol (100:50:5, v/v/v) was added to the mixture. The mixture was vortexed for 3 min and centrifuged at 3500 rpm for 10 min. The supernatant organic layer was transferred to another tube and evaporated under a gentle stream of air at 40 °C until dry. The residue was dissolved in 150 μL methanol:water (70:30, v/v) and vortex mixed. A 20 μL aliquot of the solution was injected into the LC–MS/MS system for analysis.

For the detection of 602076, 50 μL of the IS solution (500 ng/mL ZHY81018) and 50 μL of water were added to a 100 μL aliquot of rat plasma placed. The sample mixture was deproteinized with 500 μL of acetonitrile, and the precipitate was removed by centrifugation at 9500 rpm for 10 min. The supernatant (300 μL) was transferred to another tube and evaporated under a gentle stream of air at 40 °C until dry. The residue was reconstituted in 150 μL water and vortex-mixed for 3 min. A 20 μL of the aliquot of the solution was injected into the LC–MS/MS system for analysis.

2.6. Method validation

During the prestudy validation, the calibration curves were defined in three runs on the basis of duplicate assays of the spiked plasma samples, and on the same day, QC samples from three concentrations (Table 2) were determined in replicates ($n = 6$) to calculate the method's accuracy and precision. Calibration curves were constructed using a $1/x^2$ weighting linear regression of the peak-area ratios of the analyte to the IS versus the plasma concentration of the analyte. During routine analysis, each analytical run include a set of calibration samples, a set of QC samples in duplicate and the unknown samples. Extraction recovery was measured by comparing the response of the analytes spiked before and after sample preparation. Matrix effects were assessed using a method similar to that reported by Matyszewski et al. [13].

2.7. Animal studies

Sprague–Dawley (SD) rats (male, 200–250 g) were supplied by Beijing Vital River Laboratories Animal Technology Co. Ltd. Twelve rats were randomly divided into two groups and were fasted overnight but allowed free access to water before drug administration. ADF or alamifovir was dispersed in 0.5% CMC-Na and administered to rats by oral gavage (equivalent to 50 mg/kg 602076). Blood samples (0.5 mL) were withdrawn from postocular ophthalmic vein just prior to dose and at 15 min, 30 min, 1.0 h, 1.5 h, 2.0 h, 3.0 h, 4.0 h, 6.0 h, 8.0 h, 12.0 h, 24.0 h and 48.0 h after oral administration of ADF or alamifovir. 100 μL formic acid (1%) diluted with physiological saline was added to each sample to stabilize the parent compound. Plasma was separated from each sample by centrifugation at 3500 rpm for 10 min and frozen at −20 °C until analysis.

2.8. Data analysis

The pharmacokinetic parameters were calculated with non-compartment methods using Microsoft Excel 2003. The maximum plasma concentration (C_{max}) and the corresponding time (T_{max}) were obtained from observed data. The terminal elimination rate constant (K_e) was estimated with least-squares regression of values in the terminal log-linear region of plasma concentration–time curves, and the terminal elimination half-life ($t_{1/2}$) was calculated to be $0.693/K_e$. The area under the curve from time zero to the last sampling time (AUC_{0-t}) was determined using the linear trapezoidal rule.

3. Results and discussion

3.1. LC–MS/MS optimization

ESI–MS/MS was used to analyze the compounds. To quantify the analytes using the MRM mode, the full scan and product ion spectra of the analytes and IS were investigated. The chemical properties of ADF are significantly different from those of its active metabolite

Table 2
Precision and accuracy for the analysis of ADF and 602076 in quality control (QC) samples ($n = 3$ days, 6 replicates per day) in rat plasma.

	Concentration (ng/mL)		RSD(%)		Relative error (%)
	Added	Found	Intra-day	Inter-day	
ADF	5.0	5.1	3.8	14.7	1.9
	50.0	44.7	3.3	4.9	−10.6
	500.0	509.3	6.7	14.3	1.7
602076	5.0	5.0	4.9	3.2	0.2
	100.0	102.6	6.1	2.6	2.6
	1000.0	1020.4	4.0	4.4	2.0

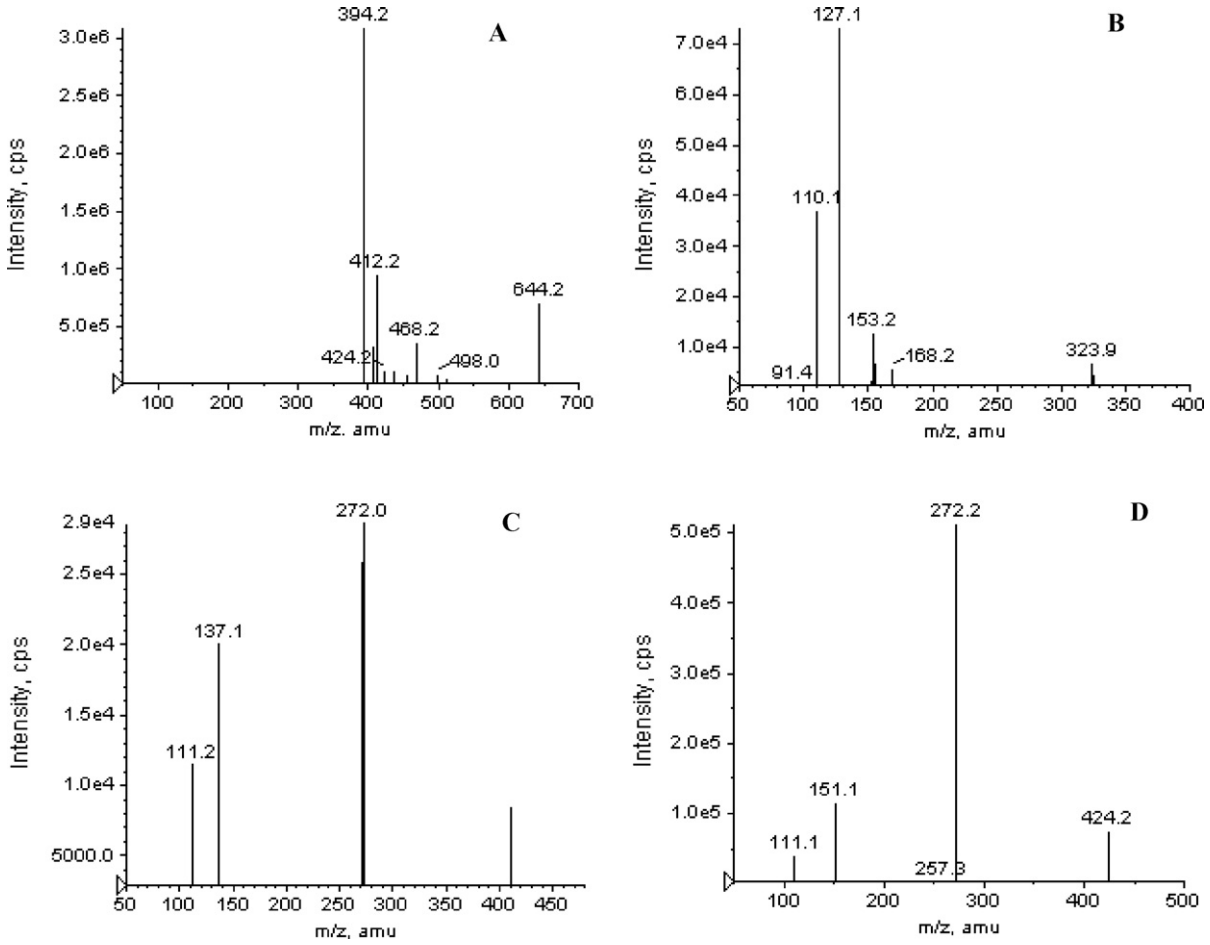

Fig. 2. Product ion mass spectra of the protonated and deprotonated molecules of ADF (A), gliclazide (B), 602076 (C) and ZHY81018 (D).

602076. While negative ESI gave excellent sensitivity for 602076, positive ionization gave increased sensitivity for ADF relative to negative mode. The optimized mobile phase conditions for chromatography and ESI were also dissimilar for ADF and 602076. Thus, two sets of liquid chromatography and ionization modes were used to determine the concentration of ADF and 602076 in rat plasma, separately.

While the protonated peak was the primary forms of the molecular ion for ADF, the deprotonated peak was the predominant form of the molecular ion for 602076. The dominant fragment observed for ADF in positive ESI was at *m*/*z* 394 (Fig. 2A), hence was selected as the product ion for quantitation. The product ion scan spectra of deprotonated molecular for 602076 showed several major fragment ions at *m*/*z* 111, 137 and 272 (Fig. 2C). The fragment ion *m*/*z* 272, formed by breaking the single carbon—nitrogen bond in the side chain, was present in the greatest abundance. The fragment ion at *m*/*z* 137 showed a relative intensity of about 65% of the base peak and *m*/*z* 111 showed less than 40%. The most abundant fragment ion at *m*/*z* 272 was selected for MRM analysis for 602076. Fig. 2 displays product ion spectra of the protonated and deprotonated molecules of ADF, 602076 and their corresponding IS.

In optimizing the LC system for the detection of 602076, chromatographic separation was tested on several C_{18} columns to achieve the best efficiency and peak shape: Phenomenex Gemini (150 mm × 2.0 mm, 5 μm), Capcell Pak MG (150 mm × 2.0 mm, 5 μm), Pinnacle II (150 mm × 2.1 mm, 5 μm) and Discovery (50 mm × 2.1 mm, 5 μm). The Capcell Pak MG C_{18} column (150 mm × 2.0 mm, 5 μm) gave good peak shape and satisfactory efficiency when acetonitrile:water (20:80, v/v) was used as the mobile phase. Different mobile phases were evaluated to improve LC separation and enhance MS sensitivity. Acetonitrile was selected as the organic modifier because its ability to ionize 602076 was superior to that of methanol. Moreover, the addition of ammonium acetate (5 mM), formic acid or acetic acid in the mobile phase greatly reduced signal intensity and resulted in peak tailing for 602076. Thus, an isocratic system with a mobile phase consisting of acetonitrile and water (20:80, v/v) was optimal for 602076 with respect to peak shape and mass spectral response.

While the asymmetrical peak was acquired on the Capcell Pak MG C_{18} column (150 mm × 2.0 mm, 5 μm) for ADF, the Phenomenex Gemini C_{18} column (150 mm × 2.0 mm, 5 μm) gave good peak shape and satisfactory efficiency under the conditions tested. For ADF, methanol and acetonitrile were tested as the organic modifier, and we found that the ability of methanol to ionize ADF was superior to that of acetonitrile. In addition, formic acid was selected as an acid modifier because of its advantage over acetic acid in preventing peak tailing. Thus, an isocratic system with a mobile phase consisting of methanol:water:formic acid (70:30:0.1, v/v/v) was optimal for ADF with respect to peak shape and mass spectral response. Under these chromatographic conditions, the retention times for ADF and gliclazide were approximately 3.3 and 2.6 min, respectively.

3.2. Internal standard selection

Although a stable isotope-labeled compound would be an ideal IS for quantitation in complex matrices in LC–MS/MS analysis, it is not readily available in most laboratories. Hence, structural

Table 3
Stability data for ADF and 602076 in rat plasma under different storage conditions ($n = 3$).

	Storage conditions	Added C (ng/mL)	Found C (ng/mL)	RSD (%)	Relative error (%)
ADF	Short-term (6 h at 24 °C)	5.0	4.5	1.9	−10.3
		50.0	44.3	3.5	−11.3
		500.0	444.3	2.6	−11.1
	Long-term (25 days at −20 °C)	5.0	4.4	4.3	−11.2
		50.0	50.2	10.3	0.40
		500.0	548.7	1.5	9.73
	Three freeze/thaw cycles	5.0	4.7	5.1	−5.8
		50.0	46.9	7.9	−6.1
		500.0	486.3	5.8	−2.7
	Autosampler for 24 h (24 °C)	5.0	4.8	6.7	−4.5
		50.0	45.6	3.6	−8.7
		500.0	497.7	1.7	−0.5
602076	Short-term (6 h at 24 °C)	5.0	5.4	1.9	8.3
		100.0	104.0	3.1	4.3
		1000.0	1036.7	2.8	3.7
	Long-term (25 days at −20 °C)	5.0	4.3	1.9	−13.3
		100.0	109.3	10.4	1.6
		1000.0	1042.7	1.7	0.1
	Three freeze/thaw cycles	5.0	5.2	4.4	4.0
		100.0	109.3	1.4	9.3
		1000.0	1042.7	5.7	4.3
	Autosampler for 24 h (24 °C)	5.0	5.1	3.7	1.9
		100.0	105.3	1.1	5.3
		1000.0	1050.0	1.7	5.0

analogues were screened to find suitable compounds for use as IS. ZHY81018, an analogue of 602076, was finally selected as the IS for the determination of 602076. However, the structural analogue of ADF was not readily available in our case. Therefore we screened other compounds for use as an IS for the determination of ADF. Gliclazide was found to be feasible and acceptable owing to its good correction for ADF.

3.3. Optimization of sample preparation

In this study, ADF were prepared by LLE. A number of organic solvents such as ethyl acetate, ethyl ether:dichloromethane (3:2, v/v), ethyl ether and *n*-hexane:dichloromethane:isopropanol (100:50:5, v/v/v) were evaluated for use in the LLE method. The results showed that *n*-hexane:dichloromethane:isopropanol (100:50:5, v/v/v) was preferable for ADF.

The largely polar character of 602076 makes it difficult to extract from plasma with organic solvents. In the present work, protein precipitation was used for the extraction of 602076 from plasma, which offered satisfactory extraction recoveries for the analytes. Moreover, when acetonitrile was chosen for protein precipitation, the extraction recovery was higher than when methanol was used.

3.4. Assay specificity and matrix effect

Method specificity was demonstrated by comparing the MRM chromatograms of blank samples with those of spiked samples. No interference was detected from endogenous substances within the analytes and IS (Figs. 3 and 4).

Co-eluting matrix compounds, in the plasma samples, may reduce or enhance the ion intensity of the analytes and affect the reproducibility and accuracy of the assay. The matrix effect was assessed as follows: to the blank matrix from five different individuals, analytes were added at three concentrations (low, middle, and high), making a total of 15 samples. These samples were subjected to the analytical procedure and compared with the standard working solutions.

The relative matrix effect of ADF was 93.1–113.1%, 93.6–111.1%, and 89.3–105.4% at the concentrations of 5, 50, and 500 ng/ml, respectively. The relative matrix effect of 602076 was 85.2–110.8%, 95.0–100.1%, and 89.0–96.0% at the concentrations of 5, 100, and 1000 ng/ml, respectively. It indicated that the matrix effects had no practical effect on the quantification of ADF and 602076.

3.5. Linearity of calibration curves and lower limit of quantification

The linear range was 2.5–500 ng/mL for ADF and 2.5–1000 ng/mL for 602076 in the rat plasma with correlation coefficients of >0.995. The lower limit of quantification, defined as the lowest concentration measured with ±15% accuracy and ≤15% precision, was 2.5 ng/mL for both ADF and 602076.

3.6. Precision, accuracy and extraction recovery

Assay precision and accuracy were determined by using QC samples at three concentrations in replicate ($n = 6$) by performing complete analytical runs on the same day and on three consecutive days. The data from these QC samples were analyzed using one-way analysis of variance. The results are summarized in Table 2.

The average extraction recoveries for ADF were 78.4 ± 2.3%, 78.1 ± 7.4% and 89.4 ± 4.0% at the concentrations of 5.0, 50, and 500 ng/mL, respectively. For 602076, the mean recoveries were 69.3 ± 3.1%, 62.4 ± 1.5% and 61.6 ± 0.5% at the concentrations of 5.0, 100, and 1000 ng/mL, respectively. The extraction recovery of the IS was 93.2 ± 8.7% (gliclazide) and 95.8 ± 3.9% (ZHY81018).

3.7. Stability

The stability of ADF and 602076 in rat plasma was investigated under a variety of storage and process conditions. ADF was found to be unstable in rat plasma: the analyte decreased by about 20% after 1.0 h of storage at room temperature. Therefore, it was required to add a stabilizer to the sample. Formic acid (0.5% and 1%), acetic acid (0.5% and 1%) and Vitamin C (50 mg/mL) were compared as

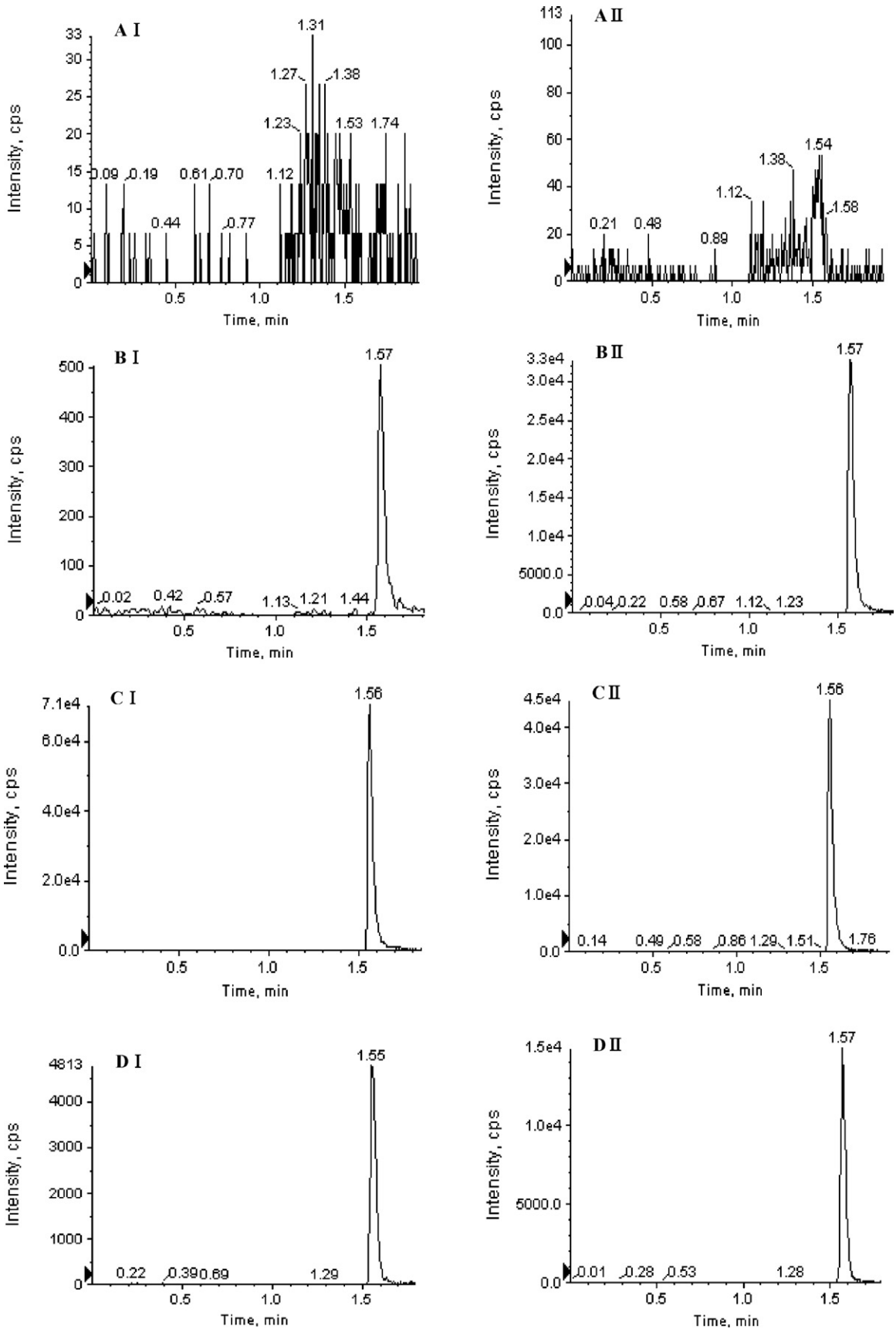

Fig. 3. Representative MRM chromatograms for 602076 (I) and IS ZHY81018 (II) in rat plasma: (A) blank plasma sample; (B) blank plasma sample spiked with 602076 at the lowest limit of quantification (2.5 ng/mL) and IS (500 ng/mL); (C) plasma sample obtained from a rat 1.0 h after oral administration of ADF (equivalent to 50 mg/kg 602076); and (D) plasma sample obtained from a rat 1.0 h after oral administration of alamifovir (equivalent to 50 mg/kg 602076).

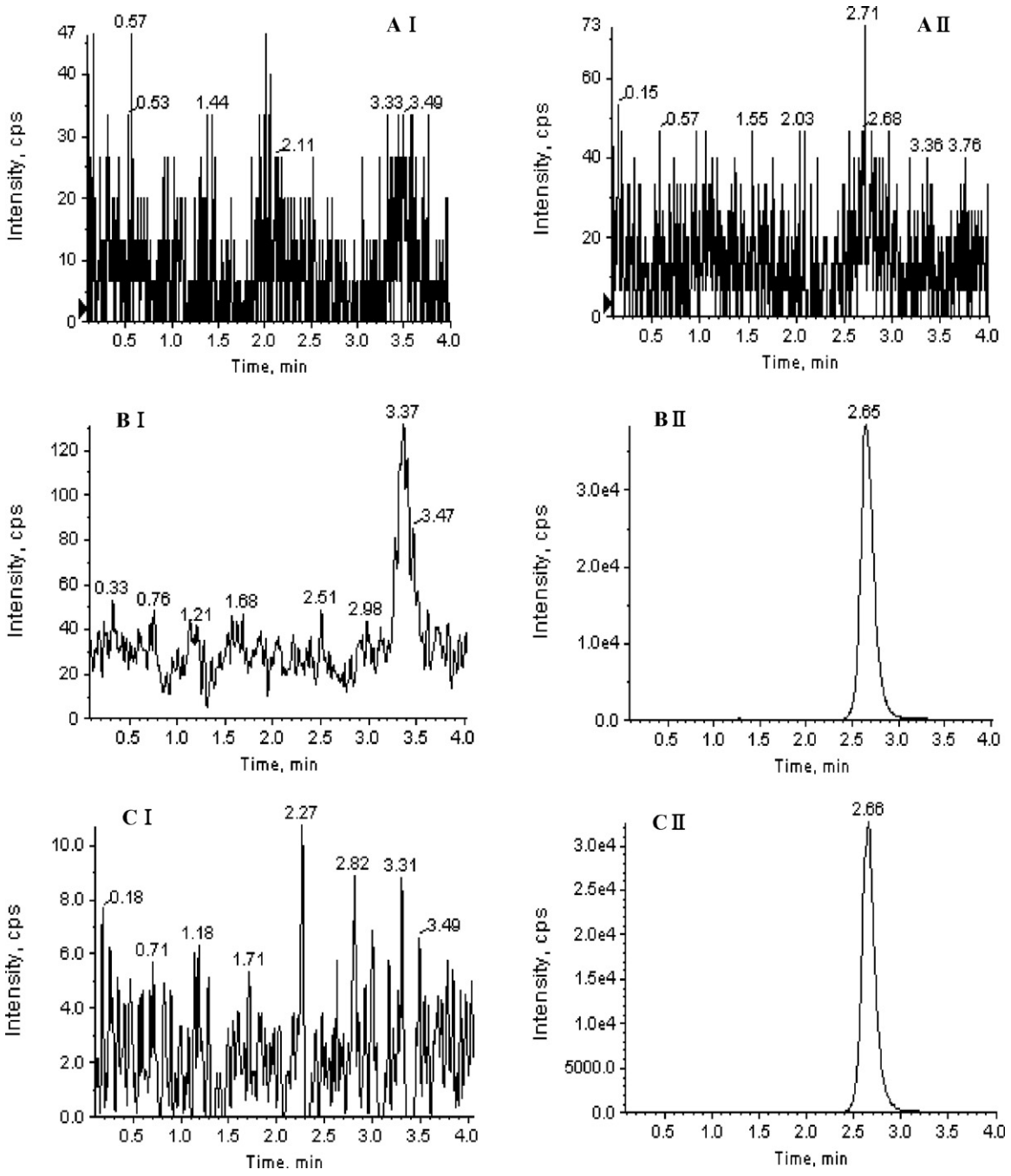

Fig. 4. Representative MRM chromatograms for ADF (I) and IS gliclazide (II) in rat plasma: (A) blank plasma sample for ADF and IS; (B) blank plasma sample spiked with ADF at the lowest limit of quantification (2.50 ng/mL) and IS (2500 ng/mL); and (C) plasma sample obtained from a rat 6.0 h after oral administration of ADF (equivalent to 50 mg/kg 602076).

stabilizers. The ADF samples with 1% formic acid were found to be stable after being stored at room temperature for 6 h. Stability data are enumerated in Table 3.

3.8. Application of the method

After validation, the LC–MS/MS methods were used to determine ADF and 602076 concentrations in plasma samples after oral administration of ADF or alamifovir (equivalent to 50 mg/kg 602076) to two groups SD rats. It was noted that orally administrated ADF could be efficiently cleaved in rat bodies to produce 602076, which was detected in plasma at 15 min post-dose, and no unchanged drug ADF was detected in the plasma samples. Fig. 5 displays the mean plasma concentration–time curve of 602076 for the two ester prodrugs. The mean maximum plasma concentration (C_{max}) was 1181.00 ± 296.52 and 224.50 ± 94.04 ng/mL, and the time to reach maximum concentration (T_{max}) was 1.46 ± 0.84 and 0.54 ± 0.25 h for ADF and alamifovir, respectively. The half-life ($t_{1/2}$) was found to be 5.59 ± 3.08 and 12.53 ± 4.21 h for ADF and alamifovir, respectively. The AUC_{0-t} for ADF and alamifovir was 3844.85 ± 714.83 and 1301.03 ± 600.94 ng·h/mL, respectively. The oral bioavailability of ADF was about 3 times higher than that of alamifovir, which indicating that ADF would be favorable for the further development.

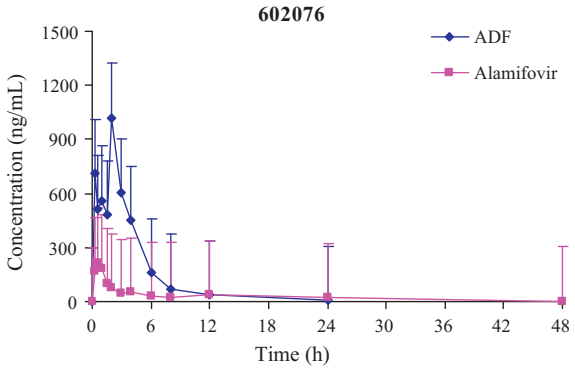

Fig. 5. Mean plasma concentration–time profiles of 602076 after oral administration of ADF or alamifovir (equivalent to 50 mg/kg 602076) to SD rats ($n = 6$).

4. Conclusion

In this study, the LC–MS/MS methods were first developed and validated for the quantification of ADF and its active metabolite 602076 in rat plasma. Owing to their disparate chemical properties, separate LC conditions and mass spectrometric ionization modes were employed for the analysis of ADF and 602076. The methods have been successfully applied to pharmacokinetic studies of 602076 after oral administration of ADF or alamifovir to the rats. The results show that ADF is rapidly metabolized to its active metabolite 602076 after oral absorption, with no detectable unchanged drug. The higher oral bioavailability of ADF supports the further development of this prodrug candidate.

Acknowledgement

This work was supported by a grant from the National Natural Science Foundation of China (No. 81001468).

References

[1] D. Lavanchy, Hepatitis B virus epidemiology, disease burden, treatment, and current and emerging prevention and control measures, J. Viral Hepat. 11 (2004) 97–107.
[2] P. Ocama, C.K. Opio, W.M. Lee, Hepatitis B virus infection: current status, Am. J. Med. 118 (2005) 1413.e15–1413.e22.
[3] R.P. Iyer, S. Padmanabhan, G.R. Zhang, J.D. Morrey, B.E. Korba, Nucleotide analogs as novel anti-hepatitis B virus agents, Curr. Opin. Pharmacol. 5 (2005) 520–528.
[4] P.K. Arora, V.M. Patil, S.P. Gupta, A QSAR study on some series of anti-hepatitis B virus (HBV) agents, Biomed. Inf. 4 (9) (2010) 417–420.
[5] H. Kwon, A.S. Lok, Hepatitis B therapy, Gastroenterol. Herpetol. 8 (2011) 275–284.
[6] V. Calvaruso, A. Craxì, Fibrosis in chronic viral hepatitis, Best Pract. Res. Clin. Gastroenterol. 25 (2011) 219–230.
[7] S.K. Ono-Nita, N. Kato, Y. Shiratori, F.J. Carrilho, M. Omata, Novel nucleoside analogue MCC-478 (LY582563) is effective against wild-type or lamivudine-resistant hepatitis B virus, Antimicrob. Agents Chemother. 46 (2002) 2602–2605.
[8] N. Kamiya, A. Kubota, Y. Iwase, K. Sekiya, M. Ubasawa, S. Yuasa, Antiviral activities of MCC-478, a novel and specific inhibitor of hepatitis B virus, Antimicrob. Agents Chemother. 46 (2002) 2872–2877.
[9] D.K.W. Soon, S.L. Lowe, C.H. Teng, K.P. Yeo, J. McGill, S.D. Wise, Safety and efficacy of alamifovir in patients with chronic hepatitis B virus infection, J. Hepatol. 41 (2004) 852–858.
[10] C. Chan, E. Abu-Raddad, G. Golor, H. Watanabe, A. Sasaki, K.P. Yeo, D. Soon, V.P. Sinha, S.D. Flanagan, M.M. He, S.D. Wise, Clinical pharmacokinetics of alamifovir and its metabolites, Antimicrob. Agents Chemother. 49 (2005) 1813–1822.
[11] Y.G. Wang, X.H. He, B.H. Zhong, Design, synthesis and biological activity of prodrugs of alamifovir analogs, Chin. J. Med. Chem. 20 (2010) 484–489.
[12] D. Wu, J.Q. Niu, X.Y. Wu, Y.H. Ding, B.H. Zhong, X.W. Feng, Anti-hepatitis B virus activity and toxicity of a novel nucleoside analogues *in vitro*, J. Jilin Univ. 33 (2007) 422–426.
[13] B.K. Matuszewski, M.L. Constanzer, C.M. Chavez-Eng, Strategies for the assessment of matrix effect in quantitative bioanalytical methods based on HPLC/MS/MS, Anal. Chem. 75 (2003) 3019–3030.

Journal of Pharmaceutical and Biomedical Analysis 61 (2012) 78–85

Contents lists available at SciVerse ScienceDirect

Journal of Pharmaceutical and Biomedical Analysis

journal homepage: www.elsevier.com/locate/jpba

Bioavailability study of triamterene and xipamide using urinary pharmacokinetic data following single oral dose of each drug or their combination

Hadir M. Maher[a,b,*], Rasha M. Youssef[a], Eman I. El-Kimary[a], Ekram M. Hassan[a,c], Magda A. Barary[a]

[a] Faculty of Pharmacy, Department of Pharmaceutical Analytical Chemistry, University of Alexandria, El-Messalah, Alexandria 21521, Egypt
[b] College of Pharmacy, Department of Pharmaceutical Chemistry, King Saud University, Riyadh 11495, P.O. Box 22452, Saudi Arabia
[c] Faculty of Pharmacy, Department of Pharmaceutical Analytical Chemistry, Beirut Arab University, Beirut, Lebanon

ARTICLE INFO

Article history:
Received 3 October 2011
Received in revised form
26 November 2011
Accepted 28 November 2011
Available online 6 December 2011

Keywords:
Triamterene
Xipamide
Urine analysis
Pharmacokinetics
HPLC–DAD

ABSTRACT

An efficient chromatographic method for the simultaneous determination of triamterene (TRI) and xipamide (XIP) in urine samples, based on high performance liquid chromatography with photodiode array detector (HPLC–DAD) has been developed. The HPLC separation was performed on a RP stainless-steel C-18 analytical column (250 mm × 4.6 mm, 5 μm) with a gradient elution system of 0.05 M phosphate buffer adjusted to pH 4.0 and methanol as the mobile phase. The method was used to determine the urinary excretion profile and to calculate different urinary pharmacokinetic parameters following oral dose of their combination compared with single oral doses of each drug and hence comparing their bioavailability. Quantitation was performed using chlorthalidone as internal standard. The calibration graphs of each drug were rectilinear in the range of 0.2–40 μg/mL urine for TRI and 0.2–15 μg/mL urine for XIP. An HPLC–DAD method was also successfully developed for the simultaneous determination of the investigated drugs in pharmaceutical preparations. The methods were validated in terms of linearity, accuracy, precision, selectivity, limits of detection and quantitation and other aspects of analytical validation.

© 2011 Elsevier B.V. All rights reserved.

1. Introduction

Triamterene (TRI) is a mild diuretic belonging to the potassium-sparing family. TRI alone is relatively inefficient as an antihypertensive drug. Thus it is usually co-administered with some other, more potent diuretics (e.g. a thiazide or anthranilic acid derivative). This combination has a synergistic effect. When TRI is given alone in the treatment of edema, the oral dosage range is 150–250 mg daily. After oral administration, about 30–70% of the dose is excreted in urine, mainly as the sulfate conjugate of *p*-hydroxytriamterene, with about 5–10% of the dose as unchanged drug [1]. In urine, TRI has been determined using different techniques [2–9]. Only few of the previously published reports [3,8,9] describe the urinary excretion profile of TRI of which, no suitable HPLC method with photodiode array detection was reported for studying the urinary excretion profile of TRI either alone or in combination with xipamide.

Xipamide (XIP) is a sulfonamide diuretic drug used for the treatment of high blood pressure and edema [10]. The common dose of xipamide is 20–40 mg day^{-1} with a maximum dose of 80 mg day^{-1} and the maximum diuresis is between 3 and 4.5 h. About 88% of a dose is excreted in the urine with about 50% as unchanged drug and 30% as xipamide-*O*-glucuronide [1]. XIP has been determined in urine using different methods [11–20]. Only one report [11] illustrates its urinary excretion till 6 h, but no reports, to our knowledge, have been reported for studying its urinary excretion profile up to 24 h either alone or in combination with triamterene diuretic.

The toxicity of TRI/XIP combination is less than that reported for the individual constituents [21]. Literature review revealed that only one report is available for the determination of mixed tablets of TRI and XIP which comprises spectrophotometric and densitometric methods [22].

Recently, diuretics have been abused in sports with weight classes, such as weightlifting, wrestling and boxing when athletes try to reduce their body weight in order to qualify for lower weight classes. It is also reported that athletes use diuretics to avoid detection of doping agents by reducing their urine concentration. Accordingly, the determination of diuretics in biological samples is a very important issue in doping control. The analysis of these drugs in physiological samples usually requires some form of preparation. Liquid–liquid [11] and solid phase [14,15] extractions are extensively used to separate the diuretics from the protein matrix and endogenous compounds. These procedures are however time-consuming and frequently incomplete recoveries are attained.

* Corresponding author at: Faculty of Pharmacy, Department of Pharmaceutical Analytical Chemistry, University of Alexandria, El-Messalah, Alexandria 21521, Egypt. Tel.: +20 3 4871317; fax: +20 3 4873273.
E-mail address: hadirrona@yahoo.com (H.M. Maher).

0731-7085/$ – see front matter © 2011 Elsevier B.V. All rights reserved.
doi:10.1016/j.jpba.2011.11.032

Table 1
Gradient HPLC system for the simultaneous determination of TRI and XIP in urine.

Time (min)	Methanol (solvent A)%	Flow rate (mL/min)
0–7	40	1
7–8	40–60	1–2
8–12	60	2

In the present work, HPLC–DAD methods are proposed for the determination of either TRI or XIP or their combination excreted unchanged in urine and for reporting their urinary excretion profiles after single oral dose of each drug or their combination up to 24-h post-dose. This is seemingly the first available method for comparing the bioavailability of the combined dosage form relative to the individual single component preparations. Furthermore, the proposed methods involve direct injection of urine samples only after protein precipitation which simplifies the determination of the two diuretics without time consuming extraction procedures and in a short analysis time. Finally, in view of the fact that there is no published HPLC method for the simultaneous determination of TRI and XIP in combined tablets, the development of rapid, sensitive, reproducible and selective analytical HPLC method would greatly aid in the determination of the binary mixture in bulk samples or tablets.

2. Experimental

2.1. Materials and reagents

Pharmaceutical grade triamterene and xipamide were kindly provided by EIPICO Pharmaceutical Industries Company, Cairo, Egypt. Analytical-reagent grade chemicals were used in all experiments. HPLC grade methanol, acetonitrile (Labscan Ltd., Dublin, Ireland), disodium hydrogen phosphate, orthophosphoric acid (BDH Laboratory Suppliers, Poole, England) and sodium hydroxide (El-Nasr Chemical Ind. Co., Egypt) were used. Fresh double distilled water was used throughout the analysis. The pharmaceutical preparations used were Diurexan® (Meda pharmaceuticals, England, 20 mg XIP/tablet), laboratory made capsules containing 60 mg TRI/capsule was prepared for bioavailability study and clinical comparison and Epitens® (EIPICO, Egypt, 30 mg TRI and 10 mg XIP/tablet).

2.2. Instrumentation and chromatographic conditions

The HPLC–DAD system (Agilent, Germany) consisted of Quaternary pump G1311A which comprises a solvent cabinet, Vacuum Degasser G1322A and a four-channel gradient pump; Diode Array and Multiple Wavelength detector G1315D. The LC system is equipped with Thermostated Column Compartment G1316A and Manual Injector which uses a Rheodyne 7725i7-port sample injection valve and fitted with a 20 μL sample loop. All are Agilent 1200 Series. LC separations were performed on an Agilent Zobrax Eclipse SB-C8 analytical column (250 mm × 4.6 mm, 5 μm). The column was thermostated at 25 °C during analysis.

For the determination of TRI or XIP in urine, a mobile phase consisting of methanol and 0.05 M aqueous phosphate buffer adjusted to pH 4 using 2% orthophosphoric acid in a ratio of 40:60 and 80:20 (v/v) was used for the determination of TRI and XIP, respectively at a flow rate of 1 mL/min. However, for the simultaneous urinary determination of TRI and XIP, a gradient system was applied. The elution gradient used was summarized in Table 1. On the other hand, acetonitrile and 0.05 M disodium hydrogen phosphate buffer (pH 4) in a ratio of (40:60, v/v) was used as a mobile phase for the analysis of the drugs in their tablets.

All the mobile phases used were degassed and filtered by passing through a 0.45 μm pore size membrane filter (Millipore, Milford, MA, USA) prior to use. The samples were also filtered using 0.45-μm disposable filters.

2.3. Preparation of stock solutions

Stock solutions of 200 μg/mL TRI or XIP in methanol were used for urine analysis. In tablets, acetonitrile was used instead. In addition, stock solutions of chlorthalidone 200 μg/mL in methanol were used as internal standard (IS) in urine analysis.

2.4. Construction of calibration graphs

2.4.1. Determination of TRI and/or XIP in urine

Appropriate volumes of the stock solutions of TRI or XIP were separately transferred into 10-mL volumetric flasks. Portions of 0.5 mL of chlorthalidone stock solution were separately added to each flask then diluted with methanol to obtain working solutions. Blank urine samples of 1 mL were spiked with 1 mL of the prepared working solutions of TRI or XIP to get concentrations within the linearity ranges mentioned in Table 2. The samples were then centrifuged for 5 min at 4000 rpm. The centrifugate was filtered using 0.45-μm disposable filters and a 20 μL aliquot of the filtrate was then injected in triplicates and chromatographed under the abovementioned conditions (Section 2.2). The peak area ratios of each drug versus the internal standard were plotted against the corresponding concentrations to obtain the calibration graph for each compound.

2.4.2. Determination of TRI and XIP in tablets

Appropriate volumes of the prepared stock solutions were separately transferred into 10-mL volumetric flasks, completed to 4 mL using acetonitrile and then diluted to the mark with phosphate buffer to obtain working solutions of suitable concentrations corresponding to the linearity ranges stated in Table 2. Twenty microliter portions of each concentration of working standards were injected in triplicates and chromatographed under the chromatographic conditions mentioned before. The peak area of each concentration was plotted against the corresponding concentration to obtain the calibration graph for each compound.

2.5. Analysis of urine samples

Volumes of 1 mL methanol containing 10 μg chlorthalidone (IS) were added to 1 mL of each thawed urine sample and centrifuged for 5 min at 4000 rpm. The centrifugate was filtered using 0.45-μm disposable filters and a 20 μL aliquot of the filtrate was then injected in triplicates and chromatographed under the abovementioned conditions (Section 2.2).

2.6. Assay of tablets

A total of 10 tablets (Epitens® tablets, EIPICO, Egypt, containing 30 mg TRI and 10 mg XIP per tablet) were finely powdered. An accurately weighed quantity of the powder equivalent to 20 mg TRI and 6.67 mg XIP was transferred into a 100-mL volumetric flask and extracted using about 60 mL acetonitrile, in an ultrasonic bath for 30 min, completed to volume with the same solvent and filtered. One milliliter aliquots of the filtrate were separately transferred into 10-mL volumetric flasks and diluted to volume with the mobile phase specified for tablet assay to prepare tablet solutions containing 20 μg/mL TRI and 6.67 μg/mL XIP. The prepared solutions were then treated as under construction of calibration graph (Section 2.4.2).

Table 2
Regression and statistical parameters for the determination of TRI and XIP in urine samples and tablets using the proposed HPLC methods.

Parameter	Urine		Tablets	
	TRI	XIP	TRI	XIP
Linearity range (μg/mL urine)	0.2–40	0.2–15	0.2–40	0.1–14
LOQ (μg/mL urine)	0.15	0.18	0.18	0.09
LOD (μg/mL urine)	0.05	0.06	0.06	0.03
Intercept[a]	14.17	2.67	−4.89	−3.47
Slope[a]	54.83	55.14	28.94	133.30
Correlation coefficient	0.9994	0.9999	0.9999	0.9993
S_a	18.06	5.53	6.13	28.28
S_b	0.96	0.463	0.27	2.61
$S_{y/x}$	33.69	9.86	8.82	40.69
a/S_a[b]	0.78	0.48	0.80	0.12
$S_b{}^2$	0.92	0.21	7.51×10^{-2}	13.03
S_b%	1.75	0.83	0.95	1.96
F	3233.89	14214.82	11166.09	1363.11
Significance F	5.73×10^{-9}	2.97×10^{-8}	8.95×10^{-5}	7.33×10^{-4}

S_a: standard deviation of intercept; S_b: standard deviation of slope; $S_{y/x}$: standard deviation of residuals; LOD: limit of detection; LOQ: limit of quantitation.

[a] Regression equation for the ratio of peak area of the analyte to that of the internal standard against concentration of the analyte provided that the internal standard (chlorthalidone) is kept constant at concentration of 10 μg/mL urine.

[b] Theoretical value of $t\,(a/S_a) = 2.31$ at the 95% confidence level.

2.7. Human studies

2.7.1. Selection of subjects

On the basis of acceptable medical histories indicating freedom from disease conditions and of normal findings in physical and laboratory investigations, six healthy adult male subjects aged 25–32 years and with bodyweight of 67–92 kg were selected to participate in the study.

2.7.2. Dosage scheduling and samples

All the volunteers received three separate treatments as follows: single oral dose administration of TRI (One laboratory made capsule containing 60 mg TRI) or XIP (One Diurexan® tablet equivalent to 20 mg XIP) or their combination (Two Epitens® tablets equivalent to 60 mg TRI and 20 mg XIP). A washout period of one week was maintained between each two successive treatments. Drug medication was administered orally early in the morning with 250 mL of water after overnight fasting. Urine samples were collected at appropriate time intervals post-dose, and analyzed as described under analysis of urine samples (Section 2.5).

Urine samples were collected before administration and according to the time intervals of 0–2, 2–4, 4–6, 6–8, 8–10, 10–12, 12–14, 14–16, 16–18, 18–20, 20–22 and 22–24-h post dosing. The volume of urine collected during sampling time from the volunteers was measured. Representative samples of urine (20 mL) were stored, in glass bottles, at −20 °C until analysis. At the time of analysis, the samples were thawed and analyzed for TRI and/or XIP content by the proposed HPLC methods. The obtained urinary excretion profiles were used to determine various pharmacokinetic parameters.

3. Results and discussion

3.1. Optimization of HPLC conditions

In order to maximize the resolution and sensitivity of the proposed HPLC assay for the urinary determination of either TRI or XIP alone or TRI and XIP in combination, different experimental conditions were studied and optimized. This was performed at a detection wavelength of 220 nm which provided the best sensitivity based on the UV absorption spectra for both drugs [1].

3.1.1. Type and ratio of organic modifier

Methanol and acetonitrile were tried as organic modifiers. It was found that the type of organic modifier greatly affected the retention time of TRI and XIP.

Experimental trials revealed that TRI could not be well separated from the peaks of un-retained urine compounds when using acetonitrile in the mobile phase. Thus methanol was used instead. However, methanol caused stronger retention of XIP on the column and consequently its elution at longer retention time compared with TRI. As a result, determination of TRI or XIP alone, with optimum resolution within reasonable total running time, was achieved using isocratic system of 40 and 80% methanol, respectively.

On the other hand, being of different chemical properties, it was not possible to resolve a combination of TRI and XIP in urine in the same run using isocratic conditions. It was noticed that the capacity factor (k) significantly decreased for TRI as the methanol concentration rose and methanol content of more than 45% in the mobile phase would prevent the resolution of TRI peak from urine peaks. So after TRI had been completely eluted using 40% methanol for 7 min, methanol % was increased to fasten the elution of XIP with acceptable peak shape. Consequently, the gradient elution system described in Table 1 was successfully adopted for the simultaneous separation and determination of TRI and XIP in urine (Fig. 1).

Nevertheless, isocratic elution using acetonitrile was applied for the separation of TRI and XIP in tablets. This could be attributed to that the use of acetonitrile in the mobile phase allowed the elution of both TRI and XIP at reasonable retention time without the need of application of gradient elution system. Optimum resolution within reasonable run time (7.56 min) was achieved using 40% acetonitrile (Fig. 2). At lower concentrations of acetonitrile, longer retention times were obtained resulting in tailing and distortion of the peak shape. Increasing acetonitrile concentrations led to overlap of TRI peak with the solvent front due to the decrease in the retention time.

3.1.2. pH of the aqueous phase

Phosphate buffer at various pH values ranging between 3 and 7 (adjusted with orthophosphoric acid or sodium hydroxide) was used to study the influence of pH of the aqueous phase on the determination of TRI and XIP. It was observed that as the pH values increased, retention time of TRI was increased while that of XIP was slightly decreased. In addition, higher pH values caused decreased sensitivity for TRI and distortion of the shape of XIP peak.

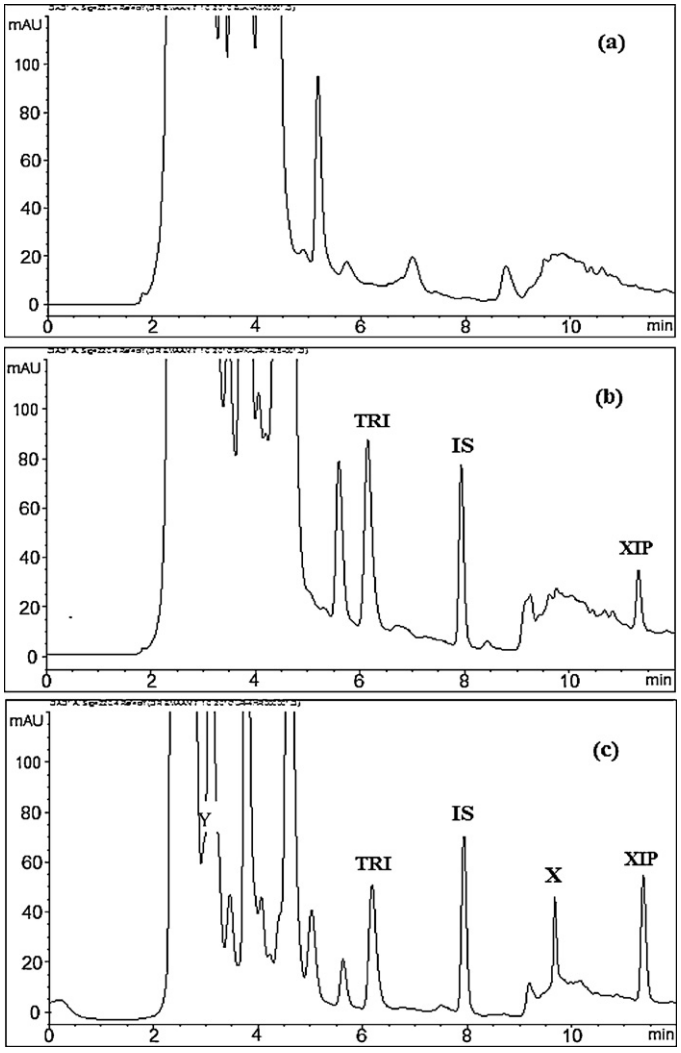

Fig. 1. HPLC chromatograms at 220 nm for blank urine sample (a), urine spiked with 5 μg/mL TRI and 2.5 μg/mL XIP (b) and urine sample obtained from a volunteer 4 h after administration of combined TRI and XIP tablets (Y is TRI metabolite, X is XIP metabolite, IS is chlorthalidone internal standard).

Noisy baseline was obtained when analyzing urine samples at pH values 6 or more together with asymmetric and forked XIP peak. Thus, pH 4 was chosen as intermediate pH providing maximum peak sharpness and symmetry.

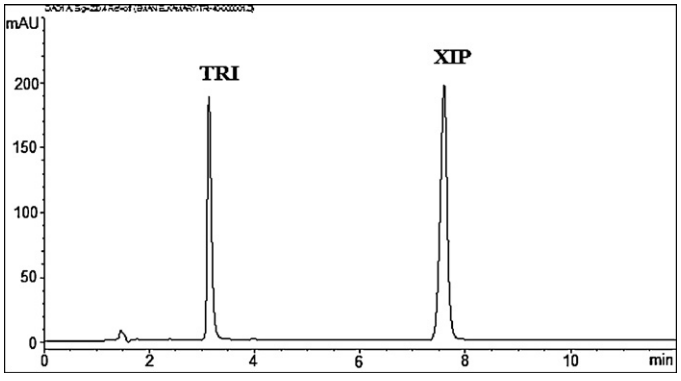

Fig. 2. A typical chromatogram of a 20 μL injection of a standard mixture of 40 μg/mL TRI and 13.5 μg/mL XIP using the optimized chromatographic conditions.

3.2. Validation

3.2.1. Linearity

Under the optimal experimental chromatographic conditions, linear relationships were obtained between the peak area ratio of the analyte (TRI or XIP) to that of the internal standard within the concentration ranges mentioned in Table 2. Meanwhile, the determination of TRI and XIP in tablets depends on the use of peak area to construct the calibration graphs within the concentration ranges presented in Table 2. Good regression lines show high values for both (r) and (F) values [23]. Statistical parameters and linearity results [23–25] are depicted in Table 2.

3.2.2. Limits of detection and quantitation

Limit of detection (LOD) and limit of quantitation (LOQ) values for each drug were calculated [25] and presented in Table 2.

3.2.3. Accuracy

Accuracy of the method was tested by fortification of blank urine samples with the two analytes or preparation of synthetic mixtures at five different known levels for urine and tablet analysis, respectively. This was followed by analysis, and determination of the recovery of each analyte. Urinary data for these experiments are shown in Table 3. Good results were obtained, with average recoveries ranging from 96.04 to 102.04%. Good accuracy was obtained since the maximum deviation from the nominal concentration fulfills the requirements for bioassays and is suitable for our purpose [26].

In addition, the average mean % recoveries from synthetic mixtures ± SD were: 101.31 ± 0.55 (TRI) and 99.33 ± 1.34 (XIP). The good accuracy was proposed by the good values of the percentage recoveries together with the small values of the percentage relative error, E_r (%) < 2%.

3.2.4. Precision

In order to assess the within-day precision, five replicate determinations for each concentration of the two drugs over the working concentration ranges were conducted in the spiked urine or synthetic mixtures. The between-day precision was similarly evaluated on several days (n = 5) over two weeks and no more than one assay per day for each concentration. The results are summarized in Table 3. Precision, expressed as percentage relative standard deviation RSD (%), was usually lower than 4.5% in the spiked urine [26] or 2.1% for synthetic mixtures indicating the high precision of the proposed methods.

3.2.5. Selectivity

The selectivity of the method was assessed by carrying out the chromatographic procedure on different lots of blank urine samples (after protein precipitation using methanol). No interfering peaks were detected at the retention times of the analytes, indicating no interference from the endogenous substances (Fig. 1).

The stability of the column was not affected by the injection of urine samples (after de-proteinization). Both resolution as well as the retention time of the drugs' peaks remained constant over three weeks of work.

In addition, spectral purities of TRI and XIP chromatographic peaks analyzed whether in urine or tablet sample solutions were evaluated using the UV spectra recorded by the DAD. The purity angle was within the purity threshold limit in all of the analyzed samples, indicating that no additional peaks were co-eluted with each of the analyte evidencing the ability of the method to assess the analytes of interest in urine or tablets without any interference from endogenous components of the urine or co-formulated adjuvants.

Table 3
Intra-day and inter-day precision and accuracy for the simultaneous determination of TRI and XIP in combination in spiked urine samples using the proposed HPLC method.

Drug	Added conc. (μg/mL urine)	Intra-day			Inter-day		
		Mean % recovery ± SD	RSD (%)	E_r(%)	Mean % recovery ± SD	RSD (%)	E_r(%)
TRI	0.3	101.39 ± 2.64	2.61	1.39	98.61 ± 3.86	3.92	−1.39
	2	97.35 ± 2.49	2.56	−2.65	102.04 ± 2.55	2.52	2.04
	10	98.66 ± 1.95	1.98	−1.34	100.24 ± 2.82	2.81	0.24
	20	100.84 ± 2.32	2.30	0.84	99.17 ± 1.50	1.51	−0.83
	40	101.03 ± 1.82	1.81	1.03	98.88 ± 1.67	1.69	−1.12
XIP	0.2	97.36 ± 3.15	3.23	−2.64	96.04 ± 4.13	4.30	−3.96
	1	100.34 ± 3.05	3.04	0.34	101.57 ± 3.26	3.21	1.57
	5	98.81 ± 2.52	2.55	−1.19	99.25 ± 1.95	1.97	−0.75
	10	101.49 ± 1.46	1.44	1.49	100.48 ± 2.35	2.34	0.48
	15	98.98 ± 1.73	1.75	−1.02	99.64 ± 2.16	2.17	−0.36

Mean ± standard deviation of five determinations.

3.3. Human studies

The described HPLC methods have been applied to the measurement of urinary levels after a minimum single dose administration of TRI (60 mg TRI/laboratory made capsule) or XIP (20 mg XIP/Diurexan tablet) or their combination Epitens® tablets (60 mg TRI and 20 mg XIP) to six human volunteers.

Fig. 1c represents the chromatogram of urine sample obtained from a volunteer 4 h after the administration of the combined dosage form. The calculated TRI and XIP concentrations were found to be 5.02 and 3.41 μg/mL urine, respectively. The retention time of unchanged TRI and XIP was 6.16 and 11.37 min, respectively. The peak appearing at 3.08 min, which was detected until at least 24 h after dosing, taking into account its high intensity in all the analyzed samples and the similarity of its UV absorption spectrum to that of TRI, probably corresponds to p-hydroxytriamterene, the main metabolite of triamterene [1]. Also, a new peak appearing at a retention time of 9.67 min was suggested to be for XIP metabolite as it has been observed only after XIP administration. Because of its high intensity in all the collected samples, this peak is probably due to XIP main metabolite, xipamide-*O*-glucuronide [1]. It has been noticed that this peak's intensity is always related to the intensity of XIP peak in addition to the similarity between their UV absorption spectra.

3.3.1. Urinary excretion studies

The estimation of bioavailability on the basis of appearance of drug in the urine is an attractive alternative to blood sampling because it represents a non-invasive method. The method is useful for drugs that are extensively excreted un-metabolized in the urine, such as certain thiazide diuretics and sulfonamides. Often a less-sensitive analytical method is required for measuring urine concentrations compared with blood concentrations. If the urine concentrations are low, the use of larger sample volumes is relatively easy. The main disadvantage of urinary excretion studies is the long time required for the collection of samples. In addition, the subjects must be careful to completely void at each collection time and to avoid accidentally discarding any samples. The three major parameters examined in urinary excretion bioavailability studies are the cumulative amount of drug excreted un-metabolized in the urine ($\sum A_e$), the maximum urinary excretion rate (R_{max}) and the time of maximum excretion rate (T_{max}). In simple pharmacokinetic models, the rate of appearance of drug in urine is proportional to its concentration in the systemic circulation. Thus, the values for T_{max} and R_{max} for urine studies are analogous to the T_{max} and C_{max} values derived from blood level studies. The value of T_{max} decreases as the absorption rate of the drug increases, and R_{max} increases as the rate and/or the extent of absorption increases. The value for $\sum A_e$ is related to the area under the curve and increases as the extent of absorption increases [27].

The cumulative amount of drug excreted un-metabolized in the urine up to each sample collection time t_s ($\sum A_{e_{0-t_s}}$) is calculated by multiplying the concentration (μg/mL urine) with the urine volume of the respective sample in each collection interval (in hours) and summing up all intervals up to time t_s. Moreover, the observed total amount of the drug recovered in the urine from time 0 up to 24 h ($A_{e_{0-24}}$) was determined by multiplying the concentration with the urine volume of the respective sample in each collection interval and summing up all intervals after dosing subsequently. The fraction of orally administered drug in urine within 24 h (f_e/f) was calculated by dividing $A_{e_{0-24}}$ by the dose of the drug administered.

The calculation of R is based on Eq. (1):

$$R = \frac{\Sigma A_{e_1} - \Sigma A_{e_2}}{t_2 - t_1} \quad (1)$$

where $\sum A_{e_1}$ and $\sum A_{e_2}$ represent the cumulative amount of drug recovered in the urine samples obtained at sampling times up to t_1 and t_2, respectively. When constructing a plot of R versus time, or for the determination of R_{max}, the values for time are taken to be the midpoint of the urine collection period, that is, the midpoint between t_1 and t_2.

The following pharmacokinetic parameters were subsequently determined from urinary excretion rate versus time curve like the maximal renal excretion rate (R_{max}), the midpoint of the respective collection interval associated with the maximal observed excretion rate (t_{max}) and the area under the renal excretion rate curve from time 0 to the last measured rate ($AURC_{0-t_z}$).

$AURC_{0-t_z}$ was calculated using the linear trapezoidal rule. The renal elimination rate constant (k_{el}) was assessed by ln-linear regression of the terminal segment of the excretion rate versus time curve. The optimal regression fit was determined using at least the three last excretion rates as the period of the highest possible coefficient of correlation. The negative value of the slope of the fitted linear regression line represents k_{el} and Ln 2 divided by k_{el} denoting the terminal elimination half-life ($t_{1/2}$) [28,29].

3.3.2. Statistical analysis

The mean and standard deviation (SD) values of all the pharmacokinetic parameters were calculated and given in tabulated format (Tables 4 and 5). Paired *t*-test was performed for all the urinary parameters at 5% level of significance. This test indicates whether the differences between the pharmacokinetic parameters obtained during different treatments are significant or not. All the statistical analyses were done using the excel program.

3.3.3. TRI alone and in combination with XIP

The urinary excretion profile of TRI after its administration either alone or in combination with XIP for six volunteers is presented in comparative graphical form in Fig. 3. Both cumulative amount of TRI excreted (%) and urinary excretion rate versus mid

Table 4
Mean urinary parameters of TRI following administration of TRI alone and in combination with XIP from the in vivo study in six volunteers.

Parameters	TRI alone (mean ± SD)	TRI and XIP combination (mean ± SD)	p-Values*
R_{max} (mg/h)	0.33 ± 0.05	0.50 ± 0.11	0.038
t_{max} (h)	3.00 ± 1.41	3.80 ± 1.10	0.177
$A_{e_{0-24}}$ (mg)	2.94 ± 0.20	3.94 ± 0.17	0.035
f_e/f (%)	4.89 ± 1.77	6.57 ± 2.29	0.027
$AURC_{0-24}$ (mg)	2.93 ± 0.40	3.94 ± 0.81	0.042
k_{el} (h^{-1})	0.115 ± 0.108	0.142 ± 0.083	0.832
$t_{1/2}$ (h)	6.027 ± 2.202	4.881 ± 2.076	0.375

* p-Value at 5% level of significance.

Table 5
Mean urinary parameters of XIP following administration of XIP alone and in combination with TRI from the in vivo study in six volunteers.

Parameters	XIP alone (mean ± SD)	XIP and TRI combination (mean ± SD)	p-Values*
R_{max} (mg/h)	1.79 ± 0.13	1.93 ± 0.10	0.629
t_{max} (h)	4.20 ± 1.09	5.40 ± 0.89	0.208
$A_{e_{0-24}}$ (mg)	10.82 ± 1.56	9.91 ± 1.95	0.218
f_e/f (%)	54.11 ± 8.50	49.32 ± 9.52	0.721
$AURC_{0-24}$ (mg)	10.86 ± 1.80	9.89 ± 1.05	0.202
k_{el} (h^{-1})	0.069 ± 0.018	0.084 ± 0.033	0.630
$t_{1/2}$ (h)	10.031 ± 2.151	8.262 ± 2.101	0.548

* p-Value at 5% level of significance.

point of time interval following the administration of TRI alone and in combination with XIP are presented in Figs. 3a and b, respectively. The mean urinary excretion pharmacokinetic data calculated after oral administration of a single dose of TRI and its combination with XIP is presented in comparative form in Table 4.

Approximately 4.89 ± 1.77% of TRI was eliminated in a period of 24 h after dosing of TRI alone while this amount was increased up to about 6.57 ± 2.29% after administration of TRI with XIP. This difference was statistically significant ($p < 0.05$, Table 4). Considering the urinary excretion rate of TRI, an increase in R_{max} from 0.33 ± 0.05 to 0.50 ± 0.11 was observed after administration of TRI alone and in combination with XIP, respectively, indicating differences in initial rates of absorption of TRI from the two formulations. This observed change in R_{max} for TRI was statistically significant ($p < 0.05$). Both $A_{e_{0-24}}$ and $AURC_{0-24}$ showed a statistically significant increase ($p < 0.05$) from 2.94 ± 0.20 to 3.94 ± 0.17 and from 2.93 ± 0.40 to 3.94 ± 0.81 when TRI was dosed alone or in combination with XIP, respectively. Other pharmacokinetic parameters such as T_{max} (h), k_{el} (h^{-1}) and $t_{1/2}$ (h) for TRI were also determined. Table 4 indicated that the changes of T_{max}, k_{el} and $t_{1/2}$ were not

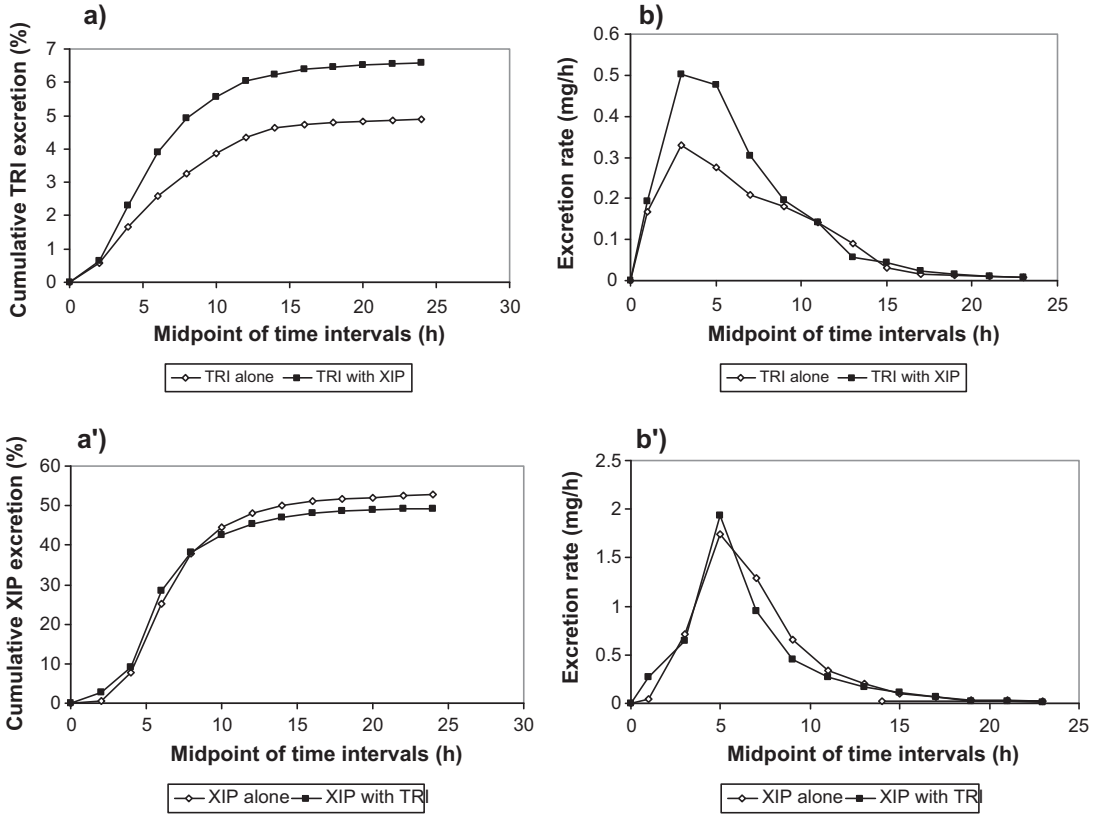

Fig. 3. Comparison of cumulative TRI and XIP excreted (%), (a and a′) and rate of excretion, (b and b′) following administration of TRI or XIP alone and TRI and XIP in combination in six volunteers.

Table 6
Assay results for the determination of TRI and XIP in tablets using the proposed HPLC method.

Epitens® tablets	TRI		XIP	
	HPLC method	Reference method [22]	HPLC method	Reference method [22]
Mean % recovery ± SD	100.45 ± 0.90	100.94 ± 1.51	98.31 ± 1.39	99.72 ± 0.65
RSD (%)	0.90	1.49	1.42	0.66
E_r (%)	0.45	0.94	−1.69	−0.38
t	–	0.63	–	2.05
F	–	2.78	–	4.53

Mean ± standard deviation of five determinations.
Theoretical values of t and F are 2.31 and 6.39, respectively, at 95% confidence limit.

significant ($p > 0.05$). This may be attributed to individual variations in the nature, rate of absorption and metabolic rate. All these observed changes in R_{max}, f_e/f, $A_{e_{0-24}}$ and $AURC_{0-24}$ after administration of TRI alone and in combination with XIP indicates an increase in the bioavailability of TRI from the combined formulation. Since the time of occurrence of mean peak excretion rates of TRI either after its administration alone or in combination with XIP was similar, the initial rates of drug bioavailability were probably similar. The extent of drug bioavailability was assessed by comparing the areas under the drug excretion rate-time curves after administration of the combination formulation with those after administration of the formulation containing the drug alone, taken as the reference. In the case of TRI, comparison of the total areas under the drug excretion rate-time curve indicated that the bioavailability of TRI from the combination formulation was 134% of that from the formulation containing the drug alone.

Differences in the bioavailability of TRI from different formulations have been reported by Tannenbaum et al. who showed that the drug was threefold more bioavailable from a tablet combination formulation with hydrochlorothiazide than from a capsule formulation, and by Stuber et al. who showed that bioavailability parameters of triamterene from three different formulations differed but correlated with in vitro dissolution data [30].

3.3.4. XIP alone and in combination with TRI

Urinary excretion pattern of XIP including cumulative amount of XIP excreted (%) and urinary excretion rate versus mid point of time interval following the administration of XIP alone and in combination with TRI are illustrated in Fig. 3a′ and b′.

Different pharmacokinetic parameters from urinary data of XIP were calculated from the rate of excretion of XIP versus midpoint of time interval curve using the excel program and are tabulated in Table 5. From this, the mean values of R_{max} were found to be 1.79 ± 0.13 mg/h for XIP alone and 1.93 ± 0.10 mg/h for XIP and TRI combination indicating that the initial rate of drug excretion was increased after administration of XIP with TRI in combination compared to administration of the drug alone; however, this difference was not statistically significant ($p > 0.05$). The mean values of $A_{e_{0-24}}$ for XIP were slightly reduced from 10.82 ± 1.56 mg to 9.91 ± 1.95 mg for individual and combination therapies which were comparable as this reduction was not statistically significant ($p > 0.05$). The value of f_e/f was found to be 54.11 ± 8.50% for XIP alone and 49.32 ± 9.52% for XIP and TRI combination which were also comparable. This slight decrease in the value of f_e/f was not statistically significant ($p > 0.05$). Other pharmacokinetic parameters such as T_{max} (h), $AURC_{0-24}$ (mg), k_{el} (h^{-1}) and $t_{1/2}$ (h) were also determined. From Table 5, it is clear that only slight changes in the values of T_{max}, R_{max}, $A_{e_{0-24}}$, f_e/f, $AURC_{0-24}$, k_{el} and $t_{1/2}$ were observed and these changes were not significant ($p > 0.05$), and presumably represents the normal inter-subject variability, indicating comparable bioavailability of XIP from the combination product compared to its single component formulation. The initial rates of bioavailability of XIP after its administration alone or in combination with TRI were probably comparable which is indicated by similar times of occurrence of R_{max}. The relative bioavailability of XIP was calculated using $AURC_{0-24}$ values taking its single component formulation as a reference and was found to be 91.07%.

3.4. Assay of tablets

Commercially available tablets (Epitens® tablets) were assayed by the proposed HPLC method. The results obtained for the two drugs were satisfactory and were in a good agreement with the label claim (Table 6). The RSD (%) and E_r (%) for the assay results showed high precision and accuracy of the proposed method. In addition, the results obtained using the proposed HPLC method were statistically compared with those obtained with the reported HPTLC method [22]. The two methods gave more or less concordant results with respect to their precision (F-test) and accuracy (t-test) where the calculated values did not exceed the theoretical values for either of the two drugs. This indicates that there is no significant difference between the proposed method and the reference one.

4. Conclusion

Simple, sensitive and specific HPLC–DAD methods were developed for estimation of TRI and/or XIP excreted in urine at their therapeutic levels. The proposed methods were successfully used to obtain urinary excretion data for TRI and XIP after administration of a single oral dose of each drug and their combination formulations in healthy human volunteers. With the proposed procedures, the urinary concentration of the two drugs could be determined up to 24 h post dose making the assay suitable for pharmacokinetic studies and routine drug monitoring. Various pharmacokinetic parameters were calculated using urinary excretion data of each drug either alone or in combination.

The present study has utilized a simple in vivo study, based on urinary pharmacokinetics to demonstrate the effect of formulating the two drugs, TRI and XIP, on their bioavailability compared to their individual dosage forms. It was found that the combination did not greatly affect the bioavailability of XIP. On the other hand, a significant increase in the bioavailability of TRI was observed from the combined formulation compared to its single one. The results of the studies reported in this paper and the cited literature [30] suggested that because of their physicochemical properties, the bioavailability of some thiazides and triamterene needs to be evaluated whenever new formulations of these drugs are produced.

In addition, a rapid and reliable isocratic HPLC–DAD method has been developed and validated for determination of TRI and XIP in their combined dosage form. Short chromatographic run time (8 min) allows the analysis of a large number of samples in a short period of time. In addition, there are no previously reported HPLC methods for the simultaneous determination of TRI and XIP in tablets making the proposed method of great interest for routine sample analysis and quality control of TRI and XIP mixture.

References

[1] A.C. Moffat, M.D. Osselton, B. Widdop, Clarke's Analysis of Drugs and Poisons, 3rd ed., 2004, London.
[2] I.D. Merás, A.E. Mansilla, F.S. López, M.J. Rodríguez Gómez, Determination of triamterene and leucovorin in biological fluids by UV derivative-spectrophotometry and partial least-squares (PLS-1) calibration, J. Pharm. Biomed. Anal. 27 (2002) 81–90.
[3] C. Horstkötter, S. Kober, H. Spahn-Langguth, E. Mutschler, G. Blaschke, Determination of triamterene and its main metabolite hydroxytriamterene sulfate in human urine by capillary electrophoresis using ultraviolet absorbance and laser-induced fluorescence detection, J. Chromatogr. B 769 (2002) 107–117.
[4] K. Tolba, D. Belder, Fast quantitative determination of diuretic drugs in tablets and human urine by microchip electrophoresis with native fluorescence detection, Electrophoresis 28 (2007) 2934–2941.
[5] J.M. Pulgarín, A.A. Molina, P.F. López, Direct determination of triamterene in urine by matrix isopotential synchronous fluorescence spectrometry, Anal. Chim. Acta 326 (1996) 117–126.
[6] J.M. Pulgarıín, A.A. Molina, P.F. López, Simultaneous direct determination of amiloride and triamterene in urine using isopotential fluorometry, Anal. Biochem. 292 (2001) 59–68.
[7] M.L. Luis, J.M.G. Fraga, A.I. Jiménez, F. Jiménez, O. Hernández, J.J. Arias, Application of PLS regression to fluorimetric data for the determination of furosemide and triamterene in pharmaceutical preparations and triamterene in urine, Talanta 62 (2004) 307–316.
[8] P. Campíns Falcó, R. Herráez-Hernández, A. Sevillano-Cabeza, Determination of triamterene in urine by HPLC using fluorescence detection and column-switching, Chromatographia 38 (1994) 29–34.
[9] S. Carda-Broch, J.S. Esteve-Romero, M.C. García-Alvarez-Coque, Chromatographic determination of diuretics in urine samples using hybrid micellar mobile phases with fluorimetric detection, Anal. Chim. Acta 375 (1998) 143–154.
[10] S.C. Sweetman, Martindale, The Complete Drug Reference, 36th ed., The Pharmaceutical Press, 2009.
[11] M. Legorburu, R. Alonso, R. Jiménez, Determination of the non-thiazide diuretic xipamide in pharmaceuticals and urine by HPLC with amperometric detection, J. Liq. Chromatogr. Relat. Technol. 22 (1999) 735–746.
[12] M.J. Ruiz-Angel, J.R. Torres-Lapasió, M.C. Garcia-Alvarez-Coque, Effects of pH and the presence of micelles on the resolution of diuretics by reversed-phase liquid chromatography, J. Chromatogr. A 1022 (2004) 51–65.
[13] D. Thieme, J. Grosse, R. Lang, R.K. Mueller, A. Wahl, Screening confirmation and quantitation of diuretics in urine for doping control analysis by high-performance liquid chromatography–atmospheric pressure ionisation tandem mass spectrometry, J. Chromatogr. B 757 (2001) 49–57.
[14] Y. Qin, X.B. Wang, C. Wang, M. Zhao, M.T. Wu, Y.X. Xu, S.Q. Peng, Application of high-performance liquid chromatography–mass spectrometry to detection of diuretics in human urine, J. Chromatogr. B 794 (2003) 193–203.
[15] C. Goebel, G.J. Trout, R. Kazlauskas, Rapid screening method for diuretics in doping control using automated solid phase extraction and liquid chromatography–electrospray tandem mass spectrometry, Anal. Chim. Acta 502 (2004) 65–74.
[16] K. Deventer, F.T. Delbeke, K. Roels, P. Van Eenoo, Screening for 18 diuretics and probenecid in doping analysis by liquid chromatography–tandem mass spectrometry, Biomed. Chromatogr. 16 (2002) 529–535.
[17] K. Deventer, P. Van Eenoo, F.T. Delbeke, Simultaneous determination of beta-blocking agents and diuretics in doping analysis by liquid chromatography/mass spectrometry with scan-to-scan polarity switching, Rapid Commun. Mass Spectrom. 19 (2005) 90–98.
[18] L. Politi, L. Morini, A. Polettini, A direct screening procedure for diuretics in human urine by liquid chromatography–tandem mass spectrometry with information dependent acquisition, Clin. Chim. Acta 386 (2007) 46–52.
[19] J. Thörngren, F. Östervall, M. Garle, A high-throughput multicomponent screening method for diuretics masking agents, central nervous system (CNS) stimulants and opiates in human urine by UPLC–MS/MS, J. Mass Spectrom. 43 (2008) 980–992.
[20] Y. Kim, K. Han, K. Paeng, Determination of xipamide metabolite in human urine by high-performance liquid chromatography/diode-array detection high-performance liquid chromatography/electrospray ionization mass spectrometry and gas chromatography/mass spectrometry, Rapid Commun. Mass Spectrom. 18 (2004) 2505–2512.
[21] Diuretic and antihypertensive composition comprising xipamide and triamterene, United States Patent 4,490,368, www.freepatentsonline.com.
[22] N.E. Wagieh, S.S. Abbas, M. Abdelkawy, M.M. Abdelrahman, Spectrophotometric and spectrodensitometric determination of triamterene and xipamide in pure form and in pharmaceutical formulation, Drug Test. Anal. 2 (2010) 113–121.
[23] P. Armitage, G. Berry, Statistical Methods in Medical Research, 3rd ed., Blackwell Scientific Publications, Oxford, England, 1994.
[24] J.N. Miller, J.C. Miller, Statistics and Chemometrics for Analytical Chemistry, 4th ed., Prentice Hall, Harlow, England, 2000.
[25] The United States Pharmacopeia, 32nd ed., The National Formulary, 27th ed., United States Pharmacopeial Convention, Inc., 2009.
[26] U.S. Department of Health and Human Services, Food and Drug Administration, Center for Drug Evaluation and Research (CDER): Guidance for Industry, Bioanalytical Method Validation, May 2001, Internet at http://www.fda.gov/cder/guidance/index.htm.
[27] J. Swarbrick, Encyclopedia of Pharmaceutical Technology, vol. 1, 3rd ed., PharmaceuTech, Inc., Pinehurst, NC, USA, 2007.
[28] R. Gieschke, Half-life, in: W. Cawello (Ed.), Parameters for Compartment-free Pharmacokinetics, Aachen Shaker, 1999, pp. 39–58.
[29] C.F. Faruquee, M.D. Ashikullah, M.A.K. Azad, M.D.I. Rayhan, S. Parveen, Interaction study between levofloxacin and omeprazole using urinary pharmacokinetic data, Pak. J. Pharm. Sci. 23 (2010) 143–148.
[30] R.R. Brodie, L.F. Chasseaud, A. Darragh, T. Taylor, L.M. Walmsley, Bioavailability of bemetizide and triamterene from a combination formulation, Biopharm. Drug Dispos. 3 (1982) 361–370.

Journal of Pharmaceutical and Biomedical Analysis 61 (2012) 86–92

Contents lists available at SciVerse ScienceDirect

Journal of Pharmaceutical and Biomedical Analysis

journal homepage: www.elsevier.com/locate/jpba

Method development and validation for rapid quantification of hydroxychloroquine in human blood using liquid chromatography–tandem mass spectrometry

Ling-Zhi Wang[a,*], Rina Yue-Ling Ong[b], Tan-Min Chin[a,c], Win-Lwin Thuya[a], Seow-Ching Wan[a], Andrea Li-Ann Wong[c], Sui-Yung Chan[b], Paul C. Ho[b], Boon-Cher Goh[a,c]

[a] Cancer Science Institute of Singapore, National University of Singapore, Singapore
[b] Department of Pharmacy, National University of Singapore, Singapore
[c] Department of Haematology & Oncology, The National University Health System, Singapore

ARTICLE INFO

Article history:
Received 27 September 2011
Received in revised form
23 November 2011
Accepted 28 November 2011
Available online 8 December 2011

Keywords:
Hydroxychloroquine
Rapid
Quantification
LC–MS/MS
Human blood

ABSTRACT

A novel and specific liquid chromatography–tandem mass spectrometric method (LC–MS/MS) was developed and validated for the quantification of hydroxychloroquine in human blood using its stable labeled isotope, hydroxychloroquine-d4 as the internal standard. Chromatographic separation of analytes was achieved using an Agilent ZORBAX Eclipse XDB – C8 analytical HPLC column (50 mm × 2.1 mm, 5 μm). The mobile phase comprising water containing 0.1% formic acid–acetonitrile (94:6, v/v) was delivered isocratically at a flow rate of 0.5 mL/min. The column effluent was detected by API 4000 triple quadrupole mass spectrometer using electrospray ionization (ESI) and monitored by multiple reaction monitoring with positive mode. The precursor to product ion transitions of m/z 336 → 247 and m/z 340 → 251 were used to measure the analyte and IS, respectively. The assay demonstrated a good linear dynamic range of 5–2000 ng/mL for hydroxychloroquine in human blood, with coefficient of determination (r^2) of ≥0.9999. The values for intra-day and inter-day precisions of hydroxychloroquine were ≤7.86% with the accuracies ranged from 93.8% to 107.6%. The chromatographic run time was 3 min, making it possible to achieve a high throughput analysis. This method was used as a bio-analytical tool in a phase I clinical trial to quantify blood hydroxychloroquine concentrations in patients with non-small cell lung cancer receiving both hydroxychloroquine and gefitinib in their treatment.

© 2011 Elsevier B.V. All rights reserved.

1. Introduction

Hydroxychloroquine (HCQ), a widely used antimalarial drug, also shows beneficial effect in lupus erythematosus and acute or chronic rheumatoid arthritis [1,2]. Recently, preliminary data obtained from an ongoing phase I clinical trial indicated that a combination of HCQ and gefitinib may potentially delay or reverse the acquired resistance to gefitinib [3]. Gefitinib (Iressa®), a small molecule orally bioavailable tyrosine kinase inhibitor (TKIs) of the epidermal growth factor receptor (EGFR) tyrosine kinsase (TK) domain is a targeted therapeutic agent for the treatment of non-small cell lung cancer (NSCLC) [4–7]. The predominance of EGFR signaling pathway in NSCLC makes gefitinib a useful salvage therapy option and has been shown to improve survival, compared to placebo, in Asian patients when administered after failure of the first or second line chemotherapy for advanced NSCLC. Nevertheless, all patients who are benefited from TKI treatment ultimately develop resistance to therapy manifesting as progression of their cancer, after which there remains very few therapeutic options [3]. Hence, co-administration of HCQ and gefitinib has been proposed to improve the clinical efficacy of gefitinib. Therefore, in order to ascertain the safety of the proposed drug combination, it is desirable to examine the pharmacokinetics of HCQ when co-administered with gefitinib.

In the previous pharmacokinetic studies, HCQ has been shown to have a long terminal elimination half-life up to 40 days [8–14]. Hence, a steady state blood level of HCQ could only be attained after six months of HCQ treatment [14]. In addition, HCQ has been suggested to be a cytochrome P450 2D6 (CYP2D6) enzyme inhibitor, as demonstrated by its probable drug interaction in the concurrent administration of metoprolol, a CYP2D6 enzyme substrate [15]. Hence, gefitinib, as a CYP2D6 enzyme substrate [4–7,16], could also possibly elicit drug–drug interactions at the CYP2D6 enzyme level, which would be undesirable in the clinical setting.

To date, two assays of HCQ have been developed using HPLC with fluorescence detection, but with a long run time of 15 min

* Corresponding author at: Cancer Science Institute of Singapore, National University of Singapore, CeLS Buiding Level 2, 28 Medical Drive, Singapore 117456, Singapore. Tel.: +65 65165475; fax: +65 67775545.
E-mail address: csiwl@nus.edu.sg (L.-Z. Wang).

0731-7085/$ – see front matter © 2011 Elsevier B.V. All rights reserved.
doi:10.1016/j.jpba.2011.11.034

[17,18]. Hence, there is a need to develop a more efficient bioanalytical method for HCQ monitoring in the clinical setting. As HCQ concentrates in the human erythrocytes, human blood was used as the biological matrix for the bioanalytical method validation for determination of HCQ concentrations. A novel and specific LC–MS/MS method was therefore developed and validated for the determination of HCQ in patient blood samples.

2. Materials and methods

2.1. Chemicals and reagents

Hydroxychloroquine sulphate (98% pure by HPLC) and internal standard (IS), hydroxychloroquine-d4 sulphate (batch number 10-ELZ-1872, 98% pure by HPLC) were obtained from Toronto Research Chemicals Inc. (North York, Ontario, Canada). Formic acid (98–100%), methanol and acetonitrile (HPLC grade) were obtained from Merck (Darmstadt, Germany). Milli-Q water was obtained from a Milli-Q Plus system (Millipore, Milford, MA, USA). Zinc sulphate stock (10%, w/v, aq) solution was prepared by dilution of 18.9 g salt in 100 mL Mill-Q water. Drug-free (blank) human blood was obtained from healthy donors from the National University Hospital, Singapore.

2.2. Sample collection

This phase I clinical trial was approved by the Institutional Ethics Review Board of the National University Health System, National University of Singapore, and informed consents were obtained from all participating patients. Human blood samples were collected from thirteen patients with advanced NSCLC enrolled to a phase I clinical trial at National University Hospital, Singapore. An oral dose of gefinitib (250 mg) and HCQ (either 400 mg or 600 mg) were administered daily. On day 35 of the first chemotherapy cycle, blood samples were collected at time points 0, 2, 3, 4, 5, 7 and 24 h after gefinitib and HCQ administration. The blood samples collected were mixed with heparin to prevent coagulation and stored at −80 °C prior to bio-analysis.

2.3. LC–MS/MS instrumentation

Chromatographic analysis was performed on a high-performance liquid chromatography (HPLC) system, which comprised Agilent 1100 series binary pump, degasser and autosampler (Agilent Technologies, Germany). Chromatographic separation of analytes was achieved using an Agilent ZORBAX Eclipse XDB – C8 analytical reversed-phase HPLC column (50 mm × 2.1 mm, 5 μm; Agilent Technologies, USA). The column temperature was kept at 25 °C. The mobile phase, comprising of water containing 0.1% (v/v) formic acid–acetonitrile (94:6, v/v) was delivered isocratically at a fixed flow rate of 0.5 mL/min. The column effluents were detected by API 4000 triple quadrupole mass spectrometer (Applied Biosystems, MDS SCIEX, Ontario, Canada) using multiple reaction monitoring (MRM).

2.4. Construction of standard curve and sample preparation

Stock solutions of HCQ and IS were prepared in 50% (v/v) methanol in water as 1 mg/mL. Eight working solutions of hydroxychloroquine were prepared by serial dilution with 50% (v/v) methanol in water to achieve concentrations of 0.025, 0.1, 0.25, 0.5, 1.0, 2.5, 5.0 and 10.0 μg/mL. The working solution of the internal standard, HCQ-d4 was prepared as 2.5 μg/mL working solution. Similarly, the three working solutions of the quality control (QC) samples were prepared by serial dilution with 50% (v/v) methanol to achieve concentrations of 0.075, 3.75 and 7.5 μg/mL. All stock solutions and working solutions were stored at −20 °C.

For each chromatographic run, calibrators were freshly prepared. 50 μL of blank human blood was added to the 1.5 mL polypropylene (PP) tube in which 10 μL of working solution of HCQ was spiked and followed by adding 10 μL of IS working solution and 60 μL of Milli-Q water. The tube was vortexed for 30 s. Subsequently, 150 μL of 100% acetonitrile was added to initiate simple direct precipitation of proteins in the human blood sample. The mixture in the tube was then vigorously vortexed for 1 min, followed by centrifugation at 30,000 × *g* for 20 min at 4 °C. Thereafter, 50 μL of the supernatant was transferred to another 1.5 mL polypropylene (PP) centrifuge tube and dried in vacuum for 30 min at 60 °C using concentrator plus (Eppendorf AG, 22331 Hamburg Germany). The dried supernatant was then reconstituted with 100 μL of the mobile phase and a volume of 10 μL was injected per run for quantitative analysis by LC–MS/MS.

The standard calibration curve covering the range of 5–2000 ng/mL was constructed with eight concentrations and the linearity was validated using quality control (QC) samples at three levels for HCQ. The calibrators for HCQ were prepared at the following concentrations of 5, 20, 50, 100, 200, 500, 1000 and 2000 ng/mL. HCQ concentrations of unknown blood samples were back-calculated from the weighted ($1/x$) linear least-squares fitted line of peak area ratio of HCQ to the IS, HCQ-d4 versus standard concentrations. Quantification of patient samples was derived and calculated using interpolation within the standard calibration curve.

2.5. Validation description

A full method validation was performed according to guidelines for bio-analytical method validation by the United States Food and Drug Administration Regulations [19].

The accuracy and precision were validated by analyzing QC samples of hydroxychloroquine at the nominal concentrations of 15, 750 and 1500 ng/mL. Five determinations were performed at each QC sample level. Intra-day accuracy and precision were determined by performing a standard calibration curve with QC samples at three different concentrations, in quintuplicate on a single day. Inter-day accuracy and precision were determined by performing standard calibration curves with QC samples on five separate days. Accuracy was calculated as a percentage of the mean value measured over the nominal value at each concentration whereas precision was expressed in terms of coefficient of variation (CV), defined as a percentage of the standard deviation divided by the mean. The lower limit of detection (LLOD) was defined as the lowest concentration at which the analytical assay can reliably differentiate signal of the analyte peak from background noise ($S/N \geq 3$). The lower limit of quantification (LLOQ) was defined as the lowest calibrator with an interday coefficient of variation <20% with an accuracy of 80–120% [20].

2.6. Dilution validation

In the quantification of hydroxychloroquine in the blood samples of the thirteen patients, there were patient samples that exceeded 2000 ng/mL, the highest limit of quantification in the linear dynamic range of the standard calibration curve. Hence, the samples were repeated using 25 μL of blood sample diluted with 25 μL of blank human blood, instead of 50 μL of blood sample as mentioned earlier in Section 2.4. The procedure was validated with spiked samples at three different concentrations at 2500, 3000 and 4000 ng/mL. The working solutions of HCQ prepared for these three concentrations were 12.5, 15 and 20 μg/mL. The sample preparation method was identical to that mentioned in Section 2.4, with

the exception that the 25 μL of spiked blood sample was diluted with 25 μL of blank human blood, with a dilution factor of two. The procedure was repeated in quintuplicate at each concentration.

2.7. Matrix effect and recovery

To investigate possible effect of the matrix on the quantification of the analyte, QC samples were prepared in quintuplicate at each concentration. Matrix effect (ME) is a common and detrimental phenomenon in LC–MS or LC–MS/MS procedures and can be evaluated accurately according to the following formula:

$$\text{ME (\%)} = \frac{\text{peak area in matrix}}{\text{peak area in neat standard}} \times 100 \quad (1)$$

When ME (%) is equal to 100, this indicates no matrix effect for current LC–MS/MS conditions and sample preparation procedures. Deviations of ME (%) below or above 100 indicate ion suppression or ion enhancement, respectively.

Recovery experiments were also performed in quintuplicate at each QC sample concentration. The samples were analyzed for recovery based on the ratio of the peak area of the analyte in the tube spiked before extraction against that in the tube spiked after extraction and also ratio of the peak area of the IS in the tube spiked before extraction against that in the tube spiked after extraction.

In our current validation procedure, the concentration levels evaluated were at 15, 750 and 1500 ng/mL for HCQ and 500 ng/mL for the internal standard. Three separate sets were prepared. The first set (Set A) was to determine the MS/MS response for neat standard HCQ and IS. The second set (Set B) consisted of the analytes spiked into blood from five different donors after extraction. By comparing the absolute area of Set B against those of Set A, the matrix effect (ion suppression or enhancement) associated with a given lot of blood can be measured. The third set (Set C) was prepared using the same five blood sources as in Set B, but the analytes were spiked into blood before the extraction process. Absolute recovery was determined by comparing the peak area of Set C with those of Set B.

2.8. Stability

Stability of the analytes in the human blood was determined using QC samples in triplicate at each concentration for HCQ.

2.8.1. Freeze and thaw stability

Three, six and nine freeze–thaw cycles were selected for testing the stability. For each set (e.g. three, six and nine freeze–thaw cycles), three aliquots of each QC concentration were prepared in human blood in accordance to the preparative steps stipulated in Section 2.4, stored at −80 °C for 24 h and thawed unassisted at room temperature. Upon completion of thawing, the samples were refrozen at −80 °C for 24 h. The freeze–thaw cycle was then repeated for a total of two, five and eight times respectively to execute three, six and nine freeze–thaw cycles for analysis of stability.

2.8.2. Bench-top stability

Intervals of 4, 8 and 24 h were selected for the analysis of stability. Three aliquots of each QC concentration were prepared in human blood in accordance to the preparative steps stipulated in Section 2.4 and conducted bench-top. Stability was assessed during the resident time in the auto-plate sampler (+4 °C) by taking three repeated measurements at 4, 8 and 24 h.

2.9. Measurement of hydroxychloroquine in human blood

This sensitive, rapid and robust method was successfully applied in a pharmacokinetic study of HCQ for thirteen lung cancer patients receiving an oral daily dose of gefitinib (250 mg) and HCQ (either 400 mg or 600 mg). Prior to sample preparation, the frozen samples were thawed unassisted at room temperature. Sample preparation procedures as stipulated in Section 2.4 were carried out.

3. Results and discussion

3.1. LC–MS/MS optimization

The mass spectrometry parameters were optimized to achieve efficient detection sensitivity. HCQ and its IS were first nebulized by nitrogen gas and introduced into the detector at 400 °C. The analytes were declustered at a potential of 86 V and analyzed by an electrospray interface in positive ionization mode of 5500 V. The optimized collision energy of HCQ and IS was 29 V. The collision cell exit potential was 14 V. Multiple reaction monitoring (MRM) was employed to monitor the precursor ions and product ions as they passed through the mass spectrometer. The optimal mass transitions were 336.4 > 247.3 m/z for HCQ and 340.3 > 251.1 m/z for IS (Fig. 1).

No interfering peaks at the retention time of HCQ and the IS were detected after injection of patient blank blood samples. Under the optimized conditions, the entire chromatographic run was completed within 3 min, with both HCQ and the IS being co-eluted at 1.8 min (Fig. 2).

In the process of optimizing the chromatographic analysis, several critical factors must be considered for realizing a rapid analysis. The selection of HPLC column for the analysis is important in achieving an appropriate chromatographic elution and symmetric peak resulting in better sensitivity of the method. In this study, an octyl (C8) silyl column was found to provide adequate hydrophobicity for the elution of the analytes. In addition, mobile phase was another dominant factor during the optimization. 0.1% formic acid added in mobile phase was able to provide good peak shape and sufficient signal intensity. Lowering pH also enhanced the protonation efficiency of the analytes in the positive ionization mode and improved the resolution of the chromatographic peak. Besides, a low concentration (0.1%) of formic acid was used to preserve the lifespan of the column and also to avoid the possible ionization suppression due to higher concentrations. Compared to methanol, acetonitrile was chosen because it demonstrated better peak symmetry. The final component of the mobile phase was optimized at 94:6 (v/v) ratio of water containing 0.1% formic acid–acetonitrile. This optimal mobile phase could provide an appropriate partition for analytes. Finally, flow rate was altered to achieve a rapid chromatographic run time (<5 min) and also to ensure that the elution of the analytes with retention time far from dead volume to avoid potential interference from endogenous residues from the human blood.

3.2. Extraction protocol optimization

Hydroxychloroquine was extracted using simple protein precipitation with 100% acetonitrile. The extraction efficiency of HCQ was initially evaluated with four different extraction precipitants (1. 100% acetonitrile; 2. 100% methanol; 3. 10% aqueous zinc sulphate solution in acetonitrile (5:95, v/v); 4. 10% aqueous zinc sulphate solution in methanol (5:95, w/v)). The ratio of precipitant to blood was set as 3:1 (v/v). The resulting chromatograms of samples are shown in Fig. 3. The results indicated that 100% acetonitrile was the best choice for achieving most intensive mass signal of the analyte. This result was also supported by our previous study in which as high as 99.9% plasma protein can be removed with 3 fold of 100% acetonitrile as a precipitant [21]. Contrarily, it showed that the addition of 0.5% zinc sulphate resulted in significant severe decay

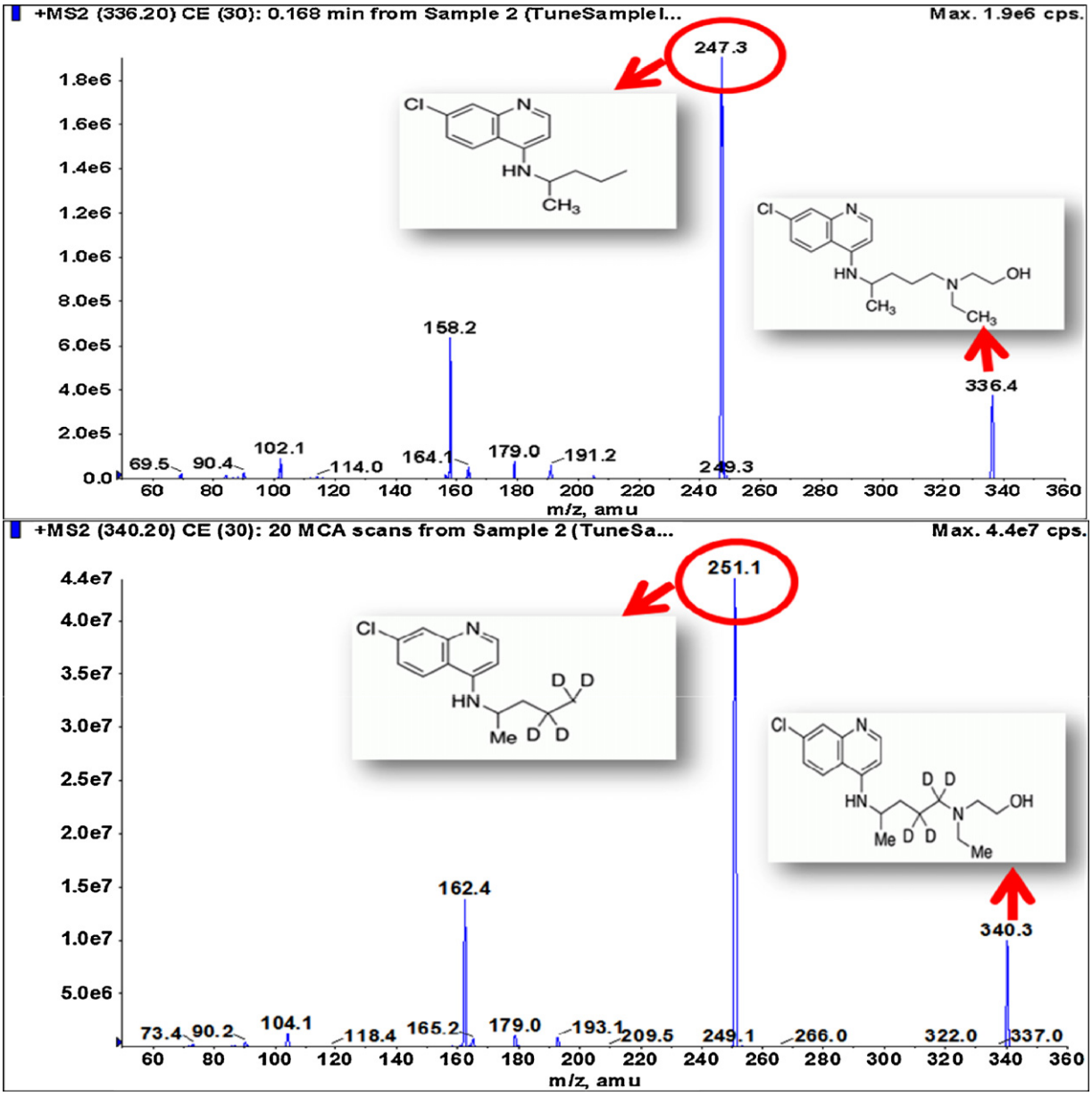

Fig. 1. Product mass spectra of hydroxychloroquine (upper) and IS (lower).

of mass signal even though zinc sulphate can efficiently remove the plasma protein evaluated by spectrophotometric method [22]. However, zinc sulphate can cause severe mass signal suppression and an excessive source contamination. Nevertheless, zinc sulphate still can be used as protein precipitant but an extra solid phase extraction must be followed up to remove the salts which are very harmful to LC–MS analysis [23,24]. Hence, 3-fold volume of acetonitrile was optimized as the precipitant throughout this LC–MS/MS method development and validation procedure.

3.3. Selectivity and linearity

The good selectivity for the optimized method was observed from the chromatograms of the human blood samples from thirteen patients. No significant interference peak was detected when IS was spiked into human blank blood (Fig. 2-1A and 1B). A chromatographic peak of HCQ was clearly identified at LLOD of 2 ng/mL.

The linearity was observed within the dynamic range of 5–2000 ng/mL for HCQ. The accuracy at LLOQ of 5 ng/mL was within 20% which met the requirement of FDA regulations. A weighting factor of $1/x$ (x is the concentration of HCQ) was adopted to minimize the effect of deviation from the slope of the curve at lower concentrations. This is because there is a bigger variance at a higher concentration. When weighed according to $1/x$ least-square linear regression, the mean coefficient of determination (r^2) was found to be 0.9999 for HCQ. The high coefficient of determination implies a very strong correlation between the peak area ratio and concentration of HCQ. A typical equation of the calibration curves was as follow: $y = 0.0175x - 0.0299$, where y represents the ratios of HCQ peak area to that of IS and x represents the blood concentrations of HCQ.

3.4. Accuracy and precision

Intra-day and inter-day method validation was executed using QC samples of at low, medium and high concentrations (15, 750 and 1500 ng/mL). The intra-day and inter-day accuracy and precision were well within 15% stipulated by the US FDA guidelines. Accuracy

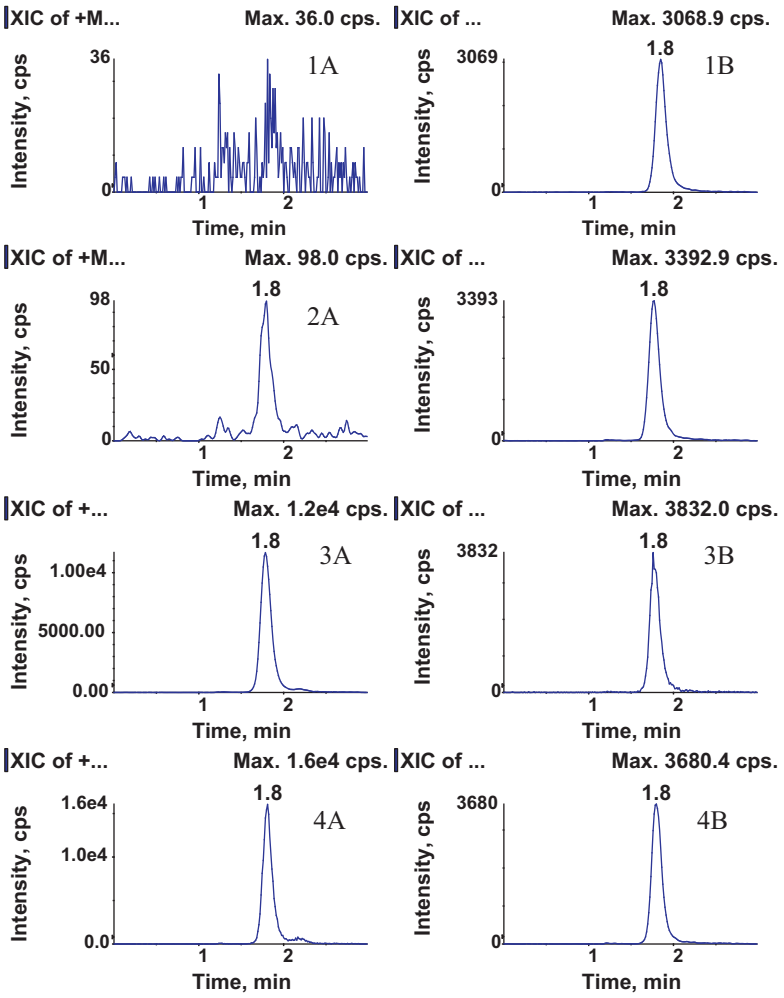

Fig. 2. Representative chromatograms of hydroxychloroquine (A) and IS (B). 1: blank blood; 2: LLOQ in blank blood; 3: patient plasma taken before ingestion of HCQ on day 35; 4: patient plasma taken 4 h after ingestion of HCQ on day 35.

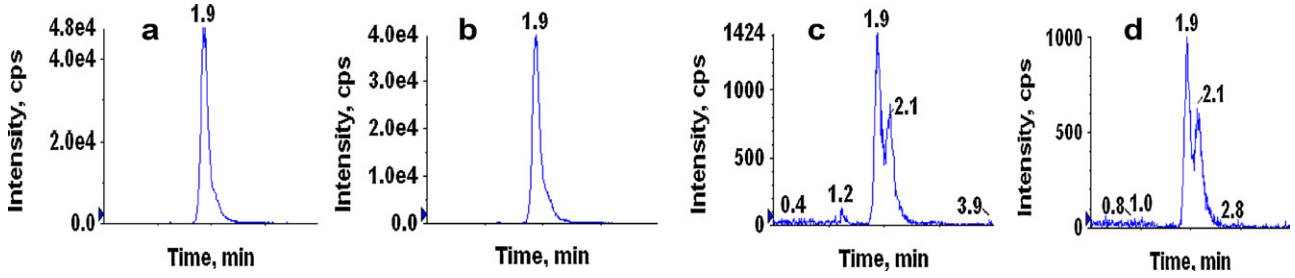

Fig. 3. The extraction efficiency of hydroxychloroquine for four different extraction precipitants (1: 100% acetonitrile; 2: 100% methanol; 3: 10% aqueous zinc sulphate solution in acetonitrile (5:95, w/v); 4: 10% aqueous zinc sulphate solution in methanol (5:95, w/v)).

Table 1
Intra-day and inter-day validation of the determination of HCQ.

HCQ		Norminal conc. (ng/mL)		
		15	750	1500
Intra-day (n^a = 5)				
Found conc. (ng/mL)	Mean ± SD	14.1 ± 0.4	752.5 ± 20.7	1536.9 ± 29.3
	Precision (%)	2.8	2.8	1.9
	Accuracy (%)	94.0	100.3	102.5
Inter-day (n^a = 5)				
Found conc. (ng/mL)	Mean ± SD	15.0 ± 1.2	747.3 ± 19.4	1614.0 ± 55.5
	Precision (%)	8.0	2.6	3.4
	Accuracy (%)	100.0	99.6	107.6

[a] Represents the number of determination.

Table 2
Dilution effect on the accuracies and precisions of concentrations over HLOQ.

Over-range (ng/mL)	Dilution factor	Expected conc. (ng/mL)	Back calculated conc. (ng/mL)	Accuracy (%)	Precision (%)
2500	2	1250	2564.0	102.6	1.6
3000	2	1500	3133.3	104.4	2.5
4000	2	2000	4207.3	105.2	2.4

was within 10% from the actual QC concentration while precision was <10% (Table 1).

In the process of quantifying the NSCLC patient samples, there were a number of samples which contained HCQ concentrations that far exceeded the highest limit of quantification (HLOQ, 2000 ng/mL) of the standard calibration curve. These samples were diluted with blank human blood with a dilution factor of 2. The actual HCQ concentrations in these patient samples were then back calculated by multiplying the quantified concentrations by two (the dilution factor). The quantified concentrations were ensured to be within 10% of the spiked concentrations. Validation of this dilution process was done with spiked samples at three concentrations at 2500, 3000 and 4000 ng/mL, in quintuplicate. Accuracy was within 10% from the nominal concentrations while precision was high, with a CV of <3% (Table 2). With the validation of this dilution method, the patient samples were hence quantified by diluting blood sample 2 fold. As a result, no assumption on the linear relationship of the standard calibration curve at concentration exceeding 2000 ng/mL is made and this ensures accurate determination of the concentrations of HCQ in the thirteen patient samples.

3.5. Matrix effect and recovery

Ion suppression or enhancement, a form of matrix effect, remains an inherent problem in LC–MS/MS analysis and could be the result of interference of endogenous substances from the biological matrices (e.g. human blood) or exogenous substances during sample preparation (e.g. polymers from PP tubes) [25]. Matrix effect was evaluated with QC samples made in duplicate. There was minimal matrix effect on HCQ and IS as the percentages of the analytes in the matrix-based tube as compared to the analytes in reference tube were in the range of 93–100.6% (Table 3). The findings indicated the absence of significant ion suppression or enhancement effect exists (Table 4).

Recovery effect was evaluated with QC samples executed in quintuplicate. The relative recoveries of HCQ and IS were all greater than 92.0%. Recovery is based on the ratio of the peak area of the analytes in the tube spiked before extraction against that in the tube spiked after extraction. This essentially evaluates the efficiency of the extraction protocol that was being optimized. Since the recoveries were well within 10% of the nominal concentration, the results indicated that the extraction protocol is efficient and complete.

3.6. Stability

Validation of the stability of HCQ in human blood was done with QC samples in triplicate at the low, medium and high concentrations (15, 750 and 1500 ng/mL). The QC samples were prepared in blank human blood in accordance to the extraction protocol as indicated in Section 2.4 before the analysis and stored at −80 °C until analysis. Bench-top stability was assessed at 4, 8 and 24 h. Effects of temperature on short-term stability were also assessed by storing the samples at a room temperature of +25 °C, refrigerator temperature of +4 °C and freezer temperature of −80 °C. Freeze–thaw stability was also assessed after 3, 6 and 9 freeze–thaw cycles. QC samples of HCQ showed no signs of significant degradation in all experiments as the accuracy were well within 15% of the nominal concentrations.

The stability study of HCQ in human blood showed reliable stability behaviour as the accuracy of all the samples were within acceptance criterion of ±15% of nominal concentrations. Bench-top stability findings indicated reliable stability behaviour under the regular bench-top experimental conditions. Samples can remain at bench-top for up to 24 h, without showing significant losses in the quantified values. The samples were also stable in human blood for up to nine freeze–thaw cycles.

Table 3
Matrix effect and recovery of hydroxychloroquine and hydroxychloroquine-d4.

Nominal conc. (ng/mL)	Matrix effect[a] (%) (n = 5)		Recovery[b] (%) (n = 5)	
	HCQ	HCQ-d4	HCQ	HCQ-d4
15	93.0	100.6	92.4	93.9
750	96.9	97.0	95.5	100.3
1500	93.7	93.2	103.2	106.6

[a] Expressed as the percentages of HCQ and HCQ-d4 present in the matrix-based tube as compared to the analytes in reference tub.
[b] Expressed as the ratio of the peak area of the analytes in the tube spiked before extraction against that in the tube spiked after extraction.

Table 4
Stability assessment of hydroxychloroquine.

Conditions	QC samples		
	15 (ng/mL)	750 (ng/mL)	1500 (ng/mL)
Auto-sampler (+4 °C)			
4 h	95.3	97.2	98.3
8 h	96.6	97.6	99.7
24 h	103.4	99.8	99.5
Bench-top (room temp, +25 °C)			
4 h	97.4	98.5	97.5
8 h	96.3	100.0	100.7
24 h	95.7	99.7	103.0
Freeze–thaw (−80 °C)			
3 cycles	95.7	100.8	102.0
6 cycles	100.6	101.7	101.8
9 cycles	98.7	99.5	100.2

3.7. Application of validated LC–MS/MS method

The developed method for the quantification of HCQ in human blood was successfully applied in a phase I clinical trial, in which

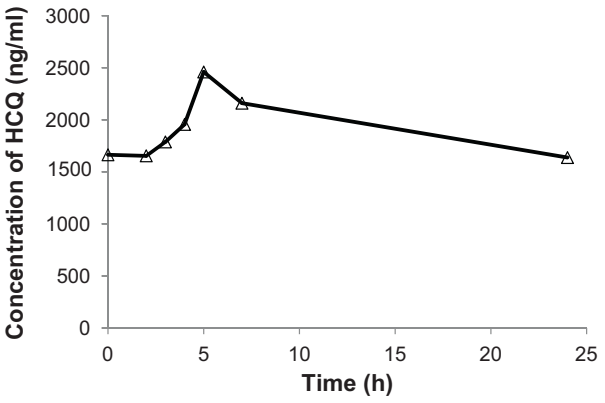

Fig. 4. Concentration–time profiles of hydroxychloroquine of a patient on day 35 after ingestion of 600 mg of hydroxychloroquine daily.

the blood samples of thirteen patients were quantified for the concentrations of HCQ. The concentration–time profiles of blood HCQ of a patient on day 35 after ingestion of 600 mg of HCQ daily was described in Fig. 4. The rapid chromatographic run time of 3 min facilitated a high analysis throughput, with the ability to quantify a larger number of clinical samples in a shorter time frame.

4. Conclusions

In summary, a simple, novel, rapid and specific LC–MS/MS assay for the quantification of hydroxychloroquine in human blood was developed and fully validated as per FDA guidelines. This method offers significant advantages over those previously reported, in terms of shorter run time (3.0 min), improved sensitivity and selectivity and simpler sample preparation. Excellent linearity was demonstrated within the range of 5–2000 ng/mL. Accuracy and precision were well within FDA guidelines of <15%. The method was also successfully utilized for the quantification of HCQ in human blood in an ongoing phase I clinical trial to determine the pharmacokinetics of HCQ in NSCLC patients.

Acknowledgements

This work was supported by the National Research Foundation of Singapore (Experimental Therapeutics Program) and the National Medical Research Council of Singapore (NMRC/CSA/021/2010).

References

[1] C.F. Lacy, L.L. Armstrong, Drug Information Handbook with International Trade Names Index, 19th ed., Lexicomp, 2010, pp. 818–820.
[2] Micromedex® Healthcare Series. Available from: http://www.thomsonhc.com.libproxy1.nus.edu.sg/hcs/librarian/ND_T/HCS/ND_PR/Main/CS/F31D18/DUPLICATIONSHIELDSYNC/087B62/ND_PG/PRIH/ND_B/HCS/SBK/3/ND_P/Main/PFActionId/hcs.common.RetrieveDocumentCommon/DocId/2557/ContentSetId/31#adultDosageSection.
[3] National University Hospital (NUH), Massachusetts General Hospital (MGH), AstraZeneca, Hydroxychloroquine and Gefitinib to treat Lung Cancer, 2008. Available from: http://clinicaltrials.gov/ct2/show/NCT00809237.
[4] H.C. Swaisland, M.V. Cantarini, R. Fuhr, A. Holt, Exploring the relationship between expression of cytochrome P450 enzymes and gefitinib pharmacokinetics, Clin. Pharmacokinet. 45 (2006) 633–644.
[5] D. McKillop, A.D. McCormick, A. Millar, G.S. Miles, P.J. Phillips, M. Hutchison, Cytochrome P450-dependent metabolism of gefitinib, Xenobiotica 35 (2005) 39–50.
[6] D. McKillop, A.D. McCormick, G.S. Miles, P.J. Phillips, K.J. Pickup, N. Bushby, M. Hutchison, In vitro metabolism of gefitinib in human liver microsomes, Xenobiotica 34 (2004) 983–1000.
[7] J. Li, M. Zhao, P. He, M. Hidalgo, S.D. Baker, Differential metabolism of gefitinib and erlotinib by human cytochrome P450 enzymes, Clin. Cancer Res. 13 (2007) 3731–3737.
[8] T. Munster, J.P. Gibbs, D. Shen, B.A. Baethge, G.R. Botstein, J. Caldwell, F. Dietz, R. Ettlinger, H.E. Golden, H. Lindsley, G.E. McLaughlin, L.W. Moreland, W.N. Roberts, T.W. Rooney, B. Rothschild, M. Sack, A.I. Sebba, M. Weisman, K.E. Welch, D. Yocum, D.E. Furst, Hydroxychloroquine concentration–response relationships in patients with rheumatoid arthritis, Arthritis Rheum. 46 (2002) 1460–1469.
[9] S.J. Carmichael, B. Charles, S.E. Tett, Population pharmacokinetics of hydroxychloroquine in patients with rheumatoid arthritis, Ther. Drug Monit. 25 (2003) 671–681.
[10] D.R. Miller, J.J. Fiechtner, J.R. Carpenter, R.R. Brown, R.M. Stroshane, V.J. Stecher, Plasma hydroxychloroquine concentrations and efficacy in rheumatoid arthritis, Arthritis Rheum. 30 (1987) 567–571.
[11] N. Costedoat-Chalumeau, Z. Amoura, J.S. Hulot, G. Aymard, G. Leroux, D. Marra, P. Lechat, J.C. Piette, Very low blood hydroxychloroquine concentration as an objective marker of poor adherence to treatment of systemic lupus erythematosus, Ann. Rheum. Dis. 66 (2007) 821–824.
[12] N. Costedoat-Chalumeau, Z. Amoura, J.S. Hulot, H.A. Hammoud, G. Aymard, P. Cacoub, C. Francès, B. Wechsler, L.T. Huong du, P. Ghillani, L. Musset, P. Lechat, J.C. Piette, Low blood concentration of hydroxychloroquine is a marker for and predictor of disease exacerbations in patients with systemic lupus erythematosus, Arthritis Rheum. 54 (2006) 3284–3290.
[13] H.S. Lim, J.S. Im, J.Y. Cho, K.S. Bae, T.A. Klein, J.S. Yeom, T.S. Kim, J.S. Choi, I.J. Jang, J.W. Park, Pharmacokinetics of hydroxychloroquine and its clinical implications in chemoprophylaxis against malaria caused by *Plasmodium vivax*, Antimicrob. Agents Chemother. 53 (2009) 1468–1475.
[14] S.E. Tett, D.J. Cutler, R.O. Day, K.F. Brown, Bioavailability of hydroxychloroquine tablets in healthy volunteers, Br. J. Clin. Pharmacol. 27 (1989) 771–779.
[15] M. Somer, J. Kallio, U. Pesonen, K. Pyykkö, R. Huupponen, M. Scheinin, Influence of hydroxychloroquine on the bioavailability of oral metoprolol, Br. J. Clin. Pharmacol. 49 (2000) 549–554.
[16] H.C. Swaisland, M. Ranson, R.P. Smith, J. Leadbetter, A. Laight, D. McKillop, M.J. Wild, Pharmacokinetic drug interactions of gefitinib with rifampicin, itraconazole and metoprolol, Clin. Pharmacokinet. 44 (2005) 1067–1081.
[17] R.R. Brown, R.M. Stroshane, D.P. Benziger, High-performance liquid chromatographic assay for hydroxychloroquine and three of its major metabolites, desethylhydroxychloroquine, desethylchloroquine and bidesethylchloroquine, in human plasma, J. Chromatogr. 377 (1986) 454–459.
[18] S.E. Tett, D.J. Cutler, K.F. Brown, High performance liquid chromatographic assay for hydroxychloroquine and metabolites in blood and plasma, using a stationary phase of poly (styrenedivinylbenzene) and a mobile phase at pH 11, with fluorimetric detection, J. Chromatogr. 344 (1985) 241–248.
[19] Guidance for Industry, Bioanalytical Method Validation. Available from: http://www.fda.gov/downloads/Drugs/GuidanceComplianceRegulatoryInformation/Guidances/ucm070107.pdf.
[20] L.Z. Wang, L.S.U. Lee, W.L. Thuya, G.H. Soon, L.R. Kong, P.L. Nye, E.J.D. Lee, C. Flexner, B.C. Goh, Simultaneous determination of raltegravir and raltegravir glucuronide in human plasma by liquid chromatography–tandem mass spectrometric method, J. Chromatogr. B 46 (2011) 202–208.
[21] L.Z. Wang, M.Y. Lim, T.M. Chin, W.L. Thuya, P.L. Nye, A. Wong, S.Y. Chan, B.C. Goh, P.C. Ho, Rapid determination of gefitinib and its main metabolite, O-desmethyl gefitinib in human plasma using liquid chromatography–tandem mass spectrometry, J. Mass Spectrom. 879 (2011) 2155–2161.
[22] C. Polson, P. Sarkar, B. Incledon, V. Raguvaran, R. Grant, Optimization of protein precipitation based upon effectiveness of protein removal and ionization effect in liquid chromatography–tandem mass spectrometry, J. Chromatogr. B 785 (2003) 263–275.
[23] M. Josefsson, I. Rydberg, Determination of methylphenidate and ritalinic acid in blood, plasma and oral fluid from adolescents and adults using protein precipitation and liquid chromatography tandem mass spectrometry—a method applied on clinical and forensic investigations, J. Pharm. Biomed. Anal. 55 (2011) 1050–1059.
[24] N. Manoa, M. Satoa, M. Nozawab, Y. Matsumotoa, M. Moria, H. Yamaguchia, J. Gotoa, M. Shimadaa, An accurate quantitative LC/ESI–MS/MS method for sirolimus in human whole blood, J. Chromatogr. B 879 (2011) 987–992.
[25] B.K. Matuszewski, M.L. Constanzer, C.M. Chavez-Eng., Strategies for the assessment of matrix effect in quantitative bioanalytical methods based on HPLC–MS/MS, Anal. Chem. 75 (2003) 3019–3030.

Journal of Pharmaceutical and Biomedical Analysis 61 (2012) 93–99

Contents lists available at SciVerse ScienceDirect

Journal of Pharmaceutical and Biomedical Analysis

journal homepage: www.elsevier.com/locate/jpba

Determination of piperazine-type stimulants in human urine by means of microextraction in packed sorbent and high performance liquid chromatography-diode array detection

I.E.D. Moreno[a], B.M. da Fonseca[a], M. Barroso[b,*], S. Costa[b], J.A. Queiroz[a], E. Gallardo[a]

[a] CICS-UBI - Centro de Investigação em Ciências da Saúde, Universidade da Beira Interior, Av. Infante D. Henrique, 6201-556 Covilhã, Portugal
[b] Serviço de Toxicologia Forense, Instituto Nacional de Medicina Legal–Delegação do Sul, Rua Manuel Bento de Sousa, 3, 1150-219 Lisboa, Portugal

ARTICLE INFO

Article history:
Received 6 October 2011
Received in revised form 4 December 2011
Accepted 6 December 2011
Available online 13 December 2011

Keywords:
Microextraction by packed sorbent
Piperazines
HPLC-DAD
Urine

ABSTRACT

A method using microextraction by packed sorbent (MEPS) and high performance liquid chromatography-diode array detection (HPLC-DAD) is described for the determination of piperazine-type stimulants in human urine. The studied compounds were 1-benzylpiperazine (BZP), 1-(3-trifluoromethylphenyl) piperazine (TFMPP), 1-(3-chlorophenyl) piperazine (mCPP) and 1-(4-methoxyphenyl) piperazine (MeOPP); 1-(2-chlorophenyl)-piperazine (oCPP) was used as internal standard (IS).

The factors which might influence the extraction were screened previously using the fractional factorial design approach, and none of them influenced significantly the process.

The procedure was linear for concentrations ranging from 0.1 (lower limit of quantitation – LLOQ) to 5 μg/mL, with determination coefficients (R^2) higher than 0.99 for all analytes in all runs. The limits of detection were 0.1 μg/mL for BZP and TFMPP, while for MeOPP and mCPP 0.05 μg/mL was obtained. Intra- and interday precision ranged from 1 to 14%, and accuracy was within a ±15% interval for all analytes, fulfilling the criteria normally accepted in bioanalytical method validation. Under the optimized conditions, extraction efficiency was higher than 80% for all analytes, except BZP (50%).

MEPS showed to be a rapid (<2 min) and simple procedure for the determination of piperazine-type stimulants in human urine, allowing reducing the handling time and costs usually associated to this type of analysis. Furthermore, the fact that only 0.1 mL of sample is required make this method a valuable and powerful tool for drug monitoring in human urine in situations where those compounds are involved, for instance in forensic scenarios.

© 2011 Elsevier B.V. All rights reserved.

1. Introduction

The term "designer drugs" refers to modified substances, both natural and synthetic, or completely designed molecular structures presenting psychotropic effects [1]. These new "designer drugs" can be divided into several subgroups, including piperazine derivatives [1], from which the most prominent are 1-benzylpiperazine (BZP), 1-(3-trifluoromethylphenyl)piperazine (TFMPP), 1-(3-chlorophenyl)piperazine (mCPP) and 1-(4-methoxyphenyl)piperazine (MeOPP) [2,3] (Fig. 1). Piperazine was originally used in veterinary medicine to treat parasitic infections, while its derivatives are extensively used as recreational drugs all over the world, despite their prohibition in several countries [4]. The mixture of BZP and TFMPP produces effects similar to those of MDMA [5,6]. The action of piperazine-type compounds involves serotonin (5-HT) uptake inhibition and 5-HT1 receptor agonistic effects [3,6], and they may act as stimulants producing euphoria [7]. The best pharmacologically characterized piperazine is mCPP, a known metabolite of the antidepressant drugs trazodone and nefazodone, which acts by increasing the extracellular levels of dopamine, serotonin and noradrenalin [7–9].

The elimination of piperazines occurs mainly through the kidney, and for the most lipophilic drugs (mCPP and TFMPP) less than 1% of the dose is eliminated unchanged in urine [10,11]. TFMPP is largely metabolized by the body and excreted in urine [8,12], with 4-hydroxy-TFMPP as its main metabolite [5,10]. Concerning BZP, it is not extensively metabolized, and is excreted unchanged in the urine [10].

Staack et al. [12] reported that some metabolites are excreted as sulphuric and/or glucuronic acid conjugates, and have been detected in urine 48 h after administration.

* Corresponding author. Tel.: +351 218811800; fax: +351 218850078.
E-mail address: mbarroso@dlinml.mj.pt (M. Barroso).

0731-7085/$ – see front matter © 2011 Elsevier B.V. All rights reserved.
doi:10.1016/j.jpba.2011.12.004

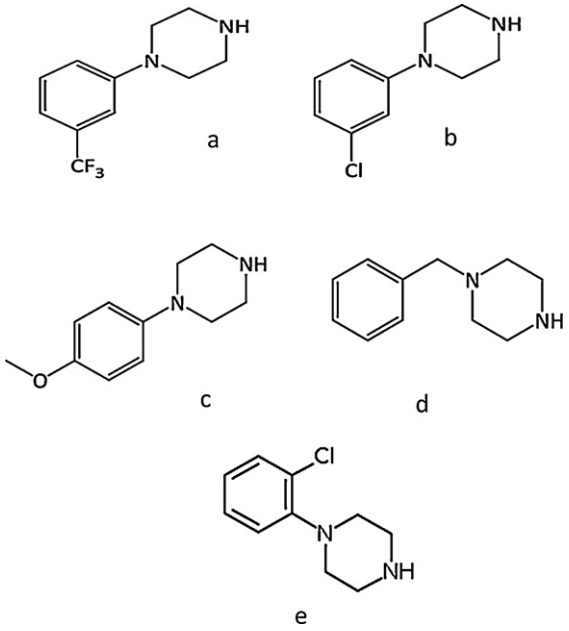

Fig. 1. Structural formulae of the studied piperazines: TFMPP (a), mCPP (b), MeOPP (c), BZP (d), and IS (e).

A few papers have been published on the analysis of those compounds in biological specimens, namely the detection of BZP, 4-methylenedioxibenzylpiperazine (MDBP), TFMPP, mCPP, and MeOPP in blood, plasma and urine [1,9,12,13]; and of TFMPP, mCPP and MeOPP in hair [7]. In those articles, sample preparation was performed mainly by means of liquid-liquid extraction (LLE) [9] or solid-phase extraction (SPE) [1,7]. However, those sample preparation procedures are often time-consuming, laborious and expensive; in addition, they present deleterious effects on the environment as well, due to the high amounts of organic solvents that need to be used and discarded.

Microextraction by packed sorbent (MEPS) appears to be a good alternative to solve those problems. This recent technique for sample preparation is based on the miniaturization of conventional SPE, using a gas-tight syringe as the extraction device; this allows the online coupling to either gas or liquid chromatographic systems without modifications in the extracting device [14,15].

Several applications have been published on the use of this technique, namely the detection of 2,4,6-trichloroanisole and 2,4,6-tribromoanisole in wine [16], organic pollutants, parabens and triclosan in wastewater [17,18], and polycyclic aromatic hydrocarbons in water [19]. Biological samples have also been analysed using MEPS, namely blood, serum or plasma for risperidone, antidepressants, olomoucine and ropivacaine [20–23], and urine for the detection of cotinine [24]. However, its application to the analysis of piperazines in biological samples has not been published yet. High efficiencies are usually obtained (60–90%) using MEPS, and it is possible to use a wide range of sample volumes. The extraction time is reduced, and the use of organic solvents is minimal [15,21–23]; furthermore, the packing material can be reused, allowing several extractions to be performed using the same device [15,23]. One feature concerning MEPS is that the extraction conditions should be optimized previously, in order to obtain maximum efficiency and less interference by matrix constituents. The number of factors that need to be optimized is often high, and therefore factorial design appears to be a good way of designing the whole experiment; indeed, it allows planning the entire procedure, aiming at investigating the effect of the controlled factors on the response [25]. In addition, the extent at which the several variables interact with each other can be also documented using a minimal number of experiments [25].

This paper describes the use of MEPS for sample preparation in the quantitative determination of piperazines (BZP, TFMPP, mCPP and MeOPP) in human urine, allowing reducing the sample preparation time to less than 2 min.

2. Experimental

2.1. Standards and reagents

The analytical standards of BZP dihydrochloride, TFMPP hydrochloride and mCPP were purchased from Lipomed (Arlesheim, Switzerland) as 1 mg/mL solutions; MeOPP dihydrochloride and oCPP hydrochloride (internal standard, IS) were purchased from Sigma–Aldrich (Steinheim, Germany). Ammonium formate and acetic acid (50% purity) were acquired from Sigma–Aldrich (Switzerland). Methanol (HPLC grade) was obtained from Merck Co (Darmstadt, Germany). Ammonium hydroxide (analytical grade) was obtained from J.T. Baker (Holland). Ultrapure water was obtained from a Milli-Q System (Millipore, Billerica, MA, USA). MEPS 100–250 μL syringe and MEPS BIN (Barrel insert and Needle) M_1 (4 mg; 80% C_8 and 20% SCX) (SGE Analytical Science, Australia) were purchased from ILC (Porto, Portugal).

Stock solutions of MeOPP and oCPP were prepared at 1 mg/mL by weighing 10 mg of the compound in a 10 mL volumetric flask, and filling up to volume with methanol. Working solutions at 10 and 1 μg/mL were prepared for all analytes by proper dilution of the stock solutions with methanol. A working solution of the IS at 10 μg/mL was prepared also in methanol. All these solutions were stored in amber glass vials and light protected between 2 and 8 °C.

To prepare the 5 mM ammonium formate solution (pH 6.4), 315.3 mg of ammonium formate was weighed in a volumetric flask and a final volume of 1 L was obtained with ultrapure water.

2.2. Biological samples

Drug-free urine samples were provided by laboratory staff.

2.3. Liquid chromatographic conditions

Analyses were carried out using an HPLC system (Agilent 1290 Infinity LC) equipped with an Agilent 1290 Infinity Detector (G4212A DAD). The piperazines were separated in a Zorbax 300 SB-C_{18} (5 μm, 4.6 mm × 150 mm) column (Agilent) at 25 °C with a mobile phase consisting of 5 mM ammonium formate (pH 6.4)-methanol (55:45, v/v), using the isocratic mode at a flow rate of 0.8 mL/min. The mobile phase was filtered under vacuum (0.2 μm hydrophilic polypropylene filter) and degassed in an ultrasonic bath before use. The monitored wavelengths were 211 for BZP, 208 for mCPP, 236 for MeOPP, and 246 nm for TFMPP and IS, and their retention times were, in minutes, 6.0, 7.8, 4.8, 9.8 and 7.4 respectively.

2.4. Sorbent activation

The sorbent was manually activated with 100 μL of methanol followed by 100 μL of water before its first use.

2.5. Sample preparation

For the optimization study, 4-mL aliquots of urine were spiked with all compounds at 4 μg/mL, slightly agitated for 15 min and stored light protected until extraction by MEPS.

The extraction procedure has been previously optimized (see Section 3.1), and the final conditions are the following.

Table 1
Design matrix for the 2_V^{5-1} fractional factorial design showing the independent variables (experimental factors) expressed in real values and experimental peak area ratios as dependent variable.

Std order[a]	Experimental factors					Response			
	Sample dilution	Strokes	% Acetic acid	% MeOH wash	% NH_4OH elution	MeOPP	BZP	mCPP	TFMPP
1	2	2	5	100	5	0.694	0.398	1.037	0.824
2	2	8	1	100	5	0.712	0.318	1.176	0.962
3	2	8	1	10	1	0.748	0.540	1.054	0.936
4	4	2	5	10	5	0.442	0.297	0.707	0.710
5	4	2	1	10	1	0.070	0.530	0.892	0.724
6	2	2	1	10	5	0.541	0.321	0.704	0.725
7	2	2	1	100	1	0.021	0.066	0.233	0.203
8	4	8	5	100	5	0.273	0.373	0.462	0.349
9	4	8	1	10	5	1.016	0.383	1.427	1.362
10	2	2	5	10	1	0.332	0.566	0.734	0.651
11	4	8	1	100	1	0.067	0.385	0.483	0.384
12	4	2	1	100	5	0.622	0.342	0.963	0.864
13	2	8	5	100	1	0.760	0.544	0.994	1.017
14	4	8	5	10	1	0.321	0.606	1.030	0.905
15	4	2	5	100	1	0.574	0.503	0.641	0.531
16	2	8	5	10	5	0.587	0.327	0.802	0.724

[a] The experiments are listed in standard order (std order), although they have been performed in random order. In the above matrix, each row represents an experimental run.

Twenty-five microliters of the IS solution (10 μg/mL) was added to 0.1 mL urine previously diluted with 0.1 mL of deionized water in a glass tube, and the sample was slightly vortex-mixed for 30 s. Then, it was manually drawn through the sorbent and ejected in the same vial 8 times (strokes) at a flow rate of 10 μL/s. The sorbent was washed with 250 μL of 1% acetic acid and 100 μL of 10% methanol in water to remove matrix-borne interferences. The analytes were eluted with 50 μL of 5% ammonia in methanol, and injected into the chromatographic system. After each extraction, the sorbent was washed sequentially with 5× 250 μL methanol and 4× 250 μL water. This step aimed at decreasing memory effects, conditioning simultaneously the sorbent for the next extraction. Under these optimal conditions, each sorbent could be used for about 100 extractions.

2.6. Fractional factorial design

The conditions for MEPS extraction were studied by means of the fractional factorial design methodology. The peak area of each analyte after extraction by MEPS was divided by the peak area of the same analyte obtained after a daily injection of a standard mixture containing all compounds [in order to compensate injection differences ($n = 3$)]; this peak area ratio was used as the measured response (dependent variable).

At an initial stage, the factors (independent variables) which could affect analyte extraction, as well as their interactions, were screened by means of a two-level-five factor half fractional factorial design (2_V^{5-1}) [26]. The factors were selected according to the literature [15], and were studied at two levels, low (−1) and high (+1). The studied factors and respective levels (low; high) were sample dilution (2; 4), number of sample aspirations through the device (strokes) (2; 8), amount of acetic acid (%) for sorbent activation (1; 5), percentage of methanol to remove interferences (washing step) (10; 100) and amount of ammonia (%) in the eluting solvent (methanol) (1; 5). It should be stressed that if a full factorial design (2^5) had been used in this particular study, it would require 32 experiments to be conducted in order to cover all possible combinations of factors' levels. However, many of those experiments would evaluate higher order interactions, which are usually negligible in routine practice [26]. In addition, the used approach has the advantage that less effort is spent in obtaining the same amount of data, saving time and money. Therefore, the number of experiments is reduced by combining the main effects with the higher order interactions; this is made in the assumption that those interactions are not likely to be of significance, and the observed effects are due to the main effects only. Likewise, the second order interactions are confounded with the third order interactions.

The independent variables, the corresponding values for the low and high levels, and the obtained matrix for this screening design are shown in Table 1. These experiments were carried out in a random order, to avoid the influence of noise factors and minimizing systematic errors.

The experimental design matrices were performed and evaluated using the MINITAB® statistical software, version 15.

3. Results and discussion

3.1. Optimization of the extraction parameters

Using a cationic exchange sorbent M_1 (SCX), the parameters susceptible of influencing the extraction process (and their respective levels) [sample dilution (2 and 4), strokes (2 and 8), sorbent activation with acetic acid (1 and 5%, v/v), amount of methanol in the washing step (10 and 100%, v/v) and the amount of ammonia on analytes elution (1 and 5%, v/v)] were studied using the fractional factorial design approach.

The experimental results obtained for this screening design under the different conditions of the studied factors are shown in Table 1.

These results were interpreted considering the Pareto Chart of main effects and linked interactions, which graphically displays the magnitudes of the effects. At the studied levels, none of the factors or interactions influenced significantly the response, and this was verified for all analytes (data not shown). Therefore, the factors could be set at the most convenient values, that is, those which originated a better response, despite the lack of statistical significance of the observed effect. In addition, a compromise had to be established, since the best levels of the factors were not the same for all analytes. For instance, the amount of ammonia in the eluting solvent had a slightly negative effect on BZP extraction, meaning that the extraction efficiency for this compound decreased with the increase from 1 to 5%. However, the opposite happened for the remaining analytes, and therefore 5% was chosen for the elution.

The final extraction conditions were therefore a sample dilution of 1:2, 8 strokes, the sorbent was activated with 1% of acetic acid, the interferences were washed out with 10% methanol and the analytes were eluted with 5% of ammonia in methanol. It should be stressed that the fractional factorial design allowed the reduction

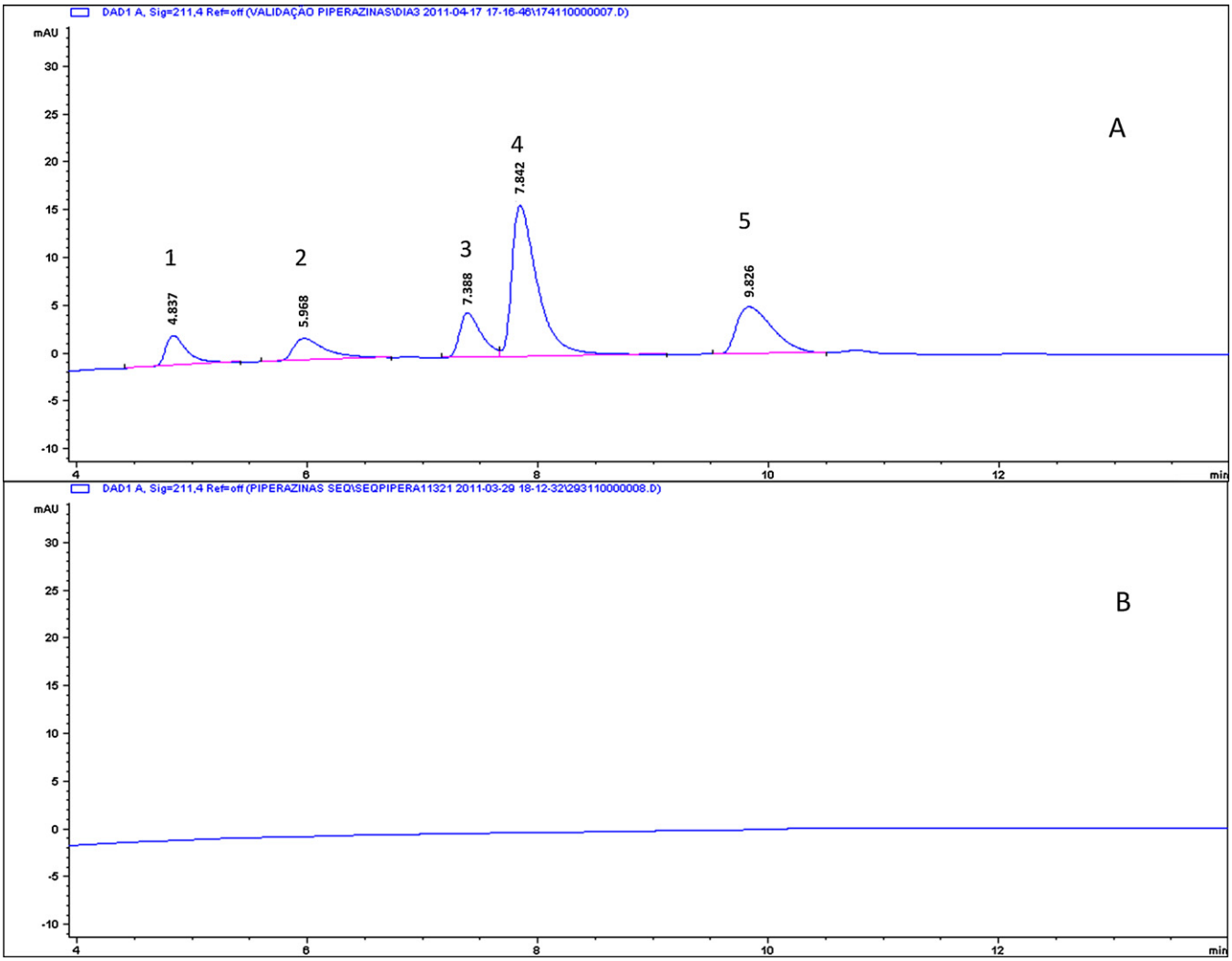

Fig. 2. Chromatogram of a blank (B) and a sample spiked with all analytes (A) (5 μg/mL). MeOPP (1), BZP (2), IS (3), mCPP (4) and TFMPP (5).

of the number of experiments, which would be much higher if a univariate approach had been used.

Using this optimized procedure sample preparation could be performed in less than 2 min, and this is an overwhelming advantage when compared to other sample preparation approaches, namely LLE and SPE.

3.2. Method validation

The described method was fully validated according to the guiding principles of the Food and Drug Administration (FDA) [27] and International Conference on Harmonization (ICH) [28]. The studied parameters were selectivity, linearity and calibration model, limits, intra- and interday precision and accuracy, recovery and stability.

3.2.1. Selectivity

The method's selectivity was evaluated by analysis of blank urine samples, which were checked for interferences at the retention times of the studied compounds. In addition, several other abused drugs [including amphetamines (amphetamine, methamphetamine, MDMA, MDA, MBDB, MDEA), opiates (morphine, codeine, 6-acetylmorphine, tramadol) and cocaine and metabolites (cocaine, benzoylecgonine, ecgonine methyl ester)], medicines (piracetam, trazodone, ketoprofen), alkaloids (papaverine, nicotine, narceine) and caffeine were also tested. No interferences from endogenous substances were observed, and the other compounds presented different retention times and/or could not be detected using our method's conditions. Fig. 2 shows a chromatogram of a blank and a sample spiked with all analytes.

3.2.2. Calibration curves and limits

To evaluate the method's linearity, urine samples spiked at final concentrations ranging from 0.1 to 5 μg/mL were prepared and analysed by the described procedure (eight calibrators evenly distributed, five replicates). Along with each calibration curve, a zero sample (blank sample with internal standard) and two quality control samples at medium (MQC: 1.5 μg/mL) and high (HQC: 3.5 μg/mL) concentrations ($n = 3$) were also analysed.

Calibration curves were obtained by plotting the peak-area ratio between each analyte and the internal standard against analyte concentration. Due to the wide calibration range and to compensate for heterocedasticity, weighted least squares regressions had to be adopted. Six weighting factors were evaluated for each analyte ($1/\sqrt{x}$, $1/x$, $1/x^2$, $1/\sqrt{y}$, $1/y$, $1/y^2$), and the one which originated the best results was selected taking into account the data obtained during the assessment of the interday precision and accuracy [7]. Using each of those factors, the mean relative errors of each calibrator were calculated and their absolute value was summed. The weighting factor for which the sum of errors was smaller (presenting simultaneously a mean R^2 value of at least 0.99) was selected

Table 2
Linearity data.

	Weight	Linear range (μg/mL)	Linearity		R^2	LLOQ (μg/mL)[b]
			Slope[a]	Intercept[a]		
MeOPP	$1/x^2$	0.1–5	0.7008 ± 0.0506	−0.0290 ± 0.0068	0.9927 ± 0.0030	0.1
BZP	$1/x^2$	0.1–5	0.4272 ± 0.0407	0.0387 ± 0.0787	0.9948 ± 0.0026	0.1
mCPP	$1/y$	0.1–5	2.4443 ± 0.2663	−0.0992 ± 0.0683	0.9948 ± 0.0018	0.1
TFMPP	$1/x$	0.1–5	1.1305 ± 0.2190	−0.0112 ± 0.0361	0.9960 ± 0.0024	0.1

[a] Mean values ± standard deviation.
[b] Lower limit of quantitation.

for each analyte. These factors were $1/x^2$ for MeOPP and BZP, $1/x$ for TFMPP and $1/y$ for mCPP.

By means of these weighted least squares regressions, linear relationships were obtained, and the calibrators' accuracy [mean relative error (bias) between measured and spiked concentrations] was in accordance with the above-mentioned criteria (±15% for all concentrations, except at the lower limit of quantitation – LLOQ – for which ±20% was accepted). Calibration data is shown in Table 2.

The LLOQ was defined as the lowest piperazine concentration that could be measured with adequate precision (coefficient of variation of less than 20%) and accuracy (within ±20% of the nominal concentration), and were determined by analysing six replicates of spiked urine samples independent from those of the calibration curve. These limits have been found to be 0.1 μg/mL for all analytes. The limits of detection (LOD), defined as the lowest tested concentration yielding a signal-to-noise ratio of at least 3, were 0.05 μg/mL for MeOPP and mCPP and 0.1 μg/mL for the remaining compounds.

These limits are satisfactory, particularly when compared to those obtained by other authors. For instance, Vorce et al. [29] have obtained the same values (0.1 μg/mL) using LC–MS, while Dickson et al. [30] obtained lower limits (0.025 μg/mL) using GC–MS. However, it should be taken into account that in this latter study the authors have used a significantly higher sample volume (2 mL), whereas in our method only 0.1 mL of sample is used. Other authors [4] have also utilized a higher sample volume, and therefore our obtained limits are comparable. Furthermore, a less sensitive detector is used in our method, which highlights the power of the developed sample preparation procedure herein described.

Moreover, these limits are adequate for monitoring those compounds routinely, since their concentrations in urine samples usually fall within the dynamic range of the assay.

3.2.3. Intra- and interday precision and accuracy

Intra-day precision and accuracy were evaluated at 6 concentration levels (0.1, 0.25, 0.5, 1, 3 and 5 μg/mL) using spiked samples prepared and analysed as mentioned above (six replicates for each concentration). The obtained coefficients of variation (CVs) were in general lower than 15% for all the compounds at all tested concentrations, presenting a mean relative error within a ±12% interval. These results are presented in Table 3.

Interday precision and accuracy were evaluated at eight concentrations within a 5-day period. The calculated CVs were lower than 15% for all compounds at all concentration levels, while accuracy (in terms of mean relative error) was within a ±7% interval. These data are presented in Table 4. In addition, combined intra- and interday precision was assessed by analysis of the quality control samples (1.5 and 3.5 μg/mL) analysed in triplicate over the same 5-day period (15 measurements); the obtained CVs were always lower than 15% for all analytes, and the relative error was within a ±6% interval from the target concentration.

3.2.4. Extraction efficiency

For recovery studies, six replicates of two concentrations (2 and 4 μg/mL) were analysed by the described optimized method. The obtained peak areas were compared to those obtained by injecting the same amount of the analytes in methanol (100% recovery). The absolute recoveries (%) (2; 4 μg/mL) were as follows: MeOPP (83.7; 74.0); mCPP (99.6; 95.1); TFMPP (100.5; 100.1) and BZP (61.2; 52.0).

These values are excellent when compared to other extraction techniques like SPE [1], where 70% efficiency was obtained for all piperazines, and LLE [31], which presented 80% efficiency for mCPP. However, the determination of piperazines in urine samples by means of MEPS has not been published in the literature yet, and therefore we cannot compare our results.

3.2.5. Stability

In order to study stability in processed samples, urine was spiked with 1.5 and 3.5 μg/mL of all compounds, and extracted using the above mentioned procedure ($n = 3$). However, after extraction the extract was left standing at room temperature in the autosampler for 24 h. Those samples were compared to freshly prepared samples, and the obtained coefficients of variation were less than 12% for all compounds, meaning that the analytes are stable in the extracts for at least 24 h at room temperature.

Short-term stability was evaluated at the same concentration levels ($n = 3$). Urine samples were spiked and were left at room temperature for 24 h. These were compared to samples prepared and analysed in the same day; the obtained coefficients of variation

Table 3
Intra-day precision and accuracy ($n = 6$).

Compound	Spiked[a]	Measured[a]	CV[b] (%)	RE[c] (%)
MeOPP	0.1	0.10	6.44	4.27
	0.25	0.25	7.53	1.16
	0.5	0.47	3.89	−5.74
	1	1.01	2.74	1.34
	3	3.00	7.46	−0.09
	5	5.31	2.21	6.13
BZP	0.1	0.11	5.41	10.51
	0.25	0.28	7.63	11.68
	0.5	0.46	16.62	−8.67
	1	0.92	12.01	−7.90
	3	2.93	7.79	−2.44
	5	5.33	0.80	6.44
mCPP	0.1	0.10	4.63	−1.63
	0.25	0.24	5.04	−5.35
	0.5	0.46	7.58	−7.85
	1	1.03	4.14	2.91
	3	3.08	4.89	2.51
	5	5.36	1.38	7.14
TFMPP	0.1	0.09	8.73	−8.24
	0.25	0.24	10.76	−2.27
	0.5	0.55	9.12	10.41
	1	1.06	7.74	6.45
	3	3.06	7.33	1.85
	5	5.09	1.13	1.86

[a] All concentrations in μg/mL.
[b] Coefficient of variation.
[c] Relative error [(spiked concentration-nominal concentration/nominal concentration) × 100].

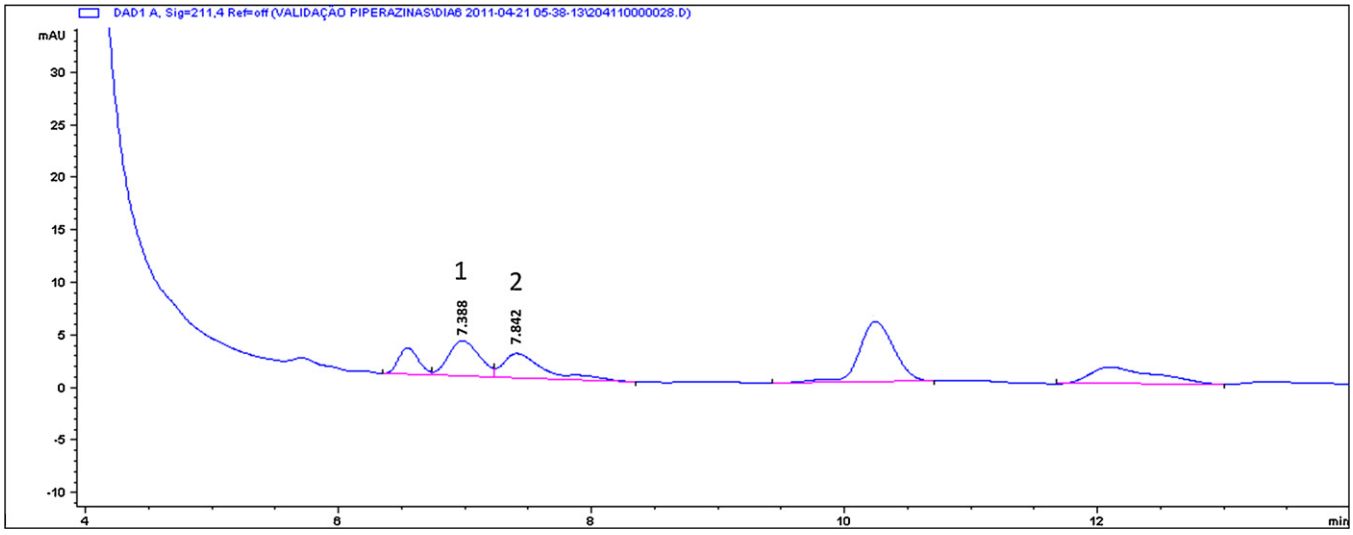

Fig. 3. Chromatogram of an authentic sample positive for mCPP (0.22 μg/mL). IS (1) and mCPP (2).

Table 4
Inter-day precision and accuracy ($n = 5$).

Compound	Spiked[a]	Measured[a]	CV[b] (%)	RE[c] (%)
MeOPP	0.1	0.10	2.81	−1.99
	0.25	0.24	5.57	2.67
	0.5	0.47	9.78	6.56
	1	1.01	7.63	−1.31
	2	2.01	6.42	−0.55
	3	2.94	9.44	1.91
	4	4.11	6.61	−2.73
	5	5.20	4.77	−3.77
BZP	0.1	0.10	2.99	0.34
	0.25	0.26	7.34	−2.75
	0.5	0.49	8.80	1.97
	1	0.95	5.12	5.40
	2	2.01	6.94	−0.47
	3	2.96	4.67	1.33
	4	4.11	5.70	−2.73
	5	5.13	2.38	−2.53
mCPP	0.1	0.11	11.00	6.80
	0.25	0.22	5.66	−4.98
	0.5	0.50	15.00	−3.85
	1	1.04	10.45	2.30
	2	2.04	5.70	5.52
	3	2.95	7.72	−0.47
	4	3.99	8.05	−6.60
	5	5.08	2.25	2.88
TFMPP	0.1	0.10	8.64	2.48
	0.25	0.24	8.35	3.63
	0.5	0.50	5.60	0.37
	1	1.03	9.62	−3.32
	2	2.12	5.17	−5.78
	3	2.99	6.29	0.45
	4	4.08	2.47	−1.87
	5	4.82	3.08	3.82

[a] All concentrations in μg/mL.
[b] Coefficient of variation.
[c] Relative error [(spiked concentration-nominal concentration/nominal concentration) × 100].

were less than 7% for all compounds, meaning that the analytes are stable in the samples for at least 24 h at room temperature.

To study freeze and thaw stability, urine samples were spiked with 1.5 and 3.5 μg/mL of all compounds and were stored at the intended storage temperature for 24 h. After this period they were thawed unassisted at room temperature, and then re-frozen for 12–24 h under the same conditions. This freeze/thaw cycle was repeated twice more, and the samples were analysed after the third cycle. These samples were compared to freshly prepared ones, and the analytes were stable for at least 3 freeze/thaw cycles (the obtained coefficients of variation were less than 8% for all compounds).

3.2.6. Method applicability

After validation, the herein described procedure was applied to an authentic sample obtained from the Psychiatry Department of the local Hospital (Centro Hospitalar Cova da Beira, E.P.E., Covilhã, Portugal), belonging to a 22-year-old female undergoing treatment with trazodone. This sample was analysed by the described procedure, and the trazodone metabolite mCPP was detected at a concentration of 0.22 ± 0.02 μg/mL ($n = 3$). Fig. 3 shows the chromatogram obtained by analysis of this sample. Authentic samples positive for the remaining analytes have not been obtained yet.

4. Conclusions

A rapid, sensitive, selective, and accurate MEPS method was developed and fully validated for the determination of piperazines in human urine samples. The analyses were carried out using reduced sample volumes (0.1 mL), which provides a significant advantage, particularly when there is little sample availability, enabling further exams to be performed on the same sample. The factorial design approach was useful in the optimization process, as it enabled the reduction of the number of experiments. In addition, it allowed concluding that none of the studied factors or interactions had significant influence on the response, and therefore the factors' levels could be set at the most convenient values.

The fact that low detection and quantitation limits were obtained in reduced sample volumes enables the detection of small amounts of the compounds, which makes this procedure useful for those laboratories performing routine urine analysis.

References

[1] A. Wohlfarth, W. Weinmann, S. Dresen, LC-MS/MS screening method for designer amphetamines, tryptamines, and piperazines in serum, Anal. Bioanal. Chem. 396 (2010) 2403–2414.
[2] D. Boer, I. Bosman, I. Hidvégi, C. Manzoni, A. Benko, J. dos Reys, R. Maes, Piperazine-like compounds: a new group of designer drugs-of-abuse on the European market, Forensic Sci. Int. 121 (2001) 47–56.
[3] R. Staack, L. Paul, D. Schmid, G. Roider, B. Rolf, Proof of a 1-(3-chlorophenyl)piperazine (mCPP) intake: use as adulterant of cocaine resulting in drug-drug interactions? J. Chromatogr. B 855 (2007) 127–133.

[4] U. Antia, H.S. Lee, R.R. Kydd, M.D. Tingle, B.R. Russell, Pharmacokinetics of 'party pill' drug N-benzylpiperazine (BZP) in healthy human participants, Forensic Sci. Int. 186 (2009) 63–67.
[5] M. Baumann, R. Clark, A. Budzynski, J. Partilla, B. Blough, R. Rothman, N-substituted piperazines abused by humans mimic the molecular mechanism of 3,4-methylenedioxymethamphetamine (MDMA, or 'Ecstasy'), Neuropsychopharmacology 30 (2005) 550–560.
[6] W. Romão, P. Lalli, M. Franco, G. Sanvido, N. Schwab, R. Lanaro, L. Costa, B. Sabino, M.I. Bueno, G. de Sa, R. Daroda, V. Souza, M. Eberlin, Chemical profile of meta-chlorophenylpiperazine (m-CPP) in ecstasy tablets by easy ambient sonic-spray ionization, X-ray fluorescence, ion mobility mass spectrometry and NMR, Anal. Bioanal. Chem. 400 (2011) 3053–3064.
[7] M. Barroso, S. Costa, M. Dias, D.N. Vieira, J.A. Queiroz, M. López-Rivadulla, Analysis of phenylpiperazine-like stimulants in human hair as trimethylsilyl derivatives by gas chromatography–mass spectrometry, J. Chromatogr. A 1217 (2010) 6274–6280.
[8] R. Staack, H. Maurer, Metabolism of designer drugs of abuse, Curr. Drug Metab. 6 (2005) 259–274.
[9] G.T. Vatassery, L.A. Holden, D.K. Hazel, M.W. Dysken, Determination of trazodone and its metabolite, 1-m-chlorophenyl-piperazine, in human plasma and red blood cell samples by HPLC, Clin. Biochem. 30 (1997) 149–153.
[10] S. Costa, Métodos de análise de piperazinas em fluidos biológicos (Dissertação de Mestrado), Universidade de Aveiro, Aveiro, 2007.
[11] J.C. Lin, R.K Jan, H. Lee, M.A. Jensen, R.R. Kydd, B.R. Russell, Determining the subjective and physiological effects of BZP combined with TFMPP in human males, Psychopharmacology 214 (2011) 761–768.
[12] R. Staack, G. Fritschi, H. Maurer, New designer drug 1-(3-trifluoromethylphenyl) piperazine (TFMPP): gas chromatography/mass spectrometry and liquid chromatography/mass spectrometry studies on its phase I and II metabolism and on its toxicological detection in rat urine, J. Mass Spectrom. 38 (2003) 971–981.
[13] U. Antia, M. Tingle, B. Russell, Validation of an LC–MS method for the detection and quantification of BZP and TFMPP and their hydroxylated metabolites in human plasma and its application to the pharmacokinetic study of TFMPP in humans, J. Forensic Sci. 55 (2010) 1311–1318.
[14] H. Miyaguchi, Y. Iwata, T. Kanamori, K. Tsujikawa, K. Kuwayama, H. Inoue, Rapid identification and quantification of methamphetamine and amphetamine in hair by gas chromatography/mass spectrometry coupled with micropulverized extraction, aqueous acetylation and microextraction by packed sorbent, J. Chromatogr. A 1216 (2009) 4063–4070.
[15] M. Abdel-Rehim, Recent advances in microextraction by packed sorbent for bioanalysis, J. Chromatogr. A 1217 (2010) 2569–2580.
[16] S. Jonsson, J. Hagberg, B. Van Bavel, Determination of 2,4,6-trichloroanisole and 2,4,6-tribromoanisole in wine using microextraction in packed syringe and gas chromatography-mass spectrometry, J. Agric. Food Chem. 56 (2008) 4962–4967.
[17] A. Prieto, S. Schrader, M. Moeder, Determination of organic priority pollutants and emerging compounds in wastewater and snow samples using multiresidue protocols on the basis of microextraction by packed sorbents coupled to large volume injection gas chromatography–mass spectrometry analysis, J. Chromatogr. A 1217 (2010) 6002–6011.
[18] I. González-Mariño, J.B. Quintana, I. Rodríguez, S. Schrader, M. Moeder, Fully automated determination of parabens, triclosan and methyl triclosan in wastewater by microextraction by packed sorbents and gas chromatography–mass spectrometry, Anal. Chim. Acta 684 (2011) 50–57.
[19] A. El-Beqqali, A. Kussak, M. Abdel-Rehim, Fast and sensitive environmental analysis utilizing microextraction in packed syringe online with gas chromatography–mass spectrometry: determination of polycyclic aromatic hydrocarbons in water, J. Chromatogr. A 1114 (2006) 234–238.
[20] A. Chaves, F. Leandro, J. Carris, M.E. Queiroz, Microextraction in packed sorbent for analysis of antidepressants in human plasma by liquid chromatography and spectrophotometric detection, J. Chromatogr. B 878 (2010) 2123–2129.
[21] M. Abdel-Rehim, P. Skansen, M. Vita, Z. Hassan, L. Blomberg, M. Hassan, Microextraction in packed syringe/liquid chromatography/electrospray tandem mass spectrometry for quantification of olomoucine in human plasma samples, Anal. Chim. Acta 539 (2005) 35–39.
[22] M.A. Saracino, A. de Palma, G. Boncompagni, M.A. Raggi, Analysis of risperidone and its metabolite in plasma and saliva by LC with coulometric detection and a novel MEPS procedure, Talanta 81 (2010) 1547–1553.
[23] M. Abdel-Rehim, Z. Altun, L. Blomberg, Microextraction in packed syringe (MEPS) for liquid and gas chromatographic applications. Part II—Determination of ropivacaine and its metabolites in human plasma samples using MEPS with liquid chromatography/tandem mass spectrometry, J. Mass Spectrom. 39 (2004) 1488–1493.
[24] F. Lafay, E. Vulliet, M. Flament-Waton, Contribution of microextraction in packed sorbent for the analysis of cotinine in human urine by GC–MS, Anal. Bioanal. Chem. 396 (2010) 937–941.
[25] S. Costa, M. Barroso, A. Castañera, M. Dias, Design of experiments, a powerful tool for method development in forensic toxicology: application to the optimization of urinary morphine 3-glucuronide acid hydrolysis, Anal. Bioanal. Chem. 396 (2010) 2533–2542.
[26] J. Miller, J. Miller, Statistics and Chemometrics for Analytical Chemistry, 5th ed., Pearson Education/Prentice-Hall, Harrow, 2000.
[27] U.S. Department of Health and Human Services, Food and Drug Administration, Guidance for Industry: Bioanalytical Method Validation, May 2001. http://www.fda.gov/downloads/Drugs/GuidanceCompilanceRegulatoryInformation/Guidances/ucm070107.pdf [accessed 29.03.11].
[28] International Conference on Harmonization (ICH). Validation of Analytical Procedures: Methodology ICH Q2 B, 2005. http://www.ich.org/LOB/media/MEDIA417.pdf [accessed 29.03.11].
[29] S.P. Vorce, J.M. Holler, B. Levine, M.R. Past, Detection of 1-benzylpiperazine and 1-(3-trifluoromethylphenyl)-piperazine in urine analysis specimens using GC–MS and LC–ESI-MS, J. Anal. Toxicol. 32 (2008) 444–450.
[30] A.J. Dickson, S.P. Vorce, J.M. Holler, T.P. Lyons, Detection of 1-benzylpiperazine, 1-(3-trifluoromethylphenyl)-piperazine, and 1-(3-chlorophenyl)-piperazine in 3,4-methylenedioxymethamphetamine-positive urine samples, J. Anal. Toxicol. 34 (2010) 464–469.
[31] B.N. Patel, N. Sharma, M. Sanya, P.S. Shrivasta, High throughput and sensitive determination of trazodone and its primary metabolite, m-chlorophenylpiperazine, in human plasma by liquid chromatography–tandem mass spectrometry, J. Chromatogr. B 871 (2008) 44–54.

Journal of Pharmaceutical and Biomedical Analysis 61 (2012) 100–107

Contents lists available at SciVerse ScienceDirect

Journal of Pharmaceutical and Biomedical Analysis

journal homepage: www.elsevier.com/locate/jpba

Assessment of the stereoselective fungal biotransformation of albendazole and its analysis by HPLC in polar organic mode

Viviane Cangerana Hilário[a], Daniel Blascke Carrão[a], Thiago Barth[b], Keyller Bastos Borges[c], Niege Araçari Jacometti Cardoso Furtado[d], Mônica Tallarico Pupo[d], Anderson Rodrigo Moraes de Oliveira[a,*]

[a] Departamento de Química, Faculdade de Filosofia, Ciências e Letras de Ribeirão Preto, Universidade de São Paulo, 14040-901, Ribeirão Preto, SP, Brazil
[b] Departamento de Física e Química, Faculdade de Ciências Farmacêuticas de Ribeirão Preto, Universidade de São Paulo, 14040-903, Ribeirão Preto, SP, Brazil
[c] Departamento de Ciências Naturais, Universidade Federal de São João del Rei, Campus Dom Bosco, Praça Dom Helvécio 74, Fábricas, 36301-160, São João del Rei, MG, Brazil
[d] Departamento de Ciências Farmacêuticas, Faculdade de Ciências Farmacêuticas de Ribeirão Preto, Universidade de São Paulo, 14040-903, Ribeirão Preto, SP, Brazil

ARTICLE INFO

Article history:
Received 9 August 2011
Received in revised form
11 December 2011
Accepted 13 December 2011
Available online 21 December 2011

Keywords:
Chiral analysis
Stereoselective fungal biotransformation
Polar organic mode
Albendazole
Ricobendazole

ABSTRACT

A high-performance liquid chromatographic method using polar organic mode was developed to analyze albendazole (ABZ), albendazole sulfone ($ABZSO_2$) and the chiral and active metabolite albendazole sulfoxide (ABZSOX, ricobendazole) that was further applied in stereoselective fungal biotransformation studies. The chromatographic separation was performed on a Chiralpak AS column using acetonitrile:ethanol (97:3, v/v) plus 0.2% triethylamine and 0.2% acetic acid as the mobile phase at a flow rate of 0.5 mL min^{-1}. The present study employed hollow fiber liquid-phase microextraction as sample preparation. The method showed to be linear over the concentration range of 25–5000 ng mL^{-1} for each ABZSOX enantiomer, 200–10,000 ng mL^{-1} for ABZ and 50–1000 ng mL^{-1} for $ABZSO_2$ metabolite with correlation coefficient (r) > 0.9934. The mean recoveries for ABZ, *rac*-ABZSOX and $ABZSO_2$ were, respectively, 9%, 33% and 20% with relative standard deviation below 10%. Within-day and between-day precision and accuracy assays for these analytes were studied at three concentration levels and were lower than 15%. This study opens the door regarding the possibility of using fungi in obtaining of the active metabolite ricobendazole. *Nigrospora sphaerica* (Sacc.) E. W. Mason (SS67), *Pestalotiopsis foedans* (VR8), *Papulaspora immersa* Hotson (SS13) and *Mucor rouxii* were able to stereoselectively metabolize ABZ into its chiral metabolite. Among them, the fungus *Mucor rouxii* was the most efficient in the production of (+)-ABZSOX.

© 2011 Elsevier B.V. All rights reserved.

1. Introduction

Chiral interaction is often a typical attribute of enzymatic reactions, messenger–receptor interactions and metabolic activities. It may differ interspecifically and even from one individual to another one. As a result, metabolic and regulatory processes mediated by the biological system are susceptible to stereochemistry and different responses can be often observed when comparing the activities of a pair of enantiomers [1]. Currently, there are several drugs marketed as racemic mixtures, however, the pharmacokinetic and pharmacodynamic profiles of the enantiomers have revealed to be different. Albendazole (ABZ) is a wide spectrum antihelminthic drug. It is a prochiral drug which action resides mostly in its sulfoxide metabolite, albendazole sulfoxide (ABZSOX) [2]. In human liver, ABZ is oxidized to the active and chiral ABZSOX metabolite by flavin monooxygenases and mainly by the cytochrome CYP3A4. ABZSOX is then oxidized to the inactive albendazole sulfone ($ABZSO_2$) metabolite [3]. Nowadays, ABZSOX is marketed as a racemic mixture under the generic name ricobendazole. Studies have shown that the disposition of the enantiomers of ricobendazole in human or animals is stereospecific [4–10].

Despite the interest in the activities of the ABZSOX enantiomers, there are a few studies employing the isolated enantiomers. Fernandez et al. [11] studied the antihelminthic activity of *rac*-ABZSOX in mice infected with *Trichinella spiralis*. The study showed that at low concentrations of *rac*-ABZSOX, (+)-ABZSOX and (−)-ABZSOX, only the (+)-ABZSOX promoted a significant reduction of the parasite viability.

The cytochrome isoform (CYP) and the flavin monooxygenases (FMO) act differently in the oxidation of ABZ. Some studies have showed that FMO-dependent *S*-oxidation outcome in the predominant formation of (+)-ABZSOX, while CYP2C6 and/or CYP2A1 favor the (−)-enantiomer production. In addition, CYP3A yields comparable quantities of (±)-enantiomers. The contribution of CYP and FMO

* Corresponding author at: Departamento de Química, Faculdade de Filosofia, Ciências e Letras de Ribeirão Preto–USP - Av. dos Bandeirantes 3900, Zip code: 14040-901, Ribeirão Preto, SP, Brazil. Tel.: +55 16 36020388; fax: +55 16 36024838.
E-mail address: deoliveira@usp.br (A.R.M. de Oliveira).

0731-7085/$ – see front matter © 2011 Elsevier B.V. All rights reserved.
doi:10.1016/j.jpba.2011.12.012

to the sulfoxidation of ABZ varies according to the animal species considered. It can explain the differences in the (±) ratios observed between the species [12–15].

There are several studies that use chiral HPLC to analyze the ABZSOX enantiomers in biological matrices. The methods employed in these studies have been based on normal [4,5] or reversed [13,16,17] phase modes of separation. The most drawbacks faced by these modes are, respectively, the amount of apolar organic solvent employed and the difficulty to analyze the ABZ due to its low solubility in water. Based on that, the polar organic mode can be a pronounced alternative to analyze ABZ and its metabolites that present different solubilities in the same analytical run. In polar organic mode, the amount of organic solvent used is usually low, due to the low flow rate employed. Of further interest in this regard, in this mode there is no presence of toxic apolar organic solvents, once the solvents used are potentially able to be recycled and, also, the analytes can be lastly concentrated because these solvents are easily evaporated [18,19].

Microorganisms can catalyze practically every type of reactions in nearly all classes of compounds. As a result, microorganisms and their enzymes are widely employed in the biotransformation of compounds and modification of the structures of abundantly available prototype compounds [20]. Microbial biotransformations are important steps to introduce functional groups into inaccessible sites of the molecules and, thereby, to produce rare structures. The reactions also involve high degrees of regio- and stereo-selectivities and require mild reaction conditions. Microbial cultures, particularly some fungi, can metabolize drugs in a manner similar to mammalian systems [21–23].

Based on this context, the aim of this work was to develop a new chiral HPLC method using the polar organic mode to analyze ABZ and its metabolites after stereoselective fungal biotransformation. Additionally, it was intended to come up with a new approach to obtain the pure ricobendazole enantiomer using fungi as catalyst.

2. Experimental

2.1. Chemicals and reagents

Standard stock solutions of ABZ (analytical standard), ABZSOX (purity ≥ 98%) and $ABZSO_2$ (analytical standard) (bought from Sigma–Aldrich, Steinheim, Germany and Toronto Research Chemicals, Toronto, Canada) were prepared at the concentration of 1000 μg mL^{-1} in methanol. Calibration curve solutions of *rac*-ABZSOX at concentrations of 2, 8, 20, 40, 200 and 400 μg mL^{-1} and ABZ at concentrations of 8, 20, 30, 40, 200 and 400 μg mL^{-1} and $ABZSO_2$ at concentrations of 2, 4, 8, 10, 20 and 40 μg mL^{-1} were obtained by dilutions in the same solvent. All these solutions were stored at −20 °C.

The solvents (analytical grade) used in hollow fiber liquid-phase microextraction (HF-LPME) procedure and in the biotransformation procedure were: 1-octanol (Sigma–Aldrich, Steinheim, Germany) and *N*,*N*-dimethylformamide (Mundial Química, Ribeirão Preto, São Paulo, Brazil).

The reagents (analytical grade) potassium chloride, monosodium phosphate ($NaH_2PO_4{\cdot}1H_2O$) and disodium phosphate ($Na_2PO_4{\cdot}2H_2O$), magnesium sulfate ($MgSO_4{\cdot}7H_2O$) and iron sulfate ($FeSO_4{\cdot}7H_2O$) were obtained from Merck (Darmstadt, Germany). Sodium hydroxide was obtained from Nuclear (Diadema, São Paulo, Brazil), hydrochloric acid and acetic acid were obtained from Zilquímica (Ribeirão Preto, São Paulo, Brazil) and phosphoric acid was obtained from Labsynth (Diadema, São Paulo, Brazil). Potato dextrose agar, sucrose, malt extract, dextrose, triptone and yeast extract were obtained from Acumedia (Lansing, MI, USA). Water used to prepare the solutions was purified using a Milli-Q plus system (Millipore, Bedford, MA, USA).

HPLC grade ethanol, methanol, acetonitrile, isopropanol and acetic acid were purchased from Merck (Darmstadt, Germany) and from J.T. Baker (Philipsburg, NJ, USA). Diethylamine and triethylamine were obtained from Fluka (Buchs, Switzerland).

2.2. Chromatographic and extraction conditions

Analyzes were conducted using a Shimadzu (Kyoto, Japan) liquid chromatograph, equipped with an LC-AT_{VP} solvent pump unit and an SPD-$10A_{VP}$ UV–visible detector operating at 290 nm. Injections were performed manually through a 20 μL loop with a Rheodyne model 7125 injector (Rheodyne, Cotati, CA, USA). Data were monitored using a controller model SCL 10A. The software for data acquisition was the LC Solution, version 1.22 SP1 (Shimadzu, Kyoto, Japan). The resolution of the ABZ, $ABZSO_2$ and the enantiomers of ABZSOX using the polar organic mode was evaluated at 23 ± 2 °C on six chiral columns, i.e. Chiralpak AS-H (150 mm × 4.6 mm, 5 μm particle size), Chiralpak AS (250 mm × 4.6 mm, 10 μm particle size), Chiralcel OJ-H (150 mm × 4.6 mm, 5 μm particle size), Chiralcel OD-H (150 mm × 4.6 mm, 5 μm particle size), Chirobiotic T (150 mm × 4.6 mm, 5 μm particle size) and Chirobiotic V (150 mm × 4.6 mm, 5 μm particle size) (purchased from Chiral Technologies, Exton, PA, USA and from Astec, Advanced Separation Technologies, Whippany, NJ, USA). A C18 column (4.6 mm × 12.5 mm, 5 μm particle size, Merck, Darmstadt, Germany) was used as guard column.

Accurel PP Q3/2 porous polypropylene hollow fiber was purchased from Membrana (Wuppertal, Germany). The inner diameter of the fiber was 600 μm, the thickness of the wall was 200 μm, and the pore size was 0.2 μm. The Vibrax VXR agitator used in HF-LPME procedure was obtained from IKA (Staufen, Germany).

2.3. Elution order

To establish the elution order, the pure enantiomers of ABZSOX were isolated by semipreparative analysis and collected using the conditions described previously in literature [4]. Next, the pure ABZSOX enantiomers were injected separately into the chromatographic system under the conditions established in the present paper. Then, the retention times of the enantiomers from both studies were compared and the elution order established.

2.4. Hollow fiber liquid-phase microextraction (HF-LPME) procedure

The format of the HF-LPME system was based on a previous work developed by Magalhães and Bonato [24]. The condition employed in the HF-LPME procedure to extract the ABZ and its metabolites from culture medium was based on a paper recently published by our group [25]. Nevertheless, the condition employed to extract the analytes and to analyze them in the current paper has been slightly modified, once the previous paper did not analyze ABZ. The best condition was achieved using as donor phase 1 mL liquid culture medium, 2.8 mL of 0.50 mol L^{-1} phosphate buffer pH 7.0 and 0.20 mL of a 4 mg mL^{-1} sodium metabisulfite. The organic solvent employed was 1-octanol and the length of the polypropylene fiber was 15 cm. The acceptor solution employed was 0.10 mol L^{-1} HCl. The extraction was performed during 50 min at room temperature (23 ± 2 °C) at 1500 rpm. After extraction, 50 μL of the acceptor solution was withdrawn using a microsyringe, transferred to a conic vial and evaporated to dryness under a gentle stream of compressed air at room temperature. The residues were dissolved in 50 μL of the mobile phase and 20 μL aliquot was injected into

the chromatographic system. After each extraction, the fiber was replaced by a new one to avoid any carryover.

2.5. Validation of the method

Since there is no specific guide that recommends the analysis of drugs and metabolites in culture medium, it was decided to follow, as close as possible, the FDA guideline [26] that recommends the analysis of drugs and metabolites in biological fluids. This requirement was followed due to the complexity of the culture medium matrix.

The linearity of the method was performed in triplicate and the results were weighted by $1/x^2$. The results of the linearity were weighted because the residual analysis of the analytical curve showed a heteroscedasticity behavior [27]. In addition, the linearity of the calibration curve was assessed by ANOVA Lack of fit test using a p value of 0.05. MINITAB Release, version 14.1 (State College, PA, USA) was used to perform the statistical analysis. Analytical curves ($n = 3$) were obtained by spiking aliquots of 1 mL liquid culture medium with standard solutions of ABZSOX in the concentration range of 25, 100, 250, 500, 2500 and 5000 ng mL^{-1} for each enantiomer. In the analysis of the ABZ and $ABZSO_2$ metabolite, the concentration range was, respectively, 200, 500, 750, 5000, 10000 ng mL^{-1} and 50, 100, 200, 250, 500, 1000 ng mL^{-1}. The limit of quantification (LOQ) was defined as the lowest concentration that could be determined with accuracy and precision below 20% over five analytical run and it was obtained using liquid culture medium samples (1 mL) spiked with 25 ng mL^{-1}, 200 ng mL^{-1} and 50 ng mL^{-1} of ABZSOX enantiomers, ABZ and $ABZSO_2$, respectively.

Precision was expressed as relative standard deviation and accuracy as percent of deviation between the true (nominal concentration) and the measured value (obtained concentration), i.e. relative error (RE%). To assess within-day precision and accuracy, replicate analyses ($n = 5$) of 1 mL of liquid culture medium spiked at concentrations of 100, 500 and 2500 ng mL^{-1} of each ABZSOX enantiomer, 100, 250 and 500 ng mL^{-1} of the $ABZSO_2$ metabolite and 500, 1000 and 5000 ng mL^{-1} of the ABZ was performed. For between-day assays, liquid culture medium samples of each concentration were analyzed for 3 consecutive days ($n = 5$) [26].

The absolute recovery of each analyte extracted from the liquid culture medium samples spiked with the concentrations of 500, 1000 and 10,000 ng mL^{-1} for ABZ, 100, 500 and 5000 ng mL^{-1} for each ABZSOX enantiomer and 100, 250 and 1000 ng mL^{-1} for $ABZSO_2$ metabolite ($n = 3$, for each concentration) was determined using calibration curves obtained from the data of the analytes not submitted to microextraction. The recovery was expressed as percentage of the amount extracted and the relative standard deviation was evaluated.

Stability tests for each analyte were performed in four different ways, i.e. (i) long-term controlled temperature stability at 30 °C; (ii) long-term frozen stability; (iii) freeze–thaw cycle stability and (iv) Short-term room temperature stability. For each analyte it was used a low concentration (500 ng mL^{-1} for ABZ; 100 ng mL^{-1} for each ABZSOX enantiomer and $ABZSO_2$) and a high concentration (5000 ng mL^{-1} for ABZ; 2500 ng mL^{-1} for each ABZSOX enantiomers and 500 ng mL^{-1} $ABZSO_2$) all in six-fold. The protocol used in these assessments was the one described by the FDA guideline [26]. The analyte peak areas obtained from stability tests were compared with the peak areas obtained with freshly prepared samples. Student's t-test was applied, with the level of significance set at $p \leq 0.05$.

2.6. Fungus isolation and maintenance

The selected strains of endophytic fungi were *Glomerella cingulata* (VA1) isolated from *Viguiera arenaria*; *Pestalotiopsis foedans* (VR8) isolated from *Viguiera robusta*; *Papulaspora immersa* Hotson (SS13), *Fusarium oxysporum* (SS50) and *Nigrospora sphaerica* (Sacc.) E.W. Mason (SS67) isolated from *Smallanthus sonchifolius*. The studied fungi were isolated and identified by rDNA sequences as previously described [28]. The fungi have been maintained as agar plugs in sterile water, or in glycerol:water (8:2, v/v) solution or in silica gel (6–12 mesh, grade 40, desiccant activated) at 10 °C. The strain has been deposited in the Academic Laboratory of Chemistry of Microorganisms, Faculty of Pharmaceutical Sciences of Ribeirão Preto (University de São Paulo, Ribeirão Preto, Brazil).

The filamentous fungus *Mucor rouxii* strain NRRL 1894 was obtained as a courtesy of Dr. C.W. Hesseltine (Northern Utilization Research and Development Division, ARS, USDA, Peoria, IL, USA) and belongs to a collection of fungal cultures of the Departamento de Biologia da Faculdade de Filosofia, Ciências e Letras de Ribeirão Preto, University of São Paulo. The microorganism is stored as a conidial suspension on silica gel (6–12 mesh, grade 40, desiccant activated) at 4 °C and on slants of solid oatmeal baby food consisting of 0.4% (w/v) oatmeal and 1.8% (w/v) agar.

2.7. Biotransformation study

The biotransformation study was performed according to the procedure previously described by our group [29–32]. Three discs of 0.5 cm of diameter containing the fungal mycelia were aseptically transferred to 9.0 cm diameter petri dishes containing PDA and allowed to grow for 6 days at 25 °C. After that, three uniform discs of 0.5 cm diameter of the fungus mycelia studied was cut with a transfer tube (Fischers Scientific, Pittsburgh, USA) and then inoculated in 50 mL Falcon tubes containing 10 mL of pre-fermentative medium (10.0 g malt extract, 10.0 g dextrose, 5.0 g triptone and 3.0 g yeast extract and deionized water to 1 L; pH was adjusted to 6.2 with a solution of 0.50 mol L^{-1} HCl) that was used for the appropriate growth of the microorganism. Finally, the mycelium was completely transferred to a 125 mL Erlenmeyer flask containing 80 mL of modified Czapek medium (25.0 g sucrose, 2.0 g $NaNO_3$, 1.0 g KH_2PO_4, 0.5 g $MgSO_4 \cdot 7H_2O$, 0.5 g KCl, 0.01 g $FeSO_4 \cdot 7H_2O$, and deionized water to 1.0 L, pH adjusted to 5.0 with a solution of 1.0 mol L^{-1} HCl). At this point, ABZ (2 mg) was dissolved in 200 μL of *N*,*N*-dimethylformamide and added to modified Czapek medium. The cultures were incubated for 144 h at 30 °C, with shaking at 120 rpm. Control tubes consisted of culture broth without ABZ and the fungus, sterile medium with ABZ without the fungus and fungal mycelium of the studied endophytic fungus.

The kinetic studies were presented as log concentration versus collecting interval (hours) profiles. In addition, the results obtained in the biotransformation process were also expressed as enantiomeric excess (*ee*), determined by the equation: $ee = (A - B/A + B) \times 100$; where A is the enantiomer with higher concentration and B is the enantiomer with lower concentration. The efficiency of the biotransformation process was calculated (in percentage). It was performed quantifying the amount *rac*-ABZSOX in the culture medium and correlating this amount with the initial amount of ABZ.

3. Results and discussion

3.1. Chromatographic separation

One of the aims of this work was to develop a new chiral HPLC method for the chiral separation of ABZSOX using the polar organic mode. In addition, it was intended the analysis of the parent drug, ABZ and the other metabolite, $ABZSO_2$ in a short time interval in the same analytical run. Therefore, six chiral stationary phases were evaluated (based on polysaccharide derivatives and macrocyclic

Table 1
Relative standard deviation of the retention time and of the resolution after 15 injections during 3 consecutive days.

Days	Relative standard deviation (RSD%)						
	Retention time				Resolution		
	$ABZSO_2$	ABZ	(−)-ABZSOX	(+)-ABZSOX	Rs_1	Rs_2	Rs_3
1	0.27	0.50	0.82	0.90	2.4	0.9	2.4
2	0.16	0.16	0.30	0.70	2.2	1.1	1.7
3	0.18	0.23	0.39	0.61	2.0	0.9	1.3

Rs_1, RSD of the resolution between the peaks $ABZSO_2$/ABZ; Rs_2, RSD of the resolution between the peaks ABZ/(−)-ABZSOX; Rs_3, RSD of the resolution between the peaks (±)ABZSOX.

antibiotics). To evaluate these columns in polar organic mode, a screening was performed using methanol, acetonitrile and ethanol or a mixture of these organic solvents. Initially, each column was evaluated with 100% of each organic solvent and the resolution was determined. Afterward, the presence of additives (triethylamine, diethylamine and acetic acid) was evaluated at the concentrations of 0.05%, 0.1%, 0.2%, 0.3% and 0.4%. The additives were evaluated separately, followed by the evaluation of mixtures of them. If the resolution was not yet acceptable, the next step was to perform a mixture of two solvents. Initially 50% of each solvent was evaluated and then, little modifications in the solvent proportions were performed trying to get a better resolution between the analytes. After evaluating all these columns and conditions, the best chiral separation of ABZSOX was accomplished on the Chirobiotic V column using acetonitrile: methanol (93:7, v/v) + 0.2% acetic acid as mobile phase and on the Chiralpak AS column using acetonitrile:ethanol (97:3, v/v) + 0.2% triethylamine and 0.2% acetic acid as the mobile phase. In both conditions, the flow rate employed was 0.5 mL min^{-1}. By employing the Chirobiotic V column, the resolution between the enantiomers was 2.0. However, at this condition there was a co-elution between the ABZ and $ABZSO_2$ peaks. By using the Chiralpak AS column, the resolution between the enantiomers was slightly lower, Rs = 1.6. However the separation between the ABZ and $ABZSO_2$ was possible with an analytical run time below 18 min. Fig. 1 shows a typical chromatogram obtained from ABZ, ABZSOX enantiomers and $ABZSO_2$. It is important to mention that the temperature control is very important in separations by HPLC employing the polar organic mode. At the present study, due to the lack of a column oven, the laboratory temperature was strictly kept at 23 ± 2 °C. By ensuring the analysis temperature, the retention time and the resolution of the analytes presented a RSD% below 1.0% and 2.5%, respectively, during 3 consecutive days (Table 1). In our study, it was realized that the addition of acid and basic additives revealed a great influence in the chiral separation of ABZSOX, since little modifications in the established proportion of triethylamine and acetic acid had negative effect in the resolution of the analytes. It has been demonstrated that acidic and basic additives could be employed to improve the separation of the enantiomers, decreasing peak broadening arising from unwanted interactions between polar solutes and the stationary phase [18]. The effect of such improvement can be a result of the isolated modifier or a sum of the two modifiers. The influence of acidic additives can be attributed to either a minimization of interactions that are nonspecific with non-selective parts of the polymer or the silica support, or to an increased retention of the analytes that can interact with the additive (ionic pair formation) and lead to a better interaction with the stationary phase. The effect of amine additive has been ascribed to a restriction of modifier access required to displace bound analytes on free silanol groups [18].

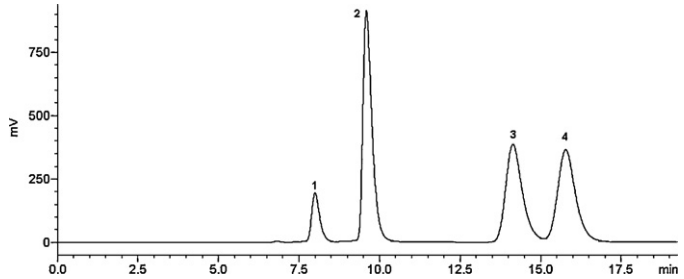

Fig. 1. Chromatogram of the analytes after HPLC optimization. $ABZSO_2$ (1), ABZ (2), (−)-ABZSOX (3) and (+)-ABZSOX (4). Chromatographic conditions described in Section 3.1.

3.2. Sample preparation

Recently our research group has developed a method to analyze the ABZSOX enantiomers in liquid culture medium using HF-LPME and capillary electrophoresis [25]. In order to use a microextraction technique and to reduce the use of organic solvents in the analytical chemistry HF-LPME was employed as sample preparation. HF-LPME is a microextraction technique developed by Pedersen-Bjergaard and Rasmussen in 1999 [33]. This technique presents several advantages such as low cost, low consume of organic solvent, high selectivity and the possibility to perform several extractions (up to 36) at the same time [34]. Since it was quantified other analytes in addition to ABZSOX, the whole HF-LPME was again optimized (data not shown). The parameters evaluated were (n = 3): type of organic solvent, extraction time, salt addition, sample pH, sample stirring and acceptor solution. The differences among the HF-LPME procedures in the present study compared to our previous published paper was the amount of salt added, the acceptor solution and the extraction pH. At the present paper, salt was not employed, once the salt addition increased the amount of interferent extracted from the liquid culture medium leading to bias in the results. Another modification was in the sample pH and in the acceptor solution concentration. It was used pH 7 instead of pH 10 and the concentration of the acceptor solution was 0.10 mol L^{-1} instead of 1 mol L^{-1}. Since the mechanism of separation between the techniques is different, these little modifications were necessary to achieve the best extraction condition. It is worth to mention that in our previous CE method the acceptor solution was directly injected in the CE equipment. The best extraction condition accomplished is described in Section 2.4.

3.3. Method validation and elution order of the enantiomers

The method showed to be linear over the concentration range of 25–5000 ng mL^{-1} for each ABZSOX enantiomer, 200–10,000 ng mL^{-1} for ABZ and 50–1000 ng mL^{-1} for $ABZSO_2$ metabolite with correlation coefficient (r) ≥ 0.9934 and relative error for each point below 15% (Table 2). The mean recoveries for ABZ, *rac*-ABZSOX and $ABZSO_2$ were, respectively, 9%, 33% and 20% with relative standard deviation below 10% (Table 2). Despite the low recovery values presented by this method, it is in agreement with several other methods that use a microextraction technique as sample preparation [35,36]. In addition, in

Table 2
Recovery and linearity of the developed method.

Analytes	Recovery		Linearity				
	(%)	RSD (%)[a]	Range (ng mL^{-1})	Linear equation[b]	r[c]	ANOVA lack of fit	
						F value	p Value
ABZ	8.8	8.9	200–10,000	$y = 131.21x - 1779.34$	0.9962	4.69	0.065
(−)-ABZSOX	34.0	5.2	25–5000	$y = 967.25x + 5339.62$	0.9975	0.02	0.999
(+)-ABZSOX	33.5	4.7	25–5000	$y = 962.51x + 4963.35$	0.9974	0.06	0.993
$ABZSO_2$	20.4	6.7	50–1000	$y = 683.18x - 16575.75$	0.9934	3.90	0.068

[a] RSD, relative standard deviation.
[b] Back-calculation of standard resulted relative errors lower than 15%.
[c] r, coefficient of correlation.

Table 3
Within-day[a] precision and accuracy of the developed method.

Analytes	Nominal concentrations (ng mL^{-1})	Obtained concentrations (ng mL^{-1})	Accuracy RE[b] (%)	Precision RSD[c] (%)
ABZ	500/1000/5000	452.0/1100.9/4902.6	−9.6/10.1/−1.9	2.5/4.4/7.2
(−)-ABZSOX	100/500/2500	96.6/518.2/2555.1	−3.4/3.6/2.2	7.1/4.4/8.6
(+)-ABZSOX	100/500/2500	97.2/515.4/2546.6	−2.8/3.1/1.9	7.4/4.6/8.6
$ABZSO_2$	100/250/500	94.3/254.5/542.3	−5.7/1.8/8.5	1.8/2.4/4.5

[a] The within-day precision and accuracy were performed in five-fold ($n = 5$).
[b] RE, relative error expressed as a percentage (%).
[c] RSD, relative standard deviation expressed as a percentage (%).

Table 4
Between-day[a] precision and accuracy of the developed method.

Analytes	Nominal concentrations (ng mL^{-1})	Obtained concentrations (ng mL^{-1})	Accuracy relative error[b] (%)	Precision RSD[c] (%)
ABZ	500/1000/5000	483.3/1055.1/4869.8	−3.3/5.5/−2.6	7.5/5.8/7.8
(−)-ABZSOX	100/500/2500	97.8/506.1/2572.8	−2.2/1.2/2.9	5.1/5.3/7.1
(+)-ABZSOX	100/500/2500	98.3/504.7/2569.9	−1.7/0.9/2.8	5.2/5.3/7.1
$ABZSO_2$	100/250/500	93.6/251.2/533.8	−6.4/0.5/6.7	2.6/4.1/4.8

[a] The between-day precision and accuracy were performed on three different days in five-fold ($n = 5$).
[b] RE, relative error expressed as a percentage (%).
[c] RSD, relative standard deviation expressed as a percentage (%).

biotransformation studies the amount of substrate added to the medium (ABZ, 2 mg) is very high. So, it was suggested that the range established in the linearity for these analytes is in agreement with other biotransformation studies published in the literature [29–32]. However, it should be addressed that concentrations below the LOQ of the analytes cannot be quantified. The lowest concentration quantified by the validated method was 25 ng mL^{-1} for each ABZSOX enantiomer, 200 ng mL^{-1} for ABZ and 50 ng mL^{-1} for $ABZSO_2$ with RSD% and relative error lower than 11%. The precision and accuracy for within-day and between-day precision is described in Tables 3 and 4, respectively. Neither relative standard deviations nor relative errors exceeded a value of 15%, in agreement with the FDA guideline recommendation [25]. The stability test showed no statistically significant difference with p values ≥ 0.08, 0.07, 0.06 and 0.08 for freeze–thaw cycles, 30 °C during 6 days, long term frozen and short-term room temperature stability tests (Table 5).

The elution order of the ABZSOX was inverted when compared to the elution order described by Lanchote et al. [4]. In this previous study the authors showed that the first enantiomer to elute shows the configuration (+) and the second (−). In the present work, employing the Chiralpak AS column in polar organic mode, the first enantiomer presented configuration (−) and the second (+). Therefore, the first peak corresponds to (−)-ABZSOX and the second to (+)-ABZSOX. In addition, a previous study performed by our group spiking liquid culture medium with pure enantiomers showed no racemization during the extraction procedure or during the conditions of biotransformation [24].

3.4. Stereoselective fungal biotransformation study

Based on the structures of the metabolites, it is expected that the ABZ substrate is initially converted to ABZSOX, which then can be converted to $ABZSO_2$. The ABZSOX metabolite is also known as

Table 5
Stability test ($n = 6$) of the developed method.

Stability	ABZ		(−)-ABZSOX		(+)-ABZSOX		$ABZSO_2$	
	Concentrations (ng mL^{-1})							
	500	5000	100	2500	100	2500	100	500
	p value[b]							
Freeze–thaw cycles[a]	0.96	0.08	0.22	0.24	0.27	0.25	0.21	0.21
30 °C during 7 days[a]	0.07	0.48	0.84	0.14	0.79	0.14	0.67	0.61
Long term frozen[a]	0.24	0.12	0.24	0.31	0.26	0.30	0.06	0.46
Room temperature[a]	0.66	0.06	0.08	0.33	0.09	0.32	0.56	0.45

[a] n = Number of determinations.
[b] Level of significance set at $p \leq 0.05$.

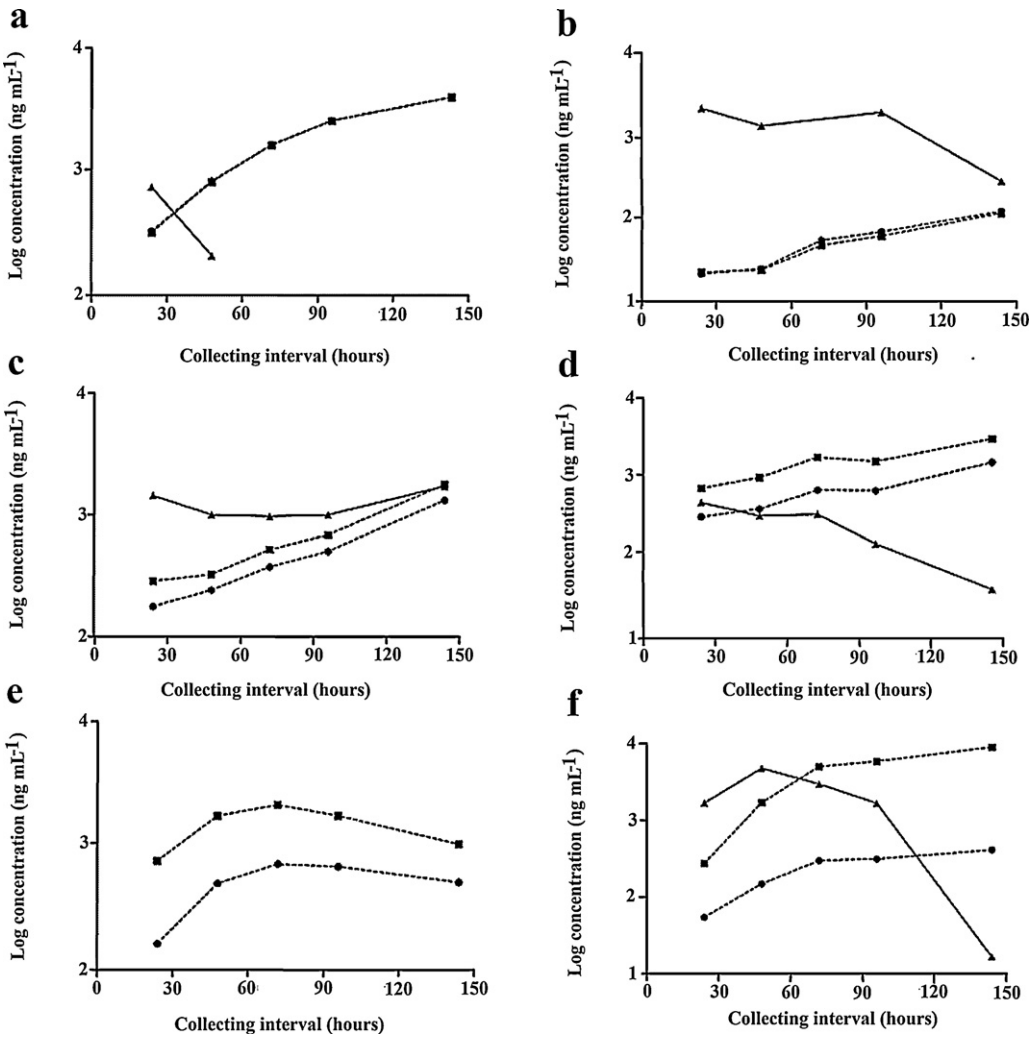

Fig. 2. Log concentration–time graphics referring to the biotransformation process of ABZ by fungi: (a) *Glomerella cingulata* (VA1), (b) *Fusarium oxysporum* (SS50), (c) *Nigrospora sphaerica* (Sacc.) E.W. Mason (SS67), (d) *Pestalotiopsis foedans* (VR8), (e) *Papulaspora immersa* Hotson (SS13) and (f) *Mucor rouxii* (NRRL 1894). (▲)-ABZ; (■)-(+)-ABZSOX; (●)-(−)-ABZSOX.

ricobendazole and it is available in the market as a more potent antihelminthic drug than ABZ.

In previous studies, researchers have used different filamentous fungi to study the biotransformation of ABZ. The filamentous fungus *Cunninghamella blakesleeana* (NCIM 687) biotransformed ABZ into three metabolites. Two metabolites were predicted to be ABZSOX and $ABZSO_2$, the major mammalian metabolites previously reported. A new *N*-methylated metabolite of ABZSOX was also produced, where the methylation took place on the *N*-atom of the imidazole ring system [37].

Under the studied conditions, all evaluated fungi were able to biotransform ABZ to ABZSOX, however the formation of $ABZSO_2$ was not observed. Probably, the formation of $ABZSO_2$ was not detected because it involves a sequence of reactions, i.e., oxidation of *S* followed by another oxidation reaction in this same atom.

The endophytic fungus *G. cingulata* (VA1) consumed all substrate (ABZ) in 48 h and high concentrations of (±)-ABZSOX was found, but the biotransformation of ABZ was not significantly stereoselective (Fig. 2a). In the same way, the fungus *F. oxysporum* (SS50) was not able to biotransform ABZ into (−)-ABZSOX or (+)-ABZSOX stereoselectively. The process of biotransformation was not efficient presenting low concentrations of (−)-ABZSOX and (+)-ABZSOX metabolites (Fig. 2b).

The maximal formation of ABZSOX employing the *N. sphaerica* (Sacc.) E.W. Mason (SS67) fungus was observed within 144 h of incubation. The concentrations of (+)-ABZSOX and (−)-ABZSOX metabolites increased along the incubation time (Fig. 2c). The formation of (+)-ABZSOX was slightly higher than (−)-ABZSOX with an enantiomeric excess about 15% (Fig. 3a). The maximal efficiency of formation for (−)-ABZSOX and (+)-ABZSOX were 10.45 and 14.12% at 144 h of incubation, respectively (Fig. 3b). The endophytic fungus *P. foedans* (VR8) was able to biotransform ABZ with higher intensity after 144 h of incubation (Fig. 2d). The high enantiomeric excess for the (+)-ABZSOX was observed after 72 h of incubation (Fig. 3a). The maximal efficiency of formation of (−)-ABZSOX and (+)-ABZSOX were 12.24 and 24.04% at 144 h of incubation, respectively (Fig. 3b). Employing the *P. immersa* Hotson (SS13) fungus, the concentration of ABZSOX increased until 72 h and then it started to decrease (Fig. 2e). The formation of (+)-ABZSOX metabolite was higher than the formation of (−)-ABZSOX metabolite (Fig. 3a) with a peak of enantiomeric excess in 24 h. The maximal efficiency of formation of (−)-ABZSOX and (+)-ABZSOX was 5.58 and 16.63% at 72 h of incubation, respectively (Fig. 3b).

The *M. rouxii* (NRRL 1894) fungus efficiently biotransformed ABZ into ABZSOX. Among all evaluated fungi, *M. rouxii* (NRRL 1894) showed higher formation of (+)-ABZSOX (Fig. 2f). This fungus presented the highest enantiomeric excess for (+)-ABZSOX metabolite

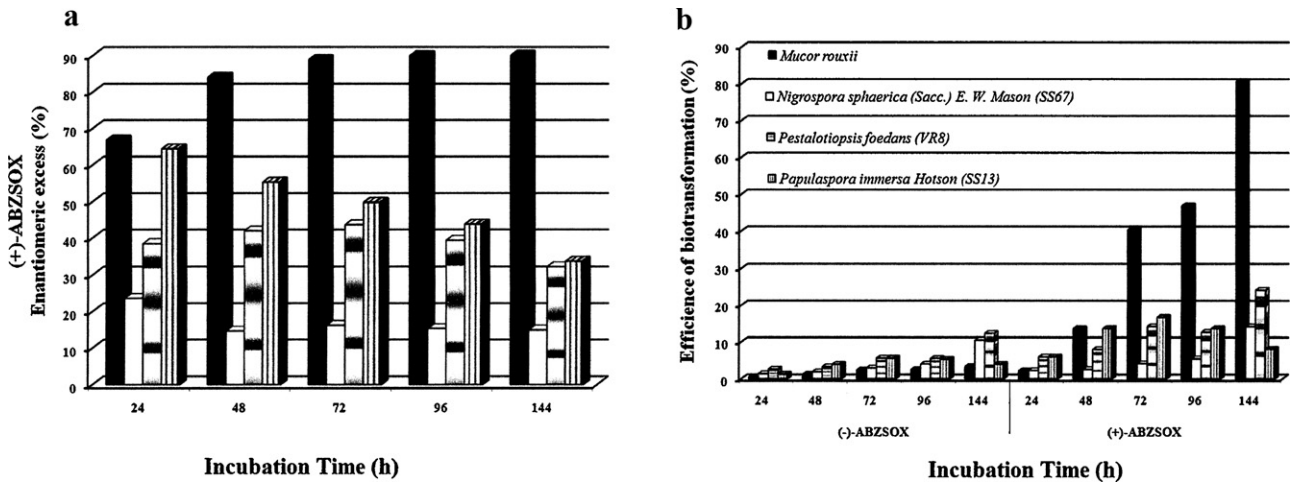

Fig. 3. (a) Graphic of the enantiomeric excess for (+)-ABZSOX in the incubation period; (b) efficiency of the biotransformation process for the fungi *Nigrospora sphaerica* (Sacc.) E.W. Mason (SS67), *Pestalotiopsis foedans* (VR8), *Papulaspora immersa* Hotson (SS13) and *Mucor rouxii* (NRRL 1894) in the incubation period.

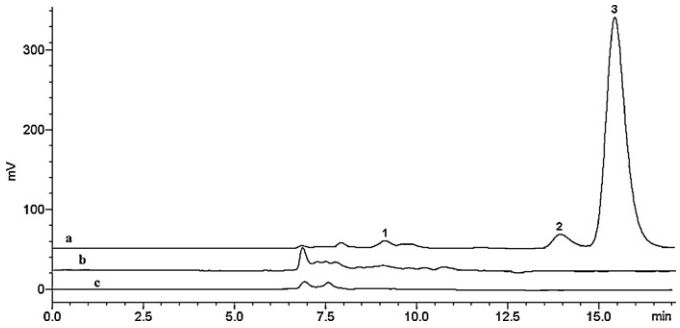

Fig. 4. (a) Representative chromatogram of the fungus *M. rouxii* (NRRL 1894) after 144 h of incubation with ABZ; (b) representative chromatogram of liquid Czapek medium (control) incubated with the *M. rouxii* (NRRL 1894) showing that this fungus did not produce any secondary metabolites in the retention time of the analytes; (c) chromatogram of blank liquid Czapek medium without the *Mucor rouxii* (NRRL 1894). ABZ (1); (−)-ABZSOX (2) and (+)-ABZSOX (3). Chromatographic and extraction conditions described in Sections 3.1 and 3.2, respectively.

in the biotransformation process (Fig. 3a). The maximal efficiency of formation for (−)-ABZSOX and (+)-ABZSOX was 3.28 and 80.61% at 144 h of incubation, respectively. Among all the studied fungi, *M. rouxii* (NRRL 1894) was the most efficient in the production of (+)-ABZSOX (Fig. 3b). Fig. 4 shows typical chromatograms obtained from the biotransformation process employing the fungus *M. rouxii* (NRRL 1894).

Regarding the reproducibility of the biotransformation by the proposed fungi, there are some papers showing that the sulfoxidation reactions are common by endophytic fungi [29,30]. In addition, due to the high degree of enantiomeric excess obtained by the *M. rouxii* fungus, the biotransformation was performed again employing this fungus. The results showed an enantiomeric excess of 87.0% which was very close to the first obtained result (80.6%).

4. Conclusions

This paper describes for the first time an enantioselective method for the simultaneous analysis of ABZ, ABZSOX enantiomers and $ABZSO_2$ by HPLC–UV, employing the polar organic mode, in combination with HF-LPME. Compared with other HPLC methods reported in literature [4–9,16,17], this one shows as advantages shorter analysis time for all analytes and the use of a simple and environmentally friendly sample preparation procedure. This method was successfully employed to study the biotransformation of ABZ by different fungi. In addition, the results showed the possibility of obtaining the ricobendazole drug using fungi as catalytic agent. Some fungi showed a high degree of enantioselectivity expressed by the enantiomeric excess. Between them, the fungus *M. roxii* (NRRL 1894) may be an excellent alternative to obtain the (+)-ABZSOX enantiomer with good efficiency of biotransformation.

Acknowledgments

The authors are grateful to Fundação de Amparo a Pesquisa do Estado de São Paulo (FAPESP) and to CNPq (Conselho Nacional de Desenvolvimento Científico e Tecnológico) for financial support and for granting a research fellowship.

References

[1] N.M. Maier, P. Franco, W.J. Lindner, Separation of enantiomers: needs, challenges, perspectives, J. Chromatogr. A 906 (2001) 3–33.
[2] O.M. Takayanagui, Therapy for neurocysticercosis, Expert Rev. Neurother. 4 (2004) 129–139.
[3] H.C. Rawden, G.O. Kokwaro, S.A. Ward, G. Edwards, Relative contribution of cytochromes P-450 and flavin-containing monoxygenases to the metabolism of albendazole by human liver microsomes, Br. J. Clin. Pharmacol. 49 (2000) 313–322.
[4] V.L. Lanchote, M.P.C. Marques, O.M. Takayanagui, R. de Carvalho, F.O. Paias, P.S. Bonato, Simultaneous determination of albendazole sulfoxide enantiomers and albendazole sulfone in plasma, J. Chromatogr. B 709 (1998) 273–279.
[5] F.O. Paias, V.L. Lanchote, O.M. Takayanagui, P.S. Bonato, Enantioselective Analysis of albendazole sulfoxide in plasma using the chiral stationary phase, Chirality 9 (1997) 722–726.
[6] V.L. Lanchote, O.M. Takayanagui, F.H. Mateus, Enantioselective renal excretion of albendazole metabolites in patients with Neurocysticercosis, Chirality 16 (2004) 520–525.
[7] B.P.S. Capece, G. Castells, C. Godoy, M. Arboix, C. Cristòfol, Pharmacokinetics of albendazole sulfoxide enantiomers administered in racemic form and separately in rats, Vet. J. 177 (2008) 297–299.
[8] J. Velík, V. Baliharová, L. Skálová, B. Szotáková, V. Wsól, J. Lamka, Stereospecific biotransformation of albendazole in mouflon and rat-isolated hepatocytes, J. Vet. Pharmacol. Ther. 26 (2003) 297–302.
[9] J. Velík, V. Baliharová, L. Skálová, B. Szotáková, V. Wsól, J. Lamka, Liver microsomal biotransformation of albendazole in deer, cattle, sheep and pig and some related wild breeds, J. Vet. Pharmacol. Ther. 28 (2005) 377–384.
[10] M.P. Marques, O.M. Takayanagui, P.S. Bonato, S.R.C.J. Santos, V.L. Lanchote, Enantioselective kinetic disposition of albendazole sulfoxide in patients with neurocysticercosis, Chirality 11 (1999) 218–223.
[11] B.F. Fernandez, S.R. Iniguez, J.J. Torrado, Ex vivo anthelmintic activity of albendazole-sulphoxide enantiomers, J. Parasitol. 90 (2004) 407–409.
[12] P. Moroni, T. Buronfosse, C. Longin-Sauvageon, P. Delatour, E. Benoit, Chiral sulfoxidation of albendazole by the flavin adenine dinucleotide-containing and cytochrome P450-dependent monooxygenases from rat-liver microsomes, Drug Metab. Dispos. 23 (1995) 160–164.
[13] P. Delatour, E. Benoit, M. Caude, A. Tambute, Species-differences in the generation of the chiral sulfoxide metabolite of albendazole in sheep and rats, Chirality 2 (1990) 156–160.

[14] P. Delatour, E. Benoit, S. Besse, A. Boukraa, Comparative enantioselectivity in the sulfoxidation of albendazole in man, dogs and rats, Xenobiotica 21 (1991) 217–221.
[15] P. Delatour, F. Garnier, E. Benoit, I. Caude, Chiral behavior of the metabolite albendazole sulfoxide in sheep, goats and cattle, Res. Vet. Sci. 50 (1991) 134–138.
[16] M. Lienne, M. Caude, R. Rosset, A. Tambute, P. Delatour, Direct separation of albendazole sulfoxide enantiomers by liquid-chromatography on a chiral column deriving from (S)-N-(3,5-dinitrobenzoyl) tyrosine – application to enantiomeric assays on plasma samples, Chirality 1 (1989) 142–153.
[17] K.R.A. Belaz, Q.B. Cass, R.V. Oliveira, Determination of albendazole metabolites by direct injection of bovine plasma and multidimensional achiral–chiral high performance liquid chromatography, Talanta 76 (2008) 146–153.
[18] B. Chankvetadze, I. Kartozia, C. Yamamoto, Y. Okamoto, Comparative enantioseparation of selected chiral drugs on four different polysaccharide-type chiral stationary phases using polar organic mobile phases, J. Pharm. Biomed. Anal. 27 (2002) 467–478.
[19] N. Matthijs, M. Maftouh, Y.V. Heyden, Screening approach for chiral separation of pharmaceuticals IV. Polar organic solvent chromatography, J. Chromatogr. A 1111 (2006) 48–61.
[20] K.B. Borges, W.S. Borges, R. Durán-Patrón, M.T. Pupo, P.S. Bonato, I.G. Collado, Stereoselective biotransformations using fungi as biocatalysts, Tetrahedron Asymmetr. 20 (2009) 385–397.
[21] A.M. Clark, C.D. Hufford, Use of microorganisms for the study of drug-metabolim – an update, Med. Res. Rev. 11 (1991) 473–501.
[22] E.A. Abourashed, A.M. Clark, C.D. Hufford, Microbial models of mammalian metabolism of xenobiotics: an updated review, Curr. Med. Chem. 6 (1999) 359–374.
[23] W.S. Borges, K.B. Borges, P.S. Bonato, S. Said, M.T. Pupo, Endophytic fungi: natural products, enzymes and biotransformation reactions, Curr. Org. Chem. 13 (2009) 1137–1163.
[24] I.R.S. Magalhães, P.S. Bonato, Two-step liquid-phase microextraction and high-performance liquid chromatography for the simultaneous analysis of the enantiomers of mefloquine and its main metabolite carboxymefloquine in plasma, Anal. Bioanal. Chem. 393 (2009) 1805–1813.
[25] D.B. Carrão, K.B. Borges, T. Barth, M.T. Pupo, P.S. Bonato, A.R.M. De Oliveira, Capillary electrophoresis and hollow fiber liquid-phase microextraction for the enantioselective determination of albendazole sulfoxide after biotransformation of albendazole by an endophytic fungus, Electrophoresis 32 (2011) 2746–2756.
[26] U.S. Department of Health & Human Services (2001) US Food and Drug Administration. http://www.fda.gov/downloads/Drugs/GuidanceComplianceRegulatoryInformation/Guidances/UCM070107.pdf. Accessed in 26 March 2011.
[27] A.M. Almeida, M.M. Castel-Branco, A.C. Falcão, Linear regression for calibration lines revisited: weighting schemes for bioanalytical methods, J. Chromatogr. B 774 (2002) 215–222.
[28] D.O. Guimarães, W.S. Borges, C.Y. Kawano, P.H. Ribeiro, G.H. Goldman, A. Nomizo, O.H. Thiemann, G. Oliva, N.P. Lopes, M.T. Pupo, Biological activities from extracts of endophytic fungi isolated from *Viguiera arenaria* and *Tithonia diversifolia*, FEMS Immunol. Med. Microbiol. 52 (2008) 134–144.
[29] K.B. Borges, W.S. Borges, M.T. Pupo, P.S. Bonato, Endophytic fungi as models for the stereoselective biotransformation of thioridazine, Appl. Microbiol. Biotechnol. 77 (2007) 669–674.
[30] K.B. Borges, W.S. Borges, M.T. Pupo, P.S. Bonato, Stereoselective analysis of thioridazine-2-sulfoxide and thioridazine-5-sulfoxide: an investigation of rac-thioridazine biotransformation by some endophytic fungi, J. Pharm. Biomed. Anal. 46 (2008) 945–952.
[31] K.B. Borges, A.R.M. De Oliveira, T. Barth, V.A.P. Jabor, M.T. Pupo, P.S. Bonato, LC-MS-MS determination of ibuprofen, 2-hydroxyibuprofen enantiomers, and carboxyibuprofen stereoisomers for application in biotransformation studies employing endophytic fungi, Anal. Bioanal. Chem. 399 (2011) 915–925.
[32] L.I. de Jesus, N.C.P. Albuquerque, K.B. Borges, R.A. Simões, L.A. Calixto, N.A.J.C. Furtado, C.M. De Gaitani, M.T. Pupo, A.R.M. De Oliveira, Enantioselective fungal biotransformation of risperidone in liquid culture medium by capillary electrophoresis and hollow fiber liquid-phase microextraction, Electrophoresis 32 (2011) 2765–2775.
[33] S. Pedersen-Bjergaard, K.E. Rasmussen, Liquid–liquid–liquid microextraction for sample preparation of biological fluids prior to capillary electrophoresis, Anal. Chem. 71 (1999) 2650–2656.
[34] A.R.M. De Oliveira, I.R.S. Magalhães, F.J.M. Santana, P.S. Bonato, Liquid-phase microextraction (LPME): fundamentals and applications to the analysis of drugs in biological samples, Quím. Nova 31 (2008) 637–644.
[35] R.A. Simões, A.R.M. De Oliveira, P.S. Bonato, Hollow fiber-based liquid-phase microextraction (HF-LPME) of isradipine and its main metabolite followed by chiral HPLC analysis: application to an in vitro biotransformation study, Anal. Bioanal. Chem. 399 (2011) 2435–2443.
[36] I.R.S. Magalhães, V.A.P. Jabor, A.M. Faria, C.H. Collins, I.C.S.F. Jardim, P.S. Bonato, Determination of β-artemether and its main metabolite dihydroartemisinin in plasma employing liquid-phase microextraction prior to liquid chromatographic-tandem mass spectrometric analysis, Talanta 81 (2010) 941–947.
[37] G.S. Prasad, S. Girisham, S.M. Reddy, K. Srisailam, Biotransformation of albendazole by fungi, World J. Microbiol. Biotechnol. 24 (2008) 1565–1571.

Journal of Pharmaceutical and Biomedical Analysis 61 (2012) 108–113

Contents lists available at SciVerse ScienceDirect

Journal of Pharmaceutical and Biomedical Analysis

journal homepage: www.elsevier.com/locate/jpba

Development of an UPLC–MS/MS method for the determination of antibiotic ertapenem on dried blood spots

Giancarlo la Marca[a,b,*,1], Elisa Giocaliere[a,1], Fabio Villanelli[a,1], Sabrina Malvagia[a], Silvia Funghini[a], Daniela Ombrone[a], Luca Filippi[c], Marina De Gaudio[d], Maurizio De Martino[d], Luisa Galli[d]

[a] Meyer Children's Hospital, Mass Spectrometry Lab, Florence, Italy
[b] Department of Pharmacology, University of Florence, Florence, Italy
[c] Meyer Children's Hospital, Neonatal Intensive Care Unit, Florence, Italy
[d] Department of Sciences for Woman and Child's Health, University of Florence, Florence, Italy

ARTICLE INFO

Article history:
Received 7 October 2011
Received in revised form
14 December 2011
Accepted 14 December 2011
Available online 23 December 2011

Keywords:
Ertapenem
Carbapenem
DBS
UPLC–MS/MS

ABSTRACT

Ertapenem (Invanz®) is a newly developed carbapenem β-lactam antimicrobial agent. The drug usage in pediatric age needs an accurate drug monitoring for effective patient management. The aim of this study was to evaluate the use of dried blood spot (DBS) specimens to measure ertapenem concentration during treatment. The analysis was performed by UPLC–MS/MS operating in multiple reaction monitoring (MRM) mode. The calibration curve in matrix was linear in the concentration range of 0.5–100 mg/L with correlation coefficient value higher than 0.997. Performance parameters of this method like lower limit of detection (LLOD, 0.2 mg/L), lower limit of quantification (LLOQ, 0.5 mg/L), matrix effect (20%), intra- and inter-day imprecision (CV within than 15%) and accuracy (between 94 and 155%) of drug concentrations have been evaluated. The drug stability at different temperatures was tested for one month, to evaluate the risks of sample delivery at different climatic conditions.

The reported method allows now ertapenem analysis and offers many advantages for patients including the possibility of collecting samples at home.

This new assay is both precise and accurate and is especially suitable for therapeutic drug monitoring and pharmacokinetic studies in neonates in whom obtaining larger blood samples is not convenient or possible.

© 2011 Elsevier B.V. All rights reserved.

1. Introduction

Ertapenem is a carbapenem antibiotic with a broad spectrum activity and stability against a wide range of β-lactamases. It has limited activity against *Pseudomonas aeruginosa*, enterococci and methicillin-resistant *Staphylococcus aureus* and therefore its use is suggested in moderate-severe community-acquired infections, rather than in nosocomial infections. Since ertapenem has a good penetration into intra-abdominal organs and interstitial fluid, it has been suggested as a therapeutic option in patients with complicated bacterial infections [1]. Recently, internationally guidelines recommended ertapenem (as other carbapenems) as an alternative option for the treatment of complicated intra-abdominal infections (cIAIs) in adults and children aged ≥3 months [2].

The role of ertapenem in the treatment of complicated bacterial infections in children is, up to now, very limited. Since it has *in vitro* activity against the majority of the extended-spectrum beta-lactamase (ESBL)-producing *Escherichia coli* and *Klebsiella* species, its use in complicated urinary tract infections (cUTIs), other than in cIAIs, is under investigation [3]. At the present, some infectious disease specialists suggest that ertapenem could be a good therapeutic option in complicated community-acquired bacterial infections, reserving the use of antipseudomonal carbapenems for infections where *Pseudomonas aeruginosa* is frequently implicated, thus reducing the selective pressure on the selection of carbapenem-resistant *Pseudomonas* spp.

Ertapenem has a favorable pharmacokinetic (PK) profile that allows once-daily (OD) administration in adults after intravenous and intramuscular administration. Data on PK profile in children younger than 12 years showed that clearance of ertapenem is about 2-fold higher as compared to adults [4]. Consequently, the recommended intravenous dosage is 1 g OD in patients aged ≥13 years and 15 mg/kg twice-daily (to a maximum of 1 g/day) in children aged 3 months to 12 years [4].

* Corresponding author at: Meyer Children's Hospital, Mass Spectrometry Lab, Florence, Italy. Tel.: +39 0555662988; fax: +39 0555662489.
E-mail address: g.lamarca@meyer.it (G. la Marca).
[1] These authors equally contributed to this work.

0731-7085/$ – see front matter © 2011 Elsevier B.V. All rights reserved.
doi:10.1016/j.jpba.2011.12.018

To the best of our knowledge, no pediatric data on ertapenem PK profile in newborns and children younger than 3 months, nor PK data after intramuscular administration are available.

Several LC-UV methods have been reported in literature for the determination of carbapenem antibiotics both in biological samples such as plasma, serum, urine, bronchial secretions and in tissue samples. On the other hand, only few LC–MS methods have been published for the identification and quantization of carbapenem compounds or their degradation products [5–8]. As is well known, PK studies are difficult to perform in younger children, since they require collection of many blood samples in the same day with a considerable discomfort for the patients. Thus, an attracting and potential method to easily obtain samples for PK studies in children is collection of whole blood samples onto filter paper (dried blood spot or DBS). DBS specimens are commonly used for neonatal screening of metabolic diseases, cystic fibrosis and hypothyroidism in micro-blood samples. Some studies recently evaluated the use of DBS for therapeutic drug monitoring (TDM) and toxicology in adults [9,10]. Some studies, also from our group, applied the DBS technique to evaluate drug concentrations in newborns, infants and children [11–15]. These reports showed that the accuracy of TDM studies using DBS is comparable to that of traditional TDM studies on plasma which require larger blood volumes. The UPLC–MS/MS method, here described, represents a robust, highly specific and sensitive approach to quantify ertapenem on dried blood spots. Sensitivity enhancement, required in quantitative analysis, and also selectivity are obtained acquiring multiple transition pairs.

2. Materials and methods

2.1. Standards

Ertapenem was provided by Merck Sharp and Dohme (Rome, Italy). A stock solution of 1 g/L was prepared in water and stored at −80 °C in different aliquots for no longer than six months. Successive dilutions were made using HPLC grade water. All chemicals and solvents were of the highest purity available from commercial sources and used without any further purification. Analytical grade methanol, acetonitrile and water were purchased from Panreac (Barcelona, Spain).

2.2. Sample preparation

Spiking studies were conducted using a pool of human blood from healthy donors; we evaluated linearity by analyzing fortified 3.2 mm dried blood spots prepared at 0.5, 1.5, 10, 50 and 100 mg/L on filter paper (903®, Whatman GmbH, Dassel Germany). The amount of blood used to prepare spots was 20 μL in order to produce homogeneous spots [16].

DBS samples were stored at −20 °C in a sealed plastic bag containing desiccant until analysis. One 3.2 mm diameter disk (containing about 3.3–3.4 μL of blood) was punched from each DBS sample and extracted with 200 μL of a 30/70 of water/methanol (v/v) solution. Samples were put in an orbital shaker and kept at 37 °C for 25 min. The extracts were transferred into a new 96-well plate and analyzed immediately.

2.3. Validation procedures

The method was validated in terms of linearity, precision, accuracy, extraction recovery, matrix effect and stability. Calibration curve was prepared by spotting on filter paper spiked human control blood to obtain concentrations of 0, 0.5, 1.5, 5, 10, 20, 50 and 100 mg/L. Intra-day precision data were evaluated by ten replicate analysis of five different ertapenem concentrations on the same day. Inter-day precision data were determined by the analysis of five different ertapenem concentrations on 10 different days.

To calculate the linear regression, the peak area was plotted against the drug concentration in milligrams per liter.

The stability study on DBS samples was evaluated up to one month after storage at −20 °C, +4 °C, room temperature and +37 °C.

2.4. Mass spectrometry

The samples and the calibration curve samples were analyzed on a Agilent (Waldbronn, Germany) 6430 bench-top Triple-Quad Mass Spectrometer equipped with an Electrospray source (ESI); the ESI source operated in positive ion mode, using the following setting: capillary voltage 5000 V, fragmentor voltage 80 V for each transition, drying gas flow 9 L/min of nitrogen, temperature 325 °C, nebulizer gas 35 psi. The following transitions were monitored in MRM mode: m/z 476.2 > 432.2 (quantifier), m/z 476.2 > 390.1 (qualifier) and m/z 476.2 > 233.1 (qualifier). Optimal collision energies were found at 20, 18, and 18 V, and the resulting cell acceleration voltage was +7 V for all transitions.

The quantitation experiments were undertaken by using a Series 1290 Infinity LC System (Agilent Technologies, Waldbronn, Germany) UHPLC Capillary Pump coupled to an Agilent 6430, both being fully controlled from the Mass Hunter data system.

The analytical column was an Agilent Zorbax Eclipse Plus C18, Rapid Resolution 1.8 μm, 2.1 mm × 50 mm (Agilent Technologies, Waldbronn, Germany) operating at 0.4 mL/min flow rate and using water (A) and acetonitrile (B) both containing 0.1% formic acid as mobile phase. The column was maintained at 60 °C during the run. The chromatographic separation was obtained using a fast gradient starting from a 95% of solution A and 5% of solution B. The 95% of organic solvent was reached in 1 min and maintained for 15 s; initial conditions were restored in 5 s and the column equilibrated for 1 min. The total running time was 2.2 min long and the ertapenem retention time was fixed to 1.04 min. The eluent from the column was directed into the Electrospray source without split. Three microliters of the extracted sample were injected for the UPLC–MS/MS experiments.

System control, data acquisition and interpretation were made with the Agilent Mass Hunter software (Version B.04.00) software including the Qualitative package (for chromatographic and spectral interpretation) and the Quantitative Software (for quantitative information generation). Calibration curves were set up with the Mass Hunter Quantitative program using a linear least-square regression non-weighted.

3. Results and discussion

Dried blood spot sampling is increasingly becoming a good alternative to traditional plasma samples for biochemical analysis. The emerging technology offers great opportunities for improved patient care especially in the pediatric population where is generally difficult and unethical to obtain sufficient number of blood samples.

In this work, we have developed a method for the analysis of ertapenem concentrations in UPLC–MS/MS performed with only a few drops of blood and therefore very appealing for its application in pharmacokinetic studies involving infants and very young children. Fig. 1 shows the MS/MS spectrum obtained by fragmenting the precursor ion (476.2 Th) of ertapenem under the above described conditions. From these experiments, the resulting most selective ion-pair transition for the quantitative experiment (MRM) was 476.2 > 432.2 while 476.2 > 390.1 and 476.2 > 233.1 were used as qualifier transitions.

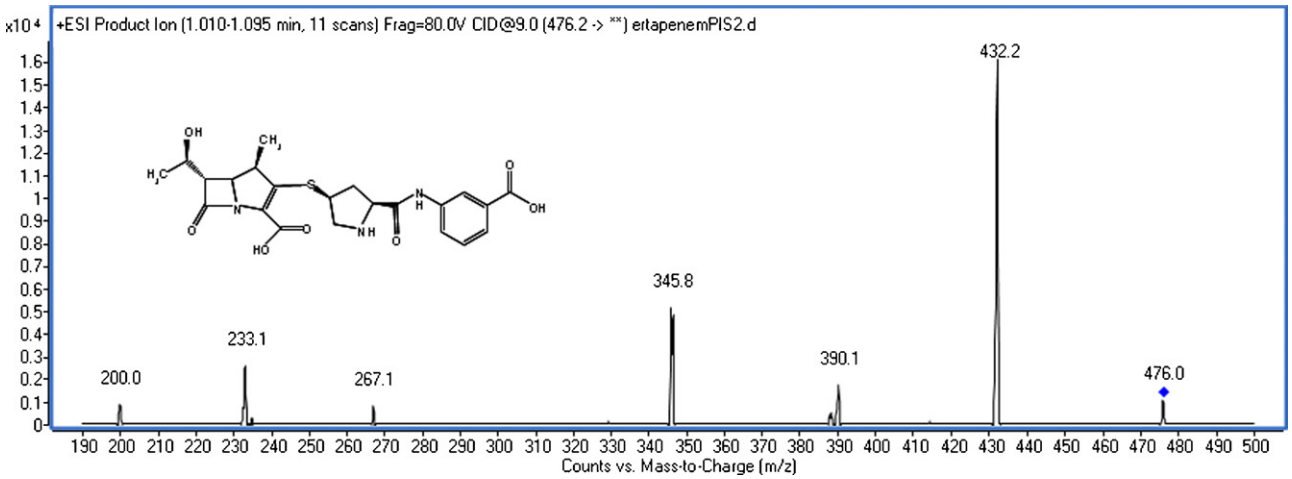

Fig. 1. Product ion scan and molecular structure of ertapenem.

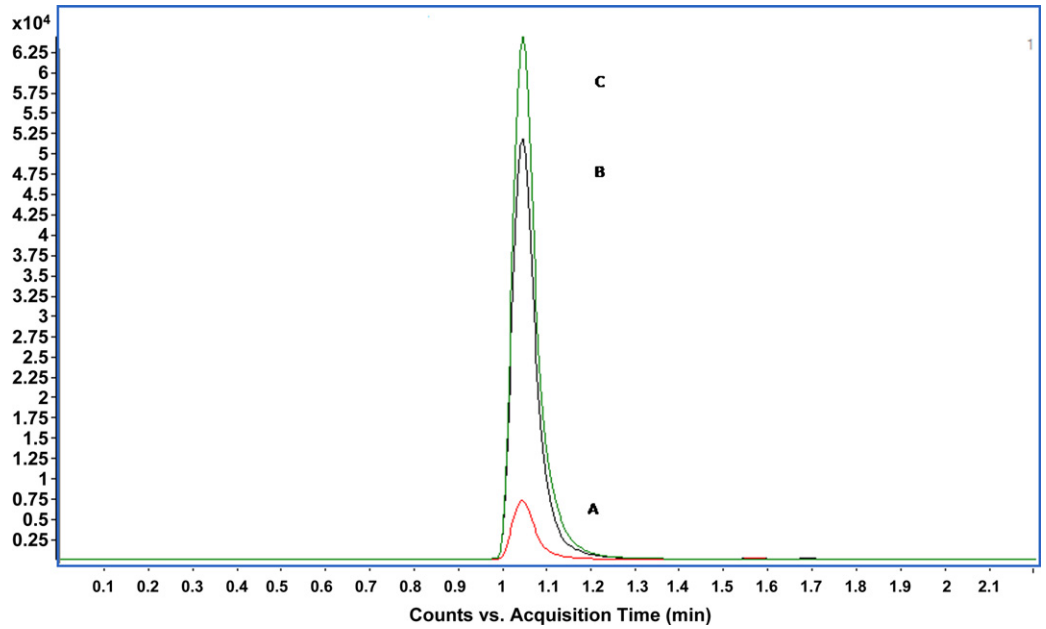

Fig. 2. Comparison among the chromatograms from a blank solvent sample spiked with ertapenem (5 mg/L) (C) *versus* a ertapenem standard solution (5 mg/L) 70/30 of methanol/water added to an extracted DBS blank sample (B) and an extracted DBS fortified with 5 mg/L of ertapenem (A).

Once the transitions were chosen, sample preparation was optimized adjusting many variables in the extraction process such as extraction solution composition, volume, time and temperature.

Different extraction solutions were examined and compared with the objective of choosing the best extraction mixture. The organic solvents used were methanol or acetonitrile with different percentages of water (from 50 to 10%). The more efficient extraction solution, with the highest extraction yield, was found to be 30/70 of water/methanol (v/v). The volume of extraction solution (200 μL) was chosen in order to combine high extraction capacity with a minimal sample dilution. A successive extraction using the same conditions on the exhausted spot produced less than 10% compared to the first one.We studied the extraction time between 10 and 60 min but no subsequent increase in the peak area was reached after 25 min (data not shown). Additionally, extraction temperature was test at 25 °C, 37 °C and 60 °C. The best extraction yield occurred at 37 °C.

Evaluation of drug extraction procedure from DBS, expressed as the ratio of the areas of the drug fortified DBS extract to that of blank DBS spiked after extraction was determined to be 15% (Fig. 2, traces A and B).

Table 1
Intra- and inter-day ertapenem reproducibility on DBS assessed by % CV calculations.

Intraday				
Expected concentration (mg/L)	Mean ($n = 10$)	SD	%CV	Accuracy %
0.5	0.78	0.04	5.12	155
1.5	1.70	0.12	7.05	113
10	10.47	0.68	6.49	105
50	47.44	2.04	4.30	95
100	102.56	7.53	7.34	103
Interday				
Expected concentration (mg/L)	Mean ($n = 10 \times 3$)	SD	%CV	Accuracy %
0.5	0.53	0.05	9.43	105
1.5	1.49	0.22	14.77	99
10	10.70	1.59	14.86	107
50	46.90	1.60	3.41	94
100	99.44	3.31	3.32	99

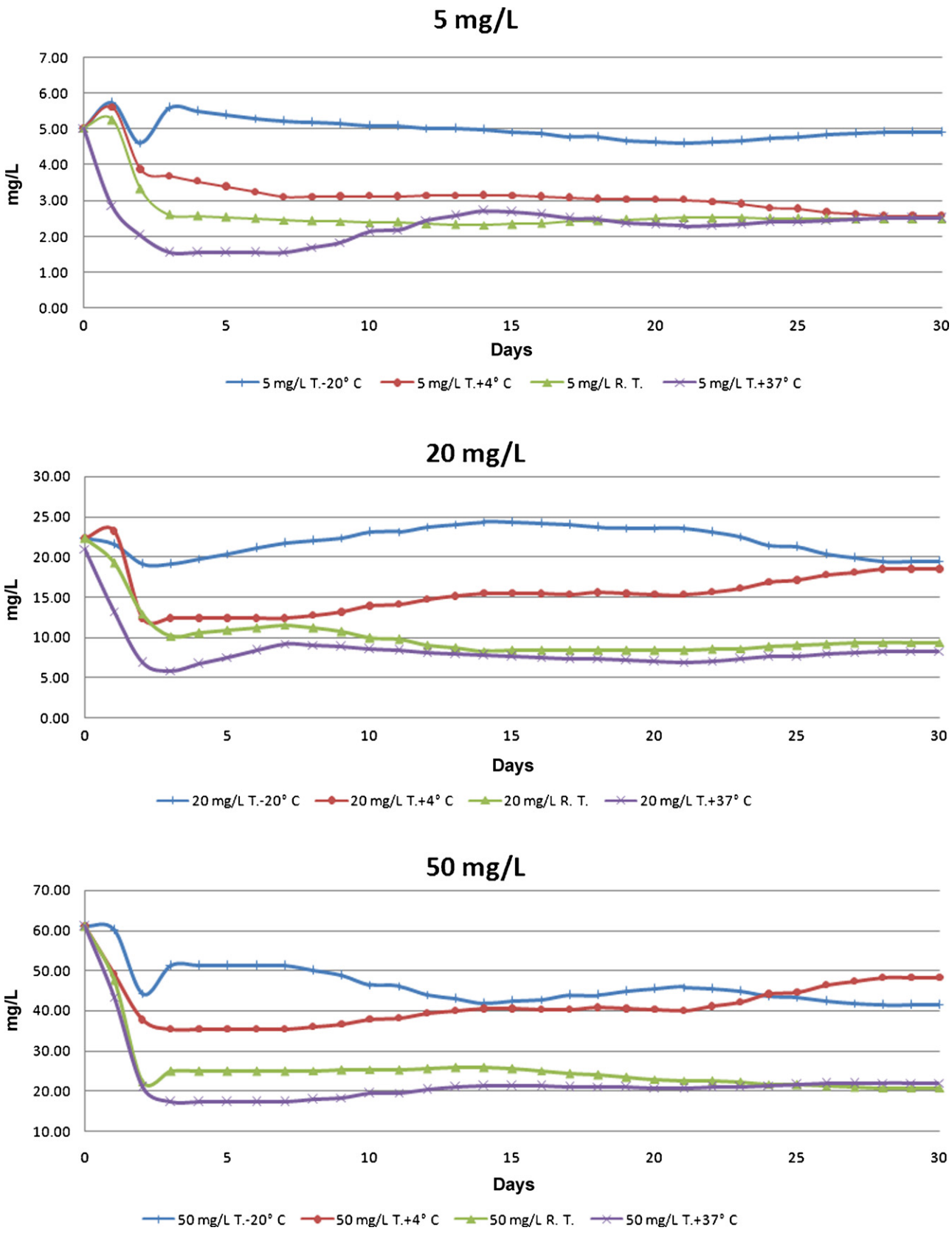

Fig. 3. Stability of ertapenem investigated at 4 different temperatures: −20 °C, +4 °C, room temperature and +37 °C for a month by repeat injection of 3 DBS spiked samples (5, 20, and 50 mg/L).

The difference between (B) and (A) could be due to a significant portion of drug bounded to the blood proteins, as reported from Musson et al. [17]. This suggested us that the extraction solution is able to extract the total free ertapenem from DBS.

We tested also different times to equilibrate the sample after the ertapenem standard spiking (data not shown) to verify the influence of time in the protein binding on the free drug portion. The equilibration time range investigated was from 20 to 120 min at room temperature but any changes in the extracted concentration were observed. Therefore after 20 min of equilibration, each spiked blood sample was spotted on filter paper.

Matrix effect is shown by the ratio of extracted DBS sample spiked post-extraction and spiked solvent sample (Fig. 2, traces B and C); this value represents a loss of 20% of the analyte signal (ion suppression) due to alterations in ionization efficiency.

One of the most important features for screening method is a fast runtime analysis. It allows processing many samples in a short period of time. Moreover the resolution is another fundamental parameter and the column we used was a 1.8 μm stationary phase column, coupled to a superior specificity of a triple quadrupole system operating in MS/MS mode. The injection volume was maintained low to avoid the system contamination from the matrix interferences and column over loading. In this new method the original sample is approximately 60 times diluted and the sample amount injected is 0.172 μL. In these conditions the sensitivity achieved is enough to afford the analyzed samples, obtaining robust performances, with the lowest sample preparation possible. Ertapenem was retained by the column enough to be separated from the salts, which represents the main ion suppression source for biological samples analysis. Inter-assay variability of calibration data obtained over concentrations of 0.5–100 mg/L was monitored on 4 consecutive weeks. The average slope, intercept, and coefficient of linear regression (r^2) were 964, −427 and 0.9987 (SD ± 0.001, range 0.9970–0.9999). A correlation coefficient >0.9950 is generally considered as the evidence of an acceptable fit of the data to the regression line.

In order to evaluate punching location impact and the homogeneity of drug distribution, experiments on several spots from the same drop of blood have been performed; no significant differences were detected. This fact is due to the low spotted volume on paper (20 μL) as elsewhere reported [17].

In order to assess the robustness of the method, five spiked levels were used (0.5, 1.5, 10, 50 and 100 mg/L) and each was processed ten times in one day, resulting in an intra-day repeatability below 7% for all values (Table 1). The inter-day repeatability obtained in four separate assays for four weeks was better than 15% (Table 1). The limit of detection (LOD) and lower limit of quantification (LLOQ) of this method were determined from the coefficient of variation of a known concentration of reference standards. The LOD for this assay, calculated from 5 times the noise level of the response, in DBS was 0.2 mg/L. The LLOQ for this assay calculated from 15 times the noise level of the response, is 0.5 mg/L.

We investigated the effect of storage time and storage temperature at four different concentration levels (0.5, 5, 20 and 50 mg/L) on spiked DBS samples. Ertapenem seems to be not stable under the tested temperatures (+4 °C, room temperature and +37 °C), with the exception of −20 °C (Fig. 3). In literature data related to the ertapenem stability reported a rapid degradation in solution and for long-term storage freeze at −20 °C is required [7,16]. Data related to the LLOQ (0.5 mg/L) stability are not shown in Fig. 3, because of the drug concentration after 24 h decreased under the limit of quantification. Usually the DBS sampling procedure helps the molecule stabilization, allowing collection, shipping and delivery at room temperature [16,18]. In this case the DBS sampling advantage remains, but the shipment must be performed at −20 °C.

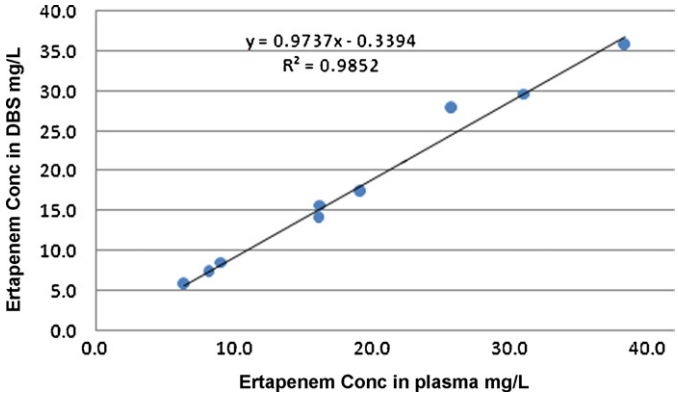

Fig. 4. Relationship between ertapenem levels in plasma and corresponding dried blood spots. Values represent the mean of duplicate experiments.

To verify the correlation between data obtained on dried blood spot and plasma, since no patients receiving ertapenem were available, three different blood samples at distinct hematocrit levels (low, medium and high) from healthy donors were selected.

For each blood sample three aliquots were prepared and spiked at 5, 10 and 20 mg/L of ertapenem. Samples were equilibrated for 20 min, then 20 μL of blood were spotted on paper and the remaining blood was centrifuged to obtain plasma. The DBS samples were extracted as reported in Section 2; 200 μL of extraction mixture were added to 2 μL of plasma, vortexed and centrifuged to precipitate proteins. Three microliters of supernatant were injected. A good correlation (R^2 = 0.9850) between ertapenem plasma and ertapenem levels measured in the corresponding DBS after real haematocrit correction was observed (Fig. 4). This confirms the validity of DBS analysis as an alternative to plasma drug.

The method will be helpful in processing large number of samples for patient's treatment monitoring at follow-up. Use of DBS for sampling requires little volume of blood spotted and dried on card, with great advantages over conventional plasma sampling being less invasive, particularly in pediatric population.

4. Conclusions

The use of DBS offers an easy way of collecting, storing, and shipping samples and is a non-invasive method because blood can be obtained from finger pricks sampling.

In order to keep stability for long term storage, ertapenem should be stored at low temperature (−20 °C).

A good correlation between drug levels measured in plasma and in the corresponding DBS after correction for real hematocrit was observed.

In this work, we developed a method for the "on DBS assay" of ertapenem by using UPLC–MS/MS. It could be considered very appealing for its application for TDM or in pharmacokinetic studies involving infants and very young children.

References

[1] M.E. Falagas, G. Peppas, G.C. Makris, D.E. Karageorgopoulos, D.K. Matthaiou, Meta-analysis: ertapenem for complicated intra-abdominal infections, Aliment. Pharmacol. Ther. 27 (2008) 919–931.
[2] J.S. Solomkin, J.E. Mazuski, J.S. Bradley, K.A. Rodvold, E.J. Goldstein, E.J. Baron, P.J. O'Neill, A.W. Chow, E.P. Dellinger, S.R. Eachempati, S. Gorbach, M. Hilfiker, A.K. May, A.B. Nathens, R.G. Sawyer, J.G. Bartlett, Diagnosis and management of complicated intra-abdominal infection in adults and children: guidelines by the Surgical Infection Society and the Infectious Diseases Society of America, Clin. Infect Dis. 50 (2010) 133–164.
[3] N. Dalgic, M. Sancar, B. Bayraktar, E. Dincer, S. Pelit, Ertapenem for the treatment of urinary tract infections caused by extended-spectrum β-lactamase-producing bacteria in children, Scand. J. Infect Dis. 43 (2011) 339–343.

[4] S.M. Abdel-Rahman, G.L. Kearns, S. Topelberg, R.F. Jacobs, G.C. Mistry, A. Majumdar, Y. Xu, J.A. Wagner, C.J. Kitchen, M. Groff, G. Herman, J.L. Blumer, Pharmacokinetics and tolerability of single-dose intravenous ertapenem in infants, children, and adolescents, Pediatr. Infect Dis. J. 29 (2010) 1072–1076.
[5] Z. Zhao, X.Z. Qin, R.A. Reed, Identification by LC/MSn of degradated of a novel carbapenem antibiotic in an aqueous matrix, J. Pharm. Biomed. Anal. 29 (2002) 173–181.
[6] M.W.R. Pletz, M. Rau, J. Bulitta, A. De Roux, O. Burkhardt, G. Kruse, M. Kurowski, C.E. Nord, H. Lode, Ertapenem pharmacokinetics and impact on intestinal microflora, in comparison to those of ceftriaxone, after multiple dosing in male and female volunteers, Antimicrob. Agents Chemother. 48 (2004) 3765–3772.
[7] T. Koal, M. Deters, K. Resch, V. Kaever, Quantification of the carbapenem antibiotic ertapenem in human plasma by a validated liquid chromatography–mass spectrometry method, Clin. Chim. Acta 364 (2006) 239–245.
[8] S. Lefeuvre, N. Venisse, S. Marchand, M. Bachelet, W. Couet, A simple and sensitive liquid chromatography-tandem mass spectrometry assay for the quantification of ertapenem in microdialysate, J. Chromatogr. B: Analyt. Technol. Biomed. Life Sci. 862 (2008) 242–245.
[9] G. Emmons, M. Rowland, Pharmacokinetic considerations as to when to use dried blood spot sampling, Bioanalysis 2 (2010) 1791–1796.
[10] L. Filippi, C. Poggi, G. la Marca, S. Furlanetto, P. Fiorini, G. Cavallaro, A. Plantulli, G. Donzelli, R. Guerrini, Oral topiramate in neonates with hypoxicischemic encephalopathy treated with hypothermia: a safety study, J. Pediatr. 157 (2010) 361–366.
[11] N. Spooner, Dried blood spot sampling for quantitative bioanalysis: time for a revolution? Bioanalysis 2 (2010) 1781.
[12] N. Spooner, Y. Ramakrishnan, M. Barfield, O. Dewit, S. Miller, Use of DBS sample collection to determine circulating drug concentrations in clinical trials: practicalities and considerations, Bioanalysis 2 (2010) 1515–1522.
[13] G. la Marca, S. Malvagia, L. Filippi, P. Fiorini, M. Innocenti, F. Luceri, G. Pieraccini, G. Moneti, S. Francese, F.R. Dani, R. Guerrini, Rapid assay of topiramate in dried blood spots by a new liquid chromatography–tandem mass spectrometric method, J. Pharm. Biomed. Anal. 48 (2008) 1392–1396.
[14] G. la Marca, S. Malvagia, L. Filippi, M. Innocenti, A. Rosati, M. Falchi, S. Pellacani, G. Moneti, R. Guerrini, Rapid assay of rufinamide in dried blood spots by a new liquid chromatography-tandem mass spectrometric method, J. Pharm. Biomed. Anal. 54 (2011) 192–197.
[15] G. la Marca, S. Malvagia, L. Filippi, F. Luceri, G. Moneti, R. Guerrini, A new rapid micromethod for the assay of phenobarbital from dried blood spots by LC–tandem mass spectrometry, Epilepsia 50 (2009) 2658–2662.
[16] W. Li, F.L. Tse, Dried blood spot sampling in combination with LC–MS/MS for quantitative analysis of small molecules, Biomed. Chromatogr. 24 (2010) 49–65.
[17] D.G. Musson, K.L. Birk, C.J. Kitchen, J. Zhang, J.Y. Hsieh, W. Fang, A.K. Majumdar, J.D. Rogers, Assay methodology for the quantitation of unbound ertapenem, a new carbapenem antibiotic, in human plasma, J. Chromatogr. B: Analyt. Technol. Biomed. Life Sci. 783 (2003) 1–9.
[18] R. Garcia Boy, J. Henseler, R. Mattern, G. Skopp, Determination of morphine and 6-acetylmorphine in blood with use of dried blood spots, Ther. Drug Monit. 30 (2008) 733–739.

Journal of Pharmaceutical and Biomedical Analysis 61 (2012) 114–121

Contents lists available at SciVerse ScienceDirect

Journal of Pharmaceutical and Biomedical Analysis

journal homepage: www.elsevier.com/locate/jpba

Updating a near-infrared multivariate calibration model formed with lab-prepared pharmaceutical tablet types to new tablet types in full production

Jeremy A. Farrell, Kevin Higgins, John H. Kalivas*

Department of Chemistry, Idaho State University, Pocatello, ID 83209, United States

ARTICLE INFO

Article history:
Received 22 July 2011
Received in revised form 1 November 2011
Accepted 4 November 2011
Available online 17 November 2011

Keywords:
Multivariate calibration
Tikhonov regularization
Calibration standardization and maintenance
Model-updating
NIR spectroscopy

ABSTRACT

Determining active pharmaceutical ingredient (API) tablet concentrations rapidly and efficiently is of great importance to the pharmaceutical industry in order to assure quality control. Using near-infrared (NIR) spectra measured on tablets in conjunction with multivariate calibration has been shown to meet these objectives. However, the calibration is typically developed under one set of conditions (primary conditions) and new tablets are produced under different measurement conditions (secondary conditions). Hence, the accuracy of multivariate calibration is limited due to differences between primary and secondary conditions such as tablet variances (composition, dosage, and production processes and precision), different instruments, and/or new environmental conditions. This study evaluates application of Tikhonov regularization (TR) to update NIR calibration models developed in a controlled primary laboratory setting to predict API tablet concentrations manufactured in full production where conditions and tablets are significantly different than in the laboratory. With just a few new tablets from full production, it is found that TR provides reduced prediction errors by as much as 64% in one situation compared to no model-updating. TR prediction errors are reduced by as much as 51% compared to local centering, another calibration maintenance method. The TR updated primary models are also found to predict as well as a full calibration model formed in the secondary conditions.

© 2011 Elsevier B.V. All rights reserved.

1. Introduction

In the pharmaceutical industry, it is important to rapidly determine tablet concentrations of the active pharmaceutical ingredient (API) for efficient quality control. It is well documented in the literature that near-infrared (NIR) spectroscopy in conjunction with multivariate calibration [1,2] can meet these goals under controlled conditions [3–13]. Specifically, in multivariate calibration, pharmaceutical samples, e.g., tablets, with known API content, or another chemical or physical tablet attribute, are prepared under a variety of controlled chemical, physical, instrumental, and environmental conditions. Near-infrared spectra are measured on these tablets and a mathematical relationship (*primary* model) is obtained relating the API content to the spectra. The model is now used to determine (predict) the API content of new tablets. The next section details the mathematics.

A problem with any calibration is that measurement conditions, as well as tablet characteristics, inevitably deviate from those spanned by the original primary calibration. These differences can be due to chemical, physical, instrumental, and/or environmental changes. Changes from the primary conditions shall be referred to as the *secondary* conditions. If an NIR calibration model is not adapted to the new conditions, it will not accurately determine API concentrations (or another calibrated chemical or physical tablet attribute) of tablets produced and measured in the new conditions [14,15]. Thus, methods are needed to solve this calibration maintenance problem. The goal of calibration maintenance, also referred to as calibration transfer or standardization, is to maintain the primary model for accurate API determinations of samples measured in secondary conditions. Various approaches have been presented in order to accomplish calibration maintenance and are well reviewed [16,17].

One approach, and the focus of this paper, is model-updating. This approach augments new secondary sample spectra and the corresponding API concentrations to the original primary data thereby allowing an updated model to be formed. The updated model can now be used to determine sample API concentrations. With model-updating, new spectral variances not present in the primary conditions can be corrected for, including new spectrally responding species. Many samples would be needed to span the new conditions in order to offset the many samples already existing in the primary set. However, this essentially amounts to a full recalibration. A simpler approach is to augment with only a few new samples [18–31]. However, many of these studies did not weight the new samples from the secondary conditions. Without proper

* Corresponding author. Tel.: +1 208 282 2726; fax: +1 208 282 4373.
E-mail addresses: farrjere@isu.edu (J.A. Farrell), higgkevi@Isu.edu (K. Higgins), kalijohn@isu.edu (J.H. Kalivas).

0731-7085/$ – see front matter © 2011 Elsevier B.V. All rights reserved.
doi:10.1016/j.jpba.2011.11.003

weighting of these new samples, too much emphasis will be put on the larger number of primary calibration samples. In work with weighting, the weights were determined by methods based on a single criterion and tended to be empirical (rule of thumb) [24–28]. However, the newly developed Tikhonov regularization (TR) methods (described in the next section) [29–31], provide a systematic methodology for determining weights based on multicriteria.

A few studies have been performed dealing with calibration maintenance issues for pharmaceutical quantitative multivariate calibration with NIR spectroscopy [32–34]. However, these studies focus on transfer between instruments. It is desirable to be able to determine the API content of different tablet types produced and measured in different conditions.

Presented in this paper are results from applying TR to a NIR pharmaceutical data set from the literature [13]. This data set has tablets prepared in a laboratory setting (primary conditions) and tablets produced in full production (secondary conditions). The approach used in this paper is to first form a primary calibration set of tablets from the tablets prepared and measured in a laboratory setting. The primary set spans simple tablet variances. The method of TR is then used to provide model-updating from the laboratory prepared samples to determine API content of tablets obtained in full production where different tablet types and other physical properties exist. New full production tablet API determination errors from the updated model are compared to the errors from a full RR calibration using a large number of full production reference samples. It is shown that the TR updated model attains similar accuracy with substantially fewer tablets from the secondary condition (full production).

2. Materials and methods

2.1. Model-updating

2.1.1. Primary calibration

A commonly used mathematical relationship for multivariate calibration is

$$\mathbf{y} = \mathbf{X}\mathbf{b} + \mathbf{e} \tag{1}$$

where $\mathbf{y}$ is an $m \times 1$ vector of quantitative information for the analyte, m is the number of samples, $\mathbf{X}$ is an $m \times n$ matrix of spectra measured over n wavelengths, $\mathbf{b}$ is an $n \times 1$ model vector, and $\mathbf{e}$ is the $m \times 1$ vector of normally distributed errors with mean zero and covariance matrix $\sigma^2\mathbf{I}$ with $\mathbf{I}$ being the $m \times m$ identity matrix [1,2]. Multivariate calibration seeks to estimate $\mathbf{b}$, by $\hat{\mathbf{b}} = \mathbf{X}^{+}\mathbf{y}$ where $\mathbf{X}^{+}$ is a generalized inverse of $\mathbf{X}$. Once $\hat{\mathbf{b}}$ is determined, it is then used to predict new samples by $\hat{y} = \mathbf{x}^T\hat{\mathbf{b}}$ where the superscript T signifies the matrix algebra transpose operation. If $\mathbf{X}$ does not properly span measurement and sample conditions, then predictions with the estimated model vector will be in error.

2.1.2. Calibration maintenance by model-updating

For multivariate calibration maintenance, the sample matrix $\mathbf{X}$ needs to be augmented with samples measured in the new conditions. In the case of pharmaceutical tablets, where $\mathbf{X}$ has been measured in a laboratory setting for tablets designed and produced in the laboratory, a few tablets manufactured in full production need to be included in order to update to the new conditions. Mathematically, this is denoted as augmentation by $\begin{pmatrix}\mathbf{X}\\ \mathbf{M}\end{pmatrix}$, where $\mathbf{M}$ is an $s \times n$ matrix of spectra and s is the number of samples measured in the new secondary conditions. These samples would be spectroscopically measured in the secondary condition and reference values for the API content would need to be respectively augmented to $\mathbf{y}$. Eq. (1) is modified to $\begin{pmatrix}\mathbf{y}\\ \mathbf{y_M}\end{pmatrix} = \begin{pmatrix}\mathbf{X}\\ \mathbf{M}\end{pmatrix}\mathbf{b} + \mathbf{e}$ where $\mathbf{y_M}$ is an $s \times 1$ vector of quantitative analyte reference information. If the number of secondary samples augmenting the primary calibration is large, then essentially a full recalibration is performed with no gain in efficiency. However, if the number of samples is small, then the new model vector will be biased towards the primary condition due to the majority of the samples spanning the primary condition. With TR (described next), a simple weighing scheme is used for a small set of samples from the secondary condition thereby reducing the primary condition bias.

2.1.3. Tikhonov regularization

Tikhonov regularization in its simplest form for multivariate calibration without maintenance (also known as TR in standard form and ridge regression (RR) [2,35]) is expressed as $\begin{pmatrix}\mathbf{y}\\ \mathbf{0}\end{pmatrix} = \begin{pmatrix}\mathbf{X}\\ \eta\mathbf{I}\end{pmatrix}\mathbf{b} + \mathbf{e}$, with solution $\hat{\mathbf{b}} = (\mathbf{X}^T\mathbf{X} + \eta^2\mathbf{I})^{-1}\mathbf{X}^T\mathbf{y}$ satisfying $\min(\|\mathbf{X}\mathbf{b} - \mathbf{y}\|_2^2 + \eta^2\|\mathbf{b}\|_2^2)$ where the superscript -1 denotes the matrix inverse operation, $\|\bullet\|_2$ represents the Euclidean vector norm (2-norm), $\mathbf{I}$ is the identity matrix of size $n \times n$, $\mathbf{0}$ is an $n \times 1$ zero vector, and η is a meta-parameter ($0 \le \eta$) that provides numerical stability to the inverse operation and regulates the magnitude of the model vector. If too large of a model is formed (small η values), then the RR model overfits the data. Similarly, if too small of a model vector is formed (large η value), the RR model underfits the data. When $\eta = 0$, the least squares solution is obtained. Various approaches have been used to determine an acceptable value for η. One approach is to plot the 2-norm of the model against the root mean square error of calibration (RMSEC) to form an L-shaped curve (L-curve) [2,29–31,35]. Acceptable values of η are those with models in the corner region of the L-curves. These models represent those with an acceptable trade-off in bias and variance (harmonious models). Further discussion of selecting the meta-parameter value is found in Section 3 where alternative graphical approaches are presented and discussed.

For calibration maintenance, new secondary samples are weighted to minimize the number of samples needed to update to the new conditions. In this case, RR is modified to the TR variant $\begin{pmatrix}\mathbf{y}\\ \mathbf{0}\\ \lambda\mathbf{y}_\mathrm{M}\end{pmatrix} = \begin{pmatrix}\mathbf{X}\\ \eta\mathbf{I}\\ \lambda\mathbf{M}\end{pmatrix}\mathbf{b} + \mathbf{e}$ with solution $\hat{\mathbf{b}} = (\mathbf{X}^T\mathbf{X} + \eta^2\mathbf{I} + \lambda^2\mathbf{M}^T\mathbf{M})^{-1}(\mathbf{X}^T\mathbf{y} + \lambda^2\mathbf{M}^T\mathbf{y_M})$ satisfying the condition

$$\min(\|\mathbf{X}\mathbf{b} - \mathbf{y}\|_2^2 + \eta^2\|\mathbf{b}\|_2^2 + \lambda^2\|\mathbf{M}\mathbf{b} - \mathbf{y}_M\|_2^2) \tag{2}$$

where λ is the weight for the secondary condition samples with $0 \le \lambda$. This TR variant is referred to as TR2 and now two meta-parameters must be determined. As with RR, graphical L-curves can be used including additional L-curves formed by plotting the model 2-norm against the RMSE of predicting $\mathbf{M}$ (RMSEM) [29–31]. Section 3 further elaborates. When the λ weight is set to zero, then Eq. (2) amounts to forming a RR model.

Other TR variants have been formed and evaluated, including an approach that provides maintenance and wavelength selection simultaneously [30,31]. A general form is satisfying the condition $\min(\|\mathbf{X}\mathbf{b} - \mathbf{y}\|_a^a + \eta^b\|\mathbf{L}\mathbf{b} - \mathbf{y}_L\|_b^b + \lambda^c\|\mathbf{M}\mathbf{b} - \mathbf{y}_M\|_c^c)$ where a, b, and c are typically 1 (1-norm) and/or 2 (2-norm). Only the TR2 format in Eq. (2) is evaluated in this study with $a = b = c = 2$, $\mathbf{L} = \mathbf{I}$, and $\mathbf{y}_\mathrm{L} = \mathbf{0}$.

2.2. Software

MATLAB 2010b (The MathWorks, Natick, MA) TR programs used in previous TR work [29–31] are used in this study.

2.3. Data centering

Local mean centering was used where **X**, **y**, **M**, and $\mathbf{y_M}$ are column wise centered to respective means. Validation samples of the secondary conditions are centered to the mean of **M** prior to prediction.

2.4. Tablet data set

The pharmaceutical tablet data used in this study is that described in Ref. [13] and available for downloading [36]. Raman and NIR spectra are obtainable and the NIR data set is used in this paper. Briefly, the data set consists of 310 Escitolopram tablets measured in the range of 4000–14,000 cm^{-1} (700–2500 nm) with a resolution of 16 cm^{-1} for a total of 404 wavelengths. Tablets are subdivided into four types (type 1, type 2, type 3, and type 4) based on total tablet weights of 90, 125, 188, and 250 mg. Because tablet types have different total weights, respective tablet types have different shapes and sizes with tablet thicknesses ranging from 2.9 to 4.3 mm. Each tablet type can be further subdivided into three production batches labeled as laboratory, pilot, and full. There are 30 tablets for each batch tablet type combination. All tablet API values were determined by high performance liquid chromatography (HPLC) with an estimated relative error of 3.5% [13]. Tablet API contents are in units of w/w%. All laboratory tablets have been stamped with a tablet press using only one punch. The pilot and full production tablets are produced in a tablet press with a total of 40 different punches [13]. Laboratory tablets are used for the primary conditions and full batch tablets are used for the secondary conditions as this is a desirable industrial situation. The laboratory batch is referred to as lab batch. Ref. [13] should be further consulted for the lab and full batch tablet specifications for each tablet type and other experimental parameters.

2.5. Primary, secondary, and validation samples

From the 30 lab type 1 tablets, 15 random tablets are always part of the primary **X** and **y**. Type 1 is always included as it is the only type with about 5% API. Tablet types 2–4 are approximately 8% API. The other tablets included in the primary **X** and **y** consist of various combinations of one, two, or three of the tablet types 2–4. For each lab tablet type included, 15 random tablets were selected. The remaining 15 tablets of each lab tablet type are then used to validate the corresponding primary RR models.

Full batch tablets are set to the secondary condition. From the secondary conditions, tablets are needed for **M** and $\mathbf{y_M}$, a full calibration set, and an independent validation set. As with the primary condition, type 1 tablets are always included. When two tablet types are used to form **M** and $\mathbf{y_M}$, two random tablets are selected from the 30 full batch type 1 tablets and depending on the situation, two random tablets from the respective 30 type 2, type 3, or type 4 tablets. To form respective full secondary calibration sets, tablets selected for **M** are used in conjunction with 13 additional random tablets of each corresponding secondary full batch tablet type. These secondary calibration sets are used to form RR models based in the secondary space.

In order to test how well a given RR or TR2 model predicts in the full batch secondary condition, a validation set needs to be formed [1,2]. Samples present in the validation set are not used in building the model and can therefore be used to check how well the model predicts. Validation sets relative to the design of **M** and $\mathbf{y_M}$ are formed by using the remaining 15 respective tablets of the same type combinations used for **M** and $\mathbf{y_M}$. The same respective validation samples are used to test all primary RR models, secondary RR models, and TR2 updated models.

2.6. Meta-parameter values

The η values ranged exponentially from1000 to 0 with 80 values and λ ranged exponentially from 1000 to 0 with 100 values.

3. Results and discussion

3.1. Principle component analysis

Plotted in Fig. 1 is the score plot of the spectra for the lab and full batches and all four tablet types using principle component PC1 and PC2. Global mean centering was performed (spectra centered to the mean of all batch and tablet types). From the PC plot, spectroscopic differences are demonstrated between the two batches. Within in each batch, differences between the tablet types are also observed. From the PC plot, it is expected that if the lab batch is used to form the primary calibration, the model will not accurately predict the full batch. Thus, calibration maintenance will be needed. Of the possible primary and secondary batch tablet situations, only a few representative situations are presented.

3.2. Determining meta-parameters

In modeling, it has been noted that a common problem consists of insufficient human intervention [37–41]. Too much reliance is often placed on automatic black-box procedures and graphical assessments are considered as not necessary. Graphical assessments assist in detecting model discrepancies, i.e., statistical measures need to be consistent for a selected set of modeling conditions. With graphical analysis, multiple modeling criteria can be visualized simultaneously allowing for proper assessment. As previously noted, TR meta-parameters can be selected from graphical assessment of L-curves using multiple criteria. For the RR format of TR, there is only one meta-parameter. Thus, only one L-curve is formed when the model vector 2-norm (an indicator of prediction variance) is plotted against the RMSEC (an indicator of prediction bias) while varying the meta-parameter. Other bias and variance measures can be used to form additional single L-curve to further substantiate meta-parameter selection [2].

For TR2, there are two meta-parameters to determine. In initial TR2 calibration maintenance work [29], multiple L-curves are formed on one plot for one set of bias and variance indicators. Shown in Fig. 2a are L-curves for the model 2-norm plotted against RMSEC with tablet types 1 and 2 in the primary condition and tablet types 1 and 2 in the secondary condition. Each L-curve (color) is

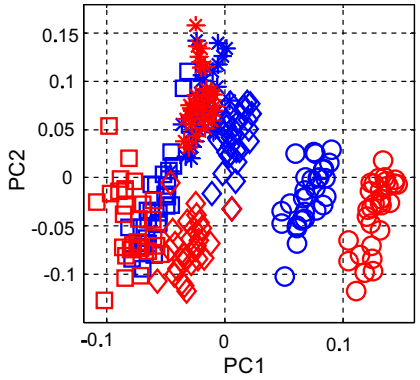

Fig. 1. (a) PCA score plot of lab and full batches with all four tablet types. (Red) lab batch tablets and (blue) full batch tablets with (asterisk) type 1, (circle) type 2, (diamond) type 3, and (square) type 4. PC1 and PC2, respectively account for 88.04% and 3.89% of the variance. Spectra were centered to the mean of all spectra. (For interpretation of the references to color in text, the reader is referred to the web version of the article.)

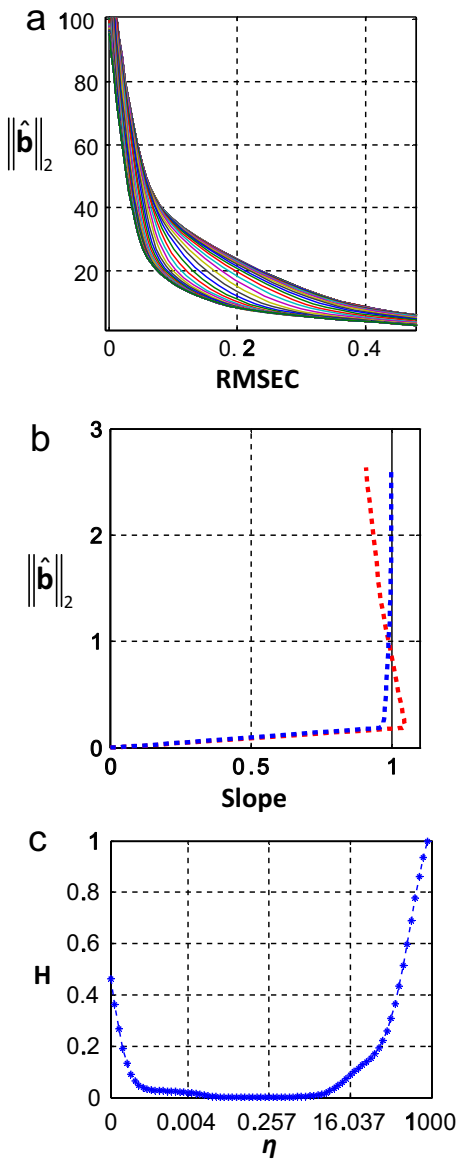

Fig. 2. Model merits for selecting meta-parameters using for primary calibration spectra in **X** tablet types 1 and 2 and secondary spectra in **M** are also tablet types 1 and 2. (a) TR2 L-curves for the model 2-norm plotted against RMSEC. Each color is a λ value while each point on an L-curve is a η value. (b) TR2 slope L-curve plots at λ = 54.29 while varying η with (red) primary samples in **X** and (blue) secondary samples in **M**. Intercepts are from plotting predicted values against reference values. A similar plot is obtained for the slope. (c) TR2 H values at λ = 54.29 while varying η. (For interpretation of the references to color in text, the reader is referred to the web version of the article.)

a λ value while each point on an L-curve is a η value. As with other studies using TR variants, L-curves converging in the lower left region are models best for predicting primary calibration spectra. The L-curves converging in the upper part are models best for the secondary condition represented by **M**. Other TR2 L-curve sets can be plotted using other bias and variance measures. As with RR, these different L-curve sets can be used to further substantiate meta-parameter selections. While meta-parameter selection is possible using the L-curve process initially described [29] and later improved [30,31], additional graphical process would be beneficial.

Graphical alternatives presented in this paper use images of RMSEC, RMSEM, model vector 2-norm, and other bias and variance measures. In this way, the bias variance tradeoff is better simultaneously assessed with respect to the two meta-parameters λ and η. An example is given in Fig. 3 for the same primary and secondary situation in Fig. 2 showing that the bias variance tradeoff trends seen in Fig. 2 are more apparent with the images. Images in Fig. 3 are: (a) RMSEC, (b) RMSEM, (c) 2-norm, and (d) RMSE of validation (RMSEV). Several observations are evident. First, all four figures show similar respective image trends across all η values when λ is small (approximately 0.002 or smaller). Convergence to the same respective image values across different ranges of η values begins with λ less than 1.00. Specifically, when the weight given to the secondary conditions is small in Eq. (2), the secondary conditions are essentially not included and the model is not updated. This consistent region amounts to using RR with local centering where the validation set (new samples) are centered to the mean of **M**. Several studies have shown that local centering is a useful method for calibration maintenance with pharmaceutical and other spectroscopic data [32,33,41–43]. Model merit values shown in Table 2 for this tablet situation indicate that local centering is not as effective as using TR2. However, in other tablet situations, local centering is more effective as evident from modeling merits listed in Table 2. Aspects of local centering are discussed in each of the following secondary condition situation sections.

Another observation of the images in Fig. 3 is that at larger λ and smaller η values (lower right corner), the RMSEM values are low. However, model vector 2-norms are some of the largest indicating overfitted models and larger η values are actually needed. If the η values are too large, the RMSEC values substantially degrade (upper right corner). This indicates that an intermediate region is necessary representing the proper tradeoff between predicting in the primary and secondary conditions. One could box in values as shown by the green box in Fig. 3b where RMSEM values are low, RMSEC values are not too large, and the 2-norm is not too small or large. Predictions from this region would be averaged for the final prediction. The RMSEV image in Fig. 3d shows that these are indeed good combinations of the two meta-parameters, albeit other combinations also provide low RMSEC values.

Alternatively, there are gradients of model merits in the regions of larger η and λ values and various L-curves can be plotted holding η constant or other L-curves formed by holding λ constant. The white lines and arrows in Fig. 3b refer to these ranges of meta-parameter values. While the 2-norm gradient is difficult to observe in Fig. 3c, when the intermediate regions are imaged, the gradient becomes more apparent. Which η or λ is held constant is not critical as long as each is within the intermediate region.

Table 1 shows results for the model-updating situation in Fig. 2. Values for respective slopes, intercepts, and R^2 are from plotting predicted values against reference values. Results from using the traditional L-curve approach indicate that improved predications are obtained compared to no model-updating. While models in corner regions predict the validation set well, improvements are possible. Specifically, regardless of which meta-parameter is held constant, L-curve corners do not identify the best meta-parameters residing in the upper part of L-curves with larger model vector 2-norms. In past studies, secondary conditions requiring updating have been less complicated such as a temperature effect or an instrument effect. With the tablet data set, differences between primary and secondary conditions are more complicated which could be why better models are formed in the L-curve portion with greater model vector 2-norms. Increasing the model 2-norm is analogous to increasing the number of factors for partial least squares (PLS) in order span a greater portion of the calibration space.

Conversely, respective primary and secondary slope and intercept L-curves identify the better meta-parameters, albeit, L-curve corners behave similar to R^2 and prediction error L-curves. The difference is that when slope and intercept model merit values for the primary and secondary conditions are plotted, there is a

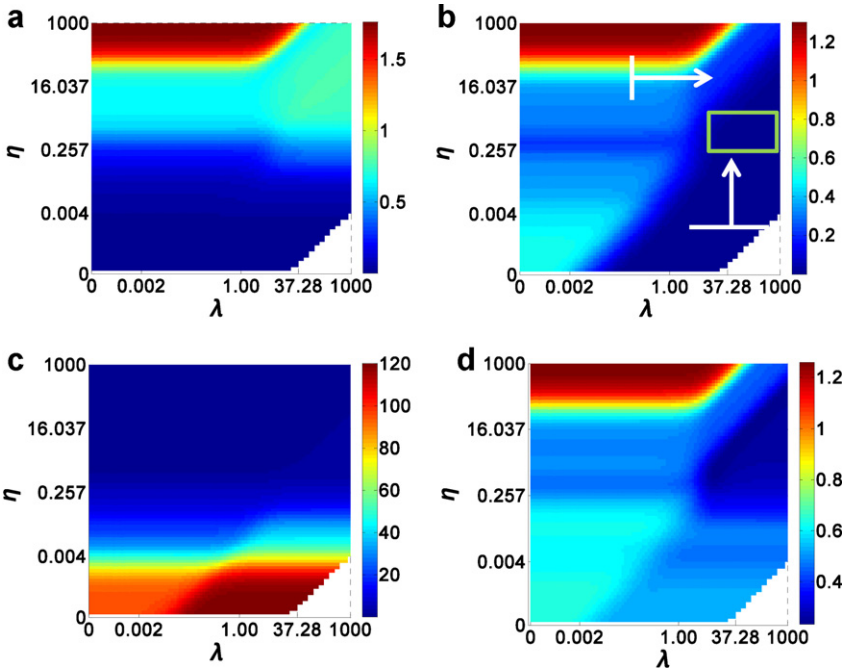

Fig. 3. TR2 image plots for the situation in Fig. 2. (a) RMSEC, (b) RMSEM, (c) model vector 2-norm, and (d) RMSEV. The green box denotes ranges of good η and λ values to obtain an average prediction for the box. The white arrows denote η and λ values ranges to select from for holding one constant while varying the other to obtain respective single L-curves.

region where the primary and secondary curves intersect indicating that this model is functioning similarly to both conditions. Shown in Fig. 2b is the slope L-curve holding λ constant. A similar plot is obtained for the intercept L-curve. The point of intersection in Fig. 2b is an appropriate η value, or the η value closest to the intersection. In this case, $\eta = 10.61$. A similar plot is obtained holding η constant and varying λ. Results tabulated in Table 1 show that this new process is functional. This observation of intersecting L-curves at the appropriate meta-parameters has not been previously observed because such plots were not formed in other TR2 studies. However, if this approach is not applicable, L-curve corner regions in the traditional mode could be used.

In previous work with TR2 and calibration maintenance [30,31], it was found that for a selected η value, model vectors converge to the same shape for best prediction of the samples in **M** (low RMSEM). A different shape is best for predicting the samples in **X** (low RMSEC). Within each converged model vector, the model vector 2-norm changes as λ varies. Thus, the better model is that with the smallest 2-norm and still correlated to the previous model vector. Using such a process, confirms the meta-parameter selections from Fig. 2b.

Another approach previously developed for meta-parameter selection [38] was evaluated for this data set. This approach has not been applied to TR2 in past work. Because the goal is selection of meta-parameters that provide an acceptable bias variance tradeoff, a harmonious criterion (H) was developed. This merit combines a bias measure such as the RMSEM with the model vector 2-norm (or another variance measure) into a single merit. For this work, the H value for the ith, jth combination of η and λ is computed by $H_{i,j} = (\mathrm{RMSEM}_{i,j}/\mathrm{RMSEM}_{\max})^2 + (\|\hat{\mathbf{b}}_{i,j}\|_2/\|\hat{\mathbf{b}}_{\max}\|)^2$ where max represents the corresponding maximum value. The lowest H value is normally taken as the best combination. However, the goal of using H is to find meta-parameters balancing the bias variance tradeoff [38]. Because not all combinations achieve such a balance, the global minimum of the H values from the corresponding H image (not shown) may not be best, i.e., the global minimum can lie in a region not bounded by larger H values while holding one meta-parameter fixed and varying the other. Thus, a λ is first selected where the tradeoff is obvious, i.e., a U-shaped region in the H image. Plotted in Fig. 2c is the H value varying across η showing this U-shape and several η values could be selected, as also noted in the RMSEV image. Tabulated in Table 1 are model merit values using the η value at the minimum of this single H plot instead of the minimum for the all possible combinations of η and λ making up the H image. The H image highlights the same region in Fig. 3d with the lowest RMSEV values as the region with the lowest H values.

It should be noted that larger η and λ values than those used to form Fig. 3 could be utilized, but essentially, the images in upper right corners of Fig. 3 just extend, i.e., respective imaged model merit values have converged. Also, the white areas in Fig. 3 correspond to η and λ that do not allow a model to be formed, i.e., the matrix $(\mathbf{X}^T\mathbf{X} + \eta^2\mathbf{I} + \lambda^2\mathbf{M}^T\mathbf{M})$ is not full rank and hence, the inverse

Table 1
Model merits for predicting secondary tablets 1 and 2. Results presented are from selecting meta-parameters by varying η with a constant λ. Unless noted otherwise, selection of η for TR2 is by the point of intersecting slope and intercept L-curves. The RR models are selected by the L-curve corner.

Method	$\|\hat{b}\|_2$	RMSEC	RMSEM	RMSEV	Slope	Intercept	R^2	Relative error[a]	η	λ
TR2	1.01	0.7643	0.0817	0.2363	0.9252	0.5140	0.9688	3.5	10.61	54.29
TR2 (L-curve)	0.20	0.7453	0.2041	0.4309	0.9193	0.7730	0.9169	6.4	72.27	54.29
TR2 (H)	2.10	0.7306	0.0140	0.2641	0.9577	0.1711	0.9657	3.9	1.70	154.29
RR local centering	2.70	0.4684	0.2452	0.4870	0.8086	1.5991	0.9352	7.3	0.58	80
RR no update	16.40	0.0964	–	0.6528	1.1029	−1.1834	0.9249	9.8	0.03	59-

[a] Relative error, 100 times RMSEV divided by mean validation API content (6.6952%) [13].

Table 2
Model merits for primary and secondary tablet types 1 and 2 RR calibration models predicting respective primary and secondary validation tablet types 1 and 2. RR models are selected by the L-curve corner.

Batch	$\|\hat{b}\|_2$	RMSEC	RMSEV	Slope	Intercept	R^2	Relative error[a]	η
Lab	16.40	0.0964	0.2756	1.0152	−0.1067	0.9715	4.1	0.0359
Full	1.34	0.2050	0.2390	0.9754	0.0986	0.9684	3.6	0.215

[a] Relative error, 100 times RMSEV divided by mean validation API content (6.6952%) [13].

is not computable. Essentially, for each η value, there is a large enough λ value where the matrix is no longer full rank.

Summarizing, the graphical approach to meta-parameter selection is to choose an η or λ value across transition areas in the upper or far right regions of respective RSEC, RMSEM and model vector 2-norm images. From here, various L-curves can be plotted fixing one meta-parameter and varying the other using the model vector 2-norm, respective slope, intercepts, R^2, prediction errors, and successive correlations for the primary and secondary samples. Meta-parameters that balance the tradeoffs between these merits are selected. The focus should be on meta-parameters where primary and secondary slope and intercept L-curves intersect. If such an intersection does not form, then the L-curve corner regions in conjunction with successive model correlations are used. Further confirmation of meta-parameter selection is obtained by plotting H and obtaining the U-curve.

3.3. Updating to tablet types 1 and 2

The previous section detailed meta-parameter selection processes for model-updating to secondary condition tablet types 1 and 2 as an example. Results presented in Table 2 reveal that TR is indeed able to update the model. Specifically, the model built for the primary laboratory samples is not able to predict in the new conditions (RR without updating). With two samples of tablet types 1 and 2 each, TR2 is able to update the model to predict in the secondary condition with substantially reduced error and better model merits. Using the traditional L-curve corner approach to select a model also performs better than no updating. The H value similarly provides a model predicting better than no updating and has improved model merits over TR2 with L-curve selection.

As previously noted in Section 3.2, local centering has been found to provide significant advantages in multivariate calibration and as well as pharmaceutical maintenance and other situations. Briefly, local centering consist of not mean centering new samples to the mean of the calibration set in **X**, but instead, new samples are mean centered relative to a representative mean of the secondary conditions. After new samples are locally centered, the API concentration can be predicted with the RR calibration model vector formed in the primary conditions. For example, the mean of the four samples in **M** is used to center validation samples in the secondary condition. For TR2, this amounts to removing the third term in Eq. (2) and L-curves (or the new intersection process) would be evaluated with $\lambda = 0$ at the far left in Fig. 3 images (or at any $\lambda \leq 0.002$ as previously described in Section 3.2). By local centering, secondary condition effects can be removed and in some cases, negate the need for calibration maintenance. Tabulated in Table 1 are model merit values for local centering showing it is not able to reduce prediction errors to the level of TR2 with **M** weighted by λ.

There are two main differences between predicting secondary validation samples using RR with global centering (no updating) and RR with local centering. One is that with global centering, validation samples are centered to the mean of **X** before prediction by RR whereas with local centering, validation samples are centered to the mean of **M** before prediction by RR. Results in Table 1 demonstrate the advantage of local centering. The other primary difference is that with local centering, model merit L-curves for **M** can be computed and used to assist in selecting the one RR meta-parameter η ($\lambda = 0$). Forming a RR model with the assistance of **M** clearly assists in identifying the correct RR model. Secondary samples in **M** could be centered to the mean of **X** and predicted to form an RMSEM and other model merits to select the respective RR model. A RR model selected this way would probably be intermediate to the RR model selected without **M** and the RR model selected with local centering of **M**. Such RR selected model would probably perform better than the typical global RR model. However, since local centering is well documented to provide better predictions, centering **M** to the mean of **X** to assist in selecting a RR model was not studied.

In addition to the special case of TR with local centering, $\lambda = 1$ represents another special case of TR2. For the images in Fig. 3, this situation corresponds to RR without any weighting, i.e., local centering **M** and augmenting the primary calibration samples with **M**. From the images in Fig. 3 and results listed in Table 1, it is clear that weighting significantly improves predictions errors and other model merit values. Another approach to augmenting the primary samples is to first augment and then mean center across both sets of samples, i.e., subtracting the mean of the combined spectra in **X** and **M**. This amounts to a form of global mean centering and was not studied.

Lastly, listed in Table 2 are model merits for RR models formed with primary calibration samples to predict primary validation samples and RR models formed with secondary calibration samples to predict secondary validation samples. The RR full calibration models predict similarly. Comparing model merits of the RR full batch model predicting full batch validation samples in Table 2 to TR2 updated models in Table 1 shows that TR2 can form models with similar model merits. The similar results are obtained with substantially fewer calibration samples than the full calibration in the full batch secondary condition.

Tables 1 and 2 also list the relative prediction errors computed as 100 times the RMSEV divided by the mean API content for the validation set [13]. The reference HPLC relative error is estimated to be 3.5%. The full batch RR model formed with 30 calibration tablets shows a similar prediction result to the HPLC relative error. Two of the TR2 approaches are equivalent to the HPLC error. This observation indicates the need for appropriate meta-parameter selection. However, all three TR2 methods substantially improve over local centering and no updating.

3.4. Other primary and secondary conditions

Other primary and secondary tablet situations were evaluated but not reported as trends were not uniquely different than that already reported. For example, using the same primary tablets, but changing the secondary tablets to 1 and 3, has similar model merit trends as that observed for updating to tablet types 1 and 2. In this case, secondary tablet type 3 is not part of the primary calibration space. Specifically, the RMSEM and the model vector 2-norm images are essentially the same as in Fig. 3. The trends for the RMSEC and RMSEV are similar but not as closely matched to those in Fig. 3. These image trends are true for other model-updating situations studied. The small variations in the RMSEC and RMSEV images probably stem from varying the secondary conditions for a

fixed primary condition and TR2 forming models to reduce prediction errors for **M**. Thus, final models will not predict the primary **X** the same. In some situations, the process of fixing η and varying λ is not as obvious to determine. Instead, selecting one λ from a range and varying η is used to form L-curves.

Unlike for secondary tablets 1 and 2, the RMSEM image (not shown) for secondary tablets 1 and 3 indicates a local RR model can be formed with low prediction errors for **M**. The RMSEV image confirms that local centering and predicting with the RR model formed for the primary conditions does provide low prediction errors. For other tablet situations, the local centering would sometimes prove useful and for others it would not. The RMSEM image always indicated when to use local centering. Generally, the new meta-parameter selection approach of intersecting L-curves could be used. When no intersection occurred, the traditional L-curve corners and *H* values would only be used. As with the previous situation depicted in Fig. 3, an average prediction within a box could be used for a final prediction in other situations. A box would be bordered by large RMSEC values above it, the larger RMSEM values to the left, and the larger 2-norm values below it.

4. Conclusion

A new observation of L-curve meta-parameter selection has been noted and found useful for this data set. For most of the tablet cases studied, the new approach worked adequately. Thus, it should prove useful in other calibration maintenance situations. Combining normalized RMSEM values with model vector 2-norms to form H model merit values was evaluated and found to assist in meta-parameter selection. It was found to agree well with other meta-parameter selection approaches in that a model was selected from the pool of models deemed acceptable. Another approach noted in this paper, but not studied, is to use images to locate an acceptable trade-off region and average the prediction in the localized region such as the green box in Fig. 3b. Images of model merits were found to provide easier interpretation on how TR2 works as meta-parameters vary and facilitate sensible selection of those meta-parameters. It should be noted that a cross-validation (CV) approach was not studied as with the 8000 meta-parameter combinations used, CV would be time intensive. Once a range of workable meta-parameters is determined, a CV approach could be used.

Other modeling updating situations were studied, but are not reported in this paper. Result trends are similar to those reported in Tables 1 and 2 and TR2 often performed better than local centering. The TR2 approach offers a relatively easy method of calibration updating control as a prediction model can be formed with laboratory produced tablets and then used in full production by updating with just a few full production tablets.

A TR variant not studied in this paper is TR2-1 [30]. In this case, wavelengths are selected simultaneously as the model is updated, i.e., the updated model formed will have model vector coefficients equal to zero and non-zero coefficients for selected wavelengths. The TR2-1 approach is similar to Eq. (2) except a vector 1-norm is used for the model vector and η is raised to the first power instead of squaring. In past calibration maintenance studies, TR2-1 either improved on TR2 results or performed similarly. The same would be expected here. As with TR2, two special cases are contained within TR2-1. When $\lambda = 0$, there is no updating and wavelength selected models are obtained with local centering used for prediction.

To date, this tablet data set has been the most difficult to work with as several factors are involved in causing the need to update the primary model. Specifically, PCA shows that there is a batch effect and several tablet effects. As previously noted, there is also a tablet press punch difference [13]. In the present work, only one meta-parameter weight is used to update all the secondary conditions represented in **M**. Future work would involve using meta-parameters to weight separate tablet effects and another to weight the batch effect. This is difficult to accomplish as additional meta-parameters would have to be determined.

Acknowledgements

This material is based upon work supported by the National Science Foundation under Grant No. CHE-0715149 (co-funded by the MPS Chemistry and DMS Statistical Divisions, and by the NSPA Program) and is gratefully acknowledged by the authors.

References

[1] T. Næs, T. Isaksson, T. Fern, T. Davies, A User Friendly Guide to Multivariate Calibration and Classification, NIR Publications, Chichester, 2002.
[2] J.H. Kalivas, Calibration methodologies, in: S.D. Brown, R. Tauler, B. Walczak (Eds.), Comprehensive Chemometrics: Chemical and Biochemical Data Analysis, Elsevier, Amsterdam, The Netherlands, 2009, pp. 1–32.
[3] Y. Hu, A. Erxleben, A.G. Ryder, P. McArdle, Quantitative analysis of sulfathiazole polymorphs in ternary mixtures by attenuated total reflectance infrared, near-infrared and Raman spectroscopy, J. Pharm. Biomed. Anal. 53 (2010) 412–420.
[4] E.W. Ciurczak, J. Dremen, Pharmaceutical and Medical Applications of Near-Infrared Spectroscopy, CRC Press, Boca Raton, FL, 2010.
[5] J.C. Menezes, A.P. Ferreira, L.O. Rodrigues, L.P. Brás, Chemometrics role within the PAT context: examples from primary pharmaceutical manufacturing, in: S.D. Brown, R. Tauler, B. Walczak (Eds.), Comprehensive Chemometrics: Chemical and Biochemical Data Analysis, Elsevier, Amsterdam, The Netherlands, 2009.
[6] O.Ye. Rodionova, Ya.V. Sokovikov, A.L. Pomerantsev, Quality control of packed raw materials in pharmaceutical industry, Anal. Chim. Acta 642 (2009) 222–227.
[7] M. Blanco, M. Bautista, M. Alcalá, Preparing calibration sets for use in pharmaceutical analysis by NIR spectroscopy, J. Pharm. Sci. 97 (2008) 1236–1245.
[8] Y. Zheng, X. Lai, S.W. Bruun, H. Ipsen, J.N. Larsen, H. Løwenstein, I. Søndergaard, S. Jacobsen, Determination of moisture content of lyophilized allergen vaccines by NIR spectroscopy, J. Pharm. Biomed. Anal. 46 (2008) 592–596.
[9] Y. Roggo, P. Chalus, L. Maurer, C. Lema-Martinez, A. Edmond, N. Jent, A review of near infrared spectroscopy and chemometrics in pharmaceutical technologies, J. Pharm. Biomed. Anal. 44 (2007) 683–700.
[10] R.P. Cogdill, J.K. Drennen III, Near infrared spectroscopy in the pharmaceutical industry, NIR News 23–26 (2005) 23–26.
[11] K.A. Bakeev, Process Analytical Technology: Spectroscopic Tools and Implementation Strategies for the Chemical and Pharmaceutical Industries, Blackwell Publishing, Oxford, 2005.
[12] M.P. Freitas, A. Sabadin, L.M. Silva, F.M. Giannotti, D.A. do Couto, E. Tonhi, R.S. Medeiros, G.L. Coco, V.F.T. Russoand, J.A. Martins, Prediction of drug dissolution profiles from tablets using NIR diffuse reflectance spectroscopy: a rapid and nondestructive method, J. Pharm. Biomed. Anal. 39 (2005) 17–21.
[13] M. Dyrby, S.B. Engelsen, L. Nørgaard, M. Bruhn, L. Lundsberg-Nielsen, Chemometric quantitation of the active substance3 (containing C≡N) pharmaceutical tablet using near-infrared (NIR) transmittance and NIR FT-IR Raman spectra, Appl. Spectrosc. 56 (2002) 579–585.
[14] D. Xiang, M. Konigsberger, B. Wabuyela, K. Hornung, J. Cheney, Development of robust quantitative methods of near-infrared spectroscopy for rapid pharmaceutical determination of content uniformity in complex tablet matrix, Analyst 134 (2009) 1405–1415.
[15] B. Igne, S. Talwar, J.K. Drennen III, C.A. Anderson, Improvement of pharmaceutical near infrared calibrations by empirical target distribution optimization, J. Near Infrared Spectrosc. 19 (2011) 1–14.
[16] R.P. Cogdill, C.A. Anderson, J.K. Drennen III, Process analytical technology case study, Part III: calibration monitoring and transfer, AAPS PharmSciTech 6 (2005) E284–E297.
[17] S.D. Brown, Transfer of multivariate calibration models, in: S.D. Brown, R. Tauler, B. Walczak (Eds.), Comprehensive Chemometrics: Chemical and Biochemical Data Analysis, Elsevier, Amsterdam, The Netherlands, 2009, pp. 345–377.
[18] K. Maruo, T. Oota, M. Tsurugi, T. Nakagawa, H. Arimoto, M. Hayakawa, M. Tamura, Y. Ozaki, Y. Yamada, Noninvasive near-infrared blood glucose monitoring using a calibration model built by a numerical simulation method: trial application to patients in an intensive care unit, Appl. Spectrosc. 60 (2006) 1423–1431.
[19] Y. Wang, D.J. Veltkamp, B.R. Kowalski, Multivariate instrument standardization, Anal. Chem. 63 (1991) 2750–2756.
[20] K.E. Kramer, G.W. Small, Blank augmentation protocol for improving the robustness of multivariate calibrations, Appl. Spectrosc. 61 (2007) 497–506.
[21] Y. Sulub, G.W. Small, Spectral simulation methodology for calibration transfer of near-infrared spectra, Appl. Spectrosc. 61 (2007) 406–413.
[22] A. Condolfi, D.L. Massart, Model-updating for the identification of NIR spectra from a pharmaceutical excipient, Appl. Spectrosc. 54 (2000) 48–53.

[23] C.M. Wehlburg, D.M. Haaland, D.K. Melgaard, L.E. Martin, New hybrid algorithm for maintaining multivariate quantitative calibrations of a near-infrared spectrometer, Appl. Spectrosc. 56 (2002) 605–614.
[24] S. Wold, Exponentially weighted moving principal components analysis and projections to latent structures, Chemom. Intell. Lab. Syst. 23 (1984) 149–161.
[25] C.L. Stork, B.R. Kowalski, Weighting schemes for updating regression models – a theoretical approach, Chemom. Intell. Lab. Syst. 48 (1999) 151–166.
[26] X. Capron, B. Walczak, O.E. de Noord, D.L. Massart, Selection and weighting of samples in multivariate regression model-updating, Chemom. Intell. Lab. Syst. 76 (2005) 205–214.
[27] K. Helland, H.A. Berntsen, O.S. Borgen, H. Martens, Recursive algorithm for partial least squares, Chemom. Intell. Lab. Syst. 14 (1991) 129–137.
[28] B.S. Dayal, J.F. MacGregor, Recursive exponentially weighted PLS and its applications to adaptive control and prediction, J. Process Control 7 (1997) 169–179.
[29] J.H. Kalivas, G.S. Siano, E. Andries, H.C. Goicoechea, Calibration maintenance and transfer using Tikhonov regularization approaches, Appl. Spectrosc. 63 (2009) 800–809.
[30] M.R. Kunz, J.H. Kalivas, E. Andries, Model-updating for spectral calibration maintenance and transfer using 1-norm variants of Tikhonov regularization, Anal. Chem. 89 (2010) 3642–3649.
[31] M.R. Kunz, J. Ottaway, J.H. Kalivas, C.A. Georgiou, G.A. Mousdis, Updating a synchronous fluorescence spectroscopic virgin olive oil adulteration calibration to a new geographical region, J. Agric. Food Chem. 59 (2011) 1051–1057.
[32] H. Leion, S. Folestad, M. Josefson, A. Sparén, Evaluation of basic algorithms for transferring quantitative multivariate calibrations between scanning grating and FT-IR spectrometers, J. Pharm. Biomed. Anal. 37 (2005) 47–55.
[33] E.L. Bergman, H. Brage, M. Josefson, O. Svensson, A. Sparén, Transfer of NIR calibrations for pharmaceutical formulations between different instruments, J. Pharm. Biomed. Anal. 41 (2006) 89–98.
[34] M. Boiret, L. Meunier, Y.M. Ginot, Tablet potency of tianeptine in coated tablets by near infrared spectroscopy: model optimization, calibration transfer and confidence intervals, J. Pharm. Biomed. Anal. 54 (2011) 510–516.
[35] R.C. Aster, B. Borchers, C.H. Thurber, Parameter Estimation and Inverse Problems, Elsevier, Amsterdam, The Netherlands, 2005.
[36] http://www.models.life.ku.dk/Tablet (accessed 15.04.11).
[37] R. Kiralj, M.C. Ferreira, Is your QSAR/QSPR descriptor real or trash? J. Chemom. 24 (2010) 681–693.
[38] R.L. Green, J.H. Kalivas, Graphical diagnostics for regression model determination with consideration of the bias/variance trade-off, Chemom. Intell. Lab. Syst. 60 (2002) 173–188.
[39] H.V. Henderson, P.F. Velleman, Building multiple regression models interactively, Biometrics 37 (1981) 391–411.
[40] R.D. Cook, S. Weisberg, Regression diagnostics with dynamic graphics, Technometrics 31 (1989) 277–291.
[41] R.D. Cook, Graphics: Ideas for Studying Regression Through Graphics, Wiley, New York, 1998.
[42] C.E. Anderson, J.H. Kalivas, Fundamentals of calibration transfer through procrustes analysis, Appl. Spectrosc. 53 (1999) 1268–1276.
[43] H. Swierenga, W.G. Haanstra, A.P. de Weijer, L.M.C. Buydens, Comparison of two different approaches toward model transferability in NIR spectroscopy, Appl. Spectrosc. 52 (1998) 7–16.

Journal of Pharmaceutical and Biomedical Analysis 61 (2012) 122–135

Contents lists available at SciVerse ScienceDirect

Journal of Pharmaceutical and Biomedical Analysis

journal homepage: www.elsevier.com/locate/jpba

Synthesis, full chemical characterisation and development of validated methods for the quantification of the components found in the evolved "*legal high*" NRG-2

Osama I.G. Khreit[a], Craig Irving[b], Elke Schmidt[c], John A. Parkinson[b], Niamh Nic Daeid[d], Oliver B. Sutcliffe[a,*]

[a] *Strathclyde Institute of Pharmacy and Biomedical Sciences (SIPBS), University of Strathclyde, 161 Cathedral Street, Glasgow G4 0RE, UK*
[b] *WestCHEM Department of Pure and Applied Chemistry, University of Strathclyde, 295 Cathedral Street, Glasgow G1 1XL, UK*
[c] *Cancer Research UK Formulation Unit, Strathclyde Institute of Pharmacy and Biomedical Sciences (SIPBS), University of Strathclyde, 161 Cathedral Street, Glasgow G4 0RE, UK*
[d] *Centre for Forensic Science, WestCHEM Department of Pure and Applied Chemistry, University of Strathclyde, 204 George Street, Glasgow G1 1XW, UK*

ARTICLE INFO

Article history:
Received 30 September 2011
Received in revised form 1 November 2011
Accepted 5 November 2011
Available online 11 November 2011

Keywords:
NRG-2
4-MEC
4-MBC
Cathinones
HPLC

ABSTRACT

The recent global increase in the abuse of 4′-methylmethcathinone (mephedrone) and related compounds has developed a requirement for full chemical characterisation of these products. This work presents full synthetic and chemical characterisation data for the hydrobromide salts of two mephedrone derivatives: 4′-methyl-N-ethylcathinone (4-MEC) and 4′-methyl-N-benzylcathinone (4-MBC) which have been identified in samples of the "legal high" NRG-2. The first fully validated chromatographic methods for the detection and quantitative analysis of these substances both in their pure form and in the presence of a number of common adulterants used in illicit drug manufacture is also reported.

© 2011 Elsevier B.V. All rights reserved.

1. Introduction

In the last few years there has been a striking increase in the sale of "*legal highs*" [1]. These chemicals may be bought through the Internet at low cost and are sometimes pure compounds which display highly similar chemical structures to existing controlled substances within the phenethylamine class.

(±)-4′-Methylmethcathinone or (±)-mephedrone (**3a**, 4-MMC) [2–12] is a synthetic β-ketoamphetamine that is structurally similar to methcathinone (**4**, R=Me), related to cathinone (**4**, R=H), a psychoactive compound found in Khat. (±)-Mephedrone has recently emerged in drug seizures, as a "*legal high*" replacement for controlled stimulants, including amphetamines such as methamphetamine (**5**) and MDMA (**6**) (Scheme 1). (±)-Mephedrone is now a substance controlled by legislation in the United Kingdom, Germany, Norway, Sweden, the Netherlands, Finland, Romania, Republic of Ireland, Denmark, Canada and Israel. Since the legislative change, a number of evolved "*legal high*" products, such as NRG-1 (naphyrone, **7**) and NRG-2, which are advertised to contain legal mephedrone substitutes, have become available. However, many of these have been reported to contain structurally related cathinone derivatives that are themselves controlled substances [13–15].

The prevalence of these cathinone-derived "*legal high*" drugs has given rise to both legal and analytical challenges in the identification of these substances. Thus, robust analytical profiling and the development of validated methods of testing are required. Although two groups have previously reported the detection and selected analytical information (such as NMR [13,14], MS [13,14] and IR [14] data) of (±)-4′-methyl-*N*-ethylcathinone (**3b**, 4-MEC) in samples of NRG-2 [13] and bulk powders seized by law enforcement agencies [14], however, there has been no comprehensive analytical profiling of a pure reference sample or the development of a validated chromatographic method for this substance. This paper seeks to address this matter by presenting the complete chemical synthesis, key physicochemical parameters (Log *P*, pK_a) and full structural elucidation of (±)-4′-methyl-*N*-ethylcathinone (**3b**) by NMR, IR, UV and MS. The synthesis and characterisation of a novel structurally-related derivative (±)-4′-methyl-N-benzylcathinone (3c, 4-MBC), which has been identified in seized samples of NRG-2 is also reported. A fully validated chromatographic method for the detection and quantitative analysis of these two substances, both in their pure form and in the presence of common adulterants is presented and evaluated using sourced samples of NRG-2.

* Corresponding author. Tel.: +44 141 548 4968; fax: +44 141 552 2562.
E-mail address: oliver.sutcliffe@strath.ac.uk (O.B. Sutcliffe).

0731-7085/$ – see front matter © 2011 Elsevier B.V. All rights reserved.
doi:10.1016/j.jpba.2011.11.004

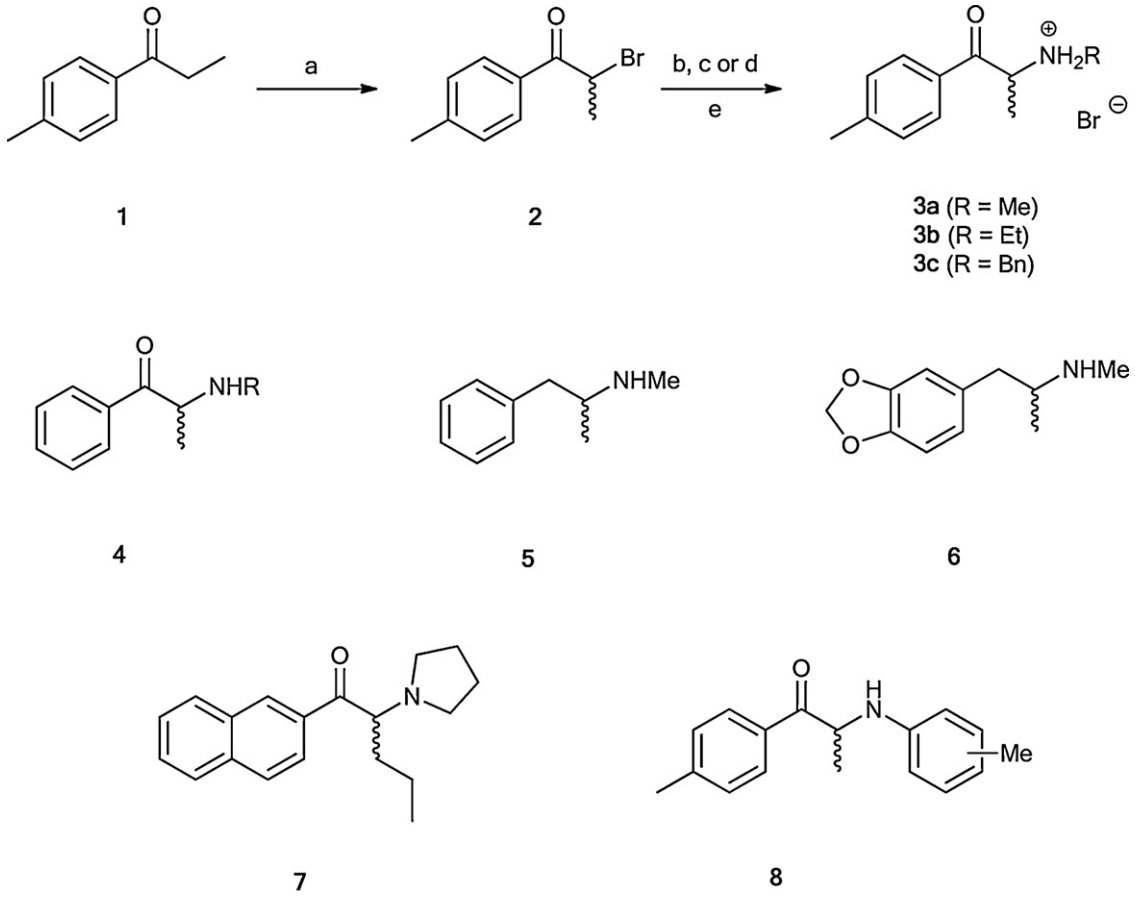

Scheme 1. *Reagents and conditions:* (a) Br_2/HBr (48% in water)/CH_2Cl_2/rt/1 h (99.6%); (b) $MeNH_2$·HCl/NEt_3/CH_2Cl_2/rt/24 h; (c) $EtNH_2$·HCl/NEt_3/CH_2Cl_2/rt/24 h; (d) $BnNH_2$/$CHCl_3$/Δ/24 h; (e) HBr (33% in AcOH)/AcOH/rt/1 h (67.4% (**3a**), 41.5% (**3b**) and 27.2% (**3c**) from **2**).

2. Experimental

All reagents were of commercial quality (obtained from Sigma–Aldrich, Gillingham, UK or Alfa-Aesar, Heysham, UK) and used without further purification. Solvents were dried, where necessary, using standard procedures. (±)-4′-Methyl-2-bromopropiophenone (**2**) and (±)-4′-methylmethcathinone hydrobromide (**3a**, 4-MMC) were prepared using the methods reported previously [12]. ^1H and ^{13}C NMR spectra were acquired on both JEOL AS-400 (JEOL, Tokyo, Japan) and Bruker Avance 400 (Bruker, Karlsruhe, Germany) NMR spectrometers operating at a proton resonance frequency of 400 MHz. Infrared spectra were obtained in the range 4000–400 cm^{-1} using a ThermoScientific Nicolet iS10ATR-FTIR instrument (ThermoScientific, Rochester, USA). Mass spectra were recorded on a ThermoScientific LTQ ORBITRAP mass spectrometer (ThermoScientific, Rochester, USA) using electrospray ionisation. Ultraviolet spectra were obtained using a Unicam 300 UV spectrophotometer (ThermoScientific, Rochester, USA). Thin-Layer Chromatography (TLC) was carried out on aluminium-backed SiO_2 plates (Merck, Darmstadt, Germany) and spots were visualised using ultra-violet light (254 nm). Microanalysis was carried out using a PerkinElmer 2400 Series II elemental analyser (PerkinElmer, San Jose, USA). Melting points were determined using differential scanning calorimetry (DSC; Netzsch STA449 C, Netzsch-Gerätebau, Wolverhampton, UK). Optical rotation values $[\alpha]_D^{22}$ (10^{-1} deg cm^2 g^{-1}) were performed on a Bellingham & Stanley ADP-220 polarimeter (Bellingham & Stanley, Tunbridge Wells, UK). Log *P* and pK_a values were determined on a Sirius T3 instrument (Sirius Analytical Instruments, Forest Row, UK). Calculated Log *P* and pK_a values were determined using Pipeline Pilot software, Vers. 7.5 (Accelrys, San Diego, USA).

2.1. Synthesis of (±)-4′-methyl-N-ethylcathinone hydrobromide (*3b*, 4-MEC)

The title compound was prepared using the method reported by Sutcliffe et al. [12] with the following modifications: To a suspension of (±)-4′-methyl-2-bromopropiophenone (**2**, 4.54 g, 20 mmol) and ethylamine hydrochloride (1.63 g, 20 mmol) in dichloromethane (40 mL) was added triethylamine (5.58 mL, 40 mmol). The mixture was stirred at room temperature overnight and then acidified (pH ~ 1) with 6 M hydrochloric acid (50 mL). The aqueous layer was washed with dichloromethane (3× 50 mL), basified (pH ~ 10) with 5 M sodium hydroxide (*circa* 100 mL) and then re-extracted with dichloromethane (3× 50 mL). The combined organic fractions were dried ($MgSO_4$) and concentrated *in vacuo* to give a viscous yellow oil. The oil was dissolved in glacial acetic acid (2 mL), treated with hydrobromic acid (33% solution in acetic acid, 5 mL) and stirred at room temperature for 1 h. The mixture was diluted with diethyl ether (100 mL) and stirred until a pale beige solid formed (*circa* 30 min). The crude product was filtered, washed with diethyl ether and recrystallised from acetone to afford (±)-*4′-methyl-N-ethylcathinone hydrobromide* (2.26 g, 41.5% from **2**) as a colourless powder. Mpt. (acetone) 206.08 °C; R_f [SiO_2, EtOAc:*n*-hexane (1:3)] = 0.10; $[\alpha]_D^{22}$ = 0 (*c* = 0.5 g/100 mL, MeOH); found: C, 52.90; H, 6.65; N, 4.95. $C_{12}H_{18}BrNO$ requires C, 52.95; H, 6.67 and N, 5.15%; UV (EtOH): λ_{max} = 260.0 nm (*A* = 0.693, *c* = 1.02 × 10^{-3} g/100 mL); IR (ATR-FTIR): 2735.4 (NH_2^+),

1687.3 (C=O), 1605.4 cm^{-1} (C=C); ^1H NMR (400 MHz, 60 °C, d_6-DMSO) δ^1H (ppm) = 8.92 (2H, br s, CH(**NH_2^+**CH_2CH_3)CH_3); 7.98 (2H, d, J = 8.4 Hz, AA′BB′), 7.41 (2H, d, J = 8.4 Hz, AA′BB′), 5.21 (1H, q, J = 6.8 Hz, **CH**($NH_2^+CH_2CH_3$)CH_3), 3.04 (2H, dq, J = 12.4, 7.2 Hz, CH(NH_2^+**CH_2**CH_3)CH_3), 2.42 (3H, s, Ar**CH_3**), 1.53 (3H, d, J = 7.2 Hz, CH(NH_2^+ CH_2CH_3)**CH_3**) and 1.28 ppm (3H, t, J = 7.2 Hz, CH(NH_2^+ CH_2**CH_3**)CH_3); ^{13}C NMR (100 MHz, 60 °C, d_6-DMSO) $\delta^{13}C$ (ppm) = 195.5 (C=O, C1), 145.2 (ArC, C4′), 130.2 (ArC, C1′), 129.4 (2 × ArC, C3′/C5′), 128.6 (2 × ArCH, C2′/C6′), 56.5 (**CH**CH_3, C2), 40.2 (NH_2^+**CH_2**CH_3, C4); 20.9 ($ArCH_3$, C7′), 15.7 (CH**CH_3**, C3) and 10.8 ppm ($NH_2^+CH_2$**CH_3**, C5); LRMS (ESI+, 70 eV): m/z = 192 (34%, $[M+H]^+$), 174 (100), 159 (30), 145 (57), 131 (16), 119 (25) and 91 (6); HRMS (ESI+, 70 eV) calculated for [M+H] $C_{12}H_{18}NO$: 192.1383, found: 192.1381.

2.2. Synthesis of (±)-4′-methyl-N-benzylcathinone hydrobromide (*3c*, 4-MBC)

The title compound was prepared using the method for (**3b**) with the following modifications: to a solution of (±)-4′-methyl-2-bromopropiophenone (**2**, 4.54 g, 20 mmol) in chloroform (40 mL) was added benzylamine (4.36 mL, 40 mmol). The mixture was heated at reflux overnight, cooled, filtered and then acidified (pH ∼ 1) with 6 M hydrochloric acid (50 mL). The aqueous layer was washed with chloroform (3× 50 mL), basified (pH ∼ 10) with 5 M sodium hydroxide (*circa* 100 mL) and then re-extracted with chloroform (3× 50 mL). The combined organic fractions were dried ($MgSO_4$) and concentrated *in vacuo* to give a viscous orange oil. The crude product was purified by gravity column chromatography [SiO_2, EtOAc:*n*-hexane (1:6)] to give a yellow oil. The oil was dissolved in glacial acetic acid (2 mL), treated with hydrobromic acid (33% solution in acetic acid, 5 mL) and stirred at room temperature for 1 h. The mixture was diluted with diethyl ether (100 mL) and stirred until a pale beige solid formed (*circa* 30 min). The crude product was filtered, washed with diethyl ether and recrystallised from acetone to afford (±)-*4′-methyl-N-benzylcathinone hydrobromide* (1.82 g, 27.2% from **2**) as an off-white powder. Mpt. (acetone) 219.48 °C; R_f [SiO_2, EtOAc:*n*-hexane (1:3)] = 0.11; $[\alpha]_D^{22}$ = 0 (c = 0.5 g/100 mL, MeOH); found: C, 61.06; H, 6.03; N, 3.99. $C_{17}H_{20}BrNO$ requires C, 61.09; H, 6.03 and N, 4.19%; UV (EtOH): λ_{max} = 260.0 nm (A = 0.498, $c = 1.04 \times 10^{-3}$ g/100 mL); IR (ATR-FTIR): 2770.6 (NH_2^+), 1683.9 (C=O), 1604.5 cm^{-1} (C=C); ^1H NMR (400 MHz, 60 °C, d_6-DMSO) δ^1H (ppm) = 9.40 (2H, br s, CH(**NH_2^+**CH_2Ph)CH_3); 7.93 (2H, d, J = 8.2 Hz, AA′BB′), 7.55–7.57 (2H, m, Ar–H), 7.45–7.41 (5H, m, Ar–H and AA′BB′ overlapping signals), 5.27 (1H, q, J = 7.2 Hz, **CH**($NH_2^+CH_2$Ph)CH_3), 4.21 (2H, dd, J = 7.2, 12.8 Hz, CH(NH_2^+**CH_2**Ph)CH_3), 2.42 (3H, s, Ar**CH_3**) and 1.53 ppm (3H, d, J = 7.2 Hz, CH($NH_2^+CH_2$Ph)**CH_3**); ^{13}C NMR (100 MHz, 60 °C, d_6-DMSO) $\delta^{13}C$ (ppm) = 195.1 (C=O, C1), 145.2 (ArC, C4′), 131.5 (ArC, C5), 130.2 (ArC, C1′), 129.8 (2 × ArCH, C7/C9), 129.4 (2 × ArCH, C3′/C5′), 128.8 (ArCH, C8), 128.6 (2 × ArCH, C2′/C6′), 128.3 (2 × ArCH, C6/C10), 57.0 (**CH**CH_3, C2), 48.7 (NH_2^+**CH_2**Ph, C4), 20.9 ($ArCH_3$, C7′) and 15.7 ppm (CH**CH_3**, C3); LRMS (ESI+, 70 eV): m/z = 254 (34%, $[M+H]^+$), 236 (10), 146 (7), 119 (3) and 91 (100); HRMS (ESI+, 70 eV) calculated for [M+H] $C_{17}H_{20}NO$: 254.1539, found: 254.1537.

2.3. High performance liquid chromatography (HPLC)

Reverse phase high-performance liquid chromatography was performed with an integrated Agilent HP Series 1100 Liquid Chromatograph (Agilent Technologies, Wokingham, UK) fitted with an in-line degasser, 100-place autoinjector and single channel, tunable UV absorbance detector (264 nm). Data analysis was carried out using ChemStation for LC (Ver. 10.02) software (Agilent Technologies, Wokingham, UK). The flow rate was 0.8 mL min^{-1} with an injection volume of 10 μL. Six replicate injections of each calibration standard were performed. The stationary phase (ACE 3 C_{18}, 150 mm × 4.6 mm i.d., particle size: 3 μm) used in the study was obtained from HiChrom Limited (Reading, UK). The column was fitted with a guard cartridge (ACE 3 C_{18}) and maintained at an isothermal temperature of 22 °C with an Agilent HP Series 1100 column oven with a programmable controller (Agilent Technologies, Wokingham, UK).

Preparation of aqueous ammonium formate buffer (10 mM, pH 3.5 ± 0.02): 1.30 g ammonium formate was dissolved in 1.8 L ultra-pure deionised water and the pH of the solution adjusted by dropwise addition of formic acid (98–100%) to pH 3.5 (±0.02). The mixture was transferred to a 2 L clear glass volumetric flask and diluted to volume with ultra-pure deionised water. The mobile phases were prepared by separately mixing volumes of the formate buffer and organic modifier in the appropriate proportions denoted in Section 3. Prior to use, all mobile phases were vacuum filtered through a 0.45 mm pore filter paper and degassed for 10 min at 25 °C using an ultrasonic bath.

Calibration standards (pure substances): 2.0 mg 4-MMC (**3a**), 4-MEC (**3b**), 4-MBC (**3c**) were weighed accurately into separate 100.0 mL clear glass volumetric flasks and diluted to volume with mobile phase to give solutions containing the components at 20.0 μg mL^{-1}. These solutions were then further diluted with mobile phase to give calibration standards containing 10.0 μg mL^{-1}, 5.0 μg mL^{-1}, 2.5 μg mL^{-1}, 1 μg mL^{-1} and 0.5 μg mL^{-1} of each analyte.

Calibration standards (adulterants study): 2.0 mg of each component (caffeine, 4-MMC (**3a**), 4-MEC (**3b**), benzocaine, 4-MBC (**3c**), sucrose, glucose, mannitol and lactose) were weighed accurately into 100.0 mL clear glass volumetric flask and diluted to volume with mobile phase to give solutions containing all components at 20.0 μg mL^{-1}. This solution was then further diluted with mobile phase to give calibration standards containing 10.0 μg mL^{-1}, 5.0 μg mL^{-1}, 2.5 μg mL^{-1}, 1 μg mL^{-1} and 0.5 μg mL^{-1} of each analyte.

Test solutions: three samples of NRG-2 were obtained from three independent Internet vendors as white crystalline powders in clear zip-lock bags. 10.0 mg of each substance was weighed (in triplicate) accurately into a 100.0 mL clear glass volumetric flask and diluted to volume with mobile phase. This solution was then further diluted (1:10) with mobile phase to give the test solution.

2.4. Liquid chromatography–mass spectrometry (LC–MS)

Liquid chromatography–mass spectrometry data were acquired using a Finnigan LTQ Orbitrap instrument (Thermo-Fisher Corporation, Hemel Hempstead, UK). Sample analysis was carried out in positive ion (ESI) detection mode. The mass scanning range was 50–1250 m/z, while the capillary temperature was 250 °C and the sheath and auxiliary gas flow rates were 30 and 10, respectively (units not specified by the manufacturer). The LC–MS system (controlled by Xcalibur Ver. 2.0, Thermo-Fisher Corporation, Hemel Hempstead, UK) was run in binary gradient mode. Solvent A was aqueous ammonium formate buffer (10 mM, pH 3.5 ± 0.02) and solvent B was methanol; the flow rate was 0.3 mL min^{-1}. An ACE 3 C_{18} (150 mm × 4.6 mm i.d., particle size: 3 μm) column (HiChrom Limited, Reading, UK) was used for all analyses. The gradient programme was as follows: 10% B (0 min) to 60% B at 7 min to 60% B at 20 min to 10% B at 25 min.

Test solutions: three samples of NRG-2 were obtained from three independent Internet vendors as white crystalline powders in clear zip-lock bags. 5.0 mg of each substance was weighed (in triplicate) accurately into a 100.0 mL clear glass volumetric flask

and diluted to volume with deionised water. This solution was then further diluted (1:10) with deionised water to give the test solution.

2.5. Supplementary information

The supplementary information relating to this work contains the LRMS, 2D [^{1}H, ^{13}C] HMBC, HMQC and [^{1}H, ^{1}H] COSY NMR data for the synthesised compounds (**3b**) and (**3c**).

3. Results and discussion

Reference samples of the two mephedrone derivatives (±)-4′-methyl-*N*-ethylcathinone (**3b**, 4-MEC) and (±)-4′-methyl-*N*-benzylcathinone (**3c**, 4-MBC) were prepared as their corresponding hydrobromide salts. The synthesis of both racemic target compounds was achieved using a modification of the previously reported method from (±)-4′-methyl-2-bromopropiophenone (**2**) in 41.5% and 27.2% yield respectively (Scheme 1) [12]. Both compounds were obtained as stable, colourless to off-white powders after recrystallisation from acetone and exhibited an optical rotation $[\alpha]_D^{22}$ of 0 (c = 0.5 g/100 mL, MeOH). The purity of the derivatives was confirmed by elemental analysis. Analysis of (**3b**) revealed 52.90% (C), 6.65% (H) and 4.95% (N) which corresponded very closely to the theoretical percentage for the hydrobromide salt (52.95% (C), 6.67% (H) and 5.15% (N)). Similarly (**3c**) gave 61.06% (C), 6.03% (H) and 3.99% (N) which was in agreement with its expected theoretical compositions (61.09% (C), 6.03% (H) and 4.19% (N)). The melting points for (**3b** and **3c**) were determined by differential scanning calorimetry (DSC) and gave sharp melting points at 206.08 and 219.48 °C respectively. Additionally, the pK_a and Log P values (**3b**, pK_a = 8.88; Log P = 2.38; **3c**, pK_a = 7.44; Log P = 4.64) were determined for each derivative using a Sirius T3 instrument and are in good agreement with the calculated values (**3b**, pK_a = 8.41; Log P = 2.36; **3c**, pK_a = 5.95; Log P = 3.59) determined by Pipeline Pilot software (Accelrys, Vers. 7.5).

The ^{1}H NMR spectrum of (±)-4′-methyl-*N*-ethylcathinone (**3b**) (obtained at 60 °C in d_6-DMSO,[1] Fig. 1a) showed the characteristic AA′BB′ aromatic system for an unsymmetrically *para*-disubstituted aromatic system (δ^1H = 7.98 ppm, AA′BB′, 2H, d, J = 8.4 Hz; δ^1H = 7.41 ppm, AA′BB′, 2H, d, J = 8.4 Hz), a deshielded one-hydrogen quartet at δ^1H = 5.21 ppm (**CH**($NH_2^+CH_2CH_3$)CH_3, J = 6.8 Hz), a deshielded two-hydrogen doublet of quartets at δ^1H = 3.04 ppm (CH(NH_2^+**CH_2**CH_3)CH_3, J = 12.4, 7.2 Hz), characteristic of an A_3X_2 system with additional geminal coupling of the prochiral hydrogens proximal to the chiral centre, a slightly deshielded methyl singlet attributable to the methyl group attached to the aromatic ring (Ar**CH_3**, δ^1H = 2.42 ppm), a methyl doublet (CH($NH_2^+CH_2CH_3$)**CH_3**, δ^1H = 1.53 ppm, J = 7.2 Hz) and finally a three-hydrogen A_2X_3 triplet (CH($NH_2^+CH_2$**CH_3**)CH_3, J = 7.2 Hz) at δ^1H = 1.28 ppm. Unlike the previously reported spectra (which were run in D_2O [13,14]) a broad signal at δ^1H = 8.92 ppm was consistently observed and corresponded to the ammonium salt protons. It was noted that in D_2O (**3b**) gave rise to an NMR spectrum consistent with that obtained by Brandt et al. [13] and Janovics et al. [14] where the signal for the ammonium salt protons is absent due to rapid exchange with the solvent confirming that the synthesised (±)-4′-methyl-*N*-ethylcathinone sample is identical to the material obtained by the other researchers.

The ^{13}C NMR spectrum (obtained at 60 °C in d_6-DMSO, Fig. 1b) supports the assertion that the sample of (**3b**) is predominantly pure with 10 distinct carbon signals. Full spectral analysis using both 2D [^{1}H, ^{13}C] HMQC and HMBC methods (see supplementary information) allowed unambiguous assignment of all carbon and hydrogen resonances. For (**3b**) the *N*-CH_2**CH_3** resonance (δ^1H = 1.28 ppm, C5) gave a ^2J correlation to C4 (δ^1H = 3.04 ppm) which in turn gave a ^3J correlation to C2. This characteristic pattern for the *N*-ethyl group was further confirmed through 2D [^{1}H, ^{1}H] COSY NMR data (see supplementary information). The resonance for C2 is in turn coupled to the methyl doublet (C3) and in the 2D [^{1}H, ^{13}C] HMBC NMR spectrum the protons of the methyl resonance (δ^1H = 1.53 ppm) are coupled to a deshielded carbon (δ^{13}C = 195.5 ppm, C1) completing the assignment of the 2-aminoethyl-propan-1-one side chain. Further couplings in the 2D [^{1}H, ^{13}C] HMBC NMR spectrum between H2′/H6′ and C1 (^3J) supports placement of the propan-1-one side chain at C1′ on the aromatic nucleus (between C6′ and C2′) and correlations between H2′/H6′ and H3′/H5′ confirmed the AA′BB′ aromatic system. The methyl singlet at δ^1H = 2.42 ppm (C7′) exhibits a ^3J [^{1}H, ^{13}C] HMBC correlation to C3′/C5′ and a ^2J correlation to C4′ concluding the assignment of all resonances (Table 1).

In the case of (±)-4′-methyl-*N*-benzylcathinone (**3c**) the ^{1}H NMR spectrum (obtained at 60 °C in d_6-DMSO, Fig. 2a) showed the characteristic centrosymmetric AA′BB′ spin system for an unsymmetrically *para*-disubstituted aromatic ring (δ^1H = 7.93 ppm, AA′BB′, 2H, d, J = 8.4 Hz), where the partner AA′BB′ resonance (*circa* δ^1H = 7.41 ppm) appeared co-incident with the resonances associated with protons on the *N*-benzyl group (δ^1H = 7.41–7.45 ppm, 5H, multiplet). Additionally, aromatic signals appeared at δ^1H = 7.55–7.57 ppm (2H, m), a deshielded one-hydrogen quartet was present at δ^1H = 5.27 ppm (**CH**($NH_2^+CH_2$Ph)CH_3, J = 7.2 Hz), together with a deshielded two-hydrogen doublet of doublets at δ^1H = 4.21 ppm (CH(NH_2^+**CH_2**Ph)CH_3, J = 12.8, 7.2 Hz) (characteristic of the non-equivalent hydrogens with additional geminal coupling, on the benzylmethylene carbon proximal to the chiral centre), a slightly deshielded methyl singlet attributable to the methyl group attached to the aromatic ring (Ar**CH_3**, δ^1H = 2.42 ppm), a methyl doublet (CH($NH_2^+$$CH_2$Ph)**$CH_3$**, δ^1H = 1.53 ppm, J = 7.2 Hz) and finally a broad signal at δ^1H = 9.40 ppm for the exchangeable ammonium salt protons, which is consistent with other reported cathinone derivatives [12] (Table 2).

The ^{13}C NMR spectrum (obtained at 60 °C in d_6-DMSO, Fig. 2b) also supports that the synthesised reference sample of (**3c**) is predominantly pure with 13 distinct carbon signals. Full spectral analysis using both 2D [^{1}H, ^{13}C] HMQC and HMBC methods (see supplementary information) allowed assignment of the carbon and hydrogen resonance. For (**3c**) the *N*-**CH_2**Ph resonance (δ^1H = 4.21 ppm, C4) gave a ^3J correlation to C2 (δ^1H = 5.27 ppm) which in turn gave a ^2J correlation to C1 and C3. The resonances for the benzyl moiety should exhibit the characteristic doublet of doublets (2H, C6/C10), doublet of doublets (2H, C7/C9) and triplet (1H, C8) multiplicities. However, these resonances appear as two complex multiplets: δ^1H = 7.44 (C7/C9 and C8 with ^2J correlation to C6/C10) and 7.56 ppm (C6/C10 with ^2J correlation to C7/C9) respectively. The complex splitting of the aromatic resonances observed in the aromatic region of the ^{1}H NMR spectrum is not uncommon in benzyl-substituted compounds and is ascribed to second-order splitting effects [16]. The resonance for C2 is in turn coupled to the methyl doublet (C3) and in the [^{1}H, ^{13}C] HMBC NMR spectrum the protons of the methyl resonance (δ^1H = 1.53 ppm) are coupled to a deshielded carbon (δ^{13}C = 195.1 ppm, C1) concluding the assignment of the 2-aminobenzyl-propan-1-one side chain. Further couplings in the [^{1}H, ^{13}C] HMBC NMR spectrum between

[1] All ^{1}H NMR spectra were recorded at 60 °C to ensure that the signal for the protons situated on the chiral centre (C2, *circa* 5.2–5.3 ppm) which broadens and coalesces at ambient temperature was fully resolved. The chemical shifts of all signals were observed to be consistent at both ambient (25 °C) and high (60 °C) temperatures. For consistency the ^{13}C NMR spectra were obtained under analogous conditions. Samples were filtered prior to analysis.

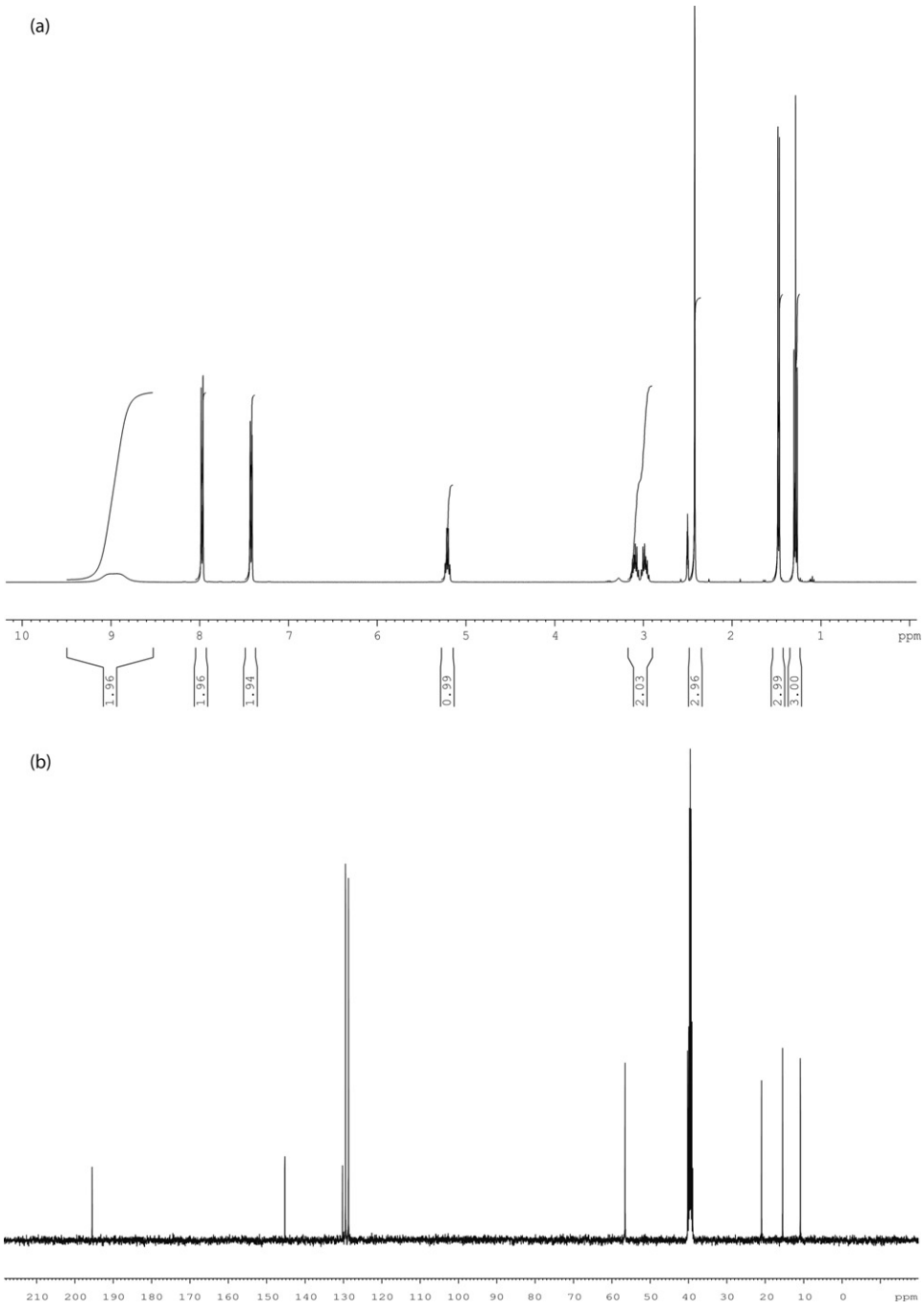

Fig. 1. (a) ^{1}H NMR spectrum (400 MHz, d_6-DMSO, 60 °C) and (b) ^{13}C NMR spectrum (100 MHz, d_6-DMSO, 60 °C) of (±)-4′-methyl-*N*-ethylcathinone.HBr (**3b**).

H2′/H6′ and C1 (^{3}J) once again supports placement of the propan-1-one side chain at C1′ on the second aromatic nucleus (between C6′ and C2′) and correlations between H2′/H6′ and H3′/H5′ confirmed the AA′BB′ aromatic system. The methyl singlet at δ^{1}H = 2.42 ppm (C7′) exhibits a ^{3}J [^{1}H, ^{13}C] HMBC correlation to C3′/C5′ and a ^{2}J correlation to C4′ completing the assignment of all resonances for (**3c**) and is consistent with the data observed for structurally related cathinones [12].

The HRESIMS analysis of (±)-4′-methyl-*N*-ethylcathinone hydrobromide (**3b**) gave an [M+H]$^{+}$ peak at m/z = 192.1381 (calculated for $C_{12}H_{18}NO$ = 192.1383) supporting the molecular formula of $C_{12}H_{17}NO$ and the identity of the sample as (±)-MEC. The mass spectrum (which is in agreement with the data reported by both Brandt et al. [13] and Janovics et al. [14]) of (**3b**) is shown in Fig. 3a and exhibits an [M+H]$^{+}$ parent ion (m/z = 192.1381) of moderate abundance (34%, $C_{12}H_{18}NO$), with the observed fragment ions (through collision induced decomposition) at m/z = 174.1276 (100%, calculated for $C_{12}H_{16}N$ = 174.1277), 159.1041 (30%, calculated for $C_{11}H_{13}N$ = 159.1043), 145.0885 (57%, calculated for $C_{10}H_{11}N$ = 145.0886), 131.0729 (16%, calculated for C_9H_9N = 131.0730), 119.0855 (25%, calculated for C_9H_{11} = 119.0855) and 91.0542 (6%, calculated for C_7H_7 = 91.0542). The novel *N*-benzyl derivative (**3c**) was also analysed using HRESIMS and gave an [M+H]$^{+}$ peak at m/z = 254.1537 (calculated

Table 1
^{1}H (400 MHz), ^{13}C (100 MHz) NMR spectral data and ^{1}H–^{13}C long-range correlations of (±)-4′-methyl-*N*-ethylcathinone.HBr (**3b**) in d_6-DMSO. Chemical shifts (δ) in ppm; coupling constants (J) in Hz.

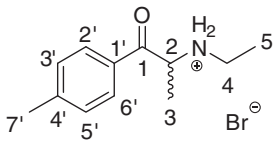

Position	^{1}H	^{13}C	^{2}J	^{3}J
1	–	195.5	–	–
2	5.21 q, J = 6.8	56.5	C1, C3	N**CH$_2$**CH$_3$
3	1.53 d, J = 7.2	15.7	C2	C1
4	3.04 dq, J = 12.4, 7.2	40.2	–	C2
5	1.28 t, J = 7.2	10.8	C4	–
1′	–	130.2	–	–
2′/6′	7.98 d, J = 8.2	128.6	C3′/C5′	C2′/C6′, C4′, C1
3′/5′	7.41 d, J = 8.2	129.4	C2′/C6′	C3′/C5′, C1′
4′	–	145.2	–	–
7′	2.42 s	20.9	C4′	C3′/C5′
NH_2^+	8.92 br s	–	–	–

Table 2
^{1}H (400 MHz), ^{13}C (100 MHz) NMR spectral data and ^{1}H–^{13}C long-range correlations of (±)-4′-methyl-*N*-benzylcathinone.HBr (**3c**) in d_6-DMSO. Chemical shifts (δ) in ppm; coupling constants (J) in Hz.

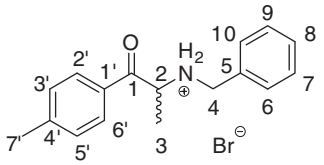

Position	^{1}H	^{13}C	^{2}J	^{3}J
1	–	195.1	–	–
2	5.27 q, J = 7.2	57.0	C1, C3	N**CH$_2$**Ph
3	1.53 d, J = 7.2	15.7	C2	C1
4	4.21 dd, J = 7.2, 12.8	48.7	–	C2
5	–	131.5	–	–
6/10	7.56, m[a]	128.3	C7, C9	–
7/9	7.44, m[b]	129.8	C6, C10	–
8		128.8	–	–
1′	–	130.2	–	–
2′/6′	7.93 d, J = 8.2	128.6	C3′/C5′	C2′/C6′, C4′, C1
3′/5′	7.41 d, J = 8.2[c]	129.4	C2′/C6′	C3′/C5′, C1′
4′	–	145.2	–	–
7′	2.42 s	20.9	C4′	C3′/C5′
NH_2^+	9.40 br s	–	–	–

[a] Expected multiplicity would be a 2H doublet of doublets (C6/C10).
[b] Co-incident resonances. Expected multiplicity would be a 2H triplet (or doublet of doublets, C7/C9) and a 1H triplet (C8).
[c] Expected coupling constant based upon the C2′/C6′ measured value.

for $C_{17}H_{20}NO$ = 254.1539) confirming the molecular formula of $C_{17}H_{19}NO$ and the identity of the sample as (±)-4′-methyl-*N*-benzylcathinone. The mass spectrum of (**3c**) is shown in Fig. 3b and also exhibits a moderately abundant $[M+H]^+$ parent ion (m/z = 254.1537, 34%, $C_{17}H_{20}NO$), with the observed CID fragment ions at m/z = 236.1433 (10%, calculated for $C_{17}H_{18}N$ = 236.1434), 146.0964 (7%, calculated for $C_{10}H_{12}N$ = 146.0964), 119.0855 (3%, calculated for C_9H_{11} = 119.0855) and 91.0542 (100%, calculated for C_7H_7 = 91.0542).

The infrared spectra of (±)-4′-methyl-*N*-ethylcathinone (**3b**, Fig. 4) and (±)-4′-methyl-*N*-benzylcathinone (**3c**, Fig. 5) were collected on an attenuated total reflection infrared (ATR-FTIR) spectrometer. The spectra show strong C=O absorption bands at 1687.3 (**3b**) and 1683.9 (**3c**) cm^{-1} respectively. Additionally both samples exhibit broad C=C absorptions at 1605.4 (**3b**) and 1604.5 (**3c**) cm^{-1}, indicative of an aromatic nucleus, and 2735.4 (**3b**) and 2770.6 (**3c**) cm^{-1} due to the NH_2^+ stretch, which is consistent with the spectra previously obtained for (±)-mephedrone [12] and 4-MEC [14].

The theoretical wavelength of maximum absorbance (as calculated from Scott's Rules [17]) of both derivatives was determined to be 256 nm. The ultraviolet spectrum of (±)-4′-methyl-*N*-ethylcathinone (**3b**) obtained in absolute ethanol (Fig. 6a, denoted by —) is in good agreement with the theoretical value and shows λ_{max} at 260.0 nm (A = 0.693, $c = 1.02 \times 10^{-3}$ g/100 mL). Spectra exhibiting a slight bathochromic shift (*circa* 4 nm) due to the solvent effect were obtained for (**3b**) in deionised water (λ_{max} = 264.0 nm, A = 0.621, $c = 1.04 \times 10^{-3}$ g/100 mL) or 0.1 M aqueous hydrochloric acid (λ_{max} = 264.0 nm, A = 0.607, $c = 1.04 \times 10^{-3}$ g/100 mL). In 0.1 M aqueous sodium hydroxide a hypsochromic shift (with a slight hyperchromic shift reduction in absorbance intensity) to 260.0 nm (A = 0.555, $c = 1.04 \times 10^{-3}$ g/100 mL) was observed in the spectrum of (**3b**) and may be due to a change in the ionisation of the sample. Similar ultraviolet spectra and wavelength maxima were obtained for the corresponding *N*-benzyl derivative (**3c**, Fig. 6a–d, denoted by - - -), though the UV absorbance intensity of 4-MBC was observed to be approximately 25% lower than 4-MEC in each

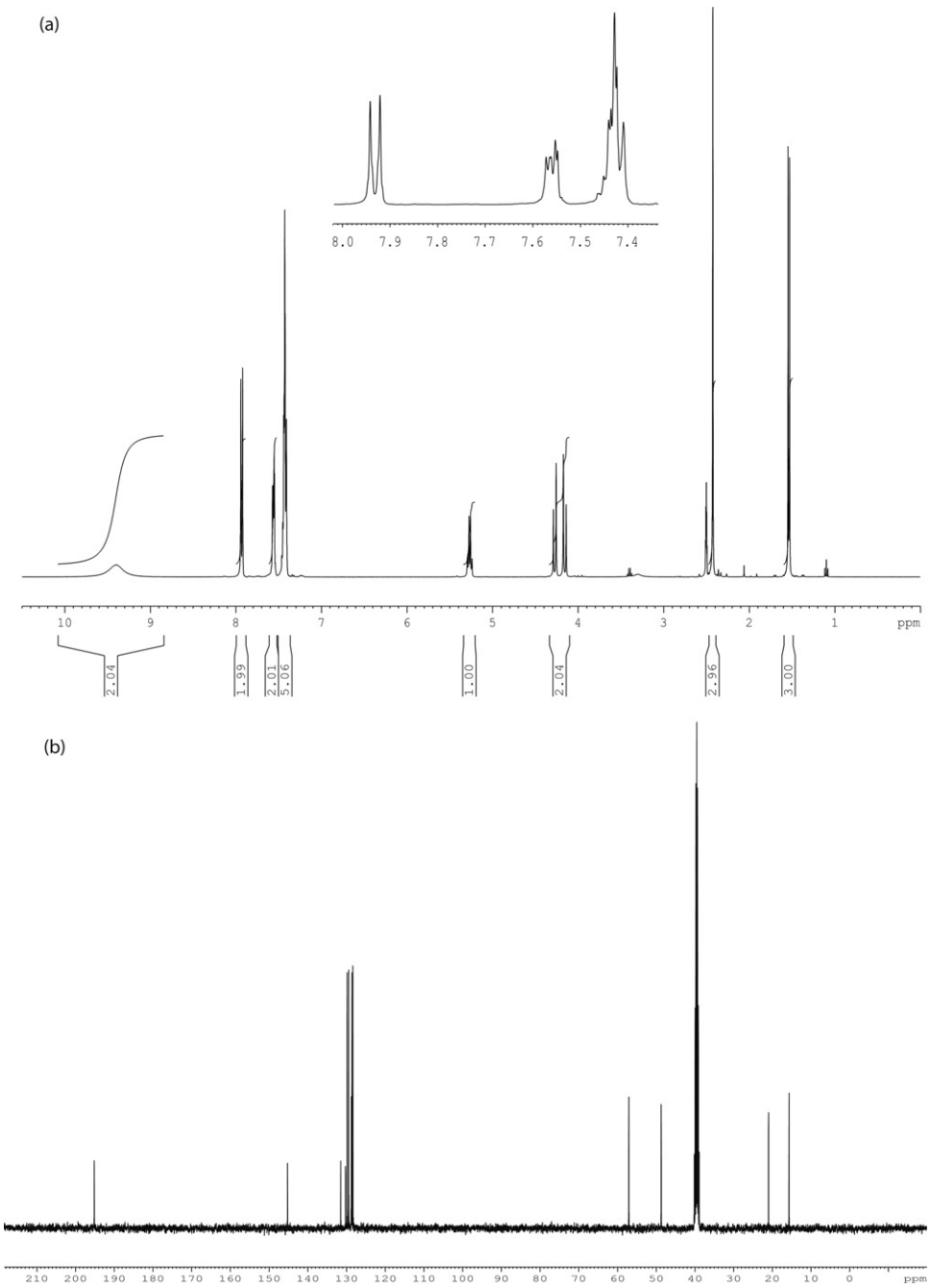

Fig. 2. (a) ^{1}H NMR spectrum (400 MHz, d_6-DMSO, 60 °C) and (b) ^{13}C NMR spectrum (100 MHz, d_6-DMSO, 60 °C) of (±)-4′-methyl-*N*-benzylcathinone.HBr (**3c**).

case. The UV data for both derivatives, which is consistent with that obtained for (±)-mephedrone (**3a**) [12], is summarised in Table 3.

Previous researchers have reported utilising HPLC and LC–MS techniques to determine (±)-mephedrone for quality control [12,18,19], toxicological [20–22] and bioanalytical [23–24] screening purposes. However, no fully validated liquid chromatographic methods (or limits of detection and quantification) for the mephedrone derivatives 4-MEC (**3b**) and 4-MBC (**3c**), or for the analysis of NRG-2 products, have been published. The recently

Table 3
Ultraviolet spectral data of (±)-4′-methyl-*N*-ethylcathinone.HBr (**3b**) and (±)-4′-methyl-*N*-benzylcathinone.HBr (**3c**).

	(±)-4′-Methyl-*N*-ethylcathinone hydrobromide (**3b**)				(±)-4′-Methyl-*N*-benzylcathinone hydrobromide (**3c**)			
Solvent	EtOH	H_2O	0.1 M HCl	0.1 M NaOH	EtOH	H_2O	0.1 M HCl	0.1 M NaOH
Concn. (g/100 mL)	1.02×10^{-3}	1.04×10^{-3}	1.04×10^{-3}	1.04×10^{-3}	1.04×10^{-3}	1.06×10^{-3}	1.06×10^{-3}	1.06×10^{-3}
λ_{max} (nm)	260.0	264.0	264.0	260.0	260.0	264.0	264.0	260.0
Absorbance (A)	0.693	0.621	0.607	0.555	0.498	0.475	0.466	0.426

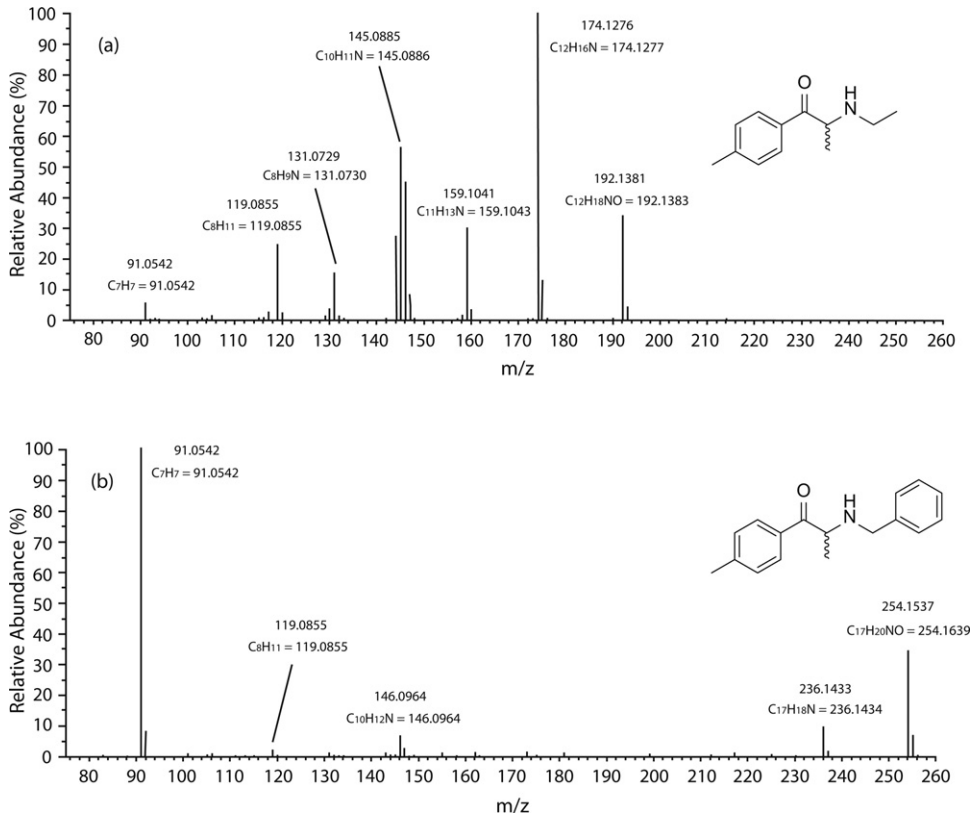

Fig. 3. HRESIMS spectra of (a) (±)-4′-methyl-*N*-ethylcathinone.HBr (**3b**) and (b) (±)-4′-methyl-*N*-benzylcathinone.HBr (**3c**).

published, validated HPLC method [12] (which can detect (±)-mephedrone at levels of 0.08 μg mL^{-1}) was further developed and re-validated to screen for (±)-mephedrone (**3a**) and the two structurally related derivatives: 4-MEC (**3b**) and 4-MBC (**3c**). The UV detection wavelength was changed to 264 nm and mobile phase composition was modified by increasing the percentage of organic modifier to 46% (v/v), to ensure both optimal detection of the analytes and a rapid analysis time. The three methcathinone derivatives eluted at 3.8 (**3a**), 4.2 (**3b**) and 11.5 (**3c**) min respectively (Fig. 7a–c) with a slight peak tailing ($A_s \sim 1.2$–1.4) observed in

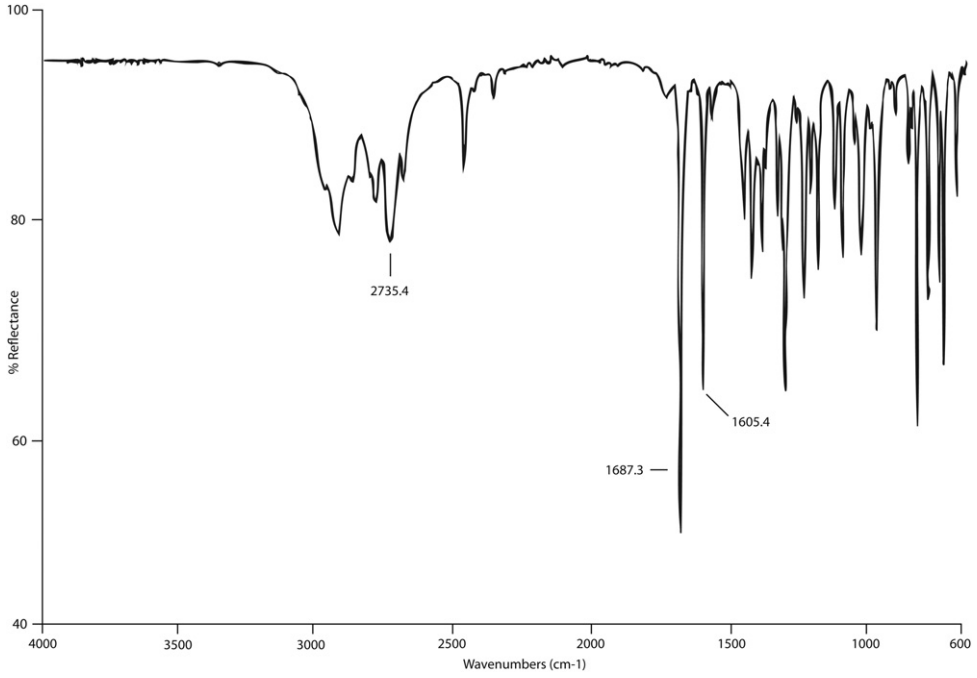

Fig. 4. ATR-FTIR spectrum of (±)-4′-methyl-*N*-ethylcathinone.HBr (**3b**).

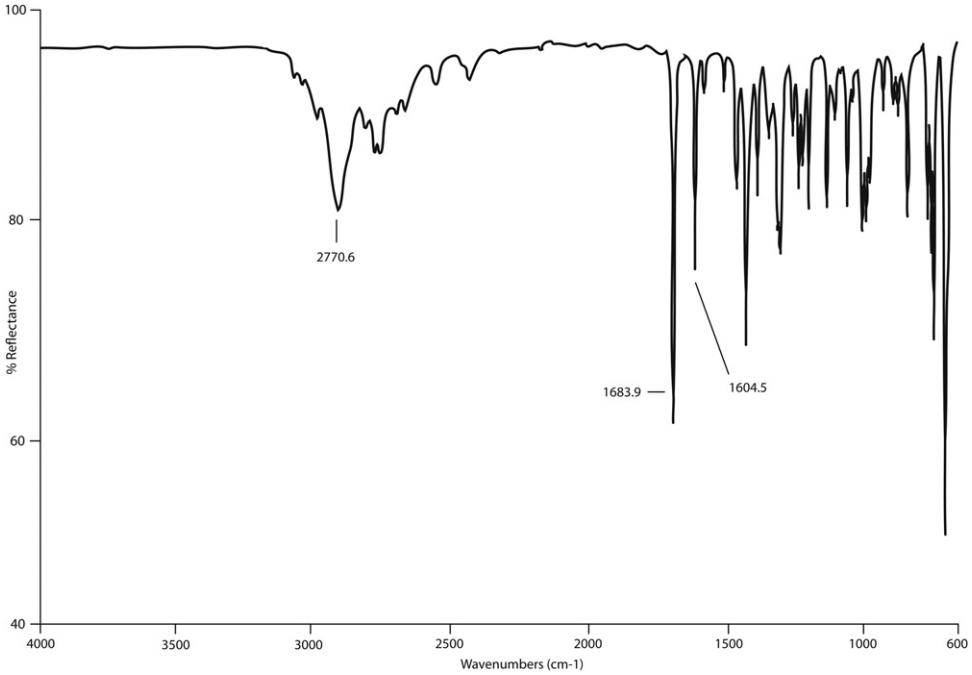

Fig. 5. ATR-FTIR spectrum of (±)-4′-methyl-*N*-benzylcathinone.HBr (**3c**).

each case. Calibration standards were prepared and demonstrated a linear response ($r^2 = 0.999$) over a 0.5–10 μg mL^{-1} range with excellent repeatability in each case (RSD = 0.08–1.80%, $n = 6$). The limits of detection and quantification were determined to be 0.03 and 0.09 (for **3a**), 0.03 and 0.08 (for **3b**) and 0.05 and 0.14 μg mL^{-1} (for **3c**) respectively, which is more sensitive than the previously reported method [12]. The validation parameters for the three analytes are summarised in Table 4.

The method was further developed to screen for methcathinones (**3a**–**3c**) in the presence of a number of common diluents. The diluents chosen for the study were caffeine, benzocaine (based upon the data reported by Brandt et al. on the analysis of "*street*" samples of NRG-2 [13]), sucrose, glucose, mannitol and lactose. The mobile phase composition utilised for the quantification of the pure substances was suitable to ensure a rapid analysis time (*circa* 13 min) and baseline resolution between the analytes (Fig. 7d). The validation parameters for the chromatographic method are summarised in Table 5. All five strongly UV-absorbing components (**3a**, **3b**, **3c**, caffeine and benzocaine) demonstrated a linear response ($r^2 = 0.999$–1) over a 0.5–10 μg mL^{-1} range with excellent repeatability (RSD = 0.03–1.90%, $n = 6$) and limits of detection (0.02 μg mL^{-1}) and quantification (0.05–0.09 μg mL^{-1}) respectively. The UV-inactive analytes (sucrose, glucose, mannitol and lactose) were shown not to interfere with the five target analytes.

Three NRG-2 samples obtained from Internet vendors were all purported to be >99% pure and to contain 1 g of NRG-2. The samples were arbitrarily labelled NRG-2-A, NRG-2-B and NRG-2-C. Preliminary LC–MS analysis (Fig. 8) indicated

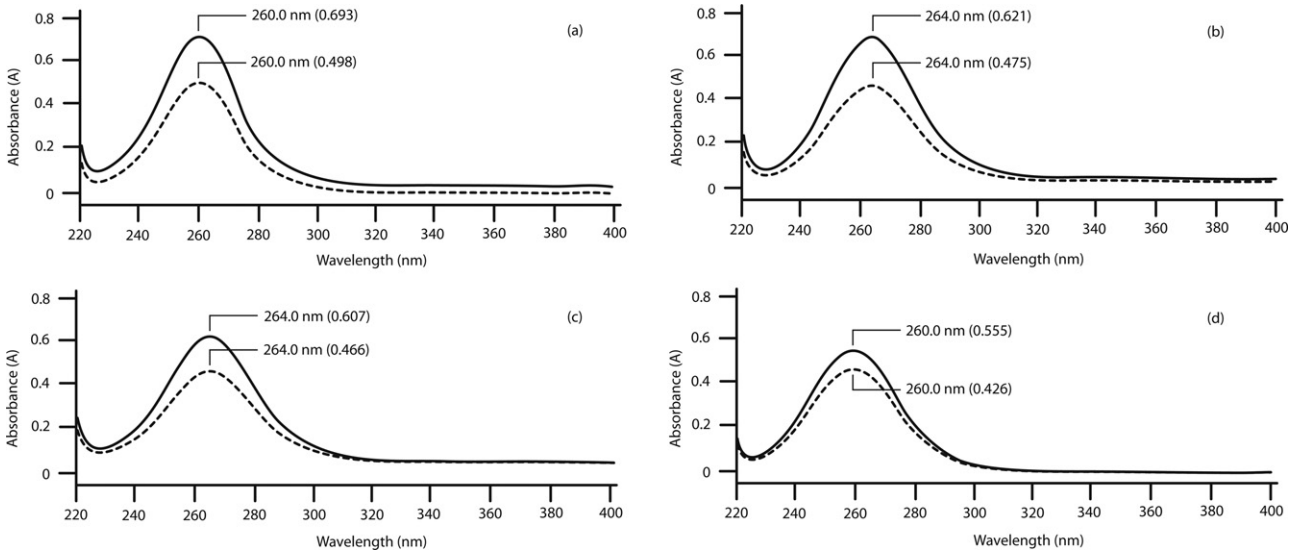

Fig. 6. UV spectra of (±)-4′-methyl-*N*-ethylcathinone.HBr (**3b**, —) and (±)-4′-methyl-*N*-benzylcathinone.HBr (**3c**, - - -) in (a) EtOH: **3b**, $c = 1.02 \times 10^{-3}$ g/100 mL; **3c**, $c = 1.04 \times 10^{-3}$ g/100 mL; (b) H_2O: **3b**, $c = 1.04 \times 10^{-3}$ g/100 mL; **3c**, $c = 1.06 \times 10^{-3}$ g/100 mL; (c) 0.1 M aqueous HCl: **3b**, $c = 1.04 \times 10^{-3}$ g/100 mL; **3c**, $c = 1.06 \times 10^{-3}$ g/100 mL and (d) 0.1 M aqueous NaOH: **3b**, $c = 1.04 \times 10^{-3}$ g/100 mL; **3c**, $c = 1.06 \times 10^{-3}$ g/100 mL.

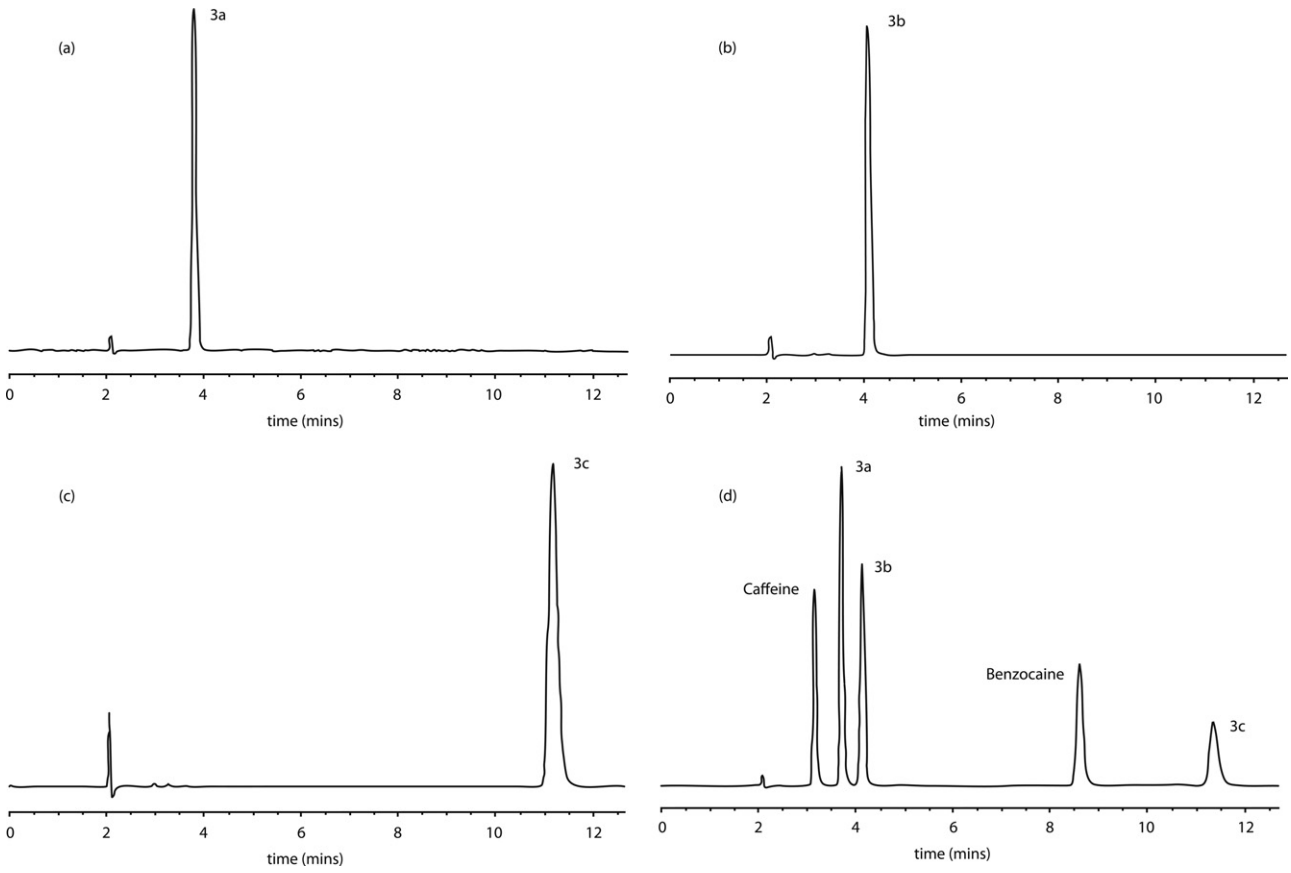

Fig. 7. Representative chromatograms of solutions containing: (a) (±)-mephedrone.HBr (**3a**, 5 μg mL^{-1}); (b) (±)-4′-methyl-*N*-ethylcathinone.HBr (**3b**, 5 μg mL^{-1}); (c) (±)-4′-methyl-*N*-benzylcathinone.HBr (**3c**, 5 μg mL^{-1}) and (d) caffeine (5 μg mL^{-1}); (±)-mephedrone.HBr (**3a**, 5 μg mL^{-1}), (±)-4′-methyl-*N*-ethylcathinone.HBr (**3b**, 5 μg mL^{-1}), benzocaine (5 μg mL^{-1}) and (±)-4′-methyl-*N*-benzylcathinone.HBr (**3c**, 5 μg mL^{-1}) obtained using ACE 3 C_{18} column (150 mm × 4.6 mm i.d., particle size: 3 μm); mobile phase: methanol:10 mM ammonium formate (pH 3.5) (46:54); detector wavelength: 264 nm; t_0 (2.2 min) was determined from the t_R of a solution of uracil.

Table 4
Summary of validation data for the quantification of (±)-mephedrone.HBr (**3a**), (±)-4′-methyl-*N*-ethylcathinone.HBr (**3b**) and (±)-4′-methyl-*N*-benzylcathinone.HBr (**3c**) obtained using ACE 3 C_{18} column (150 mm × 4.6 mm i.d., particle size: 3 μm); mobile phase: methanol:10 mM ammonium formate (pH 3.5) (46:54); detector wavelength: 264 nm.

	(**3a**)	(**3b**)	(**3c**)
t_R (min) (t_0 = 2.2 min[a])	3.8	4.2	11.6
RRT[b]	1	1.11	3.03
Capacity factor (k')	0.73	0.91	4.23
Response factor (RRF)[c]	1	0.8	0.43
N (plates)	13,500 (90,000)[f]	14,450 (96,333)[f]	20,100 (134,000)[f]
H (m)	1.11×10^{-5}	1.04×10^{-5}	7.46×10^{-6}
Resolution (R_s)	–	–	–
Symmetry factor (A_s)	1.4	1.32	1.22
LOD[d] (μg mL^{-1})	0.03	0.03	0.05
LOQ[e] (μg mL^{-1})	0.09	0.08	0.14
Co-efficient of regression (r^2)	0.999[g]	0.999[h]	0.999[i]
Precision (% RSD) (n = 6)			
10 μg mL^{-1}	0.72	1.80	1.30
5 μg mL^{-1}	0.23	0.50	0.88
2.5 μg mL^{-1}	0.62	0.66	0.97
1 μg mL^{-1}	0.21	0.12	0.30
0.5 μg mL^{-1}	0.60	0.08	0.24

[a] Determined from the retention time of uracil eluting from the column.
[b] Relative retention time (with respect to (±)-mephedrone, **3a**).
[c] Relative response factor (with respect to (±)-mephedrone, **3a**).
[d] Limit of detection (based on the standard deviation of the response and the slope).
[e] Limit of quantification (based on the standard deviation of the response and the slope).
[f] N expressed in plates per m.
[g] $y = 50.933x - 1.2239$.
[h] $y = 33.324x - 0.7367$.
[i] $y = 11.530x - 0.636$.

Table 5
Summary of validation data for the quantification of (±)-mephedrone.HBr (**3a**), (±)-4′-methyl-*N*-ethylcathinone.HBr (**3b**) and (±)-4′-methyl-*N*-benzylcathinone.HBr (**3c**) in the presence of common adulterants using ACE 3 C_{18} column (150 mm × 4.6 mm i.d., particle size: 3 μm); mobile phase: methanol:10 mM ammonium formate (pH 3.5) (46:54); detector wavelength: 264 nm.

	Caffeine	(**3a**)[e,f]	(**3b**)	Benzocaine	(**3c**)
t_R (min) (t_0 = 2.2 min[a])	3.2	3.8	4.2	8.5	11.6
RRT[b]	0.84	1	1.11	2.24	3.05
Capacity factor (k')	0.45	0.73	0.91	2.86	4.27
Response factor (RRF)	0.55	1	0.58	0.79	0.58
Resolution (R_s)	–	4.4	3.1	23.7	9.4
Symmetry factor (A_s)	0.97	0.99	0.99	0.98	0.88
LOD[c] (μg mL^{-1})	0.02	0.02	0.02	0.02	0.02
LOQ[d] (μg mL^{-1})	0.05	0.07	0.07	0.05	0.09
Co-efficient of regression (r^2)	1[g]	0.999[h]	0.999[i]	1[j]	0.999[k]
Precision (% RSD) (n = 6)					
10 μg mL^{-1}	0.21	0.10	0.19	0.14	0.46
5 μg mL^{-1}	0.29	0.10	1.00	0.29	0.54
2.5 μg mL^{-1}	1.54	1.17	0.07	0.52	0.03
1 μg mL^{-1}	0.49	0.07	0.81	0.43	1.90
0.5 μg mL^{-1}	0.74	0.03	1.76	0.75	1.65

[a] Determined from the retention time of uracil eluting from the column.
[b] Relative retention time.
[c] Limit of detection (based on the standard deviation of the response and the slope).
[d] Limit of quantification (based on the standard deviation of the response and the slope).
[e] N = 90,833 plates per m.
[f] $H = 1.10 \times 10^{-5}$ m.
[g] $y = 17.195x + 0.2407$.
[h] $y = 56.714x - 1.2765$.
[i] $y = 21.91x - 0.7506$.
[j] $y = 19.861x - 0.7602$.
[k] $y = 36.834x - 0.6905$.

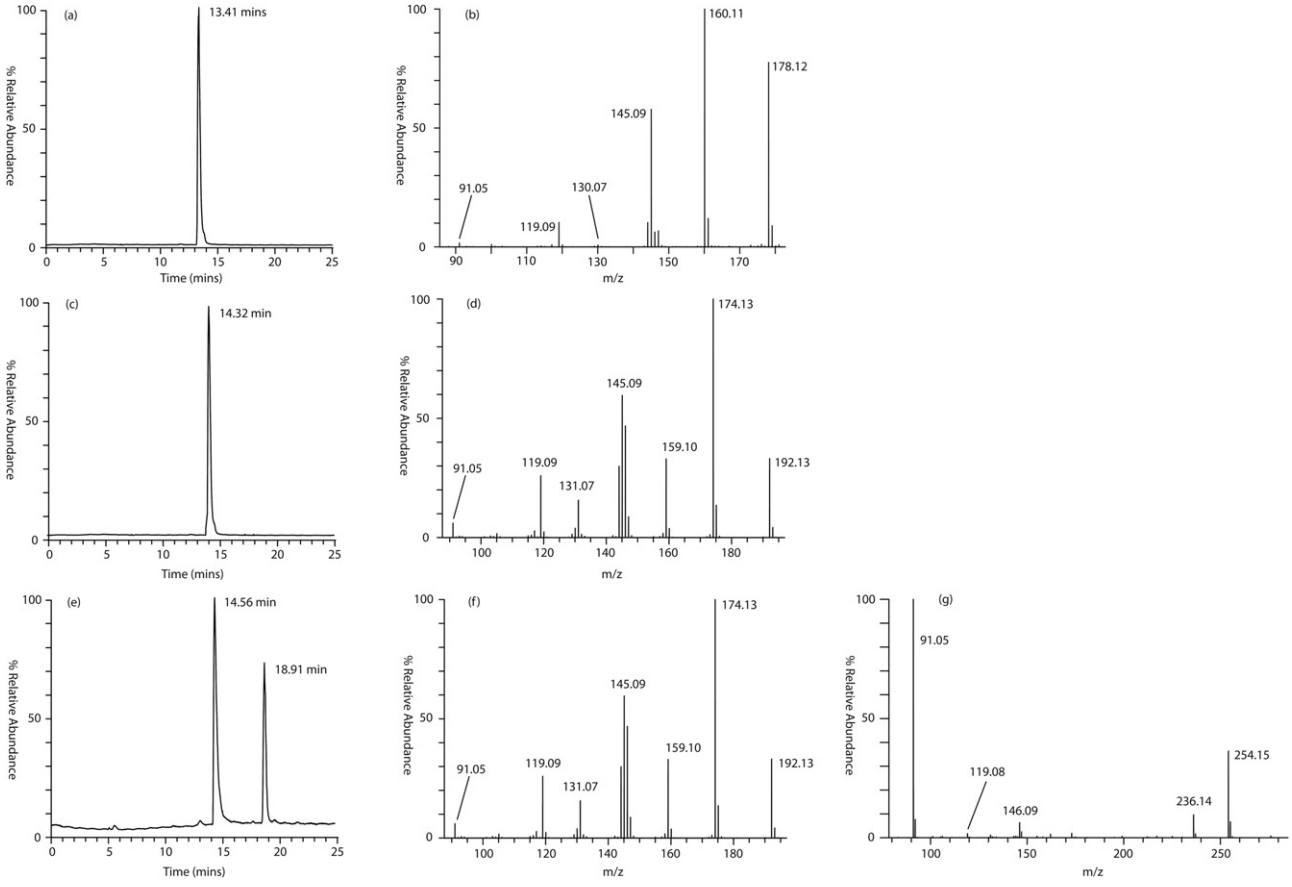

Fig. 8. LC–MS analysis of three NRG-2 products obtained using ACE 3 C_{18} column (150 mm × 4.6 mm i.d., particle size: 3 μm); mobile phase and gradient programme (see Section 2.4 for details): (a) LC chromatogram for NRG-2-A; (b) ESI mass spectrum (+ve ion mode) of peak (t_R = 13.41 min) corresponding to mephedrone (**3a**, $[M+H]^+$ = 178.12); (c) LC chromatogram for NRG-2-B; (d) ESI mass spectrum (+ve ion mode) of peak (t_R = 14.32 min) corresponding to 4-MEC (**3b**, $[M+H]^+$ = 192.14); (e) LC chromatogram for NRG-2-C; (f) ESI mass spectrum (+ve ion mode) of peak (t_R = 14.56 min) corresponding to 4-MEC (**3b**, $[M+H]^+$ = 192.14); (g) ESI mass spectrum (+ve ion mode) of peak (t_R = 18.91 min) corresponding to 4-MBC (**3c**, $[M+H]^+$ = 254.15).

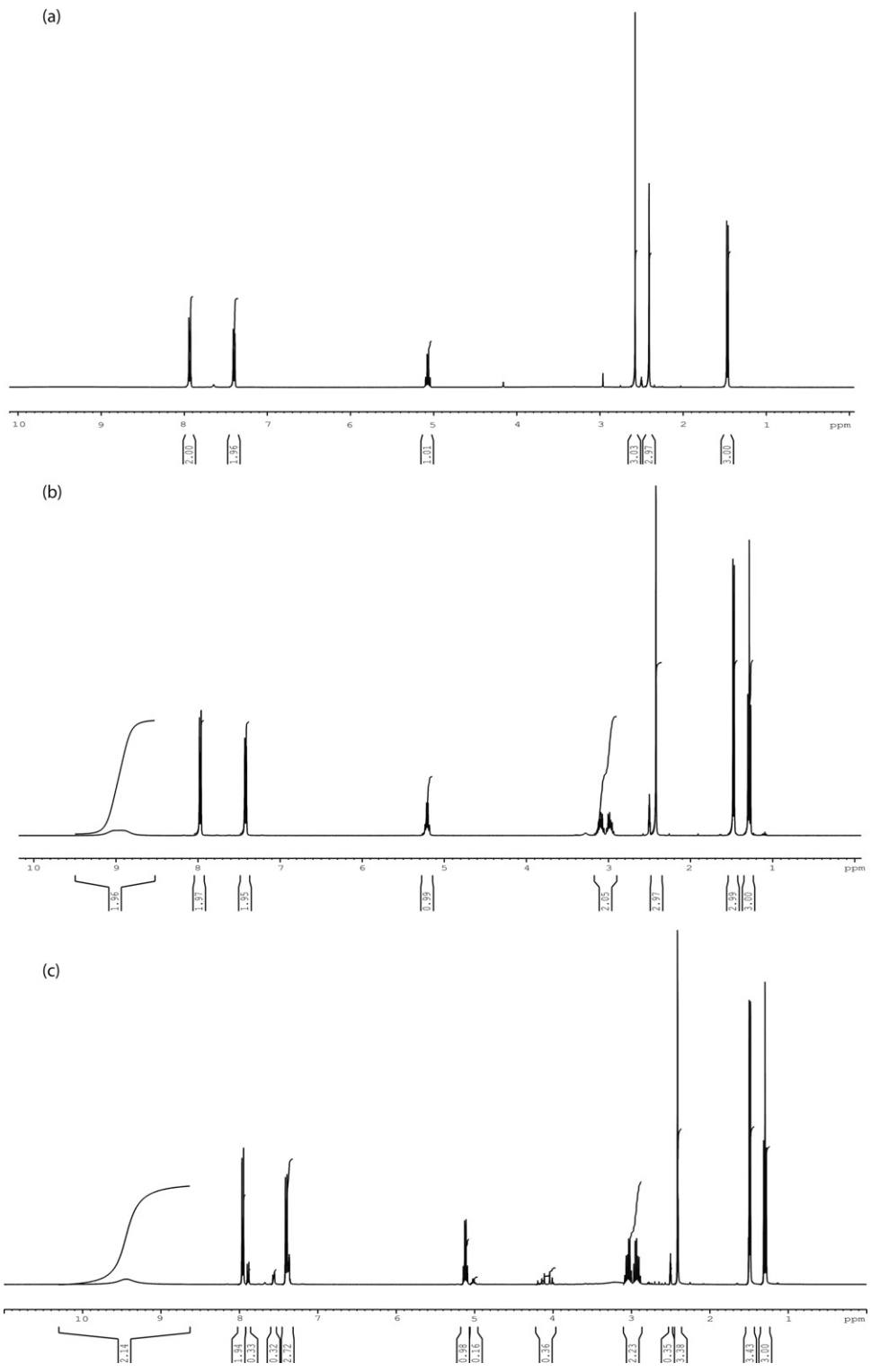

Fig. 9. ^{1}H NMR spectra (400 MHz, d_6-DMSO, 60 °C) of (a) NRG-2-A; (b) NRG-2-B and (c) NRG-2-C.

that two of the samples contained single components (NRG-2-A: t_R = 13.41 min, m/z = 178.12 $[M+H]^+$; NRG-2-B: t_R = 14.32 min, m/z = 192.14 $[M+H]^+$) and one contained two compounds (NRG-2-C: t_R = 14.56 min [major], m/z = 192.14 $[M+H]^+$; t_R = 18.91 min [minor], m/z = 254.15 $[M+H]^+$). Additional ^{1}H NMR analysis (conducted at 60 °C in d_6-DMSO) of NRG-2-A gave a spectrum (Fig. 9a) consistent with (±)-mephedrone (**3a**, 4-MMC) [12] thus confirming its identity.[2] The second sample, NRG-2-B, also exhibited the classical AA′BB′ pattern typical of an unsymmetrical *para*-disubstituted

[2] The spectrum obtained was consistent with the previously reported data [12]. However, the signal corresponding to the ammonium salt protons at *circa* δ^{1}H = 9.35 ppm was too broad to be observed.

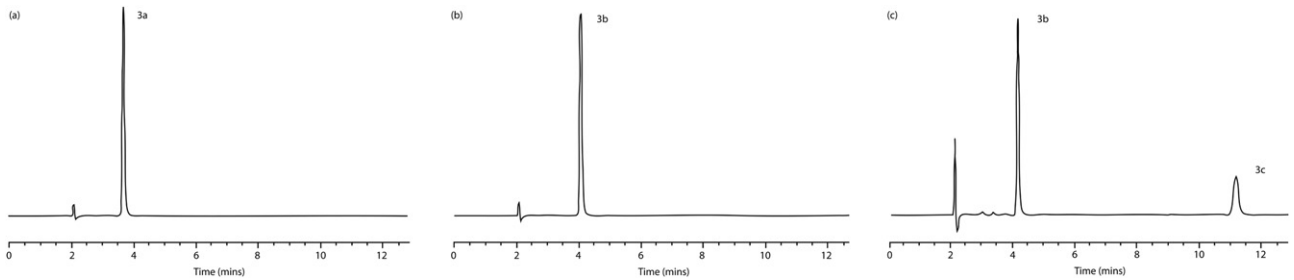

Fig. 10. Representative chromatograms of solutions containing: (a) NRG-2-A (10 μg mL^{-1}); (b) NRG-2-B (10 μg mL^{-1}) and (c) NRG-2-C (10 μg mL^{-1}) obtained using ACE 3 C_{18} column (150 mm × 4.6 mm i.d., particle size: 3 μm); mobile phase: methanol:10 mM ammonium formate (pH 3.5) (46:54); detector wavelength: 264 nm; t_0 (2.2 min) was determined from the t_R of a solution of uracil.

aromatic ring together with a quartet at δ^1H = 5.21 ppm (corresponding to the chiral C2-centre) and a deshielded singlet (*circa* δ^1H = 2.4 ppm) attributable to a methyl group attached to an aromatic ring. Taken together, these data are characteristic of a mephedrone-like structure [12] (Fig. 9b). In addition the ^{1}H NMR spectrum exhibited signals at δ^1H = 1.28 ppm and 3.04 ppm, which are characteristic of an ethyl side chain, where the methylene group demonstrates additional geminal coupling to the chiral centre at C2. This data indicates that the second sample is likely to contain the previously reported (±)-4′-methyl-*N*-ethylcathinone (**3b**, 4-MEC) and is in agreement with the data previously reported by other researchers [13,14].

The LC–MS data for NRG-2-C shows that the sample contains two components (Fig. 8). The major component (t_R = 14.56 min, m/z = 192.14 $[M+H]^+$) gives both a mass spectrum and characteristic signals in the ^{1}H NMR spectrum (Fig. 9c) that are both consistent with the data obtained for (±)-4′-methyl-*N*-ethylcathinone (**3b**, 4-MEC) thus confirming its identity and presence in the sample. The minor component (t_R = 18.91 min) gives a mass spectrum containing a molecular ion (m/z = 254.15 $[M+H]^+$) with a pattern of fragment ions, similar to (**3a**) and (**3b**), at m/z = 236.14, 146.09, 119.08 and 91.05 indicating a mephedrone-like structural motif and therefore two possible isomeric structures namely (±)-4′-methyl-*N*-benzylcathinone (**3c**, 4-MBC) or the (±)-4′-methyl-*N*-tolylcathinone derivative (**8**) (Scheme 1). The ^{1}H NMR spectrum (Fig. 9c) indicates that the minor component is a structurally related mephedrone derivative due to the characteristic signals at δ^1H ∼ 7.89 ppm (AA′BB′ system where the partner signal at δ^1H ∼ 7.4 ppm appears co-incident with other aromatic resonances), δ^1H ∼ 2.40 ppm (methyl group attached to an aromatic ring), δ^1H ∼ 5.01 ppm (corresponding to the proton attached to the chiral C2-centre) with additional aromatic signals (*circa* δ^1H = 7.36–7.38 and 7.55–7.57 ppm) for a second aromatic ring. The presence of a doublet of doublets (*circa* δ^1H = 4.08 ppm), which is distinctive of an isolated methylene group exhibiting geminal coupling to the chiral centre at C2 (*cf.* 4-MEC), and the absence of an additional deshielded singlet (*circa* δ^1H = 2.4 ppm) attributable to a second aromatic methyl group, confirms that the structure of the minor component is likely to be (±)-4′-methyl-*N*-benzylcathinone (**3c**, 4-MBC) rather than the isomeric derivative (±)-4′-methyl-*N*-tolylcathinone (**8**).

The three "*street*" samples of NRG-2 were analysed using the validated adulterants method at a concentration of 10 μg mL^{-1}. The results (Fig. 10) confirm that two of the samples contained single components (NRG-2-A: t_R = 3.8 min, mephedrone, 93.98%, %RSD = 0.05%, n = 3; Fig. 10a; NRG-2-B: t_R = 4.2 min, 4-MEC, 85.58%, %RSD = 0.02%, n = 3; Fig. 10b), one contained two (NRG-2-C: t_R = 4.2 min [major, 4-MEC, 77.47%, %RSD = 0.17%, n = 3] and t_R = 11.5 min [minor, 4-MBC, 10.05%, %RSD = 0.03%, n = 3], Fig. 10c) and all the samples are predominately pure with none of the common diluents reported by Brandt et al. [13] being present. This study indicates that this protocol can been considered suitable for the rapid analysis of these products.

4. Conclusions

A comprehensive analytical profiling and development of validated methods for the detection and quantitative analysis of two mephedrone-derivatives: 4-MEC (**3b**) and 4-MBC (**3c**) either in their pure form or in the presence of common excipients is reported. It is envisaged that the data presented will be valuable as a reference point for future analysis of these and related compounds as they emerge on the illicit drug market.

Acknowledgement

The authors gratefully acknowledge financial support of this work through the Libyan Cultural Bureau for the provision of a studentship for O.I.G.K.

Appendix A. Supplementary data

Supplementary data associated with this article can be found, in the online version, at doi:10.1016/j.jpba.2011.11.004.

References

[1] J. Hillebrand, D. Olszewski, R. Sedefov, Legal highs on the Internet, Subst. Use Misuse 45 (2010) 330–340.
[2] F. Schifano, A. Albanese, S. Fergus, J.L. Stair, P. Deluca, O. Corazza, Z. Davey, J. Corkery, H. Siemann, N. Scherbaum, M. Farre, M. Torrens, Z. Demetrovics, H.A. Ghodse, Mephedrone (4-methylmethcathinone; meow meow): chemical, pharmacological and clinical issues, Psychopharmacology 214 (2011) 593–602.
[3] M.R. Meyer, F.T. Peters, H.H. Maurer, Metabolism of the new designer drug mephedrone and toxicological detection of the beta keto designer drugs mephedrone, butylone and methylone in urine, Ann. Toxicol. Anal. 21 (2009) 22–23.
[4] P.I. Dargan, R. Sedefov, A. Gallegos, D.M. Wood, The pharmacology and toxicology of the synthetic cathinone mephedrone (4-methylmethcathinone), Drug Test. Anal. 3 (2011) 464–465.
[5] J.P. Kelly, Cathinone derivatives: a review of their chemistry, pharmacology and toxicology, Drug Test. Anal. 3 (2011) 439–453.
[6] A.J. Dickson, S.P. Vorce, B. Levine, M.R. Past, Multiple-drug toxicity caused by the coadministration of 4-methylmethcathinone (mephedrone) and heroin, J. Anal. Toxicol. 34 (2010) 162–168.
[7] D.M. Wood, S. Davis, M. Puchnarewicz, J. Button, R. Archer, H. Ovaska, J. Ramsey, T. Lee, D.W. Holt, P.I. Dargan, Recreational use of mephedrone (4-methylmethcathinone, 4-MMC) with associated sympathomimetic toxicity, J. Med. Toxicol. 6 (2010) 327–330.
[8] H. Torrance, G. Cooper, The detection of mephedrone (4-methylmethcathinone) in 4 fatalities in Scotland, Forensic Sci. Int. 202 (2010) e62–e63.
[9] A. Camilleri, M.R. Johnston, M. Brennan, S. Davis, D.G.E. Caldicott, Chemical analysis of four capsules containing the controlled substance analogues 4-methylmethcathinone, 2-fluoromethamphetamine, alpha-phthalimidopropiophenone and *N*-ethylcathinone, Forensic Sci. Int. 197 (2010) 59–66.

[10] J. Deruiter, L. Hayes, A. Valaer, C.R. Clark, F.T. Noggle, Methcathinone and designer analogues: synthesis, stereochemical analysis, and analytical properties, J. Chromatogr. Sci. 32 (1994) 552–564.
[11] S. Gibbons, M. Zloh, An analysis of the '*legal high*' mephedrone, Bioorg. Med. Chem. Lett. 20 (2010) 4135–4139.
[12] E.Y. Santali, A.-K. Cadogan, N. Nic Daeid, K.A. Savage, O.B. Sutcliffe, Synthesis, full chemical characterisation and development of validated methods for the quantification of (±)-4′-methylmethcathinone (mephedrone): a new "*legal high*", J. Pharm. Biomed. Anal. 56 (2011) 246–255.
[13] S.D. Brandt, S. Freeman, H.R. Sumnall, F. Measham, J. Cole, Analyses of second generation "*legal highs*" in the UK: initial findings, Drug Test. Anal. 2 (2010) 377–382.
[14] P. Janovics, A. Varadi, L. Toelgyesi, S. Lohner, J. Nemeth-Palotas, H. Koszegi-Szalai, Identification and characterization of the new designer drug 4′-methylethcathinone (4-MEC) and elaboration of a novel liquid chromatography–tandem mass spectrometry (LC–MS/MS) screening method for seven different methcathinone analogs, Forensic Sci. Int. 210 (2011) 213–220.
[15] S.D. Brandt, S. Freeman, H.R. Sumnall, F. Measham, J. Cole, Analysis of NRG "legal high" in the UK: identification and formation of novel cathinones, Drug Test. Anal. 3 (2011) 569–575.
[16] N.E. Jacobson, NMR Spectroscopy Explained: Simplified Theory, Applications and Examples for Organic Chemistry and Structural Biology, John Wiley & Sons Inc., Hoboken, NJ, 2007.
[17] A.I. Scott, Interpretation of the Ultraviolet Spectra of Natural Products, Pergamon, New York, 1964.
[18] N. Singh, P. Day, V.R. Katta, G.P. Mohammed, W.J. Lough, LC purity and related substances screening for mephedrone, J. Pharm. Pharmacol. 62 (2010) 1209–1210.
[19] C. Rambabu, S.V. Rao, A.B. Babu, Qualitative analysis of mephedrone in bulk and pharmaceutical formulations by reverse phase high performance liquid chromatography, Rasayan J. Chem. 3 (2010) 796–799.
[20] D.M. Wood, S. Davis, S.L. Greene, J. Button, D.W. Holt, J. Ramsey, P.I. Dargan, Case series of individuals with analytically confirmed acute mephedrone toxicity, Clin. Toxicol. 48 (2010) 924–927.
[21] P.D. Maskell, G. De Paoli, C. Seneviratne, D.J. Pounder, Mephedrone (4-methylmethcathinone)-related deaths, J. Anal. Toxicol. 35 (2011) 188–191.
[22] L.K. Sorensen, Determination of cathinones and related ephedrines in forensic whole-blood samples by liquid-chromatography–electrospray tandem mass spectrometry, J. Chromatogr. B 879 (2011) 727–736.
[23] D.K. Wissenbach, M.R. Meyer, D. Remane, A.A. Philipp, A.A. Weber, H.H. Maurer, Drugs of abuse screening in urine as part of a metabolite-based LC–MS*n* screening concept, Anal. Bioanal. Chem. 400 (2011) 3481–3489.
[24] C. Bell, C. George, A.T. Kicman, A. Traynor, Development of a rapid LC–MS/MS method for direct urinalysis of designer drugs, Drug Test. Anal. 3 (2011) 496–504.

Journal of Pharmaceutical and Biomedical Analysis 61 (2012) 136–141

Contents lists available at SciVerse ScienceDirect

Journal of Pharmaceutical and Biomedical Analysis

journal homepage: www.elsevier.com/locate/jpba

Solid-state NMR and IR characterization of commercial xenogeneic biomaterials used as bone substitutes

Joanna Kolmas*, Maciej Szwaja, Waclaw Kolodziejski

Medical University of Warsaw, Faculty of Pharmacy, Department of Inorganic and Analytical Chemistry, ul. Banacha 1, 02-097 Warsaw, Poland

ARTICLE INFO

Article history:
Received 27 May 2011
Received in revised form 5 November 2011
Accepted 7 November 2011
Available online 25 November 2011

Keywords:
Bone substitute
Xenogeneic biomaterial
Biological apatite
Solid-state NMR
Infrared spectroscopy
Powder diffraction

ABSTRACT

Three commercial xenogeneic biomaterials (Gen-Os, Apatos Spongiosa and Apatos Cortical; all from Tecnoss Dental, Torino, Italy) originated from porcine bone were characterized by various analytical methods, such as powder X-ray diffraction (XRD), thermogravimetry (TGA), high-resolution solid-state nuclear magnetic resonance (ssNMR) and infrared spectroscopy (FT-IR). The studies were focused on structural properties and chemical compositions of the samples. It was found that the main constituents of the analyzed biomaterials were nanocrystalline apatite mineral, organic collagenous matrix and water. For comparison, synthetic carbonated hydroxyapatite and natural collagen type I from bovine tendon were used. Differences in various physicochemical parameters such as crystal size, specific surface area, concentration of structural hydroxyl groups, contents of CO_3^{2-} and HPO_4^{2-} ions and their location were discussed. It was shown that various techniques of ssNMR and elaborate analysis of the FT-IR spectra, applied together, provide valuable information on xenogeneic biomaterials.

© 2011 Elsevier B.V. All rights reserved.

1. Introduction

Xenogeneic biomaterials, mainly of bovine and porcine origin, are widely used as bone substitutes in the reconstructive surgery. Their similarity to human bone tissue and effective methods of removing immunogenic factors allowed to use those materials with good efficacy [1,2].

The main components of porcine and bovine bone are biological apatite and collagen type I. Collagen is a crystalline fibroprotein with unusual amino acid composition. Its structure is determined by Gly-X-Y sequences and significant amount of Hyp and Pro. In bone, apatite crystallites are deposited almost exclusively within the collagen fibrils.

Biological apatites were found to be carbonated hydroxyapatites [3], in which CO_3^{2-} ions are substituted for PO_4^{3-} ions (major form, type B substitution) and OH^- (inferior form, type A substitution). They contain also water molecules and various extraneous components, such as Mg^{2+}, Na^+, K^+, F^-, Cl^-, citrate or HPO_4^{2-} ions, located in the crystal lattice and on the crystal surface. In the mineralized tissues (bone, dentin and dental cementum), the crystal surface serves as interface between the mineral and the organic matrix. The structure and chemical composition of the crystal surface are therefore crucial for the bioactivity and biocompatibility of apatites used as biomaterials [3,4].

Consequently, crystal interior and surface of apatitic biomaterials should be properly monitored. Therefore, spectroscopic methods have been applied, such as solid-state nuclear magnetic resonance (ssNMR) and Fourier-transformed infrared (FT-IR) vibrational spectroscopy. They are adequately sensitive, site-specific and very convenient, because sample preparation is non-destructive and very easy. Furthermore, ssNMR and FT-IR include many techniques, which can be employed for various purposes.

Although several articles have already been published on the physicochemical properties of synthetic and biological apatites, only a few works were devoted to commercial xenogeneic materials used for bone repair [5–8]. This fact motivated us to perform elaborate characterization of unstudied yet, but commonly approved and utilized xenogeneic biomaterials by means of solid-state NMR and FT-IR spectroscopies assisted by powder X-ray diffraction (XRD) and thermogravimetry (TGA). The reported spectroscopic analyses are semiquantitative and aimed at structural comparison of the examined materials. They have this important advantage that the samples do not require any chemical pretreatment, so those methods are not invasive and do not interfere in the material structure. So far, the xenogeneic biomaterials have not been investigated using ssNMR and we show that this

* Corresponding author. Tel.: +48 22 5720755; fax: +48 22 5720784.
E-mail address: joanna.kolmas@wum.edu.pl (J. Kolmas).

0731-7085/$ – see front matter © 2011 Elsevier B.V. All rights reserved.
doi:10.1016/j.jpba.2011.11.008

Table 1
Conditions of the solid-state NMR measurements.

Experiment	Rotor diameter (mm)	MAS rate (kHz)	Contact time (ms)	Recycle delay (s)
$^{1}H \rightarrow {}^{13}C$ CP	4.0	7.5	2	10
$^{1}H \rightarrow {}^{31}P$ CP	4.0	7.5	1	10
^{31}P	4.0[a]	7.5[a]	–	600
BD	2.5[b]	30[b]		
$^{31}P \rightarrow {}^{1}H$ CP	4.0	7.0	2	600
^{1}H BD	2.5	30	–	10

[a] SSA measurements.
[b] Structural studies.

spectroscopy provides important information, e.g. on intracrystalline apatite hydroxyls, which cannot be obtained any other way.

2. Experimental

2.1. Samples

Three popular commercial xenografts of porcine origin: Gen-Os (GO), Apatos Spongiosa (AS) and Apatos Cortical (AC), were purchased from Tecnoss Dental (Torino, Italy). These materials are often used in dental surgery, because of their similar properties to autogenic bone. Each substance was available as granulate consisted of thin flakes with a particle size of 0.3–1.0 mm (Figure 1S in Supplementary Materials). AS and AC were produced from trabecular and cortical porcine bone, respectively. According to the products specification, the Apatos materials were characterized by different resorption time and in both cases collagen contained in the raw bone was degraded during a manufacturing process. Gen-Os was made of porcine bone, both cortical (25%) and trabecular (75%). Unlike Apatos, it was described as containing intact bone proteins, predominantly collagen type I. However, according to manufacturer, all the pathogenic elements were eliminated by special unspecified treatment. The GO, AS and AC samples were taken out straightaway from sealed vials and analyzed as they were, without any chemical or mechanical pretreatment.

Moreover, synthetic carbonated hydroxyapatite (CHA) with ca. 6 wt.% of carbonates, produced by the wet method [9], and collagen type I from bovine tendon (Sigma–Aldrich, Steinheim, Germany) were applied as standards for comparative analysis.

2.2. Analytical methods

The phase composition and crystallinity of our samples were examined by X-ray diffraction (XRD; Bruker D8 Discover diffractometer, Karlsruhe, Germany) using Cu Kα radiation (λ = 1.54 Å). The XRD patterns were also used to calculate crystal dimensions (using Scherrer's formula).

Solid-state NMR spectra were recorded at room temperature using a Bruker Avance 400 WB spectrometer at proton, ^{31}P and ^{13}C resonance frequencies of 400, 160 and 100 MHz, respectively (Bruker, Rheinstetten, Germany). We used Bruker proprietary double-bearing MAS probes and zirconia rotors, spun by dry air. Conventional pulse-acquire (Bloch-decay; BD) and cross-polarization (CP) experiments were performed. Structural hydroxyl groups in apatites were counted using the inverse $^{31}P \rightarrow {}^{1}H$ CP technique, previously described in [10]. Specific surface areas (SSA) of apatites were estimated from their ^{31}P BD and CP linewidths [11], measured at the MAS rate of 7.5 kHz. The ^{31}P and $^{1}H/{}^{13}C$ chemical shifts were externally referenced to 85% H_3PO_4 and TMS, respectively. Other experimental conditions are presented in Table 1. The peak deconvolutions were done using a line fitting subroutine of the ACD/SpecMenager NMR program (Advanced Chemistry Developments 2007).

FT-IR spectra were recorded from KBr pellets in the 400–4000 cm^{-1} range using a Spectrum 1000 spectrometer (Perkin Elmer, Cambridge, UK) with spectral resolution of 4 cm^{-1} and 32 scans. They were processed using GRAMS/AI 8.0 software (Thermo Scientific 2008).

The water, organic matrix and mineral contents were determined from the total mass loss using the thermogravimetric method (TGA). The samples were heated continuously in air from 30 to 600 °C at a rate of 5 K/min using Du Pont Thermal Analyst System 2100 (Du Pont Instruments, Twin Lakes, WI, USA).

3. Results and discussion

3.1. XRD and TGA analyses

Fig. 1 shows the XRD patterns of the analyzed samples and the CHA reference material. As expected, all the XRD peaks correspond to the standard apatite crystal structure and any additional peaks are not observed from other crystalline calcium phosphates. However, the obtained peaks are broad and weakly resolved, indicating low crystallinity. Dimensions of the apatite crystals have been estimated using Scherrer's formula [6]. According to this estimation, all three biomaterials contain nanocrystalline apatites with the average crystal sizes similar to those in bone mineral [12] (platelets 18–31 nm long and 6–10 nm wide, see Table 1S in Supplementary Materials). The CHA standard occurred nanocrystalline as well.

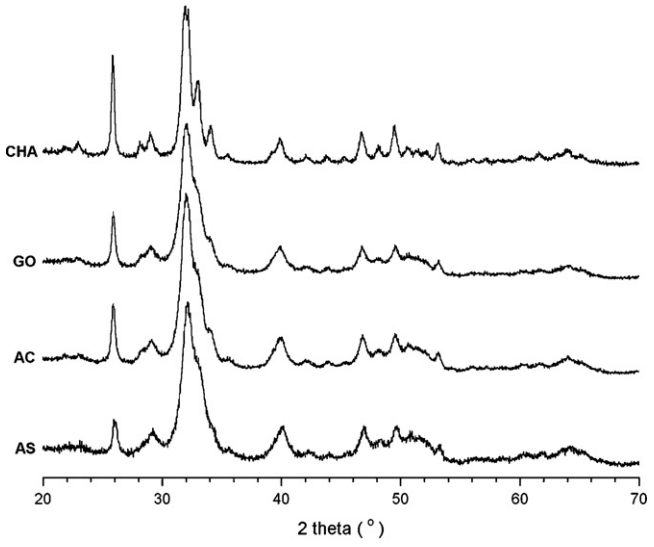

Fig. 1. XRD patterns of the analyzed samples.

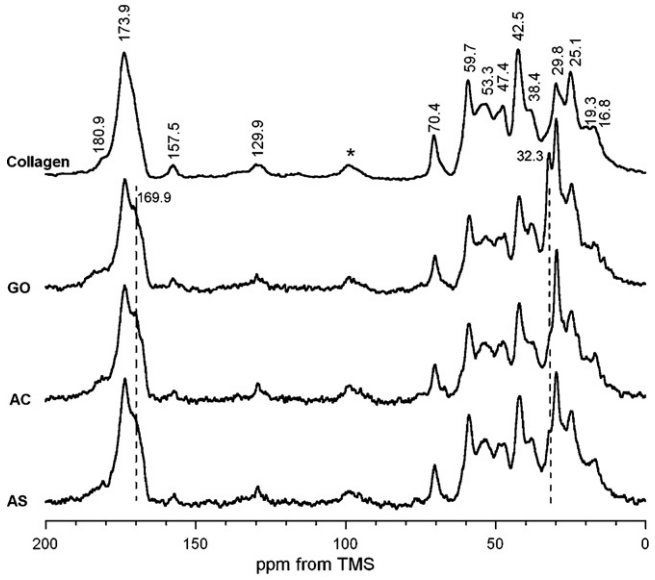

Fig. 2. ^{13}C CP/MAS NMR spectra of the analyzed biomaterials and collagen.

General chemical composition of the studied biomaterials was determined using TGA. The contents of water, organic matrix and apatite mineral were 6.5–10.4, 15.7–22.4 and 67.3–77.7 wt.%, respectively. The highest levels of water, organic matrix and apatite mineral were found in GO, AS and AC, respectively. The lowest levels of water, organic matrix and apatite mineral were found in AC, AS and GO, respectively.

3.2. Solid-state NMR measurements

The $^{1}H \rightarrow {}^{13}C$ CP/MAS NMR spectroscopy was found useful in the analysis of carbonates and organic matrix. As shown in Fig. 2, the spectra of the biomaterials are poorly resolved. There are two regions of interest: the 0–70 ppm region, characteristic for amino acid residues and that around 170 ppm, specific both for carbonyl groups of the organic matrix and for apatite carbonates. The GO, AC and AS spectra are essentially similar, showing main peaks with the same chemical shifts (Table 2) and analogous intensity ratios (Fig. 2). Worth attention is only the difference in the relative intensities of peaks at ca. 32 ppm, assigned to C_β of Lys. In the GO spectrum this line is easily noticeable and satisfactorily resolved, while for AC and AS it is hardly visible. However, the $^{1}H \rightarrow {}^{13}C$ CP/MAS NMR spectra of the studied biomaterials show significant differences in comparison to that of collagen type I. The formerly mentioned signal at 32.3 ppm is not revealed in the collagen spectrum. Most spectacular feature of the collagen spectrum is that the peak at 42.5 ppm from C_α of Gly is predominant, whereas in the GO, AC and AS spectra the most intensive is the peak at 29.8 ppm from C_β of Pro. It can be inferred that some thermal or chemical treatment of animal bone applied to prepare those biomaterials caused changes in its protein structure.

Table 2
Main ^{13}C CP/MAS NMR signals from collagen type I, GO, AC and AS. All chemical schifts are given in ppm.

Average	Collagen	AS	AC	GO	Assignment [13]
180.9	180.9	180.9	180.9	181.0	C=O (proteins)
173.7	173.9	173.5	173.5	173.8	C=O (proteins)
169.8	–	169.8	169.7	169.9	C=O (carbonates)
157.3	157.5	157.0	157.0	157.5	Arg C_ε
129.9	129.9	129.8	129.9	129.8	Phe C
70.4	70.4	70.2	70.5	70.3	Hyp C_γ
59.0	59.7	58.9	58.9	58.6	Pro C_α, Hyp C_α, Hyp C_δ
53.4	53.1	53.7	53.5	53.1	Ala C_α
47.1	47.4	47.2	47.0	46.9	Pro C_δ
42.2	42.5	42.0	42.1	42.2	Gly C_α
37.9	38.4	38.0	37.7	37.3	Hyp C_β
32.3	–	32.5	32.4	32.1	Lys C_β
29.8	29.8	30.0	29.8	29.7	Pro C_β
24.8	25.1	24.6	24.7	24.6	Pro C_γ
19.5	19.3	19.6	19.7	19.4	Leu C_δ
16.8	16.8	16.8	16.5	16.9	Ala C_β

Overall, the carbon-13 spectra indicate that all the studied biomaterials contain organic matrix composed mainly of collagenous proteins [13]. Considering low sensitivity of ^{13}C CP/MAS NMR and satisfactory appearance of the protein peaks it can be concluded that the content of the organic matrix is significant even in AC and AS, in contrast to the producer information on those products.

Furthermore, the ^{13}C CP/MAS NMR experiments were capable of detecting carbonates from apatite present in all three xenogeneic materials. The broad organic carbonyl signals from those biomaterials, observed at ca. 174 ppm (Figure 2S in Supplementary Materials), contain on their low-frequency slopes clear-cut features at ca. 170 and 168 ppm from inorganic carbonates [14]. They can be tentatively assigned to carbonates of type B and A, respectively. Of course, those resonances are absent in the collagen spectrum.

^{31}P MAS NMR spectra of apatites generally contain a single peak at 3.1 ± 0.2 ppm [11] and so do the spectra of the studied biomaterials. Under fast MAS at 30 kHz it is possible to note signal asymmetry caused by a small peak at 1.2 ppm, better disclosed by line fitting (Figure 3S in Electronic Supplementary Materials). According to the literature, this weak signal can be attributed to the HPO_4^{2-} ions or specific $\equiv PO_xH$ groups located on the crystal surface [11,15,16] (the symbol $\equiv$ designates embedding in the crystal surface). The amounts of phosphorus, incorporated in the acidic phosphate species were estimated, from the areas of the corresponding fitted peaks: 13.8, 8.2 and 5.3% in AS, AC and GO, respectively. Thus, the apatite mineral of Apatos Spongiosa is the richest in the acidic phosphate constituents residing on the crystal surface.

Specific surface areas (SSA) of apatites in the studied biomaterials could not have been determined by the standard method based on gas adsorption (BET). The obstacle to the BET measurement was the presence of a substantial amount of organic matrix. Therefore, as in our previous work [11], the SSA values were estimated by comparison of the ^{31}P CP and BD linewidths (FWHM), measured at MAS of 7.5 kHz. For AS, AC and GO we got SSA of ca. 100 $m^2\,g^{-1}$, quite similar to that of bone (ca. 94 $m^2\,g^{-1}$ [11]).

More information on the structure of the studied materials could be provided by ^{1}H MAS NMR. In the AS, AC and GO spectra (Fig. 3), there are broad massive signals from water at ca. 5 ppm and sharper peaks between 0.2 and 2.0 ppm, mainly from the organic matrix. The latter region has been assigned by comparison to the collagen and CHA spectra, considering that the total carbonate content in apatites of AS, AC and GO was only ca. 5 wt.% (Figure 4S and Table 2S in Supplementary Materials). The most interesting is the seeming absence of a peak at ca. 0.0 ppm from the structural hydroxyl groups of apatite (Fig. 3), while such peak is clearly visible at 0.12 ppm for CHA (Figure 4S in Supplementary Materials). Closer inspection of the spectra in Fig. 3 reveals a weak hump at ca. 0 ppm, the best discernible for AC, worse for AS and nearly invisible for GO. Unfortunately, such weak appearance of the resonance from the structural hydroxyl groups rendered their estimation impossible using regular proton MAS NMR.

Thus, either the analyzed biomaterials were deficient in the structural hydroxyl groups or the organic matrix interfered with their detection. The problem was reminiscent of that for bone

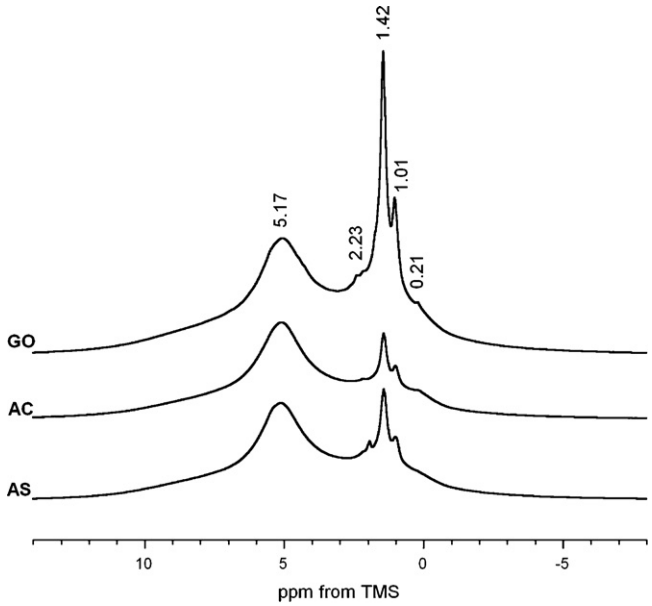

Fig. 3. Proton BD/MAS NMR spectra of the studied biomaterials.

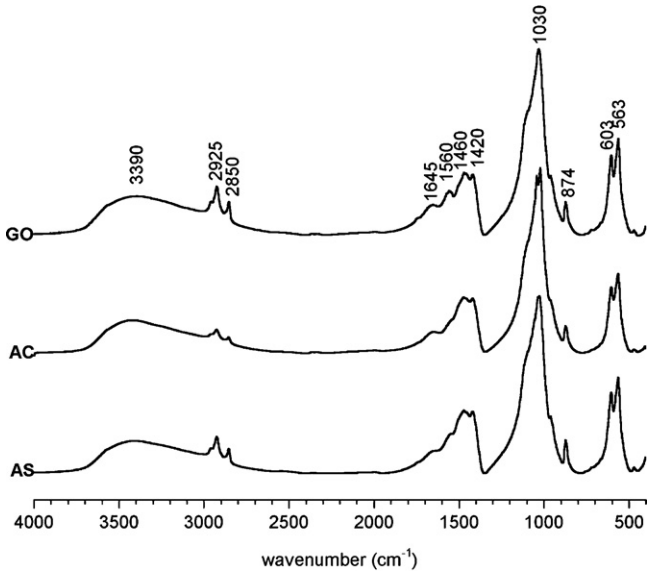

Fig. 5. FT-IR transmission spectra of the studied biomaterials.

[17], so to solve it, an unconventional, inverse cross-polarization from phosphorus-31 to protons was used. A profound discussion of this method was presented in our previous work [10]. A typical $^{31}P \rightarrow {}^{1}H$ CP/MAS NMR spectrum recorded in the present work (Fig. 4) consists of 0.1 and 5.1 ppm peaks from structural hydroxyl groups and adsorbed water, respectively. Now, the hydroxyl peak is very well exposed and resolved, because organic peaks have been suppressed. The mineral content, necessary for the counting of the structural hydroxyl groups, was determined using TGA. Considering the mineral content, sample weight in the NMR rotor and the hydroxyl peak area, contents of the structural hydroxyl groups were calculated. The results are 20, 24 and 25% of the apatitic stoichiometric value for GO, AC and AS, respectively. Those amounts are quite close to 21% determined by Cho et al. for unprocessed bone [18]. It is noteworthy, that the deconvolution of the water signal has revealed an extra line at ca. 7.7 ppm, which can be assigned to moderately acidic P–OH groups.

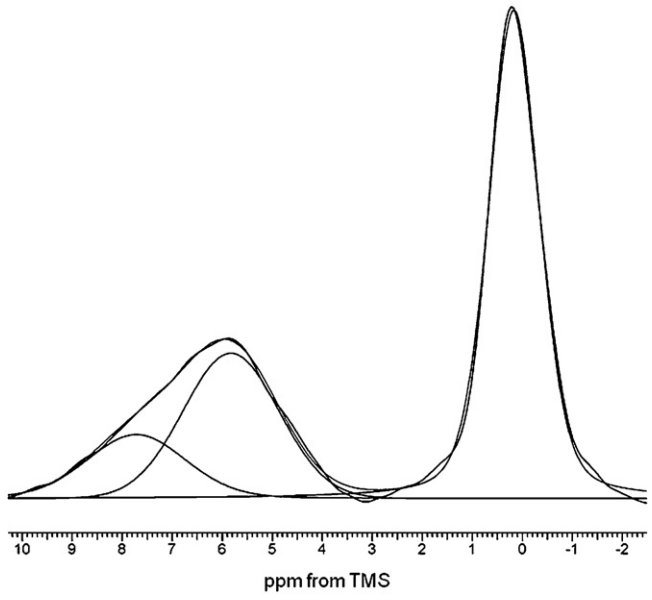

Fig. 4. A representative $^{31}P \rightarrow {}^{1}H$ CP/MAS NMR spectrum of the studied biomaterials recorded for AS and deconvoluted into three lines from structural hydroxyl groups, adsorbed water and surface P–OH groups at 0.1, 5.7 and 7.7 ppm, respectively.

3.3. FT-IR spectroscopy

All the IR spectra (Fig. 5) were recorded in the typical, transmission mode. In the spectra of the studied biomaterials, bands from both the mineral part and the organic matrix were found [19–28]. There are prominent phosphate ($\nu_1 + \nu_3$) and ν_4 bands in the 900–1200 and 480–700 cm^{-1} regions, respectively. A broad 2800–3800 cm^{-1} band observed in all the spectra originates from water and the organic matrix (amide A and B bands). The AS, AC and GO spectra are devoid of a characteristic band at 3570 cm^{-1} from the structural hydroxyl groups of apatite. Besides, this band is not revealed in the CHA spectrum (Figure 5S in Supplementary Materials). The bands at 2925 and 2850 cm^{-1} from CH_3 and CH_2 groups, respectively, are prominent, so the presence of the organic matrix in AS, AC and GO is beyond dispute (Fig. 5). This observation is in accordance with the formerly presented conclusions of our NMR analysis. By visual inspection of those bands it is feasible to appraise the studied biomaterials by order of their organic contents in: GO > AS > AC. This order is in agreement with the TGA results.

Analysis of the 1700–1300 cm^{-1} region is not trivial. Serious problems are with the water bending band at 1645 cm^{-1}, which is superimposed on the amide I band from proteins, and with the carbonate ν_3 bands, which coincide with other protein bands. However, for the carbonate analysis, the collagen spectrum was subtracted from the spectra of the studied materials (see Figure 6S and Table 2S in Supplementary Material). Then, it was possible to estimate carbonates of type A and B using a method described by Clasen and Ruyter [23]. The respective values are equal to ca. 1 and 4 wt.%. Those results are no more than rough estimates because of the aforementioned subtraction of the collagen spectrum. After all, they are in accordance with the average total carbonate concentration in human bone mineral [17].

In order to precisely examine carbonates present in the apatite of the studied biomaterials, curve fittings of the carbonate ν_2 region from 840 to 890 cm^{-1} have been done (Fig. 6, Table 3). The bands were assigned according to the literature [19,21–23]. Absorption coefficients of those bands are unknown, so the following discussion will be limited to qualitative comparisons. Thus,

Table 3
Curve fitting results for the ν_2-CO_3^{2-} domain and the accompanying HPO_4^{2-} band. Band positions are given in wavenumbers (cm^{-1}). Carbonate band areas denote their contributions to the total domain area, given in percent. Areas of the HPO_4^{2-} bands at ca. 856 cm^{-1} were divided by the total area of the corresponding ν_4-phosphate region and expressed in percent.

AC		AS		GO		CHA		Assignment
Position	Area	Position	Area	Position	Area	Position	Area	
ν_2 bands of CO_3^{2-} ions								
883.7	4.6	883.0	6.6	882.2	8.5	–	0.0	Carbonates from the crystal surface
878.4	27.6	878.6	25.3	878.5	21.4	878.4	30.4	A1-type carbonates
872.4	30.8	872.4	35.3	872.5	35.7	872.5	34.0	B-type carbonates
867.1	20.9	867.1	20.3	867.3	21.5	866.9	15.9	Labile carbonates
862.0	16.1	862.0	12.5	862.1	12.9	862.6	19.7	A2-type carbonates
HPO_4^{2-} ions								
855.5	0.688	856.0	0.837	855.8	0.472	854.9	0.165	HPO_4^{2-} ions from the crystal surface

Table 4
Curve fitting results for the ν_4-PO_4^{3-} domain and the accompanying librational bands from water and hydroxyl groups. Band positions are given in wavenumbers (cm^{-1}). Phosphate band areas denote their contributions to the total domain area, given in percent. Areas of the OH^- bands at ca. 632 cm^{-1} and of the water bands at ca. 670 cm^{-1} were divided by the total area of the corresponding phosphate ν_4 region and expressed in percent.

AC		AS		GO		CHA		Assignment
Position	Area	Position	Area	Position	Area	Position	Area	
ν_4 bands of PO_4^{3-} ions								
612.6	12.9	617.3	9.6	617.0	10.6	612.3	14.6	Labile PO_4^{3-} environment
601.6	25.5	601.9	24.1	602.1	23.2	602.3	25.6	Regular apatitic PO_4^{3-} environment
581.2	7.0	582.5	8.0	582.8	6.0	582.5	10.6	Regular apatitic PO_4^{3-}
564.5	25.6	565.0	28.0	565.2	27.7	565.0	29.0	Regular apatitic PO_4^{3-}
551.2	29.0	550.0	30.3	550.1	32.5	550.0	20.1	HPO_4^{2-} ions buried in the crystal lattice
OH^- ions								
631.9	10.4	632.0	14.9	634.2	10.3	631.0	13.7	OH^-, librational mode
Water								
670.0	1.9	670.0	1.9	667.8	2.3	670.1	0.7	Water, librational mode

considering areas of the peak at 872.5 cm^{-1}, the contents of the B-type carbonates, which replace phosphate ions, can be reported in the following order: AC < AS ≈ GO. Carbonates of type A substitute structural hydroxyl groups occupying apatite channels. They have two subtypes, A1 and A2, differing by their arrangement against the crystallographic *c*-axis and giving bands at ca. 878.5 and 862.2 cm^{-1}, respectively [19,22]. Considering areas of those bands, one can report contents of both carbonate A subtypes in the series: AC > AS ≈ GO. Then, labile carbonates (presumably located in a hydrated layer on the crystal surface) can be evaluated on the basis of the band at 867 cm^{-1}. Their contents were found similar in all three biomaterials.

Finally, the 855 cm^{-1} band from the HPO_4^{2-} ions on the crystal surface indicates the following concentration sequence: AS > AC > GO. The latter series is in agreement with our former NMR results.

Information on the apatite phosphates is easier to obtain from the analysis of the ν_4-PO_4^{3-} domain than the ($\nu_1 + \nu_3$)-PO_4^{3-} domain. In fact, curve fitting in the former region is simpler than in the latter. The ν_4 phosphate bands in the 480–700 cm^{-1} region (Fig. 7) were analyzed using assignments given in former works [20,25–28]. As before, the evaluation is only approximate. Looking at the PO_4^{3-} and HPO_4^{2-} band areas reported in Table 4, one comes to the conclusion that their contributions to the total phosphate ν_4-region are very similar for all the studied biomaterials. In particular, this is true for regular apatitic PO_4^{3-} environment and for labile phosphates, probably located in the surface hydrated layer.

The IR analysis of the 480–700 spectral region provides also information (Table 4) on structural hydroxyl groups (a band at ca. 632 cm^{-1}) and water (a band at 670 cm^{-1}). One gets the following concentration series: AS > AC ≈ GO for structural hydroxyl groups and GO > AC ≈ AS for water. The discussed sequences are slightly different than those expected from the TGA measurements,

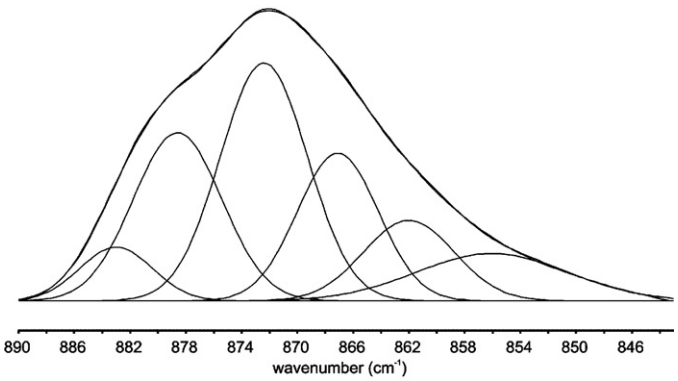

Fig. 6. Curve fitting for the carbonate ν_2 bands of AC.

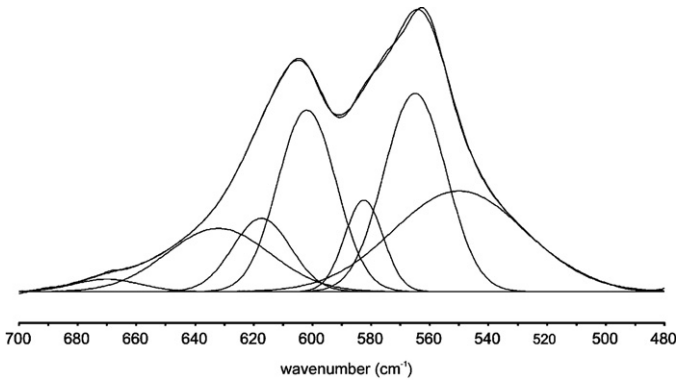

Fig. 7. Curve fitting for the phosphate ν_4 bands of AC.

because of the specificity of the respective librational bands. However, it has been confirmed that AS and GO contain the largest amounts of structural hydroxyl groups and water, respectively.

4. Conclusions

In the present work XRD, TGA, ssNMR and FT-IR were applied to study the chemical structure and composition of popular commercial xenogeneic biomaterials (GO, AS and AC), produced from porcine bone and used as bone substitutes.

The highest levels of water, organic matrix and apatite mineral were found in GO, AS and AC, respectively. The lowest levels of water, organic matrix and apatite mineral were found in AC, AS and GO, respectively.

All the studied biomaterials contained organic matrix composed mainly of collagenous proteins but with the amino acid composition different than that in pure collagen type I. Apparently, the manufacturing process has affected the protein structure, which existed in raw bone. Furthermore, amino acid compositions of the AS and AC proteins were different from those of GO.

All three biomaterials contained nanocrystalline apatites with mean crystal sizes and specific surfaces areas (SSA) similar to those in bone mineral. The apatite mineral of the studied biomaterials was deficient in structural hydroxyl groups, practically to the same degree as that of bone. It contained ca. 1 and 4 wt.% of A-type and B-type carbonates, respectively, so should be classified as carbonated apatite of mixed type AB. The studied biomaterials had similar concentrations of labile carbonates, located in the hydrated layer on the apatite crystal surface. The apatite mineral of the studied biomaterials contained HPO_4^{2-} ions embedded in the crystal surface (similar fractions) and apatitic HPO_4^{2-} ions, buried in the crystal lattice (AS > AC > GO). Generally, the acidic phosphates in the apatite mineral exhibited moderate acidity.

It was shown that solid-state NMR and FT-IR spectroscopies, applied together and accompanied by elaborate curve fitting analysis, provide valuable information on xenogeneic biomaterials.

Acknowledgment

The Medical University of Warsaw is acknowledged for financial support (FW-23/N/2011).

Appendix A. Supplementary data

Supplementary data associated with this article can be found, in the online version, at doi:10.1016/j.jpba.2011.11.008.

References

[1] Ch. Tudor, S. Srour, M. Thorwarth, P. Stockmann, F.W. Neukam, E. Nkenke, K.A. Schlegel, E. Felszeghy, Bone regeneration in osseous defects—application of particulated human and bovine materials, Oral Surg. Oral Med. Oral Pathol. Oral Radiol. Endod. 105 (2008) 430–436.
[2] U. Nannmark, L. Sennerby, The bone tissue responses to prehydrated and collagenated cortico-cancellous porcine bone grafts: a study in rabbit maxillary defects, Clin. Implant Dent. Relat. Res. 10 (2008) 264–270.
[3] J.C. Elliott, Structure and Chemistry of the Apatites and Other Calcium Orthophosphates, Elsevier, Amsterdam, 1994.
[4] Ch. Rey, C. Combes, C. Drouet, H. Sfihi, Chemical Diversity of Apatites, Adv. Sci. Technol. 49 (2006) 27–36.
[5] M. Figueiredo, J. Henriques, G. Martins, F. Guerra, F. Judas, H. Figueiredo, Physicochemical characterization of biomaterials commonly used in dentistry as bone substitutes—comparison with human bone, J. Biomed. Mater. Res. B 92 (2010) 409–419.
[6] D. Tadic, M. Epple, A thorough physiochemical characterization of 14 calcium phosphate-based bone substitution materials in comparison to natural bone, Biomaterials 25 (2004) 987–994.
[7] G.A. da Cruz, S. de Toledo, E.A. Sallum, A.F.M. de Lima, Morphological and chemical analysis of bone substitutes by scanning electron microscopy and microanalysis by spectroscopy of dispersion energy, Braz. Dent. J. 18 (2007) 129–133.
[8] T. Accorsi-Mendonça, M.B. Conz, T.C. Barros, L.A. de Sena, G. de Almeida Soares, J.M. Granjeiro, Physicochemical characterization of two deproteinized bovine xenografts, Braz. Oral Res. 22 (2008) 5–10.
[9] A. Ślósarczyk, Z. Paszkiewicz, Cz. Paluszkiewicz, FTIR and XRD evaluation of carbonated hydroxyapatite powders synthesized by wet methods, J. Mol. Struct. 744–747 (2005) 657–661.
[10] J. Kolmas, W. Kolodziejski, Concentration of hydroxyl groups in dental apatites: a solid-state ^{1}H MAS NMR study using inverse $^{31}P \rightarrow {}^1H$ cross-polarization, Chem. Commun. (2007) 4390–4392.
[11] J. Kolmas, A. Ślósarczyk, A. Wojtowicz, W. Kolodziejski, Estimation of the specific surface area of apatites in human mineralized tissues using ^{31}P MAS NMR, Solid State NMR 32 (2007) 53–58.
[12] S.V. Dorozhkin, Nanosized and nanocrystalline calcium orthophosphates, Acta Biomater. 6 (2010) 715–734.
[13] D. Huster, Solid-state NMR studies of collagen structure and dynamics in isolated fibrils and in biological tissues, Ann. Rep. NMR Spectrosc. 64 (2008) 127–159.
[14] K. Beshah, C. Rey, M.J. Glimcher, M. Shimizu, R.G. Griffin, Solid state carbon-13 and proton NMR studies of carbonate-containing calcium phosphates and enamel, J. Solid State Chem. 85 (1990) 71–81.
[15] M. Jarlbring, D.E. Sandström, O.N. Antzutkin, W. Forsling, Characterization of active phosphorus surface sites at synthetic carbonate-free fluorapatite using single-pulse ^{1}H, ^{31}P, and ^{31}P CP MAS NMR, Langmuir 22 (2006) 4787–4792.
[16] Y. Wu, M.J. Glimcher, C. Rey, J.L. Ackerman, A unique protonated phosphate group in bone mineral not present in synthetic phosphates: identification by phosphorus-31 solid state NMR spectroscopy, J. Mol. Biol. 244 (1994) 423–435.
[17] W. Kolodziejski, Solid-state NMR of bone, Top. Curr. Chem. 246 (2005) 235–270.
[18] G. Cho, Y. Wu, J.L. Ackerman, Detection of hydroxyl ions in bone mineral by solid-state NMR spectroscopy, Science 300 (2003) 1123–1127.
[19] A. Kaflak, A. Ślosarczyk, W. Kolodziejski, A comparative study of carbonate bands from nanocrystalline carbonated hydroxyapatites using FT-IR spectroscopy in the transmission and photoacoustic modes, J. Mol. Struct. 997 (2011) 7–14.
[20] A. Kaflak, W. Kolodziejski, Complementary information of water and hydroxyl groups in nanocrystalline carbonated hydroxyapatites from TGA, NMR and IR measurements, J. Mol. Struct. 990 (2011) 263–270.
[21] Ch. Rey, B. Collins, T. Goehl, I.R. Dickson, M.J. Glimcher, The carbonate environment in bone mineral, a resolution-enhanced Fourier transform infrared spectroscopy study, Calcif. Tissue Int. 45 (1989) 157–164.
[22] M.E. Fleet, Y. Xiaoyang, P.L. King, Accommodation of the carbonate ion in apatite: an FTIR and X-ray structure study of crystals synthesized at 2–4 GPa, Am. Mineral. 89 (2004) 1422–1432.
[23] A.B.S. Clasen, I.E. Ruyter, Quantitative determination of type A and type B carbonate in human deciduous and permanent enamel by means of Fourier transform infrared spectrometry, Adv. Dent. Res. 11 (1997) 523–527.
[24] K. Belbachir, R. Noreen, G. Gouspillou, C. Petibois, Collagen types analysis and differentiation by FTIR spectroscopy, Anal. Bioanal. Chem. 395 (2009) 829–837.
[25] D. Magne, P. Weiss, J.-M. Bouler, O. Laboux, G. Daclusi, Study of the maturation of the organic (type I collagen) and mineral (nonstoichiometric apatite) constituents of a calcified tissue (dentin) as a function of location: a Fourier transform infrared microspectroscopic investigation, J. Bone Miner. Res. 16 (2001) 750–756.
[26] D. Eichert, C. Drouet, H. Sfihi, C. Rey, C. Combes, Nanocrystalline Apatite-based Biomaterials, Nova Science Publishers, Inc., New York, 2009.
[27] L.M. Miller, V. Vairavamurthy, M.R. Chance, R. Mendelsohn, E.P. Paschalis, F. Betts, A.L. Boskey, In situ analysis of minerals content and crystallinity in bone using infrared micro-spectroscopy of the ν_4 PO_4^{3-} vibration, Biochim. Biophys. Acta 1527 (2001) 11–19.
[28] Ch. Rey, M. Shimizu, B. Collins, M.J. Glimcher, Resolution enhanced FT-IR spectroscopy study of the environment of phosphate ions in the early deposits of a solid phase of calcium-phosphate in bone and enamel, and their evolution with age. I. Investigation in the ν_4 PO_4 domain, Calcif. Tissue Int. 46 (1990) 384–394.

Journal of Pharmaceutical and Biomedical Analysis 61 (2012) 142–149

Contents lists available at SciVerse ScienceDirect

Journal of Pharmaceutical and Biomedical Analysis

journal homepage: www.elsevier.com/locate/jpba

Chromatographic fingerprint analysis of yohimbe bark and related dietary supplements using UHPLC/UV/MS

Jianghao Sun, Pei Chen*

U.S. Department of Agriculture, Agricultural Research Service, Beltsville Human Nutrition Research Center, Food Composition and Methods Development Laboratory, Beltsville, MD, USA

ARTICLE INFO

Article history:
Received 30 August 2011
Received in revised form 9 November 2011
Accepted 11 November 2011
Available online 20 November 2011

Keywords:
Fingerprint
UHPLC
Yohimbe
Yohimbine
Dietary supplements

ABSTRACT

A practical ultra high-performance liquid chromatography (UHPLC) method was developed for fingerprint analysis of and determination of yohimbine in yohimbe barks and related dietary supplements. Good separation was achieved using a Waters Acquity BEH C_{18} column with gradient elution using 0.1% (v/v) aqueous ammonium hydroxide and 0.1% ammonium hydroxide in methanol as the mobile phases. The study is the first reported chromatographic method that separates corynanthine from yohimbine in yohimbe bark extract. The chromatographic fingerprint analysis was applied to the analysis of 18 yohimbe commercial dietary supplement samples. Quantitation of yohimbine, the traditional method for analysis of yohimbe barks, were also performed to evaluate the results of the fingerprint analysis. Wide variability was observed in fingerprints and yohimbine content among yohimbe dietary supplement samples. For most of the dietary supplements, the yohimbine content was not consistent with the label claims.

© 2011 Published by Elsevier B.V.

1. Introduction

Yohimbine is an active indole alkaloid with sexual stimulant and aphrodisiac effects found naturally in *Pausinystalia yohimbe* (K. Schumann, Yohimbe) [1]. It has been used as a prescription medicine for the treatment of erectile dysfunction in the United States as the hydrochloride form [2]. Commercial dietary supplements of yohimbe bark are widely used as over-the-counter dietary supplements for the treatment of sexual dysfunction and enhancement of sexual satisfaction [3]. Reported side effects for yohimbine are involved in elevated systolic blood pressure and heart rate as well as anxiety, headache, and increased urinary output [4–7]. The main active chemical present in yohimbe bark are indole alkaloids including yohimbine, α-yohimibine, β-yohimbine, ψ-yohimbine, allo-yohimbine, ajmalicine, tetrohydroaltonine, yohimbic acid, corynanthine and some other minor constituents with same skeleton but different substitutional groups [8,1]. Several analytical methods, including thin layer chromatography [9], high performance liquid chromatography [2,10], non-aqueous capillary electrophoresis [11], and high performance liquid chromatography tandem mass spectrometry [8,12] have been reported for the analysis of yohimbine in barks, dietary supplements, and bio-fluids. However, the methods reported to date are suitable for analysis of yohimbine in pharmaceutical preparations, they are not appropriate for the analysis of yohimbine barks or dietary supplements based on yohimbine barks due to the fact that these methods cannot resolve the yohimbine peak from the corynanthine peak in their chromatograms. The structures of yohimbine and corynanthine are shown in Fig. 1. Corynanthine not only has the same mass as yohimbine, its fragmentation pathway is also the same as yohimbine [8,10]. Thus, neither selected ion monitoring (SIM), selected reaction monitoring (SRM), multiple reaction monitoring (MRM), nor isotope-dilution mass spectrometry can differentiate between the two. All previous reports measured the combined peaks of yohimbine and corynanthine from yohimbe bark extract as the yohimbine peak, either knowingly or unknowingly [10]. In addition, these methods were either not fully compatible with mass spectrometry due to the use of triethylamine (2 mM) [10], hexanesulphonic acid (2.5 mM) [13], or phosphate buffer (39 mM) [13] and/or used toxic reagents [10] (chloroform and triethylamine).

For pharmaceutical preparations, targeted analysis, such as quantitation of yohimbine, is enough for quality assessment. For complex botanicals, such as yohimbe bark extracts, quantitation of a single or selected targeted compound usually does not provide the whole picture. For this reason, the chromatographic fingerprint technology was accepted by the WHO as a strategy for identification and quality evaluation of herbal medicines in 1991 [14].

In the presented work, an ultra high-performance liquid chromatography (UHPLC) method has been developed for qualitative (fingerprinting) and quantitative (yohimbine) analysis of yohimbe bark and related dietary supplements. The method is fully compatible with mass spectrometry and shows superiority in resolution,

* Corresponding author. Tel.: +1 301 504 8144; fax: +1 301 504 8314.
E-mail address: pei.chen@ars.usda.gov (P. Chen).

0731-7085/$ – see front matter © 2011 Published by Elsevier B.V.
doi:10.1016/j.jpba.2011.11.013

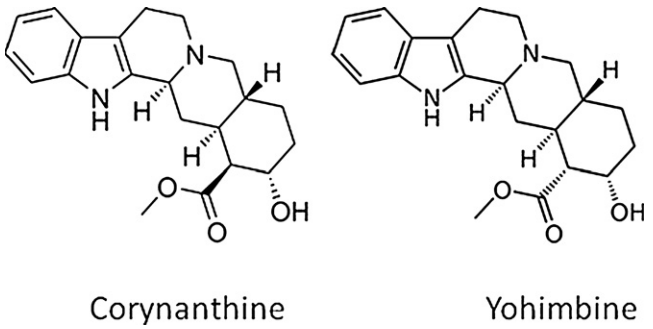

Fig. 1. The structures of corynanthine and yohimbine.

analytical time, and solvent consumption compared to previously reported methods. It is the first reported LC/UV/MS method that is capable of resolving corynanthine from yohimbine in yohimbe bark extracts. The method was successfully applied to the analysis of yohimbine in two yohimbe barks and 18 dietary supplements samples.

2. Experimental

2.1. Chemicals and reagents

Water, acetonitrile, methanol, and ammonium hydroxide (Assay 20–22% as NH_3) of Optima grade were purchased from Fisher Scientific (Pittsburgh, PA, USA). Formic acid of mass spectrometry grade was purchased from Sigma–Aldrich (St. Louis, MO, USA). Yohimbine hydrochloride was obtained from Sigma (purity > 98%, St. Louis, MO, USA). Corynanthine, α-yohimbine, yohimbic acid, ajmalincine and tetrohydroaltonine were purchased from ChromaDex (Irvine, CA, USA). All chemicals were stored in the refrigerator as required to ensure stability.

2.2. Standards solution

The yohimbine standard was accurately weighed and then dissolved in an appropriate volume of 1% NH_4OH–methanol to produce corresponding stock solutions. The working standard solution of yohimbine for the calibration curve was prepared by serial dilution of the stock solution with methanol in six concentration increments ranging from 0.11 to 214 μg/mL. Quality control (QC) samples were prepared from the stock solutions at 85.7 μg/mL, 21.4 μg/mL, and 10.7 μg/mL. All stock and working solutions were maintained at −20 °C.

2.3. Yohimbe bark samples and commercial dietary supplements

Authentic yohimbe (*Pausinystalia johimbe*) bark was purchased from American Herbal Pharmacopoeia (AHP, Certificate #374). Eighteen yohimbe dietary supplements were purchased from local stores and the internet. Five dietary supplements are in tablet form, seven are in capsule form, and six are in liquid form.

2.4. Chromatographic and mass spectrometric conditions

Samples were analyzed on an Agilent 1200 HPLC rapid resolution HPLC system (Agilent Technologies, Palo Alto, CA) consisting of a binary pump with a vacuum degasser, a thermostatted column compartment, a temperature-controlled well plate autosampler, and a diode array detector (DAD). A Waters Acquity BEH C_{18} (Waters Corporation, Milford, MA, USA, 1.7 μm particle size, 100 mm × 2.0 mm) UPLC reversed-phase column, in combination with an in-line column filter (Analytical Scientific Instruments, El Sobrante, CA), was used for the separation. Chromatographic separation was achieved using a gradient elution system consisting of (A) 0.1% NH_4OH in water (v/v) and (B) 0.1% NH_4OH in methanol (v/v). A gradient elution program was employed as follows: 20–35% B at 0–15 min, 35–65% B at 15–30 min, 65–70% B at 30–45 min, and then to 95% B at 50 min with a flow rate of 0.3 mL/min. The post-run time for re-equilibrating the system was set for 7 min. The DAD was set at 280 nm with a band width of 16 nm. The UV spectra were continuously recorded from 190 to 400 nm.

MS analysis was performed on an Orbitrap-XL high resolution mass spectrometer (Thermo Fisher Scientific Inc., Waltham, MA), equipped with electrospray ionization source; the interface was operated in positive ion mode over the range of m/z 100–700. The following conditions were used: sheath gas flow rate, 80 arb. units; aux gas flow rate, 10 arb. units; spray voltage, 4.50 kV; heated capillary temperature, 220 °C; capillary voltage, 34 V; tube lens offset, 25 V. The normalized collision energy was 30% for the MS/MS scan.

2.5. Sample preparation

Yohimbe bark samples were ground into fine powders using an IKA A11 grinder (IKA® Works, Inc., Wilmington, NC) with a knife blade. The contents of capsules of commercial dietary supplement samples were emptied into a bottle and thoroughly mixed. Tablets of commercial dietary supplement samples were ground into fine powders using a Retsch RM100 grinder (Retsch Inc., Newtown, PA). All the samples were passed through a 60-mesh sieve. Fifty mg of yohimbe bark or portions equivalent to 50 mg of yohimbe bark of each commercial sample (according to their labels) were carefully weighed into 15 mL centrifuge tubes and were moistened with 1 mL NH_4OH (20–22%). Ten milliliter MeOH then was added and sonicated for 20 min, and then centrifuged for 5 min at 5000 rpm. The supernatant was filtered through a 0.20 μm PVDF syringe filter (VWR Scientific, Seattle, WA). For liquid samples, the samples were diluted 10 times with methanol–water–concentrated ammonium hydroxide (60:40:1, v/v/v) and filtered. The injection volume for HPLC analysis is 2 μL.

2.6. Method evaluation

The limits of detection (LOD) and quantitation (LOQ) were defined as the lowest concentrations of analytes in a sample that can be detected and quantified. These LOD and LOQ limits were determined on the basis of signal-to-noise ratios (S/N) of 3:1 and 10:1, respectively. The precision was evaluated by intra-day and inter-day percent relative standard deviation % (RSD). The intra-day and inter-day variability was evaluated by analyzing QC samples at three different concentration levels (estimated at 5.36 μg/mL, 21.42 μg/mL, and 85.68 μg/mL). The intra-day precision and accuracy was calculated by analyzing QC samples in six replicates at each concentration. The analyses for calculation of inter-day precision were performed in each concentration for five consecutive days.

2.7. Fingerprint and chemometric analysis

Characteristic peaks chromatographic fingerprinting (CPCF) was used in this study. The CPCF approach initially selects the chromatogram of an authentic sample as the reference fingerprint (RF, in this study, yohimbe bark from AHP was used). The most obvious or characteristic peak of the RF was selected as the reference peak (RP, the yohimbine peak in this case). The areas of all other peaks in the chromatogram were normalized against the area of the RP and the ratios of the peaks are entered into a peak table. Then chromatograms from each sample were compared to the RF one-by-one and the corresponding peaks are entered into the peak table. After

all chromatograms are entered, the peak table is used for PCA analysis. The detailed process has been discussed previously [15,16]. The final peak table is imported into Solo (Eigenvector Research, Inc., Wenatchee, WA) for chemometric analysis. Normalize (2-Norm, length = 1) and mean center were used for data reprocessing before principal component analysis (PCA) was performed.

3. Results and discussion

3.1. Investigation of extraction solvents

The extraction solvents were optimized according to the extraction efficiency of yohimbine. Five solvent systems, methanol/NH_4OH (99:1), methanol/HCOOH (99:1), methanol/H_2O/HCOOH (60:40:1), ethanol/NH_4OH (99:1), and chloroform/NH_4OH (99:1) were investigated with the sonication at room temperature for 1 h and compared with the reference extraction method (chloroform + triethylamine) described by Zanolari et al. [10]. The methanol/NH_4OH system was proved to be superior to the reference extraction method (supplemental Fig. A). Especially when environmental factors were considered. Therefore, methanol/NH_4OH was selected as the extraction solvent. The optimal extraction time for methanol was also investigated. The yohimbe bark powder (50 mg) was moistened with ammonium hydroxide then extracted with methanol for 10, 20, 30, and 60 min, respectively. Yohimbine was almost completely extracted within 20 min (supplemental Fig. B).

3.2. Chromatography and selectivity

One goal of this study was to develop a UHPLC/UV method that was fully compatible with mass spectrometry with solvents that were less toxic and more environment-friendly compared to previously reported methods. Therefore, NH_4OH was selected as the mobile phase modifier with a final pH of the mobile phase at 10.5 after optimization compared to triethylamine [10] (more toxic) or phosphate buffer [13] (not compatible with MS) used in other methods. A few columns (Agilent Extend C_{18}, Zirchrom PBD C_{18}, and Waters Xterra C_{18}) were screened before Waters Acquity BEH C_{18} column (2.0 mm × 100 mm, 1.7 μm) was finally selected as the column of choice. Initially, good separation appeared to be achieved for yohimbine from the adjacent isomers at 10.3 min (Fig. 2A) with ACN as mobile phase B. However, when we tried to identify corynanthine, α-yohimbine, yohimbic acid, ajmalincine, and tetrohydroaltonine using standards, corynanthine was found co-eluting with yohimbine (Fig. 2B). Despite our best efforts, corynanthine cannot be separated from yohimbine if ACN was used as mobile phase B even with an optimized and longer gradient (Fig. 2C). In the end, a combination of MeOH as mobile phase B and a longer gradient elution achieved the separation. Column temperature was set at 60 °C. The maximum column pressure during the analysis was always below 500 Bar at the flow rate of 0.3 mL/min. It allowed the use of the Agilent 1200 Rapid Resolution HPLC (600 bar maximum) for the analysis. If a higher pressure LC system, such as Waters Acquity or Agilent 1290 system is available, a 0.5 mL/min flow rate can be used to have a shorter analysis time and probably even better resolution. The developed method gave good separation for all the indole alkaloids in yohimbe bark extract (Fig. 3) and their identification is listed in Table 1.

A UV or DAD detector is sensitive enough for quantify yohimbine in the extracts of yohimbe barks and related dietary supplements. Due to the numerous isomeric indole alkaloids existing in the extracts of yohimbe barks and related dietary supplements, the advantage of the specificity provided by a MS is very limited, unless the sample is contaminated or mixed with other interfering materials. Therefore, the mass spectrometer was only used in the initial method development to confirm the identities of yohimbine and some of other indole alkaloids, to compare the MS fragmentations of yohimbine and corynanthine and to prove the method is fully compatible with MS should the need arise.

3.3. Fingerprint analysis of yohimbe bark and related dietary supplements

Although the quantitation result can confirm the yohimbine content in a sample, there is no way to know how similar a commercial dietary supplement sample is to a raw plant material by quantitation of a single component. Fingerprinting and chemometric analysis, on the other hand, can show the chemical similarities between commercial dietary supplements and the reference plant material. Both mass spectroscopic and chromatographic fingerprints have been successfully used for quality assessment of botanicals in previous studies [15–18]. Due to the large amount of isomeric indole alkaloids existing in the yohimbe bark extract, MS fingerprinting was not appropriate for this study since many isomers would show up as a single entity in a mass spectral fingerprint. Thus, chromatographic fingerprinting was used.

There are basically two sources of variation contained in chromatographic fingerprints. One comes from the experimental process, and the other from the samples themselves. The main variations arising from the experimental process are retention time shifts that make the comparison of fingerprints acquired from different systems or at different times difficult for PCA analysis. A retention time alignment step is usually needed for the PCA to be successful. Despite efforts from various studies, computerized peak alignment programs have had only limited success, as discussed in a previous study [15]. The biggest advantage of the characteristic peak fingerprinting approach is that it is nearly fool-proof, as the retention time shifts introduced by the instruments and other experimental conditions (fluctuation of the temperatures, the reagents used, the columns, etc.) can be minimized. The peaks entered into the characteristic table are listed in Table 1.

Principal Components Analysis (PCA) was used to process the chromatographic fingerprints generated. PCA is an unsupervised mathematical procedure that transforms a number of possibly correlated variables into a smaller number of uncorrelated variables called principal components. Its operation can be thought of as revealing the internal structure of the data in a way which best explains the variance in the data.

For the commercial yohimbe bark dietary supplements investigated, the yohimbine and other contents of quite a few samples were very low. These samples were excused from the fingerprinting analysis. Of the remaining samples, most are clustered together with the yohimbe bark plant materials, confirming that they were made from natural yohimbe barks (Fig. 4). Two samples, YS07 and YS09, were outliers.

YS08 is separated from the rest on PC1. The PCA loading for the PC1 indicated peak 8 is mainly responsible for the separation (Fig. 5). What it means is that a higher peak 8 relative to the RS yohimbine will give a higher PC1 score, thus, move the position of the sample to the right of the PCA score plot. The chromatogram of YS07 confirmed its higher peak 8 compared to others (Fig. 6). Careful examination of chromatogram revealed the peak 8 in YS08 had a slight different retention time (27.9 min) compared to yohimbe bark (28.07 min) and YS09 (28.09 min). Although retention time shit of 0.2 min is not unusual between different chromatographic runs, even for the same sample, it is still intriguing enough for further investigation. The m/z for the peak is 286.1432 with a calculated formula $C_{17}H_{19}O_3N$ (−2.13 ppm). Compound search using SciFinder (CAS, Columbus, OH) generated thousands of returns. The label of YS07 indicated BioPerine® (5 mg/serving) was added to the

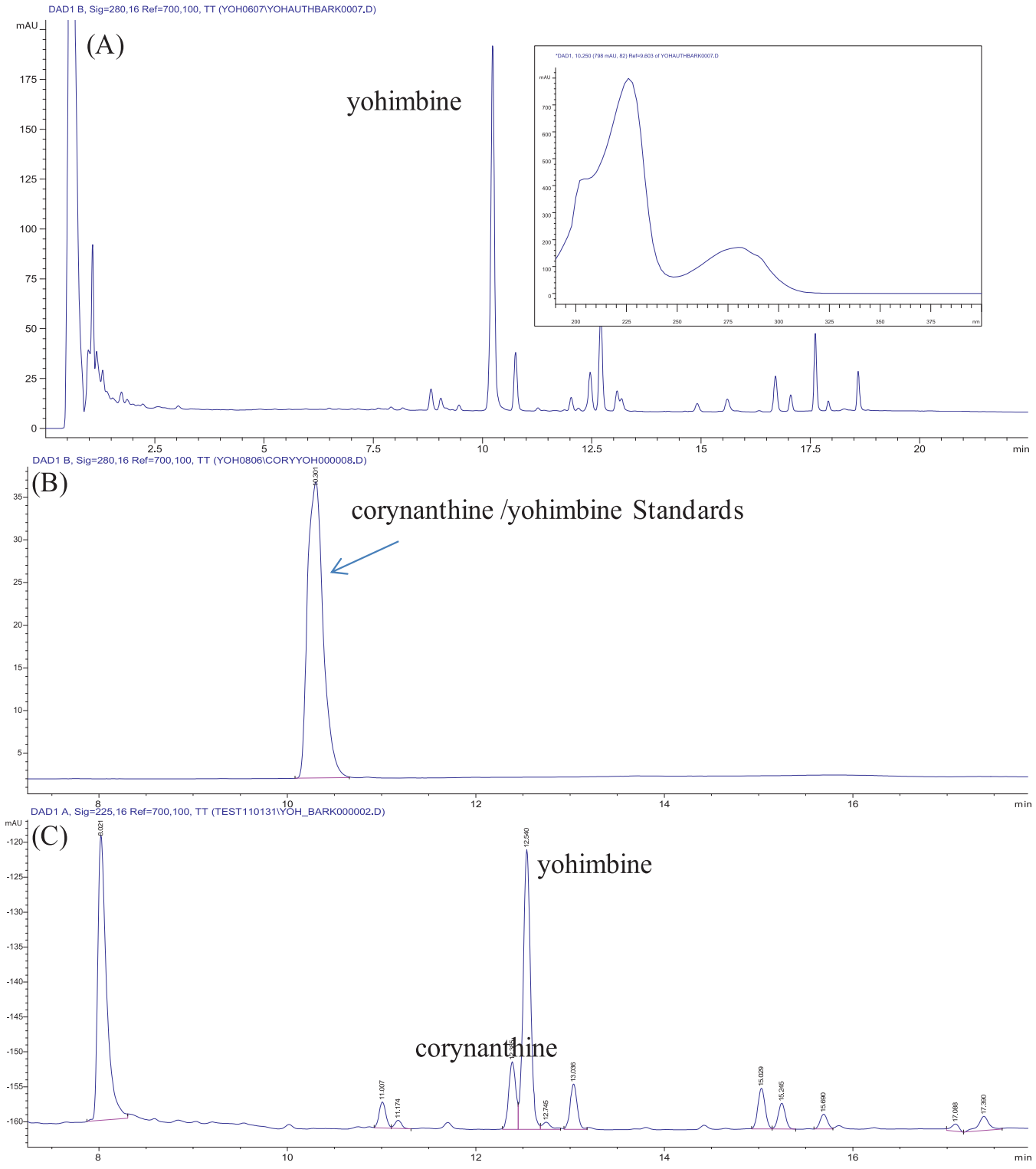

Fig. 2. The separation of yohimbine in yohimbe bark extract using ACN as mobile phase B (UV 280: (A) initial method; (B) segment of co-elution of corynanthine and yohimbine of (A); (C) optimized method).

yohimbe bark extract. BioPerine® is a standardized extract from the fruit of *Piper nigrum* L. (black pepper) or *Piper longum* L. (long pepper) that contains 95 percent of piperine. The MS^2 spectrum of the peak gives a single *m*/*z* at 201, the MS^3 spectrum of the peak (286 > 201) produces 3 major product ions at *m*/*z* 115, 143, and 171 (Fig. 7) that confirms the identity of the peak eluted at 27.9 min is piperine. According to the label, YS07 contains 5 mg BioPerine® and 5 mg of yohimbine per serving (250 mg standardized extracts, 2% yohimbine). The quantitation result showed a yohimbine content of 0.65 mg/serving. Although the CPFP used a wrong peak as peak 8, it still successfully separated YS07 from other yohimbe dietary supplements. With further investigation, it helped to identify the chemical component responsible for the difference between YS07 and the rest of the samples.

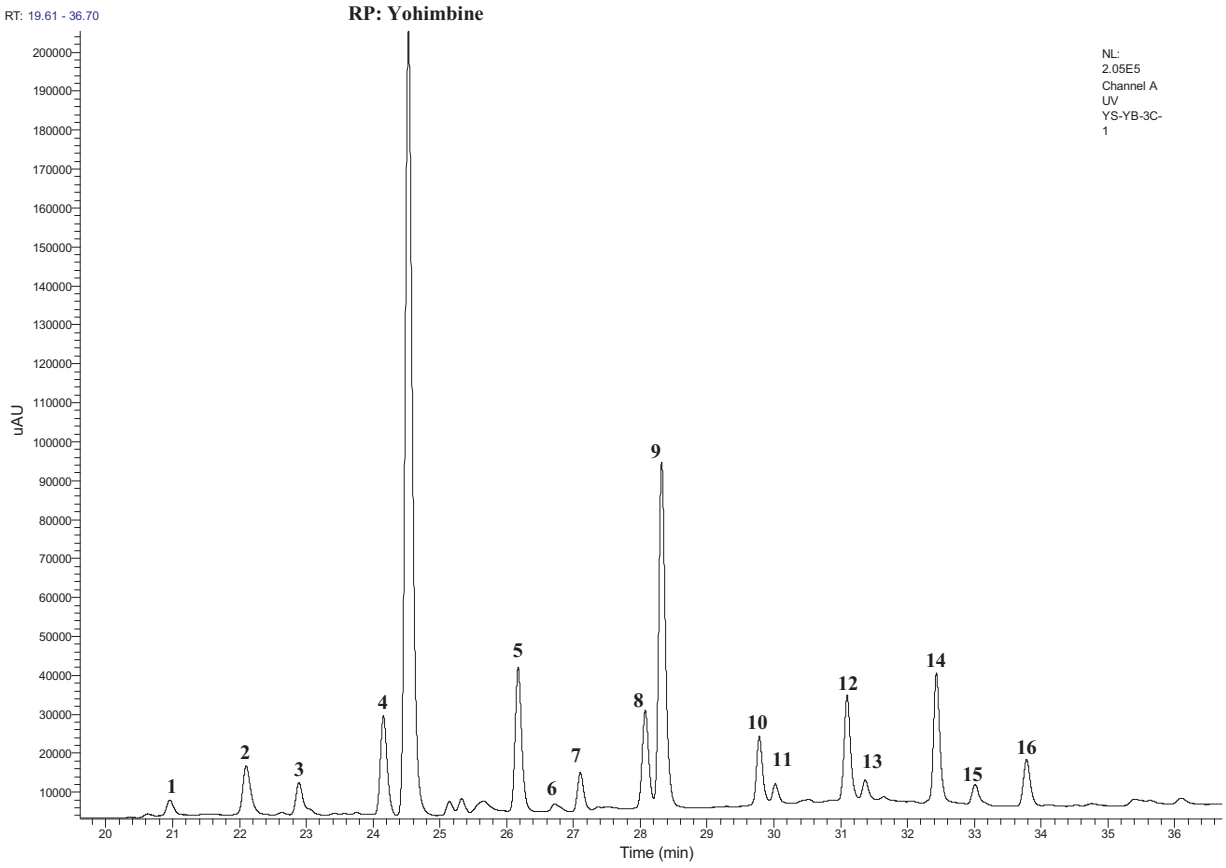

Fig. 3. The chromatogram of the developed UHPLC/UV method for analysis of yohimbe bark extract (peak identification is listed in Table 1).

Sample YS09 is separated from the rest on both PC1 and PC2. According to the PC2 loading, peak 4, 5, 7, and 14 are mainly responsible for the higher PC2 score. An examination of its chromatogram (Fig. 7) shows that the peaks 4, 5, 7, and14 are significantly higher compared to those of the authentic yohimbe bark, and it is the reason YS09 is positioned above the others. The higher peak 8 is the reason YS09 is positioned to the right of the rest (except of YS07). Every peak (from 1 to 16) has been double checked by MS and they are all correct. Obviously, the yohimbe indole alkaloids of YS09 are the same as the authentic yohimbe bark, but the composition of these indole alkaloids are different, however. The total non-yohimbine indole alkaoids (peak 1 to peak 16) content of the authentic yohimbe bark was about 120% of its yohimbine content (assuming all indole alkaloids had the same absorbance at UV 280 as yohimbine) and most of the dietary supplements ranged from 80% to 150%. For YS09, however, total non-yohimbine indole alkaloids content was about 400% of its yohimbine content. Sample YS09 is the only sample that its yohimbine content agrees with its label claim, but its total yohimbine-like indole alkaloids is much higher compared to the authentic bark with the same amount of yohimbine.

3.4. Quantitation of yohimbine

Traditionally, yohimbe barks were evaluated based quantitation of the yohimbine content. The approach was applied with the

Table 1
Indole alkaloids in AHP yohimbe bark used in the peak table for PCA.

Peak No.	Retention time	Formula $[M+H]^+$	Measured mass	Calcd. mass	Mass error (ppm)	Possible identification
1	20.96	$C_{21}H_{27}N_2O_3$	343.2012	343.2016	−0.42	Cilostamide or isomer
2	22.10	$C_{21}H_{27}N_2O_3$	355.2014	355.2016	−0.23	Yohimbine isomer
3	22.89	$C_{21}H_{27}N_2O_3$	355.2014	355.2016	−0.23	Yohimbine isomer
4	24.15	$C_{21}H_{27}N_2O_3$	355.2016	355.2016	−0.05	Corynanthine
RP	24.53	$C_{21}H_{27}N_2O_3$	355.2013	355.2016	−0.36	Yohimbine
5	25.15	$C_{21}H_{25}N_2O_3$	355.2016	355.2016	−0.02	Yohimbine isomer
6	25.33	$C_{21}H_{27}N_2O_3$	355.2012	355.2016	−0.42	Yohimbine isomer
7	26.17	$C_{21}H_{27}N_2O_3$	355.2015	355.2016	−0.08	Yohimbine isomer
8	26.71	$C_{21}H_{27}N_2O_3$	355.2012	355.2016	−0.39	Yohimbine isomer
9	27.10	$C_{21}H_{27}N_2O_3$	355.2015	355.2016	−0.14	Yohimbine isomer
10	28.07	$C_{21}H_{27}N_2O_3$	355.2013	355.2016	−0.33	α-Yohimbine
11	28.32	$C_{21}H_{29}N_2O_3$	357.2169	357.2173	−0.35	Dihydrositsirikine or isomer
12	29.78	$C_{21}H_{29}N_2O_3$	357.2170	357.2173	−0.23	Dihydrositsirikine or isomer
13	31.10	$C_{21}H_{25}N_2O_3$	353.1856	353.1860	−0.39	Ajmalicine
14	32.43	$C_{22}H_{29}N_2O_3$	369.2176	369.2173	−0.9	Methyl–yohimbine or isomer
15	33.01	$C_{21}H_{25}N_2O_3$	353.1857	353.1860	−0.29	Tetrohydroaltonine
16	33.78	$C_{22}H_{29}N_2O_3$	369.2171	369.2173	−0.17	Methyl–yohimbine or isomer

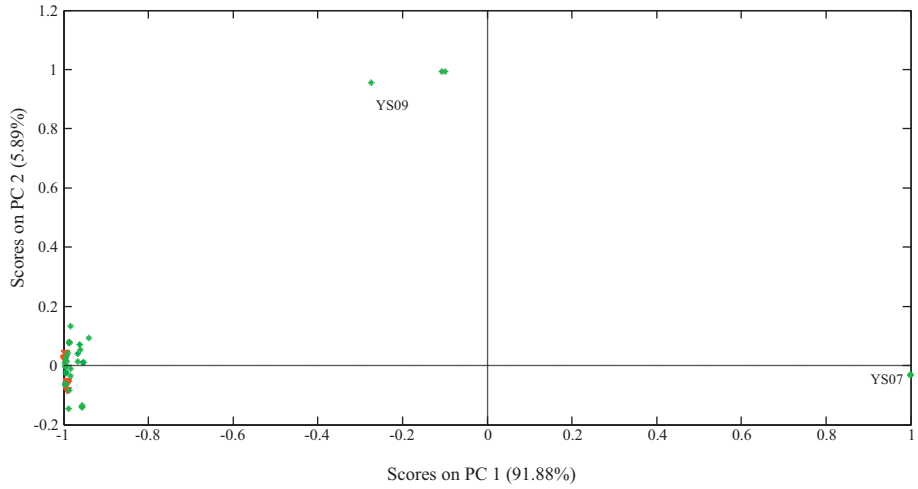

Fig. 4. PCA score plot of yohimbe bark plant materials (▼) and yohimbe bark dietary supplements (*). (YS-07 and YS-09 are both solid form YBDSs.)

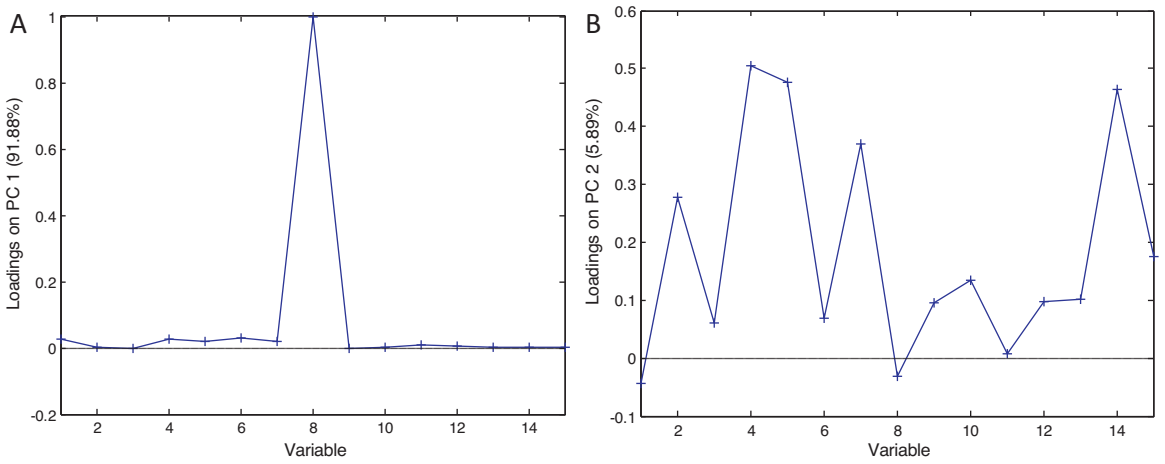

Fig. 5. PCA loading plot of yohimbe bark plant materials and yohimbe bark dietary supplements.

Table 2
The intra- and inter-day precisions of quantitation of yohimbine in yohimbe bark extract.

Concentration ($\mu g\,mL^{-1}$)	Intra-day ($n=6$)			Inter-day ($n=5$)		
	Found	RSD[a] (%)	Accuracy (%)	Found	RSD (%)	Accuracy (%)
5.36	5.33 ± 0.065	1.22	99.59	5.34 ± 0.016	0.29	99.70
21.42	20.83 ± 0.29	1.40	97.24	21.08 ± 0.26	1.22	98.40
85.68	83.56 ± 0.23	0.27	97.53	83.28 ± 0.52	0.63	97.20

[a] RSD (%) = (SD/mean) × 100.

Table 3
The measurement results of yohimbine in yohimbe bark and dietary supplements ($n=3$).[a]

Samples	Sample type	Yohimbine[b] (mg/g or mg/mL)	Yohimbine content (mg/serving)	Label claimed yohimbe bark per serving (mg)	Equivalent to AHP bark (mg/serving)
YL03	Liquid	2.40 ± 0.01	2.40 ± 0.01	1000	172.04
YL06	Liquid	0.14 ± 0.01	0.14 ± 0.01	333	10.04
YS01	Tablet	0.54 ± 0.01	0.68 ± 0.05	800	48.75
YS02	Capsule	0.96 ± 0.01	0.52 ± 0.05	–	37.26
YS03	Capsule	16.54 ± 0.18	9.93 ± 0.11	500	711.83
YS04	Capsule	5.49 ± 0.09	4.14 ± 0.06	750	296.77
YS06	Capsule	1.78 ± 0.01	1.59 ± 0.09	600	113.98
YS07	Tablet	0.15 ± 0.00	0.65 ± 0.00	250	46.59
YS08	Capsule	0.88 ± 0.03	1.09 ± 0.04	1200	78.14
YS09	Capsule	8.89 ± 0.05	5.33 ± 0.02	400	382.08
YS10	Tablet	7.46 ± 0.02	18.8 ± 0.12	750	1347.67
YS11	Capsule	12.67 ± 0.01	3.91 ± 0.00	–	308.60
YS12	Tablet	0.51 ± 0.18	0.70 ± 0.00	100	50.18
YR	AHP bark	13.95 ± 0.18	–	–	–

[a] Yohimbine contents were below LOQ in 4 liquid (YL01–03, 05) and 1 solid (YS05) dietary supplement samples.
[b] mg/g (mass to mass) for solid samples and mg/mL for liquid samples.

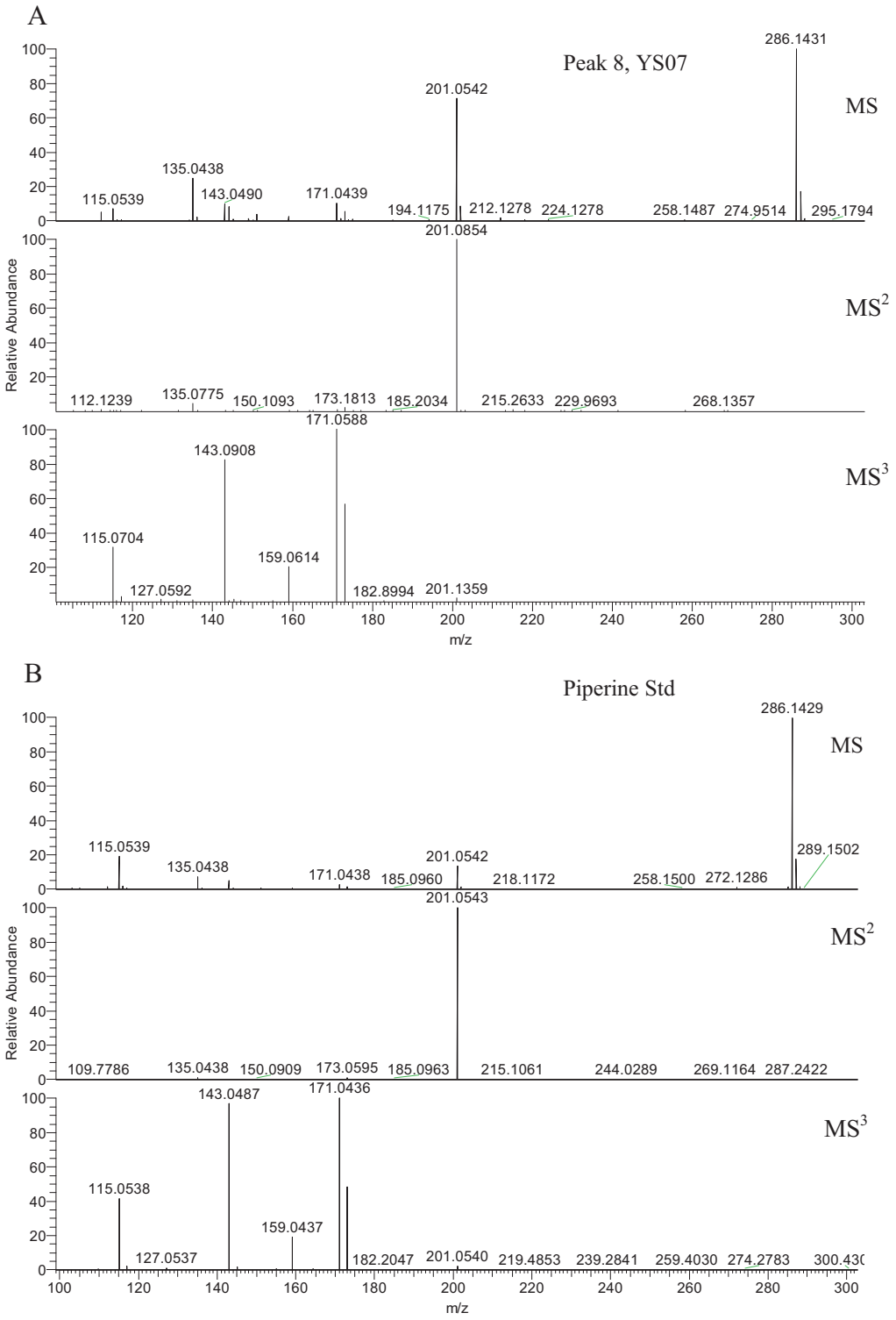

Fig. 6. The LC/DAD chromatograms of yohimbe bark, YS07, and YS09.

newly developed UHPLC method. An external standard method was used for the quantitation of yohimbine. The calibration curve is $y = 0.078x - 0.001$ with excellent linearity (r^2) was 0.9993. The range was from 0.11 to 214.1 μg/mL. The limit of detection (LOD) was 26.8 ng/mL and the limit of quantification (LOQ) was 80.4 ng/mL with an injection volume of 2 μL. The results of inter-day and intra-day precisions are shown in Table 2. The stability study showed that the yohimbine in the samples was relatively stable at room temperature (~90% of the original assay) and 5 °C (~98% of the original assay) for at least 3 weeks. The contents of yohimbine in yohimbe bark and dietary supplements are listed in Table 3 and vary greatly among the different commercial yohimbe

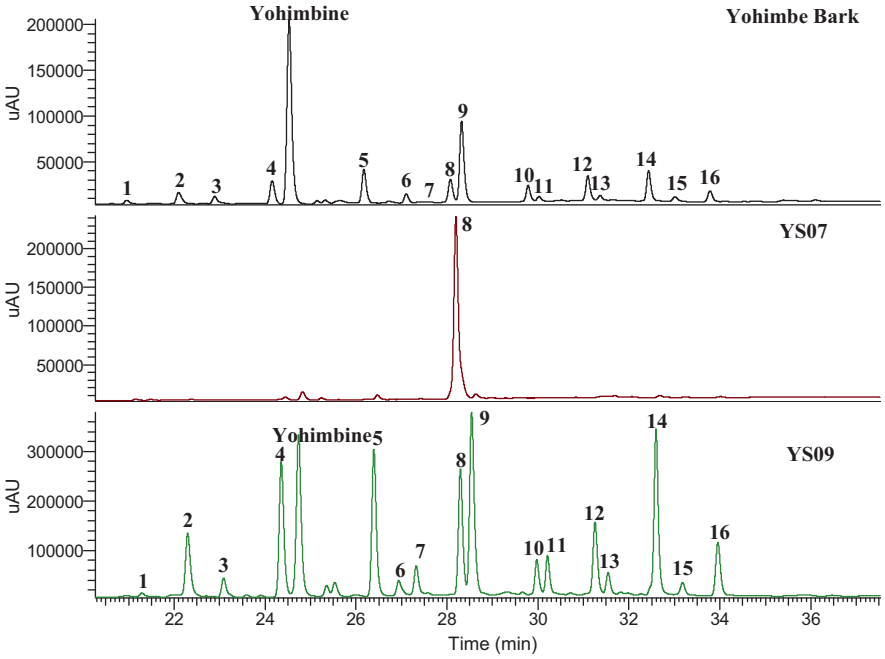

Fig. 7. The comparison of the peak at 27.9 min of YS07 (top) and piperine standard (bottom).

dietary supplements. Among the liquid samples, YL03 and YL06 contained about 3% and 17% of the label claims, respectively. The yohimbine contents were not detectable in the other 4 samples. For solid samples, only sample YS09 agreed with the label claim, two samples contained more yohimbe bark compared to the label claims (YS03, 140% and YS10, 180%), the rest ranged from 6% to 50% of the label claims except YS05 which did not have any detectable amount of yohimbine.

4. Conclusion

An environmental-friendly UHPLC method was developed using a C_{18} reverse-phase UHPLC column. The mobile phases used were fully compatible with mass spectrometry and this is the first reported chromatographic method that is capable of separation of corynanthine from yohimbine. The method was applied to the analysis of authentic yohimbe bark from American AHP and commercially available dietary supplements. The results show that the yohimbine content in commercial dietary supplements varies greatly. Moreover, quantitation of yohimbine by itself may not give the whole picture of the quality of the yohimbe dietary supplement under investigation. A combination of quantitation of yohimbine and fingerprinting analysis is the best way to assess the quality of yohimbe dietary supplements.

Acknowledgments

This research is supported by the Agricultural Research Service of the U.S. Department of Agriculture and an Interagency Agreement with the Office of Dietary Supplements of the National Institutes of Health.

Appendix A. Supplementary data

Supplementary data associated with this article can be found, in the online version, at doi:10.1016/j.jpba.2011.11.013.

References

[1] G.A. Lambert, W.J. Lang, E. Friedman, E. Meller, S. Gershon, Eur. J. Pharmacol. 49 (1978) 39–48.
[2] S. Mittal, K.S. Alexander, D. Dollimore, Drug Dev. Ind. Pharm. 26 (2000) 1059–1065.
[3] S.E. Drewes, J. George, F. Khan, Phytochemistry 62 (2003) 1019–1025.
[4] S.W. Tam, M. Worcel, M. Wyllie, Pharmacol. Ther. 91 (2001) 215–243.
[5] C. Teloken, E.L. Rhoden, P. Sogari, M. Dambros, C.A. Souto, J. Urol. 159 (1998) 122–124.
[6] M. Scherr, D. Schwerthoeffer, T. Froboese, F. Castrop, J. Bauml, Fortschr. Neurol. Psychiatr. 77 (2009) 585–590.
[7] N.R. Musso, C. Vergassola, A. Pende, G. Lotti, Am. J. Hypertens. 8 (1995) 565–571.
[8] J.H. Sun, A. Baker, P. Chen, Rapid Commun. Mass Spectrom. 25 (2011) 2591–2602.
[9] A.K. Ho, D.B. Hoffman, S. Gershon, H.H. Loh, Arch. Int. Pharmacodyn. Ther. 194 (1971) 304–315.
[10] B. Zanolari, K. Ndjoko, J.R. Ioset, A. Marston, K. Hostettmann, Phytochem. Anal. 14 (2003) 193–201.
[11] Q. Chen, P. Li, Z. Zhang, K. Li, J. Liu, Q. Li, J. Sep. Sci. 31 (2008) 2211–2218.
[12] Y. Zhang, Z. Huang, L. Ding, H. Yan, M. Wang, S. Zhu, J. Sep. Sci. 33 (2010) 2109–2114.
[13] I. Gerasimenko, Y. Sheludko, M. Unger, J. Stockigt, Phytochem. Anal. 12 (2001) 96–103.
[14] WHO, Document No. WHO/TRM/91.4, World Health Organization, Geneva, 1991.
[15] P. Chen, M. Ozcan, J. Harnly, Anal. Bioanal. Chem. 389 (2007) 251–261.
[16] P. Chen, F. Song, L.Z. Lin, J. Aoac. Int. 92 (2009) 624–632.
[17] P. Chen, L.Z. Lin, J.M. Harnly, J. Aoac. Int. 93 (2010) 1148–1154.
[18] P. Chen, J.M. Harnly, P.B. Harrington, J. AOAC Int. 94 (2011) 90–99.

Journal of Pharmaceutical and Biomedical Analysis 61 (2012) 150–155

Contents lists available at SciVerse ScienceDirect

Journal of Pharmaceutical and Biomedical Analysis

journal homepage: www.elsevier.com/locate/jpba

Determination of semduramicin in poultry feed additive, premixture and compound feed by liquid chromatography and UV spectrophotometric detection after post-column derivatisation

Ursula Vincent*, Federica Serano, María José González de la Huebra, Christoph von Holst

European Commission, Joint Research Centre, Institute for Reference Materials and Measurements (EC-JRC-IRMM), Retieseweg 111, B-2440 Geel, Belgium

ARTICLE INFO

Article history:
Received 1 September 2011
Accepted 13 November 2011
Available online 22 November 2011

Keywords:
Ionophore coccidiostats
Semduramicin
Feed
Single-laboratory validation
Ruggedness test

ABSTRACT

A new, simple and fit for purpose method based on liquid chromatography with UV spectrophotometric detection and post-column derivatisation (LC-UV-PCD) for the determination of semduramicin in poultry compound feed, premixtures and feed additive as well as its discrimination from other coccidiostats in poultry compound feed has been developed and single-laboratory validated. The concentration levels of the target analyte at which the validation experiments have been carried out varied between 12.8 and 51.3 mg kg^{-1} in compound feed, covering the authorised levels of semduramicin according to European Union legislation. Furthermore, the method has been validated for a premixture sample containing semduramicin at 3 g kg^{-1} and the feed additive containing semduramicin at 51 g kg^{-1}. The method developed involved a simple extraction of the coccidiostats with acetonitrile from the feed samples followed by a filtration of the supernatants. The resulting supernatants were submitted to chromatographic analysis. When analysing the feed additive and the premixture samples, the extraction solution was appropriately diluted prior to LC-UV-PCD analysis. The analytes were quantified through an external calibration curve prepared with pure semduramicin standards. The relative standard deviations for repeatability and for intermediate precision varied from 2.4 to 8.8% and from 2.6 to 8.8%, respectively, and the values for the relative recovery rate ranged from 89 to 95%. The limit of detection (LOD) and limit of quantification (LOQ) were estimated to be below 1 mg kg^{-1} and 3 mg kg^{-1}, respectively. Moreover, the results showed a comparable performance profile, when using methyl isobutyl ketone instead of acetonitrile as extraction solvent.Based on the obtained method performance characteristics, the method is considered suitable for the determination of semduramicin in poultry compound feed at authorised level, in premixtures and in the feed additive, hence allowing the enforcement of the European Union legislation regarding the control and the monitoring in feedingstuffs.

© 2011 Elsevier B.V. All rights reserved.

1. Introduction

Feed additives are authorised within the European Union according to the procedures laid down in Regulation EC (No) 1831/2003 [1]. This legislation foresees that specific conditions of the use of the feed additive are established individually for each product via Commission Regulations. Semduramicin is an ionophore coccidiostat, which is authorised as feed additive for chickens for fattening and corresponding details regarding the application of semduramicin are specified in Commission Regulation (EC) No 1443/2006 [2]. Coccidiostats belong to the group of feed additives, where the authorisation is granted exclusively to a specific preparation (Aviax 5%) containing semduramicin as active substance at a defined concentration level. In the case of semduramicin, the preparation, which is the actual feed additive, contains soybean mill run as major component with a mass fraction of about 85%, sodium aluminosilicate, mineral oil, sodium carbonate as minor components and the active substance semduramicin at a concentration of 51.3 g kg^{-1}. Furthermore the Commission Regulation specifies the inclusion level of the active substance in complete feedingstuffs, which ranges from 20 to 25 mg kg^{-1}. Often, feed additives containing coccidiostats are incorporated in feedingstuffs via premixtures, in order to ensure a homogenous distribution of the active substance in the final product. In addition, Regulation EC (No) 1831/2003 requires detailed labelling of these feed additives and corresponding premixtures including the content of the active substance in these products. In order to establish whether feed samples comply with legal requirements and to check correct labelling, there is a strong need for analytical methods that can be easily applied by official feed laboratories. Analytical methods suitable for official control purposes need to be validated against the criteria established by Regulation 882/2004 [3].

* Corresponding author.
E-mail address: ursula.vincent@ec.europa.eu (U. Vincent).

0731-7085/$ – see front matter © 2011 Elsevier B.V. All rights reserved.
doi:10.1016/j.jpba.2011.11.017

For the determination of coccidiostats in feedingstuffs at authorised level various standard methods exist, namely (1) the Community methods [4] for diclazuril, halofuginone, robenidine and lasalocid, (2) the ISO standard ISO 14183 for monensin, narasin and salinomycin [5], (3) the European standard 15782 for nicarbazin [6,7] and (4) the European standard 15781 for maduramicin [8,9]. In order to provide the official control laboratories with a corresponding method for the determination of semduramicin, the European Commission requested the standardisation of such a method via a mandate to the European Committee for Standardisation (CEN). The method presented in this paper is one of the analytical methods targeted within a Commission mandate to CEN (M 382/2005). For the determination of this analyte in complete feedingstuffs the authors of this study already developed and validated another method based on reverse phase high performance liquid chromatography coupled to mass spectrometry (HPLC–MS) [10,11]. The objective of this paper is to present the results of the development and validation of an alternative method, which utilises HPLC coupled to UV detection after post column derivatisation (LC-UV-PCD). Due to the instrumentation required, this method can be easily implemented by official laboratories that already apply the above mentioned methods for the determination of other coccidiostats. Furthermore, the aim of the research was to develop and validate an analytical method that is not only applicable to compound feedingstuffs but also to premixtures and the specific feed additive authorised [2]. Additionally it was important to avoid chlorinated solvents often used in the sample preparation step and to demonstrate that the presence of other authorised ionophore coccidiostats (monensin, lasalocid, maduramicin, narasin and salinomycin) potentially present in the samples does not interfere with the quantification of semduramicin.

2. Materials and methods

2.1. Reagents and solvents

All chemicals and solvents used were of analytical purity and suitable for HPLC.

Semduramicin sodium (SEM) was obtained from Phibro Animal Health (Fairfield, NJ, USA), maduramicin ammonium (MAD) from Alpharma (Willow Island, USA) and monensin sodium (MON) from Calbiochem (Merck Sciences, Darmstadt, Germany). Salinomycin sodium (SAL), narasin A (NAR A) and lasalocid sodium (LAS) were obtained from Sigma–Aldrich (St. Louis, MO, USA). The feed additive Aviax 5% was obtained through a feed producer.

Acetonitrile HPLC grade (ACN), methyl isobutyl ketone (MIBK) and methanol HPLC grade (MeOH) were from Merck Sciences (Darmstadt, Germany). Sulfuric acid, minimum 98% purity was from VWR BDH Prolabo, dimethylaminobenzaldehyde (DMAB), minimum 99% purity, formic acid, minimum 98% purity, and ammonium formate, minimum 99% purity were from Sigma–Aldrich (Steinheim, Germany). Pure water (H_2O) (18.2 $M\Omega\,cm^{-1}$ quality), which was used for the preparation of all the aqueous solutions, was obtained from a MilliQ Plus 185 System (Millipore, Molsheim, F).

2.2. Standard solutions and test samples

2.2.1. Standard solutions

A 1 $mg\,ml^{-1}$ semduramicin standard solution was prepared in methanol and used for the preparation of the calibration curve at 3.5 $\mu g\,ml^{-1}$, 7.0 $\mu g\,ml^{-1}$, 10.5 $\mu g\,ml^{-1}$, 14.0 $\mu g\,ml^{-1}$ and 17.5 $\mu g\,ml^{-1}$. A solution containing narasin A, salinomycin sodium, monensin sodium, lasalocid sodium and maduramicin ammonium at 200 $\mu g\,ml^{-1}$, 200 $\mu g\,ml^{-1}$, 480 $\mu g\,ml^{-1}$, 500 $\mu g\,ml^{-1}$ and 20 $\mu g\,ml^{-1}$, respectively, was prepared in acetonitrile and used for the spiking of the blank feed samples as described in Section 2.2.2.

Table 1
Concentration of the additional ionophore coccidistats in the compound feed samples. These substances may interfere with the quantification of semduramicin and have been added to the samples at the maximum levels of unavoidable carry-over of coccidiostats or histomonostats in non target feed established by European Union legislation.

	Concentration ($mg\,kg^{-1}$)
Lasalocid sodium	1.25
Narasin	0.7
Salinomycin sodium	0.7
Monensin sodium	1.25
Maduramicin ammonium alpha	0.05

2.2.2. Test samples

Compound feed samples: Commercial compound feedingstuff for poultry was selected, which was analysed by liquid chromatography coupled to triple quadrupole mass spectrometry [12] prior to use to demonstrate the absence of the target analytes. The preparation procedure included spiking experiments with the feed additive Aviax 5% [2] and the other ionophore coccidiostats. In detail, 25 ± 0.1 g of the compound feed samples were spiked with 6.25 mg or 12.5 mg or 25 mg of Aviax 5%. By taking into account the exact authorised concentration of semduramicin (51.3 $g\,kg^{-1}$) in the feed additive the target concentrations of this substance in the feed samples were 12.8 $mg\,kg^{-1}$, 25.7 $mg\,kg^{-1}$ and 51.3 $mg\,kg^{-1}$, corresponding to approximately (1) half of the maximum authorised concentration (MAC), (2) the MAC and (3) twice the MAC, respectively. In addition, all samples were fortified with a mixture of the above mentioned five other coccidiostats dissolved in ACN as specified in the previous section. The target concentrations of these analytes (Table 1) were the maximum levels of unavoidable carry-over of coccidiostats or histomonostats in non target feed established by European Union legislation [13]. The fortified samples were left for 1 h to ensure a satisfactory penetration of the interfering ionophore coccidiostats into the feed matrix.

For the robustness study, 5.00 ± 0.01 g portions of the commercial poultry blank feed were spiked with semduramicin at maximum authorised concentration and with the five potentially interfering coccidiostats at 1% cross-contamination level. The samples were then extracted with 15 ml ACN.

Premixtures: A premixture sample was obtained from a recognised proficiency testing provider [14] without semduramicin and mixed with Aviax 5%, thereby diluting the target analyte by a factor of about 15. For the validation exercise the premixture samples were individually spiked with appropriate amounts of Aviax 5% to achieve a target concentration of semduramicin in the premixture of 3.07 $g\,kg^{-1}$.

Feed additive: The feed additive Aviax 5% was used without further treatment. The target concentration of semduramicin in the feed additive was 51.3 $g\,kg^{-1}$ as specified in the Regulation authorising the feed additive [2].

Table 2 shows an overview of the different test samples included in the validation study.

2.3. Analytical procedure

2.3.1. Sample preparation

25.0 ± 0.1 g of the compound feed samples were suspended in 80 ml of ACN. For the analysis of premixtures and of the feed additive, 5.00 ± 0.1 g and 0.3 ± 0.001 g of the samples were suspended in 15 ml of ACN, respectively.

Table 2
Composition of test samples used for the validation of the method. Compound feed samples 1, 2 and 3 and the premixture have been fortified with the feed additive Aviax 5%. MAC = maximal authorised concentration of semduramicin in compound feed, which is 50 mg kg^{-1}.

	Interfering coccidiostats	Target SEM concentrations					
		0	0.5 MAC	MAC	2 MAC	3 g kg^{-1}	51 g kg^{-1}
Blank feed		X					
Compound feed 1	X		X				
Compound feed 2	X			X			
Compound feed 3	X				X		
Premixture						X	
Aviax 5%							X

Samples from the three matrices were extracted using an identical procedure, i.e. the suspensions were treated with a shaker (GFL 3018, Gesellschaft für Labortechnick mbH, Burgwedel, Germany) for 30 min at 150 min^{-1}. The suspensions were let stand until a clear supernatant was obtained which was then filtered through a 0.2 μm Acrodisc® PSF syringe Nylon filter (Pall Europe Limited, UK) and subjected to HPLC analysis without further sample purification. The filtered extracts from premixtures and feed additives were diluted 150 times in acetonitrile prior to HPLC analysis.

For the analysis of compound feed samples the alternative extraction solvent MIBK was included in the research in order to address the occasionally reported worldwide shortage of ACN. When using MIBK, the protocol had to be slightly adapted: 25 ± 0.1 g of the compound feed samples were suspended in 80 ml of MIBK and treated with the shaker as previously described. Then, a 2 ml aliquot of supernatant was evaporated to dryness and re-suspended in 2 ml ACN prior to filtration and HPLC analysis.

2.3.2. LC-UV-PCD conditions

All measurements were performed on a HPLC 1100 Agilent Technology (Diegm, Belgium) equipped with variable wavelength detection and coupled to a post-column derivatisation device composed of a post-column reactor operating at 92 °C with a 1.5–2.0 ml reaction stainless steel coil and a post-column reagent pump model 426 (Grace Alltech Associate Inc., Lokeren, Belgium) allowing a flow capacity from 0.5 to 2.0 ml min^{-1}.

The column used was a reverse phase Inerstil ODS-3® C18 (150 mm × 4.6 mm, 5 μm particle size) column from GL Sciences, Inc. (Tokyo, Japan) equipped with a Prevail® C18 guard column 7.5 mm × 4.6 mm, 5 μm particle size from Grace Alltech Associate Inc. (Lokeren, Belgium) and the separation was performed in isocratic conditions. The HPLC mobile phase selected after optimisation of the separation was composed of a 90:10 (v:v) mixture of MeOH and a 100 mM ammonium formate solution. The pH of the ammonium formate solution was adjusted at 3 with formic acid. The injection volume was 100 μl. The chromatographic flow rate was 0.7 ml min^{-1} and the UV detection was carried out at 598 nm. The column temperature was 38 °C. For the post column reaction, the mobile phase was methanol containing 3% (v/v) sulfuric acid and 3% (g/v) DMAB. The flow rate was 0.9 ml min^{-1} and the reactor temperature was 92 °C.

The semduramicin concentration in the test samples was quantified against an external calibration line established using the standard solutions of semduramicin (Section 2.2.1) corresponding to initial concentrations in the feedingstuff of 11.2 mg kg^{-1}, 22.4 mg kg^{-1}, 33.6 mg kg^{-1}, 44.8 mg kg^{-1} and 56.0 mg kg^{-1}.

2.4. Method validation

The method was validated taking into account various internationally recognised guidelines [15,16] including Commission Decision 657/2002 [17], which is actually designed for residues in food of animal origin. This is due to the fact that there is no specific validation guideline for feed samples. The validation of the method included the estimation of the limit of detection (LOD), limit of quantification (LOQ), precision under repeatability and intermediate conditions and the trueness. Also the ruggedness of the method was tested applying a factorial design approach.

The statistical assessments were done using commercially available software packages, namely Statistica®, Version 10 (StatSoft, Tulsa, OK, USA) for the factorial design and MINITAB™, Version 15 (Minitab Inc., State College, PA, USA) for the assessment of the precision of the method.

The validation study was performed on compound feed samples, premixtures and the feed additive Aviax 5% as shown in Table 2.

For establishing fitness for purpose criteria for the precision we calculated the HORRAT value, which is the ratio of the experimentally obtained values of the standard deviation obtained in the single laboratory validation and the target standard deviation calculated by the Horwitz equation [18,19]. The obtained precision was considered acceptable when the HORRAT value was below 1.3.

The trueness of the method was considered acceptable when the measured values for the relative recovery rate were above 80% and below 110% [17].

3. Results and discussion

3.1. Development/optimisation of the HPLC conditions

Semduramicin cannot be directly detected by UV spectrophotometry because of the absence in its chemical structure of a suitable chromophore group (Fig. 1). Post-column derivatisation therefore appears as one appropriate means to detect this analyte as in the case of other ionophore coccidiostats [5,8]. The post-column reagents vanillin and dimethylaminobenzaldehyde, prepared in methanolic sulfuric acid, react with the carboxylic acid ionophores at elevated temperatures leading to the formation of a coloured complex (Komarowsky reaction). This characteristic has been the basis for the determination of some coccidiostats such as monensin, narasin and salinomycin [5,20] and of the study presented in this paper as well.

One of the challenges of post-column derivatisation of the ionophore coccidiostats consists of the different derivatisation yield obtained depending on the ionophore. In particular the following two aspects need to be considered, namely (1) the fact that the authorised concentration of monensin in poultry feed is up to 4 times higher than the one for semduramicin and (2) the observation that the signal obtained for monensin is much more intense than the one obtained for semduramicin in an equimolar mixture. Therefore, the optimised HPLC conditions required sufficient chromatographic separation of semduramicin from the other coccidiostats in order to allow the determination of semduramicin in the presence of monensin, narasin, salinomycin, maduramicin and lasalocid.

When optimising the HPLC method, different parameters were varied to investigate their impact on the separation of

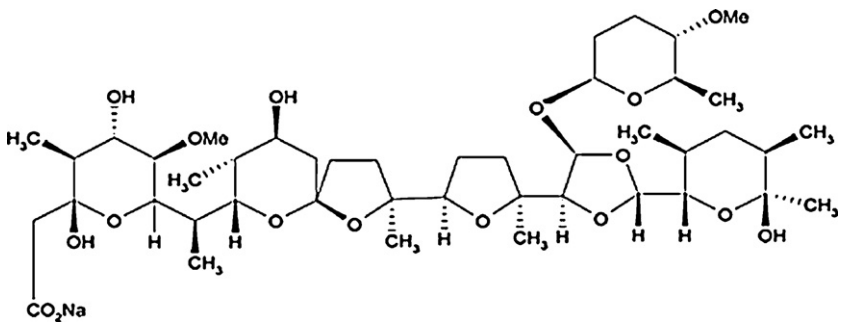

Fig. 1. Chemical structure of semduramicin.

semduramicin from other coccidiostats and the retention time of the analyte. Applying a factorial design revealed that best results were obtained with the buffer ammonium formate compared to ammonium hydroxide. The statistical assessment also showed that a water content of 10% in the mobile phase gained best results, whereas worse results were observed when the water content was above 20%, since semduramicin did not elute anymore at these conditions. Furthermore, the statistical evaluation showed that methanol as organic component of the mobile phase allowed for sufficient separation of semduramicin from the interfering substances. Addition of ACN to the organic component of the mobile phase up to a percentage volume of 50% did not significantly improve the chromatographic conditions, whereas higher portions of ACN had a negative influence on the chromatography. Based on the results from these experiments, the HPLC parameters were adjusted as specified in the experimental section of this paper. An example of a chromatogram of poultry compound feed is given in Fig. 2.

3.2. Single-laboratory validation

3.2.1. Selectivity

All blank samples including the blank material spiked with the potentially interfering coccidiostats did not generate a signal at the target retention time of semduramicin, thus demonstrating sufficient selectivity of the method.

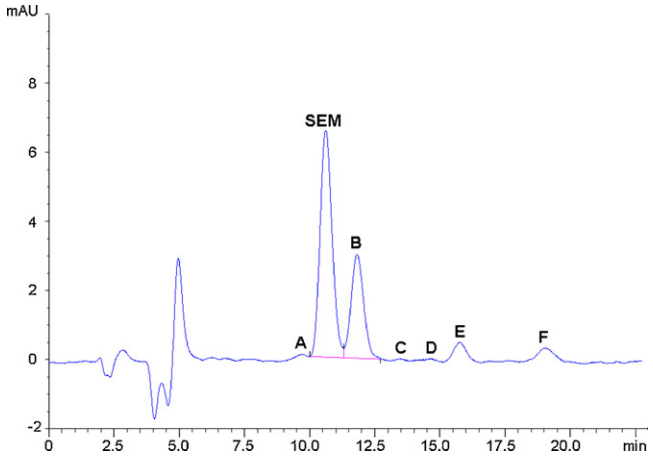

Fig. 2. Typical chromatogram for the separation of semduramicin (SEM) at 25 mg kg^{-1} from monensin, narasin, maduramicin, lasalocid and salinomycin at 1% cross-contamination level, in a commercial poultry feed spiked with Aviax 5% and with the other ionophore coccidiostats as described in Section 2.2.2; SEM – signal from semduramicin, A – signal from monensin sodium B; B – signal from monensin sodium A; C – signal from lasalocid sodium; D – signal from maduramicin ammonium; E – signal from salinomycin sodium and F – signal from narasin.

3.2.2. Sensitivity

The limits of detection (LODs) and limits of quantification (LOQs) were less relevant in the frame of this work, since the scope of the method was the determination of semduramicin at authorised concentration in compound poultry feed, in premixtures and in the feed additive, thus at relatively high concentration. Nevertheless an estimation of the LOD and LOQ of the method was performed using the calibration regression lines established [21]. The LOD and the LOQ of the method were estimated to be 1 mg kg^{-1} and 3 mg kg^{-1}, respectively, confirming that the method is sensitive enough to determine semduramicin in compound feed at 12.5 mg kg^{-1}, which was the lowest concentration included in this study.

3.2.3. Linearity and working range

A standard calibration curve was prepared by injecting into the LC system the standard solutions as described under Section 2.2.1 on each day of the validation phase. Each calibrant was injected six times. The coefficient of determination R^2 was above 0.9995 and the test of the residuals did not show any statistical trend. The evaluation of matrix effect on the calibration was not relevant. Previous work in our laboratory demonstrated that when using LC-UV-PCD no significant differences exist when quantifying semduramicin through a matrix-matched calibration curve versus a standard calibration curve.

3.2.4. Precision

The precision of the method was determined according to ISO standard 5725-3 [16] under different circumstances, namely repeatability conditions where independent experiments were carried out on the same day by the same operator using the same instrumentation and intermediate conditions where the experiments were repeated on different days. In this study, triplicate analyses were done on each day and this exercise was performed on three different days. The independent measurements included the whole analytical procedure, i.e. sample preparation and LC measurement. From each experiment, aliquots were injected into the LC system six times and average values from the six measurements were calculated for further statistical assessment. In total, the experimental design delivered results from nine experiments for each combination of the matrix and the semduramicin concentration. The measured semduramicin concentrations were then subjected to analysis of variance (ANOVA) to calculate the precision under repeatability and intermediate conditions.

The results of the statistical evaluation are shown in Table 3. The obtained relative standard deviation for repeatability (RSD_r) varied from 2.6% to 8.8% and the relative standard deviation of intermediate precision ($RSD_{Int.}$) ranged from 2.6% to 8.8%. In all cases the HORRAT values were below 1.3, thus indicating that the precision of the method fulfilled the criteria. As recommended by ISO standard 5725 [16] the data were also evaluated to establish whether a concentration independent precision of the method for

Table 3
Results from the statistical evaluation for semduramicin in compound poultry feed, premixture and feed additive samples. *ACN* has been used as extraction solvent. The target values have been calculated based on the spiking experiments and the mean values have been calculated from the results of the validation experiments.

	Target value (mg kg^{-1}) of semduramicin	Mean value (mg kg^{-1}) of semduramicin	RR (%)	S_r	RSD_r (%)	$S_{Int.}$	$RSD_{Int.}$ (%)	Horrat value
Compound feed 1	12.8	11.4	89	0.9	7.7	0.9	7.7	0.7
Compound feed 2	25.7	24.4	95	2.1	8.8	2.1	8.8	0.9
Compound feed 3	51.3	48.9	95	1.2	2.4	1.9	3.9	0.3
Premixture	3076	2795	91	73	2.6	73	2.6	0.5
Feed additive (Aviax 5%)	51,300	47,550	93	1347	2.8	2085	4.4	0.9

S_r: standard deviation for repeatability; RSD_r (%): relative standard deviation for repeatability; S_{Int}: standard deviation for intermediate precision; $RSD_{Int.}$ (%): relative standard deviation for intermediate precision. RR (%): percentage relative recovery rate.

Table 4
Results from the statistical evaluation for semduramicin in compound poultry samples. *MIBK* has been used as extraction solvent. The target values have been calculated based on the spiking experiments and the mean values have been calculated from the results of the validation experiments.

	Target value (mg kg^{-1}) of semduramicin	Mean value (mg kg^{-1}) of semduramicin	RR (%)	S_r	RSD_r (%)	$S_{Int.}$	$RSD_{Int.}$ (%)	Horrat value
Compound feed 1	12.8	11.6	90	0.9	8.0	1.3	11	0.7
Compound feed 2	25.7	23.7	92	1.1	4.8	1.1	4.8	0.5
Compound feed 3	51.3	50.9	99	2.3	4.5	3.9	7.6	0.5

S_r: standard deviation for repeatability; RSD_r (%): relative standard deviation for repeatability; S_{Int}: standard deviation for intermediate precision; $RSD_{Int.}$ (%): relative standard deviation for intermediate precision; RR (%): percentage relative recovery rate.

semduramicin in poultry compound feed could be calculated. This was possible since (1) the values for the intermediate precision estimate varied within a relatively small range and (2) there was no clear trend between the relative standard deviation and the concentration (Table 3). All measured concentrations were first divided by the respective mean values given in Table 3, in order to obtain normalised data. These data were subsequently subjected to ANOVA, obtaining an estimate for the concentration independent value for the relative intermediate precision of 5.6%. The value was considered acceptable for the intended use of the method.

3.2.5. Trueness estimated from the obtained recovery rates

The validation study also delivered acceptable results for the trueness, since the obtained values for the recovery rate varied from 89 to 95% as shown in Table 3. In addition, the data did not reveal any trend between the estimated trueness and the concentration or the matrix, indicating the robustness of the method.

3.2.6. Performance profile of the method with the alternative extraction solvent MIBK

The results from the statistical assessment when using MIBK as extraction solvent are shown in Table 4. The values for the RSD_r varied between 4.5 and 8% and the corresponding values for the $RSD_{Int.}$ varied between 4.8 and 11%, thus indicating that these values were very close to the corresponding data from the experiments with ACN as shown in Table 3. In addition, the HORRAT value was in all cases below the critical value of 1.3 showing an acceptable performance profile of the alternative method with MIBK. The concentration independent value for the intermediate precision was 8.2%. Acceptable values were also obtained for the estimated trueness, since the percentage recovery rate varied between 90 and 99%. Based on the obtained performance profile we concluded that the alternative method with MIBK was also fit for the intended purpose.

3.3. Robustness

The robustness of the method was tested by varying the experimental parameters at two levels according to an experimental design and to establish the influence of these variations on the measured recovery rate of semduramicin. Six parameters were identified and selected to perform the robustness study for the method, namely (1) the pore size of the filters used for the sample preparation, (2) the agitation speed for the extraction, (3) the proportion of methanol and ammonium formate in the mobile phase, (4) the HPLC column temperature, (5) the HPLC flow rate and (6) the temperature of the post-column derivatisation device. Equidistant deviations of the parameters from the experimental conditions of the method protocol towards lower and higher values were selected. For instance, the agitation speed of the shaker in the method protocol is 150 min^{-1} and the lower and higher values of this parameter in the robustness test were set at 100 and 200 min^{-1}, respectively. Just for the pore size of the filters only one additional size of 0.45 μm was included in the study. The variations of all parameters are shown in Table 5. 16 different combinations of the variations of the factors were selected in such a manner that the effects of the six parameters could be investigated independently from each other. 8 experiments were performed in duplicate in order to calculate the analytical error which was required to check for significance of the measured effects. In total the experimental design consisted of 24 experiments.

Table 5
Suitable range to be tested for the different parameters for the robustness study.

Parameter	Minimum value	Maximum value
Pore size of the filters (μm)	0.2	0.45
Agitation speed (min^{-1})	100	200
Composition of mobile phase	Methanol: 890 ml/ammonium formate (ml): 110 ml	Methanol: 910 ml/ammonium formate (ml): 90 ml
	110	90
HPLC column temperature (°C)	36	40
HPLC flow rate (ml min^{-1})	0.6	0.8
PCD device temperature (°C)	90	94

PCD: post-column derivatisation.

The statistical assessment revealed that the recovery rate was not affected by the variation of three parameters, which were the pore size of the filter, the agitation speed of the shaker and the HPLC column temperature. Significant effects were however observed for the other parameters. In detail, lower values for the recovery rate were observed, when (1) the buffer content was 110 ml instead of 90 ml, or (2) the flow rate was 0.8 instead of 0.6 ml min^{-1}, or (3) the temperature of the post-column reaction device was 90 instead of 94 °C. In consequence, the exact implementation of the method protocol requires particular attention to these parameters, since the deviations from the target value may have an adverse effect on the recovery rate of the protocol. In contrast, the exact adjustment of the first mentioned parameters was less critical.

4. Conclusion

A new HPLC method with spectrophotometric UV detection and post-column derivatisation for the detection and quantification of semduramicin sodium in poultry compound feed, premixture and feed additive has been developed and single-laboratory validated. Also the presence of potential interfering ionophore coccidiostats has been taken into account. The results of the validation study confirmed satisfactory values for the selectivity, sensitivity, precision, and trueness of the developed method. Therefore it was concluded that the method was fit for the purpose to be used in the frame of official control of the presence of semduramicin at authorised level in poultry compound feed, premixture and feed additive.

References

[1] Regulation (EC) No 1831/2003 of the European Parliament and of the Council of 22 September 2003 on additives for use in animal nutrition, Official J. Eur. Union L268 (2003) 29–43.
[2] Commission Regulation (EC) No 1443/2006 of 29 September 2006 concerning the permanent authorisations of certain additives in feedingstuffs and an authorisation for 10 years for a coccidiostat, Official J. Eur. Union L271 (2006).
[3] Regulation (EC) No 882/2004 of the European Parliament and of the Council of 29 April 2004 on official controls performed to ensure the verification of compliance with feed and food law, animal health and animal welfare rules, Official J. Eur. Union L165 (2004) 1–141.
[4] Commission Regulation (EC) No 152/2009 of 27 January 2009 laying down the methods of sampling and analysis for the official control of feed, Official J. Eur. Union L54 (2009) 1–130.
[5] ISO 14183: Animal Feeding Stuffs – Determination of Monensin, Narasin and Salinomycin Content – Liquid Chromatographic Method Using Post-Column Derivatisation, ISO Copyright Office, Case postale 56, CH-1211 Geneva 20, 2005.
[6] European Standard 15782: Animal Feeding Stuffs – Determination of Nicarbazin – High Performance Liquid Chromatographic Method, CEN, Avenue Marnix 17, B-1000 Brussels, 2009.
[7] J. de Jong, M. Tomassen, J. Driessen, H. Keukens, H.-A. Putzka, G. Brambilla, Liquid chromatographic method for nicarbazin in broiler feeds and premixtures: development, validation, and interlaboratory study, J. AOAC Int. 87 (2004) 1269–1277.
[8] European Standard 15781: Animal Feeding Stuffs – Determination of Maduramicin Ammonium by Reversed-Phase HPLC Using Post-Column Derivatisation, CEN, Avenue Marnix 17, B-1000 Brussels, 2009.
[9] J. de Jong, B. Stoisser, K. Wagner, M. Tomassen, J. Driessen, P. Hofmann, H.-A. Putzka, Determination of maduramicin in feedingstuffs and premixtures by liquid chromatography: development, validation, and interlaboratory study, J. AOAC Int. 87 (2004) 1033–1041.
[10] M.J. Gonzalez de la Huebra, U. Vincent, C. von Holst, Determination of semduramicin in poultry feed at authorized level by liquid chromatography single quadrupole mass spectrometry, J. Pharm. Biomed. 53 (2010) 860–868.
[11] M.J. Gonzalez de la Huebra, U. Vincent, C. von Holst, Inter-laboratory comparison of an analytical method for the determination of the feed additive semduramicin in poultry feed at authorised level by liquid chromatography single quadrupole mass spectrometry, Food Addit. Contam. 28 (2011) 35–43.
[12] U. Vincent, Z. Ezerskis, M. Chedin, C. von Holst, Determination of ionophore coccidiostats in feeding stuffs by liquid chromatography–tandem mass spectrometry. Part II. Application to cross-contamination levels and non-targeted feed, J. Pharm. Biomed. 54 (2011) 526–534.
[13] Commission Directive 2009/8/EC of 10 February 2009 amending Annex I to Directive 2002/32/EC of the European Parliament and of the Council as regards maximum levels of unavoidable carry-over of coccidiostats or histomonostats in non target feed, Official J. Eur. Union L40 (2009) 19–25.
[14] FAPAS, Proficiency Testing Schemes, The Food and Environment Research Agency, Sand Hutton, York, UK, 2010.
[15] M. Thompson, S.L.R. Ellison, R. Wood, Harmonized guidelines for single laboratory validation of methods of analysis, Pure Appl. Chem. 74 (2002) 835–855.
[16] ISO 5725-3:1994(E), Accuracy (Trueness and Precision) of Measurement Methods and Results. Part 3. Intermediate Measures of the Precision of a Standard Measurement Method, ISO Standards, Geneva, ICS 03.120 30, 1994, pp. 1–25.
[17] Commission Decision of 12 August 2002 implementing Council Directive 96/23/EC concerning the performance of analytical methods and the interpretation of results (2002/657/EC), Official J. Eur. Comm. L221 (2002) 8–36.
[18] W. Horwitz, R. Albert, Performance characteristics of methods of analysis used for regulatory purposes. Part II. Pesticide formulations, J. AOAC Int. 74 (1991) 718–744.
[19] W. Horwitz, R. Albert, The Horwitz Ratio (HorRat): a useful index of method performance with respect to precision, J. AOAC Int. 89 (2006) 1095–1109.
[20] W.J. Blanchflower, D.A. Rice, J.T.G. Hamilton, Simultaneous high-performance liquid chromatographic determination of monensin, narasin and salinomycin in feeds using post-column derivatisation, Analyst 110 (1985) 1283–1287.
[21] J.N. Miller, J.C. Miller, Statistics and Chemometrics for Analytical Chemistry, fifth ed., Pearson Education Limited, Harlow, 2005.

Journal of Pharmaceutical and Biomedical Analysis 61 (2012) 156–164

Contents lists available at SciVerse ScienceDirect

Journal of Pharmaceutical and Biomedical Analysis

journal homepage: www.elsevier.com/locate/jpba

The site-specific basicity of thyroid hormones and their precursors as regulators of their biological functions

Gergő Tóth, Sándor Hosztafi, Zsuzsanna Kovács, Béla Noszál*

Department of Pharmaceutical Chemistry, Semmelweis University, Research Group of Drugs of Abuse and Doping Agents, Hungarian Academy of Sciences, Budapest H-1092, Hőgyes Endre u. 9, Hungary

ARTICLE INFO

Article history:
Received 29 October 2011
Received in revised form
18 November 2011
Accepted 20 November 2011
Available online 28 November 2011

Keywords:
NMR
Thyroxine
Protonation constants
Thyroid hormone biosynthesis
Microspeciation

ABSTRACT

The complete macro- and microequilibrium analyses of thyroxine, liothyronine, reverse liothyronine and their biological precursors – diiodotyrosine, monoiodotyrosine and tyrosine are presented. Their biosyntheses, receptor- and transport protein-binding are shown to be distinctively dependent on the phenolate basicity. The protonation macroconstants were determined by ^{1}H NMR-pH and/or UV-pH titrations. Microconstants of the minor microspecies were determined by deductive methods, in which O-methylated and carboxymethylated derivatives were synthesized, and the combination of their NMR-pH and UV-pH titration provided the experimental base to evaluate all the microconstants. NMR-pH profiles, macro-, and microscopic protonation schemes, and species-specific diagrams are included.

Biosyntheses of the thyroid hormones take place by oxidative coupling of two iodotyrosine residues catalyzed by thyreoperoxidase in thyreoglobulin. On the grounds of our phenolate microconstants of precursors the thyroxine over liothyronine ratio needs to be 9:1 after their biosynthesis in thyroid gland, which is in good agreement with biochemical data. The microconstants show that the phenolates are in proton donor (–OH) form in liothyronine whereas they occur in proton acceptor ($-O^-$) form in thyroxine at the pH of blood. These facts explain several facts that have previously been empirically known: the affinity of liothyronine for the receptor is higher than that of thyroxine, the affinity of thyroxine for the transport proteins is higher than that of liothyronine and the selectivity of thyroxine for the OATP1C1 organic anion transporter is higher than that of liothyronine.

© 2011 Elsevier B.V. All rights reserved.

1. Introduction

Thyroxine (3,5,3′,5′-tetraiodothyronine, T4), liothyronine (3,5,3′-triiodo L-thyronine, T3) and "reverse" liothyronine (3,3′,5′-triiodo L-thyronine, rT3), the thyroid hormones are formed in the human thyroid gland by iodination and coupling reactions of tyrosine (Tyr) [1,2]. T4 contains four iodine atoms, and is formed upon coupling of two diiodotyrosine (DIT) molecules. T3 and rT3 contain three iodine atoms, and are formed by coupling DIT with monoiodotyrosine (MIT). T3 and rT3 are produced during the peripheral metabolism primarily when T4 is converted to T3 or rT3 [3]. The normal daily T4 production is between 70 and 90 mg, while that of T3 is between 3 and 8 mg by the thyroid gland. Eighty percent of the daily production of T3 is produced by deiodination of T4 in extrathyroidal tissues [4].

Following biosynthesis, T3 and T4 bind to transport proteins in blood. The main transport proteins are the thyroxine-binding globulin (TBG), transthyretin (TTR) and human serum albumin (HSA). T4 is bound more tightly than T3 to each of these proteins [5,6]. Only the unbound hormones have biological activity, the amount and ratio of the free T3 and T4 is therefore important. Approximately 0.03% of total T4 and 0.3% of total T3 in serum are circulating in a free form.

The deiodinase enzymes, as well as the receptors are located intracellularly. Thus, the action and conversion of thyroid hormone require transport across the cell membrane. Thyroid hormones are very lipophilic substances (T4: $\log P = 6.14$; T3: $\log P = 5.21$ [7]) they are therefore able to cross the plasma membrane of target cells with passive diffusion. Nevertheless, many active iodothyronine transporters have been identified (e.g. the OATP1C1, OATP14 organic anion transporter and the amino acid transporter LAT-1), and it is now widely accepted that the cellular uptake is effected by energy dependent, carrier-mediated processes [8].

After the membrane transport T3 binds the thyroid hormone receptors (a type of nuclear receptors), and it modulates the transcription of specific genes. T3 is the biologically active hormone, whereas rT3 is assumed to have no biological activity. T4 is believed to be a prohormone, T3 is more active, and the affinity of T3 for the receptor is 5-fold higher than that of T4 [9]. The thyroid hormones are crucial for the normal development of the central nervous

* Corresponding author. Tel.: +36 06 1 217 0891; fax: +36 06 1 217 0891.
E-mail address: nosbel@gytk.sote.hu (B. Noszál).

0731-7085/$ – see front matter © 2011 Elsevier B.V. All rights reserved.
doi:10.1016/j.jpba.2011.11.020

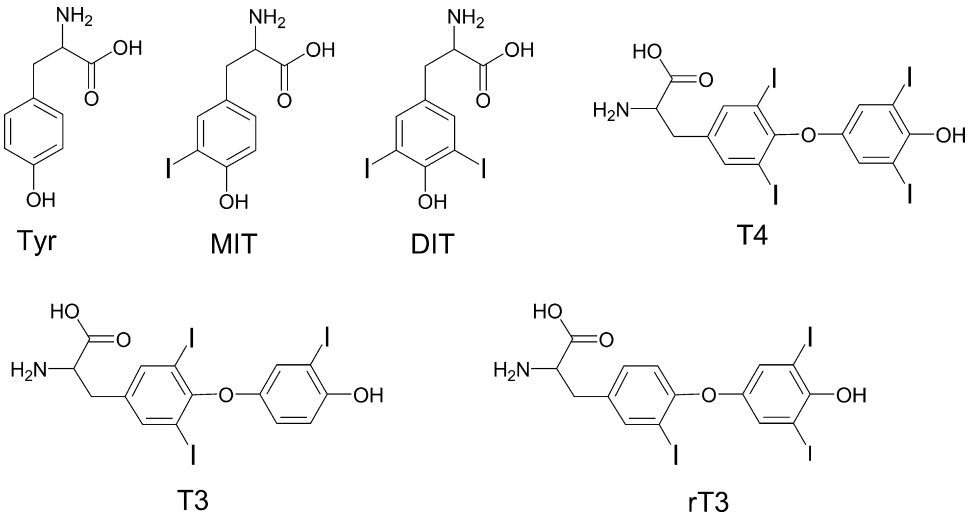

Fig. 1. Constitutional formulas of the thyroid hormones and their precursors studied.

system (CNS) in infants, the skeletal growth in children, and also for the normal function of multiple organ systems in adults [10].

It was our goal to characterize the acid–base properties of the thyroid hormones and their precursors at the site-specific level, and to find possible relationships between the basicities determined and the biological functions of the molecules. The structure of the thyroid hormones and their precursors are in Fig. 1.

Macroscopic equilibrium constants (expressed either as dissociation constants pK_a or protonation constants $\log K$) of multiprotic molecules depict the acid–base properties of the compound as a whole. They hold information on the site of the protonation in exceptional cases only. Site-specific, submolecular basicities can be obtained when microconstants are determined [11]. The site-specific acid–base properties of thyroid hormones and their precursors are therefore of fundamental importance to understand their biosynthesis, and their binding behavior in thyroid gland and in periphery. Knowledge of protonation macro- and microconstant is essential to understand the ADME properties since absorption and distribution are highly affected by the protonation state of the compound.

The thyroid hormones are of very poor solubility in aqueous media and most watermiscible solvents, which is the obvious cause of the controversy in their reported protonation macroconstants [12,13]. The exceptions are the two macroconstants of T4, which were determined by a fast UV-pH titration technique by Comer et al. [14]. The mixed-solvent procedure is a common approach for $\log K$ determination of poorly soluble molecules, and the methanol–water mixture is the most commonly used cosolvent system. This method is based on the determination of apparent protonation constants in solvent mixtures of gradually changing composition, the aqueous $\log K$ is then obtained by extrapolation [15,16]. This method could not be used for $\log K$ determination of our molecules due to the insolubility of the thyroid hormones in several solvent mixtures, including DMSO and methanol.

We therefore used ^{1}H NMR titration in water, applying thousands of transients, especially in the acidic pH region where our compounds exhibit the poorest solubility. Several important molecules have been characterized by NMR-pH titration [17,18]. This method offers a number of advantages. For example, high field NMR can distinguish between peaks of the parent compound and its possible decomposition products and other impurities, and the chemical shift is independent of the concentration. 2–32 transients are typically coadded in a ^{1}H NMR spectrum; but the signal/noise ratio can be improved upon increasing the number of transients. For the thyroid hormone and precursor molecules at low pH about 6000 transients were necessary to discern the proton signals.

NMR-pH titration is ideally suited for the determination of protonation microconstants, because each basic center can usually be followed by the protonation shift of an adjacent NMR nucleus [19]. In our investigated compounds all NMR nuclei are multiple influenced, their chemical shifts reflect to some extent the protonation of every basic center. Thus, in order to quantitate the site-specific protonation, we also introduced model molecules with reduced number of basic centers and/or methods that are selective for the protonation of a particular basic group.

The phenolate protonation could be selectively monitored by UV-pH titration at the absorption maximum near 290 nm (depending on the compound studied). Concerning molecules with minor microspecies of inferiorly low concentration, the contribution of such microspecies to the UV signal can be insignificant. In such cases the deductive method is the only approach to determine the protonation microconstants. Model compound(s) synthesized in the deductive method mimic the minor protonation isomer, and the macroconstant(s) of the auxiliary compound are then introduced into the microscopic protonation scheme of the main compound. It has been shown in many works [20,21] that electronic effects of a carboxylic (–COOH) group and a carboxylic ester (–COOR); and those of an aromatic hydroxyl (–OH) group and a phenol ether (–OR) are virtually identical on the adjoining moieties. We synthesized the carboxylic esters, the phenol ethers, and the O-methyl-carboxymethyl esters of our investigated compounds, and determined the $\log K$ values of all these compounds by NMR-pH titration.

The microspeciation of tyrosine is well-known [22,23]. In order to ensure identical circumstances for direct comparison we also determined all the tyrosine microconstants. Yamazaki et al. determined two macroconstants of monoiodotyrosine and diiodotyrosine, and four microconstants of monoiodotyrosine by spectrophotometric and potentiometric titration [24]. Gemmill and Tata examined the apparent ionization constants of the phenolate of thyroid hormones by UV-pH titration [25,26].

Although the physiological effects and many physicochemical characteristics of thyroid hormones are well known, no previous

report was devoted to their microspeciation, in spite of the fact that ADME behavior, receptor binding and other biological processes depend on the acid–base properties.

Here we report the macroscopic and microscopic acid–base properties of thyroid hormones and their precursors, which allowed the interpretation of their biochemical functions at the site-specific level.

2. Materials and methods

2.1. Materials

L-Tyrosine, L-diiodotyrosine, L-monoiodotyrosine, L-thyroxine, L-liothyronine, L-thyroxine sodium salt, liothyronine sodium salt, 3,3′,5′-triiodo L-thyronine, chloroacetic acid, dimethyl sulfate, DMSO-d_6 and D_2O (99.8 atom% D) were obtained from Sigma–Aldrich Co. Formic acid, acetic anhydride and methanol were obtained from Molar. Dichloroacetic acid was obtained from Fluka. Other chemicals of analytical grade were purchased from commercial suppliers and used without further purification. All solutions for the titration were prepared from bidistilled Millipore water (specific conductivity: 1.1 $\mu S\,cm^{-1}$).

2.2. Synthesis of derivatives with reduced number of basic site(s)

The O-methyl ether of Tyr, MIT, DIT, T3 and T4 were prepared by a modified literature procedure of the synthesis of O-methyl-tyrosine in three steps [27]. In the first step N-formyl derivatives were synthesized. The substance was treated with 85% formic acid and acetic anhydride. The reaction mixture was stirred for 3 h at room temperature and at the end of the reaction the solution was evaporated under reduced pressure.

In the second step O-methyl-N-formyl derivatives were synthesized. The N-formyl derivative was dissolved in 4 M NaOH and then treated successively with 4 M NaOH and dimethyl sulfate with stirring, the addition was repeated five times. Stirring was continued for 2 h at room temperature. The solution was then treated with a small amount of ammonia, and stirring was continued for 30 min. Then the solution was acidified with 4 M HCl, and the crystals were collected.

In the third step O-methyl derivatives were synthesized. The O-methyl-N-formyl derivative was hydrolyzed with 3 M HCl for 4 h. If the substance has not dissolved, the mixture was heated up to 60 °C. The solution was evaporated under reduced pressure Tyr, MIT and T3 methyl ethers were prepared. For DIT and T4 methyl ethers, the solution was neutralized with ammonia, and the resulting crystals were collected.

The carboxymethyl ester of Tyr, MIT, DIT, T3 and T4 and O-methyl-carboxymethyl ester of Tyr, MIT, DIT, T3 and T4 were synthesized according to literature applying direct esterification of D-tyrosine [28].

To a mixture of amino acid and MeOH thionyl chloride was added dropwise. The reaction mixture was refluxed for 4 h and then the methanol was evaporated resulting in the HCl salt of the amino acid ester. The structure of the synthesized compounds was confirmed by ^{1}H NMR spectra in DMSO-d_6 and D_2O. To the best of our knowledge, 5 of the molecules (N-formyl-O-methyl-monoiodotyrosine, N-formyl-O-methyl-thyroxine, N-formyl-O-methyl-liothyronine, O-methyl-carboxymethyl-thyroxine and O-methyl-carboxymethyl-liothyronine) are unregistered, new compounds in the literature. ^{1}H NMR assignments in DMSO-d_6 and HRMS data of the new synthesized compounds are as follows:

N-formyl-O-methyl-monoiodotyrosine
2.739 dd 1H (CH_2); 2.903 dd 1H (CH_2); 3.795 s 3H (O–CH_3); 4.433 m 1H (CH); 6.850 dd 1H (Ar1); 7.030 d 1H (Ar2); 7.537 d 1H (Ar3); 7.989 s 1H (formyl CH); 8.340 d 1H formyl NH
HRMS (ESI-TOF$^+$) m/z calcd [M+H$^+$] 349.9811, found 349.9815.

N-formyl-O-methyl-thyroxine
2.718 dd 1H (CH_2); 3.026 dd 1H (CH_2); 3.810 s 3H (O–CH3); 4.506 m 1H (CH); 7.088 s 2H (Ar1); 7.840 s 2H (Ar2); 7.985 s 1H (formyl CH); 8.321 d 1H (formyl NH)
HRMS (ESI-TOF$^+$) m/z calcd [M+H$^+$] 819.6972, found 819.6969.

N-formyl-O-methyl-liothyronine
2.816 dd 1H (CH_2); 3.046 dd 1H (CH_2); 3.803 s 3H (O–CH3); 4.522 m 1H (CH); 6.772 dd 1H (Ar1); 6.911 d 1H (Ar2); 7.198 d 1H (Ar3); 7.969 s 2H (Ar4); 7.989 s 1H (formyl CH) 8.350 d 1H (formyl NH)
HRMS (ESI-TOF$^+$) m/z calcd [M+H$^+$] 693.8006, found 693.8001.

O-methyl-carboxymethyl-thyroxine
2.968 dd 1H (CH_2); 3.276 dd 1H (CH_2); 3.660 s 3H (COO–CH_3); 3.805 s 3H (O–CH_3); 4.076 m 1H (CH); 7.090 s 2H (Ar1); 7.845 s 2H (Ar2)
HRMS (ESI-TOF$^+$) m/z calcd [M+H$^+$] 804.7180, found 804.7186.

O-methyl-carboxymethyl-liothyronine
3.059 dd 1H (CH_2); 3.290 dd 1H (CH_2); 3.658 s 3H (COO–CH_3); 3.800 s 3H (O–CH_3); 4.122 m 1H (CH); 6.668 dd 1H (Ar1); 6.902 d 1H (Ar2); 7.192 d 1H (Ar3); 7.964 s 2H (Ar4)
HRMS (ESI-TOF$^+$) m/z calcd [M+H$^+$] 678.8213, found 678.8216.

2.3. ^{1}H NMR titration

The ^{1}H NMR spectra were recorded at 600 MHz on a Varian Inova NMR spectrometer, equipped with a broadband inverse detection pulse field gradient probehead. Spectra were recorded at 25.0 ± 0.1 °C and referenced to internal DSS. The titrations were carried out at constant ionic strength (I = 0.15 mol/dm^3, auxiliary electrolyte: KCl) in 5% D_2O–95% H_2O mixtures. This deuterium concentration proved to be enough for the spectrometer lock system. Using such a small amount of D_2O, the shift of pH-scale is within the deviation limit (0.02 pH unit), according to the Gross–Butler–Purlee theory [29,30]. Processing of NMR-data has been done with both VNMRJ 2.2C and the MestRe-C software (2.3a version, http://www.mestrec.com). To suppress the signal from water, the double pulse field gradient spin echo (dpfgse) sequence was used.

For pH-measurement a Metrohm 6.0234.110 combined glass electrode was used in the pH range 3–12.5. pH data (except for pH < 3) are pH meter readings based upon NIST primary standards: 0.05 M potassium tetraoxalate (pH = 1.68), 0.05 M potassium hydrogen phthalate (pH = 4.01), 0.025 M KH_2PO_4 + 0.025 M Na_2HPO_4 (pH = 6.87) and 0.01 M borax (pH = 9.18). In order to avoid the glass electrode distortion at pH < 3, in situ NMR-pH indicator molecules dichloroacetic acid and chloroacetic acid were used. The pH of the solution was determined from the actual chemical shift of the appropriate indicator molecule [31], using Eq. (1):

$$\mathrm{pH} = \log\ K_{\mathrm{ind}} + \log\ \frac{\delta_{\mathrm{ind}}^{\mathrm{obs}} - \delta_{\mathrm{Hind}}}{\delta_{\mathrm{ind}} - \delta_{\mathrm{ind}}^{\mathrm{obs}}} \quad (1)$$

where K_{ind} is the protonation constant of the indicator (1.14 for dichloroacetic acid and 2.70 for chloroacetic acid), δ_{ind} and δ_{Hind} are the chemical shift of the species in subscript (δ_{ind} = 6.050, δ_{Hind} = 6.345 for dichloroacetic acid; δ_{ind} = 4.049, δ_{Hind} = 4.280 for chloroacetic acid), $\delta_{\mathrm{ind}}^{\mathrm{obs}}$ is the observed chemical shift.

The FID was digitized into 56,000 data points. For MIT, DIT, Tyr and related compounds 8–16 transients were coadded at each pH, whereas for rT3, T3, T4 and related compounds 128–256 transients were coadded at alkaline pH, and thousands at acidic pHs. The spectra were referenced to DSS.

For the titration of Tyr, MIT, DIT and their related compounds 1.0–1.5 mM solutions were used, for T4, T3, rT3 and related compounds 0.1 mM were used due to poor solubility. At 0.15 M ionic strength acidic and basic stock solutions were prepared with

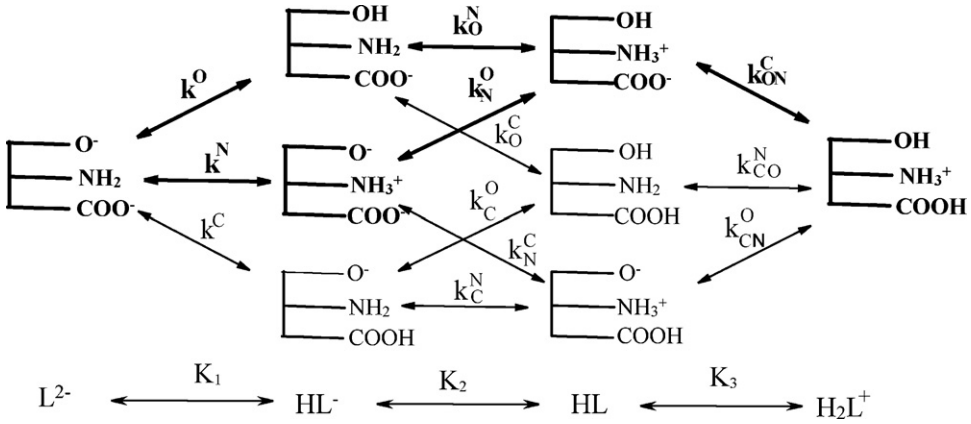

Fig. 2. The micro- and macrospeciation schemes of the examined compounds, where microconstants with superscript O, N and C belong to the phenolate, amino and carboxylate site, respectively, and K_1, K_2 and K_3 are stepwise macroconstants. The superscript on the microconstant indicate the protonating site, while the subscript (if any) stand for the site already protonated. The main (de)protonation pathway is marked with bold arrows.

concentrations of 0.1 M HCl/NaOH and 0.05 M KCl to ensure 0.15 M ionic strength. In case of the easily decomposing, base-sensitive ester derivatives, 0.14 M KCl basic stock solution was prepared and titrated with 0.01/0.02 M HCl and NaOH, to keep the ionic strength below 0.16 M. The peaks of C-methyl derivatives are safely discernible up to pH 11.

The NMR-pH datasets were fitted with Statistica 6.0, nonlinear estimations and user-specified regression module to determine protonation macroconstants from individual carbon-bound hydrogen chemical shifts. Multiple fitting was performed with Opium program and Origin 8.0.

2.4. UV-pH titration

Titrations were carried out on a Jasco V-550 diode-array spectrometer and 1 cm cuvettes at 25.0 °C. The pH of the solutions was adjusted and measured as in the NMR-pH titrations. The solute concentration was 0.2 mM for Tyr, MIT and 2 nM only for T3. This concentration is high enough for UV-pH titration, because the molar absorptivity of T3 is high. Absorption spectra were recorded between 250 and 350 nm, and the wavelength was chosen so that absorptions of the acidic and basic forms are as different as possible. UV-pH datasets were fitted with Statistica 6.0 and Origin 8.0.

2.5. HRMS analysis

Accurate mass data were acquired on an Agilent 6230 time-of-flight mass spectrometer equipped with a Jet Stream electrospray ion source in positive ion mode. Injections of 0.1–0.3 μl were directed to the mass spectrometer at a flow rate 0.5 ml/min (70% methanol–water mixture, 0.1% formic acid), using an Agilent 1260 Infinity HPLC system. Jet Stream parameters: drying gas (N_2) flow and temperature: 10.0 l/min and 325 °C, respectively; nebulizer gas (N_2) pressure: 10 psi; capillary voltage: 4000 V; sheath gas flow and temperature: 325 °C and 7.5 l/min; TOFMS parameters: fragmentor voltage: 170 V; skimmer potential: 170 V; OCT 1 RF Vpp: 750 V. Full-scan mass spectra were acquired over the m/z range 100–2500 at an acquisition rate of 250 ms/spectrum and processed by Agilent MassHunter B.03.01 software.

3. Results

All the parent compounds studied are triprotic ones, with phenolate, amino and carboxylate protonation sites. Being a triprotic molecule, the total number of microspecies and microconstants are 8 and 12, respectively, as shown in Fig. 2.

The relationships between the macro- and microconstants are as follows:

$$K_1 = k^{O} + k^{N} + k^{C} \quad (2)$$

$$K_1K_2 = k^{O}k^{N}_{O} + k^{O}k^{C}_{O} + k^{N}k^{C}_{N} = k^{O}k^{N}_{O} + k^{C}k^{O}_{C} + k^{C}k^{N}_{C} = \ldots \quad (3)$$

$$K_1K_2K_3 = k^{O}k^{N}_{O}k^{C}_{N,O} = k^{C}k^{N}_{C}k^{O}_{C,N} = \ldots \quad (4)$$

In order to characterize the basicity-modifying effect between two moieties, the pair–interactivity parameter can be defined. The pair–interactivity parameter quantitates how much the protonation of a basic site reduces the basicity of the other basic site. Three interactivity parameters occur in our triprotic compounds. The pair–interactivity parameter can be formulated in terms of basicity ratios, or their logarithmic derivatives:

$$E^{N-C} = \frac{k^{N}}{k^{N}_{C}} = \frac{k^{C}}{k^{C}_{N}} \quad (5)$$

$$\log\ E^{N-C} = \log\ k^{N} - \log\ k^{N}_{C} = \log\ k^{C} - k^{C}_{N} = \ldots \quad (6)$$

The $\log E$ values are the best transferable parameters between molecules having analogous moieties [32].

3.1. Determination of the macroconstants

Evaluation of the protonation constants from ^{1}H NMR-pH titration curves was based on the principle that non-exchanging NMR nuclei near the basic site sense different electronic environments upon protonation. All carbon-bound protons could be observed, except for thyroxine, O-methyl-thyroxine, carboxymethyl-thyroxine and carboxymethyl-liothyronine, where the protons of 2H and 3H intensities could be observed only. Signals of the 1H intensities and multiplets protons provided no discernible signals, due to the sparing solubility. Nevertheless the macroconstant determination could be carried out without difficulties. Since protonation processes are fast on the NMR time scale, the observed chemical shift of a nucleus can be expressed as a weighted average of chemical shifts of the non-protonated and protonated form. Weighting factors are the mole fractions.

$$\delta^{obs.} = \delta_{L^{2-}}\chi_{L^{2-}} + \delta_{HL^{-}}\chi_{HL^{-}} + \delta_{H_2L}\chi_{H_2L} + \delta_{H_3L^{+}}\chi_{H_3L^{+}}$$

$$= \frac{\delta_{L^{2-}} + \delta_{HL^{-}}K_1[H^{+}] + \delta_{H_2L}K_1K_2[H]^2 + \delta_{H_3L^{+}}K_1K_2K_3[H]^3}{1 + K_1[H^{+}] + K_1K_2[H]^2 + K_1K_2K_3[H]^3} \quad (7)$$

where $\delta^{obs.}$ is the observed chemical shift, L^{2-}, HL^{-}, H_2L and H_3L^{+} are the non-protonated, mono-, di-, and triprotonated

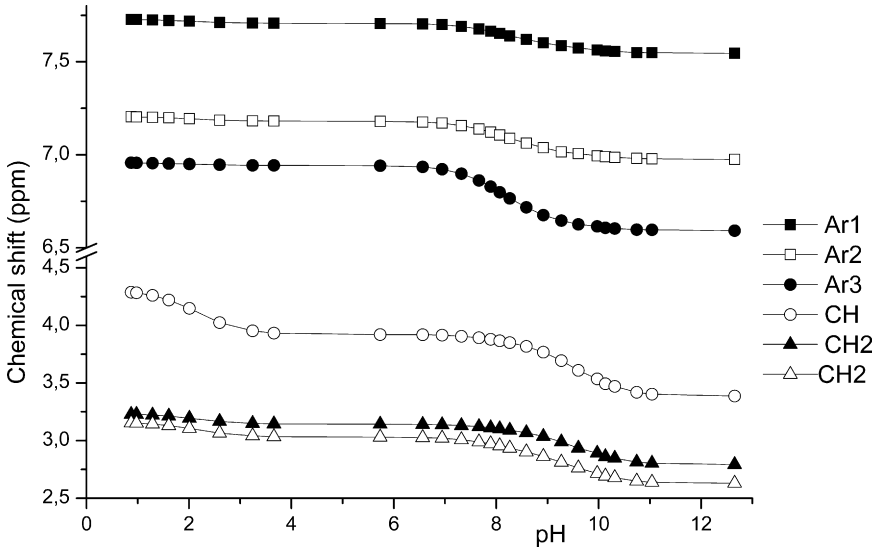

Fig. 3. Chemical shift of the observed protons in MIT as a function of pH; solid lines are the computer fits.

macrospecies, respectively, $\delta_{L^{2-}}$, $\delta_{HL^{-}}$, δ_{H_2L} and $\delta_{H_3L^{+}}$ are the chemical shifts of the species in subscript.

As an example Fig. 3 shows the NMR-pH profiles of the nuclei in MIT. The protonation macroconstants are summarized in Tables 1 and 2.

The stepwise macroconstants show that the carboxylate protonations take place in highly separated manner, as indicated by the $\log K_3$ values of the parent molecules and $\log K_2$ of the O-methyl derivatives. The introduction of iodine atom(s) reduces the basicity of the molecule, expressed mainly in the $\log K_2$ value of the parent compounds. Differences between the DIT macroconstants exceed three $\log K$ units, and the T4 and rT3 macroconstants exceed two $\log K$ units.

The $\log K$ values of dimethyl-liothyronine and dimethyl-thyroxine were immeasurable, due to the sparing solubility. The knowledge of $\log K$ values of O-methyl-liothyronine is not necessary to calculate the complete set of T3 microconstants, because the $\log k^{O}$ value of this molecule was determined by UV–pH titration and the interactivity parameter between the amino and carboxylate is known.

3.2. Determination of the protonation microconstants by UV–pH titration

Protonation microconstants can be determined by spectroscopic methods, provided that concentrations of the related microspecies are commensurable. Phenolate microconstants can be usually determined by UV–pH titration, because the pH dependence of the spectrum is influenced selectively by the protonation of the phenolate group near 290 nm. This statement is verified by the existence of an isosbestic point in the UV–pH titration curves series. We could measure the $\log k^{O}$ value of Tyr, MIT and T3. In our other molecules the difference between the amino and phenolate basicities is greater; the phenolate microconstants are therefore immeasurable by this method.

At pH > 5 the status of the carboxylate does not change, the compounds can be handled therefore as diprotic ones.

The mole fraction of the species protonated at the phenolate group ($\alpha_{OH(pH)}$) can be expressed in terms of the protonation microconstants and hydrogen ion concentrations [33], in relation to the measured UV absorbances:

$$\alpha_{OH(pH)} = \frac{k^{O}[H^+] + k^{O}k_{O}^{N}[H^+]^2}{1 + k^{O}[H^+] + k^{N}[H^+] + k^{O}k_{O}^{N}[H^+]^2} = \frac{A_{O^-} - A_{pH}}{A_{O^-} - A_{OH}} \quad (8)$$

where A_{O^-} is the absorbance of the species deprotonated at the phenolate group, A_{OH} is the absorbance of the species protonated at the phenolate group and A_{pH} is the absorbance of the solution at a particular pH where the phenolate is partially protonated.

We can calculate the k^{O} microconstant using the relationships between the macroconstants and microconstants as follows:

$$K_1 = k^{O} + k^{N} \quad (9)$$

$$K_1K_2 = k^{O}k_{O}^{N} = k^{N}k_{N}^{O} \quad (10)$$

$$k^{O} = \frac{\alpha_{OH(pH)}(1 + K_1[H^+] + K_1K_2[H^+]^2) - K_1K_2[H^+]^2}{[H^+]} \quad (11)$$

K_1 and K_2 protonation macroconstants are known quantities from our NMR-pH titrations. Fig. 4A shows the pH-dependent UV spectra of MIT, and Fig. 4B the phenolate mole fraction of MIT as a function of pH. The log k^{O} values of Tyr, MIT, T3 and the other calculated microconstants are summarized in Table 3.

3.3. The complete microspeciation of Tyr, MIT, DIT, T3 and T4

For the determination of the 12 microconstants of each of the title molecules, our evaluation process utilized four types of data:

- macroconstants of the compound in question;
- macroconstants of derivatives with reduced number of basic site(s);

Table 1
The protonation macroconstants of the parent molecules studied.

	Tyr	MIT	DIT	T4	T3	rT3
$\log K_1$	10.17 ± 0.02	9.63 ± 0.01	9.41 ± 0.01	8.60 ± 0.03	8.87 ± 0.05	9.01 ± 0.03
$\log K_2$	9.06 ± 0.03	8.12 ± 0.01	6.23 ± 0.02	6.59 ± 0.03	8.20 ± 0.05	6.71 ± 0.03
$\log K_3$	2.27 ± 0.03	2.16 ± 0.01	2.07 ± 0.02	2.01 ± 0.06	2.03 ± 0.03	2.04 ± 0.03

Table 2
The protonation macroconstants of the O-methyl-, carboxymethyl-, and dimethyl-derivatives.

	Tyr	MIT	DIT	T3	T4
O-methyl					
$\log K_1$	9.21 ± 0.01	9.01 ± 0.01	8.79 ± 0.01	–	8.55 ± 0.02
$\log K_2$	2.25 ± 0.02	2.19 ± 0.02	2.07 ± 0.04	–	2.05 ± 0.05
C-methyl					
$\log K_1$	9.78 ± 0.01	8.47 ± 0.02	7.46 ± 0.04	8.42 ± 0.03	6.90 ± 0.03
$\log K_2$	7.17 ± 0.01	6.95 ± 0.02	5.87 ± 0.04	6.63 ± 0.04	6.25 ± 0.03
Dimethyl					
$\log K_1$	7.19 ± 0.01	7.00 ± 0.02	6.79 ± 0.03	–	–

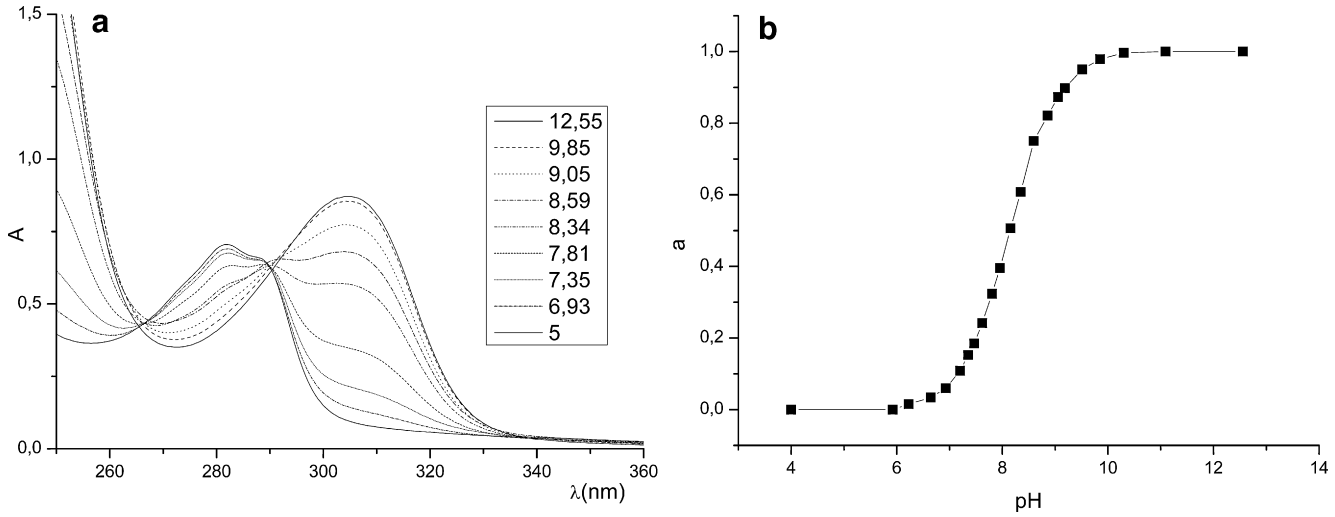

Fig. 4. (A) UV-pH titration of MIT and (B) phenolate mole fraction of MIT.

- the results of the UV-pH titration; and
- the interactivity parameter between the amino and the carboxylate group.

In accordance with the protonation scheme in Fig. 2, and the relationships in Eqs. (2)–(4), the microconstants could be obtained as follows:

1. $\log K_3 = k^{C}_{N,O}$, since the protonation along the $k^{C}_{N,O}$ arrow overwhelmingly predominates over the $k^{O}_{C,N}$ and $k^{N}_{O,C}$ processes.
2. $k^{N}_{O,C}$ is the macroconstant of the dimethyl derivatives.
3. k^{N}_{O} and k^{C}_{O} are the respective K_1 and K_2 macroconstants of the O-methyl derivatives.
4. k^{O}_{C} could be calculated from the macroconstants of the C-methyl derivatives using the value of $k^{N}_{O,C}$.
5. k^{O} and k^{C} could be obtained from Eq. (4).
6. k^{N} could be calculated from Eq. (2).
7. Other microconstants could be obtained from Eqs. (4) and (6).

Concerning thyroxine, the macroconstants of the O-methyl and C-methyl derivatives could be determined, whereas the extremely poor solubility of the dimethyl derivative precluded the determination of the $\log K$ value. Nevertheless $k^{N}_{O,C}$ could be obtained using the amino–carboxylate interactivity parameter of DIT. Thus the complete microconstant set of thyroxine could also be calculated.

Four microconstants of liothyronine (k^{O}, k^{N}, k^{O}_{N}, k^{N}_{O}) from UV-pH titration and macroconstants of the C-methyl derivative were determined. Using the interactivity parameter between the amino and carboxylate group of DIT, $k^{N}_{O,C}$ and then all the other microconstants could be calculated. The protonation microconstants and interactivity parameters of Tyr, MIT, DIT, T3 and T4 are summarized in Table 4.

Table 3
The microconstants from UV-pH titration.

	Tyr	MIT	T3
$\log k^{O}$	10.03 ± 0.01	8.72 ± 0.03	8.43 ± 0.02
$\log k^{N}$	9.61	9.57	8.67
$\log k^{O}_{N}$	9.62	8.18	8.40
$\log k^{N}_{O}$	9.20	9.03	8.64
$\log E^{O-N}$	0.41	0.54	0.03

Table 4
The protonation microconstants and interactivity parameters of Tyr, MIT, DIT, T3 and T4.

	TYR	MIT	DIT	T3	T4
Phenolate microconstants					
$\log k^{O}$	10.04	8.71	6.85	8.43	6.64
$\log k^{O}_{N}$	9.65	8.18	6.23	8.40	6.59
$\log k^{O}_{C}$	9.76	8.42	6.54	8.41	6.60
$\log k^{O}_{C,N}$	9.37	7.89	5.92	8.38	6.55
Amino microconstants					
$\log k^{N}$	9.58	9.57	9.41	8.67	8.60
$\log k^{N}_{O}$	9.19	9.04	8.79	8.64	8.55
$\log k^{N}_{C}$	7.58	7.53	7.41	6.67	6.60
$\log k^{N}_{O,C}$	7.19	7.00	6.79	6.64	6.55
Carboxylate microconstants					
$\log k^{C}$	4.55	4.49	4.37	4.05	4.05
$\log k^{C}_{O}$	4.27	4.20	4.06	4.03	4.01
$\log k^{C}_{N}$	2.55	2.45	2.37	2.05	2.05
$\log k^{C}_{N,O}$	2.27	2.16	2.06	2.03	2.01
Interactivity parameters					
$\log E^{O-N}$	0.39	0.53	0.62	0.03	0.05
$\log E^{N-C}$	2.00	2.04	2.00	2.00	2.00
$\log E^{O-C}$	0.28	0.29	0.31	0.02	0.04

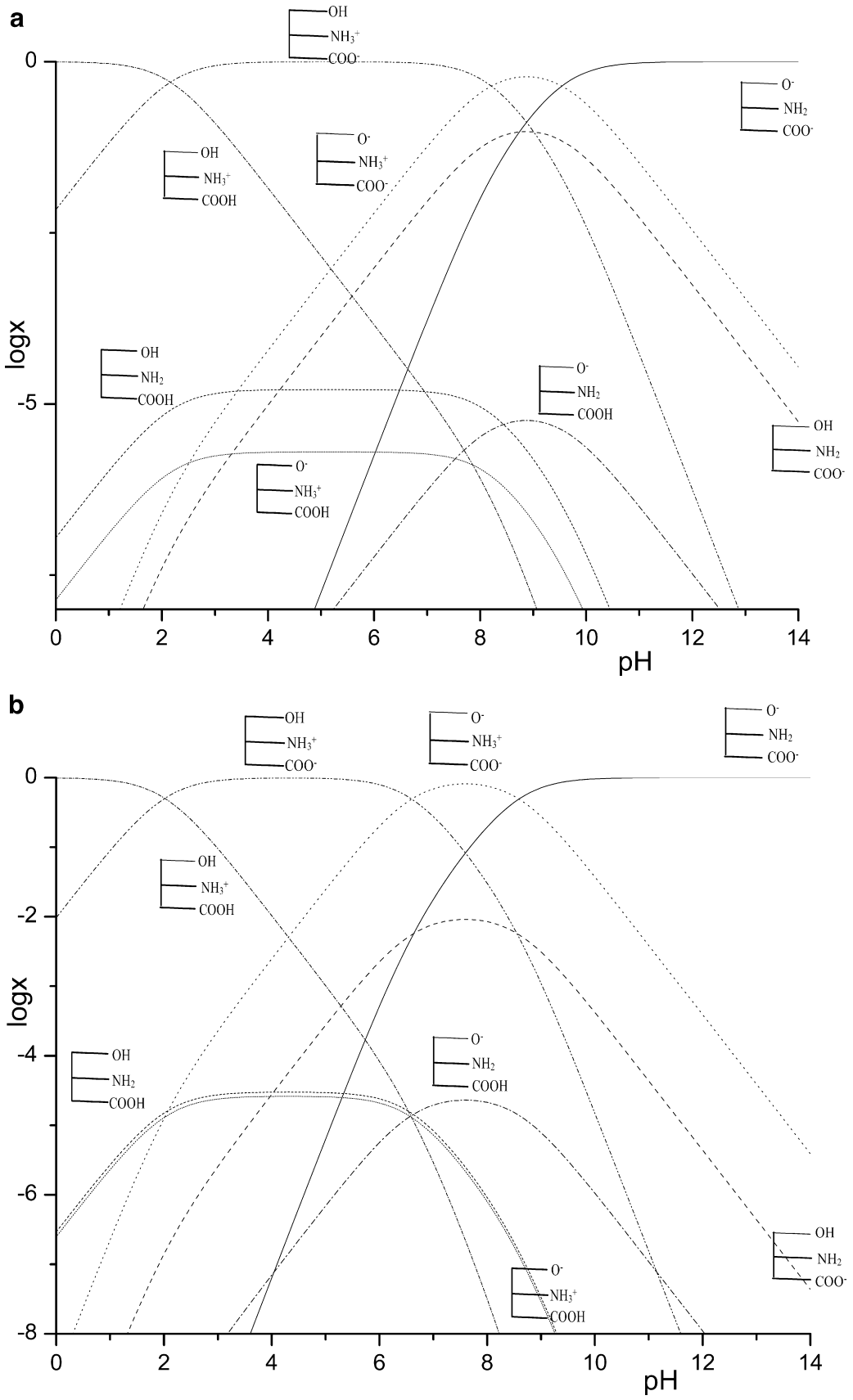

Fig. 5. (A) Logarithmic distribution diagram for all the microspecies of MIT. (B) Logartihmic distribution diagram for all the microspecies of T4.

4. Discussion

The pH-dependent distribution diagrams of the eight microspecies of all compounds studied could be constructed on the basis of our determined protonation microconstants. As an example Fig. 5 shows the distribution diagram of MIT (Fig. 5A) and T4 (Fig. 5B). The iodine atom reduces the basicity of every protonating group, mainly the phenolate. Introduction of a second iodine atom into the aromatic ring exerts an even further enhanced basicity-decreasing effect on the phenolate site. As a secondary effect, the interactivity between the phenolate and amino as well as the phenolate and carboxylate sites are increased, due to the reduced electron density at the aromatic ring and (to a lesser extent) aliphatic chain. In fact, the k^{O} constants in Tyr, MIT and DIT are 10.04, 8.71, and 6.85, respectively, showing the 1.3 and 1.9 drops in log *k* units upon the respective first and second iodination. The phenolate–amino interactivity parameters along the Tyr, MIT and DIT order shows the respective 0.4, 0.5, and 0.6 (rounded) values. The phenolate–carboxylate interactivity values are necessarily smaller than the phenolate–amino ones, since the actually protonating oxygen of the carboxylate moiety is separated by one extra bond, relative to the phenolate–amino nitrogen distance. As a consequence, the changes in the phenolate–carboxylate interactivity parameters are also smaller. Comparison of our interactivity parameters with the analogous data determined by Martin et al. [22] and Kiss and Tóth [23] shows high similarity. The 0.04 difference between the carboxylate–phenolate interactivity parameters is within the error margin, due to the propagation of uncertainty. A larger difference can be observed between our values and those determined by Yamazaki et al. [24], although their phenolate–amino interactivity also increases upon iodination.

As a result of our phenolate microconstants, the aromatic hydroxyl group of DIT exists in the deprotonated form (phenolate) in 93% at the pH of the blood plasma (pH 7.40). The analogous value of MIT is 14% only. The biosynthesis of the thyroid hormones is a complex, enzyme-catalyzed process, but it has long been generally accepted that anionic iodotyrosine residues are required for their biosynthesis [34]. On the grounds of our phenolate microconstants 90% of the biochemically produced thyroid hormones needs to be T4 (formed by linking of two molecules of DIT), which is in good agreement with 95% in physiological data [9]. The microconstant of DIT shows that this molecule is largely ionized at the pH of the thyroid gland; providing plausible explanation why T4 is the main thyroid hormone, which is formed under physiological conditions.

Interpretation of the thyroid hormone–receptor binding can also be improved using the microspeciation data. In the process of receptor binding *sine qua non* conditions are the complementary stereochemistry and appropriate state of protonation. Iodine atoms in the 3 and 5 positions are inevitably necessary for the biological effect, while rT3 is inactive. Also, the 3′ monosubstituted compounds are more potent than the 3′, 5′ disubstituted ones (the affinity of T3 for the receptor exceeds 5 times that of T4) [9]. Iodination of the outer ring decreases the phenolate basicity and increases the portion of the phenolate in the anionic form. Our pH-dependent distribution diagrams show that thyroxine mainly exist at the blood pH in the (O^-, NH_3^+, COO^-) form, whereas T3, the biologically active, receptor-binding hormone mainly occurs in the (OH, NH_3^+, COO^-) state. These data imply that the biological activity needs the phenolate in its neutral, proton donor form. T3 is more active than T4, and 3′-isopropyl-3,5-di-iodothyronine (which bears a less acidic –OH) is also more potent than T3 [9,35–37].

The protonation state of the site influences the binding propensity to transport proteins too, showing, however, an opposite tendency. The affinity for transport proteins has been reported to be dependent on the number and position of the iodine atom [8]. T4 binds the main transport proteins (TBG, TTR, HSA) with higher affinity [6], indicating that the phenolate which exists in the anionic form in T4 at the blood pH, acts as a proton acceptor [37]. Anion transporter proteins, such as OATP1C1 especially prefer T4 and rT3, in which the phenolate predominantly exists in the ionized form, and can act as proton acceptor [5].

Relationships at the submolecular level were found between the site-specific basicities and biosynthesis, receptor-, and transport protein-binding for thyroid hormones and their precursors.

Acknowledgement

This work was supported by the National Scientific Research Fund of Hungary, OTKA K7380.

References

[1] S.R. Chemburkar, K.C. Deming, R.E. Reddy, Chemistry of thyroxine: an historical perspective and recent progress on its synthesis, Tetrahedron 66 (2010) 1955–1962.
[2] P. Kopp, L. Pesce, J.C. Solis-S., Pendred syndrome and iodide transport in the thyroid, Trends Endocrinol. Metab. 19 (2008) 260–268.
[3] H. Nagao, T. Imazu, H. Hayashi, K. Takahashi, K. Minato, Influence of thyroidectomy on thyroxine metabolism and turnover rate in rats, J. Endocrinol. 210 (2011) 117–123.
[4] R. Bunevičius, G. Kažanavičius, R. Žalinkevičius, A.J. Prange Jr., Effects of thyroxine as compared with thyroxine plus triiodothyronine in patients with hypothyroidism, N. Engl. J. Med. 340 (1999) 424–429.
[5] E.C.H. Friesema, J. Jansen, T.J. Visser, Thyroid hormone transporters, Biochem. Soc. Trans. 33 (2005) 228–232.
[6] Å.K.R. Ulla Feldt-Rasmussen, Thyroid Hormone Transport and Actions, in: G.E> Krassas, S.A. Rivkees, W. Kiess (Eds.), Diseases of the Thyroid in Childhood and Adolescence, vol. 11, Karger, Basel, 2007, pp. 80–103.
[7] Marvin program 5.3.8. http://www.chemaxon.com, 2010.
[8] G. Hennemann, R. Docter, E.C. Friesema, M. de Jong, E.P. Krenning, T.J. Visser, Plasma membrane transport of thyroid hormones and its role in thyroid hormone metabolism and bioavailability, Endocr. Rev. 22 (2001) 451–476.
[9] L.S. Goodman, A. Gilman, L.L. Brunton, J.S. Lazo, K.L. Parker, Goodman & Gilman's the pharmacological basis of therapeutics, 11th ed., McGraw-Hill, New York, 2006.
[10] V. Cody, Thyroid hormone interactions: molecular conformation, protein binding, and hormone action, Endocr. Rev. 1 (1980) 140–166.
[11] B. Noszal, Acid–base properties of bioligands, in: K. Burger (Ed.), Biocoordination Chemistry: Coordination Equilibra in Biologically Active System, Ellis Horwood, Chichester, UK, 1990.
[12] E. Collance, M. Paris, Physical chemistry of thyroid hormones. II. Effect of dimethyl sulfoxide concentration on protonation constants measured in water–dimethylsulfoxide media containing 0.5 M sodium perchlorate. Extrapolation to aqueous medium, Bull. Soc. Chim. Fr. 7–8I (1983) I-149–I-154.
[13] K. Florey (Ed.), Analytical Profiles of Drug Substances, vol. 5, Academic Press, New York, 1976, pp. 225–282.
[14] J.E.A. Comer, K.J. Box, Using measured p*K*(a), Log *P* and solubility to investigate supersaturation and predict BCS class, Curr. Drug Metab. 9 (2008) 869–878.
[15] K. Mazák, A. Nemes, B. Noszál, Proton speciation and microspeciation of vinpocetine and related compounds in aqueous and biomimetic media, Pharm. Res. 16 (1999) 1757–1763.
[16] G. Völgyi, R. Ruiz, K. Box, J. Comer, E. Bosch, K. Takács-Novák, Potentiometric and spectrophotometric p*K*a determination of water-insoluble compounds: validation study in a new cosolvent system, Anal. Chim. Acta 583 (2007) 418–428.
[17] A. Marosi, Z. Kovács, S. Béni, J. Kökösi, B. Noszál, Triprotic acid–base microequilibria and pharmacokinetic sequelae of cetirizine, Eur. J. Pharm. Sci. 37 (2009) 321–328.
[18] Z. Szakács, S. Béni, Z. Varga, L. Örfi, G. Kéri, B. Noszál, Acid–base profiling of imatinib (Gleevec) and its fragments, J. Med. Chem. 48 (2005) 249–255.
[19] Z. Szakács, M. Kraszni, B. Noszál, Determination of microscopic acid–base parameters from NMR-pH titrations, Anal. Bioanal. Chem. 378 (2004) 1428–1448.
[20] L. Elbert, Determination of double ions in solutions of ampholytes, Z. Phys. Chem. 121 (1926) 385–400.
[21] J.T. Edsall, J. Wyman, Biophysical Chemistry, Academic press, New York, 1958.
[22] R.B. Martin, J.T. Edsall, D.B. Wetlaufer, B.R. Hollingworth, A complete ionization scheme for tyrosine, and the ionization constants of some tyrosine derivatives, J. Biol. Chem. 233 (1958) 1429–1435.
[23] T. Kiss, B. Tóth, Microscopic dissociation processes of some tyrosine derivatives, Talanta 29 (1982) 539–544.
[24] F. Yamazaki, K. Fujiki, Y. Murata, The ionization constants of organic compounds: I. The microscopic ionization constants of tyrosine and related compounds, Bull. Chem. Soc. Jpn. 38 (1965) 8–12.
[25] C.L. Gemmill, The apparent ionization constants of the phenolic hydroxyl groups of thyroxine and related compounds, Arch. Biochem. Biophys. 54 (1955) 359–367.

[26] J.R. Tata, An unusual property of thyroxine and other iodophenols, Biochem. J. 72 (1959) 214–222.
[27] N. Izumiya, A. Nagamatsu, Walden inversion of amino acids. VI. The synthesis of D-surnamine (N-methyl-D-tyrosine), Bull. Chem. Soc. Jpn. 25 (1952) 265–267.
[28] K. Ishigami, R. Katsuta, C. Shibata, Y. Hayakawa, H. Watanabe, T. Kitahara, Synthesis and structure revision of tyroscherin, and bioactivities of its stereoisomers against IGF-1-dependent tumor cells, Tetrahedron 65 (2009) 3629–3638.
[29] E.L. Purlee, On the solvent isotope effect of deuterium in aqueous acid solutions, J. Am. Chem. Soc. 81 (1959) 263–272.
[30] P.K. Glasoe, F.A. Long, Use of glass electrodes to measure acidities in deuterium oxide, J. Phys. Chem. 64 (1960) 188–190.
[31] Z. Szakács, G. Hägele, R. Tyka, 1H/31P NMR pH indicator series to eliminate the glass electrode in NMR spectroscopic p*K*a determinations, Anal. Chim. Acta 522 (2004) 247–258.
[32] Z. Szakács, B. Noszál, Protonation microequilibrium treatment of polybasic compounds with any possible symmetry, J. Math. Chem. 26 (1999) 139–155.
[33] P.J. Niebergall, R.L. Schnaare, E.T. Sugita, Spectral determination of microdissociation constants, J. Pharm. Sci. 61 (1972) 232–234.
[34] J.J.M. De Vijlder, M.T. Den Hartog, Anionic iodotyrosine residues are required for iodothyronine synthesis, Eur. J. Endocrinol. 138 (1998) 227–231.
[35] M.B. Bolger, E.C. Jorgensen, Molecular interactions between thyroid hormone analogs and the rat liver nuclear receptor. Partitioning of equilibrium binding free energy changes into substituent group interactions, J. Biol. Chem. 255 (1980) 10271–10278.
[36] T.A. Andrea, S.W. Dietrich, W.J. Murray, P.A. Kollman, E.C. Jorgensen, S. Rothenberg, A model for thyroid hormone–receptor interactions, J. Med. Chem. 22 (1979) 221–232.
[37] R. Somack, T.A. Andrea, E.C. Jorgensen, Thyroid hormone binding to human serum prealbumin and rat liver nuclear receptor: kinetics, contribution of the hormone phenolic hydroxyl group, and accommodation of hormone side-chain bulk, Biochemistry 21 (1982) 163–170.

Journal of Pharmaceutical and Biomedical Analysis 61 (2012) 165–175

Contents lists available at SciVerse ScienceDirect

Journal of Pharmaceutical and Biomedical Analysis

journal homepage: www.elsevier.com/locate/jpba

Highly efficient, selective, sensitive and stability indicating RP-HPLC–UV method for the quantitative determination of potential impurities and characterization of four novel impurities in eslicarbazepine acetate active pharmaceutical ingredient by LC/ESI-IT/MS/MS

Saji Thomas[a,*], Amber Bharti[a], Pawan Kumar Maddhesia[a], Sanjeev Shandilya[a], Ashutosh Agarwal[a], Dharamvir[b], Sujay Biswas[b], Vikas Bhansal[b], Ashish Kumar Gupta[b], Praveen Kumar Tewari[b], Chandra S. Mathela[c]

[a] Jubilant Life Sciences Ltd., Analytical Research Department, R&D Centre, C-26, Sector – 59, Noida, Uttar Pradesh 201 301, India
[b] Jubilant Life Sciences Ltd., Chemical Research Department, R&D Centre, C-26, Sector – 59, Noida, Uttar Pradesh 201 301, India
[c] Department of Chemistry, Kumaun University, D.S.B. Campus, Nainital, Uttarakhand 263 001, India

ARTICLE INFO

Article history:
Received 30 August 2011
Received in revised form
19 November 2011
Accepted 23 November 2011
Available online 1 December 2011

Keywords:
Eslicarbazepine acetate
Characterization
LC/MS/MS
Impurity
Validation

ABSTRACT

A novel, sensitive, selective and stability indicating LC–UV method was developed for the determination of potential impurities of eslicarbazepine acetate. High performance liquid chromatographic investigation of eslicarbazepine acetate laboratory sample revealed the presence of several impurities. Three impurities were characterized rapidly and four impurities were found to be unknown. The unknown impurities were identified by liquid chromatography coupled with electrospray ionization, ion trap mass spectrometry (LC/ESI-IT/MS/MS). Structural confirmation of these impurities was unambiguously carried out by synthesis followed by characterization using nuclear magnetic resonance spectroscopy (NMR), infrared spectroscopy (FT–IR) and mass spectrometry (MS). Based on the spectroscopic, spectrometric and elemental analysis data unknown impurities were characterized as 5-acetyl-5,11-dihydro-10*H*-dibenzo [*b*,*f*]azepin-10-one, *N*-acetyl-5*H*-dibenzo[*b*,*f*]azepine-5-carboxamide, 5-acetyl-10,11-dihydro-5*H*-dibenzo[*b*,*f*]azepin-10-yl acetate and 5-acetyl-5*H*-dibenzo[*b*,*f*]azepin-10-yl acetate. The newly developed LC–UV method was validated according to ICH guidelines considering eleven potential impurities and four new impurities to demonstrate specificity, precision, linearity, accuracy and stability indicating nature of the method. The newly developed method was found to be highly efficient, selective, sensitive and stability indicating. A plausible pathway for the formation of four new impurities is proposed.

© 2011 Elsevier B.V. All rights reserved.

1. Introduction

Eslicarbazepine acetate is chemically *S*-(−)-10-acetoxy-10,11-dihydro-5*H*-dibenzo[*b*,*f*] azepine-5-carboxamide acetate (Fig. 1a). It is a second generation antiepileptic drug to oxcarbazepine and a third generation drug to carbamazepine. It is a prodrug to eslicarbazepine (Fig. 1b) also an active metabolite of oxcarbazepine. The structural modification was made to improve efficacy, safety and to prevent formation of toxic epoxide metabolite. Eslicarbazepine acetate is rapidly and extensively metabolized to eslicarbazepine which is responsible for pharmacological activity [1–4]. It is used as add on therapy in refractory partial epilepsy and in bipolar disorder.

A very few methods have been reported in literature for the analysis of eslicarbazepine acetate drug substance. Validated chiral HPLC method for the estimation of (*R*)-enantiomer in eslicarbazepine acetate has been reported recently [5]. Chromatographic conditions have been mentioned for the analysis of eslicarbazepine acetate but not fully disclosed [6]. LC methods were not reported in any of the pharmacopoeias. Extensive literature survey reveals that no reference exists for the quantitative determination of impurities by a stability indicating HPLC method and characterization of unknown impurities of eslicarbazepine acetate drug substance. Hence it was felt necessary to develop an accurate, rapid, selective and sensitive stability indicating LC method for the determination of eslicarbazepine acetate impurities.

Objective of the current study was to develop a stability indicating LC–UV method for the quantitative determination of impurities in eslicarbazepine acetate and characterization of four

* Corresponding author. Tel.: +91 120 4362210; fax: +91 120 2580033.
E-mail address: saji_thomas@jubl.com (S. Thomas).

0731-7085/$ – see front matter © 2011 Elsevier B.V. All rights reserved.
doi:10.1016/j.jpba.2011.11.024

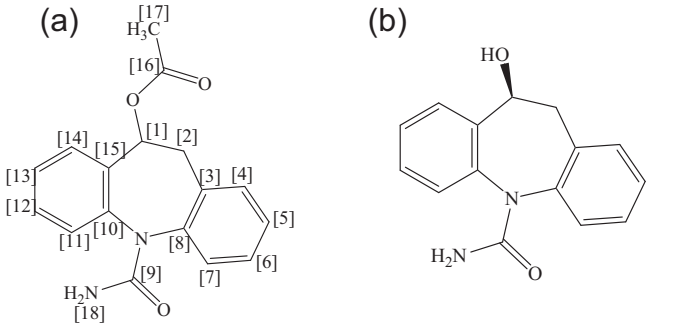

Fig. 1. (a) Eslicarbazepine acetate and (b) eslicarbazepine. Numbering has been assigned for NMR characterization.

unknown impurities detected in several batches of eslicarbazepine acetate in the range of 0.09–0.13%. ICH guidelines indicate that unknown impurities at or above 0.05% in the drug substance require identification [7] depending on the maximum daily dosage. Presence of impurities in drug substance can have significant impact on the quality, safety and efficacy of drug products. Further characterization of impurities is also required to ascertain that an impurity does not have genotoxic concern. Impurities were identified using LC–MS/MS and the proposed structures were further unambiguously confirmed by independent synthesis followed by characterization using NMR and IR techniques. Method was validated as per ICH guidelines [8]. A plausible mechanism for the formation of new impurities is also being proposed in this paper. To the best of our knowledge this is the first paper to report a stability indicating LC–UV method for the quantitative determination of impurities and the impurities characterized are novel impurities in eslicarbazepine acetate.

2. Experimental

2.1. Materials and reagents

Sample of eslicarbazepine acetate API (batch No. SLB-crude) and standards of Imp-1, Imp-2, Imp-3, Imp-4, Imp-5, Imp-6, Imp-7, Imp-8, Imp-9, Imp-10 and Imp-11 were obtained from Chemical Research and Development Department, Jubilant Life Sciences Limited (Noida, India). Deionized water was prepared using a Milli-Q plus water purification system from Millipore (Bedford, MA, USA). HPLC grade methanol, acetonitrile, analytical reagent grade potassium dihydrogen phosphate, ammonium bicarbonate, sodium hydroxide, hydrochloric acid, hydrogen peroxide and ortho phosphoric acid were purchased from Merck India Limited (Mumbai, India). Dimethyl sulphoxide-d6 (for NMR) was purchased from Sigma–Aldrich Corporation (St. Louis, MO, USA). Potassium bromide FT–IR grade was purchased from Merck KGaA (Darmstadt, Germany).

2.2. High performance liquid chromatography

Samples were analysed on a Waters alliance 2690 separation module equipped with 2487 UV detector and 2996 PDA detector for stress study (Waters corporation, MA, USA) using a symmetry shield RP-8, (250 mm × 4.6 mm, 5 μm, Waters corporation, MA, USA). Mobile phase A consisted, 10 mM potassium dihydrogen phosphate adjusted to pH 5.0 ± 0.05 with sodium hydroxide solution–acetonitrile (95:5, v/v) and mobile phase B consisted acetonitrile–water (80:20, v/v) in gradient mode (T_{min}A:B) $T_0$70:30, T_{15}65:35, T_{20}50:50, T_{40}30:70, T_{55}70:30, T_{60}70:30. The flow rate was set to 1.0 mL/min with detector wavelength fixed at 215 nm. The injection volume was 10 μL for a sample concentration of 400 μg/mL prepared in diluent (mobile phase A–acetonitrile, 50:50, v/v). Detector wavelength was fixed at 215 nm and the column temperature was maintained at 35 °C throughout the analysis.

2.3. Liquid chromatography–tandem mass spectrometry (LC–MS/MS).

The equipment and chromatographic conditions used for LC–MS investigation were exactly same as described under Section 2.2. Mobile phase A consisted 10 mM ammonium bicarbonate–acetonitrile (95:5, v/v) and mobile phase B consisted, acetonitrile–water (80:20, v/v) in gradient mode (T_{min}A:B) $T_0$70:30, T_{15}65:35, T_{20}50:50, T_{40}30:70, T_{55}70:30, T_{60}70:30.

The MS and MS/MS studies were performed on Thermo LCQ-Advantage and Xcalibur software (Thermo Electron, San Jose, CA, USA) using electrospray ionization source, atmospheric pressure ionization (APCI) and ion trap mass spectrometer. The typical electrospray source conditions were: spray voltage, 5 kV, capillary voltage, 15–20 V, heated capillary temperature 250 °C, tube lens offset voltage 20 V, sheath gas (N_2) pressure, 20 psi and helium was used as damping gas. In the full scan MS^2 mode, collision energies of 15–35 eV and isolation width of 5 amu were used. The excitation time was 30 ms, the isolated ions were then subjected to a supplementary AC signal to resonantly excite hence causing collision induced dissociation (CID). The collision energies of 15–35 eV and isolation width of 5 were used.

2.4. Sample preparation for forced degradation studies

Stress degradation studies were performed as per ICH guidelines Q1 (R2) to demonstrate the stability indicating nature and specificity of the proposed method. About 20 mg each of eslicarbazepine acetate sample was transferred into four separate 50 mL volumetric flasks and subjected to forced degradation study under acidic (0.5 N HCl, room temperature, 1 h), basic (0.015 N NaOH, room temperature, 2 min) and in water (80 °C for 3 h). The stressed samples of acid and base degradation were neutralized with NaOH and HCl respectively and made up to volume with diluent. Oxidative degradation was carried out using 30% hydrogen peroxide (80 °C for 2 h). Solid state stability of the drug substance was carried out by (a) thermal degradation at 105 °C for 24 h and (b) photolytic degradation was performed by keeping 500 mg of each solid sample in two separate loss on drying bottles (LOD, dark control and photolytic exposure) in photo stability chamber model TP 0000090G (Thermo Lab equipments Pvt. Ltd., Mumbai, India). Samples were exposed to get a minimum exposure of 1.2 million lx hours for light and 200 W h/m^2 for ultraviolet region. Samples were withdrawn at appropriate times and subjected to LC analysis using 400 μg/mL sample concentration. Accelerated and long term stability studies on solid samples were also carried to establish the retest period of drug substance to know the effect of storage conditions at different atmospheric conditions in a stability chamber (Binder GmbH, Tuttlingen, Germany).

2.5. NMR spectroscopy

^1H and ^{13}C NMR spectra were recorded at 399.957 MHz and 100.432 MHz respectively, using a Bruker AVANCE 400 MHz spectrometer (Bruker, Fallanden, Switzerland) equipped with a 5 mm BBO probe and a z-gradient shim system. The ^1H spectra were recorded with 1 s pulse repetition time using 30° flip angle, while ^{13}C spectra were recorded with power gated decoupling

Table 1
Potential impurities of eslicarbamazepine acetate.

S. No.	Structure	Mol Wt.	IUPAC name	Code	Origin
1	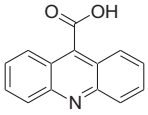	223.23	Acridine-9-carboxylic acid	Imp-1	Degradation
2	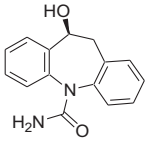	254.28	(*10S*)-10-Hydroxy-10,11-dihydro-5*H*-dibenzo[*b*,*f*]azepine-5-carboxamide	Imp-2	Process and degradation
3	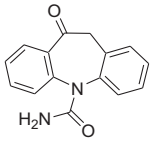	252.27	10-Oxo-10,11-dihydro-5*H*-dibenzo[*b*,*f*]azepine-5-carboxamide	Imp-3	Process
4	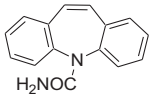	236.27	Dibenzo[*b*,*f*]azepine-5-carboxamide	Imp-4	Process
5	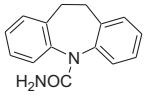	238.28	10,11-Dihydro-dibenzo[*b*,*f*]azepine-5-carboxamide	Imp-5	Process
6	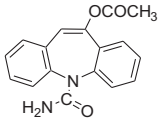	294.30	10-Acetoxy-5*H*-dibenzo[*b*,*f*]azepine-5-carboxamide	Imp-6	Process
7	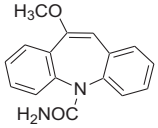	266.29	10-Methoxy-dibenzo[*b*,*f*]azepine-5-carboxamide	Imp-7	Process
8	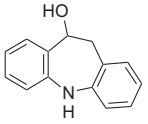	211.26	10,11-Dihydro-5*H*-dibenzo[*b*,*f*]azepin-10-ol	Imp-8	Process
9	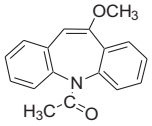	265.31	10-Methoxy-dibenzo[*b*,*f*]azepin-5-yl acetate	Imp-9	Process
10	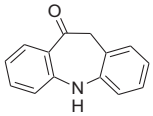	209.24	5,11-Dihydro-10-*H*-dibenzo [*b*,*f*]azepin-10-one	Imp-10	Process
11	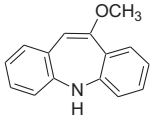	223.27	10-Methoxy-5*H*-dibenzo[*b*,*f*]azepine	Imp-11	Process

using 30° flip angle with repetition time of 2 s. Samples were dissolved in dimethyl sulfoxide-d6. The ^{1}H and ^{13}C chemical shift values were reported on the δ scale in ppm relative to DMSO-d6 (2.50 ppm). All spectra were recorded with sample spinning.

2.6. FT–IR spectroscopy

The IR spectrum was recorded in the solid state as KBr powder dispersion using Nicolet FT–IR model AVTAR 370 (Thermo Electron Scientific Instruments, Madison, WI, USA) with a DTGBS KBr

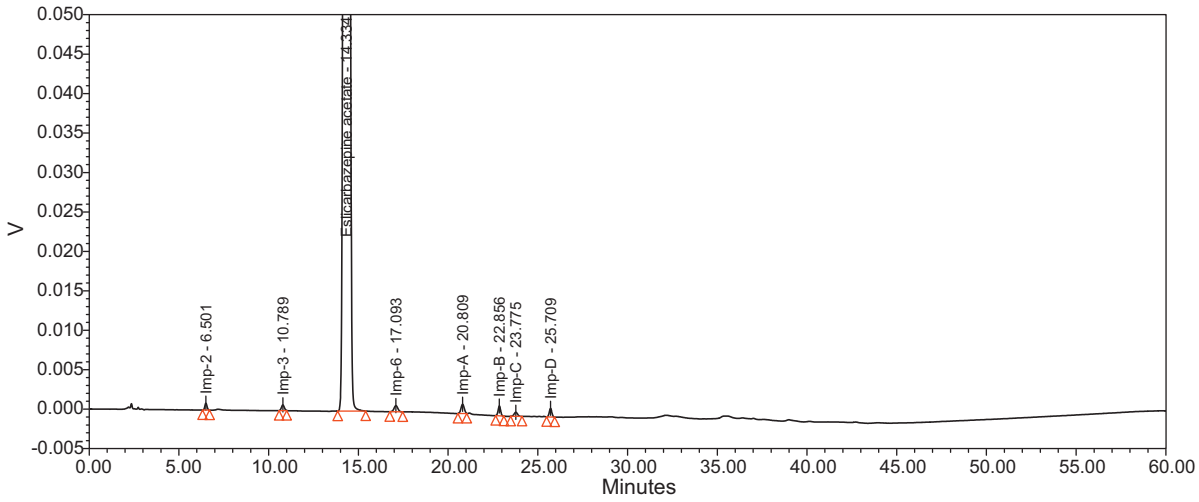

Fig. 2. Chromatogram of eslicarbazepine acetate crude sample.

detector. Data were collected between 400 and 4000 cm^{-1}, with a resolution of 4.0 cm^{-1}. A total of 16 scans were obtained and processed using the OMNIC software version 6.0.

2.7. Preparation of stock solutions for method validation

A test preparation of 400 μg/mL of eslicarbazepine acetate API sample was prepared by dissolving in diluent (buffer–acetonitrile, 50:50). A stock solution of impurities was prepared by dissolving 5 mg each of Imp-1, Imp-2, Imp-3, Imp-4, Imp-5, Imp-6, Imp-7, Imp-8, Imp-9, Imp-10, Imp-11, Imp-A, Imp-B, Imp-C and Imp-D and 5 mg of eslicarbazepine acetate in diluent and made up to 25 mL with diluent. Transferred 5 mL of each individual stock solution into a 100 mL volumetric flask and made up to volume with diluent. From this stock solution standard solution of 0.60 μg/mL of each impurity and 0.60 μg/mL of eslicarbazepine acetate was prepared. This standard solution was also used for checking solution stability and robustness parameters.

3. Results and discussion

3.1. Method development

The main objective of method development was to achieve efficient separation between eslicarbazepine acetate and know impurities (Table 1). The main difficulty was to obtain sufficient selectivity and sensitivity of impurities due to the similar chemical structure of eslicarbazepine and most of the impurities. The resolution between eslicarbazepine acetate, Imp-4 and Imp-5 were poor when different stationary phase viz; C 18, and phenyl were used in different mobile phases containing buffers like dipotassium hydrogen orthophosphate, ammonium acetate or combination of these two with pH ranging from 4 to 6 using organic modifiers such as methanol, acetonitrile and isopropyl alcohol in the mobile phases. Use of symmetry shield-RP8 column, use of acetonitrile–water mixture as mobile phase-B and column temperature 35 °C, was significant in achieving the desired resolution of eslicarbazepine acetate, Imp-4 and Imp-5. Optimum resolution between Imp-4, Imp-5, and Imp-C, Imp-8 were achieved when pH of buffer was adjusted to 5.0. After several trials for gradient profile, chromatographic conditions were finalized as described under section high performance liquid chromatography. The LC–MS compatible method was optimized using ammonium acetate bicarbonate buffer as other volatile buffers such as ammonium formate and ammonium acetate could not give steady base line.

3.2. Identification of unknown impurities by LC–ESI/MS/MS

HPLC analysis of eslicarbazepine acetate (Fig. 2) revealed the presence of seven impurities ranging from 0.09% to 0.13% consistently in several batches. RRTs of all known impurities (Table 1) were compared and found that four impurities at RRTs 1.45, 1.59, 1.66 and 1.79 were unknown and marked as Imp-A, Imp-B, Imp-C and Imp-D respectively. A LC–ESI/MS method as described in Section 2.4 was used to identify these impurities. Mass spectral data showed protonated molecular ion peaks at *m/z* 252, *m/z* 279, *m/z* 296 and *m/z* 294 for Imp-A, Imp-B, Imp-C and Imp-D respectively. Prior to characterization of impurities, LC–MS/MS data of eslicarbazepine acetate was generated to understand the fragmentation pattern. The MS^2 spectrum obtained for eslicarbazepine acetate parent ion at *m/z* 297 (Fig. 3a), showed a prominent peak at *m/z* 237 (Fig. 3b) which can be attributed to the neutral loss of ethenone (CH_2=C=O, 42 amu) due to the formation of metastable ion at *m/z* 255 followed by loss of water. The product ion at *m/z* 237 was further subjected to MS^3 analysis, which gave daughter ions at *m/z* 220 and *m/z* 194 (Fig. 3c). Formation of these product ions can be attributed to the loss of ammonia (NH_3, 17 amu) and iminomethanone (HN=C=O, 43 amu) as depicted in Fig. 4a.

The protonated molecular ion of Imp-A was obtained at *m/z* 252 and M + Na at *m/z* 274 (Fig. 3d). MS^2 analysis showed a major fragment at *m/z* 210 (Fig. 3e) due to the neutral loss of ethenone (CH_2=C=O, 42 amu). MS^3 analysis of the precursor ion at *m/z* 210 gave fragment at *m/z* 182 (Fig. 3f) due to the loss of carbon monoxide (CO, 28 amu). A critical inspection of molecular ion along with the fragmentation pattern in both MS^2 and MS^3 spectrum indicated that Imp-A contains an *N*-acetyl functional group and the structure for Imp-A can be proposed as 5-acetyl-5,11-dihydro-10*H*-dibenzo[*b,f*]azepin-10-one. A plausible fragmentation pattern showing the formation of these daughter ions is depicted in Fig. 4b.

Imp-B showed protonated molecular ion peak at *m/z* 279 and M + Na at *m/z* 301 (Fig. 3g). The MS^2 analysis of Imp-B showed daughter ions at *m/z* 237 and *m/z* 220 (Fig. 3h) which can be attributed due to the loss of ethenone and ammonia respectively. The MS^3 spectrum showed a major fragment at *m/z* 194 was due to the neutral loss of iminomethanone (NH=C=O, 43 amu). Based on the LC–MS/MS data the structure of this impurity was proposed as *N*-acetyl-5*H*-dibenzo[*b,f*] azepine-5-carboxamide. A plausible

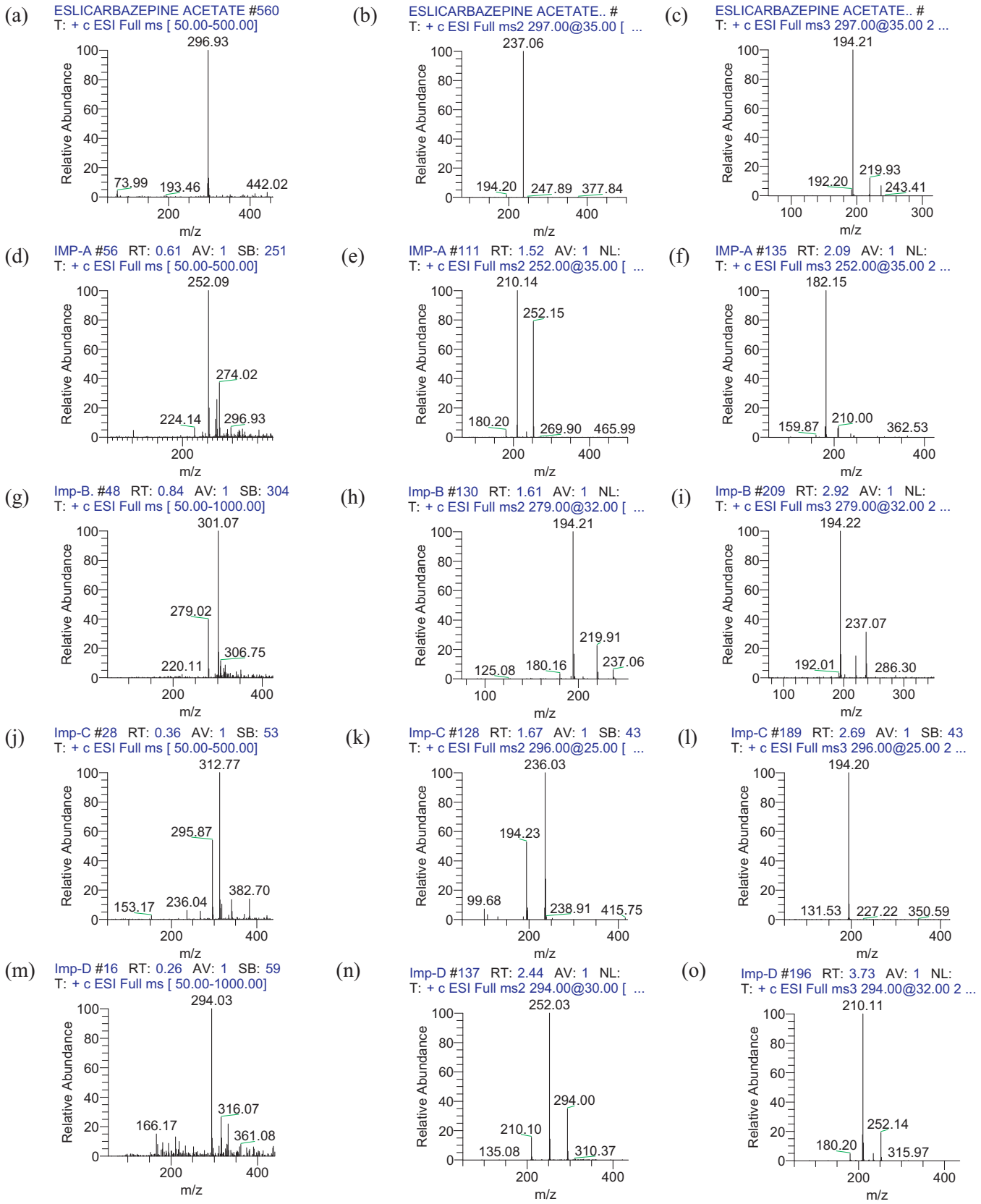

Fig. 3. (a) Mass spectra eslicarbazepine acetate showing [M + H] (at *m/z* 297), (b) MS^2 spectrum of *m/z* 297, (c) MS^3 spectrum of product ion at *m/z* 237, (d) Mass spectra of Imp-A showing [M + Na] (at *m/z* 274) and [M + H] (at *m/z* 252), (e)MS^2 spectrum of *m/z* 252, (f) MS^3 spectrum of product ion at *m/z* 210, (g) Mass spectra of Imp-B showing [M + Na] (at *m/z* 301) and [M + H] (at *m/z* 279), (h) MS^2 spectrum of *m/z* 279, (i) MS^3 spectrum of product ion at *m/z* 237, (j) Mass spectra of Imp-C showing [M + NH_4] (at *m/z* 313) and [M + H] (at *m/z* 296), (k) MS^2 spectrum of *m/z* 296, (l) MS^3 spectrum of product ion at *m/z* 236, (m) Mass spectra of Imp-D showing [M + Na] (at *m/z* 316) and [M + H] (at *m/z* 294), (n) MS^2 spectrum of *m/z* 294 and (o) MS^3 spectrum of product ion at *m/z* 252.

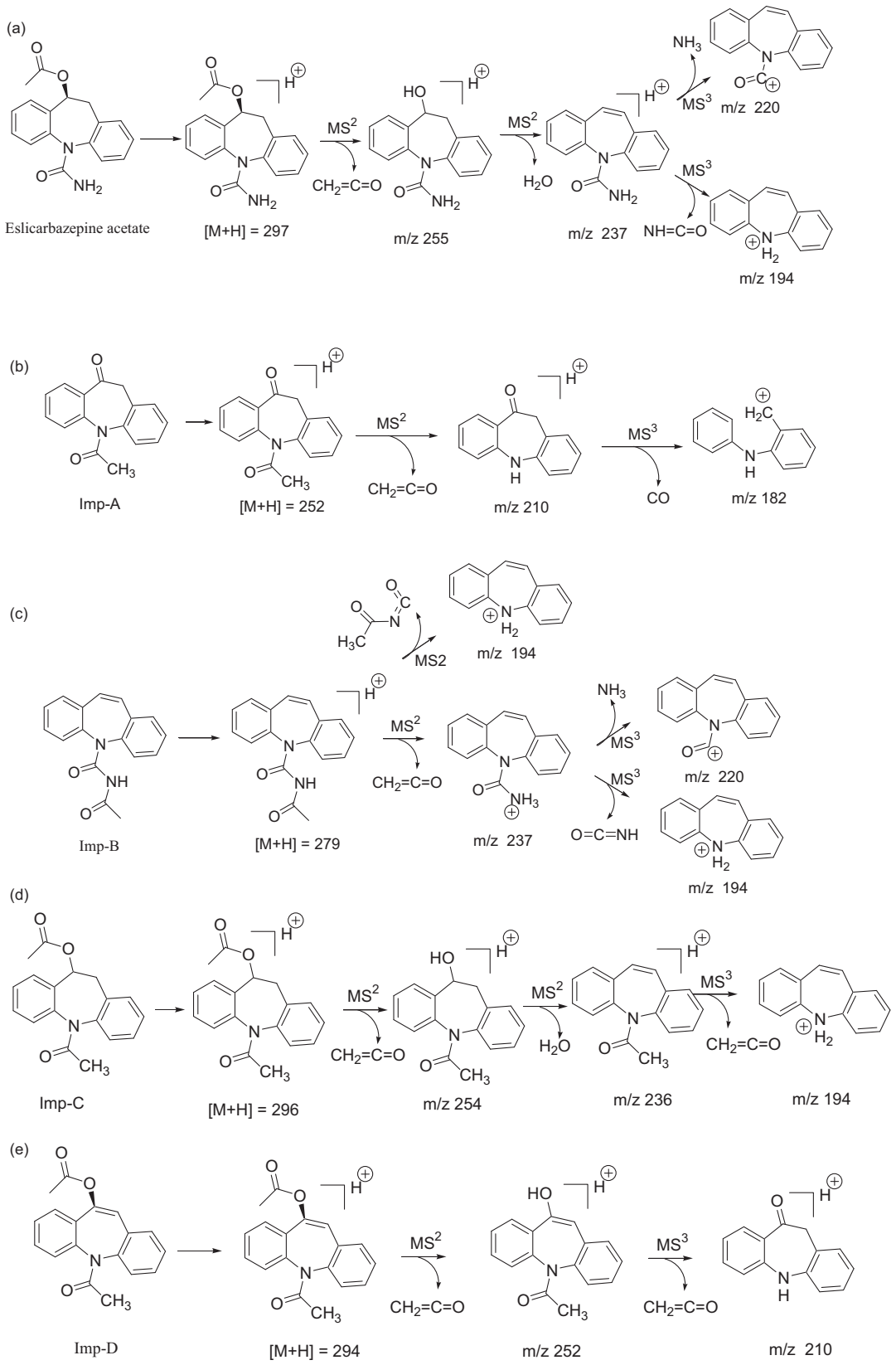

Fig. 4. Plausible pathway showing the formation of product ions of (a) eslicarbazepine acetate, (b) Imp-A, (c) Imp-B, (d) Imp-C and (e) Imp-D.

fragmentation pattern showing the formation of these daughter ions is depicted in Fig. 4c.

The full scan spectra of impurity-C showed its protonated molecular ion at *m*/*z* 296 and M + NH_4 at *m*/*z* 313 (Fig. 3j). The MS^2 analysis of impurity-B showed daughter ion peak at *m*/*z* 236 (Fig. 3k) which was formed due to the loss of water (H_2O, 18 amu) from the metastable product ion at *m*/*z* 254 formed due to the loss of ethenone (CH_2=C=O, 42 amu) from the parent ion. MS^3 analysis

Table 2
Method validation summary report.

Parameter	Imp-1	Imp-2	Imp-3	Eslicarbazepine acetate	Imp-4	Imp-5	Imp-6	Imp-7	Imp-A	Imp-B	Imp-C	Imp-8	Imp-D	Imp-9	Imp-10	Imp-11
System suitability																
RT	2.70	6.49	10.80	14.35	15.80	16.37	17.12	20.18	20.82	22.87	23.79	24.14	25.72	27.86	30.23	39.22
RRT	0.19	0.45	0.75	1.00	1.10	1.14	1.19	1.41	1.45	1.59	1.66	1.68	1.79	1.94	2.11	2.73
R_s	–	21.25	15.92	10.45	3.85	1.47	1.89	8.12	1.84	6.67	2.94	1.11	5.84	7.64	7.63	25.36
Linearity																
r	0.9993	0.9995	0.9994	0.9991	0.9994	0.9994	0.9994	0.9994	0.9994	0.9994	0.9993	0.9994	0.9995	0.9994	0.9995	0.9994
Slope	145,376	202,214	205,407	176,494	294,124	232,870	258,461	271,544	207,675	293,899	171,602	272,262	261,456	288,292	220,009	273,401
Intercept	−237	−227	−277	226	−271	−489	−267	−7.92	70.29	−76	−192	−330	−268	−375	−20	−788
Detection limit (μg/mL)	0.020	0.020	0.020	0.020	0.020	0.020	0.020	0.020	0.020	0.020	0.020	0.020	0.020	0.020	0.020	0.020
Quantitation limit (μg/mL)	0.060	0.060	0.060	0.060	0.060	0.060	0.060	0.060	0.060	0.060	0.060	0.060	0.060	0.060	0.060	0.060
Precision (QL)	0.52	1.77	1.71	2.33	0.94	0.86	0.70	2.79	2.31	0.95	2.05	1.14	0.65	1.92	1.29	2.17
% RSD ($n = 6$)																
Repeatability (intra day)	2.86	2.86	2.67	NA	3.33	3.10	2.67	3.31	3.57	2.70	5.33	2.86	3.60	2.86	3.00	1.02
% RSD ($n = 6$)																
Intermediate precision (inter day)	5.33	2.14	2.00	NA	5.33	3.57	3.13	4.67	3.33	4.00	4.01	2.14	3.32	3.00	5.03	3.33
% RSD ($n = 12$)																
Accuracy at QL level ($n = 3$)																
Amount added (μg/mL)	0.060	0.060	0.060	0.060	0.061	0.060	0.060	0.061	0.062	0.060	0.061	0.062	0.061	0.061	0.062	0.062
Amount recovered (μg/mL)	0.057	0.061	0.061	0.061	0.060	0.059	0.062	0.063	0.063	0.058	0.060	0.060	0.058	0.058	0.058	0.062
% Recovery	95.00	101.67	101.67	101.67	98.36	98.33	103.33	103.28	101.61	96.67	98.36	96.77	95.08	95.08	93.55	100.00
% RSD	0.00	0.00	0.00	0.32	4.33	0.00	0.00	4.22	0.64	0.00	0.00	0.00	0.00	4.33	0.00	0.00
Accuracy at 100% level ($n = 3$)																
Amount added (μg/mL)	0.600	0.592	0.600	0.612	0.596	0.600	0.596	0.600	0.600	0.596	0.568	0.596	0.596	0.592	0.596	0.596
Amount recovered (μg/mL)	0.564	0.564	0.588	0.632	0.580	0.580	0.564	0.580	0.576	0.588	0.560	0.560	0.576	0.568	0.584	0.572
% Recovery	94.00	95.27	98.00	103.27	97.32	96.67	94.63	96.67	96.00	98.66	98.59	93.96	96.64	95.95	97.99	95.97
% RSD	0.44	0.43	0.38	1.21	0.02	0.41	0.45	0.43	0.00	0.41	0.82	0.79	0.37	0.42	1.82	0.41
Accuracy at 150% level ($n = 3$)																
Amount added (μg/mL)	0.900	0.888	0.900	0.916	0.892	0.900	0.892	0.900	0.896	0.892	0.852	0.892	0.888	0.888	0.896	0.892
Amount recovered (μg/mL)	0.856	0.844	0.888	0.912	0.876	0.876	0.848	0.872	0.860	0.884	0.844	0.844	0.868	0.852	0.872	0.864
% Recovery	95.11	95.05	98.67	99.56	98.21	97.33	95.07	96.89	95.98	99.10	99.06	94.62	97.75	95.95	97.32	96.86
% RSD	0.95	0.78	0.51	0.70	0.68	0.89	0.68	0.43	0.46	0.77	0.97	0.90	0.51	0.68	0.68	0.91

n, number of determinations; RT, retention time; RRT, relative retention time; R_s, USP resolution; r, correlation coefficient.

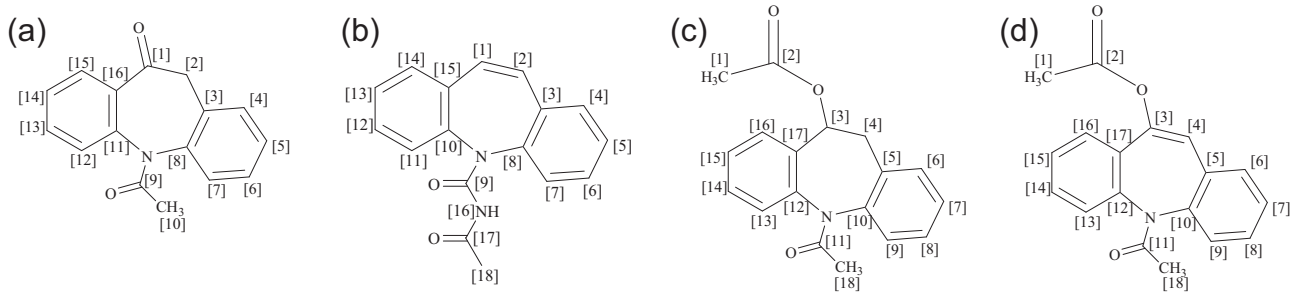

Fig. 5. New impurities of eslicarbazepine acetate, (a) Imp-A, (b) Imp-B, (c) Imp-C and (d) Imp-D. Numbering has been assigned for NMR characterization.

gave fragment at *m*/*z* 194 due to the loss of ethenone (CH_2=C=O, 42 amu) (Fig. 3l). Based on LC–MS/MS analysis this impurity was suspected to be 5-acetyl-10,11-dihydro-5*H*-dibenzo[*b*,*f*] azepin-10-yl acetate (Fig. 4d). A plausible fragmentation pattern showing the formation of these daughter ions is depicted in Fig. 4d.

The full scan spectra of impurity-D showed its protonated molecular ion at *m*/*z* 294 (Fig. 3m). The MS^2 analysis of impurity-D showed daughter ion peak at *m*/*z* 252 which can be attributed to the neutral loss of ethenone from O-acetyl moiety (CH_2=C=O, 42 amu). The MS^3 analysis of the precursor ion of *m*/*z* 210 due to the loss of ethenone from *N*-acetyl moiety (CH_2=C=O, 42 amu). Based on LC–MS/MS analysis this impurity was suspected to be the 5-acetyl-5*H*-dibenzo[*b*,*f*]azepin-10-yl acetate. Proposed fragmentation pattern showing the formation of these daughter ions is depicted in Fig. 4e.

3.3. Synthesis and structural elucidation of Imp-A, Imp-B, Imp-C and Imp-D

Based on the proposed structure of impurities by LC–MS/MS, Imp-A, Imp-B, Imp-C and Imp-D were independently synthesized and used for further structural confirmation by NMR and FT–IR techniques (Fig. 5). Synthesized impurities were analysed by HPLC method as described under Section 2.2 and the purity was found to be 95.2%, 97.6%, 98.2% and 97.9% for Imp-A, Imp-B, Imp-C and Imp-D respectively. The MS^2 spectra obtained for synthesized authentic compounds of impurities using direct infusion mode was found to be exactly same as MS^2 spectra of impurities obtained from on-line LC–MS/MS analysis.

3.3.1. Synthesis of Imp-A

10-Methoxy-5*H*-dibenzo[*b*,*f*]azepine is acetylated using acetic anhydride in presence of triethylamine and toluene as solvent to obtain 1-(10-methoxy-5*H*-dibenzo[*b*,*f*]azepin-5-yl)ethanone. Which is hydrolysed using 1 N HCl in toluene medium to obtain 5-acetyl-5,11-dihydro-10*H*-dibenzo[*b*,*f*]azepin-10-one. ^{1}H NMR (400 MHz, DMSO-d6): 2.01 (br s, 3H, 10), 3.80–3.84 (br s, 2H, 2), 7.35–7.48, 7.66–7.94 (m, 8H, 5, 7, 12, 14, 4, 6, 13, 15). ^{13}C-NMR (100 MHz, DMSO-d6): 23.40 (10), 48.88 (2), 120.75, 122.24, 128.51, 129.88, 130.34, 130.59 (7, 12, 5, 14, 6, 13, 4, 15), 135.12 (3, 16), 141.34, 142.88 (8, 11), 169.41 (9), 192.78 (1). IR; C=O str. (1678.64, 1666.74), C=C str. (1597.28, 1489.52), C—H str. (2872.19, 2963.94).

3.3.2. Synthesis of Imp-B

A suspension of eslicarbazepine acetate (2 g) and zinc chloride in acetic anhydride (30 mL) was heated to 80–85 °C and stirred at this temperature for 16 h. After reaction completion, the reaction mixture was concentrated under vacuum. The residue was diluted in a mixture of dichloromethane and water. The organic layer was washed with 5% sodium bicarbonate solution followed by concentration of aqueous layer under vacuum to get a crude mass which was purified by column chromatography to get *N*-acetyl-5*H*-dibenzo[*b*,*f*]azepine-5-carboxamide. ^{1}H-NMR (400 MHz, DMSO-d6): 2.44 (s, 3H, 18), 6.98 (br s, 2H, 1, 2), 7.17 (br s, 1H, 16), 7.42–7.51 (m, 8H, 4, 5, 6, 7, 11, 12, 13, 14). ^{13}C-NMR (100 MHz, DMSO-d6): 24.74 (18), 129.96 (1, 2, 4, 5, 6, 7, 11, 12, 13, 14, 3, 15), 151.59 (8, 10), 172.99 (9, 17). IR; >C=O str. (1711.69, 1670.83), C=C str. (1482.86), N—H str. (3272.64).

3.3.3. Synthesis of Imp-C

5-Acetyl-5,11-dihydro-10H-dibenzo[*b*,*f*]azepin-10-one was reduced using sodium borohydride in methanol to obtain 1-(10-hydroxy-10,11-dihydro-5H-dibenzo[*b*,*f*]azepin-5-yl)ethanone. Which on acetylation using acetic anhydride, in presence of dimethyl pyridine, triethylamine using dichloromethane as solvent to obtain 5-acetyl-10,11-dihydro-5H-dibenzo[b,f]azepin-10-yl acetate. ^{1}H-NMR (400 MHz, DMSO-d6): 2.03, 2.09 (s, 3H × 2, 1, 18), 3.07–3.20, 3.55–3.58 (m, 2H, 4), 6.00 6.07 (br s, 1H, 3), 7.12–7.45 (m, 8H, 6, 7, 8, 9, 13, 14, 15, 16). ^{13}C-NMR (100 MHz, DMSO-d6): 21.21, 22.94 (1, 18), 35.93 (4), 71.89 (3), 127.39, 128.57, 128.66, 128.70, 130.93, 131.25, 131.93 (7, 15, 9, 13, 6, 14, 16, 8), 134.14, 140.46 (5, 17), 142.34, 142.82 (10, 12), 170.38, 170.58 (2, 11). IR; >C=O str. (1674.35, 1735.55), C=C str. (1602.36, 1490.76).

3.3.4. Synthesis of Imp-D

1-(10-Hydroxy-dibenzo[*b*,*f*]azepin-5-yl)-ethanone is acetylated using acetic anhydride in presence of triethylamine and dimethylamino pyridine using dichloromethane as solvent to obtain 5-acetyl-5*H*-dibenzo[*b*,*f*]azepin-10-yl acetate which is recrystallised from isopropyl alcohol to obtain pure Imp-D. ^{1}H-NMR (400 MHz, DMSO-d6): 1.80, 2.31 (s, 3H × 2, 1, 18), 6.96 (s, 1H, 4), 7.34–7.69 (m, 8H, 6, 7, 8, 9, 13, 14, 15, 16). ^{13}C-NMR (100 MHz, DMSO-d6): 21.22, 22.28 (1, 18), 120.41 (4), 125.65–132.46 (6, 7, 8, 9, 13, 14, 15, 16), 140.66 (5, 17), 147.29 (3, 10, 12), 169.46, 170.10 (2, 11). IR; >C=O str. (1760.73, 1766.74), C=C str. (1593.19, 1486.95), C—H str. (3060.16).

3.4. Formation of Imp-A, Imp-C and Imp-D

During the synthesis of eslicarbazepine acetate, unreacted methoxy iminostilbene present in intermediate Ia (methoxy carbamazepine) undergo acid hydrolysis resulting in the formation of intermediate IIIa and IVa (Keto-enol) which on further acetylation leads to the formation of Imp-A, Imp-C and Imp-D. The presence of carbamazepine in oxcarbazepine was found to contribute the formation of Imp-B. The synthetic scheme of plausible formation of Imp-B, Imp-A, Imp-C and Imp-D is depicted in Fig. 6b and c respectively.

3.5. Results of forced degradation and identification of major degradant impurities

Eslicarbazepine acetate was found to be susceptible to acidic, alkaline and oxidative stress conditions and mild degradation was

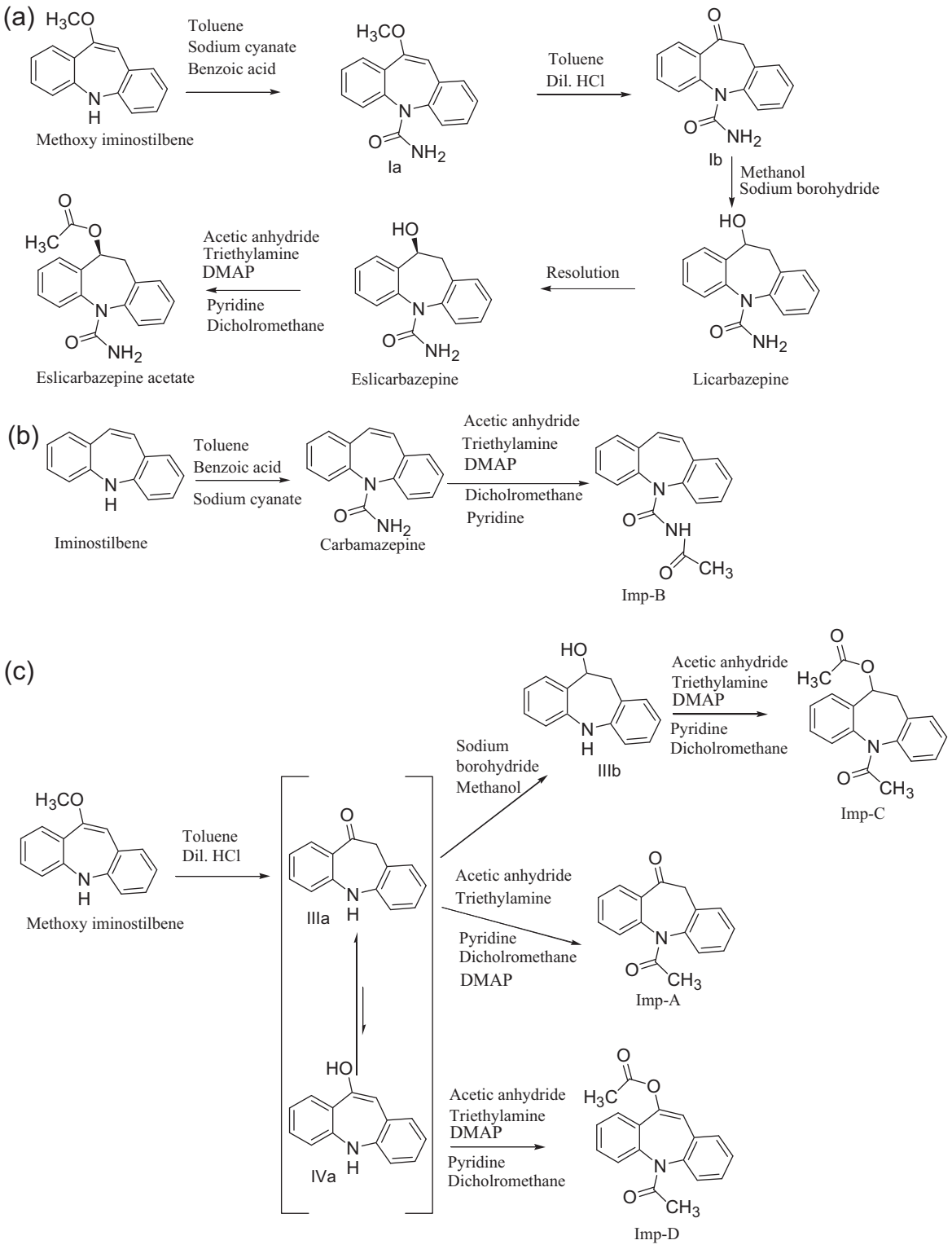

Fig. 6. (a) Scheme for the synthesis of eslicarbazepine acetate, (b) plausible scheme for the formation of Imp-B and (c) plausible scheme for the formation of Imp-A, Imp-C and Imp-D.

observed in aqueous hydrolysis. In acidic alkaline and oxidative hydrolysis, major impurity formed at RRT 0.45 was identified as eslicarbazepine (Imp-2) formed due to the hydrolysis of acetyl moiety in the drug. Solid state stress study confirmed that molecule is stable in thermal, photolytic conditions. Samples from three batches were packed in double polyethylene bags, then packaged in HDPE bottles and kept for stability studies under long-term ($25\pm2\,^{\circ}C, 60\pm5\%$ RH) and accelerated conditions ($40\pm2\,^{\circ}C, 75\pm5\%$ RH) for three months. HPLC analysis at regular intervals (1, 2, 3 months) demonstrated satisfactory resistance to degradation under solid state conditions. From the degradation studies and peak purity test results derived from PDA detector it was confirmed that

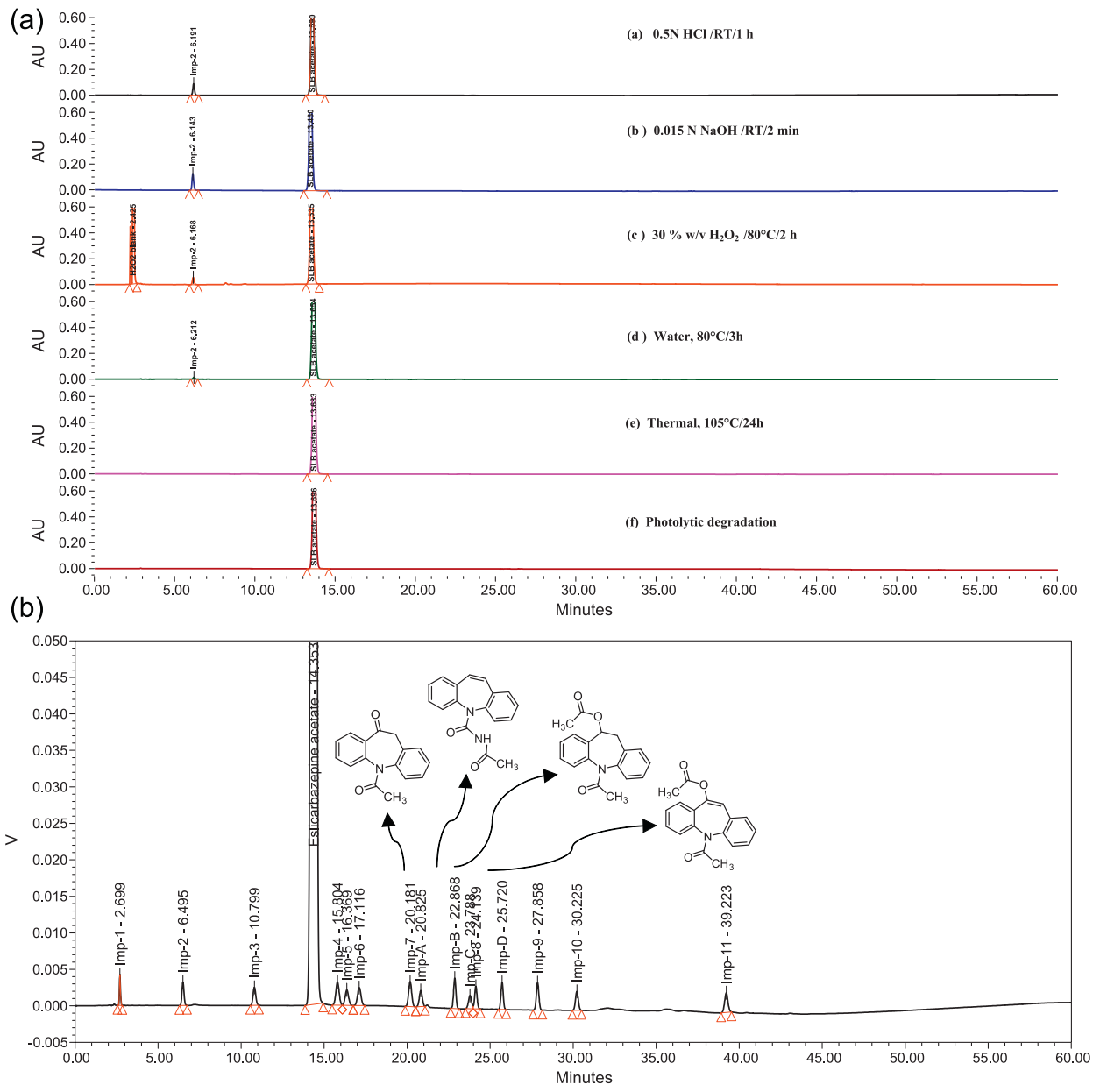

Fig. 7. (A) Typical chromatogram of eslicarbazepine acetate under stress conditions: (a) acid hydrolysis, (b) base hydrolysis, (c) oxidative degradation, (d) water hydrolysis, (e) thermal degradation and (f) photolytic degradation. (B) Chromatogram of eslicarbazepine spiked with impurities.

the spectral purity of eslicarbazepine acetate peak was homogenous thus confirmed the stability indicating power of the newly developed method.

4. Method validation

The newly developed method was validated for sensitivity, linearity, precision and accuracy, robustness and system suitability according to ICH guidelines. The peak capacity of the method for peaks eluting up to 40 min gradient time was found to be about 211 demonstrating the high efficiency of the newly developed method. Validation study was carried out for Imp-1, Imp-2, Imp-3, Imp-4, Imp-5, Imp-6, Imp-7, Imp-8, Imp-9, Imp-10, Imp-11, Imp-A, Imp-B, Imp-C and Imp-D. The system suitability and selectivity were checked by injecting 400 μg/mL of eslicarbazepine acetate solution containing 0.6 μg/mL of all impurities monitored throughout the validation. Method validation results are summarized in Table 2.

4.1. Sensitivity

Sensitivity was determined by establishing the detection limit (DL) and quantitation limit (QL) for all impurities and eslicarbazepine acetate by injecting a series of dilute solutions with known concentrations. The limit of detection and the limit of quantitation were about 0.005% and 0.015% of analyte concentration i.e. 400 μg/mL respectively. The relative standard deviation for QL concentration for all impurities was below 3%.

4.2. Linearity and range

A linearity test solution for related substance method was prepared by diluting the impurity stock solution to the required concentrations. The solutions were prepared at six concentration levels. From QL to 150% of the permitted maximum level of the impurity (i.e. 0.06 μg/mL, 0.3 μg/mL, 0.45 μg/mL, 0.60 μg/mL, 0.75 μg/mL, 0.90 μg/mL) was subjected to linear regression

analysis with the least squares method. Calibration equation obtained from regression analysis was used to calculate the corresponding predicted responses. The residuals and sum of the residual squares were calculated from the predicted responses. The correlation coefficient obtained was greater than 0.999 for all impurities. The result showed an excellent correlation between the peak and concentration of all impurities. The range of the method was from 0.06 μg/mL to 0.90 μg/mL of the analyte concentration (400 μg/mL).

4.3. Precision and accuracy

The precision of the related substances method was checked by injecting six individual preparations of (400 μg/mL) eslicarbazepine acetate spiked with 0.60 μg/mL each impurities Percentage RSD for peak areas of each impurity was calculated and the study was also determined by performing the same procedures on a different day (inter-day precision). The intermediate precision of the method was also evaluated by a different analyst and different instrument in the same laboratory. % RSD of areas of each impurity was within 6.0, confirming good precision at low level of the developed analytical method. The accuracy of the method was evaluated in triplicate at QL, 100% level (0.6 μg/mL) and 150% level (0.90 μg/mL). The percentage recovery of all impurities in drug substance has been calculated. Chromatogram of eslicarbazepine acetate spiked with fifteen impurities was depicted in Fig. 7B.

4.4. Robustness

To determine the robustness of the method, experimental conditions were deliberately changed. Close observation of analysis results of deliberately changed chromatographic conditions viz; flow rate (1.0 ± 0.1 mL/min), pH (3 ± 0.2), mobile phase composition (mobile phase A; ± 10% acetonitrile, mobile phase B; ± 10% water) and column temperature (35 ± 2 °C) revealed that resolution between eslicarbazepine acetate and Imp-4 was greater than 2.0 and no significant change in relative retention time for all impurities in spiked sample illustrating the robustness of the method.

4.5. Solution stability and mobile phase stability

The solution stability of eslicarbazepine acetate and its related impurities was carried out by leaving both spiked and unspiked sample solutions in tightly capped HPLC vials at 25 °C for 24 h in an auto sampler. Content of each impurity was determined against freshly prepared standard solution. No significant changes were observed in the content of any of the impurities. The solution stability and mobile phase stability experiment data confirms that the sample solutions and mobile phases used during related substance determination were stable for at least 24 h and 72 h, respectively.

5. Conclusion

In this study, four unknown impurities in eslicarbazepine acetate drug substance were identified using LC–UV and LC–ESI/IT–MS techniques using a newly developed HPLC method. Proposed structures of these impurities were confirmed by independent synthesis followed by structural elucidation using NMR, FT–IR and MS techniques. Imp-A was characterized as 5-acetyl-5,11-dihydro-10*H*-dibenzo[*b*,*f*]azepin-10-one. Imp-B was characterized as *N*-acetyl-5*H*-dibenzo[*b*,*f*]azepine-5-carboxamide. Imp-C was characterized as 5-acetyl-10,11-dihydro-5*H*-dibenzo [*b*,*f*]azepin-10-yl acetate and Imp-D was characterized as 5-acetyl-5*H*-dibenzo[*b*,*f*]azepin-10-yl acetate. Major impurity formed during acidic and alkaline stress conditions was identified as eslicarbazepine. The LC–UV method was validated as per ICH guidelines. Newly developed HPLC method was found to be simple, sensitive, selective, cost effective and stability indicating. Detection limit for impurities was found to be as low as 0.005% and was found to have excellent resolution for fifteen impurities indicating high sensitivity and selectivity of the validated method.

Acknowledgements

The authors are thankful to the management of Jubilant Life Sciences Limited for providing necessary facilities. Authors would like to thank Mr. Saroj Paul, Dr. Subhash Chandra Joshi, Dr. Hawaldar Maurya, Ms. Samreen Siddiqui and Mr. Sandeep Kanwar for their co-operation in carrying out this work.

References

[1] G. Alves, I. Figueiredo, M. Castel-Branco, A. Loureiro, A. Fortuna, A. Falcao, M. Caramona, Enantioselective HPLC–UV method for determination of eslicarbazepine acetate (BIA 2-093) and its metabolites in human plasma, Biomed. Chromatogr. 21 (2007) 1127–1134.
[2] G. Alves, A. Fortuna, J. Sousa, R. Direito, A. Almeida, M. Rocha, A. Falcao, P. Soares-da-Silva, Enantioselective assay for therapeutic drug monitoring of eslicarbazepine acetate: no interference with carbamazepine and its metabolites, Ther. Drug Monit. 32 (2010) 512–516.
[3] A. Fortuna, J. Sousa, G. Alves, A. Falcao, P. Soares-da-Silva, Development and validation of an HPLC–UV method for the simultaneous quantification of carbamazepine, oxcarbazepine, eslicarbazepine acetate and their main metabolites in human plasma, Anal. Bioanal. Chem. 397 (2010) 1605–1615.
[4] L. Almeida, P. Soares-da-Silva, Eslicarbazepine acetate (BIA 2-093), Neurotherapeutics 4 (2007) 88–96.
[5] M.K. Mone, K.B. Chandrasekhar, Development of liquid chromatographic enantiomer separation methods and validation for the estimation of (*R*)-enantiomer in eslicarbazepine acetate, J. Pharm. Biomed. Anal. 54 (2011) 248–251.
[6] K.J. Prabahar, P.B. Kulkarni, S.B. Sawant, N.D. Limbekar, Glenmark generics limited, United States patent 0173893 A1 (2010).
[7] ICH Guidelines, Q3A (R2), Impurities in new drug substances, October 25, 2006.
[8] ICH Guidelines, Q2 (R1), Validation of analytical procedures: test and methodology, November, 2005.

Journal of Pharmaceutical and Biomedical Analysis 61 (2012) 176–183

Contents lists available at SciVerse ScienceDirect

Journal of Pharmaceutical and Biomedical Analysis

journal homepage: www.elsevier.com/locate/jpba

Measurement of drug diffusivities in pharmaceutical solvents using Taylor dispersion analysis

Fengbin Ye, Henrik Jensen, Susan W. Larsen, Anan Yaghmur, Claus Larsen, Jesper Østergaard *

Department of Pharmaceutics and Analytical Chemistry, Faculty of Pharmaceutical Sciences, University of Copenhagen, Universitetsparken 2, DK-2100 Copenhagen, Denmark

ARTICLE INFO

Article history:
Received 20 June 2011
Received in revised form
25 November 2011
Accepted 27 November 2011
Available online 6 December 2011

Keywords:
Diffusion coefficient
Hydrodynamic radius
Molecular size
Taylor dispersion analysis
Viscosity

ABSTRACT

Knowledge of drug diffusivity is of key importance in the understanding of a number of pharmaceutical and biological processes. However, experimentally determined diffusion coefficients and hydrodynamic radii are only reported for a limited number of drug substances. In this work, Taylor dispersion analysis conducted using capillary electrophoresis instrumentation coupled with a UV imaging detector, with two detection windows along the capillary, is introduced as a powerful method for the determination of drug diffusivities in nanoliter samples. Several potential advantages associated with applying two detection windows instead of one window as done in most previous studies were identified. Overall diffusion coefficient measurements performed using two detection windows are more robust and correction for changes in flow rate and sample volume is not required. The experimental conditions applied were suboptimal for performing single detection window measurements due to the relatively large sample volumes and may be optimized to alleviate the need for tedious correction procedures for this setup. The diffusivities of eleven aromatic compounds in water at 25 °C were determined, and showed a good agreement with the literature values. Furthermore, the diffusivities and hydrodynamic radii of four selected drug substances were determined in acetonitrile, methanol, isopropyl myristate, medium chain triglyceride, and propylene glycol in addition to water. The solvent viscosity was determined simultaneously along with the measurement of analyte diffusivity. Drug diffusivities decreased with increasing solvent viscosity. Taylor dispersion analysis is a robust, simple and automated method of quantification of diffusion coefficients even in media with a relatively higher viscosity than water.

© 2011 Elsevier B.V. All rights reserved.

1. Introduction

Diffusion is the transport of matter due to the random thermal motion of molecules and a spatial gradient in chemical potential. This mass transport process is of paramount importance to the pharmaceutical sciences [1,2]. The diffusion of drug substances through biological membranes is fundamental to drug absorption and elimination processes within the body. Diffusion plays an important role in various separation processes, e.g., dialysis, sedimentation and ultrafiltration. Equally important, the release from drug delivery systems often involves a diffusion component. Pertinent examples include the achievement of controlled drug release through rate-controlling membranes or polymer matrix-based systems [1,3].

The diffusivity (diffusion coefficient, D) of a drug substance in an isotropic solvent is related to the size (hydrodynamic radius, R_h) of the molecule and the properties of the diffusion medium as often expressed through the Stokes–Einstein equation:

$$D = \frac{k_B T}{6\pi\eta R_h} \quad (1)$$

where k_B is the Boltzmann constant, T is the absolute temperature, and η is the viscosity of solution, respectively. Despite the importance of the diffusion coefficient or effective size of a drug substance in various biological and pharmaceutical matrices, this physicochemical parameter is not commonly determined experimentally. This is, at least in part, related to the fact that measurement of diffusion coefficients is mostly cumbersome and time consuming. Diffusion coefficients of substances in solution may be determined using the diffusion cell method [4,5], optical methods (e.g. dynamic light scattering) [6,7], spectroscopic methods (e.g. NMR techniques) [8,9], or Taylor Dispersion Analysis (TDA) [7,10–19].

The TDA methodology is based on the studies by Taylor [20] and, subsequently, Aris [21] on dispersion of analytes subjected to Poiseuille laminar flow conditions in a tube. The parabolic flow profile causes the analyte molecules in the tube to move with different velocities according to their radial position in the tube or capillary which consequently lead to analyte dispersion. The degree of

Abbreviations: CE, Capillary electrophoresis; IPM, Isopropyl myristate; MCT, Medium chain triglyceride; PG, propylene glycol; TDA, Taylor dispersion analysis.

* Corresponding author. Tel.: +45 35336138; fax: +45 35336030.
E-mail address: joe@farma.ku.dk (J. Østergaard).

0731-7085/$ – see front matter © 2011 Elsevier B.V. All rights reserved.
doi:10.1016/j.jpba.2011.11.030

dispersion of the analyte plug is dependent on the diffusivity of the analyte leading to redistribution over the tubular cross section (see Supplementary Data for details on TDA theory).

TDA is a simple, relatively rapid and absolute (calibration is not required) method for determination of diffusion coefficients [12]. TDA can be implemented using standard equipment such as High Performance Liquid Chromatography (HPLC), Flow Injection Analysis (FIA) and Capillary Electrophoresis (CE). In particular, commercially available CE instrumentation utilizing narrow bore fused silica capillaries and providing convenient autosampling and detection possibilities has been found well-suited for TDA studies and has contributed to the recent renewed interest in the technology. TDA has been used to assess the diffusivity of small molecules [11,17,22,23], macromolecules [11,12,15,16,18,24], as well as colloidal particles [13,25]. Also, TDA was successfully introduced to characterize complexation phenomena [14,26]. Recently, TDA studies utilizing two detection points along the capillary have been reported [7,16,18,25]. However, the potential advantages associated with having more than one detection window have hitherto not been investigated.

The present studies were undertaken to characterize further the feasibility of TDA for the measurement of diffusion coefficients and estimation of hydrodynamic radii of drug substances in selected pharmaceutical media. A UV imaging detector allowing two detection windows along the capillary connected to a commercially available CE instrument was used for the investigations. The effects of varying the experimental parameters, capillary dimensions, flow rates, and sample volumes, were studied highlighting the need for suitable corrections due to the ramp in fluid velocity and the finite width of the sample zone. In this context, several advantages of having two detection windows were identified. Using optimized experimental conditions, the diffusion coefficients of 11 low-molecular-weight analytes (mostly drug substances) in water were determined and compared to literature data. Most studies using TDA for the determination of molecular diffusion coefficients have been conducted in aqueous solutions. Consequently, it was found of interest to evaluate the feasibility of quantifying drug substance diffusivities in additional 5 pharmaceutically relevant media, including the more viscous isopropyl myristate (IPM), medium chain triglyceride (MCT), and propylene glycol (PG). In addition to the diffusion coefficients, measurements of vehicle viscosity were simultaneously attained by the TDA method.

2. Experimental

2.1. Chemicals and sample preparation

Phenol, *p*-nitrophenol, (R/S)-ibuprofen, (R/S)-warfarin, and salicylic acid were obtained from Sigma–Aldrich (St. Louis, MO, USA). Benzoic acid, histidine, isopropyl myristate (IPM), and propylene glycol (PG) were purchased from Fluka–Chemie (Buchs, Switzerland). L-Phenylalanine and L-tryptophan were obtained from Calbiochem–Novabiochem (Läufelfingen, Switzerland). Bupivacaine hydrochloride and lidocaine were obtained from Unikem (Copenhagen, Denmark). Benzene was obtained from J. T. Baker (Deventer, Holland). Toluene was obtained from Applichem (Darmstadt, Germany). Medium chain triglyceride (MCT, Myritol 318 PH) was kindly donated by Broste A/S (Lyngby, Denmark). Sodium dihydrogen phosphate monohydrate was obtained from Merck (Darmstadt, Germany). HPLC-grade methanol (MeOH) and acetonitrile (CH_3CN) were obtained from BDH (Poole, England). The free base of bupivacaine used was obtained from the corresponding hydrochloride as previously described [27]. All other chemicals were used as received. Throughout the experiments, purified water from a Milli-Q deionization unit (Millipore, Bedford, MA, USA) was used. All solutions were prepared by dissolving the analyte in the appropriate volume of water, organic or pharmaceutical solvent at ambient temperature. Ibuprofen was poorly soluble in water (0.12 mg/mL at 25 °C) [28]. Therefore, the saturated aqueous solution was prepared and filtered prior to TDA measurement.

2.2. Instrumentation

All TDA and solvent viscosity measurements were conducted on an Agilent ^{3D}CE instrument (Agilent Technologies, Waldbronn, Germany) with an external pressure source attached. An Actipix D100 UV area imaging detector (Paraytec Ltd., York, UK) was used for detection at two windows along the capillary. The capillaries were taken out of the Agilent CE cassette and looped into Actipix detector as detailed elsewhere [16]. The temperature of the capillary cartridge was set at 25 °C. The UV absorbance signals from each of the detection windows were recorded with Actipix control software (version 1.2). UV detection was performed at wavelengths of 200, 214 or 254 nm. The detection windows were 1.5 cm in width and produced by burning off the polyimide coating. Fused silica capillaries (Polymicro Technologies, Phoenix, AZ, USA) were cut to a total length of 90.2 cm and prepared with lengths of 30.7 and 50.9 cm to the centre of the first and the second detection windows, respectively.

2.3. TDA measurements

New capillaries were conditioned with 1 M NaOH and water for 30 min each. Between two injections, the capillary was flushed with dispersion media for 2 min (water, MeOH, and CH_3CN) or 10 min (IPM, MCT, and PG). In case of the more viscous and greasy solvents (IPM, MCT, and PG), the capillary was cleaned by flushing with 96% (v/v) ethanol after measurements. Sample injection was hydrodynamically performed from the inlet side of the capillary by applying a pressure of 50 mbar (from 1 to 20 s) or 1000 mbar (from 9 to 24 s) for the more viscous media. Mobilization pressures of 50, 100, 150, 200, 250, 300, and 1000 mbar were applied with a dispersion medium filled vial in the inlet position to force the sample plug through the capillary. Each sample was analyzed 6 times unless otherwise noted. The experimental temperature next to the capillary loop was measured using a Fluke 1522 temperature probe (Fluke Corporation, American Fork, UT, USA).

2.4. Determination of the capillary radius

Capillary radii, R_c, were measured using the modified Hagen–Poiseuille method [13,17]:

$$u = \frac{R_c^2\ \Delta P}{8\eta L_t} \quad (2)$$

where u is the flow rate, η is the viscosity of water, ΔP is the pressure difference between the inlet and outlet of the capillary, and L_t is the total length of capillary. The capillary was first filled with water (η = 0.933 mPa s at 23 °C [29]) by flushing the capillary for 10 min. Then a small plug of phenol sample (0.2 mg/mL in water) was hydrodynamically injected (50 mbar, 7 s) and replaced by forcing water through the capillary at ambient (known) temperature and a pressure drop of 50 mbar. The flow rate was determined by measuring the capillary length and the residence time of the phenol sample between the two detection windows. The measurements were repeated 6 times, yielding a capillary radius that varied less than 1%. The average of these measurements was taken as the capillary radius.

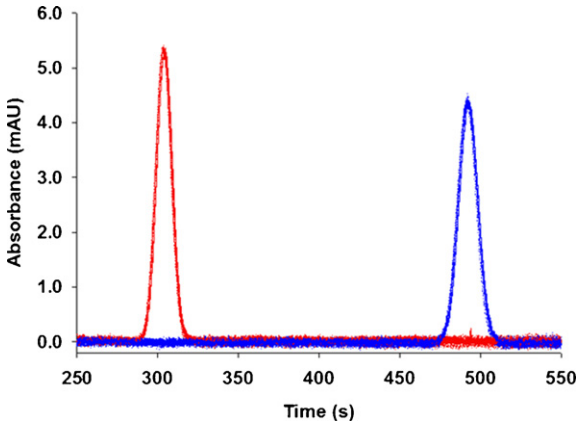

Fig. 1. Six superimposed dispersion profiles of 0.2 mg/mL phenol in water detected at 254 nm. The injected sample (33 nL (50 mbar for 7 s)) was forced through the capillary tube by a pressure drop of 50 mbar. Total length of the 75.6 μm i.d. capillary was 90.2 cm, with 30.7 and 50.9 cm to the first (red trace) and the second (blue trace) detection windows, respectively.

3. Results

3.1. Initial studies

3.1.1. Initial measurements

Measurements of diffusivities by Taylor dispersion were performed using commercially available capillary electrophoresis instrumentation equipped with a UV imaging detector and standard fused silica capillaries. Fig. 1 shows six superimposed dispersion profiles of phenol in water recorded by the UV imaging detector having two detection windows along the capillary. Phenol samples in water were introduced by pressure (50 mbar for 7 s) into the capillary (90.2 cm × 75.6 μm i.d.) followed by a mobilization pressure of 50 mbar (flow rate 1.1 mm/s) to force the peaks past the detection windows. This allowed an experiment to be completed in 10 min (Fig. 1). Analyte dispersion was apparent as a decrease in height and broadening of the second peak as compared to the first. The repeatability of the temporal variances (σ^2) and the peak appearance times (t_R) in terms of relative standard deviations determined using this initial setup was less than 1% ($n = 6$) for both the detection windows.

3.1.2. Calculation of diffusion coefficients

The peak maximum time and temporal variance of each peak were obtained from the Actipix software. Good agreement was observed between the t_R and σ^2 values read from the Actipix software and the values calculated by fitting UV traces to a Gaussian 4-parameter function using the software SigmaPlot 9.0 (Systat, Point Richmond, CA, USA) [14]:

$$y = y_0 + a \cdot e^{-1/2(t-t_R/\sigma)^2} \quad (3)$$

where y is the detector response, y_0 is the detector offset from the baseline, a is a proportionality constant, and t is the time variable. The resident times were identical and the temporal variances differed less than 3% when the initial conditions were applied (90.2 cm × 75.6 μm i.d., 30.7 and 50.9 cm to the first and second detection windows, respectively; mobilization pressure 50 mbar ($n = 12$)). Hereafter, the Actipix software was used for the calculation of t_R and σ^2 in all subsequent experiments.

The phenol diffusivity was calculated by applying the Aris equations (Eqs. (S5) and (S6)) in order to examine the effect of using one *versus* two detection windows. The approach of Aris was preferred for calculation of D to the simpler expression Eq. (S7), because axial diffusion could not be neglected, i.e. Taylor conditions were not fulfilled. When a single detection window was used, corrections for the initial ramp in flow velocity and the width of the injected plug were performed to account for experimental non-idealities due to sample injection using Eqs. (S10)–(S14) [10,17,24] as detailed in the Supplementary Data. For the one window TDA experiments, large differences between uncorrected and corrected D values were observed, as large as 25% and 15% for the first and second detection window, respectively. This was observed for an injection volume of 33 nL (50 mbar for 7 s), which corresponded to 2.5% and 1.5% of the capillary volume from the inlet to detection point for the first and second detection window, respectively. The corrections for the width of sample zone and the initial ramp were not made when both detection windows were used for TDA. Analysis of the dispersion profiles in Fig. 1 applying data from both detection windows resulted in a diffusivity of phenol in water at 23 °C of 9.56×10^{-10} m^2 s^{-1} (10.1×10^{-10} m^2 s^{-1} when recalculated to 25 °C), as compared to the reported values of 10.0×10^{-10} m^2 s^{-1} (average) at 25 °C [22,23,29].

3.2. Importance of experimental parameters

3.2.1. Pressure gradient and capillary dimensions

To evaluate the effects of flow rate (mobilization pressure) and capillary inner diameter (i.d.) on the measured diffusivity, the dispersion of phenol in water as a function of mobilization pressure in 52.8 and 75.6 μm i.d. capillaries was investigated. Both the t_R and σ^2 values of the observed peaks decrease as the mobilization pressure is increased. The repeatability was slightly worse at higher mobilization pressures as compared to 50 mbar, nevertheless in all cases the relative standard deviations were less than 8% (see Table S1 in Supplementary Data). Note that the deviation also included the variability in temperature (<1 °C).

Fig. 2 shows that D values determined using both detection windows are less affected by changes in the flow velocity than those determined using a single detection window. The apparent D values obtained using a single detection window increase with the flow rate even after performing the corrections (Eqs. (S10)–(S14)). This dependence on flow rate is also strongly related to the capillary length from the inlet to the detection window (L_D), the errors being most pronounced for the shorter L_D (Fig. 2). In cases of two detection windows, the measured D is largely independent of the flow rate (increase < 15%) in the range applied as would be expected.

3.2.2. Effects of sample volume

To assess the effect of sample volume, V_i (sample width), phenol diffusivity in water as a function of the injection volume was studied at two mobilization pressures (50 and 150 mbar (1.1 mm/s and 3.1 mm/s)) in the 75.6 μm i.d. capillary. It was observed that the sample residence time slightly decreased with increasing V_i; however, the difference was less than 5%. At a larger injection volume (>90 nL), deviation from the Gaussian peak shape was apparent. On the other hand, smaller injection volumes (<15 nL (50 mbar for 3 s)) also lead to poorer repeatability (see Table S2 in Supplementary Data).

Fig. 3 shows the uncorrected diffusivities and diffusivities of phenol determined using different correction approaches. In all experiments, the injected volumes constituted less than 3.2% and 5.2% of the inlet-to-detection point capillary volume for the first and second detection window, respectively. An injection volume of 10 nL corresponded to 0.7% and 0.4% of the inlet-to-detection point capillary volume for the first and second detection window, respectively, in Fig. 3. It is apparent that when only a single detection window is applied, the uncorrected D values decrease with increasing injection volume independent of the applied flow rate. At a flow rate of 1.1 mm/s, the deviation from the accepted diffusion coefficient (10.0×10^{-10} m^2 s^{-1} at 25 °C) increases rapidly with the

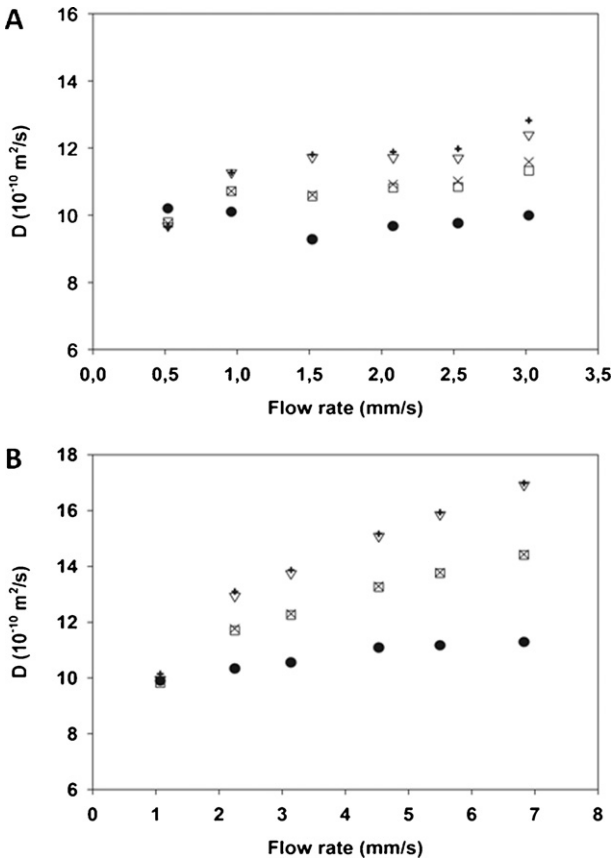

Fig. 2. Effect of the flow rate on the diffusivity of phenol in water at (A) 52.8 μm and (B) 75.6 μm inner diameter capillaries. Experimental data were determined from (▽, +) the first detection window, (□, ×) the second detection window, and (●) two detection windows. For a single detection window, the finite volume of the injected sample was corrected using (▽, □) Alizadeh et al. method (Eqs. (S10) and (S11)) or (+, ×) Cottet et al. method (Eqs. (S12) and (S13)); the initial ramp in flow velocity was corrected using Eq. (S14). Hydrodynamic injection was performed at a pressure of 50 mbar for 7 s. The injection volume V_i was 8 nL and 33 nL for the 52.8 μm and 75.6 μm inner diameter capillaries, respectively. Total length of capillaries was 90.2 cm, with 30.7 and 50.9 cm to the first and the second detection windows, respectively. The capillary volumes from the inlet to the detection points were 0.7 and 1.1 μL (1.4 and 2.3 μL) for the first and second detection windows, respectively for the 52.8 μm (75.6 μm) inner diameter capillary.

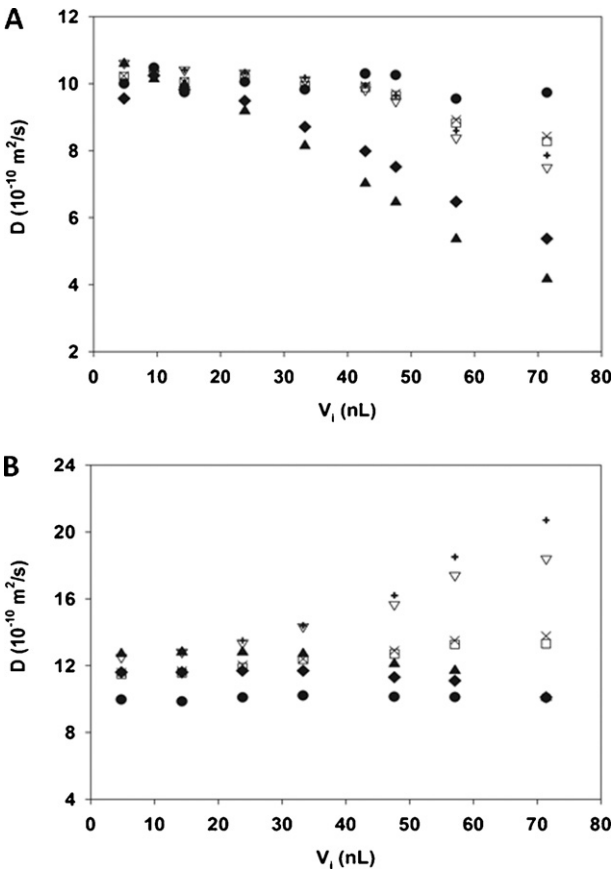

Fig. 3. Effects of injection volume and the calculation method on the determination of diffusivity of phenol in water at two mobilization pressures of (A) 50 mbar (1.1 mm/s) and (B) 150 mbar (3.1 mm/s). Experimental data were obtained from (▽, +, ▲) the first detection window, (□, ×, ♦) the second detection window, and (●) two detection windows. For a single detection window, both the (▲, ♦) uncorrected and (▽, +, □, ×) corrected diffusivities were given. The correction for the finite volume of the injected sample was performed using (▽, □) Alizadeh et al. method (Eqs. (S10) and (S11)) or (+, ×) Cottet et al. method (Eqs. (S12) and (S13)); the initial ramp in flow velocity was corrected using Eq. (S14). Total length of the 75.6 μm i.d. capillary was 90.2 cm, with 30.7 and 50.9 cm to the first and the second detection windows, respectively. The capillary volumes from the inlet to the detection points were 1.4 and 2.3 μL for the first and second detection windows, respectively. The injection volume V_i investigated ranged from 5 to 72 nL.

injection volume (Fig. 3A) whereas at a flow rate of 3.1 mm/s the decrease in D with increasing injection volume largely compensates for the offset (error) due to the higher flow rate (Figs. 2 and 3B). For the flow rate of 1.1 mm/s the correction approaches of Cottet et al. and Alizadeh et al. improve the D values determined and are successful for correction until an injection volume of 43 nL with the specific conditions applied (injection volume, flow rate and capillary dimensions). In contrast the correction procedures seem to significantly overcorrect the diffusivities using a flow rate of 3.1 mm/s. Overall, the deviation from the accepted diffusion coefficient increases with the injection volume when only a single detection window is applied (Fig. 3), even though the corrections of the width of sample zone and the initial ramp have been made (Eqs. (S10)–(S14)). Also the deviations are dependent on the length of the capillary from the inlet to the detection window, with larger errors at shorter L_D. As an alternative approach, when a single detection window is applied, the value of σ^2 at $V_i = 0$ can be obtained by extrapolation following a quadratic dependence [10]. According to correction Eq. (S11) used to correct for the width of the injected sample zone, thus taking advantage of the series of injections with varying sample volume, a more accurate D value (9.6×10^{-10} m^2 s^{-1} at 23 °C) is obtained using the extrapolated σ^2 and the residence time corrected for the initial ramp (Fig. S1 in Supplementary Data) as have previously shown by Sharma [17]. Fig. 3 demonstrates that applying two detection windows allows more accurate measurement of D as compared to using only a single detection window. The differences in measured D values using different injection volumes (5–72 nL) are less than 10% for both mobilization pressures applying data from the two detection windows (Fig. 3).

3.3. Molecular properties

3.3.1. Measurement of diffusivities in water

Table 1 summarizes the diffusion coefficients of eleven small aromatic compounds in water. The TDA measurements were executed using the optimized conditions exploiting two detection windows (90.2 cm × 75.6 μm i.d., 30.7 and 50.9 cm to the first and second detection windows, respectively; hydrodynamic injection 50 mbar for 7 s; mobilization pressure 50 mbar). The relative standard deviations were within 5% with the exceptions of histidine and warfarin (Table 1). In order to compare the measurements to the literature values at 25 °C, the results obtained were recalculated to 25 °C using the Stokes–Einstein equation (Eq. (1)). In water,

Table 1
Diffusion coefficients (D) in water at 25 °C obtained using Taylor dispersion analysis ($n = 8$).[a]

Compounds	Concentration (mg/mL)	$D \pm$ SD (10^{-10} m^2 s^{-1})	RSD (%)	Literature values (10^{-10} m^2 s^{-1})
Tryptophan	0.2	6.55 ± 0.3	4.1	6.31[b], 6.59[c]
Phenylalanine	0.2	7.07 ± 0.2	2.8	7.08[b], 7.05[c]
Histidine	0.2	7.33 ± 0.6	7.7	7.33[b]
Benzene	0.02	11.1 ± 0.2	1.9	10.9[d]
Toluene	0.02	9.43 ± 0.2	2.1	9.15[d], 9.3[e]
Phenol	0.2	10.1 ± 0.4	3.5	9.91[f], 9.98[g], 10.2[h]
p-Nitrophenol	0.2	9.33 ± 0.5	5.0	9.19[g]
Benzoic acid	0.2	10.1 ± 0.4	4.5	10.1[i]
Salicylic acid	0.2	10.5 ± 0.4	4.2	11.0[i]
Ibuprofen	Saturated	7.13 ± 0.3	4.7	7.02[j]
Warfarin	0.015	5.54 ± 0.3	5.4	4.90[k]

[a] Measurements performed in 90.2 cm × 75.6 μm i.d. capillary; hydrodynamic injection of 33 nL; the mobilization pressure was 50 mbar.
[b] TDA measurement [11].
[c] Diffusion cell measurement [5].
[d] Open tube elution measurement [30].
[e] Interferometric measurement [31].
[f] Calculated from literature data (23 °C) determined by TDA [22].
[g] TDA measurement [23].
[h] Calculated from literature data (20 °C) [29].
[i] Mass transfer measurement [32].
[j] Calculated from literature data (23 °C) [4].
[k] Computer simulation [33].

adsorption of lidocaine and bupivacaine onto the uncoated fused-silica capillary wall was observed as peak tailing in the TDA measurements. Thus, the diffusivities of lidocaine and bupivacaine were measured in a 67 mM phosphate buffer (pH 7.4) instead of water (Table 2).

3.3.2. Measurement of diffusivities in selected pharmaceutical solvents

The possibility of using TDA for the determination of diffusion coefficients in more challenging, pharmaceutically applied media was investigated. Methanol and acetonitrile solutions were analyzed using the experimental conditions developed for the measurements in water. Capillary wall adsorption of ibuprofen dissolved in acetronitrile prohibited analysis. For the more viscous solvents (IPM, MCT, and PG), a higher mobilization pressure of 1000 mbar was applied to force the sample zone through the capillary. After measurements, the remaining dispersion medium adhering to the capillary was removed by flushing with 96% (v/v) ethanol. The D values of the four selected drugs in the pharmaceutically relevant media are listed in Table 2. The diffusivities of the drug substances decrease as the viscosity of the dispersion media is increased. For example, the diffusion coefficient of phenol is reduced more than 70-fold in PG as compared to acetonitrile.

3.3.3. Measurement of solvent viscosity

The use of CE instrumentation for the measurement of the relative viscosities of aqueous solutions is well established [34,35]. Under laminar flow conditions, the flow velocity is related to the viscosity of the medium and the pressure difference between the inlet and outlet of the capillary, following the expression of Eq. (2). The uncertainty of capillary dimensions, the time required rising to the applied pressure, and the accuracy of pressure may be sources of error associated with using Eq. (2) for the determination of solvent viscosity [35]. Thus, most often, the solvent viscosity is obtained using water as a reference. When two detection windows are positioned along the capillary, the relative solvent viscosity can be calculated from:

$$\eta = \frac{\eta_{water} \times (t_{2,s} - t_{1,s})}{t_{2,water} - t_{1,water}} \quad (4)$$

where η_{water} and η are the viscosities of water and the solvent to be measured, respectively, $t_{1,s}$ and $t_{2,s}$ are the times required for the analyte in the solvent to be measured to reach detection windows 1 and 2, respectively, and $t_{1,water}$ and $t_{2,water}$ are the times required for the analyte in water to reach the detection windows 1 and 2, respectively.

The viscosities of the organic solvents, methanol and acetonitrile, and pharmaceutical media, IPM, MCT and PG determined using the TDA setup (90.2 cm × 75.6 μm i.d.; 30.7 and 50.9 cm to the first and second detection windows, respectively) are given in Table 3, along with the literature values for comparison. The viscosities listed originate from the very same experiments that were used for the determination of the diffusivity of phenol in the 5 solvents. The relative standard deviations on the viscosity measurements were less than 1% ($n = 8$).

Table 2
Diffusion coefficients (D) and hydrodynamic radii (R_h) obtained using Taylor dispersion analysis in various pharmaceutical solvents ($n = 8$).

Solvent	Phenol		Lidocaine		Ibuprofen		Bupivacaine	
	$D \pm$ SD (10^{-10} m^2 s^{-1})	R_h (Å)	$D \pm$ SD (10^{-10} m^2 s^{-1})	R_h (Å)	$D \pm$ SD (10^{-10} m^2 s^{-1})	R_h (Å)	$D \pm$ SD (10^{-10} m^2 s^{-1})	R_h (Å)
CH_3CN	26.7 ± 2.5	2.3	17.5 ± 1.1	3.6	ND[a]	ND[a]	15.5 ± 1.0	4.0
MeOH	15.8 ± 0.8	2.4	10.1 ± 0.5	3.7	10.4 ± 0.5	3.6	8.47 ± 0.3	4.5
H_2O	9.56 ± 0.3	2.4	5.52 ± 0.2[b]	4.2[b]	6.76 ± 0.32	3.5	5.02 ± 0.3[b]	4.6[b]
IPM	1.51 ± 0.08	2.8	1.65 ± 0.09	2.5	1.07 ± 0.05	3.8	1.47 ± 0.06	2.8
MCT	0.71 ± 0.03	1.3	0.43 ± 0.01	2.1	0.33 ± 0.01	2.7	0.44 ± 0.02	2.0
PG	0.37 ± 0.03	1.3	0.18 ± 0.01	2.6	0.16 ± 0.01	2.9	0.13 ± 0.005	3.4
Calculated[c]		2.8		3.9		3.7		4.2

[a] Not determined due to capillary wall adsorption.
[b] Values obtained in 67 mM phosphate buffer (pH 7.4).
[c] Calculated using group contribution method [33].

Table 3
Viscosities of organic solvents and oils obtained using CE instrumentation and Taylor dispersion analysis setup ($n = 8$).

Solvents	Pressure (mbar)	Viscosity ± SD (mPa s)	Literature data (mPa s)
CH_3CN	50	0.35 ± 0.001	0.34 [36] (25 °C)
MeOH	50	0.57 ± 0.001	0.55 [37] (23 °C)
IPM	1000	5.19 ± 0.006	5-7 [38] (25 °C)
MCT	1000	24.0 ± 0.2	23 [39] (25 °C)
PG	1000	44.8 ± 0.3	40.6 [29] (25 °C)

4. Discussion

4.1. Initial studies

The CE instrument equipped with a UV imaging detector provided good estimates of phenol diffusivity and satisfactory repeatability using the method TDA. The proprietary Actipix software algorithm and the 4-parameter Gaussian function (Eq. (3)) provided equivalent results with respect to t_R and σ^2 at the tested conditions. This is of significant advantage allowing a simple and automated procedure for data analysis. The Aris approach (Eqs. (S5) and (S6)) avoids the limitations of having Taylor conditions and allows for a wide use in terms of measuring diffusion coefficients. The differences in measured D values using the analysis of Taylor and Aris were less than 3% when Taylor conditions were satisfied.

4.2. Importance of experimental parameters

The data analysis revealed that the flow rate (mobilization pressure) and the injection volume had significant effects on the determined D values only when data from a single detection window was used; the setup used in most TDA studies until now. The diffusivity of phenol in water is a physical chemical property independent of the experimental conditions such as flow rate and capillary dimensions. The deviations from the accepted value ($10.0 \times 10^{-10}\ m^2\ s^{-1}$) significantly increase with increasing the flow rate and/or the injection volume when a single detection window is available only, and the changes are more pronounced in shorter than longer capillaries (Figs. 2 and 3). An interesting and so far unexplained exception to this is the experiments performed with varying injection volumes and a flow rate of 3.1 mm/s in the 75.6 μm i.d. capillary where the uncorrected diffusivity approaches the accepted D for phenol with increasing injection volume (Fig. 3B).

The difference between the correction approaches suggested by Cottet et al. and Alizadeh et al. is that Alizadeh et al. considered the origin of time when the first molecules enter into the capillary while Cottet et al. considered the origin of time after the injection when all sample molecules are introduced in the capillary and the mobilization pressure is applied [10,12,24]. The proposed methods for the correction of the finite injected volume perform almost similarly using the experimental settings of the current study (Fig. 3). The corrections for the finite width of the injected sample plug (Eqs. (S10)–(S13)) and the initial ramp in flow velocity (Eq. (S14)) are insufficient to account for these experimental non-idealities in the conducted experiments. Sharma et al. reached a similar conclusion in their single-detection window TDA studies comparing concentration pulses (injection plugs as in the current study) and fronts [17]. We are currently not able to explain the reason for under (flow rate 1.1 mm/s) and overcorrection (flow rate 3.1 mm/s) of diffusivities observed in Fig. 3A and B, respectively. Calculations, however, showed that the determined diffusivities are quite sensitive to errors in the injection volumes (calculated using Eq. (S15)).

In contrast, application of two detection windows almost completely eliminates the deviations due to variations of the flow rate and the injected volume (Figs. 2 and 3). Similar results were obtained applying two capillaries with different inner diameters using the two-detection-window setup (Fig. 2). However, to minimize errors, it will be advantageous to use experimentally measured capillary radii for determining the D values instead of the specified value from the manufacturer in most cases. It has to be noted that the experimental conditions investigated here were optimized for the two-detection-window setup rather than for the single-detection-window setup. Most of the injected sample volumes were large (>1% of capillary volume until the detection point) and suboptimal relative to the sample volumes normally applied in a single-detection-window setting. It is apparent from Fig. 3 that minimizing the sample volume leads to more accurate D values and thus a better performance of the single-detection-window approach.

At a given mean flow rate, the deviations/errors in residence time and temporal variance due to the finite width of the sample have a linear and a quadratic dependence on the injected sample volume (Eqs. (S10) and (S11)), respectively. The absolute magnitude of the error introduced due to the finite sample volume is the same for the two individual detection windows along the capillary and, thus, the deviation from the actual diffusivity is larger for the shorter capillary. Equally, according to the correction for the initial ramp in flow rate (Eq. (S14)), the impact of the ramp time will be more substantial at shorter residence times. These errors introduced due to the experimental setup are cancelled out when two detection windows are used. The advantages associated with exploiting the two-detection-window as compared to the traditional one-detection-window approach include increased robustness, better accuracy, and simpler data analysis, because the corrections for effects of the initial ramp and sample volume are not needed.

4.3. Molecular properties

4.3.1. Measurement of diffusivities in water

Overall the experimental diffusion coefficients in water agree well with previously reported D values (Table 1). The experimental methods reported in the literature, such as diffusion cells, interferometry, mass transfer measurements, and TDA, give a precision less than 10% [22,23,30–32]. The relatively large deviation observed for warfarin (Table 1) might be due to the fact that the literature data was obtained using an empirical correlation, which may lead to deviations of more than 20% [33,40].

4.3.2. Measurement of diffusivities in selected pharmaceutical solvents

The obtained results presented in Table 2 reveal the successful approach of utilizing TDA with two detection windows for determining diffusion coefficients in the selected pharmaceutical media. In the organic and pharmaceutical solvents investigated, analyte diffusivities were obtained with an analysis time of less than 30 min consuming only a few nanoliters of sample. Literature values for comparison were not available. However, the data set appears internally consistent.

The diffusion coefficient is related to the analyte molecular size and to solvent properties. The measured diffusion coefficients plotted against the reciprocal of the molecular sizes ($1/R$) are shown in Fig. 4. The drug substances are assumed to be spherical structures, and their molecular volumes are estimated by the group contribution method [33]. The analyte diffusivities correlate satisfactorily with respect to their molecular sizes in acetonitrile, methanol and water. Linear regressions of $1/R$ vs. diffusion coefficients show that the slopes decrease as the solvent viscosity is increased, with the values of the slopes being $7.0 \times 10^{-19}\ m^3/s$ ($R^2 = 0.94$) for acetonitrile, $4.0 \times 10^{-19}\ m^3/s$ ($R^2 = 0.89$) for methanol, and $2.4 \times 10^{-19}\ m^3/s$ ($R^2 = 0.84$) for water. This was expected since the slope is inversely

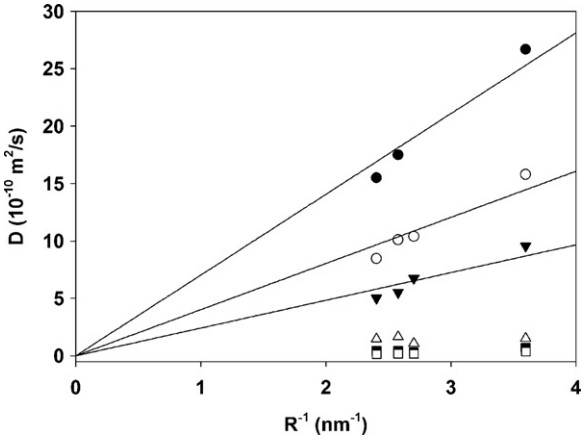

Fig. 4. The effects of molecular size (R, calculated radius) of drug substances (phenol, ibuprofen, lidocaine, and bupivacaine) on diffusion coefficients in (●) acetonitrile, (○) methanol, (▼) water, (△) IPM, (■) MCT, and (□) PG. The solid lines represent linear fits of the experimental data.

related to the solvent viscosity consistent with the Stokes–Einstein equation (Eq. (1)). Fig. 4 shows that the molecular size range spanned by the investigated analytes is too small to produce a measurable effect on diffusivity in the solvent with a viscosity much higher than water (IPM, MCT, and PG).

In general, the diffusion coefficients are inversely proportional to viscosities according to Eq. (1). Linear fits of the experimental diffusivities *versus* the reciprocal of the determined solvent viscosities are performed as shown in Fig. 5. The corrections are well represented by straight lines ($R^2 > 0.99$ in all cases). The regression values for the slopes are 9.2×10^{-10}, 6.0×10^{-10}, 5.9×10^{-10}, and 5.2×10^{-10} mPa m^2 for phenol, ibuprofen, lidocaine, and bupivacaine, respectively, correlating with the reciprocal of the hydrodynamic radius of the molecules (Table 2). However, irrespective of this overall correlation, it is of interest to observe that the hydrodynamic radii of the drugs are different in various pharmaceutical solvents as shown in Table 2. Generally, the larger hydrodynamic radii of drugs are observed in water and methanol, with an exception of phenol and ibuprofen in IPM. The possible explanation may be a result of analyte solvation. Any attractive analyte–solvent interaction, such as hydrogen bonding, would lower the diffusivity of the drug substance, hence, resulting in a larger estimated hydrodynamic radius using Eq. (1). In support of this, the work of Easteal et al. shows that diffusion coefficients (hydrodynamic radius) depend significantly on both general

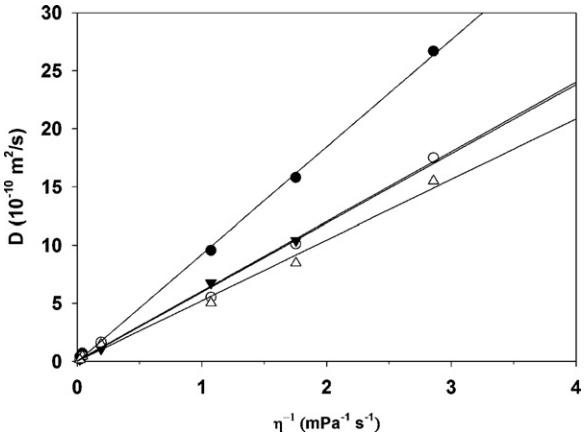

Fig. 5. Plots of the experimental diffusivities *versus* the reciprocal of the determined solvent viscosities. Four drug substances represented were (●) phenol, (▼) ibuprofen, (○) lidocaine, and (△) bupivacaine.

(dipolar) and specific (hydrogen bonding) interactions between analyte and the surrounding solvent [41].

4.3.3. Measurement of solvent viscosity

The results depicted in Table 3 show that the capillary Taylor dispersion method can also be used for measurement of solvent viscosity. In fact the viscosities listed in Table 3 originate from the very same experiments that were used for determining the diffusivity of phenol in the 5 solvents, thus making TDA a very efficient analysis method. Good agreements are also obtained in comparison of the values measured by other methods [36–39]. Note that, as expected, our data are slightly higher than the reported values in literature owing to the temperature difference (Table 3). Although CE instrumentation has been extensively used to determine the viscosity of aqueous solutions; this is, to the best of our knowledge, the first time that a CE system is applied for measuring more viscous samples like oils. The conducted studies clearly demonstrate that determination of solvent viscosity and analyte diffusivity can be achieved in a single measurement within a reasonable time. This may be of interest in various pharmaceutical applications including the development of injectable oil-based depot formulations, which is of particular interest in our laboratory.

5. Conclusion

The application of a capillary electrophoresis system equipped with a UV imaging detector, with two detection windows along the capillary for TDA, offers the capability for a rapid and effective determination of drug diffusivities in pharmaceutically relevant media. The advantages associated with using two detection windows as compared to the traditional setup with a single detection window were identified; measurements utilizing two detection windows are much less sensitive to changes in flow rate and injection volume. Also the corrections for the parameters (initial ramp and sample volume) are not needed, thus, data analysis can be simplified. The experimental conditions explored were suboptimal for instrumental setups applying only a single detection window. The results obtained indicate that better results may be obtained with smaller sample volumes for the single-detection-window setup. Good agreement was observed between the measured diffusivities for 11 analytes in water using two detection points and literature values. It is shown that solvent viscosity can also be obtained from the diffusion coefficient TDA measurements. The feasibility of measuring drug diffusivity in oils may be of importance in studies of the mechanisms of drug release from oil depot formulations. TDA provides a simple and robust method for providing information on basic physicochemical properties such as diffusivity and viscosity. These parameters are essential in the characterization and development of drug substances, formulations and delivery systems.

Acknowledgment

This work was supported by The Danish Medical Research Council.

Appendix A. Supplementary data

Supplementary data associated with this article can be found, in the online version, at doi:10.1016/j.jpba.2011.11.030.

References

[1] G.L. Amidon, P.I. Lee, E.M. Topp, Transport Processes in Pharmaceutical Systems, Marcel Dekker, New York, 2000.
[2] P.J. Sinko, Martin's Physical Pharmacy and Pharmaceutical Sciences, Lippincoot, Philadelphia, 2009.

[3] R. Baker, Controlled Release of Biologically Active Agents, Wiley, New York, 1986.
[4] L.P. de Almeida, S. Simoes, P. Brito, A. Portugal, M. Figueiredo, Modeling dissolution of sparingly soluble multisized powders, J. Pharm. Sci. 86 (1997) 726–732.
[5] L.G. Longsworth, Diffusion measurements, at 25-Degrees, of aqueous solutions of amino acids, peptides and sugars, J. Am. Chem. Soc. 75 (1953) 5705–5709.
[6] T.M. Kole, C.J. Richards, M.R. Fisch, Evolution of the diffusion coefficient and correlation length of aqueous solutions of C(12)E(6), J. Phys. Chem. 98 (1994) 4949–4954.
[7] A. Hawe, W.L. Hulse, W. Jiskoot, R.T. Forbes, Taylor dispersion analysis compared to dynamic light scattering for the size analysis of therapeutic peptides and proteins and their aggregates, Pharm. Res. 28 (2011) 2302–2310.
[8] P.C. Griffith, P. Stilbs, A.M. Howe, T. Cosgrove, A self-diffusion study of the complex formed by sodium dodecyl sulfate and gelatin in aqueous solutions, Langmuir 12 (1996) 2884–2893.
[9] H. Walderhaug, A.L. Kjoniksen, B. Nystrom, Diffusion of poly(ethylene oxide) chains in gelling and nongelling aqueous mixtures of ethyl(hydroxyethyl)cellulose and a surfactant by pulsed field gradient NMR, J. Phys. Chem. B 101 (1997) 8892–8897.
[10] A. Alizadeh, C.A. Nieto de Castro, W.A. Wakeham, The theory of the Taylor dispersion technique for liquid diffusivity measurements, Int. J. Thermophys. 1 (1980) 243–284.
[11] M.S. Bello, R. Rezzonico, P.G. Righetti, Use of Taylor–Aris dispersion for measurement of a solute diffusion coefficient in thin capillaries, Science 266 (1994) 773–776.
[12] H. Cottet, J.P. Biron, L. Cipelletti, R. Matmour, M. Martin, Determination of individual diffusion coefficients in evolving binary mixtures by Taylor dispersion analysis: application to the monitoring of polymer reaction, Anal. Chem. 82 (2010) 1793–1802.
[13] F. d'Orlye, A. Varenne, P. Gareil, Determination of nanoparticle diffusion coefficients by Taylor dispersion analysis using a capillary electrophoresis instrument, J. Chromatogr. A 1204 (2008) 226–232.
[14] H. Jensen, J. Østergaard, Flow induced dispersion analysis quantifies noncovalent interactions in nanoliter samples, J. Am. Chem. Soc. 132 (2010) 4070–4071.
[15] T. Le Saux, H. Cottet, Size-based characterization by the coupling of capillary electrophoresis to Taylor dispersion analysis, Anal. Chem. 80 (2008) 1829–1832.
[16] J. Østergaard, H. Jensen, Simultaneous evaluation of ligand binding properties and protein size by electrophoresis and Taylor dispersion in capillaries, Anal. Chem. 81 (2009) 8644–8648.
[17] U. Sharma, N.J. Gleason, J.D. Carbeck, Diffusivity of solutes measured in glass capillaries using Taylor's analysis of dispersion and a commercial CE instrument, Anal. Chem. 77 (2005) 806–813.
[18] W.L. Hulse, R.T. Forbes, A nanolitre method to determine the hydrodynamic radius of proteins and small molecules by Taylor dispersion analysis, Int. J. Pharm. 411 (2011) 64–68.
[19] V. Wernert, R. Bouchet, R. Denoyel, Influence of molecule size on its transport properties through a porous medium, Anal. Chem. 82 (2010) 2668–2679.
[20] G. Taylor, Dispersion of soluble matter in solvent flowing slowly through a tube, Proc. R. Soc. Lond. Ser. A 219 (1953) 186–203.
[21] R. Aris, On the dispersion of a solute in a fluid flowing through a tube, Proc. R. Soc. Lond. Ser. A 235 (1956) 67–77.
[22] R. Castillo, C. Garza, J. Orozco, Mutual diffusion coefficients in the water rich region of water phenol mixtures and their relation to aggregate formation, J. Phys. Chem. 96 (1992) 1475–1478.
[23] R. Niesner, A. Heintz, Diffusion coefficients of aromatics in aqueous solution, J. Chem. Eng. Data 45 (2000) 1121–1124.
[24] H. Cottet, M. Martin, A. Papillaud, E. Souaid, H. Collet, A. Commeyras, Determination of dendrigraft poly-L-lysine diffusion coefficients by Taylor dispersion analysis, Biomacromolecules 8 (2007) 3235–3243.
[25] U. Franzen, C. Vermehren, H. Jensen, J. Østergaard, Physicochemical characterization of a PEGylated liposomal drug formulation using capillary electrophoresis, Electrophoresis 32 (2011) 738–748.
[26] A. Bielejewska, A. Bylina, K. Duszczyk, M. Fialkowski, R. Holyst, Evaluation of ligand–selector interaction from effective diffusion coefficient, Anal. Chem. 82 (2010) 5463–5469.
[27] D.B. Larsen, H. Parshad, K. Fredholt, C. Larsen, Characteristics of drug substances in oily solutions. Drug release rate, partitioning and solubility, Int. J. Pharm. 232 (2002) 107–117.
[28] J. Nerurkar, J.W. Beach, M.O. Park, H.W. Jun, Solubility of (+/−)-ibuprofen and S (+/−)-ibuprofen in the presence of cosolvents and cyclodextrins, Pharm. Dev. Technol. 10 (2005) 413–421.
[29] D.R. Lide, Handbook of Chemistry and Physics, CRC Press, 2009.
[30] K.E. Gustafson, R.M. Dickhut, Molecular diffusivity of polycyclic aromatic hydrocarbons in aqueous solution, J. Chem. Eng. Data 39 (1994) 281–285.
[31] V. Daniel, J.G. Albright, Interdiffusion coefficients, densities, and viscosities of $KNO_2 + H_2O$ and $KClO_3 + H_2O$ at 25 Degrees, J. Chem. Eng. Data 40 (1995) 519–522.
[32] J.M.P.Q. Delgado, Molecular diffusion coefficients of organic compounds in water at different temperatures, J. Phase Equilib. Diff. 28 (2007) 427–432.
[33] C.R. Wilke, P. Chang, Correlation of diffusion coefficients in dilute solutions, Am. Inst. Chem. Eng. J. 1 (1955) 264–270.
[34] J. Østergaard, C. Schou, C. Larsen, N.H.H. Heegaard, Effect of dextran as a run buffer additive in drug-protein binding studies using capillary electrophoresis frontal analysis, Anal. Chem. 75 (2003) 207–214.
[35] X.J. Peng, G.M. Bebault, S.L. Sacks, D.D.Y. Chen, Quantitative description of analyte migration behavior based on the dynamic complexation model in capillary electrophoresis, Can. J. Chem. 75 (1997) 507–517.
[36] J.W. Thompson, T.J. Kaiser, J.W. Jorgenson, Viscosity measurements of methanol–water and acetonitrile–water mixtures at pressures up to 3500 bar using a novel capillary time-of-flight viscometer, J. Chromatogr. A 1134 (2006) 201–209.
[37] L.C. Richard, A.H. Chris, H.E. King Jr., High pressure viscosity of glass forming liquids measured by the centrifugal force diamond anvil cell viscometer, J. Phys. Chem. 97 (1993) 2355–2361.
[38] A. Wade, P.J. Weller, Handbook of Pharmaceutical Excipients, The Pharmaceutical Press, London, 1994.
[39] D.B. Larsen, K. Fredholt, C. Larsen, Addition of hydrogen bond donating excipients to oil solution: effect on in vitro drug release rate and viscosity, Eur. J. Pharm. Sci. 13 (2001) 403–410.
[40] J.W. Li, P.W. Carr, Accuracy of empirical correlations for estimating diffusion coefficients in aqueous organic mixtures, Anal. Chem. 69 (1997) 2530–2536.
[41] A.J. Easteal, L.A. Woolf, Solute solvent interaction effects on tracer diffusion coefficients, J. Chem. Soc. Faraday Tran. 1 (80) (1984) 1287–1295.

Journal of Pharmaceutical and Biomedical Analysis 61 (2012) 184–190

Contents lists available at SciVerse ScienceDirect

Journal of Pharmaceutical and Biomedical Analysis

journal homepage: www.elsevier.com/locate/jpba

Chromatography approaches for early screening of the phospholipidosis-inducing potential of pharmaceuticals

Zhengjin Jiang[a,*], John Reilly[b]

[a] Department of Pharmacy and Guangdong Province Key Laboratory of Pharmacodynamic Constituents of Traditional Chinese Medicine & New Drug Research, Jinan University, Guangzhou 510632, China
[b] Novartis Institutes for BioMedical Research Inc., 250 Massachusetts Avenue, Cambridge, MA 02139, USA

ARTICLE INFO

Article history:
Received 13 November 2011
Received in revised form
29 November 2011
Accepted 30 November 2011
Available online 8 December 2011

Keywords:
Drug phospholipidosis-inducing potential
Volume of distribution
Phospholipidosis
Surfactant vesicle electrokinetic chromatography

ABSTRACT

Drug-induced phospholipidosis (PLD) is an excessive accumulation of polar phospholipids within cells as a result of medical treatment. Even though a direct link between *in vitro* drug-induced PLD and toxicity in humans has not yet been firmly established, the development of PLD during preclinical testing in animals is a recognized problem in the pharmaceutical industry and can delay or abort the development process. Therefore, it is of interest to investigate the potential PLD risk of candidates at an early stage of the drug discovery process. In this work, a high throughput physicochemical approach, which is based on measuring the retention factors of the test compound within several different separation systems, was developed for screening phospholipidosis-inducing potential (PLIP) of pharmaceuticals. The measured retention factors of 36 drugs were compared with literature data on PLIP risk from three different sources. It is clearly shown that there is a statistical correlation between the chromatographic retention parameters of tested drugs and their PLIP risk. In conclusion, the retention factor ($\log k_{AOT}$) observed on a docusate sodium salt (AOT) surfactant vesicle electrokinetic chromatography (EKC) system and the logarithm of the volume of distribution ($\log V_d$) calculated from immobilized artificial membrane chromatography at pH 7.4 (CHI $IAM_{7.4}$) and HSA binding value (% HSA) can provide primary profile prediction for a large number of drug candidates early in the drug discovery process with minimal resources. The observations are that the higher the value of both $\log k_{AOT}$ and $\log V_d$, the higher the PLIP risk, and we would recommend this dual approach.

© 2011 Elsevier B.V. All rights reserved.

1. Introduction

Drug-induced phospholipidosis (PLD) is characterized by the excessive intracellular accumulation of phospholipids within lysosomes as a result of medical treatment. Although it remains uncertain whether there is a direct link between *in vitro* drug-induced PLD and adverse drug reactions in humans such drugs may have, it does not exclude the possibility that drug-induced PLD is a contributing factor in toxicity. There are circumstances in which induction of PLD occurs concurrent with toxicity [1–6]. The Food and Drug Administration (FDA) has acknowledged that drug-induced PLD is an adverse drug reaction that warrants both additional guidelines and research into the molecular mechanisms that govern this biological response [7,8]. The development of PLD during preclinical testing in animals is a recognized problem in the pharmaceutical industry and can delay or abort the development process. Therefore, it is of interest to investigate the potential PLD risk of candidates at an early stage of the drug discovery process [9]. Conventional *in vivo* methods for assessing phospholipidosis, which involve histological evaluation and confirmation by electron microscopy and/or a biochemical assay of tissue phospholipid content, are generally time-consuming, expensive, low throughput and can even raise ethical issues in respect to an industry trend to reduce and refine animal testing. Therefore, developing *in vitro* or *in silico* high throughput methods to estimate the PLD inducing potency (PLIP) of compounds would help guide drug candidate selection and assist decision making in drug discovery. Recently, numerous *in vitro* cell-based assay systems have been published for assessing the morphology of PLD using various cell systems coupled with either electron microscopy [10,11], fluorescent probes [12–15] or gene expression analysis [16]. However, these cell-based methods are still not always suitable for compound screening in

Abbreviations: AOT, docusate sodium salt; CADs, cationic amphiphillic drugs; CHI $IAM_{7.4}$, chromatographic hydrophobicity index values referring to immobilized artificial membrane chromatography at pH 7.4; CMC, the critical micelle concentration; EKC, electrokinetic chromatography; % HSA, HSA binding value; IAM, immobilized artificial membrane; $\log D_{7.4}$, logarithm of the octanol–water partition coefficient at pH 7.4; PLD, phospholipidosis; PLIP, phospholipidosis-inducing potential; V_d, calculated volume of distribution.

* Corresponding author. Tel.: +86 2085223604; fax: +86 2085224766.
E-mail address: jzjjackson@hotmail.com (Z. Jiang).

0731-7085/$ – see front matter © 2011 Elsevier B.V. All rights reserved.
doi:10.1016/j.jpba.2011.11.033

the early stage of drug discovery due to their complexity and low throughput.

While the mechanism of drug-induced PLD is still not truly understood, the current view in favor is that the drug may inhibit phospholipases due to binding to the substrate phospholipid, rendering the cell unable to break down phospholipids. This was supported by the recent demonstration of a very good correlation between phospholipidosis and the strength of drug–phospholipid interaction [17]. So far, PLD has been associated most commonly with cationic amphiphillic drugs (CADs), which contain both a hydrophobic domain, which is typically an aromatic and/or aliphatic ring structure, and a hydrophilic domain that is positively charged at physiological pH [2,3,18,19]. Electrostatic and hydrophobic/hydrophilic interaction between CADs and cellular membranes are believed to be two major contributors to PLD. This provides a theoretical basis for *in vitro* or *in silico* physicochemical approaches for predicting the phospholipidosis inducing potential (PLIP) of drugs [17,20,21]. Computational models that use multiple physical–chemical parameters, such as pKa and log *P*, have been successfully performed for predicting phospholipidosis on selected compounds [20,21]. However such models are often proprietary and are built with limited data sets. Recently Vitovic et al. predicted the PLIP risk of a series of drugs by measuring the drug–phospholipid complex formation observed by their effects on the critical micelle concentration (CMC) of a short-chain acidic phospholipids on the surface tension activity [17]. Unfortunately many labs do not currently have this technology. Later, Zhou et al. improved the method by determining the shift of CMC of a short-chain acidic phospholipids using the fluorescence probe Prodan. This method offered a fast, reliable, and cost-effective screening tool for early prediction of the PLIP risk [22]. Chromatographic techniques are widespread within the pharmaceutical industry and hold great promise for studying PLIP since they can effectively mimic drug–membrane interactions [23–31]. For example, immobilized artificial membrane (IAM) chromatography has been evaluated as a permeability screen method [23–27]. In particular the chromatographic hydrophobicity index values referring to IAM chromatography at pH 7.4 (CHI $IAM_{7.4}$) values have been shown to correlate well with the PLD data based on cell-based fluorescence-labeled lipid accumulation assay [32]. Electrokinetic chromatography (EKC) with either liposome or surfactant unilamellar vesicles as a pseudostationary phase has also been used to estimate membrane affinity related properties of drug candidates, such as intestinal absorption, volume distribution, blood brain barrier permeability [28–31].

In this work, several physicochemical parameters measured using chromatographic methods, namely the retention factor within a docusate sodium salt (AOT) vesicle EKC system (k_{AOT}), CHI $IAM_{7.4}$, the logarithm of the octanol–water partition coefficient at pH 7.4 ($\mathrm{Log}\,D_{7.4}$) and the logarithm of volume of distribution ($\log V_d$) calculated from CHI $IAM_{7.4}$ and HSA binding value (% HSA), were evaluated as high throughput, relatively easy, cost-effective, and predictive screening models for the PLIP risk. 36 commercial drugs assayed with fluorescence-labeled lipid accumulation with quantitative or qualitative literature PLIP data were selected as test compounds.

2. Experiments

2.1. Instruments

All CE experiments were carried out on the Beckman P/ACE MDQ system (Munich, Germany) equipped with diode array UV detector and a temperature control system (25 °C for all experiments). A 32 Karat™ Software Version 5.0 was used for instrument control, data acquisition and data handling. The fused-silica capillaries with a dimension of 50 μm I.D. (375 μm O. D.) and 37.5 cm total length (29 cm effective length) were purchased from Beckman Instruments (Hallow, Worcestershire, UK). All HPLC experiments were performed on the Waters Alliance 2695 HPLC System (Milford, MA, USA) equipped with 2487 dual wavelength absorbance detector. Regis IAM PC DD2 column (100 mm × 4.6 mm I.D., 10 μm particle size) and Chiral-HSA column (50 mm × 3.0 mm I.D., 3 μm particle size) were obtained from Hichrom Limited (Reading, Berkshire, UK). Gemini C_{18} column (50 mm × 3.0 mm I.D., 3 μm particle size) was purchased from Phenomenex (Macclesfield, Cheshire, UK).

2.2. Materials

The ammonium acetate, ammonium formate, docusate sodium salt (AOT), 4-[2-hydroxyethyl]-1-piperazineethanesulfonic acid (HEPES) and all *n*-alkylphenones were analytical grade reagents and purchased from Sigma–Aldrich (Gillingham, UK). All drugs listed in Table 1 were obtained from Sigma–Aldrich or provided by Novartis GDC Department (Horsham, UK). Sodium hydroxide (1 M and 0.1 M), HCl solution (1 M), HPLC-grade methanol and acetonitrile were purchased from Fisher Scientific (Leicestershire, UK). The water used throughout all experiments was purified using an Elga water purifier (Bucks, UK).

2.3. Methods

2.3.1. Preparation of solutions

Stock solutions of 50 mM ammonium acetate and 25 mM HEPES were prepared in advance and stored in the refrigerator. The buffer pH of both solutions was adjusted to 7.4 with NaOH solution (1 M) and HCl solution (1 M). All CE experiments were performed using 25 mM HEPES (pH 7.4), while HPLC experiments were carried out in gradient mode using 100% 50 mM ammonium acetate (pH 7.4) buffer as mobile phase A and 100% acetonitrile (CHI $IAM_{7.4}$ analysis and $\mathrm{Log}\,D_{7.4}$ analysis) or 2-propanol (HSA binding analysis) as mobile phase B. The 1% (w/v) AOT surfactant vesicle solutions were prepared by following reported methods [30]. In brief, the double-tailed anionic surfactant AOT was dissolved into a solution containing 85% 25 mM HEPES stock solution and 15% methanol (v/v) due to its lack of solubility in purely aqueous solutions. After the vesicle solutions were brought up to volume with HEPES stock solution, they were vortex mixed for a further 30 min in order to control the size polydispersity and to ensure a relatively equilibrated vesicle size and size distribution. The final surfactant vesicle solution was allowed to stand for 24 h after preparation to ensure equilibration and was filtered using a 0.25 μm nylon syringe filter prior to analysis. Sample solutions were made through dilution of the solid sample with methanol to provide a final concentration around 1 mg mL^{-1}.

2.3.2. VEKC experiments

New capillaries were flushed first with NaOH solution (1.0 M) for 1 h, followed by acetonitrile, water, and running buffer for 30 min each. Between runs, the capillaries were flushed for 0.5 min at 50 psi with NaOH (0.1 M), water and vesicle running buffer, respectively. The capillaries were thermostated at 25 °C. All separations were detected at λ = 254 nm (230 nm or 214 nm) depending on the UV absorbance of analyte. Sample introduction was performed hydrodynamically at 0.2 psi for 3 s, and the applied voltage of the separations was 20 kV.

Table 1
List of selected drugs and their physicochemical parameters measured by chromatographic methods.

Name	Log k_{AOT}	CHIIAM$_{7.4}$	Log $D_{7.4}$	% HSA	Log V_d	PLIP risk[20]	Refs.
Amiodarone	2.23	71.08	7.83	99.49	3.40	High	[6,17,19,21,37,38]
Chloroquine	1.71	56.12	0.22	73.98	1.87	High	[3,8,15,17,20,21,38]
Fluoxetine	2.00	56.97	1.69	94.40	1.62	High	[2,5,8,17,21]
Clomipramine	2.00	59.16	2.70	95.58	1.83	High	[3,5,17,21]
Imipramine	1.77	54.21	1.47	86.92	1.51	High	[3,8,16,17,21,42,43]
Tamoxifen	2.39	62.06	4.68	99.27	1.74	High	[2,8,17,21]
Amitriptyline	1.82	56.75	2.40	89.90	1.74	High	[8,15,17,21]
Maprotiline	1.86	61.46	1.59	91.41	2.34	High	[5,15,17,21,41]
Mianserin	1.56	50.11	3.56	93.46	0.94	High	[15,17,21]
Nortriptiline	1.97	59.24	1.61	90.87	2.04	High	[15,17,21]
Propranolol	1.45	53.29	0.95	65.13	1.62	High	[3,8,15,17,21]
Quinidine	1.02	50.58	0.70	59.08	1.38	High	[8,17,21,39]
Disopyramide	0.46	36.09	0.24	13.65	0.57	High	[16,17,21,14]
Zimelidine	1.79	51.24	1.97	88.60	1.18	High	[5,21]
Mepacrine	1.96	68.10	1.35	94.27	3.41	High	[5,21]
Labetalol	1.24	48.66	0.68	65.98	1.18	Medium	[8,17,21]
Lidocaine	0.35	34.08	2.65	17.11	0.47	Medium	[17,21]
Procaine	0.27	27.88	−0.18	70.98	0.03	Medium	[17,21,32]
Famotidine	0.12	20.13	−0.88	17.30	0.03	Low	[17,21]
Atropine	0.36	35.56	−0.30	14.46	0.54	Low	[17,21]
Atenolol	0.05	16.43	−1.21	9.10	−0.02	Low	[17,21]
Ampicillin	−1.00	−12.65	−0.59	11.14	−0.33	No	[17,21]
Furosemide	−0.88	15.89	0.24	99.65	−1.37	No	[17,21]
Ketoprofen	−0.88	16.59	0.38	98.62	−1.05	No	[17,40]
Tetracycline	−0.52	40.50	−0.24	36.86	0.73	No	[17,20,21,32]
Warfarine	−0.91	18.34	0.55	97.22/97.88	−0.80	No	[17,21]
Acetaminophen	−1.06	−10.06	−1.27	10.17	−0.31	No	[8,17,20,21,32]
Citalopram	1.75	51.08	1.52	82.71	1.26	High	[5,8,17,21]
Sertraline	1.62	48.01	1.44	66.44	1.12	+[a]	[8,16,43]
Haloperidol	2.18	68.55	2.70	97.13	3.30	+[a]	[8,16,14]
Trimipramine	1.91	55.96	3.08	88.69	1.68	+[a]	[41]
Diazepam	0.62	37.63	2.89	95.87	−0.04	−[a]	[20]
Bupivacaine	0.90	44.69	3.50	39.00	0.99	−[a]	[17]
Buspirone	0.68	36.48	2.34	72.21	0.36	−[a]	[17,20]
Verapamil	1.36	46.07	2.64	84.37	0.82	+[a]	[40]
Sotalol	0.11	13.41	−1.12	11.28	−0.08	−[a]	[8,16,14,43]

[a] Predicted PLIP risk from log k_{AOT} and log V_d in this study. + and − represent positive control and negative control, respectively.

2.3.3. Calculation of retention factors

Retention factors of the compounds in EKC were measured as previously reported [30]:

$$k_{neutral} = \frac{(t_R - t_{eof})}{t_{eof}(1 - (t_R/t_{ves}))} \quad (1)$$

$$k_{charged} = \frac{(t_R - (t_0 t_{eof}/t'_{eof}))}{(t_0 t_{eof}/t'_{eof})(1 - (t_R/t_{ves}))} \quad (2)$$

where t'_{eof}, t_{eof}, t_0 and t_R are the electroosmotic flow and the migration time of analytes in CZE system (buffer containing 85% 25 mM pH 7.4 HEPES stock solution and 15% methanol (v/v)) and EKC system (1% (w/v) AOT surfactant vesicle buffer), respectively. The elution time of AOT vesicles (t_{ves}) was determined using a co-injected vesicle marker decanophenone. All samples were run in triplicate and the mean value was used for further correlation.

2.4. Measurements of other physicochemical parameters

A method described by Valko et al. [33] was used to measure the CHI IAM$_{7.4}$ values of all test drugs on Regis IAM PC DD2 column where the stationary phase support is immobilized phosphatidylcholine. The gradient was: 0 min/0% B, 6.0 min/100% B, 6.5 min/100% B, 7.0 min/0% B, 9.0 min/0% B. The mobile phase flow rate was 1.0 mL/min. With a set of alkylphenone standards, the gradient retention times can be converted to CHI IAM$_{7.4}$, which approximates to an acetonitrile concentration at which an equal distribution of compound can be achieved between the mobile phase and IAM. Similarly, HSA binding value (% HSA) of all test drugs were determined by a fast gradient HPLC method (cycle time 15 min), originally described by Valko et al. [34] on a Chiral-HSA column. The gradient was: 0 min/0% B, 4.5 min/30% B, 9.0 min/30% B, 9.5 min/0% B, 15.0 min/0% B. The mobile phase flow rate was 1.2 mL/min. The HSA binding values were derived from the gradient retention times which were then converted to the logarithm of the equilibrium constants (log K_{HSA}) using data from a calibration set of molecules (carbamazapine, nicardipine, warfarin, diclofenc and ketoprofen). Log $D_{7.4}$ was measured on Gemini C18 column following a methodology originally described by Kerns et al. [35]. The gradient was: 0 min/0% B, 2.5 min/95% B, 4.0 min/95% B, 4.1 min/0% B, 5.5 min/0% B. The mobile phase flow rate was 1.0 mL/min. A set of standards (atenolol, metoprolol, labetolol, diltiazem and triphenylene) was selected and a calibration graph of retention time versus Log $D_{7.4}$ (literature) was constructed. The *in vitro* volume of distribution (V_d) of all selected drugs were calculated by following the reported method of Hollosy et al. [36].

3. Results and discussions

Previous *in silico* physicochemical approaches for predicting the PLIP risk have shown that the physicochemical characteristics of many drugs may be associated with the PLIP [15,17,20]. Among all investigated physicochemical descriptors, pKa and log *P* showed a strong prediction for the PLIP risk of drugs. This indicates that both hydrophobicity/lipophilicity interactions and unique electrostatic interactions between drugs and phospholipids played major roles in the PLIP. As both of these interactions are also the two most important mechanisms involved in separation science, this provides the rationale for investigating the PLIP using separation methods currently available. The IAM has been extensively used

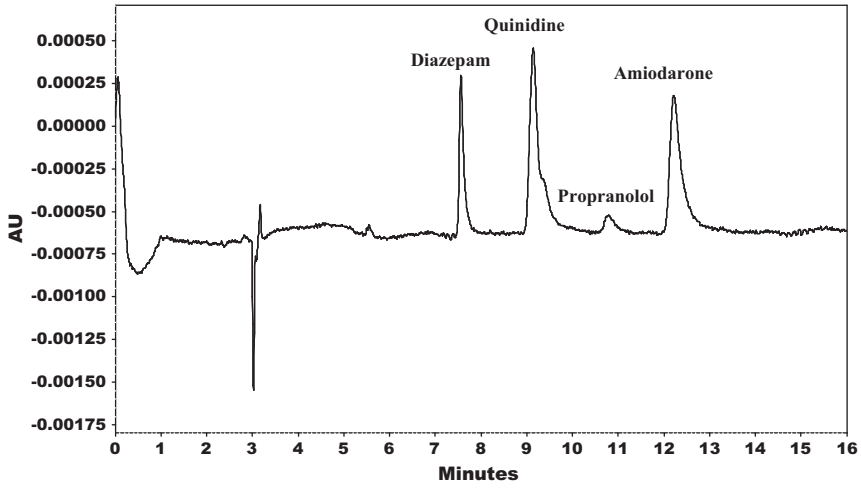

Fig. 1. Separation of four drugs with AOT vesicle EKC. Conditions: fused-silica capillary, 50 μm I.D. (375 μm O.D.) × 37.5 cm (29 cm effective length); injection by a pressure of 0.2 psi for 3 s; column was thermostated at 25 °C; applied voltage, 20 kV; current, 23 μA; detection at λ = 254 nm (or 214 or 230 nm).

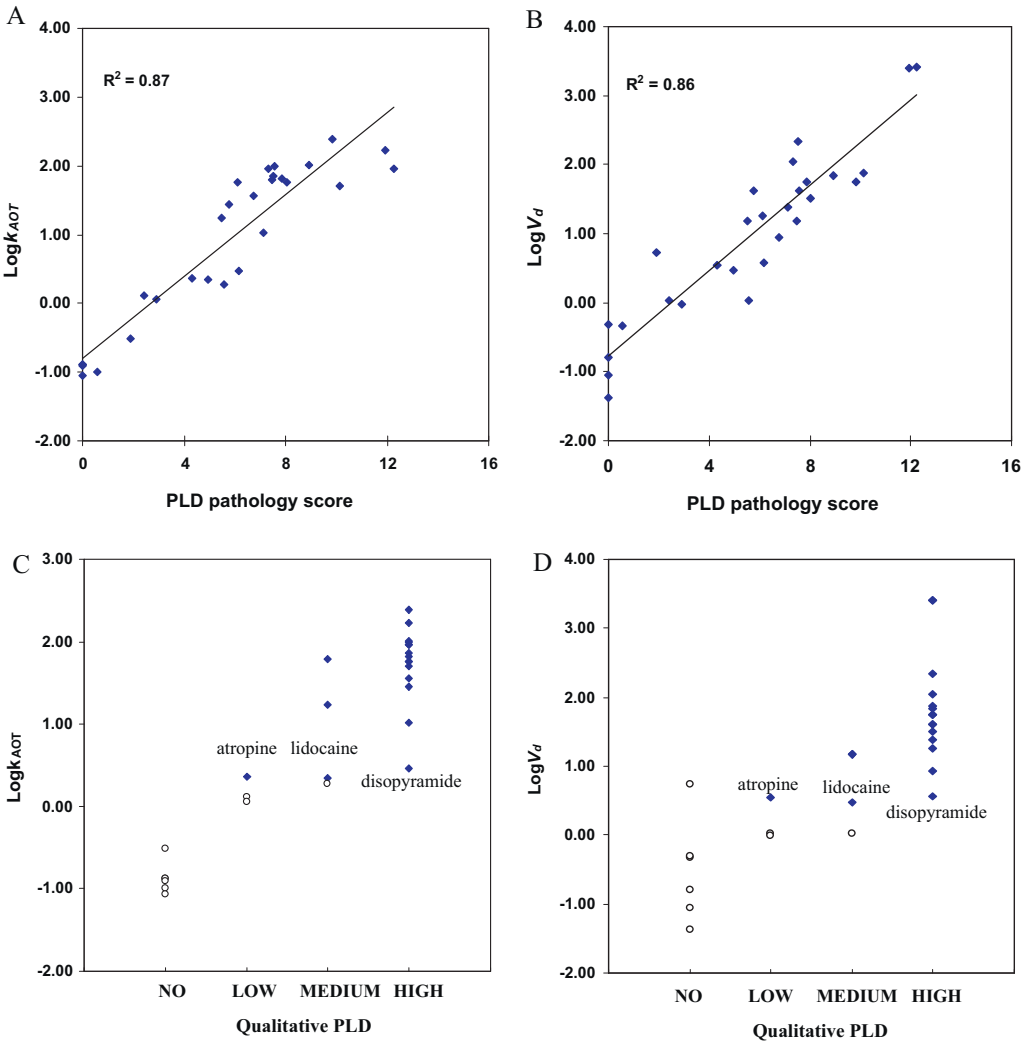

Fig. 2. (A) Correlation between log k_{AOT} and PLD pathology score assessed by Tomizawa et al.; (B) correlation between log V_d and PLD pathology score assessed by Tomizawa et al.; (C) correlation between log k_{AOT} and qualitative PLD score predicted by Tomizawa et al.; (D) correlation between log V_d and qualitative PLD score predicted by Tomizawa et al.; the PLD pathology scores were obtained from [21].

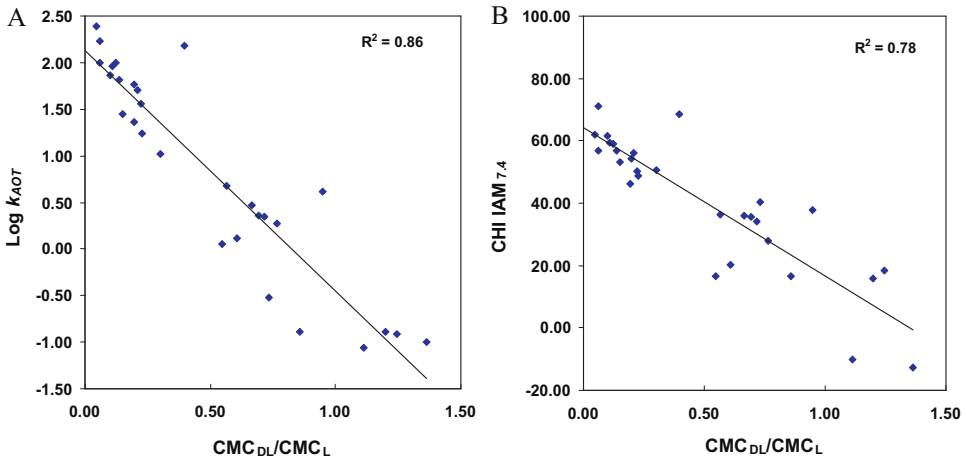

Fig. 3. (A) Correlation between log k_{AOT} and the CMC_{DL}/CMC_L value measured by Vitovic et al.; (B) Correlation between CHI $IAM_{7.4}$ and the CMC_{DL}/CMC_L value measured by Vitovic et al.; the CMC_{DL}/CMC_L values were obtained from [17].

for studying drug–cell membrane interactions. However, because of the limited commercial accessibility to membrane columns composed of negatively charged phospholipids other than neutral phosphatidylcholine, such evaluations are limited. Based on our previous work [30], a surfactant EKC method with negatively charged AOT vesicles, where both hydrophobicity/lipophilicity interactions and electrostatic interactions between the compound and AOT vesicle contribute to the resulting retention of compounds, was successfully used for predicting the lung tissue affinity of inhaled drugs. Therefore, this method was also evaluated in the current work for PLIP risk prediction.

Fig. 1 shows the separation of amiodarone, propranolol, quinidine and diazepam, which has very different potencies to induce PLD, with AOT vesicle EKC method. The four compounds can be separated rapidly (within 14 min) and the results are reproducible. More importantly, their resulting calculated retention factors, which represent the interaction between drug and AOT vesicle, are quantitatively different and appear to reflect the degree of PLIP risk of four compounds tested. Amiodarone, which is one of the most PLIP compound, exhibited highest retention (k_{AOT} = 2.23) [6,19,37,38]. Propranolol [3,15,21] and quinidine [21,39], which have been found to induce PLD *in vivo* and in cell lines, exhibit relatively lower retention (k_{AOT} = 1.45 and 1.02, respectively). The retention factor of diazepam is significantly lower than for amiodarone (k_{AOT} = 0.62). This drug is not considered to induce PLD *in vivo* [20]. Noticeably, the log V_d value also exhibited the same order (amiodarone > propranolol > quinidine > diazepam).

In order to evaluate the predictability of PLIP based on AOT vesicle EKC system and calculated log V_d, 36 compounds, whose PLIP risk have been evaluated by Tomizawa and Vitovič et al. [8,17,21] using either fluorescence-labeled lipid accumulation assay or physicochemical assays, were collected for this research. The quantitative or qualitative scores in these methods were correlated to the logarithm of the retention factors (log k_{AOT}) within AOT vesicle system and the calculated log V_d. All physicochemical properties (log k_{AOT}, Log $D_{7.4}$, CHI $IAM_{7.4}$, % HSA and log V_d) were measured using chromatographic approaches and summarized in Table 1.

We firstly compared our chromatographic results with the PLD pathology scores assessed by a fluorescence-labeled lipid accumulation cell culture assay by Tomizawa et al. [21]. 28 compounds were used for this evaluation. The correlation between Log $D_{7.4}$ and such scores is very poor (figure not shown), which has been expected since the Log $D_{7.4}$ does not consider the contribution of electrostatic interactions. However, as can be seen from Fig. 2A, there is a strong correlation between the values of log k_{AOT} and their PLD pathology scores (r^2 = 0.87). A similar strong correlation is also observed in Fig. 2B between the values of log V_d and their PLD pathology scores (r^2 = 0.86). In brief, it appears that the higher the log k_{AOT} and/or log V_d value, the higher the PLD pathology scores. Based on a prediction tree model of PLIP using two parameters, *i.e.*, the net charge of a given molecular (NC) and *C* log *P* [21], Tomizawa et al. gave tested compounds a PLIP risk rating as follows: none, low, medium and high. They also divided all tested compound into two groups, positive control (*i.e.*, that which indicates a compound can cause PLD) and negative control (*i.e.*, that which indicates a compound cannot cause PLD), based on the computational predictions of PLD risk. We therefore also compared our results with such qualitative scores. In Fig. 2C and D, the open circle and closed square are used to refer to the positive control group and the negative control group, respectively. If we defined a log k_{AOT} value = 1.0 as threshold, most positive control compounds assigned by Tomizawa et al. will appear above it. The three exceptions are disopyramide, atropine and lidocaine. Disopyramide, whose log k_{AOT} value is very low (0.46), whereas Tomizawa et al. assigned it as a high PLIP risk compound, has some controversial results from other previous *in vitro* results [16,14]. Both Sawada and Kasahara predicted negative control for disopyramide with either cell-based toxicogenomic assay [16] or phosphatidylcholine-conjugated dye (NBD-PC) fluorescence-labeled lipid accumulation assay [14]. Both lidocaine and atropine were initially reported to induce PLD in cell cultures by Tomizawa et al. [21]. However, no drug induced PLD has been reported with these two compounds in either humans or animals. Recently, Vitovič et al. also assessed PLIP of these two drugs by their effect on the critical micelle concentration (CMC) of short-chain acidic phospholipid [17]. For both compounds, quite high CMC_{DL}/CMC_L value (CMC_{DL} is the CMC for drug/lipid complex and CMC_L is the CMC of the phospholipids) was obtained, which refer to relatively low PLIP risk. Similarly, we investigated the correlations between log V_d and qualitative PLIP scores. As can be seen in Fig. 2D, there is also a good correlation between two methods. We could also define a threshold value (log V_d = 1.0), which will divide all compounds into two groups. All compounds with a log V_d > 1.0 have been classified as positive control by Tomizawa et al., whereas most compounds (except disopyramide, atropine and lidocaine) with a log V_d < 1.0 have been classified as negative control. With such defined threshold values from both methods, we predicted the PILP risk of several drugs (sertraline, sotalol, haloperidol, trimipramine, diazepam, bupivacaine, buspirone and verapamil). Based on their log k_{AOT} and log V_d value, four drugs (sertraline, haloperidol, trimipramine and verapamil) were expected to be positive controls,

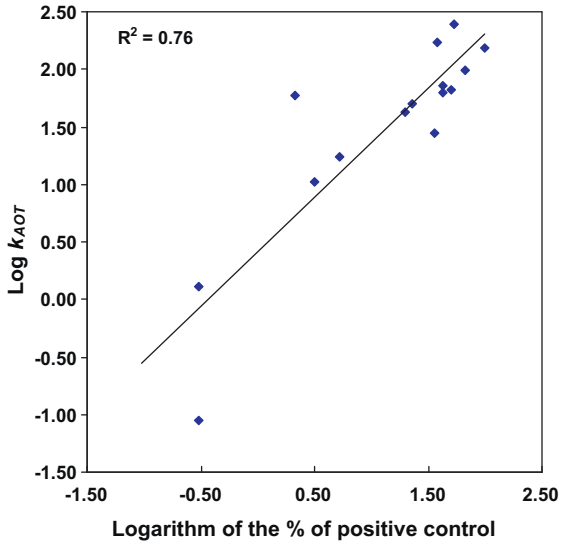

Fig. 4. Correlation between $\log k_{AOT}$ and the logarithm of the % of positive control. The % of positive control data was obtained from [8].

whereas the other four drugs (sotalol, diazepam, bupivacaine and buspirone) were expected to be negative controls. When we come across independent data demonstrating PLD for all these compounds in humans or experimental animals or cultured cells, the drug-induced PLD was observed with at least one assaying model for all four predicted positive compounds [8,16,40–42]. No PLD was observed or reported for all predicted negative control compounds [8,16,17,20,40,43].

We also compared our data with the CMC_{DL}/CMC_L value measured by Vitovic et al. [17]. Their data directly assessed the formation of drug–lipid complexes and compared very well with literature data on PLIP risk. Fig. 3A is a plot of $\log k_{AOT}$ of 29 compounds against their CMC_{DL}/CMC_L values. A strong correlation ($r^2 = 0.86$) was observed. CHI $IAM_{7.4}$ data also showed a good correlation ($r^2 = 0.78$) with the CMC_{DL}/CMC_L value (Fig. 3B). The lower correlation value compared to that of $\log k_{AOT}$ may be attributed to the relatively weaker electrostatic interaction of zwitterionic phosphatidylcholine (PC) group and single layer phospholipids structure. These correlations are encouraging as it demonstrates how effective our $\log k_{AOT}$ method is in assessing the formation of drug–negatively charged lipid interactions.

Recently, Cerep offered a rapid high content analysis assay to assess drug-induced PLD in HepG2 cells with an automated fluorescent microscope [8]. The client compound data from the PLD assay are expressed as fold over background (1% DMSO, solvent) and the percentage of the positive control (sertraline). This methodology showed good predictability for compounds that have been shown in literature to induce PLD [8]. In order to further examine the predictability of PLIP based on AOT vesicle EKC system, we also compared $\log k_{AOT}$ with the measured percentage of the positive control values from Cerep's application note (Fig. 4). The correlation between the two methods is very good ($r^2 = 0.74$). Notably, Cerep assessment only assigned a low PLIP risks to chloroquinine, which is well-known to cause PLD in animals and in humans [3,15,20,38]. The predicted PLIP risk for amiodarone, which is also known to cause PLD in the lungs in humans and animals [6,19,37,38], is also only moderate. Additionally, only low PLIP risks were predicted by the Cerep methodology for the antidepressants imipramine and citalopram, which have been reported to induce PLD in several organs in experimental animal models [41,43]. In contrast, our methods measured a high $\log k_{AOT}$ and $\log V_d$ values for all four compounds and predicted them to be relatively high PLIP risk. Such inconsistent results have been often observed when different PLIP prediction methods were evaluated [17,21,42]. This is largely attributed to the complexity of phospholipidosis. For example, the PLIP of drug *in vivo* or cell-based *in vitro* depends not only on the inherent PLD-inducing potency of the compounds, but also on the dose or concentration, its metabolism and the duration time [17,44]. In order to reduce the number of false negative results due to low drug concentration, a range of concentrations of each compound is often used in cell-based *in vitro* assays, for example gene expression analysis [42]. This will limit the throughput of the analysis. In this respect, our chromatography based approaches show two advantages. Firstly, they are rapid and high throughput since only one drug concentration is needed for each test compound. Secondly, it is very sensitive and can accurately identify compounds capable of causing PLD at a low concentration. Normally, less than 1 mg of compound is needed for both tests.

4. Conclusions

A simple and rapid physicochemical screening approach based on chromatographic methods was developed for predicting the potential of compounds to induce PLD. Our results exhibited good correlation with literature data on various PLIP risk assessment approaches. It is clearly evident that a statistical correlation does exist between both $\log k_{AOT}$ and $\log V_d$ value of tested drugs and their PLIP risk. The benefit will increase confidence in assessing the PLIP risk by routinely using both values. The short run times, high reproducibility, high selectivity and low sample and solvent cost also make these methods ideal high throughput approaches for PLIP risk screening.

Due to the complexity of phospholipidosis, it is noted that there will be exceptions using these methods and therefore they cannot effectively model all other specialized mechanisms, such as drug metabolism or drugs affecting proteins and enzymes function etc. However, bearing in mind these limitations, the $\log k_{AOT}$ and $\log V_d$ methods can provide a rapid, robust, reproducible and sensitive *in vitro* trend analysis for a large number of drug candidates early in the drug discovery process with minimal resources.

Acknowledgements

We thank Juha-Matti Alakoskela for kindly providing the CMC_{DL}/CMC_L values of test compounds. We thank the program for New Century Excellent Talents in University (NCET 10-0121), the Fundamental Research Funds for the Central Universities and the 211 Project of Jinan University for funding support.

References

[1] N. Anderson, J. Borlak, Drug-induced phospholipidosis, FEBS Lett. 580 (2006) 5533–5540.
[2] M.J. Reasor, S. Kacew, Drug-induced phospholipidosis: are there functional consequences? Exp. Biol. Med. 226 (2001) 825–830.
[3] U.P. Kodavanti, H.M. Mehendale, Cationic amphiphilic drugs and phospholipid storage disorder, Pharmacol. Rev. 42 (1990) 327–354.
[4] W.H. Halliwell, Cationic amphiphilic drug-induced phospholipidosis, Toxicol. Pathol. 25 (1997) 53–60.
[5] M.J. Reasor, A review of the biology and toxicologic implications of the induction of lysosomal lamellar bodies by drugs, Toxicol. Appl. Pharmacol. 97 (1989) 47–56.
[6] M.J. Reasor, C.L. Ogle, S. Kacew, Amiodarone-induced pulmonary toxicity in rats: biochemical and pharmacological characteristics, Toxicol. Appl. Pharmacol. 97 (1989) 124–133.
[7] B.R. Berridge, L.A. Chatman, M. Odin, A.E. Schultze, P.E. Losco, J.T. Meehan, T. Peters, S.L. Vonderfecht, Phospholipidosis in nonclinical toxicity studies, Toxicol. Pathol. 35 (2007) 325.
[8] Cerep, Phospholipidosis, ADME-Tox Application note 2009.
[9] J.-M. Alakoskela, P. Vitovič, P.J. Kinnunen, Screening for the drug–phospholipidosis interaction: correlation to phospholipidosis, ChemMedChem 4 (2009) 1224–1251.

[10] F. Van Bambeke, C. Gerbaux, J.M. Michot, M.B. d'Yvoire, J.P. Montenez, P.M. Tulkens, Lysosomal alterations induced in cultured rat fibroblasts by long-term exposure to low concentrations of azithromycin, J. Antimicrob. Chemother. 42 (1998) 761–767.
[11] K.Y. Hostetler, J. Vandeberg, K.A. Aldern, G.T. Brophy, Effect of amiodarone on the phospholipid and lamellar body content of lymphoblasts *in vitro* and peripheral blood lymphocytes *in vivo*, Biochem. Pharmacol. 41 (1991) 1007–1013.
[12] R.J. Gum, D. Hickman, J.A. Fagerland, M.A. Heindel, G.D. Gagne, J.M. Schmidt, M.R. Michaelides, S.K. Davidsen, R.G. Ulrich, Analysis of two matrix metalloproteinase inhibitors and their metabolites for induction of phospholipidosis in rat and human hepatocytes, Biochem. Pharmacol. 62 (2001) 1661–1673.
[13] R.G. Ulrich, K.S. Kilgore, E.L. Sun, C.T. Cramer, L.C. Ginsberg, An *in vitro* fluorescence assay for the detection of drug-induced cytoplasmic lamellar bodies, Toxicol. Methods 1 (1991) 89–105.
[14] T. Kasahara, K. Tomita, H. Murano, T. Harada, K. Tsubakimoto, T. Ogihara, S. Ohnishi, C. Kakinuma, Establishment of an *in vitro* high-throughput screening assay for detecting phospholipidosis-inducing potential, Toxicol. Sci. 90 (2006) 133–141.
[15] J.K. Morelli, M. Buehrle, F. Pognan, L.R. Barone, W. Fieles, P.J. Ciaccio, Validation of an *in vitro* screen for phospholipidosis using a high content biology platform, Cell Biol. Toxicol. 22 (2006) 15–27.
[16] H. Sawada, K. Takami, S. Asahi, A toxicogenomic approach to drug-induced phospholipidosis: analysis of its induction mechanism and establishment of a novel *in vitro* screening system, Toxicol. Sci. 83 (2005) 282–292.
[17] P. Vitovic, J.M. Alakoskela, P.K.J. Kinnunen, Assessment of drug–lipid complex formation by a high-throughput langmuir-balance and correlation to phospholipidosis, J. Med. Chem. 51 (2008) 1842–1848.
[18] M.J. Reasor, K.L. Hastings, R.G. Ulrich, Drug-induced phospholipidosis: issues and future directions, Expert Opin. Drug Saf. 5 (2006) 567–583.
[19] U.P. Kodavanti, H.M. Mehendale, Amiodarone- and desethylamiodarone-induced pulmonary phospholipidosis, inhibition of phospholipases *in vivo*, and alteration of [^{14}C] amiodarone uptake by perfused lung, Am. J. Respir. Cell Mol. Biol. 4 (1991) 369–378.
[20] J.P.H.T.M. Ploemen, J. Kelder, T. Hafmans, H. van de Sandt, J.A. van Burgsteden, P.J.M. Salemink, E. Van Esch, Exp Use of physicochemical calculation of pKa and *C* log *P* to predict phospholipidosis-inducing potential, Toxicol. Pathol. 55 (2004) 347–355.
[21] K. Tomizawa, K. Sugano, H. Yamada, I. Horii, Physicochemical and cell-based approach for early screening of phospholipidosis-induced potential, J. Toxicol. Sci. 31 (2006) 315–324.
[22] L. Zhou, G. Geraci, S. Hess, L. Yang, J. Wang, U. Argika, Predicting phospholipidosis: a fluorescence noncell based *in vitro* assay for the determination of drug–phospholipid complex formation in early drug discovery, Anal. Chem. 83 (2011) 6980–6987.
[23] A. Adejare, A. El-Gendy, Prediction of intestinal and blood brain barrier permeability utilizing immobilized artifical membrane chromatography, in: Abstracts of Papers of the American Chemical Society, vol. 228, 2004, p. U960.
[24] H.L. Liu, S.W. Ong, L. Glunz, C. Pidgeon, Predicting drug–membrane interactions by HPLC: structural requirements of chromatographic surfaces, Anal. Chem. 67 (1995) 3550–3557.
[25] C. Pidgeon, S.W.Ong, H.L. Liu, X.X. Qiu, M. Pidgeon, A.H. Dantzig, J. Munroe, W.J. Hornback, J.S. Kasher, L. Glunz, T. Szczerba, IAM chromatography: an *in vitro* screen for predicting drug membrane permeability, J. Med. Chem. 38 (1995) 590–594.
[26] A. Reichel, D.J. Begley, Potential of immobilized artificial membranes for predicting drug penetration across the blood–brain barrier, Pharm. Res. 15 (1998) 1270–1274.
[27] A. Taillardat-Bertschinger, C.A.M. Martinet, P.A. Carrupt, M. Reist, G. Caron, R. Fruttero, B. Testa, Molecular factors influencing retention on immobilized artificial membranes (IAM) compared to partitioning in liposomes and *n*-octanol, Pharm. Res. 19 (2002) 729–737.
[28] J.M. Carrozzino, M.G. Khaledi, Interaction of basic drugs with lipid bilayers using liposome electrokinetic chromatography, Pharm. Res. 21 (2004) 2327–2335.
[29] J.M. Carrozzino, M.G. Khaledi, pH Effects on drug interactions with lipid bilayers by liposome electrokinetic chromatography, J. Chromatogr. A 1079 (2005) 307–316.
[30] Z. Jiang, J. Reilly, B. Everatt, A method for rapidly predicting drug tissue distribution using surfactant vesicle electrokinetic chromatography, Electrophoresis 29 (2008) 3674–3684.
[31] R.J. Pascoe, J.A. Masucci, J.P. Foley, Investigation of vesicle electrokinetic chromatography as an *in vitro* assay for the estimation of intestinal permeability of pharmaceutical drug candidates, Electrophoresis 27 (2006) 793–804.
[32] A. Casartelli, M. Bonato, P. Cristofori, F. Crivellente, G. Dal Negro, I. Masotto, C. Mutinelli, K. Valko, V. Bonfante, A cell-based approach for the early assessment of the phospholipidogenic potential in pharmaceutical research and drug development, Cell Biol. Toxicol. 19 (2003) 161–176.
[33] K. Valko, C.M. Du, C.D. Bevan, D.P. Reynolds, M.H. Abraham, Rapid-gradient HPLC method for measuring drug interactions with immobilized artificial membrane: comparison with other lipophilicity measures, J. Pharm. Sci. 89 (2000) 1085–1096.
[34] K. Valko, S. Nunhuck, C. Bevan, M.H. Abraham, D.P. Reyncilds, Fast gradient HPLC method to determine compounds binding to human serum albumin. Relationships with octanol/water and immobilized artificial membrane lipophilicity, J. Pharm. Sci. 92 (2003) 2236–2248.
[35] E.H. Kerns, L. Di, S. Petusky, T. Kleintop, D. Huryn, O. McConnell, G. Carter, Pharmaceutical profiling method for lipophilicity and integrity using LC/MS, J. Chromatogr. B 791 (2003) 381–388.
[36] F. Hollosy, K. Valko, A. Hersey, S. Nunhuck, G. Keri, C. Bevan, Estimation of volume of distribution in humans from high throughput HPLC-based measurements of human serum albumin binding and immobilized artificial membrane partitioning, J. Med. Chem. 49 (2006) 6958–6971.
[37] M.J. Reasor, C.M. McCloud, M. DiMatteo, R. Schafer, A. Ima, I. Lemaire, Effects of amiodarone-induced phospholipidosis on pulmonary host defense functions in rats, Proc. Soc. Exp. Biol. Med. 211 (1996) 346–352.
[38] M.J. Reasor, S. Kacew, Amiodarone pulmonary toxicity: morphologic and biochemical features, Proc. Soc. Exp. Biol. Med. 196 (1991) 1–7.
[39] M. Jägel, R. Lüllmann-Rauch, Lipidosis-like alterations in cultured macrophages exposed to local anaesthetics, Arch. Toxicol. 55 (1984) 229–232.
[40] R. Lüllmann-Rauch, G.H. Reil, Fenfluramine-induced ultrastructural alterations in tissues of rats and guinea pigs, Naunyn Schmiedeberg's Arch. Pharmacol. 285 (1974) 175–184.
[41] Z.L. Xia, G. Ying, A.L. Hansson, H. Karlsson, Y. Xie, A. Bergstrand, J.W. DePierre, L. Nässberger, Antidepressant-induced lipidosis with special reference to tricyclic compounds, Prog. Neurobiol. 60 (2000) 501–512.
[42] P. Nioi, B.K. Perry, E.J. Wang, Y.Z. Gu, R.D. Snyder, *In vitro* detection of drug-induced phospholipidosis using gene expression and fluorescent phospholipid-based methodologies, Toxicol. Sci. 99 (2007) 162–173.
[43] A.S. Pappu, P.J. Yazaki, K.Y. Hostetler, Inhibition of purified lysosomal phospholipase A1 by various beta andrenergic blockers, Biochem. Pharmacol. 34 (1985) 521–524.
[44] D.K. Monteith, R.E. Morgan, B. Halstead, *In vitro* assays and biomarkers for drug-induced phospholipidosis, Expert Opin. Drug Metab. Toxicol. 2 (2006) 687–696.

Journal of Pharmaceutical and Biomedical Analysis 61 (2012) 191–198

Contents lists available at SciVerse ScienceDirect

Journal of Pharmaceutical and Biomedical Analysis

journal homepage: www.elsevier.com/locate/jpba

Libraries, classifiers, and quantifiers: A comparison of chemometric methods for the analysis of Raman spectra of contaminated pharmaceutical materials

Connie M. Gryniewicz-Ruzicka*, Jason D. Rodriguez, Sergey Arzhantsev, Lucinda F. Buhse, John F. Kauffman

FDA, Division of Pharmaceutical Analysis, 1114 Market St., St. Louis, MO 63101, United States

ARTICLE INFO

Article history:
Received 29 September 2011
Received in revised form
30 November 2011
Accepted 1 December 2011
Available online 9 December 2011

Keywords:
Rapid screening
Raman spectroscopy
Spectral library
SIMCA
PLS

ABSTRACT

In this study, pharmaceutical grade sorbitol was used as a model system for comparison of Raman based library spectral correlation methods with more sophisticated methods of chemometric data analysis. Both crystallizing sorbitol (CS) and non-crystallizing sorbitol (NCS) from several manufacturers were examined. The Raman spectrum of each sample was collected and identified by correlation with a spectral library that included the CS spectrum but not the NCS spectrum. The average hit quality index (HQI) for the measured NCS spectra and the library CS spectrum was 0.966 whereas the average HQI for the measured CS spectra was 0.991. Both HQIs exceeded the 0.950 threshold that is commonly used for material verification. To enhance the discrimination between CS and NCS, a CS/NCS classification model was constructed using soft independent modeling of class analogies (SIMCA). SIMCA was able to positively identify CS and NCS solutions with no mis-classifications. When CS was adulterated with low levels (0–5%) of ethylene glycol (EG) and diethylene glycol (DEG), the HQI values of the measured spectra and the CS library spectrum were still above 0.950. When the CS SIMCA model was applied to adulterated CS spectra, it determined that CS samples with adulterant levels as low as 2% were outside of the CS class. A quantitative PLS model was also applied to EG adulterated CS and resulted in a detection limit of 0.9% for EG. The results obtained from these studies highlight the importance of selecting an appropriate data analysis process for the detection of low level adulterants in pharmaceutical raw materials using Raman spectroscopic screening methods.

Published by Elsevier B.V.

1. Introduction

Globalization of the pharmaceutical supply chain appears to be increasing the risk that consumers will be exposed to contaminated, counterfeited, mislabeled, or otherwise sub-standard drug products [1–4]. Recently several imported materials have been found to be adulterated with contaminants that threaten public health and safety, and in some cases the adulteration appears to be economically motivated. One potential approach to reducing the threat of product adulteration is to develop analytical methods for materials screening that are rapid, sensitive, and selective for economically motivated adulterants (EMAs). Spectroscopic methods are particularly appealing for this application because portable instruments are becoming increasingly common and they can be used to screen samples in the field.

Raman spectroscopy offers detailed chemical and structural information and requires minimal sample preparation. These attributes make Raman spectroscopy efficient and effective for a wide range of pharmaceutical applications, including identity testing of pharmaceutical raw materials [5–10]. There are two fundamental types of library-based spectral correlation methods that can be implemented: identification and verification. Identification methods are designed to compare the spectrum of a material with all spectra contained in a spectral library. Verification methods, on the other hand, compare the spectrum of the sample under study to a predetermined reference spectrum. Both methods can utilize the hit-quality index (HQI) as a figure of merit to characterize the correlation between two spectra. Verification tests typically use a minimum HQI threshold, usually 0.95, to assign a “Pass” or “Fail” determination to the sample under study. As we have discussed in a previous paper, verification tests, while widely used in the pharmaceutical industry for screening of pharmaceutical ingredients, have a wide range of sensitivities to the presence of impurities and adulterants (i.e., contaminants) [10]. The intrinsic sensitivity of a particular ingredient/adulterant system has been found to depend on the Raman scattering cross section of the adulterant relative to the ingredient [10].

* Corresponding author at: FDA, Division of Pharmaceutical Analysis, 1114 Market St., Room 1002, St. Louis, MO 63101, United States. Tel.: +1 314 539 3843; fax: +1 314 539 2113.
E-mail address: connie.ruzicka@fda.hhs.gov (C.M. Gryniewicz-Ruzicka).

0731-7085/$ – see front matter. Published by Elsevier B.V.
doi:10.1016/j.jpba.2011.12.002

Whereas library methods deal primarily with qualitative assessments, more rigorous multivariate calibration models can be developed to obtain quantitative information about the adulterant and the composition of pharmaceutical raw materials. Partial least squares regression (PLS) is a widely used multivariate calibration algorithm that maximizes the covariance between a set of calibration standard sample spectra and their known compositions. Previous studies from our group have demonstrated the use of Raman spectroscopy as a rapid screening method for the determination of diethylene glycol in glycerin [11–13]. The validity of a quantitative calibration model used for prediction depends, in part, on how well the calibration set represents the composition of the expected test samples. The adulterant must be properly identified in order to apply the appropriate quantitative PLS model. If multiple adulterants are expected, numerous PLS models may need to be constructed. One of the main disadvantages of PLS models over the aforementioned library-based spectral correlation methods is that PLS model development requires considerable effort and expertise while library-based spectral correlation methods require little or no expertise.

A rather intermediate approach is to use chemometric classification methods as qualitative screening techniques to determine whether a sample is authentic or adulterated. Mathematical models are developed using a training data set consisting of samples assigned to predefined classes. The classification model is used to predict the class of an unknown sample by comparing the sample to a previously analyzed experience set, in which the classes are already known. Samples not predicted in the authentic class may be adulterated and therefore would be subject to further laboratory analysis for identity and purity confirmation.

In this paper, we will discuss the varying sensitivities of each of the data analysis methods discussed above. In this study, pharmaceutical grade sorbitol was used as a model compound for comparison of Raman based library methods to chemometric methods that require more extensive training sets. Sorbitol can be found in two forms: crystallizing (CS) or non-crystallizing sorbitol (NCS). NCS contains small amounts of polyols (i.e., maltitol) to help prevent crystallization. Both CS and NCS forms are potential candidates for EMA with such adulterants as ethylene glycol (EG) and diethylene glycol (DEG). DEG and EG are both poisonous, inexpensive chemicals that have similar physical and chemical properties to that of sorbitol [14]. The potential presence of trace levels of EG, which may be produced during the hydrogenation process used to manufacture sorbitol [14], suggests that a procedure should be used to screen for the presence of DEG and EG resulting either from adulteration or from the manufacturing process. Sorbitol solutions of both forms were obtained from several manufacturers and each adulterated with low levels (0–5%) of EG and DEG. The EG adulterated samples were analyzed using library spectral correlation methods, chemometric classification methods, and PLS models, whereas the DEG samples were only used in the spectral correlation and classification studies. The library spectral correlation method using CS sorbitol as the reference material was applied to an independent test set of CS, NCS, and adulterated test samples. The HQI values calculated for each sample were used to determine the form (CS or NCS) and quality (authentic or adulterated) of the sorbitol samples. For the classification studies, a soft independent modeling of class analogy (SIMCA) model was developed to identify the type of form of sorbitol and that same model was used to distinguish between authentic and adulterated sorbitol solutions. A quantitative PLS model was constructed using EG adulterated CS sorbitol. The same independent test set used in the spectral library correlation methods was analyzed by using the qualitative SIMCA and quantitative PLS models. The performance and sensitivity of each of the data analysis methods were evaluated and compared.

2. Experimental

2.1. Materials

USP grade 70% crystallizing sorbitol solution by weight and NF grade sorbitol powder, used in the development of the PLS model, were purchased from Spectrum Chemicals and Laboratory Products (New Brunswick, NJ, USA). Reagent grade ethylene glycol (EG) was acquired from Sigma–Aldrich (Saint Louis, MO, USA) and reagent grade diethylene glycol (DEG) was purchased from Fisher Scientific (Fair Lawn, NJ, USA). The water contents of as-received crystallizing sorbitol solution, sorbitol powder, EG and DEG were determined by Karl Fischer titration to be 30.01, 0.40, 0.06, and 0.04% respectively. Nine USP grade 70% crystallizing sorbitol solutions (CS) were obtained from six manufacturers and five USP grade 70% non-crystallizing sorbitol solutions (NCS) were obtained from two different manufacturers. All sorbitol solutions received from the same manufacturer were from different lots. To vary the water content of a sample, Millipore Milli-Q (18 MΩ cm) water was added. Disposable plastic CVD-UV cuvettes with a 1 cm path length and cuvette covers were purchased from Ocean Optics (Dunedin, FL, USA).

2.2. Sample preparation

The CS sorbitol solutions were labeled A through G, with sample G representing three different lots from the same manufacturer. The NCS solutions were labeled H and I. Sample H and I represent two and three lots, respectively, and each sample was obtained from different manufacturers. For library and classification methods, two sets of samples were prepared for each of the CS and NCS solutions, one using EG as the adulterant and one using DEG. Each sample set contained five individual solutions that were prepared gravimetrically with adulterant compositions of 0.0, 0.5, 1.0, 2.5, and 5.0%.

For the PLS studies, four sorbitol–water binary solutions containing approximately 65, 68, 70, and 72% sorbitol by weight were used in the preparation of the calibration standards. The 70% sorbitol solution was used as received. Stock solutions of 65 and 68% sorbitol were prepared by dilution of the 70% sorbitol solution with water. Sorbitol powder was dissolved in water to prepare the 72% sorbitol solution by weight. The binary solutions were agitated on an orbital shaker at $35 \pm 1\,^{\circ}C$ and 100 rpm (Thermo Forma, model 420, bench-top incubator orbital shaker, Thermo Electron Corporation, Marietta, OH, USA) for approximately two hours to aid in the dissolution of the sorbitol powder and to ensure a thorough mixing of the viscous solutions. The stock solutions were allowed to cool to room temperature before proceeding with the preparation of the EG adulterated calibration standards.

Ternary mixtures with EG were prepared gravimetrically from each sorbitol–water stock solution, and all concentrations are reported in weight percent. The calibration set was comprised of 34 samples. Thirty-two of the calibration samples were prepared from the 65, 68, 70, and 72% sorbitol stock solutions with each stock solution having calibration standards composed of EG compositions of 0, 0.5, 1, 2, 3, 5, 10, and 25%. The additional two calibration samples were pure components of water and EG. The validation set was comprised of 47 test samples, of which 45 were the same low level adulterated EG samples prepared for the library and classification studies. The two additional validation samples included an authentic 70% sorbitol solution (Sample "J") and a low level (4%) EG adulterated sample (Sample "K") that was prepared from the 70% crystallizing sorbitol solution used in the preparation of the calibration samples. The ternary mixtures of the calibration and validation sets were agitated on an orbital shaker at $50 \pm 1\,^{\circ}C$ and 100 rpm for approximately ninety minutes and vortexed to ensure thorough

mixing of the viscous solutions. The samples were transferred to disposable cuvettes while warm and then allowed to cool to room temperature overnight before proceeding with Raman analysis.

2.3. Raman spectroscopy

Raman spectra were recorded using a B&W Tek MiniRAM II portable Raman spectrometer. The portable unit was equipped with a fiber optic probe, a 785 nm diode laser excitation source with a maximum output power of approximately 275 mW at the sample and a thermoelectrically cooled 2048 pixel CCD detector. The spectrometer was operated on AC power and controlled by a Microsoft Excel-based user interface developed in-house. All reported spectra were measured with the fiber optic probe in a backscattering geometry (B&W Tek Model BCR100A sample holder, Newark, DE). The average spectral resolution of the instrument was estimated to be 8 cm^{-1}.

For the library analysis, the library reference spectrum for each pure component (sorbitol sample J, EG, DEG) was acquired by taking the average spectrum of 25 replicate runs. Each run featured a sample acquisition time of 2 s, and the sample cuvette was removed and replaced prior to each run to ensure random sampling. Raman spectra for all sorbitol samples were collected in the spectral range of 250–3050 cm^{-1}. The full spectral range was used in the development of PLS and classification models while the 250–2000 cm^{-1} region was used for the spectral correlation calculations. The truncated range was selected for the spectral correlation method because of the variability in the noise in the region above 2000 cm^{-1} that can influence the HQI calculation. The exposure time was set to 1.5 s per scan, and each spectrum is the average of 13 scans for a total integration time of 19.5 s. A background scan with the same integration time was collected before each sample acquisition to remove dark noise.

Forty-six Raman spectra from the 38 unique sorbitol/EG/water compositions comprised the calibration set for PLS model development, which included 5 replicate measurements of the 70% sorbitol solution, 99.9% EG, and water samples. Approximately 115 Raman spectra were used for the validation set, which included duplicate measurements of each of the EG adulterated sorbitol sample sets, 5 replicate measurements of each of the nine CS solutions, and 10 replicate measurements each of validation samples "J" and "K". The replicate measurements of samples "J" and "K" were used to determine method precision, the critical level and the detection limit of EG for the PLS model. In field applications, the critical level is the pass/fail decision threshold, and is an essential parameter for field deployment [12]. The library and classification studies were conducted using the spectral data collected for the EG PLS model in addition to the 50 Raman spectra acquired for the low level DEG adulterated sorbitol samples.

2.4. Data analysis

Raman spectra were analyzed by first subtracting the measured background spectrum from the sample spectrum. For the library analysis, each test sample spectrum was compared to the reference spectrum of each pure component using the HQI, which was calculated using the spectral correlation algorithm:

$$\mathrm{HQI} = \frac{(Library \cdot Test)^2}{(Library \cdot Library)(Test \cdot Test)} \quad (1)$$

where *Library* indicates the preprocessed library reference spectrum and *Test* indicates the preprocessed spectrum of the test mixture sample under study. The HQI defined in Eq. (1) is the square of the spectral covariance between the library and test spectra normalized by the squared norms of the two spectral vectors (i.e., the square of the spectral correlation coefficient). This form of the HQI was used in three earlier studies where a more in-depth explanation and background is given [10,15,16]. It is similar to the traditional (Grams Spectral ID) correlation algorithm [17] but features two key differences. First, the scalar product of the spectral vectors is not subtracted from 1, resulting in a scale in which 1.000 indicates perfect correlation and 0 indicates poor correlation. Secondly, the spectra used for the HQI calculation in Eq. (1) are not mean-centered prior to the HQI calculation. Rather, all spectra used for library analysis undergo first derivative preprocessing prior to the HQI calculation. The derivative spectra are calculated using a 2nd order, 11-point Gram polynomial convolution filter. As described previously, first derivative processing provides model-free baseline reduction, which, in turn, increases the discriminating ability of the HQI [10]. For the library sensitivity analysis, we used Table Curve 2D (SYSTAT Software Inc., Richmond, CA) to generate HQI sensitivity plots (shown in Fig. 4) to quantitatively determine the sensitivity of the HQI to the presence of adulterants.

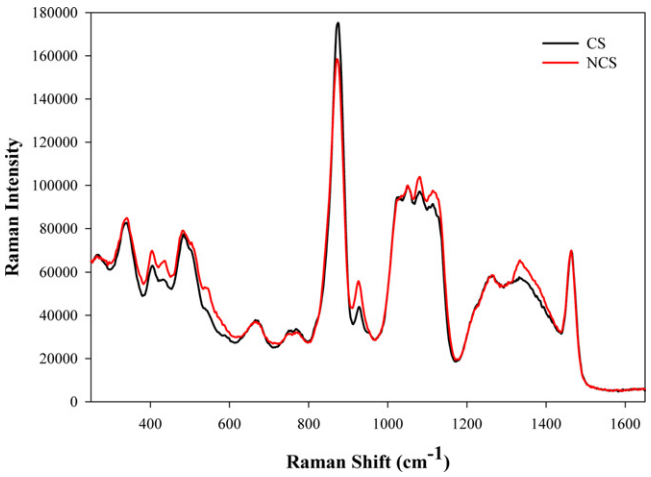

Fig. 1. Raman spectra of 70% crystallizing (CS) and 70% non-crystallizing (NCS) sorbitol solutions.

Chemometric models were developed using the Pirouette® multivariate data analysis program (Infometrix, Inc., Bothell, WA). Standard normal variate scaling (SNV) was applied to normalize the spectra and the resulting data sets were mean centered. Classification studies were preformed using SIMCA, whereas the EG adulterant quantification model was developed using PLS. PLS regression was applied to develop a correlation between the spectra and the sorbitol, EG, and water compositions. Leave one out cross validation (LOOCV) was used to assess the predictive ability of the calibration model. The model performance was also evaluated using the root mean squared error of prediction (RMSEP) and the number of latent variables in the model was optimized on the basis of RMSEP.

3. Results and analysis

3.1. Sorbitol forms

The most significant Raman features observed for sorbitol occur in the 250–1650 cm^{-1} spectral region. The Raman spectra of CS and NCS in this region are overlaid and shown in Fig. 1. Similar Raman features are observed in both forms of sorbitol solutions throughout the spectral region with only minor differences in peak intensities. Differences in peak intensities between the sorbitol solutions can be attributed to the addition of other polyols to NCS. Characteristic Raman bands for either form of sorbitol occur between 430 and 500 cm^{-1}, bands between 800 and 900 cm^{-1} and a group of bands in the spectral region between 1000 and 1150 cm^{-1}, which are due

Table 1
Calculated HQI values for (a) 70% crystallizing sorbitol (CS) and (b) 70% non-crystallizing sorbitol. The HQI values listed in the table are averages from 5 independent spectral measurements.

Sample	HQI	St. Dev.
(A) Crystallizing sorbitol (CS)		
A	0.993	0.002
B	0.992	0.001
C	0.992	0.001
D	0.991	0.000
E	0.991	0.001
F	0.990	0.000
G-01	0.990	0.000
G-02	0.991	0.000
G-03	0.991	0.000
Average	*0.991*	
(B) Non-crystallizing sorbitol (NCS)		
H-01	0.978	0.000
H-02	0.979	0.000
I-01	0.954	0.000
I-02	0.969	0.001
I-03	0.949	0.000
Average	*0.966*	

to (CCO) bending vibration, the in-phase (CCO) stretching vibration and the out-of-phase (CCO) stretching vibration, respectively [5].

Spectral correlation was used to study the Raman data acquired for the CS and NCS solutions. The verification mode operates by comparing the spectrum of each sample to a predetermined reference spectrum. A minimum HQI threshold of 0.950 was used to assign a "Pass" or "Fail" determination to the sample under study. Sample "J", a 70% crystallizing sorbitol solution, was used as the library reference spectrum. Table 1A and B list the average HQI values and the standard deviations for 5 independent spectral measurements of each CS and NCS sorbitol samples, respectively. The average HQI value for the nine CS solutions obtained from six different manufacturers was 0.991. Because the HQI values for samples A through G were greater than the 0.950 threshold, they were positively identified as 70% crystallizing sorbitol solutions. The average HQI for the group of NCS samples was 0.966. The variability observed for the HQI values of the NCS samples can be attributed to the polyol additives, which can vary by manufacturer and from lot to lot. Although small intensity variations were observed between the Raman spectra of CS and NCS solutions, in Fig. 1, the HQI values for the NCS samples, H and I, were above the 0.950 threshold with the exception of I-03 (HQI = 0.949), indicating that they are consistent with CS, when they are actually NCS. As a result, this indicates that the library verification method lacks the sensitivity to distinguish between the different forms of sorbitol.

The Raman data for CS and NCS, used in the library verification method for the identification of sorbitol form, was also analyzed using classification methods. Since some degree of inherent clustering related to sorbitol form was observed in preliminary studies using principal component analysis (PCA), the data were further analyzed using SIMCA analysis. SIMCA is a supervised pattern recognition method [18]. Objects in one group or class exhibit similar behavior and as a result the similarities of the class can be modeled. Training sets are assigned for classes and independent PCA models are constructed for each class. The residual difference between a spectrum and each class is then used in the classification of a sample. Class borders, which are 95% probability clouds, are defined around the samples of the classes. Positive identification of a sample to a class is made only if it falls within the 95% probability cloud of one of the classes. Samples falling outside the class borders are considered as outliers.

Classification of sorbitol was by form (CS or NCS), and samples were randomly assigned to either the calibration or validation set. Thirty-five Raman spectra obtained from four CS (A, C, F, and G-01) and three NCS (H-02, I-01, and I-02) solutions were used to develop the two PCA models used in the SIMCA method. The SIMCA model was then used to classify the remaining 35 spectra of the CS and NCS test samples. The classification results are shown in the scores plot of Fig. 2. Class projections are used to illustrate the ability of SIMCA to differentiate Raman data based on the first two principal components. A two dimensional plot of PC 1 versus PC 2 shows good class separation of the CS and NCS sorbitol samples. The validation samples, denoted as triangles (CS) and hexagons (NCS) in Fig. 2, cluster nicely with calibration samples used to develop the CS (circles) and NCS (squares) PCA models. The SIMCA model offered good class separation, zero misclassifications, and tight clustering among the CS group. A larger spread was observed for the NCS samples that may be attributed to the variability of the polyol additives from the different manufacturers. NCS solutions having similar polyol additives or from the same manufacturer may be identified as a result of their close proximity in clustering. The interclass Euclidean distance between centers of the CS and NCS groups was determined to be 3.2. An interclass distance greater than 3 is generally considered a good indicator of well-separated classes in a SIMCA model [19]. On the basis of these results, and unlike the spectral correlation method, the SIMCA approach has the necessary discriminating power and sensitivity to be useful in indentifying the form of liquid sorbitol solutions.

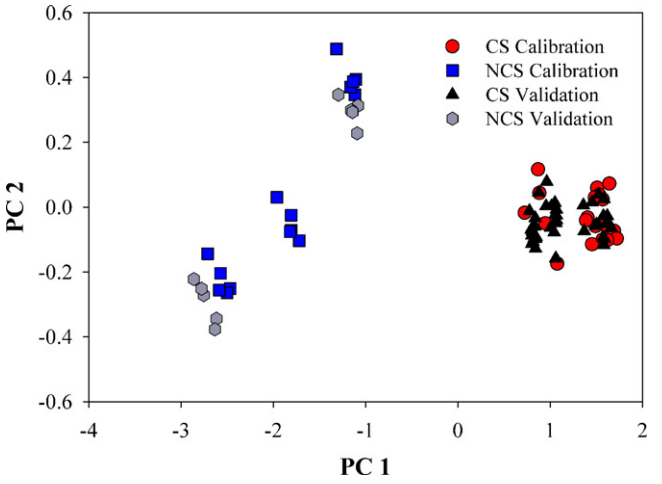

Fig. 2. Score plot of PC 1 versus PC 2 of the SIMCA classes for 70% crystallizing (CS) and 70% non-crystallizing (NCS) sorbitol.

3.2. Adulterated sorbitol

Raman spectra in the 250–1650 cm^{-1} region for adulterated CS solutions and the pure component spectrum for the adulterant (DEG or EG) are offset and shown in Fig. 3. For the sake of simplicity, only the adulterated CS spectra will be discussed, however, similar results were observed for the adulterated NCS samples. The pure component spectra of EG and DEG both share regions of common spectral features to that of the CS solution. One exception is that of the peak at ~822 cm^{-1} which arises from the OC_2H_4 moiety of DEG [20]. Significant overlap between the CS solution and the 5% adulterated sorbitol samples are observed. Key spectral differences in the bands between 900 and 1200 cm^{-1} and the 1200–1500 cm^{-1} spectral regions of the adulterated sorbitol samples can be attributed to the CH bending and C—O stretching modes, respectively, of the EG and DEG adulterants [20–22]. A shift to higher frequency and an increase in intensity of the 874 cm^{-1} Raman band of the 5% EG adulterated sorbitol sample can be attributed to the C—C stretching of the EG adulterant. The slight increase in baseline in the region just below the 874 cm^{-1} peak in

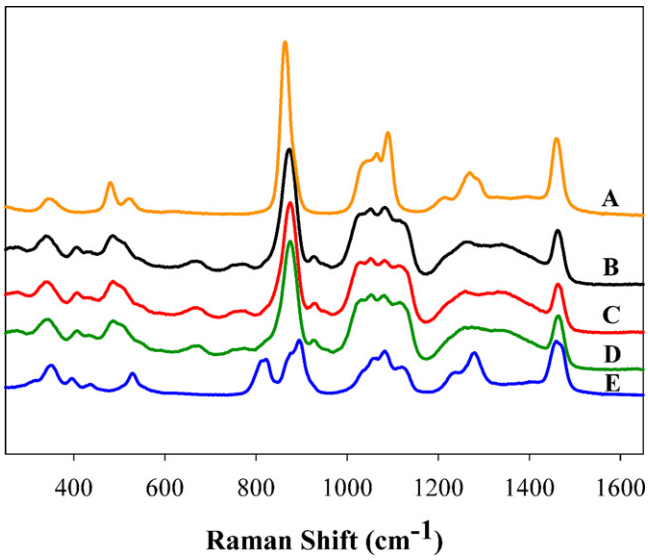

Fig. 3. Raman spectra of (a) pure EG, (b) 5% EG adulterated CS, (c) CS, (d) 5% DEG adulterated CS and e) pure DEG.

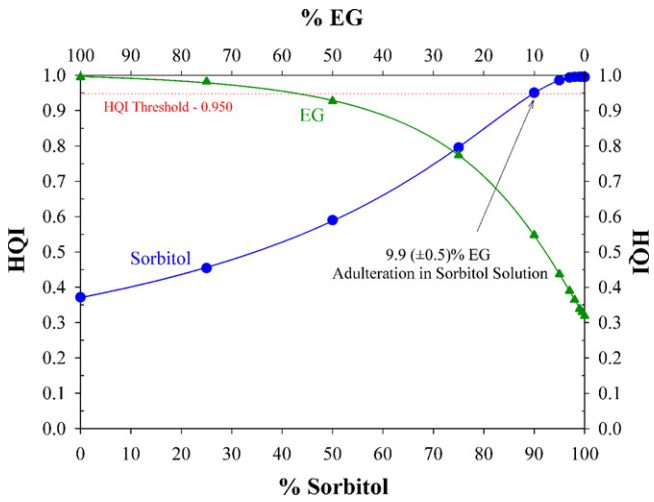

Fig. 4. HQI plot for EG and CS sorbitol.

the DEG adulterated sample results from a "growing-in" of the feature due to the OC_2H_4 moiety of DEG [20–22]. The extent of spectral overlap (and only slight differences apparent to the unaided eye) in Fig. 3 for the CS and adulterated CS solutions requires the use of chemometric methods to improve the sensitivity and selectivity of low level adulterants.

The nine CS solutions used in the sorbitol form studies were adulterated with low levels (0.0–5.0%) of EG and DEG. The Raman spectra acquired for the CS and adulterated CS solutions were analyzed using the spectral library verification method. The HQI threshold was set to 0.950 and sample J was again used as the CS reference spectrum. Table 2A and B list the average HQI values and the standard deviations for 5 independent spectral measurements of the EG and DEG adulterated sorbitol samples, respectively. As mentioned earlier, the average HQI value for the authentic CS solutions is 0.991. As the adulterant composition increases, a slight decrease in the HQI values for both EG and DEG adulterated samples are observed. When 5% of an EG or DEG adulterant is present in a CS solution, the average HQI values decrease to 0.971 and 0.988, respectively. These values are still above the 0.950 level that is often used as the "Pass" threshold, indicating that the spectral correlation method is susceptible to passing adulterated samples.

To study the sensitivity of spectral library methods, a series of EG adulterated sorbitol samples were prepared using sample J as the stock sorbitol solution. Eleven test samples were prepared with EG adulterant compositions in the range of 0–100%. Their Raman spectra were acquired and two separate HQI values were computed for each test sample. The first HQI value was calculated by comparing the test sample spectrum to the reference spectrum of CS sample J, while the second HQI value was determined using the reference spectrum of pure EG. The resulting HQIs for each sample were plotted as a function of sample composition [10]. The results are shown in the HQI plot of Fig. 4. The dashed-line in Fig. 4 represents the 0.950 HQI threshold level. The composition at which the HQI of a sample equals this level provides a measure of the sensitivity of the spectral correlation to the EG adulterant composition. According to the plot in Fig. 4, the HQI value for a sample does not drop below the 0.950 threshold until the EG adulterant composition is greater than ~10%. This indicates that the spectral correlation method lacks the sensitivity to detect low level adulterants and samples containing up to ~10% EG adulterant will still be assigned a "Pass" with verification-type spectral library correlation methods.

Table 2
Calculated HQI values for CS solutions adulterated with (a) EG and (b) DEG. The HQI values listed in the table are averages from 5 independent spectral measurements.

	Crystallizing sorbitol (CS)	
	HQI	St. Dev.
(A) (%) EG adulterant		
0.0	0.992	0.001
0.5	0.991	0.001
1.0	0.989	0.002
2.5	0.984	0.001
5.0	0.971	0.001
(B) (%) DEG adulterant		
0.0	0.991	0.000
0.5	0.992	0.000
1.0	0.992	0.000
2.5	0.991	0.001
5.0	0.988	0.001

Even though similar Raman spectral features are observed between the CS and NCS sorbitol solutions, the SIMCA classification method has been shown to be effective in correctly classifying sorbitol samples based on form. The PCA model used to classify CS solutions from the SIMCA sorbitol form method was applied to the 136 Raman spectra of authentic and low level EG and DEG adulterated CS samples that were collected during the spectral library studies. The PCA model was used to determine the sensitivity of the SIMCA classification method for low level adulterants. The PCA model is a one class-classifier method in which authentic CS solutions would be correctly identified by falling within the 95% probability cloud. Any samples falling outside this region would be termed as outliers and could consist of adulterated, non-crystallizing or non-sorbitol samples. The classification results are illustrated in the scores plot of Fig. 5. A two dimensional plot of PC 2 versus PC 3 shows good class separation by adulterant with EG adulterated samples directed along the PC 2 axis and the DEG samples located along the PC 3 axis. The samples along each axis also cluster by adulterant composition. CS samples having low level (0.5–1.0%) adulterants can sometimes fall within the 95% probability cloud and be positively identified as authentic CS solutions.

The prediction performance of the CS classification model can be assessed using the four following parameters, sensitivity, specificity, precision, and the total accuracy [23,24]. The definitions of the four parameters are as follows:

$$\text{Accuracy} = \frac{\text{TN} + \text{TP}}{\text{TP} + \text{FN} + \text{TN} + \text{FP}} \quad (2)$$

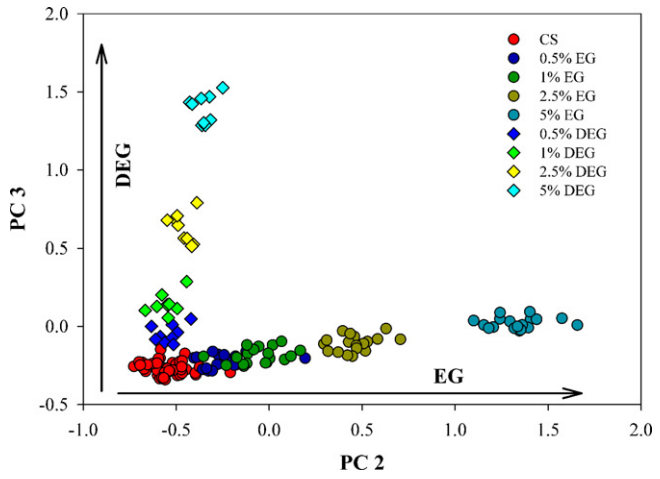

Fig. 5. Score plot of PC 2 versus PC 3 of the PCA for 70% crystallizing (CS) sorbitol applied to low level adulterated EG and DEG CS samples.

$$\text{Sensitivity} = \frac{\text{TP}}{\text{TP} + \text{FN}} \quad (3)$$

$$\text{Specificity} = \frac{\text{TN}}{\text{TN} + \text{FP}} \quad (4)$$

$$\text{Precision} = \frac{\text{TP}}{\text{TP} + \text{FP}} \quad (5)$$

TP, TN, FN, and FP denote the true positive, the true negative, the false negative and the false positive, respectively. Note that the true positive refers to a pure 70% crystallizing sorbitol solutions (CS) and the true negative is a known adulterated sample. The accuracy of the SIMCA classification model was assessed based on the number of false positive and false negative results. A false positive result occurs when a sample is wrongly identified as belonging to a specific class (adulterated sample being predicted as authentic); conversely, a false negative result occurs when a sample that does belong to a class is not classified as such (an authentic sample being predicted as adulterated). A false positive result may be considered the more serious of the two because it results in failure to detect adulteration whereas false negatives may be corrected by applying subsequent testing using alternative analytical methods. A comparison on the performance of the CS classification model for adulterant composition threshold levels set at 0, 1.0, and 2.5% are given in Table 3. The ideal composition threshold would be set at the limit of detection (LOD) for the adulterant based on a 95% confidence limit. Regardless of the composition threshold, the CS classification model had 100% sensitivity and correctly identified all authentic CS solutions as 70% crystallizing sorbitol. Adulterant composition thresholds below 2% resulted in a wide range of values for accuracy, specificity, and precision. The variability observed in these parameters confirms that the classification model is not adequate for identifying the presence of EG or DEG adulterants below concentrations of ~2% in CS solutions, but is still quite an improvement over the verification-type spectral correlation method.

Table 3
Performance of the CS classification model for different EG adulterant composition thresholds. The values represent the percentage of samples passing the specified criteria.

	EG adulterant composition threshold		
	0.0%	1.0%	2.5%
Accuracy	65.3	85.0	97.9
Sensitivity	100.0	100.0	100.0
Specificity	45.3	77.1	96.5
Precision	51.3	69.6	95.2

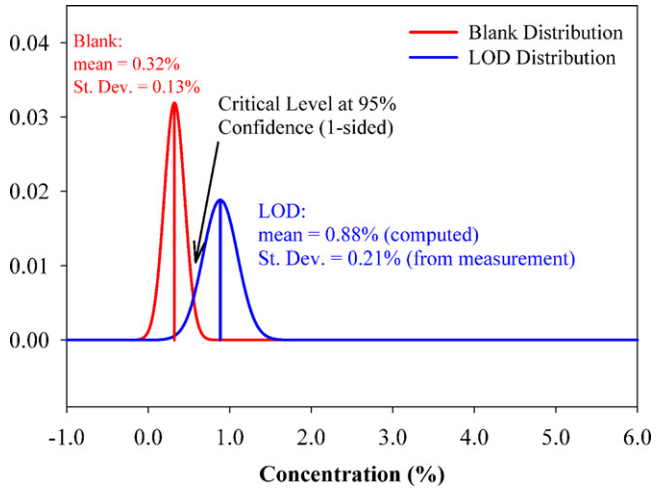

Fig. 6. Pictorial representation of determination of critical level (CL) and limit of detection (LOD). Gaussian distribution functions for chemometric predictions of a blank and a sample with low concentration of EG.

Multivariate calibration methods have been demonstrated to have the sensitivity to detect low level adulterants in raw materials [12]. Quantification of the EG adulterant in CS sorbitol solutions was performed using PLS. The PLS model was developed using the series of EG adulterated sorbitol samples from the spectral library sensitivity studies. The PLS calibration plot for EG used 4 latent variables and exhibited excellent linearity, with a slope of 0.9999, an intercept of 0.0027 and a linear correlation coefficient (R^2) of 0.9999. The root mean squared error of calibration (RMSEC) and the root mean squared error of cross validation (RMSECV) for EG was 0.33 and 0.44%, respectively. The authentic CS and EG adulterated CS samples used in the library and classification methods were used as an independent test set for the PLS model. The RMSEP of EG for the test set was 0.41% and reflects the average error between the model prediction and the reference EG composition.

The method developed by Currie was used to establish the limit of detection for the PLS model [25]. Ten replicate measurements and predictions of an authentic CS solution (sample J) and a 4% EG sample (sample K) were performed using the quantitative PLS model. The average and the standard deviation for the predicted EG compositions for samples J and K were $0.32 \pm 0.13\%$ and $3.80 \pm 0.21\%$, respectively. The procedure for establishing the CL and LOD is illustrated graphically in Fig. 6. The replicate measurements of sample J were used to estimate the normal distribution of predictions when no EG is present, and the replicate measurements of sample K were used to estimate the normal distribution of predictions when a low level of EG is present. The CL is based on the distribution of blank predictions and is typically the upper limit of the one-sided interval that includes 95% of the blank distribution area. The CL is the detection threshold, and a blank sample would be expected to pass 95% of the time, with a 5% rate of type I error (false failure of a blank sample). The LOD can then be estimated as the concentration that will have a type II error rate of 5% (false pass of a sample with an adulterant concentration at the detection limit).

The distribution for a sample with an adulterant concentration at the limit of detection was estimated from the standard deviation of a sample with a low-level adulterant concentration, and the center of the distribution was selected so that 95% of its area is above the CL. Thus, when the CL is used as the pass/fail threshold, the type I and type II error rates are both 5%, where the type II rate is specified for a sample with a concentration at the LOD. The CL and LOD for EG from the quantitative PLS model were determined to be 0.53 and 0.88%, respectively.

4. Discussion

EMAs are typically selected because their appearance, physical properties and chemical properties are similar to those of the targeted authentic material. Thus EMAs may also have similar Raman spectral features as those of a targeted authentic material and at low levels of adulteration, spectral differences may not always be observed by visual inspection (cf. Fig. 3) or spectral correlation methods (Fig. 4). The minimum amount of adulterant that can be detected by the spectral library methods is dependent on the intrinsic spectral properties of the materials involved [10]. In the case of sorbitol, the minor spectral differences attributed to the polyols or to the EG or DEG low level (<5%) adulterants were not significant and the spectral correlations for the adulterated samples resulted in HQI values above the 0.950 level used as the "Pass" threshold. Only when the EG adulterant compositions were greater than 10% did the HQI values fall outside the "Pass" threshold, thus making library verification methods susceptible to passing adulterated samples.

Chemometric classification methods exhibit enhanced sensitivity to detecting minor spectral differences. The SIMCA method can successfully differentiate between the two forms of sorbitol (CS or NCS) as well as discriminate between authentic and adulterated sorbitol samples with adulterant levels as low as ~2%. The classification model is not adulterant-specific, so that it is able to detect sorbitol adulteration even if the adulterant is not known in advance. For example, the CS form classification model was developed only using 70% CS solutions, but was able to identify EG, DEG and even diluted CS solutions as outliers or suspect samples. This is a significant difference between classification methods and PLS methods. Adulterant identification can only be made using classification methods if separate classes, that include adulterant information, are included in the SIMCA model. Implementation of this model would require the establishment of a large, authentic sample database that would include multiple lots from each sorbitol manufacturer. On-site analysis can be performed using portable Raman instruments, and with the application of chemometric calibration transfer methods, the SIMCA classification model can be utilized across multiple Raman instruments.

Despite being labor intensive and time consuming to develop, PLS models offer the highest sensitivity for the detection of low level adulterants (~0.88% EG). PLS models are matrix dependent and, as a result, the identity of the adulterant as well as the form of sorbitol must be known in order to execute the appropriate model. For example, a test set containing EG adulterated NCS samples predicted using the EG adulterated CS sorbitol PLS model, described earlier, resulted in a RMSEP of 1.19%. This error was approximately three times greater than that observed for the test set containing the EG adulterated CS samples (0.41%). In this case, the authentic NCS samples would fail the rapid screening test and need to undergo further analysis using the appropriate USP methods. Similar to the SIMCA classification method, the PLS model could be used with portable Raman instruments for on-site analysis. However, the chemometric calibration transfer procedures would be more cumbersome requiring more calibration standards and additional instrument set up time.

5. Conclusion

Confirmation of the authenticity of a pharmaceutical raw material is an increasing challenge for the pharmaceutical industry. In this paper we have explored the capabilities of three commonly used data analysis procedures. Although Raman spectral libraries are perhaps the most commonly used method for qualitative analysis in the pharmaceutical industry and are straightforward and require little or no expertise, they lack the sensitivity to correctly identify the correct form of sorbitol and even adulterants especially if the adulterant present has a similar structure. Chemometric methods, while requiring more expertise and more complex method development, feature enhanced sensitivity and specificity required for distinguishing differences in the chemical compositions of authentic and adulterated samples. For SIMCA classification methods, the identity of the adulterant does not have to be known and EG and DEG adulterated samples were flagged as suspicious when the adulterant compositions were greater than ~2%. Quantification of the EG adulterant by PLS resulted in the lowest limit of detection (~0.9% EG in CS), however, the model development was time consuming and also required the identity of the adulterant. Thus, the results obtained from these feasibility studies highlight the importance of selecting an appropriate data analysis process for balancing the desired limit of detection and the ease of method development when using portable rapid screening methods for the identification of low level adulterants in pharmaceutical raw materials.

Disclaimer

The findings and conclusions of this article have not been formally disseminated by the Food and Drug Administration and should not be construed to represent any Agency determination or policy.

References

[1] A. Coukell, Public Meeting on Economically Motivated Adulteration, College Park, MD, 2009.
[2] M. Guerrini, D. Beccati, Z. Shriver, A. Naggi, K. Viswanathan, A. Bisio, I. Capila, J.C. Lansing, S. Guglieri, B. Fraser, A. Al-Hakim, N.S. Gunay, Z. Zhang, L. Robinson, L. Buhse, M. Nasr, J. Woodcock, R. Langer, G. Venkataraman, R.J. Linhardt, B. Casu, G. Torri, R. Sasisekharan, Oversulfated chondroitin sulfate is a contaminant in heparin associated with adverse clinical events, Nat. Biotechnol. 26 (2008) 669–675.
[3] R. Lutter, Public Meeting on Economically Motivated Adulteration, College Park, MD, 2009.
[4] J. Woo, S. Wolfgang, H. Batista, The effect of globalization of drug manufacturing, production, and sourcing and challenges for American drug safety, Clin. Pharmacol. Ther. 83 (2008) 494–497.
[5] M. de Veij, P. Vandenabeele, T. De Beer, J.P. Remon, L. Moens, Reference database of Raman spectra of pharmaceutical excipients, J. Raman Spectrosc. 40 (2009) 297–307.
[6] A.L. Enculescu, J.R. Steiginga, Raman spectroscopy – a powerful tool for non-routine analysis of pharmaceuticals, Am. Pharm. Rev. 5 (2002) 81–82, 84-86, 88.
[7] R.L. Green, C.D. Brown, Raw-material authentication using a handheld Raman spectrometer, Pharm. Technol. 32 (2008) 148, 150, 152, 154, 156, 158, 160, 162.
[8] R.L. Green, R. Brush, W. Jalenak, C.D. Brown, Verification methods for 198 common raw materials using a handheld Raman spectrometer, Pharm. Technol. 33 (2009) 72–82.
[9] R.L. McCreery, A.J. Horn, J. Spencer, E. Jefferson, Noninvasive identification of materials inside USP vials with Raman spectroscopy and a Raman spectral library, J. Pharm. Sci. 87 (1998) 1–8.
[10] J.D. Rodriguez, B.J. Westenberger, L.F. Buhse, J.F. Kauffman, Quantitative evaluation of the sensitivity of library-based Raman spectral correlation methods, Anal. Chem. 83 (2011) 4061–4067.
[11] C.M. Gryniewicz, J.A. Spencer, M. Hankins, J.F. Kauffman, Spectroscopic methods for rapid determination of diethylene glycol in glycerin, Am. Pharm. Rev. 10 (2007) 24–30.
[12] C.M. Gryniewicz-Ruzicka, S. Arzhantsev, L.N. Pelster, B.J. Westenberger, L.F. Buhse, J.F. Kauffman, Multivariate calibration and instrument standardization for the rapid detection of diethylene glycol in glycerin by Raman spectroscopy, Appl. Spectrosc. 65 (2011) 334–341.
[13] J.F. Kauffman, C.M. Gryniewicz-Ruzicka, S. Arzhantsev, J.D. Dunn, J.A. Spencer, S. Wolfgang, X. Li, L.N. Pelster, B.J. Westenberger, L.F. Buhse, Pharmaceutical surveillance with rapid spectroscopic screening technologies, Am. Pharm. Rev. 13 (2010) 58–62, 64.
[14] C. Sheehan, H. Wang, K. Moore, R. Lafaver, J. Griffiths, Tools to ensure safe medicines: new monograph tests in USP-NF, J. Excipients Food Chem. 1 (2010) 33–39.
[15] J. Kauffman, J.D. Rodriguez, L.F. Buhse, Spectral preprocessing for Raman library searching, Am. Pharm. Rev. 14 (2011) 34–40.
[16] J.D. Rodriguez, B.J. Westenberger, L.F. Buhse, J.F. Kauffman, Standardization of Raman spectra for transfer of spectral libraries across different instruments, Analyst 14 (2011) 4232–4240.

[17] Spectral ID Users Guide, Glactic Industries Corporation, Salem, NH, (1998) 1198.
[18] R.G. Brereton, Chemometrics For Pattern Recognition, John Wiley & Sons, West Sussex, 2009.
[19] A. Mannig, N.A. Baldauf, L.A. Rodriguez-Romo, A.E. Yousef, L.E. Rodriguez-Saona, Differentiation of Salmonella enterica serovars and strains in cultures and food using infrared spectroscopic and microspectroscopic techniques combined with soft independent modeling of class analogy pattern recognition analysis, J. Food Prot. 71 (2008) 2249–2256.
[20] M.K. Ahmed, M.P. McLeod, J. Nezivar, A.W. Giuliani, Fourier transform infrared and near-infrared spectroscopic methods for the detection of toxic diethylene glycol (DEG) contaminant in glycerin based cough syrup, Spectroscopy 24 (2010) 601–608.
[21] I. Auzanneau, D. Combes, A. Zwick, Raman spectroscopic analysis of the effect of polyhydric alcohols on water, J. Raman Spectrosc. 22 (1991) 227–231.
[22] K. Krishnan, R.S. Krishnan, Raman and infrared spectra of ethylene glycol, Proc. Indian Acad. Sci. Sect. A 64 (1966) 111–122.
[23] C.D. Brown, H.T. Davis, Receiver operating characteristics curves and related decision measures: a tutorial, Chemom. Intell. Lab. Syst. 80 (2006) 24–38.
[24] T. Fawcett, An introduction to ROC analysis, Pattern Recogn. Lett. 27 (2006) 861–874.
[25] L.A. Currie, Limits for qualitative detection and quantitative determination. Application to radiochemistry, Anal. Chem. 40 (1968) 586–593.

Journal of Pharmaceutical and Biomedical Analysis 61 (2012) 199–206

Contents lists available at SciVerse ScienceDirect

Journal of Pharmaceutical and Biomedical Analysis

journal homepage: www.elsevier.com/locate/jpba

Preparative separation of dryofragin and aspidin BB from *Dryopteris fragrans* extracts by macroporous resin column chromatography

Xiao-Juan Li[a,b], Yu-Jie Fu[a,b,*], Meng Luo[a,b], Wei Wang[a,b], Lin Zhang[a,b], Chun-Jian Zhao[a,b], Yuan-Gang Zu[a,b]

[a] Key Laboratory of Forest Plant Ecology, Ministry of Education, Northeast Forestry University, 150040 Harbin, PR China
[b] Engineering Research Center of Forest Bio-Preparation, Ministry of Education, Northeast Forestry University, 150040 Harbin, PR China

ARTICLE INFO

Article history:
Received 4 August 2011
Received in revised form 2 December 2011
Accepted 2 December 2011
Available online 13 December 2011

Keywords:
Aspidin BB
Column chromatography
Dryofragin
Macroporous resins
Separation

ABSTRACT

A simple, efficient and environment-friendly chromatographic separation method was developed for preparative separation and enrichment of dryofragin and aspidin BB from *Dryopteris fragrans*. The adsorption properties of twelve macroporous adsorption resins were evaluated. The three selected resins were further screened depending on the separation performance of their packed columns, in which AB-8 resin showed better separation efficiency for dryofragin and aspidin BB. In order to maximize column efficiency, the operating parameters (flow rate, ethanol concentration and volume) of the resin column chromatography were optimized and compared with the conventional resin column adsorption. After preparative separation and enrichment on resin column chromatography, the contents of dryofragin and aspidin BB in the product were 8.39- and 5.99-fold increased with recovery yields of 91.22% and 75.64%, respectively. Moreover, the regenerated adsorbent exhibited excellent reusability within at least five cycles of adsorption/desorption. It suggested that multi-targets would be enriched effectively by resin column chromatography.

© 2011 Elsevier B.V. All rights reserved.

1. Introduction

Dryopteris fragrans (L.) schott, known as Xianglinmaojue in China, is a deciduous perennial herb belonging to the family Dryopteridaceae and widely distributed in Asia-temperate, Europe and North America. It is characterized by distinctive appearance of retaining withered fronds and normally occurs on talus slopes and cliff crevices [1]. Infusions and decoctions of its aerial parts have been historically used in folk medicine for treating various dermatosis in the northeast China, such as psoriasis, acne, erythra, dermatitis. Especially in Wu Da Lian Chi (Heilongjiang province, China), it has been brought to market as an important product for the therapy of beriberi. Moreover, the local residents also employed extraction solution to wash hair for getting rid of scurf and relieving itching [2]. In a word, this species is attracting more and more attention due to these beneficial effects. In agreement with the prescribed folk medicine remedy, two groups have already confirmed the antipsoriatic activity of its solvent extract in rats [3–5]. *D. fragrans* also has been reported as an effective agent of antibacterial, antioxidant, analgesic, anti-tumour as well as antirheumatic arthritis [6–10].

Phloroglucinols are typical active compounds for nearly all species of *Dryopteris* [11]. Dryofragin and aspidin BB, are major phloroglucinols in *D. fragrans*, whose chemical structures are shown in Fig. 1. To the best of our knowledge, dryofragin is a characteristic compound in *D. fragrans* and the only filicinic acid-sesquiterpene [12]. Both dryofragin and aspidin BB are ichthyotoxic compounds and exhibit potential application in treating S180 sarcoma, Lewis lung cancer and HepA liver cancer [13]. Moreover, aspidin BB also can significantly suppress two-stage mouse skin carcinogenesis in vivo [10,14] and fatty acid synthase which is highly expressed in most common human carcinomas [15], and exerted strong anthelmintic activity [16] as well as Epstein–Barr virus inhibitory activity [10]. In view of these beneficial effects, the application of low-cost technology to obtain the compounds aforementioned from *D. fragrans* is indispensable for in-depth pharmacological research and clinical trials.

In preparative enrichment of active components, various physical and chemical techniques have been successfully applied, such as liquid–liquid extraction [17,18], precipitation [19], membrane filtration [20], adsorption [21] and so forth. Among those methods, liquid–liquid extraction and precipitation are recognized as low resolution separation techniques due to their lack of specificity. Besides, the consumption of organic solvent and the environmental

* Corresponding author. Tel.: +86 451 82190535; fax: +86 451 82190535.
E-mail address: yujie_fu2002@yahoo.com (Y.-J. Fu).

0731-7085/$ – see front matter © 2011 Elsevier B.V. All rights reserved.
doi:10.1016/j.jpba.2011.12.003

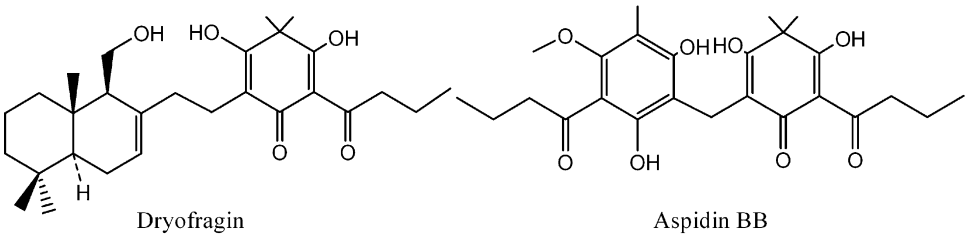

Fig. 1. Chemical structure of dryofragin and aspidin BB.

impact of their disposal may also be an important bottleneck. Membrane acts as a selectively permeable barrier to separate target substance. However, it has some limitations that need to be overcome, such as membrane fouling, sedimentation pollution and the high cost of post-operation [22]. Silica gel (SiO_2) [23], alumina (Al_2O_3) [24] and resin [25] are adsorbents commonly used for column chromatography. Among of them, the reusability of silica gel and alumina is much lower than resin, and resin column adsorption uses ethanol–water system as elution solvent in place of unfriendly solvents such as chloroform, methanol and ethyl acetate. Comparatively, taking economy and environment into account, resin seems to be more suitable for preparative enrichment due to its special characteristics such as high mechanical strength, good acid and alkali resistance, various surface functional groups, porous availability, high surface area and easy regeneration. Moreover, resin is endowed with selective adsorption properties through electrostatic force, hydrogen bonding interaction, complexation, size sieving action, etc. Nowadays, resin column adsorption has been widely used in separation and enrichment of bioactive substances, including flavonoids [26], polyphenols [27], alkaloids [28], saponins [29] and other components extracted from plant materials.

In an attempt to improve separation efficiency between different target compounds, we developed a new usage of resin column. Chromatography combined with resin column adsorption is the basis of this methodology. In this method, sample was loaded on the top layer of the resin column whose mechanism is similar to combined size-exclusion and reversed-phase chromatography. This usage of resin column has many advantages over conventional matrices, on the one hand, continuous adsorption and desorption increased the number of theoretical plates of resin column, on the other hand, it makes good use of sieve classification property of resin. These multiple modes of interaction offer a unique ability to separate compounds. In separation process, compounds with different sizes and polarities gradually separated from each other with a changing eluent composition. Thus, much more target products were preconcentrated separately within one unit operation. This methodology is controlled by a number of parameters relating to the resin properties (e.g. surface area, average pore diameter), the multi-target products (e.g. molecular weight, hydrophobicity, and conformational characteristics) and the interactions between stationary and mobile phases (e.g. flow rate, concentration and volume of ethanol solution). In our previous research, four taxoids were preparative separation by this type of resin column [30]. There is no report on using resin column chromatography to separate and enrich dryofragin and aspidin BB from extracts of *D. fragrans* as yet. In this study, the relating parameters of selected strategy were optimized for maximizing enrichment ratio, separation efficiency and recovery coefficient. The separation and enrichment efficiency of this methodology was compared with the traditional usage under the optimal conditions. The regenerability and reusability of the selected resin were also investigated.

2. Experimental

2.1. Chemicals and reagents

Standards of dryofragin and aspidin BB were isolated from *D. fragrans* in our laboratory with the purity more than 98% separately, and the structures were identified by comparing the spectral data (UV, MS, ^{1}H NMR and ^{13}C NMR) with previous literature [10]. Methanol and acetonitrile of chromatographic grade were purchased from J & K Chemical Ltd. (China). Phosphoric acid was chromatographic grade (Tianjin Kermel Chemical Reagent Co., Ltd., China). Ethanol was analytical grade obtained from Beijing Chemical Reagents Co. (Beijing, China). Deionized water was purified by a Milli-Q Water Purification system (Millipore, MA, USA). All solutions prepared for HPLC were filtered through 0.45 μm nylon membranes prior to use.

2.2. Adsorbents

Macroporous resins including AB-8, D101, D3520, H103, H1020 and NKA2 were obtained from Chemical Plant of Nankai University (Tianjin, China), while AL-1, FL-1, FL-3 resins from Nankai Hecheng S&T Co., Ltd. (Tianjin, China) and HPD-600, HPD-826, HPD-D resins were supplied by Cangzhou Bonchem Co., Ltd. (Hebei, China). Their physical and chemical properties are summarized in Table 1. The resins were pre-treated according to the manufacturer's recommendation so as to remove the monomers and porogenic agents trapped inside the pores during the synthesis process. In brief, before the adsorption experiments, the weighed resins were soaked in ethanol overnight, subsequently washed with 95% ethanol by circumfluence until there was no residue after distillation, and then washed by deionized water until the ethanol was thoroughly replaced by deionized water. The moisture contents of the tested resins were determined by drying the beads at 80 °C to constant weight in a drying oven for over 24 h.

2.3. Sample preparation

The aerial parts of *D. fragrans* were purchased from Wu Da Lian Chi (China), and were authenticated by Professor Shaoquan Nie from the Key Laboratory of Forest Plant Ecology, Ministry of Education, Northeast Forestry University, China. Dried materials of *D. fragrans* were powdered by a disintegrator (HX-200A, Yongkang Hardware and Medical Instrument Plant, China) and then sieved (20–40 mesh). One kilogram of *D. fragrans* powder was extracted with 8000 mL of ethanol–water (80:20, v/v) solution in an ultrasonic bath (Kunshan Ultrasonic Instrument, China) for 45 min, repeated three times. The filtered solutions were gathered and concentrated to dryness by removing the ethanol solvent using a rotary evaporator device (RE52AA, Shanghai Huxi Instrument Co., China) at 50 °C. The contents of dryofragin and aspidin BB in extracts were 4.10 mg/g and 9.50 mg/g, respectively. The extracts obtained were

Table 1
Chemical and physical properties of the tested resins.

Trade name	Functional group	Surface area (m^2/g)	Average pore diameter (nm)	Particle diameter (mm)	Polarity	Moisture content
H1020	Polystyrene	700–1000	8.9–9.0	–	Non-polar	53
H103	Polystyrene	1000–1100	8.5–9.5	0.315–1.25	Non-polar	54
D101	Polystyrene	400–600	10.0–12.0	0.2–0.6	Non-polar	71
D3520	Polystyrene	480–520	12.0–17.0	0.315–1.25	Non-polar	78
HPD-D	Crosslinked-polystyrene	650–750	9.0–11.0	0.3–1.25	Non-polar	76
FL-3	Ester group	80–120	15.0–20.0	0.3–1.25	Non-polar	70
AL-1	Polystyrene	250–290	12.0–17.0	0.3–1.25	Weak-polar	76
AB-8	Polystyrene	480–520	13.0–14.0	0.3–1.25	Weak-polar	69
HPD-826	Polystyrene	500–600	9.0–10.0	0.3–1.25	Middle-polar	73
HPD-600	Acylamino polystyrene	550–600	8.0–10.0	0.3–1.25	Polar	77
NKA2	Polystyrene	160–200	14.5–15.5	0.3–1.25	Polar	49
FL-1	Amino-carbonyl group	100–120	14.0–15.0	0.3–1.25	Strong-polar	71

diluted to appropriate concentration with 50% ethanol as sample solution for the subsequent experiments.

2.4. HPLC analysis of dryofragin and aspidin BB

The concentration of dryofragin and aspidin BB was determined at 35 °C by using a Jasco liquid chromatographic system (Jasco company, Japan) equipped with a Jasco UV-1575 intelligent UV/VIS Detector and a Jasco PU-1580 intelligent HPLC pump. Chromatographic separation was carried out on a HiQ Sil C18W reversed-phase column (250 mm × 4.6 mm i.d., 5 μm, Welch Materials Inc., USA). The mobile phase acetonitrile–water–phosphoric acid (86:13.5:0.5, v/v/v) was filtered through a 0.45 μm membrane filter (Millipore, USA), and deaerated ultrasonically prior to use. Dryofragin and aspidin BB were quantified at a wavelength of 280 nm. The flow rate was 1 mL/min, the injection volume was 10 μL. The retention time of dryofragin and aspidin BB was 31.60 and 37.62 min, respectively. The chromatographic peaks of the analytes were confirmed by comparing their retention time and UV spectrum with those of the reference compounds. Seven experimental points were employed for establishing a calibration curve. The regression lines for dryofragin and aspidin BB were $Y = 81{,}99{,}152.3976X + 19{,}525.8174$ ($R^2 = 0.9983$, $n = 7$), $Y = 1{,}30{,}27{,}971.5256X + 3671.8966$ ($R^2 = 0.9985$, $n = 7$), respectively, where Y is the peak area of analyte, and X is the concentration of analyte (mg/mL). All sample solutions were centrifuged at 12,000 rpm for 10 min prior to HPLC analysis.

2.5. Adsorption properties of different resins for dryofragin and aspidin BB

Macroporous resins with different chemical and physical constraints would selectively adsorb and desorb constituents from sample solutions. For maximizing enrichment ratio of both target compounds, the adsorption properties of different resins towards dryofragin and aspidin BB were investigated. Batch static adsorption tests were performed as follows: pre-weighed quantities of hydrated resins (equal to 1 g in dry weight) and 30 ml sample solution obtained in Section 2.3 were added into 100 mL conical flasks. The flasks were shaken (130 rpm) in a constant temperature shaker at 30 °C for 6 h. Subsequently take them apart by filtration. The filtrate was analyzed by HPLC. The resin after adsorption was desorbed with 30 mL ethanol. The flasks were shaken (130 rpm) for 4 h at a constant temperature of 30 °C. Then desorption solution was analyzed by HPLC.

The preliminary selection of resins was evaluated based on the adsorption and desorption capacities, and ratio of desorption. The equations were as follows:

Adsorption evaluation

$$Q_e = \frac{(C_0 - C_e)V_i}{W} \quad (1)$$

where Q_e is the adsorption capacity at adsorption equilibrium (mg/g resin); C_0 and C_e are the initial and equilibrium concentrations of solute in the solutions, respectively (mg/mL). V_i is the volume of sample solution, and W is the weight of the dry resin.

Desorption evaluation

$$D = \frac{C_d V_d}{(C_0 - C_e)V_i} \times 100\% \quad (2)$$

$$Q_d = \frac{C_d V_d}{W} \quad (3)$$

where Q_d is the desorption capacity after adsorption equilibrium (mg/g resin); D is the desorption ratio (%); C_d is the concentration of solute in the desorption solution (mg/mL); V_d is the volume of the desorption solution (mL); C_0, C_e, W and V_i are the same as described above.

2.6. Resin column chromatography

Resin column chromatography tests were carried out on lab-scale glass columns (20 mm i.d. × 300 mm) wet-packed with 15 g (wet weight) resin. Two grams sample is dissolved with a small amount of ethanol in an evaporating dish, and 5 g (wet weight) resin was added into it, then placed the evaporating dish on a water bath at 45 °C till the sample was absolutely adsorbed to the resin and no solution left. The resins with sample were loaded on the top of the prepared resin column. The bed volume (BV) of the resin (equal to 20 g of wet resin) was 20 mL and the length of resin bed was 12.0 cm.

The separation properties of the three selected resins were further evaluated by resin column chromatography test. After loading sample, different concentrations of ethanol (50%, 60%, 70%, 80%, 90% and anhydrous ethanol) were used to desorb the target compounds successively at a flow rate of 3 BV/h. The elution volume of each concentration was 5 BV. Concentrations of dryofragin and aspidin BB in desorption solution were determined by HPLC.

In order to determine the suitable elution procedures for enrichment and separation of dryofragin and aspidin BB, according to the test result above, a gradient elution was performed as follows: after the sample loading, gradient elution using different concentrations of ethanol (70%, 80%, 85%, 90% and 95%) was conducted to enrich and separate dryofragin and aspidin BB, at a constant flow rate of 3.0 BV/h. The elution volume of each ethanol concentration was adjusted under the guidance of HPLC. After determining suitable elution procedures, the flow rate 6 RV/h was chosen for the following tests in order to shorten the operation time. Dryofragin and

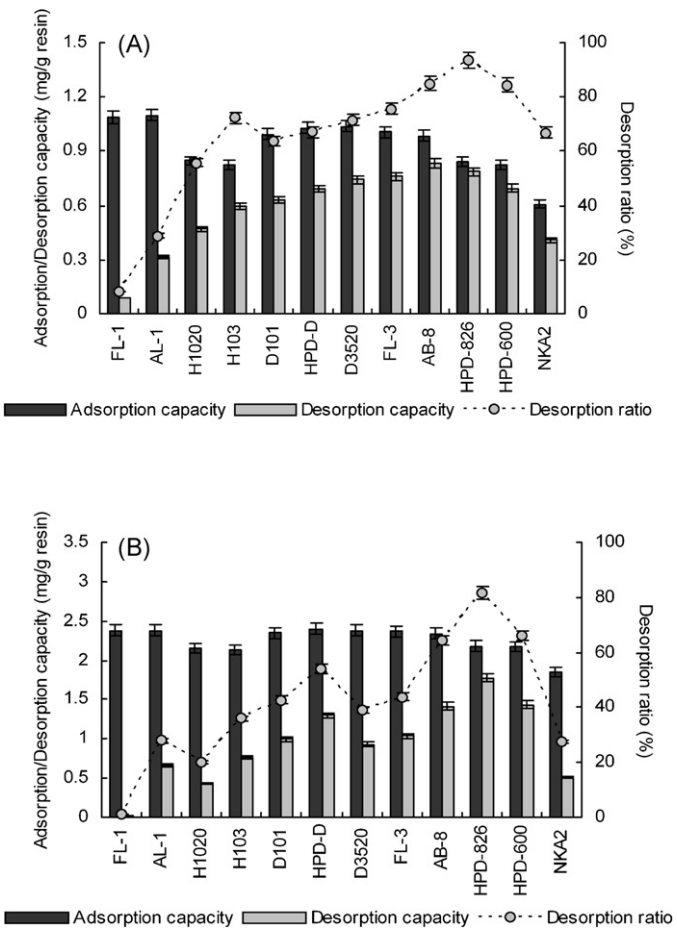

Fig. 2. Adsorption and desorption capacities, desorption ratio of dryofragin (A) and aspidin BB (B) on different resins.

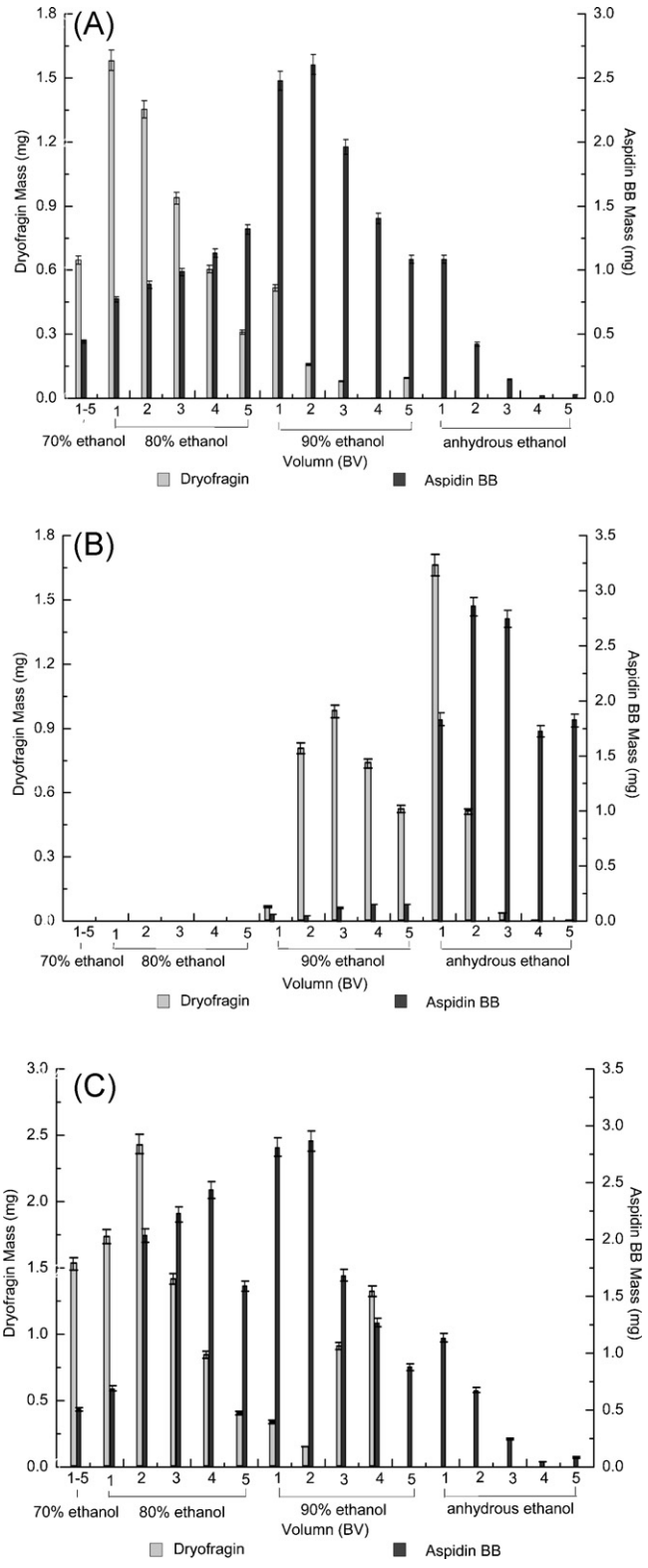

Fig. 3. Separation performance of dryofragin and aspidin BB using HPD-826 (A), AB-8 (B) and HPD-600 (C) resins column chromatography (flow rate 3 BV/h).

aspidin BB in the desorption solution were analyzed by HPLC and then concentrated to dryness under vacuum.

2.7. Resin column adsorption

The separation and enrichment of dryofragin and aspidin BB by resin column chromatography in this paper was compared with the resin column adsorption. This test was carried out in a glass column (20 mm i.d. × 300 mm) packed with selected resin. The bed volume (BV) and length of resin bed were the same as described in Section 2.6. The dried extract (2.0 g) obtained in Section 2.3 was dissolved with 50% ethanol as sample solution. The sample solution flows through the glass column at a flow rate of 1.0 BV/h, and subsequently the sample distributed in the whole resin column. The elution process was performed under the optimized conditions of resin column chromatography. Dryofragin and aspidin BB in the eluent were detected by HPLC and then concentrated to dryness under vacuum.

2.8. Regeneration of exhausted AB-8 resin

After each run on the AB-8 adsorbent, the column was subjected to a regeneration procedure in preparation for the next cycle. The regenerative protocol was performed as follows: 3 BV anhydrous ethanol were used for removing the residua in the resin at a flow rate of 1.5 BV/h, and 6 BV deionized water were to equilibrate column at a flow rate of 2 BV/h. To verify the performance of the adsorbent after regeneration, the AB-8 column was subjected to 5 cycles for separation and enrichment of dryofragin and aspidin BB successively, each cycle followed the protocol described above.

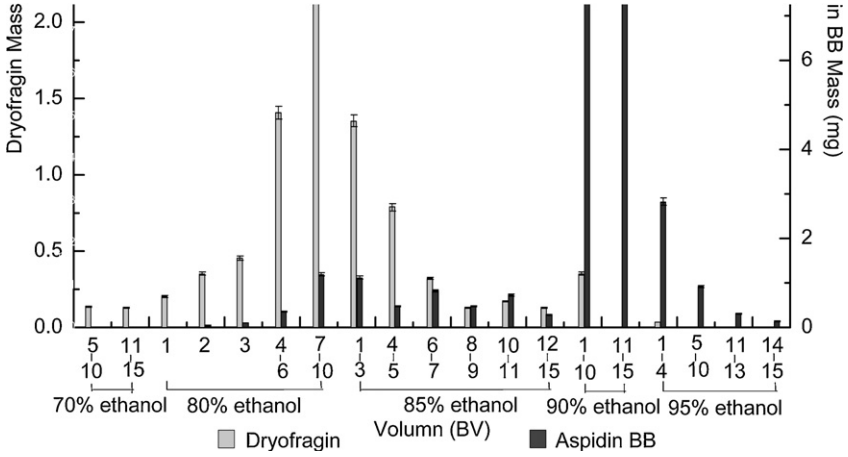

Fig. 4. Effects of the operating factors (concentration and volume of ethanol solution) on resin column chromatography for separation of dryofragin and aspidin BB (flow rate 3 BV/h).

3. Results and discussion

3.1. Adsorption properties of different resins for dryofragin and aspidin BB

As shown in Fig. 2, the adsorption capacity of different resins towards dryofragin and aspidin BB was indistinct. Taking desorption performance of resins into account, AB-8, HPD-826 and HPD-600 resins showed higher desorption capacity and desorption ratio than the other resins. This not only correlates with the physical and chemical properties of adsorbent, but also with the polarity and size of adsorbate. Resins with similar polarity to solute exhibited better adsorption ability. Moreover, suitable dimensional structure of resins (surface area, average pore diameter, etc.) is the other key factor for selecting proper resins.

Among the tested resins, low-polar (non-polar and weak-polar) resins exhibited the relatively better adsorption capacity because of their similar polarity with low-polar compounds dryofragin and aspidin BB. However, taking desorption performance of resins into account, AB-8 showed higher desorption capacity and desorption ratio than the other seven low-polar resins, as illustrated in Fig. 2 and Table 1. It possessed a weak affinity for solute so that the desorption performance of dryofragin and aspidin BB on AB-8 resin was actually notable. Among the tested polar resins (middle-polar, polar and strong-polar), the adsorption capability towards dryofragin and aspidin BB was primarily by means of physical instead of chemical forces. The middle-polar resin HPD-826 and polar resin HPD600 had relatively better adsorption and desorption capability, because their average pore diameters and surface area are more suitable for adsorption and desorption of dryofragin and aspidin BB. Therefore, AB-8, HPD-826 and HPD-600 resins were selected to further investigate their separation performance towards dryofragin and aspidin BB.

3.2. Separation performance of the three selected resins towards dryofragin and aspidin BB

Separation properties of the three selected resins towards dryofragin and aspidin BB were shown in Fig. 3. On the whole, as the resin polarity (AB-8, HPD-826 and HPD-600) increased, the affinity of dryofragin and aspidin BB for the resin column decreased so that polar solvents can more effectively compete with polar sites on the resin surface for dryofragin and aspidin BB. In Fig. 3(A), although some dryofragin could be desorbed with 70% ethanol, most of it was washed by 80% ethanol. Aspidin BB was mainly

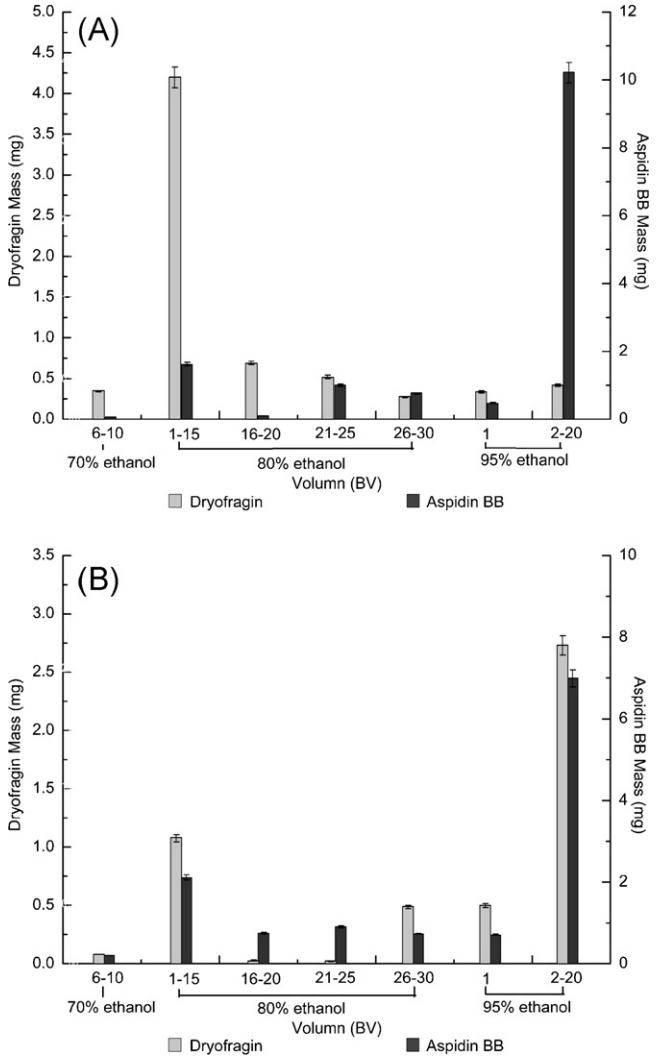

Fig. 5. Comparison of resin column chromatography (A) and resin column adsorption (B) on AB-8 resin column for separation of dryofragin and aspidin BB (flow rate 6 BV/h).

desorbed with 80% and 90% ethanol. It indicated that dryofragin and aspidin BB could not be separated well from each other on HPD-826. In Fig. 3(B), dryofragin was almost desorbed completely with 90% ethanol on AB-8 resin column, and most of aspidin BB was collected in anhydrous ethanol. The intersection of both compounds focused on the first two bed volume of anhydrous ethanol. Compared with HPD-826, AB-8 exhibited relatively sharper and narrower peak of each analyte. Meanwhile, dryofragin and aspidin BB were co-eluted in almost all elution fractions on HPD-600 (Fig. 3(C)). This result was ascribed to reversed-phase effect between weak-polarity molecular and polarity stationary phase which gave birth to retain action (i.e. tailing peak). Consequently, AB-8 resin was selected as the most suitable resin for separating and enriching dryofragin and aspidin BB in the following tests.

3.3. Effects of the operating factors on resin column chromatography

As can be seen in Fig. 4, dryofragin was hardly desorbed from AB-8 resin with 70% ethanol, when the concentration of ethanol changed into 80%, the desorption of dryofragin increased sharply and reached a peak value, and the remaining dryofragin was almost completely eluted by 85% ethanol. Comparatively, small amount of aspidin BB was eluted within the ranges of concentration of ethanol from 80% to 85%. The desorption of aspidin BB reached maximum value when the concentration of ethanol was 90%, while the concentration of ethanol increased to 95%, the few dryofragin left was completely eluted. Hence, dryofragin should be washed by more 80% ethanol in order to separate from aspidin BB. According to HPLC analysis, the optimum elution scheme was 10 BV 70% ethanol for eluting impurities, 30 BV 80% ethanol for dryofragin and 20 BV 95% ethanol for aspidin BB. Meanwhile, the flow rate 6 RV/h was chosen for the following tests in order to shorten the operation time for large-scale preparative enrichment.

Table 2
Results of the optimization method for both phloroglucinols separation and enrichment on AB-8 resin column chromatography ($n = 3$).

Concentration of ethanol (%)	BV	M	Dryofragin		Aspidin BB	
			M	C	M	C
70	10	350	0.36	0.10	0.06	0.02
80	30	170	5.85	3.44	3.50	2.06
95	20	190	1.09	0.58	10.81	5.69

M, mass of product (mg); *C*, content in product (%).

As shown in Fig. 5(A), when the flow rate increase to 6 BV/h, the enrichment and separation efficiency of AB-8 resin towards dryofragin and aspidin BB was still excellent. A faster flow rate decreased time consumption. Therefore, 6 BV/h was selected as the proper desorption flow rate in view of separation efficiency and time consumption.

Considering both contents and recoveries, the optimal enrichment and separation conditions for dryofragin and aspidin BB on AB-8 resin column chromatography were confirmed as follows: resin column with 2.0 g sample was eluted by 70% ethanol 10 BV for removing impurities, 80% ethanol 30 BV was selected to wash dryofragin and 95% ethanol 20 BV to elute aspidin BB, the flow rate was 6 BV/h, the results are listed in Table 2. The corresponding chromatograms of samples before and after separation were shown in Fig. 6, most of impurities were removed by 70% ethanol, and the relative contents of both target products were improved distinctly. After dynamic separation on AB-8 resin column chromatography, the contents of dryofragin and aspidin BB in the product were 34.4 and 56.9 mg/g, respectively, which were 8.39- and 5.99-fold increased. Their recoveries were 91.22% and 75.64%, respectively.

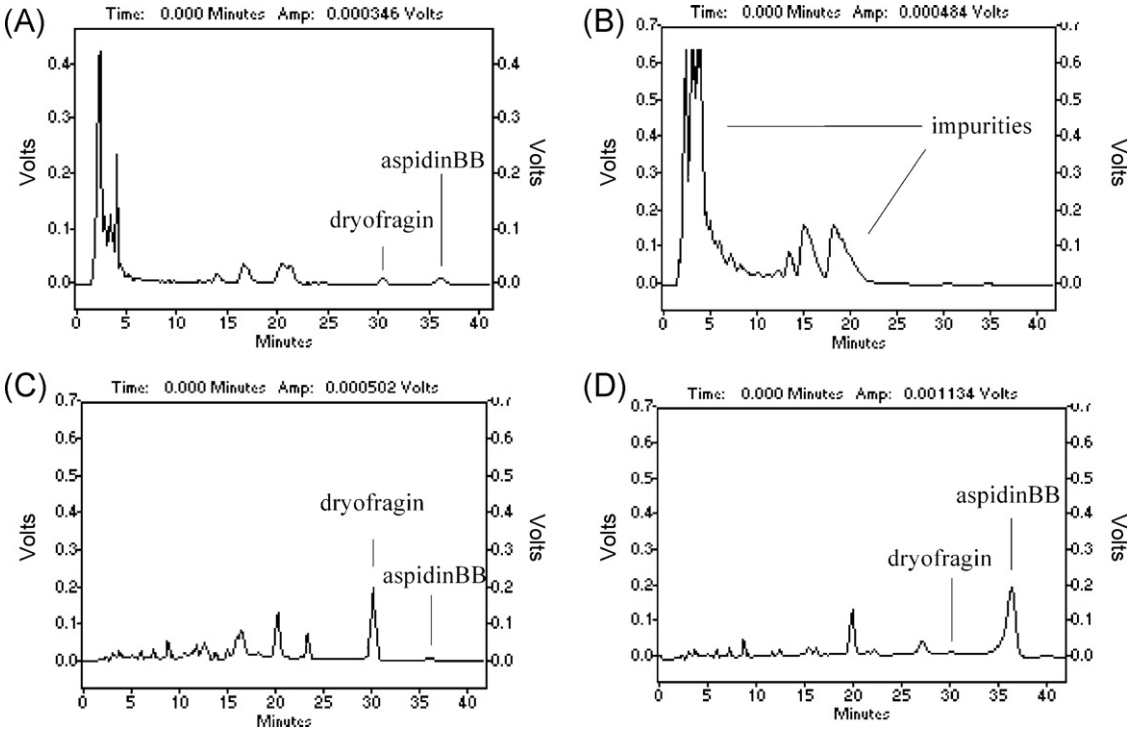

Fig. 6. Chromatograms of samples before treatment (A) and samples eluted by 70% ethanol (B), 80% ethanol (C) and 95% ethanol (D).

Table 3
Results of reusability on AB-8 adsorbent.

Target product	Concentration of ethanol (%)	BV	1 cycle	3 cycles	5 cycles
Dryofragin (mg)	80	1–15	4.3	4.19	3.98
Aspidin BB (mg)	95	2–20	10.32	10.13	9.85

3.4. Comparison of resin column chromatography and resin column adsorption for column efficiency

Resin column adsorption has been proved to own many advantages such as low cost, high efficiency and simple procedure, as compared with conventional methods [26]. As an efficient preconcentration method, resin column adsorption has attracted growing interest for large-scale preparative separation and enrichment secondary metabolites from plant materials. In present study, it was found that resin column chromatography and resin column adsorption shared an evident specialty to selectively adsorb and recover constituents from aqueous solutions as well as from nonaqueous due to electrostatic force, intermolecular interaction, size sieving action, etc. In our research, for comparing, resin column adsorption was also used to separate and enrich dryofragin and aspidin BB from *D. fragrans* at the optimized conditions. In Fig. 5(B), as concentration of ethanol solution increased, the desorption ability of solution increased, the changing trend of dryofragin and aspidin BB was similar. As shown comparatively in Fig. 5, the enrichment efficiency of resin column chromatography towards both targets was similar to that of resin column adsorption, while there is little or no separation between dryofragin and aspidin BB by resin column adsorption. The maximal difference between resin column chromatography and resin column adsorption is that the former exerts the mechanism of chromatography. Resin column chromatography exploits the advantage of solvent gradients, continuous adsorption and desorption increased the number of theoretical plates of resin column, it was possible to overcome the difficulty of the separation posed by the similar adsorption of the multi-targets. The results above revealed the comparative advantages of resin column chromatography in the separation of dryofragin and aspidin BB.

3.5. Reusability of AB-8 resin

For potential practical applications, the regeneration and reuse of the adsorbent should be considered. The separation and enrichment performance of dryofragin and aspidin BB on the regenerated resin was determined for 5 cycles. Table 3 summarized the results. It indicated that the adsorbent could be reused for separating and enriching dryofragin and aspidin BB up to 5 times without compromising its function, which is auspicious for dryofragin and aspidin BB production.

4. Conclusion

In current study, resin column chromatography was successfully applied to preparative separation and enrichment of dryofragin and aspidin BB from *D. fragrans*. The adsorption feature of dryofragin and aspidin BB onto twelve macroporous resins with different chemical and physical properties were investigated and AB-8 resin exhibited higher separation efficiency than other resins. The operating parameters of resin column chromatography were optimized for maximizing multi-target products yield. Under the optimal condition, the contents of dryofragin and aspidin BB in the product were 8.39-fold and 5.99-fold increased with recovery yields of 91.22% and 75.64%, respectively. This study substantiated that the separation efficiency of resin column chromatography for dryofragin and aspidin BB is superior to resin column adsorption. Recently, more and more new structure modified macroporous resins come forth, and they can be used in this manner for the preparative separation of natural compounds in the future research.

Acknowledgements

The authors gratefully acknowledge the financial supports by Special Fund of Forestry Industrial Research for Public Welfare of China (201004040), Agricultural Science and Technology Achievements Transformation Fund Program (2009GB23600514), Heilongjiang Province Science Foundation for Excellent Youths (JC200704), Project for Distinguished Teacher Abroad, Chinese Ministry of Education (MS2010DBLY031), the Key Program for Science and Technology Development of Harbin (2009AA3BS083) and NEFU Foundation for Excellent Doctoral Project (GRAP09).

References

[1] Z.W. Ao, G.F. Li, Ferns of Heilongjiang Province, Northeast Forestry University Press, Harbin, 1990, p. 121.
[2] Y. Chang, Progress on research of *Dryopteris fragrans* (L.) schott in domestic and aboard, Northern Hortic. 4 (2009) 113–115.
[3] Z.B. Shen, Z.X. Jin, D.L. Zhang, J.J. Liu, T. Sun, Pharmacological study on psoriasis of *Dryoperis fragrans*, Chin. Tradit. Herb. Drugs 33 (2002) 448–449.
[4] R. Luo, Z.X. Jin, Y.P. Zhang, Study on pharmacological of *Dryoperis fragrans* liniment, J. Harbin Univ. Comm. (Nat. Sci. Ed.) 19 (2003) 388–390.
[5] H.Z. Li, Z.B. Shen, Y. Zhao, N. Jiang, D.L. Zhang, Effect of *Dryoperis fragrans* ointment on experimental *Tinea corporis* in rats, J. Chin. Med. Mater. 28 (2005) 941–942.
[6] Z.B. Shen, Y.L. Ma, W.X. Jiang, W.L. Li, Inhibitory activity of *Dryoperis fragrans* extract against fungi, Chin. Tradit. Herb. Drugs 36 (2005) 735–736.
[7] Y.L. Zhang, W.M. Zeng, H.R. Wang, L. Zhu, H.L. Xu, H.X. Kuang, Study on antioxidant of Lignans from *Dryoperis fragrans*, Chin. Tradit. Herb. Drugs 39 (2008) 343–346.
[8] H.R. Wang, R. Wang, H.L. Xu, Y.L. Zhang, Analgesic effect of *Dryoperis fragrans* (L.) schott, J. Qiqihar Med. Coll. 29 (2008) 2443–2444.
[9] Y.L. Zhang, H.Y. Fu, Y.Y. Zhang, Q.Y. Song, W.H. Xu, H.X. Kuang, Chemical components from *Dryoperis fragrans* and their cytotoxicity, Chin. Tradit. Herb. Drugs 39 (2008) 648–651.
[10] H. Ito, T. Muranaka, K. Mori, Z.X. Jin, H. Tokuda, H. Nishino, T. Yoshida, Ichthyotoxic phloroglucinol derivatives from *Dryoperis fragrans* and their anti-tumor promoting activity, Chem. Pharm. Bull. 48 (2000) 1190–1195.
[11] C.J. Widén, C. Fraser-Jenkins, T. Reichstein, M. Gibby, J. Sarvela, Phloroglucinol derivatives in Dryopteris sect. Fibrillosae and related taxa (Pteridophyta Dryopteridaceae), Ann. Bot. Fenn. 33 (1996) 69–100.
[12] H. Ito, T. Muranaka, K. Mori, Z.X. Jin, H. Tokuda, Dryofragin and aspidin PB, piscicidal components from *Dryoperis fragrans*, Chem. Pharm. Bull. 45 (1997) 1720–1722.
[13] Z.B. Shen, Z.X. Jin, Application of *Dryopteris fragrans* phloroglucinol extract, 392 European Patent 101066261 (2010).
[14] G.J. Kapadia, H. Tokuda, T. Konoshima, M. Takasaki, J. Takayasu, H. Nishino, Anti-tumor promoting activity of *Dryopteris phlorophenone* derivatives, Cancer Lett. 105 (1996) 161–165.
[15] M.K. Na, J.P. Jang, B.S. Min, S.J. Lee, M.S. Lee, B.Y. Kim, W.K. Oh, J.S. Ahn, Fatty acid synthase inhibitory activity of acylphloroglucinols isolated from *Dryopteris crassirhizoma*, Bioorg. Med. Chem. Lett. 16 (2006) 4738–4742.
[16] L.G. Magalhães, G.J. Kapadia, L.R. Silva Tonuci, S.C. Caixeta, N.A. Parreira, V. Rodrigues, A.A. Da Silva Filho, In vitro schistosomicidal effects of some phloroglucinol derivatives from *Dryopteris* species against *Schistosoma mansoni* adult worms, Parasitol. Res. 106 (2010) 395–401.
[17] J. Rajesh Kumar, H.I. Lee, J.Y. Lee, J.S. Kim, J.S. Sohn, Comparison of liquid–liquid extraction studies on platinum(IV) from acidic solutions using bis(2,4,4-trimethylpentyl) monothiophosphinic acid, Sep. Purif. Technol. 63 (2008) 184–190.
[18] L.H. Wang, Y.H. Mei, F. Wang, X.S. Liu, Y. Chen, A novel and efficient method combining SFE and liquid–liquid extraction for separation of coumarins from *Angelica dahurica*, Sep. Purif. Technol. 77 (2011) 397–401.
[19] E.P. Byrne, J.J. Fitzpatrick, Investigation of how agitation during precipitation, and subsequent processing affects the particle size distribution and separation of α-lactalbumin enriched whey protein precipitates, Biochem. Eng. J. 10 (2002) 17–25.
[20] P. Priyananda, V. Chen, Separation of residual fatty acids from aqueous solutions using an agitated solution of protein and membrane filtration, Sep. Purif. Technol. 48 (2006) 113–120.
[21] Y.F. Liu, J.X. Liu, X.F. Chen, Y.W. Liu, D.L. Di, Preparative separation and purification of lycopene from tomato skins extracts by macroporous adsorption resins, Food Chem. 123 (2010) 1027–1034.
[22] Y.G. Park, Effect of ozonation for reducing membrane-fouling in the UF membrane, Desalination 147 (2002) 43–48.

[23] D.S. Tang, L. Zhang, H.L. Chena, Y.R. Liang, J.L. Lu, H.L. Liang, X.Q. Zheng, Extraction and purification of solanesol from tobacco. I. Extraction and silica gel column chromatography separation of solanesol, Sep. Purif. Technol. 56 (2007) 291–295.
[24] A.A. White, Separation and purification of cyclic nucleotides by alumina column chromatography, Methods Enzymol. 38 (1974) 41–46.
[25] Y.J. Fu, Y.G. Zu, W. Liu, T. Efferth, N.J. Zhang, X.N. Liu, Y. Kong, Optimization of luteolin separation from pigeonpea [*Cajanus cajan* (L.) Millsp.] leaves by macroporous resins, J. Chromatogr. A 1137 (2006) 145–152.
[26] W. Liu, S. Zhang, Y.G. Zu, Y.J. Fu, W. Mac, D.Y. Zhang, Y. Kong, X.J. Li, Preliminary enrichment and separation of genistein and apigenin from extracts of pigeon pea roots by macroporous resins, Bioresour. Technol. 101 (2010) 4667–4675.
[27] Z.L. Ai, Y.H. Wang, H. Wang, J. Guo, J.T. Cui, Absorption of polyphenols from apple pomace by macroporous absorbent resins, Trans. Chin. Soc. Agric. Eng. 23 (2007) 245–248.
[28] J.M. Huang, J.X. Guo, W.S. Chen, B. Lu, M.M. Sun, G.L. Duan, Adsorption properties and application of macroporous resin for purification of alkaloids in *Aconitum kusnezoffii*, Fudan Univ. J. Med. Sci. 30 (2003) 267–269.
[29] Y. Kong, M.M. Yan, W. Liu, C.Y. Chen, B.S. Zhao, Y.G. Zu, Y.J. Fu, M. Luo, M. Wink, Preparative enrichment and separation of astragalosides from Radix Astragali extracts using macroporous resins, J. Sep. Sci. 33 (2010) 2278–2286.
[30] R. Sun, K. Fu, Y.J. Fu, Y.G. Zu, Y. Wang, M. Luo, S.M. Li, H. Luo, Z.N. Li, Preparative separation and enrichment of four taxoids from *Taxus chinensis* needles extracts by macroporous resin column chromatography, J. Sep. Sci. 33 (2010) 2278–2286.

Journal of Pharmaceutical and Biomedical Analysis 61 (2012) 207–214

Contents lists available at SciVerse ScienceDirect

Journal of Pharmaceutical and Biomedical Analysis

journal homepage: www.elsevier.com/locate/jpba

Validated high performance thin layer chromatographic method for simultaneous quantification of major iridoids in *Vitex trifolia* and their antioxidant studies

Neerja Tiwari[a], Suaib Luqman[b], Nusrat Masood[b], Madan M. Gupta[a,*]

[a] *Analytical Chemistry Department, Central Institute of Medicinal and Aromatic Plants, Lucknow 226015, India*
[b] *Molecular Bioprospection Department, Central Institute of Medicinal and Aromatic Plants, Lucknow 226015, India*

ARTICLE INFO

Article history:
Received 16 September 2011
Received in revised form 5 December 2011
Accepted 8 December 2011
Available online 17 December 2011

Keywords:
Vitex trifolia
Vitex negundo
HPTLC
Iridoids
Antioxidant

ABSTRACT

Negundoside (**1**), agnuside (**2**) and 6′-*p*-hydroxy benzoyl mussaenosidic acid (**3**) are known bioactive metabolites in *Vitex trifolia*. In the present study a simple precise and reproducible method was developed for simultaneous quantitation of NS (**1**), AS (**2**) and HMA (**3**) and the antioxidant capacity of above markers has also been determined. Marker compounds have been resolved using silica gel 60 F_{254} plates, petroleum ether (60–80)/toluene/acetone/water (10:10:80:2 v/v/v/v) as the mobile phases. The method does not employ any derivatisation procedure and can be used as a quality control tool for routine analysis of drugs *V. trifolia* and *V. negundo* together with their commercial extracts. NS (**1**), AS (**2**) and HMA (**3**) showed significant activity in DPPH and NO radical scavenging assays.

© 2011 Elsevier B.V. All rights reserved.

1. Introduction

Vitex trifolia L. (Verbenaceae) is a tropical shrub widespread in Pacific–Asian countries such as India, Sri Lanka, China, Phillippines, Indonesia, North Australia, New Caledonia and French Polynesia [1,2]. Amongst the genus *Vitex* which include approximately 200 species in the tropical region, *V. trifolia* is widely employed by Pacific Islanders to cure numerous illnesses. In New Caledonia, Rotuma and Solomon islands, the leaves of *V. trifolia* are used as a remedy against severe headaches after heating and rubbing on forehead, or taken as an infusion [2–4]. The stems of *V. trifolia* are used for the treatment of dysentery in Papua New Guinea [5]. Previous studies have reported insecticidal [6] and antibacterial [7] activities of *V. trifolia* extracts. Aqueous and ethanol extracts of *V. trifolia* have also revealed significant hepatoprotective activity against CCl_4 induced liver damage in male Wistar rats [8]. Genus *Vitex* is a rich source of iridoids which are well known for hepatoprotective activity.

Negundoside (**1**) [9], agnuside (**2**) [10] and 6′-*p*-hydroxy benzoyl mussaenosidic acid (**3**) [11] (Fig. 1) are the major active constituents of *V. trifolia* and *Vitex negundo*. *V. negundo* is used in several commercial formulations viz. Acne-n-Pimple Cream, Joint Care B cream, Muscle and Joint Rub, Pilex tablet and cream, Rumalaya gel and tablets, V-Gel (Himalaya Drug Co., Bangalore, India), Jigrine (Hamdard Laboratories, New Delhi, India), Itone (Dey's Medical, Kolkata, India) [12–23]. Reported HPLC [24,25] and HPTLC [26] methods are suitable for single iridoid analysis and lacks sensitivity and resolution in the analysis of complex isomeric iridoid mixture. HPTLC is the method commonly applied for the identification assay and stability study of herbal raw materials and formulations. Currently HPTLC emerge as an alternative to HPLC because of far less solvent consumption, reduction of the analysis time, cost of analysis, besides being eco friendly. HPTLC method also facilitates repeated detection (scanning) of the chromatograms with same or different parameters.

No information related to simultaneous quantification of iridoids NS (**1**), AS (**2**) and HMA (**3**) in *V. trifolia* has ever been reported. In the present investigation an attempt has been made to develop a validated rapid, simple, precise and accurate method for simultaneous quantification of these three important IGs in *V. trifolia*. Antioxidant potential of these markers has also been evaluated. The developed method may be applied for quantification of NS (**1**), AS (**2**) and HMA (**3**) in *V. negundo* also.

Abbreviations: IG, iridoid glycoside; VT, *v. trifolia*; VN, *v. negundo*; NS, negundoside; AS, agnuside; HMA, 6′-p-hydroxybenzoyl mussaenosidic acid; DPPH, 1,1-diphenyl-2-picrylhydrazyl; FRAP, ferrous reducing antioxidant potential.

* Corresponding author at: Analytical Chemistry Department, Central Institute of Medicinal and Aromatic Plants, Lucknow 226015, India. Fax: +91 522 2342666.
E-mail address: guptammg@rediffmail.com (M.M. Gupta).

0731-7085/$ – see front matter © 2011 Elsevier B.V. All rights reserved.
doi:10.1016/j.jpba.2011.12.007

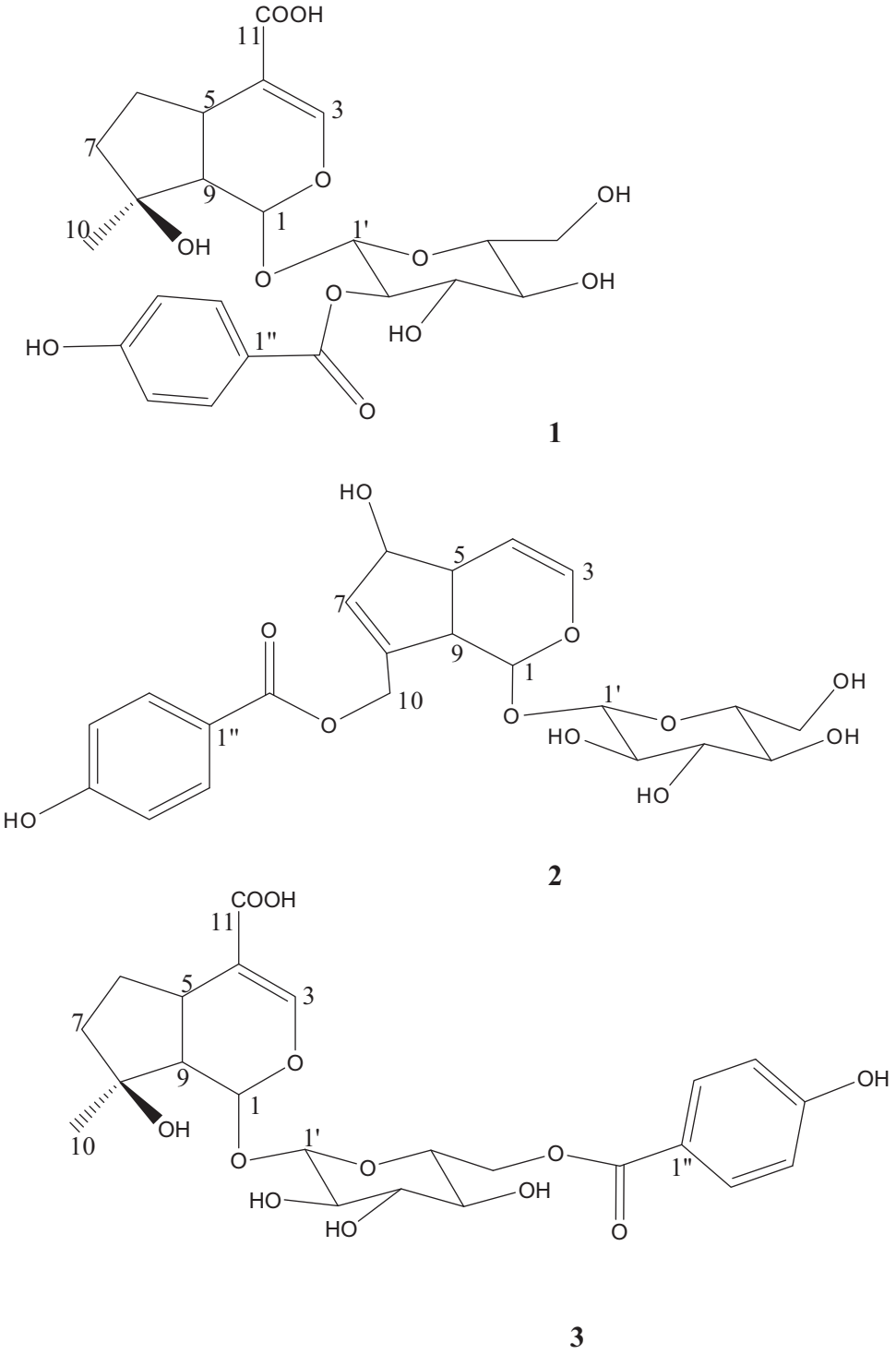

Fig. 1. Structures of NS (**1**), AS (**2**) and HMA (**3**).

2. Materials and method

2.1. Solvents, chemicals and reference standards

The markers negundoside (**1**), agnuside (**2**) and 6′-*p*-hydroxy benzoyl mussaenosidic acid (**3**), used for analysis, were of 99% purity (determined by HPLC and spectral analysis). Markers **1**–**3** were isolated in the lab from *V. trifolia* and identified by comparison of NMR and other spectral properties [9–11]. TLC plates (Silica gel 60 F_{254}), silica gel (60–120 mesh) for column chromatography and HPLC grade solvents were purchased from m/s Merck (Mumbai, India). 1,1-Diphenyl, 2-picryl hydrazyl (DPPH), ferrous sulphate, sodium nitroprusside, sulphanilamide, phosphoric acid, naphthyl ethelene diamine, sodium phosphate, ammonium molybdate, dimethyl suphoxide (DMSO), ascorbic acid, quercetin, ferric chloride, 2,2′-bipyridyl were obtained from Sigma–Aldrich Chemical Company, USA. Plant materials of *Vitex* species were collected from Lucknow in March 2009 and authenticated by Botany and

Pharmacognosy Department of CIMAP, Lucknow (India). Voucher specimens of *V. trifolia* (no. 9417) and *V. negundo* (no. 13507) have been deposited in the herbarium of the institute.

2.2. Extraction and isolation of reference compounds (IGs) from V. trifolia

Air-dried and finely powdered aerial parts of the plant (2.45 kg) were exhaustively extracted at room temperature (25 ± 3 °C) using methanol (5 × 10 L, 5 times) and combined extracts were concentrated to give brown gummy residue (500 g). This methanolic extract was suspended in water and partitioned with *n*-hexane, chloroform and *n*-butanol. The *n*-butanol fraction was concentrated in vaccum to afford brown residue (250 g). This residue was chromatographed over a silica gel column (1.5 kg, 60–120 mesh, Merck, India, column dimensions – 225 cm, 7.5 cm.) eluting with chloroform, followed by increasing concentrations of methanol. Fractions eluted with chloroform, methanol, 9:1 were dissolved in minimum amount of chloroform followed by drop by drop addition of methanol, until slight turbidity appeared; the mixture was than kept at 23 °C to crystallize agnuside (**2**). Later fractions eluted with chloroform, methanol, 17:3 were further chromatographed using preparative HPLC (MeOH:H_2O, 60:40; flow rate, 15 mL/min) which led us to the isolation of negundoside (**1**) and 6′ *p*- hydroxyl benzoyl massaenosidic acid (**3**). The structure elucidation of IGs (Fig. 1) was performed with the help of UV, ^{1}H NMR, ^{13}C NMR, 2D experiments (HSQC, HMBC, COSY and NOESY) and mass (ESI-MS) analysis and confirmed as reported earlier [9–11].

Negundoside (NS) was obtained as white crystalline substance (200 mg); ^{13}C NMR (75 MHz, MeOD): δ 95.89 (C-1), 151.17 (C-3), 113.66 (C-4), 31.03 (C-5), 30.09 (C-6), 41.21 (C-7), 79.81 (C-8), 52.29 (C-9), 24.30 (C-10), 169.97 (C-11), 97.77 (C-1′), 74.84 (C-2′), 75.95 (C-3′), 71.66 (C-4′), 78.34 (C-5′), 62.64 (C-6′), 167.29 (C=O) 122.08 (C-1″), 132.17 (C-2″, 6″), 116.13 (C-3″, 5″), 163.22 (C-4″); EIMS m/z: 519 $[M+Na]^+$ ($C_{23}H_{28}O_{12}$), 497 $[M+H]^+$.

Agnuside (AS) was obtained as white crystalline substance (500 mg); ^{13}C NMR (75 MHz, Pyr): δ 96.96 (C-1), 140.76 (C-3), 104.55 (C-4), 45.30 (C-5), 81.87 (C-6), 131.93 (C-7), 141.90 (C-8), 47.55 (C-9), 62.67 (C-10), 99.21 (C-1′), 73.89 (C-2′), 76.95 (C-3′), 70.46 (C-4′), 77.25 (C-5′), 61.75 (C-6′), 166.85 (C=O), 121.10 (C-1″), 131.46 (C-2″, 6″), 115.27 (C-3″, 5″), 162.69 (C-4″); EIMS m/z: 489 $[M+Na]^+$ ($C_{22}H_{26}O_{11}$), 465 $[M-H]^+$.

6′ *p*-Hydroxybenzoyl mussaenosidic acid (HMA) was obtained as viscous mass (250 mg); ^{13}C NMR (75 MHz, Pyr): δ 95.92 (C-1), 151.00 (C-3), 113.71 (C-4), 32.96 (C-5), 31.03 (C-6), 40.28 (C-7), 79.87 (C-8), 52.31 (C-9), 25.62 (C-10), 169.83 (C-11), 100.78 (C-1′), 74.93 (C-2′), 75.77 (C-3′), 71.65 (C-4′), 78.47 (C-5′), 64.43 (C-6′), 166.75 (C=O), 121.73 (C-1″), 132.81 (C-2″, 6″), 116.25 (C-3″, 5″), 163.72 (C-4″); EIMS m/z: 519 $[M+Na]^+$ ($C_{23}H_{28}O_{12}$), 497 $[M+H]^+$, 495 $[M-H]^+$.

2.3. Standard stock solution and sample preparation

Powdered plant parts (200 mg each) were extracted with 40 mL different solvents by microwave extraction method at 50 °C and 350 W for 10 min to choose most suitable solvent for further analysis. For content determination, amount of plant parts were adjusted to perform the quantification above LOQ level. Methanol was preferred due to high extractive value (Table 1). For all extractions weight of extracting plant part was optimized to ascertain all the quantification above LOQ levels. Different techniques like cold percolation (kept for 24 h at 30 °C) microwave extraction (at 50 °C and 350 W for 10 min), sonication (for 30 min at 50 °C) and hot extraction (at boiling water bath for 30 min) methods were tried to optimize extraction technique. Microwave extraction was found to be most appropriate (Table 2). The extracts were concentrated on a rotavapour to afford different extracts. Different plant parts were also analyzed for the content of markers. Leaves have highest content of IGs. The standards solution of markers **1**–**3** were prepared by dissolving accurately weighed 1.0 mg of the sample in 1 mL of methanol as a stock solution (1 mg/mL) and stored at 4 °C. These standards were further diluted and mixed as per the requirements to obtain a desired concentration for quantification. The concentrations of reference standards used for calibration were in the range of 333–2000 ng/band. The known volumes of mixed standards were spotted on the TLC plates to prepare 6 point calibration curves.

Table 1
Extraction efficiency of different solvent for chemical markers.[a]

Solvent	Amount of compounds quantified[b] (%, w/w)					
	NS (**1**)	SD	AS (**2**)	SD	HMA (**3**)	SD
Hexane	ND	–	ND	–	ND	–
Chloroform	ND	–	ND	–	ND	–
Methanol	0.79	0.06	1.17	0.03	0.47	0.05
Water	0.65	0.05	0.88	0.05	0.36	0.04

[a] Microwave extraction at 50 °C and 350 W for 10 min.
[b] Plant dry weight basis.

2.4. Antioxidant activity

Five assay protocols, 1,1 diphenyl-2picrylhydrazyl (DPPH) [27], NO scavenging [28], total antioxidant capacity (TAC) [29], ferric ion reducing antioxidant power (FRAP) [30] and reducing Potential (RP) [31] were used for the evaluation of antioxidant property of **1–3** as described below. Quercetin, a flavonoid, well known for its strong antioxidant property was used as a positive control (Hi Media Prod. No. RM 6191, 98% Pure).

2.4.1. DPPH discolouration assay

DPPH radical scavenging assay was investigated according to the method of Chung et al. [27]. DPPH radical react with suitable reducing agents losing colour. The resulting decolourization is stoichiometric with respect to number of electrons captured which was measured at 517 nm after incubation at 30 °C for 20 min.

2.4.2. NO scavenging assay

Nitric oxide scavenging activity was measured following the method of Marcocci et al. [28]. The absorbance of chromophore formed during diazotization of the nitrile with sulphanilamide and subsequent coupling with naphthylethelene diamine was measured at 546 nm. IC_{50} values were obtained from the plot drawn concentrations in microgram versus percentage inhibition.

2.4.3. Total antioxidant capacity (TAC)

Total antioxidant capacity was evaluated following the method of Preito et al. [29]. The total antioxidant potential of the molecules and extract was calculated based on the formation of

Table 2
Extraction efficiency of different techniques for chemical markers.[a]

Techniques[c]	Amount of compounds quantified[b] (%, w/w)					
	NS (**1**)	SD	AS (**2**)	SD	HMA (**3**)	SD
Cold	0.54	0.08	0.80	0.06	0.41	0.11
Sonication	0.74	0.05	0.85	0.05	0.46	0.04
Hot	0.64	0.10	0.95	0.08	0.43	0.06
Microwave	0.79	0.06	1.18	0.03	0.48	0.05

[a] Plant dry weight basis.
[b] Methanol was used as solvent.
[c] Cold, kept for 24 h at 30 °C; sonication, for 30 min at 50 °C; hot, boiling water bath for 30 min; microwave, 50 °C and 350 W for 10 min.

phosphomolybdenum complex. Samples were incubated at 95 °C for 90 min. After cooling at room temperature, absorbance was measured at 695 nm. Ascorbic acid was used as standard and total antioxidant capacity was expressed as ascorbic acid equivalents.

2.4.4. Ferric ion reducing antioxidant power (FRAP)

Ferric ion reducing antioxidant power was assessed according to the method of Luqman, et al. [30]. At low pH ferric to ferrous ion reduction forms a coloured ferrous–tripyridyltriazine (Fe^{2+}/TPTZ) complex. FRAP values were obtained by comparing the absorbance change at 593 nm in test reaction mixtures with those containing ferrous ions in known concentration. Absorbance of Fe^{2+}/TPTZ-complex was recorded after incubation at 37 °C for 5 min. Ferric sulphate was used as standard and ferric ion reducing power was expressed as ferric sulphate equivalents.

2.4.5. Reducing potential (RP)

Reducing potential of test compounds was estimated following the method of Yen and Chen [31]. Absorbance was recorded at 700 nm. The absorbance measured is a direct reflection of the reducing power of the test samples.

2.5. Instrumentation

Preparative HPLC (Shimadzu, Japan) consisting column (Supelcosil LC-18, 21.2 mm × 250 mm, 12 μm), pumps LC-8A and PDA detector was used for isolation and purification of reference compound (IG). Precoated TLC silica gel 60 F_{254}, (10 cm × 10 cm, 20 cm × 10 cm, E. Merck, Darmastadt, Germany) were used for optimization of analytical protocol. Vario system, TLC Scanner winCATS-III, Reprostar 3, twin trough chamber, immersion device III, TLC plate heater (Camag, Muttenz, Switzerland) were used for digital image scanning for HPTLC method development and validation. NMR spectra were recorded in deuterated methanol and pyridine with TMS as internal standard using 300 MHz spectrometer (Avance, Bruker, Switzerland). ESI-MS spectra were obtained on LCMS-2010EV (Shimadzu, Japan) hyphenated to LC system (LC-20AD, CTO-20A, SIL-10AF, SPDM20A, and ABM-20A).

2.6. Chromatographic conditions

Standard solutions of markers and extracts along with spiked samples of plant extracts were applied to precoated silica gel 60 F_{254} TLC plates, with the help of automatic TLC sampler IV (ATS IV), at a rate of 125 nL/s, in the form of 5 mm band. Plates were developed in a twin trough chamber saturated for 15 min in the solvent system, petroleum ether (60–80)/toluene/acetone/water (10:10:80:2 v/v/v/v). The developed plates were air dried at 25 °C. The dried plates were used by a Camag Video Documentation system in conjunction with the Reprostar 3 for imaging and archiving the thin layer chromatograms. The object was captured at 254 nm via win CATS software.

2.7. Chromatographic procedure

Standard mixture, all the analytes and sample solutions were applied band wise (band length 5 mm; delivery speed, 125 nL/S; track distance 8 mm; and distance from left and lower edge, 15 mm) to TLC plates. Plates were developed at 25 ± 2 °C in a CAMAG twin trough developing chamber using the solvent system petroleum ether (60–80)/toluene/acetone/water (10:10:80:2 v/v/v/v). The plates were scanned after drying at 263 nm by Camag TLC scanner III at a wavelength of 263 nm keeping a slit width of 6.00 mm × 0.45 mm micro, scanning speed 20 mm/s, data resolution 100 mm/step and D_2 lamp in absorption/reflectance mode. The HPTLC chromatograms of the extracts of *V. trifolia* and *V. negundo* are shown in Fig. 3 (segments B and C). Photo documented HPTLC plate taken at UV light and after derivatisation represents standard **1**–**3** in *V. trifolia* and *V. negundo* extracts (Figs. 2 and 3).

2.8. Method validation

2.8.1. Precision, repeatability and accuracy

For providing linearity six calibration points were analyzed over the range of 333–2000 ng/band. For each point three measurements were made to improve the repeatability. Intra and inter day variation and repeatability were chosen to determine the precision of developed method. For intraday variable test, the mixed standard solutions were analyzed for five replicates for three consecutive days. To examine the repeatability, three different working solutions were prepared from the same sample of different extracts of *V. trifolia*. The % RSD was taken as a measure of precision and repeatability. The inter and intra day precisions were calculated by the measurement of peak area of reference standard. Variations were expressed by the % RSD [32]. Recovery test was used to evaluate the accuracy of this method. Known amount of

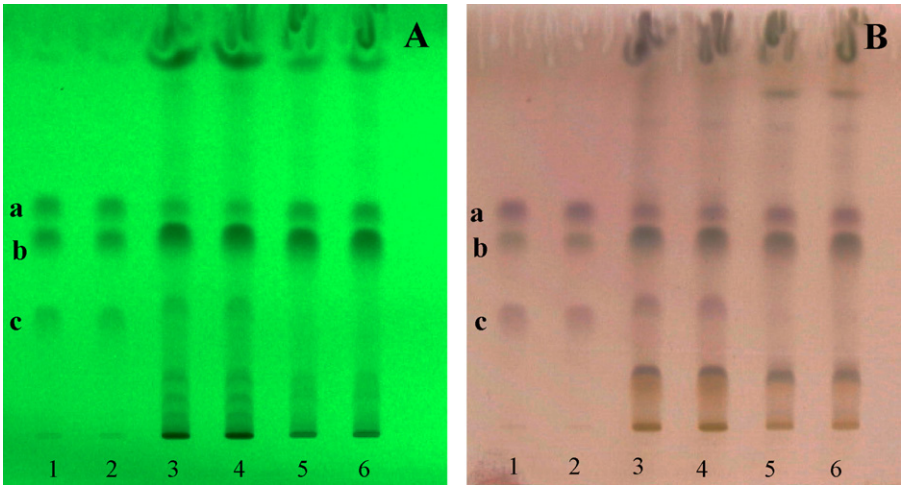

Fig. 2. Photo-documentation at 254 nm (A), and after derivatization in white radiation (B). Track assignment for HPTLC Plate 1–2, standard track: mixture of NS (a), AS (b) and 6′HMA (c); 3–4 leaf extract of *V. trifolia*; 5–6 leaf extract of *V. negundo*.

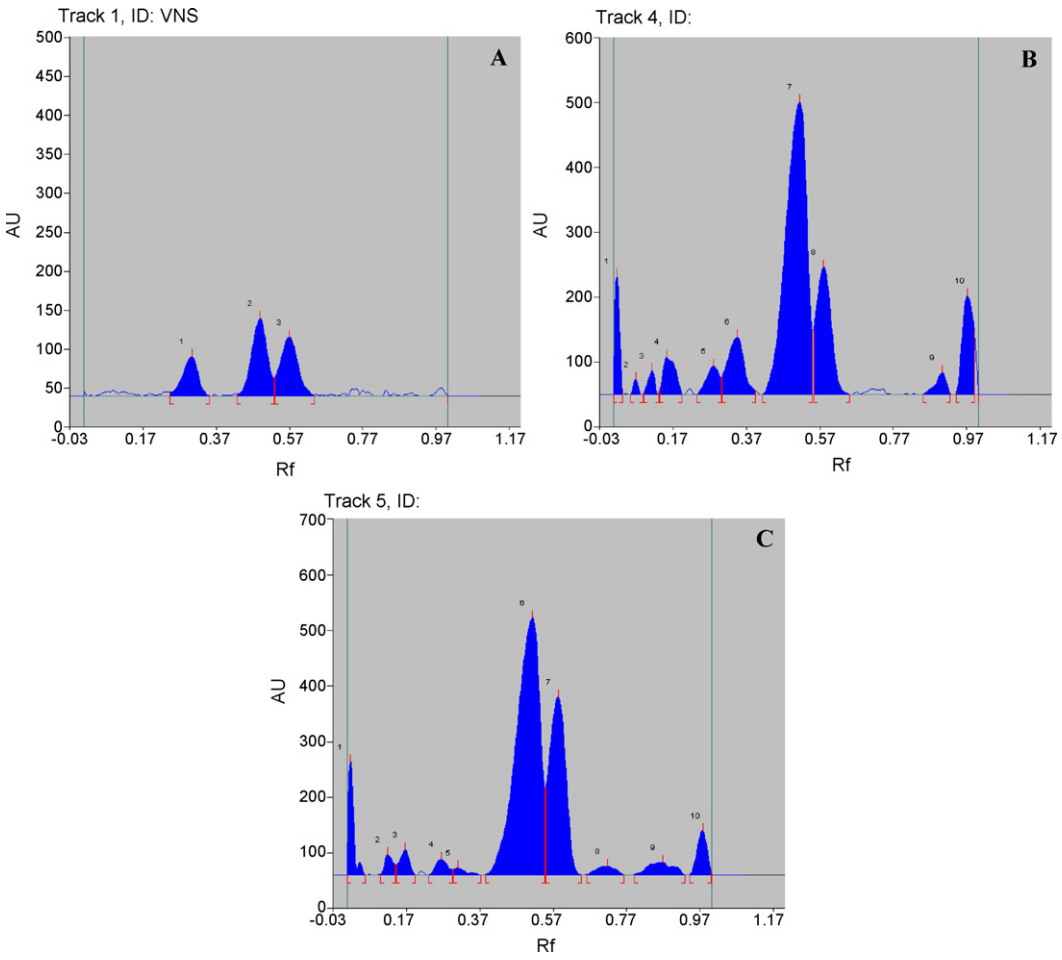

Fig. 3. The representative HPTLC chromatograms of mixtures of standards (A), *V. trifolia* leaf extract (B), *V. negundo* leaf extract (C).

investigated compounds were added to accurately weighed portion of *V. trifolia* methanolic extract and analyzed. The recovery percentage was calculated by using the formula: recovery (%) = (amount found − original amount)/amount spiked × 100% [33].

2.8.2. Specificity

The specificity of the method was ascertained by analyzing standards and sample. The bands for the three IGs **1–3** in samples were confirmed by comparing the R_f and spectra of the spot with that of standard. The peak purity of individual **1**, **2**, and **3** was assessed by comparing the spectra at peak start, peak apex and peak end of the band.

2.8.3. Robustness of the method

Mobile phases having different compositions such as petroleum ether (60–80)/toluene/acetone/water (10:8:82:2 v/v/v), (10:12:78:2 v/v/v) and (12:10:80:2 v/v/v) were tried to run the chromatograms for marker compounds **1–3**. The amount of mobile phase, temperature, and relative humidity were varied in the range of ±5%. The plates were pre washed by methanol and activated at 60 ± 5 °C for 5, 10, and 15 min, respectively, prior to chromatography. Time from spotting to chromatography and from chromatography to scanning was varied between 0, 30, 60, and 90 min. Robustness of the method was carried out at three different concentration levels: 333, 667, and 1000 ng/spot for markers. At a time only one parameter was varied while the rest were kept constant. The effects on the results i.e. peak areas were examined.

3. Result and discussion

3.1. Optimization of chromatographic conditions

Initially attempts were made to separate and standardize these three compounds using a solvent system consisting of a medium polar and a high polar solvent, but due to difference of only point of attachment in **1** and **3** (isomeric structures) and almost similar skeletal structures of **1–3** the separation could not be achieved. Various solvent systems were tried and it has been found that a solvent system consisting of petroleum ether (60–80), acetone and water gives well separated profile for **1–3** in standard mixture as well as extract, but spots of markers were diffused. That is why ether was replaced by many solvents and it was found that toluene gives symmetrical but less separated spots of markers **1–3**. Finally a solvent system consisting of petroleum ether, toluene, acetone and water was found to be ideal for fine separation and non diffused spots to quantify NS (**1**), AS (**2**) and HMA (**3**) in *Vitex* species. Determined mean R_f of **1–3** were as; NS (**1**) 0.53 ± 0.01, AS (**2**) 0.47 ± 0.01 and HMA (**3**) 0.32 ± 0.01 (Table 3).

Matching of R_f of IGs in the sample with those of reference standards and identification of these three compounds were further confirmed by in situ spectra of the above bands of the densitogram. UV maxima of NS, AS and HMA were found to be at 260, 264 and 267 nm. The experimental conditions such as mobile phase composition, scan mode, scan speed and wavelength of detection were optimized to provide accurate and precise results. The derivatisation of the plate imparts variations at various stages like the amount

Table 3
Statistical analysis of calibration curves in the HPTLC determination of IGs.[a,b,c]

Parameters	NS (**1**)	AS (**2**)	HMA (**3**)
R_f value	0.53 ± 0.01	0.47 ± 0.01	0.32 ± 0.01
Slope	7.921 ± 0.06358	9.081 ± 0.08000	4.266 ± 0.04254
95% confidence limits of slope	7.854–8.218	8.900–9.319	4.235–4.372
Intercept	2450–2800	2481–2921	688.4–922.5
95% confidence limits of intercept	7.786–8.056	8.912–9.251	4.176–4.356
F (value of Fisher test)	15519	12886	10057
Goodness of fit ($S_{y,x}$)	153.5	193.2	102.7
Coefficient of determination (r^2)	0.9990	0.9988	0.9984
LOD (ng)	58.14	63.83	72.22
LOQ (ng)	193.79	212.75	240.74

[a] Concentration range = 333–2000 ng.
[b] Number of concentration levels = 6.
[c] For all equations the significance levels $p < 0.0001$.

Table 4
Recovery study to evaluate accuracy of the method.

Compounds	Amount in sample (ng)	Spiked amount (ng)	Recovery%	Average recovery	RSD%
NS	760	333	93.41	93.94	1.84
(**1**)		667	92.43		
		1000	95.99		
AS	1150	333	95.01	97.61	2.32
(**2**)		667	98.35		
		1000	99.47		
HMA	470	333	95.22	96.60	3.62
(**3**)		667	93.87		
		1000	100.70		

and concentration of spraying reagent, immersion or spraying time, drying after derivatisation, heating (time and temperature) and waiting time before detection. Therefore, in the present investigation an attempt has been made to develop an accurate and reproducible TLC method without derivatisation for the analysis of NS, AS and HMA in *V. trifolia* and *V. negundo*. The relationship between the peak areas and amount of standard applied showed good linearity.

3.2. Method validation

3.2.1. Precision, repeatability and accuracy

The goodness of fit for all standards was found within the test range of 0.9984–0.9990. The developed method also had good accuracy with extraction recovery of 93.94–97.61% (Table 4). The LODs and LOQs were determined by following the ICH guidelines. The linear regression data, LOD and LOQ are listed in Table 3. The precision of marker compounds was determined above LOQ level ($n = 5$) and % RSD was found within acceptance.

Repeatability of the developed method was evaluated at three concentrations levels (333, 667 and 1000 ng/band). % RSDs were found below 5% which demonstrated good precision of proposed method (Table 5).

3.2.2. Linearity

The linearity was evaluated by analyzing all the markers (**1–3**) at 6 calibration points and for each point three measurements were made. In HPTLC method, the calibration graphs found to be linear.

3.2.3. Specificity

The absence of any interfering peak indicated that the method is specific. Peak purity of spectra at peak start, peak apex and peak end of the band was *r* (start, middle); 0.9991, 0.9994, 0.9981 and *r* (middle, end); 0.9998, 0.9989, 0.9989, for NS, AS and HMA, respectively (Table 6). Good correlation was also obtained between standards and sample overlay spectra (>0.99).

3.2.4. Robustness of the method

The robustness test for all the marker compounds (**1–3**) was carried out by HPTLC methods and the % RSD was found to be <3.0% (Table 7). Separation was not effected by changing scanning wavelength ±5 nm.

Table 5
Inter- and intraday precision of markers.[a]

Compounds	Concentration (ng/band)	Precision					
		Instrumental		Intraday		Interday	
		RSD (%)	Mean RSD (%)	RSD (%)	Mean RSD (%)	RSD (%)	Mean RSD (%)
NS	333	0.94	0.85	1.01	1.09	1.24	1.22
(**1**)	667	0.83		0. 99		1.22	
	1000	0.79		1.11		1.19	
AS	333	0.93	0.86	1.12	1.06	1.22	1.27
(**2**)	667	0.89		1.05		1.34	
	1000	0.75		1.10		1.24	
HMA	333	0.80	0.79	0.87	0.91	1.21	1.21
(**3**)	667	0.86		0.95		1.19	
	1000	0.72		0.92		1.23	

[a] $n = 5$.

Table 6
Peak purity test for markers.

Compounds	$r(s, m)$[a]		$r(m, e)$[b]	
	Standard track	Sample track	Standard track	Sample track
NS (**1**)	0.9997	0.9991	0.9999	0.9998
AS (**2**)	0.9995	0.9994	0.9996	0.9989
HMA (**3**)	0.9998	0.9981	0.9999	0.9989

[a] Correlation of spectrum at start of peak with spectrum at the centre of peak.
[b] Correlation of spectrum at centre of peak with spectrum at the end of peak.

Table 7
Robustness testing of the HPTLC method.

Parameters	RSD of peak area%		
	NS (**1**)	AS (**2**)	HMA (**3**)
Mobile phase composition	0.46	0.86	0.78
Time gap between spotting and plate development	0.21	0.26	0.26
Wavelength ±5 nm	2.87	2.47	2.26

3.3. Quantification of IGs in V. trifolia and V. negundo

The developed HPTLC methods were applied for quantitative determination of NS, AS and HMA in different plant parts of *V. trifolia* and *V. negundo* (Table 3). Typical HPTLC chromatograms of reference compounds with samples are shown in Fig. 3. The identification of the investigated compounds was carried out by comparison of their R_f and spectra with those obtained under the same conditions (**3**).

3.4. Biological activity

3.4.1. DPPH radical scavenging

As shown in Fig. 4, all the molecules scavenge DPPH radicals effectively. Activity order of molecules for DPPH radical scavenging activity was found to be AS > NS > HMA. IC_{50} values of NS, AS and HMA are 9.96, 9.81 and 10.31 μg, respectively (Fig. 4A).

3.4.2. Nitric oxide radical Scavenging

Nitric oxide inhibitory assay result showed that all the tested molecules were active in nitric oxide radical inhibition. Amongst NS, AS and HMA, HMA showed maximum scavenging capacity. IC_{50} values of NS, AS and HMA are 16.25, 12.90 and 13.51 μg, respectively (Fig. 4B).

3.4.3. Total antioxidant capacity (TAC)

NS and HMA were found to be inactive in TAC assay while AS showed some activity. This may be due to approximately same structures of NS and HMA. Some structural features are quite different in AS, which may be the cause of TAC activity (Fig. 4C).

3.4.4. Reducing potential (RP) and ferric ion reducing antioxidant power (FRAP)

NS, AS and HMA did not show significant activity in both RP and FRAP assays. In FRAP assay the order was HMA > AS > NS (Fig. 4D and E).

4. Concluding remarks

Statistical analysis has proved that proposed HPTLC method is simple, rapid, specific and accurate which can be performed without any special pretreatment. Method validation proved that it is

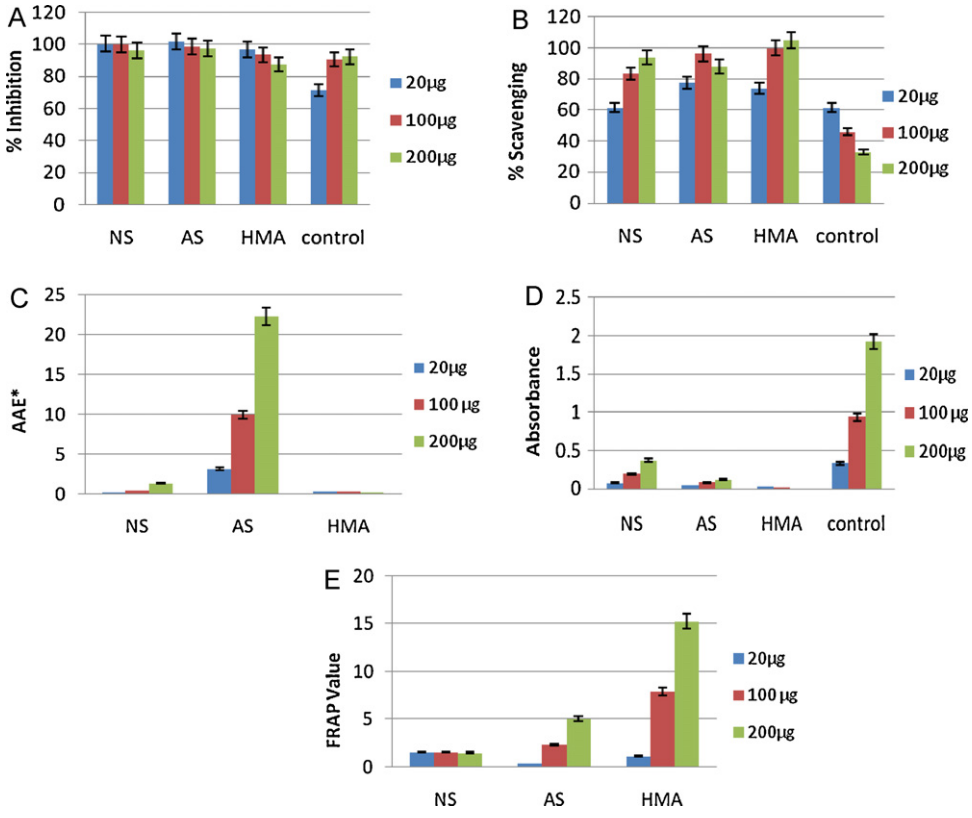

Fig. 4. In vitro antioxidant effect of NS, AS and HMA in (A) DPPH discolouration, (B) NO free radical scavenging, (C) total antioxidant capacity, (D) reducing power determination and (E) FRAP assay.

Table 8
% Content of markers in different plant parts of *V. trifolia* (VT) and *V. negundo* (VN).

Plant part[b]	% Content[a]					
	NS (**1**)	SD	AS (**2**)	SD	HMA (**3**)	SD
VT-L	0.79	0.060	1.18	0.030	0.48	0.050
VT-R	0.13	0.002	0.12	0.002	0.10	0.002
VT-S	0.06	0.003	0.10	0.002	0.04	0.001
VT-F	0.02	0.001	0.03	0.003	0.01	0.003
VN-L	0.96	0.075	0.58	0.028	0.06	0.002
VN-R	0.07	0.004	0.18	0.005	0.02	0.003
VN-S	0.03	0.003	0.02	0.005	0.01	0.002

[a] Plant dry weight basis.
[b] L: leaves; R: root; S: stem; F: fruit.

selective and reproducible. This is the first detailed study on the simultaneous quantification of IGs NS (**1**), AS (**2**) and HMA (**3**) in *Vitex species*. A comparative study of *V. trifolia* and *V. negundo* revealed that NS is higher in *V. negundo* than in *V. trifolia* and AS is higher in *V. trifolia* while HMA is very low in *V. negundo* (Table 8). This method may be applied for the quality control of formulations based on these plants. The antioxidant activity results showed that these markers have proton donating ability and could serve as free radical scavengers.

Acknowledgements

The authors thank to Director, CIMAP for keen interest during the course of work. One of the authors (N. Tiwari) is thankful to CSIR (New Delhi) for the award of senior research fellowship.

References

[1] P. Morat, Labiatae (Mabberley, D.J. and de Kok, R.P.J.) in Flore de la Nouvelle-Calédonie, Muséum Naional d'Histoire Naturelle, Paris, France, 2004, pp. 34–36.
[2] R.P.J. Kok (de), The genus *Vitex L.* (Lamiaceae) in New Guinea and the South Pacific Islands, Kew Bull. 62 (2007) 587–603.
[3] W. Mc Clatchey, The ethnopharmacopoeia of Rotuma, J. Ethnopharmacol. 50 (1996) 147–156.
[4] J. Rageau, Les plantes médicinales de la Nouvelle-Calédonie. Travaux et documents de l'ORSTOM ORSTOM, vol. 23, Nouvelle-Calédonie, Noumea, 1973, pp. 104–105.
[5] D.K. Holdsworth, Medicinal plants of Papua New Guinea South Pacific Commission Technical Paper, vol. 175, Noumea, New Caledonia, 1977, p. 65.
[6] K. Kannathasan, A. Senthilkumar, M. Chandrasekaran, V. Venkatesalu, Differential larvicidal efficacy of four species of Vitex against *Culex quinquefasciatus* larvae, Parasitology Res. 101 (2007) 1721–1723.
[7] M.M Hossain, N. Paula, M.H. Sohrab, E. Rahman, M.A. Rashid, Antibacterial activity of *Vitex trifolia*, Fitoterapia 72 (2001) 695–697.
[8] B.K. Manjunatha, S.M. Vidya, Hepatoprotective activity of *Vitex trifolia* against carbon tetrachloride-induced hepatic damage, Ind. J. Pharm. Sci. 70 (2008) 241–245.
[9] C.K. Sehgal, S.C. Taneja, K.L. Dhar, C.K. Atal, Phytochemistry 21 (1982) 363–366.
[10] S. Suksamrarn, S. Kumcharoen, A. Suksamrarn, Iridoids of *Vitex limonifolia*, Planta Med. 65 (1999) 392–393.
[11] C.K. Sehgal, S.C. Taneja, K.L. Dhar, C.K. Atal, Phytochemistry 22 (1983) 1036–1038.
[12] G. Ravichandran, V.S. Bharadwaj, S.A. Kolhapure, Evaluation of efficacy and safety of acne-n-pimple cream in acne vulgaris, Antiseptic 101 (2004) 249–254.
[13] M.V. Venkataranganna, S. Gopumadhavan, S.K. Mitra, S.D. Anturlikar, Anti-inflammatory activity of jointCare B, a polyherbal formulation, Ind. Drugs 37 (2000) 543–546.
[14] S. Rajanna, S.A. Kolhapure, Evaluation of the efficacy and safety of muscle & joint rub in the treatment of sprains, contusions and inflammatory musculoskeletal disorders, Antiseptic 102 (2005) 389–393.
[15] M. Sahu, P. Srivastava, Clinical study of pilex combination therapy vs conventional ayurvedic therapy in the management of haemorrhoids, Ind. Pract. 54 (2001) 799–805.
[16] S.S. Reddy, M. Nagabhushanam, R.M. Rao, Role of pilex tablets and ointment in the treatment of piles and fissures, Probe 23 (1984) 213–217.
[17] N. Dutta, M.N. Bhattacharya, Clinical trial of rumalaya in some rheumatic conditions, Probe 13 (1974) 57–70.
[18] A. Sharma, S.A. Kolhapure, Evaluation of the efficacy and safety of rumalaya gel in the management of acute and chronic inflammatory musculoskeletal disorders: an open, prospective, noncomparative, phase III clinical trial, Med. Update 12 (2005) 39–45.
[19] R.N. Chakravaty, Therapeutic studies on rumalaya in orthopaedic practice, Probe 17 (1978) 323–326.
[20] I. Singh, Evaluation of v-gel in vaginitis and cervicitis, Antiseptic 98 (2001) 6–9.
[21] A. Ahmad, K.K. Pillai, A.K. Najmi, S.J. Ahmad, S.N. Pal, D.K. Balani, Evaluation of hepatoprotective potential of jigrine post-treatment against thioacetamide induced hepatic damage, J. Ethnopharmacol. 79 (2002) 35–41.
[22] A.K. Najmi, K.K. Pillai, S.N. Pal, M. Aqil, Free radical scavenging and hepatoprotective activity of jigrine against galactosamine induced hepatopathy in rats, J. Ethnopharmacol. 97 (2005) 521–525.
[23] A. Mitra, A. Gupta, D. Mukhopadhyay, An extended clinical study with herbal eye drops preparation, Antiseptic 83 (1986) 567–569.
[24] P.J. Lokhande, J.K. Verma, Quantification of negundoside in *Vitex negundo* Linn. leaf powder by high-performance liquid chromatography, Acta Chromatogr. 22 (2010) 591–597.
[25] E. Hoberg, B. Meier, O. Sticher, An analytical high performance liquid chromatographic method for the determination of agnuside and p-hydroxybenzoic acid contents in Agni-casti fructus, Phytochem. Anal. 11 (2000) 327–329.
[26] P.J. Lokhande, J.K. Verma, Quantification of negundoside in *Vitex negundo* Linn. leaf by high-performance thin-layer chromatography, J. Planar Chromatogr. 22 (2009) 225–228.
[27] Y.C. Chung, C.T. Chang, W.W. Chao, C.F. Lin, S.T. Chou, Antioxidative activity and safety of the 50% ethanolic extract from red bean fermented by *Bacillus subtilis* IMR-NK1, J. Agric. Food Chem. 50 (2002) 2454–2458.
[28] L. Marcocci, J.J. Maguire, M.T. Droy-Lafaix, L. Packer, The nitric oxide-scavenging properties of *Ginkgo biloba* extract EGb 761, Biochem. Biophys. Res. Comm. 201 (1994) 748–755.
[29] P. Preito, M. Pineda, Aguilar, Spectrophotometric quantitation of antioxidant capacity through the formation of a phosphomolybdenum complex: specific application to the determination of vitamin E, Anal. Biochem. 269 (1999) 337–341.
[30] S. Luqman, R. Kumar, S. Kaushik, S. Srivastava, M.P. Darokar, S.P.S. Khanuja, Ind. J. Biochem. Biophys. 46 (2009) 122–125.
[31] G.C. Yen, H.Y. Chen, Antioxidant activity of various tea extracts in relation to their antimutagenicity, J. Agric. Food Chem. 43 (1995) 27–32.
[32] W. Steven, Analytical Methods: A Statistical Perspective on the ICH Q2A and Q2B Guidelines for Validation of Analytical Methods, vol. 19, Biopharm International, Rockville, MD, USA, 2006.
[33] X.-W. Cao, J. Li, S.-B. Chen, X.-B. Li, P.-G. Xiao, S.-L. Chen, D.-J. Yang, Simultaneous determination of nine nucleosides and nucleobases in different Fritillaria species by HPLC-diode array detector, J. Sep. Sci. 33 (2010) 1587–1594.

Journal of Pharmaceutical and Biomedical Analysis 61 (2012) 215–223

Contents lists available at SciVerse ScienceDirect

Journal of Pharmaceutical and Biomedical Analysis

journal homepage: www.elsevier.com/locate/jpba

Forced degradation study of thiocolchicoside: Characterization of its degradation products

Del Grosso Erika*, Aprile Silvio, Grosa Giorgio

Dipartimento di Scienze Chimiche, Alimentari, Farmaceutiche e Farmacologiche and Drug and Food Biotechnology Centre, Università degli Studi del Piemonte Orientale "Amedeo Avogadro", Largo Donegani 2, 28100 Novara, Italy

ARTICLE INFO

Article history:
Received 27 September 2011
Received in revised form 7 December 2011
Accepted 9 December 2011
Available online 17 December 2011

Keywords:
Thiocolchicoside
Forced degradation
Degradation products
LC–MS
LC–MS^n

ABSTRACT

Thiocolchicoside (TCC, *N*-[1,2-dimethoxy-10-methylsulphanyl-9-oxo-3-(3,4,5-trihydroxy-6-hydroxymethyl-tetrahydropyran-2-yloxy)-5,6,7,9-tetrahydro-benzo[a]heptalen-7-yl]-acetamide) was subjected to hydrolytic, oxidative, and photolytic stresses. TCC underwent degradation in acidic, basic, and oxidative conditions, while it was stable toward other stress conditions. The degradation products (**DPs**) were detected and their separation was achieved on a SGE Wakosil C18RS 5 μm (250 * 4.6 mm; SGE) column employing a gradient LC–MS method for a total time of analysis of 18 min. The mass fragmentation pathways of both thiocolchicoside and its degradation products were established using LC–MS experiments assigning the structures to the **DPs**. In particular, five **DPs** were identified as: **D1SO** (*N*-[1,2-dimethoxy-10-methylsulphoxide-9-oxo-3-(3,4,5-trihydroxy-6-hydroxymethyl-tetrahydropyran-2-yloxy)-5,6,7,9-tetrahydro-benzo[a]heptalen-7-yl]-acetamide), **D1SO$_2$** (*N*-[1,2-dimethoxy-10-methylsulphone-9-oxo-3-(3,4,5-trihydroxy-6-hydroxymethyl-tetrahydropyran-2-yloxy)-5,6,7,9-tetrahydro-benzo[a]heptalen-7-yl]-acetamide), **D2** ([1,2-dimethoxy-10-methylsulphanyl-9-oxo-3-(3,4,5-trihydroxy-6-hydroxymethyl-tetrahydropyran-2-yloxy)-5,6,7,9-tetrahydro-benzo[a]heptalen-7-yl]-amine), **D3** (*N*-[1,2-dimethoxy-3-hydroxy-10-methylsulphanyl-9-oxo-5,6,7,9-tetrahydro-benzo[a]heptalen-7-yl]-acetamide or 3-*O*-demethylthiocolchicine), **D4** ([1,2-dimethoxy-3-hydroxy-10-methylsulphanyl-9-oxo-5,6,7,9-tetrahydro-benzo[a]heptalen-7-yl]-amine or *N*-deacetyl-3-*O*-demethylthiocochicine). Moreover, the structures of **DPs** were confirmed by synthesis of the reference standards which were fully characterized by MS, NMR, IR analyses. Finally a comprehensive degradation scheme of TCC was proposed allowing to outline **D1SO** and **D3** as the indicators of its stability for oxidative and hydrolytic stress conditions.

© 2011 Elsevier B.V. All rights reserved.

1. Introduction

Thiocolchicoside (TCC) is a semi-synthetic sulphur derivative of colchicoside (CC, Fig. 1), a naturally occurring glucoside present in the *Colchicum autumnale* and in the Gloriosa superba plants. TCC has a selective affinity for γ-amino-butyric acid (GABA) receptors and acts on muscular contracture by activating the GABA-nergic inhibitory pathways [1,2]. For these properties TCC has been used for over 35 years and it is currently prescribed as a potent myorelaxant drug in the treatment of painful muscle contractions in acute and chronic rheumatic conditions, in traumatology, and especially in patients with acute low back pain (e.g. Muscoril®, Miotens®, Muscoflex®). Additionally, TCC is being the reference compound for the design and synthesis of a variety of novel compounds with the same activity [3,4]. From the analytical point of view, only one paper dealing with the separation of the TCC from synthetic impurities and other alkaloids structurally related to colchicine scaffold, such as colchicoside, thiocolchicine, colchicine, 3-*O*-demethyl-thiocolchicine, *N*-formyl-*N*-deacetyl-thiocolchicoside, and *N*-formyl-*N*-deacetyl-thiocolchicine, was published so far [5]. Moreover, in the Indian Pharmacopeia 2010 monograph of thiocolchicoside [6] a normal phase LC method was reported for the determination of the synthetic impurities, colchicoside and *N*-formyl-*N*-deacetyl-thiocolchicoside, while a RP-LC method was used for the quantification of TCC; however none of these methods are stability indicating and the formation of degradation products is not addressed.

Since TCC is also frequently administered in combined therapy with anti-inflammatory agents (e.g. ketoprofen, diclofenac, betamethasone, and floctafenine), the literature reports several analytical methods (e.g. HPLC, TLC-densitometry) describing the determination of TCC in the corresponding pharmaceutical formulations [7–12]. In addition to these data, very recently works from Umarkar et al. [13] and Jadhav et al. [14] described different

* Corresponding author. Tel.: +39 321 375758; fax: +39 321 375621.
E-mail address: erika.delgrosso@pharm.unipmn.it (D.G. Erika).

0731-7085/$ – see front matter © 2011 Elsevier B.V. All rights reserved.
doi:10.1016/j.jpba.2011.12.008

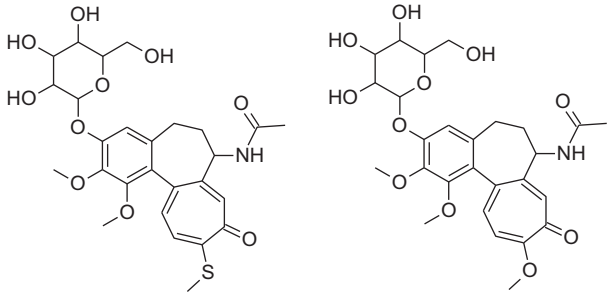

Fig. 1. Chemical structures of thiocolchicoside (TCC) and colchicoside (CC).

RP-HPLC methods applied as stability indicating methods for the determination of TCC in capsule dosage forms and for the simultaneous determination of TCC and diclofenac in tablet dosage forms respectively; nevertheless, even there are reported stress experiments in different conditions, and the chromatographic separation is similar to that reported in the Indian Pharmacopeia there is no indication about the structures and the quantification of the degradants. Although the degradation of TCC was also studied by Vargas et al. [15] describing its photolability, however, at the best of our knowledge, a comprehensive forced degradation study was not so far reported. Indeed, the lack of data on TCC API (active pharmaceutical ingredient) intrinsic stability and on its degradation products have prevented the evaluation of a stability indicating method for the quantification of TCC API and its **DPs**. On the other hand ICH guideline mentioned that forced decomposition studies should be carried out on the drug substance so as to establish the inherent stability characteristics and degradation pathways to support the stability-indicating power of the proposed analytical procedures. Taken together these considerations prompted us to perform a forced degradation study of TCC using LC–MS and LC–MS^n experiments to identify and predict the structures of the degradation products and to establish the degradation pathways of the TCC; the synthesis and physicochemical characterization of the degradation products were also presented.

2. Experimental

2.1. Reagents and chemicals

Methanol, acetonitrile (both HPLC grade), dichloromethane (>99.9%), formic acid (96%), *m*-chloroperbenzoic acid (*m*CPBA, 75%), sodium hydroxide (pellets), concentrated hydrochloric acid (37%), concentrated ammonia solution (33%), 1,1′-azobis(cyclohexane–carbonitrile, 98%), ferric chloride ($FeCl_3$, 97%), copper (II) sulphate pentahydrate ($CuSO_4{\cdot}5H_2O$, >97%) and 30% hydrogen peroxide (H_2O_2) were purchased from Sigma–Aldrich (Milano, Italy). Samples of TCC were kindly gifted by Indena s.p.a. (Milano, Italy). Water was purified by Milli-Q instrument (Millipore Corp., Bedford, MA, USA). Silica gel 60 (70–230 Mesh) for column chromatography was purchased from Merck (Darmstadt, Germany). TLC was carried out on plates with a layer thickness of 0.25 mm (Merck silica gel 60 F254). All chemicals were used without further purification.

2.2. Preparation of TCC stock solution

A 0.25 mg ml^{-1} stock solution of standard TCC (batch no. 744/44/B, CoA no. 1030/1319) was prepared in acetonitrile. The solution was stored at 4 °C and resulted stable throughout the study. The stability of the stock solution was assessed just after the preparation with analyses in triplicate, at the end of our study (2 weeks) and also after one month of storage.

2.3. LC–MS and LC–MS^n analysis

The analyses were performed using a Surveyor HPLC system (Thermo Finnigan, San Josè, CA, USA) equipped with a quaternary pump, a Surveyor AS autosampler, a vacuum degasser and a column heater (25 °C) connected to a Thermo Finnigan LCQ Deca XP *plus* Ion Trap Mass Spectrometer from Thermo Finnigan (San Josè, CA, USA) equipped with an electrospray ion source (ESI). The chromatographic separations were performed on a SGE Wakosil C18RS (5 μm, 250 * 4.6 mm, SGE) column. The mobile phase (flow rate 0.8 ml min^{-1}) consisting of solvent A ammonium formate buffer (10 mM; pH 3) – solvent B acetonitrile was set to A:B; 90:10, *v/v* at the start of analysis. The elution was then performed by a linear gradient from 10% to 30% solvent B in 2 min, from 30% to 70% solvent B for other 8 min, maintained at 70% solvent B for 2 min and then to 10% solvent B in 0.5 min and maintained at 10% solvent B for 7.5 min. The total time of each analysis was 18 min. The eluants were filtered through a 0.45-μm pore size polyvinylidene difluoride membrane filter before use. The injection volume was 20 μl.

The eluate was injected into the electrospray ion source with a splitting of 20% and the MS and MS^n spectra were acquired and interpreted using the Xcalibur® software. Operating conditions on the ion trap mass spectrometer in positive polarity were as follows: spray voltage, 5.3 kV; source current, 80 μA; capillary temperature, 350 °C; capillary voltage, 3 V; tube lens offset, 10 V; sheath gas flow (N_2), 60 A.U. Data were acquired in MS, MS/MS and MS^n scanning mode; the full spectra were recorded in the range 100–750 *m/z*; for all MS/MS and MS^n experiments the precursor isolation window was set at 1 atomic mass unit (a.m.u.) and the collision energy was optimized at 27–33%.

2.4. Spectroscopic analyses

^1H and ^{13}C NMR experiments were performed on a JEOL Eclipse ECP 300 FT MHz spectrometer (Jeol Ltd. Tokyo, Japan) operating at 7.05 T. Chemical shifts are reported in part per million (ppm) downfield from TMS and all the spectra were recorded on d_6-DMSO solutions of the analytes. FT-IR experiments were performed on an AVATAR 370 FT-IR (Thermo Fisher Scientific, Madison WI, USA) spectrophotometer and were recorded on thin pellets of compound and KBr. The melting point experiments were performed on a BUCHI Melting Point B-540.

2.5. Stress studies

For acidic degradation studies 750 μl of 0.5 N HCl solution was added to 250 μl of the TCC stock solution. This solution was allowed to stand at 70 °C and was analyzed after 30 min, 4, 24, 48 h. Prior to analysis, 200 μl of the acidified solution were added to a corresponding volume of the ammonium formate buffer (10 mM; pH 3).

For basic degradation studies 750 μl of 0.05 N NaOH solution were added to 250 μl of the TCC stock solution. This solution was heated at 50 °C and was analyzed after 24 h. Prior to analysis, 200 μl of the reaction mixture were added to a corresponding volume of the ammonium formate buffer (10 mM; pH 3).

For oxidative degradation studies three different protocols were used to assess the stability in the presence of (a) H_2O_2, (b) radical initiator, and (c) transition metals.

(a) 100 μl of 0.075%H_2O_2 solution were added to 500 μl of the TCC stock solution. This solution was allowed to stand at room

temperature and was analyzed after 2 h. Prior to analysis, 200 μl of each solution were added to a corresponding volume of the distilled water. (b) 750 μl of 60 mM 1,1′-azobis(cyclohexane–carbonitrile) solution, (c) 750 μl of 1.5 mM $FeCl_3$ or 1.5 mM $CuSO_4$ solutions were added to 250 μl of the TCC stock solution. These solutions were allowed to stand at room temperature and were analyzed after 72 h. Prior to analysis, 200 μl of each solution were added to an equal volume of distilled water and centrifuged at 5400 × g for 5 min.

For photodegradation studies 500 μl of the TCC stock solution were exposed to UV-light (254 nm) and sunlight (1400 W/m^2) for 30 min and 1 month respectively. Prior to analysis, 200 μl of the solution were added to an equal volume of distilled water. For comparison, a TCC stock solution was treated with the same procedure without the addition of the stress agent.

Degradation conditions are summarized in Table 1.

2.6. Synthesis of degradation products

2.6.1. N-[1,2-dimethoxy-10-methylsulphoxide-9-oxo-3-(3,4,5-trihydroxy-6-hydroxymethyl tetrahydropyran-2-yloxy)-5,6,7,9-tetrahydro-benzo[a]heptalen-7-yl]-acetamide (D1SO)

TCC (100 mg, 0.18 mmol) was dissolved in 8 ml of methanol and the mixture was stirred until its complete dissolution. *m*CPBA (70%, 43.5 mg, 0.18 mmol) was then added and the mixture was reacted 8 h under stirring at room temperature. At the end of the reaction (monitored by TLC: dichloromethane–methanol 7:3), the solvent was evaporated under reduced pressure. The residue was purified by gravity column chromatography using dichloromethane–methanol 95:5 and then 9:1 as eluant to give pure **D1SO** as a pair of stereoisomers (69.5 mg, 67% yield).

HPLC purity: 93.6%, IR ν_{max}: 2923.7, 2358.7, 1642.3, 1548.6, 1074.8 cm^{-1}.

2.6.2. N-[1,2-dimethoxy-10-methylsulphone-9-oxo-3-(3,4,5-trihydroxy-6-hydroxymethyl-tetrahydropyran-2-yloxy)-5,6,7,9-tetrahydro-benzo[a]heptalen-7-yl]-acetamide (D1SO2)

TCC (100 mg, 0.18 mmol) was dissolved in 8 ml of methanol and the mixture was stirred until its complete dissolution. *m*CPBA (70%, 100 mg, 0.41 mmol) was then added and the mixture was reacted 8 h under stirring at room temperature. At the end of the reaction (monitored by TLC: dichloromethane–methanol 7:3), the solvent was evaporated under reduced pressure. The residue was purified by gravity column chromatography using dichloromethane–methanol 95:5 and then 9:1 as eluant to give pure **D1SO2**, (62.2 mg, 61% yield).

HPLC purity: 95.4%, IR ν_{max}: 2359.7, 1521.4,1645.8, 1524.4, 1076.3 cm^{-1}, mp: 207 °C.

Table 1
Stress conditions applied in the forced degradation study of thiocolchicoside (TCC).

Stressor	Temperature (°C)	Time of the analysis
HCl 0.5 N	70	30 min, 4, 24, 48 h
NaOH 0.05 N	50	24 h
H_2O_2 0.075%	RT	2 h
Radical initiator	RT	72 h
Transition metals	RT	72 h
UV light	RT	30 min
Sunlight	RT	1 month

2.6.3. [1,2-Dimethoxy-10-methylsulphanyl-9-oxo-3-(3,4,5-trihydroxy-6-hydroxymethyl-tetrahydropyran-2-yloxy)-5,6,7,9-tetrahydro-benzo[a]heptalen-7-yl]-amine (D2)

0.5 N hydrochloric acid solution (60 ml) was added to TCC (600 mg, 1.07 mmol) and the mixture was reacted 15 days under stirring at room temperature. At the end of the reaction, the mixture was neutralized with 10 N sodium hydroxide solution and submitted to lyophilisation. The residue was first purified by gravity column chromatography using dichloromethane–methanol 95:5 as eluant to give impure compound **D2**. Afterwards a second purification by gravity column chromatography using dichloromethane-methanol 9:1 as eluant gave pure compound **D2** in a small yield (12.9 mg, 2.3% yield).

HPLC purity: 98.9%, IR ν_{max}: 2924.1, 2359.1, 2320.2, 1077.5 cm^{-1}, mp: 173 °C.

2.6.4. N-[1,2-dimethoxy-3-hydroxy-10-methylsulphanyl-9-oxo-5,6,7,9-tetrahydro-benzo[a]heptalen-7-yl]-acetamide or 3-O-demethylthiocolchicine (D3)

TCC (50 mg, 0.09 mmol) was dissolved in 1 N HCl solution (3.5 ml) and the mixture was stirred to reflux for 1 h, until a yellow precipitate was formed. The precipitate was filtered and dried in vacuum obtaining compound **D3** (102 mg, 72% yield).

HPLC purity: 97.5%, IR ν_{max}: 2939.0, 1638.6, 1547.2, 1310.9, and 1013.9 cm^{-1}, mp: 303 °C.

2.6.5. [1,2-Dimethoxy-3-hydroxy-10-methylsulphanyl-9-oxo-5,6,7,9-tetrahydro-benzo[a]heptalen-7-yl]-amine or N-deacetyl-3-O-demethylthiocochicine (D4)

TCC (50 mg, 0.09 mmol) was dissolved in 5 N HCl (12.5 ml) and stirred to reflux for 2 h. The end of the reaction was monitored by the disappearance of the starting material as ascertained by TLC (dichloromethane–methanol 8:2). Appropriate volumes of 10 N and then 1 N NaOH solutions were added until the mixture reached pH ∼8 observing the solution red turning yellow. The mixture was diluted with ethyl acetate and the organic layer was washed with brine, dried over anhydrous sodium sulphate, filtered and the solvent evaporated under reduced pressure obtaining pure **D4** (21 mg, 64% yield).

HPLC purity: 99.5%, IR ν_{max}: 3255.3, 2359.1, 2320.2, 1310.9, and 1013.9 cm^{-1}, mp: 181 °C.

3. Results and discussion

3.1. LC-MS^n studies on TCC

Mass spectrometry source conditions were optimized by flow injections analysis (FIA) of the TCC standard solution. Initially either positive and negative analyses were performed showing the latter a complex pattern due to the presence of the formate adducts ($[M+45]^-$) and not easily interpretable MS^2 and MS^n spectra (data not shown); on the contrary the positive ionization furnished only the protonated molecule ($[M+H]^+$) and simple sequential fragmentation pathways, either in MS^2 and MS^n spectra. Liquid chromatography conditions were set up using ammonium formate buffer (10 mM; pH 3) – acetonitrile as a mobile phase. Ammonium formate salt was chosen for its known volatility and compatibility with the MS spectrometer. It is worth of mention that using ammonium acetate we experienced a relevant in-source ion suppression effects. Finally the acidic pH was selected to improve the ionization of the analytes in the ionic source.

The method was optimized performing a non-linear gradient from 10% to 70% of acetonitrile to set the retention time of the TCC peak to 7.03 min, suitable to determine both polar and lipophilic **DPs** (Fig. 2).

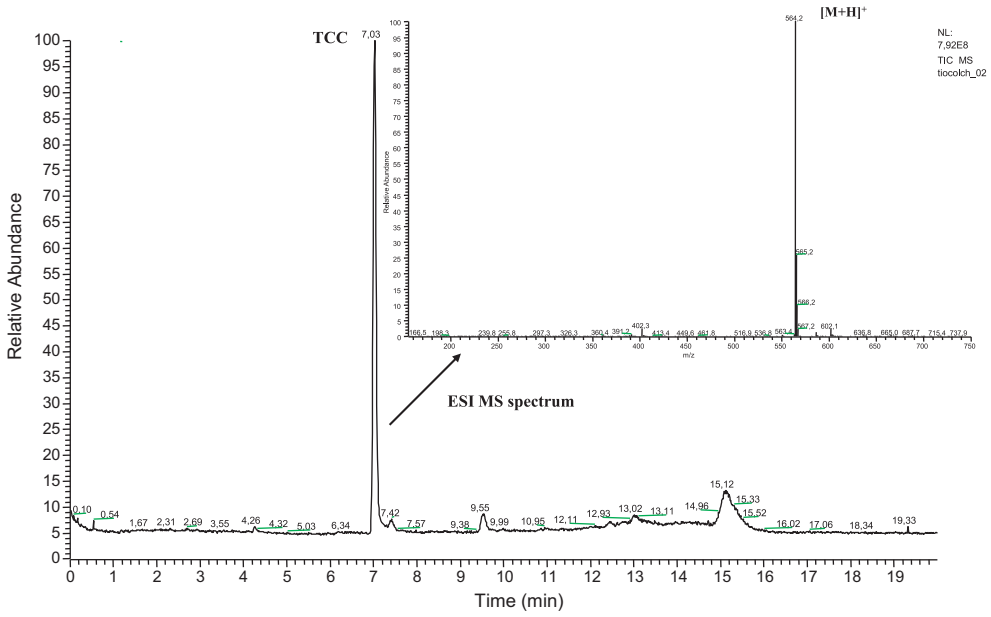

Fig. 2. LC-ESI chromatogram of TCC.

The positive MS, MS^2 and MS^3 spectra of TCC and the structure of its main fragment ions are showed in Fig. 3. The base peak of TCC was observed predominantly as $[M+H]^+$ at *m/z* 564 (range 100–750 *m/z*); moreover a $[M+Na]^+$ adduct at *m/z* 586 was generally observed at a lower abundance. In addition to the molecular species of TCC there is a diagnostic fragment ion in the MS^2 spectrum at *m/z* 402 ($[M+H-162]^+$) due to the loss of the glucoside group. Moreover the fragment ions at *m/z* 384 ($[M+H-162-18]^+$), 360 ($[M+H-162-42]^+$), 354 ($[M+H-162-48]^+$), and 343 ($[M+H-162-59]^+$) displayed at the MS^3 stage could be associated with the loss of the following fragments respectively: a neutral molecule of water, a neutral ketene (CH_2CO) from the amide chain, a neutral CH_3SH (methanethiol) from the methylthio group, and a neutral acetamide molecule (NH_2COCH_3).

All these fragments were important indicators both of the presence or of the absence of these functional groups in the **DPs**. LC–MS total ion chromatograms were then obtained from TCC samples submitted to the stress conditions described above (Table 1). For each peak, a signal representing a $[M+H]^+$ value was observed in the positive full scan mode; afterward, the LC–MS^n data arising from these ions gave further information for the structural assignments.

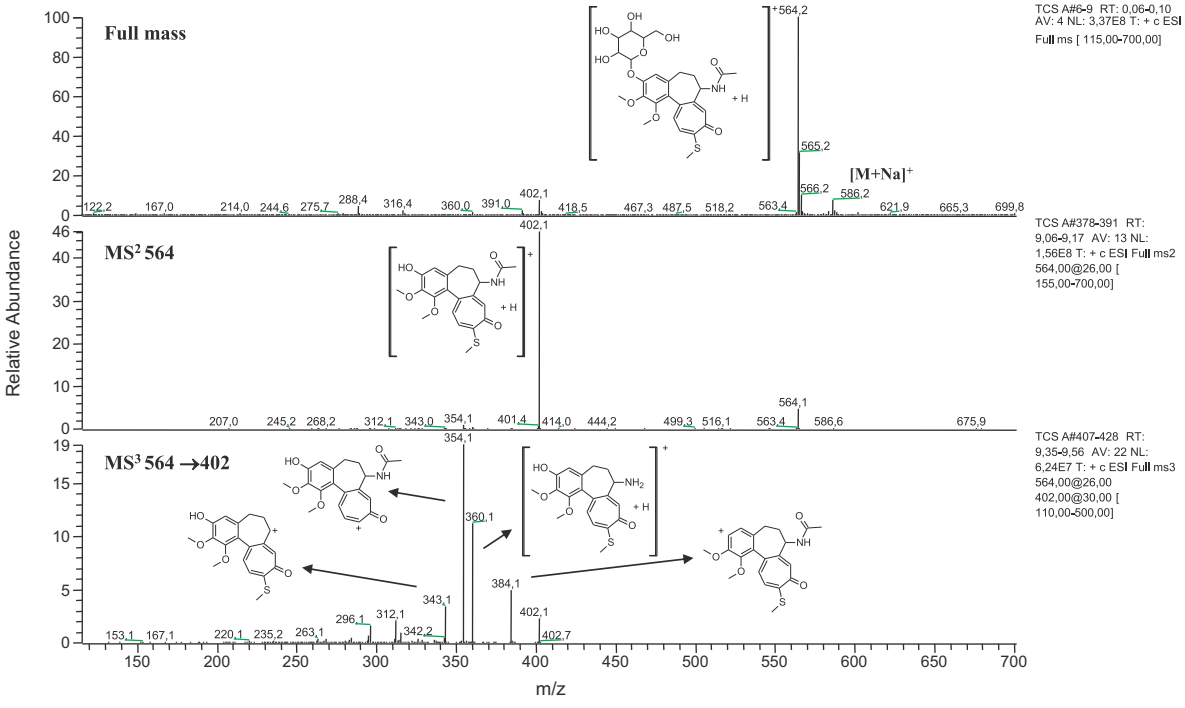

Fig. 3. TCC positive MS, MS^2 and MS^3 spectra.

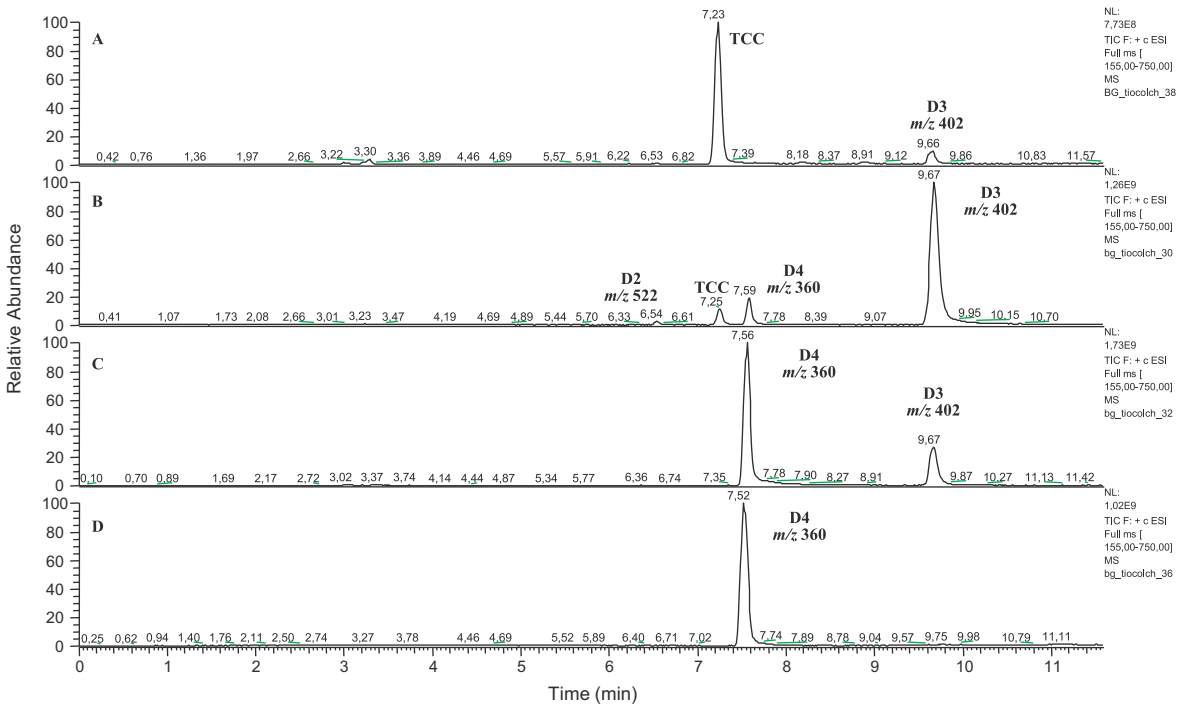

Fig. 4. LC–MS chromatograms of the degradation in 0.5 N HCl at 70 °C: (A) 30 min; (B) 4 h; (C) 24 h; (D) 48 h.

3.2. LC–MS data of TCC forced degradation

3.2.1. Acidic degradation

Under acidic conditions different chemical reactions on TCC structure, such as hydrolysis of the amide chain and/or the cleavage of the β-glycosidic bond could be expected.

In the presence of 0.5 N HCl, at 70 °C, the formation of a peak at a retention time of 9.66 min was evident after 30 min (Fig. 4A); thus its positive MS spectrum gave rise to the base peak at *m*/*z* 402 (−162 a.m.u. with respect to TCC), corresponding to the TCC aglycone (**D3**). **D3** intensity increased and after 4 h the TCC peak dramatically decreased while two other peaks were present in the chromatogram (6.54 and 7.59 min respectively, Fig. 4B). The MS spectrum of the peak at 6.54 min presented a protonated molecule at *m*/*z* 522 (−42 a.m.u. with respect to TCC), possibly arising from *N*-deacetylation reaction (**D2**); the MS spectrum of the peak at 7.59 min showed an ion at *m*/*z* 360 (−204 a.m.u. with respect to TCC), probably corresponding to a structure with the free amino group on the TCC aglycone (**D4**).

After 24 h **D2** and TCC completely disappeared being **D4** predominant with respect to **D3** (Fig. 4**C**); **D4** was then the only **DP** after 48 h (Fig. 4D). These results suggested that **D3** could be considered the degradation product indicator of stability in the acidic conditions while **D2** and **D4** were secondary **DPs**.

3.2.2. Basic degradation

The experiments were performed in 0.05 N NaOH solution at 50 °C; after 24 h there was a major peak at a retention time of 9.64 min (*m*/*z* 402) corresponding to **D3** (Fig. 5); for longer time of reaction or in severe conditions (1 N NaOH), TCC underwent a rather complete degradation. These data clearly indicates that **D3** could be considered the indicator of stability in hydrolytic conditions.

It is worth mentioning that, on the contrary one might expect, in our experiments the position more susceptible of alkaline hydrolysis resulted the β-glycosidic bond and not the acetamide moiety.

3.2.3. Oxidative degradation

Oxidative degradation studies were performed using three different stress conditions. In the presence of 60 mM radical initiator 1,1′-azobis(cyclohexane–carbonitrile) solution or the transition metals (1.5 mM $FeCl_3$ or 1.5 mM $CuSO_4$) no degradation occurred also for long time (72 h). Conversely, in the presence of H_2O_2 a very fast degradation was observed: indeed with 5% or 0.5% H_2O_2 at room temperature the complete degradation of TCC occurred in 15 min (data not shown). The forced degradation was then repeated with 0.075% H_2O_2 and the analyses were performed after 2 h: in this case the formation of two different degradation products at retention times 6.40 (**D1SO**, Fig. 6) and 6.75 min (**D1SO2**, Fig. 6) with a *m*/*z* 580 and 596 ($[M+H]^+$) respectively were present. The difference of +16 and +32 a.m.u. with respect to the TCC protonated molecule suggested the insertion of one or two oxygen atoms: possibly the sulphur atom was the target of the oxidation giving the sulfoxide and the sulphone derivatives respectively (**D1SO** and **$D1SO_2$**, Fig. 6); after 4 h a complete degradation occurred.

3.2.4. Photodegradation

For photodegradation studies, TCC solutions were exposed to UV-light and sunlight for 30 min and 1 month respectively: in these conditions no degradation occurred (data not shown).

3.3. MS^n data of the degradation products

3.3.1. ***D1SO*** *(m/z 580)*

The MS^2 spectrum of the ion at *m*/*z* 580 presented the ions at *m*/*z* 562 $[M+H-18]^+$, 516 $[M+H-64]^+$, 418 $[M+H-162]^+$, and 400 $[M+H-180]^+$: the fragments at −162 and −180 a.m.u. confirmed the presence of the sugar moiety while the fragment at −64 a.m.u. was attributable to the loss of a neutral $HSOCH_3$ group; the MS^3 spectrum on the *m*/*z* 562 confirmed the loss of the neutral ketene from the amide function (*m*/*z* 520, $[M+H-18-42]^+$) and the loss of the sugar (*m*/*z* 400, $[M+H-18-162]^+$) while the MS^3 spectrum of the ion at *m*/*z* 418 further confirmed the loss of a $HSOCH_3$ group to give

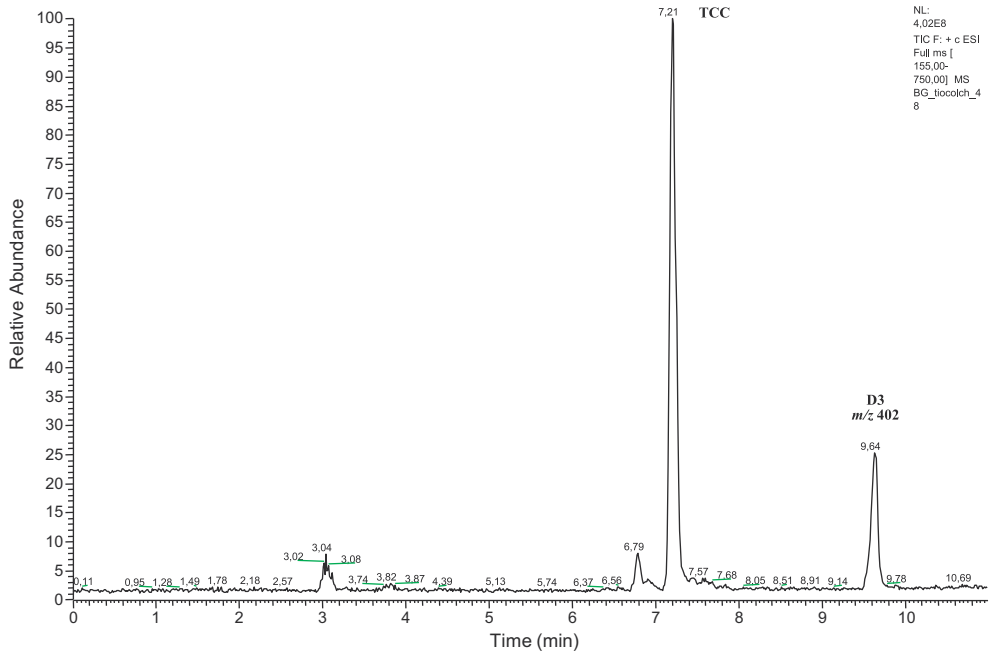

Fig. 5. LC–MS chromatograms of the degradation in NaOH: 0.05 N, 50 °C, 24 h.

the ion at *m*/*z* 354 ([M+H−162–64]$^+$) and the loss of a neutral H_2O molecule (*m*/*z* 400, [M+H−162–18]$^+$); from these data we assigned the structure of the *N*-[1,2-dimethoxy-10-methylsulphoxide-9-oxo-3-(3,4,5-trihydroxy-6-hydroxymethyl-tetrahydropyran-2-yloxy)-5,6,7,9-tetrahydro-benzo[a]heptalen-7-yl]-acetamide (see supplemental data).

3.3.2. ***D1SO2*** *(m/z 596)*

The MS^2 spectrum of the ion at *m*/*z* 596 presented the ions at *m*/*z* 434 [M+H−162]$^+$ (base peak), 392 [M+H−204]$^+$, and 354 [M+H−242]$^+$: the fragment at −162 a.m.u. confirmed the presence of the sugar moiety while the fragments at −204 and at −242 a.m.u. were attributable to a the simultaneous loss of the sugar and the amide function or a $-SO_2CH_3$ group respectively; the MS^3 spectrum of the ion at *m*/*z* 434 confirmed the loss of a HSO_2CH_3 molecule to give the ion at *m*/*z* 354 ([M+H−162–80]$^+$) and the loss of the neutral ketene from the amide function (*m*/*z* 392, [M+H−162–42]$^+$); from these data we assigned the structure of the *N*-[1,2-dimethoxy-10-methylsulphone-9-oxo-3-(3,4,5-trihydroxy-6-hydroxymethyl-tetrahydropyran-2-yloxy)-5,6,7,9-tetrahydro-benzo[a]heptalen-7-yl]-acetamide (see supplemental data).

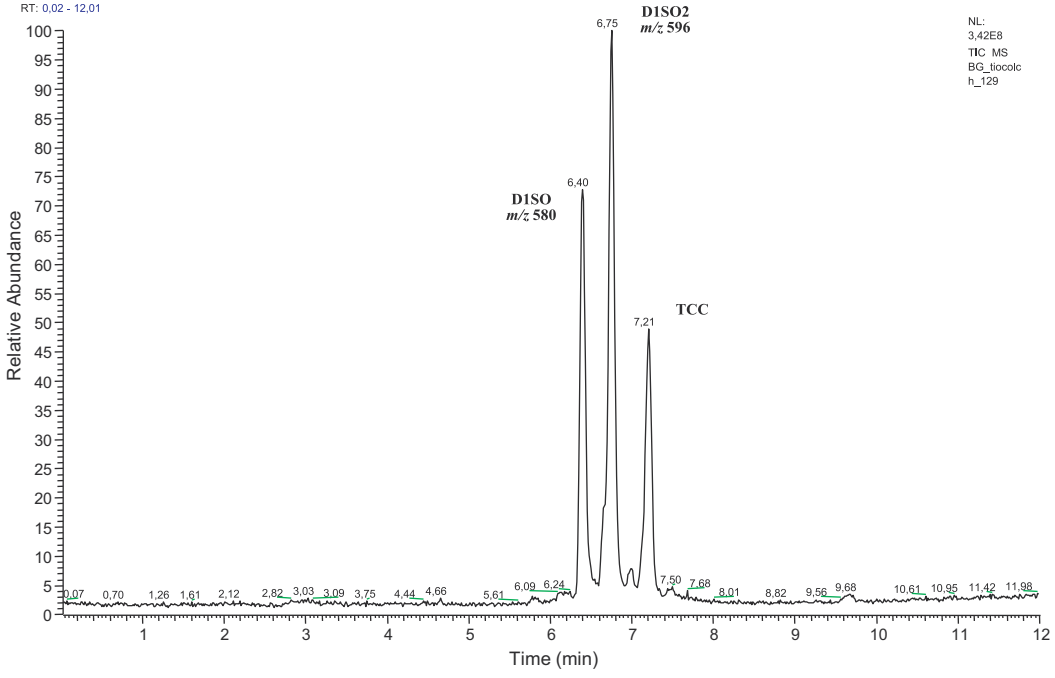

Fig. 6. LC–MS chromatograms of the degradation in 0.075% H_2O_2 at room temperature after 2 h.

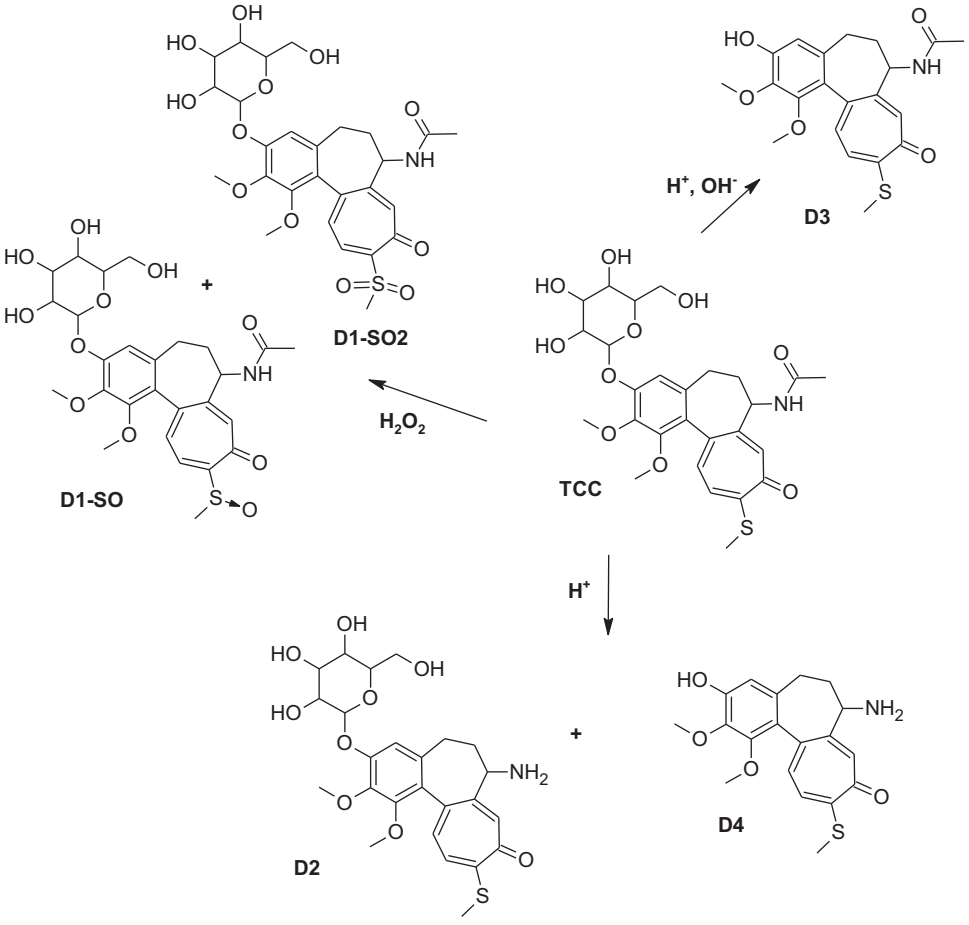

Scheme 1. Degradation pathways of TCC.

3.3.3. ***D2*** *(m/z 522)*

The MS^2 spectrum of the ion at *m/z* 522 presented the fragments at −162 a.m.u. diagnostic for the presence of the sugar moiety (*m/z* 360 $[M+H-162]^+$), and at −17 a.m.u. indicative of the presence of the free amine group (*m/z* 505 $[M+H-17]^+$); the MS^3 spectrum of the ion at *m/z* 360 confirmed the presence of the free amine group (*m/z* 343; $[M+H-162-17]^+$), the presence of a $-SCH_3$ group (*m/z* 313 $[M+H-162-47]^+$) and the simultaneous loss of a $-SCH_3$ and $-NH_2$ groups (*m/z* 296; $[M+H-162-64]^+$; these data allowed to assign the structure of the [1,2-dimethoxy-10-methylsulphanyl-9-oxo-3-(3,4,5-trihydroxy-6-hydroxymethyl-tetrahydropyran-2-yloxy)-5,6,7,9-tetrahydro-benzo[a]heptalen-7-yl]-amine (see supplemental data).

3.3.4. ***D3*** *(m/z 402)*

The MS^2 spectrum of the ion at *m/z* 402 presented no fragment at −162 a.m.u. confirming the absence of the sugar moiety, while there were present the ions at *m/z* 360 ($[M+H-42]^+$) and 343 ($[M+H-59]^+$) and at *m/z* 354 ($[M+H-48]^+$, base peak) that indicated the presence of the other functional groups of the TCC (acetamido and thiomethyl groups respectively) and the ions at *m/z* 384, 312 and 296 corresponding to the fragments $[M+H-18]^+$, $[M+H-60]^+$ and $[M+H-108]^+$; the MS^3 spectrum of the ion at *m/z* 354 gave many ions referable to the following losses: *m/z* 336 $[M+H-48-18]^+$, *m/z* 326 $[M+H-48-28]^+$, *m/z* 312 $[M+H-48-42]^+$, *m/z* 295 $[M+H-48-59]^+$, *m/z* 284 $[M+H-48-70]^+$, *m/z* 267 $[M+H-48-87]^+$, *m/z* 263 $[M+H-48-91]^+$, *m/z* 235 $[M+H-48-119]^+$; on the basis of these data we assigned the structure of the *N*-[1,2-dimethoxy-3-hydroxy-10-methylsulphanyl-9-oxo-5,6,7,9-tetrahydro-benzo[a]heptalen-7-yl]-acetamide or 3-*O*-demethylthiocolchicine (see supplemental data).

3.3.5. ***D4*** *(m/z 360)*

The MS^2 spectrum of the ion at *m/z* 360 did not present the fragments at −162 a.m.u. and at −42 a.m.u. confirming the absence of the sugar and the acetyl moieties respectively, while there were the ions at *m/z* 343 ($[M+H-17]^+$, base peak), 332 ($[M+H-28]^+$), 313 ($[M+H-47]^+$) and 296 ($[M+H-64]^+$) indicating the presence of the primary amine, the keto, and the methylthio groups respectively; the MS^3 spectrum of the ion at *m/z* 343 gave many ions referable to the following typical losses: *m/z* 328 $[M+H-17-15]^+$, *m/z* 315 $[M+H-17-28]^+$, *m/z* 311 $[M+H-17-31]^+$, *m/z* 296 $[M+H-17-47]^+$, *m/z* 269 $[M+H-17-74]^+$. These data allowed to assign the structure of the [1,2-dimethoxy-10-*methylsulphanyl*-9-oxo-3-(3,4,5-trihydroxy-6-hydroxymethyl-tetrahydropyran-2-yloxy)-5,6,7,9-tetrahydro-benzo[a]heptalen-7-yl]-amine (see supplemental data).

Taken together, the data obtained from the forced degradation study allowed to propose the degradation scheme, reported in Scheme 1, in which the hydrolysis and the oxidation were the main degradation pathways. Since **D3** and **D1SO** were both the first degradation products observed during the degradation process, they could be considered the indicators of stability for hydrolytic

and oxidative stresses respectively. Indeed the presence of **D3** was observed in different lots of TCC (data not shown).

3.4. Syntheses

The synthesis of the degradation products was performed either to confirm their structures and to obtain the standards for the development and validation of stability indicating analytical methods.

For the syntheses of the oxidative degradation products (**D1SO** and **D1SO2**), *m*CPBA at different concentrations was used as the oxidizing agent allowing to obtain the sulphoxide or sulphone derivatives in a good yield and with a high purity.

The syntheses of the **D3** and **D4** were performed on the bases of the forced degradation data; indeed, the synthetic protocol was optimized by adjusting the hydrochloric acid concentration and the time of reaction to obtain the desired products in good yield and in a high purity.

The synthesis of compound **D2** was more difficult. Indeed, starting from TCC, the amide hydrolysis (*N*-deacetylation) is the only reaction needed to obtain **D2**; this reaction could be made using hydrazine 85% [16], acylases [17] or strong bases (e.g. NaOH in methanol or MeONa). However all these reagents failed to provide the desired product **D2**, leading always to **D3** with a complex mixture of byproducts. It is important to point out that this behavior was in accordance with the forced degradation data. On the bases of these results the synthesis of **D2** was performed from TCC by hydrolysis at room temperature in 0.5 N HCl solution. The reaction was carefully monitored and stopped when the initial formation of **D4** was observed; **D2** was finally isolated and purified in a poor yield but with a very high purity.

All the synthesized products were structurally characterized by ^{1}H NMR, ^{13}C NMR, and FT-IR analyses (see supplemental data).

3.4.1. NMR and IR characterization

To confirm the structures of the synthetic degradation products NMR (^{1}H- and ^{13}C in D_6-DMSO) and FT-IR spectra were acquired starting from the analysis of TCC [18]. ^{1}H-spectrum of TCC was characterized by the presence of the signals of the methyl groups at δ 1.83 (H-17, —$COCH_3$) and at δ 2.39 (H-18, —SCH_3), of the acetamido group as a doublet at δ 8.62 (NH, —NHCO) and of the protons of the sugar moiety as complex multiplets at δ 4.90–3.70; the ^{13}C-spectrum was characterized by the presence of the signals of the methyl groups at δ 1.83 (C-17, —$COCH_3$) and at δ 2.39 (C-18, —SCH_3), of the acetamido group at δ 169.58 (C-16, —NHCO) and of the sugar group at δ 100.78 (C-1′), 73.85 (C-2′), 77.61 (C-3′), 70.42 (C-4′), 77.33 (C-5′), 61.29 (C-6′).

In the **D1SO** and **D1SO2** spectra the signals of H-18 and C-18 (—SCH_3) were present as downfield shifts with respect to TCC (+0.78 and +0.92 for the ^{1}H NMR and +26.01 and +28.11 for the ^{13}C NMR respectively); in the **D3** and **D4** spectra the signals of H-1′/6′, the glucoside-OH and the C-1′/6′ were absent; moreover, in the **D4** spectra the absence of the signals of H-17, C-16 and C-17 (—$COCH_3$) and the corresponding upfield of the —NH signal with respect to TCC (−6.62) in the ^{1}H NMR confirmed the presence of free amine; in the **D2** spectra the absence of the signals of H-17, C-16 and C-17 (—$COCH_3$) and the corresponding upfield of the —NH signal with respect to TCC (−6.72) in the ^{1}H NMR confirmed the presence of free amine. All these data are summarized in supplemental data 6 and 7. Finally FT-IR spectra further confirmed the structure assignments of the synthetic degradation products: indeed the diagnostic absorption band at 1680–1630 cm^{-1} attributable to the stretching of the carbonyl group and the diagnostic absorption band at 1570–1515 cm^{-1} attributable to the NH-deformation and the C—N stretching of the acetamido moiety is present in the spectra of **TCC**, **D3**, **D1SO** and **D1SO2**, the same was absent in the case of **D2** and **D4**.

4. Conclusions

In this study a forced degradation study of TCC was performed to assess its inherent chemical stability. For this purpose an LC-ESI–MS^n method has been developed and five degradation products were characterized by mass spectral data and confirmed by synthesis.

Two main degradation pathways of TCC were elucidated (hydrolytic and oxidative conditions) identifying the corresponding **DPs**; among these, **D1SO** and **D3** could be considered the indicators of TCC stability and they will be introduced in the development and validation of HPLC–UV stability indicating methods for determination of TCC in drug substance and drug product.

Acknowledgment

This work was supported by M.I.U.R.-PRIN 2009, Italy.

Appendix A. Supplementary data

Supplementary data associated with this article can be found, in the online version, at doi:10.1016/j.jpba.2011.12.008.

References

[1] M. Carta, L. Murru, P. Botta, G. Talani, G.P. Sechi, P.L. De Riu, E. Sanna, G. Biggio, The muscle relaxant thiocolchicoside is an antagonist of $GABA_A$ receptor function in the central nervous system, Neuropharmacology 51 (2006) 805–815.
[2] M.P. Mascia, E. Bachis, N. Obili, E. Maciocco, G.A. Cocco, G.P. Sechi, G. Biggio, Thiocolchicoside inhibits the activity of various subtypes of recombinant $GABA_A$ receptors expressed in *Xenopus laevis* oocytes, Eur. J. Pharmacol. 558 (2007) 37–42.
[3] M.L. Gelmi, D. Pocar, G. Pontremoli, S. Pellegrino, E. Bombardelli, G. Fontana, A. Riva, W. Balduini, S. Carloni, M. Cimino, F. Johnson, 3-Demethoxy-3-glycosylaminothiocolchicines: synthesis of a new class of putative muscle relaxant compounds, J. Med. Chem. 49 (2006) 5571–5577.
[4] M.L. Gelmi, G. Fontana, D. Pocar, G. Pontremoli, S. Pellegrino, E. Bombardelli, A. Riva, W. Balduini, S. Carloni, M. Cimino, Novel 3-*O*-glycosyl-3-demethylthiocolchicines as ligands for glycine and γ-aminobutyric acid receptors, J. Med. Chem. 50 (2007) 2245–2248.
[5] A. Rosso, S. Zuccaro, Determination of alkaloids from the colchicine family by reversed-phase high-performance liquid chromatography, J. Chromatogr. A 825 (1998) 96–101.
[6] Indian Pharmacopeia 2010, Thiocolchicoside monograph.
[7] R. Anacardio, O. Perilli, F. Pagnanelli, S. Bartolini, M.M. Gentile, P. Mazzeo, G. Carlucci, Physicochemical compatibility between thiocolchicoside injections (Miotens®) and pharmaceutical products frequently used for combined therapy, Farmaco 57 (2002) 925–930.
[8] N.A. El-Ragehy, M.M. Ellaithy, M.A. El-Ghobashy, Determination of thiocolchicoside in its binary mixtures (thiocolchicoside-glafenine and thiocolchicoside-floctafenine) by TLC-densitometry, Farmaco 58 (2003) 463–468.
[9] S.M. Bhavsar, D.M. Patel, A.P. Khandhar, C.N. Patel, Validated RP-HPLC method for simultaneous estimation of lornoxicam and thiocolchicoside in solid dosage form, J. Chem. Pharm. Res. 2 (2010) 563–572.
[10] S.B. Wankhede, S.S. Zambare, S.S. Chitlange, Estimation of thiocolchicoside and ketoprofen in pharmaceutical dosage form by spectrophotometric methods, J. Pharm. Res. 3 (2010) 707–710.
[11] V.S. Raymane, S.V. Ghandi, U.P. Patil, M.R. Sengar, High-performance thin-layer chromatography determination of etoricoxib and thiocolchicoside in combined tablet dosage form, J. AOAC Int. 93 (2010) 783–786.
[12] S.S. Chitlange, P.S. Shinde, G.R. Pawbake, S.B. Wankhede, Simultaneous estimation of thiocolchicoside and aceclofenac in pharmaceutical dosage form by spectrophotometric and LC method, Der Pharmacia Lettre 2 (2010) 86–93.
[13] A.R. Umarkar, N.S. Rewatkar, D.R. Chaple, L.T. Thote, S.B. Chaudhari, M.R. Bhurat, Stability indicating RP-HPLC method for estimation of thiocolchicoside in capsule dosage forms, RJPBCS 2 (2011) 750–756.
[14] S.D. Jadhav, S.R. Butle, S.D. Patil, P.K. Jagtap, Validated stability indicating RP-HPLC method for simultaneous determination and in vitro dissolution studies

of thiocolchicoside and diclofenac potassium from tablet dosage form, Arab. J. Chem. (2011), doi:10.1016/j.arab.jc.2011.01.018.
[15] F. Vargas, H. Mendez, A. Fuentes, J. Sequera, G. Fraile, M. Velásquez, G. Cáceres, K. Cuello, Photosensitizing activity of thiocolchicoside: photochemical and *in vitro* phototoxicity studies, Pharmazie 56 (2001) 83–88.
[16] H.K. Chenault, J. Dahmer, G.M. Whitesides, Kinetic resolution of unnatural and rarely occurring amino acids: enantioselective hydrolysis of N-acyl amino acids catalysed by acilase I, J. Am. Chem. Soc. 111 (1989) 6354–6364.
[17] D.D. Keith, J.A. Tortora, R. Yang, Synthesis of L-2-amino-4-methoxy-trans-but-3-enoic acid, J. Org. Chem. 43 (1978) 3711–3713.
[18] F. Clerici, S. Mottadelli, L.M. Rossi, 1H- and 13-C-NMR spectra of thiocolchicine and derivatives: a complete analysis, J. Nat. Prod. 58 (1995) 259–263.

Journal of Pharmaceutical and Biomedical Analysis 61 (2012) 224–229

Contents lists available at SciVerse ScienceDirect

Journal of Pharmaceutical and Biomedical Analysis

journal homepage: www.elsevier.com/locate/jpba

A method for identifying the origin of chondroitin sulfate with near infrared spectroscopy

Hengchang Zang[a], Lian Li[a], Fengshan Wang[a,*], Qiong Yi[b], Qin Dong[a], Chunxiao Sun[c], Jinfeng Wang[a]

[a] National Glycoengineering Research Center and School of Pharmaceutical Science, Shandong University, No. 44 Wenhuaxi Road, Jinan 250012, China
[b] Dongcheng Biochemicals Limited Company, Yantai 264006, China
[c] Shandong Freda Biopharm Limited Company, Jinan 250012, China

ARTICLE INFO

Article history:
Received 14 August 2011
Received in revised form 2 November 2011
Accepted 11 December 2011
Available online 19 December 2011

Keywords:
Chondroitin sulfate
Near infrared spectroscopy
Origin identification
SVM

ABSTRACT

The object of this study was to explore the feasibility of support vector machine (SVM) to identify the origin of chondroitin sulfate (CS) by near infrared spectroscopy. 96 batches CS from three different origins were collected in this research, 66 batches of which were chosen for training set by Kennard–Stone (KS) method and the rest were used for testing. Through the comparison of pretreatment methods of standard normal variate transformation (SNV), multiplicative scatter correction (MSC), Savitzky-Golay (SG) smoothing and derivative with SG smoothing, a SVM discrimination model was constructed, of which the prediction result is 100% accurate with the pretreatment of first derivative and SG smoothing with 15 points. The result indicated that it had great potential using SVM to identify the origin of CS.
© 2011 Elsevier B.V. All rights reserved.

1. Introduction

Chondroitin sulfate is an anionic linear polysaccharide which is composed alternatively by D-glucuronic acid and differently sulfated residues of *N*-acetyl-D-galactosamine linked by $\beta(1–3)$ bonds (Fig. 1) [1]. Chondroitin sulfate A (CS-A) and chondroitin sulfate C (CS-C) are the main compositions in commercially available products. It is widely distributed in mammals and invertebrates [2]. Commercial CS is mainly from shark, pork, and bovine; for the great profit there are some products out of accord with the actual origin in the markets. Also with the appearance of risk about bovine spongiform encephalopathy, foot-and-mouth disease, and other animal diseases, it makes people realize the importance of identifying the origin of CS. Meanwhile because of religious issue, CS from pork was restricted to use in some places. Most of all, the structure of CS varies with different sources, so the biological and pharmacological will be different [3]. The most commonly used methods for identifying the origin of CS are the DNA fragment method [3], chemical compositional analysis method [4], and NMR method [3].

Near infrared spectroscopy (NIRS) is a fast and non-destructive method, and it has been successfully used in glycosaminoglycans [5,6]. NIR spectra are mainly composed of overtone and combination bands caused by C–H, N–H, and O–H functional groups [7–13]. CS is abundant in these groups above and different CS of origins has different kinds of CS and different proportions [14,15], hence it is feasible for us to use NIRS to identify the origin of CS.

The pretreatment for raw spectrum includes SNV, MSC, SG smoothing, derivative [16], etc. SNV is used to correct the effects for multiplicative interference of scatter and particle size as well as MSC. The main advantage of SG smoothing is that it preserves features of the raw spectra such as relative peak of wave, width, which are usually flattened by other smoothing techniques. The derivative approach can eliminate baseline drift, wipe out interference of other background, discriminate overlapping peaks and improve resolution and sensitivity of spectra, but it will decrease the signal-to-noise ratio, so the approach is often used with SG smoothing [9,12,17,18]. The NIR spectrum often contains enormous variables, so the selection of variables is very important. Some reasons are listed as follows. Firstly, organic matter has distinct spectral region based on different chemical structure. Secondly, external variables like temperature, pressure will influence the calibration model. Thirdly, in order to solve collinearity between spectral variables and eliminate the variables that are useless, (noise) is necessary. And last, variable selection will decrease the test time and the cost of instrument [19]. So, variables highly relevant with the analysis purpose should be selected and that are unnecessary should be cut down to improve the robustness of model [20]. There are some variable selection methods including manual approaches, successive projections algorithm-linear discriminant analysis (SPA-LDA) [21], uninformative variable elimination (UVE), simulated annealing (SA), artificial neural networks (ANN), genetic algorithm (GA) [19], which were recently compared in Ref. [22] and difference factor (Q_s) [23] which was based on the standard deviation.

* Corresponding author. Tel.: +86 0531 88380288.
E-mail address: fswang@sdu.edu.cn (F. Wang).

0731-7085/$ – see front matter © 2011 Elsevier B.V. All rights reserved.
doi:10.1016/j.jpba.2011.12.011

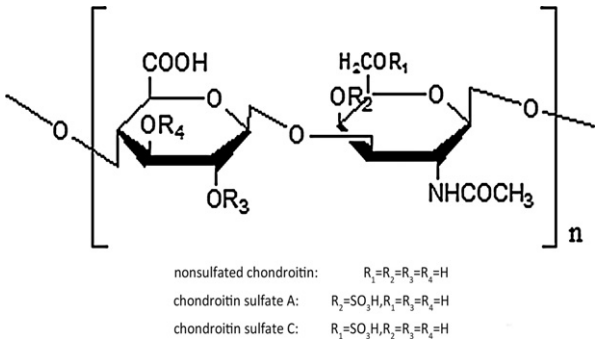

Fig. 1. Constitutional unit of chondroitin sulfate.

SVM proposed by Vapnik is based on the statistical learning theory of structural risk minimization in Vapnik-Chervonenkis dimension [24]. SVM is a powerful method, and it has been used in many fields such as combinatorial chemistry [25], drug design [26], medicine assay [27], biodiesel analysis [9,17], food safety [18] gasoline classification [28], and so on [8,10]. It is superior in small sample research with high dimensions for discrimination analysis.

This study was aimed to construct a support vector classification (SVC) model to predict the origin of three different CS to demonstrate the feasibility of NIRS for identifying the origin of CS, and different pretreatment methods and spectral regions were compared on the performance of SVM model.

2. Materials and methods

2.1. Materials

2.1.1. Samples

Ninety-six batches of CS samples were obtained from Yantai Dongcheng Biochemicals Limited Company of Shandong Province in China. CS was from bovine cartilage, porcine cartilage, and shark cartilage separately. There were 35 samples from different batches of porcine CS and shark CS, respectively, and 26 samples from disparate batches of bovine CS.

2.1.2. Other chemicals

Chondroitinase ABC was from Sigma, shark CS standard substance was from European Pharmacopeia (EP), bovine CS standard substance was from United States Pharmacopeia (USP), porcine CS standard substance was from National Institute for the Control of Pharmaceutical and Biological Products of China (NICPBP). All the other reagents were analytical grade.

2.2. Methods

2.2.1. HPLC method

HPLC equipment was from Dionex (pump mod. LPG3400SD, UV detector mod. VWD3100, software Chromeleon V. 6.80). The samples were analyzed by strong anion-exchange separation using a 250 mm × 4.6 mm stainless-steel column Hypersil SAX (from Thermo Fisher Scientific Inc.) and the UV detector was set at 232 nm. The mobile phase consisted of pH 3.5 hydrochloric acid solution (mobile phase A) and 2 M sodium chloride solution (pH = 3.5, mobile phase B). The elution was isocratic for the first 4 min at 100% of phase A, changed to 50/50 (v/v) A/B in following 41 min at a flow rate of 1 ml/min. The column temperature was maintained at 35 °C.

Three batches of samples were chosen from each origin of CS by random sampling method. About 100 mg CS samples were dissolved in 10 ml deionized water and filtrated through a 0.45 μm membrane, then 100 μl filtrate was treated with 100 μl of chondroitinase ABC (0.1 U 100 μl^{-1}) in 800 μl Tris buffer pH 8.0 at 37 °C for 1 h. The reaction was blocked by boiling the solution for 5 min. The solution was centrifuged at 10,000 rpm for 20 min and then the supernatant was further filtrated through a 0.45 μm membrane. Finally, 20 μl filtrate was injected into HPLC for analysis.

2.2.2. Reference method

The origins of cartilage were all identified by very experienced workers to guarantee the origins of CS samples, and all the samples were produced in accordance with GMP requirements, and the source can be traced back.

2.2.3. NIR method

2.2.3.1. Apparatus. CS samples were scanned by Fourier-transform near infrared spectroscopy (Antaris MX, Thermo Fisher, USA) with InGaAs detector and the system software RUSULT which was used to collect NIR data.

2.2.3.2. NIR measurement. The spectra were collected at room temperature (about 23 °C) and the humidity was steady in the laboratory. All samples were loaded in glass vials, and each spectrum was the average of 32 scans with a resolution 4 cm^{-1} using fiber optic probe. The spectral range was between 10,000 cm^{-1} and 4000 cm^{-1}, and background spectrum (32 scans) was taken before measurement of every sample in order to eliminate the effect caused by background. The measurement time of each sample was less than 1 min.

2.2.3.3. Data processing. SVM_GUI v2.0 written by faruto was downloaded from http://www.matlabsky.com/thread-9333-1-1.html. The programs were run in the soft system MATLAB2010a (Mathworks Inc., USA). The Unscrambler (CAMO, Norway) software was used for the pretreatment of raw data.

2.2.3.4. Sample dividing. The samples were divided into two sets, including training set and testing set. There were several methods used for sample dividing like random sampling (RS) method, KS algorithm method [29], and sample set partitioning based on joint *x–y* distances (SPXY) method [30]. In this study, two subsets were selected by software based on KS in MATLAB with the program written by Michal Daszykowski in the University of Silesia.

There were 66 samples in training subset including 25 shark CS, 25 porcine CS and 16 bovine CS and 30 samples in the remaining testing subset including 10 shark CS, 10 porcine CS and 10 bovine CS.

2.2.3.5. Spectral transform. All the 96 spectra were pretreated by four different spectral transform methods. They were SG smoothing with 15 points, first derivative and SG smoothing with 15 points (SG-1st derivative), MSC and SNV, all of which were taken in Unscrambler 9.7.

2.2.3.6. Selection of spectra region. In this study, the value Q_s was used to select the spectra region [23], the equation was as follows:

$$Q_s = \frac{S_{ter}}{S_{tra}} \quad (1)$$

where S_{ter} is the standard deviation of mean absorption at the same wave number of each CS origin and S_{tra} is the mean absorption of standard deviation at the same wave number of each CS origin.

In the research, upper quartile of the full spectra wavenumbers was set as threshold value.

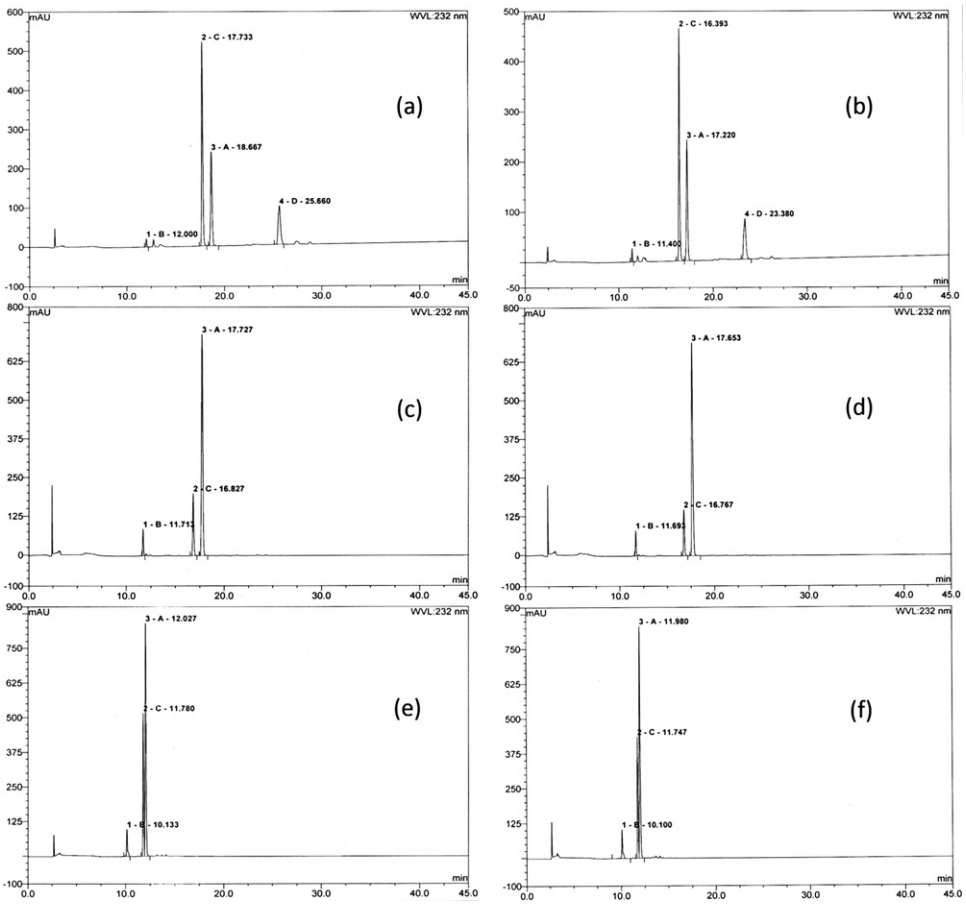

Fig. 2. Chromatogram of CS from different origins separated by HPLC at 232 nm (a) shark CS from EP, (b) shark CS sample, (c) porcine CS from NICPBP, (d) porcine CS sample, (e) bovine CS from USP, and (f) bovine CS sample.

2.2.3.7. Model efficiency estimation. In order to characterize prediction ability of a created classification model, the recognition rate and rejection rate were used. The equations were as follows:

$$\text{recognition rate} = \frac{N_r}{N_1} \times 100\% \quad (2)$$

$$\text{rejection rate} = \frac{N_{re}}{N_2} \times 100\% \quad (3)$$

where N_r refers to the number of rightly recognized samples of its own origin; N_1 refers to the number of samples of its own origin; N_{re} refers to the number of rightly refused samples of other origins; N_2 refers to the number of samples of other origins.

2.2.4. SVM classification

A function called radial basis function (RBF) was selected as kernel function in this study, which can be used to handle the problem of nonlinearity between case labels and attributes, and a "grid-search" was employed to identify c and γ with fivefold (5-fold) cross-validation [31]. Moreover, the parameter of recognition rate and rejection rate were applied to evaluate the SVM model.

3. Results and discussion

3.1. HPLC results

Fig. 2 shows the chromatogram of CS from three different origins with a good resolution of peaks. It indicates that CSs from different origins are mainly constituted of different percentages of disaccharides monosulfated in positions 4 and 6 of *N*-acetyl-D-galactosamine. Table 1 shows the average percentages of disaccharides unit of CS-A and CS-C from three origins. It demonstrates the feasibility to use NIR to identify the origin of CS.

Table 1
Percentages of disaccharides unit of CS-A and CS-C from three different origins.

Disaccharides unit of CS	Beef trachea (%)		Porcine trachea (%)		Shark cartilage (%)	
	A[a]	B[b]	A	B	A	B
ΔdiA4S[c]	56.7	64.2 ± 1.0	79.6	80.1 ± 1.2	29.6	31.0 ± 0.8
ΔdiA6S[d]	33.0	28.4 ± 0.1	16.5	14.7 ± 0.1	39.2	49.2 ± 1.2

The data were from three independent experiments.
[a] Percentages were from Ref. [14].
[b] Percentages were evaluated by HPLC.
[c] ΔdiA4S = α-ΔUA-1 → 3-GalNAc(4SO_4); UA, D-glucuronic acid; GalNAc, *N*-acetyl-D-galactosamine monosulfated at position 4.
[d] ΔdiA6S S = α-ΔUA-1 → 3-GalNAc(6SO_4); UA, D-glucuronic acid; GalNAc, *N*-acetyl-D-galactosamine monosulfated at position 6.

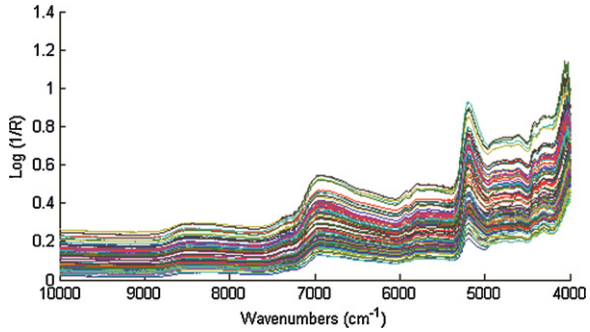

Fig. 3. Raw spectra of 96 samples.

3.2. Spectra investigation

Fig. 3 shows the spectra of 96 different batches from three origins, and it indicates that it is difficult to find specific bands in raw NIR spectra. It is composed of overtones and combinations of fundamental vibrational groups. In Fig. 3 the spectra have baseline drift caused by the particle size and light scatter. In order to solve the problem, some spectral transform methods were introduced including SG smoothing with 15 points, SG-1st derivative, MSC and SNV (Fig. 4). SG smoothing had little effect on baseline drift because the raw spectra were very smooth. MSC and SNV are used to eliminate the effect caused by particle size, because the particle size was a little different, the pretreatment furnished better results. SG-1st derivative was used to eliminate the noise and separate the overlapping peak; as a result the peaks became more apparent.

3.3. Selection of spectra region

The spectral region was selected based on the method 2.2.3.6, and the spectral regions which could reflect the difference above the dotted line were selected shown in Fig. 5. From Fig. 5, one can see that SG smoothing made no difference to the raw spectra. MSC and SNV had the same effect on the raw spectra, but the threshold values were quite different from each other. The Q_s value for MSC and SNV were 30.64 and 0.98. MSC amplifying the difference among difference origins got the highest Q_s SG-1st derivative gave some dispersive wavenumber regions which were different from others; maybe this was because the SG-1st derivative enhanced the signal to noise ratio, then some useful variables were extracted.

3.4. Prediction capability of SVM model

SVM model was established based on the full spectra region and the selected spectra region. RBF kernel was a first choice especially when the relation between origins and variables was nonlinear. A PLS-DA method was used which based on linear relation, but the results were not good. The polynomial kernel has more hyperparameters which influenced the complexity of model selection than the RBF kernel. So a RBF kernel was selected. The parameter recognition rate and rejection rate were used to evaluate the model, and the higher the recognition rate and rejection rate were, the better the model was. Table 2 shows the recognition rate and rejection rate of SVM model based on full spectra region with different spectral pretreatment. Table 3 showed the recognition rate and rejection rate of SVM model based on selected spectra region with different spectral pretreatment. Table 2 and 3 indicated that pretreatment was necessary and best result could be obtained with SG-1st derivative and MSC. But the result of SG-1st derivative was better than MSC, because useful variables were extracted and the differences among three origins were amplified. The pretreatment was easy to master, while doing MSC pretreatment, a suitable "ideal spectrum" had to be selected, it brought about some difficulties for blind test. SNV and MSC were both used to eliminate the negative influence caused by particle size and light scatter, but SNV had worse results than MSC. It could be explained that the difference of classes were reduced by SNV. Table 4 shows the average recognition rate and rejection rate of different SVM models. Prediction capability of SVM model based on selected spectra region was lower than that based on full spectra except SG-1st derivative

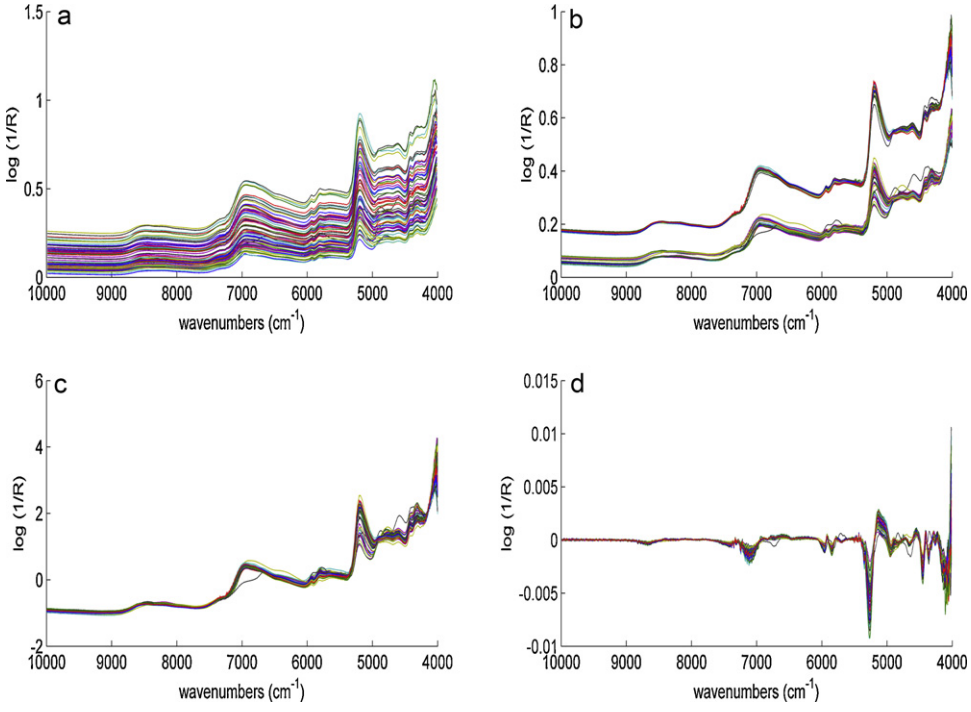

Fig. 4. Chondroitin sulfate spectra after different pretreatment methods (a) SG with 15 points, (b) MSC, (C) SNV, and (d) SG-1st derivative.

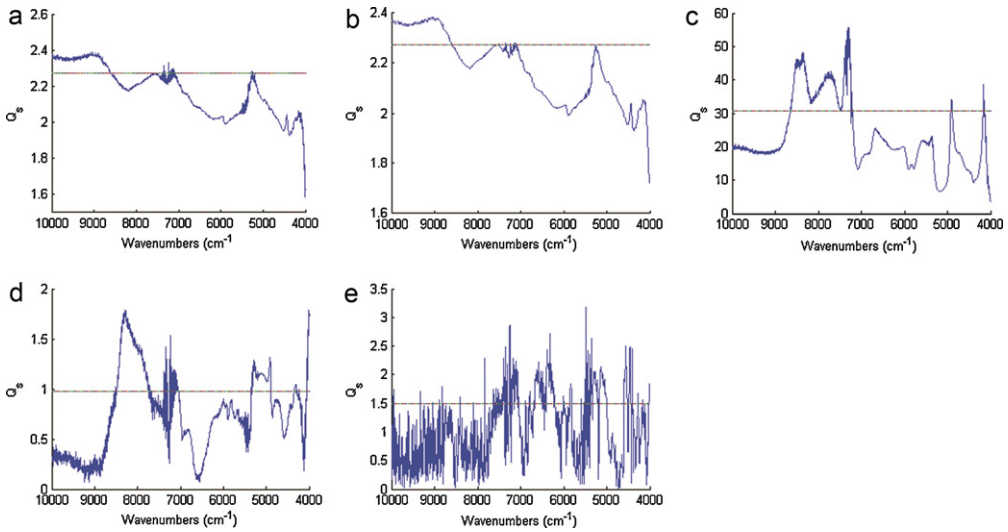

Fig. 5. Spectra region selection based on different pretreatment (a) raw spectra, (b) SG with 15 points, (c) MSC, (d) SNV, and (e) SG-1st derivative.

Table 2
Recognition rate and rejection rate of SVM model based on full spectral region with different pretreatment methods.

Pretreat method	Bovine		Porcine		Shark	
	Recognition rate (%)	Rejection rate (%)	Recognition rate (%)	Rejection rate (%)	Recognition rate (%)	Rejection rate (%)
Raw spectra	90	95	90	95	100	100
SG-1st derivative	100	100	100	100	100	100
SNV	90	95	90	95	100	100
MSC	100	100	100	100	100	100
SG smoothing	90	95	90	95	100	100

Table 3
Recognition rate and rejection rate of SVM model based on selected spectral region with different pretreatment methods.

Pretreat method	Bovine		Porcine		Shark	
	Recognition rate (%)	Rejection rate (%)	Recognition rate (%)	Rejection rate (%)	Recognition rate (%)	Rejection rate (%)
Raw spectra	60	95	90	80	100	100
SG-1st derivative	100	100	100	100	100	100
SNV	90	90	90	95	90	100
MSC	100	100	100	100	100	100
SG smoothing	50	75	50	75	100	100

Table 4
Average recognition rate and rejection rate of different SVM models.

Pretreat method	Full spectral region		Selected region	
	Average recognition rate (%)	Average rejection rate (%)	Average recognition rate (%)	Average rejection rate (%)
Raw spectra	93.33	96.67	83.33	91.67
SG-1st derivative	100	100	100	100
SNV	96.67	96.67	90	95
MSC	100	100	100	100
SG smoothing	93.33	96.67	75	83.33

and MSC SVM model. It indicated that SG smoothing, SNV made no means to extract useful variables. MSC had a good result, but it brought a little difficulty in choosing a suitable "ideal spectrum". Compared with SG-1st derivative SVM model based on full spectra and selected spectra, it manifested the selected spectra was characteristic region for discrimination, and the search time spending on selected spectra model was shorter. So it was a good model for discriminating different origins.

4. Conclusion

The results demonstrated the feasibility to use near infrared spectroscopy to identify CS of different origins. Compared with different SVM models based on different pretreatment methods, SG-1st derivative SVM model based selected spectra had the best result. The recognition rate and rejection rate were both 100%, and the selected spectra can provide a good advice for special

equipment research to reduce the cost of apparatus. The method is fast and non-destructive, so it can be used for quality assurance in factory.

Considering the number of sample was not large enough and all samples were from one factory, the model needs optimization and further confirmation in the future.

Acknowledgements

We are grateful for financial support from National Glycoengineering Research Center of China and Shandong institute for Drug Control. Then our thanks will goes to Yantai Dongcheng Biochemicals Limited Company of Shandong Province in China for providing CS samples. Additionally, we also express our gratitude to Guo Tingting for her good suggestions.

References

[1] F.N. Lamari, N.K. Karamanos, Structure of chondroitin sulfate, in: V. Nicola (Ed.), Advances in Pharmacology, Academic Press, 2006, pp. 33–48.
[2] R. Lauder, Complement Ther. Med. 17 (2009) 56–62.
[3] N. Volpi, J. Pharm. Sci. 96 (2007) 3168–3180.
[4] S. Sakai, E. Otake, T. Toida, Y. Goda, Chem. Pharm. Bull. 55 (2007) 299–303.
[5] C.X. Sun, H.C. Zang, X.M. Liu, Q. Dong, L. Li, F.S. Wang, L.Y. Sui, J. Pharm. Biomed. Anal. 51 (2010) 1060–1063.
[6] Q. Dong, H.C. Zang, A.H. Liu, G.L. Yang, C.X. Sun, L.Y. Sui, P. Wang, L. Li, J. Pharm. Biomed. Anal. 53 (2010) 274–278.
[7] Y. Roggo, P. Chalus, L. Maurer, C. Lema-Martinez, A. Edmond, N. Jent, J. Pharm. Biomed. Anal. 44 (2007) 683–700.
[8] R.M. Balabin, E.I. Lomakina, Analyst 136 (2011) 1703–1712.
[9] R.M. Balabin, R.Z. Safieva, Anal. Chim. Acta 689 (2011) 190–197.
[10] M.P. Freitas, A. Sabadin, L.M. Silva, F.M. Giannotti, D.A. do Couto, E. Tonhi, R.S. Medeiros, G.L. Coco, V.F.T. Russo, J.A. Martins, J. Pharm. Biomed. Anal. 39 (2005) 17–21.
[11] R.M. Balabin, R.Z. Safieva, E.I. Lomakina, Microchem. J. 98 (2011) 121–128.
[12] R.M. Balabin, E.I. Lomakina, R.Z. Safieva, Fuel 90 (2011) 2007–2015.
[13] R.M. Balabin, R.Z. Syunyaev, T. Schmid, J. Stadler, E.I. Lomakina, R. Zenobi, Energy Fuels 25 (2010) 189–196.
[14] N. Volpi, Carbohydr. Polym. 55 (2004) 273–281.
[15] L. Silva, Adv. Pharmacol. 53 (2006) 21–31.
[16] W.Z. Lu, Modern Near Infrared Spectroscopy Analytical Technology, second ed., China Petrochemical Press, Beijing, 2007.
[17] R.M. Balabin, R.Z. Safieva, Energy Fuels 25 (2011) 2373–2382.
[18] R.M. Balabin, S.V. Smirnov, Talanta 85 (2011) 562–568.
[19] X.B. Zou, J.W. Zhao, M.J. Povey, M. Holmes, M. Hanpin, Anal. Chim. Acta 667 (2010) 14–32.
[20] K. Kjeldahl, R. Bro, J. Chemometr. 24 (2010).
[21] M.J.C. Pontes, R.K.H. Galvão, M.C.U. Araújo, P.N.T. Moreira, O.D.P. Neto, G.E. José, T.C.B. Saldanha, Chemometr. Intell. Lab. 78 (2005) 11–18.
[22] R.M. Balabin, S.V. Smirnov, Anal. Chim. Acta 692 (2011) 63–72.
[23] T.T. Guo, W.J. Wu, Q. Su, S.J. Wang, D. An, Trans. Chin. Soc. Agric. Mach. 40 (2009) 87–92.
[24] W.C. Lu, N.Y. Chen, C.Z. Ye, G.Z. Li, Comput. Appl. Chem. 6 (2002).
[25] M.W.B. Trotter, B.F. Buxton, S.B. Holden, Meas. Contr. 34 (2001) 235–239.
[26] R. Burbidge, M. Trotter, B. Buxton, S. Holden, Comput. Chem. 26 (2001) 5–14.
[27] C. Bodson, W. Dewé, P. Hubert, L. Delattre, J. Pharm. Biomed. Anal. 41 (2006) 783–790.
[28] R.M. Balabin, R.Z. Safieva, E.I. Lomakina, Anal. Chim. Acta 671 (2010) 27–35.
[29] R.W. Kennard, L.A. Stone, Technometrics (1969) 137–148.
[30] R.K.H. Galvão, M.C.U. Araujo, G.E. José, M.J.C. Pontes, E.C. Silva, T.C.B. Saldanha, Talanta 67 (2005) 736–740.
[31] C. Hsu, C. Chang, C. Lin, Citeseer (2003).

Journal of Pharmaceutical and Biomedical Analysis 61 (2012) 230–236

Contents lists available at SciVerse ScienceDirect

Journal of Pharmaceutical and Biomedical Analysis

journal homepage: www.elsevier.com/locate/jpba

Development of chromatographic methods for the determination of genotoxic impurities in cloperastine fendizoate

Antonia García[a], Francisco J. Rupérez[a], Florencia Ceppa[a,b], Federica Pellati[b], Coral Barbas[a,*]

[a] Center for Metabolomics and Bioanalysis (CEMBIO), Facultad de Farmacia, Universidad San Pablo-CEU, Urbanización Montepríncipe, Boadilla del Monte, 28668 Madrid, Spain
[b] Department of Pharmaceutical Sciences, University of Modena and Reggio Emilia, Via G. Campi 183, 41125 Modena, Italy

ARTICLE INFO

Article history:
Received 18 November 2011
Received in revised form
10 December 2011
Accepted 13 December 2011
Available online 19 December 2011

Keywords:
Cloperastine fendizoate
Genotoxic impurities
Sulfonate esters
Alkyl halides
Threshold of toxicological concern
Limit test
HPLC
GC

ABSTRACT

The classification of an impurity of a drug substance as genotoxic means that the "threshold of toxicological concern" (TTC) value of 1.5 μg/day intake, considered to be associated with an acceptable risk, should be the admissible limit in the raw material and that leads to new analytical challenges. In this study, reliable chromatographic methods were developed and applied as limit tests for the control of three genotoxic impurities (GTIs) in cloperastine fendizoate, drug widely used as an antitussive active pharmaceutical ingredient (API). In particular, GC–MS was applied to the determination of one alkyl halide (2-chloroethanol, 2-CE), while HPLC-DAD was selected for the analysis of two sulfonate esters (methyl *p*-toluenesulfonate, MPTS, and 2-chloroethyl *p*-toluenesulfonate, CEPTS).

Regarding GC–MS, strong anion-exchange (SAX)-SPE was applied to remove fendizoate from the sample solutions, due its low volatility and its high amount in the raw material. The GC–MS analysis was performed on a Factor Four VF-23ms capillary column (30 m × 0.25 mm I.D., film thickness 0.25 μm, Varian). Single ion-monitoring (SIM) detection mode was set at *m/z* 80.

In the case of HPLC-DAD, a suitable optimization of the chromatographic conditions was carried out in order to obtain a good separation of the impurity peaks from the drug substance peaks. The optimized method utilizes a SymmetryShield RP_8 column (250 mm × 4.6 mm, 5 μm, Waters) kept at 50 °C, with phosphate buffer (pH 3.0; 10 mM)–methanol (containing 10% ACN) (45:55, v/v) as the mobile phase, at the flow-rate of 1.7 mL/min and UV detection at 227 nm. The required sensitivity level was achieved by injecting 80 μL of sample solution, purified from fendizoate by SAX-SPE, followed by a 1:1 (v/v) dilution of the SPE eluate with water.

For both GC–MS and HPLC-DAD, the method validation was performed in relation to specificity and limit of detection (LOD), as required by ICH guidelines in relation to limit assays. The developed methods were successfully applied for the determination of GTIs in five different batches of cloperastine fendizoate. In all the analyzed batches, the three target GTIs were below the concentration limit.

© 2012 Elsevier B.V. All rights reserved.

1. Introduction

D,L-Cloperastine, i.e. 1-{2-[(4-chloro-phenyl)-phenyl-methoxy]-ethyl}-piperidine, is a drug with a central antitussive effect and it is also endowed with an antihistaminic (sharing an ethylamine moiety with H_1 receptor antagonists) and papaverine-like activity similar to codeine, but without its narcotic effects [1]. Pharmacological studies have shown that this compound acts on the cough center, without depressing the respiratory center [1]. The initial response at the therapeutic dose range (10–20 mg three times daily for adults) is 20–30 min after oral administration [1]. Moreover, the duration of action of a single dose of cloperastine is 3–4 h [1]. Cloperastine is used both as hydrochloride and fendizoate (Fig. 1) salts in view of its good tolerability and availability as syrup, drop and tablet formulations (the last being only for adult administration) [1]. A pharmacological and clinical overview of cloperastine in the treatment of cough indicated that this compound can be safely used in a wide section of population (children, adolescents and adults), according to the indications on the labelling and appropriate medical evaluation [1].

The manufacturing synthesis of cloperastine consists of four steps, as shown in Fig. 2. At the end of this synthetic route, the hydrochloride salt can be easily converted into the fendizoate salt by reaction with fendizoic acid. In the second step of the overall synthesis (Fig. 2), *p*-toluenesulfonic acid, used to introduce a good leaving group in the reagent, reacting with both 2-chloroethanol (2-CE) and methanol (which is present in the reaction mixture), can

Abbreviations: 2-CE, 2-chloroethanol; MPTS, methyl *p*-toluenesulfonate; CEPTS, 2-chloroethyl *p*-toluenesulfonate; API, active pharmaceutical ingredient; GTI, genotoxic impurity; SS, solvent solution.

* Corresponding author. Tel.: +34 913724711; fax: +34 913510474.
E-mail address: cbarbas@ceu.es (C. Barbas).

0731-7085/$ – see front matter © 2012 Elsevier B.V. All rights reserved.
doi:10.1016/j.jpba.2011.12.014

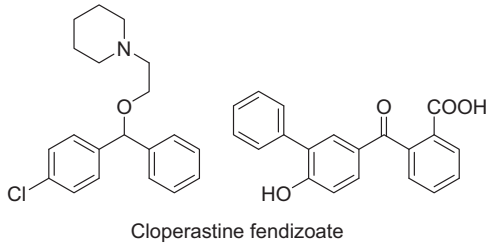

Fig. 1. Chemical structure of cloperastine fendizoate.

originate two alkyl esters of aryl sulfonic acids [2,3], namely methyl *p*-toluenesulfonate (MPTS) and 2-chloroethyl *p*-toluenesulfonate (CEPTS). The reaction between short-chain alcoholic solvents and sulfonic acids to give sulfonate esters has already been described in the literature [2,4,5]. In these systems, sulfonic acid ester formation occurs in a two stage equilibrium reaction (Fig. 3), based on the protonation of the alcohol to form an oxonium ion, followed by nucleophilic displacement of the hydroxonium moiety by sulfonate anion, which produces the alkyl sulfonate [2,4,5]. Significant concentration of protonated alcohol is needed for the reaction to proceed by this pathway [2]. In fact, alcohols are weakly acidic and so not readily protonated [2]. Moreover, the sulfonate anion is a poor nucleophile, owing to delocalization of the negative charge over the three oxygen atoms, and any water formed during the reaction has the potential to hydrolize any ester to its constituents acid and alcohol [2]. Even though the formation of sulfonate esters in this kind of system is kinetically slow and typically unfavored [2], trace amounts of these compounds could be produced following this pathway [6]. Sulfonate esters are known to be DNA reactive genotoxins and possibly carcinogenic alkylating agents [3,7,8].

Furthermore, alkyl halides, such 2-CE, frequently used as reagents in chemical synthesis of active pharmaceutical ingredients (APIs), are well-known alkylating agents [3,7,9]. Any unreacted 2-CE is an obvious potential genotoxic impurity (GTI) in cloperastine fendizoate. On the other hand, MPTS and CEPTS, which can be considered as by-products of the reaction, may also occur as GTIs into the final API.

GTIs may induce genetic mutations, chromosomal rearrangements or breaks [3], and have the potential to cause cancer in humans [3]. Therefore, exposure to even low levels of such impurities in API is of significant toxicological concern [3].

The potential presence of GTIs in APIs has attracted the attention of regulatory authorities [10,11]. In 2006, the European Medicines Agency (EMEA)'s Committee for Medicinal Products for Human Use (CHMP) has published guidelines regarding the limits for GTIs [12]. A "Threshold of Toxicological Concern" (TTC) approaches has been proposed, that refers to a threshold exposure level to compounds which will not pose a significant risk of carcinogenicity or other toxic effects [10,11,13]. A TTC value of 1.5 μg/person/day intake of GTI is considered to be associated with acceptable risk [10,11]. The concentration limit in ppm of GTI permitted in a drug substance is the ratio of TTC (μg/day) and daily dose (g/day).

The concentration limit for a GTI is the key factor in determining the sensitivity requirements for the analytical method to be used [10,11]. The analytical technique selection can be performed by dividing GTIs into two groups based on their volatility [3,10,11].

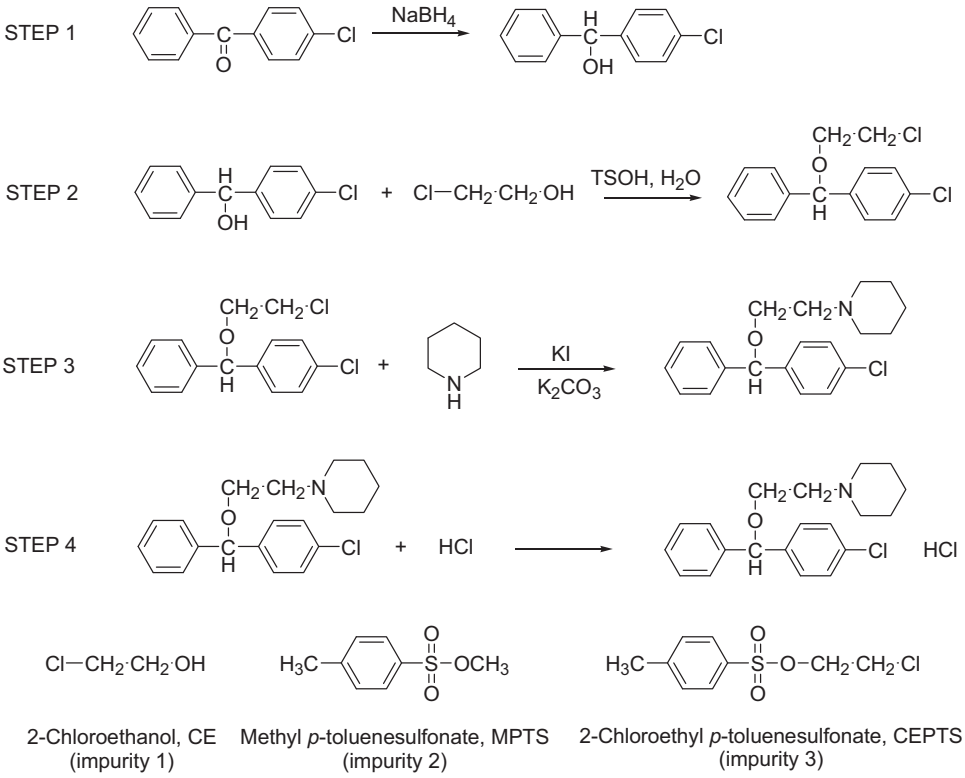

Fig. 2. Manufacturing process of cloperastine, showing the three GTIs originated from step 2.

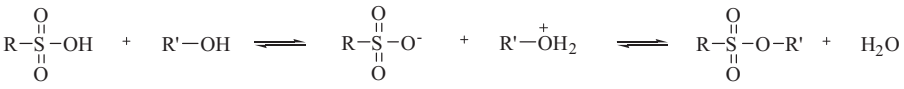

Fig. 3. Formation of sulfonate esters from a sulfonic acid and a short-chain aliphatic alcohol.

HPLC-UV shall be selected for non-volatile GTIs as the first choice due to the technical simplicity and availability [3,11]. Volatile GTIs can be analyzed by GC with flame ionization detector (FID) or other more specific detectors, such as ECD or NPD [3,10,11]. GC–MS, operating in the single ion-monitoring (SIM) mode, offers the most sensitive and selective detection, reduced background noise and it is less prone to interferences for low level analysis of GTIs [3,10,11].

In the case of cloperastine, GC–MS and HPLC–MS/MS have been described in the literature for the analysis of this active compound in human plasma [14,15]. However, final API determination methods are not suitable for GTI determination, since the concentration limit to be detected is much lower [11]. In the light of all the above, the aim of this work was the development of a suitable chromatographic technique for the reliable limit test of the three GTIs of cloperastine fendizoate encountered in the manufacturing process.

2. Experimental

2.1. Chemicals and solvents

Cloperastine fendizoate standard (HPLC purity 99.9%) and cloperastine fendizoate raw material (5 different batches) were kindly provided by CINFA S.A. (Pamplona, Spain). 2-CE (HPLC purity 99%) was from Panreac (Barcelona, Spain). MPTS (HPLC purity 98%) and CEPTS (HPLC purity 97%) were from Aldrich (Madrid, Spain). *p*-Toluenesulfonic acid, HPLC grade methanol and acetonitrile (ACN) were purchased from Sigma (Madrid, Spain). Phosphoric acid (H_3PO_4) (85%) was from Carlo Erba Reagenti (Milan, Italy). KOH and ammonia (30%) were from Panreac. Water was purified with a Milli-Q plus system from Millipore (Bedford, MA, USA).

2.2. Chromatographic systems and conditions

GC–MS analyses were performed on a 7890 gas chromatograph (Agilent Technologies, Waldbronn, Germany), coupled with a 5975 C single quadrupole mass spectrometer (Agilent Technologies). Compounds were separated on a Factor Four VF-23ms capillary column (30 m × 0.25 mm I.D., film thickness 0.25 μm, Varian). The initial column temperature was set at 60 °C, then programmed at 10 °C min^{-1} to 250 °C, which was held for 20 min. The total analysis time was 39 min. The injection volume was 3.0 μL, with a split ratio 3:1. Helium was used as the carrier gas at a flow-rate 0.8 mL/min. Injector, ion-source and quadrupole temperature was set at 250, 230 and 150 °C, respectively. MS detection was performed with electron impact (EI) mode at 70 eV, over the *m*/*z* range 49–80. SIM acquisition mode was performed at *m*/*z* 80 for 2-CE.

HPLC-DAD analyses were carried out on a System Gold apparatus (Beckman-Coulter, Palo Alto, CA, USA), consisting of a binary pump (Mod. 126), an automatic injector, a thermostatted column compartment (Mod 507) and a diode-array detector (DAD, Mod. 168). The optimized method was performed on a SymmetryShield RP-8 column (250 mm × 4.6 mm I.D., 5 μm, Waters). The mobile phase consisted of phosphate buffer (pH 3.0; 10 mM)–methanol (containing 10% ACN) (45:55, v/v), under isocratic conditions. The column temperature was set at 50 °C. The flow-rate was 1.7 mL/min. The injection volume was 80 μL. UV detection was set at 227 nm. The total analysis time was 15 min.

2.3. GC standard solutions and sample preparation

The solvent solution (SS) used in GC–MS for both 2-CE standard and samples of cloperastine fendizoate was basified methanol, which was prepared by adding 500 μL of ammonia to 250 mL of methanol (pH = 9.0). 2-CE stock solution was prepared by weighing approximately 10.0 mg of this substance and dissolving it with SS in a 10 mL volumetric flask. The concentration of the impurity in this solution was 1000 mg/L. An intermediate solution of 2-CE at 10 mg/L was prepared by dilution of its stock solution with SS. Working solutions of 2-CE at 100, 25 and 10 μg/L were prepared from the intermediate solution by further dilution with SS.

In the case of cloperastine fendizoate samples, a weighed amount of active principle (approximately 50.0 mg) was put in a 25 mL volumetric flask and diluted to volume with SS (2000 mg/L).

2.4. HPLC standard solutions and sample preparation

The SS used in HPLC-DAD for both MPTS and CEPTS standards and samples of cloperastine fendizoate was basified methanol (pH = 9.0). MTPS and CEPTS stock solutions were prepared by approximately weighing 10.0 mg of these compounds, which were dissolved with SS in a 10 mL volumetric flask (1000 mg/L). An intermediate solution of MTPS and CEPTS at 100 mg/L was prepared by dilution of its stock solution with SS. Working solutions of MTPS and CEPTS at 1000, 100 and 25 μg/L were prepared by further dilutions with SS.

In the case of cloperastine fendizoate samples, a weighed amount of active principle (approximately 50.0 mg) was put in a 25 mL volumetric flask and diluted to volume with SS (2000 mg/L).

All the solutions were filtered with 0.45 μm nylon filters prior to the injection.

2.5. Sample purification

Solid-phase extraction (SPE) was applied to remove fendizoate from cloperastine fendizoate solutions before GC–MS and HPLC-DAD analyses. The Discovery DSC-SAX cartridge (1 g, 6 mL) (Supelco, Bellefonte, PA, USA) was prepared by pre-washing with 12 mL of SS, using a vacuum manifold. The cloperastine fendizoate solution (6 mL) was then loaded and the eluate was collected into a HPLC vial and subjected to HPLC-DAD analysis to check the efficiency of the purification procedure. The GC–MS analysis was performed only in case of complete removal of fendizoate from the samples. In the case of HPLC-DAD analysis, the SPE eluate was further diluted 1:1 (v/v) with water before the injection into the HPLC system.

2.6. Method validation

The method validation was performed in relation to specificity and limit of detection (LOD), since the developed methods are intended as limit assays for the determination of GTIs in a final API [16]. These parameters were validated in agreement with the international requirements for analytical techniques for the quality control of pharmaceuticals (ICH guidelines) [16].

In particular, specificity was demonstrated by obtaining positive results from samples containing the target GTIs, coupled with negative results from samples (blanks) which do not contain these analytes. In agreement with ICH guidelines, representative chromatograms were selected to demonstrate specificity and individual components were appropriately labeled. Furthermore, peak purity tests were carried out by both GC–MS and HPLC-DAD to show that the analyte chromatographic peak was not attributable to more than one component.

Regarding LOD, it was evaluated considering the analyte concentration that would yield a signal-to-noise (S/N) value of 3. The LOD values were experimentally verified by injections of standard solutions of the compounds at the LOD concentrations.

2.7. Software

The GC system was monitored using the ChemStation G1701 (E.02.00493) MSD software (Agilent Technologies). For peak

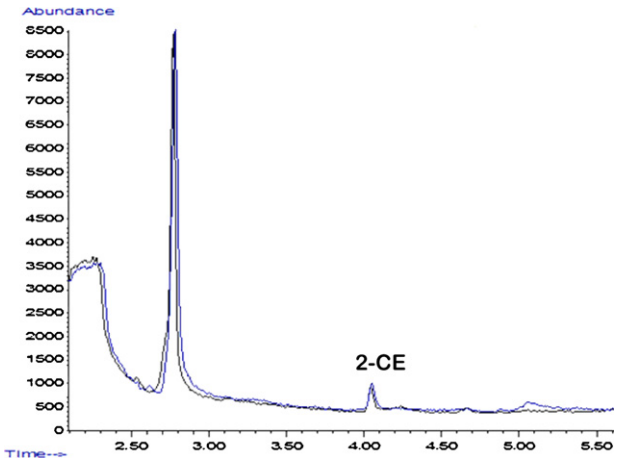

Fig. 4. GC–MS analysis of 2-CE at 25 μg/L, before (black line) and after SAX-SPE (blue line). Column: Factor Four VF-23ms (30 m × 0.25 mm I.D., film thickness 0.25 μm, Varian). Carrier gas: helium. Program temperature: initial 60 °C, then at 10 °C min^{-1} to 250 °C, held for 20 min. Flow-rate: 0.8 mL/min. Injection volume: 3.0 μL, with a split ratio 3:1. MS detection: SIM at *m*/*z* 80. (For interpretation of the references to color in this figure legend, the reader is referred to the web version of the article.)

identification the NIST 2 (2008) mass spectral database was used. The software for controlling the HPLC instrument and for processing its data was 32 carats (8.0) (Beckman-Coulter). The validation calculations were carried out with Microsoft Excel 2003 version Office Package.

3. Results and discussion

3.1. GC–MS method development

The first step of method development for the determination of GTIs in APIs is the appropriate selection of the analytical instrumentation, based on the molecular structure of the analytes and on the target concentration limit [3,10,11]. Based on the TTC limit of 1.5 μg/person/day and on the maximum adult daily dose for cloperastine fendizoate of 106.2 mg/person, its GTIs are required to be controlled at a concentration limit of 14 μg/g (ppm) in the raw material (drug substance), corresponding to 28 μg/L (ppb) in solution.

For GTIs represented by sulfonate esters and alkyl halides, analysts have often relied on the volatility of these alkylating agents and thus GC methodologies based on sensitive and selective MS detection have been developed [8,9]. In the case of alkyl and aryl sulfonic acids, derivatization has sometimes been employed before GC–MS [8]. In the light of this, GC–MS was initially selected in this study as a suitable technique for the determination of the three target GTIs in cloperastine fendizoate. However, due to the low volatility of fendizoate (m.p. 262–264 °C) and its high amount in the raw material, it was necessary to remove it from the samples before GC–MS analysis. For this reason a SPE procedure was carried out, based on the use of a strong anion-exchanger (SAX) on silica-based particles. For the GC–MS separation, a Factor Four VF-23ms capillary column, characterized by a highly substituted cyanopropyl stationary phase, was selected.

Preliminary GC–MS analyses of SAX-SPE purified solutions, containing cloperastine and related GTIs, showed a dramatic decrease in the peak intensity of MPTS, which was paralleled by the presence of new chromatographic peaks, which were not identifiable using the available mass spectra database. On the contrary, the chromatographic profile of 2-CE and CEPTS was not affected. This behaviour indicated that a degradation of MPTS occurred under the applied experimental conditions, that was thought to be caused by hydrolysis of the ester bond in the injection liner [8,17]. The degradation product of MPTS was further subjected to HPLC-DAD analysis, obtaining a good match with the retention time and UV spectrum of *p*-toluenesulfonic acid. The higher steric hindrance of the alkyl chain of CEPTS prevented the hydrolysis reaction of the ester bond of this compound.

To avoid laborious and time-consuming derivatization procedures, GC–MS was finally selected for the determination of 2-CE, which possesses a good volatility and chemical stability under the applied experimental conditions, while HPLC was considered to be more suitable for the analysis of MPTS and CEPTS. In order to achieve the required sensitivity level, MS detection was performed in the SIM mode. Although the fragment at *m*/*z* 49, which can be attributed to the α-cleavage of 2-CE, was considered the most suitable for the detection of this compound, several other interfering fragments were observed in the same region of the mass spectrum.

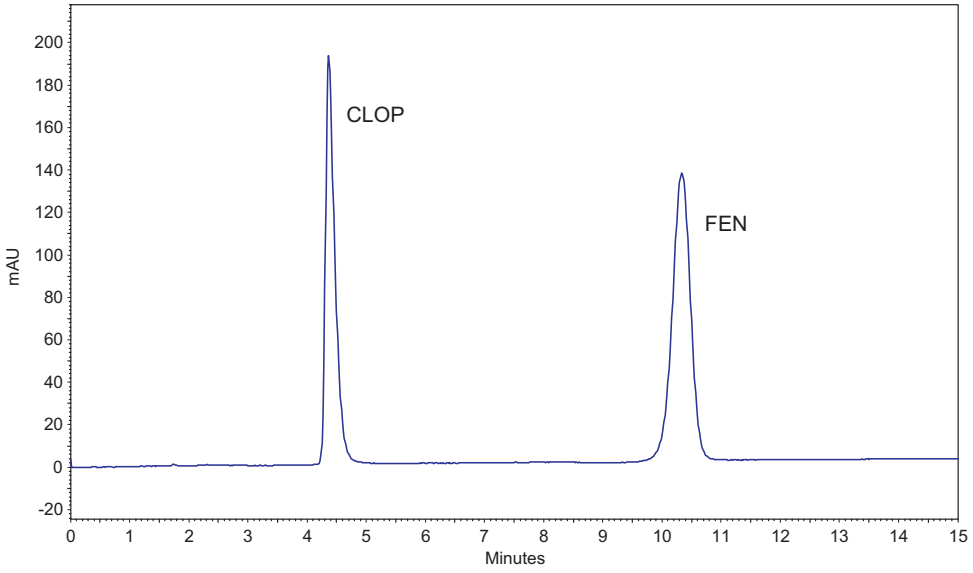

Fig. 5. HPLC-DAD analysis of cloperastine (CLOP) fendizoate (FEN) at 100 mg/L. Column: SymmetryShield RP_8 (250 mm × 4.6 mm, 5 μm, Waters). Mobile phase: phosphate buffer (pH 3.0; 10 mM)–methanol (45:55, v/v). Column temperature: 50 °C. Flow-rate: 1.7 mL/min. Injection volume: 15 μL. UV detection: 227 nm.

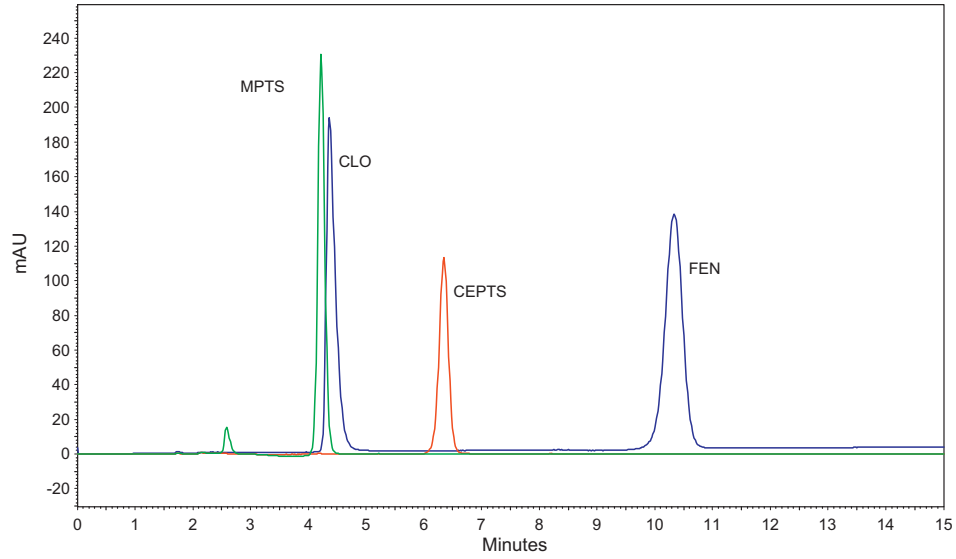

Fig. 6. HPLC-DAD analysis of cloperastine (CLOP) fendizoate (FEN) (blue line), MPTS (green line) and CEPTS (red line) at 100 mg/L. Column: SymmetryShield RP_8 (250 mm × 4.6 mm, 5 μm, Waters). Mobile phase: phosphate buffer (pH 3.0; 10 mM)–methanol (45:55, v/v). Column temperature: 50 °C. Flow-rate: 1.7 mL/min. Injection volume: 15 μL. UV detection: 227 nm. (For interpretation of the references to color in this figure legend, the reader is referred to the web version of the article.)

Therefore, SIM detection was performed at *m*/*z* 80, corresponding to the molecular ion of 2-CE. Fig. 4 shows the chromatograms obtained by the GC–MS analysis of a solution of 2-CE at 25 μg/L, before and after SAX-SPE.

3.2. HPLC-DAD method development

HPLC, almost exclusively in the reversed-phase mode, remains a key separation technique for those impurities that are insufficiently volatile and/or thermally labile for reliable GC analysis [3,10,11]. UV detector is the most widely used in pharmaceutical analysis and the most accessible in many laboratories [3,11]. Therefore, HPLC-UV represents the preferred choice for impurity analysis whenever feasible [3,11]. MPTS and other sulfonate esters have been previously analyzed in drug substances by means of HPLC–MS [17]. However, trace analysis HPLC–MS methods are generally undesired in the manufacturing environment, because of the complexity, cost and potential lack of robustness [3]. In view of the instrument simplicity, stability and availability, HPLC-DAD was therefore evaluated for the analysis of MPTS and CEPTS. Because ppm levels of GTIs are in the matrix with an extremely high level of API, a good separation of the analyte peaks from the main component is a critical aspect of the method development [3,18].

In this study, different stationary phases were evaluated to achieve a good separation of the impurity peaks from the drug substance peak. In order to obtain a short analysis time, various reversed-phase C_8 columns were tested, including Zorbax Eclipse XDB-C_8 150 mm × 4.6 mm, 5 μm, (Agilent Technologies, Santa Clara CA, USA), Discovery C_8 150 mm × 4.6 mm, 5 μm (Supelco, Bellefonte PA, USA), Nucleosil 100 C_8 150 mm × 4.6 mm, 5 μm (Teknokroma, Sant Cugat del Vallés, Spain), SymmetryShield RP_8 250 mm × 4.6 mm, 5 μm, (Waters, Milford MA, USA) and Luna

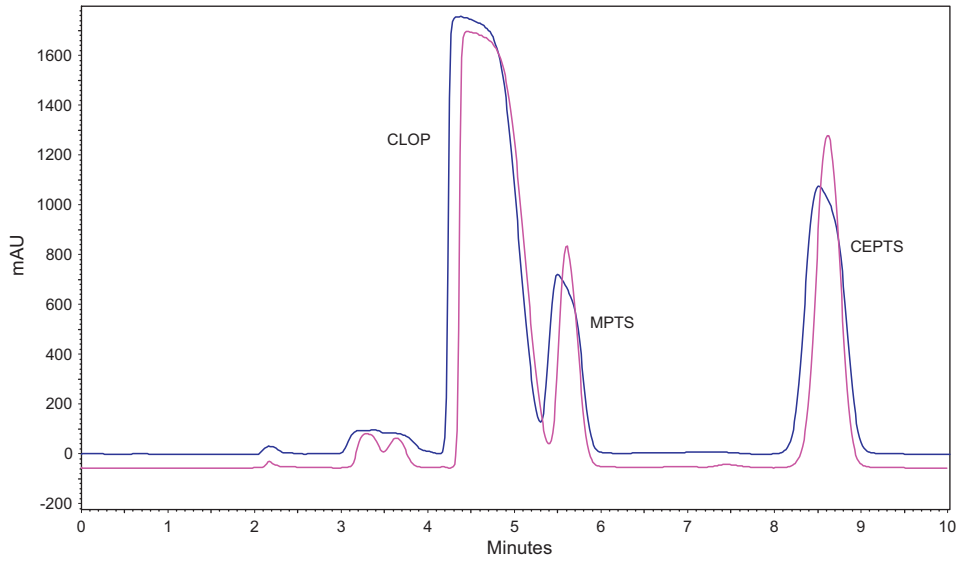

Fig. 7. HPLC-DAD analysis of cloperastine (CLOP) fendizoate (FEN) at 2000 mg/L, MPTS and CEPTS at 1000 mg/L, after SAX-SPE (blue line) and further water dilution (1:1, v/v) (pink line). Column: SymmetryShield RP_8 (250 mm × 4.6 mm, 5 μm, Waters). Mobile phase: phosphate buffer (pH 3.0; 10 mM)–methanol (with 10% ACN) (45:55, v/v). Column temperature: 50 °C. Flow-rate: 1.7 mL/min. Injection volume: 80 μL. UV detection: 227 nm. (For interpretation of the references to color in this figure legend, the reader is referred to the web version of the article.)

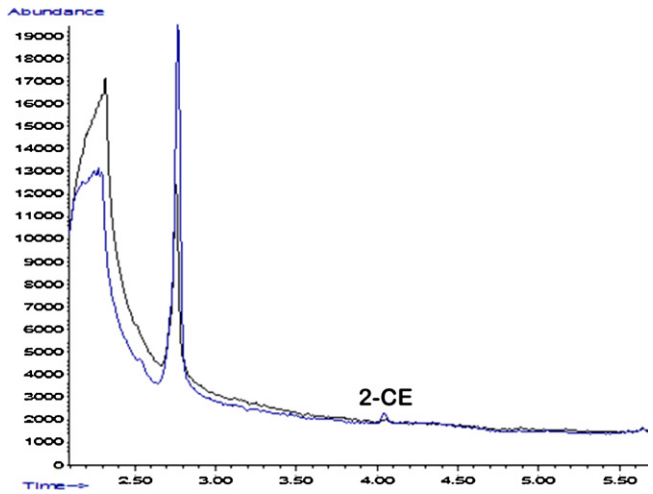

Fig. 8. GC–MS analysis of a blank solution (SS) (black line) and 2-CE at 10 μg/L (blue line). Column: Factor Four VF-23ms (30 m × 0.25 mm I.D., film thickness 0.25 μm, Varian). Carrier gas: helium. Program temperature: initial 60 °C, then at 10 °C min^{-1} to 250 °C, held for 20 min. Flow-rate: 0.8 mL/min. Injection volume: 3.0 μL, with a split ratio 3:1. MS detection: SIM at *m/z* 80. (For interpretation of the references to color in this figure legend, the reader is referred to the web version of the article.)

C_8 250 mm × 4.6 mm, 5 μm, (Phenomenex, Torrance CA, USA). The tested columns were checked under the same conditions, with a mobile phase consisting of phosphate buffer (pH 3.0; 10 mM)–methanol (45:55, v/v) and all of them were kept at 50 °C during the analysis. The flow-rate was set at 1.7 mL/min when the column was 250 mm long, and 1.0 mL/min for 150 mm. The injection volume was 15 μL. UV detection was set at 227 nm. The preliminary assays were developed by running the API (cloperastine fendizoate) only, at the concentration 100 mg/L.

With the Discovery C_8 column the peaks of cloperastine and fendizoate were overlapped. The Eclipse XDB-C_8 and Nucleosil 100 C_8 columns were not found to be suitable as the chromatographic peaks were broad and tailed. On the SymmetryShield RP_8 and Luna C_8 columns, the peaks of cloperastine and fendizoate were well separated in a short analysis time. The SymmetryShield RP_8 was finally selected, showing the best resolution of cloperastine and fendizoate peaks in a short analysis time (Fig. 5). This reversed-phase stationary phase is based on a polar group technology that "shields" the silica residual silanol surface from highly basic analytes. The reduced silanol activity for the SymmetryShield RP_8 column significantly improves the peak shape and the resolution.

The selected column was then tested by overlapping the chromatograms of cloperastine fendizoate (100 mg/L) with those of MTPS and CEPTS (100 mg/L). The results indicated a co-elution of cloperastine and MPTS (Fig. 6) at around 4.2 min. Therefore, changes in the composition of the mobile phase were applied, including phosphate buffer pH (2.5 and 6.5) and addition of a small percentage of ACN (5-10%) to the organic phase in order to modify its eluotropic power. Of the tested conditions, the last one allowed the best resolution between the drug substance peaks and its impurities. The chromatographic parameters were therefore identified as follows: column SymmetryShield RP_8 (250 mm × 4.6 mm, 5 μm, Waters) kept at 50 °C, with phosphate buffer (pH 3.0; 10 mM)–methanol (containing 10% ACN) (45:55, v/v) as the mobile phase at the flow-rate of 1.7 mL/min and UV detection at 227 nm.

The final optimization of the HPLC conditions was carried out to ensure the detection of MTPS and CEPTS at the concentration limit of 14 ppm in the drug substance. The first strategy was to increase the concentration of the GTIs in solution, by preparing test solutions containing higher amount of cloperastine fendizoate. However, the reduced solubility of the API in the SS precluded this possibility. The second strategy was based on an increase in the injection volume up to 80 μL that led to a rapid saturation of the chromatographic column, mainly due to the high amount of fendizoate injected into the HPLC system. This problem was solved by purifying the sample solution from fendizoate by SAX-SPE (with the same procedure previously described for GC–MS), followed by a 1:1 (v/v) dilution of the SPE eluate with water to improve the peak shapes of the chromatographic peaks. Under the optimized conditions, peaks of MTPS and CEPTS, eluting at around 5.6 and 8.6 min, showed good separation from the drug substance peak and improved symmetry. A representative chromatogram of the separation of the target compounds at the optimized working conditions is shown in Fig. 7. Cloperastine peak, eluting at around 4.5 min, was found to be asymmetric, due to the injection of a high volume (80 μL) of a concentrate sample solution (2000 mg/L).

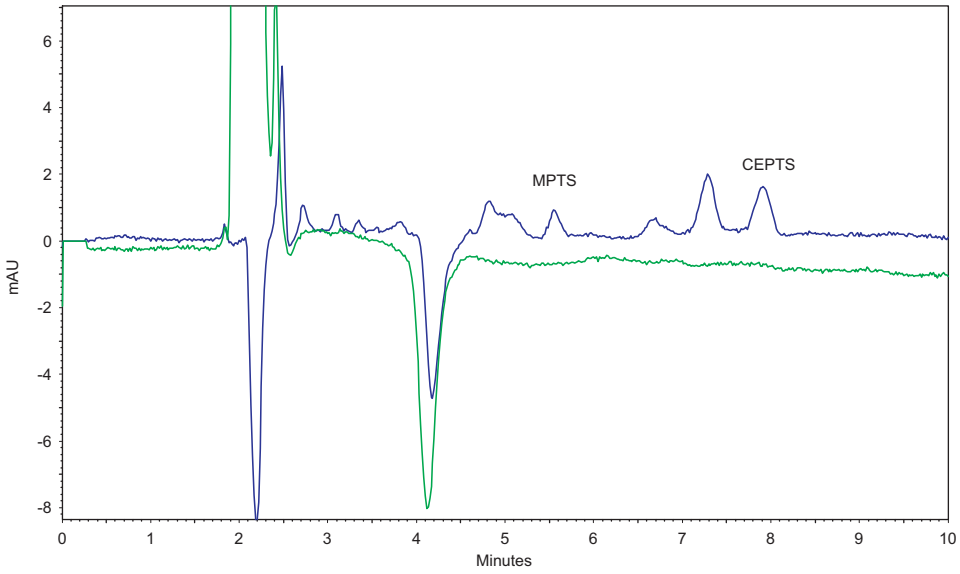

Fig. 9. HPLC-DAD analysis of a blank solution (SS) (green line), and MTPS and CEPTS at 25 μg/L (blue line). Column: SymmetryShield RP_8 (250 mm × 4.6 mm, 5 μm, Waters). Mobile phase: phosphate buffer (pH 3.0; 10 mM)–methanol (45:55, v/v). Column temperature: 50 °C. Flow-rate: 1.7 mL/min. Injection volume: 80 μL. UV detection: 227 nm. (For interpretation of the references to color in this figure legend, the reader is referred to the web version of the article.)

3.3. Method validation and application to real samples

Regarding specificity of the GC–MS method, Fig. 8 shows the results obtained by the analysis of a blank solution (SS) and a working solution of 2-CE, at the concentration 10 μg/L (ppb) in solution. SS eluted at around 2.8 min, while 2-CE eluted at around 4.1 min. Interfering peaks were not observed in the GC–MS chromatogram. Retention time for cloperastine in GC–MS was 19.0 min, but it was detected only in the full scan mode. Furthermore, peak purity tests were performed using the MS detector to demonstrate that the analyte chromatographic peak was pure and not attributable to more than one component. The LOD value for 2-CE was calculated from *S*/*N* data generated from six injections of a solution of this analyte at 100 μg/L; the LOD value was found to be 1.7 mg/L (ppm) in the raw material, corresponding to 3.5 μg/L (ppb) in solution.

In relation to MTPS and CEPTS, Fig. 9 shows the HPLC-DAD chromatograms obtained by the analysis of a blank solution (SS) and a working solution of MTPS and CEPTS, at the concentration of 25 μg/L. The blank solution did not show interfering peaks at the retention times corresponding to the target impurities. The peak purity tests, which were performed using DAD, indicated that the chromatographic peaks were pure. The LOD values were evaluated from *S*/*N* data generated from six injections of a solution of MTPS and CEPTS at 25 μg/L. For MTPS, the LOD value was found to be 11.2 mg/L (ppm) in the raw material, corresponding to 22.3 μg/L (ppb) in solution, while for CEPTS the LOD value was 2.1 mg/L (ppm) in the raw material, corresponding to 4.2 μg/L (ppb) in solution. It is noteworthy that the LOD values for the three impurities were below the required concentration limit (14 ppm) for GTIs in cloperastine fendizoate.

The developed methods were successfully applied for the determination of the target GTIs in five different batches of cloperastine fendizoate raw material. In all the batches, the three impurities were below the concentration limit previously specified. Moreover, only CEPTS could be detected in four batches, but in all cases below the specification.

4. Conclusion

Due to the different physical and chemical properties of the three target GTIs of cloperastine fendizoate, the possibility to develop one chromatographic technique for the simultaneous analysis of one alkyl halide and two sulfonate esters was precluded. Therefore, GC–MS was applied for the determination of 2-CE, while HPLC-DAD was selected for the analysis of sulfonate esters. In order to achieve the concentration levels specified by current regulations, the GC–MS method required the purification of sample solutions from fendizoate by SAX-SPE and SIM detection mode. In the case of HPLC-DAD, the high injection volume necessitated a SAX-SPE purification of samples, followed by dilution of the SPE eluate with water. The methods were validated for specificity and LOD, and applied to the analysis of GTIs in batches of cloperastine fendizoate raw material. The described analytical methods are cost-effective, direct and convenient quality control tools for the limit tests of GTIs in cloperastine fendizoate.

Acknowledgments

This work was carried out thanks to the LLP/Erasmus Program (Faculty of Pharmacy, University of Modena and Reggio Emilia, area code 12.5 Pharmacy, Coordinator Prof. Federica Pellati), which offered Dr. Florencia Ceppa the possibility to carry out her master thesis in the lab of Prof. Coral Barbas. The authors are also grateful to Cinfa Laboratories for providing the test materials.

References

[1] M.A. Catania, S. Cuzzocrea, Pharmacological and clinical overview of cloperastine in treatment of cough, Ther. Clin. Risk Manage. 7 (2011) 83–92.
[2] D.P. Elder, D.J. Snodin, Drug substance presented as sulfonic acid salts: overview of utility, safety and regulation, J. Pharm. Pharmacol. 61 (2009) 269–278.
[3] D.Q. Liu, M. Sun, A.S. Kord, Recent advances in trace analysis of pharmaceutical genotoxic impurities, J. Pharm. Biomed. Anal. 51 (2010) 999–1014.
[4] A. Teasdale, S.C. Eyley, E. Delaney, K. Jacq, K. Taylor-Worth, A. Lipczynski, V. Reif, D.P. Elder, K.L. Facchine, S. Golec, R.S. Oestrich, P. Sandra, F. David, Mechanism and processing parameters affecting the formation of methyl methanesulfonate from methanol and methanesulfonic acid: an illustrative example for sulfonate ester impurity formation, Org. Process Res. Dev. 13 (2009) 429–433.
[5] A. Teasdale, E. Delaney, S.C. Eyley, K. Jacq, K. Taylor-Worth, A. Lipczynski, W. Hoffmann, V. Reif, D.P. Elder, K.L. Facchine, S. Golec, R.S. Oestrich, P. Sandra, F. David, A detailed study of sulfonate ester formation and solvolysis reaction rates and application toward establishing sulfonate ester control in pharmaceutical manufacturing processes, Org. Process Res. Dev. 14 (2010) 999–1007.
[6] D.J. Snodin, Residues of genotoxic alkyl mesylates in mesylate salt drug substance: real or imaginary problems? Regul. Toxicol. Pharmacol. 45 (2006) 79–90.
[7] Z. Sobol, M.E. Engel, E. Rubitzki, W.W. Ku, J. Aubrecht, R.H. Schiestl, Genotoxic profiles of common alkyl halides and esters with alkylating activity, Mutat. Res. 633 (2007) 80–94.
[8] D.P. Elder, A. Teasdale, A.M. Lipczynski, Control and analysis of alkyl and aryl sulfonic acids in novel active pharmaceutical ingredients (APIs), J. Pharm. Biomed. Anal. 46 (2008) 1–8.
[9] D.P. Elder, A.M. Lipczynski, A. Teasdale, Control and analysis of alkyl and benzyl halides and other reactive organohalides as potential genotoxic impurities in active pharmaceutical ingredients (APIs), J. Pharm. Biomed. Anal. 48 (2008) 497–507.
[10] A. Giordani, W. Kobel, H.U. Gally, Overall impact of the regulatory requirements for genotoxic impurities on the drug development process, Eur. J. Pharm. Sci. 43 (2011) 1–15.
[11] N.V.V.S.S. Raman, A.V.S.S. Prasad, K. Ratnakar Reddy, Strategies for the identification, control and determination of genotoxic impurities in drug substance: a pharmaceutical industry perspective, J. Pharm. Biomed. Anal. 55 (2011) 662–667.
[12] European Medicines Agency, Committee for Medicinal Products for Human Use, Guideline on the limits of genotoxic impurities, CPMP/SWP/5199/02, EMEA/CHMP/QWP/251344/2006, 2006.
[13] E.J. Delaney, An impact analysis of the application of the threshold of toxicological concern concept to pharmaceuticals, Regul. Toxicol. Pharmacol. 49 (2007) 107–124.
[14] C. Husegawa, T. Kumazawa, X.-P. Lee, M. Fujishiro, A. Kuriki, A. Marumo, H. Seno, K. Sato, Simultaneous determination of ten antihistamine drugs in human plasma using pipette tip solid-phase extraction and gas chromatography/mass spectrometry, Rapid Commun. Mass Spectrom. 20 (2006) 537–543.
[15] H. Li, C. Zhang, J. Wang, Y. Jiang, J.P. Fawcett, J. Gu, Simultaneous quantitation of paracetamol, caffeine, pseudoephedrine, chlorpheniramine and cloperastine in human plasma by liquid chromatography–tandem mass spectrometry, J. Pharm. Biomed. Anal. 51 (2010) 716–722.
[16] International Conference on Harmonization of Technical Requirements for the Registration of Pharmaceuticals for Human Use (ICH), Guideline Q2(R1)-Validation of Analytical Procedures: Text and Methodology, 2005.
[17] G.E. Taylor, M. Gosling, A. Pearce, Low level determination of *p*-toluensulfonate and benzenesulfonate esters in drug substance by high performance liquid chromatography/mass spectrometry, J. Chromatogr. A 1119 (2006) 231–237.
[18] P.R. Kakadiya, B. Pratapa Reddy, V. Singh, S. Ganguly, T.G. Chandrashekhar, D.K. Singh, Low level determinations of methyl methanesulfonate and ethyl methanesulfonate impurities in Lopinavir and Ritonavir active pharmaceutical ingredients by LC/MS/MS using electrospray ionization, J. Pharm. Biomed. Anal. 55 (2011) 379–384.

Journal of Pharmaceutical and Biomedical Analysis 61 (2012) 237–241

Contents lists available at SciVerse ScienceDirect

Journal of Pharmaceutical and Biomedical Analysis

journal homepage: www.elsevier.com/locate/jpba

Short communication

Determination of cinacalcet hydrochloride in human plasma by liquid chromatography–tandem mass spectrometry

Fen Yang[1], Hongyun Wang[1], Qian Zhao, Hongzhong Liu, Pei Hu, Ji Jiang*

Clinical Pharmacology Research Center, Peking Union Medical College Hospital and Chinese Academy of Medical Sciences, Beijing 100730, China

ARTICLE INFO

Article history:
Received 20 May 2011
Received in revised form 18 October 2011
Accepted 19 October 2011
Available online 25 October 2011

Keywords:
Cinacalcet hydrochloride
Calcimimetic agent
SPE
LC–MS/MS
MRM

ABSTRACT

A sensitive and selective high-performance liquid chromatography–tandem mass spectrometry (HPLC–MS/MS) method was developed to determine the cinacalcet hydrochloride in human plasma. The analyte was extracted from plasma samples using a 96-well plate automatic solid-phase extraction (SPE) device and chromatographed on an Inertsil SIL-150 (2.1 mm × 50 mm, i.d. 5 μm) column using acetonitrile–water–formic acid (90:10:1) as the mobile phase with an isocratic flow rate of 0.35 mL/min. The detection was performed on a triple quadrupole tandem mass spectrometer in multiple reaction monitoring (MRM) mode using positive electrospray ionization (ESI). The method was validated over the concentration range of 0.1–25 ng/mL. The indicators of inter- and intra-day precision (RSD%) were all within 15.1%, and the accuracy (RE%) was within ±15%. The lower limit of quantitation (LLOQ) was 0.1 ng/mL. The average extraction recovery was 51.7%, and the detection was not affected by the matrix. The method was successfully applied to a pharmacokinetic study of cinacalcet hydrochloride in healthy Chinese volunteers.

© 2011 Published by Elsevier B.V.

1. Introduction

Patients with chronic kidney disease (CKD) often exhibit a combination of increased serum parathyroid hormone (PTH) levels, disordered calcium and phosphorus, and parathyroid hyperplasia commonly referred to as secondary hyperparathyroidism (SHPT) [1]. SHPT develops early and worsens as kidney function decreases [2]. HPT-associated disturbances in PTH and mineral metabolism in patients receiving dialysis contribute to an increased risk of mortality as well as vascular calcification and skeletal abnormalities collectively known as CKD-mineral and bone disorder. Traditional treatment options, including dietary phosphorus restriction, phosphorus-binding agents, calcium supplementation and 1,25-dihydroxy vitamin-D sterols, have proven inadequate in successfully controlling all aspects of SHPT [3].

Cinacalcet hydrochloride (hereinafter referred to as cinacalcet or KRN1493) is a calcimimetic agent that activates the calcium-sensing receptor on the surface of parathyroid cells and that inhibits parathyroid hormone (PTH) secretion [4]. It was approved for the treatment of SHPT in patients with chronic kidney disease (CKD) receiving dialysis and for the treatment of hypercalcaemia in patients with parathyroid carcinoma [5].

To our knowledge, there have been several reports [6–9] concerning the determination of KRN1493 in human plasma samples using the LC–MS/MS method. In these methods, KRN1493 was extracted using solid phase extraction (SPE) techniques [6,8] and 500 μL of plasma sample was required [7]. A lower limit of quantitation of 0.1 ng/mL was used in all the above methods, which was sufficient for pharmacokinetic studies of cinacalcet hydrochloride. The present study describes an assay for the determination of KRN1493 using LC–MS/MS in MRM mode. This method requires 250 μL of plasma sample, and the analyte was extracted using a 96-well plate automatic solid-phase extraction (SPE) device. The running time for each sample was only 2.2 min. In brief, the present method has advantages over the old methods that include the small plasma volume required, high-throughput sample preparation and a short running time. Furthermore, this method was validated according to FDA guidelines [10], and was successfully applied to pharmacokinetic studies of KRN1493 in healthy Chinese volunteers.

2. Materials and methods

2.1. Chemical reagents

KRN1493 (Fig. 1A) was supplied by Kirin Kunpeng (China) Biopharmaceutical Co., Ltd. Fendiline (internal standard, (IS), Fig. 1B)

* Corresponding author. Tel.: +86 10 8806 8357; fax: +86 10 8806 8864.
E-mail address: pk.frosh@gmail.com (J. Jiang).
[1] These authors contributed equally to this work and should be considered as co-first authors.

0731-7085/$ – see front matter © 2011 Published by Elsevier B.V.
doi:10.1016/j.jpba.2011.10.022

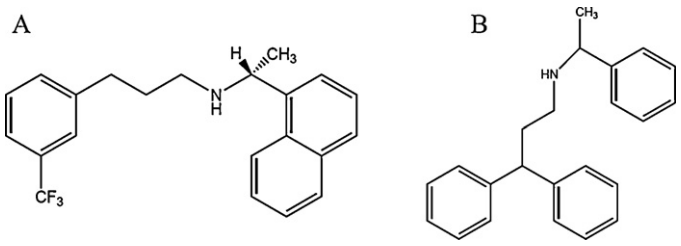

Fig. 1. Chemical structure of KRN1493 (A, MW 357) and internal standard fendiline (B, MW 315).

was purchased from Sigma–Aldrich (USA). Methanol and acetonitrile (HPLC grade) were purchased from Honeywell Burdick & Jackson (Muskegon, ML, USA). Formic acid and aqueous ammonia (both of analytical grades) were purchased from Sinopharm Chemical Reagent Co., Ltd. (Beijing, China). HPLC grade water was obtained using a Milli Q system (Millipore, Bedford, USA). Drug-free human plasma was supplied by the Peking Union Medical College Hospital blood bank.

2.2. HPLC

The chromatographic separation was carried out on a Waters Alliance 2690 liquid chromatography system (Waters, USA). An Inertsil SIL-150 column (2.1 mm × 50 mm, i.d. 5 μm, GL Sciences, Japan) and a guard column, an Inertsil SIL-150 (3.0 mm × 50 mm, i.d. 5 μm, GL Sciences, Japan) were used for all the separations. The mobile phase consisted of acetonitrile–water–formic acid (90:10:1, v/v/v). The samples were delivered at a flow rate of 0.35 mL/min, and the injection volume was 10 μL.

2.3. MS

A mass spectrometric analysis was performed using an API 3000 triple quadruple mass spectrometer from Applied Biosystems Sciex (Toronto, Canada) equipped with an electro-spray ionization (ESI) source operating in positive mode. Detection was achieved in multiple reaction monitoring (MRM) mode with a dwell time of 200 ms for each transition. The MRM transitions of KRN1493 and the IS were 358.1 → 155.1 and 316.0 → 212.1, respectively. The mass spectrometric conditions were optimized as follows: source temperature, 300 °C; curtain gas, 6 units; nebulizer gas, 5 units; auxiliary gas (7000 units); collision gas, 8 units; ion spray voltage, 5000 V; declustering potential, 38 V for KRN1493 and 66 V for the IS; collision energy, 35 eV for KRN1493 and 30 eV for the IS. Ultrahigh-purity nitrogen gas was used as the collision gas. Data acquisition and processing were performed using Analyst software (version 1.4).

2.4. Preparation of standard solutions, calibration standards and quality controls

Stock solutions of KRN1493 were prepared in duplicate in methanol at a concentration of 1 mg/mL, one for calibration curve samples and the other for quality control (QC) samples. The stock solution of internal standard (IS) was prepared as above to obtain a concentration of 1 mg/mL. Fresh working solutions were prepared by diluting the appropriate stock solution to a concentration of 10 μg/mL for KRN1493 and 100 ng/mL for the IS. Calibration standards were prepared by diluting the corresponding working solutions with drug-free human plasma. The final concentrations of KRN1493 in plasma were 0.1, 0.25, 0.5, 1, 2, 5, 10 and 25 ng/mL. Six pools of quality control (QC) samples were prepared by spiking blank plasma with KRN1493 at concentrations of 0.1 (LLOQ), 0.2 (LQC), 2 (MQC), 20 (HQC), 25 (ULOQ) and 1000 ng/mL. All stock solutions and working solutions were stored at 4 °C, and all quality control samples were stored at −30 °C. Calibration standards were freshly prepared for each experiment.

2.5. Samples preparation

In all, 250 μL of plasma was spiked with 25 μL of IS (100 ng/mL) and 500 μL of 0.3 M aqueous ammonia. The mixture was vortexed for 30 s, centrifuged for 5 min (at 13,000 rpm) and applied to a Bond Elut C18 96-well plate (100 mg/1 mL) (Varian, Palo Alto, California). The plate was then washed with 500 μL of 5 mM aqueous ammonia and 500 μL of 5 mM aqueous ammonia/methanol (8:2, v/v) and finally eluted with 1 mL of acetonitrile. The elute was evaporated to dryness under a stream of nitrogen at room temperature. The residues were dissolved in 200 μL of acetonitrile and vortexed for 1 min. Finally, 10 μL of the sample was injected for a LC–MS/MS analysis.

2.6. Method validation

Validation of this method was performed in compliance with the FDA guidelines for biological method validation [6], including validating the selectivity, calibration curve performance, accuracy and precision, LLOQ, stability of the analytes at various test conditions, recovery and the matrix effect.

Selectivity was assessed by comparing the chromatograms of drug-free human plasma from 9 different lots with the corresponding spiked plasma to test for endogenous interferences.

The calibration curves were constructed using 8 non-zero standards ranging from 0.1 to 25 ng/mL. The linearity of the relationship between the peak area ratio and the concentration was demonstrated by the correlation coefficient (R) obtained for the linear regression. The relative standard deviations were calculated for all calibration curve slopes. The intra- and inter-day assays of the method were evaluated by assessing 6 replicate QC samples at three concentration levels including LLOQ, MQC and ULOQ. The relative standard deviation (RSD%) and relative error (RE%) were calculated.

The stability of the KRN1493 stock solution and the working solution was calculated by comparing the average peak ratio of KRN1493 to the IS for solutions stored at 4 °C for 3 months with those of freshly prepared solutions at the same concentrations. The post-extraction stability was investigated by comparing the concentration of the extracted QC samples after being kept in the autosampler for 24 h with the initial concentrations. The freeze–thaw stability was determined by comparing the values for QC samples subjected to 3 freeze/thaw cycles (from −30 °C to 25 °C) with those of freshly prepared QC samples. Long-term storage stability was investigated by assessing QC samples stored at −30 °C for 112 days, including the LQC, HQC and 1000 ng/mL QC samples that were diluted to 10 ng/mL with drug-free plasma before extraction.

The extraction recovery of KRN1493 was expressed as the ratio of A (the average area ratio of KRN1493 to the IS from the extracted samples) to B (the average area ratio of KRN1493 to the IS from the samples spiked with analyte post-extraction) at the same concentration.

To determine any matrix effects in the method, blank plasma samples from 6 different lots were used to prepare the QC samples at 3 concentrations, and the matrix effect was evaluated using the average peak areas in spiked samples post-extraction to those of the corresponding working solutions at same concentrations (n = 6).

2.7. Data treatment

Data acquisition was performed using Analyst software (version 1.4). The descriptive statistics (mean, SD, RSD% and RE%) were

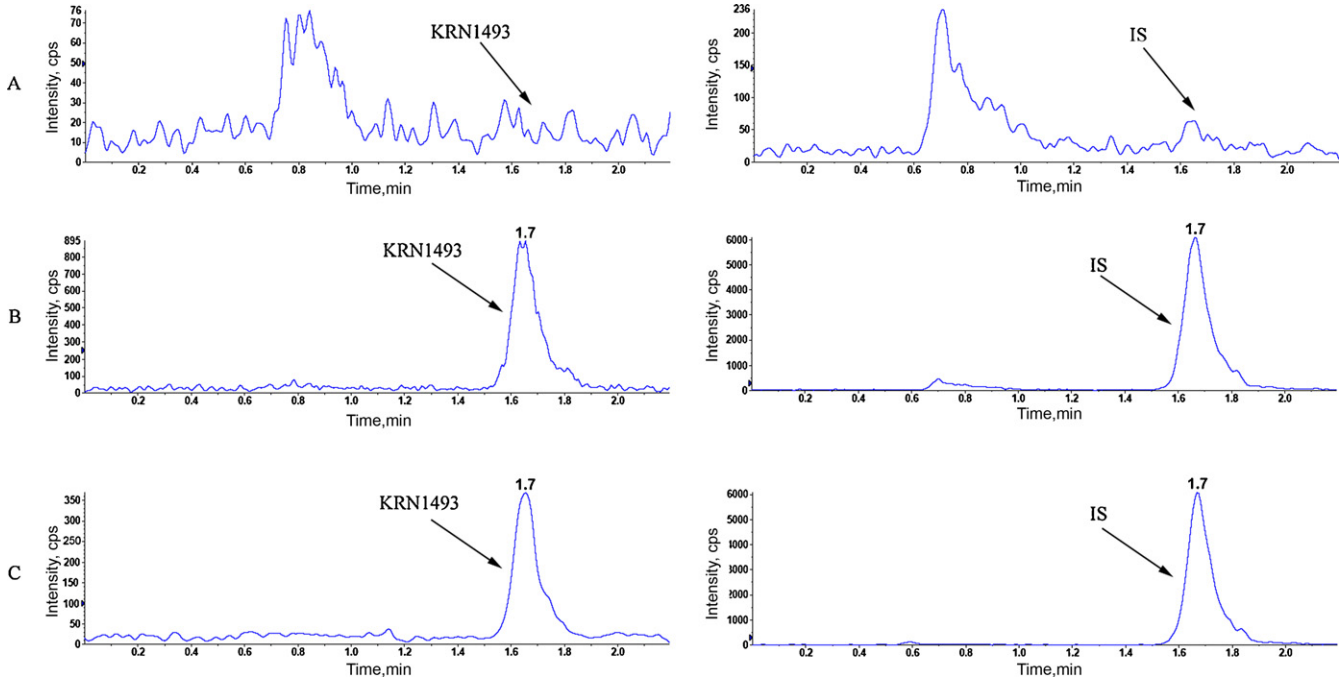

Fig. 2. Representative MRM chromatograms of KRN 1493 and IS from (A) a blank plasma sample without any analyte and internal standard added; (B) a real sample collected at 120 h after oral administration of 120 mg cinacalcet hydrochloride (0.26 ng/mL); (C) the LLOQ sample (0.1 ng/mL).

calculated using Watson LIMS (version 7.3). The calibration curve was created by plotting the peak area ratio of the analyte to the internal standard versus the plasma concentration. A weighted $1/y_2$ linear regression of the type $y = ax + b$ was used, where x represented the concentration and y represented the peak area ratio. The concentrations of the QC samples and the unknown samples were calculated by interpolation using the calibration curve.

3. Results and discussion

3.1. Chromatographic analysis

Pharmacokinetic studies involve the analysis of a large number of biological samples, so a high-throughput method is needed to perform this type of analysis. The extraction method described in this paper, using an automatic SPE device, is efficient, less laborious, rapid and reproducible. The analytes were extracted more efficiently under basic conditions. Though the extraction recovery was not particularly high, the lower limit of quantitation of the method was satisfactory for the clinical study.

To avoid interference from other compounds (exogenous or endogenous) that may co-elute with the analytes, the instrument's MRM scan mode was selected to ensure high specificity. The ionization of the analytes was achieved using an ESI ion source operated in positive mode.

The protonated ion of each analyte was selected as the precursor ion, and the most abundant or specific fragment ion was chosen as the product ion in the MRM acquisition. To obtain the highest and most stable signal response for the MRM transition, the mass spectrometric parameters were optimized, including the ion spray voltage, source temperature, nebulizer gas, collision gas and collision energy. Furthermore, good separation from interference of matrix was obtained by optimizing the mobile phase system, including the choice and the ratios of the solvents.

3.2. Method validation

3.2.1. Selectivity

Representative MRM chromatograms (Fig. 2A) of blank plasma from 9 different lots, plasma sample spiked with drugs and a real human plasma sample (Fig. 2B) were obtained under the selected analytical conditions. The results demonstrate that no significant interference from endogenous substances was found at the retention times of the analyte and the IS.

3.2.2. Sensitivity

The lower limit of quantitation (LLOQ) was defined as the concentration of the lowest non-zero calibration standard, which met the acceptance criteria for accuracy and precision of 17% (RSD%) and 1.8% (RE%). The LLOQ was set at 0.1 ng/mL, and a typical chromatogram of a plasma sample containing 0.1 ng/mL KRN1493 is shown in Fig. 2C.

3.2.3. Linearity, precision and accuracy

The calibration curves were validated over the concentration range of 0.1–25 ng/mL in human plasma. The correlation coefficients for all of the curves were greater than 0.99, and the deviations of the concentrations back-calculated from their nominal values were within ±15%.

The intra- and inter-day precision and accuracy of the method were determined from the analysis of 6 QC samples at three different concentrations, and the results are summarized in Table 1. The method was reliable and reproducible, evidenced by an RSD% below 20% for LLOQ and below 15% for MQC and ULOQ.

3.2.4. Stability

The KRN1493 stock solutions and working solutions were stable at 4 °C for 3 months. The stability of the analyte in human plasma was investigated under a variety of storage and processing conditions, and it was found to be stable under the following conditions: at 10 °C for 24 h post-extraction; after 3 cycles freeze/thaw (from

Table 1
Intra- and inter-day accuracy and precision of quality control samples.

	Inter-day (ng/mL)			Intra-day (ng/mL)		
	LLOQ (0.1000)	MQC (2.000)	ULOQ 25.00)	LLOQ 0.1000)	MQC (2.000)	ULOQ (25.00)
Mean	0.0876	1.966	23.35	0.0946	1.932	24.90
SD	0.01	0.12	0.92	0.01	0.111	1.57
Precision (RSD%)	14.7	6.4	3.9	15.1	5.5	6.3
Accuracy (RE%)	−12.4	−1.7	−6.6	−5.4	−3.4	−0.4
n	6	6	6	18	18	18

Table 2
Stability results of QC samples at different conditions ($n = 3$).

Stability tests	Initial conc. ± SD (ng/mL)	Found conc. ± SD (ng/mL)	Precision (RSD%)	Accuracy (RE%)
Stock solution (4 °C for 3 months)	2.78[a]	2.83[a]	2.8	2.0
Work solution (4 °C for 3 months)	0.34[b]	0.35[b]	1.6	−2.6
Post-extraction (10 °C for 24 h)	0.2148 ± 0.01	0.1948 ± 0.02	9.3	−9.3
	20.09 ± 0.19	17.80 ± 0.63	3.5	−11.4
Freeze thaw (from −30 °C to 25 °C, 3 cycles)	0.1964 ± 0.02	0.1775 ± 0.01	5.0	−9.6
	20.15 ± 0.75	19.09 ± 0.16	0.8	−5.3
	0.1995 ± 0.01	0.2009 ± 0.02	9.1	0.7
Long term (−30 °C for 112 days)	20.47 ± 0.95	22.15 ± 0.23	1.0	8.2
	1026 ± 28	1113 ± 25	2.3	8.4

[a] Peak area ratio of KRN1493 to IS (25 ng/mL of KRN1493).
[b] Peak area ratio of KRN1493 to IS (0.1 ng/mL of KRN1493).

−30 °C to 25 °C); and at −30 °C for 112 days. The stability results are summarized in Table 2.

3.2.5. Recovery and matrix effects

An automatic SPE method was used in the extraction of the analyte and the IS. The extraction recoveries of KRN1493 were 46.5%, 65.7% and 56.8% for the low, medium and high concentration QC samples ($n = 5$), and the extraction recovery of the IS was 55.6%.

No apparent matrix effect was found in the determination of KRN1493. The values were 103.2%, 108.3% and 106.7% for the 3 QC samples (LQC, MQC and HQC).

3.2.6. Carryover test

The MRM chromatogram of a blank sample (with added IS and without KRN1493) analyzed following five consecutive analyses of ULOQ samples showed no apparent carryover using the present method.

3.3. Application of the method in a pharmacokinetic study

This HPLC/MS/MS method was used to evaluate a pharmacokinetic study of KRN1493 in human plasma. This was a phase I, single center, open-label study with 3 parallel groups and a single period used to assess the pharmacokinetics of KRN1493 in healthy Chinese subjects. Thirty healthy Chinese volunteers were enrolled and randomized into 3 groups ($n = 10$). The subjects in each group received a single oral dose of 25, 50 or 100 mg cinacalcet hydrochloride. Plasma samples were collected pre-dose and at 0.5, 1, 1.5, 2, 2.5, 3, 3.5, 4, 5, 6, 8, 12, 24, 36, 48, 72, 96 and 120 h post-dose and assayed by the validated method. The mean plasma concentration–time curves of KRN1493 are shown in Fig. 3. The pharmacokinetic parameters of KRN1493 in healthy Chinese subjects after a single oral administration of 50 mg of cinacalcet hydrochloride are compared with those acquired in western subjects [9] at the same dose level in Table 3. The T_{max} of KRN1493 was approximately 4.5–5 h in both studies; however, faster elimination was observed in Chinese subjects. The mean $AUC_{0\to t}$, $AUC_{0\to\infty}$ and C_{max} in Chinese subjects were higher than those in western subjects, which may be explained by the differences in body weight between the Chinese and western subjects.

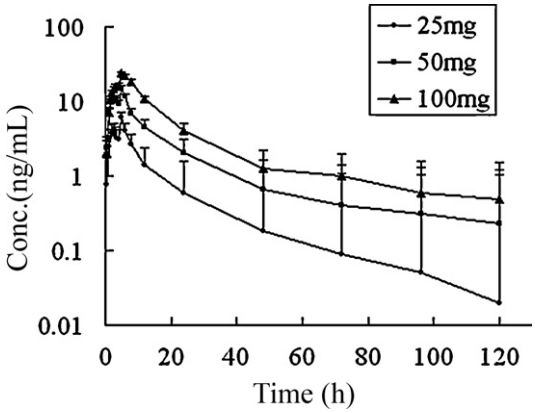

Fig. 3. Mean plasma concentration–time curves of KRN1493 after single oral administration of 25 mg, 50 mg and 100 mg cinacalcet hydrochloride ($n = 10$).

Table 3
Comparison of pharmacokinetic parameters of KRN1493 between Chinese and western volunteers at 50 mg dose of cinacalcet hydrochloride (mean ± SD).

	Chinese volunteers	Western volunteers [9]
Number (*n*)	10	6
Race	Chinese	White and black
Weight (kg)	83.3 ± 8.21	61.4 ± 9.75
Age (y)	50.8 ± 2.64	22.6 ± 1.9
$AUC_{0\to t}$ (ng h mL^{-1})	187 ± 70.7	156 ± 105
$AUC_{0\to\infty}$ (ng h mL^{-1})	205 ± 83.05	181 ± 131
C_{max} (ng/mL)	17 ± 6.33	11.9 ± 6.62
T_{max} (h)	4.55 ± 1.62	5 ± 3.8
$t_{1/2}$ (h)	37.1 ± 14.67	49.2 ± 35.4

$AUC_{0\to t}$, area under the concentration–time curve (AUC) from 0 to time *t*; $AUC_{0\to\infty}$, AUC from 0 to infinity; C_{max}, maximum plasma concentration; T_{max}, time to C_{max}; $t_{1/2}$, terminal half-life.

4. Conclusions

A rapid, sensitive and selective HPLC–MS-MS method has been developed and validated for the determination of KRN1493 in human plasma. The method, using an automatic SPE method for the extraction of KRN1493 and the IS from plasma, is sensitive, specific

and accurate. The present method was successfully applied in pharmacokinetic studies of KRN1493 in healthy Chinese volunteers.

Acknowledgment

The authors thank Kirin Kunpeng (China) Biopharmaceutical Co. Ltd. for supplying the cinacalcet hydrochloride.

References

[1] M. Rodriguez, E. Nemeth, D. Martin, The calcium-sensing receptor: a key factor in the pathogenesis of secondary hyperparathyroidism, Am. J. Physiol. Renal. Physiol. 288 (2005) F253–F264.
[2] I. Martinez, R. Saracho, J. Montenegro, F. Llach, The importance of dietary calcium and phosphorous in the secondary hyperparathyroidism of patients with early renal failure, Am. J. Kidney Dis. 29 (1997) 496–502.
[3] E.W. Young, J.M. Albert, S. Satayathum, D.A. Goodkin, R.L. Pisoni, T. Akiba, T. Akizawa, K. Kurokawa, J. Bommer, L. Piera, F.K. Port, Predictors and consequences of altered mineral metabolism: the Dialysis Outcomes and Practice Patterns Study, Kidney Int. 67 (2005) 1179–1187.
[4] M. Fukagawa, S. Yumita, T. Akizawa, E. Uchida, Y. Tsukamoto, M. Iwasaki, S. Koshikawa, KRN1493 study group, cinacalcet (KRN1493) effectively decreases the serum intact PTH level with favorable control of the serum phosphorus and calcium levels in Japanese dialysis patients, Nephrol. Dial. Transplant. 23 (2008) 328–335.
[5] E. Zitt, M. Rix, P. Ureña Torres, D. Fouque, S.H. Jacobson, F. Pétavy, B. Dehmel, M. Ryba, Effectiveness of cinacalcet in patients with recurrent/persistent secondary hyperparathyroidism following parathyroidectomy: results of the ECHO study, Nephrol. Dial. Transplant. 26 (2011) 1956–1961.
[6] N. Ohashi, T. Uematsu, S. Nagashima, M. Kanamaru, A. Togawa, A. Hishida, E. Uchida, T. Akizawa, S. Koshikawa, The calcimimetic agent KRN 1493 lowers plasma parathyroid hormone and ionized calcium concentrations in patients with chronic renal failure on haemodialysis both on the day of haemodialysis and on the day without haemodialysis, Br. J. Clin. Pharmacol. 57 (2004) 726–734.
[7] D. Padhi, R.Z. Harris, M. Salfi, J.T. Sullivan, No effect of renal function or dialysis on pharmacokinetics of cinacalcet (Sensipar/Mimpara), Clin. Pharmacokinet. 44 (2005) 509–516.
[8] D. Nakashima, H. Takama, Y. Ogasawara, T. Kawakami, T. Nishitoba, S. Hoshi, E. Uchida, H. Tanaka, Effect of cinacalcet hydrochloride, a new calcimimetic agent, on the pharmacokinetics of dextromethorphan: in vitro and clinical studies, J. Clin. Pharmacol. 47 (2007) 1311–1319.
[9] D. Padhi, R.Z. Harris, M. Salfi, R.J. Noveck, J.T. Sullivan, Pharmacokinetics and pharmacodynamics of cinacalcet in hepatic impairment: phase I, open-label, parallel-group, single-dose, single-centre study, Clin. Drug Investig. 28 (2008) 635–643.
[10] Food and Drug Administration (FDA), Guidance for Industry in Bioanalytical Method Validation, Rockville, MD, USA, 2001.

Journal of Pharmaceutical and Biomedical Analysis 61 (2012) 242–246

Contents lists available at SciVerse ScienceDirect

Journal of Pharmaceutical and Biomedical Analysis

journal homepage: www.elsevier.com/locate/jpba

Short communication

Quantitative determination and pharmacokinetic study of casticin in rat plasma by liquid chromatography–mass spectrometry

Jinlong Xu[a], Qiaoyan Zhang[a], Liang Zhao[b], Ying Wang[a], Liming Xue[a], Ting Han[a], Chengjian Zheng[a], Luping Qin[a,*]

[a] Department of Pharmacognosy, School of Pharmacy, Second Military Medical University, 325 Guohe Road, Shanghai 200433, China
[b] Department of Pharmacy, Eastern Hepatobiliary Surgery Hospital, Second Military Medical University, Shanghai 200438, China

ARTICLE INFO

Article history:
Received 7 September 2011
Received in revised form 5 November 2011
Accepted 7 November 2011
Available online 26 November 2011

Keywords:
Casticin
Pharmacokinetics
Liquid chromatography
Mass spectrometry

ABSTRACT

A specific and sensitive liquid chromatography–mass spectrometry method has been developed and validated for identification and quantification of casticin in rat plasma after oral and intravenous administrations. Kaempferol was employed as an internal standard (IS). Liquid–liquid extraction using dichloromethane was applied to extract the casticin and the internal standard from plasma. Chromatographic separation was achieved on a Zorbax SB C_{18} column (100 mm × 3.0 mm, i.d.: 3.5 μm) with a mobile phase of methanol: 0.05% formic acid aqueous solution (60:40, v/v) at a flow rate of 0.4 mL/min for 10 min. The detection was performed by selected ion monitoring (SIM) mode via positive electrospray ionization (ESI) interface. The lower limit of detection (LLOD) was 7 ng/mL ($S/N = 5$). The calibration curves were linear ($r > 0.9996$) over the concentration range from 14.06 to 7187 ng/mL. Intra-day and inter-day precisions (RSD%) were within 10% and accuracy (RE%) ranged from −8.2% to 1.0%. The extraction recovery at three quality control (QC) concentrations ranged from 91% to 102%. The validated method was successfully applied to the pharmacokinetic study of casticin after both an oral and an intravenous administrations to rats and the absolute bioavailability is 45.5 ± 11.0%.

© 2011 Elsevier B.V. All rights reserved.

1. Introduction

Casticin (3′,5-dihydroxy-3,4′,6,7-tetramethoxyflavone), also named Vitexicarpin, as a major flavone component has been isolated from a number of medicinal plants of *Vitex* species, such as *Vitex trifolia* L., *Vitex agnus-castus* L. and *Vitex rotundifolia* L. It has been reported that casticin has antitumor [1–10], anti-inflammation [11–16], anti-hyperprolactinemia [17–19], antioxidant [20,21], and anti-nociceptive [19,22] properties. In recent years, this compound is considered as the major active chemical constituent for the treatment of premenstrual syndrome (PMS) in the medicinal plants of *Vitex* species [17–19,22]. In comparison with conventional drugs such as anti-inflammatory agents (ibuprofen), psychotropic drugs (selective serotonin reuptake inhibitors), estrogen and progesterone, naturally occurring products containing casticin have been extensively used to treat PMS in European for little adverse effects. Considering the anti-inflammation, anti-nociceptive, anti-hyperprolactinemia and estrogenic activities of casticin, it has a good potential to be developed as a new therapeutic reagent for PMS. For the development of casticin as a new drug, it is necessary to establish a selective and sensitive analytical method for the quantitative estimation of casticin in preclinical biopharmaceutical and clinical pharmacology studies.

Several methods for the separation and quantification of casticin have been described using high performance liquid chromatography (HPLC) with ultra-violet detection [23–25]. However, these methods mainly focused on the quantification of casticin in raw materials or pharmaceutical preparations. Few studies can be found in biological specimen. The purpose of this study was to develop a simple, rapid and reliable LC–MS assay for the determination of casticin in rat plasma and applied the assay to the pharmacokinetic study in rats after oral and intravenous administrations of casticin.

2. Experimental

2.1. Materials and reagents

Casticin (purity >98%) (calculated with normalization of area by HPLC-DAD) was isolated and purified from the seeds of *V. trifolia* L. (obtained from Sichuan Province of China) in our laboratory, and its structure was confirmed by UV, IR, MS and NMR spectroscopy. The air-dried and powdered seeds of *V. trifolia* L. were extracted with 80% EtOH for 2 h, 3 times. After removal of the

* Corresponding author. Tel.: +86 218 187 1300; fax: +86 218 187 1300.
E-mail address: qinsmmu@126.com (L. Qin).

0731-7085/$ – see front matter © 2011 Elsevier B.V. All rights reserved.
doi:10.1016/j.jpba.2011.11.006

solvent under reduced pressure, the residue was suspended in H_2O and partitioned sequentially with petroleum ether, CH_2Cl_2, EtOAc and n-butanol, respectively. The CH_2Cl_2-soluble part was subjected to silica gel (200–300 mesh, 1000 g) and eluted successively with gradient petroleum ether–EtOAc mixtures (30:1–1:1) and CCl_4–MeOH mixtures (20:1–1:1) to provide fractions. Fraction was rechromatographed on Sephadex LH-20 to give casticin. According to the UV, IR, MS and NMR spectroscopy (data not shown), it was identified as casticin. Kaempferol (purity >98%) as the internal standard was purchased from the National Institute for the Control of Pharmaceutical and Biological Products (Beijing, China). Methanol and formic acid of HPLC grade were from Burdick & Jackson (Ulsan, Korea), and water was doubly distilled in the laboratory. The other reagents were of analytical grade and obtained through commercial sources.

2.2. Instrumentation and conditions

The 1100 HPLC system consisted of a G1322A degasser, a G1311A quaternary pump, a G1367A well-plate autosampler and a G1316A thermostated column compartment. A G1946D mass spectrometer (Agilent, Santa Clara, CA, USA) equipped with an electrospray source interface was used for MS detection. Data acquisition and analysis were performed using Agilent ChemStation for LC/MSD version B.02.01. Chromatographic separation was achieved on an Agilent Zorbax SB C_{18} column (100 mm × 3.0 mm, i.d.: 3.5 μm) and eluted with a mobile phase of methanol: 0.05% formic acid aqueous solution (60:40, v/v) at a flow rate of 0.4 mL/min. The column temperature was kept at 25 °C, and the injection volume was 5 μL. The analysis time was 10 min per sample. The HPLC system was connected to the mass spectrometer via an ESI interface. The mass conditions of electrospray ionization were optimized in the positive ion detection mode as follows: capillary 4000 V, nebulizer 40 p.s.i., drying gas 11 L/min, gas temperature 350 °C and fragmentor 110 V. Selected ion monitoring (SIM) was used and the fragmentation transitions were *m*/*z* 375.1 for casticin and *m*/*z* 287.1 for kaempferol.

2.3. Preparation of calibration standards, quality control and internal standard

Stock solutions were prepared by dissolving accurate amounts of standards in methanol solution: 2.306 mg/mL of casticin and 1.010 mg/mL of kaempferol. An internal standard (IS) working solution of 20 μg/mL was obtained by diluting corresponding stock solution with methanol. The calibration standards containing casticin (14.06, 56.25, 112.5, 450.0, 900.0, 1800, 3593 and 7187 ng/mL) were prepared by spiking 50 μL of the working standard solution into 200 μL of blank rat plasma. Quality control (QC) samples were prepared in the same manner as calibration standards at concentrations of 56.25, 1800 and 7187 ng/mL. All the solutions were kept at 4 °C. The assay standard samples and quality control samples were prepared during each analysis batch.

2.4. Sample preparation

A liquid–liquid extraction (LLE) method was used for QC samples, calibration standards and rat plasma samples. After thawed to room temperature, 200 μL plasma sample was spiked with 50 μL IS solution (kaempferol, 20 μg/mL) and vortexed for 30 s in a 1.5 mL polypropylene tube. 1 mL dichloromethane were then added into the spiked samples. Extraction was performed by vigorously vortexing for 2 min and centrifuging at 10,000 rpm for 5 min. The organic layer (800 μL) was transferred into another 1.5 mL polypropylene tube and dried under a flow of nitrogen gas at room temperature. The residue was reconstituted in 100 μL methanol vortexing for 30 s and centrifuged at 10,000 rpm for 10 min. An aliquot of 5 μL was injected into the LC–MS system for analysis.

2.5. Method validation

The selectivity of the method was investigated by analyzing six individual blank rat plasma samples and compared with those obtained by spiking casticin (1800 ng/mL) and IS (20 μg/mL) into the corresponding blank plasma sample to check interference. Standard curves ranging from 14.06 to 7187 ng/mL were fitted by least-square regression using logarithm as weighting factor of the peak area ratio of casticin to IS ($\log Y$) versus plasma concentrations ($\log X$). The linearity of casticin determined in spiked rat plasma was obtained using eight calibration standards in five independent runs. The lower limit of detection (LLOD) and the lower limit of quantification (LLOQ) for each standard solution were calculated with signal-to-noise ratios of 5 and 10, respectively.

The extraction recovery was determined by calculating the ratio of the amounts of QC samples obtained against those originally spiked in the blank plasma using five replicates. The matrix effect was evaluated by comparing the response of the solution spiked with the blank processed matrix with the solution at three different QC concentrations using five replicates.

Precision and accuracy were assessed by determining the concentration of casticin in QC samples using five replicate preparations of plasma samples at three concentration levels on three separate days, using three separate sources of rat plasma. The calibration curve constructed on the same testing day was used for the quantification of each sample.

QC concentrations were used to evaluate the stability of the analytes in rat plasma under different storage conditions: long-term stability at −20 °C for 30 days, short-term stability at room temperature for 4 h, post-preparative stability at room temperature for 24 h, and three freeze–thaw cycles.

2.6. Application to pharmacokinetic study

Male Sprague-Dawley rats (220–250 g) were obtained from Sino-British Sippr/BK Lab Animal Ltd. (Shanghai, China). The animals were acclimatized to the facilities for 5 days, and then fasted with free access to water for 12 h prior to each experiment. The rats were randomized into two groups, 6 in each group: animals in group A were administered an oral dose of 400 mg/kg casticin, and animals in group B were administered a dose of 50 mg/kg casticin via the tail vein injection. The solution of casticin was dissolved in physiological saline and mixed well. Blood samples (0.5 mL) were collected into a heparinized tube via the oculi chorioideae vein before drug administration and at 10, 20, 30, 45, 60, 90, 120, 180 and 210 min after oral administration and at 0 (pre-dose), 2, 5, 10, 15, 20, 25, 30, 40, 50 and 60 min after intravenous injection administration via the tail vein. Plasma samples (200 μL) were obtained through centrifuging at 6000 rpm for 10 min and stored at −20 °C until analysis within a week.

Plasma-concentration data for individual rats were analyzed by non-compartmental analysis using the Bioavailability Program Package (BAPP, Version 2.0, Center of Drug Metabolism and Pharmacokinetics, China Pharmaceutical University).

3. Results and discussion

3.1. Method development

Due to the high sensitivity and specificity of LC–MS, it has been widely used in biological samples analysis in recent years. The developed and validated method was successfully applied to

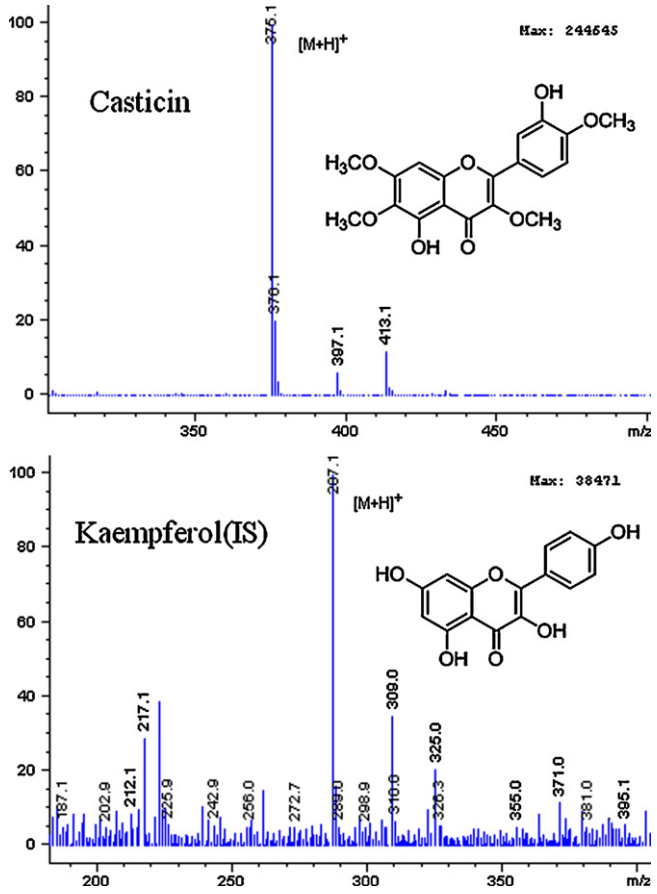

Fig. 1. Chemical structures and mass scan spectra for casticin and kaempferol (IS).

casticin analysis in rat plasma samples during preclinical investigations such as pharmacokinetic study. In order to develop a sensitive and specific LC–MS method for quantification of casticin in rat plasma, some potential factors were investigated and optimized. The response of casticin to ESI was evaluated by recording the full-scan mass spectra in both positive and negative ionization modes, and it has a good mass spectrometric response in positive ESI mode. Chemical structures and mass scan spectra for casticin and kaempferol are shown in Fig. 1. Since there are four $-OCH_3$ in chemical structure of casticin, and the $-OCH_3$ group can be changed into $-OCH_4^+$, thus casticin can easily be detected by MS using electrospray in the positive mode. Kaempferol has a good mass spectrometric response in positive and negative ESI mode, it was selected positive mode according to the mode of casticin. The most abundant fragmentation ions in the spectra ($[M+H]^+$ m/z 375.1 for casticin and $[M+H]^+$ m/z 287.1 for kaempferol) were selected for sensitive quantitation. Owing to SIM high selectivity and sensitivity, the quantification analysis was performed using it. For the aspect of internal standard selection, the analogs of kaempferol, isorhamnetin and baicalin were screened as internal standard. Based on peak shape and retention time, kaempferol was regarded as a more suitable internal standard under the chromatographic conditions.

The aim of sample preparation was to remove interferences from plasma samples with a suitable recovery rate. In the early methods at development stage, we compared and analyzed the result of liquid–liquid extraction and protein precipitation with methanol and acetonitrile for sample preparation. It was found that the interference in blank plasma cannot be eliminated when using protein precipitation method, maybe for the polarity reason. Then, several extraction solvents such as ethyl acetate, diethyl ether, trichlormethane and dichloromethane were investigated, and dichloromethane, a relatively polar solvent, was selected as the extraction agent for stable extraction recovery and less pollution. Comparatively, liquid-liquid extraction was used for sample preparation in this study, because it could not only ensure less endogenous interference, but also ensure adequate recovery and high sensitivity. In the process of sample preparation, we found that the critical operation was vortex time. It was hard to ensure a stable extraction recovery when the vortex time was too short. If the vortex time was too long, analytes would form over emulsification, and these emulsifications were difficult to remove. In the end, the vortex time was setting at 2 min.

3.2. Method validation

The representative chromatograms in SIM of casticin and kaempferol are shown in Fig. 2. The retention times of IS and casticin were approximately 4.4 and 7.8 min, respectively. No significant peaks interfering with analytes were observed in the blank rat plasma. A typical equation of the calibration curve was $y = 1.003x - 2.5195$ ($r = 0.9996$) in the range of 14.06–7187 ng/mL. LLOQ was set at 14.06 ng/mL for casticin and the signal-to-noise ratio was higher than 10-fold and the deviation was no more than 15% ($n = 5$). LLOD of casticin was obtained by diluting the solution to 7 ng/mL, and the signal-to-noise ratio was 5-fold.

The matrix effects of casticin at concentrations of 56.25, 1800 and 7187 ng/mL were 86%, 90% and 89%, respectively. The matrix effect value was 101% for IS. The results showed that there was no significant interference on the quantitation of analytes from the plasma matrix. The extraction recovery of IS was 39%.

The intra-day and inter-day precisions of this method ranged from 7.1% to 9.1% and from 7.8% to 9.7% for each QC level, respectively. The accuracy was within ±10% (data not shown).

Stability of the three analytes during the sample storing and processing procedures was fully evaluated by analysis of QC samples. The concentration variation after three freeze–thaw cycles was within ±10% of nominal concentrations, indicating that there was no significant substance loss during thawing and freezing. When the processed samples were stored at room temperature for 24 h, three analytes showed good stability as the responses varied no more than ±9% at QC concentrations. After storage at −20 °C for a whole month, the concentrations of three analytes showed no obvious substance loss (RE: 2.3–4.0%, RSD <9%). In addition, analytes were stable stored at ambient temperature for 4.0 h (RE: 1.5–6.9%, RSD <10%).

3.3. Application of the method to pharmacokinetic study

The presented method was successfully applied to quantify casticin in the plasma of rats following a single 400 mg/kg oral dose ($n = 6$) or after intravenous injection 50 mg/kg ($n = 6$). The mean plasma concentrations versus time profiles after oral and intravenous injection administrations were shown in Fig. 3. The main pharmacokinetic parameters of casticin after oral and intravenous injection administrations calculated by non-compartmental analysis were summarized in Table 1. As for oral administration, the absorption of casticin from rat gastrointestinal tract was irregular and retained individual difference in the plasma. The concentration–time curve of casticin showed obvious double-peak phenomenon. The reasons for this phenomenon might be caused by the absorption varied within different regions of the gut or enterohepatic circulation. The mean C_{max} value was 287.06 ± 40.68 ng/ml (range 244.66–325.78 ng/ml), which means casticin was not absorbed well following oral administration to rats. Considering that the oral pharmacokinetics of casticin are affected by solvent, the impact of solvent of casticin was assessed

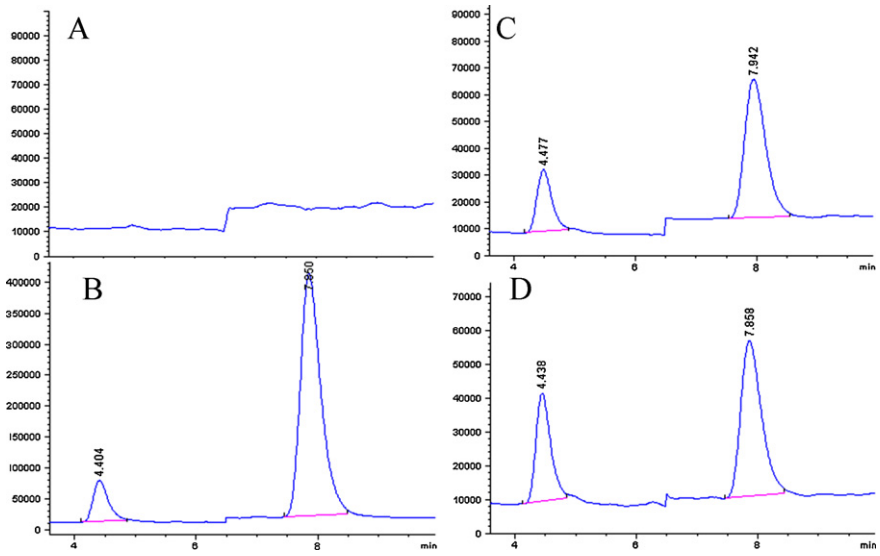

Fig. 2. Selected ionmonitoring chromatograms for (A) blank rat plasma sample, (B) blank plasma sample spiked with casticin (1800 ng/mL) and internal standard (20 μg/mL), (C) plasma sample at 45 min after oral administration with 400 mg/kg of casticin and (D) plasma sample at 15 min after intravenous administration with 50 mg/kg of casticin.

with two formulations, suspended in 0.5% CMC and solubilized with physiological saline. When 0.5% CMC casticin solution was given, casticin was not quantifiable in almost all post-dosing plasma samples except at 45 min at the dose of 400 mg/kg. Maybe the reason is that casticin was surrounded by CMC, and hard to be released and absorbed. When physiological saline solution was given, casticin can be easily detected in the rats plasma at the same dose. As for intravenous injection administration, elimination half-life was 20.86 ± 2.02 min (range 18.66–22.64 min). This result indicated that the drug was distributed and eliminated rapidly in rats. The short elimination half-life may be resulted from casticin that was easily hydroxylated in the plasma. The absolute bioavailability was 45.5 ± 11.0%, which is beneficial to drug exerting in clinical application at anti-PMS activity in the future. It was shown the standard deviation was quite big among individual rat (in Fig. 3). Further studies are needed to elucidate the absorption casticin at dose–linearity.

Table 1
The main pharmacokinetic parameters of casticin after oral (400 mg/kg) and i.v. (50 mg/kg) administrations to six rats (mean ± SD).

Parameter	Administration mode	
	Oral (400 mg/kg)	Intravenous (50 mg/kg)
C_{max} (ng/mL)	287.06 ± 40.68	12,737.82 ± 7243.88
T_{max} (min)	43.83 ± 1.47	0 (pre-dose)
$t_{1/2}$ (min)	36.48 ± 7.24	20.86 ± 2.02
$AUC_{0-\tau}$ (ng h/mL)	18,652.72 ± 4030.88	41,225.92 ± 1403.37
$AUC_{0-\infty}$ (ng h/mL)	19,179.92 ± 4325.42	42,322.12 ± 1880.98
MRT (min)	85.85 ± 9.53	11.48 ± 1.37

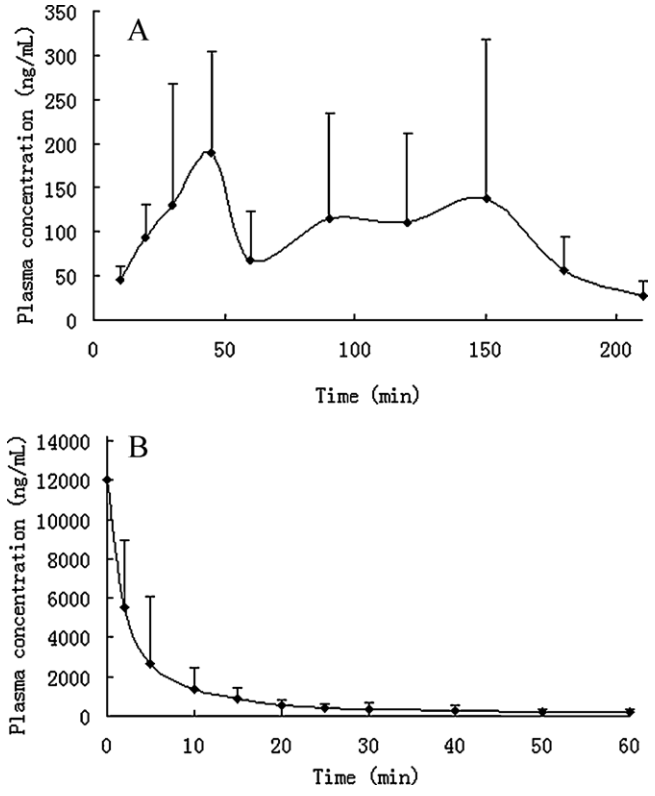

Fig. 3. Mean rats plasma concentration–time profiles of casticin after (A) an oral dose of 400 mg/kg and (B) an intravenous injection dose of 50 mg/kg (each point represents mean ± SD, $n = 6$).

4. Conclusion

A LC–MS method was developed and validated for the quantification of casticin in rat plasma. This method demonstrated a relatively short analysis time and the acceptable sensitivity, precision, accuracy, selectivity, recovery and stability. It was then successfully applied to a pharmacokinetic study of casticin after both oral and intravenous administrations. A simple and economic liquid–liquid extraction method was employed for sample preparation and showed good reproducibility. In addition, based on this validated method, the pharmacokinetic parameters of casticin were calculated, providing valuable information for future development of casticin. The absolute bioavailability is 45.5 ± 11.0% which is beneficial to drug exerting in clinical application in the future. Further studies of absorption, distribution, excretion and metabolism of casticin are underway on rats and dogs in the laboratory. Analytical methods, including this assay described here, will be applied in these studies.

Acknowledgement

This research was supported by the National Key New Drug Creation Special Programme (Grant No. 2009ZXJ09004-068).

References

[1] H.Y. Wang, B. Cai, C.B. Cui, D.Y. Zhang, B.F. Yang, Vitexicarpin, a flavonoid from *Vitex trifolia* L., induces apoptosis in K562 cells via mitochondria-controlled apoptotic pathway, Yao Xue Xue Bao 40 (2005) 27–31.
[2] K.M You, K.H. Son, H.W. Chang, S.S. Kang, H.P. Kim, Vitexicarpin, a flavonoid from the fruits of *Vitex rotundifolia*, inhibits mouse lymphocyte proliferation and growth of cell lines in vitro, Planta Med. 64 (1998) 546–550.
[3] Y.C. Song, X. Zhang, G.Y. Lei, C.X. Dang, Vitexicarpin affects proliferation and apoptosis in mutated p53 breast cancer cell, Zhong Hua Yi Xue Za Zhi 90 (2010) 703–707.
[4] W.G. Ko, T.H. Kang, S.J. Lee, N.Y. Kim, Y.C. Kim, D.H. Sohn, B.H. Lee, Polymethoxyflavonoids from Vitex rotundifolia inhibit proliferation by inducing apoptosis in human myeloid leukemia cells, Food Chem. Toxicol. 38 (2000) 861–865.
[5] M. Ono, T. Yanaka, M. Yamamoto, Y. Ito, T. Nohara, New diterpenes and norditerpenes from the fruits of *Vitex rotundifolia*, J. Nat. Prod. 65 (2002) 537–541.
[6] J. Kobayakawa, F.S. Nishimori, M. Moriyasu, Y. Matsukawa, G2-M arrest and antimitotic activity mediated by casticin, a flavonoid isolated from *Viticis fructus*, Cancer Lett. 208 (2004) 59–64.
[7] W.X Li, C.B. Cui, B. Cai, H.Y. Wang, X.S. Yao, Flavonoids from *Vitex trifolia* L. inhibit cell cycle progression at G2/M phase and induce apoptosis in mammalian cancer cells, J. Asian Nat. Prod. Res. 7 (2005) 615–626.
[8] K. Haidara, L. Zamir, Q.W. Shi, G. Batist, The flavonoid Casticin has multiple mechanisms of tumor cytotoxicity action, Cancer Lett. 242 (2006) 180–190.
[9] F. Diaz, D. Chavez, D. Lee, Q. Mi, H.B. Chai, G.T. Tan, L.B. Kardono, S. Riswan, C.R. Fairchild, R. Wild, N.R. Farnsworth, G.A. Cordell, J.M. Pezzuto, A.D. Kinghorn, Cytotoxic flavone analogues of vitexicarpin, a constituent of the leaves of Vitex negundo, J. Nat. Prod. 66 (2003) 865–867.
[10] J.K. Shen, H.P. Du, M. Yang, Y.G. Wang, J. Jin, Casticin induces leukemic cell death through apoptosis and mitotic catastrophe, Ann. Hematol. 88 (2009) 743–752.
[11] S.M. Lee, Y.J. Lee, Y.C. Kim, J.S. Kim, D.G. Kang, H.S. Lee, Vascular protective role of vitexicarpin isolated from *Vitex rotundifolia* in human umbilical vein endothelial cells, Inflammation (2011).
[12] G. Alam, S. Wahyuono, I.G. Ganjar, L. Hakim, H. Timmerman, R. Verpoorte, Tracheospasmolytic activity of viteosin-A and vitexicarpin isolated from *Vitex trifolia*, Planta Med. 68 (2002) 1047–1049.
[13] D.J. Koh, H.S. Ahn, H.S. Chung, H. Lee, Y. Kim, J.Y. Lee, D.G. Kim, M. Hong, M. Shin, H. Bae, Inhibitory effects of casticin on migration of eosinophil and expression of chemokines and adhesion molecules in A549 lung epithelial cells via NF-kappaB inactivation, J. Ethnopharmacol. 136 (2011) 399–405.
[14] L. Shan, L.P. Qin, In vivo effect of casticin on acute inflammation, Zhong Xi Yi Jie He Xue Bao 5 (2007) 573–576.
[15] S. Freitas, S. Costa, C. Azevedo, G. Carvalho, S. Freire, P. Barbosa, E. Velozo, R. Schaer, M. Tardy, R. Meyer, I. Nascimento, Flavonoids inhibit angiogenic cytokine production by human glioma cells, Phytother. Res. 25 (2011) 916–921.
[16] P. Remberg, L. Bjork, T. Hedner, O. Sterner, Characteristics, clinical effect profile and tolerability of a nasal spray preparation of *Artemisia abrotanum* L. for allergic rhinitis, Phytomedicine 11 (2004) 36–42.
[17] Y. Hu, T.T. Hou, Q.Y. Zhang, H.L. Xin, H.C. Zheng, K. Rahman, L.P. Qin, Evaluation of the estrogenic activity of the constituents in the fruits of *Vitex rotundifolia* L. for the potential treatment of premenstrual syndrome, J. Pharm. Pharmacol. 59 (2007) 1307–1312.
[18] Q. Ye, Q.Y. Zhang, C.J. Zheng, Y. Wang, L.P. Qin, Casticin, a flavonoid isolated from *Vitex rotundifolia*, inhibits prolactin release in vivo and in vitro, Acta Pharmacol. Sin. 31 (2010) 1564–1568.
[19] Y. Hu, H.L. Xin, Q.Y. Zhang, H.C. Zheng, K. Rahman, L.P. Qin, Anti-nociceptive and anti-hyperprolactinemia activities of *Fructus Viticis* and its effective fractions and chemical constituents, Phytomedicine 14 (2007) 668–674.
[20] Z. Hajdu, J. Hohmann, P. Forgo, T. Martinek, M. Dervarics, I. Zupko, G. Falkay, D. Cossuta, I. Mathe, Diterpenoids and flavonoids from the fruits of *Vitex agnus-castus* and antioxidant activity of the fruit extracts and their constituents, Phytother. Res. 21 (2007) 391–394.
[21] M.I. Choudhary, S. Jalil, S.A. Nawaz, K.M. Khan, R.B. Tareen, Antiinflammatory and lipoxygenase inhibitory compounds from *Vitex agnus-castus*, Phytother. Res. 23 (2009) 1336–1339.
[22] D.E. Webster, Y. He, S.N. Chen, G.F. Pauli, N.R. Farnsworth, Z.J. Wang, Opioidergic mechanisms underlying the actions of *Vitex agnus-castus* L, Biochem. Pharmacol. 81 (2011) 170–177.
[23] E. Hoberg, B. Meier, O. Sticher, Quantitative high performance liquid chromatographic analysis of diterpenoids in agni-casti fructus, Planta Med. 66 (2000) 352–355.
[24] E. Hoberg, B. Meier, O. Sticher, Quantitative high performance liquid chromatographic analysis of casticin in the fruits of *Vitex agnus-castus*, Pharm. Biol. 39 (2001) 57–61.
[25] A. Bilia, P. Melillo de Malgalhaes, M. Bergonzi, F. Vincieri, Simultaneous analysis of artemisinin and flavonoids of several extracts of *Artemisia annua* L. obtained from a commercial sample and a selected cultivar, Phytomedicine 13 (2006) 487–493.

Journal of Pharmaceutical and Biomedical Analysis 61 (2012) 247–251

Contents lists available at SciVerse ScienceDirect

Journal of Pharmaceutical and Biomedical Analysis

journal homepage: www.elsevier.com/locate/jpba

Short communication

Simultaneous quantitative determination and validation of quercetin glycosides with peroxynitrite-scavenging effects from *Saussurea grandifolia*

Agung Nugroho[a,b], Sang-Cheol Lim[a], Chan Mi Lee[c], Jae Sue Choi[c], Hee-Juhn Park[d,*]

[a] Department of Applied Plant Sciences, Graduate School, Sangji University, Wonju 220-702, Republic of Korea
[b] Department of Agro-industrial Technology, Faculty of Agriculture, Lambung Mangkurat University, Indonesia 70712, Indonesia
[c] Department of Food Science and Nutrition, Pukyong National University, Busan 607-737, Republic of Korea
[d] Department of Pharmaceutical Engineering, Sangji University, Wonju 220-702, Republic of Korea

ARTICLE INFO

Article history:
Received 11 October 2011
Received in revised form
10 November 2011
Accepted 14 November 2011
Available online 22 November 2011

Keywords:
Saussurea grandifolia
Compositae
Saxifragin
Peroxynitrite
HPLC

ABSTRACT

The leaves of *Saussurea grandifolia* (Compositae) are used as chwinamul, a well-known Korean mountainous vegetable, or to treat hepatitis and hematuria. Since the methanolic extract of *S. grandifolia* leaves exhibit a potent peroxynitrite-scavenging effect, phytochemical and high-performance liquid chromatographic (HPLC) analyses were employed to identify and simultaneously quantify the active components: chlorogenic acid and 3,5-di-O-caffeoylquinic acid (3,5-DQ) as caffeoylquinic acids, and quercetin, isoquercitrin (quercetin-3-glucoside), saxifragin (quercetin-5-glucoside), and rutin (quercetin-3-rutinoside). Validation of HPLC methods was performed to verify the linearity, LOD, LOQ, intra-day and inter-day variabilities, recovery, and repeatability to ensure that this method is selective, sensitive, precise, accurate and reproducible. In particular, leaves contained saxifragin with potent peroxynitrite-scavenging activity (IC_{50}, 0.67 μM) as 4.65 mg/g dry weight, which is equivalent to 33.74 mg/g extract.

© 2011 Elsevier B.V. All rights reserved.

1. Introduction

Mountainous vegetables are consumed to treat or prevent several diseases in Korea. Numerous mountainous vegetables belong to the family Compositae. Chwinamul is a representative mountainous vegetable among this family, but it refers to several species: *Aster scaber*, *Aster yomena*, *Solidago virga* var. *gigantea*, *Solidago virgaaurea* var. *asiatica*, *Saussurea grandifolia*, *Ainsliaea acerifolia*, *Ligularia fischeri*, and *Ligularia stenocephala* [1,2]. We have studied the polyphenolic substances of chwinamul, since those compounds are commonly beneficial for aging-related diseases. In particular, chwinamul contains high amounts of caffeoylquinic acids [3].

Peroxynitrite is a highly reactive oxidant that is produced from the reaction between superoxide anion radical ($^{\bullet}O_2^-$) and nitric oxide ($^{\bullet}NO$) [4]. Overproduction of peroxynitrite results in peroxidation of lipids and proteins, cytotoxicity, and neurotoxicity [5]. Furthermore, it causes hypercholesterolemia, atherosclerosis, obesity and diabetes mellitus [6–8].

S. grandifolia is a mountainous vegetable that is used in chwinamul. Since quercetin glycosides were identified from this plant during our study of polyphenolic substances with peroxynitrite-scavenging activity, high-performance liquid chromatographic (HPLC) quantitative analysis and peroxynitrite-scavenging assays of these substances were performed. Validation of the linearity, precision, accuracy and repeatability of our HPLC method was also performed to verify the present method.

2. Experimental

2.1. Plant material

S. grandifolia (Compositae) was collected in Gangwon-do province, Korea, and identified by Won-Bae Kim (National Institute of Horticultural & Herbal Science, Rural Development Administration, Korea). This plant was dried and pulverized for extraction. A voucher specimen was deposited in the Laboratory of Natural Product Chemistry, Department of Pharmaceutical Engineering, Sangji University, Korea.

2.2. Instruments and reagents

The Varian HPLC system (Varian, Walnut Creek, CA, USA) used in this study consisted of Prostar 210 solvent delivery module and Prostar 325 UV–Vis detector. A Shiseido (Chuoku, Tokyo, Japan) Capcell Pak C18 column (5 μm, 250 mm × 4.6 mm i.d.) was used as the column. Solvents used for the mobile phase were

* Corresponding author. Tel.: +82 33 730 0564; fax: +82 33 730 0564.
E-mail address: hjpark@sangji.ac.kr (H.-J. Park).

0731-7085/$ – see front matter © 2011 Elsevier B.V. All rights reserved.
doi:10.1016/j.jpba.2011.11.016

HPLC grade (J.T.Baker, Phillipsburg, NJ, USA). Reagents used for peroxynitrite-scavenging assay were as follows: diethylenetriaminepentaacetic acid (DTPA) was from Sigma Chemical Co. (St. Louis, MO, USA), dihydrorhodamine 123 (DHR 123) was from Molecular Probes (Eugene, OR, USA), peroxynitrite was from Cayman Chemicals Co. (Ann Arbor, MI, USA). Silica gel used for column chromatography was silica gel 60 (70–230 mesh, Merck, Germany) and TLC plate was Merck Kieselgel 60 F254 plate (20 cm × 20 cm, 0.25 mm thickness). TLC spots were observed under UV light.

2.3. Standard compounds

Three compounds, chlorogenic acid, saxifragin, and rutin, were isolated from *S. grandifolia* and used for HPLC analysis. The isolation of these compounds is described briefly. The dried plant material (400 g) was extracted three times with MeOH for 6 h under reflux on a heating mantle. The extracted solution was filtered and evaporated under reduced pressure to give a viscous extract, which was further lyophilized for 12 h to give the MeOH extract (weight, 55.02 g; yield, 13.75%). A portion of the MeOH extract (53 g) was suspended in 800 ml of H_2O, fractionated successively with the same volume of diethyl ether and n-butanol (BuOH), and then concentrated, respectively, to give a diethyl ether fraction (24.75 g) and BuOH fraction (19.17 g). The BuOH fraction (18.17 g) was subjected to sequential Diaion HP-20 column chromatography with water (1.5 l), 50% MeOH (1.5 l), and MeOH (1.5 l) and collected as nine 500-ml (each) fractions. SG-# 6 fraction was concentrated *in vacuo* and then chromatographed on a silica gel column (2.76 g, 4.5 cm × 35 cm) with $CHCl_3$–MeOH–H_2O (70:30:10, lower phase) to produce compound **1** (1.25 g). The combined fraction of SG-#7 and SG-#8 was dissolved in 80 ml of MeOH and allowed to stand more than 48 h to yield a precipitate of yellowish powder (compound **2**, 940 mg). The liquid phase resulted from that precipitation process was evaporated and chromatographed consecutively on ODS- and Sephadex column to produce compound **3** (460 mg). Based on their spectroscopic data (^{1}H NMR and ^{13}C NMR) which were agreeable with literatures data [9–12], those three compounds, **1**–**3**, were identified as chlorogenic acid, quercetin 5-O-β-D-glucopyranoside (saxifragin) and quercetin 3-O-α-L-rhamnopyranosyl-(1→6)-β-D-glucopyranoside (rutin), respectively. The three compounds, quercetin 5-O-β-D-glucopyranoside (isoquercitrin), 3,5-di-O-caffeoylquinic acid (3,5-DQ) and quercetin, were purchased from Sigma Co. (St. Louis, MO, USA) and used for HPLC analysis.

2.4. Chlorogenic acid

White geisha powder from MeOH, ^{1}H NMR (500 MHz, DMSO-d_6), ^{13}C NMR (125 MHz, DMSO-d_6): [9].

2.5. Saxifragin (Qc-5-glc)

Yellowish needles from MeOH, bright yellow fluorescence under UV light (365 nm), mp 264 °C, ^{1}H NMR (500 MHz, DMSO-d_6): [10], ^{13}C NMR (125 MHz, DMSO-d_6): [11].

2.6. Rutin (Qc-3-rut)

Yellowish powder from MeOH, mp 187–189 °C, ^{1}H NMR (500 MHz, DMSO-d_6), ^{13}C NMR (125 MHz, DMSO-d_6): [12].

2.7. Preparation of sample solution

A small amount of the lyophilized MeOH extract (yield: 13.75%) that was used in the isolation process was employed for HPLC quantification analysis. To comply with ICH guidelines for analytical procedures, five different concentrations (1000, 1500, 2000, 2500 and 3000 μg/ml) of sample solutions were made individually by dissolving samples in MeOH; those five solutions were then used for repeatability tests, and one of them (1500 μg/ml) was used for intra-day and inter-day variability test. Before injection onto the HPLC, all sample solutions were filtered using 0.50-μm syringe filters.

2.8. HPLC condition

Five standard compounds were dissolved in MeOH, vortexed and then dissolved completely by ultrasonicator to prepare standard solutions. The solutions were filtered using 0.50-μm syringe filters and injected onto the HPLC system. The mobile phase consisted of two solutions (A and B solutions) and flowed with a programmed gradient elution. The A solution was 0.05%-trifluoroacetic acid (TFA) aqueous solution and the B solution was 0.05% TFA in MeOH–CH_3CN (60:40). Gradient elution was programmed as follows: (A)/(B) = 85/15 (0 min) → 35/65 (35 min, hold for 10 min) → 0/100 (47 min; hold for 4 min to wash the column) → 85/15 (54 min; hold for 6 min to equilibrate the column condition). Recording of the chromatogram was set from 0 min to 37 min. The column temperature was 40 °C, and the flow rate was 1.00 ml/min. A wavelength 254 nm for detection was chosen during our consideration of the three ones, 254, 280, and 360 nm, because it was the most sensitive. That wavelength was sensitive enough to detect the two types of phenolics including caffeoylquinic acids and flavonols simultaneously.

2.9. Linearity of standard compounds

The linearity of the standard compounds was assessed. Standard solutions were prepared by serial dilution method over the range of 1.56–50.0 μg/ml (saxifragin, rutin, isoquercitrin), 2.50–80.00 μg/ml (chlorogenic acid), and 1.88–60.00 μg/ml (3,5-DQ, quercetin). Calibration equations were obtained by plotting the mean of peak area (*y* axis) versus concentration (*x* axis) for each analyte in that range. Linearity was evaluated by R^2 value.

2.10. LOD and LOQ

LOD (limit of detection) and LOQ (limit of quantification) were determined by injecting 20 μl of the serial dilution of six individual solutions onto HPLC. LODs and LOQs under the present HPLC method were determined at signal to noise (S/N) ratios of 3 and 10, respectively.

2.11. Precision, accuracy, and repeatability studies

The intra-day and inter-day variabilities were studied to assess the precision of the method. Intra-day variability was determined by analyzing within 24 h. Each solution was measured five times and the relative standard deviation (RSD) was considered a measure of precision. Accuracy was assessed by measuring the mean recovery rate (%) from the spiked sample solution versus the non-spiked solution.

2.12. Assay for peroxynitrite-scavenging activity

Peroxynitrite-scavenging effect was determined by modifying the method described by Kooy et al. [13]. This method involves monitoring the highly fluorescent rhodamine 123, which is formed rapidly from non-fluorescent DHR 123 under peroxynitrite. The rhodamine buffer (pH 7.4) consisted of 50 mM sodium phosphate dibasic, 50 mM sodium phosphate monobasic, 90 mM sodium

chloride, 5 mM potassium chloride, and 100 μM DTPA (diethylenetriaminepentaacetic acid). The final DHR 123 concentration was 5 μM. The buffer used in this assay was prepared prior to use and placed on ice. The extract was dissolved in 10% DMSO prior to use. The background and fluorescence intensities were measured 5 min after treatment with and without authentic peroxynitrite (10 μM) dissolved in 0.3 N sodium hydroxide. The fluorescenceintensity of oxidized DHR 123 was measured at excitation and emission wavelengths of 480 nm and 530 nm, respectively, using microplate fluorescencereader FL 500 (Bio-Tek Instruments Inc., Winooski, VT, USA). Peroxynitrite-scavenging activity was calculated as the final fluorescence intensity minus the background fluorescence, via the detection of DHR oxidation. L-Penicillamine was used as a positive control.

3. Results and discussion

3.1. Identification and peroxynitrite-scavenging activity

Since the MeOH extract showed a potent peroxynitrite-scavenging effect, we attempted to identify the active compounds and their quantitative levels in the extract and plant material. Three isolated compounds, chlorogenic acid [9], saxifragin [10,11] and rutin [12] were identified by comparing their spectroscopic data (^{1}H NMR and ^{13}C NMR) with literature data. Three other compounds, isoquercitrin, quercetin and 3,5-DQ were identified by comparing their retention time with the standard compounds and were confirmed again by recovery test. Therefore, these six compounds were used for the quantification; their structures are shown in Fig. 1. Among them, saxifragin, with its bright yellow fluorescent color and the structure of a flavonol 5-O-glycoside, is uncommon in natural sources. This compound was first isolated from *Saxifraga stolonifera* [10] and then from silkworm (*Bombyx mori*) [11]. As shown in Fig. 2, the four quercetin analogues and the two caffeoylquinic acids were observed on the HPLC chromatogram.

Peroxynitrite-scavenging activity was indicated by the value of IC_{50} of each extract (μg/ml) and active compound (μM). As shown in Table 1, the IC_{50}s of peroxynitrite-scavenging activity of MeOH extract and BuOH fraction were 1.09 μg/ml and 0.55 μg/ml, respectively, indicating that the active compounds were mainly in the BuOH fraction. The activity levels of isoquercitrin and saxifragin were similar based on the IC_{50} values (0.67 μM). But the IC_{50} of rutin (2.62 μM) was higher than that of those two compounds. On the other hand, the two caffeoylquinic acids, chlorogenic acid and 3,5-DQ, had significant activities with IC_{50}s of 0.84 μM and 1.00 μM. Those data demonstrated that the six compounds, which possess catechol (3,4-dihydroxyphenyl) moiety, were active more than L-penicillamine as the positive control (11.69 μM).

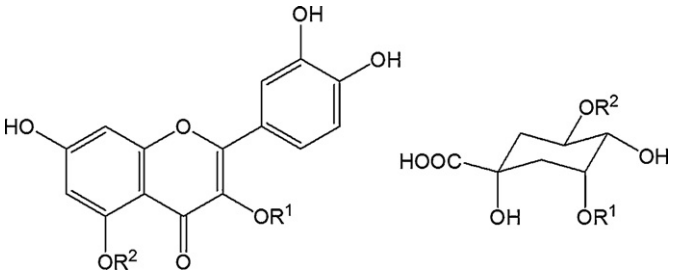

Fig. 1. Structure of six compounds identified in *S. gradifolia*. Quercetin: R^1 = OH, Isoquercitrin: R^1 = β-D-glucopyranosyl, R^2 = H, Rutin: R^1 = α-L-rhamnopyranoyl-(1 → 6)-β-D-glucopyranosyl, R^2 = H, Saxifragin: R^1 = H, R^2 = β-D-glucopyranosyl, chlorogenic acid: R^1 = H, R^2 = caffeoyl, 3,5-DQ: R^1 = caffeoyl, R^2 = caffeoyl.

3.2. Optimization of HPLC conditions

Recently, many researchers have reported HPLC quantification of bioactive compounds contained in medicinal plants or functional foods and their validation. In this research, the validation of the present HPLC method was performed to assess linearity, precision, repeatability and accuracy according to the International Conference on Harmonization (ICH) guidelines.

The HPLC conditions were investigated with regard to column, mobile phase, and detection wavelength for better HPLC chromatographic resolution. Capcell Pak C18 column (5 μm, 250 mm × 4.6 mm) was chosen because it showed more selectivity. The mobile phase system of 0.05% TFA (trifluoroacetic acid) in water (A solvent) and 0.05% TFA in MeOH–CH_3CN (60:40) (B solvent) was selected because it showed better peak shapes than the MeOH–H_2O or MeOH–CH_3CN system. Addition of TFA improved peak shapes because the acid prohibited ionization. Combination of 40 °C of column temperature and 1.00 ml/min of flow rate showed an adequate separation of the constituents. The 254 nm of detection wavelength also showed better sensitivity than other two wavelengths (280 and 360 nm) for detection of phenolic compounds, including caffeoylquinic acids and flavonols.

3.3. Validation on the HPLC method

HPLC experiments on linearity, precision, and repeatability were performed to demonstrate that the present method is selective, precise and reproducible, respectively. To determine linearity, six concentrations of each standard solution were injected: chlorogenic acid (2.50–80.00 μg/ml), saxifragin, rutin, isoquercitrin (1.56–50.00 μg/ml) and 3,5-DQ and quercetin (1.88–60.00 μg/ml). Calibration curve equations were obtained by plotting peak area versus concentrations. Since all the R^2 values were >0.999, linearity was verified. This method was sensitive for

Table 1
Peroxynitrite-scavenging effect (%) of the MeOH extract of *Saussurea grandifolia* and its constituents.

Treatment	Concentration (μg/ml)				IC_{50}
	10.0	2.0	0.40	0.080	
MeOH ext.	91.82 ± 2.41[a]	68.43 ± 0.75	35.75 ± 2.57	–	1.09 ± 0.03 μg/ml
BuOH fraction	94.04 ± 1.40	72.56 ± 4.38	53.05 ± 9.55	–	0.55 ± 0.01 μg/ml
Chlorogenic acid	–	89.70 ± 1.85	72.56 ± 4.38	53.05 ± 9.55	0.84 ± 0.11 μM
Saxifragin	–	86.40 ± 0.56	61.29 ± 1.51	19.59 ± 9.79	0.67 ± 0.03 μM
Rutin	–	72.95 ± 1.22	26.00 ± 1.58	23.20 ± 0.98	2.62 ± 0.06 μM
Isoquercitrin	–	93.23 ± 0.30	62.17 ± 5.70	19.62 ± 5.56	0.67 ± 0.04 μM
3,5-DQ	–	86.03 ± 2.31	50.53 ± 3.18	7.72 ± 4.90	1.00 ± 0.04 μM
Quercetin	–	92.81 ± 2.10	73.34 ± 1.33	19.35 ± 1.48	0.87 ± 0.01 μM
L-Penicillamine	–	55.03 ± 4.51	18.91 ± 9.89	8.75 ± 7.87	11.69 ± 0.87 μM

[a] Value represents mean ± SD; IC_{50} values are mean ± SEM (standard error of the mean); – (not tested).

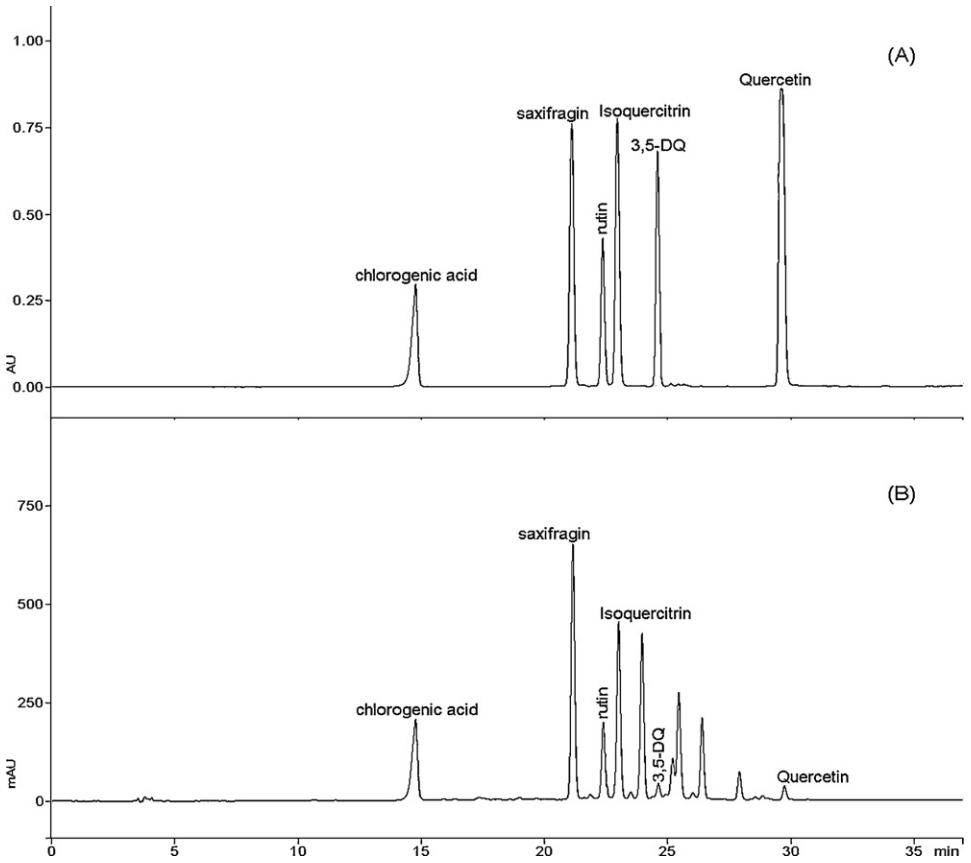

Fig. 2. (A) Chromatogram of mixed standard compounds, (B) Chromatogram of MeOH extract of *S. grandifolia*.

Table 2
Calibration curves, detection limits and quantification limits of the analytes.

Analyte	Calibration equation (linear model)[a]	Linear range (μg/ml)	R^2[b]	LOD[c] (μg/ml)	LOQ[d] (μg/ml)
Chlorogenic acid	$y = 85.929x + 11.29$	2.50–80.00	0.9998	0.74	2.47
Saxifragin	$y = 414.623x + 65.93$	1.56–50.00	0.9998	0.12	0.40
Rutin	$y = 143.532x + 15.18$	1.56–50.00	0.9999	0.42	1.34
Isoquercitrin	$y = 472.749x + 75.62$	1.56–50.00	0.9999	0.11	0.36
3,5-DQ	$y = 133.880x + 34.25$	1.88–60.00	0.9997	0.30	1.01
Quercetin	$y = 659.275x + 87.33$	1.88–60.00	0.9999	0.09	0.23

[a] y, peak area at 254 nm; x, concentration of the standard (μg/ml).
[b] R^2, correlation coefficient for 6 data points in the calibration curves ($n = 3$).
[c] LOD, limit of detection (S/N = 3).
[d] LOQ, limit of quantification (S/N = 10).

detection and quantification, since LOD and LOQ were >0.74 μg/ml and >2.47 μg/ml, respectively (Table 2).

Intra-day and inter-day variabilities were measured to assess the precision. In this test, sample solutions were injected five times to obtain RSDs. As shown in Table 3, the RSDs in intra-day and inter-day variability were <2.84% and <3.11%, respectively. The RSD in the repeatability test was <3.43%.

The recovery test, which is used to evaluate accuracy, is a method that measures the change of recovery rate (%) by addition of standard compounds to the sample solution. Accuracy was

Table 3
Analytical results of intra-day and inter-day variabilities and repeatability for the analytes of MeOH extract.

Analyte	Intra-day variability		Inter-day variability		RRT[a]		Repeatability ($n = 5$)	
	Content (mg/g)	RSD (%)	Content (mg/g)	RSD (%)	α	RSD	Content (mg/g)	RSD (%)
Chlorogenic acid	89.92	0.33	89.90	0.39	1.00	0.13	89.87	0.42
Saxifragin	30.80	0.56	30.89	0.64	1.43	0.09	30.76	0.71
Rutin	33.78	0.29	33.79	0.36	1.52	0.08	33.74	0.40
Isoquercitrin	24.53	0.45	24.51	0.58	1.56	0.08	24.46	0.63
3,5-DQ	3.55	2.24	3.57	2.44	1.66	0.06	3.51	2.74
Quercetin	1.01	2.84	1.02	3.11	2.01	0.05	0.99	3.43

[a] RRT: relative retention time.

Table 4
Recovery of each analyte as determined by standard addition method.

Analyte	Initial concentration (μg/ml)	Amount added (μg)	Concentration after addition (μg/ml)		Recovery (%)	RSD (%)
			Expected	Measured		
Chlorogenic acid	122.25	100	222.25	227.32	102.28	2.19
Saxifragin	41.92	50	91.92	95.19	103.56	1.52
Rutin	45.98	50	95.98	93.22	97.12	1.89
Isoquercitrin	33.39	25	58.39	56.25	96.34	2.22
3,5-DQ	4.83	7.50	12.33	11.90	96.51	2.14
Quercetin	1.36	3.75	5.11	5.33	104.29	1.98

The data was present as average of three determinations.

Table 5
Content of analytes.

Analyte	Content of analytes (mg/g)		
	of extract[a]	of DW[b]	RSD
Chlorogenic acid	89.87	12.35	0.42
Saxifragin	30.76	4.24	0.71
Rutin	33.74	4.65	0.40
Isoquercitrin	24.46	3.37	0.63
3,5-DQ	3.51	0.49	2.74
Quercetin	0.99	0.14	3.43

[a] Lyophilized MeOH extract.
[b] DW: dry weight of plant materials.

evaluated by calculating the mean recovery rate (%) of standard compounds from the spiked extract solution versus the non-spiked extract sample. As shown in Table 4, the mean recovery rate was between 96.34 and 104.29% and the RSD was <2.22%. These results verified that the present method for analysis of the six compounds, chlorogenic acid, 3,5-DQ, isoquercitrin, saxifragin, rutin, and quercetin of *S. grandifolia*, is selective, sensitive, accurate, precise and reproducible.

3.4. Sample analysis

Using the present verified method, six compounds were quantitatively analyzed. The contents (mg/g) are shown as the concentration in the extract and in the dried weight of plant material (DW), respectively. Of the six compounds, the content of chlorogenic acid was highest at 89.87 mg/g extract and 12.35 mg/g DW. The concentration of saxifragin was 30.76 mg/g extract and 4.24 mg/g DW, respectively, and these levels were similar to those of rutin and isoquercitrin. Compared with those levels, the contents of 3,5-DQ and quercetin were very low (Table 5).

4. Conclusions

The six compounds with a catechol (3,4-dihydroxylphenyl) moiety had potent peroxynitrite-scavenging effects and their contents in *S. grandifolia* were determined. Since overproduction of peroxynitrite causes aging-related diseases such as diabetes mellitus, obesity, hypercholesterolemia, and atherosclerosis, intake of *S. grandifolia could* contribute to the treatment or prevention of such diseases. In addition, saxifragin with its bright yellow fluorescent color could be considered as a marker compound of *S. grandifolia* because that compound is very uncommon in plant kingdom.

Acknowledgements

This research was supported by the Basic Science Research Program through the National Research Foundation of Korea (NRF) funded by the Ministry of Education, Science and Technology (# 20100021039).

References

[1] H.J. Park, Chemistry and pharmacological action of caffeoylquinic acid derivatives and pharmaceutical utilization of chwinamul (Korean Mountainous vegetable), Arch. Pharm. Res. 33 (2010) 1703–1720.
[2] A. Nugroho, J. Choi, K.R. Lee, M.S. Bachri, J.S. Choi, W.B. Kim, K.T. Lee, H.J. Park, Anti-ulcerogenic effect of the caffeoylquinic acid-rich extract from *Ligularia stenocephala* and HPLC Analysis, Biol. Pharm. Bull. 33 (2010) 493–497.
[3] A. Nugroho, K.H. Kim, K.R. Lee, M.B. Alam, J.S. Choi, W.B. Kim, H.J. Park, Qualitative and quantitative determination of the caffeoylquinic acids on the Korean mountainous vegetables used for chwinamul and their peroxynitrite-scavenging effect, Arch. Pharm. Res. 32 (2009) 1361–1367.
[4] R. Radi, J.S. Beckman, K.M. Bush, B.A. Freeman, Peroxynitrite oxidation of sulfhydryls, the cytotoxic potential of superoxide and nitric oxide, J. Biol. Chem. 266 (1991) 4244–4250.
[5] G.R. Haenen, J.B. Paquay, R.E. Korthouwer, A. Bast, Peroxynitrite scavenging by flavonoids, Biochem. Biophys. Res. Commun. 236 (1997) 591–593.
[6] M. Korda, R. Kubant, S. Patton, T. Malinski, Leptin-induced endothelial dysfunction in obesity, Am. J. Physiol. Heart Circ. Physiol. 295 (2008) 1514–1521.
[7] P. Patcher, I.G. Obrosova, J.G. Mabley, C. Szabo, Role of nitrosative stress and peroxynitrite in the pathogenesis of diabetic complications, emerging new therapeutical strategies, Curr. Med. Chem. 12 (2005) 267–275.
[8] V.R. Drel, P. Patcher, I. Vareniuk, I. Pavlov, V.V. Lyzogulbov, J.T. Grovez, I.G. Obrosova, A peroxynitrite decomposition catalyst counteracts sensory neuropathy in streptozotocin-diabetic mice, Eup. J. Pharmacol. 569 (2007) 48–58.
[9] H.A. Jung, J.C. Park, H.Y. Chung, J. Kim, J.S. Choi, Antioxidant flavonoids and chlorogenic acid from the leaves of *Eryobotrya japonica*, Arch. Pharm. Res. 22 (1999) 213–218.
[10] N. Morita, M. Shimizu, M. Arisawa, M. Koshi, Studies on the medicinal resources. XXXVI. The constituents of the leaves of *Saxifraga stolonifera* Meerburg (Saxifragaceae), Chem. Pharm. Bull. 22 (1974) 1487–1489.
[11] Y. Tamura, K. Nakajima, K. Nagayasu, C. Takabayashi, Flavonoid 5-glucosides from the cocoon shell of the silk worm *Bombyx mori*, Phytochemistry 59 (2002) 275–278.
[12] H.W. Park, N.I. Baek, S.H. Kim, B.M. Kwon, I.S. Chung, M.H. Park, S.H. Kim, D.K. Kim, Phytochemical components from the whole plants of *Arabis glabra* (L.) Bernh, Kor. J. Pharmacogn. 35 (2004) 320–323.
[13] N.W. Kooy, J.A. Royall, H. Ischiropoulos, J.S. Beckman, Peroxynitrite-mediated oxidation of dihydrorhodamine 123, Free Radic. Biol. Med. 16 (1994) 149–156.

Journal of Pharmaceutical and Biomedical Analysis 61 (2012) 252–255

Contents lists available at SciVerse ScienceDirect

Journal of Pharmaceutical and Biomedical Analysis

journal homepage: www.elsevier.com/locate/jpba

Short communication

Simultaneous determination of tetrandrine and fangchinoline in herbal medicine *Stephania tetrandra* S. Moore by liquid chromatography with electrochemical detection

Lihong Liu[a,b], Shenglan Li[a,b], Zilin Chen[a,b,*]

[a] Key Laboratory of Combinatorial Biosynthesis and Drug Discovery (Wuhan University), Ministry of Education, Wuhan 430071, China
[b] School of Pharmaceutical Sciences, Wuhan University, Wuhan 430071, China

ARTICLE INFO

Article history:
Received 18 August 2011
Received in revised form
25 November 2011
Accepted 25 November 2011
Available online 6 December 2011

Keywords:
Tetrandrine
Fangchinoline
Stephania tetrandra S. Moore
LC-ECD
Herbal medicine

ABSTRACT

A simple and selective method was developed for the simultaneous determination of tetrandrine and fangchinoline in herbal medicine by HPLC with electrochemical detection (ECD) on a bare glassy carbon electrode. The HPLC separation and ECD conditions have been optimized. The separation was carried out on a WondaSil® C18-WR column (4.6 mm × 250 mm, 5 μm), with the mobile phase of acetonitrile–ammonium acetate buffer (pH 6.5; 40 mM) (32:68, v/v) using an isocratic elution at the flow rate of 0.5 mL/min. The electrochemical detection potential was set at +0.9 V. The obtained LODs for tetrandrine and fangchinoline were 0.26 and 0.27 μmol/L, respectively. The method was successfully applied to the analysis of tetrandrine and fangchinoline contents in *Stephania tetrandra* S. Moore. It has been demonstrated that the LC-ECD method is an excellent technique for analysis of the herbal medicine. The mean recoveries were in the range of 95–105%, while the precision expressed as repetition of peak area was lower than 2.7%.

© 2011 Published by Elsevier B.V.

1. Introduction

Traditional Chinese medicines (TCMs) have been utilized to treat various diseases for centuries in China. Currently, scientists become aware that herbal medicine is an almost infinite resource for drug development, so more attention is paid on TCMs by modern pharmaceutical institutes [1]. Analysis of herbal medicine is an important technique, which affords much data in biochemical, pharmaceutical and clinical research. Because these medicinal plants usually contain complex constituents, efficient methods are required for the separation and identification of the active constituents from the matrix.

Stephania tetrandra S. Moore is a Chinese traditional medicine listed in the Chinese Pharmacopoeia [2,3]. A large number of compounds have been isolated from this plant in the past 50 years for studying the biologically active constituents [4,5]. Tetrandrine (TEN) and fangchinoline (FAN), which are isolated from the root of *Stephania tetrandra* S. Moore (Han-Fang-Ji in Chinese), have been known to have pharmacological activity such as anti-allergic, anti-inflammatory activity, anti-cancer, and hypotensive effects, inhibiting release of histamine, and reducing myocardial oxygen consumption [6–8]. In order to study pharmacological activities of TEN and FAN and to control quality of *S. tetrandra* and its products, a reliable and sensitive quantification method is needed.

Several analytical techniques are reported for determination of TEN and FAN such as TLC [9], CE [10,11], HPLC [12,13], pH-zone refining conventional high-speed countercurrent chromatography (CCC) [14] and HPLC/MS [15,16]. However, these methods suffer from various drawbacks such as time-consuming sample preparation, sophisticated instrumentation, and the requirement for a skilled operator. Thus, it is necessary to develop a rapid, simple, and inexpensive method for the TEN and FAN analysis. Electrochemical detections (ECD) provide very high sensitivity and selectivity. Recently, the hyphenation of high performance liquid chromatography with ECD draws attraction for the analysis of biological samples [17–19]. In our previous work, we have applied HPLC-ECD method for the determination of kynurenine and tryptophane in human plasma samples [20] and bavachin and isobavachalcone in Fructus Psoraleae [21].

In this paper, a simple and selective method for the analysis of TEN and FAN has been developed by liquid chromatography with electrochemical detection on a bare glassy carbon electrode. It has been demonstrated that the method has been applied to analyze the active components in real sample of herbal medicine *Stephania tetrandra* S. Moore.

* Corresponding author at: School of Pharmaceutical Sciences, Wuhan University Wuhan 430071, China. Tel.: +86 27 68759893; fax: +86 27 68759850.
E-mail address: chenzl@whu.edu.cn (Z. Chen).

0731-7085/$ – see front matter © 2011 Published by Elsevier B.V.
doi:10.1016/j.jpba.2011.11.027

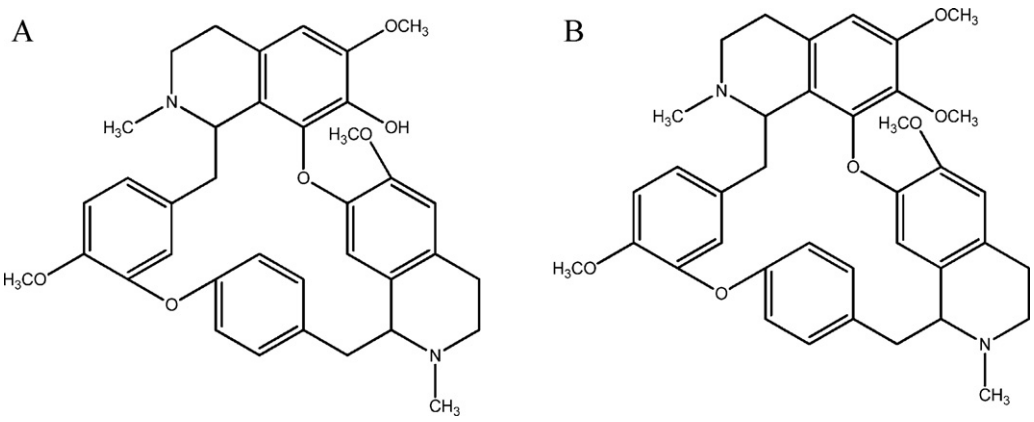

Fig. 1. Chemical structures of (A) FAN and (B) TEN.

2. Experimental

2.1. Chemicals and reagents

Tetrandrine (TET) and fangchinoline (FAN) (Fig. 1) were obtained from Aladdin Reagent Co., Ltd. (Shanghai, China). HPLC grade methanol and acetonitrile were purchased from Tedia Chemical (USA). Analytical reagents such as ammonium acetate and acetic acid were obtained from Sinopharm Chemical Reagent Co., Ltd. (Shanghai, China). All the other chemicals used were analytical reagents.

2.2. Instrumentation

The HPLC analysis was performed with a Shimadzu LC-20AT (Kyoto, Japan) equipped with a manual injector with a 20 μL sample loop. CHI 660 electrochemical workstation (CH Instrument Company, Shanghai, China) was used as an amperometric detector to control the detection potential and record the current. A three electrode system includes a 3 mm glassy carbon electrode as the working electrode, an Ag/AgCl reference electrode and a stainless steel auxiliary block as the counter electrode. The working electrode was set at potential of +0.9 V vs the Ag/AgCl reference electrode. The sensitivity of the detector was maintained at 10 μA full-scale deflection. Control and data collection/processing were handled through CHI 660 electrochemical workstation (Shanghai, China).

2.3. Preparation of GC electrode

The glassy carbon electrodes (GC, ∅ = 3 mm) were polished on a polishing pad with 0.05 μm alumina slurry, rinsed with water, ultrasonicated for 45 s in redistilled water and ethanol, respectively, and dried in air. The grassy carbon electrode was polished every day after experiment for an experiment by other researcher.

2.4. Chromatographic conditions

The HPLC analysis was carried out on WondaSil® C18-WR column (4.6 mm × 250 mm, 5 μm; GL Sciences Inc.). The flow rate was set at 0.5 mL/min. An isocratic elution was used with a mobile phase consisted of acetonitrile–ammonium acetate buffer (pH 6.5; 40 mM) (32:68, v/v). The mobile phase was filtered through a 0.22 μm nylon membrane filter prior to use.

2.5. Standard solution and sample preparation

TEN and FAN stock solutions were prepared with mobile phase and stored in a refrigerator. *Stephania tetrandra* S. Moore (Han-Fang-Ji) was bought from local pharmaceutical store. The plant sample was ground into powder, and 100 mg sample was transferred into a 25 mL volumetric EP tube. Then 15 mL methanol was added to the EP tube and the sample was ultrasonocated for 30 min. After centrifuging at 10,000 rpm for 10 min, the surpernate was collected and filtered through a 0.45 μm nylon membrane filter prior to analysis. Ultimately 20 μL of the sample solution was injected for HPLC analysis.

3. Results and discussion

3.1. Electrochemical behaviors of TEN and FAN on GCE

The differential pulse voltammetric behaviors of two alkaloids TEN and FAN on bare GCE were studied. Fig. 2 shows the electrochemical response of two alkaloids. As shown in Fig. 2, when TEN was introduced into the electrolyte, a sensitive anodic peak was observed (Fig. 2a) on bare GCE with a peak potential of 0.728 V (vs Ag/AgCl) in the supporting electrolyte. FAN was also investigated and there were two anodic peaks observed at the peak potentials of

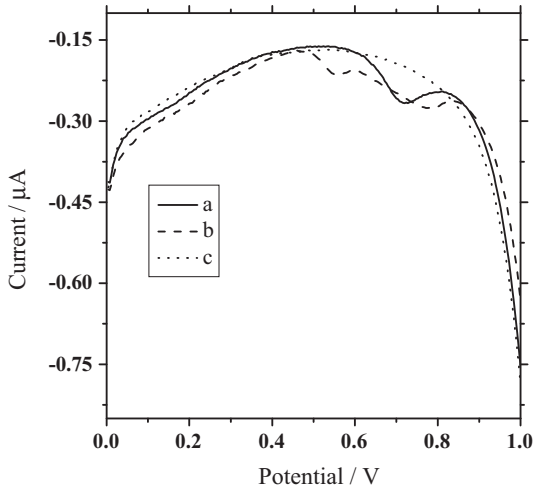

Fig. 2. Differential pulse voltammetric behaviors of two alkaloids TEN and FAN on bare GCE. (a) 9 μM TEN; (b) 9 μM FAN; (c) Blank. Scan rate: 0.1 V s^{-1}; supporting electrolyte: acetonitrile–ammonium acetate buffer (pH 6.5; 40 mM) (32:68, v/v); accumulation time: 180 s (on open-circuit).

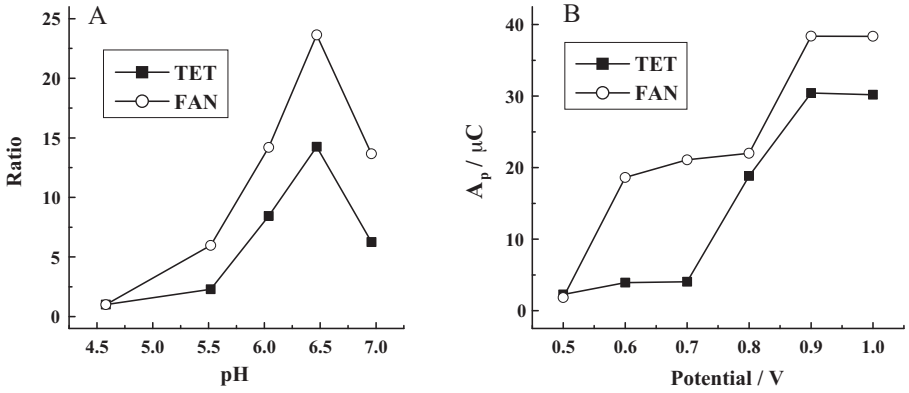

Fig. 3. (A) Effect of pH of mobile phase on the sensitivity of EC detection of TEN and FAN (*X* axis is the pH value of mobile phase. *Y* axis is the ratio between the peak areas at certain pH and the peak area at pH 4.6). (B) Electrochemical responses (peak area) of TEN and FAN at various potential settings.

0.544 V and 0.756 V (Fig. 2b). As expected, there is no anodic peak in blank electrolyte (Fig. 2c).

3.2. Optimization of HPLC-EC detection

Chromatography was performed on a WondaSil® C18-WR column. Acetonitrile and water were examined as the mobile phases at different ratio of acetonitrile to water. Acetonitrile–water (32:68, v/v) was preferred for analysis.

Although electrochemical detector is a sensitive detector, the sensitivity can be affected by the pH and ionic strength of the buffers in the mobile phase [22]. Ammonium acetate is one of the most commonly used buffers for EC detection [23,24]. We compared the sensitivity of EC detections, when different ionic strengths were used. The highest sensitivity was achieved when 40 mM ammonium acetate was used in the mobile phase. The pH value of the mobile phase was adjusted to carry out satisfactory LC separation and EC detection. Fig. 3(A) shows the effects of pH of mobile phase on the sensitivity of the EC detection in terms of TEN and FAN quantification. When pH value was at 6.5, the peak current increased significantly. The reason is probably that the electron transfer of TEN and FAN on bare GCE is easier at pH 6.5. Thus, acetonitrile–ammonium acetate (40 mM) buffer at pH 6.5 (32:68, v/v) was preferred for better EC detection sensitivity.

The applied potential was determined by comparing detection signals at different applied potentials. As shown in Fig. 3 (B), when the potential was set at +0.9 V, a higher signal was generated without interfering with background peaks. Therefore, 0.9 V was selected for subsequent experiments.

3.3. Performance of the analytical method

Under the optimum conditions, the calibration curves were calculated for more than seven concentration levels (each concentration was injected in triplicate). The oxidation current on ECD was linear with the concentration of analytes in the range of 1.3–107 μM for TEN ($R = 0.9966$) and 1.4–109 μM for FAN ($R = 0.9970$). The LODs for TEN and FAN were 0.26 μM and 0.27 μM, respectively. The repeatability of the method was also studied ($n = 4$). The obtained RSD values for peak areas and retention times were lower than 3.4% and 1.8%, respectively. These results suggest that the proposed method has good suitability, as these errors are not more critical than those obtained from conventional methods.

3.4. Analysis of Stephania tetrandra S. Moore by LC-ECD and structure identification

The contents of TEN and FAN in medicinal plant *Stephania tetrandra* S. Moore were tested by the developed method. As shown in Fig. 4, there are no any interferences resulted from the matrix in the area of analyte peaks. Therefore, analytes can be easily discriminated and quantified using EC detection. The average contents of TEN and FAN in *Stephania tetrandra* S. Moore are 0.78% and 0.40%, respectively. These results are in very good agreement with the reference [14] by LC–UV method. The results for determining TEN and FAN are listed in Table 1. As can be seen in the table, the concentrations added and found are in good agreement, and with absolute recoveries ranged from 95.0 to 105.0%.

To check the reliability of results obtained by LC-ECD method, LC/ESI-MS measurements were also applied. The LC–MS analysis was carried out on an Agilent 1100 series LC/MSD Trap-SL (Agilent, Wilmington, Germany). The mass spectra were recorded in a positive ion mode, with mass scan range 100–1000 *m/z*. As expected, only protonated ions $[M+H]^+$ (*m/z* 609 for FAN and *m/z* 623 for TEN) were generated in MS spectra (Fig. 5). It has been demonstrated that the results obtained by LC-ECD agree well with those obtained by LC–MS without interference of endogenous components.

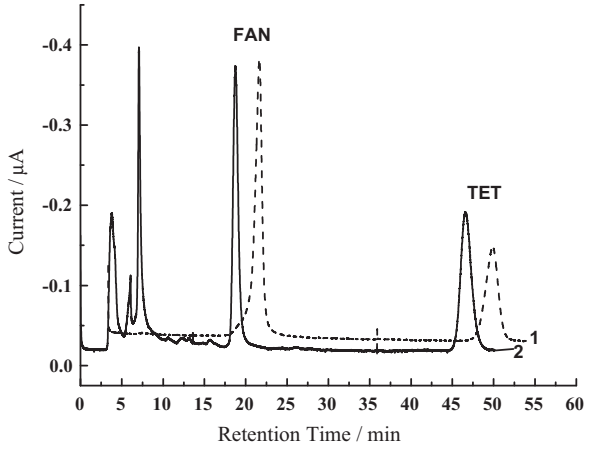

Fig. 4. Representative chromatograms for determining TEN and FAN by LC-ECD. (1) Standard solution; (2) *Stephania tetrandra* S. Moore.

Table 1
Recovery of TEN and FAN in *Stephania tetrandra* S. Moore.

Compound	Added concentration (μM)	Found concentration (μM)	Recovery (%)	RSD (%, $n = 5$)
TEN	2.7	2.8	103.7	2.7
	5.4	5.3	98.1	2.2
	16.1	16.9	105.0	1.7
	80.0	76.0	95.0	1.2
FAN	2.7	2.8	103.7	2.5
	5.5	5.7	103.6	1.9
	16.4	15.7	95.7	1.5
	50.0	47.8	95.6	1.1

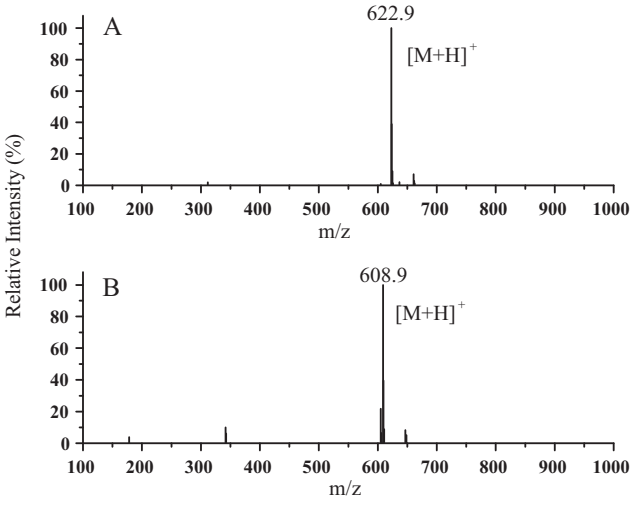

Fig. 5. MS spectra in the full scan mode of (A) FAN; (B) TEN.

4. Conclusion

In this work, a novel, simple and selective LC-ECD method has been developed for simultaneous determination of active components of TEN and FAN in the Chinese medicines. Because of the good accuracy and selectivity, the LC-ECD method is suitable for the quality control of commercial medicines containing TEN and FAN. This LC-ECD method may be used as a valuable alternative technique to LC–UV in the simultaneous determination of TEN and FAN. The method has been applied to the real sample analysis of *Stephania tetrandra* S with the average contents of TEN and FAN 0.78% and 0.40%, respectively. The specificity and accuracy of the proposed LC-ECD method has been confirmed with LC/ESI-MS.

Acknowledgements

This work was supported by the National Scientific Foundation of China (NSFC NOs. 90817103, 30973672 and 20775055), the Fundamental Research Funds for the Central Universities.

References

[1] T.H. Tsai, Analytical approaches for traditional Chinese medicines exhibiting antineoplastic activity, J. Chromatogr. B 764 (2001) 27–48.
[2] R. Sager, Tumor suppressor genes: the puzzle and the promise, Science 246 (1989) 1406–1412.
[3] D.C. Fang, W.X. Yao, G.J. Xia, L. Qu, M.X. Jiang, Studies on the calcium antagonistic action of tetrandine: I. Effects of tetrandrine on the isolated guinea pig atrium, Journal of Huazhong University of Science and Technology-Medical Science 1 (1981) 46–50.
[4] H.L. Koh, H. Wang, S. Zhou, E. Chan, S.O. Woo, Detection of aristolochic acid I, tetrandrine and fangchinoline in medicinal plants by high performance liquid chromatography and liquid chromatography/mass spectrometry, J. Pharm. Biomed. 40 (2006) 653–661.
[5] C.J. Chou, L.C. Lin, C. Peng, Y.C. Shen, C.F. Chen, Determination of tetrandrine, fangchinoline, cyclanoline and oblongine in Radix *Stephaniae tetrandrae* by HPLC, J. Chin. Med. 13 (2002) 39–48.
[6] C.L. Yang, L.Y. Guo, X.Y. Liu, H.X. Zhang, M.C. Liu, Determination of tetrandrine and fangchinoline in plasma samples using hollow fiber liquid-phase microextraction combined with high-performance liquid chromatography, J. Chromatogr. A 1164 (2007) 56–64.
[7] J.S. Lou, C.L. Zhang, Pharmacokinetic study of tetrandrine in rabbits, Chin. Trad. Herbal Drugs 24 (1993) 24–26.
[8] Y.J. Chen, Potential role of tetrandrine in cancer therapy, Acta Pharmacol. Sin. 23 (2002) 1102–1106.
[9] P.J. Davis, J.P. Rosazza, Microbial transformations of natural antitumor agents. 2. Studies with d-tetrandrine and laudanosine, J. Org. Chem. 41 (1976) 2548–2551.
[10] J.J. Yang, H. Long, H.W. Liu, A.J. Huang, Y.L. Sun, Analysis of tetrandrine and fangchinoline in traditional Chinese medicines by capillary electrophoresis, J. Chromatogr. A 811 (1998) 274–279.
[11] W.H. Gao, S.Y. Lin, A. Chen, Y. Li, X. Chen, Z. Hu, Nonaqueous capillary electrophoresis for rapid and sensitive determination of fangchinoline and tetrandrine in Radix *Stephaniae tetrandrae* and its medicinal preparations, J. Sep. Sci. 28 (2005) 639–646.
[12] J.M. Huang, J.X. Guo, G.L. Duan, Determination of 7 bio-active alkaloids in stephania plants by RP-HPLC, Acta Pharm. Sin. 33 (1998) 528–533.
[13] V.C. Joshi, B. Avula, I.A. Khan, Authentication of *Stephania tetrandra* S. Moore (Fang Ji) and differentiation of its common adulterants using microscopy and HPLC analysis, J. Nat. Med. 62 (2008) 117–121.
[14] L.J. Zhang, X. Wang, J.H. Liu, W.J. Duan, D.J. Wang, Y.L. Geng, Use of pH-zone refining countercurrent chromatography for preparative separation of fangchinoline and tetrandrine from *Stephania tetrandra*, Chromatographia 69 (2009) 959–962.
[15] R.M. Liu, F.Y. He, A.L. Sun, Separation and identification of alkaloids in *Stephania tetrandra* by capillary electrophoresis electrospray-MS/MS, Acta Pharm. Sin. 39 (2004) 363–366.
[16] N.N. Song, S.Y. Zhang, Q.S. Li, C.X. Liu, Establishment of a liquid chromatographic/mass spectrometry method for quantification of tetrandrine in rat plasma and its application to pharmacokinetic study, J. Pharm. Biomed. Anal. 48 (2008) 974–979.
[17] M.C. Liu, P. Li, Y.X. Cheng, Y.Z. Xian, C.L. Zhang, L.T. Jin, Determination of thiol compounds in rat striatum microdialysate by HPLC with a nanosized CoHCF-modified electrode, Anal. Bioanal. Chem. 380 (2004) 742–750.
[18] N. Vanbeneden, F. Delvaux, F.R. Delvaux, Determination of hydroxycinnamic acids and volatile phenols in wort and beer by isocratic high-performance liquid chromatography using electrochemical detection, J. Chromatogr. A 1136 (2006) 237–242.
[19] L. Manna, L. Valvo, P. Betto, Determination of oxidized and reduced glutathione in pharmaceuticals by reversed-phase high-performance liquid chromatography with dual electrochemical detection, J. Chromatogr. A 846 (1999) 59–64.
[20] L.H. Liu, Y. Chen, Y.L. Zhang, F. Wang, Z.L. Chen, Determination of tryptophan and kynurenine in human plasma by liquid chromatography-electrochemical detection with multi-wall carbon nanotube-modified glassy carbon electrode, Biomed. Chromatogr. 25 (2011) 938–942.
[21] Y. Li, F. Wang, Z.L. Chen, Determination of bavachin and isobavachalcone in Fructus Psoraleae by high-performance liquid chromatography with electrochemical detection, J. Sep. Sci. 34 (2011) 514–519.
[22] B. Benova, M. Adam, K. Onderkova, J. Kralovsky, M. Krajicek, Analysis of selected stilbenes in polygonum cuspidatum by HPLC coupled with coularray detection, J. Sep. Sci. 31 (2008) 2404–2409.
[23] D.J.L. Jones, C.K. Lim, D.R. Ferry, A. Gescher, Determination of quercetin in human plasma by HPLC with spectrophotometric or electrochemical detection, Biomed. Chromatogr. 12 (1998) 232–235.
[24] C. Piazza, M.G. Privitera, B. Melilli, T. Incognito, M.R. Marano, G.M. Leggio, M.A. Roxas, F. Drago, Influence of inulin on plasma isoflavone concentrations in healthy postmenopausal women, Am. J. Clin. Nutr. 86 (2007) 775–780.

Journal of Pharmaceutical and Biomedical Analysis 61 (2012) 256–264

Contents lists available at SciVerse ScienceDirect

Journal of Pharmaceutical and Biomedical Analysis

journal homepage: www.elsevier.com/locate/jpba

Short communication

Isolation and characterisation of degradant impurities in Dipyridamole formulation

B. Venkata Subbaiah[a,*], K.K. Sree Ganesh[a], G. Vamsi krishna[a], K. Vyas[a], R. Vasu Dev[b], K. Subramanyam Reddy[c]

[a] Analytical Research & Development, Dr. Reddy's Laboratories Ltd., IPD, Bachupally, Hyderabad 500 090, India
[b] Aurigene Discovery Technologies Ltd., Miyapur, Hyderabad 500 049, India
[c] Department of Chemistry, Sri Venkateswara University, Tirupati 517 502, India

ARTICLE INFO

Article history:
Received 21 July 2011
Received in revised form
23 November 2011
Accepted 26 November 2011
Available online 9 December 2011

Keywords:
Dipyridamole
Degradant impurities
Preparative HPLC
Isolation
Characterisation techniques

ABSTRACT

Dipyridamole is an antithrombotic drug. In the stability study of drug product of Dipyridamole, two unknown impurities (referred as DP-I and DP-II) were detected at levels of 0.25% and 0.54% by gradient reverse phase HPLC method. The drug product was subjected to stress to enhance the level of these impurities. An elegant isocratic preparative method was employed using a Reprosil CN column with a short run time of 14 min to isolate these impurities. The DP-I and DP-II were isolated with purities of 99.1% and 99.8% respectively. Structural studies of these impurities were undertaken using spectroscopic techniques such as IR, NMR and Mass. Based on the spectral data, the structures of DP-I and DP-II have been characterised to be 2,2′,2″,2‴-(4-hydroxy-8-(piperidin-1-yl) pyrimido [5,4-d]pyrimidine-2,6 diyl) bis(azanetriyl) tetraethanol, 4-(2-((6-(bis (2-hydroxyethyl) amino)-4, 8-di (piperidin-1-yl) pyrimido [5,4-d] pyrimidin-2-yl) (2-hydroxyethyl) amino) ethoxy)-2, 3-dihydroxy-4-oxobutanoic acid, respectively. A detailed elucidation of the structure is presented in this article.

© 2011 Elsevier B.V. All rights reserved.

1. Introduction

Pharmacological studies on Dipyridamole, 2,6-bis (diethanolamino)-4,8-dipiperidinopyrimido-[5,4-d] pyrimidine suggest that it may be used as a coronary vasodilator in clinical medicine. The known pharmacological approach for the prevention of thrombotic accidents is to use Dipyridamole in combination with Aspirin (acetylsalicylic acid). Dipyridamole is well accepted for treatment of angina pectoris and cerebrovascular diseases. The mechanism of action is to inhibit the cellular uptake and metabolism of adenosine with resulting vasodilatory and anti-aggregatory effects. Through the combination of its antiplatelet and vasodilator function, Dipyridamole probably improves tissue perfusion [1]. It has also been reported that Dipyridamole possesses antioxidant properties and attenuates the formation of reactive oxygen species in platelets and endothelial cells [2]. Recent studies reveal that combination of a very low dose of Prednisolone and Dipyridamole has exhibited significant synergistic effects in human clinical trials [3]. The same was also observed in collagen and adjuvant arthritic animal based on inhibition of additional inflammatory chemokine [4]. On the contrary, Dipyridamole did not modify the symptoms of rheumatoid arthritis in other clinical trial described by Forrest et al. [5]. In view of its wide use, the stability indicating methods for the determination of degradation products in Dipyridamole [6–8] have received much attention (Tables 1–2).

It is mandatory to identify and structurally characterise any impurity formed during production and stability, exceeding the identification threshold of 0.2% in the drug product [9–15]. For low-level impurities or degradation products, this quite often involves HPLC method development, isolation and characterisation techniques [16–19]. This paper describes the separation, isolation and characterisation of two unknown degradation impurities formed in Dipyridamole.

2. Experimental

2.1. Chemicals and reagents

Dipyridamole drug product used for investigation was obtained from the R&D of Dr. Reddy's Laboratories Ltd., Hyderabad, India. HPLC grade acetonitrile and methanol were

* Corresponding author. Tel.: +91 9963029509; fax: +91 40 44346285.
E-mail addresses: venkatasb@drreddys.com, kaushik0208@yahoo.com (B. Venkata Subbaiah).

0731-7085/$ – see front matter © 2011 Elsevier B.V. All rights reserved.
doi:10.1016/j.jpba.2011.11.028

Table 1
Fragmentation pathways and infrared data of Dipyridamole, DP-I and DP-II.

Name	Fragmentation pathways	FT-IR (cm^{-1})
Dipyridamole	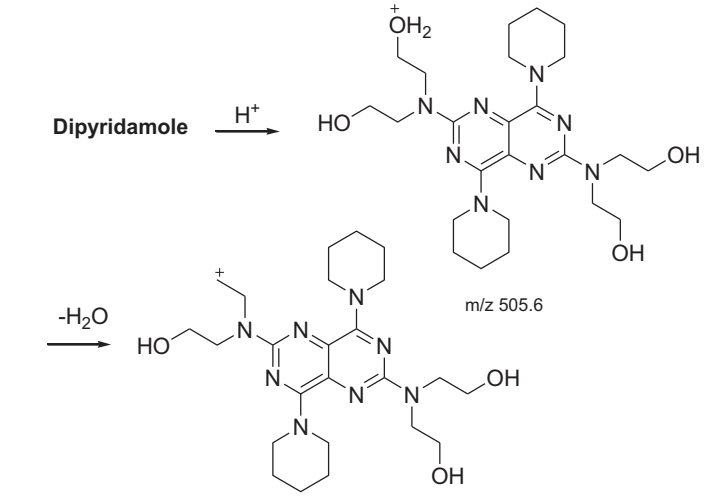	3376, 3304, 2922, 2852, 1532, 1470, 1440, 1359, 1216, 1080, 1052, 1025, 1014, 853, 760.
DP-I	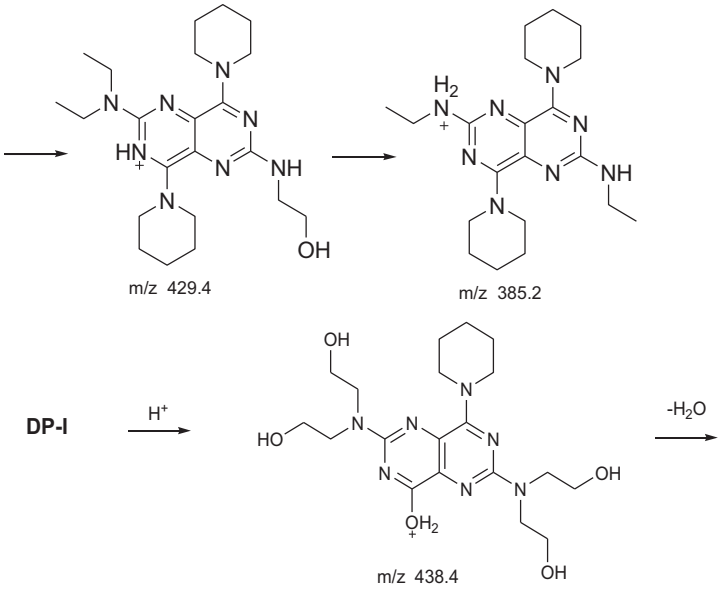	3448, 3271, 3053, 2937, 2878, 2852, 1649, 1604, 1562, 1536, 1359, 1262, 1079, 1064, 1039, 1029, 1013, 846, 801.

obtained from the Merck Co., Mumbai, India. Ultra pure water was collected from TKA Millipore water purification system. Ammonium formate, formic acid, potassium dihydrogen phosphate, sodium hydroxide were procured from Rankem India Ltd. Chloroform-d_3, methanol-d_4 and dimethyl sulphoxide-d_6 (for NMR) were purchased from Aldrich Chemical Co., USA.

2.2. High performance liquid chromatography (analytical)

Samples were analysed on Agilent HPLC-DAD system equipped with 1100 series low pressure quaternary gradient pump along with pulse dampener. An Inertsil ODS-2 column (Agilent 150 × 4.6 mm, 5 μm) was used for chromatographic separations. Mobile phase A consists of a mixture of 0.01 M KH_2PO_4 buffer,

Table 1 (*Continued*)

Name	Fragmentation pathways	FT-IR (cm^{-1})
DP-II	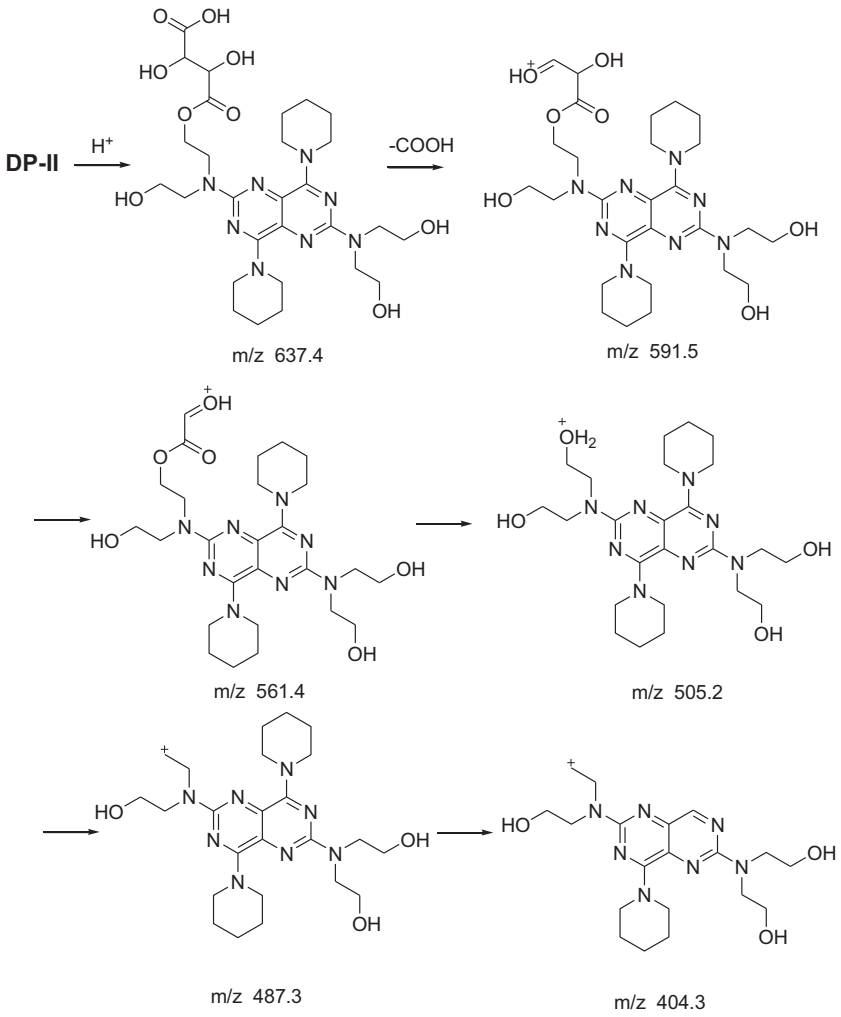	3357, 2934, 2855, 1740, 1626, 1532, 1443, 1362, 1253, 1215, 1126, 1070, 1019, 853, 754.

with the pH adjusted to 7.0 using 5% sodium hydroxide, and methanol in the ratio of 50:50 (v/v). Mobile phase B consists of methanol and 0.01 M KH_2PO_4 buffer in the ratio of 95:5 (v/v). The following gradient programme is employed: T (min)/%B (v/v): 0/0, 4/0, 25/100, 28/100, 30/0, 35/0. The sample detection was monitored at a wavelength of 295 nm. Chromatography was performed at 45 °C using a flow rate of 1 mL/min.

2.3. Forced degradation of Dipyridamole drug product

Forced degradation studies were performed on the Dipyridamole drug product with the intention of determining the conditions responsible for the formation of the degradation products. Accordingly, degradation studies were conducted by stressing with acid, base, peroxide and thermal.

2.3.1. Acid stressed degradation

200 mg equivalent of Dipyridamole drug product was dissolved in 20 mL of methanol and water in the ratio of 1:1. HCl solution (5 mL of 0.1 N) was added and refluxed for about 4 h and neutralised.

2.3.2. Base stressed degradation

200 mg equivalent of Dipyridamole drug product was dissolved in 20 mL of methanol and water in the ratio of 1:1. NaOH solution (5 mL of 0.1 N) was added and refluxed for about 4 h and neutralised.

2.3.3. Peroxide stressed degradation

200 mg equivalent of Dipyridamole drug product was dissolved in 20 mL of methanol and water in the ratio of 1:1. Hydrogen peroxide (5 mL of 6% solution) was added and maintained at 70 °C for 4 h.

2.3.4. Thermal stressed degradation

200 mg equivalent of Dipyridamole drug product was taken in a Petri dish. Water was sprinkled on the drug product and subjected to 105 °C for 3 h.

2.3.5. HPLC analyses of forced degradation samples

The degradation samples were analysed by HPLC method as described in Section 2.2. Under acid stressed conditions, DP-I and DP-II have formed up to 3.0% and 0.4%, while peroxide degradation yielded 0.6% and 1.1%, respectively. In thermal stressed condition, only DP-II was formed up to 7.7%. In base stressed condition, there

Table 2
^{1}H and ^{13}C NMR assignments for Dipyridamole, DP-I and DP-II.

Position[a]	Dipyridamole δ_C		DP-I δ_C		DP-II δ_C	
	^{1}H	^{13}C	^{1}H	^{13}C	^{1}H	^{13}C
1	–	153.2 (C)	–	146.7 (C)	–	153.2 (C)
3	–	159.3 (C)	–	160.5 (C)	–	159.3 (C)
4	–	131.9 (C)	–	128.0 (C)	–	132.1 (C)
5	–	131.9 (C)	–	128.0 (C)	–	131.8 (C)
8	–	153.2 (C)	–	146.7 (C)	–	152.8 (C)
10	–	159.3 (C)	–	158.2 (C)	–	159.3 (C)
12	3.8,s	51.7 (CH_2)	3.7,s	51.5 (CH_2)	3.95,s	51.6 (CH_2)
13	3.8,s	51.7 (CH_2)	3.6,m	51.9 (CH_2)	3.8,m	51.2 (CH_2)
14	3.7,s	59.6 (CH_2)	3.7,s	58.3 (CH_2)	4.45,t	64.0 (CH_2)
16	3.7,s	59.6 (CH_2)	3.7,s	59.9 (CH_2)	3.8,m	59.5 (CH_2)
20, 24	4.1,s	47.8 (CH_2)	–	–	3.95,s	47.6 (CH_2)
21, 23	1.7,s	24.6 (CH_2)	–	–	1.75,s	24.5 (CH_2)
22	1.7,s	25.9 (CH_2)	–	–	1.75,s	25.8 (CH_2)
26	3.8,s	51.7 (CH_2)	3.7,s	51.8 (CH_2)	3.8,m	51.2 (CH_2)
27	3.8,s	51.7 (CH_2)	3.6,m	51.8 (CH_2)	3.8,m	51.2 (CH_2)
28	3.7,s	59.6 (CH_2)	3.7,s	59.4 (CH_2)	3.8,m	59.5 (CH_2)
29	3.7,s	59.6 (CH_2)	3.7,s	59.4 (CH_2)	3.8,m	59.5 (CH_2)
32	4.1,s	47.8 (CH_2)	4.02,s	47.1 (CH_2)	4.1,s	47.9 (CH_2)
33, 35	1.7,s	24.6 (CH_2)	1.63,s	24.3 (CH_2)	1.75,s	24.5 (CH_2)
34	1.7,s	25.9 (CH_2)	1.63,s	25.9 (CH_2)	1.75,s	25.8 (CH_2)
36	4.1,s	47.8 (CH_2)	4.02,s	48.1 (CH_2)	4.1,s	47.9 (CH_2)
37	–	–	–	–	–	172.1 (C=O)
39	–	–	–	–	4.32,d	72.4 (CH)
40	–	–	–	–	4.5,d	72.2 (CH)
43	–	–	–	–	–	173.0 (C=O)

[a] Refer structural formula (Fig. 1(A)) for numbering: s, singlet; d, doublet; t, triplet; m, multiplet. The correlations shown in the ^{1}H and ^{13}C NMR columns are in agreement with HSQC and HMBC spectra.

was no significant degradation. Hence the thermal and acid degradation routes were chosen to enhance the impurities.

2.4. Sample preparation

Dipyridamole sample was prepared at a concentration of 1 mg/mL in methanol for the analytical HPLC and 50 mg/mL for the preparative HPLC analyses.

2.5. High performance liquid chromatography (preparative)

Impurities were isolated from the sample using Gilson GX281 preparative HPLC Binary system equipped with a Gilson photodiode array detector model 172 along with a Gilson analytical HPLC system. Data was collected and processed using TRILUTION LC software (ver 2.1). Approximately 50 mg/mL of sample was prepared to load on to the column. A Reprosil CN column (250 × 20 mm, 5 μm) was employed for the separation of DP-I and DP-II. The mobile phase consists of a mixture of 0.02 M ammonium acetate buffer, with the pH adjusted to 7.0 with ammonia and acetonitrile in the ratio of 70:30. The flow rate was kept at 15 mL/min. Detection was carried out at 295 nm. Desaltification procedure was used to remove the buffering agents leading to pure fractions of the impurities. The impurity fractions from several injections were pooled. The pooled fraction was concentrated by using Rotavapour (Heidolph Laboratory 4002 control) under high vacuum. The aqueous solution was lyophilized to solidify the impurities.

2.6. Mass spectrometry (LC–MS/MS)

LC–MS/MS analyses have been performed on API 4000 model Mass Spectrometre (Applied Bio systems). Analyses were performed in positive ionisation mode with turbo ion spray interface. The parametres for Ion source voltage (IS) = 5500 V, Declustering Potential (DP) = 70 V, Entrance Potential (EP) = 10 V were set with nebulizer gas as air at a pressure of 40 psi and curtain gas as nitrogen at a pressure of 25 psi. An Inertsil C8 column (250 × 4.6 mm, 5 μm) was used for the separation. Mobile phase A is a mixture, consisting of 0.01 M Ammonium formate buffer with the pH adjusted to 4.0 using formic acid and acetonitrile in the ratio of 70:30. Mobile phase B is a mixture consisting of above buffer and acetonitrile in the ratio of 55:45. The gradient conditions employed for the separation with a timed gradient programme of T (min)/%B (v/v): 0/0, 40/100, 41/0, 45/0. The flow rate was kept at 1 mL/min.

2.7. UPLC-TOF-MS

The UPLC-TOF-MS system consisted of an ACQUITY™ Ultra Performance Liquid Chromatography system and a Micro mass LCT Premier XE Mass Spectrometre (High sensitivity orthogonal time-of-flight instrument, Waters, Millford, USA) equipped with a lock mass sprayer, operating in either the positive or negative ion mode. All analyses were acquired using the lock spray to ensure accuracy and reproducibility; leucine enkephalin was used as the lock mass. Sample of concentration 0.02 mg/mL in methanol was infused in TOF-MS at a flow rate of 10 μL/min. High resolution (W mode, FWHM 10500) positive polarity scan responses were collected from m/z 100 to 1000 at a rate of 1.0 s/scan.

2.8. NMR spectroscopy

NMR experiments were performed on 400 MHz Mercury plus NMR spectrometre (Varian) in DMSO-d_6 + $CDCl_3$ and Methanol-d_4 at 25 °C. Proton and carbon chemical shifts were reported on δ scale in ppm, relative to TMS (δ = 0.00 ppm), $CDCl_3$ (δ = 77.00 ppm), CD_3OD (δ = 49.1 ppm) and DMSO (δ = 39.50 ppm) as internal standards. Standard pulse sequences provided by Varian were used for ^{1}H NMR, gradient Double Quantum – filtered Correlation Spectroscopy (gDQCOSY), gradient Heteronuclear Single Quantum

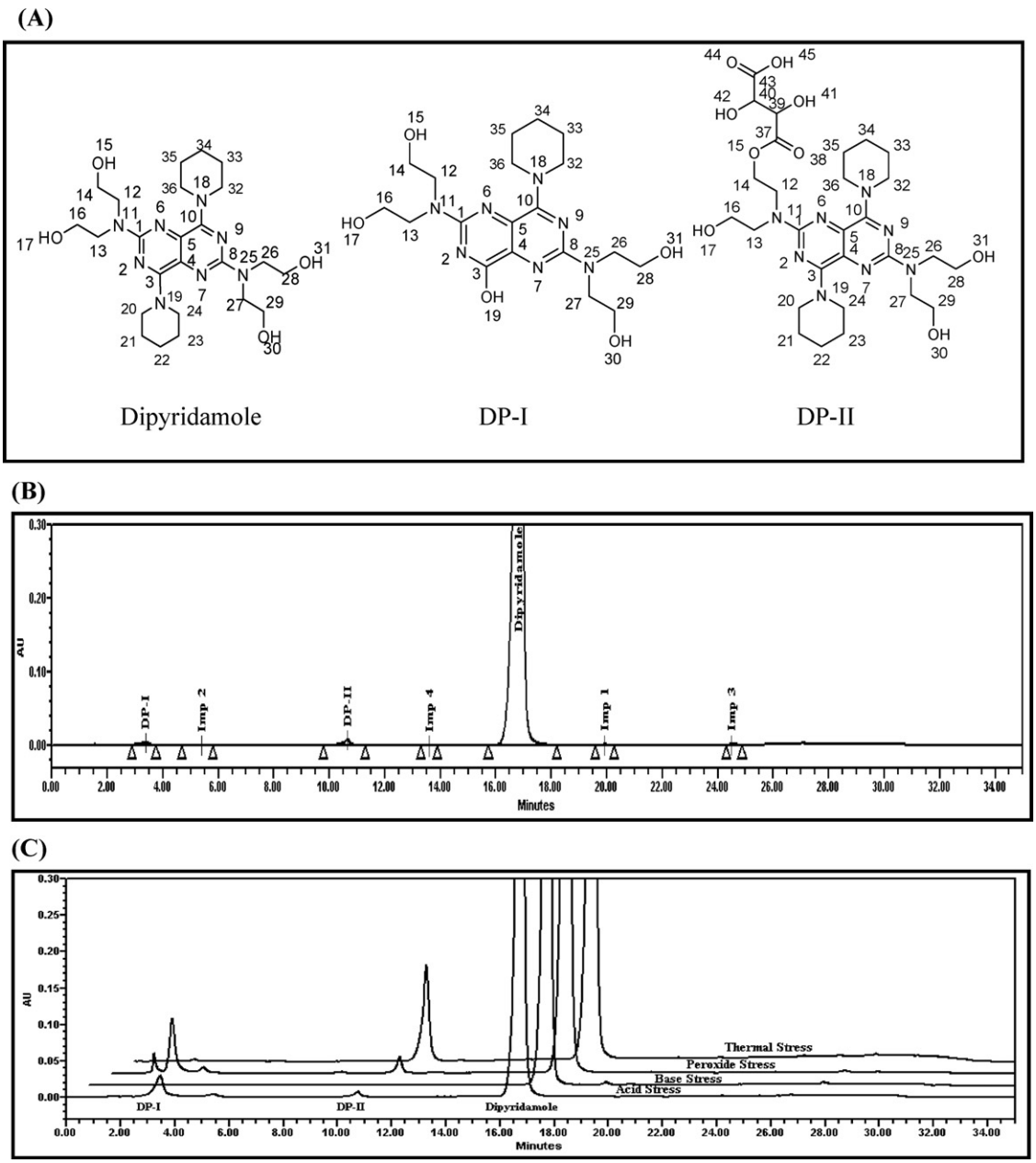

Fig. 1. (A) Chemical structures of Dipyridamole and its degradant products DP-I and DP-II. (B) HPLC stability chromatogram of Dipyridamole sample. (C) Overlay of HPLC chromatograms of Dipyridamole forced degradation studies.

Coherence spectroscopy (gHSQC) and gradient Heteronuclear Multiple Bond Correlation spectroscopy (gHMBC).

2.9. FT-IR spectroscopy

IR spectra were recorded in solid state as KBr dispersion medium using Perkin-Elmer FT-IR spectrophotometre.

3. Results and discussion

3.1. Analytical HPLC of drug product

A typical analytical HPLC chromatogram of a stability batch of Dipyridamole drug product recorded using the HPLC method as described in Section 2.2 is shown in Fig. 1(B). DP-I, DP-II and Dipyridamole elute at retention times 3.4, 10.7 and 16.8 min, respectively, while Imp-1, 2, 3 and 4 are known impurities. The representative HPLC chromatograms of the forced degradation study are shown in Fig. 1(C). The structures of these impurities and Dipyridamole are shown in Fig. 1(A). Both DP-I and DP-II are more polar with respect to Dipyridamole.

3.2. Isolation of impurities by preparative HPLC

Isolation of these impurities by preparative HPLC was a challenging job as the two target impurities were eluting very closely to the parent peak in preliminary studies. This was due to limitations of preparative chromatography, which is traditionally associated with low efficiency columns, packed with less pure silica (compared with analytical columns), unstable and packed with conventional packing technologies.

With relatively high particle size (7–10 μm) of the stationary phase used in preparative HPLC columns, it is indeed a challenging task to resolve the peaks of the target impurities from the main

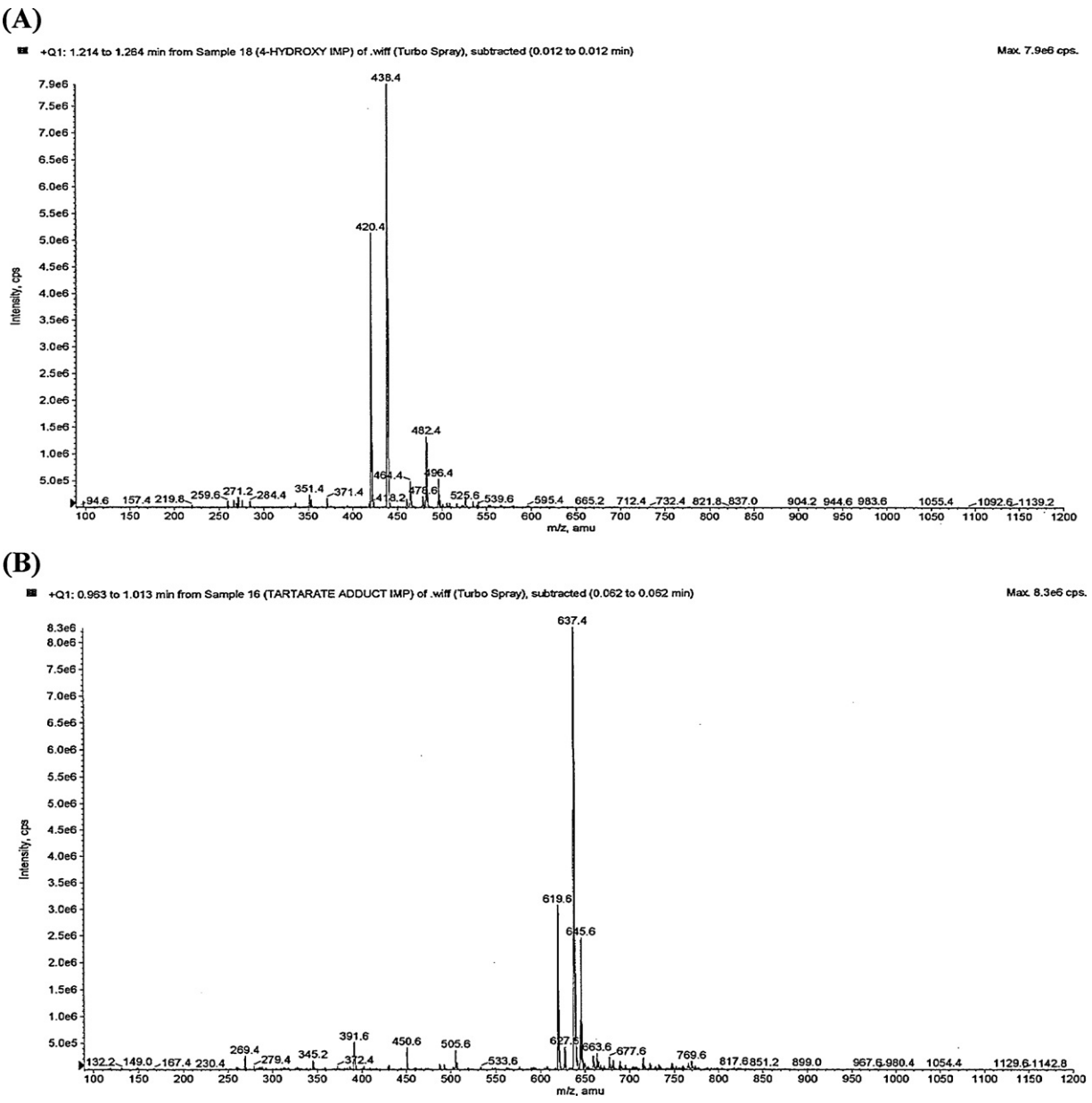

Fig. 2. (A) LC–MS data of DP-I. (B) LC–MS data of DP-II.

peak despite the maximum injection load and yet leading to isolation of impurities in sufficient quantities with high purity. Several trials were performed to achieve the required resolution. Finally an isocratic solvent system was developed with good resolution and a short runtime (14 min). The purity of DP-I and DP-II were 99.1 and 99.8% respectively and these samples were used for spectroscopic structural studies.

3.3. Structure elucidation of Dipyridamole DP-I

In the positive and negative mass spectra, the protonated and deprotonated, $[M+H]^+$ and $[M-H]^-$, molecular ions were detected at *m*/*z* 438.1 and 436.4, respectively. The even *m*/*z* number of $[M+H]^+$ and $[M+H]^-$ ions suggest that DP-I contains odd number of nitrogen atoms (nitrogen rule). From these results the molecular ion of DP-I was found to be at *m*/*z* 437. The mass difference between Dipyridamole and DP-I was found to be 68 amu.

The positive HR-MS spectrum showed protonated molecular ion at *m*/*z* 438.2453 corresponding to molecular formula $C_{19}H_{32}N_7O_5$. When compared with the molecular formula of Dipyridamole, there was a difference of C_5H_9N and an addition of one oxygen atom. The difference can be rationalised in terms of the loss of piperidine moiety and an addition of one hydroxyl group. The LC–MS data of DP-I is shown in Fig. 2(A).

The proton NMR spectra of Dipyridamole and DP-I showed three sets of signals. The ^1H NMR and ^{13}C NMR spectra of DP-I are shown in Fig. 3(A) and (B), respectively. The proton signals in DP-I were observed at 4.02 (4H), 3.6–3.7 (16H) and 1.63 ppm (6H), where as Dipyridamole showed signals at 4.1 (8H), 3.7–3.8 (16H) and 1.7 (12H) protons and the exchangeable protons were not observed. From the gDQCOSY data, it was observed that the protons at 4.02 ppm showed correlations with the proton at 1.63 ppm. These can be attributed to piperidine moiety. Further, the protons at 3.6 ppm showed correlations with the protons at 3.7 ppm corresponding to methylazanediyl diethanol moiety. In DP-I, the protons corresponding to piperidine were found to be ten, confirming that this is only one piperidine moiety. The remaining protons from

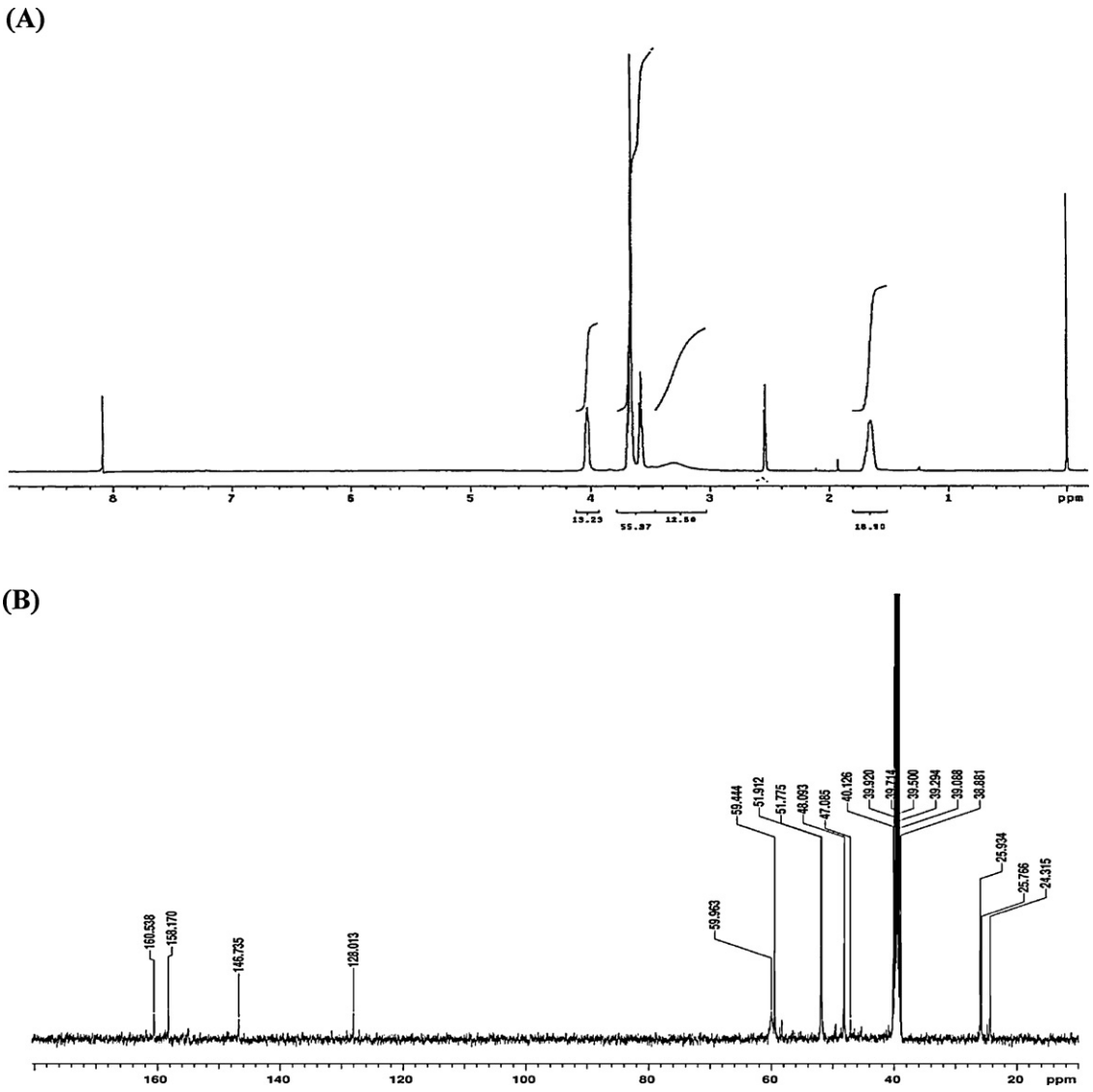

Fig. 3. (A) ^{1}H NMR spectrum of DP-I. (B) Proton decoupled ^{13}C NMR spectrum of DP-I.

methylazanediyl diethanol corresponding to sixteen were found to be intact.

The absence of piperidine group shows that there are 84 mass units less ($C_5H_{10}N$) when compared to Dipyridamole. But the MS data showed that there is only a 68 mass unit difference. This shows that there is an addition of 16 mass units after the removal of piperidine moiety. This observation indicates that the piperidine moiety was replaced by a hydroxyl group.

The above spectral data supports the assigned structure as 2,2′,2″,2‴-(4-hydroxy-8-(piperidin-1-yl)pyrimido[5,4-d]pyrimidine-2,6 diyl) bis(azanetriyl) tetraethanol (DP-I).

3.4. Structure elucidation of Dipyridamole DP-II

In the positive and negative mass spectra, the protonated $[M+H]^+$ and deprotonated $[M-H]^-$ molecular ions were detected at *m*/*z* 637.3 and 635.7, respectively. From these results the molecular ion of DP-II was found to be at *m*/*z* 636. The mass difference between Dipyridamole and DP-II was found to be 132 amu. The ES-MS–MS spectrum displayed product ions at *m*/*z* 619.6, 591.5, 561.4, 505.2, 487.3 and 404.3 in which 505.2 is the dominant fragment. The fragment ion at 505.2 suggests that the parent moiety is intact in DP-II.

The positive HR-MS spectrum showed protonated molecular ion at *m*/*z* 637.3329 corresponding to molecular formula $C_{28}H_{45}N_8O_9$. When compared with the molecular formula of Dipyridamole, there was an addition of $C_4H_4O_5$. The LC–MS data of DP-II is shown in Fig. 2(B).

The ^{1}H NMR and ^{13}C NMR spectra of DP-II are shown in Fig. 4(A) and (B), respectively. On comparison, DP-II showed two additional protons at 4.5 (1H) and 4.32 (1H) as doublets and their corresponding carbon signals were observed at 72.4 and 72.2 ppm, respectively. From the proton and carbon chemical shifts these can be attributed to oxygen attached methine groups. The ^{13}C NMR spectrum showed two carbonyl signals at 173.0 and 172.1 ppm. The protons at 4.5 and 4.32 ppm showed HMBC correlations to the carbon signals at 173.0 ppm and 172.1 ppm, respectively. From these observations the additional moiety can be attributed to tartaric acid group, which was found to be one of the excipients used in the formulation. The additional carbonyl groups were further confirmed from IR spectroscopy at 1741 cm^{-1}. Interestingly one of the carbonyls at 172.1 ppm showed additional cross peak with one of the methylene protons (4.45 ppm as a triplet) of methylazanediyl diethanol of Dipyridamole.

The above spectral data supports the assigned structure as 4-(2-((6-(bis (2-hydroxyethyl) amino)-4,8-di (piperidin-1-yl) pyrimido

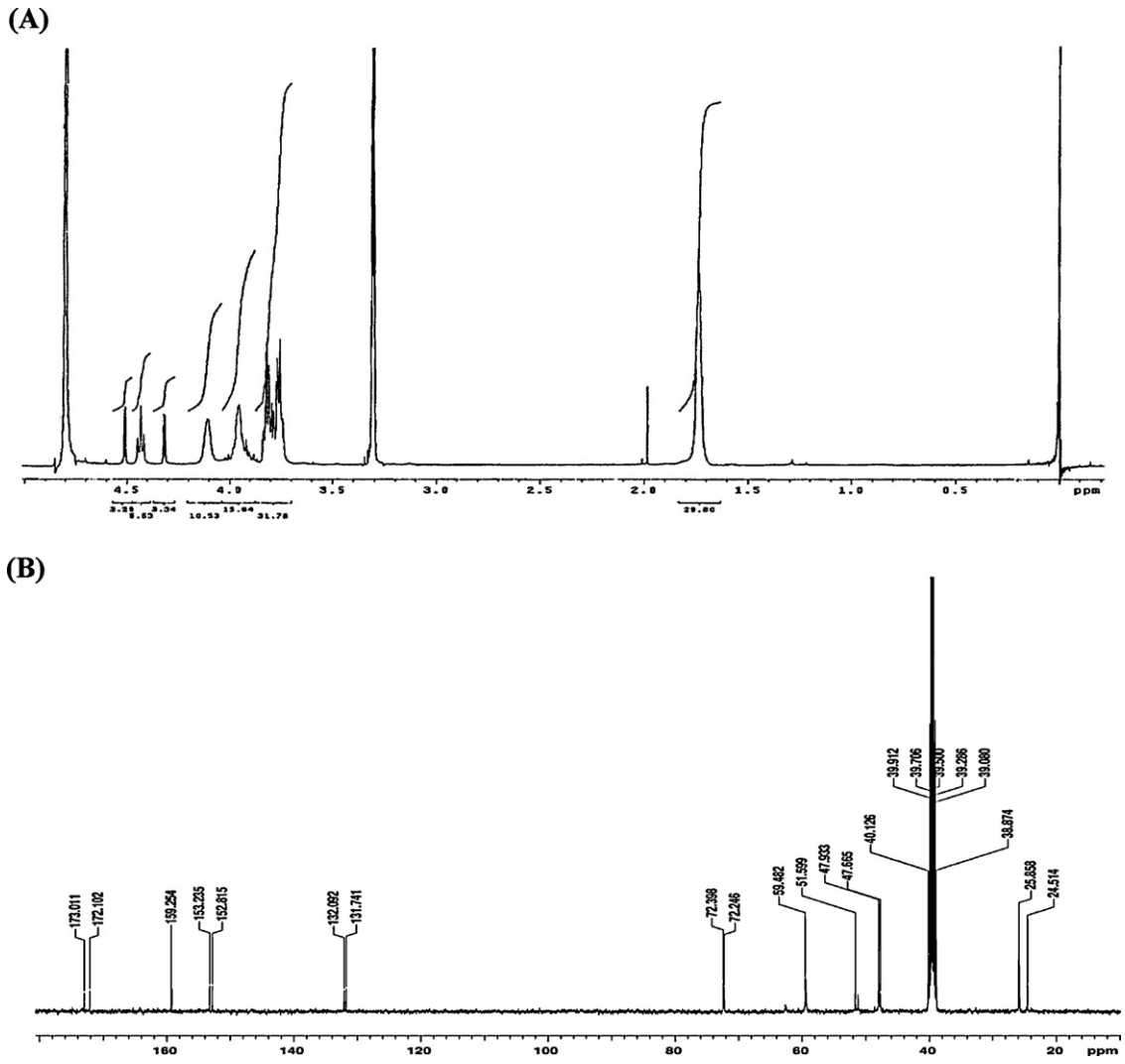

Fig. 4. (A) ^{1}H NMR spectrum of DP-II. (B) Proton decoupled ^{13}C NMR spectrum of DP-II.

[5,4-d] pyrimidin-2-yl) (2-hydroxyethyl) amino) ethoxy)-2,3-dihydroxy-4-oxobutanoic acid (DP II).

4. Conclusion

The drug product of Dipyridamole, subjected to stability studies, was evaluated for degradation products. In addition to pharmacopoeia impurities, two unknown impurities which are not reported in the literature were observed. Stress study was performed to enhance the impurities. These degradation products were isolated by a simple isocratic method and characterised by IR, NMR, MS and HRMS spectroscopic techniques. The most probable structures are proposed for these impurities based on the spectral data.

Acknowledgement

We would like to thank the management of Dr. Reddy's Laboratories Ltd. for supporting this work. Cooperation from colleagues of Research & Development and Analytical Research & Development of Dr. Reddy's Laboratories Ltd. is acknowledged.

Appendix A. Supplementary data

Supplementary data associated with this article can be found, in the online version, at doi:10.1016/j.jpba.2011.11.028.

References

[1] N.P. Stafford, A.E. Pink, A.E. White, J.R. Glenn, S. Heptinstall, Mechanisms involved in adenosine triphosphate-induced platelet aggregation in whole blood, arterioscler, Thromb. Vasc. Biol. 23 (2003) 1928–1933.
[2] S. Chakrabarti, O. Vitseva, D. Iyu, S. Varghese, J.E. Freedman, The effect of Dipyridamole on vascular cell-derived reactive oxygen species, J. Pharmacol. Exp. Ther. 315 (2005) 494–500.
[3] T.K. Kvien, E. Fjeld, B. Slatkowsky-Christensen, M. Nichols, Y. Zhang, A. Proven, et al., Efficacy and safety of a novel synergistic drug candidate, CRx-102, in hand osteoarthritis, Ann. Rheum. Dis. 67 (2008) 942–948.
[4] G.R. Zimmermann, W. Avery, A.L. Finelli, M. Farwell, C.C. Fraser, A.A. Borisy, Selective amplification of glucocorticoid anti-inflammatory activity through synergistic multi-target action of a combination drug, Arthritis Res. Ther. 11 (2009) 105–118.
[5] C.M. Forrest, T.W. Stone, G.M. Mackay, L. Oxford, N. Stoy, G. Harman, et al., Purine metabolism and clinical status of patients with rheumatoid arthritis treated with Dipyridamole, Nucleosides Nucleotides Nucleic Acids 25 (2006) 1287–1290.
[6] J. Zhang, R.B. Miller, R. Jacobus, Development and validation of a stability-indicating HPLC method for the determination of degradation products in Dipyridamole injection, Chromatographia 44 (1997) 247–252.
[7] K. Prakash, Rama Rao Kalakuntla, Jayapal Reddy Sama, Rapid and simultaneous determination of aspirin and Dipyridamole in pharmaceutical formulations by

reversed-phase high performance liquid chromatography (RP-HPLC) method, Afr. J. Pharm. Pharacol. 5 (2011) 244–251.
[8] J.H. Bridle, M.T. Brimble, A stability indicating method for Dipyridamole, Drug Dev. Ind. Pharm. 19 (1993) 371–381.
[9] International Conference on Harmonisation of Technical Requirements for Registration of Pharmaceuticals for Human Use, ICH Q3A (R2), Impurities in New Drug substances, 2006, pp. 1–15.
[10] International Conference on Harmonisation of Technical Requirements for Registration of Pharmaceuticals for Human Use, ICH Q3B (R2), Impurities in New Drug Products, 2006, pp. 1–16.
[11] International Conference on Harmonisation of Technical Requirements for Registration of Pharmaceuticals for Human use, ICH Q1A (R2) Stability Testing of New Drug Substances and Products, 2003, pp. 1–24.
[12] U.S. Food and Drug Administration Drug Stability Guidelines, February 1987.
[13] S. Görög, New safe medicines faster: the role of analytical chemistry, Trends Anal. Chem. 22 (2003) 407–415.
[14] J.A. Mollica, S. Ahuja, Cohen, Stability of Pharmaceuticals, J. J. Pharm. Sci. 67 (1978) 443–445.
[15] The United States Pharmacopeia, General notices, 25th ed., United States Pharmacopeial Convention, Inc., Rockville, MD, USA, 2000, p. 7.
[16] Satinder Ahuja, Karen Mills Alsante, Handbook of Isolation and Characterisation of Impurities in Pharmaceuticals, first ed., USA, 2003.
[17] R.J. Smith, M.L. Webb, Analyses of Drug Impurities, first ed., Blackwell Publishing, UK, 2007.
[18] S. Ahuja, Impurities Evaluation of Pharmaceuticals, first ed., Marcel Dekker, NY, 1998.
[19] Budzikiewicz Herbert, Djerassi Carl, Dudley H. Williams, Mass spectrometry of organic compounds, first ed., Holden-day, Inc., CA, 1967.

Journal of Pharmaceutical and Biomedical Analysis 61 (2012) 265–270

Contents lists available at SciVerse ScienceDirect

Journal of Pharmaceutical and Biomedical Analysis

journal homepage: www.elsevier.com/locate/jpba

Short communication

Method development and validation for optimized separation of quercetin derivatives in selected *Potentilla* species using high-performance thin-layer chromatography photodensitometry method

Michał Tomczyk[a,*], Agnieszka Bazylko[b], Jessica Bonarewicz[b]

[a] Department of Pharmacognosy, Faculty of Pharmacy, Medical University of Białystok, ul. Mickiewicza 2a, 15-230 Białystok, Poland
[b] Department of Pharmacognosy and Molecular Basis of Phytotherapy, Faculty of Pharmacy, Warsaw Medical University, ul. Banacha 1, 02-097 Warsaw, Poland

ARTICLE INFO

Article history:
Received 20 September 2011
Received in revised form 8 December 2011
Accepted 9 December 2011
Available online 17 December 2011

Keywords:
Potentilla L.
High-performance thin-layer chromatography (HPTLC)
Densitometry
Flavonoids
Quercetin derivatives

ABSTRACT

A novel HPTLC-densitometry method was developed for separation and quantitative determination of four flavonoids: quercetin 3-O-β-D-glucuropyranoside (miquelianin; QG), quercetin 3-O-β-D-glucopyranoside (isoquercitrin; IQ), quercetin 3-O-β-D-galactopyranoside (hyperoside; HYP) and quercetin 3-O-β-D-(6″-α-L-rhamnosylo)-glucopyranoside (rutin; RUT) in ethyl acetate fractions from aerial parts of selected *Potentilla* species: *P. argentea*, *P. erecta*, *Dasiphora fruticosa* (syn. *P. fruticosa*), *Drymocallis rupestris* (syn. *P. rupestris*), *P. nepalensis* var. 'Miss Wilmott' and *P. thuringiaca*. For the first time, separation of this type of flavonoids was achieved on a HPTLC DIOL F_{254} plates using a mixture consisting of ethyl acetate/methyl ethyl ketone/diisopropyl ether/formic acid (3:10:4:1, v/v/v/v). QG, IQ, HYP and RUT were determined by densitometry at 363 nm. Sensitivity, accuracy (recovery rates were between 95.0 and 101.4%) and precision (in both cases intra-day precision and inter-day precision were ≤8.0%) of the method were determined. Their amounts were calculated using the regression equations of the calibration curves which were linear in a range of 0.025–0.200 μg/spot for all investigated compounds. The amounts of marker compounds in ethyl acetate extracts of *Potentilla* species measured by the method ranged between 16.7 ± 1.1 and 41.7 ± 0.6 mg/g for QG, 15.8 ± 1.3 and 36.7 ± 1.0 mg/g for IQ, 14.5 ± 0.5 mg/g for HYP and 6.7 ± 0.3 and 27.8 ± 2.1 mg/g for RUT. The method was found to be relatively simple, specific, precise and accurate and may be used for the quality control of simultaneous determination of quercetin derivatives in *Potentilla* extracts but also in other similar plant materials.
© 2011 Elsevier B.V. All rights reserved.

1. Introduction

Plant extracts or herbal formulations are known to be complicated samples to analysis, which usually contain a multicomponent samples, and in most cases it is difficult to identify all phytoconstituents by means of common approaches. Identification and quantification of a specific marker, or a class of substances can be considered as the main application of thin-layer chromatography (TLC) technique [1]. Nowadays, modern high-performance TLC (HPTLC) technique is an efficient instrumental method and optimized quantitative HPTLC using a densitometric evaluation produce results that are analogous to those obtained with gas chromatography (GC) as well as high-performance liquid chromatography (HPLC) [2,3]. Especially for plant extracts which are complex mixtures, HPTLC seems to have some advantages over other analytical methods. HPTLC method allows for the simultaneous analysis of numerous samples using small quantities of solvents, automation, simple sample preparation, reducing the time and cost of experiment but also a fast changing of chromatographic conditions, scanning and simultaneous development of several chromatograms. HPTLC procedure does not require extensive clean-up procedures even for quantitative analysis; moreover, the availability of many sensitive and selective reagents using in postchromatographic derivatization, for confirmation of specific groups or classes of analyzed compounds, is also a great advantage of HPTLC [4,5].

Several chromatographic techniques including TLC/HPTLC have been developed to analyze flavonol-type compounds in various matrices [6–11]. In recent papers, a variety of different sorbents as well as many eluents for separation of flavonoid standards were tested. The best separation was obtained on silica and cyanopropyl-bonded silica plates developed 1D-, 2D-TLC and HPTLC techniques [12,13]. However, none of the earlier described separations of flavonoid glycosides (quercetin derivatives) did not included quercetin 3-glucuronide as well as separation on DIOL plates.

* Corresponding author. Tel.: +48 085 748 5692; fax: +48 085 748 5614.
E-mail address: tomczyk@umwb.edu.pl (M. Tomczyk).

0731-7085/$ – see front matter © 2011 Elsevier B.V. All rights reserved.
doi:10.1016/j.jpba.2011.12.010

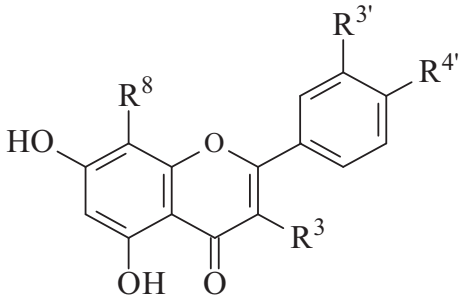

IQ	R^3 – O-glc	$R^{3'}$ – H	$R^{4'}$ – OH	R^8 – H
HYP	R^3 – O-gal	$R^{3'}$ – H	$R^{4'}$ – OH	R^8 – H
GQ	R^3 – O-glucur	$R^{3'}$ – OH	$R^{4'}$ – OH	R^8 – H
RUT	R^3 – O-rut	$R^{3'}$ – H	$R^{4'}$ – OH	R^8 – H

glc – glucose
gal – galactose
glucur – glucuronide
rut – rutinose

Fig. 1. Chemical structures of investigated compounds.

Traditionally, *Potentilla* species (Rosaceae) have attracted considerable attention and are under intense investigations. Most pharmacological effects of *Potentilla* plant material can be explained by the high amount of polyphenolic compounds present in all plant parts [14–16]. In our pilot study, for the simultaneous determination of different polyphenolics from *Potentilla* species has been developed and validated using HPTLC precoated silica gel 60F_{254} plates with toluene/ethyl formate/formic acid (6:4:1, v/v/v) [17]. Apparently, this separation was insufficient for flavonoids analysis what encouraged us for improve their separation by using a HPTLC DIOL plates. The purpose of this study was to develop a fast, selective and simplest method of separation of major flavonoids (Fig. 1) which are present in ethyl acetate fractions obtained from aerial parts of selected *Potentilla* species: *P. argentea* L., *P. erecta* (L.) RAEUSCH., *Dasiphora fruticosa* (L.) RYDB. (syn. *P. fruticosa* L.), *Drymocallis rupestris* (L.) SOJÁK (syn. *P. rupestris* L.), *P. nepalensis* HOOK var. 'Miss Wilmott' and *P. thuringiaca* BERNH. ex LINK. To our best knowledge, of note is the fact that it is the first simultaneous HPTLC-densitometric method developed for quercetin 3-glucuronide with other quercetin derivatives determination (Fig. 1). It is interesting that the first separation and quantitative determination of quercetin 3-glucuronide in plant material by using by HPTLC-densitometry have been carried out by Bazylko et al. [18]. Our analytical method was validated according to the ICH guidelines by determination of the linearity, precision, accuracy of each analyte [19,20].

2. Materials and methods

2.1. Plant material

Seeds of four species (*D. fruticosa* – index seminum/ind. sem./2566, *D. rupestris* – ind. sem. 763, *P. nepalensis* – ind. sem. 1542, *P. thuringiaca* – ind. sem. 1551, were requested from the Hortus Botanicus Universitatis Masarykianae, Brno, Czech Republic; Botanical Garden of Vilnius University, Lithuania; Hortus Botanicus Universitatis Posnaniensis, Poznań, Poland and the Giardino Botanico Alpino, Cogne, Italy. Plants were cultivated in a common plot at the Medicinal Plants Garden near Medical University of Białystok, Poland. Aerial parts of *P. argentea* and *P. erecta* were collected from Puszcza Knyszyńska, near Białystok, Poland. Voucher specimens of plants have been deposited in the Herbarium of the Department of Pharmacognosy, Medical University of Białystok, Poland and carefully authenticated by one of the author (M.T.). Collected plant materials, during June–July 2007–2010, were air-dried under shade at room temperature and then ground with an electric grinder into fine powders which were stored into airtight containers at room temperature. The list of all studied plants is given in Table 3.

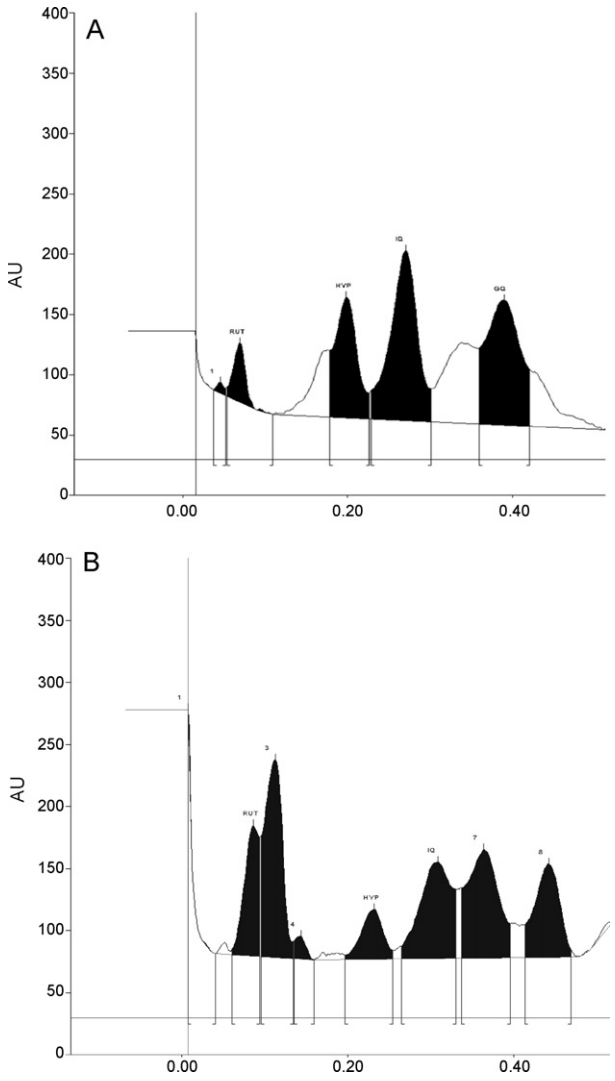

Fig. 2. Representative HPTLC profiles of ethyl acetate extracts of *D. fruticosa* (A) and *P. thuringiaca* (B) detected at λ = 363 nm.

2.2. Solvents and chemicals

Quercetin 3-glucoside (isoquercitrin) (IQ), quercetin 3-galactoside (hyperoside) (HYP) and quercetin 3-rhamnoglucoside (rutin) (RUT) were purchased from ROTH (Karlsruhe, Germany). Quercetin 3-glucuronide (QG) (purity > 96%) was isolated from willow herb (*Epilobium angustifolium* L.) and was obtained from Dr. Kiss (Department of Pharmacognosy and Molecular Basis of Phytotherapy, Faculty of Pharmacy, Medical University of Warsaw, Poland) [21]. Methanol, chloroform, diethyl ether, ethyl acetate and *n*-butanol were purchased from POCH (Gliwice, Poland).

Methyl ethyl ketone, diisopropylether and formic acid were purchased from FLUKA (Steinheim, Germany). All chemicals used for experimental procedures were of analytical grade. Milli-Q Plus (MILLIPORE, MA, USA) treated water (18.2 MΩ cm) was used throughout the analysis.

2.3. Preparation of fractions

Accurately weighed 2.0 g quantities of plant material in powder form were separately extracted with methanol (3× 50 mL) and once with 50 mL of 80% (v/v) methanol in an ultrasonicator bath (Sonic-5, POLSONIC, Poland) at controlled temperature (40 ± 2 °C) for given certain time 45 min. After solvent evaporation under reduced pressure from each sample, the methanolic extracts were diluted with water and successively partitioned between chloroform and then diethyl ether (Et_2O) and ethyl acetate (EtOAc) and finally with *n*-butanol (BuOH). The ethyl acetate extracts were filtered through a cellulose filter, a Chromafil 0-45/25 (PTFE 25 mm, 0.45 μm, MACHEREY-NAGEL, Germany). All these fractions were concentrated to dryness under vacuum (562, 95 and 7 mbar, respectively) controlled temperature (BÜCHI System, Switzerland) (temperature: 40 ± 2 °C) and subjected to lyophilization using vacuum concentrator (LABCONCO, USA) until a constant weight were obtained. The fractions yields were as follows: **1**, 2.06% (0.041 g); **2**, 1.23% (0.025 g); **3**, 1.92% (0.038 g); **4**, 1.16% (0.023 g); **5**, 0.63% (0.012 g); **6**, 0.75% (0.015 g); **7**, 1.06% (0.021 g).

2.4. Preparation of standard and sample solutions

Solutions of standards (1.0 mg/mL) – 1.0 mg of accurately weighted: QG, IQ, HYP and RUT were diluted in 1.0 mL of 80% (v/v) methanol solution. The appropriate amounts of stock solutions were diluted in 80% (v/v) methanol to obtain standard solutions containing: 0.0125, 0.025, 0.0375, 0.075 and 0.100 mg/mL. The mixture of QG, IQ, HYP and RUT was also prepared.

Solutions of fractions (2.0 mg/mL) – 2.0 mg of accurately weighted EtOAc fractions were diluted in 1.0 mL of 80% (v/v) methanol solution.

2.5. HPTLC-densitometry conditions and instrumentation

HPTLC-DIOL F_{254} silica gel glass plates (10 × 10) (E. MERCK, Darmstadt, Germany) were used without any pretreatment. Samples were applied on the plates as 5 mm bands, distance between bands 10 mm, 10 mm from the bottom edge, by means of DESAGA AS 30 automatic applicator (DESAGA, Germany). Plates were developed in ADC2 (Automatic Development Chamber) (CAMAG, Switzerland). Plates were developed using a mobile phase: ethyl acetate/methyl ethyl ketone/diisopropylether/formic acid (3:10:4:1, v/v/v/v) (distance of 7.5 cm). All chromatographical analyses were carried out at constant temperature (22 ± 1 °C) and humidity (48 ± 1%). Parameters of the development were as follows: 10 min of chamber saturation, 10 min of plate precondition, 120 s of the humidity control and 10 min of plate drying. After development, the chromatograms were scanned using a SCANNER 4 and WINCAT software (CAMAG, Switzerland).

2.5.1. Calibration and quantification

Portions of 2 μL of standard solutions (0.025, 0.050, 0.075, 0.150 and 0.200 μg/spot for all compounds) and 2 μL of the sample solution were applied to plates in triplicate. After development, the chromatograms were scanned. Densitometric detections were performed at 363 nm, for a bandwidth of 4.0 mm. The peak areas were recorded. The calibration curves of QG, IQ, HYP and RUT determined were obtained by plotting the peak areas *versus* the numbers of milligrams of standards. The amounts of compounds in samples were calculated using the regression and quadratic equations of the calibration curves. We have also decided to perform more complex evaluation to test linearity of calibration. All four curves proved to be linear by means of all common statistic tests (Lack-of-fit and Mandel's tests) used in this case, as shown in Table 1.

2.5.2. Recovery

The accuracy of the method was tested by performing recovery studies for three different concentrations (12.5, 25.0 and 37.5 ng/spot for QG, IQ, HYP and RUT). The results of the recovery study of QG, IQ, HYP and RUT by the proposed HPTLC-photodensitometric method are shown in Table 2.

2.5.3. Precision

The precision of the method was estimated on the basis of statistical evaluation for the determination of six samples. Intermediate precision was determined using three different concentrations (low, medium, high) of the mixed standards solutions. For intra-day precision, the mixed standard solutions were analyzed for three times within 1 day, whereas for inter-day precision, the standards were examined for consecutive 3 days.

2.5.4. Limit of detection (LOD) and limit of quantification (LOQ)

Limit of detection (LOD) and limit of quantitation (LOQ) values were calculated using the formulas: $3.3 \times \sigma/S$, $10 \times \sigma/S$ (σ – standard deviation of the intercept, S – the slope of the calibration curves), respectively. LOD and LOQ for each compound are shown in Table 1.

3. Results and discussion

Silica gel is by far the most frequently used layer material for phytochemical analysis by TLC and HPTLC methods. This phase has been used for separation of all classes of compounds. Unmodified silica gel and silica gel bonded phases with polar (hydrophilic bonded): cyano, amino, diol, and nonpolar (hydrophobic bonded): *n*-octadecyl groups were employed for analysis of polyphenolic compounds by TLC method. Diol plates have functional groups in the form of alcoholic hydroxyl residues [22]. So far, only few phytochemical separations on diol layer for flavonoids and other polyphenolics have been reported [23,24].

The goal of our present study was to determine major flavonoids by using of HTLC-densitometric method. Separation of selected quercetin derivatives present in ethyl acetate fractions obtained from selected *Potentilla* L. species was attempted (Fig. 2). Four flavonol-type compounds: quercetin 3-O-β-D-glucuropyranoside (miquelianin), quercetin 3O-β-D-glucopyranoside (isoquercitrin), quercetin 3-O-β-D-galactopyranoside (hyperoside) and quercetin 3-O-β-D-(6″-α-L-rhamnosylo)-glucopyranoside (rutin) (Fig. 1) were included in the comparative and qualitative study. The selection of compounds for chromatographic analyses resulted from the analysis of the incidence of particular compound groups (chemotaxonomy) in the aerial parts of plants from the genus *Potentilla* L. based on previously published literature data [14].

Optimization of our plant samples preparation was based on ultrasonication extraction at low temperature which is commonly used in the extraction of herbal samples [25]. Although higher temperature gave better extraction efficiencies, but it may also caused decomposition of phytoconstituents. The extraction with methanol and 80% (v/v) methanol at 50 °C for 30 min was chosen as preferred method. From results of preliminary experiments, the ethyl acetate fraction obtained by exhaustively extraction of aqueous solution of methanolic extract was chosen for further investigation. In our previous study, it was observed that only this fraction, in contrast to others (diethyl ether or *n*-butanolic), gave a high concentration of those constituents. Various solvent systems for the

Table 1
Statistical evaluation of calibration: calibration equations, linearity and regression diagnostics. Calibration data including R_f values, linear range (ng/spot), limit of detection (LOD; ng/spot) and limit of quantitation (LOQ); (ng/spot) for QG, IQ, HYP and RUT.

	QG	IQ	HYP	RUT
R_f values	0.42 ± 0.022	0.29 ± 0.014	0.22 ± 0.020	0.09 ± 0.006
Linear equation	$y = 20{,}020.47x - 8.93$	$y = 20{,}856.66x - 35.82$	$y = 23{,}701.34x + 58.47$	$y = 14{,}024.16x + 90.55$
Quadratic equation	$20{,}669.70x - 2865.86x^2 - 33.00$	$13{,}972.9x + 29{,}148.9x^2 + 213.20$	$26{,}949.77x - 14{,}343.15x^2 - 61.97$	$16460x - 10750x^2 + 0.29$
R^2 of linear model	0.9962	0.9868	0.9941	0.9845
Lack-of-fit test	0.1642 ($p = 0.92$)	4.895 ($p = 0.02$)	0.8969 ($p = 0.47$)	0.2498 ($p = 0.86$)
Mandel's test	0.119 ($p = 0.73$)	4.62 ($p = 0.05$)	1.5406 ($p = 0.24$)	0.8932 ($p = 0.36$)
Linear range (μg/spot)	0.025–0.200	0.025–0.200	0.025–0.200	0.025–0.200
LOD (ng/spot)	8.4	20.1	10.5	7.6
LOQ (ng/spot)	25.5	60.8	32.0	23.0

best optimization of HPTLC system and separation of all interesting compounds were tested. Our initial optimization of chromatographic separation included 9 polyphenolic compounds among which were derivatives of quercetin, kaempferol, apigenin, luteolin as well as ellagic acid and it derivative [26]. Mixtures of *n*-hexan-methyl ethyl ketone but also *n*-hexan-ethyl acetate–methyl ethyl ketone–formic acid, *n*-hexan-methyl ethyl ketone–formic acid, *n*-hexan-ethyl acetate–methyl ethyl ketone–formic acid, methyl ethyl ketone–diisopropylether–formic acid in different ratios were tried. So, finally, the focus was put on isocratic separation, as they are usually less time-consuming and are characterized by better reproducibility and repeatability. After dozens of modifications, the best separation of the above compounds was achieved using DIOL-modified silica gel plates and ethyl acetate–methyl ethyl ketone–diisopropylether–formic acid (3:10:4:1 v/v/v/v) as mobile phase. The robustness of the method was studied by determining the effects of small variation of mobile phase composition, chamber saturation, plate precondition, humidity control and plate drying periods as well as development distance. All chromatographical analyses were carried out at constant temperature (22 ± 1 °C) and humidity (48 ± 1%). In those conditions, flavonol derivatives were well separated. The identity of the bands of QG, IQ, HYP and RUT in the sample fractions was confirmed by overlaying their UV absorption spectra with those of the standards. Purity of the bands in the samples was confirmed by comparing the absorption spectra at the start, middle and end position of the bands. Using the aforementioned mobile phase, QG, IQ, HYP and RUT had R_f values of 0.42, 0.29, 0.22 and 0.09, respectively. Quantification was performed at the maximum of the absorption spectrum for all compounds (λ = 363 nm). The concentrations of QG, IQ, HYP and RUT in different samples were calculated using the regression of the calibration curves, which were linear within a range of 0.025 μg–0.200 μg/spot; $R^2 = 0.9962$; $y = 20{,}020.47x - 8.93$ for QG; $R^2 = 0.9868$; $y = 20{,}856.66x - 35.82$ for IQ; $R^2 = 0.9941$; $y = 23{,}701.34x + 58.47$ for HYP and $R^2 = 0.9845$; $y = 14{,}024.16x + 90.55$ for RUT. LOD and LOQ were respectively 8.1 and 25.5 ng/spot for QG, 20.1 and 60.8 ng/spot for IQ, 10.5 and 32.0 ng/spot for HYP and 7.6 and 23.0 ng/spot for RUT (Table 1). This indicated that the proposed method exhibits a good sensitivity for the quantification of these compounds. Statistical evaluation for the determination of six samples, intra-day and inter-day was chosen to determine the precision of the developed HPTLC assay. The intra- and inter-day precision (expressed in terms of CV [%]) were observed in the range of 0.6–8.0% and 3.8–8.0%, respectively (Table 2), which demonstrated the good precision of the analysis.

The accuracy of the proposed method was expressed as the recovery of standards added to the pre-analyzed samples. The average percentages of recovery of QG, IQ, HYP and RUT at three different levels were 97.7%, 100.6%, 95.0% and 101.4%, respectively (Table 2). Distribution of coefficients of tested compounds (α – coefficient of separation; Rs – resolution) are: RUT/HYP – $\alpha = 3.17$, Rs = 2.43; HYP/IQ – $\alpha = 1.44$, Rs = 1.03; IQ/GQ – $\alpha = 1.69$, Rs = 1.54. Their values shown that the investigated substances in the used system are well separated.

The results of quantitative determination of QG, IQ, HYP and RUT in ethyl acetate extracts from aerial parts of *Potentilla* species are presented in Table 3. The amounts of analyzed compounds measured by the method ranged between 16.7 ± 1.1 and 41.7 ± 0.6 mg/g for QG, 15.8 ± 1.3 and 36.7 ± 1.0 mg/g for IQ, 14.5 ± 0.5 mg/g for HYP and 6.7 ± 0.3 and 27.8 ± 2.1 mg/g for RUT. It is worth noting that we have confirmed the presence of quercetin 3-glucuronide (QG)

Table 2
Recovery study of QG, IQ, HYP and RUT and intermediate precision, CV [%] of the proposed HPTLC-photodensitometry method.

Compound	Amount of standard added [ng/spot]	Average amount found [ng/spot]	Recovery [%]	CV [%]	Average recovery [%]	Intra-day precision		Inter-day precision	
						ng/spot	CV [%]	ng/spot	CV [%]
QG	12.5	12.3	98.1	6.9	97.7	25.0	1.2	25.0	6.7
	25.0	24.9	99.5	6.7	± 6.8	150.0	3.3	150.0	8.0
	37.5	35.8	95.4	7.2		250.0	1.8	250.0	4.0
IQ	12.5	12.8	102.7	8.0	100.6	25.0	4.3	25.0	6.9
	25.0	24.6	98.6	7.4	± 6.7	150.0	3.0	150.0	7.8
	37.5	37.6	100.4	4.7		250.0	2.8	250.0	7.8
HYP	12.5	10.7	85.9	9.7	95.0	25.0	7.8	25.0	6.9
	25.0	24.2	96.9	10.2	± 8.2	150.0	4.6	150.0	4.0
	37.5	38.3	102.0	4.5		250.0	4.2	250.0	4.4
RUT	12.5	12.5	99.9	1.7	101.4	25.0	8.0	25.0	8.0
	25.0	25.1	100.6	4.9	± 4.3	150.0	0.6	150.0	6.4
	37.5	38.9	103.8	6.1		250.0	2.1	250.0	3.8

Table 3
QG, IQ, HYP and RUT content determined in ethyl acetate fractions of *Potentilla* species.

Sample name			Content [mg/g, w/w][b,c]							
			QG	CV [%]	IQ	CV [%]	HYP	CV [%]	RUT	CV [%]
1.	*Dasiphora fruticosa* (L.) Rydb. (syn. *Potentilla fruticosa* L.)[a]	Herb	36.9 ± 2.5	6.87	36.7 ± 1.0	2.65	14.5 ± 0.5	3.36	6.7 ± 0.3	3.98
2.	*Drymocallis rupestris* (L.) Soják (syn. *Potentilla rupestris* L.)[a]	Herb	30.9 ± 1.3	4.26	26.6 ± 2.3	8.48	ndt	–	ndt	–
3.	*Potentilla argentea* L.	Herb	31.1 ± 1.0	3.31	<LOQ	–	ndt	–	ndt	–
4.	*Potentilla erecta* (L.) *Raeusch.*	Herb	21.2 ± 1.5	7.16	<LOQ	–	ndt	–	<LOQ	–
5.	*Potentilla nepalensis Hook var.* '*Miss Wilmott*'	Leaves	16.7 ± 1.1	6.87	27.1 ± 0.8	3.05	ndt	–	12.3 ± 1.2	9.38
6.	*Potentilla nepalensis Hook var.* '*Miss Wilmott*'	Flowers	41.7 ± 0.6	1.36	15.8 ± 1.3	8.50	ndt	–	15.3 ± 1.3	8.40
7.	*Potentilla thuringiaca Bernh. ex Link*	Herb	ndt	–	33.8 ± 1.6	4.87	ndt	–	27.8 ± 2.1	7.42

ndt – compound not detected; <LOQ – under limit of quantification.
[a] Botanical nomenclature in accordance with the taxonomy of USDA/Natural Resources Conservation Service (NRCS).
[b] Mean values ± standard deviation ($n = 6$).
[c] Dry ethyl acetate extract.

in most from the analyzed samples of cinquefoils (Table 3). This also was confirmed previously by Lithuanian authors in relation to aerial parts of *D. fruticosa* where quercetin 3-glucuronide has been isolated from [27]. In addition, the compound was also described in *P. anserina* flowers [28]. Of note is the fact that the presence of the most from the analyzed of quercetin derivatives were described in investigated species from the first time.

Our results have shown that the proposed HPTLC with UV scanning photodensitometry method is suitable, being relatively simple, reproducible, specific, precise and accurate. Additionally, the method was validated for linearity, LOD, LOQ and precision, and was applied to analysis of these flavonoid compounds. The proposed method can be used for quality control of aerial parts from *Potentilla* plants and for the routine assay of simultaneous determination of QG, IQ, HYP and RUT in extracts and phytomedicines containing other *Potentilla* species. The HPTLC photodensitometry method can be applied as a chemotaxonomic tool for the rapid screening of *Potentilla* species and for the distinction between closely related taxa from the Rosaceae family.

Acknowledgements

This study was financially supported by the Polish Ministry of Science and Higher Education (Grant No. N N405 621638) and carried out with the use of CePT infrastructure financed by the European Union the European Regional Development Fund within the Operational Programme "Innovative economy" for 2007–2013.

References

[1] Sz. Nyiredy, Progress in forced-flow planar chromatography, J. Chromatogr. A 1000 (2003) 985–999.
[2] Ł. Cieśla, M. Waksmundzka-Hajnos, Two-dimensional thin-layer chromatography in the analysis of secondary plant metabolites, J. Chromatogr. A 1216 (2009) 1035–1052.
[3] M. Medić-Šarić, I. Jasprica, A. Mornar, Ž. Maleš, Application of TLC in the isolation and analysis of flavonoids, in: M. Waksmundzka-Hajnos, J. Sherma, T. Kowalska (Eds.), Thin Layer Chromatography in Phytochemistry, CRC Press Taylor & Francis Group, Boca Raton/London/New York, 2008, pp. 405–423.
[4] C.A.M. Pereira, J.H. Yariwake, F.M. Lanças, J-N. Wauters, M. Tits, L. Angenot, A HPTLC densitometric determination of flavonoids from *Passiflora alata*, *P. edulis*, *P. incarnata* and *P. caerulea* and comparison with HPLC method, Phytochem. Anal. 15 (2004) 241–248.
[5] M. Günther, P.C. Schmidt, Comparison between HPLC and HPTLC-densitometry for the determination of harpagoside from *Harpagophytum procumbens* CO_2-extracts, J. Pharm. Biomed. Anal. 37 (2005) 817–821.
[6] F. Soponar, A.C. Moţ, C. Sârbu, High-performance thin-layer chromatography and three-dimensional image analysis for the determination of rutin in pharmaceutical preparations, J. AOAC Int. 93 (2010) 804–810.
[7] M. Bartnik, K. Głowniak, A. Gromek, TLC and HPLC analysis of the flavonoid glycosides in the aerial parts of *Peucedanum tauricum* Bieb., J. Planar Chromatogr. 20 (2007) 127–130.
[8] Ž. Maleš, M. Plazibat, V.B. Vundać, I. Žuntar, K.H. Pilepić, Thin-layer chromatographic analysis of flavonoids, phenolic acids, and amino acids in some Croatian *Hypericum* taxa, J. Planar Chromatogr. 17 (2004) 280–285.
[9] V.B. Vundać, Ž. Maleš, M. Plazibat, P. Golja, B. Cetina-Čižmek, HPTLC determination of flavonoids and phenolic acids in some Croatian *Stachys* taxa, J. Planar Chromatogr. 18 (2005) 269–273.
[10] R. Nowak, TLC fingerprinting analysis of the European dog rose, J. Planar Chromatogr. 20 (2007) 43–48.
[11] P. Bhandari, N. Kumar, A.P. Gupta, B. Singh, V.K. Kaul, A rapid RP-HPTLC densitometry method for simultaneous determination of major flavonoids in important medicinal plants, J. Sep. Sci. 30 (2007) 2092–2096.
[12] G. Matysik, M. Wójciak-Kosior, Optimized method for the determination of flavonoid glycosides and aglycones, Chromatographia 61 (2005) 89–92.
[13] E. de Rijke, P. Out, W.M.A. Niessen, F. Ariese, C. Gooijer, U.A.Th. Brinkman, Analytical separation and detection methods for flavonoids, J. Chromatogr. A 1112 (2006) 31–63.
[14] M. Tomczyk, K.P. Latté, *Potentilla* – a review of its phytochemical and pharmacological profile, J. Ethnopharmacol. 122 (2009) 184–204.
[15] M. Tomczyk, A. Wiater, M. Pleszczyńska, Variation in total polyphenolics contents of aerial parts of *Potentilla* species and their anticariogenic activity, Molecules 15 (2010) 4639–4651.
[16] M. Tomczyk, A. Wiater, M. Pleszczyńska, In vitro anticariogenic effects of aerial parts of *Potentilla recta* and its phytochemical profile, Phytother. Res. 25 (2011) 343–350.
[17] M. Tomczyk, A. Bazylko, A. Staszewska, Determination of polyphenolics in extracts of *Potentilla* species by high-performance thin-layer chromatography photodensitometry method, Phytochem. Anal. 21 (2010) 174–179.
[18] A. Bazylko, A.K. Kiss, J. Kowalski, High-performance thin-layer chromatography method for quantitative determination of oenothein B and quercetin glucuronide in aqueous extract of *Epilobii angustifolii herba*, J. Chromatogr. A 1173 (2007) 146–150.
[19] ICH, Q2B Validation of analytical procedures: methodology, in: The 6th International Conference on Harmonization (ICH), November, Geneva, 2003.
[20] J. Ermer, Validation in pharmaceutical analysis. Part I: an integrated approach, J. Pharm. Biomed. Anal. 24 (2001) 755–767.
[21] A. Kiss, J. Kowalski, M.F. Melzig, Compounds from *Epilobium angustifolium* inhibit the specific metallopeptidases ACE, NEP and APN, Planta Med. 70 (2004) 919–923.
[22] J. Sherma, Sorbents and precoated layers for the analysis and isolation of primary and secondary metabolites, in: M. Waksmundzka-Hajnos, J. Sherma, T. Kowalska (Eds.), Thin Layer Chromatography in Phytochemistry, CRC Press Taylor & Francis Group, Boca Raton/London/New York, 2008, pp. 103–117.
[23] A. Bashir, M. Hamburger, M.P. Gupta, P. Solis, K. Hostettmann, Flavonol glycosides from *Monnina sylvatica*, Phytochem. 30 (1991) 3781–3784.
[24] I. Fecka, W. Cisowski, TLC determination of tannins and flavonoids in extracts from some *Erodium* species using chemically modified stationary phases, J. Planar Chromatogr. 15 (2002) 429–432.

[25] H. Bojarowicz, M.P. Marszałł, M. Wnuk, K. Goryński, A. Buciński, Determination of rutin in plant extracts and emulsions by HPLC-MS, Anal. Lett. 44 (2009) 1728–1737.
[26] A. Bazylko, M. Tomczyk, A. Flazińska, A. Lęgas, Chemical fingerprint of *Potentilla* species by using HPTLC method, J. Planar Chromatogr. 24 (2011) 441–444.
[27] G. Miliauskas, T.A. van Beek, P.R. Venskutonis, J.P.H Linssen, P. de Waard, J.R.E. Sudhölter, Antioxidant activity of *Potentilla fruticosa*, J. Sci. Food Agric. 84 (2004) 1997–2009.
[28] R. Kombal, H. Glasl, Flavan-3-ols and flavonoids from *Potentilla anserina*, Planta Med. 61 (1995) 484–485.

Journal of Pharmaceutical and Biomedical Analysis 61 (2012) 271–276

Contents lists available at SciVerse ScienceDirect

Journal of Pharmaceutical and Biomedical Analysis

journal homepage: www.elsevier.com/locate/jpba

Short communication

Development and validation of a liquid chromatographic method for purity control of clopidogrel–acetylsalicylic acid in combined oral dosage forms

Getu Kahsay, Ann Van Schepdael, Erwin Adams*

Katholieke Universiteit Leuven, Faculteit Farmaceutische Wetenschappen, Laboratorium voor Farmaceutische Analyse, O&N2, Herestraat 49, PB 923, B-3000 Leuven, Belgium

ARTICLE INFO

Article history:
Received 5 November 2011
Received in revised form
14 December 2011
Accepted 14 December 2011
Available online 23 December 2011

Keywords:
Aspirin
Clopidogrel
Reversed phase liquid chromatography
Impurities
Method development

ABSTRACT

A reversed phase liquid chromatographic method with UV detection for the simultaneous determination of clopidogrel and acetylsalicylic acid and their related substances in combined oral formulations was developed and validated. Good separation was achieved on a Luna C18 column (150 mm × 4.6 mm, 3 μm) using gradient elution at a flow rate of 1 mL/min and a column temperature of 35 °C. UV detection was performed at 220 nm. The validation was performed according to the ICH guidelines. The method proved to be specific, sensitive (LOQ = 0.975 μg/mL and 0.0384 μg/mL for clopidogrel and acetylsalicylic acid, respectively), linear in the concentration range from LOQ to 325 μg/mL for clopidogrel and from LOQ to 650 μg/mL for acetylsalicylic acid, precise (RSD values for intermediate precision <1%) and accurate with mean recovery values of 100.7% and 100.2% for clopidogrel and acetylsalicylic acid, respectively. Moreover, the solution stability and method robustness were examined. The method gives satisfactory separation of impurities of clopidogrel and acetylsalicylic acid and so it is suitable for quantification of the related substances as well as for the assay of the actives.

© 2011 Elsevier B.V. All rights reserved.

1. Introduction

Clopidogrel (CLP) and acetylsalicylic acid (ASA) (Fig. 1) are two widely used antithrombogenic agents and coadministration produces an enhanced therapeutic effect in many clinical conditions, particularly in high-risk patients with acute coronary syndromes [1]. Thus, their mechanisms are complementary and may decrease clot formation over either agent alone.

The synthesis of an active pharmaceutical ingredient (API) normally consists of several synthetic steps. The process related impurities can be formed at any step and could ultimately appear in the final drug substance. Impurities may also develop upon aging of both API and formulated APIs to medicines [2]. In addition, for an optically active single isomer drug there could be enantiomeric impurities present in the API. So, to guarantee the quality, safety and efficacy of drugs, sensitive and selective control methods are advisable. The chemical structures for impurities of CLP (usually used in its hydrogen sulfate form) and ASA are depicted in Figs. 2 and 3 [3,4].

A number of analytical methods have been reported in the literature for the individual determination of CLP or ASA. These methods include: spectrofluorimetry [5], reversed phase liquid chromatography (LC) [6–9], thin-layer chromatography [10], and spectrophotometry [11,12]. The simultaneous assay determination of CLP and ASA in tablets and capsules was also reported [13,14]. Moreover, a chemometric approach for the simultaneous estimation of CLP and ASA from combined dosage forms has been described by Rajput et al. [15]. For the determination of related substances in pharmaceutical dosage forms, several analytical methods [16,17] based on LC were reported for ASA. Concerning CLP, LC methods have been described for purity control of bulk drugs and pharmaceutical dosage forms including an enantiospecific LC method [18,19]. Both the European Pharmacopoeia (only drug substance) and United States Pharmacopeia (also drug products) describe separate LC methods for the determination of CLP and ASA and their respective impurities [3,4]. However, no LC method for the simultaneous analysis of CLP, ASA and their related substances in combined dosage forms has been reported so far. In this study, a reversed phase LC method for this purpose was developed and validated.

2. Experimental

2.1. Reagents and samples

Reference substances for CLP, ASA and their impurities, as well as Coplavix® 75/100 (combination tablets containing 75 mg of CLP/tablet and 100 mg of ASA/tablet) were kindly provided by Sanofi-Aventis Groupe (Paris, France). Two other tablet formulations containing 75 mg of CLP/tablet and 75 mg of ASA/tablet

* Corresponding author. Tel.: +32 16323444; fax: +32 16323448.
E-mail address: Erwin.Adams@pharm.kuleuven.be (E. Adams).

0731-7085/$ – see front matter © 2011 Elsevier B.V. All rights reserved.
doi:10.1016/j.jpba.2011.12.019

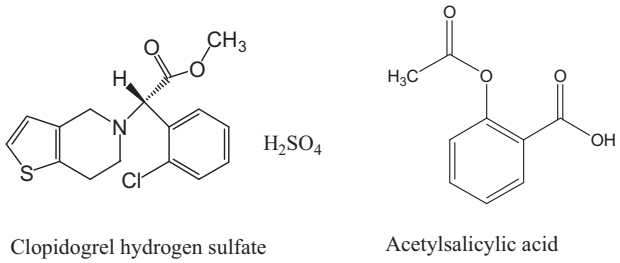

Clopidogrel hydrogen sulfate Acetylsalicylic acid

Fig. 1. Chemical structures of clopidogrel hydrogen sulfate and acetylsalicylic acid.

(Closprin® 75/75) or 150 mg of ASA/tablet (Noklot Plus® 75/150) were from Venus international (Mumbai, India) and Hetero Labs Ltd. (Kalyanpur, India), respectively. Sodium octane sulfonate monohydrate was purchased from Acros Organics (Geel, Belgium), HPLC gradient grade acetonitrile was from Fisher Scientific (Leicestershire, UK), HPLC grade methanol from Biosolve Ltd. (Valkenswaard, The Netherlands) and phosphoric acid, 98% purity from BDH (Briare, France).

2.2. Apparatus

LC analyses were performed on a Dionex Ultimate 3000 system from Dionex Softron GmbH (Germering, Germany) equipped with a high pressure pump (LPG-3400A), autosampler (WPS-3000T SL) and UV/VIS detector (MWD-3000). For data processing and acquisition, Chromeleon software version 6.80 from Dionex was used. An ultrasonicator from Branson Ultrasonics Corporation (Danbury, CT, USA) and a pH meter from Metrohm (Herisau, Switzerland) were used.

2.3. Chromatographic conditions

Chromatographic separations were achieved on a Luna C-18 (150 mm × 4.6 mm, 3 μm) column (Phenomenex, CA, USA). A Julabo

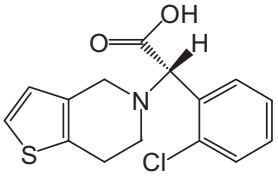

Imp. C1 (SR 26334)
(acid derivative)

Ph. Eur. : Impurity A
USP : Related compound A

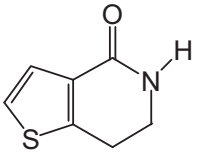

Imp. C4 (PCR 2482)

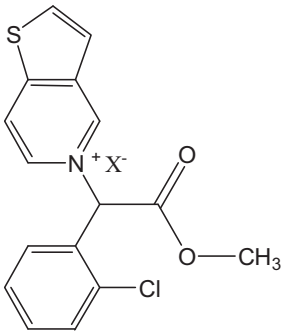

Imp. C7 (SR 26577)

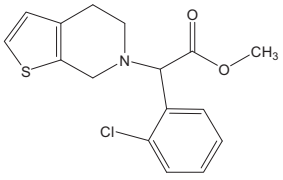

Imp. C2 (SR 24726)
(regio-isomer)

Ph. Eur. : Impurity B
USP : Related compound B

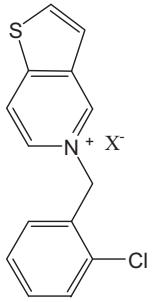

Imp. C5 (PCR 0625)

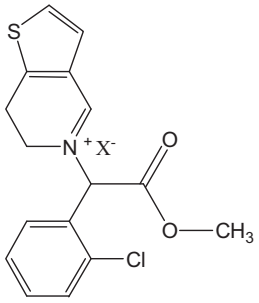

Imp. C8 (SR 120867)

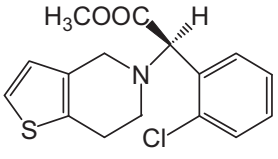

Imp. C3 (SR 25989)
(enantiomer)

Ph. Eur. : Impurity C
USP : Related compound C

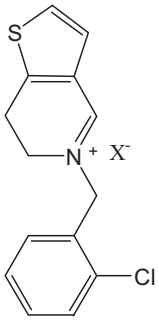

Imp. C6 (PCR 2549)

Fig. 2. Chemical structures of impurities of clopidogrel.

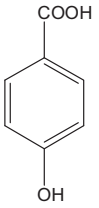

Imp. A1 = 4-hydroxybenzoic acid

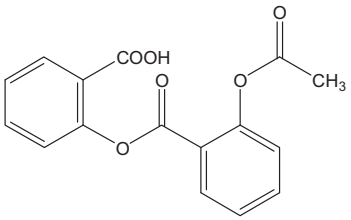

Imp. A4 = acetylsalicylsalicylic acid

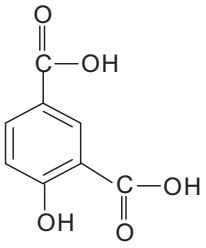

Imp. A2 = 4-hydroxyisophthalic acid

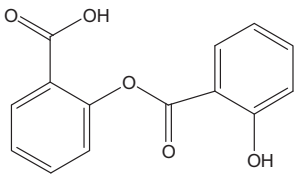

Imp. A5 = salicylsalicylic acid

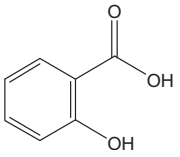

Imp. A3 = salicylic acid

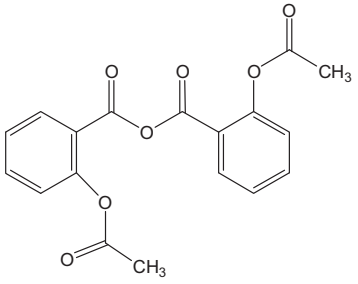

Imp. A6 = acetylsalicylic anhydride

Fig. 3. Chemical structures of impurities of acetylsalicylic acid.

EM immersion thermostat (Seelbach, Germany) was used to keep the water bath of the column at 35 °C. The mobile phase was a gradient mixture of mobile phase A (5:95 (v/v) mixture of methanol and a 1.0 g/L solution of sodium octane sulfonate monohydrate adjusted to pH 2.5 with dilute phosphoric acid) and mobile phase B (5:95 (v/v) mixture of methanol and acetonitrile) pumped at a flow rate of 1 mL/min. The gradient programme [time (min)/%B] was set as 0/10.5, 3/10.5 to 48/68.5, 68/68.5 to 80/10.5. The injection volume was set at 10 μL and the UV detection was made at 220 nm.

2.4. Assay determination of CLP and ASA

2.4.1. Preparation of sample and reference solutions

Sample solution: Twenty tablets from each Coplavix®, Closprin® and Noklot Plus® products were weighed and finely powdered with a mortar and pestle. A quantity of the powder equivalent to 20 mg of CLP and 26.67 mg (Coplavix®), 20 mg (Closprin®) or 40 mg (Noklot Plus®) of ASA was transferred into a 20.0 mL volumetric flask, sonicated with solvent mixture (mobile phase A – acetonitrile (40:60, v/v)) for ten minutes and then the solution was completed to volume with the same solvent. This solution was filtered through a 0.2 μm nylon filter (Whatman, Dassel, Germany) and 1.0 mL of the filtered solution was diluted to 10.0 mL with the solvent mixture. An aliquot of this solution was used for analysis.

Reference solutions: A stock reference solution of CLP was prepared by dissolving 26.10 mg of clopidogrel hydrogen sulfate (equivalent to 20 mg of CLP) in 20.0 mL of solvent mixture. A similar stock reference solution of ASA (20 mg/20 mL) was made. Since the content of ASA is different for the three products, 2 different dilutions were prepared: 1.0 mL of the stock reference solution of CLP and 1.0 mL of the stock reference solution of ASA were diluted to 10.0 mL (reference solution used for Coplavix® and Closprin®) while 1.0 mL of the stock reference solution of CLP and 2.0 mL of the stock reference solution of ASA were diluted to 10.0 mL with the solvent mixture (reference solution used for Noklot Plus®). For Coplavix®, peak areas of ASA reference were corrected with a factor 1.33 to compensate for the higher amount of ASA compared to Closprin® (100 mg vs. 75 mg).

2.5. Determination of related substances

2.5.1. Preparation of test and reference solutions

Test solutions: From the tablet powder used for assay, a quantity equivalent to 65 mg of CLP and 86.67 mg, 65 mg and 130 mg of ASA for Coplavix®, Closprin® and Noklot Plus®, respectively, was dissolved in a 10.0 mL volumetric flask and sonicated with the solvent mixture for 10 min. The solutions were cooled to room temperature and completed to volume with the same solvent. The solution was filtered through a 0.2 μm nylon filter to ensure the absence of particulate matter before analysis.

Reference solution: 1.0 mL of the test solution was diluted to 100.0 mL with the solvent mixture. 1.0 mL of this solution was further diluted to 10.0 mL (=0.1%) with the same solvent.

2.6. Method validation

The proposed method was validated according to the ICH guidelines [20] for its specificity, limit of detection (LOD), limit of quantification (LOQ), linearity, precision, accuracy, solution stability and robustness. Moreover, relative response factors for the impurities of CLP and ASA were also determined.

2.6.1. Specificity

The specificity of the developed method was examined for the presence of possible interference from excipients or sample matrix by overlaying chromatograms of (1) APIs spiked with impurities, (2) the drug products and (3) the blank.

2.6.2. Limit of detection (LOD) and limit of quantification (LOQ)

The LOD and LOQ for CLP and ASA were determined based on a signal-to-noise ratio of 3 and 10, respectively. Precision at the LOQ level was determined as % RSD for both APIs.

2.6.3. Linearity

Linearity was examined for the assay of the APIs and for the related substances. ASA: For the assay method, five concentrations (50 μg/mL, 100 μg/mL, 150 μg/mL, 200 μg/mL and 250 μg/mL) which cover the different concentrations of ASA in the tablets (75, 100, 150 mg/tablet) were injected. For related substances, concentrations ranging from LOQ to 650 μg/mL of the test solution were examined. CLP: Similarly, for the assay method, five concentrations ranging from 25 to 125% of the assay analyte concentration (25 μg/mL, 50 μg/mL, 75 μg/mL, 100 μg/mL and 125 μg/mL) and for the related substances concentrations ranging from LOQ to 5% of the test solution (100% = 6.5 mg/mL) were examined.

2.6.4. Precision and accuracy

Repeatability was examined by three fold analyses of two preparations of 100 μg/mL of CLP and 200 μg/mL of ASA in one day. Between days variation (intermediate precision) was examined on five consecutive days. The % RSD on the peak areas was evaluated. Accuracy of the proposed method was determined by the standard addition method on the dosage form to which known amounts of CLP and ASA standards have been added at different concentrations (CLP: 7.8 μg/mL, 15.6 μg/mL, 23.4 μg/mL; ASA: 20 μg/mL, 40 μg/mL, 60 μg/mL). The determination was carried out using three replicates at each concentration level. The accuracy was determined as percent recovery of amount of analyte added to the sample.

2.6.5. Robustness

To evaluate the robustness of the method, experimental factors that might cause variability in the method responses were examined. 4 factors (column temperature, pH, the time at which percent v/v of mobile phase B reaches its maximum and the percent v/v of mobile phase B at its plateau) were investigated. A two-level full factorial experimental design with $2^k + n$ number of runs, where k is the number of factors and n is the number of center points was applied. Thus, 19 experiments including three center points were performed in duplicate. The design was generated by using Modde 5.0 Umetrics software (Umeå, Sweden). For this test, one lower value and one higher value of the factors were used. The different values used for each factor in the design are given in Table 1. In every experiment, as response, the amount of impurities of CLP and ASA were calculated against a reference solution of 0.1%.

2.6.6. Response factors

The response factors of the impurities were determined from the ratio of the slopes of the impurities and the APIs. Solutions were prepared at concentrations from LOQ to 65 μg/mL of the test concentration for all impurities and APIs.

Table 1
Chromatographic parameter settings applied in the robustness investigation, corresponding to low (−), central (0) and high (+) levels.

Parameter	Low value (−)	Central value (0)	High value (+)
Temperature (°C)	33	35	37
pH	2.3	2.5	2.7
MP B (%, v/v)	67	68.5	70
MP B (time, min)	46	48	50

MP: mobile phase.

3. Results and discussion

3.1. Optimization of the chromatographic conditions

The starting conditions were taken from the European Pharmacopoeia monograph for clopidogrel hydrogen sulfate [3]. Three different columns have been tested for the separation of the specified and unspecified impurities of both APIs from the principal peaks: Luna C18 column (150 mm × 4.6 mm, 3 μm), Kromasil C18 column (150 mm × 4.6 mm, 5 μm) and Symmetry C18 column (150 mm × 4.6 mm, 3.9 μm). The specified impurities were better separated from the main peaks of CLP and ASA using the Luna column. Using the Kromasil column, impurity C1 and ASA were not well separated. Similarly, impurity C1 and ASA were coeluted using the Symmetry column. As a consequence, the Luna column was used for further method development and optimization. To optimize the chromatographic conditions for satisfactory separation of the APIs and their impurities, the effect of different chromatographic parameters was examined. The percentage of the organic modifier (acetonitrile) was changed from 37.5% to 80% in different gradient runs. The temperature of the column was varied from 25 °C to 40 °C (25 °C, 30 °C, 35 °C and 40 °C). Similarly the effect of pH was examined at 2.0, 2.5, 3.0 and 3.5. The concentration of the ion pairing reagent (IPR) (sodium pentane sulfonate monohydrate) was changed from 4.8 mM, 5.0 mM, 5.5 mM, 5.9 mM, 7.5 mM till 10.0 mM. Sodium pentane sulfonate monohydrate is the IPR used in the European Pharmacopoeia monograph for clopidogrel hydrogen sulfate in mobile phase A. However, not all impurities of CLP and ASA could be well separated. Changing the IPR to sodium octane sulfonate (SOS) monohydrate (investigated in the range 3.9–4.9 mM) did substantially improve the selectivity. It was found that a column temperature of 35 °C and an IPR concentration of 4.3 mM SOS in mobile phase A at pH 2.5 were the optimum conditions for the separation of the APIs and their impurities (Fig. 4).

3.2. Specificity

The specificity of the developed method was determined by examining the presence of possible interference from excipients or sample matrix. The chromatogram overlay of the spiked mixture of impurities and APIs, the drug product and the blank showed that the proposed method is specific for both APIs and their related substances as there was no interference observed. Absence of interference was verified for all forms. As the method is not enantiospecific, impurity C3 (=R-enantiomer of CLP) cannot be determined.

3.3. Limit of detection (LOD) and limit of quantification (LOQ)

The LOD and LOQ for CLP and ASA were determined by injecting a series of dilutions of known concentrations of the analytes. It was found that for CLP, the LOD and LOQ were 0.3 μg/mL and

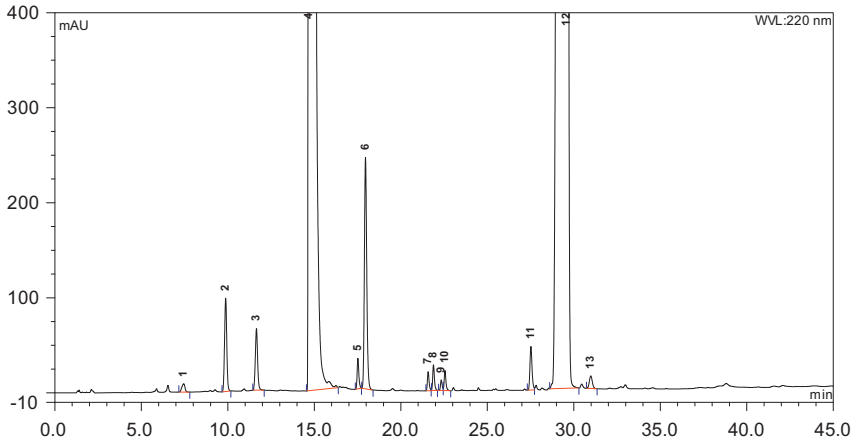

Fig. 4. Typical chromatogram of a solution of APIs spiked with all available impurities. Chromatographic conditions: see Section 2.3. **1**. Impurity A1; **2**. Impurity A2; **3**. Impurity C4; **4**. Aspirin; **5**. Impurity C1; **6**. Impurity A3; **7**. Impurity C5; **8**. Impurity C6; **9**. Impurity C7; **10**. Impurity C8; **11**. Impurity A4; **12**. Clopidogrel; **13**. Impurity C2.

1.0 μg/mL (RSD = 0.6%), respectively and for ASA, the LOD and LOQ were 0.04 μg/mL and 0.13 μg/mL (RSD = 0.6%), respectively.

3.4. Linearity

In the examined concentration ranges described under Section 2.6.3, linear responses were observed between the peak areas and the concentration of the analytes. The points in the residual plots were randomly distributed around the horizontal axis. The random dispersion of the residuals suggests that the linear model gives a good fit of the data. The coefficients of determination of the regression lines, the standard error of estimate and the linear regression equations are shown in Table 2.

3.5. Precision and accuracy

The precision of the method was evaluated as repeatability and intermediate precision. Repeatability was examined by three fold analyses of two preparations of 100 μg/mL of CLP and 200 μg/mL of ASA in one day. The RSD on the peak areas of these six determinations was not more than 0.5%. Intermediate precision was also determined for five consecutive days. The RSD on the peak areas (n = 30, 5 days) was not more than 1.0% (Table 2) suggesting that the proposed method is suitable for simultaneous analysis of CLP and ASA in combined dosage forms. In addition, the between days (intermediate) precision suggests that the developed method gave repeatable results for five consecutive days. Accuracy of the method was determined as percent recovery of a known added amount of analyte to the sample. The proposed method was found to give a mean recovery of 100.7% for CLP and 100.2% for ASA in the examined dosage form. So, the developed method gave satisfactory recoveries for both CLP and ASA.

3.6. Robustness test

A two-level full factorial experimental design was used to check the robustness of the LC method by introducing intentional variation of the experimental factors as described in Section 2.6.5. From the regression coefficient plots of the impurities it can be concluded that the percentage of impurities A1, A4, C2, C6 and C8 was not significantly (α = 0.05) affected when the chromatographic parameters were varied as shown in Table 1. Temperature and pH variations affect somewhat the percentage of impurities A2, C1, C4, C5 and C7 in the range examined. Although the effects are significant, their absolute value is small. The assay values of CLP and ASA were not affected by these small variations of the chromatographic factors investigated. Nevertheless, it is advisable to control these effects rather strictly.

3.7. Relative response factor

The results for the relative response factors of each impurity versus the APIs are shown in Table 3. The purity of the reference impurities, as given by the supplier, was taken into account.

3.8. Application to real samples

The proposed method was applied for the determination of CLP and ASA in three tablet products. The assay results are shown in Table 3. According to the USP specification, CLP or ASA tablets contain not less than 90.0% and not more than 110.0% of the labeled amount of CLP or ASA [4]. Hence, the content of ASA in the two generics (Closprin® and Noklot Plus®) does not comply with the prescribed limits stipulated by the USP. Next, impurities of CLP and ASA were quantified in the three products. The disregard limits for CLP and ASA impurities were 0.05% and 0.03%, respectively. Impurities of CLP were calculated versus the diluted CLP reference (0.1% dilution of the test solution) while impurities of ASA were calculated versus the diluted ASA reference (0.1% dilution of the test solution). The results are shown in Table 3. The level of impurity C1 in Closprin® was above the 1.2% limit of the USP monograph of CLP tablets [8]. In Closprin® and Noklot Plus®, the amount of impurity

Table 2
Results of linearity and intermediate precision determinations.

Method	APIs	Concentration range (μg/mL)	Regression equation	R^2	$S_{y,x}$	Intermediate precision (RSD, n = 30)
Assay	CLP	25–125	$y = 0.3933x - 2.1044$	0.9995	0.8	0.4
	ASA	50–250	$y = 0.3903x - 0.6833$	0.9994	0.4	0.6
Related substances	CLP	0.975–325	$y = 0.4059x + 0.1299$	1.0000	0.1	
	ASA	0.128–650	$y = 0.3000x - 0.1047$	0.9999	0.3	

Where R^2 = coefficient of determination; $S_{y,x}$ = standard error of estimate; y = mean (n = 3) peak area; x = concentration (μg/mL).

Table 3
Results for relative response factor, content and impurities determinations.

	CLP and ASA impurities (%, m/m)											Content (RSD, $n = 6$)	
	A1	A2	A3	A4	C1	C2	C4	C5	C6	C7	C8	CLP	ASA
Coplavix®	<0.03	<0.03	0.64	0.10	0.05	0.10	0.11	<0.05	0.05	<0.05	0.08	99.9 (0.5)	98.2 (1.7)
Closprin®	0.53	<0.04	20.94	<0.03	2.81	0.14	<0.05	<0.05	0.42	<0.05	0.06	96.2 (0.7)	75.5 (1.4)
Noklot Plus®	0.19	0.03	9.31	0.27	1.03	0.15	0.24	0.08	0.33	0.15	0.20	94.4 (0.3)	89.2 (0.3)
RRF	0.66	4.72	0.86	1.29	0.99	0.89	3.11	1.23	1.95	1.38	1.14	(1.00)	(1.00)

RRF: relative response factor; Ax: aspirin impurities; Cx: clopidogrel impurities.

A3 was far above the 3.0% limit prescribed in the USP monograph for coated ASA tablets.

4. Conclusion

The developed reversed phase LC method is specific, linear, sensitive, precise and accurate for the separation and determination of CLP, ASA and their impurities. As there is no official method, the LC method can be applied for routine quality control of the APIs and their related substances in combined oral dosage forms.

Acknowledgment

The authors would like to thank Sanofi-Aventis Groupe for the financial support of this work.

References

[1] G.E. Cooke, Y. Liu-Stratton, A.K. Ferketich, M.L. Moeschberger, D.J. Frid, R.D. Magorien, P.F. Bray, P.F. Binkley, P.J. Goldschmidt-Clermont, Effect of platelet antigen polymorphism on platelet inhibition by aspirin, clopidogrel, or their combination, J. Am. Coll. Cardiol. 47 (2006) 541–546.
[2] J. Roy, Pharmaceutical impurities—a mini-review, AAPS PharmSciTech 3 (2002) 1–2.
[3] European Pharmacopoeia, 7th ed., European Department for the Quality of Medicines, Strasbourg, France, 2010.
[4] United States Pharmacopeia, 32nd ed., United States Pharmacopeial Convention, Rockville, MD, 2010.
[5] P. Umapathi, S.K. Parirqoo, V. Thomas, J. Agarwal, Spectrofluorometric estimation of aspirin and dipyridamole in pure admixtures and in dosage forms, J. Pharm. Biomed. Anal. 15 (1997) 1703–1708.
[6] J. Sippel, L.L. Sfair, E.E. Schapoval, M. Steppe, New high performance liquid chromatographic method for determination of clopidogrel in coated tablets, J. AOAC Int. 91 (2008) 67–72.
[7] A. Mitakos, I. Panderi, A validated LC method for the determination of clopidogrel in pharmaceutical preparations, J. Pharm. Biomed. Anal. 28 (2002) 431–438.
[8] S. Minshan, A.G. Wilmer, W. Yu-Chien, T. Qinglin, J.M. Robert, R.S. Abu, Development and validation of a stability-indicating HPLC method for simultaneous determination of salicylic acid, betamethasone dipropionate and their related compounds in diprosalic lotion, J. Pharm. Biomed. Anal. 50 (2009) 356–361.
[9] R.V.S. Nirogi, N.K. Vishwottam, M. Shukla, K. Mudigonda, S. Maurya, R. Boosi, Quantification of clopidogrel in human plasma by sensitive liquid chromatography/tandem mass spectrometry, Rapid Commun. Mass Spectrom. 20 (2006) 1695–1700.
[10] N.S. Kamble, A. Venkatachalam, Gas chromatographic determination of clopidogrel from tablet dosage forms, Indian J. Pharm. Sci. 67 (2005) 128–129.
[11] P. Mishra, A. Dolly, Spectrophotometric methods for determination of clopidogrel in tablets, Indian J. Pharm. Sci. 67 (2005) 491–493.
[12] Z. Kokot, K. Burda, Simultaneous determination of salicylic acid and acetyl salicylic acid in aspirin delayed-release tablet formulations by second-derivative UV spectrophotometry, J. Pharm. Biomed. Anal. 18 (1998) 871–875.
[13] K. Anandakumar, T. Ayyappan, V. Raghu Raman, T. Vetrichelvan, A.S.K. Sankar, D. Nagavalli, RP-HPLC analysis of aspirin and clopidogrel bisulphate in combination, Indian J. Pharm. Sci. 69 (2007) 597–599.
[14] S.P. Sagar, Ion-pairing RP-HPLC method for simultaneous determination of aspirin and clopidogrel bisulphate in tablet and capsule dosage forms, Int. J. Pharm. Tech. Res. 2 (2010) 269–273.
[15] S.J. Rajput, R.K. George, D.B. Ruikar, Chemometric simultaneous estimation of clopidogrel bisulphate and aspirin from combined dosage form, Indian J. Pharm. Sci. 70 (2008) 450–454.
[16] G.P. McMahon, M.T. Kelly, Determination of aspirin and salicylic acid in human plasma by column-switching liquid chromatography using on-line solid-phase extraction, Anal. Chem. 70 (1998) 409–414.
[17] C. Akay, I.T. Degim, A. Sayal, A. Aydin, Y. Ozkan, H. Gul, Rapid and simultaneous determination of acetylsalicylic acid, paracetamol and their degradation and toxic impurity products by HPLC in pharmaceutical dosage forms, Turk. J. Med. Sci. 38 (2008) 167–173.
[18] D.R. Dantu, L. Kalyanarama, S.S. Shakil, P.V. Rao, A validated stability-indicating normal phase LC method for clopidogrel bisulfate and its impurities in bulk drug and pharmaceutical dosage form, J. Pharm. Biomed. Anal. 52 (2010) 160–165.
[19] Y. Gomez, E. Adams, J. Hoogmartens, Analysis of purity in 19 drug product tablets containing clopidogrel: 18 copies versus the original brand, J. Pharm. Biomed. Anal. 34 (2004) 341–348.
[20] ICH, Validation of Analytical Procedures: Text and Methodology Q2 (R1), EMEA, 2006.

Journal of Pharmaceutical and Biomedical Analysis 61 (2012) 277–283

Contents lists available at SciVerse ScienceDirect

Journal of Pharmaceutical and Biomedical Analysis

journal homepage: www.elsevier.com/locate/jpba

Mechanistic study on degradation of azelnidipine solution under radical initiator-based oxidative conditions

Eiji Ueyama [a,*], Fumie Takahashi [a], Jyunji Ohashi [a], Tomonori Konse [a], Naoyuki Kishi [a], Kenji Kano [b]

[a] Analytical and Quality Evaluation Research Laboratories, Pharmaceutical Technology Division, Daiichi Sankyo, 1-12-1, Shinomiya, Hiratsuka, Kanagawa 254-0014, Japan
[b] Division of Applied Life Sciences Graduate School of Agriculture, Kyoto University, Kitashirakawa Oiwake-cho, Sakyo-ku, Kyoto 606-8502, Japan

ARTICLE INFO

Article history:
Received 17 September 2011
Received in revised form 1 December 2011
Accepted 1 December 2011
Available online 17 December 2011

Keywords:
AIBN
Oxidation
Stability
Heavy oxygen water
Degradation product

ABSTRACT

We identified four degradants (Dg-A, Dg-B, Dg-C, Dg-D) of azelnidipine to be generated under radical initiator-based oxidative conditions and proposed the mechanistic pathway for their formation. 2,2′-Azobisisobutyronitrile was used as a radical initiator. There appeared to be two major pathways in the oxidation of the 1,4-dihydropyridine moiety. One was initiated by hydrogen abstraction from the C-4 position of the dihydropyridine ring, followed by hydrogen abstraction from the N-1 position, leading to aromatization of the dihydropyridine ring and Dg-A generation. The other was initiated by hydrogen abstraction from the N-1 position of the dihydropyridine ring followed by oxidation and hydrolysis to yield Dg-B. Furthermore, Dg-B was subjected to hydrolysis to generate Dg-C and Dg-D. It has been revealed that the rate of the Dg-B degradation was predominantly governed by the water content of the solvent used. Water participation in Dg-B degradation was proved by monitoring the incorporation of heavy oxygen atom (^{18}O) into the structure with LC–MS, in which the experiment was carried out in a medium prepared with heavy oxygen water to label ^{18}O during the hydrolysis.

© 2011 Elsevier B.V. All rights reserved.

1. Introduction

Drug substances used as pharmaceuticals have diverse molecular structures, and are therefore susceptible to many and variable degradations. Possible degradation pathways include hydrolysis, oxidation, photodegradation and complex interactions with excipients. Elucidation of the degradation pathway of a target drug is essential to develop a formulation to minimize chemical degradation and is useful to design appropriate stability testing for drug application. In addition, it is of considerable significance to develop a robust and highly selective stability-indicating method for determination of the drug and degradants to control the quality of a drug throughout a pharmaceutical development period.

Azelnidipine (AZ) (Fig. 1), the target compound in the present study, is a dihydropyridine-based calcium antagonist used to treat patients with hypertension in Japan. AZ has been shown to exert a long-lasting vasodilator action due to its long half-life in plasma [1], and it is categorized as a third-generation Ca^{2+}-channel blocker in view of such slow pharmacokinetic and pharmacodynamics profiles [2,3]. In a preliminary study, we developed a stability-indicating method for the assay of AZ with reverse-phase high-performance liquid chromatography (HPLC). To validate the stability-indicating power of the HPLC method, forced degradation studies were carried out under extreme thermal, humidified, oxidative, acidic, alkaline, and photolytic conditions. Characteristic oxidation products were generated under an oxidative condition with the radical initiator 2,2′-azobisisobutyronitrile (AIBN).

Azonitrile-based radical initiators such as AIBN and 4,4′-azobis-4-cyanovaleric acid (ACVA) are used to study the autoxidation mechanism of pharmaceuticals. Originally, this practice was proposed by Boccardi et al. [4,5]. They demonstrated that azonitrile-based radical initiators could produce primary oxidation degradation products observed by long-term storage of a drug and its pharmaceutical forms. Waterman et al. [6] and Hovorka et al. [7] reviewed the oxidative degradation of pharmaceuticals. They said that free radical-based oxidation experiments were useful to predict oxidation products by autoxidation. Recently, Alsante et al. [8] provided a "roadmap" for when and how to carry out forced degradation studies throughout drug-development stages. In that article, they strongly recommended that free radical-based oxidation experiments using azonitrile-based radical initiators should be conducted at all stages of development. Meanwhile, a benchmarking study of stress testing practices carried out in the pharmaceutical industry was conducted in 2003 [9]. According to that survey, 5 out of 20 companies (25%) used initiators such as AIBN or ACVA to predict oxidation of peroxy radicals. We believe that this percentage has probably increased. Nelson et al. explored

* Corresponding author. Tel.: +81 463 31 6888; fax: +81 463 38 3944.
E-mail address: ueyama.eiji.s2@daiichisankyo.co.jp (E. Ueyama).

0731-7085/$ – see front matter © 2011 Elsevier B.V. All rights reserved.
doi:10.1016/j.jpba.2011.12.001

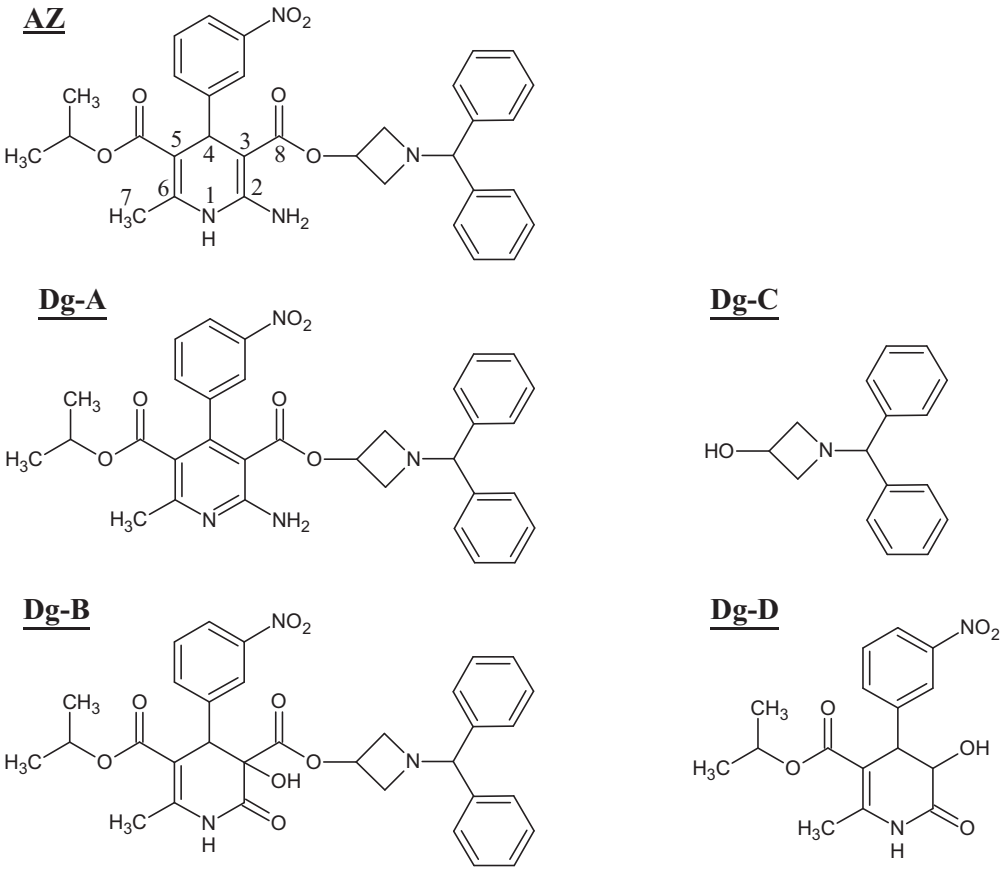

Fig. 1. Structure of azelnidipine and its degradants.

the practical implications of azonitrile-forced degradation experiments, and they provided increased clarity about several of the key parameters of the experiments [10,11]. Betigeri et al. [12] applied other hydrophilic free radical initiators such as 2,2′-azobis(-amidinopropane) dihydrochloride (AAPH) to assess the oxidative stability of drug candidates in development.

The mechanistic pathway of AZ oxidation induced by free radical-based initiators has not been published. It would be important from a scientific and pharmaceutical perspective to understand the mechanism of AZ oxidation under the radical chain oxidative condition. It would also be helpful in stabilizing a dosage form. The goal of the present study was to elucidate the radical initiator-produced oxidative degradants and the mechanistic pathway for their formation.

2. Experimental

2.1. Materials

AZ was obtained from Daiichi-Sankyo (Tokyo, Japan). Synthesized degradants Dg-A, Dg-B, Dg-C, and Dg-D were kindly donated by Ube Industries (Ube, Japan). AIBN and acetonitrile were purchased from Wako (Osaka, Japan). Heavy oxygen water (WATER-^{18}O) was purchased from Taiyo Nippon Sanso (Tokyo, Japan). All other chemicals used were of analytical grade from commercial sources.

2.2. HPLC assay

Agilent 1200 and 1100 systems equipped with a photodiode array detector were used for HPLC analyses. A Hydrosphere C18 (100 mm × 4.6 mm i.d., particle size 3 μm; YMC) was used as an analytical column. The temperature of the column was kept at 40 °C. Eluent was monitored at a wavelength of 220 nm. Mobile phase A was a mixture of 15 mM potassium dihydrogen phosphate, acetonitrile and methanol in a ratio of 8:1:1 (v/v/v), and mobile phase B was acetonitrile. The gradient elution was conducted as follows: from 0 min to 30 min, the composition of mobile phase B was increased from 20% to 75% and then maintained for 25 min at a constant flow rate of 1.0 mL/min.

2.3. Liquid chromatography–mass spectrometry (LC–MS)

LC–MS and liquid chromatography with tandem mass spectrometry (LC–MS/MS) analyses were undertaken using an Agilent 1200 system equipped with an LTQ Orbitrap XL mass spectrometer. A Cadenza CD-C18 (100 mm × 2 mm i.d., particle size 3 μm; Imtakt, Kyoto, Japan) was used as an analytical column. The temperature of the column was kept at 40 °C. Mobile phase A was 5 mM acetate buffer adjusted to pH 6.0 with 5 mM ammonium hydrogen carbonate, and mobile phase B was acetonitrile. Deuterium oxide was used as a solvent for the preparation of mobile phase A in an online hydrogen–deuterium (H/D) exchange LC–MS analyses. The gradient elution was conducted as follows: from 0 min to 1 min, the composition of mobile phase B was maintained at 40%. From 1 min to 10 min, the composition was increased from 40% to 90% and then maintained for 2 min at a constant flow rate of 0.3 mL/min. The major degradants were eluted on a chromatogram with the relative retention time of 0.31 (Dg-D), 0.33 (Dg-C), 0.83 (Dg-B), and 1.06 (Dg-A) against AZ.

For LC–MS, atmospheric pressure chemical ionization in positive polarity (Posi) for Dg-A, B, and C and negative polarity (Nega)

for Dg-D was utilized. Operating conditions on the mass spectrometer were as follows: vaporizer temperature, 400 °C; capillary temperature, 150 °C; sheath gas flow rate, 40 arb; aux gas low rate, 5 arb; source voltage, 6.00 kV; source current, 4 μA (Posi) and 5 μA (Nega); capillary voltage, 25 V (Posi) and −10 V (Nega); tube lens, 80 V (Posi) and −125 V (Nega). MS/MS data were acquired in product ion scan mode using collision energy at 14–15%.

2.4. Preparative LC

Isolation of Dg-B was undertaken using an Agilent 1200 preparative LC system. A Cadenza CD-C18 semi-preparative column (100 mm × 10 mm i.d., particle size 3 μm; Imtakt) was used for separation. Other chromatographic conditions were the same as for the LC–MS method with the following exceptions: (a) the flow rate was 5 mL/min, (b) the injection volume was 900 μL, and (c) the column temperature was ambient. Dg-B-containing fractions were collected, combined, and centrifugally evaporated.

2.5. Nuclear magnetic resonance (NMR)

NMR experiments were done using a Bruker Avance 400 MHz NMR spectrometer (Bruker, Billerica, MA, USA). All spectra were acquired on isolated sample dissolved in dimethylsulfoxide-d6 at 25 °C. Two-dimensional experiments were carried out. Double-quantum filter correlation spectroscopy (DQF-COSY) was used to establish the H—H network; edited-heteronuclear single-quantum correlation spectroscopy (edited-HSQC) revealed C—H connectivity; heteronuclear multiple-bond correlation spectroscopy (HMBC) was used to establish the C—C—H and C—C—C—H connectivity.

2.6. Oxidative degradation with AIBN

AZ and AIBN were dissolved with a mixture of water–acetonitrile (1:1, v/v) or acetonitrile, and the concentration was adjusted to 1.7 mM and 2 mM, respectively. The solution was stressed at 40 °C and sampled periodically. The sample solution was diluted fivefold with a mixture of water–acetonitrile (1:1, v/v) before analyses.

The effect of antioxidants on the rates of AIBN-initiated oxidation of AZ was investigated. An antioxidant, AZ and AIBN were dissolved with a mixture of water–acetonitrile (1:1, v/v), and the concentration adjusted to 1.7 mM, 1.7 mM and 2 mM, respectively. The solution was stressed at 40 °C and sampled periodically. The sample solution was directly injected to the HPLC system. The rate constant of each condition was obtained from the semi-logarithmic plots of % AZ remaining versus time.

2.7. Method validation for the HPLC assay

2.7.1. Linearity

Linearity test solutions for the assay of AZ were prepared at five concentrations from 10% to 150% with respect to AZ concentration (1 mg/mL).

Linearity test solutions for the assay of degradants, Dg-A, Dg-B, Dg-C, and Dg-D were prepared at eight concentrations from 0.008% to 4.0% (w/w) with respect to AZ concentration (1 mg/mL). A calibration curve was drawn by plotting the peak areas of degradants versus their corresponding concentration. The slope, *y*-intercept, residual sum of squares, and correlation coefficient were calculated.

The response factor for Dg-A, Dg-B, Dg-C, and Dg-D was calculated as the ratio of the slope of degradants and the slope of AZ obtained with linearity calibration plots.

2.7.2. Accuracy

The accuracy of the assay of degradants was evaluated in triplicate at three concentrations. The percentage recovery of these degradants was checked by injecting an AZ sample solution spiked with 0.05%, 1%, and 5% of Dg-A, Dg-B, Dg-C, and Dg-D with respect to AZ concentration (1 mg/mL).

2.7.3. Precision

The repeatability of the assay method was evaluated by carrying out six independent assays of test samples of AZ.

The repeatability of the assay of degradants was evaluated by analyzing six individual preparations of an AZ sample solution spiked with 1% of Dg-A, Dg-B, Dg-C, and Dg-D with respect to AZ concentration. The percentage relative standard deviation (RSD) of area for each degradant and AZ was calculated.

2.7.4. Limit of detection (LOD) and limit of quantification (LOQ)

The LOD and LOQ for Dg-A, Dg-B, Dg-C, Dg-D, and AZ were estimated at a signal-to-noise ratio of 3:1 and 10:1, respectively, by injecting a series of diluted solutions of known concentration. A precision study was also carried at the LOQ level by injecting six individual preparations of degradants and AZ and calculating the % RSD of the area.

3. Results and discussion

3.1. Development of a stability-indicating HPLC assay method

3.1.1. Method development

The main objectives of the chromatographic method were: (i) to get separation of the degradants generated from AZ, and (ii) that the method should be capable of resolving all impurities from each other. To separate all of the oxidative degradants, various mobile phases containing acetonitrile–aqueous phosphate buffers and acetonitrile–methanol–aqueous phosphate buffers were employed. As an intrinsic problem, insufficient separation between Dg-C and Dg-D caused by poor reproducibility of the retention time of Dg-C was noticed. Based on the identified structure (which will be mentioned below), it is anticipated that Dg-D would not have a characteristic acid dissociation constant (pK_a) in the molecule, whereas Dg-C would have a specific pK_a derived from a protonation site, a tertiary amine moiety, in the structure. Thus, we estimated the pK_a of Dg-C to be 7.6 with ACD/Labs pK_a DB software (product version 11.01; ACD/Labs, Toronto, Canada). Indeed, the retention time was drastically changed by altering the pH of the mobile phase in the vicinity of the pK_a. Consequently, it was suspected that the poor reproducibility of the retention time of Dg-C was ascribed to the pH of the mobile phase. We set the pH of the mobile phase to 5.0 to suppress the protonation of the amine moiety of Dg-C. Furthermore, it has been found that the addition of methanol causes better separation from other minor degradants. The chromatogram obtained from the oxidative stress testing of AZ is presented in Fig. 2. The major degradants were eluted on a chromatogram with the relative retention time of 0.16 (Dg-C), 0.32 (Dg-D), 0.83 (Dg-B), and 1.09 (Dg-A) against AZ.

3.1.2. Results of method validation

Linear calibration plots were obtained over the calibration ranges tested. All of correlation coefficients obtained were >0.999. Other results showed that an excellent correlation existed between the peak area and concentration of Dg-A, Dg-B, Dg-C, Dg-D, and AZ. The established response factors for Dg-A, Dg-B, Dg-C, and Dg-D were 1.36, 0.92, 1.11, and 0.82, respectively.

The percentage recovery of Dg-A, Dg-B, Dg-C, and Dg-D in drug substances was 93.1–116.8%. The % recovery and 95% confidence

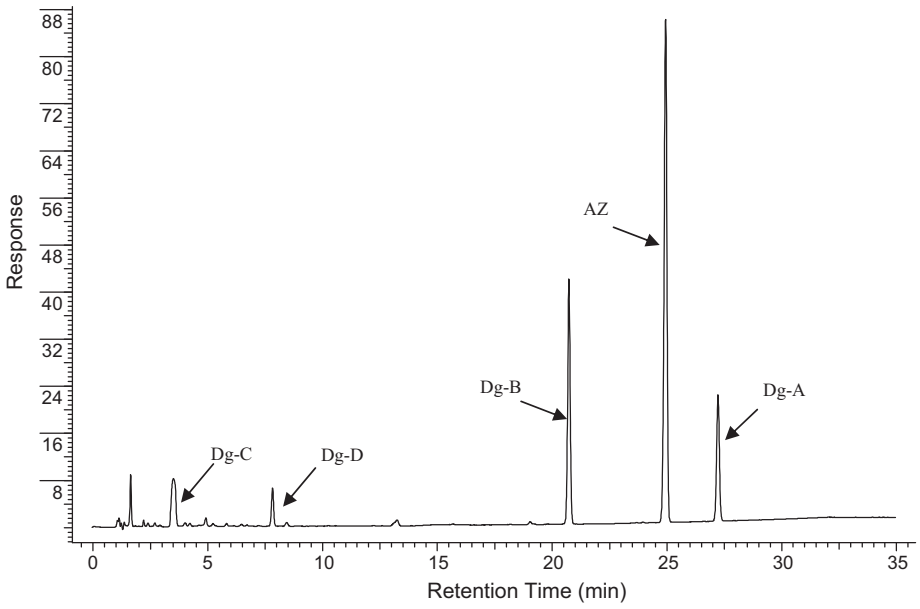

Fig. 2. HPLC chromatogram of oxidation-stressed azelnidipine held at 40 °C for 14 days with the HPLC assay method. The azelnidipine peak is denoted by "AZ" and four major degradants are indicated as Dg-A, -B, -C, and -D.

interval of the mean showed that this method was accurate for the determination of degradants.

The % RSD of area of degradants in the repeatability study was within 0.58%, confirming good repeatability of the method.

The LOD for Dg-A, Dg-C and AZ were 0.003%, and for Dg-B and Dg-D were 0.004% (w/w). The LOQ for Dg-A, Dg-B, Dg-C, Dg-D and AZ were 0.01% (w/w). The method precision for Dg-A, Dg-B, Dg-C, Dg-D, and AZ at LOQ level was <10% RSD.

It was considered that the developed stability-indicating HPLC assay method was suitable for this study to understand the degradation mechanism of AZ.

3.2. Generation and identification of degradation products

3.2.1. Generation of degradation products

At the initial stage, the major degradants Dg-A and Dg-B were mainly generated. Then, the concentration of Dg-C and Dg-D gradually increased with time. These degradants, Dg-A, Dg-B, Dg-C, and Dg-D, accounted for a large percentage of degradation products, >90% to total degradation of AZ throughout the storage period (a bar chart expressing the mass balance relationship between AZ and generated degradants under the oxidative condition at designated sampling points is shown in Fig. S1 in Supplementary material). Thus, structure elucidation of the primary degradants, Dg-A, Dg-B, Dg-C, and Dg-D, was conducted.

3.2.2. Identification of Dg-A

The characteristic fragment ions were *m*/*z* 539, 342, 222, and 167. The fragment ion with *m*/*z* 222 and 167 indicated that Dg-A retained an intact diphenyl methyl amine moiety. The major fragment ions with *m*/*z* 539 and 342 corresponded to the loss of two hydrogen atoms from each proposed fragment ion of AZ (results of LC–MS analyses are summarized in Table S1 in Supplementary material). All of results led to a pyridine-related derivative for Dg-A (Fig. 1).

3.2.3. Identification of Dg-B

The major fragment ion with *m*/*z* 582 was generated by H_2O loss from the molecular formula, and the *m*/*z* 558 ion was caused by the loss of an isopropyl moiety from Dg-B. The ion with *m*/*z* 343 corresponded to H_2O loss followed by the remaining diphenyl methyl amine moiety. Thus, these results indicated that Dg-B was another pyridine-related derivative. It was, however, not possible to fully characterize the Dg-B structure only by LC–MS analyses. Therefore, the degradation product was isolated and subjected to NMR analyses. Table 1 shows the ^1H and ^{13}C chemical shift assignment of the isolated sample. The assignment in Table 1 is limited to the dihydropyridine moiety because the NMR data of Dg-B showed similarity to those of the parent compound except position 1, 2, 4, and 3-OH. The significant difference from the parent was a proton resonance of 3-OH at 7.12 ppm that was not observed in the parent.

Table 1
^1H and ^{13}C assignments for dihydropyridine moieties of AZ and Dg-B.

Site	AZ				Dg-B			
	Type	^{13}C (ppm)	^1H (ppm)	HMBC[a]	Type	^{13}C (ppm)	^1H (ppm)	HMBC
1	>NH	–	8.83	3, 5, 7	>NH	–	10.44	3, 5, 7
2	>C=	151.7	–	4	>C=O	166.0	–	4, 7
3	>C=	76.2	–	1, 4	>C<	76.3	–	1, 4, 3-OH
4	>CH—	38.8	4.83	2, 3, 5, 6, 8, 27, 31, 32	>CH—	50.4	4.24	2, 3, 5, 6, 7, 8, 26, 27, 31, 32, 3-OH
5	>C=	102.7	–	1, 4, 7	>C=	105.3	–	1, 4, 7
6	>C=	145.2	–	4, 7	>C=	145.6	–	4, 7
7	—CH_3	18.6	2.29	1, 5, 6	—CH_3	17.8	2.34	1, 2, 5, 6
8	>C=O	167.1	–	4	>C=O	168.6	–	4, 9, 3-OH
2-NH_2	—NH_2	–	6.78	–	–	–	–	–
3-OH	–	–	–	–	—OH	–	7.12	2, 3, 4, 8

[a] Heteronuclearmultiple-bond correlations.

The edited-HSQC experiment indicated that the proton did not connect to a carbon atom. The HMBC experiment showed that the 3-OH proton correlated with C2, C3, C4, and C8 carbons. Meanwhile, the accurate mass result suggested that the difference in the molecular weight from AZ was 17-higher, which accounted for NH loss and O_2 addition. All of the data suggested that the hydroxyl group was located at the C3 position, and that C2 changed to a carbonyl carbon (Fig. 1).

3.2.4. Identification of Dg-C and Dg-D

The molecular formula of Dg-C was estimated to be $C_{16}H_{17}NO$, and the characteristic fragment ion with *m/z* 167 showed the existence of the diphenyl methyl moiety. These results led us to the structure of Dg-C (Fig. 1). Along with Dg-C generation, it was suspected that the corresponding counterpart, carboxylate form was generated. LC–MS results, however, showed the molecular formula of Dg-D to be $C_{16}H_{18}N_2O_6$, and it corresponded to a decarboxylation form not the carboxylate form (Fig. 1). The decarboxylation has been studied extensively for cases in which the carboxyl group is located at the β position to the keto group [9], and it supported the proposed structure. It was considered that Dg-C and Dg-D were secondary degradation products derived from Dg-B.

3.3. Evidence of water contribution to the AZ oxidation

The sample in lower water composition exhibited significant degradation, leading to Dg-A. Although slight degradation to Dg-B was observed, the formation rate was much lower than that of Dg-A. The sample in higher water composition showed faster Dg-B formation compared with that in the lower composition (Fig. S2 in Supplementary material). This result suggested that water played a key part in Dg-B formation. To elucidate in detail how water contributed to the degradation, the following mechanistic study was carried out. Heavy oxygen water ($H_2{}^{18}O$), which was employed as an oxygen tracer in a hydrolysis reaction, was applied to the AIBN experiments instead of H_2O. The evidence of water participation in the reaction was verified by monitoring incorporation of the heavy oxygen atom (^{18}O) into the structure of Dg-B with LC–MS. The $H_2{}^{18}O$ experiments gave very important information to characterize the reactive sites that were subject to hydrolysis and oxidation in the molecule. Dg-B yielded $[M+H]^+$ with *m/z* 602 under the $H_2{}^{18}O$ condition. The molecular weight of Dg-B was estimated to be 19-higher than that of AZ, which could be explained by NH loss and $^{16}O^{18}O$ addition. The results revealed that AZ was simultaneously subject to oxidation and hydrolysis under the oxidative condition. MS/MS spectra and the proposed fragmentation are shown in Fig. 3. Key fragment ions resulting from ^{18}O-labeled Dg-B were *m/z* 584, 345, and 319. This fragmentation suggested that $H_2{}^{16}O$ loss occurred at the beginning and a subsequent fragmentation proceeded afterwards. These fragment ions were higher by 2 in molecular weight compared with that generated from non-labeled Dg-B. The increment accounted for one ^{18}O addition. The $H_2{}^{16}O$ loss would be good evidence for the presence of a hydroxyl function composed of $-{}^{16}OH$ in the molecule. These results suggested that the C2 position was subject to hydrolysis and that the C3 position was oxidized.

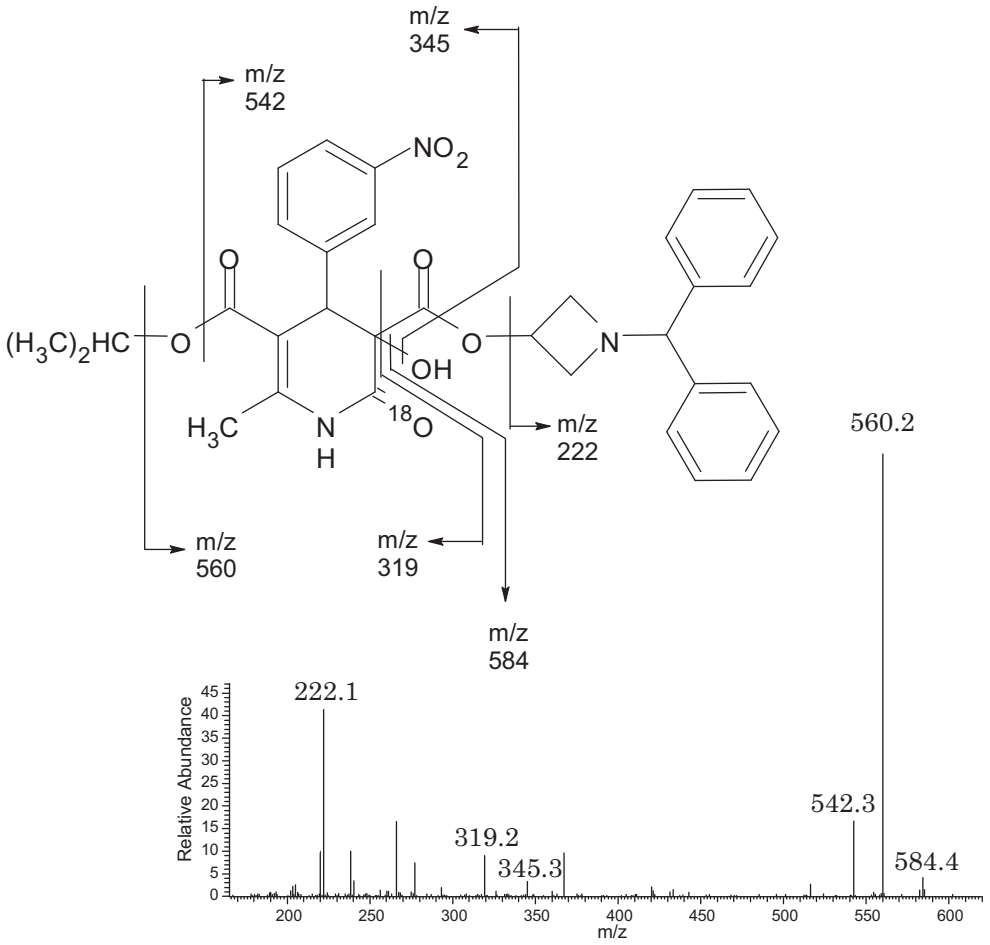

Fig. 3. MS/MS spectra and proposed fragmentation of ^{18}O-labeled Dg-B. The oxidation reaction was carried out with acetonitrile–$H_2{}^{18}O$ (1:1, v/v).

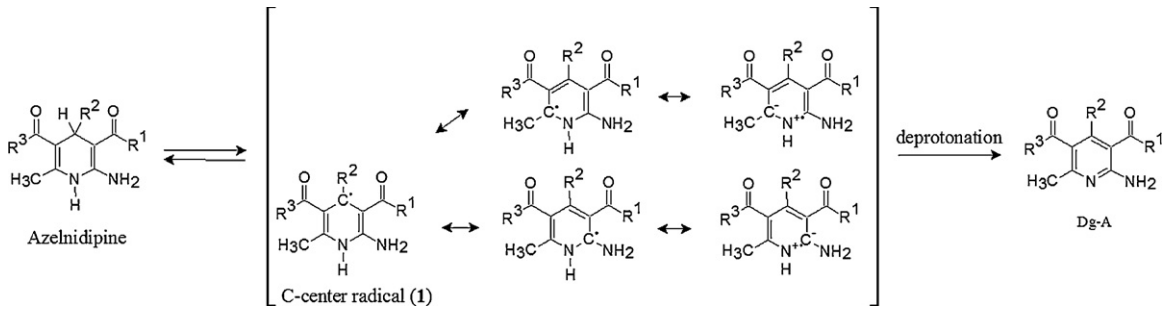

Fig. 4. Oxidation mechanism of azelnidipine via a C-center radical.

3.4. Oxidation mechanism of azelnidipine

Results of AIBN-initiated oxidation experiments supported the notion that the radical chain oxidation mechanism occurred on AZ oxidation because the use of azonitrile-type radical initiators such as AIBN or ACVA are intended to create a peroxy radical oxidation environment. To strengthen this hypothesis, the effectiveness of different antioxidants was assessed in solution by comparing the rate of AIBN-initiated oxidation in 50% (v/v) acetonitrile–water at 40 °C. Addition of antioxidants in the solution resulted in a decreasing rate of AIBN-initiated oxidation (Table S2 in Supplementary material). The effectiveness of antioxidants used under these conditions was ranked: BHT > propyl gallate > control (AIBN only). This result would suggest that AZ radical species mediate the oxidation reaction in the oxidative condition more precisely because BHT and propyl gallate, which acts as a radical scavenger, competitively prevented AZ oxidation.

Figs. 4 and 5 depict our proposed degradation mechanism of AZ under the radical initiator-based oxidative conditions. The AIBN experiments showed the predominant generation of the oxidation products Dg-A and Dg-B. It was assumed that hydrogen abstraction from the parent molecule by the peroxyl radical originated from AIBN occurred and the generated transient radical species proceeded to further reactions. We considered that AZ had possible resonance stabilization structures for the free radicals, which could be classified into two types of radical: C-center radical (**1**) (Fig. 4) and N-center radical (**2**) (Fig. 5). The C-center radical (**1**) had an unpaired electron localized prevalently in the C2, C4, or C6 position. The C-center radical (**1**) was aromatized via further one-electron oxidation and deprotonation, and this oxidation reaction generated Dg-A. Eisner et al. [13] investigated the effect of substituents introduced into a 1,4-dihydropyridine moiety on the rate of oxidation under free-radical conditions using diphenylpicrylhydrazyl. They reported that replacing hydrogen on the nitrogen (N1 position) by a methyl group did not affect the oxidation rate. The result indicated that the first step was abstraction of a hydrogen atom from the C4 position of 1,4-dihydropyridines. That result supported our proposed mechanism, in which the initiator-based free radical abstracts a hydrogen atom from the C4 position and generates a C-center radical (**1**).

The results of structure elucidation of Dg-B and water participation in the Dg-B generation step reasonably led to speculation on the generation of the N-center radical (**2**). The overall picture of the oxidation mechanism involves the N-center radical (**2**) as follows. The N-center radical (**2**) has an unpaired electron localized prevalently in the N1, C3, or C5 position. The resonance structure that has an unpaired electron localized in the C3 position is labile to react with molecular oxygen, and a transient alcohol (**3**) is generated. Furthermore, the imine moiety in the transient alcohol (**3**) undergoes hydrolysis to generate the corresponding ketone moiety. In this mechanism, the oxygen atom of the alcohol moiety is derived from the oxygen molecule, and the ketone moiety

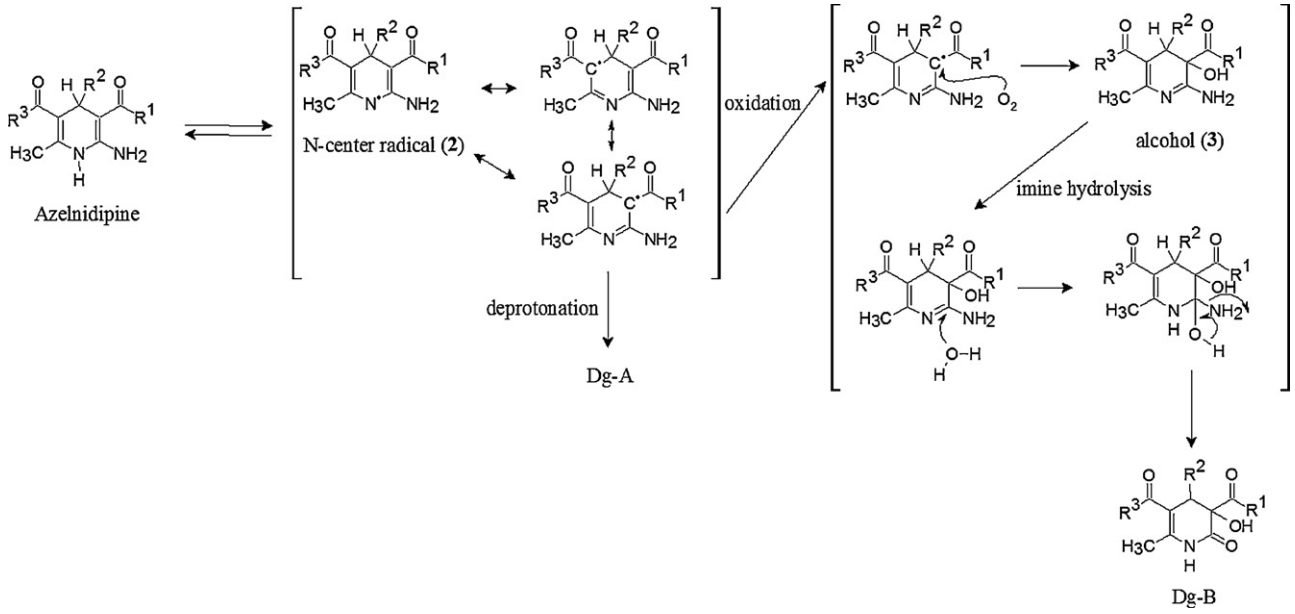

Fig. 5. Oxidation mechanism of azelnidipine via aN-center radical.

is derived from the water molecule. This mechanism is consistent with the result of the $H_2{}^{18}O$ experiment mentioned in Section 3.3. All of the results completely support this proposed mechanism involving the successive reaction of oxidation followed by hydrolysis.

4. Conclusions

A stability-indicating method that can realize separation of all oxidative degradants was developed and validated to understand the oxidation mechanism of AZ. The structure of the four major degradants of AZ generated under the oxidative conditions was characterized and mechanistic pathways proposed. The AIBN experiments provided numerous and useful information to elucidate the oxidation pathway. Furthermore, the oxidation experiment with heavy oxygen water as an oxygen tracer proved participation of water molecules in the Dg-B generation step. These findings helped to characterize the critical parameters affecting the stability of AZ and may provide useful insights into the manner of storage, formulation and analyses.

Acknowledgment

The authors thank Kanako Iwanade for supporting this work.

Appendix A. Supplementary data

Supplementary data associated with this article can be found, in the online version, at doi:10.1016/j.jpba.2011.12.001.

References

[1] K. Kuramoto, S. Ichikawa, A. Hirai, S. Kanada, T. Nakachi, T. Ogihara, Azelnidipine, amlodipine: a comparison of their pharmacokinetics and effects on ambulatory blood pressure, Hypertens. Res. 26 (2003) 201–208.
[2] K. Nakano, K. Egashira, H. Tada, Y. Kohjimoto, Y. Hirouchi, S. Kitajima, Y. Endo, X.H. Li, K. Sunagawa, A third-generation, long-acting, dihydropyridine calcium antagonist, azelnidipine, attenuates stent-associated neointimal formation in non-human primates, J. Hypertens. 24 (2006) 1881–1889.
[3] T. Toyo-Oka, W.G. Nayler, Third generation calcium entry blockers, Blood Press. 5 (1996) 206–208.
[4] G. Boccardi, C. Deleuze, M. Gachon, G. Palmisano, J.P. Vergnaud, Autoxidation of tetrazepam in tablets: prediction of degradation impurities from the oxidative behavior in solution, J. Pharm. Sci. 81 (1992) 183–185.
[5] G. Boccardi, Autoxidation of drugs: prediction of degradation impurities from results of reaction with radical chain initiators, Farmaco 49 (1994) 431–435.
[6] K.C. Waterman, R.C. Adami, K.M. Alsante, J. Hong, M.S. Landis, F. Lombardo, C.J. Roberts, Stabilization of Pharmaceuticals to oxidative degradation, Pharm. Dev. Technol. 7 (2002) 1–32.
[7] S.W. Hovorka, C. Schoneich, Oxidative degradation of pharmaceuticals: theory, mechanisms and inhibition, J. Pharm. Sci. 90 (2001) 253–269.
[8] K.M. Alsante, A. Ando, R. Brown, J. Ensing, T.D. Hatajik, W. Kong, Y. Tsuda, The role of degradant profiling in active pharmaceutical ingredients and drug products, Adv. Drug Deliv. Rev. 59 (2007) 29–37.
[9] K.M. Alsante, L. Martin, S.W. Baertschi, A stress testing benchmarking study, Pharm. Technol. 27 (2003) 60–72.
[10] E.D. Nelson, P.A. Harmon, R.C. Szymanik, M.G. Teresk, L. Li, R.A. Seburg, R.A. Reed, Evaluation of solution oxygenation requirements for azonitrile-based oxidative forced degradation studies of pharmaceutical compounds, J. Pharm. Sci. 95 (2006) 1527–1539.
[11] E.D. Nelson, G.M. Thompson, Y. Yao, H.M. Flanagan, P.A. Harmon, Solvent effects on the AIBN forced degradation of cumene: implications for forced degradation practices, J. Pharm. Sci. 98 (2009) 959–969.
[12] S. Betigeri, A. Thakur, K. Raghavan, Use of 2,2(-azobis(2-amidinopropane) dihydrochloride as a reagent tool for evaluation of oxidative stability of drugs, Pharm. Res. 22 (2005) 310–317.
[13] U. Eisner, M.M. Sadeghi, W.P. Hambright, Free radical oxidation of dihydropyridines, Tetrahedron Lett. 3 (1978) 303–306.

Journal of Pharmaceutical and Biomedical Analysis

Editors

B. Chankvetadze, Department of Chemistry, School of Exact and Natural Sciences, Tbilisi State University, 0179 Tbilisi, Georgia. E-mail: jpba_bezhan@yahoo.com

S. Görög, Chemical Works of Gedeon Richter Ltd., P.O. Box 27, H-1475 Budapest 10, Hungary. E-mail: s.gorog@richter.hu

J. Haginaka, Faculty of Pharmaceutical Sciences, Mukogawa Women's University, 11-68 Koshien Kyuban-cho, Nishinomiya 663-8179, Japan. E-mail: jpba@mukogawa-u.ac.jp

R. Moaddel, Baltimore, MD. 21224. USA. Tel: - +1-301-792-6579.

S. Pinzauti, Department of Pharmaceutical Sciences, University of Florence, Polo Scientifico, Via U. Schiff 6, 50019 Sesto Fiorentino, Italy. E-mail: pinz@unifi.it

Editorial Advisory Board

S.W. Baertschi (Indianapolis, IN, USA)
C. Barbas (Madrid, Spain)
C. Bertucci (Bologna, Italy)
F. Bressolle (Montpellier, France)
Z. Cai (Kowloon, Hong Kong)
P.S. Callery (Morgantown, WV, USA)
A. Cifuentes (Madrid, Spain)
J. Crommen (Liège, Belgium)
S. Fanali (Monterotondo Scalo, Italy)
S. Furlanetto (Florence, Italy)
M. Ganzera (Innsbruck, Austria)
R. Gotti (Bologna, Italy)
U. Holzgrabe (Würzburg, Germany)
K. Jozwiak (Lublin, Poland)
K. Kakehi (Higashi-Osaka, Japan)
R. Kaliszan (Gdansk, Poland)
S.P. Li (Macau, China)
W. Lindner (Vienna, Austria)
H. Lingeman (Amsterdam, The Netherlands)
B.K. Matuszewski (West Point, PA, USA)
N. Medlicott (Dunedin, New Zealand)
K. Nakashima (Nagasaki, Japan)
B. Noszál (Budapest, Hungary)
B.A. Olsen (Indianapolis, IN, USA)
K.W. Phinney (Gaithersburg, MD, USA)
S. Pichini (Rome, Italy)
M.A. Raggi (Bologna, Italy)
K.E. Scriba (Jena, Germany)
K. Shimada (Sendai, Japan)
S. Singh (S.A.S. Nagar, India)
E. Szökö (Budapest, Hungary)
T-H. Tsai (Taipei, Taiwan)
H. Ulrich (São Paulo, Brazil)
Y. Vander Heyden (Brussels, Belgium)
J.-L. Veuthey (Geneva, Switzerland)
I.D. Wilson (Macclesfield, UK)
G. Xu (Dalian, China)

Author enquiries
For enquiries relating to the submission of articles (including electronic submission) please visit this journals homepage at http://www.elsevier.com/locate/jpba. Contact details for questions arising after acceptance of an article, especially those relating to proofs, will be provided by the publisher. You can track accepted articles at http://www.elsevier.com/trackarticle. You can also check our Author FAQs at http://www.elsevier.com/authorFAQ and/or contact Customer Support via http://support.elsevier.com.

Funding body agreements and policies
Elsevier has established agreements and developed policies to allow authors whose articles appear in journals published by Elsevier, to comply with potential manuscript archiving requirements as specified as conditions of their grant awards. To learn more about existing agreements and policies please visit http://www.elsevier.com/fundingbodies

Orders, claims, and journal enquiries: please contact the Elsevier Customer Service Department nearest you:
St. Louis: Elsevier Customer Service Department, 3251 Riverport Lane, Maryland Heights, MO 63043, USA; phone: (877) 8397126 [toll free within the USA]; (+1) (314) 4478878 [outside the USA]; fax: (+1) (314) 4478077; e-mail: JournalCustomerService-usa@elsevier.com
Oxford: Elsevier Customer Service Department, The Boulevard, Langford Lane, Kidlington, Oxford OX5 1GB, UK; phone: (+44) (1865) 843434; fax: (+44) (1865) 843970; e-mail: JournalsCustomerServiceEMEA@elsevier.com
Tokyo: Elsevier Customer Service Department, 4F Higashi-Azabu, 1-Chome Bldg, 1-9-15 Higashi-Azabu, Minato-ku, Tokyo 106-0044, Japan; phone: (+81) (3) 5561 5037; fax: (+81) (3) 5561 5047; e-mail: JournalsCustomerServiceJapan@elsevier.com
Singapore: Elsevier Customer Service Department, 3 Killiney Road, #08-01 Winsland House I, Singapore 239519; phone: (+65) 63490222; fax: (+65) 67331510; e-mail: JournalsCustomerServiceAPAC@elsevier.com